



Inductively Coupled Plasma Spectrometry and its Applications

SECOND EDITION

Edited by Steve J. Hill



Blackwell
Publishing

Inductively Coupled Plasma Spectrometry and its Applications

Analytical Chemistry

Series Editors: *Alan J. Handley*
John M. Chalmers

A series which presents the current state of the art of chosen sectors of analytical chemistry. Written at professional and reference level, it is directed at analytical chemists, environmental scientists, food scientists, pharmaceutical scientists, earth scientists, petrochemists and polymer chemists. Each volume in the series provides an accessible source of information on the essential principles, instrumentation, methodology and applications of a particular analytical technique.

Titles in the Series:

Spectrochemical Analysis Using Infrared Multichannel Detectors

Edited by Rohit Bhargava

Spectroscopy in Process Analysis

Edited by John M. Chalmers

Atomic Spectroscopy in Elemental Analysis

Edited by Michael Cullen

Extraction methods in Organic Analysis

Edited by Alan J. Handley

Gas Chromatographic Techniques and Applications

Edited by Alan J. Handley

Inductively Coupled Plasma Spectrometry and its Applications 2nd Edition

Edited by Steve J. Hill

Pharmaceutical Analysis

Edited by David C. Lee and Michael Webb

Chemical Analysis of Contaminated Land

Edited by Clive Thompson and Paul Nathanail

Environmental Toxicity Testing

Edited by K. Clive Thompson, Kirit Wadhia and Andreas Loibner

Design and Analysis in Chemical Research

Edited by Roy Tranter

Inductively Coupled Plasma Spectrometry and its Applications

Edited by

Steve J. Hill

School of Earth, Ocean and Environmental Sciences
University of Plymouth
Plymouth, UK



Blackwell
Publishing

© 2007 by Blackwell Publishing Ltd

Editorial Offices:

Blackwell Publishing Ltd, 9600 Garsington Road, Oxford OX4 2DQ, UK

Tel: +44 (0)1865 776868

Blackwell Publishing Professional, 2121 State Avenue, Ames, Iowa 50014-8300, USA

Tel: +1 515 292 0140

Blackwell Publishing Asia Pty Ltd, 550 Swanston Street, Carlton, Victoria 3053, Australia

Tel: +61 (0)3 8359 1011

The right of the Author to be identified as the Author of this Work has been asserted in accordance with the Copyright, Designs and Patents Act 1988.

All rights reserved. No part of this publication may be reproduced, stored in a retrieval system, or transmitted, in any form or by any means, electronic, mechanical, photocopying, recording or otherwise, except as permitted by the UK Copyright, Designs and Patents Act 1988, without the prior permission of the publisher.

First published 2006 by Blackwell Publishing Ltd

ISBN-13: 978-1-4051-3594-8

ISBN-10: 1-4051-3594-8

Library of Congress Cataloging-in-Publication Data is available

A catalogue record for this title is available from the British Library

Set in 10/12 pt Minion by Charon Tec Ltd (A Macmillan Company), Chennai, India

Printed and bound in Singapore by Markono Print Media Pte Ltd

The publisher's policy is to use permanent paper from mills that operate a sustainable forestry policy, and which has been manufactured from pulp processed using acid-free and elementary chlorine-free practices. Furthermore, the publisher ensures that the text paper and cover board used have met acceptable environmental accreditation standards.

For further information on Blackwell Publishing, visit our web site:

www.blackwellpublishing.com

Contents

<i>Contributors</i>	<i>xv</i>
<i>Preface</i>	<i>xix</i>
1 Introduction – A Forward-Looking Perspective Gary M. Hieftje	1
1.1 Introduction	1
1.2 Extrapolation of past and current trends	2
1.2.1 Influences from science and technology	2
1.2.2 Influences from society, politics, and the economy	4
1.2.3 Past and current trends in atomic spectrometry	5
1.3 Influence of technology transfer	6
1.3.1 Electronics and data manipulation	6
1.3.2 Metal-binding structures	7
1.3.3 Novel separation methods	7
1.3.4 Detector technologies	8
1.4 Strengths and weaknesses of ICP-AES and ICP-MS	8
1.4.1 Strengths and weaknesses of ICP-AES	10
1.4.2 Strengths and weaknesses of ICP-MS	12
1.4.3 ICP limitations	13
1.5 Potential directions in ICP spectrometry	15
1.6 Concluding considerations	21
References	22
2 Fundamental Principles of Inductively Coupled Plasmas	27
Jean-Michel Mermet	
2.1 Principles to inductively coupled plasma generation	27

2.2	Equilibrium in a plasma	29
2.3	Line intensities	31
2.4	Line profiles	32
2.5	Temperature definitions	34
2.6	Temperature measurements	35
2.6.1	Kinetic temperature measurement	35
2.6.2	Rotational temperature measurement	36
2.6.3	Excitation temperature	38
2.6.3.1	Boltzmann plot	39
2.6.3.2	Line pair method	40
2.6.4	Electron temperature	41
2.7	Electron number density measurement	42
2.8	Ionic to atomic line intensity ratio	43
2.9	Active methods	44
2.9.1	Laser-induced fluorescence	45
2.9.2	Light scattering	45
2.10	Spatial profiles	46
2.11	Temperature and electron number densities observed in analytical ICPs	47
2.12	Plasma perturbation	48
2.13	Multiline diagnostics	49
	References	50
3	Basic Concepts and Instrumentation for Plasma Spectrometry	
	<i>Steve J. Hill, Andrew Fisher and Michael Foulkes</i>	61
3.1	Detection limits and sensitivity	61
3.1.1	ICP-Atomic emission spectrometry	61
3.1.2	Limits of detection	64
3.1.3	Axial systems	64
3.1.4	The sample introduction system	65
3.1.5	Detectors	66
3.2	Accuracy and precision	68
3.2.1	Instrumental drift	69
3.2.2	Matrix effects	70
3.2.3	Plasma effects	70
3.2.4	Spectral effects, interferences and background correction	71
3.2.5	Dynamic range	71
3.2.6	ICP-MS	72
3.3	Multi-element capability and selectivity	73
3.4	Instrumental overview	73
3.5	Radio-frequency generators	74
3.6	Torches	76
3.7	Spectrometers	79
3.7.1	Line isolation	79
3.7.2	Monochromators	81
3.7.3	Polychromators	82

3.8	Detectors	84
3.8.1	Photomultiplier tubes	84
3.8.2	Solid-state detectors	85
3.9	Nebulisers and spray chambers	86
3.10	Read-out devices, instrument control and data processing	87
3.11	Radial and axial plasmas	88
3.12	Instrumentation for high-resolution spectrometry	90
3.13	Micro-plasmas and plasma on a chip	90
	References	93
4	Aerosol Generation and Sample Transport <i>Barry L. Sharp and Ciaran O'Connor</i>	98
4.1	Introduction	98
4.2	Sample introduction characteristics of the ICP source	98
4.2.1	Particle size distribution	98
4.2.2	Plasma loading	99
4.3	Liquid aerosol generation	101
4.3.1	Pneumatic nebulization	101
4.3.1.1	Pneumatic nebulizer designs	102
4.3.1.2	Ultrasonic nebulizers	105
4.3.1.3	Alternative nebulizer designs	107
4.3.2	Spray chambers	108
4.3.2.1	Mode of operation	108
4.3.2.2	Practical designs of spray chambers	109
4.3.2.3	Desolvation	111
4.3.3	Chromatographic interfaces	112
4.4	Vapour generation	113
4.5	Electrothermal vaporization	114
4.6	Solid sampling via LA	115
4.6.1	Fundamentals	115
4.6.1.1	Ablation mechanisms	115
4.6.1.2	Elemental fractionation	116
4.6.2	Instrumentation	116
4.6.2.1	The laser	117
4.6.2.2	The ablation chamber and transport system	118
4.6.3	Sampling strategy	119
4.6.4	Quantification of LA-ICP-MS	119
4.7	Conclusion	120
	References	121
5	Fundamental Aspects of Inductively Coupled Plasma–Mass Spectrometry (ICP-MS) <i>Gavin O'Connor and E. Hywel Evans</i>	134
5.1	The ICP as an ion source	134
5.2	Ion sampling	136
5.2.1	Ion sampling interface	137
5.2.2	Ion focusing	140

5.2.3	Langmuir probe measurements	141
5.2.4	Ion kinetic energies	141
5.3	Mass analysers	142
5.3.1	Quadrupole	143
5.3.2	Magnetic sector	144
5.3.3	Double-focusing sector mass analyzer	145
5.3.4	Time of flight	146
5.3.5	Ion trap	149
5.4	Ion detection	150
5.4.1	Faraday cup collector	150
5.4.2	Electron multiplier	151
5.4.2.1	Continuous dynode	151
5.4.2.2	Discrete dynode	152
5.4.3	Channel plate	153
5.5	Instrumentation for interference removal	153
5.5.1	Cool plasma operation	153
5.5.2	Multiple reaction cell	154
5.5.3	Kinetic energy discrimination	156
	References	157
6	Use of ICP-MS for Isotope Ratio Measurements <i>Frank Vanhaecke, Lieve Balcaen and Philip Taylor</i>	160
6.1	Introduction	160
6.2	Fundamentals	160
6.2.1	Isotope ratios: general concepts	160
6.2.2	ICP-MS vs TIMS for isotope ratio measurements	164
6.3	Different sources of uncertainty affecting isotope ratios when measured using ICP-MS	170
6.3.1	Uncertainty according to International Standards Organisation–International Bureau of Weights and Measures	170
6.3.2	Sources of noise	171
6.3.3	Sources of bias	171
6.3.3.1	Mass discrimination	172
6.3.3.2	Mass scale shift	174
6.3.3.3	Background and contamination	174
6.3.3.4	Detector dead time	176
6.3.4	Optimisation of data acquisition parameters in terms of isotope ratio precision	178
6.4	ID: general concepts	178
6.4.1	Principle	179
6.4.2	Advantages and pitfalls	181
6.4.3	Optimum sample to spike mixing ratios	182
6.4.4	Spike calibration	182
6.4.5	Blank correction	183
6.4.6	ICP-IDMS: metrological and non-metrological mode of application	184

6.5	Selected applications	184
6.5.1	Introduction	184
6.5.2	Isotope dilution	185
6.5.2.1	ICP-IDMS for certification purposes/ metrological and non-metrological use of ICP-IDMS	185
6.5.2.2	ICP-IDMS combined with the application of matrix/trace separation procedures	186
6.5.2.3	Radioanalytical applications of ICP-IDMS	188
6.5.2.4	ICP-IDMS in connection with direct solid sampling	190
6.5.2.5	ICP-IDMS in elemental speciation	192
6.5.3	Tracer studies	197
6.5.3.1	Tracer studies for investigating (human) metabolism and element toxicity	197
6.5.4	Determination of natural isotope ratios	202
6.5.4.1	Geochronology and other application in the geosciences	202
6.5.4.2	Archaeometric and archaeological applications	206
6.5.4.3	Provenance determination of agricultural products	210
6.5.4.4	Environmental applications	211
6.5.4.5	Biological applications	214
6.6	General conclusions	215
	References	215
7	Alternative and Mixed Gas Plasmas <i>Andrew Fisher and Steve J. Hill</i>	226
7.1	Introduction	226
7.2	Ionization effects	229
7.3	Thermal conductivity	231
7.4	Use of alternative gases (mixed gas plasmas) in ICP-OES	232
7.4.1	Introduction of nitrogen	232
7.4.2	Introduction of hydrogen	233
7.4.3	Introduction of hydrocarbon gases	234
7.4.4	Introduction of halocarbon gases	234
7.4.5	Introduction of oxygen	234
7.4.6	Introduction of helium and other noble gases	235
7.4.7	Air plasmas for ICP-AES	236
7.4.8	Carbon dioxide plasmas	236
7.4.9	Multiple gas plasmas	237
7.5	Mixed gas plasmas for use with ICP-MS	237
7.5.1	Introduction of nitrogen	238
7.5.2	Introduction of hydrogen	239
7.5.3	Introduction of hydrocarbon gases	240
7.5.4	Introduction of oxygen	240
7.5.5	Introduction of helium and other noble gases	241
7.5.6	Air plasmas for ICP-MS	242

7.6	Low-pressure plasmas	242
7.7	Low-power plasmas	245
7.8	Conclusions	245
	References	245
8	Electrospray Ionization Mass Spectrometry: A Complementary Source for Trace Element Speciation Analysis <i>Helle R. Hansen and Spiros A. Pergantis</i>	251
8.1	Introduction	251
8.1.1	Historical aspects of ES-MS	252
8.1.2	The role of ES-MS in biomolecule analysis	253
8.2	Mechanistic aspects of electrospray ionization	254
8.2.1	Formation of charged droplets	254
8.2.2	Electrospray sources	256
8.2.3	Droplet disintegration	257
8.2.4	Gas-phase ion formation	258
8.2.5	Sampling electrosprayed ions	259
8.3	Mass analysers used with ES	259
8.3.1	Quadrupole: time-of-flight analysers	259
8.3.2	Quadrupole: ion trap mass analyser	261
8.4	Element speciation using ES-MS	262
8.4.1	Arsenic	262
8.4.1.1	Recognizing As-containing peaks by ES-MS	262
8.4.1.2	Parallel HPLC-ICP-MS and single quadrupole HPLC-ES-MS	263
8.4.1.3	Application of ES-MS/MS for identification of As species in crude matrices	264
8.4.2	Selenium	265
8.4.2.1	Recognizing Se-containing peaks by ES-MS	266
8.4.2.2	Parallel HPLC-ICP-MS and HPLC-ES single quadrupole MS	266
8.4.2.3	ES-MS/MS analysis after chromatographic purification (heart-cutting)	267
8.4.2.4	Parallel HPLC-ICP-MS and HPLC-ES-MS/MS analysis	267
8.4.2.5	Selenium-containing proteins	267
8.4.3	Antimony	269
8.4.3.1	Recognizing Sb-containing peaks by ES-MS	269
8.4.3.2	Sb interaction with biomolecules	270
8.4.3.3	Complexation behaviour of Sb	270
8.4.4	Tin	271
8.4.4.1	Recognizing Sn-containing peaks by ES-MS	271
8.5	Conclusions	273
	References	273

9	Geological Applications of Plasma Spectrometry	
	<i>Douglas L. Miles and Jennifer M. Cook</i>	277
9.1	Introduction	277
9.2	Sampling and sample preparation	279
9.2.1	Sampling	279
9.2.2	Sample preparation	281
9.2.2.1	Comminution	281
9.2.2.2	Sample decomposition and dissolution	283
9.2.2.2.1	Decomposition with acids	284
9.2.2.2.2	Decomposition by fusion	286
9.2.2.2.3	Microwave-assisted decomposition	287
9.2.2.2.4	Selective extraction schemes	289
9.3	Determination of major elements	290
9.4	Determination of trace elements	291
9.5	Determination of the rare earth and other incompatible trace elements	293
9.5.1	Background	293
9.5.2	Determination of the REEs by ICP-AES	294
9.5.3	Determination of the REEs by ICP-MS	295
9.5.4	Determination of other incompatible elements	297
9.6	Determination of gold and the PGEs	299
9.7	Measurement of isotope ratios	302
9.8	Laser ablation	304
9.8.1	Analysis of fluid inclusions	310
9.8.2	<i>In situ</i> determination of isotope ratios	311
9.9	Future trends	312
	References	315
10	Environmental and Clinical Applications of Inductively Coupled Plasma Spectrometry	
	<i>Anne P. Vonderheide, Baki B.M. Sadi, Karen L. Sutton, Jodi R. Shann and Joseph A. Caruso</i>	338
10.1	Introduction	338
10.2	Analysis of air	339
10.2.1	Introduction	339
10.2.2	Sampling	339
10.2.3	Sample preparation	340
10.2.4	Interferences	340
10.2.5	Applications	341
10.3	Analysis of water	341
10.3.1	Introduction	341
10.3.2	Sample collection and preparation	343
10.3.3	Sample clean-up and interference removal	343
10.3.4	Preconcentration	344
10.3.5	Hydride generation	344

10.3.6	Elemental speciation studies	345
10.3.7	Analysis of non-metals	346
10.4	Analysis of clinical samples	348
10.4.1	Introduction	348
10.4.2	Single element/multi-element	349
10.4.3	Types of mass spectrometers in use	349
10.4.4	Sample introduction	355
10.4.5	Speciation of elements	356
10.5	Conclusions	361
	References	361
11	Applications of Plasma Spectrometry in Food Science	
	<i>Helen M. Crews, Paul Robb and Malcolm J. Baxter</i>	387
11.1	Introduction	387
11.2	Analytical challenges	388
11.2.1	Isobaric overlap in ICP-MS	388
11.2.2	Polyatomic and doubly charged species interferences in ICP-MS	389
11.2.3	Ionization interferences in ICP-MS	391
11.2.4	Interferences in ICP-AES	392
11.2.5	Other sources of error	392
11.3	Sample collection and storage	393
11.3.1	Uncertainty associated with sampling	393
11.4	Sample preparation	393
11.4.1	Liquid foods	394
11.4.2	Meat	394
11.4.3	Fish and shellfish	394
11.4.4	Vegetables	395
11.4.5	Fruits	395
11.4.6	Fats and oils	395
11.4.7	Cereals	396
11.4.8	Mixed fruit/whole meals/diets	396
11.5	Sample pre-treatment	396
11.5.1	Samples requiring minimal pre-treatment	396
11.5.2	Digestion of foods and related samples with acid(s)	397
11.5.3	Other techniques	398
11.5.4	Pre-concentration methods and removal of interferences	399
11.6	Quantification	399
11.6.1	Practical considerations	400
11.6.2	Diet analysis	400
11.6.3	Isotope ratio measurements	401
11.7	Quality control	401
11.7.1	General observations	403
11.7.2	Instrument performance	403
11.7.3	Limits of detection	403

11.7.4	Spike and reference material recoveries	405
11.7.5	Replicate analyses	406
11.7.6	Reporting results	406
11.8	Speciation studies	406
11.8.1	Arsenic speciation	406
11.8.2	Applications using HPLC	407
11.8.3	Selenium speciation	409
11.9	Future trends	412
	References	413
	Index	423

This page intentionally left blank

Contributors

Dr Lieve Balcaen	Laboratory of Analytical Chemistry, University of Ghent, Proeftuinstraat 86, B-9000 Ghent, Belgium
Mr Malcolm J. Baxter	Central Science Laboratory, Sand Hutton, York, YO41 1LZ, UK
Professor Joseph A. Caruso	Department of Chemistry, University of Cincinnati, PO Box 210172, Cincinnati, OH 45221 0172, USA
Ms Jennifer M. Cook	British Geological Survey, Keyworth, Nottingham, NG12 5GG, UK
Dr Helen M. Crews	Central Science Laboratory, Sand Hutton, York, YO41 1LZ, UK
Dr E. Hywel Evans	School of Earth, Ocean and Environmental Sciences, University of Plymouth, Drake Circus, Plymouth, Devon, PL4 8AA, UK
Dr Andrew Fisher	School of Earth, Ocean and Environmental Sciences, University of Plymouth, Drake Circus, Plymouth, Devon, PL4 8AA, UK
Dr Michael Foulkes	School of Earth, Ocean and Environmental Sciences, University of Plymouth, Drake Circus, Plymouth, Devon, PL4 8AA, UK
Dr Helle R. Hansen	Department of Chemistry, Environmental Chemical Processes Laboratory, University of Crete, Knossou Ave, Heraklion, 71409 Greece

Prof. Gary M. Hieftje	Department of Chemistry, Indiana University, Bloomington, IN47405, USA
Prof. Steve J. Hill	School of Earth, Ocean and Environmental Sciences, University of Plymouth, Drake Circus, Plymouth, Devon, PL4 8AA, UK
Prof. Jean-Michel Mermet	Laboratoire des Sciences Analytiques, Bât. 308, Université Claude Bernard-Lyon 1, 43 bvd du 11 Novembre 1918, 69622 Villeur-banne Cedex, France
Mr Douglas L. Miles	British Geological Survey, Keyworth, Nottingham, NG12 5GG, UK
Mr Ciaran O'Connor	Analytical Atomic Spectroscopy Group, Department of Chemistry, Loughborough University, LE11 3TU, UK
Dr Gavin O'Connor	LGC, Queens Road, Teddington, Middlesex, TW11 0LY, UK
Prof. Spiros A Pergantis	Department of Chemistry, Environmental Chemical Processes Laboratory, University of Crete, Knossou Ave, Heraklion, 71409 Greece
Dr Paul Robb	Central Science Laboratory, Sand Hutton, York, YO41 1LZ, UK
Dr Baki B.M. Sadi	Department of Chemistry, University of Cincinnati, PO Box 210172, Cincinnati, OH 45221 0172, USA
Prof. Jodi R. Shann	Department of Biological Sciences, University of Cincinnati, Cincinnati, OH 45221-0006, USA
Dr Barry L. Sharp	Analytical Atomic Spectroscopy Group, Department of Chemistry, Loughborough University, LE11 3TU, UK
Dr Karen L. Sutton	Procter and Gamble Technical Centres Ltd, Rusham Park, Whitehall Lane, Egham, TW20, 9NW, UK
Dr Philip Taylor	Institute for Reference Materials and Measurements, European Commission Joint Research Centre, Retieseweg 111, B-2440 Geel, Belgium
Prof. Frank Vanhaecke	Laboratory of Analytical Chemistry, University of Ghent, Proeftuinstraat 86, B-9000 Ghent, Belgium
Dr Anne P. Vonderheide	Department of Biological Sciences, University of Cincinnati, Cincinnati, OH 45221-0006, USA

Preface

To undertake to update and revise a book that has been well received is rather a daunting task. Clearly any editor, and indeed all of the authors who contribute, would like the second edition to be even better than the first. The difficulty however is how to achieve that. The first edition of this book was perceived as a handbook for users of inductively coupled plasmas (ICPs) who wanted a better understanding of the theory, yet also wanted a practical insight of how best to approach a range of applications. These key objectives have been retained in the second edition but the focus of the book has changed so that the overall perspective is more forward looking. Much of the historical development behind the use of the techniques described in some detail in the first edition has been minimised and the emphasis is now on state-of-the-art developments and potential developments for the future.

The book has been structured into 11 chapters, each utilising the authors' expertise and experience, and providing enough detail to be useful to both the new and experienced users. The first chapter of the previous edition presented the first full account by Stan Greenfield of the early development of the ICP. This second edition starts at the other end of the spectrum and sets the scene for the rest of the book by providing a thought provoking account of both the strengths and weaknesses of ICP-AES and ICP-MS and how the impact of technology transfer is starting to effect current trends and may impact on future developments. I was delighted when Gary Hieftje accepted the challenge to write this chapter.

The rest of the book follows the same format as the first edition although there have been some important changes. Chapter 2 looks at the fundamental principles of inductively coupled plasma including details of temperature measurement and recent studies employing solid-state detectors to acquire the entire UV-visible spectra for diagnostic studies. Chapter 3 introduces the basic concepts and requirements for precise and accurate practical measurement and then overviews the instrumentation required for ICP-AES. Again however, the focus is on current developments and there are sections on high-resolution spectrometry, microplasmas and plasma on a chip technology. Chapter 4 looks in detail at sample introduction via liquid aerosol generation but also describes other forms of sample transport such as vapour generation techniques, electrothermal vaporisation and solid sample laser ablation. In Chapter 5 the focus turns to ICP-MS, covering fundamental aspects such as ion sampling, mass analysers and ion detection, prior to a more detailed consideration of the use of ICP-MS for isotope ratio measurements, including selected applications, in Chapter 6.

Another of the original objectives of this book was to provide a useful starting point when users want to try an approach or technique that is new to them. The latter part of the book is designed to help in this regard. In Chapter 7 alternative and mixed gas plasma are discussed. Some aspects of adding additional gases to the argon plasma are now used routinely in many laboratories (e.g. the addition of oxygen when using organic matrices in ICP-MS). Other approaches have remained more of academic interest but may well offer some advantage for specific applications. The following chapter on electrospray ionisation mass spectrometry again offers something additional to users of plasma spectrometry. Whilst not strictly falling within the remit of the title of this book, this technique has quickly established a major role as a complementary technique for trace metal speciation studies, particularly when there is a need to better characterise important complex metal containing species such as biomolecules. The last three chapters put all of the above into a practical context. These three chapters cover geological, environmental and clinical applications together with a detailed account of plasma spectrometry in food science. All three of these chapters have been extensively revised and updated from the first edition.

Before I finish I must express my sincere thanks to the authors who have contributed to this book. My approach, as with the first edition, was to ask internationally recognised leaders to head up each chapter. Of course such people are also very busy (and not really looking to take on yet another task), and so it is a great honour for me to look down the list of those who agreed to contribute and reflect on their expertise, wealth of experience and standing in the field. Their knowledge and insight is reflected in every chapter. I hope that the combination of all our efforts has resulted in a book that is both timely and informative, and that it provides a useful reference for those engaged in using ICPs to achieve their own scientific goals.

Steve J. Hill

Chapter 1

Introduction – A Forward-Looking Perspective

Gary M. Hieftje

1.1 Introduction

It is a distinct honor and particular pleasure to be asked to prepare the first chapter in this new edition of the popular text edited by Steve J. Hill, 'Inductively Coupled Plasma Spectrometry and Its Applications'. When asked, I was requested to consider what the future might hold for inductively coupled plasma (ICP) spectrometry. However, attempting to forecast the future in this ever-changing field is somewhat daunting. As Niels Bohr once stated, 'making successful predictions is difficult – especially when the predictions are concerned about what will happen in the future'. Moreover, there are no doubt some readers who recall an earlier time in which this author had been asked to predict the future of atomic absorption spectrometry (AAS); with tongue firmly in cheek, he extrapolated recent publications in AAS by fitting the trend to a third-order polynomial, a model that projected the demise of the technique by the year 2000 [1]. Readers are therefore urged to use with some caution the projections offered here and to make a special effort to distinguish true projections from those offered in jest.

There are some established procedures that can be employed to forecast the future. The first is to extrapolate past and current trends, both those within the field of interest (here, ICP spectrometry) and those outside that exert an influence on the directions the field might take. These external influences include those imposed by society, technology, and science. A second approach is to assess the likely impact that might arise directly from other fields of science and technology. This sort of 'technology transfer' is clearly apparent in many past and recent developments in ICP spectrometry, an obvious example being the widespread adoption of array-detector technology for multielement determinations in ICP-atomic emission spectrometry (ICP-AES).

Regrettably for the goals of this chapter, some of the most dramatic changes in any field are wholly unexpected. These 'Eureka' events are impossible to foresee or predict but can change completely the thinking of scientists in the field. Interestingly, some of these breakthrough events require some time before their impact is fully realized. An example in our own discipline is the seminal work involving end-on viewing of the ICP, some 30 years ago [2,3]. Although this pioneering work was ignored for many years, end-on emission measurement from an ICP is now widely utilized.

In this chapter, these predictive tools will be exploited to project a possible future for ICP spectrometry. Greatest emphasis will be placed on likely developments in plasma spectrometric instrumentation, since that is the area of the author's greatest expertise. We will begin with an attempt to assess and extrapolate past and current trends.

1.2 Extrapolation of past and current trends

As the American statesman and President Thomas Jefferson once said, 'I know ought to judge the future, save by the past'. Following Jefferson's lead, let us examine first the external forces that influence the directions our field might take. These influences include those from science, society, politics, and the economy.

1.2.1 Influences from science and technology

Scientific influences dictate where the demand, need, and opportunities for atomic spectrometry exist. These forces were recognized fully by Marvin Margoshes in his classical 1979 paper, 'Demand-Pull and Science-Push in Multielement Analysis' [4]. Margoshes realized that the demand ('pull') for a particular activity (in this case multielement analysis) was dictated by emerging and critical applications, whereas the second factor, a 'push', was provided by scientific innovation and discoveries.

Many of the 'pull' factors in the current environment are clear. Perhaps most prominently, bioscience is driving innovation and providing many of the resources that enable today's research to be performed. Particularly important in this regard is the study of metalloproteins and other metal-containing biologically active compounds. Indeed, the importance of this trend has spawned the new term 'metallomics' to describe the activities [5]. However, also important are materials science and nanotechnology, both of which demand multielemental analysis at every-greater sensitivity, in samples of rapidly decreasing size, and on a spatially resolved basis. Energy needs, too, are pulling our field; the metals content in fossil fuels is already of recognized importance, the nuclear-power industry requires a careful elemental inventory of its feedstock and output, and emerging technologies such as hybrid automobiles and the 'hydrogen economy' will no doubt impose additional demands.

Environmental science is already an important customer of ICP spectrometry and will no doubt continue to be so. Moreover, environmental demands and those from many other fields now require information not only on the elemental composition of samples, but also about the chemical form in which those elements are found. The importance of this 'speciation' is already documented in our community, and is on its way to becoming universally recognized in importance.

These demands (pull) on our field are coming at a time when we can expect a time compression in the life cycle of most analytical methods. Because of rapid technological developments, new techniques and instruments will continue to be introduced, to undergo the traditional development and acceptance phase, and fall into senescence as newer, even more powerful methods replace them. It is, in fact, interesting that the field of AES has endured so long [6]. The reason can be found in the continuing developments that reinforce the field. Fundamental discoveries help us to understand better the components of

our systems, from sample-introduction devices to excitation events that transpire in the ICP. In turn, these findings lead to continuous improvements in sources, sample-introduction equipment, and spectrometric systems. We will return to this point later.

Also, pulling our field along is the growing demand for information-rich methods. Because sample mixtures being examined are increasingly complex, it is now not uncommon to see employed a two-dimensional or three-dimensional separation process before an analytical measurement of each constituent is made. Especially in the bioscience area, we can expect to witness these sorts of complex schemes employed in conjunction with ICP spectrometry. Of course, the danger of such combinations is a data storm, a glut of information that must be converted in some form to knowledge. The newly emerging discipline of *informatics* will no doubt play an important role in this interpretation process.¹

Other science and technology needs include the desire for unattended and remote operation of instruments, so measurements can be made in hostile or unapproachable sites, and the need for simpler, faster, and continuous analysis. These desires are at odds with the operation of the conventional ICP spectrometer, with its high-power consumption and its need for high volumes of high-purity argon.

Just as science and technology will pull our field along because of its needs, there will also be external scientific trends that provide us with fresh opportunities and ‘push’ our field in new directions. There will probably be, for example, spin-offs from bioscience, materials science, energy, and the environment that are difficult to foresee. One possibility is the development of low-cost solid-state (diode) lasers that could be used in a number of ways, from simplifying spectral alignment in atomic emission spectrometers, to promoting selective ionization in ICP-mass spectrometry (ICP-MS), to reopening opportunities in ICP measurement by atomic fluorescence. Improvements in battery performance and energy storage might also simplify the design of ‘fieldable’ ICP spectrometers, and lessons learned from bioscience might make possible the design of miniaturized spectrometers based on mimics of the vision process. In fact, whole new generations of microspectrometers might emerge because of developments now under way in the area of nanotechnology. Combinatorial methods, already very popular in chemistry and materials science, might result in the fabrication of new components for ICP spectrometers that are now difficult to envision; also, such methods might result in the introduction of new, highly selective chelates for specific elements, and in new tools for speciation (perhaps in conjunction with bioscience in the form of highly selective aptamers) [7].

Information-rich methods and informatics itself might also simplify in a number of ways our interpretation of ICP spectrometric data. For example, such methods should make it easier to identify suitable internal standards for most elements, perhaps by combining signals from a number of different internal-standard candidates. They could also be applied to the broad range of atomic emission lines or mass-spectrometry signals that can now be acquired in a virtually simultaneous fashion by modern spectrometers. If applied properly, that broad range of signals could provide diagnostic information that would enable a spectrometer to determine if and why a spectral or matrix interference exists for a particular sample and perhaps even help determine how a spectrometer or the ICP itself could be adjusted to overcome the interference.

¹ For example, consult the web site of the Indiana University School of Informatics <http://informatics.indiana.edu/>

‘Interdisciplinarity’ is another ‘push’ that affects our field. Traditionally, analytical chemists have always functioned best when immersed in a problem they are asked to help solve. However, the importance of this cooperation is now being more widely recognized, something that should help those in atomic spectrometry perform their job better. Similarly, electronic publication, virtually instantaneous communication, and nearly free and ubiquitous computing power will make interdisciplinary collaboration even simpler. It will also foster the ultimate development of a truly self-diagnosing instrument and allow its output to be monitored remotely.

1.2.2 Influences from society, politics, and the economy

Let us now turn to external influences on our field other than those imposed by science and technology. These factors include societal, political, and economic. Unfortunately, there is at present a widespread disaffection with science. Smaller numbers of science majors are found each year in universities throughout the world, a situation that will translate into fewer scientists in the future. These shortages will place demands on every surviving laboratory and will require those who remain to be more innovative and more efficient.

Another regrettable trend that affects our field especially is low funding. A widespread misconception about atomic spectrometry is that the ICP is a ‘solved problem’ and that innovation in atomic spectrometry in general is lacking. Fewer and fewer in our discipline are being funded by major federal agencies, and graduate students considering academic careers are urged to pursue other scientific endeavors. I see no clear solution to this problem, but believe it can be mitigated by education and mutual support. Our colleagues in other areas must be made aware not only of the past achievements of ICP spectrometry but also of its continuing improvement, evolution, and excitement. Young people must be particularly encouraged and urged to introduce atomic spectrometry into other areas where its impact can be appreciated.

The ever-expanding world population will also have an influence on every aspect of science, our own work included. The global population is roughly 6 billion now and is expected to be 9 billion by the year 2050. This larger population will place, again, greater weight on efficiency, energy, and the environment, opening new opportunities (but also new responsibilities) for us.

The fact that we will have fewer students and probably scientists will increase the need for automation and better diagnostics. It might also lead to longer times for students to complete their doctoral studies, a regrettable but perhaps unavoidable trend. Lower funding by federal agencies and from the private sector will place greater demands on resources, potentially leading to stagnation. These funding shortfalls will require selective investment in only the best science.

Finally, there is the aging of the world’s population to consider. In our own field, the ‘graying of spectrochemical analysis’ could lead to a loss of our knowledge base. Already, those of us long in the field witness the reinvention of many things, an efficiency that will become more and more impossible to tolerate. There is a tendency, with the powerful literature search engines that now exist and the desktop availability of journals, to ignore the past literature (except, perhaps, for citation purposes). Every effort will have to be made to compensate for the loss of our knowledge base by exploiting the Internet and developments in

informatics more efficiently. Another impact of population aging will be elevated costs of healthcare and difficulties faced by those on fixed incomes. Again, this situation will no doubt pose problems for our discipline, but also provide it with new opportunities to improve efficiency and develop new tools that provide high-quality multielemental and speciation information but at lower cost.

1.2.3 Past and current trends in atomic spectrometry

There are several ways in which trends in atomic spectrometry can be used to predict its future. The most straightforward way, of course, is to track current or recent changes and simply to extrapolate them to future performance, figures of merit, and instrumental developments. However, an even more effective approach is to assess the strengths and weaknesses of currently available systems and to suggest how the strengths might be improved and the weaknesses overcome. In this approach, it is particularly useful to establish an ‘ideal’ standard with which the performance of existing systems can be compared [8]. Such an ideal system provides a fixed, immutable standard for comparison, and also serves to indicate not only which weaknesses are most worrisome but also how much existing strengths can be improved. In strengthening attributes and lessening shortcomings, it is appropriate to consider the impact of newly emerging or introduced technologies.

As was suggested earlier, tracing the growth and decline of individual analytical methods is valuable in gauging where a field is headed [6]. The questions that naturally emerge are: (1) What methods have endured? (2) What methods have died? and (3) What are the reasons for these changes? In the field of atomic spectrometry, the changes are fairly easy to define. Flame emission spectrometry, which was dominant in the 1950s and early 1960s, was supplanted by flame atomic absorption spectrometry (FAAS), in part because of improved nebulizer-burner systems that were introduced for FAAS but in part also because of the simplicity of locking onto desired atomic lines by means of the narrow-band emission from a hollow cathode lamp. In turn, FAAS was largely replaced by electrothermal vaporization (ETV)-AAS and by ICP-AES. ETV-AAS offered better detection limits and the ability to handle microliter sample volumes, while ICP-AES provided a considerably broader dynamic range, lower detection limits, and truly multielement capability. More recently, we have seen some of the workload traditionally handled by ETV-AES taken over by ICP-MS, again because it offers truly multielement capability and extraordinarily low detection limits.

These changes appear at first glance to support the concept involved in Velmer Fassel’s ‘Seven Stages of an Analytical Method’ [9]. These stages are outlined in Table 1.1

I would argue that Fassel’s list does not fully account for the evolutionary changes in atomic spectrometry that have occurred. In particular, it seems unlikely that immediately after we secure an improved understanding of the fundamental principles of a method, then it becomes outdated. Rather, I would modify Fassel’s Seven Stages as shown in Table 1.2. In this modified series of steps, the main change is that an improved understanding of fundamental principles leads to better instrumentation and methods which, in turn, generate better figures of merit and new systems that are introduced into the marketplace, enjoy general acceptance and widespread use, and spur further characterization of the fundamental features of the method. Only when this iterative improvement produces systems

Table 1.1 Seven stages of an analytical method

-
1. Conception of idea
 2. Design and construction of first operating apparatus
 3. Successful demonstration of idea; first publication
 4. Improvement of instrumentation; figures of merit
 5. Maturity; general acceptance; automation
 6. Improved understanding of fundamental principles
 7. Old age and senescence
-

Adapted from Fassel, V.A., Fresenius', Z. (1986) *Anal. Chem.*, **324**, 511.

Table 1.2 Seven stages of an analytical method (modified)

-
1. Conception of idea
 2. Successful demonstration and publication of idea
 3. Improvement of instrumentation; figures of merit
 4. Maturity; general acceptance; automation
 5. Improved understanding of fundamental principles;
introduction of new instrumentation
 6. Iteration of steps 3–5
 7. Old age and senescence
-

that fail to compete with new techniques and technologies does the method then enter its period of old age and senescence. At that point, it will of course be supplanted by the newer technologies. We will consider this issue in somewhat more detail shortly.

1.3 Influence of technology transfer

Advances made in other fields of science and technology will no doubt have an almost immediate impact on ICP spectrometry. Let us deal with a few of these ongoing changes and their likely impact.

1.3.1 Electronics and data manipulation

Electronic systems are being made ever faster, smaller, and less expensive. This will lead to smaller, cooler-running systems that are more likely to be portable. Further, power supplies should become more efficient and therefore less critical. At present, power supplies constitute one of the most expensive components of commercial ICP-AES or ICP-MS systems. In addition, *fast data acquisition* will become more powerful and simpler, making it possible to read detector-array chips even more rapidly and making it more straightforward to perform multi-elemental analysis on transient samples such as those produced by laser ablation, flow-injection, or chromatography. Fast data acquisition will be particularly important, of course, for inherently high-speed techniques such as time-of-flight mass spectrometry (TOFMS).

On-board data manipulation by *digital signal processing* (DSP) chips will make it possible for an instrument to process increasingly complex data arrays and to devise strategies

for characterization that permit samples to be characterized more fully and immediately. The low cost of electronic systems and *virtually free computing power* will encourage the use of redundancies so instruments become more robust. Further, as outlined earlier, *self-diagnosis* of instrumentation will become common. Lastly, the *human–computer interface*, which has already undergone a revolution of its own, will improve even further. Data displays are likely to evolve from current models that show tables and one-dimensional plots to those that display more complex patterns, more easily recognized by humans. Examples can be found in the field of informatics, in which complex data arrays are being expressed in the form of human-like faces, whose subtle expressions we as human beings have come to recognize immediately. In a similar vein, complex-data patterns are now being expressed by audible signals, in varying tones of pleasantness or dissonance, according to the ‘quality’ of incoming information. Even tactile feedback seems reasonable; just as an experienced automobile driver benefits from ‘road feel’, operators of future ICP spectrometers might obtain a sense of how an instrument is performing or the nature of a sample by means of pressure, vibration, or force applied to the operator’s hand.

1.3.2 *Metal-binding structures*

As it was suggested before, novel *lock-and-key structures* useful for elemental or speciation analysis might emerge from both materials’ science and bioscience activities. An example is the use of aptamers [7]. Simply viewed, aptamers are single-strand DNA structures that have been intentionally evolved to interact selectively with specific moieties. Most commonly applied to protein analysis, aptamers are also now being explored as vehicles for the selective tagging of smaller molecules or structures and might some day be applied to metal ions, oxyanions, and other chemical systems currently of interest to ICP spectrometrists. This capability would be a tremendous aid in speciation, since the aptamer would entrap the original species in its native state, thereby avoiding alterations in speciation such as now occur in chromatography or when other conventional methods of separation are used.

Single-strand DNA aptamers are evolved by a repeated process of selection and amplification. A combinatorial sort of approach is initially employed to produce a broad range of DNA structures, which are then collectively allowed to interact with the target species. Those DNA structures that successfully bind with the target are then trapped by a suitable method, while the others are discarded. The DNA species that had been trapped are then denatured, to release the target species, and the DNA strands themselves amplified by the polymerase chain reaction (PCR). The expanded group of DNA molecules is then ‘renatured’ and allowed to interact once again with the target species. This process of amplification and selectivity refinement then continues until the desired degree of specificity is achieved.

1.3.3 *Novel separations methods*

The need to analyze samples of ever-increasing complexity might require atomic spectrometrists to become familiar with and employ additional separations’ methods in the future. Especially in the field of metallomics, high-efficiency, multi-dimensional separations will no doubt be necessary. In protein characterization, for example, instruments are now being used

that begin with a two-dimensional separation by means of liquid chromatography (LC). In this process, a first LC column that provides a relatively slow separation is followed by a second column that separates on a much faster time scale but by means of an alternative mode of affinity. As a peak elutes from the first column, it is rapidly sent through the second, and overlapping constituents thereby hopefully resolved. The result, of course, is a much more highly defined chromatogram, a greatly increased plate capacity, and much less likely overlap of co-eluting species. Nevertheless, this preliminary two-dimensional separation, which occurs on a time scale of seconds, is now being followed by electrospray ionization and a gas-phase separation by means of ion mobility spectrometry (IMS). Unlike LC, which separates on the basis of the differential affinity of a compound for a stationary and mobile phase, IMS separates compounds on the basis of their gas-phase collisional cross-sections, and on a millisecond time scale. Consequently, even proteins having the same primary structure (amino acid sequence) but different folding (tertiary structure) can be distinguished [10]. Even this degree of separation is today not considered to be adequate, for recent practice is to follow the first IMS stage with a collision cell and a second, faster IMS unit [11,12]. Just as two-dimensional LC provides more information and greater benefits than a single stage of LC, the dual-IMS makes it far less likely that two co-emerging proteins will occur. Moreover, a collision region between the two IMS units permits proteins to be fragmented or altered to provide an additional degree of selectivity.

Conveniently, even this four-dimensional complex stage of protein analysis could be coupled to an ICP system for the analysis of a metalloprotein mixture. It should be straightforward to feed the output from the second IMS system directly into an ICP and to analyze the ICP output by either emission or high-speed MS.

1.3.4 Detector technologies

Continuing improvement in detector technologies has already had an enormous impact on ICP spectrometry and will continue to do so. Pixel densities keep on increasing, costs are lower, readout speeds are faster, sensitivities are higher, all while noise continues to drop. Moreover, technologies intended originally for optical imaging are likely to find their way into mass spectrometers. A recent example is our own work [13] in which a multiplexed array of integrating amplifiers, originally designed for use in infrared detection, was employed in conjunction with a double-focusing mass spectrometer. The result, at present, is a 128-channel detector array that is capable of examining a broad mass range at once, of interrogating each mass location in either a destructive or non-destructive way, in any mass order desired, and of integrating the incoming signal continuously. Even early generations of the array offered sensitivity that equals or betters that of conventional mass-spectrometric detectors based on electron multiplication. Similar developments in electronics and detector-array technology are likely to benefit MS in the future.

1.4 Strengths and weaknesses of ICP-AES and ICP-MS

Before listing the strengths and weaknesses of each of the ICP spectrometric techniques, it is useful to compare the two methods on the basis of the signals they generate and the relative difficulty of measuring those signals above a finite background. Modern ICP-MS

instruments produce signal levels on the order of 10^8 counts per second (cps) when a 1 part per million (ppm) solution of a given element is introduced into them. This signal level would appear to be remarkably high, until it is recalled that a 1 ppm solution of an element having a hypothetical atomic weight of 100, introduced into a nebulizer at a rate of 1 ml min^{-1} , involves the consumption of $\sim 10^{14}$ atoms s^{-1} . In other words, the efficiency of even a modern ICP-MS instrument is only approximately 10^{-4} %.

However, important is that the background in a typical ICP-MS instrument is extremely low, on the order of 1 cps or less. Consequently, the signal-to-background ratio of an ICP-MS instrument is on the order of 10^8 for a 1 ppm solution. Because background noise follows a Poisson distribution, the noise in the background should be equal to the square root of the background itself, which in the present case is also 1, making the signal-to-noise ratio expected of an ICP-MS instrument equal to 10^8 for a 1 ppm solution. If the spectrometric system behaves linearly, and it is expected to do so, the signal-to-noise ratio should therefore be unity at a concentration of 10^{-8} ppm, or 0.01 ppt. Because detection limits are ordinarily defined at a $S/N = 3$, this calculation would suggest a detection limit of 0.03 ppt for an ICP-MS instrument, roughly what is commonly quoted.

The same set of calculations for an ICP-AE spectrometer yields rather different results. Initially, one might expect that an emission measurement would be more efficient than MS. After all, in MS each ion can be detected only once, whereas a free atom or atomic ion can be repeatedly excited at rates typically approaching 10^8 times per second. Thus, 10^{14} atoms s^{-1} (the consumption rate for a 1 ppm solution) should produce as many as 10^{22} photons s^{-1} if the atoms could all be captured and detected. In contrast, measurements made in our laboratory and confirmed elsewhere suggest a more typical count rate of 10^6 per second from a high-quality photomultiplier tube, when a 1 ppm solution is introduced into the ICP. Accordingly, the efficiency of an ICP-AES system is even lower than that of ICP-MS! The reason, of course, lies in the limited time that is available to observe each atom or ion as it passes through the observation zone in the plasma (about 10^{-4} s), the relatively small solid angle of radiation that is captured (~ 0.01 sr), optical losses, and the relatively low quantum efficiency of even the best photomultiplier tubes. In both ICP-AES and ICP-MS systems, of course, there are additional losses imposed by the sample-introduction system, diffusion in the plasma, and the finite efficiencies of atom and ion formation.

Of importance also is the background that is encountered in ICP-AES. Produced in part by recombination of argon ions and electrons and by the Lorentzian wings of the many atomic spectral lines found in the plasma, this emission background in a typical spectrometer is on the order of 2×10^4 counts s^{-1} . Combined with the signal level of 10^6 cps, this calculation yields a signal-to-background ratio of 50, which is commonly encountered. The signal-to-noise ratio of the system can then, once again, be obtained by recognizing that the background should be Poisson in its statistical characteristics, to yield a noise level of just over 10^2 , and a S/N of 10^4 . This value for a 1 ppm solution then dictates a detection limit in the range of 0.3 ppb, approximately what is found.

From these crude calculations, it appears that ICP-MS enjoys an advantage in S/N over ICP-AES of a factor of 10^4 , which experience shows is about the same as the relative limits of detection. However, other conclusion can be derived:

- (1) Both systems are rather inefficient, with ICP-AES being extraordinarily so.
- (2) ICP-AES signal levels are only a factor of two or so weaker than those in ICP-MS.

- (3) Background levels in ICP-MS are far lower than those in ICP-AES.
- (4) Signal and noise characteristics are all highly dependent on instrumentation and therefore should be able to be controlled.

1.4.1 *Strengths and weaknesses of ICP-AES*

With these considerations as a backdrop, let us now examine the strengths and the weaknesses of each of the ICP spectrometric methods. The strengths of ICP-AES are listed in Table 1.3, but deserve some elaboration. As the foregoing signal analysis indicated, a sufficiently energetic environment (such as that provided by the ICP) can cause each atom to emit as many as 10^8 photons per second. This high count rate enables each atom to be examined many times, unlike in MS, and fundamentally might lead to greatly enhanced sensitivity. Indeed, this is one of the traditional reasons why atomic fluorescence spectrometry (AFS) has been offered as an alternative to emission or AAS.

In addition, ICP-AES produces an extremely line-rich spectrum, permitting spectral lines to be chosen that are ideally free from spectral overlap with those from other species and, as outlined below, can also be used for diagnostic purposes. These lines can come, of course, from either neutral atoms or atomic ions, again providing further information not only about the sample but also about the ICP itself.

Unlike in atomic MS, spatial averaging is trivial to achieve in ICP-AES. In turn, spatial averaging can improve precision, one of the principal reasons ordinarily given for employing end-on viewing and also allowing a region to be selected that is relatively free from matrix interferences [14].

The fact that some modern AES spectrometers can measure virtually all analyte atom and ion lines simultaneously from the ICP, along with emission features from the solvent, intrinsic plasma species, and those entrained from the atmosphere, opens a broad range of options for diagnostics. For example, gas-kinetic ('finger-burning') temperatures (T_g) can be estimated from the Doppler width of some lines, if a sufficiently high-resolution spectrometer is employed, or can be approximated by fitting emission features of molecular species to a Boltzmann distribution based on their rotational or vibrational progressions. Similarly, atomic or ionic excitation temperatures (T_{exc}) can be determined for analyte species such as iron or for intrinsic plasmas species such as argon, merely by fitting the normalized intensities of electronic states to the Boltzmann distribution. Electron number densities, another

Table 1.3 Strengths of AES

-
- 10^8 counts s^{-1} per atom
 - Rich spectrum; choice of spectral lines
 - Atom, ion lines
 - Straightforward spatial averaging
 - Convenient diagnostics
 - T_g , T_{exc} , n_e , $M(II)/M(I)$, MO , etc.
 - Simple instrumentation
 - Alignment (visual), familiarity
-

important plasma parameter, can be estimated from the Stark-broadened line width of either argon lines or, more commonly, the hydrogen-beta line. Atom and ion emission-intensity ratios, so valuable for gauging plasma ‘robustness’ [15] can readily be measured for magnesium, and the abundance of oxides can be determined by examining the emission from appropriate species. Moreover, all these diagnostics can be obtained on a simultaneous basis and in a spatially resolved fashion in an appropriately designed system.

Finally, ICP-AES instrumentation is familiar to most scientists and technicians, is relatively trivial to operate, and its operation can be monitored by simple visual inspection. Alignment of the ICP source and other optics can be accomplished in a straightforward fashion, since the light can be seen. As importantly, photons are *clean* and do not clutter a spectrometer when they are introduced into it.

Despite these many strengths, ICP-AES is not without its shortcomings, some of the most important of which are listed in Table 1.4. For example, the line-rich spectra, so useful for diagnostics, also produce tremendous spectral clutter, which can promote spectral interferences and make the identification of chosen spectral lines more difficult. As important, measuring such a large number of spectral intervals requires spectrometers of high resolution and either a substantial measurement time (if the intervals are measured in sequence) or an array detector that contains an enormous number of pixels (if a simultaneous spectrometer is utilized).

Further, the desired spectral features and also the spectral clutter just mentioned are superimposed on a high background, generated in part by the argon ion–electron recombination continuum, in part by molecular bands that are observed in the plasma and also from the superimposed Lorentzian wings of the large number of spectral lines emitted by the ICP. As the calculation earlier indicated, this high background compromises detection limits in ICP-AES. It also necessitates accurate background correction, again placing stringent demands on scanning systems or on the pixel density of multi-channel units.

In comparison to detectors commonly employed in MS, those used in AES are relatively inefficient and noisy. Whereas ions in MS strike the detector with relatively high energy (in sector-field systems, greater than 1 keV), photons in the ultraviolet and visible spectral regions are relatively weak (on the order of several eV). As a consequence, quantum efficiencies for photon detectors in the UV-VIS are relatively low, although strides have been made recently in solid-state devices. Moreover, this low photon energy requires that detectors in ICP-AES respond to events of similarly low energy, which makes them susceptible to thermal noise. It is for this reason that even the best solid-state detectors are ordinarily cooled to at least -40°C .

Table 1.4 Weaknesses of AES

-
- Large number of resolution elements
 - Spectral clutter (‘rich’ spectra)
 - Spectral interferences
 - High background (continuum, bands)
 - Detector noise (low work function)
 - Cannot ‘see’ some oxides, multiply charged ions
 - Cannot resolve most isotopes
-

Lastly, ICP-AES is regrettably blind to some features. Many oxides, for example, do not emit strongly, so cannot be used for diagnostic purposes. Similarly, the existence of multiply charged ions is difficult to gauge. And perhaps most importantly, isotope-induced spectral shifts for elements in the center of the Periodic Table are too small to be resolved by even the best modern spectrometers and, indeed, are smaller than the observed line widths from a typical ICP. Isotope-analysis capability is correspondingly very limited in ICP-AES.

1.4.2 Strengths and weaknesses of ICP-MS

Let us now turn to the strengths and weakness of ICP-MS. The strengths of this technique are listed in Table 1.5. In contrast to ICP-AES, isotopic information is trivial to obtain in ICP-MS. This information permits not only the determination of isotopic abundances, but also makes possible the use of isotope dilution, and the improved accuracies that accompany it. Also, isotopic patterns are extremely useful in ICP-MS to confirm the identity of sought-for elements.

Table 1.5 Strengths of atomic MS

- | |
|--|
| <ul style="list-style-type: none">● Isotopic information<ul style="list-style-type: none">– Isotope analysis, isotope dilution, diagnostics● Simple spectrum (~240 resolution elements)● High detector ‘quantum’ efficiency● Low detector background● Powerful speciation capability |
|--|

Again, unlike with ICP-AES, spectra observed in ICP-MS are quite simple. Because only the atomic mass-spectral range must be examined, 240 or so resolution elements should be all that is required. Of course, it is often desired to measure several points across each target mass-spectral peak. Even in such cases, a spectrometer offering only 1000 resolution elements should be adequate. It is perhaps for this reason that scanning instruments continue to dominate sales in the field of ICP-MS.

As was indicated above, the detection efficiency for atomic ions is extremely high, approaching unity. Moreover, those ions can be measured against an almost vanishingly low background, below 0.1 cps in the best spectrometers.

Finally, MS intrinsically provides speciation information if the right sort of source is employed. Of course, an ICP typically produces only atomic ion spectra. However, switched or tunable sources [16–19], based on glow discharges, low-power ICPs, microwave plasmas, and electrospray devices have all been explored as tools that can provide both atomic and molecular spectra. Further, it has become fairly commonplace for individuals engaged in speciation analysis to employ two spectrometers in tandem, one that utilizes an ICP source and the other an electrospray or electron-impact source. One device even feeds both sources into the same mass spectrometer [20,21].

These strengths must be weighed against the weaknesses of atomic MS, listed in Table 1.6. As was indicated above, most commercial ICP-MS units measure isotope and elements sequentially. Not only does this custom constrain the speed of analysis, it can also limit isotope-ratio precision. The problem arises because fluctuations in the ICP can be faster than

Table 1.6 Weaknesses of atomic MS

-
- Sequential isotopic measurements
 - Limited speed (for speciation, etc.)
 - Low signal levels (1 count per atom)
 - Low efficiency (1 atom in 10^7 detected)
 - Cannot ‘see’ neutrals
 - No spatial averaging in plasma
 - Complexity (vacuum, contamination, etc.)
 - Cost
-

the scanning time from one element or isotope to another. In such cases, the different peaks of interest are being measured under different ICP conditions, so precision is compromised.

Low signal levels also should be a problem in ICP-MS, since there is only one opportunity to measure each atomic ion. Further, the relatively low efficiency of most ICP-MS instruments, estimated quantitatively above, means that only about one atom in every million or so is detected.

In contrast to ICP-AES, neutral species cannot be detected in ICP-MS, limiting its diagnostic utility. Also, no spatial averaging is possible; instead, a fixed spatial location, typically 10 mm above the load coil, must be selected. As a result, it is not straightforward to use spatial averaging or to employ spatial behavior as a diagnostic. Recent studies involving modulation of the central-gas flow in the ICP, however, might offer a solution to this limitation [22].

Lastly, it is undeniable that mass spectrometers are more complex and costly than emission spectrometers. They require vacuum pumps, entrance apertures, and ion optics with which many chemists are not comfortable. Furthermore, unlike in an atomic emission spectrometer, the sample is sent directly into an ICP-MS unit, and can erode, corrode, or block orifices, collect on ion optics, and foul detectors. Moreover, an ion beam cannot be visually inspected, a fact that complicates alignment and instrument troubleshooting.

1.4.3 ICP limitations

Of course, some of the present limitations in ICP-AES and ICP-MS arise from the source itself. Some of these limitations are compiled in Table 1.7.

Table 1.7 Source limitations

-
- High background (in AES)
 - Limited signal levels
 - Spectral interferences
 - Matrix interferences
 - Incomplete atomization
 - Speciation capability
 - Virtually full atomization
 - Precision, stability
 - Sample-utilization efficiency
-

From the standpoint of AES, and as detailed earlier, the intense and complex background of the ICP promotes spectral interferences, constrains detection limits, and necessitates the use of costly high-resolution spectrometers. At the same time, signal levels generated by the plasma are undesirably low, especially for atomic MS, in which each ion can be detected only once. In part, this limited signal arises from inefficiencies in the sample-introduction equipment, but is also an unavoidable consequence of sample dilution that occurs when an aerosol is introduced into the high gas flows typical of an ICP. Moreover, there is the added complication of collecting a large solid angle of radiation in AES or in efficiently extracting ions into a mass-spectrometer interface for MS detection.

Spectral interferences, too, are a consequence of imperfections in the ICP. In AES, such interferences arise from the large number of spectral lines emitted by each element and by emission features of the plasma support gas, of sample-matrix components, and of atmospheric constituents entrained into the plasma. In ICP-MS, such interferences more commonly develop from overlaps between isotopic peaks of interest and those from polyatomic species generated from the sample material or, commonly, from a combination of atoms from the sample and the argon support gas.

Matrix interferences also affect both MS and AES, but for different reasons and in different ways. To some extent, such interferences arise from the fact that sample atomization is incomplete, even in a source with as high a thermal temperature as the ICP. More importantly, atomization is not consistent and varies from sample to sample and between samples and standards. Other matrix interferences arise in AES because of changes in plasma excitation conditions that the sample matrix generates and in MS because of 'space charge' effects. Such effects essentially involve Coulombic repulsion among ions in the beam extracted from the ICP. Because of the high ion currents in such a beam, positively charged sample ions can repel each other, so lighter ions are driven from the center of the beam and experience lower transmission efficiency.

Speciation capability is also compromised when an ICP is used because atomization, although not complete, is sufficient to mask the original chemical form in which an element was introduced.

Limited precision also is a consequence of ICP shortcomings. Whether the measurement be by AES or MS, typical precision values for the examination of a single spectral line or a single isotope are on the order of 1–5% RSD, insufficient for many applications. Some of this instability arises from the sample-introduction system, but some also from plasma tail-flame waver and from vortex instabilities that surround the plasma and induce 'whistle' noise in measured signals.

Lastly, and as outlined earlier, samples are not utilized as efficiently in the ICP as would be desired. Although recent reports [23] indicate that as many as 1 atom in 1000 can be detected by ICP-MS, few existing instrumental systems are capable of such performance. Without doubt, the ICP is still a long way from providing the single-atom detection capability that many have sought [24].

Fortunately, there appear to be ways to retain the strengths compiled in Tables 1.3 and 1.5 but to overcome the weaknesses outlined in Tables 1.4, 1.6, and 1.7. Some of these potential solutions, listed in Table 1.8, suggest possible future directions in ICP spectrometry.

Table 1.8 Potential solutions

-
- Better sample-introduction systems
 - Source with lower background (for AES)
 - Atomic resonance-line source (for AES)
 - Source with extended residence time
 - ‘Switched’ sources for speciation
 - Simultaneous-reading mass spectrometers
 - Higher-resolution emission spectrometers
 - Faster emission and mass spectrometers
 - Intelligent instrumentation
-

1.5 Potential directions in ICP spectrometry

First, sample-introduction systems must be improved further. To be sure, dramatic strides have been made in the last decade, in which it was rediscovered that reduced sample-solution flows into a pneumatic nebulizer result in dramatic improvements in efficiency [25]. Yet, many additional improvements are to be desired. For example, spray chambers with faster wash-out times are needed [26], especially for coupling with inherently transient sample-introduction techniques such as flow-injection [27]. Recent efforts to model spray chambers in a fundamental way should help in this direction [28,29]. Such fast wash-out systems should also generate higher peak signals and thereby offer better detection limits. In addition, a great deal more effort is needed in the area of solid-sample analysis, especially when each sample must be analyzed in a three-dimensional spatial fashion. Greater knowledge and improved systems for laser ablation [30–38] offer a temporary and partial solution; additional opportunity might exist because of recent developments in atmospheric-pressure glow discharges designed for sample volatilization.

Alternatives for sources that produce a lower background or those that generate atomic resonance lines directly, for AES applications, will be described in more detail below.

Atomization efficiency in the ICP could be enhanced and spectral background potentially reduced by designing a source with an extended sample-residence time. Spatially extended ICPs have already been explored [39,40] but it might be more efficient in some applications to consider a completely enclosed source [41–43], one that uses a very low flow of argon [44], or one in which atoms generated in an ICP-like source are extracted into a lower-pressure volume in which residence time is increased [45]. Not only will such schemes likely improve atomization efficiency, they will permit the AES-based measurement of atoms for longer periods, thereby promoting sensitivity.

It has already been shown that some sources can be switched or tuned in operation to provide alternately an atomic or molecular mass spectrum [17–19]. There are additional ways in which such source tuning might be employed to provide more information about the chemical composition of the sample being analyzed. With the introduction of TOFMS to the ICP arsenal, simultaneous-reading mass spectrometers are already available and have shown their capability in measuring samples more rapidly, in providing high-precision, multielement isotope ratios, and simplifying the measurement of transient samples

produced by flow-injection, laser ablation, ETV, or chromatography. These capabilities will be offered also by a new generation of multi-channel mass spectrometers [46–53] similar in concept to the multi-channel emission spectrometers that have long been on the market.

Similarly, the resolution of conventional emission spectrometers could be improved by coupling them with auxiliary front-end or back-end devices. An obvious such device is a Fabry-Perot (F-P) interferometer. However, such optical systems are ordinarily limited to only a narrow range of wavelengths, beyond which the finesse of the interferometer, and therefore its resolution, begin to suffer. Yet, alternative ways, to be described shortly, might offer a solution.

Finally, faster and more intelligent emission and mass spectrometers seem likely to be developed in the future. Continuing improvements in the speed and efficiency of multi-channel photon detectors and advances in high-speed electronics useful for TOFMS and simultaneous multi-channel mass spectrometers will likely change the face of the instrumentation market. Further, it seems reasonable that the diagnostic capability already inherent in emission spectrometry be made available also for use by a mass spectrometer. For example, a moderate-resolution emission spectrometer aligned to examine the ICP itself or the ion beam extracted from it into the first stage of a mass spectrometer could be used potentially to predict whether matrix or spectral interferences are likely to exist and, if so, to devise a means to correct them.

Let us now revisit a few of the points listed in Table 1.8, in order to clarify and amplify them. First, source background, whether from an ICP or another device, might be reduced by a number of different approaches. In many cases, these approaches were described in what would now be regarded as ancient literature. The interested reader, especially the young spectrochemist, is therefore urged to examine this earlier literature for potential clues about what might happen in the future. As a wise person once said, ‘Six months in the laboratory can save you as much as an hour of library time’.

One possible approach to narrowing detected spectral lines is portrayed in Fig. 1.1. Termed ‘selective spectral-line modulation’, this scheme provides an effective narrowing of the spectral bandpass of any optical monochromator or spectrometer with which it is combined. It involves interposing an atom reservoir between the emission source and the detector. When the concentration of atoms in the reservoir is raised and lowered, atomic absorption goes up and down accordingly. However, because only the absorption lines of atoms in the reservoir undergo this modulation, only the resonance lines corresponding to those transitions will be similarly modulated. As a result, an alternating current (AC) detector tuned to the atom-modulation frequency detects only spectral lines corresponding to the atoms being modulated. As importantly, the effective bandpass of the modulation

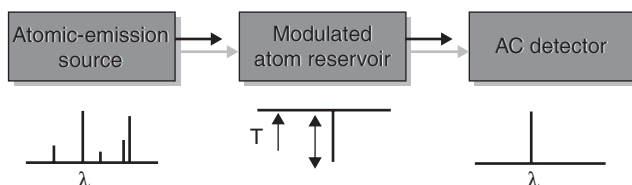


Figure 1.1 Schematic diagram of apparatus for performing selective spectral-line modulation.

process is equal to the absorption line width of atoms in the reservoir, ordinarily much narrower than a conventional monochromator or spectrometer can provide.

Of course, selective spectral-line modulation requires a modulated atom reservoir. Past studies have shown that the reservoir can be constructed from flames, hollow cathode lamps, or other kinds of glow discharges [54–58]. Understandably, however, it might be difficult to fashion a modulated atom reservoir that covers the entire suite of elements whose simultaneous determination is desired.

A similar but more direct approach would be to modulate the concentration of the analyte itself. In this concept, only the desired species (the analyte) would be modulated in concentration, so a detector tuned to the modulation frequency would ignore any direct current (DC) background or other species whose concentrations are not being varied. Regrettably, no method for true analyte modulation has yet been devised; the closest strategy is one that involves sample modulation [59]. Unfortunately, in sample modulation all species present in the sample (including those that might cause spectral or matrix interference) are modulated along with the analyte so that some selectivity is compromised.

A tandem source [16,45,60–63], shown in Fig. 1.2a and b, offers another potential solution to the source-background problem. In such a tandem source, shown in Fig. 1.2a, two devices are connected in series, each of which is intended to perform a specific function that leads to signal generation in emission or MS. For example, the first source might have the responsibility of converting a sample solution into free atoms useful for analysis, while the second source has the job of exciting or ionizing the sample atoms. In such an arrangement, each source can be tailored to perform its intended function with the greatest possible effectiveness; the result might be improved atomization efficiency, higher signal levels, lower background, and the ability to perform speciation better. In the latter

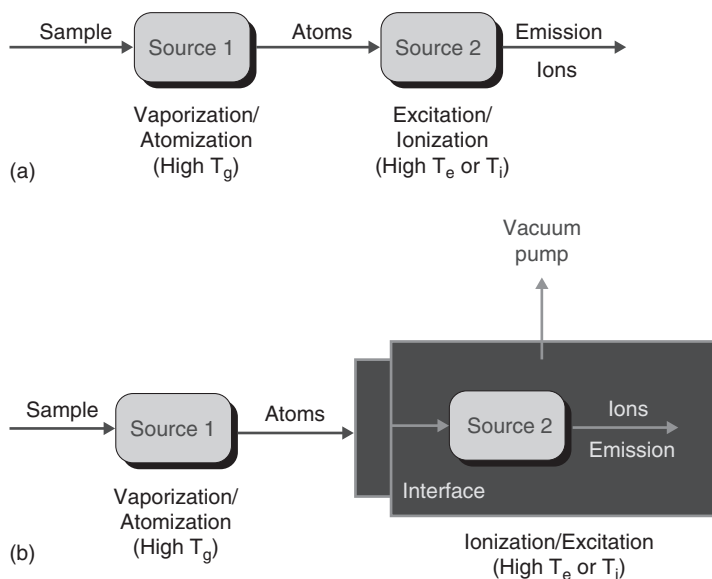


Figure 1.2 Concept of a tandem source. (a) Conventional tandem source; (b) Pressure-differential tandem source.

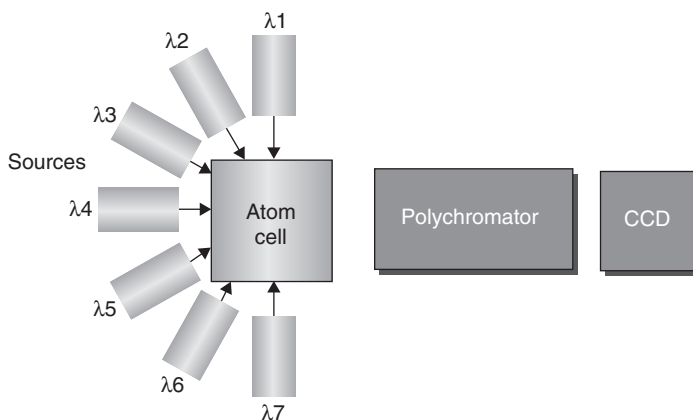


Figure 1.3 A selective-excitation source, based on atomic fluorescence spectrometry, could potentially be used to narrow the observed spectral lines from an ICP.

instance, the effective temperature (T_g) of the first source might be switched or tuned between one mode in which samples are fully atomized and another in which they are merely fragmented, so a fragmentation mass spectrum could be produced.

A modification of a tandem source, shown in Fig. 1.2b, involves introducing the effluent from the first source into a second source held at reduced pressure. Of course, a vacuum interface will be needed in this second arrangement, which might reduce efficiency somewhat. However, it is likely that the second source would exhibit under these conditions a lower background emission and possibly more efficient excitation or ionization, depending on whether emission or MS is to be employed.

Another way to achieve lower backgrounds from even an existing source such as the ICP would be to employ the selective-excitation scheme shown in Fig. 1.3. In this arrangement, which depends on the availability of a group of narrow-band excitation sources, emission from selected resonance lines in the atomization cell would be excited by external sources tuned to each respective wavelength. Of course, those familiar with the history of atomic spectrometry will realize that this arrangement is nothing more or less than atomic fluorescence, which seemed at one time to be the likely successor to AAS. Now, however, recent advances in solid-state laser technology [64–67] urges that the benefits of this arrangement be reconsidered. AFS offers a number of important advantages over emission spectrometry, including a freedom from excited-state quenching effects, more intense spectral lines, and a potentially lower background. Furthermore, as Fig. 1.3 suggests, light from all elements can be measured in a truly simultaneous fashion, by employing the charge coupled and charge injection devices (CCD or CID) based spectrometers that are already available.

Another approach based on AFS is the resonance monochromator [68–71], diagrammed in Fig. 1.4. In this case, fluorescence is not excited from atoms or ions in the ICP (or other atomization source) but rather is used to narrow the bandpass of detected radiation. Broadband light, emitted for example by an ICP in a conventional fashion, falls on an atom cloud, the concentration and composition of which is controlled. For example, if it is desired to determine cadmium, the atom cloud would consist entirely of cadmium atoms. As a result, the only radiation seen at right angles to the incoming broadband light would be fluorescence

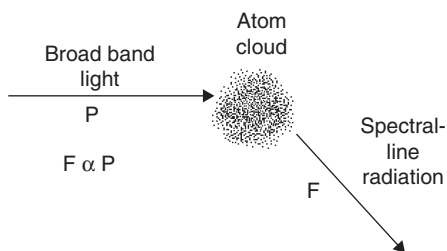


Figure 1.4 A resonance monochromator, based on atomic fluorescence, could be used to narrow the bandpass of radiation detected in ICP emission spectrometry.

corresponding to the narrow spectral lines of cadmium. Any detector or spectrometer positioned in that direction would then be selective for cadmium and would be virtually free of contributions from broadband light or other (non-cadmium) spectral features emitted by the ICP. Also, the bandpass of the detected radiation will correspond to the absorption line width of the cadmium atoms in the cloud, thereby further lessening the likelihood of spectral interference. Unfortunately, like the selective spectral-line modulation approach, the use of a resonance monochromator necessitates that an atom cell be available that contains all the elements whose determination is desired. Just as hollow cathode lamps are practically limited to emitting the spectra of only a few elements at a time, the resonance monochromator is similarly likely to be limited. For this reason, it might be desirable to employ as a resonance monochromator an alternative form of atom reservoir such as a chemical flame. Although two ICPs could also be employed, in the configuration termed ASIA (Atomizer, Source, ICP in AFS) [72], this arrangement has the disadvantage that some background features from the source ICP would be emitted also by the second source.

Let us now consider alternative spectrometers that might overcome some of the limitations expressed in Table 1.4 and in part in Table 1.6. First, a miniaturized high-resolution spectrometer might be fabricated in the fashion diagrammed in Fig. 1.5. In this concept, a F-P interferometer is employed to achieve the narrow spectral bandpass desired in an emission spectrometer. Unfortunately, as was indicated earlier, such an interferometer produces high resolution only when narrow-band, high-reflectivity multilayer dielectric coatings are employed in its fabrication. In turn, such coatings usually restrict use of the device to a narrow range of wavelengths. In the interferometer of Fig. 1.5, however, each area element of the two mirrors that constitute the interferometer is coated to provide high reflectivity for only the narrow range of wavelengths surrounding the desired spectral-line. Finesse and transmission at those wavelengths is therefore high. In addition, each corresponding location in the array also is coated with its own multilayer interference filter, to eliminate intrusion of other spectral lines from higher or lower order of the interferometer. This scheme depends, of course, on light being transmitted through the interferometer in parallel rays; however, that condition is a requirement for proper operation of the interferometer anyway. An array detector placed behind the F-P mirror combination would then detect all the desired spectral intervals at once.

Because the concept shown in Fig. 1.5 might be fabricated in a mass-produced fashion, it should not be prohibitive in cost. It should also be extremely robust, since spacing between the two mirrors and each of the transmitting elements can be fixed and

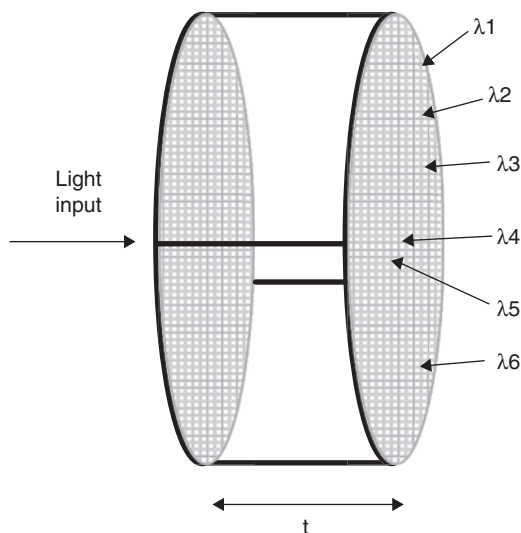


Figure 1.5 Proposed miniature spectrometer based on array of Fabry-Perot (F-P) interferometers. Each pixel in the array is comprised of a miniature F-P interferometer, with dielectric mirrors coated for high reflectivity in the spectral range of a desired atomic emission line. In series with each F-P pixel is a broader band interference filter, to block undesired orders of the F-P. Imaging the pixels onto a two-dimensional array detector then enables many spectral lines to be detected at once, and at high resolution.

therefore inherently very stable; the combination could then be affixed directly onto a detector array.

In the realm of ICP-MS, it is appropriate to question whether alternative forms or combinations of mass spectrometers are likely to make inroads on the entrenched position of the quadrupole and sector-field instruments now on the market. Three manufacturers now offer TOFMS systems, but so far those units appear to be employed for specific applications, such as when transient samples must be examined. Similarly, an ion-trap ICP mass spectrometer is commercially available, but sales to date appear to be low. The use of Fourier-transform MS in conjunction with an ICP source has been explored, but the cost of such systems seems prohibitive, and the dynamic range they offer is likely far too limited.

Perhaps the most promising alternative now on the scene is a sector-field spectrometer coupled with an array detector. Such a combination has largely been used to examine a broad mass range in a simultaneous fashion [13,46,47,49–53,73]. However, it could just as well be utilized in a ‘sequential (or windowed) slew-scan’ manner [74], similar to that of some commercial emission spectrometers. In this approach, a multi-channel array detector would examine a limited mass range at a time, with a high enough resolution (say, $R = 10\,000$) that mass-spectral overlaps are of little concern. After each spectral interval is so examined, the spectrometer could be rapidly slewed to the next spectral region, and so on. In this way, the dual benefits of high mass resolution and rapid mass-spectral acquisition would be realized.

Another potentially attractive combination is that of quadrupole MS and TOFMS. Such a combination would offer tremendous flexibility. When full-mass-range, rapid spectral

acquisition is needed, the quadrupole unit would function as either a band-reject filter or a collision cell to remove undesired species (e.g. polyatomics) from a mass spectrum. The collision cell would also serve to reduce the velocity of the incoming beam and thereby improve the duty factor of TOFMS. At the other extreme, the same combination could be used in a high-precision isotope-ratio mode on an element-by-element basis. In this mode, the quadrupole mass filter would isolate the isotopes of a specific element for transmission into the extraction zone of the TOFMS. The TOFMS would then deflect all ions except those in the mass range transmitted by the quadrupole unit; as a result, the duty factor of the TOFMS could be raised to approximately unity, so all the ions introduced into it could be determined. Because each TOF mass spectrum would be extracted at the same moment from the quadrupole filter, isotope-ratio precision should approach that limited by Poisson statistics [75].

1.6 Concluding considerations

It is hoped that the foregoing discussion offers a few attractive alternatives for instrument and technique development in the field of ICP spectrometry. Regrettably, perhaps, the narrative no doubt raises more questions than it answers. A few explicit questions are those that follow.

- Can ICP-AES remain competitive with ICP-MS?
- What is the future of ICP-TOFMS, ICP-ion trap MS, and ICP-array detector MS?
- Are there other sources that can compete with the ICP?
- How can speciation best be performed whether or not the ICP is retained as a dominant source?
- What new applications areas will appear?

In trying to answer these questions, future spectrochemists face a number of dangers and competing needs. They cannot afford to ignore applications, for if a method or new instrument has no application, of what use is it? On the other hand, it is dangerous for those in our field to become too wedded to applications; instrumentation and method development will no doubt stagnate and our field will become one of strictly service to other communities. Furthermore, we cannot afford to emphasize one source, one spectrometer, or one method. The strength of analytical science is its flexibility and we must use that flexibility to blaze new paths for the future.

We must not all follow the same paths. It is human nature, of course, and perhaps even more so for physical scientists, to pursue the most recent developments. An example over the last several years is the jump toward studying ion–molecule reactions that occur in collision and reaction cells used in ICP-MS. Slavish following of scientific trends is dangerous because it discourages pursuit of new research directions and fosters only incremental research gains. Because many people are working with the same instrumentation and following the same research paths, each person's goals must then of necessity be short term, and increments in development correspondingly small. Overall, scientific trendiness stifles innovation and creative thinking. This point was perhaps made best by the late physicist Richard Feynman, who stated 'In a less crowded field, among shorter yardsticks,

a novelist would not just have seemed bigger, he would have been bigger.' [76]. That is, in a less crowded field, the novelist (read 'scientist') could attack bigger, less fragmented problems and thereby make more important gains.

There are clear paths downhill, reflected in statements witnessed at every conference, in many discussions, and in some manuscripts. These statements are stifling, self-defeating, and destructive: 'We did that 15 years ago', 'The ICP is a solved problem', 'That will never work', 'If it isn't bioscience, it isn't important', 'That's outside my field of interest', 'It's too applied for me', 'It's too fundamental for me', 'If I didn't invent it, it's not worth doing'. The reader can no doubt add a few similar statements from personal experience.

On the other hand, we can all work to improve our field, to make it grow and retain its vibrancy. We should strive toward instruments that diagnose and correct themselves. We should aim for sub-micrometer spatial resolution in solids, in three-dimensions. We should try to measure all, the signal from every element, from every isotope, all the time. We should search for ways to take measurements even below the fundamental noise limit. We should strive to devise a truly standardless method in ICP spectrometry, especially for solids. And finally, we should try for truly multi-dimensional, information-rich analytical schemes that employ the ICP and atomic spectrometry. In the future, I hope to see our techniques and technologies utilized for the complete analysis of metalloproteins and to witness the integration of informatics and atomic spectrometry. Human-computer integration to yield 'artificial intuition' seems possible and the use of atomic spectrometry in space exploration appears to be inevitable.

In conclusion, it is useful to reiterate one of the earlier points made in this discussion, a point perhaps made most forcefully in the 1965 survey of chemistry made by the National Academy of Sciences of the United States (the 'Westheimer report'). In that report it is stated that '... many of the most important and original developments in chemistry will ... be unexpected'.

References

1. Hieftje, G.M. (1989) AAS – has it gone or where is it going. *J. Anal. Atom. Spectrom.*, **4**, 117–122.
2. Robin, J. and Trassy, C. (1975) Stimulated emission of aluminium and titanium resonance lines at very low concentrations in a HF (high frequency) argon plasma *C.R. Acad. Sc. (Paris)*, **281**, 345.
3. Lichte, F.E. and Koirtzoyhann, S.R. (1976) Induction coupled plasma emission from a different angle. *ICP. Inf. Newsl.*, **2**, 192.
4. Margoshes, M. (1979) Demand-pull and science-push in multielement analysis. *Anal. Chem.*, **51**, 1317A.
5. Fraústo da Silva, J.J.R. and Williams, R.J.P. (2001) *The Biological Chemistry of the Elements*, Oxford University Press, Oxford.
6. Hieftje, G.M. (2000) Atomic emission spectroscopy – it lasts and lasts and lasts. *J. Chem. Educ.*, **77**, 577–583.
7. Potyrailo, R.A., Conrad, R.C., Ellington, A.D. and Hieftje, G.M. (1998) Adapting selected nucleic acid ligands (Aptamers) to biosensors. *Anal. Chem.*, **70**, 3419–3425.
8. Hieftje, G.M. (1996) The future of plasma spectrochemical instrumentation. *J. Anal. Atom. Spectrom.*, **11**, 613–621.
9. Fassell, V.A. (1986) Seven stages of an analytical method. *Fres. Z. Anal. Chem.*, **324**, 511.

10. Liu, X., Plasencia, M., Ragg, S., Valentine, S.J. and Clemmer, D.E. (2004) Development of high throughput dispersive LC-ion mobility-TOFMS techniques for analysing the human plasma proteome. *Brief. Funct. Genom. Proteom.*, **3**, 177–186.
11. Koeniger, S.L., Valentine, S.J., Myung, S., Plasencia, M., Lee, Y.J. and Clemmer, D.E. (2005) Development of field modulation in a split-field drift tube for high-throughput multidimensional separations. *J. Proteome Res.*, **4**, 25–35.
12. Valentine, S.J., Koeniger, S.L. and Clemmer, D.E. (2003) A split-field drift tube for separation and efficient fragmentation of biomolecular ions. *Anal. Chem.*, **75**, 6202–6208.
13. Barnes IV, J.H., Schilling, G.D., Sperline, R., Denton, M.B., Young, E.T., Barinaga, C.J., Koppenaal, D.W. and Hieftje, G.M. (2004) Characterization of a focal plane camera fitted to a Mattauch–Herzog geometry mass spectrograph. II. Use with an inductively coupled plasma. *Anal. Chem.*, **76**, 2531–2536.
14. Galley, P.J. and Hieftje, G.M. (1994) Easily ionizable element interferences in ICP-AES Part II. Minimization of EIE effects by choice of observation volume. *Spectrochim. Acta*, **49B**, 703–724.
15. Mermet, J.M. (1991) Use of magnesium as a test element for inductively coupled plasma atomic emission spectrometry diagnostics. *Anal. Chim. Acta*, **250**, 85–94.
16. Borer, M.W. and Hieftje, G.M. (1991) Tandem sources for analytical atomic spectrometry. *Spectrochim. Acta*, **14**, 463–486.
17. Milstein, L.S., Waggoner, J.W., Sutton, K.L. and Caruso, J.A. (2000) Mixed gas helium/argon low-power/reduced-pressure ICP as a tunable ionization source for the mass spectrometric detection of organotin compounds. *Appl. Spectrosc.*, **54**, 1286–1290.
18. Marcus, R.K., Evans, E.H. and Caruso, J.A. (2000) Tunable plasma sources in analytical spectroscopy: current status and projections. *J. Anal. Atom. Spectrom.*, **15**, 1–5.
19. Lewis, C.L., Moser, M.A., Dale Jr., D.E., Huang, W., Hassell, C., King, F.L. and Majidi, V. (2003) Time-gated pulsed glow discharge: real-time chemical speciation at the elemental, structural, and molecular level for gas chromatography time-of-flight mass spectrometry. *Anal. Chem.*, **75**, 1983–1996.
20. Rosen, A.L. and Hieftje, G.M. (2004) Inductively coupled plasma mass spectrometry and electrospray mass spectrometry for speciation analysis: applications and instrumentation. *Spectrochim. Acta*, **59**, 135–146.
21. Ray, S.J. and Hieftje, G.M. (2001) Microwave plasma torch-atmospheric sampling glow discharge modulated tandem source for the sequential acquisition of molecular fragmentation and atomic mass spectra. *Anal. Chim. Acta*, **445**, 35–45.
22. McClenathan, D.M. and Hieftje, G.M. (2005) Use of rapid gas-flow modulation for improved performance in inductively coupled plasma time-of-flight mass spectrometry. *J. Anal. Atom. Spectrom.*, **20**, 1318–1325.
23. Lehn, S. Richland, W.A. (2005). Personal communication.
24. Alkemade, C.T.J. (1981) Single-atom detection. *Appl. Spectrosc.*, **35**, 1–14.
25. Olesik, J.W., Kinzer, J.A. and Harkleroad, B. (1994) Inductively coupled plasma optical emission spectrometry using nebulizers with widely different sample consumption rates. *Anal. Chem.*, **66**, 2022–2230.
26. Wu, M. and Hieftje, G.M. (1992) A new spray chamber for inductively coupled plasma spectrometry. *Appl. Spectrosc.*, **46**, 1912–1918.
27. Wu, M., Madrid, Y., Auxier, J.A. and Hieftje, G.M. (1994) New spray chamber for use in flow-injection plasma emission spectrometry. *Anal. Chim. Acta*, **286**, 155–167.
28. Schaldach, G., Berndt, H. and Sharp, B.L. (2003) An application of computational fluid dynamics (CFD) to the characterization and optimization of a cyclonic spray chamber for ICP-AES. *J. Anal. Atom. Spectrom.*, **18**, 742–750.
29. Schaldach, G., Razilov, I. and Berndt, H. (2003) Optimization of the geometry of a double-path spray chamber for inductively coupled plasma-atomic emission spectrometry by computer simulation and an evolutionary strategy. *Spectrochim. Acta B*, **58B**, 1807–1819.

30. Niemax, K. and Sdorra, W. (1990) Topics in laser spectroscopy: temporal and spatial distribution of analyte atoms and ions in microplasmas produced by laser ablation of solid samples. *Spectrochim. Acta*, **45B**, 917–926.
31. Guillon, M. and Guenther, D. (2002) Effect of particle size distribution on ICP-induced elemental fractionation in laser ablation-inductively coupled plasma-mass spectrometry. *J. Anal. Atom. Spectrom.*, **17**, 831–837.
32. Jackson, S.E. and Guenther, D. (2003) The nature and sources of laser induced isotopic fractionation in laser ablation-multicollector-inductively coupled plasma-mass spectrometry. *J. Anal. Atom. Spectrom.*, **18**, 205–212.
33. Margetic, V., Niemax, K. and Hergenroeder, R. (2003) Application of femtosecond laser ablation time-of-flight mass spectrometry to in-depth multilayer analysis. *Anal. Chem.*, **75**, 3435–3439.
34. Gonzalez, J., Liu, C., Mao, X. and Russo, R.E. (2004) UV-femtosecond laser ablation-ICP-MS for analysis of alloy samples. *J. Anal. Atom. Spectrom.*, **19**, 1165–1168.
35. Klunder, G.L., Grant, P.M., Andresen, B.D. and Russo, R.E. (2004) Direct chemical analysis of solids by laser ablation in an ion storage time-of-flight mass spectrometer. *Anal. Chem.*, **76**, 1249–1256.
36. Kuhn, H.-R. and Guenther, D. (2004) Laser ablation-ICP-MS: particle size dependent elemental composition studies on filter-collected and online measured aerosols from glass. *J. Anal. Atom. Spectrom.*, **19**, 1158–1164.
37. Bian, Q.Z., Koch, J., Lindner, H., Berndt, H., Herggenroder, R. and Niemax, K. (2005) Non-matrix matched calibration using near-IR femtosecond laser ablation inductively coupled plasma optical emission spectrometry. *J. Anal. Atom. Spectrom.*, **20**, 671–676.
38. Gonzalez, J., Liu, C., Yoo, J., Mao, X. and Russo, R.E. (2005) Double-pulse laser ablation inductively coupled plasma mass spectrometry. *Spectrochim. Acta B*, **60B**, 27–31.
39. Allen, G.M. and Coleman, D.M. (1984) Segregated sampling and excitation with a dual inductively coupled plasma. *Anal. Chem.*, **56**, 2981–2983.
40. Allen, G.M. and Coleman, D.M. (1987) Characterization of a dual inductively coupled plasma atomic emission source. *Appl. Spectrosc.*, **41**, 381–387.
41. Jahl, M.J., Jacksier, T. and Barnes, R.M. (1992) Sealed inductively coupled plasma atomic emission spectrometry: instrumentation development. *J. Anal. Atom. Spectrom.*, **7**, 653–660.
42. Gaillat, A., Barnes, R.M., Proulx, P. and Boulos, M.I. (1995) Computer simulation of enclosed inductively coupled plasma discharges Part 1. monatomic gases. *J. Anal. Atom. Spectrom.*, **10**, 935–940.
43. Gaillat, A., Barnes, R.M., Proulx, P. and Boulos, M.I. (1995) Computer simulation of enclosed inductively coupled plasma discharges Part 2. molecular gases. *J. Anal. Atom. Spectrom.*, **10**, 941–946.
44. Klostermeier, A., Engelhard, C., Evers, S., Sperling, M. and Buscher, W. (2005) New torch design for inductively coupled plasma optical emission spectrometry with minimized gas consumption. *J. Anal. Atom. Spectrom.*, **20**, 308–314.
45. Borer, M.W. and Hieftje, G.M. (1993) Design considerations for a pressure-differential tandem source for use in atomic spectrometry. *J. Anal. Atom. Spectrom.*, **8**, 333–338.
46. Hieftje, G.M., Barnes IV, J.H., Grøn, O.A., Leach, A.M., McClenathan, D.M., Ray, S.J., Solyom, D.A., Wetzel, W.C., Denton, M.B. and Koppelaar, D.W. (2001) Evolution and revolution in instrumentation for plasma-source mass spectrometry. *Pure Appl. Chem.*, **73**, 1579–1588.
47. Barnes IV, J.H., Sperline, R., Denton, M.B., Barinaga, C.J., Koppelaar, D., Young, E.T. and Hieftje, G.M. (2002) Characterization of a focal plane camera fitted to a Mattauch–Herzog geometry mass spectrograph. I. Use with a glow-discharge source. *Anal. Chem.*, **74**, 5327–5332.
48. Barnes IV, J.H., Hieftje, G.M., Denton, M.B., Sperline, R., Koppelaar, D.W. and Barinaga, C.J. (2003) A new mass spectrometry detector array capable of truly simultaneous detection. *American Laboratory – 35th Anniversary Edition*, vol. 35, pp. 15–22.

49. Barnes IV, J.H., Schilling, G.D., Sperline, R., Denton, M.B., Young, E.T., Barinaga, C.J., Koppelaar, D.W. and Hieftje, G.M. (2004) Coupling of a gas chromatograph to a simultaneous-detection inductively coupled plasma mass spectrograph for speciation of organohalide and organometallic compounds. *J. Anal. Atom. Spectrom.*, **19**, 751–756.
50. Barnes IV, J.H., Schilling, G.D., Sperline, R.P., Denton, M.B., Barinaga, C.J., Koppelaar, D.W. and Hieftje, G.M. (2004) Use of a novel array detector for the direct analysis of solid samples by laser ablation inductively coupled plasma sector-field mass spectrometry. *J. Am. Soc. Mass Spectrom.*, **15**, 769–776.
51. Barnes IV, J.H., Schilling, G.D., Stone, S.F., Sperline, R.P., Denton, M.B., Young, E.T., Barinaga, C.J., Koppelaar, D.W. and Hieftje, G.M. (2004) Simultaneous multichannel mass-specific detection for high-performance liquid chromatography using an array detector sector-field mass Spectrometer. *Anal. Bioanal. Chem.*, **380**, 227–234.
52. Koppelaar, D.W., Barinaga, C.J., Denton, M.B., Sperline, R., Hieftje, G.M., Schilling, G.D. Andrade, F.A and Barnes, J.H. (2005) Mass spectrometry detectors. *Anal. Chem.*, **77**, 419A–427A.
53. Sperline, R.P., Knight, A.K., Gresham, C.A., Koppelaar, D.W., Hieftje, G.M. and Denton, M.B. (2005) Read-noise characterization of focal plane array detectors via mean-variance analysis. *Appl. Spec.*, Submitted. **59**, 1315–1323.
54. Cochran, R.L. and Hieftje, G.M. (1977) Selective spectral-line modulation technique for high sensitivity continuum-source atomic absorption spectrometry. *Anal. Chem.*, **49**, 98–105.
55. Cochran, R.L. and Hieftje, G.M. (1978) Device for selective spectral-line modulation atomic absorption spectrometry. *Anal. Chem.*, **50**, 791–800.
56. Downey, S.W., Shabushnig, J.G. and Hieftje, G.M. (1980) Reduction of spectral interferences in flame emission spectrometry by selective spectral-line modulation. *Anal. Chim. Acta*, **121**, 165–174.
57. Downey, S.W. and Hieftje, G.M. (1982) Reduction of spectral interferences in inductively coupled plasma-atomic emission spectrometry by selective spectral-line modulation. *Anal. Chim. Acta*, **141**, 193–205.
58. Mitchell, J.C., Steele, A.W. and Hieftje, G.M. (1987) The use of discharge lamps as directly modulated atom reservoirs for selective line modulation in atomic emission spectrometry. *Anal. Chem. Acta*, **200**, 539–550.
59. Steele, A.W. and Hieftje, G.M. (1986) The use of sample modulation to simplify the experimental arrangement of selective line modulation in atomic emission spectrometry. *Appl. Spectrosc.*, **40**, 1110–1117.
60. Falk, H., Hoffman, E. and Luedko, C. (1981) Fanes (Furnace Atomic Nonthermal Excitation Spectrometry): a new emission technique with high detection power. *Spectrochim. Acta*, **36B**, 767.
61. Borer, M.W. and Hieftje, G.M. (1993) Inductively coupled plasma-microwave induced plasma tandem source for atomic emission spectrometry. *J. Anal. Atom. Spectrom.*, **8**, 339–349.
62. Pack, B.W. and Hieftje, G.M. (2000) Inductively coupled plasma-microwave induced plasma tandem source for atomic emission spectroscopy. *Appl. Spectrosc.*, **54**, 80–88.
63. Ray, S.J., Andrade, F., Gamez, G., McClenathan, D., Rogers, D., Schilling, G., Wetzel, W. and Hieftje, G.M. (2004) Plasma-source mass spectrometry for speciation analysis: state-of-the-art. *J. Chromatogr. A*, **1050**, 3–34.
64. Niemax, K., Zybin, A. and Eger, D. (2001) Tunable deep blue light for laser spectrochemistry. *Anal. Chem.*, **73**, 134A–139A.
65. Zybin, A., Koch, J., Butcher, D.J. and Niemax, K. (2004) Element-selective detection in liquid and gas chromatography by diode laser absorption spectrometry. *J. Chromatogr. A*, **1050**, 35–44.
66. Anderson, T.N., Lucht, R.P., Meyer, T.R., Roy, S. and Gord, J.R. (2005) Diode-laser-based ultraviolet-absorption sensor for high-speed detection of the hydroxyl radical. *Opt. Lett.*, **30**, 1321–1323.
67. Hecht, J. (2005) Semiconductor sources advance deeper into the ultraviolet. *Laser Focus World*, **41**, 95–96, 98–99.

68. Palermo, E.F. and Crouch, S.R. (1973) Theoretical and experimental evaluation of resonance monochromators for atomic absorption spectrometry. *Anal. Chem.*, **45**, 1594.
69. Bower, J., Bradshaw, J. and Winefordner, J. (1979) A continuum-source single-detector resonance-monochromator for atomic-absorption spectrometry. *Talanta*, **26**, 249–250.
70. Krupa, R.J., Long, G.L. and Winefordner, J.D. (1985) An ICP-excited ICP resonance monochromator and fluorescence spectrometer for the determination of trace to major sample constituents. *Spectrochim. Acta B*, **40B**, 1485–1494.
71. Hermann, G., Udem, T., Hirokawa, K. and Matsuta, H. (1994) Calculated transmission line structures of a Cu coherent forward scattering resonance monochromator (CFSRM). *Spectrochim. Acta, B*, **49B**, 355–365.
72. Greenfield, S., Salman, M.S. and Tyson, J.F. (1988) Atomizer, source, inductively coupled plasmas in atomic fluorescence spectrometry (ASIA): a study of chemical and ionization interference effects. *Spectrochim. Acta, B*, **43B**, 1087–1092.
73. Knight, A.K., Sperline, R.P., Hieftje, G.M., Young, E., Barinaga, C.J., Koppelaar, D.W. and Denton, M.B. (2002) The development of a micro-faraday array for ion detection. *Int. J. Mass Spectrom. Ion Proc.*, **215**, 131–139.
74. Stubbley, E.A. and Horlick, G. (1985) A window slew-scanning FTS for ICP emission spectrometry. *Appl. Spec.*, **39**, 5.
75. McClenathan, D.M., Ray, S.J., Wetzel, W.C. and Hieftje, G.M. (2004) Plasma source TOFMS. *Anal. Chem.*, **76**, 159A–166A.
76. Gleick, J. (1993) *Genius: The Life and Science of Richard Feynman*, Pantheon, New York.

Chapter 2

Fundamental Principles of Inductively Coupled Plasmas

Jean-Michel Mermet

2.1 Principles of inductively coupled plasma generation

A plasma is an ionized gas that is macroscopically neutral (i.e. with the same number of positive particles (ions) and negative particles (electrons)). If a monoatomic gas, X , is used, a plasma can be described by the following equilibrium:

$$X = \sum_{n=1}^q X^{n+} + \sum_{n=1}^q n e$$

where X^{n+} is an ion with n charges and e is the electron. Some properties of ideal gases such as the pressure and the volume still apply in contrast to other properties such as the viscosity and the thermal conductivity that significantly differ from those of ideal gases, because of the presence of charged particles. When argon is used as the inductively coupled plasma (ICP) plasma gas, the only Ar ions that are observed are the singly ionized Ar ions.

In contrast to a flame, it is necessary to supply an external energy in the form of an electrical field in order to ionize the gas and to sustain the plasma, which, in turn, will transmit part of this energy to the sample to atomize, ionize and excite it. Plasmas may be classified according to the kind of electrical field that is used to create and sustain the plasma:

- direct current plasma (DCP) is obtained when a direct current field is established across electrodes,
- ICP is obtained when a high-frequency (hf) field is applied through a coil,
- microwave-induced plasma (MIP) is obtained when a microwave field is applied to a cavity.

Historically, the DCP was the first described and commercialized plasma. However, the ICP is currently the most commonly used plasma because of some unique properties. Originally, the ICP was designed for the production of crystals [1,2]. The first analytical applications of the ICP were published in 1964 [3] and 1965 [4]. Various names were used (e.g. induction-coupled plasma spectrometric excitation source [4], hf plasma source [5], induction plasma [6], induction-coupled, radio-frequency (rf) plasma torch [7]), before the term ICP and its corresponding acronym, ICP, were used [8].

The gas that is used to generate the plasma (plasma gas) is argon. Like any noble gas, argon is a monoatomic element with a high ionization energy (15.76 eV), and is chemically inert. Consequently:

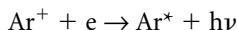
- (i) a simple spectrum is emitted by argon in contrast to a flame where primarily molecular spectra are observed;
- (ii) argon has the capability to excite and ionize most of the elements of the Periodic Table;
- (iii) no stable compounds are formed between argon and the analytes.

It should be noted, however, that some unstable molecular excited or ionized species can be formed within the plasma (e.g. ArH). They usually dissociate after their de-excitation. Argon is also the cheapest noble gas, as its concentration in the air is 1%. The only limitation in using argon is the poor thermal conductivity of this gas compared with molecular gases such as nitrogen and hydrogen.

The hf field is produced by a rf generator (see Chapter 3) and accelerates the electrons. These electrons will ionize the plasma gas:



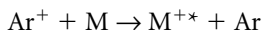
Then, through the process of radiative recombination, the argon ions are recombined with electrons to lead to excited argon atoms and to a significant background:



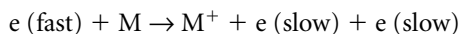
This background is mainly produced by the process of radiative recombination in the ultraviolet (UV) region, while bremsstrahlung must also be taken into consideration in the visible part of the spectrum [9,10]. Except for the resonance lines that are located at 106.7 nm and 104.8 nm, there are no argon atomic lines below 300 nm.

In atomic emission spectrometry (AES), a source will have actually two roles: the first step consists of the atomization of the sample to be analyzed so as to obtain free analyte atoms, usually in the ground state, the second step consists of a partial ionization of the analyte atoms, and of the excitation of the atoms and the ions to higher-energy states. The plasma acts as reservoir of energy provided by the rf field, and transfers this energy to an analyte, *M*. It should be noted that the atomization of a sample is a relatively long process (of the order of a few ms), while ionization and excitation are very fast processes. Various ionization and excitation processes have been suggested [11–33] resulting from the presence of species that are obtained during the plasma generation. The major species are not only the argon ions, Ar^+ , and the electrons, *e*, but also the excited argon atoms, Ar^* , with the special case of the metastable levels, Ar^m [11,13,23,34]. The main ionization processes are:

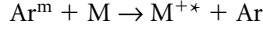
the charge-transfer ionization,



the electron-impact ionization,

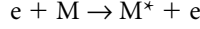


the Penning ionization,

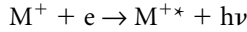


while the main excitation processes for the analyte atom are:

the electron impact excitation,



and the ion–electron radiative recombination,



It has been possible to explain the observation of species such as Mg^{+*} through the charge transfer process [21,27,30], but no general evidence has been given so far to explain the processes involved for each element. However, some simple rules can be given. Ionic lines will be more sensitive than atomic lines when their sum of ionization and excitation energies is below the ionization energy of Ar (i.e. 16 eV) [21]. This is the case for elements such as Al, Ba, Be, Ca, Ce, Co, Cr, Fe, Hf, Hg, In, Ir, La (and rare earths), Mg, Mo, Nb, Ni, Os, Pb, Sc, Sn, Sr, Ta, Th, Ti, U, V, W, Y, Zn, and Zr. Al is a good example of this rule, since the only ionic line that fulfills this requirement is the Al II 167 nm line, which is the most sensitive Al line [21]. In contrast, atomic lines are the most sensitive ones for elements such as Ag, As, Au, B, Bi, Ga, Ge, K, Li, Na, Rb, S, Sb, Se, and Si. Usually, the use of atomic lines lead to a degradation of the sensitivity. Only a few elements exhibit atomic and ionic lines of similar sensitivities, Cu, Pd, Pt, Rh, and Ni.

2.2 Equilibrium in a plasma

Two laws are used to describe equilibrium in a plasma: the Boltzmann law to describe the equilibrium between the population of the various levels within the same ionization state, including both excited and ground states, and the Saha law to describe the equilibrium between the population of two successive ionization states.

If we consider the population n_m and n_k of the excited level E_m and E_k , respectively, their ratio can be given by the Boltzmann law:

$$\frac{n_m}{n_k} = \frac{g_m \exp\left(\frac{-E_m}{kT}\right)}{g_n \exp\left(\frac{-E_k}{kT}\right)} \quad (2.1)$$

where k is the Boltzmann constant ($k = 1.380 \times 10^{-23} \text{ J K}^{-1} = 0.695 \text{ cm}^{-1} \text{ K}^{-1} = 8.617 \times 10^{-5} \text{ eV K}^{-1}$), T is the temperature of the radiation source (called here the excitation temperature) and g is the statistical weight ($g = 2J + 1$, J being the total electronic angular momentum quantum number). As the population of excited levels is proportional to the exponential of $(-E)$, the population decreases very rapidly when E increases. The

use of a plasma permits the obtaining of a high excitation temperature, typically between 3500 and 7000 K, which will increase the population of the upper levels. In the case of the ground state, $E = 0$, and:

$$\frac{n_m}{n_0} = \frac{g_m \exp\left(\frac{-E_m}{kT}\right)}{g_0} \quad (2.2)$$

In order to relate n_m to the total population of the levels of the atom (or the ion), N

$$N = n_0 + n_1 + \dots + n_m + \dots \quad (2.3)$$

it is possible to sum the terms such as $g_m \cdot \exp(-E_m/kT)$ for all possible levels and to define the partition function, Z , as follows:

$$Z = g_0 + g_1 \exp\left(\frac{-E_1}{kT}\right) + \dots + g_m \exp\left(\frac{-E_m}{kT}\right) + \dots \quad (2.4)$$

The Boltzmann law is modified to:

$$\frac{n_m}{N} = \frac{g_m \exp\left(\frac{-E_m}{kT}\right)}{Z} \quad (2.5)$$

The partition function is, therefore, a function of T . However, in the range of temperatures observed in an ICP (i.e. 3000–7000 K), this variation may be small or negligible.

The Saha equation is:

$$\frac{n_{q+1} n_e}{n_q} = \left(\frac{2Z_{q+1}}{Z_q} \right) \left(\frac{(2\pi m_0 k)^{1/2}}{h} \right)^3 T^{3/2} \exp\left(\frac{-E_{\text{ion}}}{kT}\right) \quad (2.6)$$

where k and h are the Boltzmann and Planck constants ($h = 6.626 \times 10^{-34}$ J s = 3.336×10^{-11} cm⁻¹ s), respectively, E_{ion} is the ionization energy between the q and $q + 1$ ionization states, m_0 is the electron mass, and Z is the partition function. When the densities are expressed in m⁻³, the Z equation becomes:

$$\frac{n_{q+1} n_e}{n_q} = 4.825 \times 10^{21} \left(\frac{Z_{q+1}}{Z_q} \right) T^{3/2} \exp\left(\frac{-E_{\text{ion}}}{kT}\right) \quad (2.7)$$

The temperature used in the Saha equation is called the ionization temperature.

2.3 Line intensities

If the transition occurs between an upper level, E_m and a lower level E_k , radiation is emitted whose frequency ν is given by:

$$h\nu = E_m - E_k \quad (2.8)$$

where h is the Plank constant. In AES, wavelength λ is commonly used instead of frequency with:

$$\lambda = \frac{c}{\nu} \quad (2.9)$$

where c is the velocity of light ($c = 299\,792\,458\text{ m s}^{-1}$). Wavelengths used to be expressed in angström (Å). They should be expressed in nm (10^{-9} m).

Quantitative analysis will be possible if the intensity of the line can be related to the concentration of the emitting species. The intensity of a line is proportional to:

- (i) the difference in energy between the upper level, E_m , and the lower level, E_k , of the transition,
- (ii) the population of electrons, n_m , in the upper level, E_m ,
- (iii) the number of possible transitions between E_m and E_k per unit time. This value is expressed by the transition probability A , and has been defined by Einstein. Therefore, the intensity I is proportional to:

$$I \propto (E_m - E_k) A n_m \quad (2.10)$$

As seen above, it is possible to relate the population n_m to the total population N through the Boltzmann equation. The intensity of a line can be, therefore, written as:

$$I = \Phi \left(\frac{hcg_m AN}{4\pi\lambda Z} \right) \exp \left(\frac{-E_m}{kT} \right) \quad (2.11)$$

where Φ is a coefficient to account for the emission being isotropic over a solid angle of 4π steradian.

When a radiation source is stable enough to exhibit a constant temperature, the function of partition, Z , will remain constant, and the number of atoms (or ions) N will be proportional to the concentration, c . For a given line of the element to be analyzed, g_m , A , λ , and E_m are constant. Therefore, I is proportional to c , which makes it possible to conduct quantitative analysis. In this instance, relative quantitative analysis is conducted. It should be noted that, in the case of a constant concentration of the analyte, any small variations in the characteristics of the plasma source can lead to a variation in the temperature, and a subsequent variation in the line intensity, because of the change in the population of the excited level. When considering the resonance Al I 396.15 nm line ($E_m = 25\,347\text{ cm}^{-1}$), an increase of 100 K in the temperature of the radiation source will correspond to an increase in the exponential term ($-E_m/kT$) of about 50% and 5% at 3000 and 6000 K, respectively.

This explains why good stability of the source characteristics (i.e. forward power and gas flow rates), is required so as to obtain good repeatability and reproducibility and to avoid any drift of the analytical signal.

2.4 Line profiles

The line profile is the distribution of the spectral intensity within the line. The maximum value of the line profile function is the peak intensity, and the shape of the line profile is usually represented by the width measured at half the maximum intensity. This line width, $\Delta\lambda$, is also called the full width at half maximum (FWHM). The wing of the line is the part of the line profile that is below 1% of the maximum intensity. Two major causes of line broadening explain the physical line widths, $\Delta\lambda_L$, observed for analyte lines in an ICP: the Doppler effect and the collisional broadening. The Doppler effect originates from the motion of the emitting particles, because of the kinetic temperature of the media. The velocity, v , of the particles is related to the kinetic temperature, T_{kin} :

$$v = \left(\frac{2kT_{\text{kin}}}{m} \right)^{1/2} \quad (2.12)$$

where m is the mass of the emitting particle. The FWHM corresponding to the Doppler effect, $\Delta\lambda_D$ is then:

$$\Delta\lambda_D = 7.16 \times 10^{-7} \lambda \left(\frac{T_{\text{kin}}}{M} \right)^{1/2} \quad (2.13)$$

where M is expressed in atomic mass unit.

The lowest values of the Doppler FWHMs are then for heavy elements and for wavelengths in the UV, such as Au II 200.08 nm (0.8 pm), Cd I 228.80 nm (1.2 pm), and Ba II 233.53 nm (1.2 pm) while the largest values are for light elements (e.g. Be II 313.11 nm (5.9 pm)). The actual range is 0.8–6 pm.

Collisional broadening results from the collisions between the analyte ions and atoms and the neutral Ar atoms. This broadening is also called pressure broadening, because its magnitude depends on the number of collisions, and therefore, on the pressure. Calculation is far more complex than for the Doppler effect. Calculations are usually based on the hypothesis of a Van der Waals potential; that is, the shift of the circular frequency of the emitting atoms is inversely proportional to r^6 , r being the distance between the analyte and argon atoms [35]. The a -parameter described the ratio between the two FWHM values:

$$a = \left(\frac{\Delta\lambda_{\text{vdw}}}{\Delta\lambda_D} \right) (\ln 2)^{1/2} \quad (2.14)$$

The a -parameter varies for most lines between 0.1 and 0.5 [35–36]. These a -values mean that the FWHM resulting from the pressure broadening, $\Delta\lambda_{\text{vdw}}$, is lower than that

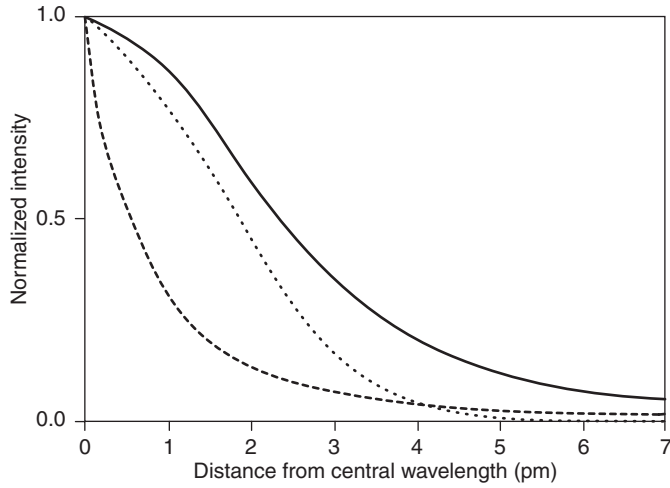


Figure 2.1 Influence of the pressure broadening (----) and the Doppler effect (.....) on the Ca II 393 nm line profile (—).

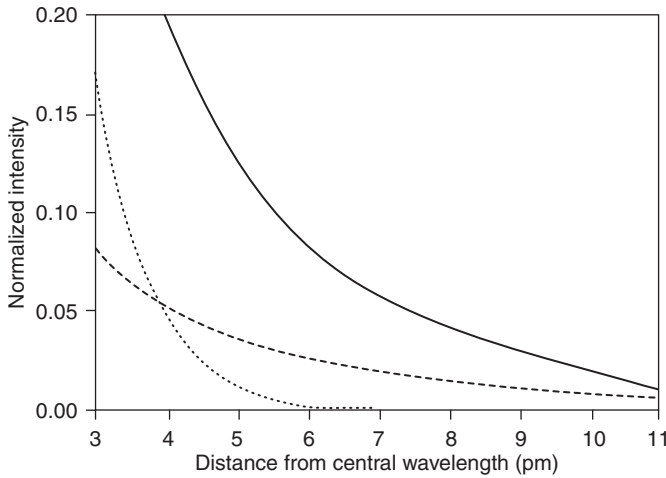


Figure 2.2 Influence of the pressure broadening (----) and the Doppler effect (.....) on the Ca II 393 nm line wing (—).

observed for the Doppler effect. In other words, the Doppler effect predominates at the FWHM level. An example of calculation is given in Fig. 2.1 for the Ca I 422.7 nm line. Compared to the values previously mentioned, the physical line width resulting from the two effects is then 0.9, 1.5, and 1.5 pm for the Au II 200.08 nm, Cd I 228.80 nm, and Ba II 233.53 nm lines, respectively, which is close to the Doppler FWHM values. In marked contrast, the pressure broadening is predominant along the wing of the lines because of the Lorentzian shape of the pressure broadening, while the Doppler broadening is described by a Gaussian profile. This contribution of the pressure broadening can be significant [35], even far from the central wavelength (Fig. 2.2). A consequence is that the wing intensity

from a sensitive line emitted by a major element can be significant compared to that of an analyte line located in its vicinity. Moreover, this can result in a background that is curved.

Stark effect results from the electrical field produced by the charged particles. The effect is very strong on hydrogen lines, in particular on the H_{β} 486.1 nm line (see Section 2.7), and significant on some Ar lines located in the 500–600 nm region. Only a few lines from other elements are sensitive to the Stark effect (e.g. the Mg I 237.6 nm line). Computation led to a Stark FWHM of 26 pm for this line, while the Doppler FWHM and the pressure broadening FWHM were 2.8 and 5.2 pm, respectively. In this case, the Doppler broadening was the smallest effect [35].

It should be noted that, in some cases, hyperfine structure can be observed for some analytical lines. Some classical examples are the Bi I 206.17 nm and the Ho II 374.82 nm lines, with a physical line width of 13.5 and 32.6 pm, respectively, while the Doppler width was only 0.8 and 1.7 pm, respectively [36].

The values of the physical line widths generally observed in the ICP can lead to specifications for the practical resolution of the dispersive system. Ideally, a practical resolution of less than 1 pm should be necessary to fully resolve the narrowest lines. In any case, two lines with a similar intensity could be totally resolved if they would be separated by a distance of at least 2 pm. Actually, the best commercially available systems provide a resolution in the UV around 5 pm [37], which means that a full separation is obtained for lines with a distance of at least 10 pm.

2.5 Temperature definitions

Several temperatures have been previously mentioned: the kinetic temperature, T_{kin} , which corresponds to the motion of the particles, the excitation temperature, T_{exc} , which describes the Boltzmann equilibrium, and the ionization temperature, T_{ion} , which describes the Saha equilibrium. It is necessary to add the electron temperature, T_e , which is related to the velocity of the free electrons. The rotational temperature, T_{rot} , is related to the vibrational–rotational excitation of molecules or radicals that are still present in the ICP, such as N_2^+ and OH. The rotational temperature is often assumed to be similar to the kinetic temperature (see Section 2.11).

Plasmas are composed of species with a very large difference in mass: the electrons and the heavy Ar particles. Following energy deposition through the hf field, the two species will exhibit fast relaxation processes towards two different Maxwellian distributions, that is, two different kinetic energies with T_e and T_{kin} , the kinetic temperature of the electrons and the heavy particles, respectively. The second process where the two sub-systems would tend to thermal equilibrium with only a single temperature is usually very slow due to the poor efficiency of the energy transfer between the electrons and the heavy particles. The ICP belongs to the category of thermal plasmas where there is a correlation between the behavior of the electrons and the heavy particles (i.e. T_{kin} tends to T_e). Thermal plasmas should be close to being in local thermodynamic equilibrium (LTE) (i.e. all the temperatures should be similar). Practically, this is not the case and it is observed that (see Section 2.11):

$$T_{\text{rot}} < T_{\text{exc}} < T_{\text{ion}} < T_e$$

Although knowledge of the various temperatures is not sufficient to explain the various processes in the ICP, their measurements are most helpful for the optimization of the plasma conditions so as to obtain good analytical performance in terms of atomization, excitation, and ionization processes.

2.6 Temperature measurements

Two different types of spectrometric methods can be used for temperature measurements: passive methods where no interaction with the plasma is produced, and active methods where a perturbation is brought to the plasma, generally by means of a laser [38]. Measurement of line emission intensities and line profiles belong to the former category, while laser scattering belongs to the latter one. Usually, passive methods can be applied to at least some commercially available ICP systems, while active methods require sophisticated devices and can only be used in some dedicated laboratories [39].

2.6.1 Kinetic temperature measurement

The kinetic temperature, T_{kin} , can be obtained by measuring the Doppler width. However, some requirements must be fulfilled:

- (i) The Doppler effect must be predominant at the FWHM level.
- (ii) The a -parameter value must be known in order to calculate the contribution of the pressure broadening in the physical line width.
- (iii) The practical resolution of the dispersive system should be lower than the physical line width.

These requirements explain why a limited number of lines can be used for this purpose, because the practical resolution of the commercially available ICP spectrometers is 5 pm at the best. Practically, only lines such as the Be I 234.61 nm [36] are used.

The first step is to measure the practical resolution (or instrumental broadening) of the dispersive system near 230 nm. The experimental (or effective) line width, $\Delta\lambda_{\text{exp}}$, is related through a quadratique function to the physical line width, $\Delta\lambda_{\text{L}}$, and to the practical resolution, $\Delta\lambda_{\text{ins}}$:

$$\Delta\lambda_{\text{exp}}^2 = \Delta\lambda_{\text{L}}^2 + \Delta\lambda_{\text{ins}}^2 \quad (2.15)$$

When the physical line width is known, it is then easy to deduce the value of the practical resolution from that of the experimental line width. Practically, because $\Delta\lambda_{\text{ins}}$ is higher than 5 pm, the use of a narrow line such as the Cd I 228.80 nm line ($\Delta\lambda_{\text{L}} = 1.5$ pm) makes it possible to obtain directly the value of $\Delta\lambda_{\text{ins}}$ from $\Delta\lambda_{\text{exp}}$, because the value of $\Delta\lambda_{\text{L}}$ becomes negligible. Once $\Delta\lambda_{\text{ins}}$ has been determined, it is then possible to measure the physical line width of the Be I 234.61 nm line using the same relation:

$$\Delta\lambda_{\text{L}}(\text{Be}) = \left[\Delta\lambda_{\text{exp}}^2 - \Delta\lambda_{\text{ins}}^2 \right]^{1/2} \quad (2.16)$$

Then, it remains to determine the contribution of the Doppler effect in the physical line width, knowing that the a -parameter is 0.1 in the case of the Be I 234.61 nm line [36].

The relation between the physical line width, the Doppler width and the pressure width is given by:

$$\Delta\lambda_L = \frac{1}{2}\Delta\lambda_{\text{vdw}} + \left(\frac{1}{4}\Delta\lambda_{\text{vdw}}^2 + \Delta\lambda_D^2 \right)^{1/2} \quad (2.17)$$

It can be then easily deduced that for the Be I line:

$$\Delta\lambda_D = \frac{\Delta\lambda_L}{1.062} \quad (2.18)$$

From Equations (2.13), (2.16), and (2.18), it can be obtained, with $M = 9.01$:

$$T_{\text{kin}} = 283.3[\Delta\lambda_{\text{exp}}^2(\text{BeI234}) - \Delta\lambda_{\text{exp}}^2(\text{CdI228})] \quad (2.19)$$

when $\Delta\lambda_{\text{ins}} \gg \Delta\lambda_{\text{exp}}$ (Cd I 228). For example, if $\Delta\lambda_{\text{exp}}$ (Be I 234) = 7 pm and $\Delta\lambda_{\text{exp}}$ (Cd I 228) = 5 pm, T_{kin} is then equal to 6700 K.

2.6.2 Rotational temperature measurement

The rotational fine structure of electronic bands such as $B^2\Sigma_u^+ - X^2\Sigma_g^+$ for N_2^+ (first negative system) and $A^2\Sigma^+ - X^2\Pi$ for OH can be used to determine the rotational temperature. To resolve the band structure, a scanning monochromator is required (i.e. a sequential system), with the best possible resolution (i.e. 5 pm). For a transition $J' - J''$, the intensity of a rotational line can be expressed as a function of either the oscillator strength, S_J , or the probability transition, A_J :

$$I = DS_J\nu^4 \exp\left(\frac{-B_v hcJ'(J' + 1)}{kT_{\text{rot}}}\right) \quad (2.20)$$

$$I = DA_J h\nu \exp\left(\frac{-B_v hcJ'(J' + 1)}{kT_{\text{rot}}}\right) \quad (2.21)$$

where ν is the wavenumber of the line, and B_v is the rotational constant belonging to the vibrational quantum number ν . The oscillator strength, S_J , is equal to:

$$S_J = K' + K'' + 1 \quad (2.22)$$

In the case of N_2^+ , two branches can be used for temperature measurements, the P and the R branches. Unlike the use of high-resolution Fourier transform spectrometry [40], the

use of dispersive systems with a resolution higher than 5 pm does not permit to resolve the hyperfine splitting of either the P or R branches, for example the P_1 , P_2 , and Q_{12} in the P branch [41–44].

It is possible to determine the rotational temperature from Equations (2.20) and (2.22) by plotting $\text{Log}[I/(K' + K'' + 1)]$ vs $K'(K' + 1)$. Practically, the value of S_j , $K' + K'' + 1$, is expressed as a function of the quantum number K'' , K'' being the assignment of the lower state, with $K' = K'' - 1$ for the P branch, and $K' = K'' + 1$ for the R branch.

$$S_j(\text{P branch}) = 2K'' \quad (2.23)$$

$$S_j(\text{R branch}) = 2(K'' + 1) \quad (2.24)$$

Similarly, the value of $K'(K' + 1)$ can be expressed as a function of K'' . In the case of the P branch:

$$K'(K' + 1) = K''(K'' - 1) \quad (2.25)$$

and for the R branch:

$$K'(K' + 1) = (K'' + 1)(K'' + 2) \quad (2.26)$$

It is then possible to plot the intensity vs K'' for the P branch:

$$\text{Ln} \frac{I}{2K''} = \text{cste} - \frac{Bhc}{kT} K''(K'' - 1) \quad (2.27)$$

and for the R branch:

$$\text{Ln} \frac{I}{2(K'' + 1)} = \text{cste} - \frac{Bhc}{kT} (K'' + 1)(K'' + 2) \quad (2.28)$$

The value of the slope is:

$$\frac{-B_v hc}{kT} = \frac{-2.983}{T} \quad (2.29)$$

The slope is equal to $-1.296/T$ when a decadic logarithm is used. Practically, the (0–0) band is used, with a bandhead located at 319.4 nm. Wavelengths of the rotational lines are available as a function of the K'' values for the R and P branches [45,46], and are given in Table 2.1. The R branch is used up to $K'' = 20$, while the P branch is used above $K'' = 18$ –20, and up to $K'' = 35$ [41]. It should be noted that, because of the even–odd alternation, line intensities with odd K'' must be multiplied by 2.

The OH spectra is more complex, because five main branches, O, P, Q, R, S can be observed with a total of 12 branches. Practically, the R_2 and Q_1 branches of the (0–0) are used [42–44,47,48]. Line assignments, wavelengths, energies [49], and transition probabilities [50] are available and are given in Table 2.2. Equation (2.21) is then used and the temperature is obtained from the plot of $\text{Log}(I\lambda/A)$ vs E , and the slope is $-0.625/T$ when the energies are expressed in cm^{-1} .

Table 2.1 K'' values, corresponding wavelengths (nm), and S_J values of the (0–0) band of the first negative system of N_2^+ , for the P and R branches, which are used for the determination of rotational temperatures

K''	P branch		R branch	
	λ	$S_J = K''(K'' - 1)$	λ	$S_J = (K'' + 1)(K'' + 2)$
6			390.49	56
7			390.40	72
8			390.29	90
9			390.19	110
10			390.08	132
11			389.97	156
12			389.85	182
13			389.73	210
16			389.33	306
18	391.35	306	389.04	380
20	391.30	380	388.74	462
21	391.29	420	388.58	506
22	391.25	462		
23	391.20	506		
24	391.15	552		
25	391.10	600		
26	391.04	650		
27	390.97	702		
28	390.91	756		
29	390.84	812		
30	390.76	870		
31	390.68	930		
32	390.60	992		
33	390.51	1056		
34	390.41	1122		
35	390.31	1190		

Alternative species have been used for the measurement of rotational temperature, in particular CH_4 [51] and N_2 [52–54].

2.6.3 Excitation temperature

The excitation temperature is deduced from the line intensity relation (Equation (2.11)). Although an absolute line intensity measurement could be performed, alternative methods are preferred, because of the difficulty of measuring absolute line intensity: calibration of the optical system, computation of the number density of the emitting species. Practically, the so-called Boltzmann plot and the line pair intensity ratio are the most commonly used method.

Table 2.2 Assignment, wavelengths (nm), energies (cm^{-1}) and transition probabilities, A , values (10^8s^{-1}) for the R_2 and Q_1 branches of the OH (0–0) band used for rotational temperature measurements

K	R_2 branch			Q_1 branch		
	λ	E	A	λ	E	A
1	308.405	32 542	2.7	307.844	32 475	0.0
2	308.023	32 643	5.7	307.995	32 543	17.0
3	307.703	32 778	8.9			
4	307.437	32 947	12.8	308.328	32 779	33.7
5				308.520	32 948	42.2
6				308.734	33 150	50.6
7	306.918	33 650	24.8			
8				309.239	33 652	67.5
9				309.534	33 952	75.8
10				309.859	34 283	84.1
11						
12						
13	306.967	35 912	49.1	311.022	35 462	100.6
14	307.114	36 393	53.2	311.477	35 915	108.8
15	307.303	36 903	57.2	311.967	36 397	125.2
16	307.553	37 440	61.3	312.493	36 906	133.3
17	307.807	38 004	65.3	313.057	37 444	141.5
18	308.125	38 594	69.3	313.689	38 008	149.6
19	308.489	39 209	73.4	314.301	38 598	157.7
20	308.901	39 847	77.4			

2.6.3.1 Boltzmann plot

The Boltzmann plot is based on the use of lines of a given element within the same ionization state. In this case, it is not necessary to know the value of the number density and of the partition function and a relative measurement of line intensities is sufficient. The temperature can be deduced from the plot of:

$$\text{Ln} \frac{I\lambda}{gA} \quad \text{vs} \quad E_{\text{exc}} \quad (2.30)$$

and the slope is equal to $-0.625/T_{\text{exc}}$ when E is expressed in cm^{-1} and equal to $-5040/T_{\text{exc}}$ when E is expressed in eV. It should be noted that the oscillator strength, f , can also be used instead of the transition probability, A . It is then necessary to plot $\text{Ln}(I\lambda^3/gf)$ vs E_{exc} . An accurate determination of the excitation temperature is obtained when a large range of excitation energies is used, and when the values of the transition probabilities are accurately known. Usually, the relation is applied over a small range of wavelengths, so that the wavelength response of the dispersive system can be considered constant.

Table 2.3 Selection of atomic Fe lines, excitation energies, E_{exc} (cm^{-1}), statistical weights of the upper excited level, g , and transition probabilities, A (10^8s^{-1}) for the determination of excitation temperature

Wavelength (nm)	E_{exc}	g	A
370.925	34 329	7	0.156
371.993	26 875	11	0.162
372.256	27 560	5	0.0497
372.762	34 547	5	0.225
373.332	27 666	3	0.062
373.486	33 695	11	0.902
373.713	27 167	9	0.142
374.826	27 560	5	0.0915
374.978	34 040	9	0.764
375.823	34 329	7	0.634

In the case of argon, lines in the 340–700 nm range have been used [12,41,51,55–60]. However, this range corresponds to a rather small range in energy (i.e. 107 500–124 750 cm^{-1}). In other words, the obtaining of a good accuracy for the argon excitation temperature is rather problematic. This is probably an explanation for the scarcity of results based on the argon species. Transition probability values for argon can be taken from the compilation of Furh and Wiese [61].

Practically, excitation temperatures are determined using injected elements. The most commonly used element is neutral iron [42,48,56–59,62–74], because the atomic lines exhibit a wide range of energy and are located at closely spaced wavelengths. Many Fe I lines are present in the 350–400 nm range. Moreover, reasonably reliable transition probabilities are available [75]. A selection of Fe I lines with corresponding λ , g , E_{exc} , and A values are given in Table 2.3. Note that the use of high energy excitation levels higher than 35 000 cm^{-1} is not recommended, because of some possible curvatures of the Boltzmann plot [63].

2.6.3.2 Line pair method

An alternative to the Boltzmann plot is the use of the line pair intensity ratio method. Two lines of the same elements in the same ionization state are used. The excitation temperature can be easily deduced from the ratio of the two line intensities, I_1 and I_2 :

$$T = \frac{1}{k} \frac{(E_1 - E_2)}{\text{Ln} \frac{g_1 A_1 \lambda_2}{g_2 A_2 \lambda_1} - \text{Ln} \frac{I_1}{I_2}} \quad (2.31)$$

with $k = 0.695 \text{ cm}^{-1} \text{ K}^{-1} = 8.617 \times 10^{-5} \text{ eV K}^{-1}$, and $e = 2.302$. The subscripts 1 and 2 refer to the first and second line intensities, respectively. Log stands for logarithm to the base 10, and Ln for the natural logarithm.

When E is given in cm^{-1} :

$$T = 1.439 \frac{(E_1 - E_2)}{\text{Ln} \frac{g_1 A_1 \lambda_2}{g_2 A_2 \lambda_1} - \text{Ln} \frac{I_1}{I_2}} \quad (2.32)$$

$$T = 0.625 \frac{(E_1 - E_2)}{\text{Log} \frac{g_1 A_1 \lambda_2}{g_2 A_2 \lambda_1} - \text{Log} \frac{I_1}{I_2}} \quad (2.33)$$

When E is given in eV:

$$T = 11\,605 \frac{(E_1 - E_2)}{\text{Ln} \frac{g_1 A_1 \lambda_2}{g_2 A_2 \lambda_1} - \text{Ln} \frac{I_1}{I_2}} \quad (2.34)$$

$$T = 5041 \frac{(E_1 - E_2)}{\text{Log} \frac{g_1 A_1 \lambda_2}{g_2 A_2 \lambda_1} - \text{Log} \frac{I_1}{I_2}} \quad (2.35)$$

The line pair method is less accurate than the Boltzmann plot. This method is mostly used to follow any possible relative variation of the excitation temperature. The accuracy is improved when the excitation energy difference is the largest possible. Several test elements have been suggested, including Fe and Ti. The Ti II 322.284 nm and the Ti II 322.424 nm lines can be used because these two lines exhibit a large energy difference, 31 114 and 43 781 cm^{-1} , respectively). Using the transition probabilities given in [76], Equation (2.33) becomes:

$$T = \frac{7920}{1.53 - \frac{\text{Log } I_{322.4}}{\text{Log } I_{322.2}}} \quad (2.36)$$

2.6.4 Electron temperature

Near 430 nm, the continuum results mainly from the radiative recombination process. It is possible to access to the electron temperature, T_e , by measuring the ratio of an argon line intensity, I_{line} , to the intensity of the adjacent continuum, I_{cont} [9,10,77]. A simplified relation between the line-to-continuum intensity ratio is:

$$\frac{I_{\text{line}}}{I_{\text{cont}}} = C_r \frac{A_m g_m}{Z_{\text{ion}}} \frac{1}{\xi T_e} \exp \left(\frac{E_{\text{ion}} - E_m}{k T_e} \right) \frac{\lambda}{\Delta \lambda} \quad (2.37)$$

where A_m is the transition probability of the argon line, g_m is the statistical weight, E_m is the excitation energy, E_{ion} is the ionization energy, Z_{ion} is the partition function of the argon

ion, C_r is a constant, and ξ is a correction factor that depends on the wavelength and the temperature. Usually the adjacent continuum is used, which means that the same wavelength, λ , can be used. The term $\Delta\lambda$ is the spectral bandpass of the system, when the continuum intensity is measured. Equation (2.37) is usually applied for the Ar I 430 nm line and the adjacent continuum, because its transition probability is known with accuracy. The values of A_m , g_m , E_m , E_{ion} , Z_{ion} , C_r , and ξ are $0.31 \times 10^6 \text{ s}^{-1}$, 14.51 eV, 15.76 eV, 5.5, 2.005×10^{-5} , and 1.8, respectively. Equation (2.37) becomes:

$$\frac{I_{\text{line}}}{I_{\text{cont}}} = \frac{3.139}{T_e} \exp\left(\frac{14\,506}{T_e}\right) \frac{430}{\Delta\lambda} \quad (2.38)$$

where $\Delta\lambda$ is expressed in nm.

2.7 Electron number density measurement

One of the most commonly used measurement of the electron number density is based on the Stark broadening of the H_β 486.1 nm line. Stark broadening is caused by the interaction of the electric field generated by the electrons and ions of the plasma and the emitting atoms. Stark broadening is very sensitive for the Balmer series lines of hydrogen, particularly the H_β 486.1 nm line, and, to a less extent on argon lines in the 500–600 nm range. From Kepple and Griem [78], a relation can be written between the FWHM (nm) due to the Stark effect, $\Delta\lambda_s$, and the electron number density (m^{-3}):

$$\Delta\lambda_s = 2.50 \times 10^{-14} \alpha_{1/2} n_e^{2/3} \quad (2.39)$$

For $T_e = 10\,000 \text{ K}$, $n_e = 10^{21} \text{ m}^{-3}$, which are typical values observed in an ICP, $\alpha_{1/2}$ is equal to 0.0803 and the corresponding $\Delta\lambda_s$ is 0.2 nm (i.e. 200 pm). It should be noted that the Doppler effect is 27 pm, assuming a kinetic temperature of 6000 K. For dispersive systems with an instrumental broadening in the range 5–10 pm, Stark effect is then predominant over the Doppler and instrumental broadening. However, for $n_e < 10^{20} \text{ m}^{-3}$, $\Delta\lambda_s < 50 \text{ pm}$. In this case, Doppler broadening cannot be longer neglected.

Several computations have been described in the literature [79,80] that relate the electron number density to the Stark FWHM. One of them [80] includes the variation of T . However, these various computations do not lead to drastically different results. The key point is the accurate measurement of the FWHM. The H_β line exhibits a central dip when its width is larger than 200 pm and an asymmetry of the two maximums on each side of the dip. The lower wavelength side shows a higher maximum. This is why in the computation proposed by Czernichowski and Chapelle [80], the FWHM is obtained by doubling the semi-half width taken on the lower wavelength side of the H_β line.

$$\log n_e = 22.578 + 1.478 \log \Delta\lambda - 0.144(\log \Delta\lambda)^2 - 0.1265 \log T_e \quad (2.40)$$

where $\Delta\lambda$ is expressed in nm and n_e in m^{-3} .

Moreover, the value of the background may be difficult to determine, because the true continuum is located far from the central wavelength. A more sophisticated approach is

the fitting of the experimental line profile to the theoretical Stark-broadened profile. Algorithms have been described [81] and the corresponding computer program has been made available [82]. Some examples of the use of the H_β line for ICP diagnostics are given in [38,56,58,59,83–85].

2.8 Ionic to atomic line intensity ratio

Most of the measurements previously described cannot easily be conducted on a commercially available ICP system. This is why there is a demand for simple experiments, which can provide information about the operating conditions of the ICP. A popular measurement is the use of the intensity ratio between an ionic line and an atomic line of the same element. The aim is to compute a theoretical ratio assuming LTE, and to compare an experimental ratio to it. Usually, atomic lines are not very sensitive to a change in the excitation conditions, while ionic lines are. Their ratio permits the normalization of the behavior of the ionic line compared to the atomic line. If the two lines are closely spaced in terms of wavelength, the ratio is independent of the detector conditions (e.g. voltage for a photomultiplier tube (PMT)).

Using the Saha equation, where T_e is involved, and the line intensity relationship where T_{exc} is involved via the Boltzmann function, the ionic to atomic line ratio I_i/I_a can be deduced:

$$\frac{I_i}{I_a} = \left(\frac{4.83 \times 10^{21}}{n_e} \right) \left(\frac{g_i A_i \lambda_a}{g_a A_a \lambda_i} \right) T_e^{3/2} \exp \left(\frac{-E_{\text{ion}}}{kT_e} \right) \exp \left(\frac{-E_{\text{exc} \cdot i} - E_{\text{exc} \cdot a}}{kT_{\text{exc}}} \right) \quad (2.41)$$

where E_{exc} is the excitation energy, and E_{ion} is the ionization energy. When LTE is assumed, $T_e = T_{\text{exc}} = T$. The a and i subscripts refer to the atomic and ionic lines, respectively.

Among the possible elements, magnesium has often been used [13,37,48,56,58,59,63,65, 83,86–111] with the following line selection: Mg II 280.270 nm (or Mg II 279.553 nm) and Mg I 285.213 nm. An advantage of this selection is the closeness of the excitation energies of the atomic and ionic lines, 35 051 and 35 669 cm^{-1} , respectively. This makes the influence of the second exponential, 0.91 for T equal to 10 000 K, 0.88 for T equal to 7000 K, almost negligible. Moreover, the accuracy on gA values is acceptable [112] with gA equal to $5.32 \times 10^8 \text{ s}^{-1}$ and to $14.85 \times 10^8 \text{ s}^{-1}$ for Mg II 280.270 and Mg I 285.213, respectively. The conversion from the Mg II 279.553 line intensity to the Mg II 280.270 line intensity is obtained by dividing the line intensity by 2, since these two lines have almost the same A values and E_{exc} , 35 761 cm^{-1} for Mg II 279.553, and differ only by the g values, 4 and 2 for Mg II 279.553 and Mg II 280.270, respectively. The wavelength closeness of the Mg I 285 and the Mg II 280 nm lines usually avoids a wavelength response correction. However, in particular with echelle grating-based dispersive systems, a correction may be necessary. This correction can be easily determined by measuring the background at the two different locations.

Assuming LTE, there is a relation between T and n_e and from the relation 2.37, the Mg II 280.270 nm/Mg I 285.213 nm line intensity ratio is then

$$\frac{I_i}{I_a} = \left(\frac{1.76 \times 10^{21}}{n_e} \right) T^{3/2} \exp \left(\frac{-88732}{T} \right) \quad (2.42)$$

Table 2.4 Temperature T (K), electron number density (m^{-3}) and Mg II 280.270 nm/Mg I 285.213 nm line intensity ratio computed assuming LTE

T	n_e (m^{-3})	I_i/I_a
6500	1.01×10^{20}	10.8
7000	2.83	11.4
7500	6.90	12.1
8000	1.51×10^{21}	12.7
8500	3.01	13.4
9000	5.57	14.1
9500	9.70	14.8
10 000	1.60×10^{22}	15.4

Table 2.5 Various line pairs for the study of the ionic-to-atomic line intensity ratios

Energy sum (eV)		Excitation energy (eV)	
Cd II 226.502	14.47	Cd I 228.802	5.42
Cr II 267.716	12.92	Cr I 357.868	3.46
Ni II 231.604	14.03	Ni I 232.138	5.61
Pb II 220.353	14.79	Pb I 217.000	5.71
Zn II 206.200	15.40	Zn I 213.857	5.80

A theoretical I_i/I_a ratio is deduced as a function of n_e (Table 2.4). Under the LTE assumption, the value of the ratio varies between 10 and 14 over the range of n_e normally observed in an ICP. Practically, the experimental ratio varies in the 1–14 range. When the experimental ratio is above a value of 8, so-called robust conditions are obtained, which means that complete atomization, excitation, and ionization processes are expected. Under these operating conditions, which usually correspond to a high rf power and a low carrier gas flow rate [48,108], matrix effects are minimized. In marked contrast, when the ratio is below a value of 4, processes are not optimized and the ICP is subject to large matrix effects. The use of the Mg ratio can also be applied to the injection of organic solvents [113]. The ratio makes it possible to locate the axial position where the vaporization and atomization have reached completion, and to determine the solvent loading to obtain a robust ICP [113].

Although the Mg II/Mg I ratio has been widely used, it may be suggested some alternative line pairs (Table 2.5).

2.9 Active methods

Active methods are based on the interaction of light with the plasma. Most often the light is emitted by a laser, which means that the light is not only monochromatic, but also is localized in a narrow beam with a high power density. By crossing the observation axis

with that of the laser beam, small probing volumes can be achieved, which leads to localized determination of plasma characteristics. Two major techniques have been used, laser-induced fluorescence spectrometry and laser-based light scattering.

2.9.1 *Laser-induced fluorescence*

Laser-induced fluorescence permits the measurement of several characteristics [114] of the ICP such as excited atom lifetimes [115,116], collisional processes [116], spatial distributions [117,118], influence of easily ionizable elements [119,120], study of aerosol transport rate [100] and clouds produced from single droplets [121], study of power-modulated ICP [99,122], study of excitation and ionization processes [123], and number densities, in particular atoms in a ground state [124]. The use of high spectral irradiance lasers permits the saturation of the atomic transition, which means that the fluorescence yield becomes independent on the laser power and of radiationless de-excitation processes. Analyte number species can be then determined from laser-induced saturated atomic fluorescence [39].

2.9.2 *Light scattering*

Light scattering is the deflection of light by particles from the main direction of the beam. The particles can be heavy (e.g. neutral argon) or light (such as electrons). Two main types of scattering are used for plasma diagnostics, Rayleigh scattering, and Thomson scattering.

Rayleigh scattering occurs when the dimensions of the particles are small compared with the wavelength of the laser. Rayleigh scattering can be explained by classical physics, and the scattered intensity varies as $1/\lambda^4$. Rayleigh scattering is proportional to the concentration of scattered species (i.e. ground-state argon atoms in an ICP). The contribution of excited argon atoms is weak. Because the ideal-gas law may be applied to a plasma, the gas temperature is then deduced from the argon atom number density [39,125]. In the case of heavy particles such as argon atoms, the thermal velocity can be neglected, particularly when compared with that of electrons. Therefore, the scattered signal is not broadened. The measuring system must be calibrated by using at least two volumes of argon gas at different but well-known temperatures. Gas at room temperature is relatively easy to obtain, but the obtaining of a well-thermostatted argon volume at higher temperatures is more problematic [125]. This problem has been overcome by using a different gas such as helium [125], whose Rayleigh cross-section is well known. As in any scattering measurements, the challenge is the detection of a very weak light intensity compared with the incident beam. Any stray light must be minimized, and taken into consideration during the calibration process. Measurement of Rayleigh scattering is not trivial, which explains why it is reserved to research laboratories with sophisticated equipments [38,39,126]. Rayleigh scattering along with Raman scattering has been used for the study of air entrainment in the ICP [127].

Thomson scattering is the scattering of incident light by free electrons. In contrast to Rayleigh scattering, theory of Thomson scattering is far more complex [128]. The intensity of the scattered signal is related to the concentration of electrons in the probed volume. Because of the high velocity of the electrons, $4 \times 10^5 \text{ m s}^{-1}$ [39], the scattered photons are

significantly Doppler-shifted. If the electrons exhibit a Maxwellian velocity distribution, a broadening of the scattered signal is observed. This Thomson scattering spectrum is centered at the incident wavelength radiation and has a Gaussian shape. The width of the Thomson scattering spectrum is related to the electron energy while the integrated spectrum is proportional to the electron number density. Therefore, Thompson scattering makes it possible to determine both electron number density and electron energy distribution. The electron temperature can be then deduced from the slope of the plot of the natural logarithm of the scattered intensity vs the square of the wavelength shift (i.e. $\ln \lambda$ vs $\Delta \lambda^2$) [39,129,130]. Because of the very weak scattered intensity and the corresponding noise in the wings of the Thomson scattering spectrum. Consequently, electron temperature is obtained with less confidence than electron number density [129]. Dedicated designs of the optical system have been described [38,39,126,131] to accommodate the weak scattered signal, the stray light, and the noise. They are usually based on the use of a detector array to measure the Thomson scattering spectrum on each side of the incident wavelength. The central channel can be used to measure the non-broadened Rayleigh scattering. Large scattering angles are used in order to minimize the so-called scattered parameter, which is related to the deviation of the velocity from a Gaussian distribution, and which leads to a distortion of the spectrum [131]. Calibration of the Thomson scattering effect can be conducted by using Rayleigh scattering [132] or Raman scattering [133].

The power of Thomson and Rayleigh scattering has been demonstrated [38,130,134–136] and compared to passive methods [38]. Influence of the power [130], of the generator frequency [136] and spatial distribution of the electron and gas temperatures [134] have been then studied. Although sophisticated and time-consuming, laser scattering-based methods have significantly improved knowledge of ICP characteristics.

2.10 Spatial profiles

Because of the presence of the central channel and the deposition of the rf energy at the edge of the plasma, large temperature and number density gradients are observed. When a lateral viewing is carried out, a probing volume is then observed, and the value of the signal intensity is averaged over the probed volume. When the observation is scanned over a lateral coordinate, x , at a given observation height, the lateral signal intensity, $I(x)$, is related to the radial intensity, $I(r)$, r being the radial coordinate, through the Abel integral equation:

$$I(x) = 2 \int_x^R \frac{I(r)r}{(x^2 - r^2)^{1/2}} dr \quad (2.43)$$

where R is the radius of the plasma. The intensity, $I(r)$ can be then deduced from the intensity, $I(x)$, via the Abel inversion:

$$I(r) = -\frac{1}{\pi} \int_r^R \frac{I'(x)}{(x^2 - r^2)^{1/2}} dx \quad (2.44)$$

Usually, the integral is evaluated numerically [9,84,98,99,137–139]. However, the plasma must be perfectly symmetric. In the case of an asymmetric plasma, the mathematical treatment is more complex [140]. Abel inversion is not an easy process, and cannot usually be performed on a commercially available ICP system. Moreover, considering the narrow size of the central channel, acceptable results without Abel inversion can be obtained concerning the radial profile of characteristics linked to the analyte. The use of absorption or fluorescence measurements makes it possible to overcome the problem of Abel inversion. Absorption measurements were used to describe the influence of easily ionizable elements on analyte signals. Three-dimensional profiles were then obtained [149], giving evidence of the change in the spatial distribution of the analyte. Similarly, the use of laser-excited fluorescence permitted the determination of the spatial profiles of analyte species [117,118].

Spatial profiles [24,25,28,53,55,56,59,60,62,64,67,70,74,77,85,98,99,108,113,117,118,141–176] can be related to the signal intensities and to the plasma characteristics (i.e. temperatures and number densities). In the case of line intensities [25,28,108,113,117,118,142–145,147–159,161,162,164,166–171,173,174,176], the most commonly used measurement is the vertical profile of the signal along the axis of the plasma. These vertical profiles are very useful to understand the appearance of the various species in the plasma (e.g. Ref. [25]) and to optimize the observation height to obtain the best signal-to-background ratio. When dealing with the observation height, a problem is the spatial reference. The top of the load coil is widely used, but there is no direct relation between this position and mechanisms in the plasma. Alternative references have been suggested, such as the injection of a visible emitting species (e.g. Na) [177], the crossing between an atomic line and an ionic line of the same element [155] and the 306.4 nm OH bullet [173]. An interesting application of vertical profiles was the concept of cross-over point [108,148,158,168]. When an element such as Na is added to an analyte, usually the Na effect corresponds to an enhancement of the analyte at low observation heights, and to depressive effects at high observation heights. This results in the presence of a cross-over point where the Na effect disappears. Unfortunately, this cross-over point is related to both the element and the analyte line. Moreover, under robust conditions [108], a constant shift of the vertical profiles is observed along the observation height instead of the cross-over point.

Lateral profiles are very useful in the case of axial viewing, not only to optimize the signal-to-background ratio but also to study the effects of easily ionizable elements on the analyte signals [106]. It should be noted that most elements exhibit a maximum at the axis position, while a few elements such as As and Se show a small dip at the axis position.

Similarly, spatial profiles of the various temperatures and number densities, in particular the electron number density have been performed [24,53,55,56,59,60,62,64,67,70,77,84,85,146,151,159,160,163,172,175]. However, the use of laser-based scattering measurements described previously, although very complex, seems to be an attractive alternative to overcome the need for Abel inversion [125–136].

2.11 Temperatures and electron number densities observed in analytical ICPs

Both the temperatures and the electron number densities are dependent on the operating conditions of the plasma, in particular the forward power and the carrier gas flow rate, on the

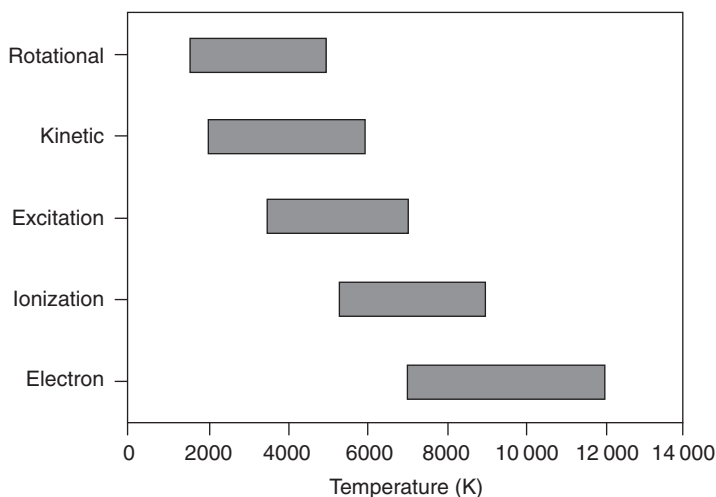


Figure 2.3 Range of the various temperatures observed in analytical ICPs.

solvent loading, on the torch design, inner diameter of the injector, and the generator characteristics (frequency). The actual range of the various temperatures that have been observed in ICPs is given in Fig. 2.3. It can be seen that $T_e > T_{\text{ion}} > T_{\text{exc}}$ while $T_{\text{kin}} > T_{\text{rot}}$. Regardless of the type of temperature, an increase is usually observed when the power increases, the carrier gas decreases, and the generator frequency decreases (e.g. Ref. [136]). A similar trend is observed for the electron number density. These results mean that some apparent small changes in the operating conditions can lead to a totally different plasma in terms of kinetic and excitation temperatures, tolerance to solvent loading, and therefore matrix effects. This is why the concept of robustness has been introduced to describe operating conditions, namely high power and low carrier gas flow rate, which leads to high temperatures, electron number densities and ionic line to atomic line intensity ratio, and consequently which minimizes matrix effects due to the plasma conditions [48,102,104,108,113].

2.12 Plasma perturbation

The rf energy is provided to the electrons, which, in turn carry this energy through the plasma via collisional processes and ionize the Ar atoms. The use of steady-state operating conditions does not provide information about the kinetics of energy delivery to the plasma and the transport inward and upward of the species responsible for excitation. An alternative is the use of plasma perturbation to study the energy transfer from the load coil to the analyte [178–195]. Power modulation has been used for this purpose. The first work was making use of a sinusoidally modulated power [178]. Although this modulation can be easily obtained by using a waveform generator, complex time-dependent signals were observed [178]. Pulsed modulation was then preferred in order to obtain a fact decrease in the power. The power could be switched off, but only during a limited period of time (e.g. 200 μs) so as to reignite the plasma [181]. An alternative was the use of a so-called step function, which

corresponds to a switch between a high and low level of power; for example, 1000 and 250 W [179], or 1000 and 500 W [180]. Moreover, with such a modulation or interruption, in addition to plasma relaxation, plasma re-excitation could also be studied [180].

Diagnostics were conducted by observing the decay of various test elements, such as an Ar line, which represents the time-behavior of the plasma, and analyte lines. In order to follow the propagation of the energy, spatially resolved measurements were performed. Time-dependence of the excitation temperature could also be followed [178]. In particular, the temporal study of the ratio of the electron temperature to the kinetic temperature made it possible to define regions where the energy was coupled to the plasma [182].

Some conclusions can be driven from these experiments:

- (1) Different time-dependent behavior was observed between Ar lines and analyte lines [187]. Several processes were suggested to explain the Ar decay lifetime: ambipolar diffusion, thermal conduction, quenching by the surrounding nitrogen, and ion–electron recombination [179].
- (2) The emission signals were out of phase with the applied power wave form.
- (3) The emission responded more rapidly after a power interruption than after a power increase [180,181].
- (4) The decay times were height dependent [99,178–181].
- (5) The coupling of energy was still occurring below and above the load coil [99,184,186].
- (6) Evidence was given for the ionization of Mg^+ by the charge transfer process [99,187].
- (7) Evaporation of the aerosol droplets and carrier gas flow rate had a significant influence on the response of elements such as Li [190] and could also be an explanation of the different behavior with Ar lines.
- (8) The electrons were kept at higher temperatures than the heavy particles, which means that a heating process was occurring, through for instance a three-body recombination process [38].

Plasma perturbation was also used in the case of atomic absorption spectrometry [194,195] and for analytical applications with laser-induced fluorescence [192,193].

2.13 Multiline diagnostics

Since the beginning of the studies on ICP-AES, non-spectral matrix interferences and mechanisms have been the subject of numerous publications. However, until recently, these studies have been based on the use of sequential optical systems or conventional polychromators (i.e. optical systems equipped with PMTs). Because a sequential system was inherently slow, and usually a single line per element was available on a polychromator, studies were performed by using one or two lines per element. It was rather difficult to deduce definitive conclusions from previously published works, because of a large variety of lines and elements that were used, without mentioning different operating parameters and even torch configurations. It is even probable that the generator design and its tuning play a role in the magnitude of matrix effects. In any case, matrix effects appeared to be complex.

The introduction of segmented charge-coupled device (CCD) detectors in the 1990s permitted the use of two to five lines per element. Matrix effect studies based on such

optical system have shown that conclusions were depending on line selection. Moreover, even lines close in excitation energies could exhibit different behaviors. The current availability of solid-state detectors such as CCD or charge injection devices (CID) that permit the acquisition of the entire UV-visible spectra has totally modified the way of conducting diagnostics in ICP-AES. It is then possible to perform experiments based on the use of a large number of lines, then covering a large range of excitation energy [196–198].

Selection of elements with line-rich spectra such as Co, Cr, Mn ... makes it possible to improve our understanding of matrix effects. It is then possible to study the effects as a function of the operating parameters, and to confirm the interest of using so-called robust conditions, along with a study of the influence of the sample introduction system. It becomes obvious that the excitation energy is not the only parameter to consider. When studying multiplets, it may be seen that the optical transition may also play a significant role. By comparing the behavior of ionic lines to that of atomic lines, it is also possible to provide evidence of some excitation/ionization processes.

References

1. Reed, T.B. (1961) Induction coupled plasmas. *J. Appl. Phys.*, **32**, 821–824.
2. Reed, T.B. (1961) Growth of refractory crystals using the induction plasma torch. *J. Appl. Phys.*, **32**, 2534–2535.
3. Greenfield, S., Jones, I.Ll. and Berry, C.T. (1964) High-pressure plasmas as spectroscopic emission sources. *Analyst*, **89**, 713–720.
4. Wendt, R.H. and Fassel, V.A. (1965) Induction coupled plasma spectrometric excitation source. *Anal. Chem.*, **37**, 920–922.
5. Hoare, H.C. and Mostyn, R.A. (1967) Emission spectrometry of solutions and powders with a high-frequency plasma source. *Anal. Chem.*, **39**, 1153–1155.
6. Biancifiori, M.A. and Bordonali, C. (1967) Utilizzazione di un plasma ad induzione nell'analisi di tracce per assorbimento atomico (Utilization of an induction plasma in the analysis of traces by atomic absorption). *La Metall. Ital.*, **8**, 631–638.
7. Veillon, C. and Margoshes, M. (1968) An evaluation of the induction-coupled, radio frequency plasma torch for atomic emission and atomic absorption spectrometry. *Spectrochim. Acta*, **23B**, 503–512.
8. Miller, R.C. and Ayen, R.J. (1969) Temperature profiles and energy balances for an inductively coupled plasma torch. *J. Appl. Phys.*, **40**, 5260–5273.
9. Batal, A., Jarosz, J. and Mermet, J.M. (1981) A spectrometric study of a 40 MHz ICP. VI. Argon continuum in the visible region of the spectrum. *Spectrochim. Acta*, **36B**, 983–992.
10. Bastiaans, G.J. and Mangold, R.A. (1985) The calculation of electron density and temperature in Ar spectroscopic plasmas from continuum and line spectra. *Spectrochim. Acta*, **40B**, 885–892.
11. Mermet, J.M. (1975) Sur les mécanismes d'excitation des éléments introduits dans un plasma HF d'argon. *C.R. Acad. Sci. Paris, Série B*, **281**, 273–275.
12. Mermet, J.M. and Trassy, C. (1977) Etude de transferts d'excitation dans un plasma induit par haute fréquence entre gaz plasmagène et éléments introduits. *Rev. Phys. Appl.*, **12**, 1219–1222.
13. Boumans, P.W.J.M. and DeBoer, F.J. (1977) An experimental study of a 1 kW, 50 MHz RF inductively coupled plasma with a pneumatic nebulizer, and a discussion of experimental evidence for a nonthermal mechanism. *Spectrochim. Acta*, **32B**, 365–395.
14. Blades, M.W. and Hieftje, G.M. (1982) On the significance of radiation trapping in the inductively coupled plasma. *Spectrochim. Acta*, **37B**, 191–197.

15. Batal, A. and Mermet, J.M. (1982) Influence of the collision processes on the energy range of analytical lines in ICP-AES. *Can. J. Spectrosc.*, **27**, 37–45.
16. Schram, D.C., Raaijmakers, I.J.M.M., van der Sijde, B., Schenkelaars, H.J.W. and Boumans, P.W.J.M. (1983) Approaches for clarifying excitation mechanisms in spectrochemical excitation sources. *Spectrochim. Acta*, **38B**, 1545–1557.
17. de Galan, L. (1984) Some considerations on the excitation mechanism in the inductively coupled argon plasma. *Spectrochim. Acta*, **39B**, 537–550.
18. Mills, J.W. and Hieftje, G.M. (1984) A detailed consideration of resonance radiation in the argon inductively coupled plasma. *Spectrochim. Acta*, **39B**, 859–866.
19. Eljoundi, A., Batal, A. and Mermet, J.M. (1985) Dielectronic recombination in the zinc spectrum observed in inductively coupled plasma atomic emission spectrometry. *Spectrochim. Acta*, **40B**, 1007–1011.
20. Hieftje, G.M., Rayson, G.D. and Olesik, J.W. (1985) A steady-state approach to excitation mechanisms in the ICP. *Spectrochim. Acta*, **40B**, 167–176.
21. Goldwasser, A. and Mermet, J.M. (1986) Contribution of the charge-transfer process to the excitation mechanisms in inductively coupled plasma atomic emission spectroscopy. *Spectrochim. Acta*, **41B**, 725–739.
22. Rayson, G.D. and Hieftje, G.M. (1986) A steady-state approach to evaluation of proposed excitation mechanisms in the analytical ICP. *Spectrochim. Acta*, **41B**, 683–697.
23. Hart, L.P., Smith, B.W. and Omenetto, N. (1986) Evaluation of argon metastable number densities in the inductively coupled plasma by continuum source absorption spectrometry. *Spectrochim. Acta*, **41B**, 1367–1380.
24. Davies, J. and Snook, R.D. (1986) Spatial emission characteristics and excitation mechanisms in the inductively coupled plasma. A review. *J. Anal. Atom. Spectrom.*, **1**, 325–330.
25. Furuta, N. (1986) Spatial emission distribution of Y0, Y I, Y II and Y III radiation in an inductively coupled plasma for the elucidation of excitation mechanisms. *Spectrochim. Acta*, **41B**, 1115–1129.
26. Marichy, M., Mermet, M. and Mermet, J.M. (1987) Relationship between detection limits and mechanisms in inductively coupled plasma atomic emission spectrometry. *J. Anal. Atom. Spectrom.*, **2**, 561–565.
27. van der Mullen, J.A.M., Raaijmakers, I.J.M.M., van Lammeren, A.C.A.P., Schram, D.C., van der Sijde, B. and Schenkelaars, H.J.W. (1987) On the charge transfer in an inductively coupled argon plasma. *Spectrochim. Acta*, **42B**, 1039–1051.
28. Rayson, G.D., Parisi, A.F. and Hieftje, G.M. (1989) Spatially resolved measurements as a vehicle for studying atomization mechanisms in an inductively coupled plasma. *Spectrochim. Acta*, **44B**, 999–1008.
29. Huang, M., Yang, P.Y., Hanselman, D.S., Monnig, C.A. and Hieftje, G.M. (1990) Verification of a Maxwellian electron-energy distribution in the inductively coupled plasma. *Spectrochim. Acta*, **45B**, 511–520.
30. Farnsworth, P.B., Smith, B.W. and Omenetto, N. (1991) An investigation of the balance of charge exchange between Mg and Ar ions in the inductively coupled plasma. *Spectrochim. Acta*, **46B**, 831–841.
31. Ogilvie, C.M. and Farnsworth, P.B. (1992) Correlation spectroscopy as a probe of excitation and ionization mechanisms in the inductively coupled plasma. *Spectrochim. Acta*, **47B**, 1389–1401.
32. Fey, F.H.A.G., Benoy, D.A., van Dongen, M.E.H. and van der Mullen, J.A.M. (1995) A model for the behaviour of analyte in the inner channel of an inductively coupled plasma. *Spectrochim. Acta*, **50B**, 51–62.
33. Schram, D.C., van der Mullen, J.A.M., de Regt, J.M., Benoy, D.A., Fey, F.H.A.G., de Grootte, F. and Jonkers, J. (1996) Fundamental description of spectrochemical inductively coupled plasma. *J. Anal. Atom. Spectrom.*, **11**, 623–632.

34. Uchida, H., Tanabe, K., Nojiri, Y., Haraguchi, H. and Fuwa, K. (1980) Measurement of meta-stable argon in an inductively coupled plasma by atomic absorption spectroscopy. *Spectrochim. Acta*, **35B**, 881–883.
35. Batal, A. and Mermet, J.M. (1981) Calculation of some line profiles in ICP-AES assuming a Van der Waals potential. *Spectrochim. Acta*, **36B**, 993–1003.
36. Boumans, P.W.J.M. and Vrakking, J.J.A.M. (1986) The widths and shapes of about 350 prominent lines of 65 elements emitted by an inductively coupled plasma. *Spectrochim. Acta*, **41B**, 1235–1275.
37. Mermet, J.M. and Poussel, E. (1995) ICP emission spectrometers: 1995 figures of merit. *Appl. Spectrosc.*, **49**, 12A–18A.
38. de Regt, J.M., de Groote, F.P.J., van der Mullen, J.A.M. and Schram, D.C. (1996) Comparison of active and passive spectroscopic methods to investigate atmospheric inductively coupled plasmas. *Spectrochim. Acta*, **51B**, 1371–1383.
39. Sesi, N.N., Hanselman, D.S., Galley, P., Horner, J., Huang, M. and Hieftje, G.M. (1997). An imaging-based instrument for fundamental plasma studies. *Spectrochim. Acta*, **52B**, 83–102.
40. Ishii, I., Cai, M., Montaser, A., Palmer, B.A. and Layman, L.R. (1994) Rotational temperatures of argon–nitrogen ICP discharges measured by high-resolution Fourier transform spectrometry. *Spectrochim. Acta*, **49B**, 1111–1119.
41. Abdallah, M.H. and Mermet, J.M. (1978) The behavior of nitrogen excited in an inductively coupled argon plasma. *J. Quant. Spectrosc. Ra.*, **19**, 83–91.
42. Abdallah, M.H. and Mermet, J.M. (1982) Comparison of temperature measurements in ICP and MIP with Ar and He as plasma gas. *Spectrochim. Acta*, **37B**, 391–397.
43. Raeymaekers, B., Broekaert, J.A.C. and Leis, F. (1988) Radially resolved rotational temperatures in nitrogen–argon, oxygen–argon, air–argon and argon inductively coupled plasmas. *Spectrochim. Acta*, **43B**, 941–949.
44. Ishii, I. and Montaser, A. (1991) A tutorial discussion on measurements of rotational temperature in inductively coupled plasmas. *Spectrochim. Acta*, **46B**, 1197–1206.
45. Childs, W.H.J. (1932) Perturbation and rotation constants of some first negative nitrogen bands. *Proc. R. Soc. Lond. Ser-A.*, **137**, 641–661.
46. Coster, D. and Brons, F. (1932) Die negativen Stickstoffbanden. *Z. Physik.*, **73**, 747–774
47. Abila, P.A. and Trassy, C. (1989) Rotational temperatures and LTE in argon ICP. *Mikrochim. Acta*, **3**, 159–168.
48. Novotny, I., Fariñas, J.C., Wan J.-L., Poussel, E. and Mermet, J.M. (1996) Effect of power and carrier gas flow rate on the tolerance to water loading in inductively coupled plasma atomic emission spectrometry. *Spectrochim. Acta*, **51B**, 1517–1526.
49. Dieke, G.H. and Crosswhite, H.M. (1962) The ultraviolet bands of OH. fundamental data. *J. Quant. Spectrosc. Radiat. Trans.*, **2**, 97–199.
50. Hui, A.K., McKeever, M.R. and Tellinghuisen, J. (1979) Temperature of Tesla discharges from OH A \rightarrow X intensity measurements. *J. Quant. Spectrosc. Radiat. Trans.*, **21**, 387–396.
51. Alder, F. and Mermet, J.M. (1973) A spectroscopic study of some radiofrequency mixed gas plasma. *Spectrochim. Acta*, **28B**, 421–433.
52. Seliskar, C.J., Miller, D.C. and Fleitz, P.A. (1987) ICP rotational spectroscopic temperature determination using N₂ and N₂⁺. *Appl. Spectrosc.*, **41**, 658–660.
53. Hasegawa, T. and Winefordner, J.D. (1987) Spatially resolved rotational and vibrational temperatures of a neutral nitrogen molecule in the inductively coupled plasma. *Spectrochim. Acta*, **42B**, 637–649.
54. Marawi, I., Bielski, B.A., Caruso, J.A. and Meeks, F.R. (1992) Measurements of inductively coupled plasma temperatures: comparison of N₂ rotational temperatures with optical pyrometry. *J. Anal. Atom. Spectrom.*, **7**, 899–903.
55. Kornblum, G.R. and de Galan, L. (1974) Arrangement for measuring spatial distributions in an argon induction-coupled RF plasma. *Spectrochim. Acta*, **29B**, 249–261.

56. Mermet, J.M. (1975) Comparaison des températures et des densités électroniques mesurées sur le gaz plasmagène et sur des éléments excités dans un plasma HF. *Spectrochim. Acta*, **30B**, 383–396.
57. Kalnicky, D.J., Kniseley, R.N. and Fassel, V.A. (1975) Inductively coupled plasma optical emission spectroscopy. Excitation temperatures experienced by analyte species. *Spectrochim. Acta*, **30B**, 511–525.
58. Kalnicky, D.J., Fassel, V.A. and Kniseley, R.N. (1977) Excitation temperatures and electron number densities experienced by analyte species in inductively coupled plasma with and without the presence of an easily ionized element. *Appl. Spectrosc.*, **31**, 137–150.
59. Jarosz, J., Mermet, J.M. and Robin, J. (1978) A spectrometric study of a 40-MHz inductively coupled plasma. III. Temperatures and electron number density. *Spectrochim. Acta*, **33B**, 55–78.
60. Uchida, H., Tanabe, K., Nojiri, Y., Haraguchi, H. and Fuwa, K. (1981) Spatial distributions of metastable argon, temperature and electron number density in an inductively coupled argon plasma. *Spectrochim. Acta*, **36B**, 711–718.
61. Furh, J.R. and Wiese, W.L. (1995–1996) Atomic transition probabilities: *CRC Handbook of Chemistry and Physics*, 76th edn, CRC Press, Boca Raton, FL.
62. Kornblum, G.R. and De Galan, L. (1977) Spatial distribution of the temperature and the number densities of electrons and atomic and ionic species in an inductively coupled RF argon plasma. *Spectrochim. Acta*, **32B**, 71–96.
63. Alder, J.F., Bombelka, R.M. and Kirkbright, G.F. (1980) Electronic excitation and ionization temperature measurements in a high-frequency inductively coupled plasma source and the influence of water vapor on plasma parameters. *Spectrochim. Acta*, **35B**, 163–175.
64. Kawaguchi, H., Ito, T. and Mizuike, A. (1981) Axial profiles of excitation and gas temperatures in an inductively coupled plasma. *Spectrochim. Acta*, **36B**, 615–623.
65. Capelle, B., Mermet, J.M. and Robin, J.P. (1982) Influence of the generator frequency on the spectral characteristics of inductively coupled plasma. *Appl. Spectrosc.*, **36**, 102–106.
66. Faires, L.M., Palmer, B.A., Engleman Jr, R. and Niemczyk, T.M. (1984) Temperature determinations in the inductively coupled plasma using a Fourier transform spectrometer. *Spectrochim. Acta*, **39B**, 819–828.
67. Furuta, N. (1985) Spatial profile measurement of ionization and excitation temperatures in an inductively coupled plasma. *Spectrochim. Acta*, **40B**, 1013–1022.
68. Blades, M.W. and Caughlin, B.L. (1985) Excitation temperature and electron density in the inductively coupled plasma – aqueous vs organic solvent introduction. *Spectrochim. Acta*, **40B**, 579–591.
69. Walker, Z. and Blades, M.W. (1986) Measurement of excited state level populations for atomic and ionic iron in the inductively coupled plasma. *Spectrochim. Acta*, **41B**, 761–775.
70. Ishii, I., Golightly, D.W. and Montaser, A. (1988) Radial excitation temperatures in argon–nitrogen inductively coupled plasmas. *J. Anal. Atom. Spectrom.*, **3**, 965–968.
71. Murillo, M. and Mermet, J.M. (1989) Improvement of the energy transfer with added-hydrogen in inductively coupled plasma atomic emission spectrometry. *Spectrochim. Acta*, **44B**, 359–366.
72. Nixon, D.E. (1990) Excitation modulation by water: effects of desolvation on line intensities, temperatures and ion–atom ratios produced by inductively coupled plasmas. *J. Anal. Atom. Spectrom.*, **5**, 531–536.
73. Montaser, A., Ishii, I., Palmer, B.A. and Layman, L.R. (1990) Line widths and temperatures of Ar–N₂ inductively coupled plasma discharges measured by high-resolution Fourier transform spectrometry. *Spectrochim. Acta*, **45B**, 603–612.
74. Kitagawa, K. and Horlick, G. (1992) Deviation of the level populations of iron atoms and ions from the Boltzmann distribution in an inductively coupled plasma. Part 1. Spatial and power dependences. *J. Anal. Atom. Spectrom.*, **7**, 1207–1219.
75. Fuhr, J.R., Martin, G.A. and Wiese, W.L. (1988) Atomic transition probabilities – iron through nickel: a critical compilation. *J. Phys. Chem. Ref. Data*, **17**(4) (suppl. 4).

76. Wiese, W.L. and Fuhr, J.R. (1975) Atomic transition probabilities for scandium and titanium. *J. Phys. Chem. Ref. Data*, **4**, 263.
77. Galley, P.J. and Hieftje, G.M. (1993) Tomographically resolved ionization temperatures and electron densities in the inductively coupled plasma determined by the line-to-continuum method. *Spectrochim. Acta*, **48B**, E1725–E1742.
78. Kepple, P. and Griem, H.R. (1968) Improved Stark profile calculations for the hydrogen lines H_{α} , H_{β} , H_{γ} and H_{δ} . *Phys. Rev.*, **173**, 317–325.
79. Hill, R.A. (1967) Fractional-intensity widths and Stark broadening formulas for the hydrogen Balmer lines. *J. Quant. Spectrosc. Radiat. Trans.*, **7**, 401–410.
80. Czernichowski, A. and Chapelle, J. (1983) Etude expérimentale de l'élargissement Stark de la raie 430.01 nm de Ar I. *Acta Phys. Pol.*, **A63**, 67–75.
81. Chan, S.K. and Montaser, A. (1989) Determination of electron number density via Stark broadening with an improved algorithm. *Spectrochim. Acta*, **44B**, 175–184.
82. Zhang, H., Hsieh, C., Ishii, I., Zeng, Z. and Montaser, A. (1994) Revised, fast, flexible algorithms for determination of electron number densities in plasma discharges. *Spectrochim. Acta*, **49B**, 817–828.
83. Caughlin, B.L. and Blades, M.W. (1984) An evaluation of ion-atom emission intensity ratios and local thermodynamic equilibrium in an argon inductively coupled plasma. *Spectrochim. Acta*, **39B**, 1583–1602.
84. Walters, P.E., Gunter, W.H. and Zeeman, P.B. (1986) Electron density characterization of 27.1 and 50 MHz inductively coupled plasmas by means of Abel corrected Stark broadened H β line profiles. *Spectrochim. Acta*, **41B**, 133–141.
85. Olesik, J.W., Den, S.-J. and Bradley, K.R. (1989) An instrumental system for simultaneous measurement of spatially resolved electron number densities in plasmas. *Appl. Spectrosc.*, **43**, 924–932.
86. Mermet, J.M. and Robin, J. (1975) Etude des interférences dans un plasma induit par haute fréquence. *Anal. Chim. Acta*, **75**, 271–279.
87. Abdallah, M.H., Mermet, J.M. and Trassy, C. (1976) Etude spectrométrique d'un plasma induit par haute fréquence. II. Etude de différents types d'effets interéléments observés. *Anal. Chim. Acta*, **84**, 329–339.
88. Savage, R.N. and Hieftje, G.M. (1980) Vaporization and ionization interferences in a miniature inductively coupled plasma. *Anal. Chem.*, **52**, 1267–1272.
89. Blades, M.W. (1982) Some considerations regarding temperature, electron density, and ionization in the argon inductively coupled plasma. *Spectrochim. Acta*, **37B**, 869–879.
90. Caughlin, B.L. and Blades, M.W. (1985) Analyte ionization in the inductively coupled plasma. *Spectrochim. Acta*, **40B**, 1539–1554.
91. Rezaaiyaan, R. and Hieftje, G.M. (1985) Analytical characteristics of a low-flow, low power inductively coupled plasma. *Anal. Chem.*, **57**, 412–415.
92. Farino, J., Miller, J.R., Smith, D.D. and Browner, R.F. (1987) Influence of solution uptake rate on signals and interferences in inductively coupled plasma optical emission spectrometry. *Anal. Chem.*, **59**, 2303–2309.
93. Webb, B.D. and Denton, M.B. (1987) Effect of torch size on a 148 MHz inductively coupled plasma atomic emission spectrometry. Part 2. Noise power studies and interferences effects. *J. Anal. Atom. Spectrom.*, **2**, 21–26.
94. Michaud-Poussel, E. and Mermet, J.M. (1987) Study of low-power 100 MHz inductively coupled plasma with special reference to the role of the frequency. *Spectrochim. Acta*, **42B**, 1163–1168.
95. Mermet, J.M. (1989) Ionic to atomic line intensity ratio and residence time in inductively coupled plasma-atomic emission spectrometry. *Spectrochim. Acta*, **44B**, 1109–1116.
96. Smith, T.R. and Bonner Denton, M. (1989) LTE conditions within the central channel of the plasma. *Appl. Spectrosc.*, **43**, 1385–1387.

97. Boumans, P.W.J.M. (1989) Detection limits for lines widely differing in hardness and intensity ratios of ionic to atomic lines measured in 50 and 100 MHz inductively coupled plasmas. *Spectrochim. Acta*, **44B**, 1285–1296.
98. Olesik, J.W. and Den, S.J. (1990) Effect of central gas flow rate and water on an argon inductively coupled plasma: spatially resolved emission, ion-atom intensity ratios and electron number densities. *Spectrochim. Acta*, **45B**, 731–752.
99. Olesik, J.W. (1990) Spatially and temporally resolved emission and fluorescence in a power modulated inductively coupled plasma. *Spectrochim. Acta*, **45B**, 975–995.
100. Bates, L.C. and Olesik, J.W. (1990) Effect of sample aerosol transport rate on inductively coupled plasma atomic emission and fluorescence. *J. Anal. Atom. Spectrom.*, **5**, 239–247.
101. Mermet, J.M. (1991) Use of magnesium as test element for inductively coupled plasma atomic emission spectrometry diagnostics. *Anal. Chim. Acta*, **250**, 85–94.
102. Poussel, E., Mermet, J.M. and Samuel, O. (1993) Simple experiments for the control, the evaluation and the diagnosis of inductively coupled plasma sequential systems. *Spectrochim. Acta*, **48B**, 743–755.
103. Matousek, J.P. and Mermet, J.M. (1993) The effect of added hydrogen in electrothermal vaporization inductively coupled plasma atomic emission spectrometry. *Spectrochim. Acta*, **48B**, 835–850.
104. Fernandez, A., Murillo, M., Carrion, N. and Mermet, J.M. (1994) Influence of operating conditions on the effects of acids in inductively coupled plasma atomic emission spectrometry. *J. Anal. Atom. Spectrom.*, **9**, 217–221.
105. Carré, M., Lebas, K., Marichy, M., Mermet, M., Poussel, E. and Mermet, J.M. (1995) Influence of the sample introduction system on acid effects in inductively coupled plasma atomic emission spectrometry. *Spectrochim. Acta*, **50B**, 271–283.
106. O'Hanlon, K., Ebdon, L. and Foulkes, M. (1996) Effect of ionizable elements on solutions and slurries in an axially viewed inductively coupled plasma. *J. Anal. Atom. Spectrom.*, **11**, 427–436.
107. Dubuisson, C., Poussel, E. and Mermet, J.M. (1997) Comparison of axially and radially viewed inductively coupled plasma atomic emission spectrometry in terms of signal-to-background ratio and matrix effects. *J. Anal. Atom. Spectrom.*, **12**, 281–286.
108. Romero, X., Poussel, E. and Mermet, J.M. (1997) The effect of sodium on analyte ionic line intensities in inductively coupled plasma atomic emission spectrometry. *Spectrochim. Acta*, **52B**, 495–502.
109. Cabalin, L.M. and Mermet, J.M. (1997) Use of normalized relative line intensities for qualitative and semiquantitative analysis in inductively coupled plasma atomic emission spectrometry using a custom segmented-array charge-coupled device detector. Part III: Application to laser ablation. *Appl. Spectrosc.*, **51**, 898–901.
110. Sartoros, C., Alary, J.F., Salin, E.D. and Mermet, J.M. (1997) An expert system program for ICP-AES system diagnosis. *Spectrochim. Acta*, **52B**, 1923–1927.
111. Dubuisson, C., Poussel, E., Mermet, J.M. and Todoli, J.L. (1998) Comparison of the effect of acetic acid with axially and radially viewed inductively coupled plasma atomic emission spectrometry: influence of the operating conditions. *J. Anal. Atom. Spectrom.*, **13**, 63–67.
112. Wiese, W.L., Smith, M.W. and Miles B.M. (1969) *Atomic Transition Probabilities, Vol. 2, Sodium Through Calcium*, National Standard Reference Data Series, National Bureau Standards, Washington DC.
113. Weir, D.G. and Blades, M.W. (1994) Characteristics of an inductively coupled argon plasma operating with organic aerosols. Part 2. Axial profiles of solvent and analyte species in a chloroform-loaded plasma. *J. Anal. Atom. Spectrom.*, **9**, 1323–1334.
114. Omenetto, N., Nikdel, S., Bradshaw, J.D., Epstein, M.S., Reeves, R.D. and Winefordner, J.D. (1979) Diagnostic and analytical studies of the inductively coupled plasma by atomic fluorescence spectrometry. *Anal. Chem.*, **51**, 1521–1525.

115. Uchida, H., Kosinski, M.A., Omenetto, N. and Winefordner, J.D. (1983) Time resolved fluorescence in an argon inductively coupled plasma: determination of excited atom lifetimes. *Spectrochim. Acta*, **38B**, 529–532.
116. Uchida, H., Kosinski, M.A., Omenetto, N. and Winefordner, J.D. (1984) Studies on lifetime measurements and collisional processes in an inductively coupled argon plasma using laser induced fluorescence. *Spectrochim. Acta*, **39B**, 63–68.
117. Huang, X., Yeah, K.S. and Winefordner, J.D. (1985) Spatial distribution profiles of Ca, Cu and Mn atoms and ions in an inductively coupled plasma by means of laser excited fluorescence. *Spectrochim. Acta*, **40B**, 1379–1386.
118. Gillson, G. and Horlick, G. (1986) Comparison of atomic fluorescence and atomic emission spatial distribution profiles in the inductively coupled plasma. *Spectrochim. Acta*, **41B**, 1323–1346.
119. Gillson, G. and Horlick, G. (1986) An atomic fluorescence study of easily ionizable element interferences in the inductively coupled plasma. *Spectrochim. Acta*, **41B**, 619–624.
120. Omenetto, N., Leong, M., Stevenson, C., Vera, J., Smith, B.W. and Winefordner, J.D. (1988) Fluorescence dip spectroscopy of sodium atoms in an inductively coupled plasma. *Spectrochim. Acta*, **43B**, 1093–1100.
121. Olesik, J.W., Kinzer, J.A. and McGowan, G.J. (1997) Observation of atom and ion clouds produced from single droplets of sample in inductively coupled plasmas by optical emission and laser-induced fluorescence imaging. *Appl. Spectrosc.*, **51**, 607–616.
122. Turk, G.C. (1992) Laser-induced fluorescence of atoms in a power-modulated inductively coupled plasma for trace detection and diagnostic study. *Appl. Spectrosc.*, **46**, 1223–1225.
123. Omenetto, N. and Matveev, O.I. (1994) Time-resolved fluorescence as a direct experimental approach to the study of excitation and ionization processes in different atom reservoirs. *Spectrochim. Acta*, **49B**, 1519–1535.
124. Gillson, G. and Horlick, G. (1986) Characterization of ground state analyte neutral atoms and ions in the inductively coupled plasma using atomic fluorescence spectrometry. *Spectrochim. Acta*, **41B**, 1299–1321.
125. Marshall, K.A. and Hieftje, G.M. (1987) Measurement of true gas kinetic temperatures in an inductively coupled plasma by laser-light scattering. *J. Anal. Atom. Spectrom.*, **2**, 567–571.
126. Huang, M., Marshall, K.A. and Hieftje, G.M. (1985) An apparatus for measuring Thomson scattering from an inductively coupled plasma. *Spectrochim. Acta*, **40B**, 1211–1217.
127. de Regt, J.M., de Groote, F.P.J., van der Mullen, J.A.M. and Schram, D.C. (1996) Air entrainment in an inductively coupled plasma measured by Raman and Rayleigh scattering. *Spectrochim. Acta*, **51B**, 1527–1534.
128. Huang, M. and Hieftje, G.M. (1985) Thomson scattering from an ICP. *Spectrochim. Acta*, **40B**, 1387–1400.
129. Marschall, K.A. and Hieftje, G.M. (1988) Thomson scattering for determining electron concentrations and temperatures in an inductively coupled plasma. 1. Assessment of the technique for a low-flow, low-power plasma. *Spectrochim. Acta*, **43B**, 841–849.
130. Huang, M. and Hieftje, G.M. (1989) Simultaneous measurement of spatially resolved electron temperatures, electron number densities and gas temperatures by laser light scattering from the inductively coupled plasma. *Spectrochim. Acta*, **44B**, 739–749.
131. Marschall, K.A. and Hieftje, G.M. (1988) Thomson scattering for determining electron concentrations and temperatures in an inductively coupled plasma. 2. Description and evaluation of a multichannel instrument. *Spectrochim. Acta*, **43B**, 851–865.
132. Huang, M., Marshall, K.A. and Hieftje, G.M. (1986) Electron temperatures and electron number densities measured by Thomson scattering in the inductively coupled plasma. *Anal. Chem.*, **58**, 207–210.
133. de Regt, J.M., Engeln, R.A.H., de Groote, F.P.J., van der Mullen, J.A.M. and Schram, D.C. (1995) Thomson scattering experiments on a 100 MHz inductively coupled plasma calibrated by Raman scattering. *Rev. Sci. Instrum.*, **66**, 3228–3233.

134. Huang, M., Hanselman, D.S., Yang, P. and Hieftje, G.M. (1992) Isocontour maps on electron temperature, electron number density and gas kinetic temperature in the Ar inductively coupled plasma obtained by laser-light Thomson and Rayleigh scattering. *Spectrochim. Acta*, **47B**, 765–785.
135. Hanselman, D.S., Sesi, N.N., Huang, M. and Hieftje, G.M. (1994) The effect of sample matrix on electron density, electron temperature and gas temperature in the argon inductively coupled plasma examined by Thomson and Rayleigh scattering. *Spectrochim. Acta*, **49B**, 495–526.
136. Huang, M., Lehn, S.A., Andrews, E.J. and Hieftje, G.M. (1997) Comparison of electron concentrations, electron temperatures, gas kinetic temperatures, and excitation temperatures in argon ICPs operated at 27 and 40 MHz. *Spectrochim. Acta*, **52B**, 1173–1193.
137. Mermet, J.M. and Robin, J. (1973) Etude de l'inversion d'Abel en vue de la mesure de la répartition de température dans un plasma inductif. *Rev. Int. Htes Temp. Réfract.*, **10**, 133–139.
138. Blades, M.W. and Horlick, G. (1980) Photodiode array measurement system for implementing Abel inversion on emission from an inductively coupled plasma. *Appl. Spectrosc.*, **34**, 696–699.
139. Choi, B.S. and Kim, H. (1982) On Abel inversions of emission data from an inductively coupled plasma. *Appl. Spectrosc.*, **36**, 71–74.
140. Blades, M.W. (1983) Assymetric Abel inversions on inductively coupled plasma spatial emission profiles collected from a photodiode array. *Appl. Spectrosc.*, **37**, 371–375.
141. Kornblum, G.F. and de Galan, L. (1977) A study of the interference of cesium and phosphate in the low-power inductively coupled radio frequency argon plasma using spatially resolved emission and absorption measurements. *Spectrochim. Acta*, **32B**, 455–478.
142. Kawaguchi, H., Ito, T., Ota, K. and Mizuike, A. (1980) Effects of matrix on spatial profiles of emission from an inductively coupled plasma. *Spectrochim. Acta*, **35B**, 199–206.
143. Omenetto, N., Nikdel, S., Reeves, R.D., Bradshaw, J., Bower, J.N. and Winefordner, J.D. (1980) Relative spatial profiles of barium ion and atom in the argon inductively coupled plasma as obtained by laser-excited fluorescence. *Spectrochim. Acta*, **35B**, 507–517.
144. Horlick, G. and Blades, M.W. (1980) Clarification of some analyte emission characteristics of the inductively coupled plasma using emission spatial profiles. *Appl. Spectrosc.*, **34**, 229–233.
145. Koirtiyohann, S.R., Jones, J.S., Jester, C.P. and Yates, D.A. (1981) Use of spatial emission profiles and a nomenclature system as aids in interpreting matrix effects in the low-power argon inductively coupled plasma. *Spectrochim. Acta*, **36B**, 49–59.
146. Kawaguchi, H., Ito, T. and Mizuike, A. (1981) Axial profiles of excitation and gas temperatures in an inductively coupled plasma. *Spectrochim. Acta*, **36B**, 615–623.
147. Blades, M.W. and Horlick, G. (1981) The vertical spatial characteristics of analyte emission in the inductively coupled plasma. *Spectrochim. Acta*, **36B**, 861–880.
148. Blades, M.W. and Horlick, G. (1981) Interferences from easily ionizable element matrices in inductively coupled plasma emission spectroscopy – a spatial study. *Spectrochim. Acta*, **36B**, 881–900.
149. Rybarczyk, J.P., Jester, C.P., Yates, D.A. and Koirtiyohann, S.R. (1982) Spatial profiles of interelement effects in the inductively coupled plasma. *Anal. Chem.*, **54**, 2162–2170.
150. Roederer, J.E., Bastiaans, G.J., Fernandez, M.A. and Fredeen, K.J. (1982) Spatial distribution of interference effects in ICP emission analysis. *Appl. Spectrosc.*, **36**, 383–389.
151. Furuta, N. and Horlick, G. (1982) Spatial characterization of analyte emission and excitation temperature in an inductively coupled plasma. *Spectrochim. Acta*, **37B**, 53–64.
152. Horlick, G. and Furuta, N. (1982) Spectrographic observation of the spatial emission structure of the inductively coupled plasma. *Spectrochim. Acta*, **37B**, 999–1008.
153. Nojiri, Y., Tanabe, K., Uchida, H., Haraguchi, H., Fuwa, K. and Winefordner, J.D. (1983) Comparison of spatial distributions of argon species number densities with calcium atom and ion in an inductively coupled argon plasma. *Spectrochim. Acta*, **38B**, 61–74.
154. Walters, P.E., Long, G.L. and Winefordner, J.D. (1984) Spatially resolved concentration studies of ground state atoms and ions in an ICP: saturated absorption spectroscopic method. *Spectrochim. Acta*, **39B**, 69–76.

155. Anderson, T.A., Burns, D.W. and Parsons, M.L. (1984) The use of emission spatial profiles for the establishment of an internal reference point in ICP-AES. *Spectrochim. Acta*, **39B**, 559–566.
156. Houk, R.S. and Olivares, J.A. (1984) General calculations of vertically-resolved emission profiles for analyte elements in inductively coupled plasmas. *Spectrochim. Acta*, **39B**, 575–587.
157. Niebergall, K., Brauer, H. and Dittrich, K. (1984) Equidensitometry – a method for plasma diagnostics. 13. Investigations of the spatial emission distribution of different spectral lines in an ICAP. *Spectrochim. Acta*, **39B**, 1225–1237.
158. Rezaaiyaan, R., Olesik, J.W. and Hieftje, G.M. (1985) Interferences in a low-flow, low-power inductively coupled plasma. *Spectrochim. Acta*, **40B**, 73–83.
159. Furuta, N., Nojiri, Y. and Fuwa, K. (1985) Spatial profile measurements of electron number densities and analyte line intensities in an inductively coupled plasma. *Spectrochim. Acta*, **40B**, 423–434.
160. Caughlin, B.L. and Blades, M.W. (1985) Spatial profiles of electron number density in the inductively coupled plasma. *Spectrochim. Acta*, **40B**, 987–993.
161. Long, S.E. and Browner, R.F. (1986) Influence of water on the spatial excitation behaviour of selected elements in the inductively coupled plasma. *Spectrochim. Acta*, **41B**, 639–649.
162. Choot, E.H. and Horlick, G. (1986) Vertical spatial emission profiles in Ar–N₂ mixed gas inductively coupled plasma. *Spectrochim. Acta*, **41B**, 889–906.
163. Choot, E.H. and Horlick, G. (1986) Spatially resolved electron density measurements in Ar, N₂–Ar and O₂–Ar ICPs using a photodiode array detection system. *Spectrochim. Acta*, **41B**, 935–945.
164. Hasegawa, T. and Winefordner, J.D. (1987) Spatial distributions of atomic and molecular species in the inductively coupled argon plasma. *Spectrochim. Acta*, **42B**, 773–789.
165. Houk, R.S., Schoer, J.K. and Crain, J.S. (1987) Deduction of arbitrary excitation temperatures for various analyte species in inductively coupled plasmas from vertically-resolved emission profiles. *Spectrochim. Acta*, **42B**, 841–852.
166. Fogg, T.R. (1988) Simple ICP spatial profiles: optimization of observation position. *Appl. Spectrosc.*, **42**, 170–172.
167. Kolczynski, J.D., Pomeroy, R.S., Jalkian, R.D. and Bonner Denton, M. (1989) Spatial and spectral imaging of plasma excitation sources. *Appl. Spectrosc.*, **43**, 887–891.
168. Olesik, J.W. and Williamsen, E.J. (1989) Easily and noneasily ionizable element matrix effects in inductively coupled plasma optical spectrometry. *Appl. Spectrosc.*, **43**, 1223–1232.
169. Li, K.P., Hwang, J.D. and Winefordner, J.D. (1990) Studies of chemical interferences in an inductively coupled plasma using moment analysis of space-resolved emission profiles. *Anal. Chem.*, **62**, 1233–1238.
170. van Berkel, W.W., Balke, J. and Maessen, F.J.M.J. (1990) Introduction of analyte-loaded poly(dithiocarbamate) into inductively coupled argon plasmas by electrothermal vaporization. Spatial emission characteristics of the resulting dry plasmas. *Spectrochim. Acta*, **45B**, 1265–1274.
171. Fister III, J.C. and Olesik, J.W. (1991) Vertical and radial emission profiles and ion-atom intensity ratios in inductively coupled plasmas: the connection to vaporizing droplets. *Spectrochim. Acta*, **46B**, 843–850.
172. Xiao Jian., Li Qingyan., Li Wenchong., Qian Haowen., Tan Jingyuan, and Zhang Zhanxia (1992) Matrix effects of easily ionized elements on the spatial distribution of electron number densities in an inductively coupled plasma using an optical fibre probe and a photodiode array spectrometer. *J. Anal. Atom. Spectrom.*, **7**, 131–134.
173. Galley, P.J. and Hieftje, G.M. (1993) The OH ‘bullet’ – a promising spatial reference for the inductively coupled plasma. *J. Anal. Atom. Spectrom.*, **8**, 715–721.
174. Weir, D.G. and Blades, M.W. (1994) Characteristics of an inductively coupled argon plasma operating with organic aerosols. Part 1. Spectral and spatial observations. *J. Anal. Atom. Spectrom.*, **9**, 1311–1322.

175. Weir, D.G.J. and Blades, M.W. (1994) The response of the inductively coupled plasma argon plasma to solvent plasma load: spatially resolved maps of electron density obtained from the intensity of one argon line. *Spectrochim. Acta*, **49B**, 1231–1250.
176. Mao, X. and Russo, R.E. (1997) Optimization and calibration of laser ablation-inductively coupled plasma atomic emission spectrometry by measuring vertical spatial intensity profiles. *J. Anal. Atom. Spectrom.*, **12**, 177–182.
177. Koirtiyohann, S.R., Jones, J.S. and Yates, D.A. (1980) Nomenclature system for the low-power argon inductively coupled plasma. *Anal. Chem.*, **52**, 1966–1968.
178. Parisi, A.F. and Hieftje, G.M. (1986) Fundamental studies in the ICP using a sinusoidally modulated power input. *Appl. Spectrosc.*, **40**, 181–185.
179. Parisi, A.F., Rayson, G.D., Hieftje, G.M. and Olesik, J.W. (1987) Temporally and spatially resolved studies in an amplitude modulated inductively coupled plasma. *Spectrochim. Acta*, **42B**, 361–376.
180. Olesik, J.W. and Bradley, K.R. (1987) Analyte excitation in the inductively coupled plasma studied by power modulation. *Spectrochim. Acta*, **42B**, 377–392.
181. Farnsworth, P.B., Rodham, D.A. and Ririe, D.W. (1987) The use of time and space-resolved emission data for fundamental studies of a pulsed ICP. *Spectrochim. Acta*, **42B**, 393–406.
182. Bydder, E.L. and Miller, G.P. (1988) A relaxation method for determining state of equilibrium and temperature ratio T_e/T_g in an argon ICPT. *Spectrochim. Acta*, **43B**, 819–829.
183. Bydder, E.L. and Miller, G.P. (1988) An experimental study of asymmetry in an argon inductively coupled plasma torch using a relaxation method. *Spectrochim. Acta*, **43B**, 1431–1442.
184. Bydder, E.L. and Miller, G.P. (1989) Excitation and kinetic equilibria in an argon inductively coupled plasma torch. 1. Coolant flow only. *Spectrochim. Acta*, **44B**, 165–174.
185. Miller, G.P. (1989) Excitation and kinetic equilibrium in an argon inductively coupled plasma. 2. Introduction of aerosol flow. *Spectrochim. Acta*, **44B**, 395–410.
186. Miller, G.P. (1990) A theoretical evaluation of the relaxation method in determining the temperature ratio T_e/T_g in an inductively coupled plasma. *Spectrochim. Acta*, **45B**, 329–331.
187. Fey, F.H.A.G., Stoffels, W.W., van der Mullen, J.A.M., van der Sijde, B. and Schram, D.C. (1991) Instantaneous and delayed responses of line intensities to interruption of the RF power in an argon inductively coupled plasma. *Spectrochim. Acta*, **46B**, 885–900.
188. Miller, G.P. (1991) A method for observing changes in radiative losses from an inductively coupled argon plasma. *Spectrochim. Acta*, **46B**, 1253–1262.
189. Miller, G.P. (1992) Long-term intensity oscillations in a pulsed inductively coupled plasma. *Spectrochim. Acta*, **47B**, 1013–1022.
190. Fey, F.H.A.G., de Regt, J.M., van der Mullen, J.A.M. and Schram, D.C. (1992) The effect of evaporation on the analyte emission intensities during power interruption in an inductively coupled plasma. *Spectrochim. Acta*, **47B**, 1447–1459.
191. Fey, F.H.A.G., Benoy, D.A., de Regt, J.M., van der Mullen, J.A.M. and Schram, D.C. (1993) Numerical simulation of the response of Li state densities to power interruption in an inductively coupled plasma. *Spectrochim. Acta*, **48B**, 1579–1592.
192. Turk, G.C., Yu, Lijian., Watters Jr, R.L. and Travis, J.C. (1992) Laser-induced ionization of atoms in a power-modulated inductively coupled plasma. *Appl. Spectrosc.*, **46**, 1217–1222.
193. Turk, G.C. (1992) Laser-induced fluorescence of atoms in a power-modulated inductively coupled plasma for trace detection and diagnostic study. *Appl. Spectrosc.*, **46**, 1223–1225.
194. Rayson, G.D. and Shen, D.Y. (1992) Application of an inductively coupled argon plasma axial viewing absorption technique using a power modulated plasma. *Spectrochim. Acta*, **47B**, 553–559.
195. Hensman, C.E., Drake, L.R. and Rayson, G.D. (1997) Characterization of analyte absorption profiles in a power-amplitude modulated inductively coupled argon plasma. *Spectrochim. Acta*, **52B**, 503–515.

196. Chan, G.C.-Y. and Hieftje, G.M. (2004) Using matrix effects as a probe for the study of the charge-transfer mechanism in inductively coupled plasma-atomic emission spectrometry. *Spectrochim. Acta*, **59B**, 163–183.
197. Iglésias, M., Vaculovic, T., Studynkova, J., Poussel, E. and Mermet, J.M. (2004) Influence of the operating conditions and of the optical transition on non-spectral matrix effects in inductively coupled plasma atomic emission spectrometry. *Spectrochim. Acta*, **59B**, 1841–1850.
198. Chan, G.C.-Y. and Hieftje, G.M. (2004) Experimental evidence of state-selective charge transfer in inductively coupled plasma-atomic emission spectrometry. *Spectrochim. Acta*, **59B**, 1007–1020.

Chapter 3

Basic Concepts and Instrumentation for Plasma Spectrometry

Steve J. Hill, Andrew Fisher and Michael Foulkes

3.1 Detection limits and sensitivity

3.1.1 ICP-Atomic emission spectrometry

When an analyte, in aerosol form, enters the central channel of the inductively coupled plasma (ICP) a number of processes occur. The sample desolvates, the matrix decomposes and the resulting analyte and solvent vapour undergoes excitation to produce molecular, atomic and ionic species in various energy states. Some of this energy is released in the form of electromagnetic radiation, of a wavelength that is characteristic of the emitting species. It is this latter property of the plasma that is utilised for analytical purposes in the ICP-emission spectrometer.

From an extended form of the Einstein equation, an expression for the absolute intensity (I_{qp}) of a spontaneous emission line originating from an electronic transition from a higher state q to lower state p can be shown to be [1]:

$$I_{qp} = \frac{d}{4\pi} A_{qp} h\nu_{qp} N_q \quad (3.1)$$

where d is the depth of source, ν_{qp} is the transition frequency, A_{qp} is the line transition probability, h is Planck's constant and N_q the number of excited level species. The relationship between N_q , A_{qp} and I_{qp} , for a given analyte emission line, λ_{qp} , illustrates the fundamental reliance on the number of emitting species, N_q , giving rise to that absolute intensity. This number is dependent on the energy transferred to the analyte and in an IC plasma this energy originates from the high temperatures maintained (*c.* 6000–8000 K). For the purposes of simplification, if it is assumed that some local thermodynamic equilibrium (LTE) is present in a plasma, then N_q is related to temperature (T) through the Boltzmann distribution:

$$N_q = \frac{N_t g_q}{Z(T)} \exp[E_q/kT] \quad (3.2)$$

Where N_i is the total number of analyte species (atom or ion), g_q is the statistical weight of the level q , $Z(T)$ is the partition function (itself dependent on temperature), k is the Boltzmann constant and E_q is the excitation energy of the level q [1].

However, there are many factors to be considered when the sensitivity, that is the net response per unit quantity of analyte, and the absolute detection limit of an element is to be measured instrumentally. Assuming the most intense interference-free analyte line is chosen (thereby maximising sensitivity for a set of given conditions), then these factors include: The physical state of the sample and the sample introduction system, the plasma operating conditions and finally the arrangement of the wavelength selection and detection unit. This latter unit (mono- or polychromator) introduces its own set of limiting factors and these include the small angle of collection of radiation by the entrance optics of the spectrometer (dependent on slit height and widths), losses of intensity due to absorption and scattering by the transmission optics and path length medium, and the efficiency of the electronic detector employed. The compromise between the use of small entrance and detector slit widths (to produce a suitable band-pass for line resolution), and the absolute intensity of radiation reaching the detector is an inherent problem with the general design of mono- and polychromator systems. As stated, these factors take account only of the 'collection of radiation' between the plasma and the detector.

The means by which the sample is introduced to the plasma, the sample introduction system, plays an equally important, if not greater part, in the overall efficiency of the instrument [2,3]. Pneumatic nebulisation and spray chamber systems, for example, are noted for their poor analyte mass transport capabilities (1–2%). In many cases, the conditions used for carrier gas and liquid sample flows are a compromise for a given sample introduction arrangement. In addition, the bore of the injector, the carrier and auxiliary gas flows, the forward power of the generator, the plasma viewing-orientation (radial or axial) and even spray chamber temperature affect both the noise and sensitivity of the instrument. It is little wonder that 'run of the mill' laboratory measurements are sometimes made well away from the optimum conditions for these instruments. The problem is compounded by the fact that, in terms of an 'instrumental response', many of the multivariate parameters employed are interdependent. For comparisons between various ICP spectrometers to be of practical use, 'optimisation' is essential; the figure of merit to be tailored accordingly; that is, sensitivity using signal and background levels, limits of detection (LODs) using signal and noise levels. Both values will give a measure of the performance of the instrument. If the noise component is small and approximately constant for a set of analyte lines then the link between sensitivity (S) for a given line (net signal-to-concentration ratio) and the LOD expressed in terms of concentration can be shown to be:

$$\text{LOD} = \frac{3\text{sd}}{S} \quad (3.3)$$

where sd is the standard deviation of the noise of the signal and the value of 3 dictates a confidence interval (CI) of 99.7% (see below). Instrument manufacturers now offer system programmes as an aid to optimising performance. The figure of merit and the variable parameters should however be carefully chosen.

A scrutiny of atomic spectrometry articles shows that interpretation of the term 'LOD' is variable and the value obtained may include the whole procedure (i.e. sampling, sample

preparation, introduction technique and analyte measurement). The LOD of an individual analytical procedure is 'the lowest amount of an analyte in a sample that can be detected but not necessarily quantified as an exact value' [4]. In the 'Guidelines for Achieving Quality in Trace Analysis' [5] the LOD is expressed as 'the concentration C_L or quantity q_L derived from the smallest measure X_L that can be detected with reasonable certainty for a given procedure. The value X_L is given by the following equation:

$$X_L = X_{bl} + KS_{bl} \quad (3.4)$$

where X_{bl} is the mean of the blank measures, S_{bl} is the standard deviation of the blank measures and K is a numerical factor chosen according to the CI required' [6].

'Instrumental LODs' should be identified as a separate set of data. The instrumental LOD may be defined as that quantity of the element which gives rise to a reading equal to three times the standard deviation of a series of at least ten determinations ($n = 10$) at or near the blank level [1]. From both a realistic and a practical point of view, these measurements should be made using the intensity from the analytical line of interest at or around the limit of determination (see below). The noise component associated with an on-peak measurement is therefore included in the determination, rather than just the blank which contains little or no analyte signal. The on-peak stability is therefore taken into account and a more reliable measure of LOD is obtained. As shown, the use of three times the standard deviation to give a CI, assuming a normal distribution, of 99.7% is preferred. It should be noted that the number of determinations, n , has a bearing on the confidence limit values. Low values of n will effectively change the probability factor associated with that of a 'normal' distribution and hence change the 'simple' standard deviation calculated. This must be taken into account [7]. Correction is performed using the values from t factor tables of CI vs degrees of freedom ($n - 1$).

$$\mu = X \pm t.sd/\sqrt{n} \quad (3.5)$$

where μ = the limiting value and X = the mean analyte value.

The concept of the detection limit has been discussed in various publications, some in greater detail than others. One earlier work of note [8] expresses the LOD as the statistical figure of merit that appraises an analytical method for the smallest detectable concentration, C_L , or absolute amount, q_L , of an analyte. As shown in Equations (3.3) and (3.4), the analyte signal is to be distinguished from the background fluctuations by employing a suitable statistical confidence to the value. However, the detection limit (C_L) may also be expressed in terms of the net signal-to-background ratio (SBR) [8]:

$$C_L = \frac{0.01K(\%RSD)_B C_0}{SBR} \quad (3.6)$$

where K is a statistical constant (either 2 or preferably 3), $\%RSD_B$ is the relative standard deviation of the fluctuations of the background expressed as a percentage; and C_0 is the concentration of the analyte giving rise to the SBR [8]. SBR is a dimensionless quantity and detection limits calculated using this approach have a reduced dependence on various instrumental parameters. This allows some comparisons to be made between instruments.

One other work of note discusses the analytical performance of the ICP in detail and again considers both the fundamental concepts and practical limitations involved [9].

Many of the parameters that govern sensitivity and LOD in ICP-AES are common to the ICP-mass spectrometer. However, those particular parameters which relate to mono- and polychromator systems in ICP-AES should be substituted for and re-evaluated in terms of, the mass collection and filtering processes employed in ICP-MS. For example, the loss of emission intensity suffered by a monochromator are analogous, in simple terms, to those losses of ion intensity associated with the physical gas sampling at the plasma-sampler interface and the quadrupole filter [10]. The definitions relating to 'instrumental' figures of merit (the LOD, limit of determination, stability and sensitivity) remain the same; being independent of the instrument employed.

3.1.2 *Limit of determination*

A note on the limit of determination should be made here to clarify the term. For an individual analytical procedure it is considered to be the lowest amount of an analyte in a sample which can be quantitatively determined with suitable uncertainty. For practical purposes, it may be taken as the amount that is equivalent to 10 times the signal-to-noise ratio [5].

3.1.3 *Axial systems*

Recent developments in optical emission spectrometry have led to a range of commercially available axially viewed instruments [11]. By collecting analyte emission from the central channel of the plasma but viewed down the tail flame (i.e. end-on), it is shown that lower LODs are obtained. In this instrument, the torch assembly and plasma are, in most cases, turned through 90° to become horizontal, with the tail flame pointing towards the collection optics. A shear gas is usually employed to cut the tip of the tail flame. This produces a flattened cross-sectional profile to clear the optical and thermal paths for axial viewing and also a means of dissipating the hot gases which are now directed at the spectrometer. One design also incorporates a cooled cone with a sampling orifice and counter flow of argon. These shield the spectrometer and help disperse the optically thick cooled plasma gases, which contain lower energy state analytes that can absorb analyte emission. More analyte emitting species are being viewed in an axial orientation than in the radial system, which results in an increase in collection efficiency. The radial system however, takes full advantage of the optically thin profile of the plasma. The ability to vary the height at which the emitting species are viewed also allows spatially dependent interferences to be avoided or reduced (e.g. easily ionisable element, EIE, effects) [12]. Viewing axially removes this degree of freedom, and by also introducing an optically thicker, end-on profile may impose some limitations on the concentration range and matrix type that may be introduced for interference-free analyte determination. The use of larger bore injectors, tailored interface designs and close attention to the operating conditions of the plasma's power and gas flows can address a number of these effects. Detection limits from axial viewing are stated to be improved by a factor of 5 to 10 (although comparisons between truly optimised systems

are not always seen and the matrices employed are sometimes simple). The performance characteristics of this instrumental arrangement have been well documented in the 'literature' and its advantages and disadvantages discussed [13,14].

3.1.4 *The sample introduction system*

The sample introduction system is known to be an important factor when particular detection limits are required [2]. The conventional pneumatic nebuliser, as stated, is rarely greater than 2% (usually nearer 1%) efficient in terms of the mass transport (mass of analyte transported to the plasma per unit mass of analyte introduced from the sample, expressed as a %). Consequently, these systems have been the focus of research for many years in an attempt to increase the number of analyte species reaching the plasma (and hence increase the sensitivity) and in reducing the noise characteristics associated with them. One problem with increasing the sample mass transport efficiency is the effect of also increasing the solvent load in the plasma which can lead to gross instability and matrix effects [15,16]. A pneumatic nebuliser, for example, concentric glass, high solids, cross-flow, etc., produces a range of aerosol particle sizes. This distribution is dramatically changed by the spray chamber–injector assembly [17], giving rise to a much reduced transport efficiency. This assembly also produces a smaller and narrower aerosol particle size distribution. One consequence of this is a reduction in the noise associated with the aerosol–plasma interaction. Sensitivity has therefore been increased and LODs lowered by developing sample introduction systems that increase the analyte mass transport while reducing both the particle size of the aerosol and the associated solvent carrier load.

Systems which offer improvements in these parameters cover a range of designs and approaches:

- (i) The ultrasonic nebuliser utilises the piezo-electric effect from a specially prepared crystal to produce an aerosol with a very small and narrow particle size distribution (approximately $<2\text{ }\mu\text{m}$). The result is that, with a greatly reduced rejection of aerosol particles by the spray chamber–injector assembly, the mass transport efficiency is improved by over an order of magnitude [18]. Such an increase would severely load the plasma based on a normal liquid flow rate of $0.5\text{--}1.0\text{ ml min}^{-1}$. However, with a combination of reduced sample flow rate and solvent vapour removal, either by 'in-line heating and condensing' or by membrane separation, only micro-crystallites and/or ultra-small aerosol particles reach the plasma. The noise characteristics associated with aerosol particles is consequently much reduced and together with the increased number of analyte particles reaching the plasma, the LOD is much improved (*c.* 100 times). The inherent benefits of this sample introduction system for organic matrices is obvious and those loading problems associated with liquids of high vapour pressure are very much reduced (if not negated); thereby extending the analytical range of the instrument. This system is not however without its problems. Memory effects associated with sample concentration and with complex matrices can be seen [19].
- (ii) LODs are notably lowered if an analyte of interest can be transformed to the gaseous state. Such is used in the hydride, cold vapour or alkylation systems as shown; for example, in the determination of arsenic mercury and cadmium [20–22]. In each case

the major analyte loss processes within the sample introduction system are removed. Three points should be noted:

- (a) in hydride and alkylation systems, gaseous by-products are generated, often in high quantities which can load and de-stabilise the plasma,
 - (b) the chemistry of the generation technique may suffer interferences some of which are quite severe, due to the presence of certain metal ions in the matrix; for example, transition ions, in particular the platinum group metals (PGMs),
 - (c) only certain elements and particular oxidation states of these elements will form stable volatile hydrides and alkyls.
- (iii) If the normal nebuliser, spray chamber and torch assembly is replaced by a direct injection nebuliser (DIN) system, improvements in LOD may be seen [23]. Some designs are termed direct injection high-efficiency nebulisers (DIHENs), to denote their 'higher efficiency' [24]. Generally, in this sample introduction system, the liquid sample is transported via a stabilised high performance, low flow pump to a capillary or micro-nebuliser of the 'venturi' design situated within the injector of the plasma torch. Small quantities ($\mu\text{l min}^{-1}$) are delivered to the DIN and the aerosol produced by a concentric argon gas flow is directed to the central channel of the plasma. The earlier designs of DIN required great attention to detail in setting up, with the liquid sample to carrier gas flow ratio being critical; in order to produce an aerosol of very small particle size and to limit noise characteristics. Interestingly, this type of nebuliser was used on the first ICPs [25] but was abandoned at the time because of its delicate construction. Its re-introduction has been brought about because of more robust designs.
- (iv) Two further approaches to direct injection systems can be considered and these rely on modifications of the aerosol production process. If a capillary is heated electrothermally so as to raise the temperature substantially above the boiling point of the liquid sample, a combined aerosol-vapour phase is produced when a suitable carrier gas flow is employed. Alternatively, if a high voltage is applied to a capillary carrying a liquid sample, it is possible to produce a finely divided aerosol within a gas flow that is stabilised by electrostatic repulsion. In the former case the nebulisation system is termed as a 'thermospray' [26] and in the latter, 'electrospray' [27]. In both cases, the analyte can be introduced directly to the plasma using a similar solvent delivery and gas carrying system to that of the DIN and consequently improvements in the LOD are noted, if attention is paid to those same critical parameters required for use with the DIN. More recently, higher flow thermosprays have been developed which has resulted in the need for a desolvation step prior to introduction to the plasma [28].

The sample introduction systems discussed here are not restricted to ICP-emission instruments and can be used to improve sensitivity and lower the LOD for mass spectrometric instruments as well.

3.1.5 Detectors

The use of photomultiplier tubes (PMTs), together with their inherent limitations; that is, non-uniform spectral response, rate-dependence (counts per second) and physical size, in ICP spectrometers has been eroded by the introduction and availability of segmented charge coupled, charge coupled and charge injection devices (SCDs, CCDs and CIDs, respectively)

[29]. The modern echelle spectrometer design, when coupled with these higher efficiency, mega-pixel devices, produces a compact polychromator with most of the advantages expected of this detector design. The benefits available include: (i) the simultaneous measurement of analytes, internal standards and background allowing a variety of correction techniques [30]), (ii) the simultaneous acquisition and storage of emission data from a sample in one run, covering the entire spectral range (or part) of the polychromator and (iii) the possibility of using non-rate dependent total counting statistics. These detectors offer improvements in the LOD of analytes through improved stability, sophisticated noise-correction techniques and photon integration.

The ion-detection system in ICP-mass spectrometry (e.g. electron multipliers, Faraday cups and Davy collectors, etc.), is a topic area in its own right, taking into account ion-collection-focusing trains, amplifier modules and specialist programmes [31].

Table 3.1 displays typical LODs for the elements obtained using radial and axial-viewed ICP-AES in comparison with the plasma mass spectrometric technique.

Table 3.1 General limits of detection for the elements using the most sensitive line in ICP-AES and most abundant isotope in quadrupole ICP-MS

Analyte	Axial ICP-AES/ $\mu\text{g dm}^{-3}$	Radial ICP-AES/ $\mu\text{g dm}^{-3}$	ICP-MS/ng dm^{-3}
Al	0.9	5	50
Sb	3	20	5
As	3	12	10
Ba	0.03	0.15	1
Be	0.05	0.1	1
Bi	—	10	1
B	—	3	70
Cd	0.2	1	5
Ca	0.01	0.1	500
Ce	—	100	1
Cr	0.5	2	5
Co	0.4	2	1
Cu	0.9	1.5	5
Ge	—	100	50
Au	—	25	5
In	—	100	1
Fe	0.3	1	100
La	—	6	5
Pb	1.5	7	1
Li	0.06	1	5
Mg	0.05	0.3	50
Mn	0.1	0.3	5
Hg	—	20	1
Mo	0.5	1	5
Ni	0.7	4	5
Pd	—	70	5
Pt	—	30	5

Table 3.1 (Continued)

Analyte	Axial ICP-AES/ $\mu\text{g dm}^{-3}$	Radial ICP-AES/ $\mu\text{g dm}^{-3}$	ICP-MS/ng dm^{-3}
K	0.3	4	500
P	4	20	1000
Se	4	16	50
Si	—	5	1000
Ag	0.5	1	5
Na	0.2	2	50
Rb	1	5	
Sr	0.02	0.2	1
S	4	15	50 000
Te	—	20	50
Tl	2	15	1
Sn	2	7	5
Ti	0.5	2	50
W	—	20	5
U	—	400	1
V	0.7	2	5
Zn	0.2	1	5
Zr	—	5	5

3.2 Accuracy and precision

While there are a number of ways of expressing accuracy [5], the simplest practical statement may be considered as the closeness to the true or accepted value of an analyte concentration. If the ability to obtain a representative sample is not in question, then the reasons for deviation from this ‘true value’, from a purely instrumental stand-point, are many and varied, and often place an analyst’s experience in the front line.

Precision can be defined as ‘the closeness of agreement between the results obtained applying the experimental procedure several times under prescribed conditions’ [5]. From an instrumental point of view, the stability requirements of those operating parameters previously discussed have a direct bearing on the precision of an analytical measurement. In practical terms, small variations in, for example, the forward power, nebuliser gas and liquid sample flow rates, can result in a change of sensitivity for an analytical line (or ion) [8]. The rate at which these operating parameters change compared with the duration and rate of analyte detection/data acquisition (integration times, period between measurements, etc.) will govern, to a greater extent the precision of a measurement [32].

A general note should be made here when considering accuracy. The incorporation of quality control checks within a full ‘assurance’ regime is necessary for the monitoring of an instrument’s performance and for the validation of any analytical procedure. The use of simple check standards for set-up procedures together with the use of suitable matrix matched certified reference materials during analytical runs will provide the analyst with a measure of confidence for any determination undertaken. The importance of such a quality regime cannot be over-stressed [33].

Improvements in precision can be obtained by the use of a suitable internal standard (IS). The purists criteria can be applied (as described later in Section 3.2.3) for IS selection, also allowing corrections to be made to the analytical accuracy. This requires ratioing of an analytical signal to an IS which has very similar characteristics to that of the analyte of interest (e.g. use of an atom or ion line, ionisation energy, emission wavelength, etc.). The introduction of CCDs and CIDs as emission detectors for the echelle (and similar) spectrometer, allows simultaneous multi-element internal standardisation measurements to be made. When linked in 'real-time', corrections for transient parameter fluctuations result in improved precision [34].

When considering mass spectrometric techniques, the purist's list should be extended to include an IS of similar mass. However, one technique that can greatly improve (when correctly applied) both precision and accuracy in ICP-MS measurements is isotope dilution analysis (IDA). The spiking of a sample with an analyte of interest is known as a standard addition procedure. If the spike contains the analyte but with an enriched isotopic abundance then a measure of the isotope ratios can be used to calculate the concentration of the analyte present. This procedure employs both internal standardisation and internal compensation as a means of correction [35].

3.2.1 *Instrumental drift*

The complexity inherent in the current designs of optical emission and mass spectrometers results in an instrument that is dependent on precision mechanical, optical and electronic engineering for its efficient performance. This performance will be severely degraded if attention is not paid to control of the inter-dependent multivariate parameters that give rise to instrumental drift. Manufacturers link performance with the thermal stability of the instrument's environment. Temperature fluctuations can cause severe instrumental drift and some measure to compensate (at least partly) for these effects can be incorporated in the overall design. While both mono- and polychromator optical systems for example are usually made as temperature compensated and controlled units, the need to site the instrument in a temperature-controlled room, isolated from vibration must be considered.

Stable power generators, gas and liquid flows are important in reducing instrumental drift effects. The advent of solid-state generators, mass-flow controllers, precision pumps and stepper motor systems have allowed improvements in stability to be realised.

The incorporation of wavelength correction techniques in the design of the optical train helps to reduce severe drift effects within the optical spectrometer (e.g. separate mercury monitoring line to give regular internal wavelength calibration). Poor on-peak stability can seriously affect accuracy and LODs, and long-term tests using a number of lines covering the entire wavelength range of the instrument should be part of any performance evaluation. The use of temperature control units for circulating the coolant water extends the stability of an instrument.

Due to the presence of both long- and short-term drift effects in instruments, which may themselves be progressive or cyclic, a continuous internal monitoring/standardisation process is required in order to maintain accuracy [36]. In the absence of all other interferences, suitable IS added to the sample and continuously monitored would be an adequate approach. The echelle polychromator-detector designs offer the means to address a number of the stated stability problems, however the sources of these problems should not be forgotten.

The stability of the plasma mass spectrometer is dependent on the same criteria as its optical cousin in terms of instrumental drift. However, its measurement of the extended lower concentration range ($\mu\text{g L}^{-1}$ and ng L^{-1} levels) and the presence of a low pressure mass filter impose stricter requirements on stability. Hence, the use of internal standardisation to correct for drift is of paramount importance in this technique [37]. In the presence of other interferent effects (e.g. spectral and matrix related) the requirements for internal standardisation become more complex and are considered under their respective headings. In addition, a number of thermally controlled units are used to improve stability. One important parameter to consider is the spray chamber temperature as this affects the mass transport of the sample. A spray chamber coolant supply is also of benefit when dealing with non-aqueous (i.e. organic), samples. Any reduction in the organic solvent temperature results in a reduction in the plasma solvent vapour load.

3.2.2 *Matrix effects*

The efficiency with which an instrument handles a sample matrix and isolates the analytes of interest is important. The mass transport efficiency from a pneumatic nebuliser spray chamber arrangement is, in part, dependent on the viscosity, surface tension, vapour pressure and density of the liquid sample. Their effect on aerosol formation should not be trivialised and has been the focus of a number of studies [2,15,16,38]. Hence, calibration using standards that are matrix-matched to samples can be an important factor to consider. The use of an IS to correct for these transport effects must be chosen with care. The IS and standard additions (SA) techniques may not always correct the final analyte value. This is particularly so for plasma emission and post-plasma sampling systems, such as ICP-MS where particular 'plasma processes' come into prominence. In terms of sample introduction system transport effects only, these correction techniques (IS and SA) are efficient.

3.2.3 *Plasma effects*

It is known that the higher temperature of the argon plasma, *c.* 6000 K, is responsible for the reduction of those major chemical interferences often seen in simpler flame emission and absorption instruments. Its greater efficiency for matrix destruction and for producing atomic and ionic species for spectral detection or mass sampling is a consequence of this higher thermal environment. However, the plasma is spatially inhomogeneous and, for example, the peak viewing height for optical emission of an analyte in a radial view system will vary depending on a number of interdependent parameters; that is, the three gas flows, forward power, the sample matrix, sample flow and whether an atom or ion line is employed for detection. The latter parameter displays this spatial dependence to a marked degree. For a given analyte under a given set of conditions, the position for peak emission will generally be in the order: atomic species (very low down in the plasma), ionic species (higher up) and the possibility of atomic species again (very high up). This effect may be rationalised in respect of the vertical change in gas kinetic temperature T_k and electron density of the central channel, the residence time for the species in the plasma and the excitation and ionisation energies of the analyte (the hard and soft line criteria)[8,39]. The reasons for careful choice of IS, to correct for plasma-based effects and to account for analyte characteristics and matrix-related processes, therefore becomes apparent in the 'light' of these variables.

A purist's criteria for selection of an IS would, as stated previously, include the use of the same line type (either ion or atom) as that of the analyte(s) of interest, an ionisation energy (IE) that is close to the analyte's and a similar emission wavelength. Frequently however, these criteria cannot always be met and a compromise with other parameters is often made.

The problems are compounded when physical post-plasma sampling techniques are employed, as in ICP-MS. The presence of certain matrix species at the plasma-sampling interface can modify the analyte ion concentration; a consequence of plasma potential and space charge effects [40]. Internal standardisation for this technique is often centred on the use of similar mass range isotopes and those of comparable IE to that of the analyte of interest. The practical result is that more than one 'IS' is chosen for the determination of a series of analytes.

3.2.4 Spectral effects, interferences and background correction

Modern optical emission spectrometers utilise a sophisticated range of mono- and polychromators to select the analyte line of interest. The term 'element specific detection' has to be carefully employed however because of those interferences which may result, even in the absence of an analyte. From research using UV-Visible Fourier Transform spectrometers [41, 42] it can be shown that fewer 'real' line overlaps occur even in the presence of line broadening phenomena such as that attributed to the Doppler and Lorentz effects. The compromise between the intensity of a specific line reaching the detector and the resolution, previously discussed, results in possible line overlap. This sets some of the gross effects of line coincidence firmly under the heading of instrumental broadening (i.e. a mono- and polychromator-based effect). It is also important to remember that molecular species can result in a spectral interference. The presence of OH, PO and SO in high concentrations in a matrix, for example, can contribute to emission in particular regions both in terms of wavelength and vertical position in the central channel, giving rise to structured background effects. Wavelength response information at and around the analyte line of interest can help to visualise the line profile and the effects of the limits of resolution (shoulder/wing effects and even gross broadening) and may allow suitable background points to be chosen for 'net signal' correction. The importance of 'net' signal measurement cannot be overemphasised. Correction for the background emission being raised because of the concomitant matrix composition, as presented, must be considered in all measurements. However, when severe spectral line overlap and molecular emission occurs, then correction using background points, internal standardisation or SA will not be effective. While some reduction from molecular emission may be achieved by judicious use of vertical profiles (if this parameter is available!) in the plasma, for major effects an alternative line is best chosen.

3.2.5 Dynamic range

The argon ICP is a spatially inhomogeneous (in terms of electron density and 'temperature'), partially ionised gas. When the nebuliser gas flow punches a hole through the plasma and produces an annulus, this spatial inhomogeneity is increased. The energy transfer processes which create and stabilise the 'fireball' (that outer region where the electron density and temperature are greatest) are extended to include the central channel. The velocity

profile of this channel gives rise to a plasma 'tube' of reduced electron density and 'temperature'; effectively a 'cooler' region [43]. The result from having an efficient atomising and exciting plasma which is cooler at the centre, is that in ICP-AES an optically thin profile is produced, and self-absorption effects are greatly reduced. The dynamic range for linear calibration of an analyte is therefore typically more than four orders of magnitude.

The ICP is also an efficient ioniser. The number of excited species present (electrons, Ar^+ , etc.) which produce analyte ions, greatly exceed those of the analyte itself. Consequently, the dynamic range experienced in ICP-MS is also large and can extend to over five orders of magnitude. The sensitivity of the two instruments are however notably different. Efficient post-plasma sampling when combined with variable mass filtering and sensitive ion detectors, allows an analyte concentration range from ng dm^{-3} up to 100s of mg dm^{-3} to be measured. The optical emission spectrometer, in contrast, usually extends from the low $\mu\text{g dm}^{-3}$ to 10s of mg dm^{-3} concentration range for a given line. These limits are of course dependent on the analyte sample type and introduction system used. To extend the range for an analyte at higher concentration, an alternative, less sensitive line can be chosen. The advantages of the newer design of polychromator-detector, that allows simultaneous measurements to be made across their spectral range, come into their own, under these conditions.

3.2.6 ICP-MS

The problems associated with the plasma matrix and analyte processes and with spectral interference are also of major concern in mass spectrometric post-plasma sampling systems. A typical quadrupole mass analyser exhibits certain practical limitations of resolution (0.1–0.5 AMU). When this resolution is high there is an effect on the number of ions reaching the detector (i.e. they decrease). Hence, the inverse effect seen in ICP-AES between resolution and light detection has some analogies in ICP-MS. As a result, spectral overlap for ions of similar mass, be they element or molecular based (termed isobaric and polyatomic, respectively) is possible. Tables of coincidence are well documented by manufacturers and researchers [44,45]. Examples of this coincidence for isobaric phenomena are ^{113}Cd and ^{113}In , and ^{40}Ca and ^{40}Ar . For polyatomic phenomena, examples include $^{40}\text{Ar}^{35}\text{Cl}^+$ on $^{75}\text{As}^+$, $^{40}\text{Ar}^{16}\text{O}^+$ on $^{56}\text{Fe}^+$ and $^{35}\text{Cl}^{16}\text{O}^+$ on $^{51}\text{V}^+$. While in general, an alternative isotope can be chosen, some analytes are mono-isotopic (e.g. ^{75}As and ^{59}Co) or may only provide isotopes of low abundance. This usually requires a change to special operating conditions or some modification of the plasma mass spectrometer (e.g. use of a mixed gas system like N_2) [46], or the use of a coupled technique such as HPLC-ICP-MS [46]. Such modifications can, however, lower the sensitivity and raise the detection limit of the analyte(s) of interest.

Developments in multi-pole mass filter design (e.g. hexapole, octapole, etc.), have attempted to address the limitations imposed by resolution, with varying success. An alternative approach to removing interferences has been the development of the reaction or collision cell interface. This utilises a multi-pole, high-frequency (hf) ion-residence cell, which allows certain gases to be introduced (e.g. CH_4 , NH_3 , He , H_2 , etc.), in order to interact with sampled portions of the analyte-containing plasma. Concomitant interfering species are removed, allowing post-cell sampling for the analyte of interest [47,48]. Detection limits for these instruments depends on the cell and gas system used and the analyte and matrix under investigation. However, typical values range from 10s of ppb down to sub-ppt. In this form,

the multi-element capability of the ICP-MS is usually compromised, but not always [48]. To date, few instruments, if any, match that of the high-resolution sector field ICP-MS. Combined magnetic and electrostatic focusing remove many of the concomitant mass problems, but their cost together with the technical expertise required to operate them still place these instruments in the specialist field.

3.3 Multi-element capability and selectivity

The ICP has made a major impact in analytical atomic spectrometry because of its multi-element capabilities. On its own the plasma is not element selective. The property of efficiently producing excited atomic and ionic species from most samples in various forms and with the reduced interferent effects compared with other techniques, allows access to most elements of the Periodic Table. There are however some exceptions. These result, in part, from practical constraints associated with the general operating conditions or cost. The use of aqueous solutions, often stabilised with acids such as HNO_3 and HCl , together with the need to operate at atmospheric pressures negates the routine estimation of carbon, nitrogen, oxygen and hydrogen. The older design of mono- and polychromator, even with a purging or vacuum facility, would rarely exceed the range 160–800 nm and in many instruments this range was much reduced; thereby restricting access to some emission lines. A few elements; for example, F, Cl and Br, and the noble gases are poorly excited or ionised unless an alternative plasma gas is used (e.g. He). Given these relatively few exceptions, it is not surprising that instruments based on the argon plasma have already made their mark in the modern analytical laboratory. It is, however, of note that the modern polychromator with a pixel based detector in ICP-emission spectrometry is extending the range of line capabilities further. One instrumental system covers the range 130 to over 1000 nm; thereby allowing halogen emission lines to be accessed.

The selectivity of a plasma instrument is brought about by the coupling with either optically (using a mono- or polychromator) or mass spectrometrically (using a quadrupole filter) isolation devices. Both these instruments have already been discussed in terms of their benefits and limitations. The selectivity of both instruments can be extended (and enhanced), if a separation technique is employed as part of the sample introduction system. Gas chromatographic and high performance liquid chromatography (HPLC) systems effectively couple with ICP-AES and ICP-MS; resulting in a rather large element-specific detector. Their combined analytical power becomes greater, allowing elemental speciation studies (i.e. the chemical form of the element), to be performed. When the impressive separation obtained with capillary electrophoresis, in terms of speed and resolution, is combined with the element specific and sensitive ICP-MS, then a potentially powerful analytical tool is obtained. Although coupled techniques are continually under development [49,50] and in some cases, their full capabilities have yet to be realised, much research interest lies in this area.

3.4 Instrumental overview

A schematic view of an ICP-AES instrument is shown in Fig. 3.1. It consists of a radio-frequency (rf) generator, a sample introduction system, a torch where the plasma is formed,

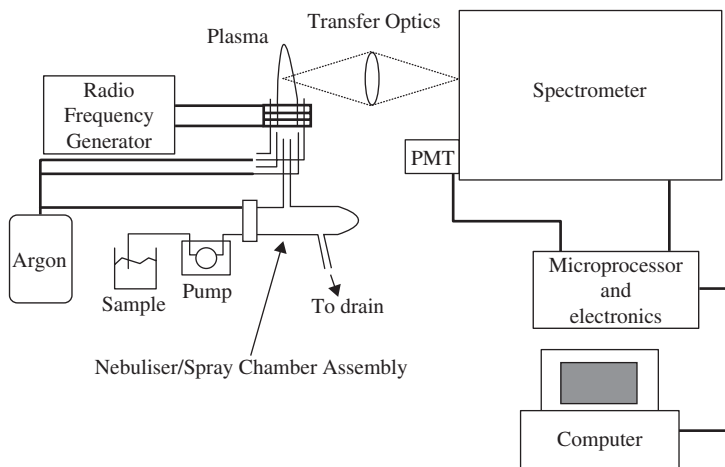


Figure 3.1 A schematic diagram of a generalised ICP-AES instrument.

a spectrometer that isolates the wavelength/wavelengths required during the analysis, a detector and a read-out device. Each of these parts will be discussed in more detail below.

3.5 Radio-frequency generators

The rf generator is a device that is used to provide the power required for the generation and sustaining of the plasma discharge. The power required for atomic emission spectrometry (AES) measurements ranges between 600 and 1800 W, depending on the sample to be analysed, the dimensions of the torch, etc. Although many generators have the capacity to reach up to at least 2000 W. Typical operational powers required for the analysis of aqueous-based solutions range from 950 to 1400 W. Higher powers may be required for the analysis of samples presented in organic solvents. The same instrumentation may be used to sustain an ICP for use with atomic fluorescence measurements, although modifications to the torch box would be required. For atomic fluorescence measurements to be made, a much lower power is generally required (300–750 W). Although many generators are capable of reaching these power levels with a great deal of accuracy and precision, others may not be calibrated for this range and these, at best, would lead to irreproducible results. The power is transferred to the argon gas by a water-cooled copper load coil that surrounds the end of the torch. The number of turns on the coil is variable, but most commercial instruments use between two and five turns. There have been reports in the literature though of seven-turn coils being used.

The frequency of operation of the generator in most commercial instruments is either 27.12 or 40.68 MHz, although instruments have been produced that used much higher frequencies (e.g. 56, 64 or even 148 MHz). The 40.68 MHz generators are generally regarded as offering improved coupling efficiency, which leads to a higher temperature and improved plasma robustness and stability. This means that the plasma is likely to be more tolerant of samples introduced in organic solvents or of the presence of gases other than argon

(e.g. hydrogen produced as a by-product during hydride generation sample introduction). In addition, because the coupling efficiency is improved, the 40.68 MHz generators produce a robust and stable plasma at a lower power output. This leads to a lower background continuum spectrum being produced and since the background signal is reduced, this often leads to an improvement in LODs. The 'skin-effect' in rf plasmas means that a higher frequency of generation gives a thinner plasma with a wider dynamic range. This is because if the plasma is thinner, there is less self-absorption, lower backgrounds and fewer interferences. Most modern instruments have a coupling efficiency (i.e. the percentage of power actually reaching the plasma) of 70–75%. Older generators were notoriously inefficient, with losses exceeding 50% being experienced. Traditionally, the 27.12 MHz generators were used but, more recently, many manufacturers have tended to utilise the advantages offered by the 40.68 MHz ones.

There are basically two types of generator, namely crystal controlled and free running. In the former, a piezo-electric crystal (quartz or Rochelle salts) is sandwiched between two metal plates. If a voltage is applied to the plates, the crystal will expand and contract with the changing polarity. This is known as the piezo-electric effect. The natural frequency of the expansion of the crystal is constant but is inversely proportional to the thickness of the crystal. Most crystals are cut so that they have a natural frequency of 13.56 MHz. A frequency multiplier (either $\times 2$ for the 27.12 MHz or $\times 3$ for the 40.68 MHz generators) generates power at the frequency required and buffer circuits and power amplification devices then amplify the power output. A directional coupler measures both the forward and reflected powers, an impedance matching network (impedance is a material's resistance to the flow of an electric current) and an induction coil are also part of the power supply to the plasma. The impedance matching network usually operated using servo-driven capacitors. For most sample types these work very well. However, for sudden changes of impedance (e.g. a change between aqueous and organic solvent introduction), the impedance matching network may not work sufficiently quickly to prevent plasma instability and possible extinction. The power from these instruments may be stabilised to better than 1% and so are extremely precise. The other kind of generator is of the free-running type. In this type of generator, the frequency of operation is controlled by components within an electrical circuit. Typically, a 40.68 MHz generator of this type will operate with a much wider uncertainty on the frequency of the power output; with a range of 40.68 ± 2 MHz being common. Free-running generators have a matching network that has no moving parts. This means that small changes in frequency brought about by sample solvents, etc. are overcome by electronic tuning. This means that they respond much more rapidly to rapid changes in impedance and hence plasmas formed from such generators are less likely to be extinguished by the introduction of organic solvents. This type of generator uses solid-state electronics and hence the need for bulky vacuum power amplifiers is removed. As a result, modern, free-running generators tend to be much more compact (smaller) than those of several years ago.

There are several different types of oscillator, including the Armstrong, the Hartley, the Colpitts, although the Hartley is really an extension of the Armstrong and the Colpitts is a further extension of this. The stability increases in the order Armstrong < Hartley < Colpitts. Further information about rf generators may be found in the literature [8].

Generators may be either water- or air-cooled. Both have advantages and disadvantages. The air cooling is obviously cheaper, but may not be as efficient. Cooling of the generators is necessary to ensure that power drift (and hence signal drift) are kept to a minimum.

3.6 Torches

When ICPs were first used for analytical measurements, there were two basic torch designs. Although they were fundamentally the same, there was a very large difference in size, and also in power and gas consumption. The differences between the Greenfield and the Fassel torches are summarised in Table 3.2. Since the Fassel design is somewhat cheaper to operate, manufacturers have almost exclusively used this style for 25 years, even though it does suffer some drawbacks in terms of robustness when compared with the Greenfield style. A schematic diagram of a typical torch is shown in Fig. 3.2. The torch consists of three concentric tubes. The outer most one is termed the plasma or coolant gas and has a typical flow rate of $11\text{--}14\text{ l min}^{-1}$ argon. It is from this gas flow that the plasma is formed. The second tube contains the intermediate or auxiliary gas, which flows at a rate of $0.5\text{--}2\text{ l min}^{-1}$

Table 3.2 Comparison of Greenfield and Fassel style torches

Greenfield	Fassel
Gas flow = $12\text{--}38\text{ l min}^{-1}$ Ar + $20\text{--}70\text{ l min}^{-1}$ N ₂	Total gas flow = $13\text{--}18\text{ l min}^{-1}$ Ar
Large dimensions (coolant tube = 29 mm)	Small dimensions (coolant tube = 20 mm)
Large injector size (at least 2 mm)	Small size injector (1.5–1.8 mm)
High power requirement (several kW)	Low power requirement (0.9–1.5 kW)
Robust – may cope with poor concentricity of tubes and tolerant of other gases	Intolerant of other gases
Expensive running costs	Cheap running costs

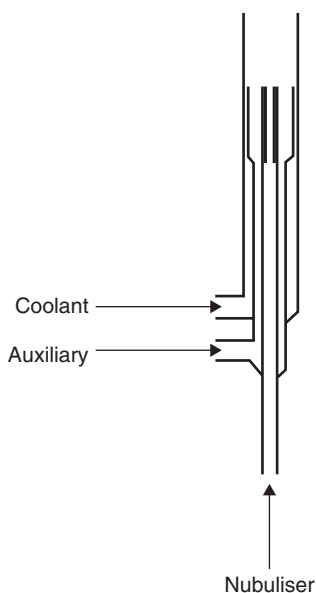


Figure 3.2 Structure of an ICP torch.

argon. The function of this gas is to lift the plasma away from the ends of the auxiliary and injector tubes, hence preventing them from melting. The innermost tube contains the nebuliser/injector gas. This flows at a rate that is dependent on the type of nebuliser present, but is typically in the range $0.5\text{--}1.5\text{ l min}^{-1}$ argon. Although most commercial torches resemble that shown in Fig. 3.2, some do have minor differences. Such minor differences include an extended coolant tube that helps decrease the amount of emission from the OH band and the insertion of a slot machined into the quartz coolant tube. This latter modification prevents light being emitted from the plasma from being absorbed or diffracted away from the detector. The one piece Fassel design also have the drawbacks of being difficult to manufacture because of the concentricity required, are not usually resistant to corrosive samples; for example, those that have hydrofluoric acid present and, if damaged, they often need replacing in their entirety or at least require repair from a skilled quartz worker. These drawbacks have led some manufacturers to preparing partially or even fully demountable torches. An example of such a device is shown in Fig. 3.3. The advantage of such a torch is that a different injector may be inserted depending on the sample type being analysed. Traditionally, the injector tube was manufactured from quartz but, as discussed previously, this is not resistant to hydrofluoric acid. Many manufacturers produce a range of injector type, some of which are still prepared from quartz, others are made from alumina, others from a different ceramic. As well as the different material used to manufacture the injector, the injector style may also differ widely. A typical Fassel injector has a bore of $1.5\text{--}1.8\text{ mm}$. This may block after extended aspiration of samples with substantial amounts of dissolved/suspended solid

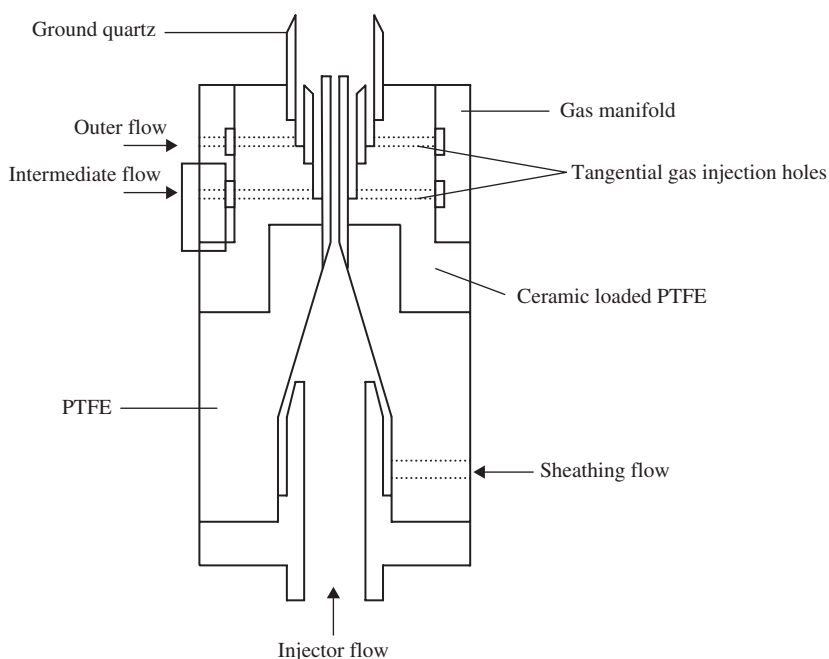


Figure 3.3 Schematic diagram of a demountable torch.

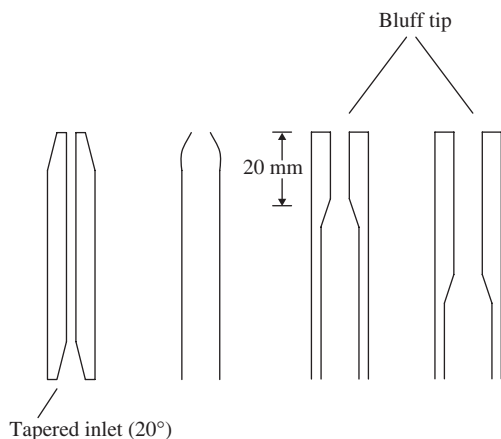


Figure 3.4 Different types of injector.

material, leading to extensive signal drift. Injector tubes with a wider bore are less likely to become blocked. These may therefore be used for much longer periods with this type of sample. The disadvantage of such injectors is that the cross section of the gas being pushed through the plasma is much larger, and hence successfully ‘punching’ the plasma can become troublesome. The internal shape of the injector can also affect the performance of the torch. Some designs are shown in Fig. 3.4. Dissolved solid material may become de-solvated and start to block some designs, especially those with sudden constrictions (e.g. design D). The laminar flow injector (design A) will enable the plasma to be ‘punched’ more readily, whilst its gently tapered design will inhibit blockage. The turbulent flow injector (design B) suffers the drawback of being easily devitrified. This means that it will have a shorter lifespan than other types. The effect of injector configuration has been exemplified recently in an article by Nham and Wiseman [51] who developed a torch for use with an axial instrument that was capable of aspirating 25% sodium chloride without blocking.

Several other modified or custom-built torches have been reported. These include fully demountable ones [52–54] and the mini- or micro-torches, otherwise known as low-flow torches. The advantage of the low-flow torches is that they consume substantially less argon and hence are cheaper to operate. The dimensions of these torches are much smaller than the standard ones, with the diameter of the coolant tube being 13 mm and the injector bore being 0.75 mm for the mini-torch [55]. This torch operated at a power of 1 kW and used a coolant flow of 81 min^{-1} argon. The micro-torch was smaller still and had a diameter of 9 mm and operated with a gas flow of 6.41 min^{-1} and at a power of 500 W [56]. The performance of these torches in terms of figures of merit were similar to the standard versions, but the reduced flow torches were more vulnerable to blockage from samples containing 1% m/m dissolved/suspended solid and also suffered from problems with respect to easily ionised elements. Yabuta and co-workers [57] have also developed a low-flow torch, that operates with a gas consumption of 51 min^{-1} and may be used with either argon, or with helium. The most recent advances in reduced gas flow torches have been summarised in a recent article by Klostermeier *et al.* [58]. This article also described a torch for use with an axial ICP-OES instrument that used a total of 11 min^{-1} argon in the plasma gas channel, but

with 40 l min^{-1} air as a coolant surrounding the whole torch. After ignition, the argon consumption was reduced to only 0.6 l min^{-1} . The power applied to form the plasma was in the range $0.75\text{--}1.2\text{ kW}$. LODs for seven elements were at or below the $\mu\text{g L}^{-1}$ level. Another approach to reducing argon consumption has been to use a water-cooled torch. This has been far from common, but an article by De Loos-Vollebregt and co-workers described a torch that used water as well as argon at a flow rate of 1.5 l min^{-1} as a coolant [59]. The plasma required modifications to be made to the load coil and sample introduction system, but at higher operating frequencies, the plasma yielded LODs similar to those obtained using conventional instrumentation.

There are also some very specialised torches that can be used for direct sample insertion or in-torch vaporisation. Here, a device onto which a sample has been placed, is inserted through the injector tube of the torch so that it becomes adjacent to the plasma. The sample becomes increasingly hot until it vaporises directly into the plasma. The insertion device is usually made either from graphite or from a very refractory metal. Examples of a rhenium in-torch vaporisation device have been described recently by Karanassios and co-workers [60,61]. Alternatively, Skinner and Salin [62] described the use of an automated pre-concentration system that deposited 15 ml of a solution metal chelates onto a direct sample insertion device made from graphite. The nebuliser entered the torch through a slot machined in the end of the coolant tube and sprayed the sample into the insertion device. The device was then heated inductively to evaporate the solvent, the nebuliser then removed, the plasma ignited and the cup raised into the plasma for AES analysis. Although the procedure was very lengthy (lasting 21 min), improvements in LODs of up to $34\,000$ were obtained. Either of these devices may be used for the direct analysis of solid samples, thereby avoiding the potential problems of contamination and the use of hazardous dissolution acids. Another advantage is that the sample has a 100% transport efficiency to the plasma, rather than the $1\text{--}2\%$ associated with conventional liquid nebulisation.

3.7 Spectrometers

3.7.1 Line isolation

The role of the spectrometer is to isolate the analytical wavelengths of interest from the light emitted from the plasma source. The vast majority of these wavelengths lie in the region of $160\text{--}860\text{ nm}$ and therefore a spectrometer should ideally be capable of determining all wavelengths in this region. Sensitivity may be enhanced at wavelengths below 200 nm by flushing the spectrometer with argon or nitrogen or by using a pump to evacuate it. This helps reduce the ingress of oxygen which may otherwise absorb the light emitted in this region of the spectrum. Some of the lines that most benefit by this include As at 193.696 and 188.979 nm and Al at 167.017 nm . Until the 1990s, the most common method for dispersion of the different wavelengths was by use of a grating, although older instruments used a prism or filters. These devices would enable only one wavelength to be focused to the detector at any one instant, before rotating to a different angle, thereby enabling another wavelength to be monitored. These devices therefore enable sequential monitoring of different wavelengths. Since the 1990s though, an alternate dispersion device has become used increasingly, since it enables numerous wavelengths to be monitored simultaneously. This obviously speeds up the rate of

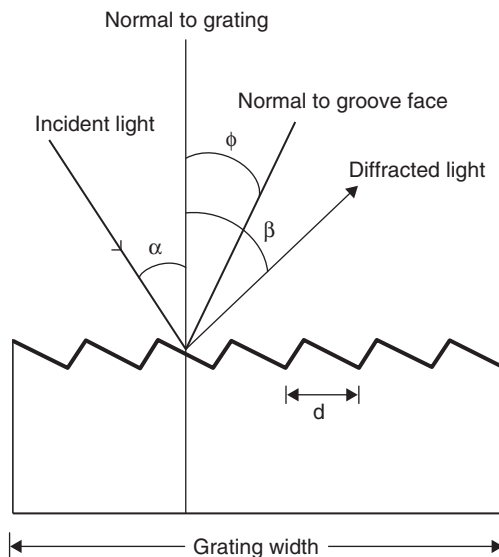


Figure 3.5 A blazed grating.

analysis and also enables real-time background correction. The device is called an echelle grating. This device will be discussed later in this section. Conventional gratings are usually of two sorts, ruled and holographic. They consist of a series of equidistant parallel grooves cut at an angle into the surface of a mirror. This is called the blazing of a grating. A schematic diagram of a blazed grating is shown in Fig. 3.5. The angle of the blaze determines the performance of the grating by reducing the problems associated with wavelengths of different orders overlapping. Light striking the grating will be diffracted to a degree that is dependent on its wavelength. The coverage of the entire spectrum may require the use of two different gratings. The density of the lines for ruled gratings is typically between 600 and 4200 lines mm^{-1} and it is this density of lines along with the focal length of the spectrometer that will determine the resolution of the instrument. A ruled grating is made by depositing a layer of aluminium on the grating blank and then using a diamond tool to rule the lines. This forms a master grating from which copies can easily be made. Modern instruments are more likely to use a holographic grating. This is made by coating the blank grating with a photosensitive material and then projecting the interference pattern of two coherent lasers to form the lines. The glass is then etched and the grating coated with aluminium to form a reflective surface. This type of grating is exceptionally free of 'ghosts' (false lines), leading to excellent stray light properties. The echelle spectrometer makes use of both a prism and a grating. Although the grating has typically only 100 lines mm^{-1} , it also has a larger angle of blaze. This means that it also has larger angles of diffraction and can be used in several spectral orders. For enhanced light transmission in the ultraviolet (UV) region, the prism is often replaced by a Schmidt cross-dispersion device. Overall, the resolution of an echelle grating is approximately an order of magnitude superior to most conventional gratings. A comparison of the two types is shown in Table 3.3. In every case, a line isolation device is present in all spectrometers.

Table 3.3 Comparison of echelle and conventional gratings

Feature	Conventional	Echelle
Focal length (m)	0.5	0.5
Groove density (lines/mm)	600–4200	75–100
Diffraction angle	10° 22′	63° 26′
Spectral order	1	~100
Resolution	62 400	75 8400
Resolving power (nm)	0.00481	0.000396

3.7.2 Monochromators

There are two broad classes of spectrometers in common use, namely monochromators and polychromators. Traditionally, the large majority of spectrometers have been sequential in nature; that is, they can only inspect one analytical wavelength at a time (hence the term monochromator). They can however scan to other wavelengths fairly rapidly. Despite the relative speed with which they can interrogate several lines, they are still much slower than a simultaneous instrument (using a polychromator). This means that sample introduction techniques that produce a transient signal (e.g. flow injection, laser ablation, electrothermal vapourisation, etc.), may only produce a signal that lasts long enough to measure one analyte. Repeat analysis of the same sample would have to be performed for other elements, which would increase the analysis time dramatically. For laser ablation, where a small amount of sample from one particular spot is used completely, the multiple sampling requirement may mean that unless the sample is completely homogeneous, effectively a different sample is analysed each firing of the laser. This means that surface mapping and depth profiling for several elements is impossible.

Background correction is very simple, but it must be stressed that the background emission and the analyte emission are measured separately and at a different time. ‘True’ background correction is therefore not available for this type of spectrometer. They have the advantage though of being able to scan to any wavelength between 160 and 860 nm so absolutely every analyte wavelength within this region is available for interrogation. They are also relatively cheap and simple to operate.

Monochromators come in two basic designs although others, far less common ones, have been developed. The Ebert monochromator makes use of a single, large front-silvered spherical mirror to focus the emitted radiation onto the grating and then re-focus only the wavelength of interest to the detector. Although very successful, the manufacture of a large single mirror was expensive and difficult. They have, therefore, largely been replaced by the Czerny-Turner style monochromator that makes use of two smaller mirrors. Schematic diagrams of these devices is shown in Fig. 3.6. Other monochromator devices have been devised, but are rarely used. Examples include the Seya-Namioka, which is used almost exclusively in the vacuum UV region (i.e. below 200 nm) and the Fastie-Ebert (which is a modified Ebert style). Boumans has given a good review of the optics of conventional monochromators [8].

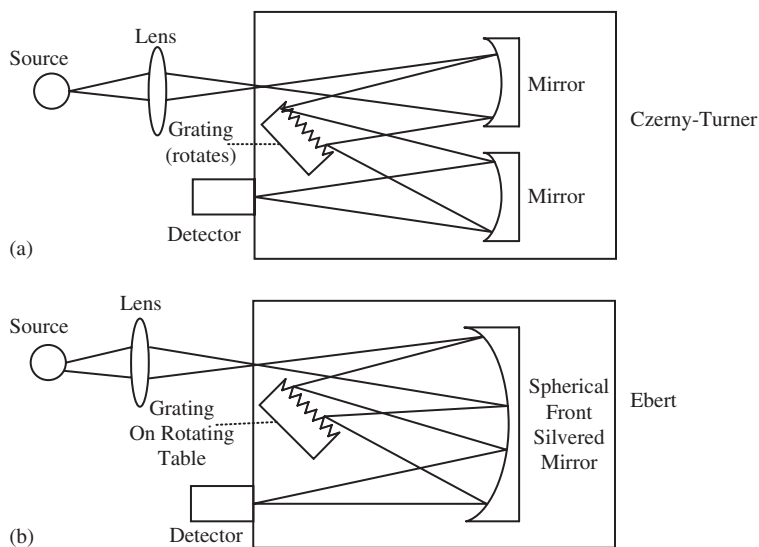


Figure 3.6 Schematic diagrams of Czerny-Turner and Ebert monochromators.

3.7.3 Polychromators

The advantage of polychromators is that they are capable of determining several analytes simultaneously. This has the advantages of giving a high sample throughput, lower running costs and the capability of using real-time background correction. In addition, the use of an IS is facilitated, which goes some way to overcome instrument drift and problems associated with the nebulisation of samples and standards that have a different viscosity/surface tension. The traditional polychromator was based on the Paschen-Runge design (depicted in Fig. 3.7). As can be seen, the line dispersive grating is still present, but rather than having only one exit slit through which the wavelength of interest is focused to the detector, there are several exit slits and several detectors all arranged at intervals around a Rowland circle. In this design, the grating is fixed on the periphery of the Rowland circle (i.e. it does not rotate). This means that the exit slits are therefore designed to allow only one specific wavelength each through to its respective detector. Since there is only a finite amount of space around the periphery of the Rowland circle, this means that the number of lines capable of being determined simultaneously is limited. A maximum of approximately 60 lines may be programmed at the time of manufacture, although most instruments use only about 30. Since the Paschen-Runge polychromator is so inflexible, the choice of lines must be made very carefully. If further lines are subsequently needed, then altering the device will prove very costly in terms of both time and expense. As can be seen in Fig. 3.7, the grating is also concave and the diameter of the Rowland circle is equal to the radius of curvature of the grating. The normal detector for monochromators and for the Paschen-Runge polychromator is the PMT. This will be discussed in more detail in the following section.

More recently, the echelle style polychromator has become extremely common with commercial instrumentation. A schematic diagram of this device is shown in Fig. 3.8. An echelle

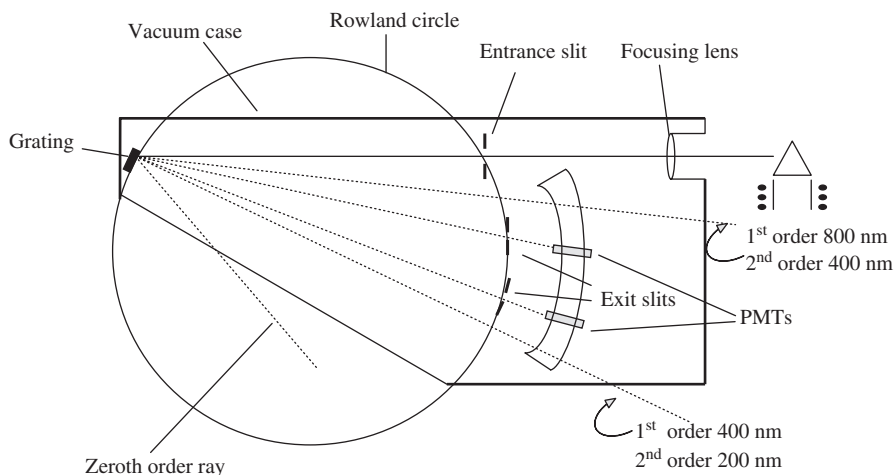


Figure 3.7 Paschen-Runge polychromator.

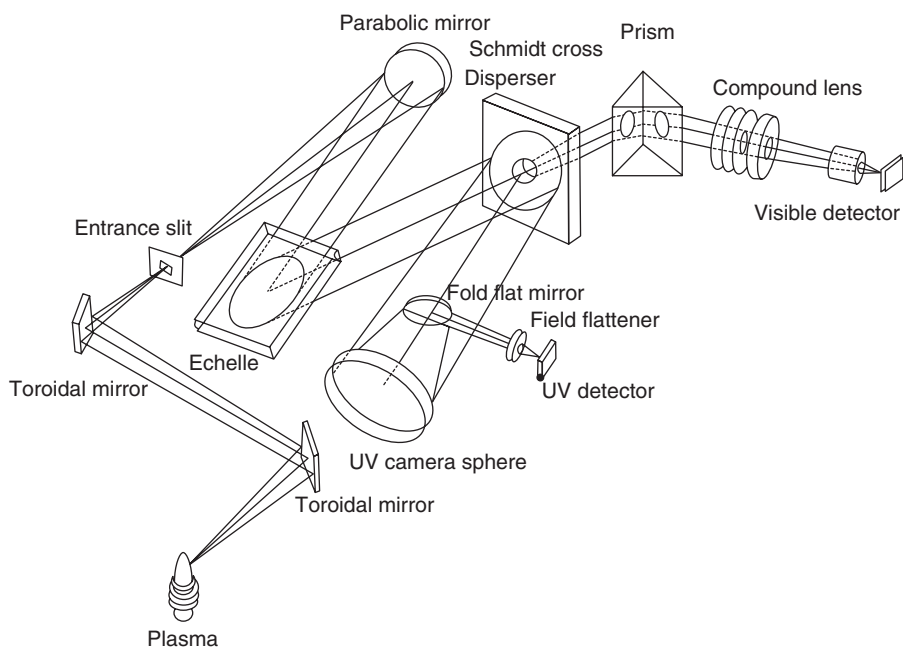


Figure 3.8 An echelle spectrometer.

instrument is far more flexible than the conventional Paschen-Runge polychromator. The echelle grating operates as described previously and diffracts light towards a Schmidt cross-disperser. This then separates the lines in the visible range of the spectrum from those in the UV. Light passing through the open centre of the optic passes to a visible detector, whilst

light reflecting from the surface of the disperser is sent to the UV detector. The surface of the Schmidt cross-disperser is a coarse grating with approximately $350\text{--}400\text{ lines mm}^{-1}$ and this separates the overlapping orders into a two-dimensional pattern, called either an echelle pattern or echellogram. Another function of the Schmidt cross-disperser is to correct for the spherical aberrations generated by the camera sphere mirror. An alternative to the Schmidt disperser is a prism. A standard prism would lose considerable energy in the UV region, but those made of calcium fluoride offer excellent UV efficiency. It achieves this because the surface of the disperser also has a small waveform on it. Other parts of the UV channel include a fold-flat mirror which deflects the UV light towards the detector and a field flattener which is a lens that ensures a good focus for the entire UV wavelength range to the detector. The visible channel of the spectrometer usually makes use of a prism to act as a further dispersion device. This too provides the two-dimensional echellogram and the light is focused using a compound lens to the detector. Two detectors are therefore necessary to cover the entire wavelength range of interest, one for the UV region and one for the visible. Instead of a PMT, that is the most common type of detector for monochromators and the Paschen-Runge polychromator, echelle spectrometers usually have a solid-state detector. There are different types of these, but they will be discussed in more detail in the following section.

3.8 Detectors

3.8.1 Photomultiplier tubes

PMTs have been used for many years as detectors for ICP-AES instrumentation. They come in two basic designs: side- and end-on viewed. An end-on viewed PMT is shown schematically in Fig. 3.9. It consists of a photo sensitive cathode and a series of dynodes, which are

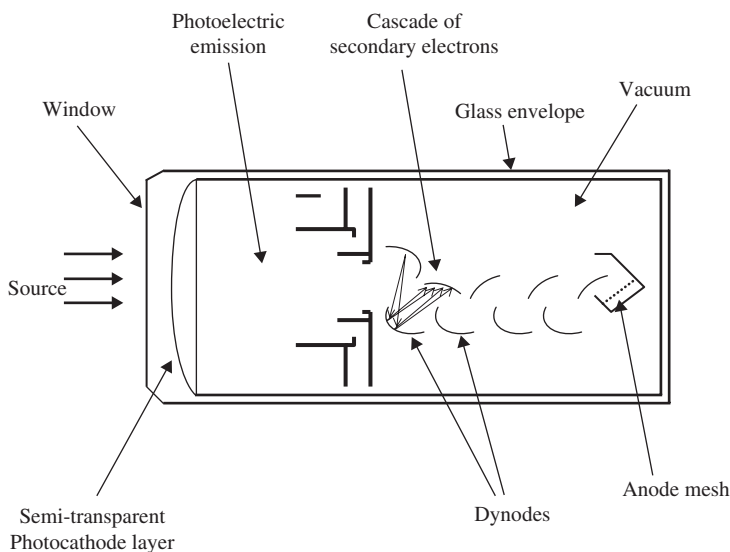


Figure 3.9 Schematic diagram of an end-on PMT.

set at increasingly positive potentials until an anode is reached. Light exits the spectrometer and strikes the cathode of the PMT. Since this is coated with a semi-conductor, it emits electrons which are accelerated down the dynode chain. Each time an electron impacts with a dynode, a number of secondary electrons are emitted. An avalanche effect is therefore established, which amplifies the signal by a factor of approximately 10^8 . By measuring the number of electrons arriving at the anode (i.e. the current), a proportional relationship between this and the number of photons impinging on the cathode (which will be proportional to the concentration of the analyte emitting those photons) can be made. Several semi-conductors have been used to coat the cathode. The most common has been gallium arsenide, because this has a relatively uniform response over a wide spectral range. Materials such as caesium–antimony or sodium–potassium–caesium–antimony compounds have also been used. These have different responses over different areas of the spectrum. Solar blind PMTs are specific for detection in the UV region. It should be noted that different semi-conductors are being developed continually and are being applied to PMT technology. In general, the goal is to improve the response time of the detector and to increase the dynamic range, sensitivity and signal-to-noise ratio.

It has been found that the end-on PMTs have a higher quantum efficiency than the side-on ones and therefore offer the opportunity for obtaining better LODs. The dark current of a PMT is the signal generated in the absence of any photons. It is caused by thermal excitation or by cosmic or radioactive rays. For superior LODs to be obtained, it is necessary to have as low a dark current as possible. Often, increasing the voltage applied to the detector increases the signal, but a concomitant increase in the dark current will manifest itself as noise and hence no overall improvement in LOD is obtained.

3.8.2 Solid-state detectors

Some of these devices were first developed over 30 years ago, but it has been only in the last 15 years that they have been used for ICP-AES instrumentation, largely for the echelle style spectrometers. The first generation of these was the one-dimensional photodiode array (PDA). The detectors were in a fixed position (just like a PMT), but they were much smaller and cheaper. Therefore, many more of them may be incorporated into a single instrument. PDAs had typically 1024 miniature detectors spread over a distance of 5–7 cm, that were capable of measuring energy over a wavelength range of 50–100 nm simultaneously. The next generation was charge-transfer devices. Charge-transfer devices is a general term for a selection of similar detectors. CCDs and CIDs have many similar attributes. Both use a metal oxide semi-conductor (MOS) to collect photo-generated charges. A detailed description of how these devices work is beyond the scope of this text, but effectively the CCD is *p*-doped whilst the CID are *n*-doped, meaning that the CCD collects electrons, whilst the CID collects holes. Early CCD detectors suffered from a problem of 'blooming'. Analytes at a very high concentration may overload a pixel and the charge would then spill over into adjacent pixels. This could potentially affect the accuracy of the determination. This problem has largely been overcome now by the use of mega-pixel detectors or by segmented CCD. SCDs are two-dimensional arrays of dimensions 13×18 mm. Unfortunately, they have the limitation of having only relatively few pixels on their surface (a few thousand). This means that although the whole spectral range can be covered, the number of analytical

lines available are fairly limited. The analyst therefore does not have complete freedom of line choice that PMT instruments could provide (e.g. if the concentration of one analyte was so large that a very insensitive alternative line was necessary), but instead could determine several analytes simultaneously. It should be noted though that such a detector is capable of determining three or four primary lines from each of approximately 70 analytes. Other advantages of this are that it had true random-access readout, a high quantum efficiency in the UV region and because it was segmented, there were no adjacent pixels for blooming to occur. Most of the noise associated with a CCD system comes from the electronics, but it also has a component from the plasma. CID systems have a much higher ($\times 10$) readout noise when compared with CCD, but do not suffer the problems of blooming. Therefore, many CID have a longer linear range when compared with CCD. The CID detectors also facilitate non-destructive readout thus allowing high-intensity signals to be acquired more frequently than lower-intensity signals which may be allowed to accumulate for longer periods to provide better signal-to-noise performance.

Quantum efficiency can be improved in many ways, but the most elegant (and most common nowadays) is by chemically removing the substrate layer (i.e. making it thinner), mounting it upside down and then illuminating it from behind. This has the effect of increasing the quantum efficiency, especially in the UV region, substantially. Front-illuminated CCD may be virtually blind below 400 nm, but the thinned, back-illuminated CCD may still have a quantum efficiency of about 40%, even at wavelengths as low as 200 nm. The newest generation of detectors (CCDs) have an array of 512×2048 pixels (i.e. a total of over 1 million pixels). These are powerful enough to determine any wavelength from around 160 to over 800 nm and have an extremely low-noise amplifier.

An excellent review of solid-state detectors, how they operate, their characteristics, flaws, etc. has been presented by Harnly and Fields [63]. Another excellent text discussing these detectors has been published in a book edited by Sweedler *et al.* [64].

Overall, both PMT and charge-transfer devices offer advantages and disadvantages. The PMT-based instruments tend to have lower background equivalent concentrations (and hence better LODs), as well as longer linear ranges. However, unless a true polychromator is used, PMT-operated instruments must act in a sequential manner. The poorer sensitivity of charge-transfer devices means however that longer counting times are required to obtain LODs equivalent to those obtained by a PMT. Therefore, although these devices are simultaneous, if low concentrations are being measured, it may take as long, if not longer to determine six to eight analytes as for a PMT-based spectrometer. Therefore, at low concentration, sample introduction techniques that produce transient signals may be equally disadvantaged for multi-element determination with both PMT and charge-transfer device detectors.

3.9 Nebulisers and spray chambers

This subject will be discussed in far more detail in Chapter 4. Essentially, the function of the nebuliser is to transform a stream of liquid sample into a nebular, a mist of droplets. There are numerous types of nebuliser available commercially. Some are specialised at the introduction of samples that have a high content of dissolved solid material and others specialise in samples that have a high level of suspended solid material. Either of these types of sample can lead to blockage of some types of pneumatic nebuliser. Some nebulisers

are self-aspirating (i.e. do not require the sample to be pumped to them), whereas others require introduction via a peristaltic pump. Many nebulisers have an optimum sample uptake rate of $1\text{--}1.5\text{ ml min}^{-1}$, whereas others can function perfectly adequately at an uptake rate of $30\text{--}50\text{ }\mu\text{l min}^{-1}$. Some nebulisers are made of glass, but others are made from an assortment of plastics so that samples containing corrosive acids may be aspirated. The type of nebuliser used will depend largely on the sample type. Although, as a general fail-safe, an analyst can use a plastic, high solids nebuliser and pump the sample to it at any rate required, the performance in terms of noise characteristics, LOD, precision, etc., is likely to be affected adversely.

The spray chamber has two basic functions. One is to separate the large droplets formed by the nebuliser from the smaller ones. The largest ones are removed to waste, whilst the smaller ones are caught in the nebuliser gas flow stream and are transported to the plasma. The transport efficiency will depend largely on the type of nebuliser and spray chamber being used, but is typically $1\text{--}2\%$ for an aqueous-based sample and somewhat higher for an organic solvent. Too much solvent entering the plasma will lead to instability and possible extinction. The other function of the spray chamber is to act as a dampener of any noise arising from sample introduction by a peristaltic pump. There are numerous types of spray chamber. Some are made of glass, others from plastics such as Ryton, so that corrosive samples may be analysed. Some have a very large surface area and volume, where sample can become trapped in dead-space, or where analyte can become adsorbed to the spray chamber surfaces. These large chambers act as better noise dampeners, but may lead to long wash out periods between samples. Others have a much smaller surface area and volume, and so they are more likely to lead to improved sensitivity and wash-out characteristics, but may also lead to a slightly noisier signal. Some spray chambers are surrounded by a jacket, through which a coolant solution flows. This tends to lead to increased stability since changes in temperature of the spray chamber will lead to differing amounts of sample nebular reaching the plasma. Again, the analyst's choice of spray chamber will depend largely on the application.

3.10 Read-out devices, instrument control and data processing

Detectors based on PMT devices produce an electrical current at the anode. This signal must then be converted into a form that may be used by either an analyst or a microcomputer. The signal is processed by an electronic circuit before it is measured by the read-out device. The electronic circuit amplifies the signal and then converts it via an analogue to digital converter (A/D converter) into a digital signal before inputting it into a microcomputer. It is the microcomputer that gives the read-out and processes all of the data. Data processing hardware for solid-state detectors is largely the same as for the PMT. These too need an A/D converter to produce data that may be understood by the computer.

Although many modern instruments have a powerful computing facility that stores results and creates reports, the data produced by PMT-based instrumentation is somewhat less flexible to manipulate post-analysis than those of the solid-state detectors. For instance, although the PMT will have detected the emission intensity at a given wavelength and perhaps also the background emission at adjacent wavelengths, it is very difficult to adjust the wavelength of the background correction slightly, if the analysts suddenly realises that it was

set incorrectly at the start of the experiment. In such cases, it may even be necessary to re-analyse the whole set of samples. For the solid-state detectors, especially the more recent ones that have a huge number of pixels, it is far more simple to re-calculate data from an experimental run without recourse to re-analysing the sample. Since an electronic photograph is essentially taken, then close to the entire spectrum can be stored on the computer and interrogated at a later date. This means that not only can background correction points be moved slightly to facilitate re-calculation of a more accurate answer, but also semi-quantitative data may be obtained for analytes that were not even on the original list. If for instance an analyst determined Cd, Cu, Pb and Zn in a series of samples, but the customer later asked for Mn too, then by simply inspecting a wavelength in the spectrum corresponding to Mn and observing the size of the emission intensity, a reasonable estimate of the Mn concentration can be made. This is especially true if one mixed standard containing all of the analytes of interest is analysed so that the scale of the Mn signal may be compared with those of the other analytes. This could potentially save the analyst a lot of time, and therefore money. Although this requires far more memory space on the computer, the advent of ever more powerful computers is making this less of a problem.

As well as performing all the data manipulation and calculations, the computer also controls the instrument data acquisition. Plasma conditions, that is power, gas flows, viewing height (if a radial ICP is being used), etc. are all controlled by the computer. Optimisation of these parameters is relatively straightforward if only one analyte is to be determined. However, since different analytes will have different optima, then a suite of analytes will usually require a compromise set of conditions. Many modern instruments have built-in algorithms that help the optimisation process. The computer will also control the autosampler and, since many autosamplers are capable of on-line dilution, then working standards may be made from one stock standard, and any sample found to have a greater concentration than the top standard may be diluted and re-analysed without any input from the analyst. Similarly, the computer may be programmed to run check standards intermittently. If these are found to drift significantly, the autosampler can be instructed to re-calibrate and then re-start analysing those samples that were after the last good check standard. Often, there are several other options available at this stage, so the analyst may choose the most favourable option from the outset. The computer therefore enables completely automated operation of the instrument. Once the data has all been acquired and the computer has performed the relevant calculations, including the calculation of concentrations, standard deviation and precision, the computer is also responsible for generating a report. The relevant data must therefore be easily down-loadable into standard word-processing and graphics packages.

Some instruments have software packages that are dedicated to the acquisition and data processing of chromatography data. Since speciation is an ever-increasing part of analytical chemistry, software specifically designed to measure time-resolved signals should be present. At worst, the instrument should have the facility to attach a chart recorder or an integrator so that a hard copy of a chromatogram can be obtained.

3. 11 Radial and axial plasmas

Traditionally, radial (side-viewed) plasmas were the norm, however in recent years, the use of axial (end-on viewed) plasmas have become very much more popular. In general, the

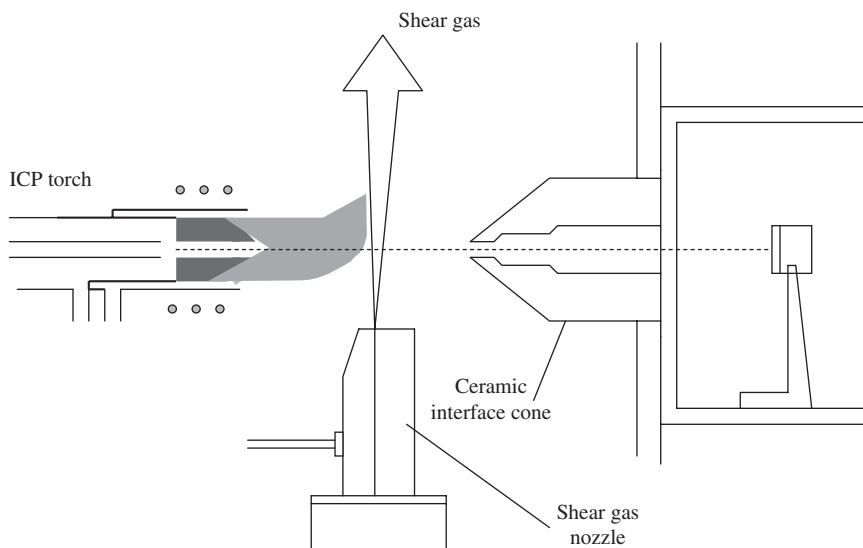


Figure 3.10 An axial ICP with shear gas.

components of each are the same, with both requiring a generator, a sample introduction system, a spectrometer, a detector and a data processing unit. The axial-viewed plasma requires either a perpendicular 'shear gas' flow that removes much of the cooler tail flame, hence removing the part of the plasma where most self-absorption occurs or, in some models, a cooled cone interface may be used. A schematic diagram of the shear gas interface is shown in Fig. 3.10. Both techniques have had their disadvantages; for example, the shear gas adds to the expense of gas consumption, whereas the cooled cone interface may suffer blockage if a sample with a very high dissolved (or suspended) solid content is analysed. These problems have largely been overcome now, with many instruments using air as the shear gas and reports of the cooled cone interfaces being capable of analysing 5% sodium chloride solution without blockage. The use of air as the shear gas will however preclude the use of lines below 190 nm. If the Al line at 167 nm is to be measured, then a shear gas of nitrogen or argon will be required. Since the flow rate of the shear gas is typically $15\text{--}20\text{ l min}^{-1}$, the gas expense would be increased considerably. The cooled cone interface uses a counter flow of argon at 2.5 l min^{-1} to displace the tail flame of the plasma away from the optical path, resulting in a longer linear range, fewer interferences and minimising wear on the interface and transfer optics. Overall, the axial plasma offers the advantage of improved LODs (typically by 4–10-fold), because the viewing volume has increased substantially. Historically, it was thought that by viewing the plasma end-on, that the dynamic range would decrease because of greater self-absorption (i.e. the plasma would be optically thick). Similarly, it was thought that there would also be a greater potential for interferences to be present and that axial systems would be limited to analysing very simple matrices (e.g. drinking water). Although it is true that the radial system gives the analyst more freedom in determining which part of the plasma the light is sampled from (which would enable them to overcome spatially dependent interferences) the problems forecast for the axial systems

have not really transpired. There has been some debate in the literature however on whether or not one configuration is any more prone to interference than the other [13,14].

3.12 Instrumentation for high-resolution spectrometry

Resolution is usually measured on the line width at half of the peak intensity. An article by Mermet has discussed the qualities related to spectra acquisition [65]. Most commercial instrumentation uses a focal length of between 0.50 and 0.75 m, and this supplies adequate resolution for most applications. Some instruments provide a longer focal length (e.g. 1.5 m), and these are more highly resolving, and hence suffer from fewer interferences. The determination of extremely line-rich analytes such as the rare earth elements or the actinides is an example, where peak overlap (interference) may occur. Resolving powers of 60 000 are typical for smaller monochromators, whereas an echelle style polychromator has a resolution of 10 times this. A 1.5 m monochromator may have a resolution of close to 500 000, depending on the number of lines blazed onto the grating. Some laboratories have reported the use of enormous monochromators (i.e. ones that have a focal length of 10 m). Although these are highly resolving, they obviously have limited use because of their sheer size and weight (they can weigh well over 100 kg). Long focal length monochromators must also be thermostated to a very precise temperature ($\pm 0.6^\circ\text{C}$) if large signal drift is not to be observed. Similarly, they are very susceptible to problems caused by vibration and are not suited to field or on-line applications. They do, however, cover large areas of the spectrum and are therefore flexible with the number of lines they can monitor. As an application, Zamzow and co-workers reported the use of an instrument that was sufficiently resolving to be able to separate the wavelengths associated with different isotopes of U around the 424.437 nm line [66]. There are other methods of obtaining high-resolution results. Baldwin *et al.* [67] described the use of an acousto-optic tunable filter (AOTF) interferometer used in combination with a Fabry-Perot interferometer. These two solid-state components were both developed for the communications industry, but offer several advantages for high-resolution spectroscopy when compared with the long focal length monochromators. Included in these advantages are their compact nature (<0.5 m), weight (<10 kg) and stability to both thermal and vibrational change. The AOTF acts as a pre-filter to select a narrow wavelength range from the polychromatic beam entering it. The output from the AOTF then enters the Fabry-Perot interferometer, where it is split into component wavelengths with very high resolution. The detailed description of how both components work may be found in the article by Baldwin and co-workers and the references therein.

It is worth noting that, as well as using sophisticated high-resolution instrumentation, interferences may be overcome by use of a chemometric technique such as Kalman filtering. An article by VanVeen and De Loos Vollebregt used Kalman filtering and found that it was far superior to the three-point background correction system and that LODs were improved by up to two orders of magnitude [68].

3.13 Micro-plasmas and plasma on a chip

Since 1999, a great deal of effort has gone into miniaturising plasmas so that they may be used on-line more readily as detectors for chromatographic separations, to make them

more portable, to consume less gas/power, etc. The overall advantages of this are that they are cheaper to operate and, since they can be mass produced, they are cheaper to purchase. This has led to the development of a wide range of miniature plasma types, including ICP, direct current plasma (DCP), microwave-induced plasma (MIP) and capacitively coupled plasmas. The use of these and others; for example, a dielectric barrier discharge, micro-hollow cathode discharge or a micro-structure electrode discharge, have been discussed by Karanassios [69]. This overview by Karanassios contains 94 references and discusses in detail the instrumentation required for these plasmas. Some of these plasmas have been formed in capillary tubes, whereas others have been formed on silicon chips. At present, there are fewer than 20 laboratories worldwide undertaking research into this area, but the publication rate has been prolific. Other reviews/overviews of this area have been published by Franzke and co-workers (56 references) [70], Broekaert and Siemens [71], who described recent developments in miniaturisation of hf plasmas, DC discharges and microwave plasmas and Broekaert (42 references) [72].

The plasmas have to be sufficiently robust to withstand the introduction of sample and sufficiently powerful to atomise/ionise the analyte efficiently. In addition, they must be confined to extremely small spaces so that damage to the chip or to the capillary is not inflicted. The first researchers to describe the application of plasmas on a chip for analytical applications was Eijkel and co-workers [73,74]. As stated previously, many of these plasmas are used as a detector for gas chromatography or for gaseous compounds. The experimental setup in the first article, is shown schematically in Fig. 3.11 and a schematic of the glass chip is shown in Fig. 3.12. In this article, the DC helium plasma was confined to a 50 nl chamber on a glass chip. Methane was the analyte and could be detected with a LOD of 600 ppm

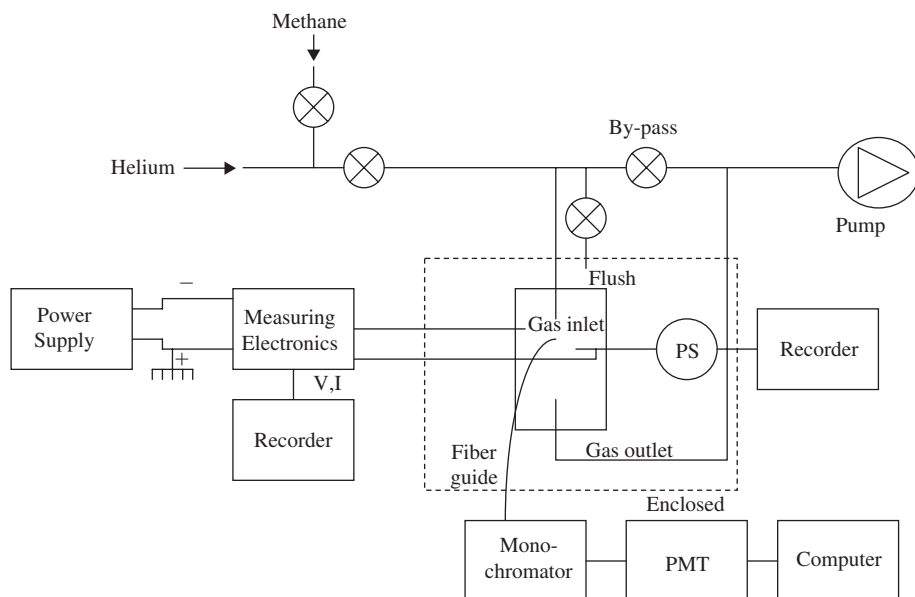


Figure 3.11 Block diagram of the measurement setup. PS: Pressure sensor; PMT: Photomultiplier tube.

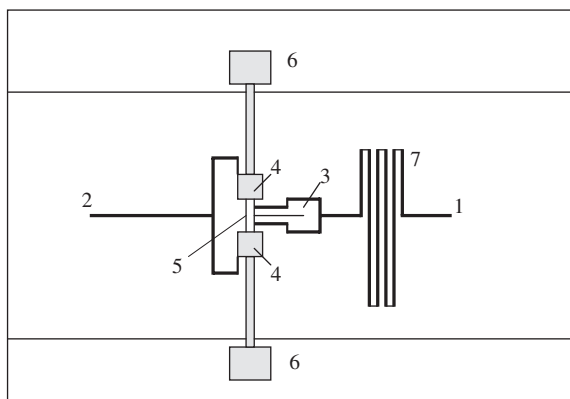


Figure 3.12 Schematic of the chip layout. 1: Gas inlet; 2: Gas outlet; 3: Pressure sensor connection; 4: Electrodes; 5: Plasma chamber; 6: Electrode connection pads; 7: Inlet channel; 8: Outlet channel.

($3 \times 10^{12} \text{ gs}^{-1}$) by monitoring the emission of the CH radical at 431.3 nm. The second article used gas chromatography to separate a mixture of five alcohols (methanol–1-pentanol) and hexane. A DC glow discharge was generated using 9 mW applied to helium flowing at 320 nl s^{-1} in a 180 nl chamber and the six C containing compounds were detected by measurement at 519 nm. The authors reported that some peak broadening was observed when compared with the response from a conventional flame ionisation detector, which was attributed to areas of dead volume, but that the response of the device remained stable over a period of at least 24 h.

Since these original articles, a plethora of others has been published that report the development of assorted plasma types in chips or in capillaries. An article by Minayeva and Hopwood described a micro-fabricated ICP on a chip for the detection of sulphur dioxide [75]. The system consisted of a planar plasma source on a glass wafer and a miniature aluminium vacuum chamber. The plasma operated at a pressure of 0.1–10 torr, a frequency of 493 MHz and at a power of 4 W. These authors reported that LODs improved with increasing power and increasing pressure; with the best LOD obtained being 45 ppb. The same authors have used Langmuir probe diagnostics on a similar plasma [76]. The neutral gas temperature was found to be nearly equal to room temperature. In addition, it was shown that between 2% and 18% of the power applied to the micro-structure was absorbed by the discharge and that the transfer of power to the discharge was most efficient at low pressure. Bass *et al.*, reported the use of a capacitively coupled helium plasma on a quartz wafer that operated at atmospheric pressure, at a frequency of 13.56 MHz, a power of 5–25 W and with a gas flow of between 17 and 150 ml min^{-1} [77]. The authors stated that the capacitive power coupling was ideal for ‘plasma on a chip’ applications because it did not require tuning or resonant structures. Schermer and co-workers described the formation of a 2.45 GHz argon-based microstrip plasma operating at atmospheric pressure for the determination of gaseous Hg species [78]. The plasma was sustained on a sapphire substrate. The authors optimised the operating conditions, for example gas flow rates ($15\text{--}60 \text{ l h}^{-1}$) and power (5–40 W), and reported that under optimal conditions, an LOD of less than 10 ng Hg l^{-1} Ar was obtainable. By introducing ferrocene into the plasma, the authors used emission from Fe as a

thermometric means to determine excitation temperatures (6000–7000 K for 10–40 W and 151h^{-1}). One of the most recent publications in this area has been by Houk's group, who generated a rf plasma in a polydimethylsiloxane chip [79]. The argon plasma operated at atmospheric pressure and with a power of 70 W at a frequency of 27.12 MHz. The plasma was viewed axially through a purged fibre optic cable. The analytical species was CF_4 at 0.1% in argon. The authors reported the chip as being easy to manufacture, to be inexpensive and being a polymer, to be more resistant to fluorocarbon gases than silicon-based chips. They speculated that it could find use in the semi-conductor industry.

References

1. Ebdon, L., Evans, E.H., Fisher, A. and Hill, S.J. (1998) *An Introduction to Analytical Atomic Spectrometry*, John Wiley, Chichester, UK.
2. Sharp, B.L. (1988) Pneumatic nebulisers and spray chambers for inductively coupled plasma spectrometry: a review. Parts 1 and 2. *J. Anal. Atom. Spectrom.*, **3**, 613–652; 939–963.
3. Mora, J., Maestre, S., Hernandis, B. and Todoli, J.L. (2003) Liquid-sample introduction in plasma spectrometry. *TrAC – Trend. Anal. Chem.*, **22**, 123–132.
4. Taylor, A. (2005) 'Quality Assurance' in *Encyclopedia of Analytical Science*, 2nd Edition. P. Worsfold, A. Townshend and C. Poole Eds. Elsevier Academic Press, Oxford, UK.
5. Sargent, M. and MacKay, G. (Eds.) (1995) *Guidelines for Achieving Quality in Trace Analysis*, Royal Society of Chemistry, Cambridge.
6. Gold, V., Loening, K.L., McNought, A.D. and Sehmi, P. *Compendium of Chemical Terminology, IUPAC Recommendations*, Blackwell Press, 1987.
7. Miller, J.N. and Miller, J.C. (2005) *Statistics and Chemometrics for Analytical Chemistry*, Pearson/Prentice Hall, Harlow, UK.
8. Boumans, P.W.J.M. (1987) Basic concepts and characteristics of ICP-AES. In *Inductively Coupled Plasma Emission Spectrometry, Part I Methodology, Instrumentation and Performance* (Ed. P.W.J.M. Boumans), Wiley-Interscience, New York.
9. Thompson, M. (1992) Analytical performance. In *Inductively Coupled Plasmas in Analytical Atomic Spectrometry* (Eds. A. Montaser and G.W. Golightly), VCH publishers, New York.
10. Jarvis, K.E., Gray, A.L. and Houk, R.S. (1992) *Handbook of Inductively Coupled Plasma Mass Spectrometry*, Blackie, Glasgow.
11. Silva, J.C.J., Santos, D.M., Cadore, S., Nobrega, J.A. and Baccan, N. (2004) Evaluation of inductively coupled plasma optical emission spectrometers with axial configuration: interfaces with end-on gas and shear gas. *Microchem. J.*, **77**, 185–190.
12. Iglesias, M., Vaculovic, T., Studynkova, J., Poussel, E. and Mermet, J.M. (2004) Influence of the operating conditions and of the optical transition on non-spectral matrix effects in inductively coupled plasma atomic emission spectrometry. *Spectrochim. Acta B*, **59**, 1841–1850.
13. Brenner, I.B. and Zander, A.T. (2000) Axially and radially viewed inductively coupled plasmas – a critical review. *Spectrochim. Acta B*, **55**, 1195–1240.
14. Dubuisson, C., Poussel, E. and Mermet, J.M. (1997) Comparison of axially and radially viewed ICP-AES in terms of signal-to-background ratio and matrix effects – plenary lecture. *J. Anal. Atom. Spectrom.*, **12**, 281–286.
15. Browner, R.F. and Boorn, A. (1982) Effects of organic-solvents in inductively coupled plasma atomic emission spectrometry. *Anal. Chem.*, **54**, 1402–1410.
16. Hu, Z.C., Hu, S.H., Gao, S., Liu, Y.S. and Lin, S.L. (2004) Volatile organic solvent induced signal enhancements in inductively coupled plasma – mass spectrometry: a case study of methanol and acetone. *Spectrochim. Acta B*, **59**, 1463–1470.

17. Ebdon, L., Foulkes, M.E. and Hill, S.J. (1989) Fundamental and comparative studies of aerosol sample introduction for solutions and slurries in atomic spectrometry. *Microchem. J.*, **40**, 30–64.
18. Desboeufs, K.V., Losno, R. and Colin, J.L. (2003) Figures of merit of pneumatic and ultrasonic sample introduction systems in inductively coupled plasma multi-channel-based emission spectrometry in an ultra clean environment. *Anal. Bioanal. Chem.*, **375**, 567–573.
19. Poitrasson, F. and Dundas, S.H. (1999) Direct isotope ratio measurement of ultra-trace lead in waters by double focussing ICP-MS with an ultrasonic nebuliser and a desolvation unit. *J. Anal. Atom. Spectrom.*, **14**, 1573–1577.
20. Grotti, M., Lagomarsino, C. and Frache, R. (2005) Multivariate study in chemical vapour generation for simultaneous determination of As, Sb, Bi, Te, Sn, Se, Te and Hg by ICP-OES. *J. Anal. Atom. Spectrom.*, **20**, 1365–1373.
21. Yang, L., Willie, S. and Sturgeon, R.E. (2005) Ultra-trace determination of mercury in water by cold vapour generation ID-MS. *J. Anal. Atom. Spectrom.*, **20**, 1226–1231.
22. Tao, S.Q. (1996) Development of novel methods for sample introduction via in-situ chemical reaction in ICP-AES and their applications. *Bunseki Kagaku*, **45**, 895–896.
23. Goitom, D., Bjorn, E., Frech, W. and de Loos-Vollebregh, M.T.C. (2005) Radial ICP characteristics for ICP-AES using direct injection or microconcentric nebulisation. *J. Anal. Atom. Spectrom.*, **20**, 645–651.
24. O'Brien, S.A.E., Chirinos, J.R., Jorabchi, K., Kahen, K., Cree, M.E. and Montaser, A. (2003) Investigation of the high efficiency nebuliser for axially and radially viewed ICP-AES. *J. Anal. Atom. Spectrom.*, **18**, 910–916.
25. Greenfield, S., Jones, I.L.I.W., Berry, C.T. and Spash, D.I. (1968) Improvements relating to spectroscopic methods and apparatus. British Patent No.1,109,602; Greenfield, S., Jones, I.L.I.W. and Berry, C.T. (1969) Plasma light source for spectroscopic investigation. US Patent No.3,467,471.
26. Zhang, X.H., Chen, D., Marquardt, R. and Koropchak, J.A. (2000) Thermospray sample introduction to atomic spectrometry. *Microchem. J.*, **66**, 17–53.
27. Huan, Y.F., Zheng, J., Feng, G.D., Zhou, J.G., Zhang, H.Q. and Jin, Q.H. (2003) New advances in solution sample introduction methods for plasma atomic spectrometry. *Chinese J. Anal. Chem.*, **31**, 490–495.
28. Ding, L., Wang, S.T., Ren, N.Q., Zhang, H.Q. and Jin, Q.H. (2003) Comparison of a low microwave-powered thermospray nebulizer and a Meinhard-pneumatic nebulizer for inductively coupled plasma-atomic emission spectrometry. *Chinese J. Anal. Chem.*, **31**, 1458–1461.
29. Mermet, J.M. (2002) Trends in instrumentation and data processing in ICP-AES – plenary lecture. *J. Anal. Atom. Spectrom.*, **17**, 1065–1071.
30. Mermet, J.M. (2004) Potential of time correlation to improve limits of detection in ICP-AES. *Can. J. Anal. Sci. Spect.*, **49**, 414–422.
31. Hoffmann, D.L., Richards, D.A., Elliott, T.R., Smart, P.L., Coath, C.D. and Hawkesworth, C.J. (2005) Characterisation of secondary electron multiplier nonlinearity using MC-ICPMS. *Int. J. Mass Spectrom.*, **244**, 97–108.
32. Montaser, A. and Golightly, G.W. (Eds.) (1992) *Inductively Coupled Plasmas in Analytical Atomic Spectrometry*, VCH publishers, New York.
33. Quevauviller, P. (2001) Accuracy and traceability in speciation analysis. In *Trace Element Speciation* (Eds. L. Ebdon, L. Pitts, R. Cornelis, H. Crews, O.F.X. Donard and P. Quevauviller), Royal Society of Chemistry, Cambridge, UK.
34. Carre, M., Excoffier, S. and Mermet, J.M. (1997) Study of the relation between the limit of detection and the limit of quantification in inductively coupled plasma spectrochemistry. *Spectrochim. Acta B*, **52**, 2043–2049.
35. Clough, R., Belt, S.T., Fairman, B., Catterick, T. and Evans, E.H. (2005) Uncertainty contributions to single and double isotope dilution mass spectrometry with HPLC-CV-MC-ICP-MS for the determination of methylmercury in fish tissue. *J. Anal. Atom. Spectrom.*, **20**, 1072–1075.

36. Marcos, A., Foulkes, M. and Hill, S.J. (2001) Application of a multi-way method to study long-term stability in ICP-AES. *J. Anal. Atom. Spectrom.*, **16**, 105–114.
37. Niemala, M., Kola, H., Peramaki, P., Piispanen, J. and Poikolainen, J. (2005) Comparison of microwave-assisted digestion methods and selection of internal standards for the determination of Rh, Pd and Pt in dust samples by ICP-MS. *Microchim. Acta*, **150**, 211–217.
38. Kahen, K., Acon, B.W. and Montaser, A. (2005) Modified Nukiyama-Tanasawa and Rizk-Lefebvre models to predict droplet size for microconcentric nebulizers with aqueous and organic solvents. *J. Anal. Atom. Spectrom.*, **20**, 631–637.
39. Chan, G.C.Y and Chan, W.T. (2003) Plasma related matrix effects in inductively coupled plasma – atomic emission spectrometry by group I and group II matrix-elements. *Spectrochim. Acta B*, **58**, 1301–1317.
40. Lehn, S.A., Huang, M., Warner, K.A., Gamez, G. and Hieftje, G.M. (2003) Spatially resolved ground-state number densities of calcium and strontium ion in an inductively coupled plasma in contact with an inductively coupled plasma mass spectrometry sampling interface. *Spectrochim. Acta B*, **58**, 1647–1662.
41. Spillane, D.E.M., Snook, R.D., Thorne, A.P. and Wheaton, J.E.G. (1987) Preliminary-results with a high-resolution inductively coupled plasma Fourier-transform spectrometer. *J. Anal. Atom. Spectrom.*, **2**, 591–594.
42. Schierle, C. and Thorne, A.P. (1995) Inductively-coupled plasma Fourier-transform spectrometry – a study of element spectra and a table of inductively-coupled plasma lines. *Spectrochim. Acta*, **50B**, 27–50.
43. Houk, R.S. and Zhai, Y. (2001) Comparison of mass spectrometric and optical measurements of temperature and electron density in the inductively coupled plasma during mass spectrometric sampling. *Spectrochim. Acta B*, **56**, 1055–1067.
44. Evans, E.H. and Giglio, J.J. (1993) Interferences in inductively coupled plasma mass-spectrometry – a review. *J. Anal. Atom. Spectrom.*, **8**, 1–18.
45. Shao, Y. and Horlick, G. (1991) Recognition of mass spectral interferences in inductively coupled plasma-mass spectrometry. *Appl. Spectrosc.*, **45**, 143–147.
46. Rattanachongkiat, S., Millward, G.E. and Foulkes, M.E. (2004) Determination of arsenic species in fish, crustacean and sediment samples from Thailand using high performance liquid chromatography (HPLC) coupled with inductively coupled plasma mass spectrometry (ICP-MS). *J. Environ. Monit.*, **6**, 254–261.
47. Koppelaar, D.W., Eiden, G.C. and Barinaga, C.J. (2004) Collision and reaction cells in atomic mass spectrometry: development, status and applications. *J. Anal. Atom. Spectrom.*, **19**, 561–570.
48. McCurdy, E. and Woods, G. (2004) The application of collision/reaction cell ICP-MS to multi-element analysis in variable sample matrices, using He as a non-reactive cell gas. *J. Anal. Atom. Spectrom.*, **19**, 607–615.
49. Sutton, K., Sutton, R.M.C. and Caruso, J.A. (1997) Inductively coupled plasma mass spectrometric detection for chromatography and capillary electrophoresis. *J. Chrom. A*, **789**, 85–126.
50. Bacon, J.R., Linge, K.L. and Van Vaeck, L. (2005) Atomic spectrometry update. Atomic mass spectrometry. *J. Anal. Atom. Spectrom.*, **20**, 763–802.
51. Nham, T.T. and Wiseman, A.G. (2003) A new torch for analysis of samples having exceptionally high total dissolved solids by axially-viewed inductively coupled plasma optical emission spectrometry. *J. Anal. Atom. Spectrom.*, **18**, 790–794.
52. Ebdon, L., Mowthorpe, D.J. and Cave, M.R. (1980) A versatile new torch for inductively coupled plasma spectrometry. *Anal. Chim. Acta*, **115**, 171–178.
53. Boumans, P.W.J.M. and Lux-Steiner, M.Ch. (1982) Modification and optimization of a 50 MHz inductively coupled argon plasma with special reference to analyses using organic-solvents. *Spectrochim. Acta*, **37B**, 97–126.

54. Brenner, I.B. and Dorfman, E. (1995) Application of conventional and low-flow torches for the analysis of xylene-based and tetralin-based petroliferous materials by argon and oxygen-argon ICP-AES. *Microchem. J.*, **52**, 81–95.
55. Savage, R.N. and Hieftje, G.M. (1981) Characteristics of the background emission-spectrum from a miniature inductively-coupled plasma. *Anal. Chim. Acta*, **123**, 319–324.
56. Weiss, A.D., Savage, R.N. and Hieftje, G.M. (1981) Development and characterization of a 9-mm inductively-coupled argon plasma source for atomic emission-spectrometry. *Anal. Chim. Acta*, **124**, 245–258.
57. Yabuta, H., Miyahara, H., Watanabe, M., Hotta, E. and Okino, A. (2002) Design and evaluation of dual inlet ICP torch for low gas consumption. *J. Anal. Atom. Spectrom.*, **17**, 1090–1095.
58. Klostermeier, A., Engelhard, C., Evers, S., Sperling, M. and Buscher, W. (2005) New torch design for inductively coupled plasma optical emission spectrometry with minimised gas consumption. *J. Anal. Atom. Spectrom.*, **20**, 308–314.
59. De Loos-Vollebregt, M.T.C., van Houtte, C.N. and Tiggelman, J.J. (1991) Analytical evaluation of a water-cooled low gas-flow torch for inductively coupled plasma atomic emission-spectrometry. *J. Anal. Atom. Spectrom.*, **6**, 323–328.
60. Badiei, H.R., Smith, A.T. and Karanassios, V. (2002) Rhenium-cup, in-torch vaporization (ITV) sample introduction for axially viewed ICP-AES and its application to the analysis of a microscopic, ng-weight solid sample. *J. Anal. Atom. Spectrom.*, **17**, 1030–1036.
61. Smith, A.T., Badiei, H.R., Evans, J.C. and Karanassios, V. (2004) Simultaneous determination of the Cd and Zn total body burden of individual, nearly microscopic, nanoliter-volume aquatic organisms (*Hyalella azteca*) by rhenium-cup in-torch vaporization (ITV) sample introduction and axially viewed ICP-AES. *Anal. Bioanal. Chem.*, **380**, 212–217.
62. Skinner, C.D. and Salin, E.D. (2003) Preconcentration and adsorption of metal chelates with analysis by direct sample insertion inductively coupled plasma atomic emission spectrometry. *J. Anal. Atom. Spectrom.*, **18**, 495–500.
63. Harnly, J.M. and Fields, R.E. (1997) Solid state array detectors for analytical spectrometry. *Appl. Spectrosc.*, **51**(9), A334–A351.
64. Sweedler, J.V., Ratzlaff, K.L. and Denton, M.B. (Eds.) (1994) *Charge Transfer Devices in Spectroscopy*, VCH publishers, New York.
65. Mermet, J.M. (2001) Qualities related to spectra acquisition in inductively coupled plasma-atomic emission spectrometry. *Spectrochim. Acta B*, **56**(9), 1657–1672.
66. Zamzow, D., Murray, G.M., D'Silva, A.P. and Edelson, M.C. (1991) High-resolution optical-emission spectroscopy of uranium hexafluoride in the argon afterglow discharge. *Appl. Spectrosc.*, **45**(8), 1318–1321.
67. Baldwin, D.P., Zamzow, D.S. and D'Silva, A.P. (1991) High-resolution spectroscopy using an acousto-optic tunable filter and a fiber-optic Fabry-Perot interferometer. *Appl. Spectrosc.*, **50**(4), 498–503.
68. VanVeen, E.H. and De Loos Vollebregt, M.T.C. (1991) Kalman filtering for data reduction in inductively coupled plasma atomic emission-spectrometry. *Anal. Chem.*, **63**(14), 1441–1448.
69. Karanassios, V. (2004) Microplasmas for chemical analysis: analytical tools or research toys? *Spectrochim. Acta B*, **59**, 909–928.
70. Franzke, J., Kunze, K., Miclea, M. and Niemax, K. (2003) Microplasmas for analytical spectrometry. *J. Anal. Atom. Spectrom.*, **18**, 802–807.
71. Broekaert, J.A.C. and Siemens, V. (2004) Some trends in the development of microplasmas for spectrochemical analysis. *Anal. Bioanal. Chem.*, **380**, 185–189.
72. Broekaert, J.A.C. (2002) The development of microplasmas for spectrochemical analysis. *Anal. Bioanal. Chem.*, **374**, 182–187.
73. Eijkel, J.C.T., Stoei, H. and Manz, A. (1999) A molecular emission detector on a chip employing a direct current microplasma. *Anal. Chem.*, **71**, 2600–2606.

-
74. Eijkel, J.C.T., Stoeri, H. and Manz, A. (2000) A dc microplasma on a chip employed as an optical emission detector for gas chromatography. *Anal. Chem.*, **72**, 2547–2552.
 75. Minayeva, O.B. and Hopwood, J.A. (2003) Microfabricated inductively coupled plasma-on-a-chip for molecular SO₂ detection: a comparison between global model and optical emission spectrometry. *J. Anal. Atom. Spectrom.*, **18**, 856–863.
 76. Minayeva, O.B. and Hopwood, J. (2003) Langmuir probe diagnostics of a microfabricated inductively coupled plasma on a chip. *J. Appl. Phys.*, **94**, 2821–2828.
 77. Bass, A., Chevalier, C. and Blades, M.W. (2001) A capacitively coupled microplasma (CC μ P) formed in a channel in a quartz wafer. *J. Anal. Atom. Spectrom.*, **16**, 919–921.
 78. Schermer, S., Bings, N.H., Bilgic, A.M., Stories, R., Voges, E. and Broekaert, J.A.C. (2003) An improved microstrip plasma for optical emission spectrometry of gaseous species. *Spectrochim. Acta*, **58**, 1585–1596.
 79. Lim, H.B., Kim, D., Jung, T., Houk, R.S. and Kim, Y. (2005) A radiofrequency plasma in a polydimethylsiloxane (PDMS) microchip. *Anal. Chim. Acta*, **545**, 119–121.

Chapter 4

Aerosol Generation and Sample Transport

Barry L. Sharp and Ciaran O' Connor

4.1 Introduction

Sample introduction is the principal means by which the analyst can tailor the performance of inductively coupled plasma–atomic emission spectrometry or mass spectrometry (ICP-AES or MS) to particular analytical tasks. Whereas formerly sample introduction was seen as a limiting part of the instrumentation, now it is this aspect that brings enormous versatility to the applications of these techniques. Interfaces for solid, liquid and gaseous samples have been described and in turn these have been coupled to a variety of separation techniques including gas chromatography (GC), liquid chromatography (LC), capillary electrophoresis (CE), gel plates and field flow fractionation. Developments in sample introduction for the ICP source have been largely responsible for bringing about convergence between the historically separate fields of elemental and organic analysis.

General accounts of sample introduction have been provided by several authors including, for liquids: Browner [1], Montaser [2], Sharp [3,4] and Mora [5]; and for solids Durrant [6], Russo [7] and Günther [8].

4.2 Sample introduction characteristics of the ICP source

4.2.1 Particle size distribution

The convention in discussing the sample aerosol is to describe the aerosol produced by the aerosol generator as the *primary aerosol*, and that entering the plasma as the *tertiary aerosol* [1,9]. It is important in any discussion of sample introduction techniques to remember that the ICP only responds to the latter, having no knowledge of any prior process.

Sample material entering the central channel of the ICP source will experience a temperature of 6–7000 K for a period of a few milliseconds [10,11]. The consequence of this is that there is a maximum size of particle that can be processed by the plasma to yield a homogeneous vapour, representative of the bulk sample composition, that can be efficiently excited and ionized. The exact particle diameter is not known and will vary depending on composition, but is generally agreed that for solution nebulisation (SN) 10 μm is close to the upper limit with particle size closer to 1 μm being preferred [12]. A high speed photographic study has shown unprocessed particles from conventional pneumatic nebulization

surviving in the Ar plasma [13]. A narrow particle size distribution is also advantageous since it facilitates optimization in terms of the height of viewing (AES), or depth of sampling (MS), provides a uniformity to the pattern of matrix interferences, and maximizes the signal-to-noise ratio [14]. Hobbs and Olesik studied the fate of individual particles passing through the ICP and provided a useful model of desolvating/vaporizing particles and their effect on the local plasma conditions and the observed analytical signal [15].

Recent work in the field of laser ablation (LA) has suggested that for the plasma to process particles in a truly composition independent fashion requires particles < 90 nm in size (based on the analysis of glass) [16]. This is well below the median diameter of the particle size distributions produced by common sample introduction systems and is therefore an impractical working standard. It is a further reminder however that the analytical signal is heavily dependent on the nature of the sample introduction process and reflects nuances that are not always obvious from cursory observation. Careful calibration, with appropriate attention to solvents and matrix composition, is required to control these subtle and sometimes unsuspected variances.

Although it is convenient to discuss particle size distributions in terms of particle diameter, the analytical signal is dependent on the mass distribution which introduces a ' d^3 ' term into the equation. It is worth noting that a $10\text{ }\mu\text{m}$ particle, which is only marginally transported and processed by the sample introduction system and plasma, contains 1000 times the analyte of the more desirable $1\text{ }\mu\text{m}$ particle. Thus, any tendency to polydispersity above a few microns is highly detrimental. Another common measure of particle size is the volume-to-surface area mean diameter or Sauter mean diameter given the symbol $D_{3,2}$ [1]. See Section 4.3.1 for some typical particle size distributions.

4.2.2 Plasma loading

The ICP is a remarkably robust source, not least because power is not directly coupled into the central channel where the sample is introduced. Nevertheless, for a given plasma power there is a maximum plasma loading that can be tolerated, above this level the plasma robustness is reduced leading to a greater propensity for matrix interferences and ultimately instability and extinction of the discharge [17]. A typical nebulizer and spray chamber combination will deliver about $20\text{ }\mu\text{l min}^{-1}$ (20 mg min^{-1}) of liquid aerosol to the plasma accompanied by an equivalent mass flux of vapour. Fig. 4.1 shows the achievable vapour loading at saturation for 1 l min^{-1} of argon (a typical sample introduction flow rate) at various temperatures. Saturation of the liquid aerosol with vapour is guaranteed by the large surface area of the aerosol and the increased vapour pressure inside the droplets due to the surface tension. The maximum rate of sample input for an aqueous aerosol has not been investigated as such, but indirect evidence from using more efficient types of sample introduction (e.g. the ultrasonic nebulizer, USN) suggest that the maximum lies within a factor of ~ 5 of this typical value. Practically the limit is more likely to be set by matrix problems rather than simple liquid flux.

The distribution between the condensed phase and the vapour phase of the sample is critical in determining how the plasma handles the sample. It is possible to inject quite large amounts of solid refractory material through the central channel (though not analytically useful) without extinguishing the plasma provided that the radio frequency (rf)

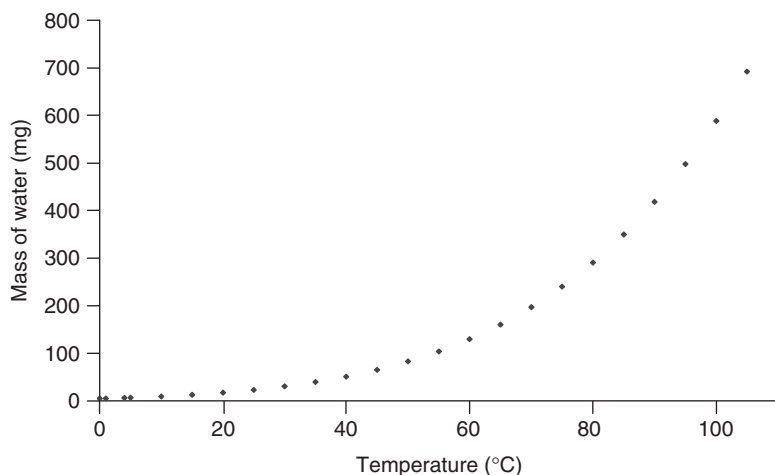


Figure 4.1 A graph showing the achievable water vapour loading at saturation for a 1 l min^{-1} Ar stream at various temperatures.

generator has a robust impedance matching capability. In contrast, a relatively small flux of volatile solvent can cause extinction of the plasma. The reasons for this are twofold. Firstly, $20 \mu\text{l min}^{-1}$ of water, for example, translates to 0.6 l min^{-1} of vapour at 7000 K, so a significant increase in the central channel flow arises when liquid is vaporized. Secondly, when this vapour is derived from a volatile solvent, it is produced low down in the central channel and can diffuse out into the energy coupling region of the discharge. A high enthalpy solvent or one that produces stable fragments can depress the electron energies to the point where the plasma equilibrium is destroyed.

The evaporation of a droplet with an initial diameter r_0 is described by the equation [14,18]:

$$r^3 = r_0^3 - 6D\sigma p_s \left[\frac{M}{\rho RT} \right]^2 t \quad (4.1)$$

where:

r is the radius at time t

D is the vapour diffusion coefficient

σ is the surface tension

p_s is the saturated vapour pressure

ρ is the density

M is the molecular weight

R is the gas constant

T is the temperature

Thus a variety of factors determine how much liquid is partitioned to the vapour phase in a given time. Vapour flux is usually controlled by cooling or aerosol 'drying', but for the reasons discussed above, care is needed when combining hot surfaces with aerosols as the

flash evaporation of large aerosol droplets produces pressure pulses that result in noise in the analytical signal.

4.3 Liquid aerosol generation

The processes of aerosol generation and transport have been widely studied and some excellent reviews produced that explore the underlying theory [1–4,19–22].

The discussion here will be restricted to identifying only the key factors so that the basis of successful designs may be understood. Whilst understanding the theory is certainly a necessary starting point, being able to produce the design in suitable materials, within tight tolerances and to an acceptable cost are equally important.

Many processes have been invoked to produce the primary aerosol [1,2,4], but commercially pneumatic nebulization and ultrasonic nebulization are the only ones that have made significant impact and so the discussion here is restricted to these types of device.

4.3.1 Pneumatic nebulization

A typical pneumatic nebulizer for ICP spectrometry operates at $0.6\text{--}1.2\text{ l min}^{-1}$ gas flow with a liquid flow rate of $0.5\text{--}1.5\text{ ml min}^{-1}$. These are here defined as *standard conditions*, lower flows, notably of the liquid, are referred to as *micro-flow conditions*.

The processes responsible for producing aerosol droplets have been extensively studied [23,24] and are qualitatively described by three mechanisms:

- Low velocity disintegration of large free, or attached, droplets of liquid (Rayleigh–Taylor instability).
- Disintegration of liquid filaments stretched out from the liquid body by the gas flow.
- Film formation followed by break up of wave-like structures formed on the surface of the film.

The gas provides the energy; surface tension provides the ‘returning’ force for the oscillations and viscosity the damping force. Thus generally, high-velocity gas combined with low surface tension and viscosity liquid produces the finest aerosols. Film-formation accounts for the smallest droplets, whilst Rayleigh–Taylor instability may lead to larger droplets.

The simplest way of pointing to effective practical design is to use a parametric model and the one most cited is that due to Nukiyama and Tanasawa [23]. However, it was not derived for the conditions used in ICP nebulizers and predicts droplet sizes that are larger than those obtained from analytical devices. A more appropriate model for concentric nebulizers, that accounts for the majority of practical devices employed, has been described by Gras *et al.* [25]:

$$D_{3,2} = 0.48d_1 \left(\frac{\sigma_1}{\rho_g V^2 d_1} \right)^{0.5} \left(\frac{Q_1 \rho_1}{Q_g \rho_g} \right)^{0.53} + 0.15d_1 \left(\frac{\eta_1}{\sigma_1 \rho_1 d_1} \right)^{0.49} \left(\frac{Q_1 \rho_1}{Q_g \rho_g} \right) \quad (4.2)$$

where:

d_l is the liquid outlet diameter (cm)

σ_l is the liquid surface tension (dyne cm^{-1})

ρ_l and ρ_g are the liquid and gas densities, respectively (g cm^{-3})

V is the difference in velocity between the liquid and gas (cm s^{-1})

Q_l and Q_g are the liquid and gas flow rates, respectively ($\text{cm}^3 \text{s}^{-1}$)

η_l is the liquid viscosity (poise)

This equation shows that to produce a fine primary aerosol requires:

- A high gas-to-liquid ratio (commensurate with the central channel flow limitation of the ICP).
- A small liquid channel diameter (this being large enough to avoid adventitious blockage).
- A small gas flow channel area to maximize V .
- Low viscosity.
- Low surface tension.
- High gas density (so Ar is more efficient than e.g. He).

The finer aerosols produced by adhering to these axioms improve transport efficiency and enable equivalent detection limits to be achieved at much lower uptake rates.

Typical *primary aerosol* drop size distributions for some common nebulizers are shown in Fig. 4.2 [2,26,27]. Note the finer aerosol produced by the high-efficiency nebulizer with the normal device.

4.3.1.1 Pneumatic nebulizer designs

A wide variety of pneumatic nebulizer designs have been described (oscillating capillary, single bore [28,29], HEN [27,30], direct injection high-efficiency nebulizer (DIHEN) [31–36], etc.), but here the focus is on devices that are commercially available and are therefore in widespread use. Pneumatic nebulizers are described by their basic geometry and thus Fig. 4.3 a–e shows the configurations for the concentric (similarly for micro-concentric), DIHEN, Babington (Cone-Spray version), cross-flow and Parallel Path designs. Choosing between

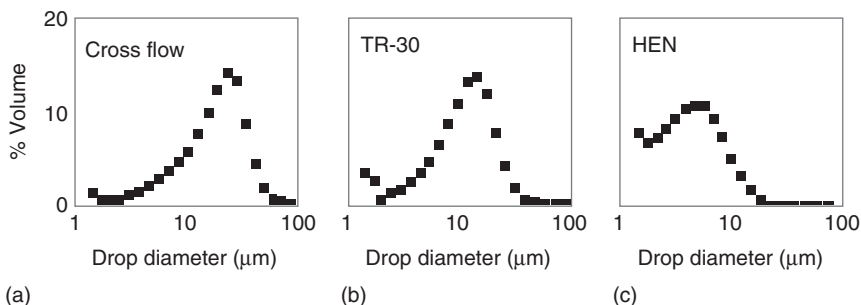


Figure 4.2 Typical particle size distribution diagrams for: (a) a cross-flow nebulizer, (b) a standard flow concentric and (c) a micro-concentric nebulizer. Revised with permission from Ref. [65].

the various types depends on the application, but as a general guide, best sensitivity and highest signal-to-noise ratio is obtained from concentric designs with high pressure and/or intermediate/reduced liquid flow (e.g. $100 \mu\text{l min}^{-1}$). The cross-flow nebulizer and Parallel Path nebulizer appear to offer improved robustness for higher matrix samples, whereas the Babington type devices work with very high matrix levels or slurries, but at slightly reduced

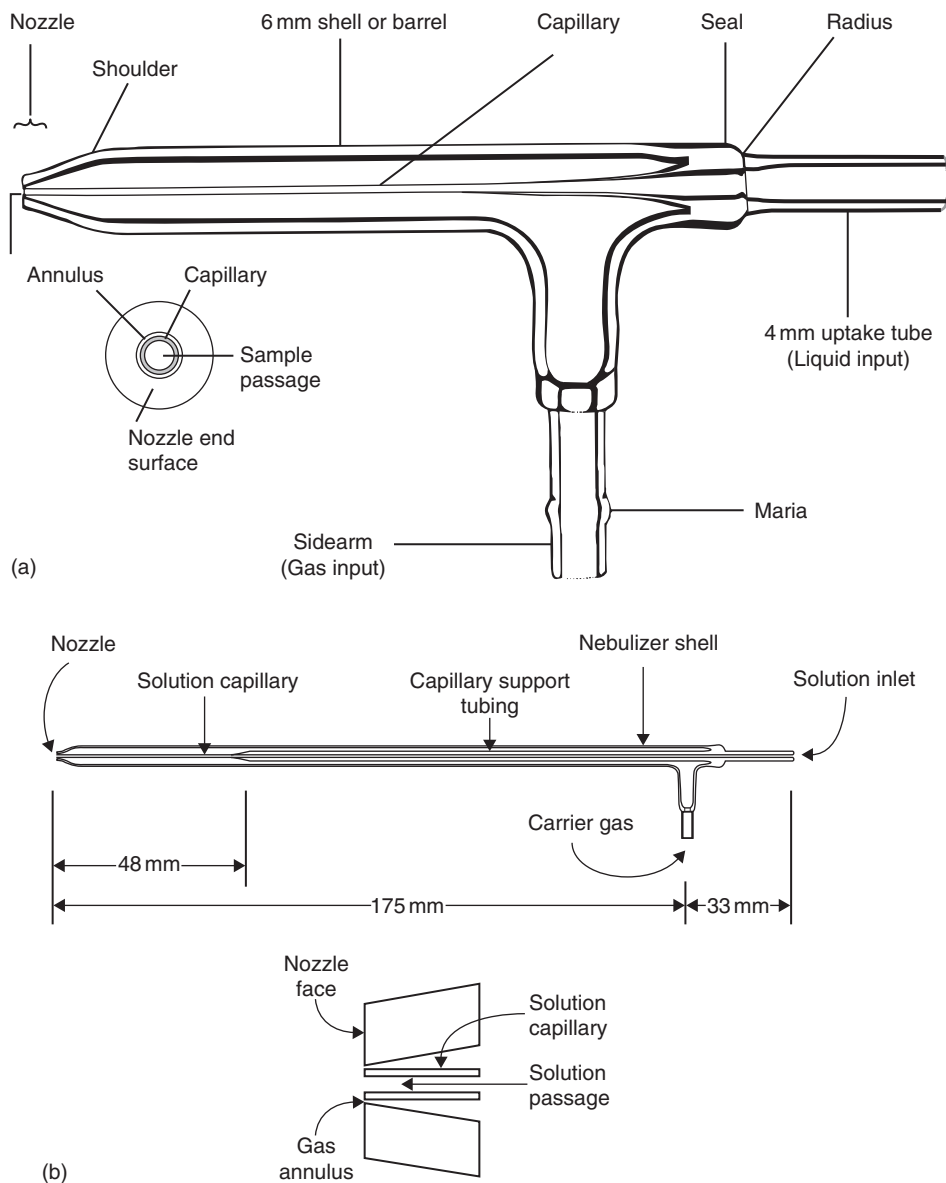


Figure 4.3 Schematic diagrams of: (a) a glass concentric nebulizer, courtesy of Meinhard Glass Products; (b) a DIHEN, courtesy of Meinhard Glass Products.

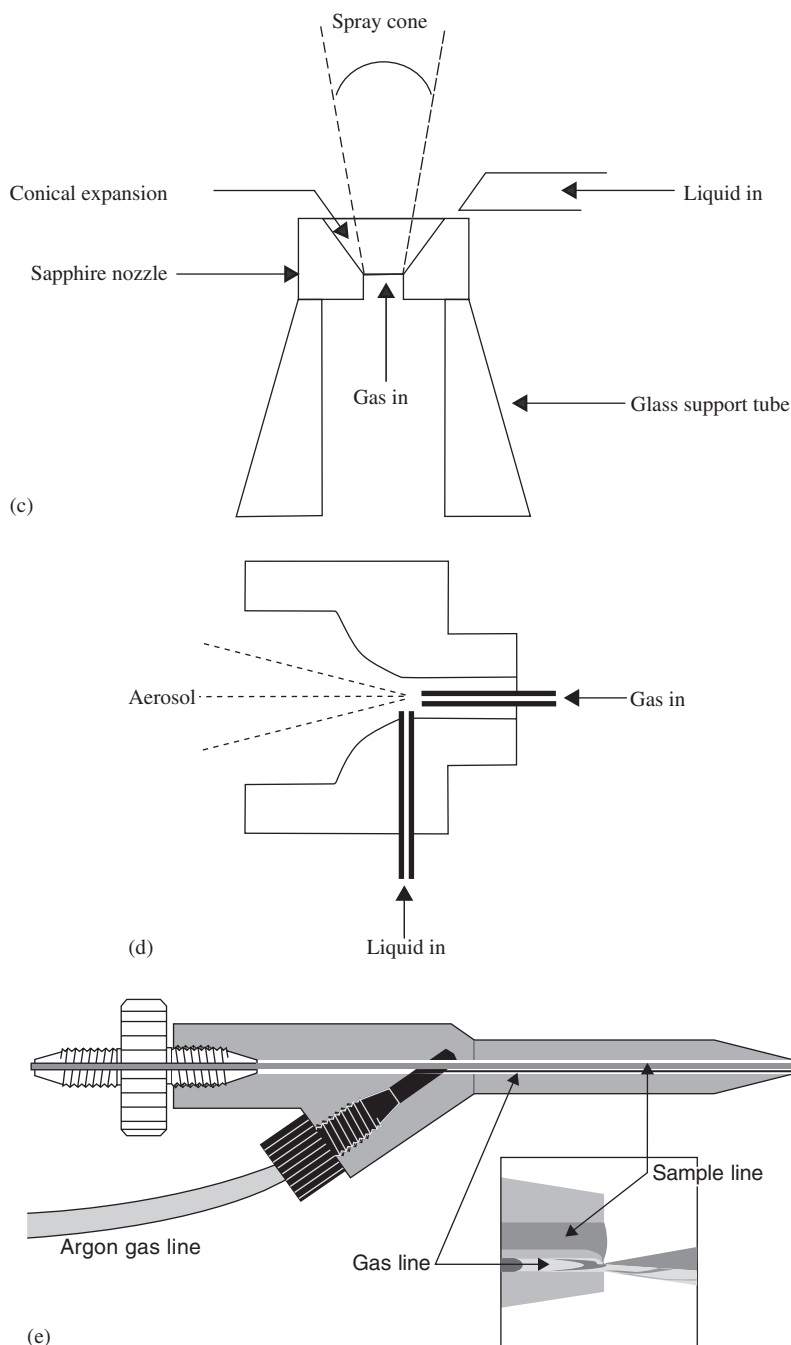


Figure 4.3 (Continued) (c) a Cone-Spray nebulizer revised from Ref. [3] with permission; (d) a cross-flow nebulizer and (e) an Enhanced Parallel Path nebulizer, courtesy of Burgener Research Inc.

Table 4.1 Characteristics of standard vs micro-flow nebulizers

Characteristic	Standard flow	Micro-flow
Uptake rate (ml min ⁻¹)	0.5–2.0	0.02–0.15
Gas flow (l min ⁻¹)	0.4–1.5	0.4–1.2
Gas pressure (psig)	20–60	20–175
Efficiency	~0.02	0.02–0.3+
Uptake tube diameter (mm)	0.2–0.35	~0.1
Gas annulus width (mm)	~0.02	≤0.02
Construction	One piece or fabricated	One piece or fabricated
Materials	Glass or inert polymer (e.g. PFA)	Glass or inert polymer (e.g. PFA)

efficiency. The Parallel Path nebulizer appears to be a hybrid between the cross-flow and Babington type and potentially combines some characteristics of each type.

Concentric nebulizers are usually constructed of one-piece, fused glass or polymer (e.g. perfluoro-alkoxyalkane, PFA), or from sapphire orifices coupled with fused silica capillaries. They come in standard format, recessed tip variant for high solids, micro-flow, high-pressure operation and direct injection. Table 4.1 summarizes some characteristics of standard vs micro-flow types.

The direct injection nebulizer (DIN) dispenses with the spray chamber and injects the aerosol directly into the base of the plasma. This has the advantages of reducing dead volume, which is useful for high-resolution chromatographic couplings, and the area of wetted surface which reduces memory effects [37] (e.g. in ultra-trace applications). The drawbacks are setting up time, and limited tolerance to high dissolved solids and these have precluded their widespread application.

Cross-flow nebulizers have largely been supplied directly by instrument manufacturers rather than third-party suppliers. The preferred construction employs a sapphire orifice for the gas jet and a polymer needle for the uptake tube in a fixed relative configuration.

Babington type nebulizers can be obtained in Cone-Spray (sapphire orifice) [3,38] or v-groove (Teflon construction) format and are the most tolerant with respect to salt or particle loading in the sample. For undemanding applications and those involving high matrix levels, which are typical of many addressed by ICP-AES, they may be the preferred option.

Table 4.2 lists some of the current commercial suppliers of nebulizers.

4.3.1.2 Ultrasonic nebulizers

USNs employ ultrasound waves in the range of 200 kHz–10 MHz to provide the energy for droplet production, rather than the gas flow. Thus the injector flow can be optimized independently of the droplet production. The waves are generated normally to the surface of a piezo-electric crystal, which in analytical devices is bonded to a chemically resistant plate (e.g. fused silica), onto which the sample is introduced. Waves can only propagate in fluid media given an adequate depth of fluid. Therefore, a small but significant depth of liquid

Table 4.2 Suppliers of nebulizers

Nebulizer type	Supplier	Location
Glass concentric	Glass Expansion Inc.	West Melbourne, Victoria, Australia www.geicp.com
	Meinhard Glass Products	Golden, Colorado, USA www.meinhard.com
	e-Pond	Vevey, Switzerland www.epond.biz
	Precision Glassblowing	Centennial, Colorado, USA www.precision-glassblowing.com
Polymer concentric	Burgener Research	Mississauga, Ontario, Canada www.burgener.com
	CPI International	Santa Rosa, California, USA www.cpiinternational.com
	Elemental Scientific Inc.	Omaha, Nebraska, USA www.elementalscientific.com
	CETAC Technologies	Omaha, Nebraska, USA www.cetac.com
Parallel Path	Glass Expansion Inc.	
Cross-Flow	e-Pond	
	Precision Glassblowing	
Direct Injection	Burgener Research	
	Precision Glassblowing	
V-groove	CPI International	
Cone-spray	Meinhard Glass Products	
	Precision Glassblowing	
	Burgener Research	
Ultrasonic	Meinhard Glass Products	
	Perkin Elmer	
	CETAC Technologies	

has to be created on the surface of the plate to allow a geyser to form from which the droplets are produced. This is usually accomplished by pumping the analyte on to the surface through a capillary tube (see Fig. 4.4). The wavelength of the waves produced for a driving frequency f (Hz) is given by [39]:

$$\lambda = \left(\frac{8\pi\sigma}{\rho f} \right)^{1/3} \quad (4.3)$$

where the symbols have the same meaning as for Equation (4.1) and the average droplet size is

$$D = 0.34\lambda \quad (4.4)$$

For a 3 MHz crystal the average droplet size is 3 μm and so transport efficiencies of ~20% are achieved rising to close to 100% when coupled to a desolvation system. Desolvation is

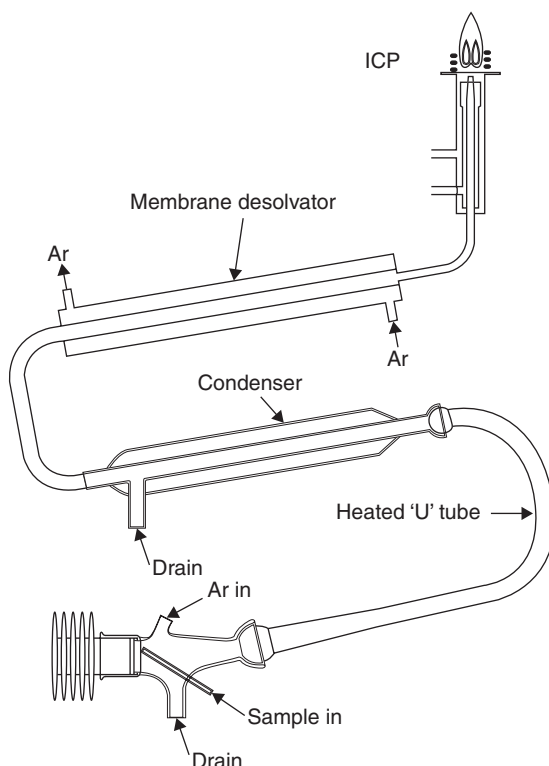


Figure 4.4 A schematic of an ultrasonic nebulizer with its associated desolvation system, courtesy of CETAC Technologies Inc.

essential unless a micro-flow [40] is fed to the plate, but stability is more readily achieved at higher flow rates.

The greater efficiency of analyte transport leads to a 10-fold improvement in detection limit providing the sample matrix is not complicated [41,42]. However, cost is much higher, wash-out times are longer, memory effects can be a problem (e.g. for Boron), and precision is lower ~2–3% because of the instability of the droplet production process.

4.3.1.3 *Alternative nebulizer designs*

Many other types of nebulizer have been described in the literature, for example, high-pressure hydraulic design [43–47], oscillating capillary [48–51], jet impact [52], thermospray [53,54], electrospray [55–57], frit nebulizer [58,59] and others, but none have found general application.

The advent of ‘lab on a chip’ and nano-spray techniques for LC and CE may in the future demand further developments in nebulizer technology.

4.3.2 *Spray chambers*

4.3.2.1 *Mode of operation*

The primary function of the spray chamber is to remove large droplets and allow only those that can be fully processed by the plasma to enter the central channel. In achieving this apparently simple goal, a wide range of complex processes occur which are variously beneficial or detrimental to analytical performance [1,2,4,5,60,61]. These processes include: modification of the aerosol particle size distribution, reduction of the aerosol concentration, modification of the phase equilibrium towards thermal equilibrium, reduction of the turbulence associated with the nebulization process and modification of the charge distribution.

The fate of droplets in a spray chamber is determined by: the particle density which impacts on droplet coalescence, notably in the near field immediately after the nebulizer; the gas flow pattern and the degree to which particles are entrained in it. Small particles, $\leq 1 \mu\text{m}$, are fully entrained in the gas flow and follow its flow paths, although they can be lost by Brownian diffusion through the static boundary gas attached to the chamber walls. Larger particles do not equilibrate their velocities with the gas flow and therefore tend to intercept on surfaces when the gas flow turns.

Conceptually the spray chamber can be divided into two zones, the near field close to the nebulizer (up to $\sim 20 \text{ mm}$), and the far field well downstream of the nebulizer, although in practise there is no sharp division between the two. In the near field, droplets have not equilibrated fully with the gas flow and in the very near field (notable within a few $100 \mu\text{m}$) the particle densities are very high. Thus rapidly moving small particles pass through a cloud of slowly accelerating large particles, but if an impact surface is placed in the path, the situation is reversed with the small particles turning with the flow and the larger particles holding their paths and passing through the now slower-moving (with respect to the axial velocity component) small particles. The consequences of this flow field are that the probability of recombination (large particles sweeping up small particles) is high and thus many small particles are lost. The small particles will also be entrained in the local flow field induced by the large particles and swept to the impact wall without being able to follow the gas flow lines. Qualitatively this model accounts for the much increased efficiency observed with micro-flow nebulizers where the particle sizes are smaller and more importantly the particle density is much lower. The process of particle loss in which large particles fail to turn with the gas flow and impact on the chamber wall, is generally referred to as flow line interception, but it includes the additional component of particle recombination and subsequent impact. The near field is also a region of strong entrainment by the nebulizer jet, resulting in the establishment of large scale re-circulating eddies in the chamber, causing deposition of liquid on the rear surfaces of the chamber and the nebulizer itself.

In the far field, most of the large particles have been lost so the aerosol density is lower and the surviving particles are approximately equilibrated with the gas flow. Losses occur through particles being transported to the walls by turbulent eddies where given sufficient momentum they cross the boundary layer and impact.

Whereas as the flow line interception process should be highly selective with respect to particle size, this selectivity is reduced by the turbulent nature of the flow and the recombination/sweeping up process. Turbulent deposition is less selective and accounts for significant loss of potentially useful aerosol. Gravitational settling may also be a factor for

large volume chambers or long conduits containing large ($>10\text{ }\mu\text{m}$) particles. Berndt [62–64] and co-workers have employed computational fluid dynamics (CFD) to model the processes in spray chambers and to optimize spray chamber design.

Although pneumatic nebulizers are variously capable of producing approximately 30–90% of the aerosol in the $<10\text{ }\mu\text{m}$ particle size range, under standard conditions the efficiency of typical spray chambers does not exceed 2–3%. The greatly reduced particle densities [65] produced by micro-flow nebulizers yields much higher transport efficiencies with 30% being typical, increasing to close to 100% with desolvation (see Section 4.3.2.3).

4.3.2.2 Practical designs of spray chambers

A variety of spray chambers have been described [4], including: Scott [66], cyclonic [67] and dual chamber designs such as the Stable Introduction System (SIS, Thermo Finnigan). These and commercial variants are available from suppliers (see Table 4.3 for a list of current products). The market is dominated by the double-pass or Scott-type design (see Fig. 4.5a) and the cyclonic design (Fig. 4.5b). Generally, the double-pass chamber provides the finest tertiary aerosol [62], whereas the cyclonic design offers higher efficiency, but with a slightly broader particle size distribution [63,64]. Materials are generally, glass, silica or polymer usually PFA. An important consideration, particularly for non-wettable surfaces, is to ensure a smooth drainage from the chamber without the generation of noise spikes due to pressure pulses.

Table 4.3 Suppliers of spray chambers and desolvation systems

Spray chamber type	Supplier	Location
Glass cyclonic	Glass Expansion Inc.	West Melbourne Vic, Australia www.geicp.com
	Elemental Scientific Inc.	Omaha, Nebraska, USA www.elementalscientific.com
	Precision Glassblowing	Centennial, Colorado, USA www.precisionglassblowing.com
	e-Pond	Vevey, Switzerland www.epond.biz
Polymer cyclonic	Glass Expansion Inc.	
	Elemental Scientific Inc.	
	Precision Glassblowing	
	CPI International	Santa Rosa, California, USA www.cpiinternational.com
Low volume cyclonic	e-Pond	
	Glass Expansion Inc.	
	Precision Glassblowing	
	e-Pond	
Scott/Double Pass	Precision Glassblowing Meinhard Glass Products	
Desolvation systems	CETAC Technologies	
	Elemental Scientific	

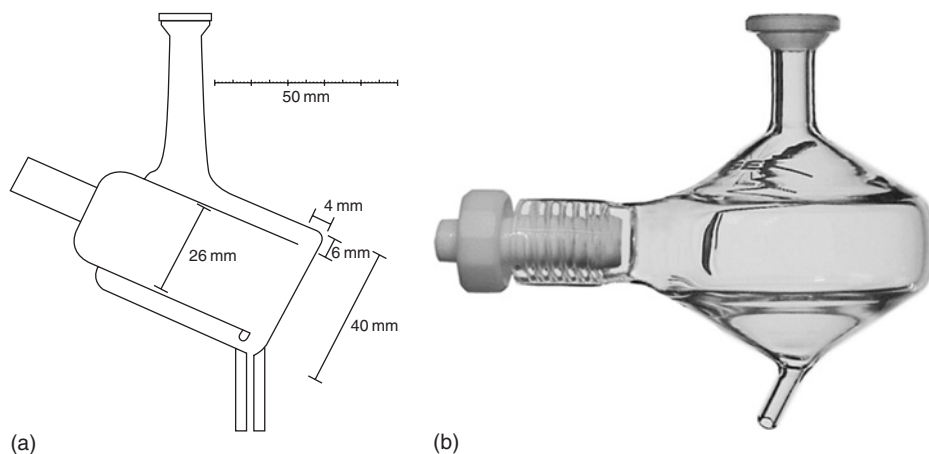


Figure 4.5 A schematic of: (a) an optimized volume double pass/scott style spray chamber, courtesy of B. L. Sharp; (b) an image of a typical glass cyclonic spray chamber, courtesy of Glass Expansion Inc.

Wash-in and wash-out time are important in determining the productivity of routine analyses and avoiding band-broadening in chromatographic coupling. There are two components to the wash-in/out time. The first component is related to the build-up and decay of the aerosol density which should be approximately equal [64]. Wash-in and wash-out times are usually defined in terms of the time taken for the signal to rise to 99%, or fall to 1% of its peak value, which is an adequate difference for routine work with samples of similar concentration. However, for more demanding applications where analyte concentration is varying by more than say an order of magnitude, or in high-accuracy isotope ratio determinations, a much longer time between samples may be necessary. The second component, only relevant to the wash-out time, is related to the chemical nature of the solvent and the analyte and is much less well understood. Here changes in the physical properties of the solvent can produce memory or ‘adaptation’ effects [68–70]; some analytes can exhibit long wash-out times due to retention on surfaces; and some can be produced in volatile form (e.g. I_2 and Th), that coat the chamber/tubing and produce measurable vapour pressure after aspiration has ceased [71].

Reducing the chamber volume reduces wash-out time, but also efficiency, because of increased surface-to-volume ratio and hence increased particle deposition. The conventional 150 mm long Scott-type chamber is certainly much larger than is required and optimized versions of this design with lengths of 80 mm and internal volumes of approximately 55 ml have been described [62]. Taylor *et al.* have described a cyclonic chamber [72] including a flow spoiler, that was later characterized by CFD [63,64], that can be optimized either for efficiency, or for wash-out time, (down to 3 s) or for best compromise performance. CFD studies and practical experience has shown that the spray chamber design has to be matched to the nebulizer. Micro-flow nebulizers are best matched to lower volume chambers and for these devices the flow geometry is more critical in determining efficiency and wash-out than for nebulizers operating under standard flow conditions. Thus, whereas for conventional systems the effect of changing the sample uptake rate is highly regulated

by the chamber processes, leading to only small changes in signal when the uptake rate is changed, a greater sensitivity to uptake rate is expected at micro-flow rates.

Isotope ratio measurements often place more emphasis on eliminating noise than achieving low limits of detection and here double-chamber designs can produce a refined aerosol that reduces plasma loading and noise thereby enabling improved measurement precision.

4.3.2.3 Desolvation

Desolvation adds complexity and cost to the sample introduction system and changes the characteristics of the plasma [73–76]. Without desolvation, the solvent – mostly water – dominates the plasma loading and only small perturbations are caused by the sample matrix. With desolvation a ‘dry’ plasma is produced, but variable sample matrix will in turn produce varying plasma loading. Although with MS detection, chilled spray chambers (typically 1–5°C) are commonly used to reduce the vapour loading and to reduce solvent-related interferences, full desolvation should only be used for specific purposes. Desolvation is employed to: reduce the solvent load with high efficiency nebulizers such as the ultrasonic design, to improve the transport efficiency, to remove or reduce spectral interferences – notably in isotope ratio measurements – and to produce a dry aerosol for calibration in LA experiments. According to Equation (4.1), a marginally transported 10 μm droplet will reduce to $\sim 1 \mu\text{m}$ in the milliseconds time scale at 60°C. A typical lifetime for a droplet in a spray chamber is of the order of 5–10 s and so desolvation does improve transport efficiency. However, it does so for both the analyte and the matrix in equal degree and therefore is not indicated as a means of improving detection limits for trace element in high matrix samples.

Small droplets tend to spontaneously evaporate because of their excess internal pressure; however, cooling due to loss of the latent heat of evaporation of the solvent, and increasing salt concentration depress the vapour pressure so that the equilibrium droplet size is finite. Heat is therefore required to drive the process to completion and this is usually accomplished by heating the spray chamber [77], although direct heating of droplets with infrared (IR) [78,79] or microwaves [79–83] has also been demonstrated. Fig. 4.1 shows that for micro-flow nebulizers it is quite possible to accommodate the entire sample flow in the vapour state at quite low temperatures (e.g. 60°C will accommodate $130 \mu\text{l min}^{-1}$ as vapour in 1 l of Ar). For the reasons indicated above, micro-nebulizers that do not produce significant wetting of the heated chamber walls (and therefore vapour pulses) are the preferred devices for primary aerosol generation.

Removal of the vapour load is usually achieved by a condenser and or a counter-flow membrane drier either of micro-porous Teflon or Nafion™ as shown in Fig. 4.6. Care is needed in setting up these devices to avoid reverse flow of the sweep gas into the sample carrier gas. Commercially available desolvating sample introduction systems are listed in Table 4.3.

Recently Todoli *et al.* have described a torch with a built-in spray chamber that provides heating of the micro-flow aerosol and 100% transport efficiency [84–88]. This configuration might be considered intermediate between a conventional nebulizer/spray chamber and a DIN.

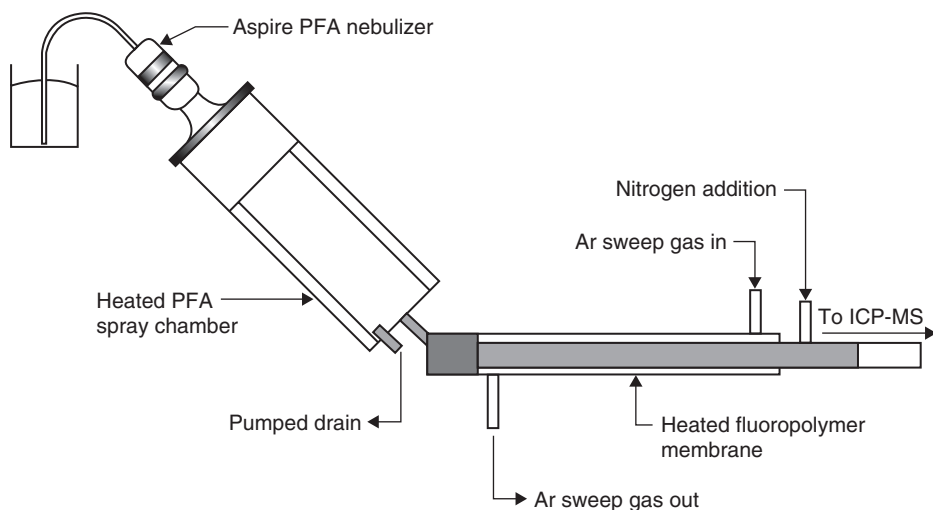


Figure 4.6 A schematic of a membrane desolvation sample introduction system, courtesy of CETAC Technologies Inc.

4.3.3 Chromatographic interfaces

The use of ICP-AES, and in particular ICP-MS, as detectors for various forms of separation has revolutionized the field of elemental speciation [89–97]. Effecting the physical coupling between the instruments has, in most cases, proved surprisingly easy. The greater difficulty has been in making the hyphenated instruments ‘talk’ to each other and developing software that can handle the output from the ICP with the same degree of refinement as is available with organic mass spectrometers. Nevertheless, fully integrated hyphenated instruments are now appearing on the market indicating the maturity of the elemental speciation technique.

Coupling a gas chromatograph to an ICP is relatively straightforward requiring only a heated transfer line to avoid condensation of the analytes [89,93,98–100]. There is a significant dilution of the ml min^{-1} column flow in the 100s of ml min^{-1} Ar injector flow, but with optimization excellent detection limits have been achieved.

Packed column high-performance liquid chromatography (HPLC) is the simplest separation technique to couple to the ICP [49,89–91,93–97,101–107] because the typical flow rates of $0.5\text{--}1.0 \text{ ml min}^{-1}$ exactly match those of standard ICP nebulizers. The nebulizer uptake tubing, kept as short as possible, is a perfectly good practical interface. The wash-in/wash-out times of the spray chamber are important in conserving the separation efficiency, but surprisingly little band broadening occurs in the aerosol phase [108]. Capillary column HPLC is slightly more demanding, but modern micro-flow nebulizers running at $30\text{--}100 \mu\text{l min}^{-1}$ handle the flows quite well.

The principal difficulty in coupling LC to the ICP source is the nature of the solvent or buffers used. Aqueous buffers at mM levels (a few 10s of ppm) are easily accommodated as are methanol/water mixtures, but high salt and/or organic content eluents and gradient elutions can cause difficulties with plasma stability and varying backgrounds. Ammonium

salts can offer an alternative, but these can also be quite volatile and produce plasma instability. Desolvation [40,103,109–111] is not an easy option because of band broadening, but hydride generation (HG) has been used to improve the detection of elements such as As [112–116].

Where modest levels of spectral interference are present (e.g. $^{75}\text{ArCl}^+$ on $^{75}\text{As}^+$ in a biological sample), the chromatographic step produces temporal discrimination of the background interferent (in this case a continuous signal is produced from chloride in the matrix) and the sample peak (the transient due to the elution of the As species). Thus background correction is automatically achieved as part of the peak integration process.

CE [72,91–93,117–131] provides the most challenging of the interfaces because, apart from the electroendosmotic flow, it is a zero flow technique. The internal volume for a typical $50\text{ cm} \times 100\text{ }\mu\text{m}$ internal diameter is only $3.9 \times 10^{-9}\text{ m}^3$, therefore a flow of $30\text{ }\mu\text{l min}^{-1}$ would displace the column volume in 8 s and induce significant laminar flow causing band broadening. A micro-nebulizer is supplied with a make-up flow, either pumped or through natural aspiration, that nullifies the suction of the nebulizer so that no pressure-driven flow occurs in the column. The make-up flow also provides the electrical connection and can be spiked with a standard to monitor system performance. Unfortunately, even a nebulizer flow of $30\text{ }\mu\text{l min}^{-1}$ causes a significant dilution of the nanolitre sample sizes typical of CE. Some CE systems can exert negative pressure on the sample reservoir end of the column and this can be used to offset part of the nebulizer suction whilst employing low make-up flow rates [72]. The limit is set by the stable operation of the nebulizer which is difficult to sustain below $\sim 10\text{ }\mu\text{l min}^{-1}$.

Recently, planar separations on gel plates and membranes have been probed using LA [132–146]. The major difficulty with this interface is quantitation, largely because of the inherent variability of gels. Another problem is the depth of the gel (0.25–0.5 mm) which is greater than the penetration depth of modern ultraviolet (UV) lasers. Membrane blotting however, concentrates the sample in a thin layer and greatly improves the sampling efficiency [143].

4.4 Vapour generation

Vapour generation is a method by which analytes present in a liquid, or sometimes a slurried solid sample [147], may be mixed with reagents that transform them into a gaseous species. The gaseous species may then be swept by a flow of Ar gas into the plasma for detection. There are several types of vapour that may be produced; for instance, Hg may be reduced to its elemental form by stannous chloride and the Hg vapour produced is detected. This technique is usually termed ‘cold vapour generation’. The other main types of vapour produced are the hydride species formed by reaction with sodium tetrahydroborate (also called sodium borohydride). This technique is referred to as hydride generation. Traditionally, the metalloid analytes such as As, Sb and Se, and to a lesser extent Bi, Ge, Pb, Sn, Te and Tl, were determined by this method where the vapour species formed were arsine (AsH_3), stibine (SbH_3), etc. The mechanism of the reduction using tetrahydroborate has been described by Howard [148]. More recently, a much larger suite of analytes (e.g. Ag, Au, Cd, Co, Cu, Ni, Sn and Zn) has also been determined using the same reagent [149], as have Pd and Pt [150]. Other reagents that have been used to form volatile vapours include sodium tetraethylborate [151].

Vapour generation of analytes into an ICP offers several advantages over conventional nebulization. Since the analyte is transformed into a gaseous state, it may be transported much more efficiently (close to 100%) to the plasma, so the sensitivity and limit of detection (LOD) tends to improve. Also, the analyte is separated from the bulk of the sample matrix, leading to fewer spectral interferences. Inevitably, there are also disadvantages associated with sample introduction of gaseous analytes. Different oxidation states of analytes produce hydrides with different efficiencies (e.g. both As^{III} and As^{V} produce a hydride), but the kinetics of the reaction are very much slower for As^{V} . Another disadvantage of the HG technique is that the presence of some other metals (e.g. platinum group metals, or some transition metals, namely Cu or Fe^{III}) in the sample may interfere with the HG process. This may be overcome in a number of ways, but the most common is to use a masking agent (i.e. an agent that 'ties up' the potential interferent) [152]. Another drawback of vapour generation is that the excess hydrogen produced during the hydride formation process is also swept into the plasma, and may cause instability.

The instrumentation required for vapour generation is fairly minimal. Commercial units may be purchased, but effectively, they amount to a peristaltic pump, a switching valve, a mixing 'T' and a gas-liquid separator. A more detailed text discussing HG has been published by Dedina and Tsalev [153], and a review discussing advances in HG coupled with atomic emission detectors has been presented by Pohl [154].

4.5 Electrothermal vaporization

Sample introduction by electrothermal vaporization (ETV) is a method that has evolved from atomic absorption measurements. Instead of direct nebulization of a liquid sample, a small volume of liquid (10–100 μl), or a few milligrams of solid material, is introduced directly into an electrothermal atomizer. The theory behind ETV may be found in other publications [155]. The atomizer is then heated resistively, by passing an electrical current through it. A ramped temperature program is used in which the sample (if it is a liquid) is first dried, then the temperature is raised so that as much of the potentially interfering matrix is removed as possible whilst ensuring that the analytes are not lost. Finally, a high-temperature vaporization step follows in which the analytes are removed from the electrothermal atomizer and enter a gas stream which transports them to the plasma. It is important to note that atomization is not required in plasma source spectrometry, and indeed it is quite difficult to conduct reactive free atoms through connecting tubing. A micro-particulate or stable molecular vapour are the preferred forms for introduction to the ICP.

The technique has the advantage of being capable of determining analytes in very small volumes of sample (<100 μl), as well as separating them from many potential interferences. In addition, transport efficiency to the plasma tends to be very high, leading to improved sensitivity and improvements in LOD of at least an order of magnitude. However, the procedure is very slow. As well as taking time to weigh (in the case of solid samples) the sample into the vaporizer, each of the stages of the temperature programme requires a finite time to complete its task. This technique produces a transient signal and so, as with LA and chromatography, a sequential scanning optical spectrometer may only be fast enough to determine one analyte per injection, and therefore simultaneous instruments are preferred. Modern quadrupole mass spectrometers however do have sufficient scanning speed to carry

out multi-element scans on signals lasting of the order of a few seconds. Since sample introduction is normally by a micro-pipette, precision is typically 3–5% rather than the 1% normally associated with sample introduction using a nebulizer. Precision for solid sampling (SS) can be worse still.

Commercial instrumentation is available, although many laboratories manufacture their own vaporizers in-house, often from redundant systems that had been used for atomic absorption spectrometry (AAS) measurements. Metal vaporizers may be used instead of carbon and a brief discussion of these has been presented by Nobrega and co-workers [156] whilst a good example of the application of ETV-ICP-MS using a metal vaporizer has been published by Parsons *et al.* [157].

Reviews of SS-ETV-ICP-MS have been prepared by Martin-Esteban and Slowikowski [158] and by Vanheacke *et al.* [159]. The analysis of micro-samples, using techniques such as ETV as a sample introduction method, has also been discussed recently by Todoli and Mermet [160].

An alternative to ETV is to use direct sample insertion (DSI). Here, the sample is loaded onto the tip of a graphite (or refractory metal) probe. This is then inserted through a modified torch so that the sample is heated directly by the plasma. Similar advantages and disadvantages are experienced as with ETV. The technique was reviewed in 1990 by Karanassios and Horlick [161] and then again, more recently, by Sing [162]. DSI and its applications have also been discussed previously in Chapter 3.

4.6 Solid sampling via LA

In 1985 Gray first realized that the material produced via LA could be transported to the ICP for efficient atomization and ionization. The analyte ions were detected by MS so creating the technique of LA-ICP-MS [163]. Twenty years later, LA is the most versatile SS technique for ICP-MS, and the general principle of the technique has not changed.

4.6.1 Fundamentals

4.6.1.1 Ablation mechanisms

In LA, material is removed from a sample placed in an ablation cell using a high-power, short-pulsed laser focused onto the sample surface. The ablated material is carried to the ICP in a continuously flowing carrier gas, which forms the injector flow for the plasma. When the sample is irradiated with laser energy, material is released in the form of particulates, electrons, atoms and ions forming a plasma plume above the ablation site. This ablation plasma plume can interact with the incident laser beam causing shielding of the sample thereby reducing the energy deliverance to the substrate.

Generally, material is removed from the sample at a depth of 0.02–5 μm [164]. Particle size distributions are much broader for aerosols generated via LA than solution nebulization (SN) and strongly correlate to the properties of the sample matrix and of the incident laser beam. It should be noted that the particle size distribution created by the LA process is not indicative of what reaches the ICP, since individual particles change size by

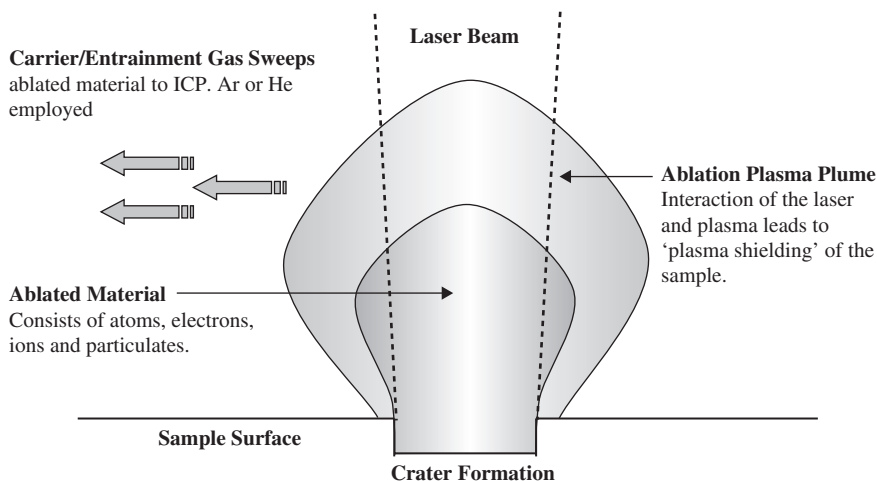


Figure 4.7 The processes involved in LA (i.e. the interaction of a high power, highly focused laser beam with a solid target).

condensation, vaporization or agglomeration with other particles [165]. The processes involved in LA are shown in Fig. 4.7.

4.6.1.2 Elemental fractionation

A few years after Gray's initial work, the most severe problems associated with LA-ICP-MS analysis were recognized; namely elemental fractionation (non-representative sampling) and a lack of certified reference materials. Without the employment of matrix matched calibration standards, elemental fractionation has dramatic implications for quantitative analysis; such calibration standards are not available for the majority of sample types.

It is now generally accepted that elemental fractionation occurs at three points in the LA-ICP-MS process; the ablation process, the transport process and the atomization/ionization process within the plasma itself. Elemental fractionation cannot be eliminated, but steps can be taken to reduce its impact. Previously, emphasis was placed on attributing fractionation to processes occurring at the LA stage; however, emphasis has now shifted towards processes occurring within the ICP; namely the incomplete vaporization of larger particles leading to selective vaporization of more volatile elements. Factors such as laser wavelength, laser pulse duration, crater morphology (depth-to-diameter) and choice of carrier gas require careful consideration since they play a vital role in determining the size of particles produced.

4.6.2 Instrumentation

A typical LA sampling system employs: a laser beam, to supply sufficient energy to the sample surface to facilitate ablation; an ablation cell, to allow containment and positioning

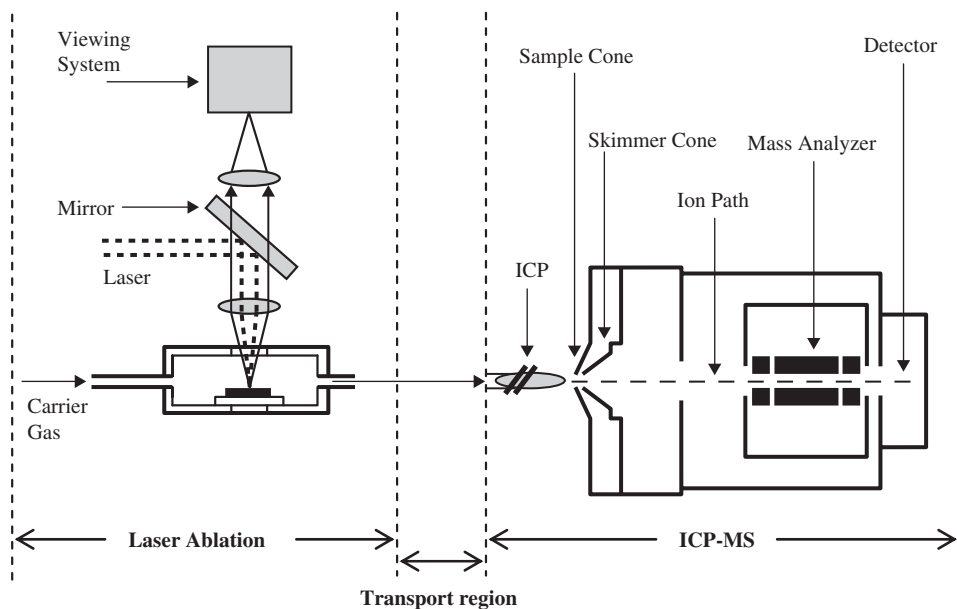


Figure 4.8 A schematic of a typical LA-ICP-MS setup.

of the sample along the x -, y - and z -axis and a transport system, to transfer the ablated sample material from the ablation site to the ICP with maximum efficiency. Fig. 4.8 shows a schematic of a typical LA-ICP-MS setup.

4.6.2.1 The laser

Ruby, excimer and neodymium-doped yttrium–aluminium–garnet (Nd:YAG) lasers have successfully been used for LA. The Nd:YAG laser is the most widely used laser source for LA-ICP-MS, due to its ease of use and robustness. The Nd:YAG laser is a solid state laser consisting of a Nd:YAG rod a few millimetres in diameter. Although the fundamental wavelength of the Nd:YAG lies at 1064 nm, a wavelength poorly absorbed by a variety of sample matrices, harmonic generation allows Nd:YAG lasers to be operated at harmonics lying in the UV such as 266 nm, and 213 nm. Although the fourth harmonic output at 266 nm is still commonly used for LA applications, the fifth harmonic output at 213 nm is more popular due to increased ablation efficiency at this shorter wavelength [166]. A Nd:YAG operating at 193 nm has recently been described and is now commercially available [167,168].

The choice of wavelength for LA has been widely discussed [164,167,169–175]. Generally speaking, it is the amount of laser energy absorbed by the sample surface, that controls the ablation yield and hence the analytical response. Therefore, the use of shorter wavelengths (UV) is considered advantageous, since it provides greater photon energy and a greater energy density in the target, for more efficient bond breaking within the sample. The use of shorter wavelengths has been shown to reduce the degree of elemental fractionation, since the ablation process occurs via a non-thermal mechanism whereupon selective vaporization

of more volatile components is reduced. The use of shorter wavelength lasers has also been shown to produce smaller particles, more readily fully processed within the ICP, and more uniform particle size distributions than the use of longer wavelengths [167,176]. Shorter wavelengths penetrate the ablation plasma plume more effectively, thus reducing plasma shielding effects and leading to a greater energy deliverance to the sample surface.

Most LA applications have been performed utilizing lasers of nanosecond pulse duration. However, there is now a developing trend towards the use of lasers of narrower pulse width, such as picosecond and femtosecond [177–186]. By utilizing narrower pulse widths elemental fractionation can be reduced, since the interaction time of the laser and sample is shorter than the phonon relaxation time of the sample. Hence, ablation occurs by a less thermal mechanism and sample heating is greatly reduced. In nanosecond LA, plasma shielding causes laser energy to be scattered and lost. This plasma shielding effect is absent in the use of femtosecond ablation since the laser pulse has ceased before formation of the carrier gas plasma; consequently there is a greater energy deliverance to the sample surface and a freer expansion of the ablated material [180,182].

4.6.2.2 *The ablation chamber and transport system*

A basic ablation chamber consists of: a gas-tight cell, ports to allow entry and exit of the carrier gas, a window to allow laser beam access and an adjustable platform on which the sample sits. Arrowsmith and Hughes have described three designs of ablation cell used for LA [187], whilst Jackson described a novel design known as a 'jet cell' [188] in which the ablation site was cooled by a high-velocity carrier gas jet, leading to a reduction in elemental fractionation.

Particles may be lost in the connective tubing between the ablation chamber and the ICP by gravitational settling or impaction with the tubing walls. Larger bore tubing could be desirable since it provides an increased ratio of gas volume to tubing wall area, minimizing losses due to impaction. Conversely, smaller diameter tubing provides increased gas velocity, reducing the overall transport time and sample loss due to gravitational settling. In practice it is necessary to reach a compromise between the two extremes to give reasonable transport efficiency.

Ar was traditionally used as a carrier gas for LA-ICP-MS. However, He is now used for the majority of applications due to improved ablation and transport [189–192]. Employment of He as a carrier gas produces smaller particles from the ablation process; such particles are transported with greater efficiency to the ICP and also more fully vaporized. The shift in particle size distribution towards smaller particles has been attributed to the physical properties of the He carrier gas including: a lower density, higher ionization energy and higher thermal conductivity. Lower density means a greater transport efficiency of ablated material away from the ablation site; whilst higher ionization energy leads to the formation of a much smaller plasma. These properties allow a faster removal of energy from the ablation site, leading to a rapid end to condensational growth of particulates [191].

4.6.3 *Sampling strategy*

The commercially available LA systems allow many different sampling strategies to be employed, these include: single spot drilling, a series of spots and a line or raster across the

Table 4.4 Suppliers of LA systems

Supplier	Location
New-wave Research	Fremont, CA, USA: www.new-wave.com
CETAC Technologies	Omaha, NE, USA: www.cetac.com
LSA LINA-Spark Applications	Cully, Switzerland: www.lina-spark.com
Lambda Physik	Göttingen, Germany: www.lambdaphysik.com

sample surface. Table 4.4 lists suppliers of LA systems. Modern systems provide a wide choice of laser spot sizes for different applications. The choice of sampling strategy will ultimately be determined by the particular application. If bulk analysis is desired, whereupon the goal is to obtain analysis representative of a whole sample, then the beam is normally focused to produce spots $>100\text{ }\mu\text{m}$ in diameter. A line or raster mode of analysis can be employed in which the laser scans across a much larger region of sample. The raster mode of analysis has been shown to significantly reduce the effects of fractionation associated with crater development. The degree of fractionation is strongly linked to the morphology of the ablation crater and increases as the aspect ratio (depth-to-diameter ratio) of the crater increases [189,193]. This has been attributed to a combination of factors including: a reduced transport efficiency from deeper depths, a confined plasma within deeper craters leading to a more thermal mechanism of ablation and finally, a reduction in laser irradiance due to changes in the effective area exposed to the laser beam.

If spatial resolution is desired, whereupon the goal is to determine the composition of discrete portions of a larger sample, then the laser beam is normally focused to produce spots $<100\text{ }\mu\text{m}$. The ability to change the ablation spot size according to application is critical and is best achieved via the use of a variable aperture placed in the laser beam path. The aperture is imaged onto the sample surface by the laser objective lens. A change in aperture diameter results in a proportional change in diameter of the imaged ablation spot. The use of such a system has the advantage that a constant energy density (fluence) on the sample surface can be maintained regardless of the ablation spot size employed. For successful implementation of this kind of imaging optics, a flat laser beam energy profile is required.

4.6.4 Quantification of LA-ICP-MS

Due to the lack of certified reference materials for the majority of sample types and the occurrence of elemental fractionation, LA-ICP-MS has been termed in the past as semi-quantitative; however, advancements in LA systems and calibration strategies now mean that accurate and precise analytical data is obtainable. Quantification via LA-ICP-MS can be accomplished by a variety of methodologies; matrix-matched direct solid ablation with external calibration, often incorporating internal standardization; simultaneous sample-standard introduction; direct liquid ablation and isotope dilution (ID).

Ablation rates vary greatly with respect to even tiny changes in sample matrix; hence, calibration via external standardization requires the use of highly matrix matched calibration standards in terms of elemental composition and physicochemical properties. Such

reference materials are not available for the majority of sample types. One solution is to add the sample or standard to a powdered matrix and press the mix into a disc [194–205], or fuse the sample into a glass bead [194,198,206,207]. Sample preparation of this type allows a more similar matrix composition between samples and standards to be obtained (matrix matching), as well as the potential addition of an internal standard element to correct for changes in ablation rates. It has been shown that the addition of modifiers to a disc or bead can increase the efficiency of the ablation process [208,209] yielding higher sensitivity and reduced elemental fractionation. Such modifiers (organic and inorganic based) improve the absorption of laser energy by the sample, subsequently leading to the formation of smaller particles more readily processed by the ICP [209].

Internal standardization provides a viable quantification technique since it allows for differences in ablated mass due to shot-to-shot variation, loss of sample in the ablation chamber and transfer line, and for incomplete vaporization of particles within the ICP. The disadvantage of internal standardization is that at least one element of known concentration, needs to be present in, or added to the sample. It is vital that this internal standard be of a homogeneous distribution throughout the sample.

Simultaneous sample-standard introduction has been successfully employed as a quantification method for LA-ICP-MS, especially in the absence of certified reference materials [210–222]. Two sample introduction lines are employed so that simultaneous introduction of an ablated sample and a nebulized standard is achieved. Careful mixing of the two aerosols is required before introduction into the ICP. Desolvation of the standard aerosol can be employed so that it more closely matches the dry aerosol produced by ablation of the sample. However, recent work in this laboratory has shown that the more standardised plasma conditions produced by employing a classical wet plasma are beneficial for routine analysis [223]. The major limitation of this technique is the different particle types and sizes produced by the different sample introduction systems.

Direct liquid ablation has been used as a calibration strategy for LA-ICP-MS. Direct ablation of a liquid standard has the advantage that the standards are cheap and easy to prepare and offer a renewed surface for ablation after each laser shot. Heterogeneous distribution of elements is not a problem if such standards are employed. Aqueous standards can be ablated with [224] or without [225] the addition of an organic chromophore to improve the absorption of laser energy and hence improve coupling between the laser beam and standard solution. Again the limiting factor is the totally different sample and standard matrix.

The sampling capabilities of LA can be combined with the powerful quantification technique of ID. There are two general approaches to LA-ICP-IDMS. One approach incorporates the isotope spike solution into a powdered sample [203–205,226], before pressing the sample/spike mixture into a pellet or disc. Another approach utilizes a simultaneous sample-standard system; here the standard aerosol, formed by solution nebulisation of an isotopically enriched spike solution, is combined with the sample aerosol before introduction to the ICP [227–229]. In both cases it is vital that equilibrium between sample and spike is reached.

4.7 Conclusion

Sample introduction techniques for ICP-AES and ICP-MS have now reached the stage where they provide practical solutions to most analytical problems. The remaining challenges are

likely to come from the life sciences where nanolitre samples are common and there is increasing need to couple powerful two-dimensional (2-D) separations to plasma source spectrometry. The use of LA in particular in this area is likely to be a growth area for future research.

References

1. Browner, R.F. (1999) *Aerosol Generation and Sample Transport, Inductively Coupled Plasma Mass Spectrometry and Its Applications*, 1st edn (Ed. S.J. Hill), Sheffield Academic Press Ltd., Sheffield (UK), Chapter 4, 98–118.
2. Montaser, A. (1998) *Inductively Coupled Plasma Mass Spectrometry*, Wiley-VCH, New York.
3. Sharp, B.L. (1988) Pneumatic nebulizers and spray chambers for inductively coupled plasma spectrometry – a review. 1. Nebulizers. *J. Anal. Atom. Spectrom.*, **3**, 613–652.
4. Sharp, B.L. (1988) Pneumatic nebulizers and spray chambers for inductively coupled plasma spectrometry – a review. 2. Spray chambers. *J. Anal. Atom. Spectrom.*, **3**, 939–963.
5. Mora, J., Maestre, S., Hernandis, V. and Todoli, J.L. (2003) Liquid-sample introduction in plasma spectrometry. *Trac-Trend Anal. Chem.*, **22**, 123–132.
6. Durrant, S.F. (1999) Laser ablation inductively coupled plasma mass spectrometry: achievements, problems, prospects. *J. Anal. Atom. Spectrom.*, **14**, 1385–1403.
7. Russo, R.E., Mao, X.L., Liu, H.C., Gonzalez, J.J. and Mao, S.S. (2002) Laser ablation in analytical chemistry – a review. *Talanta*, **57**, 425–451.
8. Günther, D., Jackson, S.E. and Longerich, H.P. (1999) Laser ablation and arc/spark solid sample introduction into inductively coupled plasma mass spectrometers. *Spectrochim. Acta B*, **54**, 381–409.
9. Farino, J. and Browner, R.F. (1984) Surface-tension effects on aerosol properties in atomic spectrometry. *Anal. Chem.*, **56**, 2709–2714.
10. Hasegawa, T., Umemoto, H., Haraguchi, C., Hsieh, C. and Montaser, A. (1992) Fundamental properties of inductively coupled plasmas. *Inductively Coupled Plasmas in Analytical Atomic Spectrometry*. 2nd edn, VCH, New York.
11. Montaser, A. and Goolightly, D.W. (1992) Assessment of the potentials and limitations of plasma sources compared to ICP discharges for analytical spectrometry. *Inductively Coupled Plasmas in Analytical Atomic Spectrometry*. 2nd edn, VCH, New York.
12. Olesik, J.W., Dziewatkoski, M.P. and McGowan, G.J. (1994) Fundamental and practical advantages of individual, monodisperse droplet sample introduction for ICP-MS, Abstracts of *Papers of the American Chemical Society*, 208, 147-ANYL.
13. Houk, R.S., Winge, R.K. and Chen, X.S. (1997) High speed photographic study of wet droplets and solid particles in the inductively coupled plasma. *J. Anal. Atom. Spectrom.*, **12**, 1139–1148.
14. Horner, J.A., Lehn, S.A. and Hieftje, G.M. (2002) Computerized simulation of aerosol-droplet desolvation in an inductively coupled plasma. *Spectrochim. Acta B*, **57**, 1025–1042.
15. Hobbs, S.E. and Olesik, J.W. (1992) Inductively coupled plasma mass-spectrometry signal fluctuations due to individual aerosol droplets and vaporizing particles. *Anal. Chem.*, **64**, 274–283.
16. Kuhn, H.R., Guillong, M. and Günther, D. (2004) Size-related vaporisation and ionisation of laser-induced glass particles in the inductively coupled plasma. *Anal. Bioanal. Chem.*, **378**, 1069–1074.
17. Todoli, J.L. and Mermet, J.M. (1998) Minimization of acid effects at low consumption rates in an axially viewed inductively coupled plasma atomic emission spectrometer by using micronebulizer-based sample introduction systems. *J. Anal. Atom. Spectrom.*, **13**, 727–734.
18. Porstendorfer, J., Gebhart, J. and Robig, G. (1977) Effect of evaporation on the size distribution of nebulized aerosols. *J. Aerosol Sci.*, **8**, 371–380.

19. Browner, R.F. and Boorn, A.W. (1984) Sample introduction – the achilles heel of atomic spectroscopy. *Anal. Chem.*, **56**, A786–A798.
20. Browner, R.F. and Boorn, A.W. (1984) Sample introduction techniques for atomic spectroscopy. *Anal. Chem.*, **56**, A875–A888.
21. Gustavsson, A. (1984) The determination of some nebulizer characteristics. *Spectrochim. Acta B*, **39**, 743–746.
22. Gustavsson, A. (1984) A tutorial review of the basic theory for and practical aspects of aerosol chambers. *Spectrochim. Acta B*, **39**, 85–94.
23. Nukiyama, S. and Tanasawa, Y. Experiments on the atomization of liquids in Air Streams, *Trans. Soc. Mech. Eng. (Japan)*, 4, 5 and 6, E. Hope, transl., Defence Research Board, Department of National Defence, Ottawa, Canada, 1950 (1938–1940).
24. Hinds, W.C. (1982) *Aerosol technology, Properties, Behaviour and Measurement of Airborne Particles*, Wiley, New York.
25. Gras, L., Alvarez, M.L. and Canals, A. (2002) Evaluation of new models for drop size distribution prediction of aerosols in atomic spectrometry: pneumatic nebulizers. *J. Anal. Atom. Spectrom.*, **17**, 524–529.
26. Maestre, S.E., Todoli, J.L. and Mermet, J.M. (2004) Evaluation of several pneumatic micronebulizers with different designs for use in ICP-AES and ICP-MS. Future directions for further improvement. *Anal. Bioanal. Chem.*, **379**, 888–899.
27. Liu, H.Y., Montaser, A., Dolan, S.P. and Schwartz, R.S. (1996) Evaluation of a low sample consumption, high-efficiency nebulizer for elemental analysis of biological samples using inductively coupled plasma mass spectrometry. *J. Anal. Atom. Spectrom.*, **11**, 307–311.
28. Hernandis, V., Todoli, J.L., Canals, A. and Sala, V. (1995) An experimental study of the behaviour of several elements in inductively coupled plasma mass spectrometry using a single bore high pressure pneumatic nebulizer. *Spectrochim. Acta B*, **50B**, 985–996.
29. Todoli, J.L., Munoz, M., Valiente, M., Hernandis, V. and Canals, A. (1994) Performance of the new single bore high pressure pneumatic nebulizer (SBHPPN) in plasma atomic emission spectrometry. *Appl. Spectrosc.*, **48**, 573–580.
30. Liu, H.Y. and Montaser, A. (1994) Phase-Doppler diagnostic studies of primary and tertiary aerosols produced by a high-efficiency nebulizer. *Anal. Chem.*, **66**, 3233–3242.
31. McLean, J.A., Zhang, H. and Montaser, A. (1998) A direct injection high-efficiency nebulizer for inductively coupled plasma mass spectrometry. *Anal. Chem.*, **70**, 1012–1020.
32. Acon, B.W., McLean, J.A. and Montaser, A. (2000) A large bore-direct injection high efficiency nebulizer for inductively coupled plasma spectrometry. *Anal. Chem.*, **72**, 1885–1893.
33. Minnich, M.G. and Montaser, A. (2000) Direct injection high efficiency nebulization in inductively coupled plasma mass spectrometry under cool and normal plasma conditions. *Appl. Spectrosc.*, **54**, 1261–1269.
34. Todoli, J.L. and Mermet, J.M. (2001) Evaluation of a direct injection high-efficiency nebulizer (DIHEN) by comparison with a high-efficiency nebulizer (HEN) coupled to a cyclonic spray chamber as a liquid sample introduction system for ICP-AES. *J. Anal. Atom. Spectrom.*, **16**, 514–520.
35. Bjorn, E., Jonsson, T. and Goitom, D. (2002) Noise characteristics and analytical precision of a direct injection high efficiency and micro concentric nebuliser for sample introduction in inductively coupled plasma mass spectrometry. *J. Anal. Atom. Spectrom.*, **17**, 1257–1263.
36. Westphal, C.S., Kahen, K., Rutkowski, W.E., Acon, B.W. and Montaser, A. Demountable direct injection high efficiency nebulizer for inductively coupled plasma mass spectrometry. *Spectrochim. Acta B*, **59**, 353–368.
37. O'Brien, S.E., McLean, J.A., Acon, B.W., Eshelman, B.J., Bauer, W.F. and Montaser, A. (2002) Determination of memory-prone elements using direct injection high efficiency nebulizer inductively coupled plasma mass spectrometry. *Appl. Spectrosc.*, **56**, 1006–1012.

38. Sharp, B.L. (1986) The Conespray Nebuliser – Method of and Apparatus for the Nebulization of Liquid and Liquid Suspensions, British Technology Group Assignment No. 8432338, UKPA 8531504.
39. Fassel, V.A. and Dickinson, G.W. (1968) Continuous ultrasonic nebulization and spectrographic analysis of molten metals. *Anal. Chem.*, **40**, 247–249.
40. Tarr, M.A., Zhu, G.X. and Browner, R.F. (1993) Microflow ultrasonic nebulizer for inductively coupled plasma atomic emission spectrometry. *Anal. Chem.*, **65**, 1689–1695.
41. Fassel, V.A. and Bear, B.R. (1986) Ultrasonic nebulization of liquid samples for analytical inductively coupled plasma atomic spectroscopy – an update. *Spectrochim. Acta B*, **41**, 1089–1113.
42. Jakubowski, N., Feldmann, I. and Stuewer, D. (1992) Analytical improvement of pneumatic nebulization in Icp-MS by desolvation. *Spectrochim. Acta B*, **47**, 107–118.
43. Berndt, H. and Yanez, J. (1996) High-temperature hydraulic high-pressure nebulization: a recent nebulization principle for sample introduction. *J. Anal. Atom. Spectrom.*, **11**, 703–712.
44. Berndt, H. and Schaldach, G. (1989) Improvement of the power of detection in ICP-OES by a new way of sample introduction (hydraulic high-pressure nebulization). *Fresen. Z. Anal. Chem.*, **335**, 367–369.
45. Berndt, H. (1989) Hydraulic high-pressure nebulization (HHPN) – a new way of (micro) sample introduction for atomic spectroscopy. *Fresen. Z. Anal. Chem.*, **334**, 644–647.
46. Jakubowski, N., Feldmann, I., Stuewer, D. and Berndt, H. (1992) Hydraulic high-pressure nebulization – application of a new nebulization system for inductively coupled plasma mass spectrometry. *Spectrochim. Acta B*, **47**, 119–129.
47. Luo, S.K. and Berndt, H. (1994) Sample introduction in ICP spectrometry by hydraulic high-pressure nebulization. *Spectrochim. Acta B*, **49**, 485–492.
48. Browner, R.F., Wang, L.Q. and May, S.W. (1994) ICP-MS with an oscillating capillary nebulizer for micro-flow liquid chromatography of Se drug metabolites, Abstracts of *Papers of the American Chemical Society*, 208, 148-ANYL.
49. Wang, L.Q., May, S.W., Browner, R.F. and Pollock, S.H. (1996) Low-flow interface for liquid chromatography inductively coupled plasma mass spectrometry speciation using an oscillating capillary nebulizer. *J. Anal. Atom. Spectrom.*, **11**, 1137–1146.
50. Hoang, T.T., May, S.W. and Browner, R.F. (2002) Developments with the oscillating capillary nebulizer – effects of spray chamber design, droplet size and turbulence on analytical signals and analyte transport efficiency of selected biochemically important organoselenium compounds. *J. Anal. Atom. Spectrom.*, **17**, 1575–1581.
51. Kirlew, P.W. and Caruso, J.A. (1998) Investigation of a modified oscillating capillary nebulizer design as an interface for CE-ICP-MS. *Appl. Spectrosc.*, **52**, 770–772.
52. Doherty, M.P. and Hieftje, G.M. (1984) Jet-impact nebulization for sample introduction in inductively coupled plasma spectrometry. *Appl. Spectrosc.*, **38**, 405–412.
53. Zhuang, Z.X., Yang, C.L., Li, B., Yang, P.Y. and Wang, X.R. (1997) Thermospray nebulization as sample introduction for inductively coupled plasma atomic emission spectrometry. *Chem. J. Chinese U.*, **18**, 1939–1943.
54. Zhang, X.H., Chen, D., Marquardt, R. and Koropchak, J.A. (2000) Thermospray sample introduction to atomic spectrometry. *Microchem. J.*, **66**, 17–53.
55. Gotz, R., Elgersma, J.W., Kraak, J.C. and Poppe, H. (1994) Application of an electrospray-interface as a new nebulizer for inductively-coupled plasma-atomic emission-spectrometry. *Spectrochim. Acta B*, **49**, 761–768.
56. Raynor, M.W., Dawson, G.D., Balcerzak, M., Pretorius, W.G. and Ebdon, L. (1997) Electrospray nebulization interface for micro-high performance liquid chromatography inductively coupled plasma mass spectrometry. *J. Anal. Atom. Spectrom.*, **12**, 1057–1064.
57. Elgersma, J.W., Kraak, J.C. and Poppe, H. (1997) Electrospray as interface in the coupling of micro high performance liquid chromatography to inductively coupled plasma atomic emission spectrometry. *J. Anal. Atom. Spectrom.*, **12**, 1065–1068.

58. Layman, L.R. and Lichte, F.E. (1982) Glass frit nebulizer for atomic spectrometry. *Anal. Chem.*, **54**, 638–642.
59. Liu, H.Y., Clifford, R.H., Dolan, S.P. and Montaser, A. (1996) Investigation of a high-efficiency nebulizer and a thimble glass frit nebulizer for elemental analysis of biological materials by inductively coupled plasma-atomic emission spectrometry. *Spectrochim. Acta B*, **51**, 27–40.
60. Maestre, S., Mora, J., Todoli, J.L. and Canals, A. (1999) Evaluation of several commercially available spray chambers for use in inductively coupled plasma atomic emission spectrometry. *J. Anal. Atom. Spectrom.*, **14**, 61–67.
61. Todoli, J.L., Maestre, S., Mora, J., Canals, A. and Hernandis, V. (2000) Comparison of several spray chambers operating at very low liquid flow rates in inductively coupled plasma atomic emission spectrometry. *Fresen. J. Anal. Chem.*, **368**, 773–779.
62. Schaldach, G., Berger, L., Razilov, I. and Berndt, H. (2002) Characterization of a double-pass spray chamber for ICP spectrometry by computer simulation (CFD). *Spectrochim. Acta B*, **57**, 1505–1520.
63. Schaldach, G., Berger, L., Razilov, I. and Berndt, H. (2002) Characterization of a cyclone spray chamber for ICP spectrometry by computer simulation. *J. Anal. Atom. Spectrom.*, **17**, 334–344.
64. Schaldach, G., Berndt, H. and Sharp, B.L. (2003) An application of computational fluid dynamics (CFD) to the characterisation and optimisation of a cyclonic spray chamber for ICP-AES. *J. Anal. Atom. Spectrom.*, **18**, 742–750.
65. Olesik, J.W., Kinzer, J.A. and Harkleroad, B. (1994) Inductively coupled plasma optical emission spectrometry using nebulizers with widely different sample consumption rates. *Anal. Chem.*, **66**, 2022–2030.
66. Scott, R.H., Fassel, V.A., Kniseley, R.N. and Nixon, D.E. (1974) Inductively coupled plasma optical emission analytical spectrometry, a compact facility for trace analysis of solutions. *Anal. Chem.*, **46**, 75–80.
67. Vieira, P.A., Zhizhuang, H., Chan, S. and Montaser, A. (1986) Evaluation of a recycling cyclone spray chamber for ICP-AES. *Appl. Spectrosc.*, **40**, 1141–1146.
68. Canals, A., Hernandis, V., Todoli, J.L. and Browner, R.F. (1995) Fundamental-studies on pneumatic generation and aerosol transport in atomic spectrometry – effect of mineral acids on emission intensity in inductively coupled plasma-atomic emission spectrometry. *Spectrochim. Acta B*, **50**, 305–321.
69. Stewart, I. and Olesik, J.W. (1998) The effect of nitric acid concentration and nebulizer gas flow rates on aerosol properties and transport rates in inductively coupled plasma sample introduction. *J. Anal. Atom. Spectrom.*, **13**, 1249–1256.
70. Jose-Luis, T.A. and Mermet, J.M. (2000) Effect of the spray chamber design on steady and transient acid interferences in inductively coupled plasma atomic emission spectrometry. *J. Anal. Atom. Spectrom.*, **15**, 863–867.
71. Al-Ammar, A., Reitznerova, E. and Barnes, R.M. (2001) Thorium and iodine memory effects in inductively coupled plasma mass spectrometry. *Fresen. J. Anal. Chem.*, **370**, 479–482.
72. Taylor, K.A., Sharp, B.L., Lewis, D.J. and Crews, H.M. (1998) Design and characterisation of a microconcentric nebuliser interface for capillary electrophoresis-inductively coupled plasma mass spectrometry. *J. Anal. Atom. Spectrom.*, **13**, 1095–1100.
73. Walters, P.E. and Barnardt, C.A. (1988) The role of desolvation and hydrogen addition on the excitation features of the inductively coupled plasma. *Spectrochim. Acta B*, **43**, 325–337.
74. Caughlin, B.L. and Blades, M.W. (1987) Effect of wet and dry nebulizer gas on the spatial distribution of electron density. *Spectrochim. Acta B*, **42**, 352–360.
75. Long, S.E. and Browner, R.F. (1988) Influence of water on conditions in the inductively coupled plasma. *Spectrochim. Acta B*, **43B**, 1461–1471.
76. Zhu, G. and Browner, R.F. (1988) Study of the influence of water vapour loading and interface pressure in inductively coupled plasma mass spectrometry. *J. Anal. Atom. Spectrom.*, **3**, 781–789.

77. Peters, G.R. and Beauchemin, D. (1993) Effect of pre-evaporating the solvent on the analytical performance of inductively coupled plasma mass spectrometry. *Spectrochim. Acta B*, **48**, 1481–1494.
78. Eastgate, A.R., Fry, R.C. and Gower, G.H. (1993) Radiation versus conduction in heated spray chamber desolvation for inductively coupled plasmas. *J. Anal. Atom. Spectrom.*, **8**, 305–308.
79. Gras, L., Mora, J., Todoli, J.L., Canals, A. and Hernandis, V. (1999) Desolvation of acid solutions in inductively coupled plasma atomic emission spectrometry by infrared radiation. Comparison with a system based on microwave radiation. *Spectrochim. Acta B*, **54**, 1321–1333.
80. Canals, A., Gras, L., Mora, J., Hernandis, V., Margineda, J., Rojo, M. and Munoz, J. (1999) Insight into the interaction of the microwave radiation with droplets of interest in analytical chemistry. *Spectrochim. Acta B*, **54**, 333–342.
81. Gras, L., Mora, J., Todoli, J.L., Canals, A. and Hernandis, V. (1999) Microwave desolvation for acid sample introduction in inductively coupled plasma atomic emission spectrometry. *Spectrochim. Acta B*, **54**, 469–480.
82. Gras, L., Mora, J., Todoli, J.L., Hernandis, V. and Canals, A. (1997) Behaviour of a desolvation system based on microwave radiation heating for use in inductively coupled plasma atomic emission spectrometry. *Spectrochim. Acta B*, **52**, 1201–1213.
83. Grindlay, G., Maestre, S., Mora, J., Hernandis, V. and Gras, L. (2005) A microwave assisted desolvation system based on the use of a TM010 cavity for inductively coupled plasma based analytical techniques. *J. Anal. Atom. Spectrom.*, **20**, 455–461.
84. Todoli, J.L. and Mermet, J.M. (2002) Influence of the spray chamber design for vapor-based liquid sample introduction at room temperature in ICP-AES. *J. Anal. Atom. Spectrom.*, **17**, 211–218.
85. Todoli, J.L. and Mermet, J.M. (2002) Towards a new compact, low consumption liquid sample introduction system for ICP-AES. *Can. J. Anal. Sci. Spect.*, **47**, 164–170.
86. Todoli, J.L. and Mermet, J.M. (2002) Study of matrix effects using an adjustable chamber volume in a torch-integrated sample introduction system (TISIS) in ICP-AES. *J. Anal. Atom. Spectrom.*, **17**, 913–921.
87. Todoli, J.L. and Mermet, J.M. (2002) New torch design with an in-built chamber for liquid sample analysis by ICP-AES. *J. Anal. Atom. Spectrom.*, **17**, 345–351.
88. Todoli, J.L. and Mermet, J.M. (2003) Optimization of the evaporation cavity in a torch integrated sample introduction system based ICP-AES system. Applications to matrix and transient effects, analysis of microsamples and analysis of certified solid samples. *J. Anal. Atom. Spectrom.*, **18**, 1185–1191.
89. Hill, S.J., Bloxham, M.J. and Worsfold, P.J. (1993) Chromatography coupled with inductively-coupled plasma-atomic emission-spectrometry and inductively-coupled plasma-mass spectrometry – a review. *J. Anal. Atom. Spectrom.*, **8**, 499–515.
90. Hill, S.J., Pitts, L.J. and Fisher, A.S. (2000) High-performance liquid chromatography-isotope dilution inductively coupled plasma mass spectrometry for speciation studies: an overview. *Trac-Trend. Anal. Chem.*, **19**, 120–126.
91. Sutton, K., Sutton, R.M.C. and Caruso, J.A. (1997) Inductively coupled plasma mass spectrometric detection for chromatography and capillary electrophoresis. *J. Chromatogr. A*, **789**, 85–126.
92. Zoorob, G.K., McKiernan, J.W. and Caruso, J.A. (1998) ICP-MS for elemental speciation studies. *Mikrochim. Acta*, **128**, 145–168.
93. Waddell, R., Lewis, C., Hang, W., Hassell, C. and Majidi, V. (2005) Inductively coupled plasma mass spectrometry for elemental speciation: applications in the new millennium. *Appl. Spectrosc. Rev.*, **40**, 33–69.
94. de Leon, C.A.P., Montes-Bayon, M. and Caruso, J.A. (2002) Elemental speciation by chromatographic separation with inductively coupled plasma mass spectrometry detection. *J. Chromatogr. A*, **974**, 1–21.
95. Montes-Bayon, M., DeNicola, K. and Caruso, J.A. (2003) Liquid chromatography-inductively coupled plasma mass spectrometry. *J. Chromatogr. A*, **1000**, 457–476.

96. Caruso, J.A. and Montes-Bayon, M. (2003) Elemental speciation studies – new directions for trace metal analysis. *Ecotox. Environ. Safe.*, **56**, 148–163.
97. Sanz-Medel, A., Montes-Bayon, M. and Sanchez, M.L.F. (2003) Trace element speciation by ICP-MS in large biomolecules and its potential for proteomics. *Anal. Bioanal. Chem.*, **377**, 236–247.
93. Bouyssiere, B., Szpunar, J. and Lobinski, R. (2002) Gas chromatography with inductively coupled plasma mass spectrometric detection in speciation analysis. *Spectrochim. Acta B*, **57**, 805–828.
99. Bouyssiere, B., Szpunar, J., Lespes, G. and Lobinski, R. (2003) Gas chromatography with inductively coupled plasma mass spectrometric detection (GC-ICP MS). *Adv. Chromatogr.*, **42**, 107–137.
100. Wuilloud, J.C.A., Wuilloud, R.G., Vonderheide, A.P. and Caruso, J.A. (2004) Gas chromatography/plasma spectrometry – an important analytical tool for elemental speciation studies. *Spectrochim. Acta B*, **59**, 755–792.
101. Huang, Z.Y., Wu, X.H., Hu, G.L., Zhuang, Z.X. and Wang, X.R. (2002) Speciation analysis with hyphenated technique of high performance liquid chromatography and inductively coupled plasma mass spectrometry. *Chinese J. Anal. Chem.*, **30**, 1387–1393.
102. Brown, A.A., Ebdon, L. and Hill, S.J. (1994) Development of a coupled liquid-chromatography isotope-dilution inductively-coupled plasma-mass spectrometry method for lead speciation. *Anal. Chim. Acta*, **286**, 391–399.
103. Cairns, W.R.L., Ebdon, L. and Hill, S.J. (1996) A high performance liquid chromatography – Inductively coupled plasma-mass spectrometry interface employing desolvation for speciation studies of platinum in chemotherapy drugs. *Fresen. J. Anal. Chem.*, **355**, 202–208.
104. Ebdon, L., Hill, S.J. and Rivas, C. (1998) Lead speciation in rainwater by isotope dilution-high performance liquid chromatography inductively coupled plasma mass spectrometry. *Spectrochim. Acta B*, **53**, 289–297.
105. Rivas, C., Ebdon, L. and Hill, S.J. (1996) Effect of different spray chambers on the determination of organotin compounds by high-performance liquid chromatography inductively coupled plasma mass spectrometry. *J. Anal. Atom. Spectrom.*, **11**, 1147–1150.
106. Rivas, C., Ebdon, L., Evans, E.H. and Hill, S.J. (1996) An evaluation of reversed-phase and ion-exchange chromatography for use with inductively coupled plasma mass spectrometry for the determination of organotin compounds. *Appl. Organomet. Chem.*, **10**, 61–68.
107. Acon, B.W., McLean, J.A. and Montaser, A. (2001) A direct injection high efficiency nebulizer interface for microbore high-performance liquid chromatography-inductively coupled plasma mass spectrometry. *J. Anal. Atom. Spectrom.*, **16**, 852–857.
108. Koropchak, J.A., Sadain, S. and Szostek, B. (1996) Dispersion of discrete sample signals within aerosol spray chambers: preliminary investigations. *Spectrochim. Acta B*, **51**, 1733–1745.
109. Bendahl, L. and Gammelgaard, B. (2005) Sample introduction systems for reversed phase LC-ICP-MS of selenium using large amounts of methanol – comparison of systems based on membrane desolvation, a spray chamber and direct injection. *J. Anal. Atom. Spectrom.*, **20**, 410–416.
110. Jensen, B.P., Gammelgaard, B., Hansen, S.H. and Andersen, J.V. (2003) Comparison of direct injection nebulizer and desolvating microconcentric nebulizer for analysis of chlorine-, bromine- and iodine-containing compounds by reversed phase HPLC with ICP-MS detection. *J. Anal. Atom. Spectrom.*, **18**, 891–896.
111. Krachler, M. and Emons, H. (2001) Speciation analysis of antimony by high-performance liquid chromatography inductively coupled plasma mass spectrometry using ultrasonic nebulization. *Anal. Chim. Acta*, **429**, 125–133.
112. Yang, H.J. and Jiang, S.J. (1995) Hydride generation inductively-coupled plasma-mass spectrometric detection of lead compounds separated by liquid-chromatography. *J. Anal. Atom. Spectrom.*, **10**, 963–967.
113. Kirby, J., Maher, W., Ellwood, M. and Krikowa, F. (2004) Arsenic species determination in biological tissues by HPLC-ICP-MS and HPLC-HG-ICP-MS. *Aust. J. Chem.*, **57**, 957–966.

114. Nakazato, T., Tao, H., Taniguchi, T. and Isshiki, K. (2002) Determination of arsenite, arsenate, and monomethylarsonic acid in seawater by ion-exclusion chromatography combined with inductively coupled plasma mass spectrometry using reaction cell and hydride generation techniques. *Talanta*, **58**, 121–132.
115. Nakazato, T., Taniguchi, T., Tao, H., Tominaga, M. and Miyazaki, A. (2000) Ion-exclusion chromatography combined with ICP-MS and hydride generation-ICP-MS for the determination of arsenic species in biological matrices. *J. Anal. Atom. Spectrom.*, **15**, 1546–1552.
116. Gomez-Ariza, J.L., Sanchez-Rodas, D., Giraldez, I. and Morales, E. (2000) Comparison of biota sample pretreatments for arsenic speciation with coupled HPLC-HG-ICP-MS. *Analyst*, **125**, 401–407.
117. Li, J.X., Umemura, T., Otake, T. and Tsunoda, K. (2001) A high-efficiency cross-flow micronebulizer interface for capillary electrophoresis and inductively coupled plasma mass spectrometry. *Anal. Chem.*, **73**, 5992–5999.
118. Michalke, B. (2005) Capillary electrophoresis-inductively coupled plasma-mass spectrometry: a report on technical principles and problem solutions, potential, and limitations of this technology as well as on examples of application. *Electrophoresis*, **26**, 1584–1597.
119. Alvarez-Llamas, G., de la Campa, M.D. and Sanz-Medel, A. (2005) ICP-MS for specific detection in capillary electrophoresis. *Trac-Trend. Anal. Chem.*, **24**, 28–36.
120. Michalke, B. (2004) Manganese speciation using capillary electrophoresis-ICP-mass spectrometry. *J. Chromatogr. A*, **1050**, 69–76.
121. Michalke, B. (2000) CE-ICP-MS: advantages and improvements in selenium speciation. *Spectroscopy*, **15**, 31–34.
122. Michalke, B. and Schramel, P. (1999) Iodine speciation in biological samples by capillary electrophoresis – inductively coupled plasma mass spectrometry. *Electrophoresis*, **20**, 2547–2553.
123. Michalke, B. (1999) Potential and limitations of capillary electrophoresis inductively coupled plasma mass spectrometry – invited lecture. *J. Anal. Atom. Spectrom.*, **14**, 1297–1302.
124. Michalke, B. and Schramel, P. (1999) Antimony speciation in environmental samples by interfacing capillary electrophoresis on-line to an inductively coupled plasma mass spectrometer. *J. Chromatogr. A*, **834**, 341–348.
125. Michalke, B. and Schramel, P. (1998) The coupling of capillary electrophoresis to ICP-MS. *Analysis*, **26**, M51–M56.
126. Michalke, B. and Schramel, P. (1998) Capillary electrophoresis interfaced to inductively coupled plasma mass spectrometry for element selective detection in arsenic speciation. *Electrophoresis*, **19**, 2220–2225.
127. Michalke, B. and Schramel, P. (1998) Selenium speciation by interfacing capillary electrophoresis with inductively coupled plasma-mass spectrometry. *Electrophoresis*, **19**, 270–275.
128. Lustig, S., Michalke, B., Beck, W. and Schramel, P. (1998) Platinum speciation with hyphenated techniques: high performance liquid chromatography and capillary electrophoresis on-line coupled to an inductively coupled plasma-mass spectrometer – application to aqueous extracts from a platinum treated soil. *Fresen. J. Anal. Chem.*, **360**, 18–25.
129. Michalke, B. and Schramel, P. (1997) Coupling of capillary electrophoresis with ICP-MS for speciation investigations. *Fresen. J. Anal. Chem.*, **357**, 594–599.
130. Michalke, B., Lustig, S. and Schramel, P. (1997) Analysis for the stability of platinum-containing species in soil samples using capillary electrophoresis interfaced on-line with inductively coupled plasma mass spectrometry. *Electrophoresis*, **18**, 196–201.
131. Michalke, B. and Schramel, P. (1996) Hyphenation of capillary electrophoresis to inductively coupled plasma mass spectrometry as an element-specific detection method for metal speciation. *J. Chromatogr. A*, **750**, 51–62.
132. Ballihaut, G., Tastet, L., Pecheyran, C., Bouyssiere, B., Donard, O., Grimaud, R. and Lobinski, R. (2005) Biosynthesis, purification and analysis of selenomethionyl calmodulin by gel

- electrophoresis-laser ablation-ICP-MS and capillary HPLC-ICP-MS peptide mapping following in-gel tryptic digestion. *J. Anal. Atom. Spectrom.*, **20**, 493–499.
133. Becker, J.S., Zoriy, M., Pickhardt, C. and Przybylski, M. (2005) Investigation of Cu-, Zn- and Fe-containing human brain proteins using isotopic-enriched tracers by LA-ICP-MS and MALDI-FT-ICR-MS. *Int. J. Mass Spectrom.*, **242**, 135–144.
134. Szpunar, J. (2005) Advances in analytical methodology for bioinorganic speciation analysis: metallomics, metalloproteomics and heteroatom-tagged proteomics and metabolomics. *Analyst*, **130**, 442–465.
135. Becker, J.S., Zoriy, M., Krause-Buchholz, U., Pickhardt, C., Przybylski, M., Pompe, W. and Rodel, G. (2004) In-gel screening of phosphorus and copper, zinc and iron in proteins of yeast mitochondria by LA-ICP-MS and identification of phosphorylated protein structures by MALDI-FT-ICR-MS after separation with two-dimensional gel electrophoresis. *J. Anal. Atom. Spectrom.*, **19**, 1236–1243.
136. Ma, R.L., McLeod, C.W., Tomlinson, K. and Poole, R.K. (2004) Speciation of protein-bound trace elements by gel electrophoresis and atomic spectrometry. *Electrophoresis*, **25**, 2469–2477.
137. Chassaing, H., Chery, C.C., Bordin, G., Vanhaecke, F. and Rodriguez, A.R. (2004) 2-Dimensional gel electrophoresis technique for yeast selenium-containing proteins – sample preparation and MS approaches for processing 2-D gel protein spots. *J. Anal. Atom. Spectrom.*, **19**, 85–95.
138. Bandura, D.R., Ornatsky, O. and Liao, L. (2004) Characterization of phosphorus content of biological samples by ICP-DRC-MS: potential tool for cancer research. *J. Anal. Atom. Spectrom.*, **19**, 96–100.
139. Becker, J.S., Zoriy, M., Pickhardt, C. and Przybylski, M. (2004) Determination of phosphorus and metals in human brain proteins after isolation by gel electrophoresis by laser ablation inductively coupled plasma source mass spectrometry. *J. Anal. Atom. Spectrom.*, **19**, 149–152.
140. Chery, C.C., Günther, D., Cornelis, R., Vanhaecke, F. and Moens, L. (2003) Detection of metals in proteins by means of polyacrylamide gel electrophoresis and laser ablation-inductively coupled plasma-mass spectrometry: application to selenium. *Electrophoresis*, **24**, 3305–3313.
141. Becker, J.S., Boulyga, S.F., Pickhardt, C., Damoc, E. and Przybylski, M. (2003) Structural identification and quantification of protein phosphorylations after gel electrophoretic separation using Fourier transform ion cyclotron resonance mass spectrometry and laser ablation inductively coupled plasma mass spectrometry. *Int. J. Mass Spectrom.*, **228**, 985–997.
142. Binet, M.R.B., Ma, R.L., McLeod, C.W. and Poole, R.K. (2003) Detection and characterization of zinc- and cadmium-binding proteins in *Escherichia coli* by gel electrophoresis and laser ablation-inductively coupled plasma-mass spectrometry. *Anal. Biochem.*, **318**, 30–38.
143. Wind, M., Feldmann, I., Jakubowski, N. and Lehmann, W.D. (2003) Spotting and quantification of phosphoproteins purified by gel electrophoresis and laser ablation-element mass spectrometry with phosphorus-31 detection. *Electrophoresis*, **24**, 1276–1280.
144. Fan, T.W.M., Pruszkowski, E. and Shuttleworth, S. (2002) Speciation of selenoproteins in Se-contaminated wildlife by gel electrophoresis and laser ablation-ICP-MS. *J. Anal. Atom. Spectrom.*, **17**, 1621–1623.
145. Evens, R.D. and Villeneuve, J.Y. (2000) A method for characterization of humic and fulvic acids by gel electrophoresis laser ablation inductively coupled plasma mass spectrometry. *J. Anal. Atom. Spectrom.*, **15**, 157–161.
146. Nielsen, J.L., Abildtrup, A., Christensen, J., Watson, P., Cox, A. and McLeod, C.W. (1998) Laser ablation inductively coupled plasma-mass spectrometry in combination with gel electrophoresis: a new strategy for speciation of metal binding serum proteins. *Spectrochim. Acta B*, **53**, 339–345.
147. Moreda-Pineiro, J., Lopez-Mahia, P., Muniategui-Lorenzo, S., Fernandez-Fernandez, E. and Prada-Rodriguez, D. (2002) Direct As, Bi, Ge, Hg and Se (IV) cold vapor/hydride generation from coal fly ash slurry samples and determination by electrothermal atomic absorption spectrometry. *Spectrochim. Acta B*, **57**(5), 883–895.

148. Howard, A.G. (1997) (Boro)hydride techniques in trace element speciation. *J. Anal. Atom. Spectrom.*, **12**(3), 267–272.
149. Duan, X.C., McLaughlin, R.L., Brindle, I.D. and Conn, A. (2002) Investigations into the generation of Ag, Au, Cd, Co, Cu, Ni, Sn and Zn by vapour generation and their determination by inductively coupled plasma atomic emission spectrometry, together with a mass spectrometric study of volatile species. Determination of Ag, Au, Co, Cu, Ni and Zn in iron. *J. Anal. Atom. Spectrom.*, **17**(3), 227–231.
150. Pohl, P. and Zyrnicki, W. (2003) Analytical features of Au, Pd and Pt chemical vapour generation inductively coupled plasma atomic emission spectrometry. *J. Anal. Atom. Spectrom.*, **18**(7), 798–801.
151. Ebdon, L., Goodall, P., Hill, S.J., Stockwell, P. and Thompson, K.C. (1994) Approach to the determination of lead by vapour generation atomic-absorption spectrometry. *J. Anal. Atom. Spectrom.*, **9**(12), 1417–1421.
152. D’Ulivo, A., Gianfranceschi, L., Lampugnani, L. and Zamboni, R. (2002) Masking agents in the determination of selenium by hydride generation technique. *Spectrochim. Acta B*, **57**(12), 2081–2094.
153. Dedina, J. and Tsalev, D. (1995). *Hydride Generation and Atomic Absorption Spectrometry*. John Wiley and Sons. Chichester, UK.
154. Pohl, P. (2004) Hydride generation – recent advances in atomic emission spectrometry. *TRAC-Trend. Anal. Chem.*, **23**(2), 87–101.
155. Welz, B. and Sperling, M. (1999) *Atomic Absorption Spectrometry*, Third, Completely Revised Edition. Wiley-VCH, Weinheim, Germany.
156. Nobrega, J.A., Rust, J., Calloway, C.P. and Jones, B.T. (2004) Use of modifiers with metal atomizers in electrothermal atomic absorption spectrometry: a short review. *Spectrochim. Acta part B*, **59**(9), 1337–1345.
157. Parsons, P.J., Zhou, Y., Palmer, C.D., Brockman, P. and Aldous, K.M. (2003) Atomization and vaporization of lead from a blood matrix using rhodium-coated tungsten filaments with pseudo-simultaneous electrothermal atomic absorption and inductively coupled plasma mass spectrometric measurements. *J. Anal. Atom. Spectrom.*, **18**(1), 4–10.
158. Martin-Esteban, A. and Slowikowski, B. (2003) Electrothermal vaporization – Inductively coupled plasma-mass spectrometry (ETV-ICP-MS): a valuable tool for direct multielement determination in solid samples. *Crit. Rev. Anal. Chem.*, **33**(1), 43–55.
159. Vanhaecke, F., Resano, M. and Moens, L. (2002) Electrothermal vaporisation ICP-mass spectrometry (ETV-ICP-MS) for the determination and speciation of trace elements in solid samples – a review of real-life applications from the author’s lab. *Anal. Bioanal. Chem.*, **374**(2), 188–195.
160. Todoli, J.L. and Mermet, J.M. (2005) Elemental analysis of liquid microsamples through inductively coupled plasma Spectrochemistry. *TRAC-Tends Anal. Chem.*, **24**(2), 107–116.
161. Karanassios, V. and Horlick, G. (1990) Direct sample insertion devices for coupled plasma spectrometry. *Spectrochim. Acta Rev.*, **13**, 89–166.
162. Sing, R. (1999) Direct sample insertion for inductively coupled plasma spectrometry. *Spectrochim. Acta Part B*, **54**(3–4), 411–441.
163. Gray, A.L. (1985) Solid sample introduction by laser ablation for inductively coupled plasma source mass spectrometry. *Analyst*, **110**, 551–556.
164. Horn, I., Guillon, M. and Günther, D. (2001) Wavelength dependent ablation rates for metals and silicate glasses using homogenized laser beam profiles – implications for LA-ICP-MS. *Appl. Surf. Sci.*, **182**, 91–102.
165. Niemax, K. (2001) LA – reflections on a very complex technique for solid sampling. *Fresen. J. Anal. Chem.*, **370**, 332–340.
166. Jeffries, T.E., Jackson, S.E. and Longerich, H.P. (1998) Application of a frequency quintupled Nd:YAG source ($\lambda = 213$ nm) for laser ablation inductively coupled plasma mass spectrometric analysis of minerals. *J. Anal. Atom. Spectrom.*, **13**, 935–940.

167. Guillon, M., Horn, I. and Günther, D. (2003) A comparison of 266 nm, 213 nm and 193 nm produced from a single solid state Nd:YAG laser for laser ablation ICP-MS. *J. Anal. Atom. Spectrom.*, **18**, 1224–1230.
168. Horn, I., Günther, D. and Guillon, M. (2003) Evaluation and design of a solid-state 193 nm OPO-Nd: YAG laser ablation system. *Spectrochim. Acta B*, **58**, 1837–1846.
169. Geertsens, C., Briand, A., Chartier, F., Lacour, J.L., Mauchien, P., Sjöstrom, S. and Mermet, J.M. (1994) Comparison between infrared and ultraviolet-laser ablation at atmospheric-pressure – implications for solid sampling inductively-coupled plasma spectrometry. *J. Anal. Atom. Spectrom.*, **9**, 17–22.
170. Jeffries, T.E., Perkins, W.T. and Pearce, N.J.G. (1995) Comparison of infrared and ultraviolet laser probe microanalysis inductively coupled plasma mass spectrometry in mineral analysis. *Analyst*, **120**, 1365–1371.
171. Liu, H.C., Borisov, O.V., Mao, X.L., Shuttleworth, S. and Russo, R.E. (2000) Pb/U fractionation during Nd:YAG 213 nm and 266 nm laser ablation sampling with inductively coupled plasma mass spectrometry. *Appl. Spectrosc.*, **54**, 1435–1442.
172. Russo, R.E., Mao, X.L., Borisov, O.V. and Liu, H.C. (2000) Influence of wavelength on fractionation in laser ablation ICP-MS. *J. Anal. Atom. Spectrom.*, **15**, 1115–1120.
173. Tenzler, D. and Becker, J.S. (2001) Studies of LA-ICP-MS on quartz glasses at different wavelengths of a Nd:YAG laser. *Fresen. J. Anal. Chem.*, **370**, 637–640.
174. Motelica-Heino, M., Le Coustumer, P. and Donard, O.F.X. (2001) Micro- and macro-scale investigation of fractionation and matrix effects in LA-ICP-MS at 1064 nm and 266 nm on glassy materials. *J. Anal. Atom. Spectrom.*, **16**, 542–550.
175. Gonzalez, J., Mao, X.L., Roy, J., Mao, S.S. and Russo, R.E. (2002) Comparison of 193, 213 and 266 nm laser ablation ICP-MS. *J. Anal. Atom. Spectrom.*, **17**, 1108–1113.
176. Guillon, M. and Günther, D. (2002) Effect of particle size distribution on ICP-induced elemental fractionation in laser ablation-inductively coupled plasma-mass spectrometry. *J. Anal. Atom. Spectrom.*, **17**, 831–837.
177. Varel, M.W.H., Rosenfeld, A., Ashkenasi, D. and Campbell, E.E.B. (1998) Femtosecond laser ablation of Sapphire: TOF analysis of ablation plume. *Appl. Surf. Sci.*, **127–129**, 128–133.
178. Mao, S.S., Mao, X.L., Greif, R. and Russo, R.E. (2000) Initiation of an early-stage plasma during picosecond laser ablation of solids. *Appl. Phys. Lett.*, **77**, 2464–2466.
179. Mao, S.S., Mao, X.L., Greif, R. and Russo, R.E. (2000) Simulation of a picosecond laser ablation plasma. *Appl. Phys. Lett.*, **76**, 3370–3372.
180. Margetic, V., Pakulev, A., Stockhaus, A., Bolshov, M., Niemax, K. and Hergenroder, R. (2000) A comparison of nanosecond and femtosecond laser-induced plasma spectroscopy of brass samples. *Spectrochim. Acta B*, **55**, 1771–1785.
181. Margetic, V., Bolshov, M., Stockhaus, A., Niemax, K. and Hergenroder, R. (2001) Depth profiling of multi-layer samples using femtosecond laser ablation. *J. Anal. Atom. Spectrom.*, **16**, 616–621.
182. Russo, R.E., Mao, X.L., Gonzalez, J.J. and Mao, S.S. (2002) Femtosecond laser ablation ICP-MS. *J. Anal. Atom. Spectrom.*, **17**, 1072–1075.
183. Poitrasson, F., Mao, X.L., Mao, S.S., Freydisier, R. and Russo, R.E. (2003) Comparison of ultraviolet femtosecond and nanosecond laser ablation inductively coupled plasma mass spectrometry analysis in glass, monazite, and zircon. *Anal. Chem.*, **75**, 6184–6190.
184. Gonzalez, J., Liu, C.Y., Mao, X.L. and Russo, R.E. (2004) UV-femtosecond laser ablation-ICP-MS for analysis of alloy samples. *J. Anal. Atom. Spectrom.*, **19**, 1165–1168.
185. Koch, J., von Bohlen, A., Hergenroder, R. and Niemax, K. (2004) Particle size distributions and compositions of aerosols produced by near-IR femto- and nanosecond laser ablation of brass. *J. Anal. Atom. Spectrom.*, **19**, 267–272.
186. Zeng, X., Mao, X.L., Greif, R. and Russo, R.E. (2005) Experimental investigation of ablation efficiency and plasma expansion during femtosecond and nanosecond laser ablation of silicon. *Appl. Phys. A-Mater.*, **80**, 237–241.

187. Arrowsmith, P. and Hughes, S.K. (1988) Entrainment and transport of laser ablated plumes for subsequent elemental analysis. *Appl. Spectrosc.*, **42**, 1231–1239.
188. Jackson, S.E., Horn, I. and Longerich, H.P. (1996) The application of laser ablation microprobe (LAM)-ICP-MS to *in situ* U–Pb zircon geochronology. *V. M. Goldschmidt Conf. J. Conf. Abstracts*, **1**, 283.
189. Eggins, S.M., Kinsley, L.P.J. and Shelley, J.M.G. (1998) Deposition and element fractionation processes during atmospheric pressure laser sampling for analysis by ICP-MS. *Appl. Surf. Sci.*, **129**, 278–286.
190. Günther, D. and Heinrich, C.A. (1999) Enhanced sensitivity in laser ablation-ICP mass spectrometry using helium–argon mixtures as aerosol carrier – plenary lecture. *J. Anal. Atom. Spectrom.*, **14**, 1363–1368.
191. Horn, I. and Günther, D. (2003) The influence of ablation carrier gasses Ar, He and Ne on the particle size distribution and transport efficiencies of laser ablation-induced aerosols: implications for LA-ICP-MS. *Appl. Surf. Sci.*, **207**, 144–157.
192. Günther, D. and Heinrich, C.A. (1999) Comparison of the ablation behaviour of 266 nm Nd:YAG and 193 nm ArF excimer lasers for LA-ICP-MS analysis. *J. Anal. Atom. Spectrom.*, **14**, 1369–1374.
193. Mank, A.J.G. and Mason, P.R.D. (1999) A critical assessment of laser ablation ICP-MS as an analytical tool for depth analysis in silica-based glass samples. *J. Anal. Atom. Spectrom.*, **14**, 1143–1153.
194. Perkins, W.T., Fuge, R. and Pearce, N.J.G. (1991) Quantitative-analysis of trace-elements in carbonates using laser ablation inductively coupled plasma mass-spectrometry. *J. Anal. Atom. Spectrom.*, **6**, 445–449.
195. Vanheuzen, A.A. and Morsink, J.B.W. (1991) Analysis of solids by laser ablation inductively coupled plasma mass-spectrometry (La-Icp-Ms). 2. Matching with a pressed pellet. *Spectrochim. Acta B*, **46**, 1819–1828.
196. Durrant, S.F. (1992) Multielemental analysis of environmental matrices by laser ablation inductively coupled plasma mass spectrometry. *Analyst*, **117**, 1585–1592.
197. Jarvis, K.E. and Williams, J.G. (1993) Laser-ablation inductively-coupled plasma-mass spectrometry (LA-ICP-MS) – a rapid technique for the direct, quantitative-determination of major, trace and rare-earth elements in geological samples, *Chem. Geol.*, **106**, 251–262.
198. Perkins, W.T., Pearce, N.J.G. and Jeffries, T.E. (1993) Laser ablation inductively coupled plasma mass-spectrometry – a new technique for the determination of trace and ultra-trace elements in silicates. *Geochim. Cosmochim. Acta*, **57**, 475–482.
199. Williams, J.G. and Jarvis, K.E. (1993) Preliminary assessment of laser ablation inductively coupled plasma mass-spectrometry for quantitative multielement determination in silicates. *J. Anal. Atom. Spectrom.*, **8**, 25–34.
200. Perkins, W.T., Pearce, N.J.G. and Westgate, J.A. (1997) The development of laser ablation ICP-MS and calibration strategies: examples from the analysis of trace elements in volcanic glass shards and sulfide minerals. *Geostd. Newslett. J. Geostd. Geoanal.*, **21**, 175–190.
201. Motelica-Heino, M., Donard, O.F.X. and Mermet, J.M. (1999) Laser ablation of synthetic geological powders using ICP-AES detection: effects of the matrix, chemical form of the analyte and laser wavelength. *J. Anal. Atom. Spectrom.*, **14**, 675–682.
202. Bellotto, V.R. and Mielekey, N. (2000) Improvements in calibration procedures for the quantitative determination of trace elements in carbonate material (mussel shells) by laser ablation ICP-MS. *Fresen. J. Anal. Chem.*, **367**, 635–640.
203. Tibi, M. and Heumann, K.G. (2003) Isotope dilution mass spectrometry as a calibration method for the analysis of trace elements in powder samples by LA-ICP-MS. *J. Anal. Atom. Spectrom.*, **18**, 1076–1081.
204. Tibi, M. and Heumann, K.G. (2003) Multi-element trace determinations in pure alkaline earth fluoride powders by high-resolution ICP-MS using wet-chemical sample preparation and laser ablation. *Anal. Bioanal. Chem.*, **377**, 126–131.

205. Boulyga, S.F. and Heumann, K.G. (2004) Comparative LA-ICP-IDMS determinations of trace elements in powdered samples using laser ablation systems with low and high ablation rates. *J. Anal. Atom. Spectrom.*, **19**, 1501–1503.
206. Vanheuzen, A.A. (1991) Analysis of solids by laser ablation inductively coupled plasma mass spectrometry (La-Icp-Ms). I. Matching with a glass matrix. *Spectrochim. Acta B*, **46**, 1803–1817.
207. Günther, D., von Quadt, A., Wirz, R., Cousin, H. and Dietrich, V.J. (2001) Elemental analyses using laser ablation-inductively coupled plasma-mass spectrometry (LA-ICP-MS) of geological samples fused with $\text{Li}_2\text{B}_4\text{O}_7$ and calibrated without matrix-matched standards. *Mikrochim. Acta*, **136**, 101–107.
208. Lee, Y.L., Chang, C.C. and Jiang, S.J. (2003) Laser ablation inductively coupled plasma mass spectrometry for the determination of trace elements in soil. *Spectrochim. Acta B*, **58**, 523–530.
209. Weis, P., Beck, H. and Günther, D. (2005) Characterizing ablation and aerosol generation during elemental fractionation on absorption modified lithium tetraborate glasses using LA-ICP-MS. *Anal. Bioanal. Chem.*, **381**, 212–224.
210. Thompson, M., Chenery, S. and Brett, L. (1989) Calibration studies in laser ablation microprobe – inductively coupled plasma atomic emission-spectrometry. *J. Anal. Atom. Spectrom.*, **4**, 11–16.
211. Baldwin, D.P., Zamzow, D.S. and Dsilva, A.P. (1994) Aerosol mass measurement and solution standard additions for quantitation in laser-ablation inductively-coupled plasma-atomic emission-spectrometry. *Anal. Chem.*, **66**, 1911–1917.
212. Cromwell, E.F. and Arrowsmith, P. (1995) Semiquantitative analysis with laser-ablation inductively-coupled plasma-mass spectrometry. *Anal. Chem.*, **67**, 131–138.
213. Günther, D., Cousin, H., Magyar, B. and Leopold, I. (1997) Calibration studies on dried aerosols for laser ablation inductively coupled plasma mass spectrometry. *J. Anal. Atom. Spectrom.*, **12**, 165–170.
214. Falk, H.F., Hattendorf, B., Kregel-Rothensee, K., Wieberneit, N. and Dannen, S.L. (1998) Calibration of laser-ablation ICP-MS. Can we use synthetic standards with pneumatic nebulization? *Fresen. J. Anal. Chem.*, **362**, 468–472.
215. Bings, N.H. (2002) Direct determination of metals in lubricating oils by laser ablation coupled to inductively coupled plasma time-of-flight mass spectrometry. *J. Anal. Atom. Spectrom.*, **17**, 759–767.
216. Leach, J.J., Allen, L.A., Aeschliman, D.B. and Houk, R.S. (1999) Calibration of laser ablation inductively coupled plasma mass spectrometry using standard additions with dried solution aerosols. *Anal. Chem.*, **71**, 440–445.
217. Bi, M., Ruiz, A.M., Smith, B.W. and Winefordner, J.D. (2000) Study of solution calibration of NIST soil and glass samples by laser ablation inductively coupled plasma mass spectrometry. *Appl. Spectrosc.*, **54**, 639–644.
218. Becker, J.S., Pickhardt, C. and Dietze, H.J. (2000) A new strategy of solution calibration in LA-ICP-MS for multielement trace analysis in geological samples. *Fresen. J. Anal. Chem.*, **368**, 173–181.
219. Horn, I., Rudnick, R.L. and McDonough, W.F. (2000) Precise elemental and isotope ratio determination by simultaneous solution nebulization and laser ablation-ICP-MS: application to U–Pb geochronology. *Chem. Geol.*, **167**, 405–425.
220. Becker, J.S., Pickhardt, C. and Dietze, H.J. (2001) Determination of trace elements in high-purity platinum by laser ablation inductively coupled plasma mass spectrometry using solution calibration. *J. Anal. Atom. Spectrom.*, **16**, 603–606.
221. Boulyga, S.F., Pickhardt, C. and Becker, J.S. (2004) New approach of solution-based calibration in laser ablation inductively coupled plasma mass spectrometry of trace elements in metals and reduction of fractionation effects. *Atom. Spectrosc.*, **25**, 53–63.
222. Halicz, L. and Günther, D. (2004) Quantitative analysis of silicates using LA-ICP-MS with liquid calibration. *J. Anal. Atom. Spectrom.*, **19**, 1539–1545.

-
223. O' Connor, C., Sharp, B.L. and Evans, P. (2006) On-line additions of aqueous standards for calibration of laser ablation inductively coupled plasma mass spectrometry: theory and comparison of wet and dry plasma conditions. *J. Anal. Atom. Spectrom.*, **21**, 556–565.
 224. Boue-Bigne, F., Masters, B.J., Crighton, J.S. and Sharp, B.L. (1999) A calibration strategy for LA-ICP-MS analysis employing aqueous standards having modified absorption coefficients. *J. Anal. Atom. Spectrom.*, **14**, 1665–1672.
 225. Günther, D., Frischnecht, R., Müschenborn, H.J., Heinrich, C.A. (1997) Direct liquid ablation – a new strategy for LA-ICP-MS microanalysis of liquids and solids. *Fresen. J. Anal. Chem.*, **359**, 390–393.
 226. Boulyga, S.F., Tibi, M., Heumann, K.G. (2004) Application of isotope-dilution laser ablation ICP-MS for direct determination of Pu concentrations in soils at pg g^{-1} levels. *Anal. Bioanal. Chem.*, **378**, 342–347.
 227. Becker, J.S., Pickhardt, C. and Pompe, W. (2004) Determination of Ag, Tl, and Pb in few milligrams of platinum nanoclusters by on-line isotope dilution in laser ablation inductively coupled plasma mass spectrometry. *Int. J. Mass Spectrom.*, **237**, 13–17.
 228. Becker, J.S. (2002) Applications of inductively coupled plasma mass spectrometry and laser ablation inductively coupled plasma mass spectrometry in materials science. *Spectrochim. Acta B*, **57**, 1805–1820.
 229. Becker, J.S. (2002) State-of-the-art and progress in precise and accurate isotope ratio measurements by ICP-MS and LA-ICP-MS – plenary lecture. *J. Anal. Atom. Spectrom.*, **17**, 1172–1185.

Chapter 5

Fundamental Aspects of Inductively Coupled Plasma – Mass Spectrometry (ICP-MS)

Gavin O'Connor and E. Hywel Evans

5.1 The ICP as an ion source

The inductively coupled plasma (ICP) was first developed by Reed [1–3] in 1960, and was first used by Greenfield *et al.* [4] for spectrochemical analysis. An atmospheric ICP is formed when an inert gas, usually argon, is introduced into a quartz torch that consists of three tubes of varying diameter. The inner tube carries the sample aerosol in a flow of argon, and the intermediate and outer tubes carry gas flows which both form the plasma and cool the torch. On entering the torch the argon is seeded with electrons by initial excitation with a tesla coil. The electrons are then accelerated in the magnetic field, induced by the application of radio-frequency (rf) energy to a copper coil surrounding the torch, collide with neutral argon atoms and ionise them. The ions and electrons continuously collide, and as long as the rf field is maintained the plasma is sustained. A diagram of a typical ICP used in ICP-MS is shown in Fig. 5.1. The shape of the ICP is of fundamental importance for its use as an ionisation and excitation source. The tangential flow of gas into the torch creates a vortex that weakens the base of the plasma. This enables the easy punching of the plasma by the nebuliser gas flow, which carries the sample into the centre of the fire-ball. The majority of the rf power is coupled into the outer region of the gas flow, which leads to a skin effect whereby the outer regions of the plasma are hotter than the central

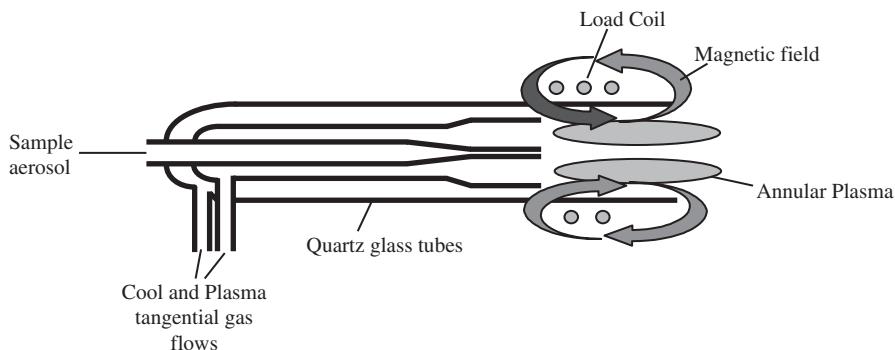
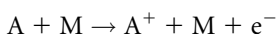
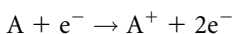


Figure 5.1 Schematic diagram of an inductively coupled plasma.

channel. The centre of the plasma is heated by conduction, convection and radiative transfer of energy from the skin.

The resulting plasma is a dense annular-shaped ball of highly excited electrons, ions, metastable and neutral species. The ionisation of the analyte in ICP-MS is a complex process that has invoked major discussion in the past [5,6] and will continue to do so in the future. The operating temperature of an ICP is between 5000 and 10 000 K. This leads to desolvation and thermal atomisation of analytes introduced into the central region of the plasma. Once atomised, ionisation may occur by a number of processes [6].

Thermal ionisation is induced by collisions among ions, atoms and free electrons in the plasma:



If an electron absorbs sufficient energy, equal to its first ionisation energy, it escapes the atomic nucleus and an ion is formed. In the ICP, the major mechanism by which ionisation occurs is thermal ionisation. When a system is in thermal equilibrium, the degree of ionisation of an atom is given by the Saha equation:

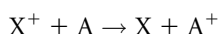
$$\frac{n_i n_e}{n_a} = 2 \frac{Z_i}{Z_a} \left(2\pi m k \frac{T}{h^2} \right)^{\frac{3}{2}} \exp(-E_i/kT) \quad (5.1)$$

where n_i , n_e and n_a are the number densities of the ions, free electrons and atoms, respectively; Z_i and Z_a are the ionic and atomic partition functions, respectively; m is the electron mass; k is the Boltzmann constant; T is the temperature; h is Planck's constant and E_i is the first ionisation energy. In this case, ionisation is effected by ion-atom and atom-atom collisions, where the energy required for ionisation is derived from thermal agitation of the particles. The degree of ionisation is dependent on the electron number density, the temperature and the ionisation energy of the element in question. Taking the average electron number density for an argon ICP to be $4 \times 10^{15} \text{ cm}^{-3}$ and the ionisation temperature to be 8730 K, then the degree of ionisation as a function of first ionisation energy, predicted by the Saha equation, is shown in Fig. 5.2. Most of the elements in the periodic table have first ionisation energies of less than 9 eV and are over 80% ionised in the ICP. A third of the elements are ionised to a lesser extent depending on their first ionisation energy, with the most poorly ionised elements being He, Ne, F, O and N (<1% ionised); Kr and Cl (1–10%); C, Br, Xe and S (10–30%) and P, I, Hg, As, Au and Pt (30–80%). Such thermal ionisation is probably the dominant mechanism of ionisation in the ICP.

Penning ionisation is caused by charge exchange between plasma gas metastable species and analyte atoms:



Charge transfer is caused by transfer of energy from an ion to an analyte ion:



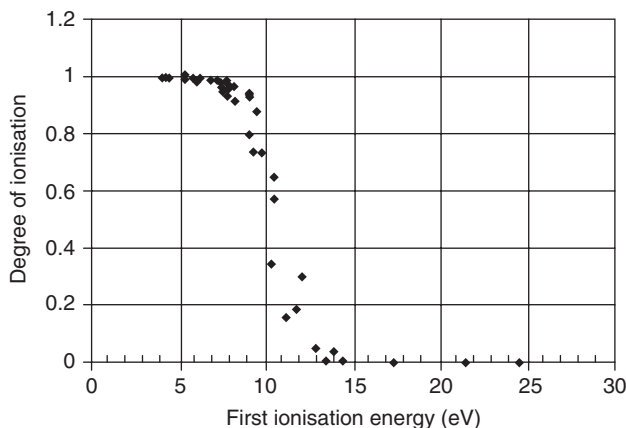


Figure 5.2 Degree of ionisation as a function of first ionisation energy as calculated by the Saha equation.

For effective penning ionisation and charge transfer to occur, the energy of the colliding species should be similar to the ionisation energy of the analyte atom. From the above processes it is easy to see how the extent to which an analyte is ionised can be influenced. Simply by changing the plasma gas, the three ionisation processes can be influenced greatly (see Chapter 7).

Atmospheric pressure ICPs have been shown to deviate from local thermal equilibrium (LTE) [7]; that is, collisions between atoms, ions and electrons do not result in an equilibrium being maintained between the various states, so the plasma does not have a uniform temperature [8]. This plasma phenomenon has led to the experimental measurement of the gas kinetic temperature (T_g) [5], the ionisation temperature (T_{ion}) [9,10], the rotational temperature (T_{rot}) [11], the excitation temperature (T_{exc}) [12] and the electron number density (n_e) [12,13], which help reflect the overall characteristics of the plasma as an ionisation source. Further investigations into the degree of analyte ionisation in an ICP have been performed by Caughlin and Blades [14].

The atmospheric pressure argon ICP is not an efficient ionisation source for elements with ionisation energies above approximately 10 eV. Spectroscopic interferences can also lead to problems in argon ICP-MS work [15]; for example, hydrochloric acid can cause problems if used in sample digestion, especially for $^{51}\text{V}^+$ and $^{75}\text{As}^+$ because of interferences by $^{35}\text{Cl}^{16}\text{O}^+$ and $^{40}\text{Ar}^{35}\text{Cl}^+$. The use of alternative gas plasmas consisting of oxygen [16–20], nitrogen [21], air [22] and helium [23,24] as well as mixed gas plasmas [25,26] have been investigated to reduce these and other matrix effects, and are discussed in Chapter 7.

5.2 Ion sampling

Ion sampling from an ICP for the purpose of mass spectrometry is complicated by the fact that the ions have to be physically transported from the atmospheric pressure plasma to the low-pressure mass analyser. This has resulted in the plasma being aligned horizontally with a water-cooled sampler, which is constructed of nickel, copper or platinum. The tip of

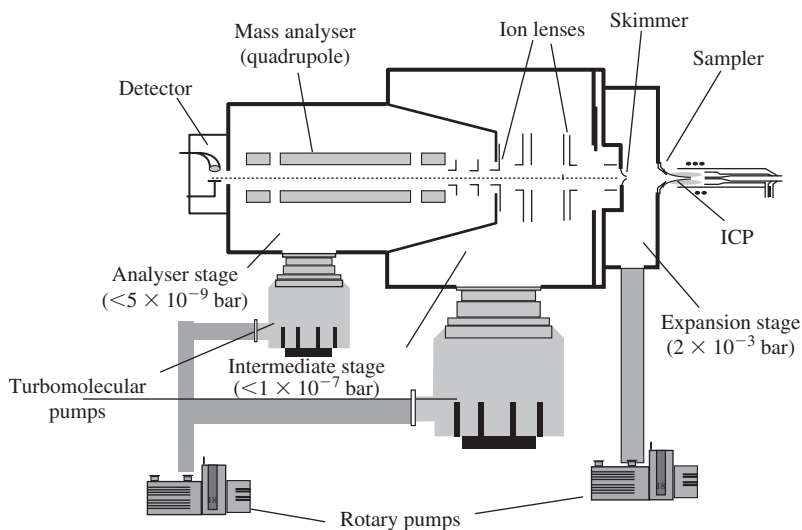


Figure 5.3 Schematic diagram of an ICP-MS.

the sampler has a small orifice (*ca.* 1 mm), which is immersed in the plasma fireball. The analyser side of the sampler is held at reduced pressure compared with the plasma, and ions are extracted from the plasma through this orifice. A diagram of an ICP-MS is shown in Fig. 5.3. A comprehensive review of the ion-sampling process for ICP-MS has been completed by Niu and Houk [27].

5.2.1 Ion sampling interface

Ion sampling interfaces for plasma source mass spectrometry have been designed using theory derived from molecular beam studies [28]. These studies give a detailed description of gas flow and kinetics, when sampled through small diameter orifices.

The sampling of the plasma gas, and hence the ions it contains, is performed through a series of chambers that are held at consecutively lower pressures. The gas is sampled and transported from an area of high pressure to an area of lower pressure through a series of small orifices. An in-depth study of the effect of orifice size and shape has been performed by Campargue [29].

On sampling the gas from atmospheric pressure to an area of lower background pressure the gas passes through a sampler orifice. On passing through this orifice the gas expands adiabatically, which causes a decrease in gas density and kinetic temperature, the enthalpy of the source gas is converted into directional flow and the gas temperature drops. The gas flow speed increases and exceeds the local speed of sound and a supersonic, free jet is formed. The free-jet structure is approximately conical in shape with its apex originating at the sampler orifice. The base of the cone is called the Mach disc and this is the region where the sampled gas collides with the background gas, causing the gas flow to become subsonic and the gas kinetic temperature to rise again. The area between the sampler orifice and the Mach disc is known as the zone of silence. It is thought that in the zone of silence the sampled gas is

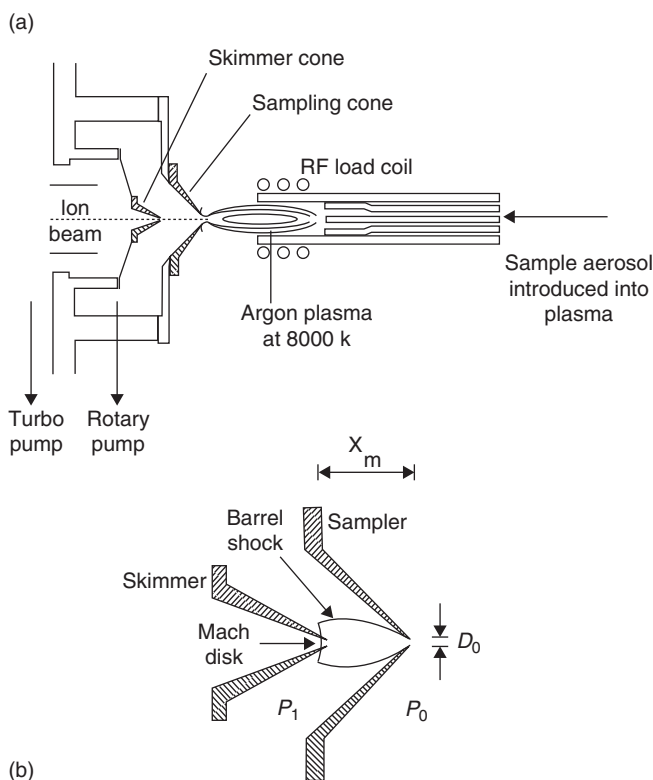


Figure 5.4 Schematic diagram of (a) the ICP-MS interface and (b) the supersonic expansion formed in the ion extraction interface of an ICP-MS.

representative of the plasma gas, so it is in this region that the second orifice, called the skimmer, is placed. Once skimmed, the ions are extracted and focused using a series of electrostatic lenses. A diagram of the ion-sampling process is shown in Fig. 5.4.

The flow of plasma gas through the sampler orifice is given by [30]:

$$U_0 = \frac{pf(\gamma)N_A D_0^2 P_0}{4(MRT_0)^{1/2}} \quad (5.2)$$

where U_0 is the flow of gas through the sampler in molecules per second, γ is the ratio of the heat capacities at constant pressure and constant volume, N_A is Avogadro's constant, D_0 is the sampler diameter (m), P_0 is the torch pressure (Pa), M is the relative molecular mass of the plasma gas (kg mol^{-1}), R is the gas constant and T_0 is the source temperature.

The function $f(\gamma)$ is given by:

$$f(\gamma) = \gamma^{1/2} \left[\frac{2}{(\gamma + 1)} \right]^{\gamma - 1/2(\gamma - 1)} \quad (5.3)$$

The position of the first Mach disc downstream from the sampler orifice is given by [29]:

$$X_m = 0.67D_0 \left(\frac{P_0}{P_1} \right)^{1/2} \quad (5.4)$$

where P_1 is the pressure in the expansion stage (Pa). In order for a representative sample to be obtained from the plasma, the skimmer orifice must be placed upstream of the first Mach disc. Campargue [29] gives the skimming distance that yields maximum beam intensity (X_s) as:

$$X_s = 0.125D_0 \left[\left(\frac{1}{Kn} \right) \left(\frac{P_0}{P_1} \right) \right]^{1/3} \quad (5.5)$$

where Kn is the Knudsen number at the sampling orifice, P_0 is the torch pressure (Pa) and P_1 is the pressure in the expansion stage. The Knudsen number is given by:

$$Kn = \frac{\lambda}{D} \quad (5.6)$$

where D is the diameter of the orifice through which the gas passes and λ is the mean free path given by [31]:

$$\lambda = \frac{\left(\frac{16}{5} \right) \eta}{NM \left(\frac{2\pi kT}{M} \right)^{1/2}} \quad (5.7)$$

where η is the viscosity co-efficient of the plasma gas, N is the number density, M is the mean molecular mass of the plasma gas (g), k is the Boltzmann constant and T is the local temperature (K) [31]. Campargue [29] has calculated this value to be approximately $0.75X_m$.

The flow of gas through the skimming orifice is related to the gas flow through the sampler by [30]:

$$U_s = U_0 f(\gamma) \left(\frac{D_s}{X_s} \right)^2 \quad (5.8)$$

where D_s is the skimmer orifice diameter and X_s is the sampler to skimmer orifice distance (m).

Hoglund and Rosengren [32] state that the flow conditions, as described in Equations (5.2)–(5.8), prevail when the pressure ratio across the sampler orifice is greater than 2, or analytically for an ideal gas when:

$$\frac{P_0}{P_1} \geq \left[\frac{\gamma + 1}{2} \right]^{\gamma/\gamma-1} \quad (5.9)$$

5.2.2 *Ion focusing*

Once the ions have entered the skimmer tip it is necessary to extract and focus the ions into the analyser. The ion-focusing lenses are crucial for the overall sensitivity of the instrument because scattered ions will not be detected. Ion focusing is achieved by subjecting the charged ions to constant electric fields. These electric fields have an accelerating effect on the ions and if the field strength is high, ions may be accelerated to such an extent that their residence time in certain analysers is not sufficient for effective mass analysis.

In order to construct an effective ion optical array it is necessary to calculate the path taken by ions in the electrostatic fields. To do this, several assumptions must be made about the conditions, electric fields and ion interactions, namely that:

- (i) An ion is a free particle with a positive charge.
- (ii) Ionic velocities are small in comparison with the speed of light.
- (iii) The density of the ion beam is not great enough to induce space charge (ion-ion repulsions).
- (iv) The presence of the ions brings about no appreciable change to the electrostatic fields they are subjected to.
- (v) Vacuum conditions are assumed to be adequate to give the ions the necessary mean free path.

Electrostatic lenses, placed in a vacuum chamber and set at specific potentials, will affect the surrounding space by causing a gradient of equipotentials in the regions between different lenses. These equipotentials are the refracting surfaces of electrostatic ion optics and are analogous to the lateral refracting surfaces of glass lenses in ordinary light optics.

A number of models are available for the calculation of the equipotential fields formed in a vacuum by the ion lenses. However, these models have been greatly enhanced by the increased speed and memory capacity of modern computers. The use of such computer models as SIMION has greatly enhanced the understanding of ion-optical design for ICP-MS, and in the hands of experts has shown the extent that space charge plays in ion focusing. The majority of studies into space charge in the ion beam for ICP-MS can be attributed to Scott Tanner, and in a recent book chapter he outlines the development of ion optics for ICP-MS [33]. Space-charge interference is caused by charge separation of the ion beam. The transition to charge flow can be attributed to a number of factors. The sampled gas stream exiting the skimmer cones consists of neutral gas and equal concentration of ions and electrons. Collisional damping of the neutral species along with the diffusion of lighter electrons from the extracted beam give rise to a charge. However, this is enhanced by the presence of the extraction optics, which will attract the positive ions while repelling the electrons. Tanner has shown that charge separation of the ion beam, in an ion optical array incorporating a photon stop, is essential for effective ion transmission. Later versions of SIMION have incorporated the ability to model some aspects of space charge. However, no model to date successfully accounts for collisional damping and the transformation to charged flow.

A recent development in ion-optical interfaces for ICP-MS is the incorporation of a hexapole collision cell between the extraction lens and the mass analyser of an ICP-MS [34]. The use of a multipole lens system has been shown to have a number of advantages

compared with conventional lens systems. Multipole lenses are high-efficiency lenses that suffer little mass bias. The lens can be placed at a slight angle, which prevents photons and neutrals from entering the analyser, hence a photon stop is not required. The effect of helium collisional gas in the hexapole has been shown to thermalise the extracted ion beam. This causes ions to exit the hexapole with a narrow spread of ion kinetic energies (2 eV), which results in enhanced resolution for the interfaced mass analyser. Collisions in the cell have also been shown to reduce polyatomic interferant ions, with the argon-based polyatomics $^{40}\text{Ar}^{16}\text{O}^+$, $^{40}\text{Ar}^{35}\text{Cl}^+$ and $^{40}\text{Ar}_2^+$ being collisionally dissociated in the cell, enabling mass analysis of ^{56}Fe , ^{75}As and ^{80}Se . Selective damping of an interfering ion is also possible with a collision cell. By careful selection of damping gases such as oxygen, argon and helium, Ar^+ , Kr^+ and Xe^+ interferences have been reduced. The advantages of the multipole collision cell have been equated to those of running with a 'shielded' or 'cool' plasma (see Chapter 7); however, the multipole interface does not suffer the reduced ionisation power of the 'cool' plasmas.

5.2.3 *Langmuir probe measurements*

The effect of plasma potential on the formation of a secondary discharge in the ion sampling interface has been investigated using a Langmuir probe, which was slowly swept through the plasma to stop the probe tip from melting [35]. It was shown that, as the plasma potential increased, the number of doubly charge ions increased and the number of argon-associated polyatomic ions decreased. It was thought that the presence of a secondary discharge in the sampling interface was causing this phenomenon [35]. The effect of load coil geometry and earthing position on plasma potential, and hence the intensity of the secondary discharge, was monitored by using a floating Langmuir probe [36]. These investigations led to probe measurements being obtained inside the interface region of an ICP-MS instrument with plasma potential, n_e and T_e being determined [37,38].

5.2.4 *Ion kinetic energies*

Ion kinetic energy measurements are important for the characterisation of plasma sources used for mass spectrometry because a spread in energies will often affect the sensitivity or resolution of the mass analyser. A quadrupole is the most common analyser used in plasma source MS, and a decrease in resolution is normally observed using this type of analyser when ions of a particular m/z exhibit a wide spread in kinetic energies. This is rather detrimental because quadrupoles are normally only capable of unit mass resolution. Ion kinetic energy measurements can be made by placing a retarding potential on the front of the mass analyser, increasing the potential gradually and obtaining an ion-stopping curve. Stopping curves for ions extracted from an argon ICP have been obtained, at different operating conditions, by applying a direct current (dc) bias to the quadrupole mass analyser. The dc bias was ramped and the plot of ion signal against the quadrupole dc offset yielded the stopping curve, which was differentiated to obtain the ion kinetic energy [39]. Ion kinetic energies have also been obtained by placing a small orifice retarding plate in front of the

mass analyser. Again stopping curves were obtained by ramping the dc offset of the retarding plate [40].

Douglas [5] has described the application of a three-lens ion-stopping grid for ion kinetic energy measurements. In his chapter he describes the necessity for removing any ion optics upstream of the measurement grid. This was deemed necessary due to the accelerating effect of the optics, which would alter the ion energies. This system was later used by Tanner [41]. In the first instance ion kinetic energies were measured in order to characterise the extent of a secondary discharge at different plasma operating conditions [39]. However, Fulford and Douglas [42] have investigated the relationship between ion mass and ion kinetic energy, and have shown that the ion kinetic energy increases linearly with ion mass in accordance with the energy imparted by the ion-sampling process in addition to the plasma potential. More recently, ion kinetic energy measurements and ion-sampling theory have been used to calculate the gas kinetic temperature of the sampled plasma [41].

Fulford and Douglas [42] have described how the ion kinetic energies of ions, extracted through a molecular beam type interface, should increase linearly in proportion to the mass, as described by:

$$E_s = \frac{M}{M_{\text{gas}}} \left(\frac{5}{2} kT_{\text{gas}} \right) + P \quad (5.10)$$

where E_s is the ion kinetic energy, M is the mass of the ion, M_{gas} is the mass of the plasma gas, k is the Boltzmann constant, T_{gas} is the gas kinetic temperature of the sampled plasma (K) and P is the plasma potential (V). This is due to the translational energy imparted by the ion-sampling process. Tanner [41] later used this linear relationship to determine T_{gas} and the plasma potential of an atmospheric pressure argon ICP. The relationship was applied to both sampled atomic and polyatomic ions, with both showing a linear increase in energy with mass. However, the polyatomic ions showed lower energies than atomic ions of the same mass.

5.3 Mass analysers

The mass analyser sorts the ions extracted from the ICP source according to their mass to charge ratio (m/z). The mass spectrum is a record of the relative numbers of ions of different m/z , which is characteristic of the analyte compound [43].

Functionally, all mass analysers perform two basic tasks:

- (i) They separate ions according to their mass to charge ratio.
- (ii) They measure the relative abundance of ions at each mass.

Successful operation of the mass analyser requires a collision-free path for ions. To achieve this, the pressure in the analyser section of the spectrometer should ideally be below 10^{-6} torr [44]. Once in the analyser the ions are sorted into discrete m/z values depending on the energy, momentum and velocity of the ions. A measurement of any two of these allows the m/z to be determined [45].

5.3.1 Quadrupole

The quadrupole mass filter is comprised of four parallel electrically conducting rods, as shown in Fig. 5.5. Opposite rods are connected and parallel rods are supplied with a dc voltage, one pair being held at $+U$ volts and the other set at $-U$ volts. The first set of rods is supplied with an rf voltage ($+V \cos \omega t$) and the second set of rods is supplied with an rf voltage out of phase by 180° ($-V \cos \omega t$). This results in the formation of an oscillating hyperbolic field in the area between the rods. As ions pass down the quadrupole analyser (z -axis) they experience transverse motion in the x and y planes and start to oscillate. The dc field tends to focus positive ions in the positive plane and defocus them in the negative plane. The rf field accelerates the ions, so that when the ions are in the negative half of the rf cycle they are accelerated towards the rods and when they are in the positive half of the rf cycle they are repelled and are accelerated away from the rods [46]. The ions oscillate with increasing amplitude until they either reach the detector or collide with the rods and become neutral. Hence, the quadrupole mass analyser has the ability to transmit certain ions and reject others depending on the stability of their path [46]. Ions, when inside the quadrupole, are forced to follow certain trajectories that are dependent on the geometry of the field, the amplitude (V_0), the angular frequency (Ω) of the alternating potential, the magnitude (U) of the dc bias applied to the rods, the m/z of the ions, the initial conditions (position and velocity) and the phase angle with which the ions enter the field. Stable ions are transmitted through the length of the quadrupole while unstable ions hit the rods.

The mass spectrum is scanned by varying U and V_0 while maintaining a constant ratio U/V_0 . The recorded mass is proportional to V_0 so that a linear increase of V_0 provides an easily calibrated linear mass scale [44].

The advantages of the quadrupole mass analyser are its relatively small size, the fact that it is not restricted to the detection of mono-energetic ions and that ions are accepted within a 60° cone around the axis so that a focusing slit is not necessary. Quadrupole mass analysers are essentially sequential instruments, although they can be used to rapidly scan over $200 m/z$ in under 1 ms.

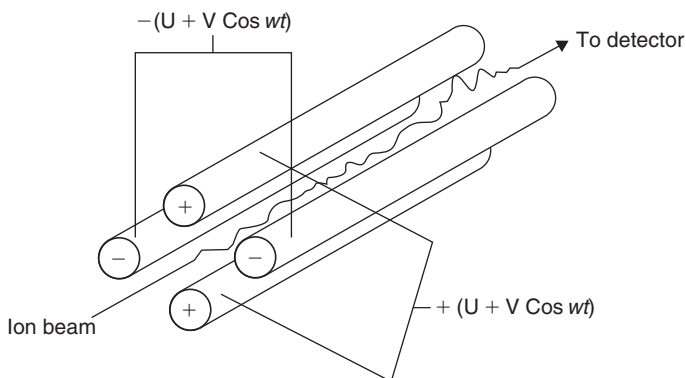


Figure 5.5 Schematic diagram of a quadrupole mass analyser.

5.3.2 Magnetic sector

In a magnetic sector analyser, ions are subjected to a magnetic field that causes the ions to be deflected along curved paths (Fig. 5.6). The ions are introduced into the analyser via a series of electrostatic slits which accelerate and focus the ions into a dense ion beam. The velocity of the ions is controlled by the potential (V) applied to the slits. As the ions enter the magnetic sector analyser they are subjected to a magnetic field parallel to the slits but perpendicular to the ion beam. This causes the ions to deviate from their initial path and curve in a circular fashion. A stable, controllable magnetic field (H) separates the components of the beam according to momentum. This causes the ion beam to separate spatially and each ion has a unique radius of curvature, or trajectory (R), according to its m/z . Only ions of a single m/z value will possess the correct trajectory to focus the ion on the exit slit to the detector. By changing the magnetic field strength, ions with differing m/z values are brought into focus at the detector slit.

The ion velocity (v) in the magnetic field is given by the following equation [47]:

$$\frac{1}{2}mv^2 = zV \quad \text{or} \quad v = \sqrt{\frac{2zV}{m}} \quad (5.11)$$

As the ions enter the magnetic field, they are subjected to a magnetic force at right angles to both the magnetic lines of force and their line of flight. This leads to a centrifugal force, leading to curvature of the ion beam:

$$\frac{mv^2}{R} = Hzv \quad (5.12)$$

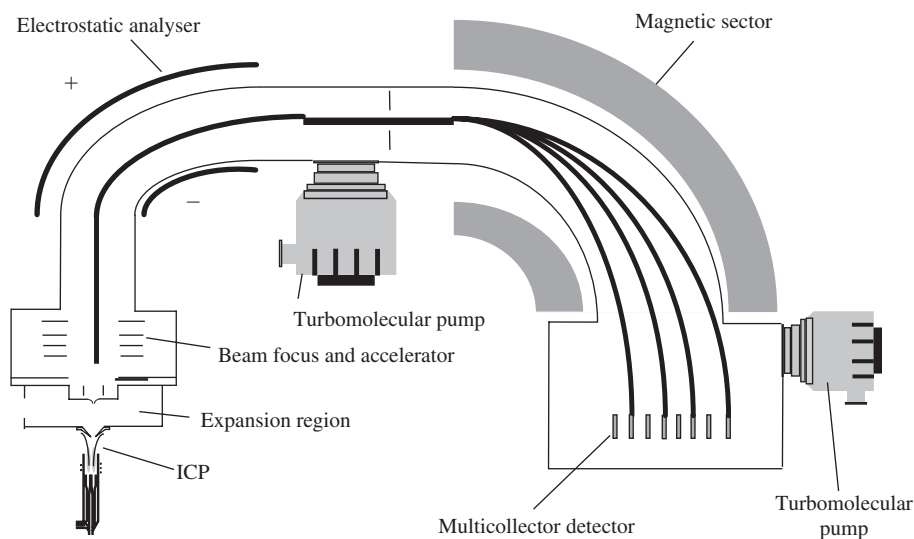


Figure 5.6 Schematic diagram of a double-focusing ICP-MS instrument operating in a low-resolution multicollector mode.

The radius of curvature of the flight path is proportional to its momentum and inversely proportional to the magnetic field strength:

$$R = \frac{mv}{zH} \quad (5.13)$$

By eliminating the velocity term (v) between Equations (5.11) and (5.13) we get:

$$R = \frac{1}{H} \sqrt{2V \left(\frac{m}{z} \right)} \quad (5.14)$$

hence, ions accelerated through an electrostatic field, uniform in nature, and then subjected to a uniform magnetic field have different radii of curvature. This leads to ions of a specific m/z value being focused onto the detector slit while all other ions hit the side of the analyser. Thus, the magnetic field classifies and separates ions into a spectrum of beams with each part of the spectrum having a different m/z ratio, where:

$$\frac{m}{z} = \frac{H^2 R^2}{2V} \quad (5.15)$$

To obtain a complete mass spectrum from a magnetic sector analyser, either the accelerating voltage (V) or the magnetic field strength (H) is varied. Each m/z ion from light to heavy is sequentially focused on the detector and hence a mass spectrum is obtained.

5.3.3 Double-focusing sector mass analyser

Single-focusing magnetic sectors, as described above, have the disadvantage that ion energies vary depending on their point of formation in the ion source. The difference in ion energy is accentuated by the accelerating voltage, which leads to peak broadening and low resolution in the single-focusing mass analyser.

Double-focusing magnetic/electrostatic sector instruments use magnetic and electrical fields to disperse ions according to their momentum and translational energy [47]. An ion entering the electrostatic field travels in a circular path of radius (R) such that the electrostatic force acting on it balances the centrifugal force. The equation of motion or transmission is:

$$\frac{mv^2}{R} = Ez \quad (5.16)$$

where E is the electrostatic field strength. Hence the radius of curvature of the ion path in the electrostatic sector is dependent on its energy and not on its mass [44]. A narrow slit placed in the image plane of the electrostatic sector can be used to transmit a narrow band of ion energies. If this sort of analyser was placed in front of a magnetic sector analyser an increase in resolution would result, but a decrease in detection would be inevitable due to the decrease

in ions exiting the electrostatic sector in comparison with ions exiting the ion source. This loss in sensitivity can be compensated for by the choice of a suitable combination of electrostatic and magnetic sectors such that the velocity dispersion is equal and opposite in the two analysers. The operation of a double-focusing mass analyser is shown in Fig. 5.6.

The narrow ion energy range transmitting the full length of a sector instrument would suggest a loss in sensitivity, compared with quadrupole mass analysers, when both are operated at the same resolution; this has not been observed in practice. This has been mainly attributed to the ion focusing requirements for the different analysers. Double-focusing mass analysers require a high-energy (3–8 kV) ion beam for effective ion transmission and resolution whereas, if such a high-energy beam was focused down a quadrupole, the ions would obtain a velocity profile too great to be affected by the hyperbolic energy fields of the quadrupole analyser, which generally requires ion energies of less than 10 eV for effective mass separation. The higher ion energy beam is less affected by space-charge interference, which causes scattering of the ion beam and has led to increased sensitivity of double-focusing instruments.

The main advantage of double-focusing analysers is their vastly superior resolution compared with quadrupole instruments. The resolution of a mass analyser can be expressed as:

$$R = \frac{M}{\Delta M}$$

where R is resolution, M is the mass of the isotope of interest and ΔM is the peak width of the isotope at 5% peak height. The increased resolution is advantageous because polyatomic ion interferences can be resolved from analyte isotopes of interest. Table 5.1 shows a number of polyatomic ion interferants and the resolution required to separate them from the elemental isotope of interest. Most quadrupole mass analysers operate with an upper resolution of 400, which enables unit mass resolution, while double-focusing instruments for ICP-MS have been operated at a resolution of 10 000, enabling peaks of fractions of a mass unit to be resolved.

Another advantage associated with focusing instruments is that ions of different mass are spatially separated on exiting the analyser. This fact has been exploited by a number of manufacturers who have developed multidetector instruments. An array of detectors is placed downstream of the analyser allowing up to 10 ions to be detected simultaneously in a low-resolution mode. This has the advantage of reducing imprecision caused by temporal fluctuations in the ion beam, thereby improving the precision of isotope ratio measurements.

5.3.4 Time of flight

Time-of-flight (TOF) mass analysers have a quite different mode of operation compared with other analysers. In conventional analysers the ion signal is a continuous beam. In TOF mass spectrometry the ion beam is pulsed so that the ions are either formed or introduced to the analyser in 'packets'. These ion packets are introduced to the field-free region of a flight tube 30–100 cm long. The principle behind TOF analysis is that, if all ions are accelerated to the same kinetic energy, each ion will acquire a characteristic velocity dependent on its m/z ratio [47]. The ion beam reaches its drift energy (2700 eV) in less than 2 cm. The ions are then

Table 5.1 Common polyatomic ion interferences with the mass analyser resolution necessary to resolve them from the analyte of interest

Analyte ion		Interfering ion		Resolution required
Nominal m/z	Accurate m/z	Nominal m/z	Accurate m/z	
^{24}Mg	23.9850	$^{12}\text{C}_2$	24.0000	1599
^{28}Si	27.9769	$^{14}\text{N}_2$	28.0060	962
^{28}Si	27.9769	$^{12}\text{C}^{16}\text{O}$	27.9949	1555
^{31}P	30.9737	$^{14}\text{N}^{16}\text{O}^1\text{H}$	31.0057	968
^{31}P	30.9737	$^{15}\text{N}^{16}\text{O}$	30.9950	1455
^{32}S	31.9721	$^{16}\text{O}_2$	31.9898	1807
^{44}Ca	43.9555	$^{12}\text{C}^{16}\text{O}_2$	43.9898	1282
^{48}Ti	47.9479	$^{32}\text{S}^{16}\text{O}$	47.9670	2511
^{51}V	50.9440	$^{35}\text{Cl}^{16}\text{O}$	50.9637	2586
^{52}Cr	51.9405	$^{35}\text{Cl}^{16}\text{O}^1\text{H}$	51.9715	1676
^{52}Cr	51.9405	$^{40}\text{Ar}^{12}\text{C}$	51.9623	2383
^{54}Fe	53.9396	$^{40}\text{Ar}^{14}\text{N}$	53.9653	2099
^{56}Fe	55.9349	$^{40}\text{Ar}^{16}\text{O}$	55.9572	2509
^{63}Cu	62.9296	$^{40}\text{Ar}^{23}\text{Na}$	62.9521	2797
^{64}Zn	63.9291	$^{32}\text{S}^{16}\text{O}_2$	63.9619	1950
^{64}Zn	63.9291	$^{32}\text{S}_2$	63.9442	4234
^{75}As	74.9216	$^{40}\text{Ar}^{35}\text{Cl}$	74.9311	7887
^{80}Se	79.9165	$^{40}\text{Ar}_2$	79.9246	9867

accelerated down the TOF tube with whatever velocity they have acquired. Each ion has a kinetic energy (zV) expressed by Equation (5.11). Because all ions have essentially the same energy at this point, their velocities are inversely proportional to the square roots of their masses. As a result, ions of different mass travel down the flight tube at different speeds, thereby separating spatially along the flight tube with lighter, faster ions reaching the detector before the heavier ions. Hence, the m/z ratio of an ion and its transit time (T , ms) through a flight distance (L , cm) under an acceleration voltage (V) are given by:

$$t = L \sqrt{\left[\left(\frac{m}{z} \right) \left(\frac{1}{2V} \right) \right]} \quad \text{or} \quad \frac{m}{z} = \frac{2VT^2}{L^2} \quad (5.17)$$

TOF mass analysers are calibrated using two ions of known mass, so exact values of L and V need not be known. The mass calibration is based on the conditions of the analyser during the entire period of measurement.

While simple in theory, the TOF analyser causes numerous problems when coupled with an ICP. The spread in ion kinetic energies caused by the ion-sampling process results in the ions entering the field-free region of the flight tube at different angles. This scattering of ions in the analyser led to poor sensitivity and resolution during preliminary investigations. This problem, along with reducing the background associated with pulsing the continuous ion beam, has been an ongoing area of research by Hieftje and co-workers [48–50]. The

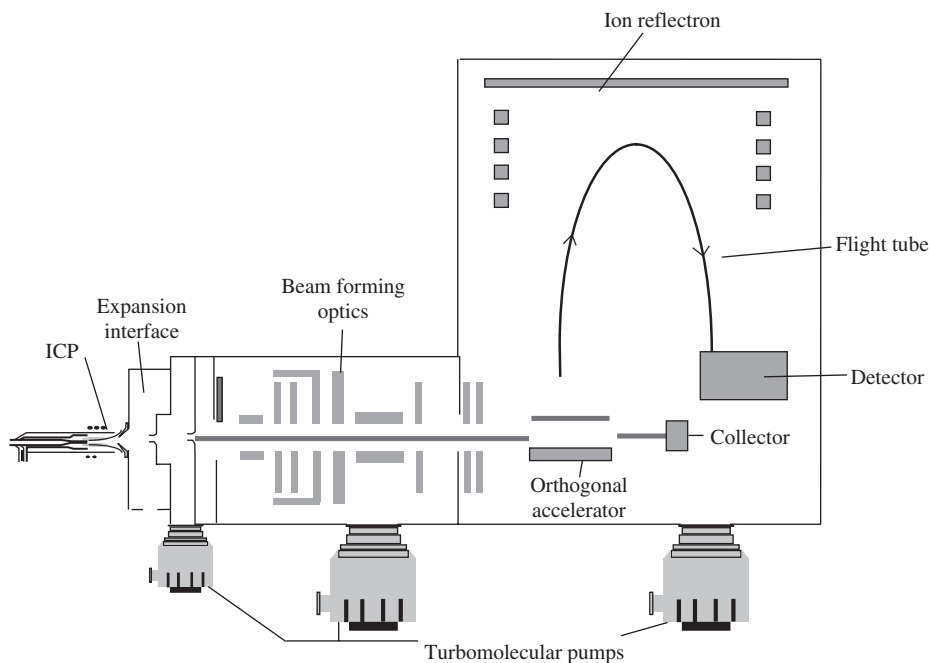


Figure 5.7 Schematic diagram of a commercially available TOF ICP-MS instrument.

incorporation of two positively biased plates, after the ion extraction interface, led to increased sensitivity for TOF-MS. This was thought to be caused by the plates steering the ions straight down the flight tube. Another difficulty with ICP-TOF-MS is that ions have to be introduced in packets. This has been achieved by using an orthogonal interface with a pulsed-repeller plate. However, background noise still remains problematic with such an interface. This background has been reduced by using a combination of quadrupole ion optics and an energy discriminator before the detector. The quadrupole lens was found to increase the instrument's sensitivity because this type of lens does not suffer the trade-off between sensitivity and resolution inherent in cylindrical ion optics. In addition, the ability to use the quadrupole as a 'gate', enabling the ion beam to be pulsed into the repeller section of the orthogonal interface, was seen to increase the signal-to-noise ratio. However, a significant background of low-energy ions still remained throughout the spectrum. This background was significantly reduced by using an energy discriminator [50]. This consisted of a potential barrier placed before the detector of the mass analyser which discriminates between low-energy background continuum ions and higher-energy background analyte ions. The solving of these and many other problems has led to the recent commercialisation of ICP-TOF-MS, a diagram of which is shown in Fig. 5.7.

The TOF analyser has a number of advantages over other analysers used for ICP-MS. The fact that all masses in the spectrum can be monitored simultaneously is the main attraction for many ICP-MS users. Even for simple multi-element analysis, scanning analysers suffer from a decrease in sensitivity as the number of ions to be monitored is increased. This is highlighted by Fig. 5.8. The fact that over 30 000 simultaneous mass spectra per

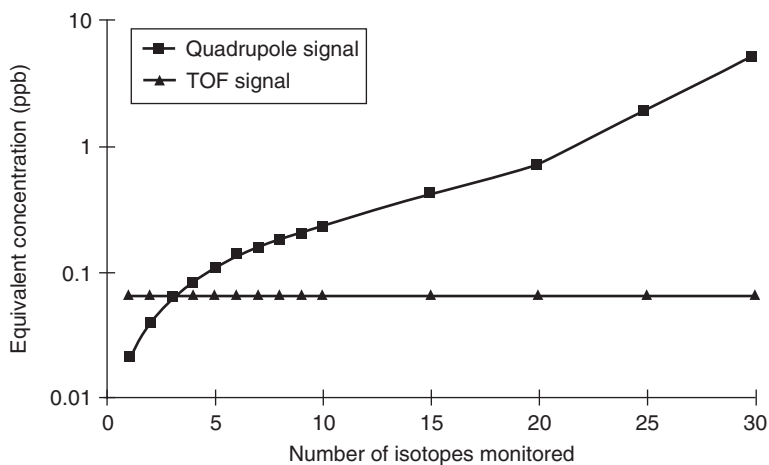


Figure 5.8 Effect of the number of ions monitored on ion signal intensity for scanning and simultaneous mass analysers.

second can be obtained by the TOF analyser has many advantages for monitoring transient signals, such as those produced by laser ablation and chromatographic, capillary electrophoresis and electrothermal vaporisation sample introduction techniques. In addition, improved isotope ratio measurements have been reported because of the elimination of noise due to temporal fluctuations in the plasma and sample introduction systems.

5.3.5 Ion trap

The most common ion trap (IT) mass spectrometer consists of a doughnut-shaped ring electrode supplied with an rf voltage and capped with two end-cap electrodes [51], as shown in Fig. 5.9. The electrodes are contained in a chamber at a pressure of 10^{-3} torr with a helium bath gas. Ions enter through a hole in the end-cap and oscillate in the trap. The stability of the oscillating ions is determined by the rf and voltage supplied to the ring electrode and the m/z of the ion. Increasing the rf amplitude causes ions of increasing m/z to destabilise and leave the trap, where they are detected. A mass spectrum is obtained by scanning the rf supply and detecting ions as they are ejected from the trap. This method of operation is known as the mass selective instability mode.

A second method of ion ejection is known as axial modulation. In this method a second rf voltage, lower in frequency than that of the ring electrode, is supplied to the end-caps. On scanning the rf amplitude on the ring electrode, causing mass selective instability, ions are sequentially brought into resonance with the rf of the end-caps. This causes an increase in translational energy of the ion and the ion is ejected from the trap. This is considered advantageous as m/z ions are ejected at much lower rf voltages than those required for mass selective instability. This has the desired effect of increasing the mass range of the analyser. In addition, selective ejection and trapping can be performed, enabling the concentration of a single ion in the trap. This process has been further developed and ion traps are now successfully used for MS-MS and MSⁿ experiments.

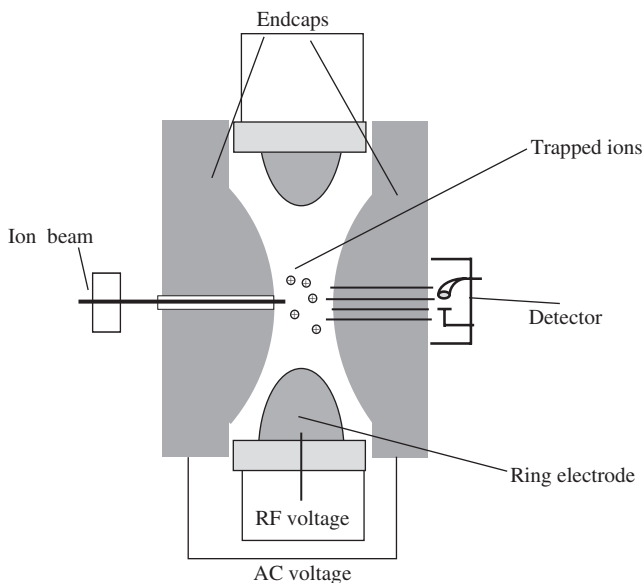


Figure 5.9 Schematic diagram of an ion-trap mass analyser.

Ion traps have received little attention as analysers for the ICP as conventional wisdom suggests that space charge in the analyser, caused by the abundance of argon ions in the ion beam, would lead to in-trap collisions and scattering of the ions. However, initial investigations by Koppenaal and co-workers have shown that advantages can be obtained by replacing the detector of a quadrupole ICP-MS with an ion-trap analyser [51]. In this instance the quadrupole acts as a linear focusing lens and not as a mass filter. The background spectra for such an instrument showed low background levels for argon and polyatomic ions normally found in the background spectra of an atmospheric ICP. Further investigations performed on an instrument without the quadrupole also yielded similar background spectra that lacked the polyatomic interferences [52]. The advantage of using the ion trap to selectively store ions of a narrow mass range while ejecting all other ions has been speculated upon. This ability enables the concentration of low levels of ions in the analyser allowing further in-trap experiments to be performed, such as the dissociation of polyatomic ions and laser optical studies of the concentrated ions.

5.4 Ion detection

On exiting from the mass analyser the ions will sequentially strike the detector. Several types of detectors are available, although the electron multiplier is the most common.

5.4.1 Faraday cup collector

This consists of a collector electrode that is surrounded by a cage. The electrode is positioned at an angle with respect to the ion beam so that ions exiting the analyser strike the

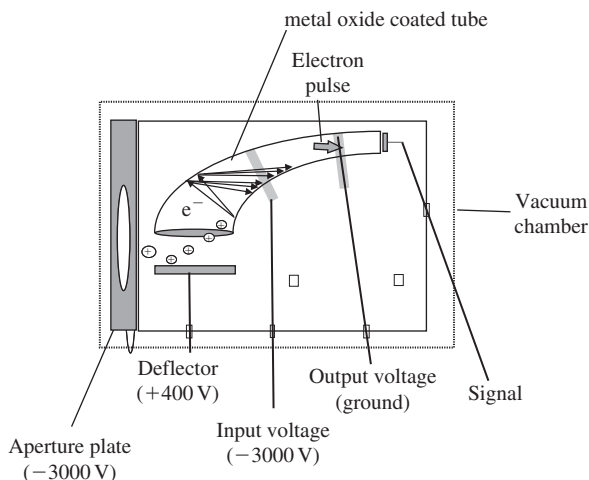


Figure 5.10 Schematic diagram of a continuous dynode electron multiplier detector.

electrode but secondary emissions are reflected away from the detector entrance. The function of the cage is to prevent detected ions and secondary electrons escaping from the detector. The electrode is connected to ground via a resistor. The ion current striking the electrode is neutralised by electron flow from ground through the resistor. This causes a potential drop, which is amplified to create a signal. Currents as low as 10^{-15} A have been successfully measured in this way [46].

5.4.2 Electron multiplier

For currents of less than 10^{-15} A an electron multiplier is necessary for detection. When the ion beam exits the analyser it strikes a conversion plate, which converts ions into electrons. The ions are drawn towards the plate by a strong voltage applied to the conversion plate. On striking the conversion plate the ions stimulate the ejection of electrons, which are accelerated by the voltage applied to the plate. The electrons are multiplied in one of two ways depending on the type of electron multiplier used.

5.4.2.1 Continuous dynode

The commonest type is the channel electron multiplier shown in Fig. 5.10. This consists of a curved glass tube of approximately 1 mm in internal diameter with an inner resistive coating and a flared end. The multiplier can be operated in one of two modes. In pulse-counting mode – the most sensitive mode of operation – a high voltage of between -2600 and -3500 V is applied to the multiplier (Fig. 5.10), which attracts ions into the funnel opening. When a positive ion strikes the inner coating, the collision results in the ejection of one or more secondary electrons from the surface. These electrons are accelerated down the tube by the potential gradient and collide with the wall, resulting in further electron

ejection. Hence, an exponential cascade of electrons rapidly builds up along the length of the tube, eventually reaching saturation towards the end of the tube, resulting in a large electron pulse and a consequent gain of 10^7 – 10^8 over the original ion collision. The electron pulses are read at the base of the multiplier and are approximately 50–100 mV and 10 ns in duration. Continuous dynode multipliers consist of a leaded glass tube which contains a series of metal oxides. The tube is curved and electrons are drawn down the tube by the potential gradient established by the resistivity of the glass. The tube is curved to stop electron feedback. A 10^5 – 10^7 increase in signal is expected; however, the major constricting factor is the background noise of the system.

Alternatively, the multiplier can be operated in analogue mode with a gain of only 10^3 – 10^4 so that the multiplier does not become saturated and the pulses vary greatly in size. In this mode the applied voltage is between -500 and -1500 V and the electron pulses are read at the collector electrode (Fig. 5.10) where they are amplified and averaged over a short time interval to allow rapid data acquisition. The greatest sensitivity is achieved with the detector in pulse-counting mode, but the detector will become saturated at counting rates above 10^6 Hz, which are encountered when the analyte is at a high concentration in the sample. If the detector is switched into analogue mode it is less sensitive but can be used for analyte concentrations that are much higher, typically up to three orders of magnitude higher than for pulse counting. Such dual-mode operation results in an extremely large linear dynamic range of up to nine orders of magnitude, but requires that two analytical scans be made to acquire all the data.

5.4.2.2 Discrete dynode

An array of discrete dynode multipliers, usually containing 15–18 dynodes, are coated with a metal oxide that has high secondary electron emission properties. The dynodes are placed in one of the two configurations, either Venetian blind or box and grid fashion. Secondary electrons emitted by the metal oxide are forced to follow a circular path by a magnetic field so they strike successive dynodes, thereby multiplying the signal (Fig. 5.11).

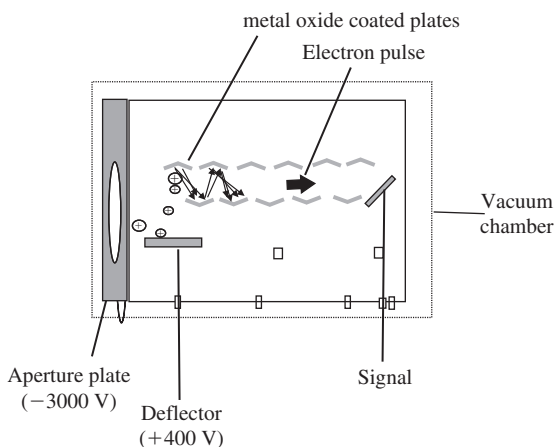


Figure 5.11 Schematic diagram of a discrete dynode electron multiplier detector.

5.4.3 Channel plate

This type of multiplier consists of an array of small channels cut in a semi-conducting material. Each channel has an entrance diameter of about 10–25 μm . The channels are coated internally with a metal oxide, so each channel acts as a micro-multiplier. To improve gain further, a series of these plates can be placed in tandem so that the multiplied electrons from the first plate are further multiplied by the second.

5.5 Instrumentation for interference removal

ICP-MS suffers from two principal types of interference, spectroscopic and non-spectroscopic [6]. Spectroscopic interferences arise when an interfering species has the same nominal m/z as the analyte of interest. The interfering species can be either an isotope of another element (which are well documented and hence easily accounted for), or a molecular ion formed between elements in the sample matrix, plasma gas, water and entrained atmospheric gases. Molecular ions are less easy to correct for since they will vary depending on the nature of the sample matrix. Some common molecular ion interferences are shown in Table 5.1. Many of these interferences can be overcome by choosing an alternative isotope of the analyte which is free from interference, although a sacrifice in sensitivity may result. As already noted a magnetic sector instrument is capable of resolving many problematic polyatomic ion interferences from the nominal analyte m/z . However, the increased cost associated with this type of instrumentation precludes its adoption in most routine laboratories; hence, alternative methods of interference reduction have been sought. A large body of research has been published on the use of chemical extraction and chromatography to separate the analyte from the matrix prior to analysis. Such hyphenated methods require additional expertise and sample preparation steps, so the development of instrumental methods of interference reduction, which require no, or minimal, extra sample preparation has been a major development aim for instrument manufacturers. To this end, three principal methods have emerged, namely cool plasma operation, multipole reaction cells and kinetic energy discrimination.

5.5.1 Cool plasma operation

Many polyatomic ions are thought to be formed in the interface due to a secondary discharge caused by capacitive coupling between the plasma and the grounded interface. The discharge can be eliminated by operating the plasma at low power, typically 600 W, and modifying the torch by inserting a grounded shield between it and the coil (Fig. 5.12) or using centre-tapped or interlaced rf coils. Under these so-called 'cool plasma' conditions [53] many polyatomic ion interferences can be eliminated (Fig. 5.13). Several drawbacks pertain with this mode of operation however: the plasma is less robust and may suffer more from non-spectroscopic matrix interferences; the cooler plasma encourages the formation of oxides and other refractory compounds, so the sensitivity of many refractory elements may be reduced and interferences due to metal oxides increased and elements with medium to high ionisation potentials are not as efficiently ionised, so sensitivity may be reduced.

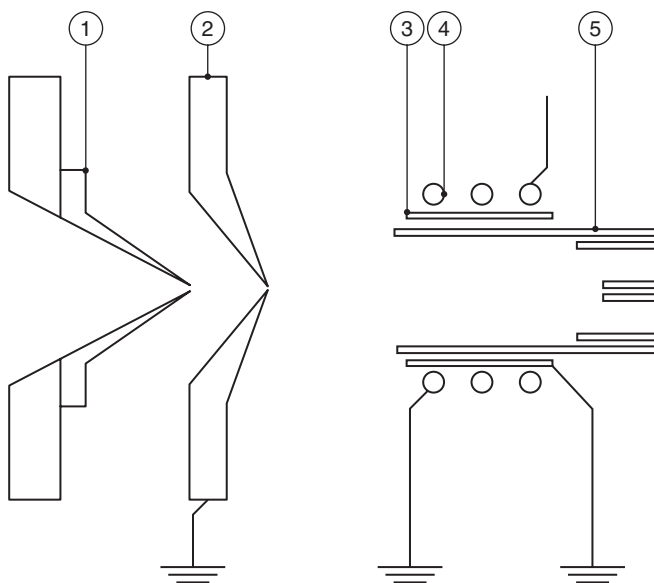
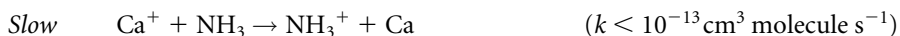


Figure 5.12 Schematic diagram of a shielded torch used for cool plasma operation: (1) skimmer cone, (2) sampling cone, (3) grounded shield plate, (4) rf work coil and (5) torch (from Ref. [53] with permission).

5.5.2 Multipole reaction cell

An alternative method of reducing molecular ions is to use a reaction cell prior to the quadrupole mass analyser. The reaction cell usually takes the form of a separate quadrupole or octopole upstream of the mass analyser (Fig. 5.14). A gas, such as hydrogen, helium or ammonia, is introduced into the cell where it either reacts with, collisionally dissociates, or neutralizes the polyatomic species or precursors. Originally the mode of operation was thought to be due primarily to intermolecular collisions; however, the role of the reaction gas is to thermalise the ion beam (i.e. collisions merely reduce the magnitude and spread in kinetic energies) and ion–molecule reactions are now known to play the primary role, so the choice of reactive gas is paramount. In the simplest form of operation a reaction gas is chosen such that it reacts efficiently with the polyatomic ion interference, but has low reaction efficiency with the analyte [54]. An example of just such a pair of charge transfer reaction is shown below:



In this case ammonia can be used as a reactive gas to neutralise Ar^+ species because the reaction efficiency is very high; however, the efficiency of the corresponding neutralisation reaction for Ca^+ is much lower, so this analyte can still be determined after elimination of the Ar^+ interference at m/z 40. The reason for this disparity in reaction rates is, that polyatomic ions, having larger collision cross-sections, undergo more collisions than the smaller analyte ions, hence reaction rates are greater. A further advantage of incorporating a multipole is that

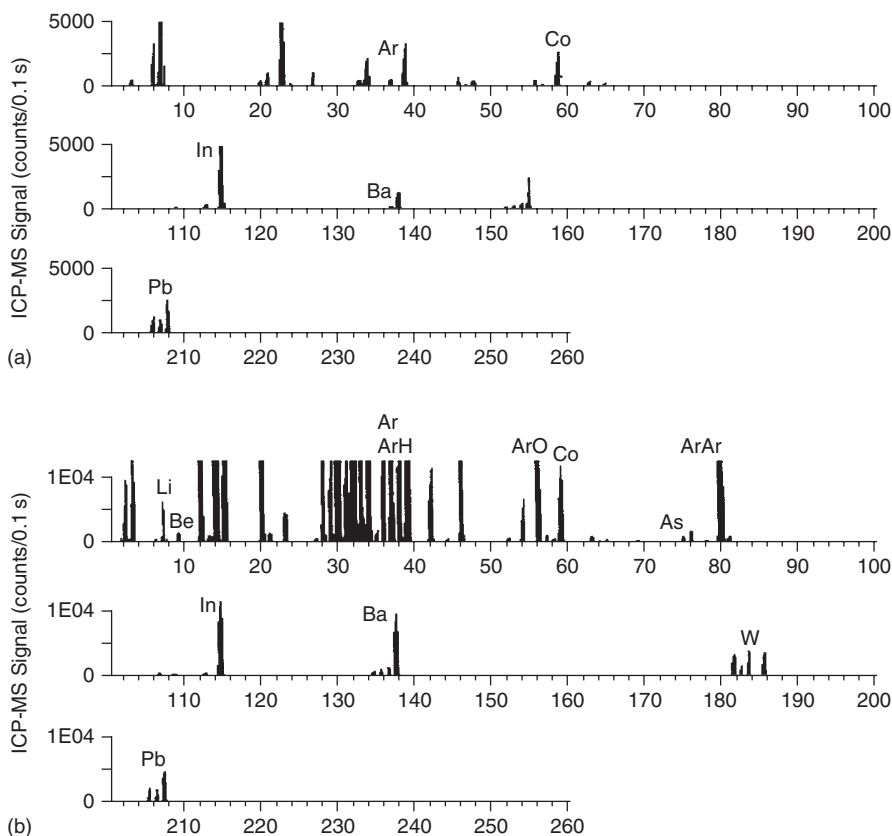


Figure 5.13 Spectrum of 10 ng/ml Li, Be, Co, As, In, Ba, W, Pb standard solution using: (a) cool and (b) conventional plasma ICP-MS conditions (from Ref. [53] with permission).

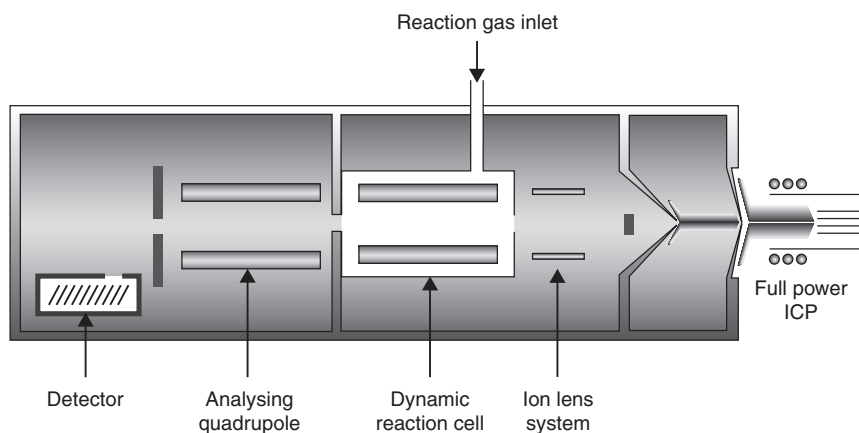


Figure 5.14 Schematic diagram of a multipole reaction cell (from Ref. [54] with permission).

it can be placed at a slight angle which prevents photons and neutrals from entering the analyser, hence a photon stop is not required, and background count rates are much lower.

It is evident from the foregoing that the reaction gas must be chosen with care for each particular analysis in order to ensure favourable ion–molecule reaction conditions for both analyte and interference. Kinetic and thermochemical data for a number of ion–molecule reactions are available in the literature [55]; however, empirical studies are always necessary to optimise performance.

A major drawback of the technique is the propensity for the reaction gas to react with other analytes, organic contaminants or polyatomic ions to form new interferences. This has been overcome by the development of a so-called dynamic reaction cell [54]. In this case, the reaction cell is an enclosed, low constant, rf amplitude quadrupole, the bandpass of which can be varied in concert with the analyser quadrupole. Dynamic scanning of the reaction cell ensures that only reactions of ions which are confined within the cell proceed, with unstable ions being rejected. Hence, only polyatomic ions at the particular m/z of interest are involved in reactions at any one time, and reactions of ions at other masses are suppressed.

5.5.3 Kinetic energy discrimination

Polyatomic ions, with their larger collision cross-sections, suffer more collisions than monoatomic analyte ions. This results in the former having lower kinetic energies, so they can be discriminated based on their different kinetic energy. For example, the $^{35}\text{Cl}^{16}\text{O}^+$ ion (ionic radius 230 pm), which overlaps with $^{51}\text{V}^+$ (ionic radius 135 pm), has a lower kinetic energy. In practice an inert gas such as helium is used as a collision gas to thermalise the ions, and a pole bias between the collision cell and quadrupole results in an effective retarding potential of ~ 2 V, which prevents the lower energy polyatomic ions from reaching the mass analyser (Fig. 5.15).

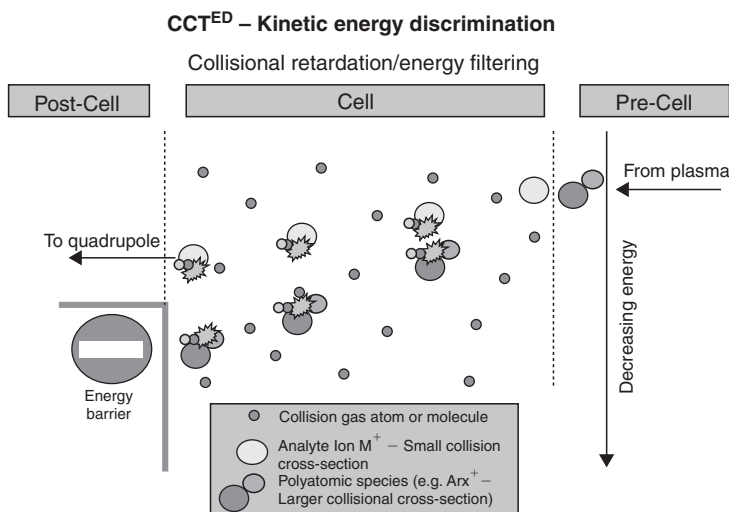


Figure 5.15 Reduction in polyatomic ion interferences by kinetic energy discrimination (Thermo Electron Corporation).

References

1. Reed, T.B. (1961) Inductively coupled plasma torch. *J. Appl. Phys.*, **32**, 821.
2. Reed, T.B. (1961) Growth of refractory crystals using the inductively coupled plasma. *J. Appl. Phys.*, **32**, 2534.
3. Reed, T.B. (1962) Plasma torches. *Int. Sci. Tech.*, **6**, 42.
4. Greenfield, S., Jones, I.L.W. and Berry, C.T. (1964) High pressure plasmas as spectrometric emission sources. *Analyst*, **89**, 713.
5. Montaser, A. and Golightly, D.W. (1992) *Inductively Coupled Plasmas in Analytical Atomic Spectrometry*, 2nd edn, VCH, New York.
6. Evans, E.H., Giglio, J.J., Castillano, T.M. and Caruso, J.A. (1995) *Inductively Coupled and Microwave Induced Plasma Sources for Mass Spectrometry*, Royal Society of Chemistry, Cambridge.
7. Smith, T.R. and Bonner Denton, M. (1989) LTE conditions within the central channel of the plasma. *Appl. Spectrosc.*, **43**, 1385.
8. Fannin, H.B., Seliskar, C.J. and Miller, D.C. (1987) Studies of energy-transfer and ionization processes in a helium ICP. *Appl. Spectrosc.*, **42**, 621.
9. Houk, R.S., Svec, H.J. and Fassel, V.A. (1981) Mass-spectrometric evidence for suprathermal ionization in an inductively coupled argon plasma. *Appl. Spectrosc.*, **35**, 380.
10. Crain, J.S., Smith, F.G. and Houk, R.S. (1990) Mass spectrometric measurement of ionization temperature in an inductively coupled plasma. *Spectrochim. Acta*, **45B**, 249.
11. Seliskar, C.J., Miller, D.C. and Fleitz, P.A. (1987) ICP rotational spectroscopic temperature determination using N_2 and N_2^+ . *Appl. Spectrosc.*, **41**, 658.
12. Blades, M.W. and Caughlin, B.L. (1985) Excitation temperature and electron-density in the inductively coupled plasma aqueous vs organic-solvent introduction. *Spectrochim. Acta*, **40B**, 579.
13. Caughlin, B.L. and Blades, M.W. (1985) Spatial profiles of electron-density in the inductively coupled plasma. *Spectrochim. Acta*, **40B**, 987.
14. Caughlin, B.L. and Blades, M.W. (1985) An evaluation of ion-atom emission intensity ratios and local thermodynamic-equilibrium in an argon inductively coupled plasma. *Spectrochim. Acta*, **40B**, 1539.
15. Evans, E.H. and Giglio, J.J. (1989) Interferences in inductively coupled plasma mass spectrometry. A review. *J. Anal. At. Spectrom.*, **4**, 299.
16. Liu, K., Kovacic, N. and Barnes, R.M. (1990) High-power oxygen inductively coupled plasma discharge for spectrochemical analysis. *Spectrochim. Acta*, **45B**, 145.
17. Yang, P. and Barnes, R.M. (1989) A low-power oxygen inductively coupled plasma for spectrochemical analysis. 2. Plasma diagnostics. *Spectrochim. Acta*, **44B**, 1093.
18. Yang, P. and Barnes, R.M. (1989) A low-power oxygen inductively coupled plasma for spectrochemical analysis. 1. Computer-simulation. *Spectrochim. Acta*, **44B**, 1081.
19. Yang, P. and Barnes, R.M. (1990) A low-power oxygen inductively coupled plasma for spectrochemical analysis. 3. Excitation mechanism. *Spectrochim. Acta*, **45B**, 157.
20. Yang, P. and Barnes, R.M. (1990) A low-power oxygen inductively coupled plasma for spectrochemical analysis. 4. Analytical features. *Spectrochim. Acta*, **45B**, 167.
21. Barnes, R.M., Kovacic, N. and Meyer, G.A. (1985) Computer simulation of a nitrogen ICP discharge. *Spectrochim. Acta*, **40B**, 907.
22. Kovacic, N., Meyer, G.A., Ke-Ling, L. and Barnes, R.M. (1985) Diagnostics in an air inductively coupled plasma. *Spectrochim. Acta*, **40B**, 903.
23. Chan, S. and Montaser, A. (1985) A helium inductively coupled plasma for atomic emission-spectrometry. *Spectrochim. Acta*, **40B**, 1467.
24. Zhang, H., Nam, S.H., Cai, M. and Montaser, A. (1996) Atmospheric-pressure helium inductively-coupled plasmas for elemental mass-spectrometry. *Appl. Spectrosc.*, **50**(4), 427.

25. Evans, E.H. and Ebdon, L. (1989) Simple approach to reducing polyatomic ion interferences on arsenic and selenium in inductively coupled plasma mass spectrometry. *J. Anal. At. Spectrom.*, **4**, 299.
26. Evans, E.H. and Ebdon, L. (1990) Effect of organic-solvents and molecular gases on polyatomic ion interferences in inductively coupled plasma mass-spectrometry. *J. Anal. At. Spectrom.*, **5**, 425.
27. Niu, H. and Houk, R.S. (1996) Fundamental-aspects of ion extraction in inductively-coupled plasma-mass spectrometry. *Spectrochim. Acta*, **51B**, 779.
28. Douglas, D.J. and French, J.B. (1988) Gas-dynamics of the inductively coupled plasma mass-spectrometry interface. *J. Anal. At. Spectrom.*, **3**, 743.
29. Campargue, R. (1984) Progress in overexpanded supersonic jets and skimmed molecular-beams in free-jet zones of silence. *J. Phys. Chem.*, **88**, 4466.
30. Gray, A.L. (1989) Visual observation of shock-waves in an inductively coupled plasma mass-spectrometry expansion stage. *J. Anal. At. Spectrom.*, **4**, 371.
31. Olivares, J.A. and Houk, R.S. (1985) Ion sampling for inductively coupled plasma mass spectrometry. *Anal. Chem.*, **57**, 2674.
32. Hoglund, A. and Rosengren, L.G. (1984) A new sensitive molecular-beam mass-spectrometer. *Int. J. Mass. Spectrom. Ion. Proc.*, **60**, 173.33.
33. Tanner, S.D. (1987) *Plasma Source Mass Spectrometry Development and Applications* (Eds G. Holland and S.D. Tanner), Royal Society of Chemistry, Cambridge.
34. Turner, P., Merren, T., Speakman, J. and Haines, C. (1997) *Plasma Source Mass Spectrometry Development and Applications* (Eds G. Holland and S.D. Tanner), Royal Society of Chemistry, Cambridge.
35. Gray, A.L., Houk, R.S. and Williams, J.G. (1987) Langmuir probe potential measurements in the plasma and their correlation with mass-spectral characteristics in inductively coupled plasma mass-spectrometry. *J. Anal. At. Spectrom.*, **2**, 13.
36. Houk, R.S., Schoer, J.K. and Crain, J.S. (1987) Plasma potential measurements for inductively coupled plasma mass-spectrometry with a center-tapped load-coil. *J. Anal. At. Spectrom.*, **2**, 283.
37. Lim, H.B. and Houk, R.S. (1990) Langmuir probe measurement of electron-temperature in a supersonic jet extracted from an inductively coupled plasma. *Spectrochim. Acta*, **45B**, 453.
38. Chambers, D.M., Poehlman, J., Yang, P. and Hieftje, G.M. (1991) Fundamental studies of the sampling process in an inductively coupled plasma mass-spectrometer. 1. Langmuir probe measurements. *Spectrochim. Acta*, **46B**, 741.
39. Olivares, J.A. and Houk, R.S. (1985) Kinetic-energy distributions of positive ions in an inductively coupled plasma mass-spectrometer. *Appl. Spectrosc.*, **39**, 1070.
40. Chambers, D.M. and Hieftje, G.M. (1991) Fundamental studies of the sampling process in an inductively coupled plasma mass-spectrometer. 2. Ion kinetic-energy measurements. *Spectrom-chim. Acta*, **46B**, 761.
41. Tanner, S.D. (1993) Plasma temperature from ion kinetic energies and implications for the source of diatomic oxide ions in inductively-coupled plasma-mass spectrometry. *J. Anal. At. Spectrom.*, **8**, 891.
42. Fulford, J.E. and Douglas, D.J. (1986) Ion kinetic energies in inductively coupled plasma mass-spectrometry (ICP-MS). *Appl. Spectrosc.*, **40**, 971.
43. Melton, C.E. (1970) *Principles of Mass Spectrometry and Negative Ions*, Marcel Dekker, New York.
44. Chapman, J.R. (1993) *Practical Organic Mass Spectrometry*, 2nd edn, John Wiley, Chichester.
45. Flesch, G.D. and Svec, H.J. (1975) *International Review of Science (Mass Spectrometry) Physical Chemistry*, Series 2, Vol. 5 (Eds A.D. Buckingham and A. Maccoll), Butterworth, London.
46. Todd, J.F.J. and Lawson, G. (1975) *International Review of Science (Mass Spectrometry) Physical Chemistry*, Series 2, Vol. 5 (Eds A.D. Buckingham and A. Maccoll), Butterworth, London.
47. Willard, H.H., Merritt, L.L., Dean, A.J. and Settle, A.F. (1988) *Instrumental Methods of Analysis*, 7th edn, Wadsworth, CA.

48. Myers, D.P., Yang, G.L.P. and Hieftje, G.M. (1994) An inductively-coupled plasma time-of-flight mass spectrometer for elemental analysis. 1. Optimization and characteristics. *J. Am. Soc. Mass Spectrom.*, **5**, 1008.
49. Myers, D.P., Li, G., Mahoney, P.P. and Hieftje, G.M. (1995) An inductively-coupled plasma time-of-flight mass spectrometer for elemental analysis. 3. Analytical performance. *J. Am. Soc. Mass Spectrom.*, **6**, 411.
50. Myers, D.P., Li, G., Mahoney, P.P. and Hieftje, G.M. (1995) An inductively-coupled plasma time-of-flight mass spectrometer for elemental analysis. 2. Direct-current quadrupole lens system for improved performance. *J. Am. Soc. Mass Spectrom.*, **6**, 400.
51. Koppenaal, D.W., Barinaga, C.J. and Smith, M.R. (1994) Performance of an inductively-coupled plasma source ion trap mass spectrometer. *J. Anal. At. Spectrom.*, **9**, 1053.
52. Barinaga, C.J., Eiden, G.C., Alexander, M.L. and Koppenaal, D.W. (1996) Analytical atomic spectroscopy using ion-trap devices. *Fresenius' J. Anal. Chem.*, **355**, 487.
53. Sakata, K. and Kawabata, K. (1994) Reduction of fundamental polyatomic ions in inductively coupled plasma mass spectrometry. *Spectrochim. Acta B*, **49**, 1027.
54. Tanner, S.D. and Baranov, V.I. (1999) Theory, design, and operation of a dynamic reaction cell for ICP-MS. *At. Spectrosc.*, **20**, 45.
55. Anicich, V.G. (1993) Evaluated bimolecular ion–molecule gas-phase kinetics of positive ions for use in modelling planetary atmospheres, cometary comae and interstellar clouds. *J. Phys. Chem. Ref. Data*, **22**, 1469.

Chapter 6

Use of ICP-MS for Isotope Ratio Measurements

Frank Vanhaecke, Lieve Balcaen and Philip Taylor

6.1 Introduction

More than 20 years after its commercial introduction (in 1983), inductively coupled plasma-mass spectrometry (ICP-MS) has evolved into a well-established technique for trace and ultra-trace element determination with >10 000 instruments in use worldwide. From the early beginnings, also isotope ratio measurements using ICP-MS were reported on, but the application range was largely limited to measuring either induced changes in the isotopic composition of a target element, for example, for calibration by means of isotope dilution (ID) or in tracer experiments, or pronounced natural variations, as are observed in the case of Pb. This was because the isotope ratio precision obtainable with most ICP-MS instruments was and still is rather poor compared to the precision achievable using thermal ionisation mass spectrometry (TIMS). The introduction of multi-collector MC-ICP-MS as a dedicated tool for isotopic analysis however, has not only bridged this gap in isotope ratio precision, but has even opened previously inaccessible application ranges. The objective of this chapter is to explain, review and illustrate the opportunities which isotopic analysis can offer in ICP-MS. Although the capabilities of MC-ICP-MS will be illustrated, also single-collector ICP-MS will receive proper attention, since it represents the vast majority (~99%) of the instrumentation used worldwide and it can be successfully used for a wide variety of applications. First, the general concepts of isotopic measurement are briefly outlined, then the application areas in which ICP-MS has a strong position are discussed, using selected applications from the literature.

6.2 Fundamentals

6.2.1 *Isotope ratios: general concepts*

In chemical measurements, isotope-specific analytical techniques, which take full advantage of the isotopic character of matter, have proven to be extremely useful and powerful tools [1]. This section outlines the principles on which such measurements are based, first in a general way, then referring specifically to ICP-MS.

Table 6.1 Examples of elements for which measurable variations in the isotopic composition occur in normal terrestrial materials [2,3,4]

Factors limiting uncertainty on representative isotopic composition as tabulated by IUPAC	Effect measurable by ICP-MS	Effect not measurable by ICP-MS
Man-made variation	Li, B, U	H, He, Kr
Natural mass fractionation	Li, B	H, C, N, O
Radioactive decay of naturally occurring radionuclides	Sr, Os, Pb	Ar

First of all, it is important to be aware of the fact that, generally speaking, isotopic abundances are constant in nature [2]. As a result, a variety of problems can be studied by using compounds in which a particular element shows an isotopic composition sufficiently different from the corresponding natural one. This is always the case when artificially produced radionuclides are employed (e.g. ^{239}Pu , ^{236}U , ^{233}U , ^{99}Tc or ^{129}I). Stable isotopes, on the other hand, must be either partially or totally isolated to be of use, unless the isotopic composition of the element under consideration shows natural variations.

Many isotopic applications make use of the assumption that the behaviour of different isotopes is chemically and physically identical (Table 6.1). This is a prerequisite for tracer and ID experiments, often practised in ICP-MS. Nevertheless, small isotopic or mass fractionation effects do occur in both natural and industrial processes [1]. The origin of such effects can be either kinetic or thermodynamic and the variations in isotopic composition they give origin to [3] are observed especially for the lighter elements (for which the relative mass differences are more outspoken), such as H, C, N, O and S. Most of these elements are not accessible for ICP-MS, but are typically studied using gas source mass spectrometry (GSMS). It is interesting to point out that with the increasing isotope ratio precision that state-of-art TIMS and MC-ICP-MS instrumentation offers, natural variations in the isotopic composition are established for an increasing number of elements and seem to be by no means restricted to the 'light' elements only. Additionally, variations in the isotopic composition of some elements may also occur as a consequence of the radioactive decay of naturally occurring long-lived radionuclides [4], nuclear reactions resulting from the interaction of cosmic rays with matter and anthropogenic activities. In addition, in some meteoritic samples, some elements show deviations from the natural isotopic composition, unknown in terrestrial samples [5]. Because of these variations, the *representative isotopic composition* [2] in 'normal terrestrial' materials cannot be defined precisely for some elements, such as Li, Sr or Pb, as can be seen from the ranges given in Table 6.2. In these cases, and for critical applications, the isotopic composition of a sample should be measured instead of using tabulated values (e.g., when performing isotope dilution mass spectrometry (IDMS)). Care should also be taken when using commercially available chemical reagents containing Li or U in isotope ratio work, because the isotopic composition of these elements may be substantially modified (depleted in ^6Li and ^{235}U , respectively) without any corresponding indication on the package [6,7].

Of all the isotope-specific analysis techniques (MS, activation analysis, optical methods and nuclear magnetic resonance spectrometry [1]), MS is by far the most versatile and powerful. It allows the relative abundances of different isotopes to be measured with unrivalled

Table 6.2 Natural variations in the relative abundances of isotopes of Li, Sr and Pb in terrestrial materials [2]

Nuclide	Lower level for isotopic abundance (%)	Upper level for isotopic abundance (%)
${}^6\text{Li}$	7.21	7.71
${}^7\text{Li}$	92.29	92.79
${}^{84}\text{Sr}$	0.55	0.58
${}^{86}\text{Sr}$	9.75	9.99
${}^{87}\text{Sr}$	6.94	7.14
${}^{88}\text{Sr}$	82.29	82.75
${}^{204}\text{Pb}$	1.04	1.65
${}^{206}\text{Pb}$	20.84	27.48
${}^{207}\text{Pb}$	17.62	23.65
${}^{208}\text{Pb}$	51.28	56.21

precision and accuracy. The specific advantages of ICP-MS in this context are discussed in Section 6.2.2.

Relative abundances cannot be measured directly. An isotope ratio (R) of an element E in a sample is, however, experimentally accessible. Such a ratio is colloquially referred to as ${}^iE/{}^jE$ (e.g. ${}^{204}\text{Pb}/{}^{208}\text{Pb}$) and is in fact a ratio of *amounts* of isotopes:

$$R = \frac{n({}^iE)}{n({}^jE)} \approx \frac{I({}^iE)}{I({}^jE)} \quad (6.1)$$

By using MS, the ion currents $I({}^iE^+)$ and $I({}^jE^+)$ can be measured easily (positive ions are only given as an example). An isotope ratio is a very robust quantity as the number of parameters which influence it are limited and their effect is generally quite small. Fig. 6.1 illustrates this robustness convincingly. There are some mass-dependent processes, however, which cause a small, but measurable bias due to the difference in mass between the isotopes measured. Nevertheless, small bias, good repeatability and reproducibility are inherent properties of isotope ratio measurements. This qualitative statement can be translated into the following quantitative expression:

$$R = \frac{n({}^iE)}{n({}^jE)} = \frac{I({}^iE^+)}{I({}^jE^+)} K_1 K_2 \dots K_z = \frac{I({}^iE^+)}{I({}^jE^+)} K_{\text{TOT}} \quad (6.2)$$

in which K_1 to K_z are correction factors related to the various sources of bias, and

$$K_{\text{TOT}} = \prod_i K_i$$

In general, K_{TOT} is fairly close (typically within 1–5%) to unity and is known with a relatively small uncertainty. Depending on the objectives of the measurement and the amount of effort that goes into the characterisation of these correction factors, different situations

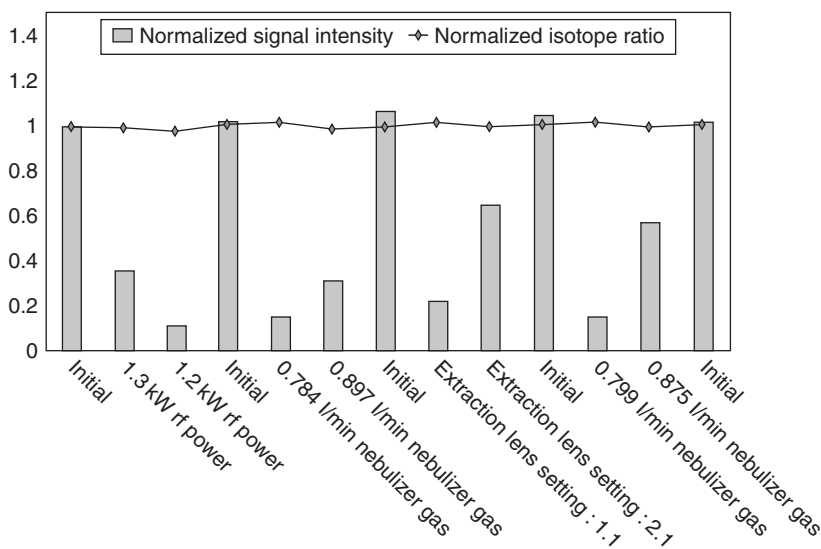


Figure 6.1 Quadrupole-based ICP-MS experiment in which the sensitivity (for Pb) is deliberately changed by varying the instrument settings and the $^{206}\text{Pb}/^{208}\text{Pb}$ isotope ratio is measured under these different conditions. The relative standard deviation (RSD) for the 13 isotope ratio results amounted to 0.5% only.

arise. In the crudest case, small correction factors are simply ignored as the specificity of the isotopic measurement can already help to unravel pathways and mechanisms; this is often the case in tracer experiments. In other cases, the correction factors are assumed to stay constant during the measurement and no effort is made to quantify them. This can, for example, be the case when applying ID if the isotope ratio of interest is determined experimentally for the sample, the spike and the blend. In another case, the objective may be a *differential* isotopic measurement, that is how different is the isotope ratio measured in a particular sample (R_X) compared to the corresponding one in another sample, the latter sample often being a(n) (internationally recognised) reference sample (R_{RS}). Such differences are often small, and therefore high reproducibility/repeatability is desired. Often the result of such a measurement is expressed in a relative way:

$$\delta(\text{‰}) = \frac{R_X - R_{RS}}{R_{RS}} 1000 \quad (6.3)$$

Such differential measurements are widespread and are applied to solve analytical problems in many different domains. Assuming constant bias (as R_X and R_{RS} are fairly similar) is of course convenient, but for critical applications, this should preferably be checked independently. One of these critical applications is the preparation of certified reference materials (CRMs). If such materials are only used as comparators (with $\delta = 0$) and they have no 'absolute' ratio, problems arise when such comparator samples are unstable or no longer available. For this reason, calibrated isotope ratios are required [8]. This calibration is accomplished by using certified isotopic reference materials or, in their absence, by calibration against gravimetric mixtures of purified and isotopically enriched materials.

6.2.2 ICP-MS vs TIMS for isotope ratio measurements

The isotopic analysis of the 'light' elements H, C, N, O and S – which show substantial natural variation in their isotopic composition due to pronounced fractionation effects, occurring as a result of the relatively large mass difference between their isotopes – is typically carried out by means of GSMS. Because of its application field, this technique is even often referred to as isotope ratio mass spectrometry (IRMS). Prior to the introduction of ICP-MS, the domain of isotopic analysis of the 'heavier' elements on the other hand, was dominated by TIMS. The terms 'lighter' and 'heavier' elements should only be considered a general description of the typical application field here, as also the isotopic composition of Li and B can be studied using TIMS [9,10], while GSMS can, for example, be used for the isotopic analysis of U (converted into UF_6) as well [11]. Especially when equipped with an MC detection system (array of Faraday collectors), TIMS is capable of providing an excellent isotope ratio precision down to $<0.01\%$ RSD [12]. Additionally, fractionation processes – the thermal ionisation of the lighter isotope(s) is somewhat faster than that of the heavier isotope(s) of the target element, such that the ion beam composition varies slightly during the course of a TIMS acquisition – are not very pronounced and are fairly well understood, such that accuracy is not gravely threatened when adequate correction is applied or when integrating the results over the entire period during which the target element is ionised from the filament (total sample evaporation). Moreover, as a result of the isolation of the analyte element during the sample preparation, necessarily preceding analysis via TIMS, and the gentle ionisation in vacuum, spectral interferences are very scarce in TIMS.

However, TIMS also shows important drawbacks. An efficient thermal ionisation is only guaranteed when the target element is chemically isolated as purely as possible from the concomitant matrix. After suitable sample preparation, μl amounts of pre-concentrated sample solution have to be applied onto a filament. During this process, additional chemicals may be added onto the filament, with the intention of facilitating ion formation. Electrodeposition of the analyte element onto the filament is sometimes used as an alternative. After complete drying, the filaments are mounted onto a sample turret, inserted into the sample introduction compartment of a TIMS instrument, which is subsequently evacuated using a vacuum pump. Therefore, often, the entire sample preparation preceding TIMS is very labour-intensive and time-consuming and requires high analyst skills. Additionally, only elements with an ionisation energy (IE) below 7.5 eV are efficiently ionised, while also volatile elements pose additional problems [13]. To some extent, however, the possibility of using negative (atomic or molecular) ions instead of the more traditional positive ions offers a solution for the aforementioned restriction to low IE elements [14].

From the beginning on, it was realised and demonstrated that ICP-MS can also be used to obtain isotopic information on the analyte elements. The ICP is a powerful ion source that also ionises elements with an IE exceeding 7.5 eV with high efficiency. Moreover, the requirements in terms of sample preparation are far less severe, as sample introduction traditionally consists of continuous nebulisation of sample solution into an ion source operated at atmospheric pressure, while the concomitant matrix may well induce signal suppression or enhancement, but does not preclude a sufficiently efficient formation of analyte ions. Due to the rather poor isotope ratio precision of quadrupole-based instruments – from $\sim 0.5\%$ with first-generation instrumentation to $\geq 0.1\%$ RSD with present-day instruments (it is worthwhile to point out that all isotope ratio precisions cited in this chapter are internal

precisions for successive measurements, unless mentioned otherwise) – the application range was however mainly limited to studying *induced* changes in the isotopic composition in the context of elemental assay by means of ID or of tracer experiments, aiming at obtaining a more profound insight into (bio)chemical or physical processes.

Although not specifically aiming at improving the isotope ratio capabilities, a meaningful improvement in the isotope ratio precision was achieved by fundamental changes to the design of ICP-MS instruments, such as the use of double-focusing sector field mass spectrometers [15] or time-of-flight (TOF) analysers [16] instead of the more traditional quadrupole filter, or the introduction of collision/reaction cells in quadrupole-based instrumentation [17].

The main advantage of sector field ICP-MS instrumentation is the possibility to avoid spectral overlap by using a higher mass resolution. Vanhaecke *et al.* [18] however, were the first to demonstrate that owing to the flat-topped (trapezoidal) peaks obtained at *low* mass resolution with this type of instrumentation, an isotope ratio precision of $\leq 0.05\%$ RSD is attainable, at least under favourable conditions, that is, two isotopes with similar abundance (isotope ratio close to unity) and at a sufficiently high analyte concentration (counting statistics not the limiting factor). ‘Sampling’ only the central part of the trapezoidal ion peak and a high peak-hopping rate were shown to be crucial to achieve optimum isotope ratio precision. When operating a sector field ICP-MS instrument at higher mass resolution, peaks of a rather triangular form are obtained, such that isotope ratio precision is somewhat deteriorated to figures similar to those for quadrupole-based instrumentation [19]. Nevertheless, the possibility to avoid spectral overlap leads to a further extension of the application range of ICP-MS and even allowed isotopic analysis of elements such as S [20], that were previously not accessible using ICP-MS.

In a later publication, Vanhaecke *et al.* [21] showed that as a result of the simultaneous introduction into and handling of the ions sampled from the ICP by the TOF analyser, also ICP-TOFMS provides the user with $\leq 0.05\%$ RSD isotope ratio precision. Moreover, it was demonstrated that the isotope ratio precision was not deteriorated in a multi-element mode and that even for transient signals with a short duration (< 10 s fwhm), a very decent isotope ratio precision (0.1% RSD) could be obtained. Despite the initial hype immediately after its commercial introduction at the end of the 1990s, ICP-TOFMS has so far not been able to obtain a reasonable share of the ICP-MS market.

Collision/reaction cells were introduced as a flexible means for tackling spectral overlap in quadrupole-based ICP-MS. These cells are positioned in-between the interface and the mass analyser and contain a multipole ($2n + 2$ rods) assembly (Fig. 6.2). Depending on the manufacturer, either a quadrupole ($n = 1$, 4 rods), hexapole ($n = 2$, 6 rods) or octopole ($n = 3$, 8 rods) set-up can be used. When such a cell is pressurised with a suitable gas, the signals of interfering ions can be reduced by orders of magnitude, thus creating interference-free conditions for the target element(s). Collision-induced dissociation (to a lesser extent), selective ion-molecule reactions and/or energy filtering are the processes responsible [17]. Alternately, by means of selective ion-molecule chemistry, an analyte ion suffering from spectral overlap can also be converted into a reaction product ion, that can be measured interference-free at another mass-to-charge ratio [22].

Moreover, Bandura *et al.* [24] showed that the temporal homogenisation of ions extracted from the ICP at slightly different moments in time, by using a non-reactive gas in a collision/reaction cell, also permits $\leq 0.05\%$ RSD isotope ratio precision to be obtained.

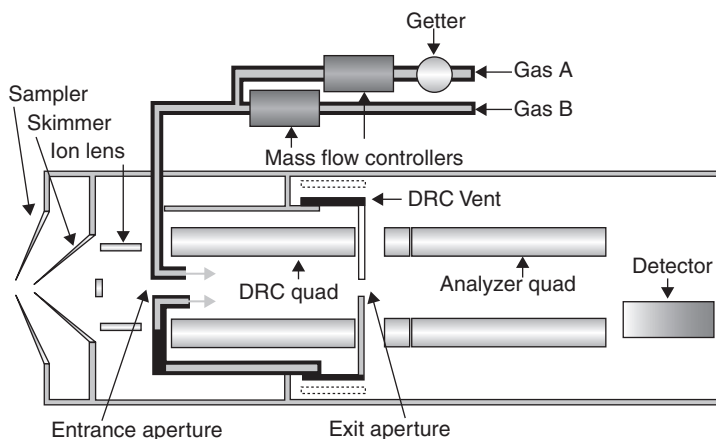


Figure 6.2 Schematic representation of a quadrupole-based instrument, equipped with a collision/reaction cell (dynamic reaction cell, DRC). The DRC is equipped with a quadrupole unit, which permits unwanted ions created inside the cell to be removed by means of mass filtering. Reaction and/or collision gases can be introduced into the DRC at ml min^{-1} gas flow rates. A getter is used to further purify the gas used (removal of O-containing gas molecules). Reproduced from [23].

Admixing a non-reactive collision gas with a reaction gas allows the benefits of collisional damping to be maintained while using the cell as a device to overcome spectral overlap [25].

The gap in isotope ratio precision between TIMS on one hand and ICP-MS on the other, was however only fully bridged with the introduction of MC-ICP-MS, wherein the ion beams of the isotopes of interest are separated from one another in space in a double-focusing sector field mass spectrometer of Nier–Johnson geometry and the beam intensities *simultaneously* measured using an array of Faraday collectors (Fig. 6.3).

As a result of short-term variations in the analyte introduction, ionisation and extraction efficiencies, the ICP ion signal is known to be rather noisy. With single-collector instrumentation, the detrimental effect this has on the isotope ratio precision is counteracted to the largest possible extent by using a high scanning or peak-hopping rate. With MC-ICP-MS, all analyte signals are monitored simultaneously. As a result, the aforementioned short-term variations in signal intensity affect all signals to the same extent, such that they should no longer deteriorate the isotope ratio precision. The VG Plasma 54 was the first commercially available MC-ICP-MS instrument [27] and immediately, isotope ratio precisions of $<0.01\%$ RSD were within reach for isotope ratios approaching unity and even for isotope ratios deviating substantially from unity (e.g. $^{235}\text{U}/^{238}\text{U}$ or $^{204}\text{Pb}/^{208}\text{Pb}$), $<0.05\%$ RSDs were obtained. In spite of its lower sensitivity, the Faraday collector is preferred over the electron multiplier for ion detection in MC-ICP-MS instrumentation, because in the counting mode, the electron multiplier suffers from dead time effects (see Section 6.3.3.4), which become increasingly more important as the isotope ratio deviates more from unity. Only if a higher sensitivity is required, one or more Faraday cups can be replaced by an electron multiplier. Present-day MC-ICP-MS instrumentation – the Neptune (from ThermoElectron) or the Nu high-resolution (HR) Plasma (from Nu instruments) – provides even more impressive isotope ratio precisions down to 0.002%

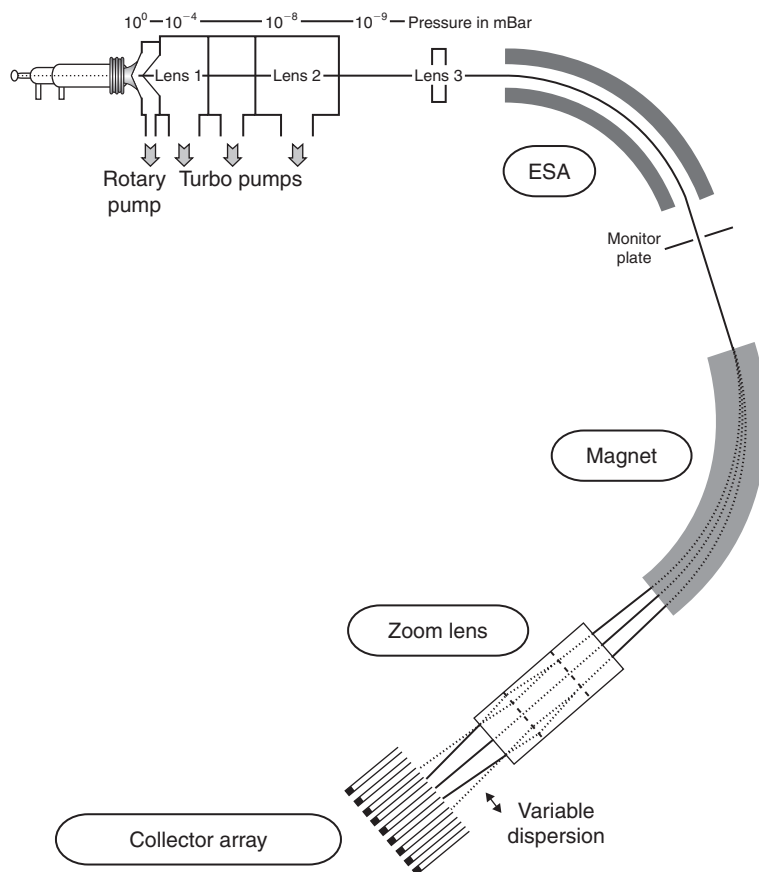


Figure 6.3 MC-ICP-MS instrumentation, with double-focusing sector field mass spectrometer of Nier Johnson geometry (electrostatic analyser ESA, followed by magnetic sector) and equipped with an array of Faraday collectors. Reproduced from [26].

RSD. This is similar to the best values reported for TIMS, while the advantages of the ICP ion source are maintained. Moreover, important instrumental developments, such as the possibility of using multiple ion counters to monitor the beam intensities of those isotopes present at low abundance and of a retardation lens to improve the abundance sensitivity and thus to improve the capabilities for reliable measurements of ‘extreme’ isotope ratios have further extended the application range of MC-ICP-MS [28]. The MC-ICP-MS instrument from GV Instruments (isoprobe) shows an alternative design and uses a hexapole collision cell pressurised with a non-reactive collision gas instead of an electrostatic sector for energy focusing [26].

However, while isotope fractionation in TIMS is rather well understood, a complete understanding of mass discrimination (defined as the deviation between the experimental result and the corresponding ‘true’ isotopic ratio) in ICP-MS is not obtained yet, although recent systematic studies already permitted a more profound insight and hence, stimulated

the development of better correction approaches (see Section 6.3.3.1). Perhaps an even more important pitfall is the occurrence of spectral interferences. Spectral overlap is often considered the most important disadvantage of ICP-MS as a technique for trace element determination and it is even more of a nuisance in isotopic analysis as here, the signals of at least *two* isotopes should be free from overlap. Additionally, the better the isotope ratio precision attainable, the more the occurrence of polyatomic ions, originating from the Ar plasma gas, entrained air, the solvent and/or the matrix, hamper isotopic analysis, as already at a much lower abundance, they will affect the result and hence, the accuracy attainable. In ICP-MS in general, high mass resolution (sector field ICP-MS) is considered the most elegant and powerful approach to overcome spectral overlap. Despite the double-focusing properties of the mass spectrometer in the Plasma 54, it could only be operated at unit mass resolution. More recent MC-ICP-MS instruments can however be operated at high mass resolution. With single-collector sector field ICP-MS, a higher mass resolution is obtained by a simultaneous decrease of the width of both a slit in-between the accelerating optics and the mass analyser (source slit) and a slit in-between the mass analyser and the detector (collector slit). This frees the analyte ion signal from that of interfering ions with either lower or higher mass, but results in triangular peak shapes (Fig. 6.4b) and hence, brings about significantly deteriorated isotope ratio precision. As very often, interfering ion(s) are all at the *same* side of the analyte mass [29], reducing the width of the source slit by moving one side only, while the width of the collector slit is not adjusted is sufficient to obtain what is sometimes referred to as 'pseudo high mass resolution' [30,31]. In this way, the analyte signal is not *completely* resolved from that of the interfering ion, but there is a small mass range where only the analyte ion contributes to the total signal intensity and where the signal displays a sufficiently wide flat section for precise isotope ratio measurement (Fig. 6.4c). At higher mass resolution, the isotope ratio precision attainable – 0.005% RSD – is barely deteriorated compared to that at low mass resolution – 0.002% RSD.

Although at first, it was claimed that for reliable isotopic analysis using MC-ICP-MS, analyte isolation was not required, this statement had to be revisited once it became clear that the concomitant matrix affects the mass discrimination in a measurable way. Hence, for highly accurate measurements, analyte isolation is still required. Still, the straightforward sample introduction into and high ionisation efficiency of the ICP ion source are sufficient advantages that have made MC-ICP-MS not only a serious competitor for TIMS [32], but have even allowed a variety of new applications that can only be successfully carried out by MC-ICP-MS [33,34]. Moreover, for less demanding applications – at least in terms of precision – less demanding sample preparation can suffice, while already immediately after the introduction of MC-ICP-MS, it was clear that even laser ablation (LA) can be used as a means of sample introduction [35], permitting direct isotopic analysis of solid materials, while offering the possibility of spatially resolved sampling. In the applications section, examples will illustrate the tremendous possibilities of MC-ICP-MS as a dedicated technique for isotopic analysis, of which currently (2006) approximately 100 instruments are in use. Self-evidently the large majority of the >10 000 ICP-MS instruments used worldwide are single-collector ICP-MS instruments, equipped with a quadrupole filter (~90%), a sector field mass spectrometer (<10%) or a TOF-analyser (maximum a few %). From the selected applications section, it will become clear that also these single-collector instruments are successfully used in isotopic analysis, at least for less demanding applications.

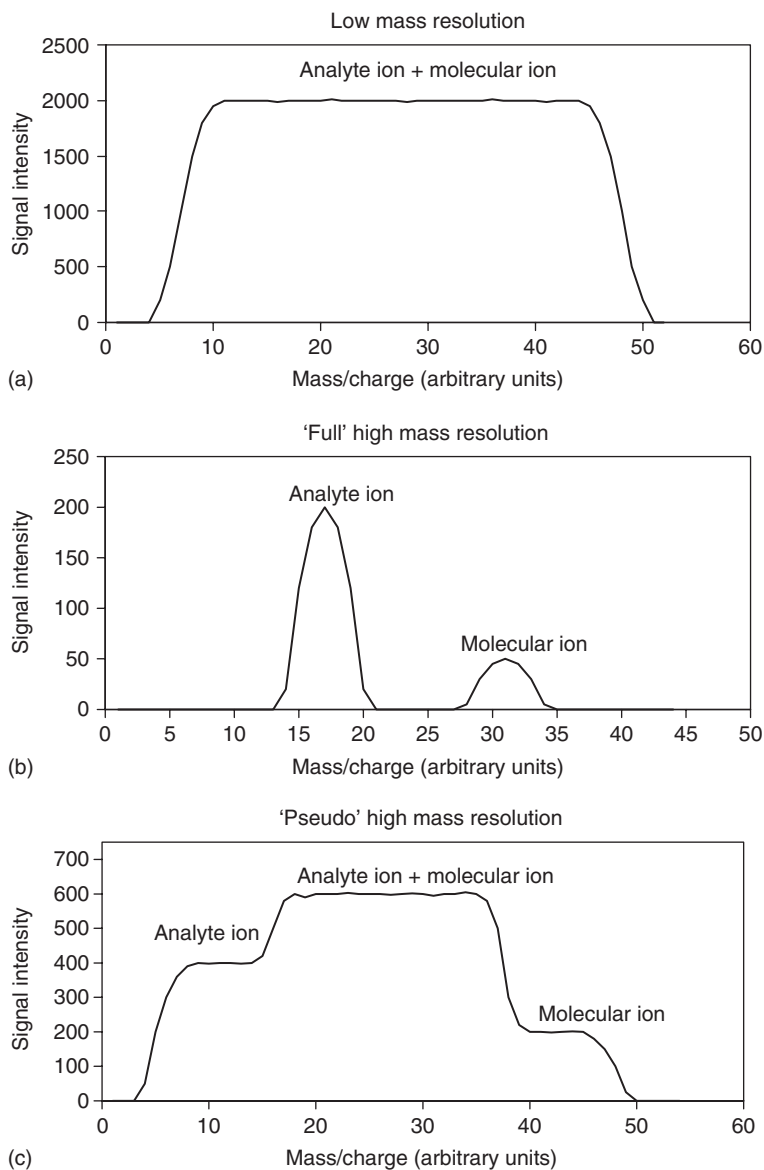


Figure 6.4 Schematical representation of the difference in the shape of the mass spectral peaks when using (a) low, (b) 'full' high and (c) 'pseudo' high mass resolution in MC-ICP-MS. The highest isotope ratio precision is obtained via static multi-collection at the flat section of the analyte signals ((a) or (c)). Reproduced from [31].

6.3 Different sources of uncertainty affecting isotope ratios when measured using ICP-MS

The quality requirements and/or expectations of isotope ratio measurements are often very high. This section discusses possible sources of uncertainty when these measurements are carried out using ICP-MS. This knowledge will help users to assess and calculate the total combined uncertainty for the measured isotope ratio.

In their reviews, Begley and Sharp [36,37] differentiate between factors that contribute to the noise of the system (the imprecision) and those that create an offset (bias). Although useful as a means of classification, in reality the factors are intertwined and it is often not possible to make a distinction between them. Before addressing the various sources of uncertainty, present-day concepts on uncertainty, which are internationally agreed upon, are first briefly outlined.

6.3.1 *Uncertainty according to International Standards Organisation–International Bureau of Weights and Measures*

The word ‘uncertainty’ is used here as defined by the ISO [38,39]. In this approach, a pragmatic stance is taken for different kinds of uncertainty: they are different depending on the way in which they are measured. Uncertainty estimates obtained from repeated measurements are said to be of type A and all other are of type B. Typical type B uncertainties are data used/derived from a certificate (of a certified reference material or of a calibrant) or originating from a separate experiment (e.g. aimed at establishing the influence of a spectral interference). For calculating the total uncertainty, both types are treated in an identical way.

Why bother about uncertainty? Because uncertainty is linked with quality. International Standards Organisation–International Bureau of Weights and Measures (ISO–BIPM) uncertainty can be seen as a way to make a more objective statement about the quality of a measurement. Vague expressions such as ‘inaccurate’, ‘fairly accurate’ or ‘highly accurate’ can then be quantified.

In the uncertainty estimation process, the first crucial step is often underestimated: to mathematically formulate the relationship between what is being measured (the measurand) and the experimental factors which have an influence. For isotope ratio and IDMS measurements, this is significantly easier compared to other methods because the relationship is simple, for example Equations (6.2) and (6.12), and the number of influencing parameters is small and they are of limited magnitude.

In the final stages, the various uncertainty sources (either type A or B) are combined to produce a *combined uncertainty*, u_c , either using the rules of error propagation or more simple approximations. If necessary, an expanded uncertainty, U , is calculated by applying a *coverage factor*, k ($U = ku_c$), depending on the level of confidence ($k = 1, 2, \dots$).

Finally, newcomers to the field of isotopic measurements need to be aware that there is a strong tradition and tendency (especially in geochemical and cosmochemical circles) to use large numbers of replicate experiments (e.g. 100 replicate measurements on a sample aliquot in a 10 min period) to reduce the standard error of the mean ($= s/\sqrt{n}$) when expressing type

A uncertainties. Although this obviously leads to impressively small numerical values, it can be quite misleading. One should be aware of, and if necessary take into account, the other (often larger) sources of uncertainty when calculating combined uncertainties.

6.3.2 Sources of noise

Different parts of the instrument are responsible for producing noise. The ICP is a noisy ion source (compared to thermal ionisation or electron impact ionisation sources) because of, for example, pulsations of the peristaltic pump, variations in the nebulisation efficiency, the gasdynamic rotation of the plasma, changes in the transfer of energy from the plasma to the sample and variation in ion extraction efficiencies. Such processes have been well described and some are identical to those occurring in ICP optical emission spectrometry. Source noise contributions can be minimised by selecting suitable data acquisition parameters for quadrupole-based or single-collector sector field instruments (see Section 6.3.4). The most efficient way to minimise the effect of source noise, however, is by using an MC instrument.

Random events also occur in detectors (electron multipliers and Faraday cups) and their associated electronics (amplifiers, counters and discriminators). More troublesome is the pick-up of noise from inside the instrument (e.g. stray radio frequency (rf) radiation) or from external sources (e.g. interfering equipment).

The effect of all of these processes is that the arrival of ions at the detector is not a continuous process but a random one. Often, one assumes that this process can be described using a Poisson distribution. Counting statistics are then said to hold and, under this assumption, for ion-counting systems an *a priori* statement can be made concerning the standard deviation of the number of counts, N :

$$\sigma_N = \sqrt{N} \quad (6.4)$$

In reality, experimental values will probably be larger than the minimal value given by Equation (6.4). By applying uncertainty propagation, the minimum standard uncertainty on the isotope ratio $R = A/B$ would be given by:

$$\left(\frac{\sigma_R}{R} \right) = \sqrt{\left(\frac{\sigma_A}{A} \right)^2 + \left(\frac{\sigma_B}{B} \right)^2} \quad (6.5)$$

in which σ_A and σ_B are the contributions from the counts observed for the respective isotopes.

6.3.3 Sources of bias

Different sources of bias are discussed in the following sections, together with methods used for correction. In most cases, correction is required to obtain reliable results.

6.3.3.1 Mass discrimination

When an instrument produces a different response for ions of different mass, this systematic error is called mass discrimination. Fig. 6.5 is a typical response curve for a quadrupole-based ICP-mass spectrometer. In the absence of any mass discrimination, this response curve would be a horizontal straight line. Typically, the mass discrimination that occurs in ICP-MS instruments is about 1% per mass unit (at mass 100), irrespective of the kind of instrumentation. As the ion kinetic energy is dependent on the mass [40], any energy-dependent process in the instrumentation (e.g. sampling of ions from the ICP, transfer of ions or detection) will lead to a mass discrimination. Compared to TIMS, mass discrimination in ICP-MS is often larger (especially at lower mass, e.g. 16% for $^6\text{Li}/^7\text{Li}$ in the case of ICP-MS [41] compared to $<1\%$ mass fractionation using TIMS [42]). Lower bias in TIMS can be the consequence of the separation of the evaporation and the ionisation step, whereby species of higher mass (e.g. $\text{Li}_2\text{B}_2\text{O}_7$ instead of LiCl) are deposited on and evaporated from the filament. Not all the sources and mechanisms of mass discrimination in ICP-MS have been unequivocally identified, but the sampling of ions from the ICP and the ion-transfer lens system have been identified as major contributors. Heumann *et al.* described the ‘nozzle effect’ as a reason of mass discrimination during plasma extraction via the sampling cone aperture [12]. Andren *et al.* carried out isotopic analysis of B deposited on the sampling and skimmer cone [43]. The results obtained confirmed the aforementioned nozzle effect and enabled the supersonic expansion of the extracted plasma gas in the expansion chamber to be identified as another important source of mass

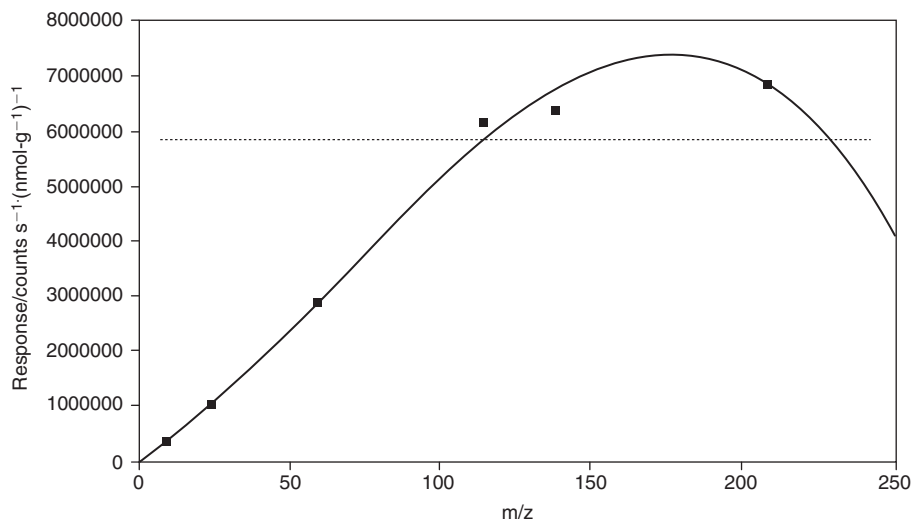


Figure 6.5 Experimental response curve for a quadrupole-based ICP-mass spectrometer. The response for the elements studied was determined using a solution containing 1 nmol g^{-1} of Be, Mg, Co, In, La and Pb, and the results obtained were corrected for differences in ionisation efficiency and isotopic abundance. The dotted line represents a hypothetical case where mass discrimination would be absent.

discrimination. Tanner *et al.* described the influence of the space-charge effects caused by the large matrix Ar^+ ion currents (μA) passing through the lens system [44]. The effect of these space-charge effects were also confirmed by isotopic analysis of deposits of various elements on the ion lenses by Andren *et al.* [43]. Burgoyne *et al.* have studied and reduced mass discrimination by applying acceleration voltages behind the skimmer [45]. For commercial instrumentation (both quadrupole and sector field), the behaviour and the magnitude of the mass discrimination across the mass range is fairly similar. Contrary to TIMS, in which a discrete amount of sample is brought into the ion source, there is a continuous introduction of new sample into the ICP. Therefore, systematic time-dependent fractionation (as with TIMS) does not occur.

Ratios can be corrected for mass discrimination using several approaches. External calibration is frequently used. For this, isotopic reference materials with known isotopic composition are used or, in their absence, samples in which the element has a natural isotopic composition. In the latter case, this can only be done for those elements for which no natural (e.g. Sr or Pb) or man-made (e.g. Li or U) variability measurable with the instrumentation used occurs (see Section 6.2). Ideally, the ratios used in the correction process should be similar to the ones being measured and a ‘*bracketing*’ approach, whereby the isotopic standard is measured before and after every sample, is recommendable. Sometimes, a known ‘internal isotope ratio’ can be used (e.g. $^{88}\text{Sr}/^{86}\text{Sr}$, which is constant in nature, to correct the $^{87}\text{Sr}/^{86}\text{Sr}$ ratio, which shows natural variations as a result of radioactive decay of ^{87}Rb into ^{87}Sr) to correct for mass discrimination. This approach can generally not be applied for ID, as an external spike has then been added. Finally, *substitute* calibration using a different element added to the sample (e.g. Tl for Pb [46,47] or Ga for Zn [48]) can also be used. Of course, this increases the measurement time required and the uncertainty obtained, at least with quadrupole-based or sector field *single*-collector instrumentation.

In case of internal correction for, or substitute calibration of the mass discrimination, a K factor can be calculated based on the ‘true’ value (R_{true} from the certificate or the IUPAC table) and the experimental result (R_{obs}) for the isotope ratio, from which a discrimination factor ε can be calculated. Several empirical models can be used for this. For data from quadrupole-based ICP-MS, it is sufficient to use a linear model, as the uncertainty on the data obtained is fairly large:

$$K = \frac{R_{\text{true}}}{R_{\text{obs}}} = (1 + \varepsilon_{\text{linear}} \Delta m) \quad (6.6)$$

With reduced uncertainty (e.g. MC-ICP-MS), the use of the linear model is no longer sufficient and the power-law (6.7) or exponential (6.8) model have to be considered [49]:

$$K = \frac{R_{\text{true}}}{R_{\text{obs}}} = (1 + \varepsilon_{\text{power}})^{\Delta m} \quad (6.7)$$

$$K = \frac{R_{\text{true}}}{R_{\text{obs}}} = e^{\varepsilon_{\text{exp}} \Delta m} \quad (6.8)$$

According to these approaches, only the mass difference between the isotopes of interest Δm determines the mass discrimination and hence, a similar mass discrimination is expected for ${}^6\text{Li}/{}^7\text{Li}$ as for ${}^{206}\text{Pb}/{}^{207}\text{Pb}$. In ICP-MS, this assumption is not correct, as mass discrimination per mass unit is higher for the lighter elements [12], which show a more pronounced *relative* difference in the masses of their isotopes. It has been demonstrated that this assumption is not even valid for neighbouring elements such as Tl and Pb once the situation is studied with the high precision offered by MC-ICP-MS [50]. Other approaches, such as that Russell's Equation (6.9) rather use the absolute mass of the isotopes involved [49]:

$$K = \frac{R_{\text{true}}}{R_{\text{obs}}} = \left(\frac{m_1}{m_2} \right)^{\beta} \quad (6.9)$$

Once ε or β is determined via a 'known' isotope ratio (e.g. using ${}^{86}\text{Sr}/{}^{88}\text{Sr}$ or ${}^{203}\text{Tl}/{}^{205}\text{Tl}$), it can be used to convert experimental results for the isotope ratio of interest (e.g. ${}^{86}\text{Sr}/{}^{87}\text{Sr}$ or ${}^{206}\text{Pb}/{}^{207}\text{Pb}$) into the corrected ('true') result on the basis of the mass difference (Δm) between the isotopes of interest or the masses of the isotopes, respectively. There is still ongoing debate as to which correction method provides the most accurate description of mass discrimination effects. This is an issue of increasing importance as a result of the continuously improving isotope ratio precision. Finally, some authors report other approaches – the generalised power law [51] or a double spike approach [52] – to provide even more accurate results. For more information on these approaches, the reader is referred to the literature. Finally, with an ideal mass spectrometer, the bias on isotope ratios would be constant across the range of isotope ratios measured. For ICP-MS, there are not many studies that have focused on this aspect in detail. Taylor *et al.* [53] have investigated this linearity for a first-generation MC instrument and have found that U isotope ratios varying between 0.01 and 1 all agreed within 0.03% with the corresponding certified value after mass discrimination correction using the same value for ε . For this purpose, they used a special set of synthetically prepared isotopic reference materials (IRMM-072). Contrary to Faraday cups, electron multipliers, and in particular continuous dynode electron multipliers, are known to have a narrower optimal operational range.

6.3.3.2 Mass scale shift

Although the reasons are different, mass scale shifts occur with both quadrupole-based and sector field instruments. For quadrupole filters, the constancy of the rf and direct current (DC) potentials is the limiting factor [36]. Since the introduction of solid state rf generators, the situation has improved. In isotope ratio work with sector field instruments, mass scale shifts also occur, for example, as a consequence of temperature changes.

6.3.3.3 Background and contamination

Here, 'background' is defined as that part of the ion current measured at a certain mass-to-charge ratio (m/z), corresponding to the isotope under investigation, not originating from this element. Background can be continuous or discontinuous. 'Contamination' is defined as

that part of the ion current measured at a certain m/z that does originate from the same element, but for which the origin either lies within the instrument or within the chemical procedure used. As it is important to know the origin of either one (in order to control it), it is meaningful to distinguish between background and contamination by studying the mass spectral region of interest and measuring and comparing the isotope ratio with the expected one, as calculated from the IUPAC tables [2]. Background can be continuous over the mass spectral region and often originates from the detector (e.g. due to photons from the ICP arriving at the multiplier). Discontinuous background is due to a spectrally interfering species (isobaric nuclide, doubly charged or polyatomic ion). Its origin can be 'instrumental', for example, due to the formation of ArO^+ and Ar_2^+ ions, or the presence of impurities in the plasma gas (e.g. Xe), or external, that is from concomitants in the sample, for example, overlap of the analyte signal with that from ArNa^+ when measuring ^{63}Cu . Such interferences also tend to deteriorate the reproducibility of the isotope ratio measured. Contamination can also be external or instrumental. Examples of instrumental contamination are memory effects occurring in the nebuliser tubing, nebuliser, spray chamber and/or interface. Such effects can occur because of the volatility of the compound (e.g. B, Hg and Os) or because of specific chemical features (e.g. Pt in solution is easily reduced in Teflon tubing and refractory elements tend to deposit on the interface). External contamination can occur in any sample preparation step, for example, contamination occurring during the sample digestion, sample storage or application of separation procedures. Of course, it is extremely important to prepare a procedural blank. In exceptional cases, spectral interferences can occur which hardly affect the isotope ratio under study. An example of this is given by Vanhaecke *et al.* [54] for the interference of SiCl^+ ions on both Cu isotopes, and the implications of this spectral overlap are discussed in more detail by Papadakis *et al.* [55].

Different approaches are used for correction of these interferences (Table 6.3). For instrumental background or instrumental contamination, it is necessary to measure a representative blank sample (e.g. at the start of or at several occasions during the measurement session) and to subtract the blank signal measured (containing the interfering signal) from the corresponding signal for subsequent samples. The software of most ICP-MS instruments caters for this. This is only possible if the blank value is sufficiently stable and representative. The magnitude of the correction should obviously be limited. For discontinuous background, originating from the sample (e.g. Mo present in a water sample, causing an MoO^+ interference on Cd isotopes), the same approach could in principle be used, but only when it is possible to prepare a 'matrix-matched' blank sample (e.g. a water sample with a

Table 6.3 Origin of and correction methods for different types of contamination and background

Type	Origin	Blank subtraction	Mathematical correction
Contamination	External sources	✓	
Contamination	Instrument	✓	
Discontinuous background	Sample	✓	✓
Discontinuous background	Instrument	✓	✓
Continuous background	Photon and electronic noise	✓	

Mo concentration identical to the sample, but self-evidently no Cd), which can be difficult. Finally, for discontinuous background, also mathematical corrections can be used to correct the ion current observed for isotope i M (e.g. ^{204}Pb) by measuring the ion current of another isotope (e.g. ^{202}Hg) of the interfering element and calculating its effect at the m/z of interest assuming natural isotopic composition for the interfering element. The same approach holds for corrections involving polyatomic species (e.g. the abundance of ArNa^+ species reflects that of argon itself). Procedural contamination is best corrected for by measuring the isotope intensities (or concentration of M) in a number of independent blank samples, for example, measuring the contamination originating from an ion-exchange separation step by preparing three independent blank separations.

6.3.3.4 Detector dead time

When using an electron multiplier operated in the pulse-counting mode (or a Daly detector), pulse pile-up leads to biased isotope ratio results, at least for isotope ratios differing from unity. Although not only the detector itself but also other parts of the detection system (amplifier, discriminator and counting system) may contribute to the bias under consideration, the global effect is commonly attributed to detector dead time. The detector dead time is the time required for the detection and electronic handling of an ion pulse. If another ion strikes the detector surface within the time required for handling the first ion pulse, the second ion will not be detected and hence, the observed count rate will be lower than the actual count rate. Typically, the detector dead times reported for ICP-MS instrumentation range from 15 to 100 ns. If the detector dead time τ can be determined accurately, these signal losses can be appropriately corrected for using Equation (6.10):

$$N_T = \frac{N_O}{1 - N_O\tau} \quad (6.10)$$

where N_O is the observed count rate, N_T is the actual count rate and τ is the detector dead time. The higher the count rate, the larger the bias observed. As isotope ratio measurements are often carried out at quite high count rates to improve the precision of the results (*cf.* Poisson counting statistics), while keeping the acquisition time at an acceptable level, an accurate determination of the detector dead time is of great importance for reliable isotope ratio results. In addition, the detector dead time should also be determined at regular time intervals since it has been observed to be influenced to a considerable extent by the age of the detector [56] and previous exposure.

A practicable method to determine the detector dead time was proposed by Russ [57]. For standard solutions of different concentration levels, a given isotope ratio differing from unity is determined with, if applicable, the automatic detector dead time correction disabled (set to zero ns). For each concentration level, plotting the 'normalised' isotope ratio (isotope ratio corrected for the detector dead time divided by the true value) as a function of the value used for the dead time correction leads to a curve. The intersection of the curves corresponding with different concentration levels supplies the analyst with the correct value for the detector dead time (Fig. 6.6). In addition, the ordinate value of the intersection point

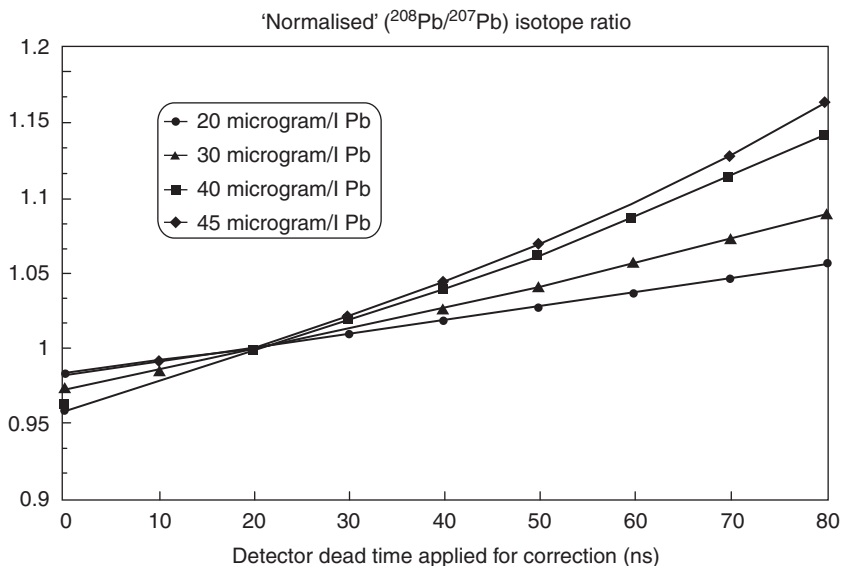


Figure 6.6 Normalised $^{208}\text{Pb}/^{207}\text{Pb}$ isotope ratio ($= [^{208}\text{Pb}/^{207}\text{Pb}]_{\text{measured}}/\text{true value}$) plotted as a function of the value applied for dead time correction of the 'raw' results, obtained for standard solutions with a Pb concentration ranging from 20 to 45 $\mu\text{g l}^{-1}$ (detector dead time ~ 20 ns). Reproduced from [59].

(deviation from unity) permits an estimation of the mass discrimination. Other methods that can be used for experimental determination of the detector dead time have been compiled and evaluated by Nelms *et al.* [58], who also indicated how the uncertainty on the dead time can be estimated.

The dead time obtained in this way is often considered as an invariable instrument parameter, which it is not. The constancy of the detector dead time across the mass range has been evaluated [59] for two commercially available and commonly used ICP-mass spectrometers: a quadrupole-based one equipped with a Channeltron–continuous dynode–electron multiplier and a sector field instrument equipped with a conversion dynode and a secondary electron multiplier with discrete dynodes. For the latter instrument, the detector dead time was found to be constant across the mass range. For the former, however, the detector dead time measured was observed to be strongly dependent on the analyte mass. This observation was attributed to a decreasing gain of Channeltron electron multipliers with increasing analyte mass. It has also been reported that, above a critical level, the gain of an electron multiplier decreases with the number of incident particles per time unit [60]. As a result, at increasingly higher count rates, an increasing fraction of the output pulses show an amplitude below the discriminator level and hence, these pulses are not detected [61,62]. This effect is called 'sag' and leads to a significant increase of the measured (or apparent) dead time at high count rates. It should be stressed that the method of determining the detector dead time described above also offers a means of detecting the appearance of sag: if sag appears for the highest concentration level used, the

corresponding curve will intersect the other curves at several rather widely dispersed points. Of course, all measurement data that are observed to be affected by sag should be discarded and not used for the determination of the detector dead time.

6.3.4 Optimisation of data acquisition parameters in terms of isotope ratio precision

As in many instrumental analytical techniques, a quantity (in this case, an isotope ratio) can be measured more precisely, if the number of observations is increased (i.e. if the measurement time is increased). Various measurement protocols can be applied, and those whereby the time actually spent on measuring the isotope ratios of interest is maximised are preferable. For this reason, peak-jumping (or peak-hopping) procedures are favoured over scanning. The data acquisition parameters that can be changed for further improving the isotope ratio precision are: the integration time (dwell time) per acquisition point, the number of acquisition points per spectral peak, the number of sweeps and possibly, the settling time of the quadrupole filter or sector field mass spectrometer. With single-collector ICP-MS instruments, the noisy character of the ICP ion source is counteracted by using a high peak-hopping or peak-jumping rate to eliminate low frequency noise from the plasma and the sample introduction system to the largest possible extent [63–65]. In the 1980s, this was already experimentally demonstrated and dwell times of typically 10–20 ms and a limited number of acquisition points per peak (even as low as one point) were advised. Later on, chemometric approaches were used to optimise the data acquisition parameters in a more systematic way and these approaches were generally observed to result in similar conclusions [66]. With shorter mass spectrometer settling times, even higher peak-hopping rates, realised by using even shorter dwell times of a few ms only, can be used [24,25]. Also for single-collector sector field ICP-MS instruments, a high peak-hopping rate was demonstrated to be crucial for obtaining the optimum isotope ratio precision [18]. The measurement time can sometimes be used more efficiently by increasing the acquisition time for (the) low-abundant isotope(s) relative to that of the higher abundant isotope(s) [66]. Finally, simultaneous monitoring of all the isotopes involved is realised in MC-ICP-MS instrumentation, which results in a superior isotope ratio precision, similar to that offered by state-of-art TIMS. MC-ICP-MS is operated in a *static* mode during the measurements, which means that nor the accelerating field nor the strength of the magnetic field are changed during data acquisition.

6.4 ID: general concepts

The concept of ‘dilution’ was first used to evaluate populations of rare bird species living on islands, that is in a closed system. Rings were put on the legs of a given number of birds, which were then released and sufficient time was allowed to elapse before capturing another flock of birds, so that ringed birds could mix randomly with unringed ones. The proportion of unringed birds to ringed specimens gave the ratio of the total population to the number of ringed ones [1].

The same principle was later used to quantify amounts of chemical compounds, first by applying radioactive isotopes and later also by using stable isotopes. This powerful technique is now applied for different purposes and using different instrumental methods to quantify the isotope ratios. Primarily, the latter has been achieved using mass spectrometry (IDMS), although other isotope-specific techniques can be used (e.g. gamma ray spectrometry in combination with neutron activation).

Contrary to many other approaches in analytical chemistry, ID makes full use of the existence of isotopes. Therefore, from a first principles point of view, quantifying chemicals via this route offers some quite unique advantages, especially for providing reference measurements. The degree to which this is possible strongly depends on the care and thoroughness with which the measurements are carried out, as is discussed in Section 6.4.6.

6.4.1 Principle

By inducing a deliberate change in a chosen isotope ratio of an element, it is possible to measure the amount or the concentration of a particular chemical compound in the sample studied. For this purpose, an amount of this chemical is added to the sample (the spiking process). The isotopic composition of the element in this spike or tracer needs to be sufficiently different from the one in the sample (Fig. 6.7).

In the simplest case, for example, for measuring the concentration of iodine in a terrestrial sample (only the isotope ^{127}I occurs in 'normal terrestrial' samples) via addition of the long-lived radionuclide ^{129}I , the following equation holds:

$$\frac{N_X}{N_Y} = R_B \quad (6.11)$$

in which R_B is the blend ratio and N_X and N_Y are the number of iodine atoms in the sample (X) and the spike (Y) solutions. The ID process has been compared to a weighing process, as the measurement process is very similar and the device used (in this case a mass spectrometer) also serves as a comparator device [67]. In the case of ID, numbers of atoms/molecules are compared.

For the more general case, in which the elements have i different isotopes, the equation can be written as follows:

$$\frac{N_X}{N_Y} = \frac{R_Y - R_B}{R_B - R_X} \frac{\sum_i (R_X)_i}{\sum_i (R_Y)_i} \quad (6.12)$$

with a particular isotope selected as the reference isotope. As $N = N_A n$ (where N_A is Avogadro's constant and n is the amount (in mol) of substance), and $n = cm$ (where c is the molar concentration and m is the mass of solution), Equation (6.12) can be written as:

$$\frac{n_X}{n_Y} = \frac{c_X m_X}{c_Y m_Y} = \frac{R_Y - R_B}{R_B - R_X} \frac{\sum_i (R_X)_i}{\sum_i (R_Y)_i} \quad (6.13)$$

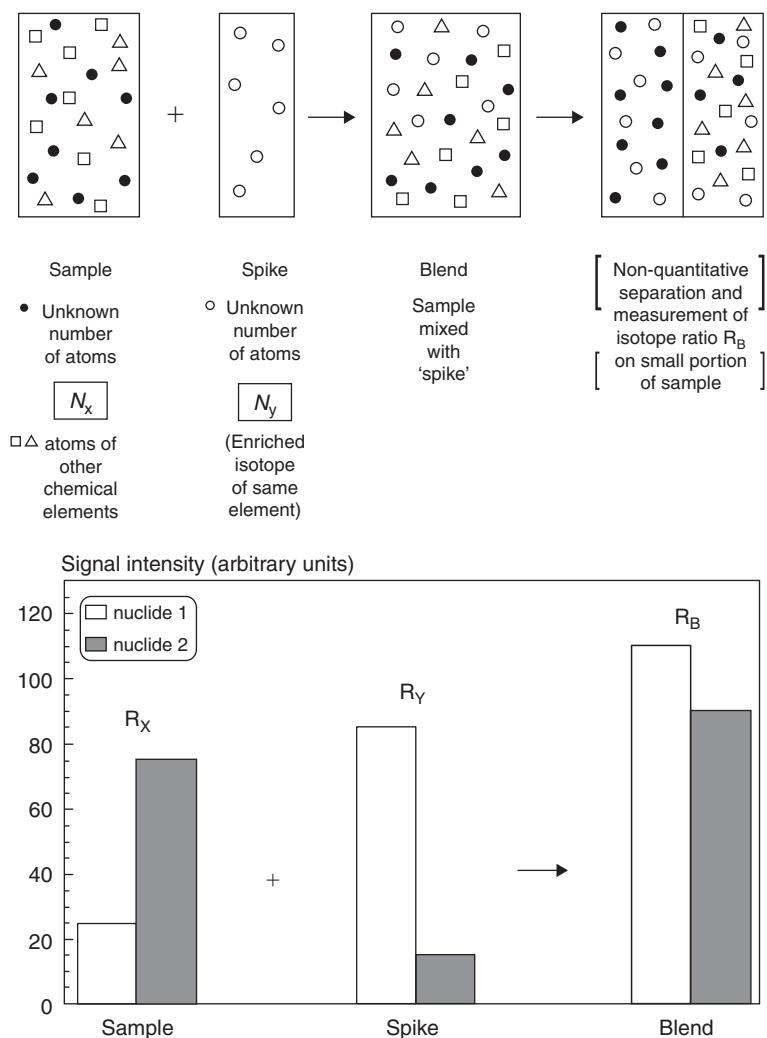


Figure 6.7 Schematic representation of the principle of IDMS.

Table 6.4 gives a numerical example. As can be seen, concentrations need to be expressed in mol g^{-1} (or mol l^{-1}) to yield correct values.

Of course, the above equation does not hold if R_X , R_Y and/or R_B are biased due to spectral interference, which often occurs in ICP-MS. For that reason, it is vital to measure R_X and compare it to the value calculated from IUPAC tabulated values. However, for some elements, such as Li, Pb and U, this approach is not possible due to the variations in natural isotopic composition. Also, the mass spectral region of interest should be carefully studied in order to ascertain that the two isotopes involved are free from spectral overlap.

If the element which has to be determined shows no natural variations in isotopic composition, while sufficient information concerning the spike material is available from the

Table 6.4 Numerical example of an IDMS experiment. A 20 g aliquot of a sample (for which the Pb concentration has to be determined) is spiked with a tracer solution (enriched in ^{206}Pb) with a Pb concentration of 10 pmol g^{-1} . In this particular example, calculation of the unknown Pb concentration was based on the $^{207}\text{Pb}/^{206}\text{Pb}$ ratios, measured for the sample (R_X), the spike (R_Y) and the mixture or blend (R_B)

Ratio	Sample	Spike	Blend
$^{204}\text{Pb}/^{206}\text{Pb}$	0.058	0.001	
$^{206}\text{Pb}/^{206}\text{Pb}$	1.000	1.000	
$^{207}\text{Pb}/^{206}\text{Pb}$	0.917	0.020	0.388
$^{208}\text{Pb}/^{206}\text{Pb}$	2.174	0.005	
ΣR_i	4.149	1.026	
Mass of solution (in g)	20	2	
Pb concentration (in pmol g^{-1})	2.813	10	

corresponding certificate or via reverse ID (see Section 6.4.4), it is not necessary to experimentally determine all isotope ratios. For this approach, Equation (6.13) can be rewritten as:

$$\frac{n_X}{n_Y} = \frac{R_Y - R_B}{R_B - R_X} \frac{f_{iY}}{f_{iX}} \quad (6.14)$$

where f_i represents the isotopic abundance of the reference isotope in the spike (Y) and in the sample (X), respectively. Numerically, Equations (6.13) and (6.14) yield identical values ($f_i = R_i/\Sigma R_i$). In another variant of Equation (6.13), mass/volume concentrations (C) are used. In this case, a correction factor for the atomic weight (A_r) needs to be applied ($c = C/A_r$). If R_X , R_Y and R_B are determined experimentally, mass discrimination is often assumed to be constant and hence, no correction for this is required. If, on the other hand, R_X is calculated on the basis of IUPAC tabulated values and/or R_Y is taken from the certificate of the spike material, the experimental value for R_B has to be corrected for mass discrimination.

Traditionally in ID, when small uncertainties are required, dilutions are made gravimetrically. Volumetric preparations of dilutions are somewhat more practicable and less time-consuming, but result in combined uncertainties on the concentrations which are in the 0.5–1% range, when no strict precautions are taken. When using gravimetry, this can be limited to 0.1%.

6.4.2 Advantages and pitfalls

The simplicity of the IDMS formula reveals some very interesting ID properties. It can, for example, be noticed that this equation does not contain a ‘sensitivity’ factor, contrary to all other calibration strategies. Most analytical instrumentation is susceptible to temporal changes in sensitivity or to matrix-induced changes in sensitivity. This effect is orders of magnitude smaller for ID compared to other calibration methods and therefore, in most cases, it is not measurable. Furthermore, because isotope ratios can be measured with high

precision (typically between 0.5% and 0.002% RSD with ICP-MS, depending on the type of instrumentation used), this results in a small uncertainty on the assay.

For Equation (6.13) to hold, it is crucial that the isotopic species added to the sample behaves identically to the one which is originally present in the sample. If not, the isotope ratios measured (e.g. after a separation procedure) will be biased. If some of the added spike disappears before isotopic equilibrium is established, isotope ratios will be biased. Very often, when measuring total element concentrations, isotopic equilibration is obtained by subjecting the sample to a strong oxidation/reduction step. However, when the objective is to measure the concentration of a certain chemical species (e.g. the amount of CH_3Hg^+), it is important not to disturb the chemical equilibrium. After isotopic equilibration, the isotope ratio in the blend is 'frozen' and this implies that it is not affected by further sample treatment. Hence, non-quantitative recovery is, for example, automatically corrected for, because any aliquot of the sample, or any dilution, still 'displays' the ratio R_B .

Typically, ID has been found to be applicable over a wide range of concentrations, from pmol to mol levels. Whereas most other calibration strategies require the preparation of a series of calibration samples, it is possible to obtain a concentration value from a single spiking process. This is due to both the sensitivity and the dynamic range of the ratio measurement technique. For ICP-MS, the former is certainly valid, but the latter is generally much less the case when using quadrupole-based ICP-MS instrumentation. Overspiking or underspiking processes, whereby the ratio N_X/N_Y is either small or large (e.g. <0.01 or >100) and which can be useful when the amount of compound to be determined is either small or large, should therefore be used with care [68–70].

6.4.3 Optimum sample to spike mixing ratios

When designing an ID experiment, some *ab initio* calculations can be done prior to the experiment. Influencing factors are the enrichment of the spike and the uncertainty with which the isotope ratios can be measured. The mathematical expression for this is given by De Bièvre [71] and the results can be graphically represented in so-called *error magnification curves*. However, these calculations are based on the assumption that the relative uncertainty for the isotope ratios for the sample, spike and blend ratios are constant across the range of ratios. Whereas this might be true in the case of thermal ionisation, this is not always the case when ICP-MS is used. Error magnification curves should therefore be interpreted with care and merely used to indicate trends. Often it is safer to use blend ratios close to unity or in the range from 0.1 to 10, especially when using electron multipliers for detection. As an approximation, the optimum blend ratio should approximate the geometric mean of the spike and sample ratio:

$$R_{B,\text{opt}} = (R_X R_Y)^{1/2}$$

6.4.4 Spike calibration

Proper assay of the amount or concentration of a compound in a sample is only possible (see Equation (6.12)) if the amount of spike added is well known. This can be accomplished

in two ways: either by using calibrated spike isotopic reference materials or by a process called reverse IDMS.

When using reverse IDMS, the spike is calibrated against a high-purity solution of the compound. Such a solution is prepared gravimetrically from a suitable material and Moody *et al.* have described a list of such inorganic compounds which are best used as they are the most likely to be available as pure compounds with known stoichiometry [72]. Often it is assumed that the element in such a sample is of natural isotopic composition (taken from [2]), but this should be checked for some elements (see Table 6.2). Such material is used as it would be too expensive to convert or assay the isotopically enriched material itself. Mathematically this 'reverse' IDMS process can be expressed as:

$$\frac{c_X m_X}{c_Z m_Z} = \frac{m_Y}{m'_Y} \frac{R_Y - R_B}{R_B - R_X} \frac{R_Z - R'_B}{R'_B - R_Y} \frac{\sum_i (R_X)_i}{\sum_i (R_Z)_i} \quad (6.15)$$

in which the subscript Z refers to the high-purity material (often the isotopic composition of the high-purity material is equal to that of the sample) and R_B and R'_B refer to the blend ratios in the mixtures X/Y and Y/Z, respectively. As can be seen, c_X can be determined from the known concentration c_Z , the ratio of masses of solutions used and the isotope ratios determined. It can be shown, when applying error propagation, that the uncertainty of c_X is virtually independent of the uncertainty of R_Y (and therefore R_Y only needs to be known approximately).

The second approach makes use of calibrated spike isotope reference materials, for which the isotope ratios as well as the concentration of the compound are well characterised. In this way, the spike calibration process is taken care of only once (i.e. by the producer of the material). An ID assay is then reduced to a single spiking operation and measurement of R_B (and possibly R_X). This avoids, as is the case for reverse IDMS, the preparation of a considerable number of samples to carry out the procedure successfully. For calibrated spike isotopic reference materials, long-term spike stability is guaranteed by putting the solutions in flame-sealed ampoules (e.g. quartz or glass). Producers of such materials prepare these isotopic reference materials from a batch of isotopically enriched material, which is chemically purified and then characterised both for concentration and isotope ratios. The raw material is converted into a stoichiometric compound (e.g. an oxide or metal) and then a gravimetric solution is prepared from this. For ultimate accuracy, the isotope ratios can be calibrated against synthetic isotope mixtures [8].

6.4.5 Blank correction

As discussed in Section 6.3.3.3, reliable isotope ratios can only be obtained if the contribution of background and contamination to the total signal intensity is appropriately corrected. When low concentrations of a compound in a sample are measured, contamination from external sources (e.g. originating from an ion-exchange separation step or from the acids or containers used) is best assessed by measuring the concentration in independently prepared blank samples. This value can be used to correct the measured concentration and the uncertainty of the correction can be taken into account when calculating the combined uncertainty.

6.4.6 ICP-IDMS: metrological and non-metrological mode of application

Often, 'IDMS measurement' is considered to be a synonym of 'reference measurement'. Such a measurement is one with a *provable* (and sufficiently small) uncertainty statement, and therefore one will be able to refer to it. Although IDMS certainly has this *potential*, not *all* measurements are (or need to be) reference measurements. IDMS can (intentionally or not) be used in a less stringent way. The long-acknowledged special IDMS reliability feature has been internationally and formally recognised by the BIPM [73]. The BIPM has identified IDMS as one of the primary methods of measurement, having the potential to yield SI-traceable values. Such a 'status' can obviously be used and misused. It is not *because* IDMS is employed that reliability follows automatically. The method needs to be applied *correctly*. Giving an objective and detailed account of the uncertainty of the measurement (although still not common practice) could make this statement much more objective and concrete [74,75].

Laboratories active in the field of reference measurements or CRMs have therefore been keen IDMS users. As their mission is producing reliable measurements, this often means being quite conservative before adopting new methods. ICP-IDMS has nevertheless been successfully applied, replacing or complementing thermal ionisation IDMS (TI-IDMS). Since in this field reliability is the primary objective (and not speed, sample throughput, etc.), such procedures often make use of off-line chemical separation steps. The reason for this is that with increasing complexity of the measurement procedure, its transparency (knowledge about sources of uncertainty) correspondingly deteriorates. Applications include the assay of elements in biological/clinical samples (blood, plasma, serum, urine), technological materials (exhaust catalysts), environmental samples (sediments, waters, particulate fall-out) and food (rice, wine). Although not its primary application field, also MC-ICP-MS is used for ID [76,77]. It provides a superior isotope ratio precision and can therefore aid reduction of the total uncertainty on the element concentrations thus determined.

Apart from these metrological applications of IDMS, many analytical chemists have discovered the assets of ICP-IDMS. As utmost reliability is not the main concern of the majority of users, too much time and effort cannot be spent on identifying and quantifying the uncertainty. Such users are nevertheless attracted by the robustness of ICP-IDMS and also by its other advantages (e.g. isotope specificity, non-quantitative chemistry, wide dynamic range, freedom of sensitivity changes). It should, however, be taken into account that applications such as on-line ICP-IDMS or flow injection ICP-IDMS lead to larger total combined uncertainties (and are therefore less suited when the aim is to establish reference values) [78–81].

6.5 Selected applications

6.5.1 Introduction

Since its commercial introduction in the early 1980s, ICP-MS has aroused great expectations, both as an elemental detector and as a device for measuring isotope ratios. At present, >10 000 ICP-mass spectrometers, most of which are quadrupole-based, are used across

the world. Although most of these instruments are operated for element determination only, an impressive number of publications has been devoted to isotope ratio determination by means of ICP-MS. Many of these applications are aimed at elemental assay by means of ID. A description of selected applications is given in Section 6.5.2. However, there is also a considerable amount of literature reporting on the use of ICP-MS for stable isotopic tracer investigations, aiming at a better understanding of (human) metabolism and heavy metal toxicity. In addition, monitoring of isotope ratios following addition of a stable tracer has also proved useful for the study of chemical reactions (and physical processes). Examples of the research involving the measurement of isotope ratios following administration of a stable tracer(s) is presented in Section 6.5.3. The amount of literature covering the use of ICP-MS for the determination of natural isotope ratios has increased exponentially with the introduction of MC-ICP-MS. A selection of such applications is discussed in Section 6.5.4.

6.5.2 *Isotope dilution*

Instead of attempting to cover the entire application range of ICP-IDMS, only a limited number of selected applications are addressed in this section. The first example is discussed in some detail and serves as an example of the metrological use of IDMS for certification purposes. Thereafter, some examples are given on how ID can be of use to assure the quality of analytical results when a matrix/trace separation procedure is included in the sample pretreatment procedure. The use of ICP-IDMS in radioanalytical work is also discussed.

6.5.2.1 *ICP-IDMS for certification purposes/metrological and non-metrological use of ICP-IDMS*

A typical application in which ID was used in conjunction with ICP-MS for certification purposes was described by Vassileva and Quérel [82]. These authors have applied ID to the certification of the contents of Cd, Cu and Pb in a rice material, that was used for round 19 of the international measurement evaluation programme (IMEP), co-ordinated by the institute for reference materials and measurements (IRMM). Rice is the main foodstuff for about half of the world's population. To protect the public health, the presence of contaminants in rice has to be carefully checked. Maximum levels of Cd and Pb in foodstuff are set in relevant regulations, such as the EC Directive 466/2001 [83]. However, also the measurement of traces of essential elements, such as Cu, is of crucial importance to estimate dietary uptake rates. It is clear that important conclusions and decisions concerning public health and/or international trade are derived from such results. Therefore, the results have to be based on measurement data of good quality and they must be traceable to a system of reference, preferably to SI. For the SI-traceable certification of the Cd, Cu and Pb mass fractions in rice, Vassileva and Quérel used ICP-IDMS in a metrological mode. Typical of this approach is the careful and systematic search for and investigation of all possible sources of bias or uncertainty. The Isotopic Certified Reference Materials (ICRM) used for IDMS purposes were IRMM-622 (^{111}Cd -enriched), IRMM-632 (^{65}Cu -enriched) and NIST SRM-991 (^{206}Pb -enriched) for Cd, Cu and Pb, respectively. Accurately weighed rice samples (~ 0.2 g) were taken into solution by acid digestion (using HNO_3 and HF), after addition of an appropriate weighed amount of

spike material. All measurements were carried out with a quadrupole-based ICP-MS instrument. The blend isotope ratios were corrected externally for mass discrimination by measuring, immediately before and after the sample solution, the ratio of interest in the material used as reference ('natural' standards or isotopic reference materials). The selection of the isotopes to be measured in the blend samples was done with respect to the availability of spike materials, the abundance of the isotopes and possible spectral interferences during measurement by ICP-MS. For Cu, medium mass resolution spectra (obtained by means of a sector field ICP-MS instrument) demonstrated that the Cu signals were not significantly affected as a result of the possible occurrence of ArNa^+ , Ba^{2+} or SiCl^+ . For Cd, the situation was less favourable, because MoO^+ interferences affected all of the Cd isotopes, except for ^{106}Cd . Although this interference contributed very little to the signals measured, the interference was corrected for on all five isotopes. The ratio $^{110}\text{Cd}/^{111}\text{Cd}$ was selected for the final certification calculations as it corresponded to the combination of the least interfered isotopes. Finally, for Pb, only one isotope (^{204}Pb) was affected by spectral overlap. The $^{201}\text{Hg}^+$ signal was monitored to correct for the contribution from $^{204}\text{Hg}^+$ to the signal intensity at a mass-to-charge ratio of 204 (~0.5% of the signal). A comparison was made between two series of IDMS experiments: a first series with so called 'non-saturated' samples (samples spiked immediately after opening of the bottles) and a second series with 'saturated' samples (samples spiked after having attained a moisture equilibrium with the laboratory atmosphere). For the determination of the water content in the rice material, two methods were investigated and compared: Karl Fischer titration [84] and the use of a drying method based on oven treatment.

The concentrations of Cu, Cd and Pb, calculated on the basis of the ID formula, were corrected for contamination effects and moisture content. The individual uncertainty components associated to these corrections were propagated together with those of the isotope ratio measurement results and resulted in a combined uncertainty. The IDMS results achieved from the two series of samples mentioned above were in excellent agreement within measurement uncertainty, irrespective of the method used to correct for moisture content. A relative expanded uncertainty ($k = 2$) below 2% was achieved for all three certified contents.

As a result of the capability of ICP-IDMS to provide highly accurate and precise results, a number of papers deal with its application for certification purposes (e.g. 75,85,86). However, if the ultimate level of accuracy is not requested, the ID approach can be made considerably more practicable and less time-consuming by making certain simplifications (e.g. by using volumetric instead of gravimetric dilution). Even under these conditions, ID shows distinct advantages over more traditional calibration approaches as (i) matrix effects, signal drift and instrument instability are to a large extent automatically corrected for and (ii) once isotopic equilibration has been established, loss of analyte does not affect the analytical result.

6.5.2.2 ICP-IDMS combined with the application of matrix/trace separation procedures

Since with ID, loss of analyte does not affect the analytical result once isotopic equilibration has taken place, IDMS is especially useful when the sample preparation procedure includes a matrix/trace separation and/or preconcentration step.

Müller and Heumann reported on the use of ID for the determination of platinum group elements (PGEs) in environmental samples by ICP-MS [87]. It is well known that the determination of PGEs by ICP-MS is often hampered by spectral interferences, originating from matrix elements. The authors decided to develop a method with quadrupole-based ICP-MS in connection with a chromatographic analyte/matrix separation and the use of the ID technique for calibration. The method could be used for Pt, Pd, Ru and Ir. Rh is mono-isotopic and could thus not be determined by the ID technique. After addition of appropriate amounts of the isotopically enriched spikes (^{194}Pt , ^{108}Pd , ^{99}Ru and ^{191}Ir) to an accurately weighed amount of sample, the samples were decomposed by using aqua regia in a high pressure asher. Silicate-containing samples were not completely dissolved by aqua regia. Therefore an additional microwave-assisted decomposition step with addition of HF was introduced for these samples. After decomposition, the samples were diluted and isolation of the PGEs by anion-exchange chromatography took place. After introduction of the isotope-diluted sample on top of the column, all interfering elements were eluted with 2 M HNO_3 and subsequently the PGEs were collected in a small fraction by using concentrated HNO_3 . The recovery of this analytical step varied strongly from one separation to the next (e.g. Pd: 19–35%). Nevertheless, accurate results could be obtained by using the ID technique, as was demonstrated by analysis of CRMs. Finally, the method developed was used for the determination of PGE concentrations in surface soil, sampled at different distances from a highway. The authors concluded that relatively high concentrations of the PGEs are established close to the highway, while an exponential decrease is found with increasing distance from the highway.

McLaren *et al.* reported on the use of ID for the determination of trace metals in sea water by ICP-MS, after preconcentration of the elements of interest on silica-immobilised 8-hydroxyquinoline [88]. After addition of appropriate amounts of the enriched spikes, the seawater sample was heated overnight at 80°C to ensure isotopic equilibration prior to passage through the column. This step was reported to be essential for accurate Cr determination. Prior to the isotope ratio measurements, the column effluent containing the trace elements of interest was heated to dryness to remove HCl, and hence, to avoid Cl-based molecular ions causing spectral overlap, and the residue was redissolved using dilute HNO_3 . For all of the elements investigated (Cd, Cu, Cr, Ni, Pb and Zn), the ID results obtained for a Coastal Water Reference Material (CASS-1) were in good agreement with the corresponding reference values, which originated from a pooling of results of a number of techniques.

Of course, the advantage that ICP-IDMS requires neither 100% recovery nor absolute isolation of the elements of interest is not restricted to *chromatographic* separation. Balcaen *et al.* determined ultra-trace amounts of Fe in AgNO_3 solutions after precipitation of Ag as AgBr [89]. The determination of Fe in AgNO_3 is of interest when this material is used in the manufacturing of photographic materials, because varying Fe concentrations can change their sensitivity. Because of its excellent sensitivity and the high sample throughput, ICP-MS was the technique of choice. However, to assure that accurate results would be obtained, a few problems had to be tackled. To prevent strong signal suppression and irreversible memory effects, the Ag concentration introduced into the instrument had to be limited. This was done by precipitating Ag as a silver halide. To be sure that an incomplete recovery of the analyte did not affect the results, the ID technique was used for calibration. The enriched spike, ^{54}Fe (99.84% isotopic abundance), available as a metal, was dissolved and appropriately diluted. The molar concentration of ^{54}Fe in this spike solution was determined by means of

reverse IDMS using a standard solution of natural isotopic composition. For the determination of Fe in the AgNO_3 samples, an accurately weighed amount of the spike solution was added to each sample. After isotopic equilibration, HBr was added to precipitate Ag as AgBr and the analyte element was separated from the AgBr precipitate by passing through a $0.45\text{ }\mu\text{m}$ polytetrafluoroethylene (PTFE) syringe filter. The filtrates obtained in this way were further diluted. All measurements were carried out using a quadrupole-based ICP-mass spectrometer. Of course, an important prerequisite for obtaining accurate results using ID is the availability of two isotopes free from spectral interferences. The reliable determination of Fe by means of ICP-MS is traditionally hindered by spectral overlap of the analyte signals with those of Ar- and Ca-based molecular ions. In this work, it was shown that the spectral interferences hampering the accurate determination of Fe with ICP-MS can be overcome by using ion/molecule chemistry in a DRC with NH_3 as a reaction gas. The detection limit obtained with this method (13 ng g^{-1}) was much better than that obtained with the more traditional approach – sample dilution and quantification by means of external calibration (1200 ng g^{-1}). Therefore, the authors decided that ID-ICP-DRC-MS is the method of choice for the determination of ultra-traces of Fe in AgNO_3 solutions. Finally, three different AgNO_3 solutions were analysed by means of the method developed. Important differences in Fe concentration could be observed between the samples, which clearly demonstrated the necessity of quality control of AgNO_3 solutions.

Yoshinaga *et al.* used ICP-IDMS for the determination of mercury in biological and environmental samples [90]. The samples of interest, human hair and sediments, were acid-digested after addition of an ^{202}Hg spike. For the analysis of sediment samples, solvent extraction and back-extraction were a part of the sample pretreatment procedure. As persistent memory effects were originally observed to jeopardise accurate isotope ratio determination and hence, reliable analysis results, the sample introduction system was thoroughly rinsed with 1 M hydrobromic acid between measurements of different solutions. The ICP-IDMS results obtained for relevant CRMs were in excellent agreement with the corresponding certified or reference values and were reported to be better than those obtained using standard addition or external calibration in terms of accuracy and precision.

6.5.2.3 Radioanalytical applications of ICP-IDMS

Since with ID not only the elemental content, but also the concentration of *specific* isotopes can be determined, ICP-IDMS is also useful in radioanalytical chemistry, particularly because ICP-MS offers significantly lower limits of detection for the determination of long-lived radionuclides than the more traditional radiometric methods, while the sample throughput can be increased tremendously [91]. However, a problem that is difficult to solve for these applications, is the isobaric interference certain nuclides suffer from. Therefore, a chemical separation of interfering elements is often required before mass spectrometric analysis.

Perna *et al.* report on the use of ID ICP-MS for the simultaneous determination of fission products (lanthanides) and actinides (Pu, Np, U, Am and Cm), after on-line removal of interfering elements via ion chromatography [92]. The determination of the concentration and isotopic abundances of long-lived radionuclides is of great importance for, among other, environmental monitoring and nuclear waste management. In the majority of these investigations, it is necessary to obtain the complete inventory of fission products and

actinides. Therefore, the authors decided to develop a method where all these nuclides could be determined simultaneously. The separation of the actinide and lanthanide elements from the interfering elements was achieved using a Dionex CS5A mixed-bed column with a mixture of 100 mM oxalic acid – 190 mM lithium hydroxide and 2 M hydrochloric acid as the eluent. To convert all the elements into a single oxidation state, 0.2 M sodium nitrite was added to all the samples before chromatographic injection. In this way, it was possible to perform quantitative determination of the total element concentrations. The quantification of the lanthanides and actinides was based on ID analysis for Nd, Am, Pu, U and Cm (using ^{150}Nd , ^{243}Am , ^{244}Pu , ^{233}U and ^{248}Cm as spikes) and on the standard additions method for the other lanthanides and Np. Detection limits for the method proposed were found to be 0.25 ng ml^{-1} for the lanthanides and 0.45 ng ml^{-1} for the actinides. The analytical procedure was validated by the use of the reference material NIST SRM 4355 as well as by using other independent techniques, and in all cases, good agreement was established between the experimental and the reference values. To verify the applicability of the method for a real sample, an irradiated nuclear fuel sample was studied and the results obtained were in good agreement with those obtained using other procedures.

Two radionuclides out of the actinides series, plutonium and americium, were also the subject of a study by Boulyga *et al.* [93]. In this work, LA ICP-MS was combined with ID for the determination of ^{239}Pu , ^{240}Pu and ^{241}Am in mosses. Mosses are often used as bioindicators. They seem to be particularly suitable for investigating atmospheric contamination as they may provide a record of the history of atmospheric fallout. As already stated before, the occurrence of spectral interferences is a limiting factor for the isotopic measurement of long-lived radionuclides at low concentrations by means of ICP-MS. Therefore, the authors decided to separate Pu and Am from the matrix and subsequently electroplate the separated Pu and Am fractions on a stainless steel target. Due to the fact that the uranium concentration in soil samples is usually significantly higher than that of plutonium, a complete separation of Pu from U is not possible. Even after separation, the determination of $^{239}\text{Pu}^+$ is hindered by spectral overlap from $^{238}\text{U}^1\text{H}^+$, if ICP-MS is used in combination with liquid standard introduction. Therefore the authors decided to make use of LA as a sample introduction technique. In this way, the uranium hydride formation could be reduced, owing to the absence of any water or water vapour during sample ablation. To correct for analyte losses during the extensive sample preparation and for fractionation effects during sample ablation, the ID technique was used for calibration. ^{242}Pu and ^{243}Am were used as spikes. From the final analysis results, obtained for moss samples collected from a bog in the eastern Italian Alps, the authors concluded that the environment at the selected sites had been contaminated with artificial transuranium elements, probably due to the global fallout after nuclear weapons tests in the 1960s.

Since the Chernobyl accident, the behaviour of ^{137}Cs in the environment has been of great interest and has been studied in detail, because, owing to its solubility and mobility, this isotope can be used as a tracer for contamination studies. Moreno *et al.* used ICP-IDMS for the determination of Cs and its isotopic composition in nuclear samples [94]. On-line ion-exchange chromatography was applied to separate Cs from Ba, because the determination of radioactive Cs isotopes suffers from isobaric interferences from natural Ba isotopes. Three different chromatographic ion-exchange columns were compared and the authors concluded that the use of a CS5 column with 1 M HNO_3 as eluent lead to the best separation in terms of precision and accuracy. The determination of Cs in highly

active nuclear wastes, was performed by ID analysis using natural ^{133}Cs as spike. The proposed method was applied to determine the burn-up of irradiated spent fuel samples and the values obtained were in good agreement with those obtained by γ -spectrometry and with simulation calculations.

6.5.2.4 ICP-IDMS in connection with direct solid sampling

ICP-IDMS is most often carried out using pneumatic nebulisation for the introduction of aqueous solutions. However, application of IDMS is also possible for direct analysis of solid samples if homogeneous mixing of the sample and spike can be achieved in the solid phase. In this section, a number of selected applications of IDMS, using electrothermal vapourisation (ETV) and LA for sample introduction are reviewed.

Resano *et al.* reported on the application of ID as a calibration method for the direct determination of Hg in different materials by means of ETV-ICP-MS [95]. Due to its toxic properties, the determination of Hg at low levels in a variety of samples, is important. Because some Hg species are very volatile, there is a risk of analyte losses if an analysis method is chosen which requires an extensive sample pretreatment. Therefore, the authors decided to use a direct solid sampling method. One of their first considerations was to develop a reliable, but universal calibration procedure, which could be used regardless of the matrix composition. Traditionally, for ETV-ICP-MS measurements, calibration is accomplished by means of aqueous standards. To remove the solvent from these standard solutions, a drying step is included in the temperature program, while matrix effects can be reduced by a selective vaporisation of the matrix components during thermal pretreatment. However, for the determination of Hg, both the drying step and the pyrolysis step, often have to be omitted to prevent analyte losses. Therefore, it is necessary to use a calibration technique that does not require the introduction of high amounts of solvent into the furnace and that is capable of dealing with matrix effects. By using ID with a Hg spike in gaseous form for calibration, the authors fulfilled both requirements. In this approach, a constant flow of gaseous Hg, isotopically enriched in ^{200}Hg and emitted by a home-made permeation tube (Fig. 6.8), was directed through the graphite furnace by means of an Ar flow, where it underwent the temperature program, in order to create exactly the same conditions as for the sample. To test the robustness of the method, three different samples with different characteristics – BCR CRM 320 River sediment, IAEA-086 Hair and a real freshwater fish sample – were studied. For all samples, the same experimental conditions could be used and satisfactory results were obtained.

Next to ETV, also laser-assisted sample introduction has the advantage of direct solid sampling without extensive sample pretreatment. Although the technique has gained increasing popularity over the last decade, there are still some problems preventing LA-ICP-MS to become a more widely adopted routine method in analytical chemistry: the occurrence of fractionation and the difficulties sometimes associated with quantification. In general, the use of matrix-matched standards for calibration is recommended, but for many applications, no matrix-matched CRMs are available. Therefore, several research groups have used alternative quantification procedures. For the determination of Ag, Tl and Pb in platinum nanoclusters by means of LA-ICP-MS, Becker *et al.* investigated the possibilities of solution-based ID for calibration [97]. Hereby, the advantages of both the direct ablation of

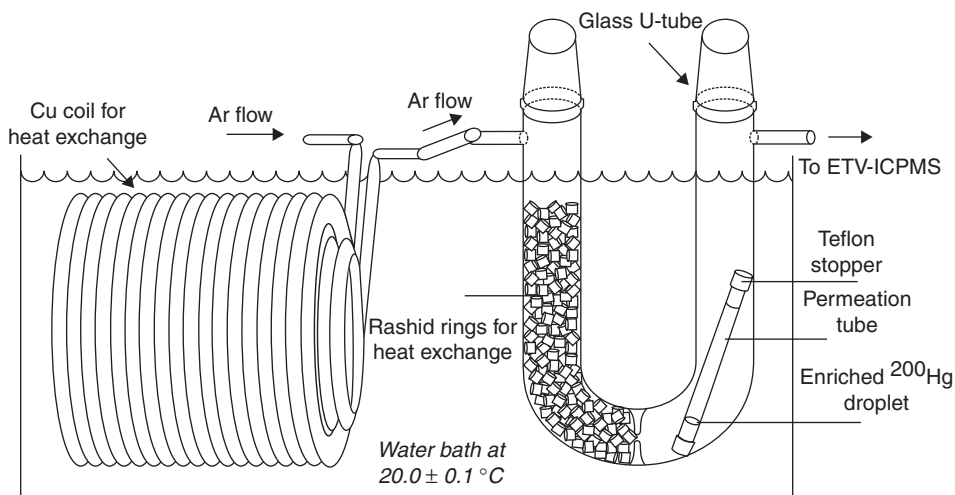


Figure 6.8 Environmental set-up for generation of the ^{200}Hg -enriched spike. Reproduced from [96].

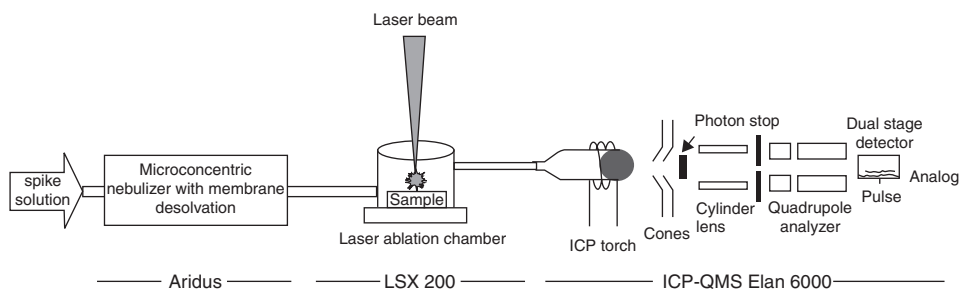


Figure 6.9 Experimental arrangement for on-line ID analysis in LA-ICP-MS. Reproduced from [97].

a solid sample by a laser beam and the calibration with aqueous standard solutions were combined. The standard solutions were nebulised with a microconcentric nebuliser with desolvator, which was coupled on-line with the LA chamber, as is shown in Fig. 6.9.

Differences in sensitivity between LA-ICP-MS and pneumatic nebulisation-ICP-MS were corrected for by using Cu as the internal standard element. For each experiment, first an isotopically enriched spike solution was nebulised. After 150s, the platinum nanocluster samples were ablated and after an additional 150s, 2% nitric acid was nebulised instead of the spike solution. The isotope ratios of interest, $^{204}\text{Pb}/^{206}\text{Pb}$, $^{107}\text{Ag}/^{109}\text{Ag}$, $^{203}\text{Tl}/^{205}\text{Tl}$ and $^{63}\text{Cu}/^{65}\text{Cu}$ were monitored during the entire experiment and elemental concentrations were calculated via the formula for ID analysis. The method developed was validated by the determination of Ag and Pb in a platinum standard reference material SRM NIST 681. Finally, the determination of Ag, Tl and Pb in a few milligram of platinum nanoclusters was accomplished and a good agreement was found between these results and those obtained via external calibration, using NIST SRM 681.

Also other research groups are working in the field of LA-ICP-IDMS. Tibi and Heumann reported on the use of ID as a universal calibration method for the accurate determination of trace elements in powder samples [98]. To investigate the figures of merit of this approach, the concentrations of Cr, Fe, Cu, Zn, Sr, Cd and Pb were determined in a set of CRMs (different organic and inorganic matrices) by means of LA-ICP-IDMS. The spike solutions were directly added to the powder samples and homogeneous suspensions were then obtained by shaking. After drying and homogenising with a Teflon pestle, the isotope diluted samples were pressed to pellets. Polyvinylalcohol powder was fixed on the back of the pellets to increase their mechanical stability. For the analysis of the pellets, a LINA-SparkTM-Atomizer was used in combination with a sector field ICP-MS. A medium mass resolution ($R = 4000$) was chosen to resolve the signals of the $^{40}\text{Ar}^{12}\text{C}^+$, $^{40}\text{Ar}^{16}\text{O}^+$ and $^{40}\text{Ar}^{16}\text{O}^1\text{H}^+$ ions, interfering with the determination of Cr and Fe at low mass resolution. The results obtained in this way were in agreement with the certified values for 28 out of the total of 32 trace element concentrations. Only for Fe and Cr in some reference materials, deviations from the certified values could be noticed. The authors explained these deviations by an inhomogeneous distribution of the corresponding spike element after drying of the isotope diluted sample. They concluded that IDMS is an extremely valuable supplement to the existing calibration procedures in LA-ICP-MS, although for a few elements, some unsolved problems remain. In other papers, the same research group applied the method for multi-element trace determinations in pure alkaline earth fluoride powders [99] and for the direct determination of halogens in powdered geological and environmental samples [100]. In both cases, the results obtained by means of LA-ICP-IDMS were in good agreement with reference values obtained by means of other techniques, or taken from the literature.

6.5.2.5 ICP-IDMS in elemental speciation

As the toxicity and mobility, and hence, the environmental and biomedical importance, of an element strongly depend on the chemical form in which it occurs, elemental speciation has become an important topic of research and efforts have been made to couple various chromatographic and electrophoretic separation methods to ICP-MS as a sensitive and element-specific multi-element detector. In particular, the coupling of high-performance liquid chromatography (HPLC) and ICP-MS, for which the liquid flow rates are fully compatible, has received considerable attention in the literature.

During an HPLC chromatographic separation process, not only the content of the different elemental species in the column effluent will vary as a function of time, but also that of other substances present at much higher concentration levels. This may lead to a variation in the degree of matrix-induced signal suppression or enhancement (matrix effects) as a function of time, such that the accuracy of analytical results obtained using external calibration may be jeopardised. In addition, as an entire HPLC separation process may take a considerable time, signal drift and instrumental instability may further adversely affect the results obtained by external calibration. In order to cope with these problems, Heumann *et al.* used ID as a calibration strategy in HPLC-ICP-MS [101]. Depending on the analytical problem at hand, they made use of either a species-specific spike or a species-unspecific spike. A schematic overview of both methods, is given in Fig. 6.10.

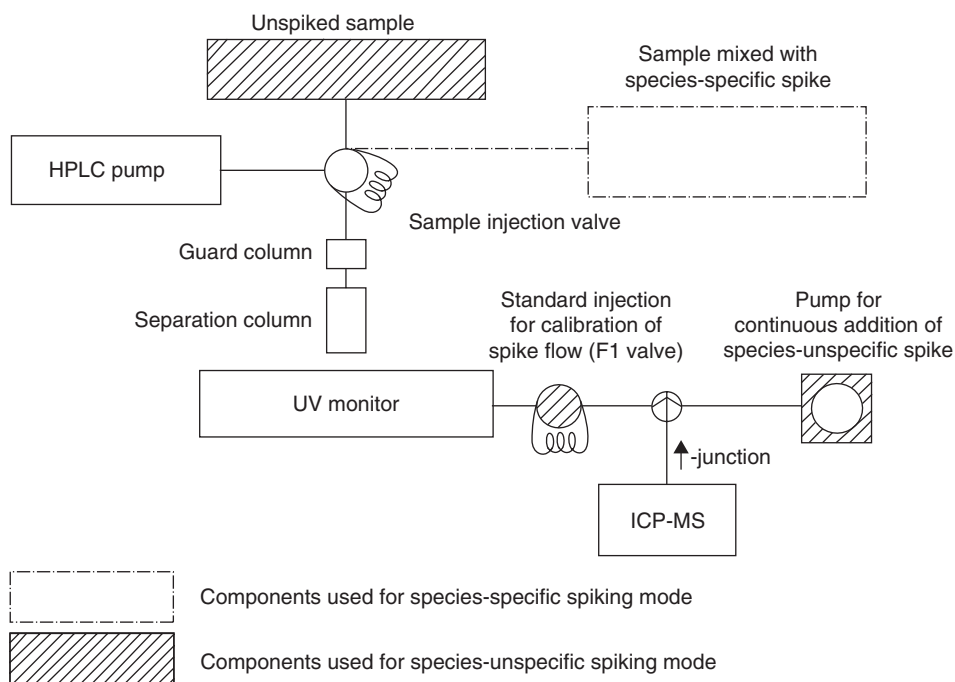


Figure 6.10 Schematic diagram of the combination of HPLC and ICP-MS for elemental speciation with species-specific or species-unspecific spiking for calibration by ID. Reproduced from [101].

For species-specific spiking, the composition and structure of the element species must be known and the spike must be available or synthesised in an isotopically labelled form of the element species to be determined. The spike has to be added to the sample before separation of the different species.

Reyes *et al.* used this approach for the determination of selenomethionine (SeMet) in selenium-enriched yeast by means of HPLC-ICP-MS [102]. Because no isotopically enriched SeMet standard is commercially available, a method was developed for the biosynthesis of ^{77}Se -labelled SeMet by yeast cultures. The yeast proteins were hydrolysed with protease XIV and the isotopically enriched SeMet was isolated by anion exchange chromatography. The isotopic composition and the concentration of the enriched SeMet spike were determined by HPLC-ICP-MS and reverse ID with a natural SeMet standard. Subsequently, the isotopically enriched SeMet solution was used for the ID analysis of SeMet in a yeast intercomparison material. To allow an accurate determination of SeMet in selenium-enriched yeast, it is important that the SeMet is quantitatively extracted without changing the identity and concentration of the original compounds. Therefore, the use of an adequate method of protein hydrolysis is critical and the authors compared several different procedures for the enzymatic extraction of SeMet from yeast samples. The results obtained after hydrolysis with Protease XIV at 37°C for 20 h, showed that between 59% and

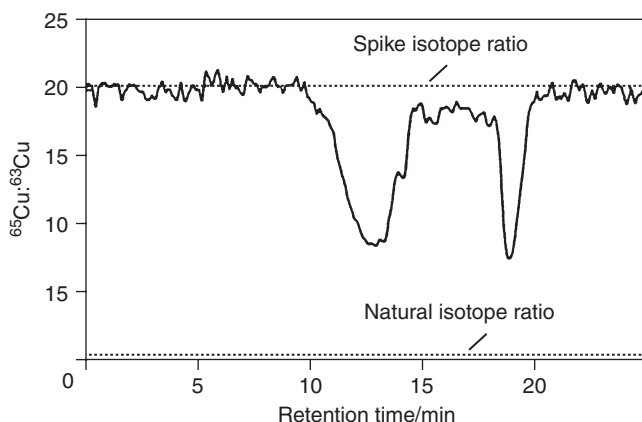


Figure 6.11 $^{65}\text{Cu}/^{63}\text{Cu}$ isotope ratio as a function of the retention time during analysis of a river water sample using a combination of HPLC, equipped with a size exclusion column (SEC), and ICP-MS, with species-unspecific spiking for ID purposes. Reproduced from [101].

65% of the total Se content was extracted as SeMet, which was in good agreement with the interlaboratory-mean value available from Ref. [103]. On the other hand, the use of an enzymatic hydrolysis during 1 min of ultrasonic extraction, resulted in lower SeMet extraction efficiencies. The authors concluded that, in spite of these lower extraction efficiencies, the potential of such fast extraction technique is great for speciation purposes and deserves further study in order to increase the SeMet extraction efficiencies. Of course, not only selenium, but also a lot of other elements have been the subject of investigation of HPLC-ICP-MS with species-specific ID, for example, Pb [104,105], Hg [106,107] and Sn [108].

For the quantification of more complex elemental species, synthesis of a species-specific spike is no longer feasible and hence, ID can only be carried out using a species-unspecific spike. In this approach, the species of interest are separated from one another using an appropriate chromatographic method and a continuous flow of enriched spike is mixed with the column effluent prior to introduction into the ICP-mass spectrometer. Since, owing to the high temperature of the ICP, the elemental response of ICP-MS is to a large extent independent of the chemical form of the element under investigation, the compound used in the preparation of this spike is of no importance as long as its isotopic composition is sufficiently different from the natural one. As is shown in Fig. 6.11 for Cu, with this approach, the isotope ratio of interest is monitored as a function of time. When no copper-containing species are eluted from the column, the measured ratio is that of the enriched spike. Cu-containing fractions of the eluent, however, shift the isotope ratio of interest in the direction of the natural isotope ratio, as can be seen from the two 'negative' peaks in the chromatogram. Finally, the original chromatogram, showing the variation of the Cu isotope ratio as a function of time, can be converted into a chromatogram, which directly displays the amount of Cu present in the effluent as a function of time. This approach is of major interest for the quantification of metal complexes with proteins in body fluids or with humic substances in waters of different origin [101].

Rottmann and Heumann used ID with a species-unspecific spike to study heavy metal interactions with dissolved organic materials in natural aquatic systems [109]. For this study, they coupled an HPLC system, equipped with an SEC column on-line, to an ultraviolet (UV) detector and an ICP-mass spectrometer. During the experiment, a spike solution was continuously pumped into a Y-junction, so that it is thoroughly mixed with the eluent flow containing the separated species. Simultaneous registration of the presence of UV-absorbing organic matter and the heavy metals in the column effluent permitted conclusions to be drawn concerning the interactions between the metals under investigation and humic substances, which form the major part of dissolved organic matter in waters of different origin. In addition, the ID approach allowed accurate quantitative information to be obtained.

For volatile species or species that can be derivatised into a volatile form, (capillary) gas chromatography ICP-MS is a powerful speciation technique. In comparison with HPLC-ICP-MS, GC-ICP-MS offers a higher resolving power, 100% introduction efficiency, allows a more stable plasma, gives rise to fewer spectral interferences as a result of the plasma being dry and leads to less sampling cone and skimmer wear. Of course, on the other hand, the application range is limited to thermally stable and volatile species and species that can be derivatised into a sufficiently volatile form. In speciation work carried out using CGC-ICP-MS, ID can be used for calibration, and similar to the situation for HPLC-ICP-MS, either a species-specific spike or a species-unspecific spike can be used.

In a recent article, Poperechna and Heumann reported on the use of species-specific ID GC-ICP-MS for the simultaneous multi-species determination of trimethyllead (Me_3Pb), monomethylmercury (MeHg) and three butyltin compounds (mono-, di- and tributyltin – MBT, DBT, TBT) in biological samples [110]. Taking into account that these compounds are highly toxic and that they can accumulate in marine animals, the development of an accurate, sensitive and simultaneous analysis method for these species is of prime importance for the quality assurance of seafood. Based on the results of previous work in this field [108,111], GC-ICP-IDMS was found to be the method of choice. Most of the isotopically-labelled spike compounds, necessary for the ID step, were commercially available (MeHg , enriched in ^{202}Hg and a mixture of the three butyltin compounds, all enriched in ^{119}Sn). Only the trimethyllead spike was not available and had to be synthesised by reaction of lead bromide with methyl-lithium (to give tetramethyllead) and subsequent addition of elementary iodine (to form Me_3PbI). The method was validated by the analysis of three biological reference materials and a sediment reference material. After careful investigation, the authors concluded that no species transformation was found under the experimental conditions used in this work and that the GC-ICP-IDMS results agreed very well with the certified values. Finally, the method developed was also applied to seafood samples, purchased from a supermarket. Interesting conclusions from this work are that the highest methylmercury contents were found in tuna fish and shark samples. For butylated tin compounds on the other hand, the highest concentrations were found in mussels, which often live in harbour areas, where contamination with butyltin compounds is more likely as TBT is/was used as an active component in paints that prevent the growth of algae and mussels on hulls of ships and in docks.

Also Rodríguez-González *et al.* developed a method for speciation analysis of butyltin compounds by GC-ICP-MS with ID for calibration [112]. They paid special attention to the possibility of species rearrangement reactions throughout the speciation procedure. By using a triple spike approach, the authors were able to calculate accurately the three butyltin concentrations plus the values of six possible interconversion yields (Fig. 6.12).

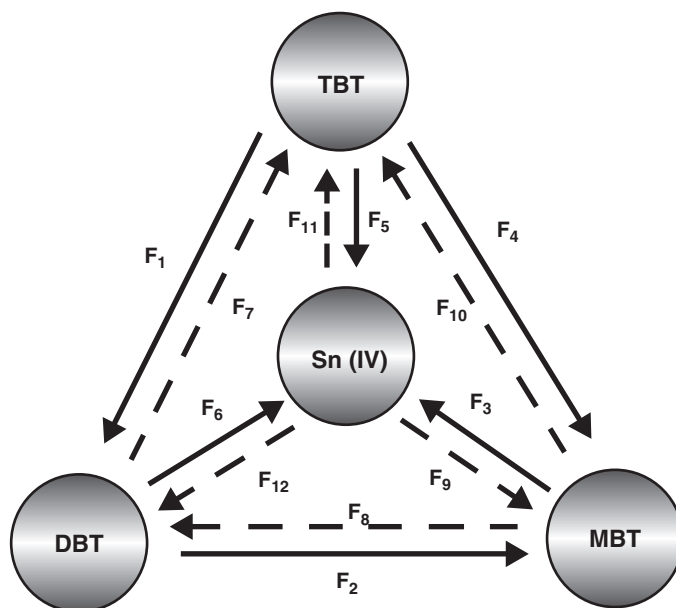


Figure 6.12 Possible interconversion pathways of the butyltin compounds. Reproduced from [112].

For the development of the triple spike approach, a spike solution containing all three butyltin species, each of them isotopically labelled with a different isotope, was synthesised and the mathematical equations required for the application of this powerful tool were developed. To evaluate the method developed, determination of butyltin compounds in the certified reference material CRM-477, was carried out after microwave-assisted extraction under different conditions. The corrected concentrations and the factors describing possible rearrangement reactions were calculated for increasing heating times from 1 to 16 min at 150 W. Only at 16 min of heating, the decomposition of DBT into MBT was clearly observed, whereas direct degradation of TBT to MBT, as well as butylation reactions, were found to be negligible under all conditions. The good agreement between the experimental values and the corresponding certified values, confirmed that the proposed triple spike methodology is able to correct for any interconversion reaction that may occur during the speciation analysis procedure of tin.

An example of the application of species-unspecific ID analysis for mercury speciation was given by Gelaude *et al.* [96]. In this work, a fast and sensitive method for the determination of methylmercury and inorganic mercury by using solid sampling ETV-ICP-MS was developed. The method is based on the fact that by means of ETV, vaporisation of these mercury species can be separated from one another in time (Fig. 6.13). For the quantification of the two peaks, different calibration approaches were investigated. Due to the fact that the inorganic mercury was vaporised simultaneously with most of the organic matrix, and consequently, the signal for the inorganic mercury was heavily suppressed, while the vaporisation of MeHg was disturbed in the presence of H_2O , the use of ID with a gaseous Hg phase was considered to be the most promising calibration approach.

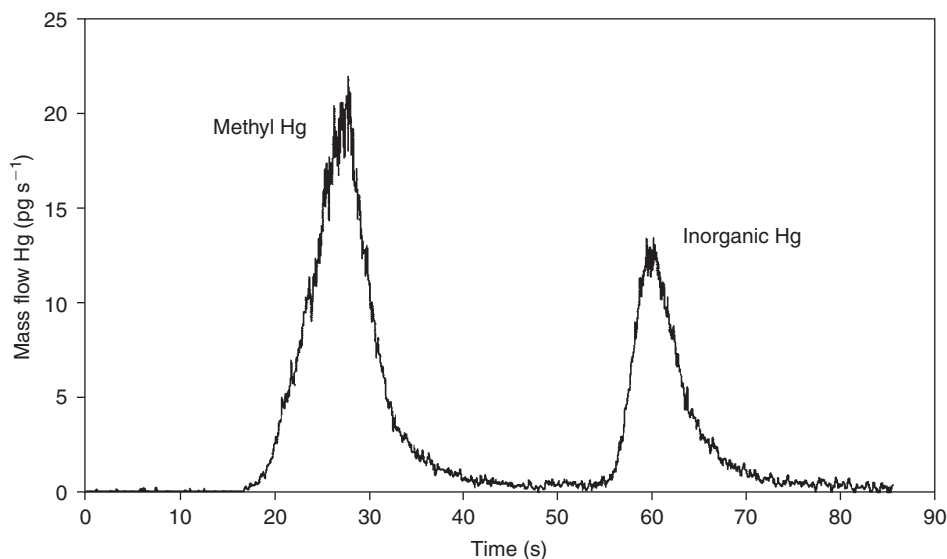


Figure 6.13 Separation of organic and inorganic mercury by means of ETV. Reproduced from [96].

The quantification of both species was carried out by mixing a stable flow of argon loaded with gaseous Hg, isotopically enriched in ^{200}Hg , which was generated by a homemade permeation tube. Moreover, by adapting the temperature of the permeation tube, the spike/sample ratio could be optimised, so that the method can also be applied to samples with a large diversity in mercury content. To assess the figures of merit of this approach, CRMs with different inorganic mercury and methylmercury contents were analysed and the results obtained were in excellent agreement with the certified values.

6.5.3 Tracer studies

6.5.3.1 Tracer studies for investigating (human) metabolism and element toxicity

Radioisotopes have been and still are frequently used as ‘tracers’ for *in vivo* diagnostic investigation and for obtaining a better insight into biochemical processes occurring on intake of either essential or toxic elements. In cases where no radioisotope of appropriate half-life exists and for safety reasons (especially when pregnant women or young children are the subject of investigation), stable tracers with an isotopic composition sufficiently different from the natural one can be used. In these instances, the change(s) in (a) selected isotope ratio(s) has/have to be monitored on administration of a tracer or spike by means of a mass spectrometric detection device. The tracers involved may be administered to the subject via the alimentary canal, the respiratory system, the integument or by injection. Traditionally, for the ‘heavier’ elements, these isotope ratio measurements were carried out

by TIMS. This, however, requires the analyte to be isolated from the matrix, which often leads to labour-intensive and time-consuming sample preparation. In addition, TIMS instrumentation is not widespread. Nutritional, toxicological and pharmacological studies have therefore benefited significantly from the introduction of ICP-MS. A number of publications have presented an overview of the use of ICP-MS for biomedical research and/or reported on the use of stable isotope tracers in this domain [113–115].

Such stable isotopic tracer experiments can be carried out in several ways as use can be made of, for example, a mass balance, single and dual tracer administration, and continuous administration. Although a considerable amount of literature on this subject is available and a variety of elements have already been studied in clinical samples (e.g. Mg, Fe, Ni, Cu, Zn, Se and U), only a limited number of selected applications are discussed here to give the reader some insight into the potential of these tracer experiments.

Karpas *et al.* evaluated the fractional absorption of U and its behaviour after gastrointestinal absorption by measuring both the concentration and the isotopic composition of U in urine after oral administration of a small dose of isotopically depleted uranium (DU) (with a ^{235}U isotopic abundance of 0.245%) to five individuals [116]. As the daily intake of U is significantly higher than often assumed, on average in the $\mu\text{g day}^{-1}$ range and sometimes substantially higher, an evaluation of the uptake of U indeed deserves considerable attention. The high sensitivity of the ICP-MS instrumentation used allowed analysis of each individual voiding, hence, detailed biokinetic studies could be carried out. The results obtained for both the U concentration and its isotopic composition indicated a fast excretion of U in the urine. Although important between subject differences could be established, the average uptake fraction obtained (0.1–0.5%) is in agreement with that observed in other studies. Isotopic analysis of the urine samples indicated a rapid decrease in the ^{235}U isotopic abundance, reaching a minimum value approaching that of the ingested U within a few hours. Thereafter, the ^{235}U isotopic abundance gradually increased until the natural value was obtained again. Taking into account this isotopic behaviour and the gastrointestinal absorption efficiency, it was possible to evaluate the accuracy of existing models for the uptake of U. On the basis of this evaluation, it could be concluded that the mechanism of U absorption and excretion is rather complex and involves exchange of ingested U and U stored in different body compartments.

Rodriguez-Cea *et al.* demonstrated that the use of a stable isotopic tracer does not only provide information on the *total* absorption of a particular element, but also on element redistribution over various body compartments and the governing mechanisms [117]. In their experiment, seven European eels (*Anguilla anguilla*) were exposed to $100 \mu\text{g l}^{-1}$ of ^{111}Cd during 3 weeks. After exposure, liver and kidney tissue of these animals was dissolved and analysed for total content and isotopic composition of the Cd present. Blank values were obtained using tissues from another group of seven eels, not exposed to ^{111}Cd . Based on the measurement data obtained, the authors were able to discriminate between Cd previously present in liver and kidney tissue and 'new' cadmium (*de novo* cadmium) that was incorporated during the 3 weeks of exposure. The results obtained indicated redistribution of Cd, as part of the original Cd present in the liver was relocated to the kidney for 'storage'. Although the mechanism by which they operate is not fully understood yet, it is known that metallothioneins (MT) – small metal-binding proteins, rich in sulphur-containing amino acids and synthesised in the liver and kidney – play an important role in metal ion transport and detoxification processes. The cytosolic fraction of liver and kidney

tissues was therefore isolated using an approach in which ultracentrifugation played the central role, the MT-containing fraction separated using SEC and subsequently, subjected to HPLC (anion exchange chromatography) – ICP-MS, which provided further quantitative information on their role in the Cd redistribution.

From these examples, it is clear that absorption or bioavailability of an element can be determined by measuring the change in its isotopic composition in relevant body fluids or tissues after orally administering an enriched isotope (a single tracer) to subjects. In order to obtain meaningful results with this approach, often some assumptions have to be made concerning the distribution of the absorbed element over various body compartments. As there is often considerable dispute or lack of information concerning this matter, a more reliable approach for these studies is the ‘double’ or ‘dual’ tracer method. In this approach, one tracer is administered orally and another intravenously, and therefore redistribution in the body is automatically compensated for and more accurate results can be obtained.

Whittaker *et al.* used the dual tracer approach to determine the absorption of Fe in normal women [118]. The results reported are part of a study investigating the necessity of iron supplements for pregnant women. An evaluation of this necessity is of importance, not only because an increased dose of iron may give origin to gastrointestinal upsets and may affect the uptake of other essential elements, but also because general prescription presents a financial burden that cannot be neglected. After having fasted overnight, a basal blood sample was taken from all subjects (non-pregnant, normal, healthy women). A 200 μg dose of $^{57}\text{FeSO}_4$ was then administered intravenously, followed by an oral dose consisting of 5 mg $^{54}\text{FeSO}_4$. In order to study the uptake (rate) of Fe in human serum, blood samples were taken at various time intervals after administration and the $^{54}\text{Fe}/^{56}\text{Fe}$ and $^{57}\text{Fe}/^{56}\text{Fe}$ isotope ratios in the serum fraction were determined by means of ICP-MS, using ETV for sample introduction. As can be seen from Fig. 6.14, immediately after administration of the dual tracer, a significant increase in the $^{57}\text{Fe}/^{56}\text{Fe}$ isotope ratio in the serum was

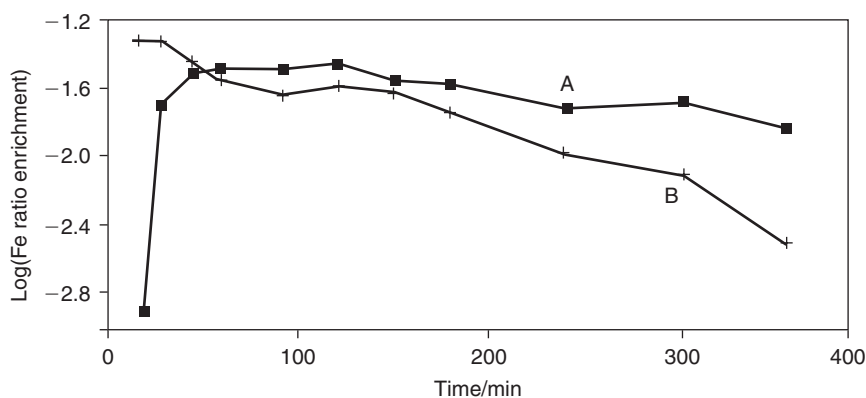


Figure 6.14 Time course of Fe isotope ratio enrichment in serum after (a) oral ^{54}Fe and (b) intravenous ^{57}Fe administration to a non-pregnant woman. The Fe isotope ratio enrichment is defined as $\log[(^{54}\text{Fe}/^{56}\text{Fe})_t - ^{54}\text{Fe}/^{56}\text{Fe}]_0$ or $^{57}\text{Fe}/^{56}\text{Fe}_t - ^{57}\text{Fe}/^{56}\text{Fe}_0$. Reproduced from [118].

observed; thereafter the $^{57}\text{Fe}/^{56}\text{Fe}$ ratio decreases gradually as a result of Fe excretion and redistribution over different body compartments. As a result of ^{54}Fe having been administered orally, the $^{54}\text{Fe}/^{56}\text{Fe}$ ratio shows a delayed but rapid increase and the ratio of interest was observed to reach a maximum after approximately 1 h. A slow decrease in the $^{54}\text{Fe}/^{56}\text{Fe}$ ratio was then observed. Measurement of both isotope ratios allowed calculation of the amount of oral Fe absorption.

It should be noted that Whittaker *et al.* performed these experiments in 1989 with a traditional quadrupole-based ICP-mass spectrometer. ETV was used for sample introduction to avoid bias of results due to the occurrence of Ar-based molecular ions (ArN^+ , ArO^+ and ArOH^+), which gave rise to important spectral overlap when using pneumatic nebulisation. However, over the last 15 years, new types of ICP-MS instruments have been developed, characterised by improved measurement capabilities and performance. For example, sector field ICP-MS and quadrupole-based ICP-mass spectrometers equipped with a reaction/collision cell have significantly improved interference removal capabilities and MC-ICP-MS provides isotope ratio precisions similar to those of TIMS. All these techniques have been applied for the determination of Fe isotope ratios in different sample types. Ingle *et al.* used single-collector sector field ICP-MS for the determination of iron isotope ratios in faeces [119]. They found good agreement between ICP-MS and TIMS results and precisions in the 0.5–1.0% RSD range were obtained. Vanhaecke *et al.* investigated the possibilities of reaction cell technology for the interference-free determination of Fe in human serum [120]. They concluded that by using an appropriate reaction gas (NH_3 or CO) and after careful optimisation of some instrumental parameters, most argon-based (and even some calcium-based) interferences can be effectively removed in a reaction cell, enabling accurate $^{54}\text{Fe}/^{56}\text{Fe}$ determination. The precisions obtained for isotope ratio measurements were similar to those reported for sector field ICP-MS. Although these single-collector instruments can produce valuable data for the estimation of iron absorption, it is clear that MC-ICP-MS is even a more useful tool. Indeed, the amount of enriched tracer(s) required for tracer experiments, is determined by several factors. A prerequisite for obtaining meaningful results is a significant difference between the isotope ratios of interest before and after administration of the tracer(s). Hence, the amount of tracer required is determined by the amount of element present in the body compartment of interest, the amount of absorption, the normal daily intake and the measurement precision, since the difference between the isotope ratio before and after administration should be more than three times the standard deviation of the basal isotope ratio. Furthermore, the price of the stable tracers has also to be taken into account. It is here that MC brings an important advantage, because the very high precision allows the use of small doses of enriched stable isotope to be administered. Additionally, nowadays, also MC instruments can be operated at higher mass resolution (Fig. 6.15), such that not only very precise, but also very accurate results can be obtained. At present, isotope ratios of Fe have already been determined by MC-ICP-MS [30,121]. The isotope ratio precision attainable was even sufficient to reveal natural isotopic variation in Fe between individuals and between sexes [122].

Comparable tracer studies have also been carried out for other metals and metalloids of biomedical/nutritional importance. Unfortunately, as is the case for Fe, also for Mg, Ca, Ni, Cu, Zn, Se and Mo accurate determination of the isotope ratios of interest is often hampered by spectral interferences. Nevertheless, several authors have reported on the use of quadrupole ICP-MS for the isotope ratio determination of these elements, after an

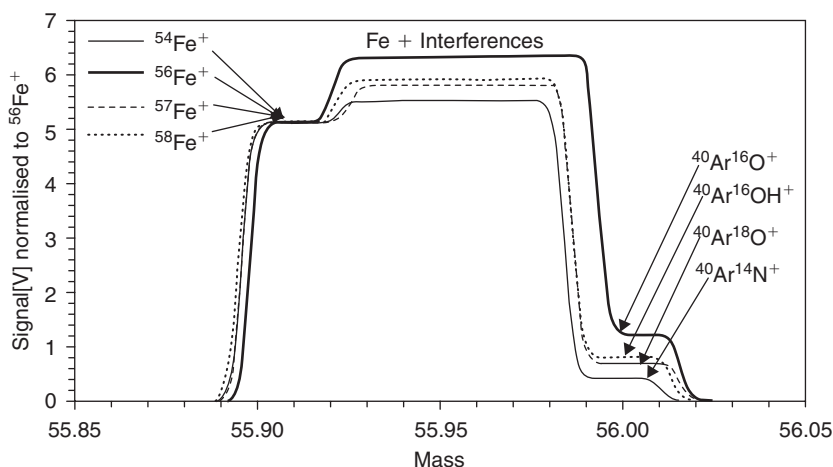


Figure 6.15 Mass scan performed with a MC-ICP-MS instrument operated at higher mass resolution, showing all Fe isotopes and their respective molecular interferences. All Fe signals were normalised to the signal of ^{56}Fe . Since the Fe isotopes have a lower mass, they enter the detector first in a scan and form the left plateau. The centre plateau consists of contributions from both the polyatomic interferences and the Fe isotopes. The right plateau is formed by the polyatomic ions only. Fe isotope ratios can be measured interference-free on the left plateau. Reproduced from [30].

appropriate sample preparation step or by using an alternative sample introduction system [e.g. 123–125]. More recently, a small number of articles on the use of single-collector and MC sector field ICP-MS for isotope ratio determinations in nutritional/biological studies have been published (e.g. [126–129]). De Wannemacker *et al.* developed a method for the quantification of Mg^{2+} transport across the intestine of tilapia fish [127]. Because the Mg^{2+} ion is involved in numerous biochemical processes, insight into the uptake and partitioning mechanisms of Mg is important. A series of experiments was designed to assess bidirectional transepithelial Mg^{2+} fluxes across the proximal intestine of tilapia fish. Two solutions (representing the lumen content and body fluid, respectively) were separated by a sheet of intestinal tissue. Both solutions contained the same concentration of Mg. In solution 1, the Mg was enriched in ^{24}Mg , while in solution 2 the Mg was enriched in ^{26}Mg . By measuring the $^{26}\text{Mg}/^{24}\text{Mg}$ isotope ratio as a function of time for both solutions, the Mg^{2+} fluxes could be determined. In spite of the numerous possibilities for spectral overlap, accurate determination of Mg isotope ratios was possible by using a sector field ICP-mass spectrometer operated at a higher mass resolution ($R = 3000$). In a study by Ingle *et al.*, MC-ICP-MS was used for the determination of total zinc and zinc isotope ratios in nitric acid digests of freeze-dried faecal material, available from a stable isotope tracer experiment [128]. In this study, the absorption of zinc from three different diet types, ‘meat’, ‘poultry and fish’ and ‘vegetarian’, was investigated using the faecal monitoring technique with ^{70}Zn as the tracer. For this study, the required within-sample precision for a ratio involving the tracer isotope was 0.4% RSD. First, the single-collector acquisition mode was tested, but the within-sample precision (typically 0.6–1.5% RSD) was insufficient for the

requirements of the study. Therefore, MC instrumentation had to be used. To separate the signal for $^{70}\text{Zn}^+$ from that for the interfering molecular ion $^{40}\text{Ar}^{14}\text{N}^{16}\text{O}^+$, the axial detector channel was operated at an increased mass resolution ($R > 2350$), while the other isotopes of interest were measured at low mass resolution using Faraday collectors. Typical within-sample precisions for acid digested faecal samples were 0.1–0.3% RSD for all ratios considered, meeting the requirements of this human study. Moreover, a good agreement was found between the ICP-MS results for acid digested solutions of the faecal samples and the results of TIMS analysis of fully cleaned up samples (from the same set). Preliminary results from the nutritional study indicated that there is no significant difference between the apparent zinc absorption from meat, poultry and vegetarian diets.

Finally, tracer studies can also be applied to investigate chemical reactions and physical processes. Ketterer and Fiorentino, for example, have used a stable tracer experiment to determine the Tl(III/I) electron self-exchange rate in aqueous HClO_4 [130]. Tl(III) ions were obtained from Tl_2O_3 enriched in ^{203}Tl (abundance ~36% in comparison with a natural abundance of 29.52%). Tl(I) was prepared from Tl reagents of natural isotopic composition. Subsequently, labelled and unlabelled reactants were mixed and stepwise separation was carried out by means of selective precipitation of Tl(I) as TlBr . In both the TlBr precipitate and the Tl(III) solution phase, the isotopic composition of Tl was determined by means of ICP-MS. The electron self-exchange rate constant, calculated on the basis of the results obtained, compared favourably with a previously published value obtained using radiolabelled (^{204}Tl) reactants.

6.5.4 Determination of natural isotope ratios

6.5.4.1 Geochronology and other applications in the geosciences

Since several decades, isotopic analysis is playing a crucial role in the geosciences: GSMS is used for isotopic analysis of the light elements H, C, N, O and S, while isotopic variations in other elements can be studied via TIMS. Traditionally, only the least demanding applications could be tackled using ICP-MS. Of the light elements typically studied using GSMS, only S has also become accessible using ICP-MS, as the spectral interferences the S isotopes suffer from (e.g. overlap of the signals of $^{32}\text{S}^+$ and $^{16}\text{O}_2^+$ at unit mass resolution) can be overcome by using a collision/reaction cell [131] or high mass resolution [20]. At present however, MC-ICP-MS is replacing TIMS for an increasing number of applications [32] and has even given new impetus to the geosciences by offering possibilities that were previously unheard of. Next to the higher sample throughput, also the high ionisation efficiency of the ICP is considered as an important advantage as some of the target elements are characterised by a relatively high IE and thus can only be analysed with TIMS via the production of negative molecular ions. Currently, articles reporting on the use of MC-ICP-MS for unravelling geological problems are published in high abundance and they provide new insights into topics as the formation of the solar system, planet accretion, climate changes over a geological timescale, volcanism and ore formation to cite only a few. Most of the articles on the use of MC-ICP-MS in geo- and cosmochemistry, however, cover highly specialised topics and were hence assessed to be beyond the scope of this chapter. Only some typical examples with a content accessible to the average reader were selected to shed some

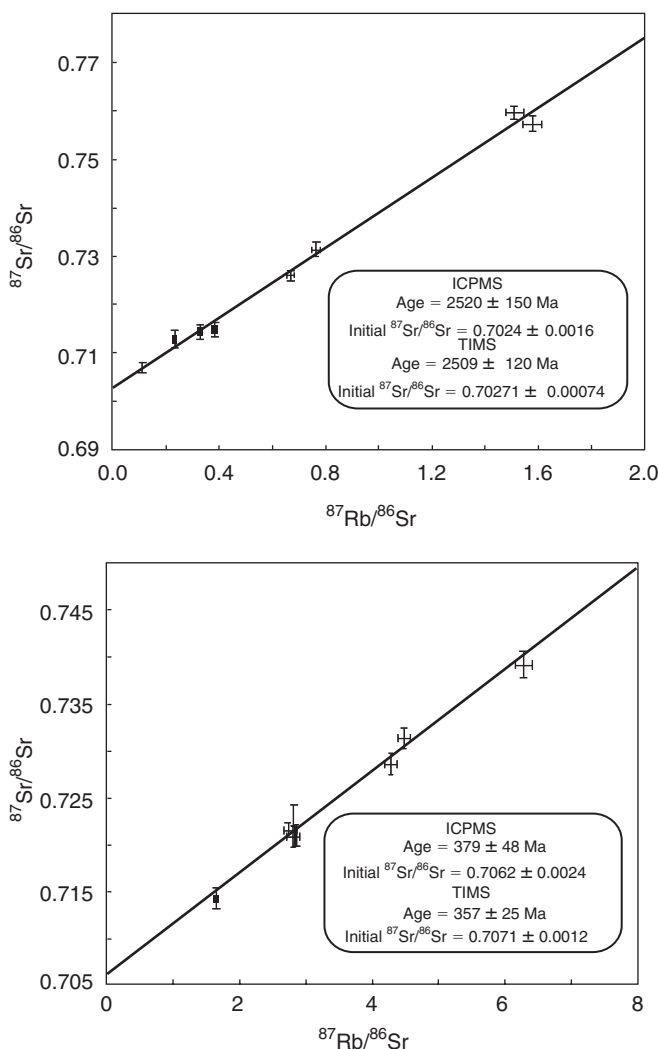


Figure 6.16 Isochrons obtained on the basis of $^{87}\text{Sr}/^{86}\text{Sr}$ isotope ratios determined using single-collector sector field ICP-MS. Ages and initial $^{87}\text{Sr}/^{86}\text{Sr}$ isotope ratios are in good agreement with the corresponding results obtained using TIMS. Reproduced from [132].

light on the possibilities of ICP-MS in this context. For a deeper insight, the reader is referred to the specialised literature. Attention will also be given to applications carried out using quadrupole-based or sector field instruments equipped with a single detector.

Elements such as Sr, Nd, Hf, Os and Pb show variations in their isotopic composition as a result of natural radioactivity. ^{87}Sr , for example, is produced as a result of the β^- -decay of the naturally occurring and long-lived ($T_{1/2} \approx 50$ billion years) radionuclide ^{87}Rb into ^{87}Sr . As a result, determination of the Rb and Sr contents and of the $^{87}\text{Sr}/^{86}\text{Sr}$ isotope ratio of whole rock samples or isolated minerals of a rock formation can be used for dating

purposes [4], at least if the system has always been closed with respect to Rb and Sr mobility. For most of these applications, a very high isotope ratio precision is required, such that this application range was almost exclusively the domain of TIMS. Nevertheless, Vanhaecke *et al.* demonstrated that in less demanding cases, also single-collector sector field ICP-MS [132] and even quadrupole-based ICP-MS [133] may provide accurate results. For the two rock formations – Nilgiri Enderbites, India (c. 2500 million years old) and Regensburg Forest Granites, Germany (c. 360 million years old) – dated, the results were in good agreement with the corresponding TIMS results (Fig. 6.16). In contrast to TIMS, where the analyte (in this case Sr) has to be isolated as purely as possible from all concomitant matrix components, separation of Sr from Rb (accomplished using cation exchange chromatography) sufficed in this context.

Even with sector field ICP-MS, this chemical separation is required since the maximum mass resolution offered by present-day instrumentation ($R = 10\,000$) is by far insufficient to resolve the spectral overlap of the signals of $^{87}\text{Sr}^+$ and $^{87}\text{Rb}^+$ (minimum mass resolution required: 300.000). Self-evidently, the less stringent sample preparation and the more straightforward sample introduction lead to a much higher sample throughput with ICP-MS. Moreover, Moens *et al.* [25] demonstrated that by using CH_3F as a reaction gas in a DRC, chemical separation of Sr and Rb prior to the measurement could be avoided. Under these conditions, Sr^+ ions are (partly) converted into SrF^+ ions, while Rb^+ ions show no reactivity towards CH_3F , such that the $^{87}\text{Sr}/^{86}\text{Sr}$ isotope ratio can be measured interference-free using the corresponding SrF^+ signals (Fig. 6.17). Ne was admixed with CH_3F to improve the isotope ratio precision by means of collisional damping.

The only drawback of this approach is that matrix-matched isotopic standards had to be used for mass discrimination correction. In a later study, Vanhaecke *et al.* [134] demonstrated, that, in general, the mass discrimination is more affected by the matrix when using a pressurised DRC. For more demanding cases of Rb–Sr dating, MC-ICP-MS can be applied. Willigers *et al.* [135] compared MC-ICP-MS and TIMS for Rb–Sr dating of biotites from the

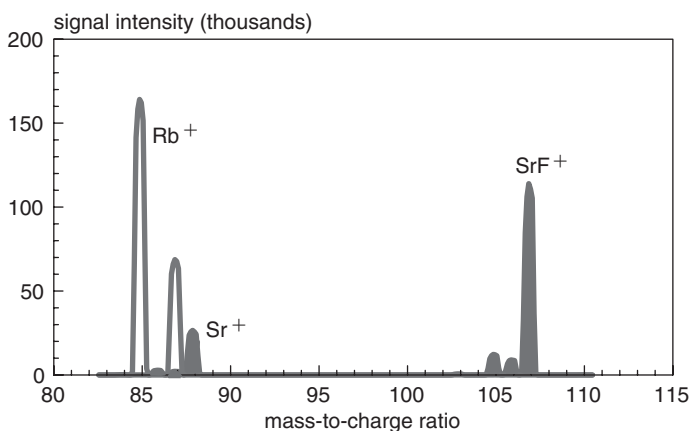


Figure 6.17 Mass spectrum obtained via quadrupole-based ICP-MS. By using CH_3F as a reaction gas in a DRC, Sr^+ ions are converted into SrF^+ ions, enabling interference-free $^{87}\text{Sr}/^{86}\text{Sr}$ isotope ratio determination. Reproduced from [25].

Oslo rift (Norway) and concluded that MC-ICP-MS was superior for this application, as the spread in the results obtained was three times smaller than that in the corresponding TIMS data. Therefore, they state that MC-ICP-MS can reveal geological information obscured by TIMS Rb–Sr age determination. Also in U–Th dating studies, MC-ICP-MS was reported to provide better precision than TIMS [136].

Next to Rb–Sr dating, several other geochronometers exist and their use is based on the same or similar general principles (e.g., Sm–Nd, Lu–Hf, Re–Os, U, Th–Pb and U-series dating [4]). Barfod *et al.* demonstrated that MC-ICP-MS permits Lu–Hf dating of sedimentary formations [137]. Selby and Creaser used LA-MC-ICP-MS for Re–Os isotopic analysis of molybdenite [138]. As a result of its high IE, isotopic analysis of Os using TIMS can only be accomplished by using the negative ion technique. Halliday used the ^{182}Hf – ^{182}W system to investigate the origin of the moon and estimate its age [139]. On the basis of isotopic analysis of lunar samples, they concluded that the moon is probably formed as a result of a collision between the young Earth and another object of similar size. On the basis of the results obtained via MC-ICP-MS, this interplanetary ‘big bang’ is estimated to have occurred approximately 50 million years after the genesis of our solar system. The Nb–Zr system (^{92}Nb decays into ^{92}Zr with a half-life of 3.6 million years) can be used for obtaining information on the timing of early solar system processes [140].

The use of LA as a means of sample introduction for MC-ICP-MS is currently receiving ample attention as it allows a substantial decrease in terms of sample preparation and consumption and/or provides the opportunity of providing spatially resolved isotopic information. Willigers *et al.*, for example, compared LA-MC-ICP-MS and TIMS for Pb–Pb dating of apatite and monazite from metamorphic rocks from West Greenland and concluded that while being vastly more rapid, LA-MC-ICP-MS provided ages identical to those obtained via conventional sample processing and subsequent TIMS analysis [141]. Nevertheless, it is necessary to point out that results obtained via LA-MC-ICP-MS have to be critically assessed and validated. Stirling *et al.*, for example, demonstrated that when using a frequency-quadrupled 266 nm Nd:YAG laser, data obtained in ^{238}U – ^{234}U – ^{230}Th dating of zircon and opal samples depended on the type of carrier gas used [142]. While with Ar, considerable elemental fractionation, affecting the ages obtained, was observed, the use of He as a carrier gas permitted accurate results to be obtained. If the necessary precautions are taken however, LA-MC-ICP-MS offers undeniable advantages compared to other approaches. Corals are late Pleistocene carbonates that have archived important information concerning sea-level changes and continental climate changes and are therefore often studied in palaeoclimate studies. Of course, for drawing meaningful conclusions, reliable dating of the corals is necessary. Dating of corals is possible using α -spectrometry, TIMS or MC-ICP-MS after digestion and further sample processing. However, only the combination of LA with MC-ICP-MS provides the high sample throughput required for *rapid* age determination and screening of uncharacterised coral samples. While the highly abundant ^{238}U was monitored using a Faraday collector, ion counters were used for the detection of the low-abundant ^{234}U , ^{235}U , ^{230}Th and ^{232}Th isotopes. Samples with an age from <10,000–600,000 years could be successfully dated [143]. The method provides results similar to those obtained via α -spectrometry, but the amount of sample required is decreased by a factor of 10,000 (!), while no sample preparation is required with LA-MC-ICP-MS. Hirata showed that LA-MC-ICP-MS shows sufficient precision to study variations in the $^{182}\text{W}/^{183}\text{W}$ isotope ratio due to radioactive decay of ^{182}Hf on samples containing as little as 20 ng of W [144].

Next to radiogenically altered isotope ratios, also isotopic variations occurring as a result of natural fractionation effects can provide information on geological processes and as a result of the use of MC-ICP-MS, such fractionation effects have been demonstrated for an increasing number of elements. It is evident that – as a result of the large *relative* mass difference between the isotopes – especially the light elements undergo isotopic fractionation in natural processes. Isotopic analysis of B via MC-ICP-MS was, for example, used to obtain information of the origin of this element present in a geothermal system [145]. Gussone *et al.* determined Ca isotope ratios in skeletal aragonite and calcite from different marine biota [146]. The Ca fractionation observed was related to the temperature at which the precipitation of CaCO_3 took place. As a result, Ca isotopic analysis shows the potential to provide information on temperature variations to be used in palaeoclimate reconstruction. Poitrasson and Freyrier studied the Fe isotopic composition of igneous rocks and observed a good correlation between the isotopic composition of Fe on one hand and the MgO and SiO_2 contents of the granitoids on the other hand [147]. This is interpreted by the authors as an indication of exsolution of late magmatic fluids from the granitic melt. Malinovsky *et al.* developed a method for precise measurement of Mo isotope ratios on the basis of which they could demonstrate that geochemical processes during weathering and transport of Mo to the oceans induce isotopic fractionation [148]. Isotopic analysis of Mo can be applied to obtain information on redox conditions in the geological past. On the basis of a study executed using MC-ICP-MS, Rouxel *et al.* conclude that a relative strong isotopic fractionation occurs during reduction of Sb(V) into Sb(III) [149]. Hence, the authors suggest that Sb isotopes can be used as palaeoredox tracers in oceanic systems.

It is necessary to point out that for these highly challenging applications, isolation of the target element from the concomitant matrix is required in order to permit accurate correction for the instrumental mass discrimination, observed in MC-ICP-MS. These chemical separations have to be carried out with the utmost care, as also this chemical processing can result in isotopic fractionation [150]. As a result, *quantitative* recovery of the target element is often an important prerequisite.

6.5.4.2 Archaeometric and archaeological applications

Provenance determination and evaluation of authenticity via isotopic analysis has been successfully used in the domain of archaeometry, with Pb being the most important target element. Pb has four stable isotopes, three of which are radiogenic: radioactive decay of ^{238}U and ^{235}U gives origin to ^{206}Pb and ^{207}Pb as end products, respectively, while the end product of radioactive decay of ^{232}Th is ^{208}Pb . ^{204}Pb is not radiogenic. Hence, the isotopic composition of lead ores varies considerably, depending on the age and the parent:daughter ratios in geological formations (see Table 6.5). As the isotopic composition of Pb is not noticeably changed during industrial processing, manufacturing of objects of art or biochemical processes, measurement of the Pb isotope ratios and comparison with database values can provide information on the provenance of archaeological objects. In this section, a number of selected applications from various fields are discussed, and should give the reader some idea of the possibilities of this approach. Moreover, the high sensitivity displayed by ICP-MS and thus, the low amount of sample required, allow this type of chemical analysis with minimal damage to the artefacts studied.

Table 6.5 $^{206}\text{Pb}/^{207}\text{Pb}$ isotope ratios of ore deposits [151]

Country	Mining district	$^{206}\text{Pb}/^{207}\text{Pb}$
USA	Missouri	1.385
	Idaho	1.052
Russia	Altay, Kazakhstan	1.131
Australia	Broken Hill	1.037
Canada	British Columbia	1.064
	New Brunswick	1.160
	Ontario	0.920
Peru	Cerro de Pasco	1.200

During dredging operations in the rivers Scheldt and Durme (Belgium), 26 copper alloy statuettes, representing Roman gods, were found. De Wannemacker *et al.* carried out Pb isotopic analysis of these artefacts using single-collector sector field ICP-MS and compared the results obtained with literature data for different Pb ore mines that were exploited during Roman times [152]. Of each statuette, a few mg of sample was taken using a stainless steel drill. The samples were acid-digested in open vessels and subjected to Pb isotopic analysis with a single-collector sector field ICP-MS instrument, operated at low mass resolution. $^{208}\text{Pb}/^{206}\text{Pb}$ and $^{207}\text{Pb}/^{206}\text{Pb}$ ratios could be determined with a precision of 0.05–0.15% RSD, while for $^{204}\text{Pb}/^{206}\text{Pb}$, a precision of 0.1–0.4% was obtained due to the lower isotopic abundance of ^{204}Pb (counting statistics). Plotting the experimental results on a bivariate plot – $^{208}\text{Pb}/^{206}\text{Pb}$ as a function of $^{207}\text{Pb}/^{206}\text{Pb}$ – on which also the isotopic fields for different ancient mining areas were indicated – provided information on the origin of the metal used in their manufacturing (Fig. 6.18). It was concluded that some statuettes were manufactured from Pb from the British islands, while for other, Pb originating from Southern Europe was used. The grouping of the statuettes thus obtained was in agreement with that obtained on the basis of stylistic investigation.

When using LA as a means of sample introduction, even less damage is inflicted to the samples investigated. Schultheis *et al.* carried out Pb isotopic analysis of historic glass samples via LA – single-collector sector field ICP-MS [153]. Mass discrimination was corrected for by using either a glass reference material NIST SRM 610 or a Pb isotopic reference material NIST SRM 981 as an external isotopic standard. The Pb isotopic composition of NIST SRM 610 was previously determined using the $^{203}\text{Tl}/^{205}\text{Tl}$ isotope ratio for mass bias correction (power law equation). This investigation led to the conclusion that the single layers of iridescent Art Nouveau lead crystal glass samples originated from different sources. In spite of the low Pb concentration in glass fragments excavated at the archaeological site of Ephesos in Turkey, Pb isotopic analysis via LA-ICP-MS provided sufficient isotope ratio precision to discriminate between fragments from different origin.

As the use of LA for sample introduction leads to transient signals and elemental fractionation may occur to some extent during the ablation process (depending on the type of LA system used), the isotope ratio precision obtained with a single-collector instrument is poorer than when using pneumatic nebulisation for sample introduction. The application

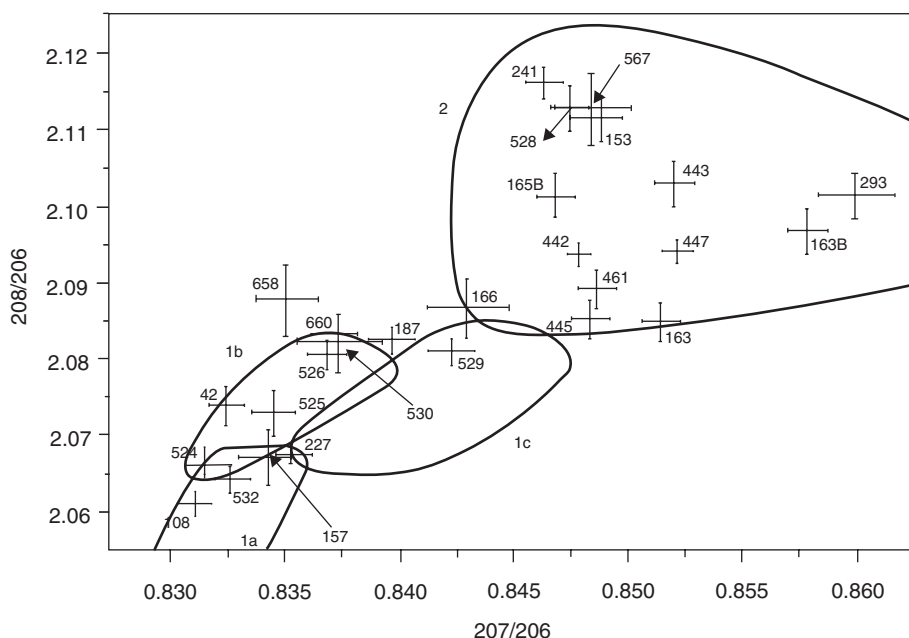


Figure 6.18 Bivariate plot – $^{208}\text{Pb}/^{206}\text{Pb}$ as a function of $^{207}\text{Pb}/^{206}\text{Pb}$ – representing the experimental results for 26 copper alloy statuettes (with corresponding uncertainties) and the lead isotopic fields for possible Pb ore sources: 1a, Laurion mining district (Greece); 1b, Kythnian mining district (Greece); 1c, Cypriot field and 2 British Islands field. Reproduced from [152].

range of LA-ICP-MS for isotopic analysis is however considerably extended by using MC-ICP-MS. LA-MC-ICP-MS was, for example, used for Pb isotopic fingerprinting of Roman silver coins [154] and for investigating metal artefacts stemming from the early Bronze Age and found in central Germany and Bohemia [155]. Next to Pb, Klein *et al.* [156] also studied the isotopic composition of Cu, present in coins from Roman times (between 16 BC and 37 AD). The Cu isotope ratio results were assessed to provide supplementary information useful in grouping and classification. Junk and Pernicka on the other hand introduced isotopic analysis of Os, which shows variations in its isotopic composition as a result of the radioactive decay of ^{187}Re and ^{190}Pt , via LA-MC-ICP-MS as a means of provenance determination of gold coins [157].

Fortunato *et al.* used MC-ICP-MS for Pb isotopic analysis of the commonly used white lead $2\text{PbCO}_3 \cdot \text{Pb}(\text{OH})_2$ pigment, originating from 16th and 17th century paintings [158]. Minute samples (50–200 μg) were taken from Old Masters' paintings of the Northern and Southern schools. On a bivariate plot ($^{207}\text{Pb}/^{204}\text{Pb}$ as a function of $^{206}\text{Pb}/^{204}\text{Pb}$), the data points for white lead pigments used by Flemish painters, such as Rubens and van Dyck form a narrow cluster that is clearly separated from the data points for the same pigment from contemporary Italian paintings (Figs. 6.19 and 6.20).

Surprisingly, comparison of the Pb isotope ratio data obtained for the Flemish paintings with information on the isotopic composition of ore samples, led to the conclusion that no

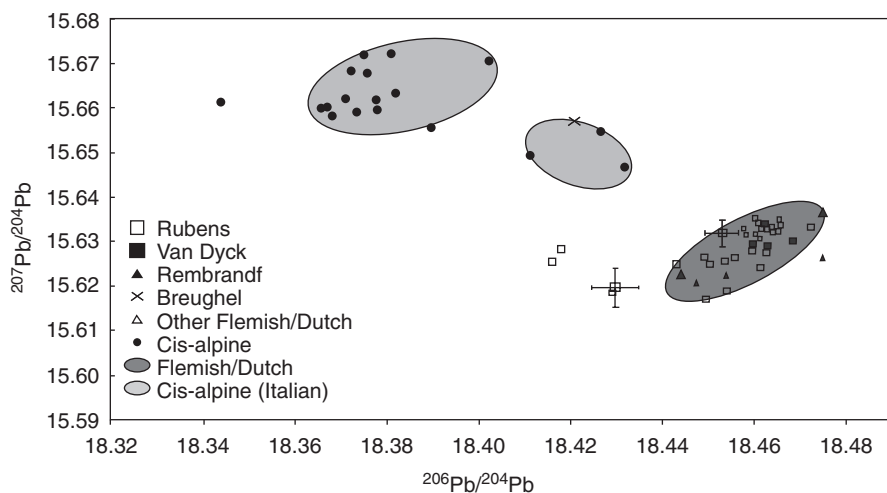


Figure 6.19 Bivariate plot – $^{207}\text{Pb}/^{204}\text{Pb}$ as a function of $^{206}\text{Pb}/^{204}\text{Pb}$ – representing the MC-ICP-MS results for white lead pigments taken from Old Masters' paintings of the Northern and Southern schools. The results for samples from Flemish/Dutch paintings form a narrow cluster, clearly separated from that of samples from cis-alpine (Italian) paintings. Reproduced from [158].

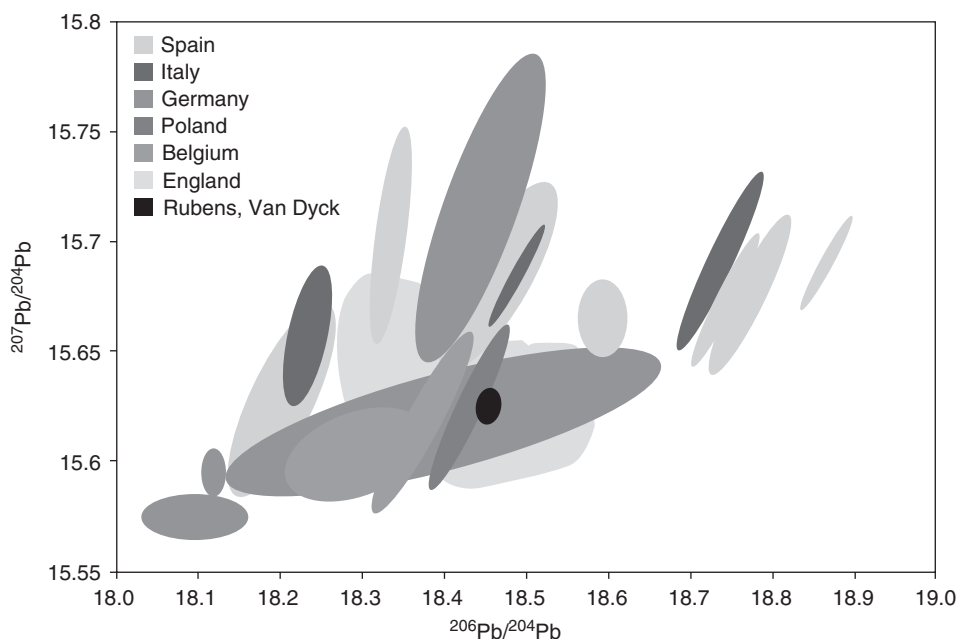


Figure 6.20 Bivariate plot – $^{207}\text{Pb}/^{204}\text{Pb}$ as a function of $^{206}\text{Pb}/^{204}\text{Pb}$ – representing isotopic fields characterising the isotopic composition of Pb from different mining areas. The Pb present in white lead pigment sampled from paintings from Rubens and van Dyck does not stem from Belgian mines. Reproduced from [158].

local ores were used in the production of the pigment, but that the ore, the Pb isolated out of the ore or the pigment itself was imported from England or Germany. This information and type of analysis can be useful in authentication studies and in revealing the history of a work of art, for example, the detection of later overpaints or retouchings.

Latkoczy *et al.* used single-collector sector field ICP-MS operated at low mass resolution for Sr isotopic analysis on 7000 year-old human skeleton remains, discovered in lower Austria [159]. The skeletons found at this Neolithic settlement showed ample evidence of a violent death. Significant differences in the $^{87}\text{Sr}/^{86}\text{Sr}$ ratio (determined with a precision better than 0.03% RSD for $n = 5$) between individuals found at the same location indicated that the human remains stem from at least two populations: this observation was interpreted as evidence for a hostile encounter with casualties between two tribes. Prohaska *et al.* used LA – single-collector ICP-MS for spatially resolved Sr isotopic analysis of teeth [160]. Despite the poorer isotope ratio due to the use of LA for sample introduction, a difference in Sr isotopic composition between dentine and enamel for an individual from the Neolithic settlement mentioned above, demonstrates a change in food source and hence, a possible migration during early childhood.

6.5.4.3 Provenance determination of agricultural products

For a growing range of agricultural products, there is a need for objective methods for determination of their geographical provenance. For wines, the geographical origin may be indicated on the bottle under the form of the AOC (*Appellation d'Origine Contrôlée*). As a result of the economical importance of the wine trade and the high prices paid for prestige wines, it is worthwhile to apply chemical methods for provenance determination and hence, for evaluating the authenticity of the indicated origin and thus to trace down fraud. These methods also play a role in the protection of terms of which the use is legally restricted to a well-defined region of origin (e.g. Champagne, Madeira, Port wine) and that are considered as a fundamental indication of quality. Isotopic analysis of elements showing natural variation in their isotopic composition can be used as a powerful tool in this context. Although in the majority of cases, this type of work is focusing on the light elements H, C, N and O, and is thus carried out using gas source MS, ICP-MS has entered this field as well. Sr is one of the elements that was investigated in this context. Almeida and Vasconcelos, for example, developed a method based on UV irradiation of wine, cation exchange chromatography to separate Sr from Rb (to avoid the isobaric overlap of the signals from ^{87}Sr and ^{87}Rb) and isotopic analysis of the Sr fraction using quadrupole-based ICP-MS [161]. Mass discrimination was corrected for by using the $^{86}\text{Sr}/^{88}\text{Sr}$ isotope ratio – which is constant in nature – as an internal standard. The precision obtained (<0.3% RSD) was sufficient to discriminate wines coming from the North of Portugal from those coming from the South of the country. Bordeaux wines (France) showed an Sr isotopic composition (or $^{87}\text{Sr}/^{86}\text{Sr}$ isotope ratio) significantly different from that of the Portuguese wines. More recently, Coetzee and Vanhaecke showed that also the $^{11}\text{B}/^{10}\text{B}$ isotope ratio that varies as a result of natural fractionation processes shows promise as a tool for discriminating wines according to geographical origin [162]. Also in this case, quadrupole-based ICP-MS was used, while sample preparation was limited to 100-fold dilution of the wine. It was shown that Bergerac (France), Valpolicella (Italy) and South African wines showed a clear difference in B isotopic

composition and on the basis of B isotopic composition, even South African wines could to some extent be distinguished from one another according to origin (Robertson, Stellenbosch or Swartland).

As a result of its superior precision, the use of MC-ICP-MS is often required or at least recommendable in provenance determination. Barbaste *et al.* reported an isotope ratio precision of 0.002–0.003% for $^{87}\text{Sr}/^{86}\text{Sr}$ isotope ratios obtained for wine and could easily distinguish between wines grown on basaltic, mixed and granitic soil areas [163]. Fortunato *et al.* reported on the use of MC-ICP-MS for Sr isotopic analysis of Emmenthal-type cheeses [164], originating from different regions (alpine and prealpine Switzerland, Bretagne, Finland, Canada and Australia). Sr isotope ratios could be determined with 0.002–0.01% precision and reflected the local geological properties of the area of production, making Sr isotopic analysis useful for provenance determination. While the Sr isotopic composition in wine or cheese reflects that of the provenance soil, Medina *et al.* showed that anthropogenic contamination governs the isotopic composition found for Pb in wine [165]. Nevertheless, they conclude that since the Pb isotopic composition is specific of the continental origin of the wine, it still can be used for certifying wine authenticity.

6.5.4.4 Environmental applications

Isotopic analysis can also shed light on the origin of environmental pollution. Kersten *et al.* measured $^{206}\text{Pb}/^{207}\text{Pb}$ isotope ratios in both sea water and sediments sampled in the Efesis Bay in Greece [166]. As a result of the vicinity of the metropolitan basin of Greater Athens, with a population exceeding 3 million, 50% of all vehicles registered in Greece and 40% of the Greek heavy industry, the Efesis Bay is heavily polluted. Due to the considerable number of anthropogenic inputs, determination of the Pb content is insufficient for determination of the principal source(s) of Pb pollution. However, as the isotopic composition of background Pb in sediments, that is the locally mined Pb and the Pb used by the local industry, and of gasoline Pb (tetraethyllead added as anti-knocking agent) differ considerably ($^{206}\text{Pb}/^{207}\text{Pb} \sim 1.06$ for gasoline in comparison with ~ 1.20 for the former sources), measurement of Pb isotope ratios in the samples of interest permitted some important conclusions to be drawn. As the Pb isotopic composition for the sediment samples was observed to be quite uniform throughout the entire bay, with a $^{206}\text{Pb}/^{207}\text{Pb}$ isotope ratio of approximately 1.17, the Pb pollution of the sediments is dominated by the industrial activities. For the dissolved Pb, however, the isotopic composition indicates that up to 70% is derived from gasoline Pb. In addition, by means of Pb isotopic analysis of sea water sampled at different locations, it could be concluded that road wash-out, discharged together with domestic sewage, is far more important as a pollution pathway than direct atmospheric deposition of gasoline Pb.

In Switzerland, unleaded gasoline was introduced in 1985. Pb isotopic analysis of lake sediment samples permitted an evaluation of the corresponding environmental consequences [167]. Lake sediment samples were accurately dated and subjected to Pb isotopic analysis by means of ICP-MS. The background $^{206}\text{Pb}/^{207}\text{Pb}$ isotope ratio (preindustrial sediment) was found to be 1.20. The emission of petrol lead additives having a $^{206}\text{Pb}/^{207}\text{Pb}$ isotope ratio of 1.04–1.10 was clearly demonstrated to have an effect on the $^{206}\text{Pb}/^{207}\text{Pb}$ isotope ratio of the sediment samples. At a depth corresponding to ~ 1980 , a minimum

value of 1.13 was reached. For younger sediments (~1990), this value was observed to have increased to 1.16.

Townsend and Snape carried out isotopic analysis of Antarctic marine sediments, sampled near the Australian station Casey [168]. Despite low Pb levels, sufficiently precise Pb isotopic analysis could be accomplished using a single-collector sector field ICP-MS instrument, owing to the capacitive decoupling of the induction coil and the ICP by means of a grounded Pt shield that boosted the signal intensity by an order of magnitude. The analysis data provided evidence for anthropogenic contamination, attributed to the runoff from a waste disposal site with abandoned lead batteries.

Pb isotopic analysis to provide insight into the origin of Pb pollution, is not restricted to 'Modern times'. Outridge *et al.* studied historical trends in the isotopic composition of Pb in the tooth tissue of beluga from the Canadian Arctic in order to assess the importance of long-range transport of industrial pollution [169]. Tooth samples of beluga were available for both modern and preindustrial (<1825) eras. Significant decreases in the $^{206}\text{Pb}/^{207}\text{Pb}$ and $^{208}\text{Pb}/^{207}\text{Pb}$ isotope ratios indicate exposure to 'anthropogenic Pb' since at least the mid-17th to late 18th centuries. This exposure has to be attributed to the development of large-scale lead–silver smelting activities in Central Europe and the New World. The industrial revolution led to a more recent decline in the isotope ratios of interest. Clearly, these isotopic changes reflect the historical changes in human uses of Pb. In addition, it is clear that the pollution associated with these changes is hemispherical in scale, such that Pb was/is also deposited in circumpolar environmental matrices and incorporated in Arctic food chains. Le Roux *et al.* sampled a peat core from the Manchester area in slices of 2 cm [170]. The peat bog was used as an archive, providing information on Pb pollution from approximately 2000 BC to 1800 AD (estimated via radiocarbon dating and ^{210}Pb dating). Apparently, Pb pollution appeared as early as 900 BC, as a result from pre-Roman mining activities. Local mining of the Pb ores continued to be the main source of pollution during the Roman era and the Middle Ages.

Although not an environmental application, Pb isotopic analysis using a similar rationale – comparison of the isotopic composition of a particular sample with that of possible sources – is also used in forensic analysis. Buttigieg *et al.* showed, for example, that on the basis of Pb isotopic analysis carried out using MC-ICP-MS, they could separate small arms projectiles from one another according to manufacturer and hence, geographical origin [171].

Gäbler and Bahr used a single-collector sector field ICP-MS instrument to determine the $^{10}\text{B}/^{11}\text{B}$ isotope ratio in surface and ground waters to detect anthropogenic input [172]. This approach is based on the fact that sodium perborate, present as a bleaching agent in detergents, shows a $^{10}\text{B}/^{11}\text{B}$ isotope ratio that differs markedly from that of geogenic B in the area of interest. The $^{10}\text{B}/^{11}\text{B}$ isotope ratio could be determined with a precision of 0.1–0.2%. A relatively small contribution from $^{40}\text{Ar}^{4+}$ to the signal intensity at a mass-to-charge ratio of 10 could be avoided by slightly adjusting the mass range scanned. The results obtained clearly demonstrated the effect of the discharge of a sewage plant on the Innerste river water (Harz region, Germany) and infiltration of the river water into some ground water observation wells.

By means of MC-ICP-MS, Cloquet *et al.* demonstrated natural isotopic fractionation effects for Cd [173]. Although the range of variation is only 0.04%, MC-ICP-MS offers an isotope ratio precision sufficient to use the isotopic composition of Cd as a tracer of the origin of anthropogenic Cd pollution in the environment.

Of course, ICP-MS is also suited to study environmental pollution with radionuclides. On the basis of $^{240}\text{Pu}/^{239}\text{Pu}$ and $^{241}\text{Pu}/^{239}\text{Pu}$ determination with sector field ICP-MS, Ketterer *et al.* [174] have estimated the contributions from global fallout and from the 1986 Chernobyl nuclear disaster (fallout characterised by higher $^{240}\text{Pu}/^{239}\text{Pu}$ and $^{241}\text{Pu}/^{239}\text{Pu}$ isotope ratios) to the Pu activity in Polish soils. The contribution of Chernobyl fallout to the total $^{239} + ^{240}\text{Pu}$ activity, calculated on the basis of a two-component mixing model ranged from $<10\%$ to $>90\%$. Especially for the Northeastern part of Poland, the contribution from the Chernobyl accident was assessed to be very high, with values approaching 100% . Sometimes, this type of application may be complicated due to the low levels in which these radionuclides may occur in environmental samples, spectral interference and/or insufficient abundance sensitivity. Izmer *et al.* have developed a method for $^{129}\text{I}/^{127}\text{I}$ isotope ratio determination in soils, coping with the problems mentioned above [175]. Iodine was released from the soil samples by means of thermal desorption in a device coupled on-line to a quadrupole-based ICP-MS instrument. The interfering signal from $^{129}\text{Xe}^+$ (Xe is present as a contamination in the Ar plasma gas) was suppressed by using a mixture of O_2 and He as reaction gases in a hexapole collision/reaction cell. $^{127}\text{I}/^{129}\text{I}$ isotope ratios down to 10^{-6} could be determined in soil samples from contaminated regions.

During the past years, there has been quite some anxiety concerning the occurrence of DU in the environment and its impact on human health. For its use as fuel in a nuclear reactor, mined uranium has to be isotopically enriched in ^{235}U . As a result of this enrichment process, also DU – this is U in which the isotopic abundance of ^{235}U is considerably lower than the natural one (approximately 0.2% instead of 0.72%) – is formed as a waste product. Since this material is characterised by an extremely high density, it is used for several purposes. Well-known is the use of this material in ammunition and projectiles, enabling these to penetrate the armoured steel of military vehicles. On impact, DU will readily burn and will be dispersed into small particles. Additionally, DU is also used in some aeroplanes to make the volume of counterweights – present in the tail and wings and used for maintaining the aircraft's centre of gravity – as small as possible. However, U is both chemically and radiologically toxic and since veterans of the Gulf war and that in former Yugoslavia, in which DU ammunition has been used, and the residents of areas where DU-containing planes have crashed had serious complaints concerning their physical and mental health, the attention for this problem has increased. Danesi *et al.* used ICP-MS for monitoring ^{234}U , ^{235}U , ^{236}U and ^{238}U in soil samples from locations in Kosovo, where DU ammunition was used during the 1999 Balkan conflict [176]. The results obtained showed that a U concentration exceeding the normal background level ($2\text{--}3\ \mu\text{g g}^{-1}$) was always accompanied by a $^{235}\text{U}/^{238}\text{U}$ isotope ratio, unequivocally identifying DU as the source. Moreover, the presence of ^{236}U in these soil samples indicated that the DU used for manufacturing the ammunition used was previously irradiated (used as fuel in a reactor) and then reprocessed. Gwiazda *et al.* demonstrated that the $^{235}\text{U}/^{238}\text{U}$ urinary isotope ratio of American Gulf war veterans injured with DU-containing fragments, or exposed to DU via inhalation, ingestion and/or wound infection could deviate from the natural isotope ratio as long as 8 years after exposure to DU [177]. These authors also demonstrated that the U concentration as such does not (always) suffice to demonstrate exposure to DU as the urinary U content may substantially vary as a result of significant differences in daily intake. In 1992, a Boeing cargo aircraft crashed into two apartment buildings in Amsterdam, the Netherlands. Afterwards, a substantial number of police officers and firemen that had been present for longer times at the

scene of the disaster experienced health problems. Exposure to the DU used in the balance weights of the aircraft was launched as a hypothesis. Based on a combination of determination of the urinary U concentration [178] and U isotopic analysis [179] for urine samples showing a U concentration higher than 50 ng/l, Bijlsma *et al.* [180] concluded that there was no indication that the health complaints were related to exposure to DU.

6.5.4.5 Biological applications

While the use of stable isotopic tracers in nutrition studies is (becoming) a well-established practice, the increased capabilities of MC-ICP-MS also open new fields of research as its high precision allows to detect and quantify natural variations in the isotopic composition as a result of natural fractionation effects for an increasing number of elements.

Walczyk and von Blanckenburg demonstrated that the isotopic composition of Fe present in human blood differs between male and female subjects [122]. Based on this initial observation, further research was carried out [181], which revealed that while blood and muscle tissue Fe have a similar isotopic composition, Fe present in the liver is isotopically heavier than that in blood. These observations contribute to a better understanding of the mechanisms of isotopic fractionation occurring in the body and a more profound insight into human iron metabolism. As their research also indicated that the isotopic composition of blood Fe reflects the individual differences in iron metabolism, it was predicted that for patients suffering from hereditary haemochromatosis, blood Fe would show an isotopic

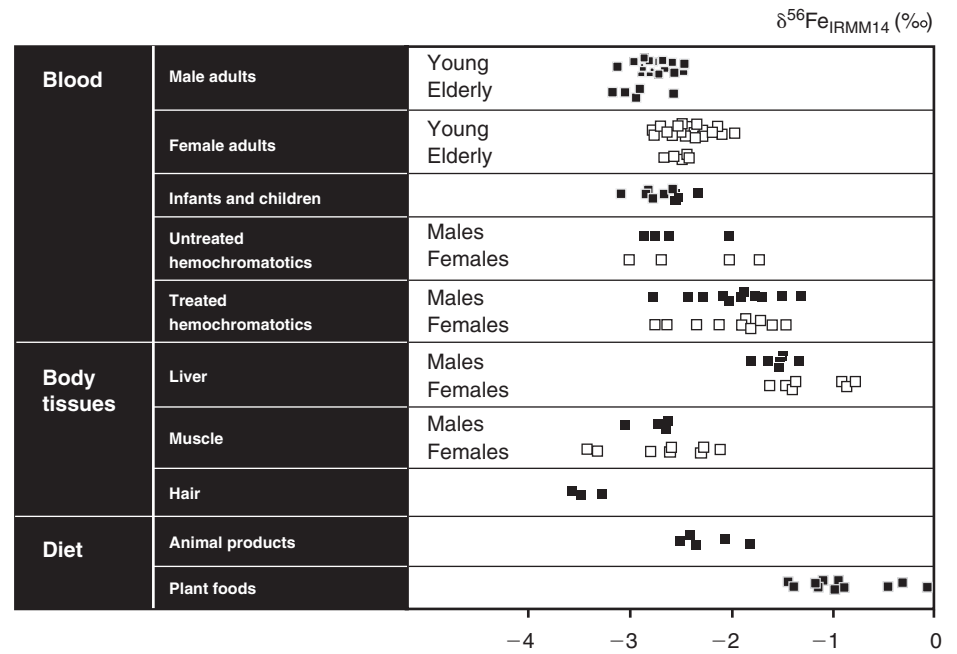


Figure 6.21 $\delta^{56}\text{Fe}$ values (with reference to the Fe isotopic reference material IRMM-014) for body tissues and fluids of male and female healthy individuals and patients suffering from hereditary haemochromatosis and for foodstuffs as obtained using MC-ICP-MS. Reprinted from [181].

composition deviating from 'normal' values. This hypothesis was confirmed experimentally, since by using MC-ICP-MS [182] it could be shown that in the blood of haemochromatosis patients the $^{56}\text{Fe}/^{54}\text{Fe}$ isotope ratio significantly exceeded that typical for healthy individuals (see Fig. 6.21). Moreover, the magnitude of this deviation was assessed to correlate with the clinical severity of the disease.

Also for Zn, it was demonstrated that isotopic fractionation occurs within the human body as a significantly different isotopic composition was found for Zn in red blood cells and in hair from the same individual, respectively [183].

Outridge *et al.* used LA-MC-ICP-MS for $^{87}\text{Sr}/^{86}\text{Sr}$ isotope ratio measurement in fish otoliths (earbones) with sub-annual resolution [184]. As the Sr isotopic composition in this tissue reflects the geochemical environment the animal resided in at the time that this calcified tissue was formed, information on the fish's life history can be obtained. Based on the same rationale, Pb isotopic analysis of tooth tissue from Atlantic walrus was applied by Outridge *et al.* to investigate the stock structure in the Canadian Arctic and Greenland [185]. Owing to the high isotope ratio precision attained, the dental Pb isotope signatures indicated that the groups of walrus live more localised than originally expected.

6.6 General conclusions

In spite of its rather poor isotope ratio precision, single-collector ICP-MS has managed to become a routine tool for isotope ratio measurement, especially for quantifying induced changes in the isotopic composition of a target element. With the introduction of and the important developments in MC instrumentation on the other hand, the use of ICP-MS for studying natural differences in the isotopic composition of target elements is no longer restricted to elements showing pronounced isotopic variation (e.g. Sr or Pb), but even the most subtle cases can now be adequately tackled. The interest for using ICP-MS for measuring isotope ratios is still growing and fascinating new application fields are being explored.

References

1. Roth, E. (1997) Critical evaluation of the use and analysis of stable isotopes. *Pure Appl. Chem.*, **69**, 1753–1828.
2. Rosman, K.J.R. and Taylor, P.D.P. (1998) IUPAC table of isotopic compositions of the elements. *Pure Appl. Chem.*, **70**, 217–235.
3. Coplen, T.B., Bohlke, J.K., De Bièvre, P., Ding, T., Holden, N.E., Hopple, J.A., Krouse, H.R., Lambert, A., Peiser, H.S., Revesz, K., Rieder, S.E., Rosman, K.J.R., Roth, E., Taylor, P.D.P., Vocke Jr., R.D. and Xiao, Y.K. (2002) Isotope-abundance variations of selected elements. *Pure Appl. Chem.*, **74**, 1987–2017.
4. Faure, G. and Mensing, T.M. (2004) *Isotopes Principles and Applications*, 3rd edn, John Wiley, New York.
5. Grégoire, D.C. (1989) Application of isotope ratios determined by ICP-MS to earth science studies. *Progr. Anal. Spectrosc.*, **12**, 433–452.
6. Qi, H.P., Coplen, T.B., Wang, Q.Z. and Wang, Y.H. (1997) Unnatural isotopic composition of lithium reagents. *Anal. Chem.*, **69**, 4076–4078.

7. Richter, S., Alonso, A., Wellum, R. and Taylor, P.D.P. (1999) The isotopic composition of commercially available uranium chemical reagents. *J. Anal. Atom. Spectrom.*, **14**, 889–891.
8. De Bièvre, P., Delaeter, J.R., Peiser, H.S. and Reed, W.P. (1993) Reference materials by isotope-ratio mass spectrometry. *Mass Spectrom. Rev.*, **12**, 143–172.
9. Sahoo, S.K. and Masuda, A. (1998) Precise determination of lithium isotopic composition by thermal ionization mass spectrometry in natural samples such as seawater. *Anal. Chim. Acta*, **370**, 215–220.
10. Zeininger, H. and Heumann, K.G. (1983) Boron isotope ratio measurement by negative thermal ionization mass-spectrometry. *Int. J. Mass Spectrom. Ion. Proc.*, **48**, 377–380.
11. Richter, S., Alonso, A., De Bolle, W., Wellum, R. and Taylor, P.D.P. (1999) Isotopic ‘fingerprints’ for natural uranium ore samples. *Int. J. Mass Spectrom.*, **193**, 9–14.
12. Heumann, K.G., Gallus, S.M., Rädlinger, G. and Vogl, J. (1998) Precision and accuracy in isotope ratio measurements by plasma source mass spectrometry. *J. Anal. Atom. Spectrom.*, **13**, 1001–1008.
13. Smith, D.H. (2000) Thermal ionization mass spectrometry (Chapter 1). In *Inorganic Mass Spectrometry – Fundamentals and Applications* (Eds. C.M. Barshick, D.C. Duckworth and D.H. Smith), Marcel Dekker Inc, New York & Basel.
14. Heumann, K.G., Eisenhut, S., Gallus, S., Hebeda, E.H., Nusko, R., Vengosh, A. and Walczyk, T. (1995) Recent developments in thermal ionization mass-spectrometric techniques for isotopic analysis – a review. *Analyst*, **120**, 1291–1299.
15. Jakubowski, N., Moens, L. and Vanhaecke, F. (1998) Sector field mass spectrometers in ICP-MS. *Spectrochim. Acta B*, **53**, 1739–1763.
16. Mahoney, P.P., Ray, S.J. and Hieftje, G.M. (1997) Time-of-flight mass spectrometry for elemental analysis. *Appl. Spectrosc.*, **51**, A16–A28.
17. Tanner, S.D., Baranov, V.I. and Bandura, D.R. (2002) Reaction cells and collision cells for ICP-MS: a tutorial review. *Spectrochim. Acta B*, **57**, 1361–1452.
18. Vanhaecke, F., Moens, L., Dams, R. and Taylor, P. (1996) Precise measurement of isotope ratios with a double-focusing magnetic sector ICP-mass spectrometer. *Anal. Chem.*, **68**, 567–569.
19. Vanhaecke, F., Moens, L., Dams, R., Papadakis, I. and Taylor, P. (1997) Applicability of high-resolution ICP-mass spectrometry for isotope ratio measurements. *Anal. Chem.*, **69**, 268–273.
20. Prohaska, T., Latkoczy, C. and Stingeder, G. (1999) Precise sulfur isotope ratio measurements in trace concentration of sulfur by inductively coupled plasma double focusing sector field mass spectrometry. *J. Anal. Atom. Spectrom.*, **14**, 1501–1504.
21. Vanhaecke, F., Moens, L., Dams, R., Allen, L. and Georgitis, S. (1999) Evaluation of the isotope ratio performance of an axial time-of-flight ICP-mass spectrometer. *Anal. Chem.*, **71**, 3297–3303.
22. Bandura, D.R., Baranov, V.I. and Tanner, S.D. (2001) Reaction chemistry and collisional processes in multipole devices for resolving isobaric interferences in ICP-MS. *Fresen. J. Anal. Chem.*, **370**, 454–470.
23. Hattendorf, B. and Günther, D. (2003) Strategies for method development for an inductively coupled plasma mass spectrometer with bandpass reaction cell. Approaches with different reaction gases for the determination of selenium. *Spectrochim. Acta B*, **58**, 1–13. See Fig. 6.2.
24. Bandura, D.R., Baranov, V.I. and Tanner, S.D. (2000) Effect of collisional damping and reactions in a dynamic reaction cell on the precision of isotope ratio measurements. *J. Anal. Atom. Spectrom.*, **15**, 921–928.
25. Moens, L.J., Vanhaecke, F.F., Bandura, D.R., Baranov, V.I. and Tanner, S.D. (2001) Elimination of isobaric interferences in ICP-MS, using ion-molecule reaction chemistry: Rb/Sr age determination of magmatic rocks, a case study. *J. Anal. Atom. Spectrom.*, **16**, 991–994.
26. Becker, J.S. (2005) Recent developments in isotope analysis by advanced mass spectrometric techniques – Plenary lecture. *J. Anal. Atom. Spectrom.*, **20**, 1173–1184.

27. Walder, A.J. and Freedman, P.A. (1992) Isotopic ratio measurement using a double focusing magnetic-sector mass analyzer with an inductively coupled plasma as an ion-source. *J. Anal. Atom. Spectrom.*, **7**, 571–575.
28. Wieser, M.E. and Schwieters, J.B. (2005) The development of multiple collector mass spectrometry for isotope ratio measurements. *Int. J. Mass. Spectrom.*, **242**, 97–115.
29. Finnigan ICP-MS Interferenz – Tabelle, version 2, May 1995.
30. Weyer, S. and Schwieters, J. (2003) High precision Fe isotope measurements with high mass resolution MC-ICPMS. *Int. J. Mass. Spectrom.*, **226**, 355–368.
31. Vanhaecke, F. and Moens, L. (2004) Overcoming spectral overlap in isotopic analysis via single- and multi-collector ICP-mass spectrometry. *Anal. Bioanal. Chem.*, **378**, 232–240.
32. Walczyk, T. (2004) TIMS vs. multicollector-ICP-MS: coexistence or struggle for survival? *Anal. Bioanal. Chem.*, **378**, 229–231.
33. Halliday, A.N., Lee, D.-C., Christensen, J., Rehkämper, M., Yi, W., Luo, X., Hall, C.M., Ballentine, C.J., Pettke, T. and Stirling, C. (1998) Applications of multiple collector-ICPMS to cosmochemistry, geochemistry, and paleoceanography. *Geochim. Cosmochim. Acta*, **62**, 910–940.
34. Rehkämper, M., Schonbachler, M. and Stirling, C.H. (2001) Multiple collector ICP-MS: introduction to instrumentation, measurement techniques and analytical capabilities. *Geostandard Newslett.*, **25**, 23–40.
35. Walder, A.J., Abell, I.D., Platzner, I. (1993) Lead isotope ratio measurement of NIST 610 glass by laser ablation inductively coupled plasma mass-spectrometry. *Spectrochim. Acta B*, **48**, 397–402.
36. Begley, I.S. and Sharp, B.L. (1994) Occurrence and reduction of noise in inductively coupled plasma mass spectrometry for enhanced precision in isotope ratio measurement. *J. Anal. Atom. Spectrom.*, **9**, 171–176.
37. Begley, I.S. and Sharp, B.L. (1997) Characterization and correction of instrumental bias in inductively coupled plasma quadrupole mass spectrometry for accurate measurement of lead isotope ratios. *J. Anal. Atom. Spectrom.*, **12**, 395–402.
38. ISO (1993) *Guide to the Expression of Uncertainty in Measurement*, 1st edn, ISO, Genève.
39. Eurachem (1995) *Quantifying Uncertainty in Chemical Measurement*, 1st edn, BSI Customer Services, London.
40. Niu, H. and Houk, R.S. (1996) Fundamental aspects of ion extraction in inductively coupled plasma mass spectrometry. *Spectrochim. Acta B*, **51**, 779–815.
41. Sun, X.F., Ting, B.T.G., Zeisel, S.H. and Janghorbani, M. (1987) Accurate measurement of stable isotopes of lithium by inductively coupled plasma mass spectrometry. *Analyst*, **112**, 1223–1228.
42. Michiels, E. and De Bièvre, P. (1983) Accurate assay of lithium by isotope-dilution mass spectrometry. *Int. J. Mass Spectrom. Ion Proc.*, **48**, 369–372.
43. Andren, H., Rodushkin, I., Stenberg, A., Malinovsky, D. and Baxter, D.C. (2004) Sources of mass bias and isotope ratio variation in multicollector ICP-MS: optimization of instrumental parameters based on experimental observations. *J. Anal. Atom. Spectrom.*, **19**, 1217–1224.
44. Tanner, S.D., Cousins, L.M. and Douglas, D.J. (1994) Reduction of space-charge effects using a three-aperture gas dynamic vacuum interface for inductively coupled plasma mass spectrometry. *Appl. Spectrosc.*, **48**, 1367–1372.
45. Burgoyne, T.W., Hieftje, G.M. and Hites, R.A. (1997) Space charge evaluation in a plasmasource mass spectrograph. *Anal. Chem.*, **69**, 485–489.
46. Longerich, H.P., Fryer, B.J. and Strong, D.F. (1987) Determination of lead isotope ratios by inductively coupled plasma mass spectrometry (ICP-MS). *Spectrochim. Acta B*, **42**, 39–48.
47. Ketterer, M.E., Peters, M.J. and Tisdale, P.J. (1991) Verification of a correction procedure for measurement of lead isotope ratios by inductively coupled plasma mass spectrometry. *J. Anal. Atom. Spectrom.*, **6**, 435–443.

48. Roehl, R., Gomez, J. and Woodhouse, L.R. (1995) Correction of mass bias drift in inductively coupled plasma mass spectrometry measurements of zinc isotope ratios using gallium as an isotope ratio internal standard. *J. Anal. Atom. Spectrom.*, **10**, 15–23.
49. Ingle, C.P., Sharp, B.L., Horstwood, M.S.A., Parrish, R.R. and Lewis, D.J. (2003) Instrument response functions, mass bias and matrix effects in isotope ratio measurements and semi-quantitative analysis by single and multi-collector ICP-MS. *J. Anal. Atom. Spectrom.*, **18**, 219–229.
50. Albarede, F., Telouk, P., Blichert-Toft, J., Boyet, M., Agranier, A. and Nelson, B. (2004) Precise and accurate isotopic measurements using multiple-collector ICPMS. *Geochim. Cosmochim. Acta*, **68**, 2725–2744.
51. Wombacher, F. and Rehkamper, M. (2003) Investigation of the mass discrimination of multiple collector ICP-MS using neodymium isotopes and the generalised power law. *J. Anal. Atom. Spectrom.*, **18**, 1371–1375.
52. Woodhead, J. (2002) A simple method for obtaining highly accurate Pb isotope data by MC-ICP-MS. *J. Anal. Atom. Spectrom.*, **17**, 1381–1385.
53. Taylor, P.D.P., De Bièvre, P., Walder, A.J. and Entwistle, A. (1995) Validation of the analytical linearity and mass discrimination correction model exhibited by a multiple collector inductively-coupled plasma-mass spectrometer by means of synthetic uranium isotope mixtures. *J. Anal. Atom. Spectrom.*, **10**, 395–398.
54. Vanhaecke, F., Vanhoe, H., Moens, L. and Dams, R. (1995) Quadrupole ICP-mass spectrometry for the determination of the aqua regia soluble content of trace metals in soil and sludge candidate reference materials. *Bull. Soc. Chim. Belge*, **104**, 653–661.
55. Papadakis, I., Taylor, P.D.P. and De Bièvre, P. (1997) Establishing an SI-traceable copper concentration in the candidate reference material MURST ISS A1 Antarctic sediment using isotope dilution as a primary method of measurement. *J. Anal. Atom. Spectrom.*, **12**, 791–796.
56. Seah, M.P. (1995) Effective dead time in pulse counting systems. *Surf. Interface Anal.*, **23**, 729–732.
57. Russ III, G.P. (1987) Isotope ratio measurements using ICP-MS. In *Applications of Inductively Coupled Plasma Mass Spectrometry* (Eds. A.R. Date and A.L. Gray), Chapman & Hall, London, pp. 90–114.
58. Nelms, S.M., Quétel, C.R., Prohaska, T., Vogl, J. and Taylor, P.D.P. (2001) Evaluation of detector dead time calculation models for ICP-MS. *J. Anal. Atom. Spectrom.*, **16**, 333–338.
59. Vanhaecke, F., De Wannemacker, G., Moens, L., Dams, R., Latkoczy, C., Prohaska, T. and Stingeder, G. (1998) Dependence of detector dead time on analyte mass number in ICP-mass spectrometry. *J. Anal. Atom. Spectrom.*, **13**, 567–571.
60. Kurz, E.A. (1979) Channel electron multipliers. *Am. Lab.*, March, 67–82.
61. Dietz, L.A. (1965) Basic properties of electron multiplier ion detection and pulse counting methods in mass spectrometry. *Rev. Sci. Instrum.*, **36**, 1763–1770.
62. Russ III, G.P. and Bazan, J.M. (1987) Isotope ratio measurements with an inductively coupled plasma-source mass spectrometer. *Spectrochim. Acta B*, **42**, 49–62.
63. Hinnert, T.A., Heithmar, E.M., Spittler, T.M. and Henshaw, J.M. (1987) Inductively coupled plasma mass spectrometric determination of lead isotopes. *Anal. Chem.*, **59**, 2658–2662.
64. Furuta, N. (1991) Optimization of the mass scanning rate for the determination of lead-isotope ratios using an inductively coupled plasma mass spectrometer. *J. Anal. Atom. Spectrom.*, **6**, 199–203.
65. Koirtyohann, S.R. (1996) Precise determination of isotopic ratios for some biologically significant elements by inductively coupled plasma mass spectroscopy. *Spectrochim. Acta B*, **49**, 1305–1311.
66. Quétel, C.R., Thomas, B., Donard, O.F.X. and Grousset, F.E. (1997) Factorial optimization of data-acquisition factors for lead isotope ratio determination by inductively coupled plasma mass spectrometry. *Spectrochim. Acta B*, **52**, 177–187.
67. De Bièvre, P. (1990) Isotope dilution mass spectrometry: what can it contribute to accuracy in trace analysis? *Fresen. J. Anal. Chem.*, **337**, 766–771.

68. Beary, E.S. and Paulsen, P.J. (1993) Selective application of chemical separations to isotope dilution inductively coupled plasma mass spectrometric analyses of standard reference materials. *Anal. Chem.*, **65**, 1602–1608.
69. Beary, E.S., Paulsen, P.J. and Fassett, J.D. (1994) Sample preparation approaches for isotope dilution inductively coupled plasma mass spectrometric certification of reference materials. *J. Anal. Atom. Spectrom.*, **9**, 1363–1369.
70. Beary, E.S. and Paulsen, P.J. (1995) Development of high-accuracy ICP-mass spectrometric procedures for the quantification of Pt, Pd, Rh and Pb in used auto catalysts. *Anal. Chem.*, **67**, 393–3201.
71. De Bièvre, P. (1994) Isotope dilution mass spectrometry (IDMS). In *Trace Element Analysis in Biological Specimens, Techniques and Instrumentation in Analytical Chemistry* Vol. 15 (Eds. R.F.M. Herber and M. Stoeppler), Elsevier, Amsterdam, pp. 169–183.
72. Moody, J.R., Greenberg, R.R., Pratt, K.W. and Rains, T.C. (1988) Recommended inorganic chemicals for calibration. *Anal. Chem.*, **60**, 1203A–1218A.
73. BIPM (1996) *Report of the 2nd Meeting*, Comité Consultatif pour la Quantité de Matière, BIPM, Sèvres.
74. Papadakis, I., Taylor, P.D.P. and De Bièvre, P. (1997) SI-traceable values for cadmium and lead concentrations in the candidate reference material, MURST-ISS A1 Antarctic sediment, by combination of ICP-MS with isotope dilution. *Anal. Chim. Acta*, **346**, 17–22.
75. Diemer, J., Quétel, C.R. and Taylor, P.D.P. (2002) Contribution to the certification of B, Cd, Cu, Mg and Pb in a synthetic water sample, by use of isotope-dilution ICP-MS, for comparison 12 of the international measurement evaluation programme. *Anal. Bioanal. Chem.*, **374**, 220–225.
76. Kent, A.J.R., Jacobsen, B., Peate, D.W., Waight, T.E. and Baker, J.A. (2004) Isotope dilution MC-ICP-MS rare earth element analysis of geochemical reference materials NIST SRM 610, NIST SRM 612, NIST SRM 614, BHVO-2G, BHVO-2, BCR-2G, JB-2, WS-E, W-2, AGV-1 and AGV-2. *Geostandard. Geoanal. Res.*, **28**, 417–429.
77. Simpson, L.A., Hearn, R. and Catterick, T. (2004) The development of a high accuracy method for the analysis of Pd, Pt and Rh in auto catalysts using a multi-collector ICP-MS. *J. Anal. Atom. Spectrom.*, **19**, 1244–1251.
78. Lásztity, A., Viczián, M., Wang, X. and Barnes, R.M. (1989) Sample analysis by on-line isotope-dilution inductively coupled plasma mass spectrometry. *J. Anal. Atom. Spectrom.*, **4**, 761–766.
79. Viczián, M., Lásztity, A., Wang, X. and Barnes, R.M. (1990) On-line isotope dilution by flow injection and inductively coupled plasma mass spectrometry. *J. Anal. Atom. Spectrom.*, **5**, 125–133.
80. Colodner, D.C., Boyle, E.A. and Edmond, J.M. (1993) Determination of rhenium and platinum in natural waters and sediments, and iridium in sediments by flow-injection isotope dilution inductively coupled plasma mass spectrometry. *Anal. Chem.*, **65**, 1419–1425.
81. Klinkenberg, H., Beeren, T., Van Borm, W., Van Der Linden, F. and Raets, M. (1993) Use of an enriched isotope as an on-line internal standard in inductively coupled plasma mass spectrometry: a reference method for a proposed determination of tellurium in industrial waste water by means of graphite-furnace atomic-absorption spectrometry. *Spectrochim. Acta B*, **48**, 649–661.
82. Vassileva, E. and Quétel, C.R. (2004) Certification measurement of the cadmium, copper and lead contents in rice using isotope dilution inductively coupled plasma mass spectrometry. *Anal. Chim. Acta*, **519**, 79–86.
83. Commission Regulation (EC) N 466/2001 of 8 March 2001 setting maximum levels for certain contaminants in foodstuff. *Official Journal of the European Communities* L077, 16/03/2001, 0001–0013.
84. Schmitt, K. and Isengard, H.D. (1998) Karl Fischer titration. A method for determining the true water content of cereals. *Fresen. J. Anal. Chem.*, **360**, 465–469.
85. Botha, A., Barzev, A.I., Linsky, S.M. and Fischer, J.L. (2005) A case study for the provision of measurement traceability and measurement uncertainty for the South African reference materials. *J. Anal. Atom. Spectrom.*, **20**, 1044–1050.

86. Myors, R.B., Nolan, A.L., Askew, S., Saxby, D.L., Hearn R. and Mackay, L.G. (2005) High-accuracy IDMS analysis of trace elements in wheat flour for the provision of reference values to a proficiency testing scheme. *J. Anal. Atom. Spectrom.*, **20**, 1051–1057.
87. Müller, M. and Heumann, K.G. (2000) Isotope dilution inductively coupled plasma quadrupole mass spectrometry in connection with a chromatographic separation for ultra trace determinations of platinum group elements (Pt, Pd, Ru, Ir) in environmental samples. *Fresen. J. Anal. Chem.*, **368**, 109–115.
88. McLaren, J.W., Myktyiuk, A.P., Willie, S.N. and Berman, S.S. (1985) Determination of trace metals in seawater by inductively coupled plasma mass spectrometry with preconcentration on silica-immobilized 8-hydroxyquinoline. *Anal. Chem.*, **57**, 2907–2911.
89. Balcaen, L., Geuens, I., Moens, L. and Vanhaecke, F. (2003) Determination of ultra-trace amounts of Fe in AgNO₃ solutions by means of isotope dilution analysis applying an inductively coupled plasma mass spectrometer equipped with a dynamic reaction cell. *Anal. Bioanal. Chem.*, **377**, 1020–1025.
90. Yoshinaga, J. and Morita, M. (1997) Determination of mercury in biological and environmental samples by inductively coupled plasma mass spectrometry with the isotope dilution technique. *J. Anal. Atom. Spectrom.*, **12**, 417–420.
91. Kim, C.-K., Seki, R., Morita, S., Yamasaki, S.-I., Tsumura, A., Takaku, Y., Igarashi, Y. and Yamamoto, M. (1991) Application of a high resolution inductively coupled plasma mass spectrometer to the measurement of long-lived radionuclides. *J. Anal. Atom. Spectrom.*, **6**, 205–209.
92. Perna, L., Bocci, F., Aldave de las Heras, L., De Pablo, J. and Betti, M. (2002) Studies on simultaneous separation and determination of lanthanides and actinides by ion chromatography inductively coupled plasma mass spectrometry combined with isotope dilution mass spectrometry. *J. Anal. Atom. Spectrom.*, **17**, 1166–1171.
93. Boulyga, S.F., Desideri, D., Meli, M.A., Testa, C. and Becker, J.S. (2003) Plutonium and americium determination in mosses by laser ablation ICP-MS combined with isotope dilution technique. *Int. J. Mass Spectrom.*, **226**, 329–339.
94. Moreno, J.M.B., Betti, M. and Nicolaou, G. (1999) Determination of caesium and its isotopic composition in nuclear samples using isotope dilution-ion chromatography-inductively coupled plasma mass spectrometry. *J. Anal. Atom. Spectrom.*, **14**, 875–879.
95. Resano, M., Gelaude, I., Dams, R. and Vanhaecke, F. (2005) Solid sampling-electrothermal vaporization-inductively coupled plasma mass spectrometry for the direct determination of Hg in different materials using isotope dilution with a gaseous phase for calibration. *Spectrochim. Acta B*, **60**, 319–326.
96. Gelaude, I., Dams, R., Resano, R., Vanhaecke, F. and Moens, L. (2002) Direct determination of methylmercury and inorganic mercury in biological materials by solid sampling-electrothermal vaporization-inductively coupled plasma–isotope dilution-mass spectrometry. *Anal. Chem.*, **74**, 3833–3842.
97. Becker, J.S., Pickhardt, C. and Pompe, W. (2004) Determination of Ag, Tl and Pb in few milligrams of platinum nanoclusters by on-line isotope dilution in laser ablation inductively coupled plasma mass spectrometry. *Int. J. Mass Spectrom.*, **237**, 13–17.
98. Tibi, M. and Heumann, K.G. (2003) Isotope dilution mass spectrometry as a calibration method for the analysis of trace elements in powder samples by LA-ICP-MS. *J. Anal. Atom. Spectrom.*, **18**, 1076–1081.
99. Tibi, M. and Heumann, K.G. (2003) Multi-element trace determinations in pure alkaline earth fluoride powders by high-resolution ICP-MS using wet-chemical sample preparation and laser ablation. *Anal. Bioanal. Chem.*, **377**, 126–131.
100. Boulyga, S.F. and Heumann, K.G. (2005) Direct determination of halogens in powdered geological and environmental samples using isotope dilution laser ablation ICP-MS. *Int. J. Mass Spectrom.*, **242**, 291–296.

101. Heumann, K.G., Rottmann, L. and Vogl, J. (1994) Elemental speciation with liquid chromatography-isotope dilution inductively coupled plasma isotope dilution mass spectrometry. *J. Anal. Atom. Spectrom.*, **9**, 1351–1355.
102. Hinojosa Reyes, L., Moreno Sanz, F., Herrero Espílez, P., Marchante-Gayón, J.M., García Alonso, J.F. and Sanz-Medel, A. (2004) Biosynthesis of isotopically enriched selenomethionine: application to its accurate determination in selenium-enriched yeast by isotope dilution analysis-HPLC-ICP-MS. *J. Anal. Atom. Spectrom.*, **19**, 1230–1235.
103. Diaz Huerta, V., Hinojosa Reyes, L., Marchante-Gayón, J.M., Fernández Sánchez, M.L. and Sanz-Medel, A. (2003) Total determination and quantitative speciation analysis of selenium in yeast and wheat flour by isotope dilution analysis ICP-MS. *J. Anal. Atom. Spectrom.*, **18**, 1243–1247.
104. Brown, A.A., Ebdon, L. and Hill, S.J. (1994) Development of a coupled liquid chromatography-isotope dilution inductively coupled plasma mass spectrometry method for lead speciation. *Anal. Chim. Acta*, **286**, 391–399.
105. Ebdon, L., Hill, S.J. and Rivas, C. (1998) Lead speciation in rain water by isotope dilution-high performance liquid chromatography-inductively coupled plasma mass spectrometry. *Spectrochim. Acta B*, **53**, 289–297.
106. Clough, R., Belt, S.T., Evans, E.H., Sutton, P., Fairman, B. and Catterick, T. (2003) Uncertainty contributions to species-specific isotope dilution analysis: Part 2. Determination of methylmercury by HPLC coupled with quadrupole and multicollector ICP-MS. *J. Anal. Atom. Spectrom.*, **18**, 1039–1046.
107. Wilken, R.D. and Falter, R. (1998) Determination of methylmercury by the species-specific isotope addition method using a newly developed HPLC-ICP-MS coupling technique with ultrasonic nebulization. *Appl. Organomet. Chem.*, **12**, 551–557.
108. Wahlen, R. and Wolff-Briche, C. (2003) Comparison of GC-ICP-MS and HPLC-ICP-MS for species-specific isotope dilution analysis of tributyltin in sediment after accelerated solvent extraction. *Anal. Bioanal. Chem.*, **377**, 140–148.
109. Rottmann, L. and Heumann, K.G. (1994) Determination of heavy metal interactions with dissolved organic materials in natural aquatic systems by coupling a high-performance liquid chromatography system with an inductively coupled plasma mass spectrometer. *Anal. Chem.*, **66**, 3709–3715.
110. Poperechna, N. and Heumann, K.G. (2005) Simultaneous multi-species determination of trimethyllead, monomethylmercury and three butyltin compounds by species-specific isotope dilution GC-ICP-MS in biological samples. *Anal. Bioanal. Chem.*, **383**, 153–139.
111. Monperrus, M., Martín-Doimeadios, R.C.R., Scancar, J., Amouroux, D. and Donard, O.F.X. (2003) Simultaneous sample preparation and species-specific isotope dilution mass spectrometry analysis of monomethylmercury and tributyltin in a certified oyster tissue. *Anal. Chem.*, **75**, 4095–4102.
112. Rodríguez-González, P., Ruiz Encinar, J., García Alonso, J.I. and Sanz-Medel, A. (2004) Development of a triple spike methodology for validation of butyltin compounds speciation analysis by isotope dilution mass spectrometry – Part I: synthesis of the spike, characterisation and development of the mathematical equations. *J. Anal. Atom. Spectrom.*, **19**, 685–691.
113. Barnes, R.M. (1996) Analytical plasma source mass spectrometry in biomedical research. *Fresen. J. Anal. Chem.*, **355**, 433–441.
114. Patriarca, M. (1996) The contribution of inductively coupled plasma mass spectrometry to biomedical research. *Microchem. J.*, **54**, 262–271.
115. Stürup, S. (2004) The use of ICPMS for stable isotope tracer studies in humans: a review. *Anal. Bioanal. Chem.*, **378**, 273–282.
116. Karpas, Z., Lorber, A., Elish, E., Kol, R., Roiz, Y., Marko, R., Katorza, E., Halicz, L., Riondato, J., Vanhaecke, F. and Moens, L. (1998) Uptake of ingested uranium after low acute intake. *Health Phys.*, **74**, 337–345.

117. Rodriguez-Cea, A., del Rosario Fernandez de la Campa, M., Garcia Alonso, J.I. and Sanz-Medel, A. (2006) The use of enriched ^{111}Cd as tracer to study *de novo* cadmium accumulation and quantitative speciation in *Anguilla Anguilla* tissues. *J. Anal. Atom. Spectrom.*, **21**, 270–278.
118. Whittaker, P.G., Lind, T., Williams, J.G. and Gray, A.L. (1989) Inductively coupled plasma mass spectrometric determination of the absorption of iron in normal women. *Analyst*, **114**, 675–678.
119. Ingle, C., Langford, N., Harvey, L.J., Dainty, J., Armah, C., Fairweather-Tait, S.J., Sharp, B.L., Crews, H.M., Rose, M. and Lewis, J. (2002) Development of a high-resolution ICP-MS method, suitable for the measurement of iron and iron isotope ratios in acid digests of faecal samples from a human nutrition study. *J. Anal. Atom. Spectrom.*, **17**, 1498–1501.
120. Vanhaecke, F., Balcaen, L., de Wannemacker, G. and Moens, L. (2002) Capabilities of inductively coupled plasma mass spectrometry for the measurement of Fe isotope ratios. *J. Anal. Atom. Spectrom.*, **17**, 933–943.
121. Schoenberg, R. and von Blanckenburg, F. (2005) An assessment of the accuracy of stable Fe isotope ratio measurements on samples with organic and inorganic matrices by high-resolution multicollector ICP-MS. *Int. J. Mass Spectrom.*, **242**, 257–272.
122. Walczyk, T. and von Blanckenburg, F. (2002) Natural iron isotope variations in human blood. *Science*, **295**, 2065–2066.
123. Yeung, G.S., Schauer, C.S. and Zlotkin, S.H. (2001) Fractional zinc absorption using a single isotope tracer. *Eur. J. Clin. Nutr.*, **55**, 1098–1103.
124. Beattie, J.H., Reid, M.D., Harvey, L.J., Dainty, J., Majsak-Newman, G. and Fairweather-Tait, S.J. (2001) Selective extraction of blood plasma exchangeable copper for isotope studies of dietary copper absorption. *Analyst*, **126**, 2225–2229.
125. Keyes, W.R. and Turnlund, J.R. (2002) Determination of molybdenum and enriched Mo stable isotope concentrations in human blood plasma by isotope dilution ICP-MS. *J. Anal. Atom. Spectrom.*, **17**, 1153–1156.
126. Stürup, S. (2000) Application of HR-ICP-MS for the simultaneous measurement of zinc isotope ratios and total zinc content in human samples. *J. Anal. Atom. Spectrom.*, **15**, 315–321.
127. De Wannemacker, G., Ronderos, A., Moens, L., Vanhaecke, F., Bijvelds, M.J.C. and Kolar, Z.I. (2001) Use of double-focusing sector field ICP-mass spectrometry in tracer experiments, aiming at the quantification of Mg^{2+} transport across the intestine of tilapia fish. *J. Anal. Atom. Spectrom.*, **16**, 581–586.
128. Ingle, C., Langford, N., Harvey, L., Dainty, J.R., Armah, C., Fairweather-Tait, S.J., Sharp, B., Rose, M., Crews, H. and Lewis, J. (2002) An ICP-MS methodology using a combined high-resolution/multi-collector detector system for the measurement of total zinc and zinc isotope ratios in faecal samples from a human nutrition study. *J. Anal. Atom. Spectrom.*, **17**, 1502–1505.
129. Field, M.P., Shapses, S., Cifuentes, M. and Sherrell, R.M. (2003) Precise and accurate determination of calcium isotope ratios in urine using HR-ICP-SFMS. *J. Anal. Atom. Spectrom.*, **18**, 727–733.
130. Ketterer, M.E. and Fiorentino, M.A. (1995) Measurement of Tl (III/I) electron self-exchange rates using enriched stable isotope labels and inductively coupled plasma mass spectrometry. *Anal. Chem.*, **67**, 4004–4009.
131. Mason, P.R.D., Kaspers, K. and van Bergen, M.J. (1999) Determination of sulfur isotope ratios and concentrations in water samples using ICP-MS incorporating hexapole ion optics. *J. Anal. Atom. Spectrom.*, **14**, 1067–1074.
132. Vanhaecke, F., De Wannemacker, G., Moens, L. and Van den haute, P. (2001) The use of sector field ICP-mass spectrometry for Rb-Sr geochronological dating. *Fresen. J. Anal. Chem.*, **371**, 915–920.
133. Vanhaecke, F., De Wannemacker, G., Moens, L. and Hertogen, J. (1999) The determination of strontium isotope ratios by means of quadrupole-based ICP-mass spectrometry: a geochronological case study. *J. Anal. Atom. Spectrom.*, **14**, 1691–1696.

134. Vanhaecke, F., Balcaen, L., Deconinck, I., De Schrijver, I., Almeida, C.M. and Moens, L. (2003) Mass discrimination in dynamic reaction cell (DRC) – ICP-mass spectrometry. *J. Anal. Atom. Spectrom.*, **18**, 1060–1065.
135. Willigers, B.J.A., Mezger, K. and Baker, J.A. (2004) Development of high precision Rb-Sr phlogopite and biotite geochronology; an alternative to Ar-40/Ar-39 tri-octahedral mica dating. *Chem. Geol.*, **213**, 339–358.
136. Robinson, L.F., Henderson, G.M. and Slowey, N.C. (2002) U-Th dating of marine isotope stage 7 in Bahamas slope sediments. *Earth Planet Sci. Lett.*, **196**, 175–187.
137. Barfod, G.H., Otero, O. and Albarède, F. (2003) Phosphate Lu–Hf geochronology. *Chem. Geol.*, **200**, 241–253.
138. Selby, D. and Creaser, R.A. (2004) Macroscale NTIMS and microscale LA-MC-ICP-MS Re-Os isotopic analysis of molybdenite: testing spatial restrictions of reliable Re-Os age determination and implications for the decoupling of Re and Os within molybdenite. *Geochim. Cosmochim. Acta*, **68**, 3897–3908.
139. Halliday, A.N. (2000) Terrestrial accretion rates and the origin of the Moon. *Earth Planet Sci. Lett.*, **176**, 17–30.
140. Schonbachler, M., Rehkämper, M., Halliday, A.N., Lee, D.C., Bourrot-Denise, M., Zanda, B., Hattendorf, B. and Günther, D. (2002) Niobium-Zirconium chronometry and early solar system development. *Science*, **295**, 1705–1708.
141. Willigers, B.J.A., Baker, J.A., Krogstad, E.J. and Peate, D.W. (2002) Precise and *in-situ* Pb–Pb dating of apatite, monazite and sphene by laser ablation multiple-collector ICP-MS. *Geochim. Cosmochim. Acta*, **66**, 1051–1066.
142. Stirling, C.H., Lee, D.C., Christensen, J.N. and Halliday, A.N. (2000) High-precision *in situ* U-238–U-234–Th-230 isotopic analysis using laser ablation multiple-collector ICP-MS. *Geochim. Cosmochim. Acta*, **64**, 3737–3750.
143. Potter, E.K., Stirling, C.H., Weichert, U.H., Halliday, A.N. and Spotl, C. (2005) Uranium-series dating of corals *in situ* with laser ablation MC-ICP-MS. *Int. J. Mass. Spec.*, **240**, 27–35.
144. Hirata, T. (2002) *In-situ* precise isotopic analysis of tungsten using laser ablation multi-collector inductively coupled plasma mass spectrometry (LA-MC-ICP-MS) with time resolved data acquisition. *J. Anal. Atom. Spectrom.*, **17**, 204–210.
145. Aggarwal, J.K., Sheppard, D., Mezger, K., and Pernicka, E. (2003) Precise and accurate determination of boron isotope ratios by multiple collector ICP-MS: origin of boron in the Ngawha geothermal system, New Zealand. *Chem. Geol.*, **199**, 331–342.
146. Gussone, N., Böhm, F., Eisenhauer, A., Dietzel, M., Heuser, A., Teichert, B.M.A., Reitner, J., Worheide, G. and Dullo, W.C. (2005) Calcium isotope fractionation in calcite and aragonite. *Geochim. Cosmochim. Acta*, **69**, 4485–4494.
147. Poitrasson, F. and Freydisse, R. (2005) Heavy iron isotope composition of granites determined by high resolution MC-ICP-MS. *Chem. Geol.*, **222**, 132–147.
148. Malinovsky, D., Rodushkin, I., Baxter, D.C., Ingri, J. and Ohlander, B. (2005) Molybdenum isotope ratio measurements on geological samples by MC-ICP-MS. *Int. J. Mass Spectrom.*, **245**, 94–107.
149. Rouxel, O., Ludden, J. and Fouquet, Y. (2003) Antimony isotopes variations in natural systems and implications for their use as geochemical tracers. *Chem. Geol.*, **200**, 25–40.
150. Maréchal, C. and Albarède, F. (2002) Ion-exchange fractionation of copper and zinc isotopes. *Geochim. Cosmochim. Acta*, **66**, 1499–1509.
151. Hall, E.S. and Murphy, E. (1993) Determination of sources of lead in tap water by inductively coupled plasma mass spectrometry. *J. Radioanal. Nucl. Chem.*, **175**, 129–138.
152. De Wannemacker, G., Vanhaecke, F., Moens, L., Van Mele, A. and Thoen, H. (2000) Lead isotopic and elemental analysis of copper alloy statuettes by double focusing sector field ICP-mass spectrometry. *J. Anal. Atom. Spectrom.*, **15**, 323–327.

153. Schultheis, G., Prohaska, T., Stingeder, G., Dietrich, K., Jembrih-Simburger, D. and Schreiner, M. (2004) Characterisation of ancient and art nouveau glass samples by Pb isotopic analysis using laser ablation coupled to a magnetic sector field inductively coupled plasma mass spectrometer (LA-ICP-SF-MS). *J. Anal. Atom. Spectrom.*, **19**, 838–843.
154. Ponting, M., Evans, J.A. and Pashley, V. (2003) Fingerprinting of Roman mints using laser-ablation MC-ICP-MS lead isotope analysis. *Archaeometry*, **45**, 591–597.
155. Niederschlag, E., Pernicka, E., Seifert, T. and Bartelheim, M. (2003) The determination of lead isotope ratios by multiple collector ICP-MS: a case study of early bronze age artefacts and their possible relation with ore deposits in the Erzgebirge. *Archaeometry*, **45**, 61–100.
156. Klein, S., Lahaye, Y., Brey, G.P. and Von Kaenel, H.M. (2004) The early Roman Imperial AES coinage II: tracing the copper sources by analysis of lead and copper isotopes – copper coins of Augustus and Tiberius. *Archaeometry*, **46**, 469–480.
157. Junk, S.A. and Pernicka, E. (2003) An assessment of osmium isotope ratios as a new tool to determine the provenance of gold with platinum-group metal inclusions. *Archaeometry*, **45**, 313–331.
158. Fortunato, G., Ritter, A. and Fabian, D. (2005) Old Masters' lead white pigments: investigations of paintings from the 16th to the 17th century using high precision lead abundance ratio. *Analyst*, **130**, 898–906.
159. Latkoczy, C., Prohaska, T., Stingeder, G. and Teschler-Nicola, M. (1998) Strontium isotope ratio measurements in prehistoric human bone samples by means of high-resolution inductively coupled plasma mass spectrometry (HR-ICP-MS). *J. Anal. Atom. Spectrom.*, **13**, 561–566.
160. Prohaska, T., Latkoczy, C., Schultheis, G., Teschler-Nicola, M. and Stingeder, G. (2002) Investigation of Sr isotope ratios in prehistoric human bones and teeth using laser ablation ICP-MS and ICP-MS after Rb/Sr separation. *J. Anal. Atom. Spectrom.*, **17**, 887–891.
161. Almeida, C.M. and Vasconcelos, M.T.S.D. (2001) ICP-MS determination of strontium isotope ratio in wine in order to be used as a fingerprint of its regional origin. *J. Anal. Atom. Spectrom.*, **16**, 607–611.
162. Coetzee, P.P. and Vanhaecke, F. (2005) Classifying wine according to geographical origin via quadrupole-based ICP-mass spectrometry measurements of boron isotope ratios. *Anal. Bioanal. Chem.*, **383**, 977–984.
163. Barbaste, M., Robinson, K., Guilfoyle, S., Medina, B. and Lobinski, R. (2002) Precise determination of the strontium isotope ratios in wine by inductively coupled plasma sector field multicollector mass spectrometry. *J. Anal. Atom. Spectrom.*, **17**, 135–137.
164. Fortunato, G., Mumic, K., Wunderli, S., Pillonel, L., Bosset, J.O. and Gremaud, G. (2004) Application of strontium isotope abundance ratios measured by MC-ICP-MS for food authentication. *J. Anal. Atom. Spectrom.*, **19**, 227–234.
165. Medina, B., Augagneur, S., Barbaste, M., Grouset, F.E. and Buat-Meard, P. (2000) Influence of atmospheric pollution on the lead content of wines. *Food Addit. Contam.*, **17**, 435–445.
166. Kersten, M., Garbe-Schönberg, C.-D., Thomsen, S., Anagnostou, C. and Sioulas, A. (1997) Source appointment of Pb pollution in the coastal waters of Efesus bay, Greece. *Environ. Sci. Technol.*, **31**, 1295–1301.
167. Moor, H.C., Schaller, T. and Sturm, M. (1996) Recent changes in stable lead isotope ratios in sediments of Lake Zug, Switzerland. *Environ. Sci. Technol.*, **30**, 2928–2933.
168. Townsend, A.T. and Snape, I. (2002) The use of Pb isotope ratios determined by magnetic sector ICP-MS for tracing Pb pollution in marine sediments near Casey Station, East Antarctica. *J. Anal. Atom. Spectrom.*, **17**, 922–928.
169. Outridge, P.M., Evans, R.D., Wagemann, R. and Stewart, R.E.A. (1997) Historical trends of heavy metals and stable lead isotopes in beluga (*Delphinapterus leucas*) and walrus (*Odobenus rosmarus rosmarus*) in the Canadian arctic. *Sci. Total Environ.*, **203**, 209–219.
170. Le Roux, G., Weiss, D., Grattan, J., Givélet, N., Krachler, M., Cheburkin, A., Rausch, N., Kober, B. and Shotyk, W. (2004) Identifying the sources and timing of ancient and medieval

- atmospheric lead pollution in England using a peat profile from Lindow bog, Manchester. *J. Environ. Monit.*, **6**, 502–510.
171. Buttigieg, G.A., Baker, M.E., Ruiz, J. and Denton, M.B. (2003) Lead isotope ratio determination for the forensic analysis of military small arms projectiles. *Anal. Chem.*, **75**, 5022–5029.
172. Gäbler, H.-E. and Bahr, A. (1999) Boron isotope ratio measurements with a double-focusing magnetic sector ICP mass spectrometer for tracing anthropogenic input into surface and ground water. *Chem. Geol.*, **156**, 323–330.
173. Cloquet, C., Rouxel, O., Carignan, J. and Libourel, G. (2005) Natural cadmium isotopic variations in eight geological reference materials (NIST SRM 2711, BCR 176, GSS-1, GXR-1, GXR-2, GSD-12, Nod-P-1, Nod-A-1) and anthropogenic samples, measured by MC-ICP-MS. *Geostandard Geoanal. Res.*, **29**, 95–106.
174. Ketterer, M.E., Hafer, K.M. and Mietelski, J.W. (2004) Assessing Chernobyl vs. global fallout contributions in soils from Poland using Plutonium atom ratios measured by inductively coupled plasma mass spectrometry. *J. Environ. Radioactiv.*, **73**, 183–201.
175. Izmer, A.V., Boulyga, S.F. and Becker, J.S. (2003) Determination of I-129/I-127 isotope ratios in liquid solutions and environmental soil samples by ICP-MS with hexapole collision cell. *J. Anal. Atom. Spectrom.*, **18**, 1339–1345.
176. Danesi, P.R., Bleise, A., Burkart, W., Cabianca, T., Campbell, M.J., Makarewicz, M., Moreno, J., Tuniz, C. and Hotchkins, M. (2003) Isotopic composition and origin of Uranium and Plutonium in selected soil samples collected in Kosovo. *J. Environ. Radioactiv.*, **64**, 121–131.
177. Gwiazda, R.H., Squibb, K., McDiarmid, M. and Smith, D. (2004) Detection of depleted uranium (DU) in urines of veterans from the 1991 Gulf War. *Health Phys.*, **86**, 12–18.
178. Vanhaecke, F., Stevens, G., De Wannemacker, G. and Moens, L. (2003) Sector field ICP-mass spectrometry for the routine determination of uranium in urine. *Can. J. Anal. Sci. Spectrosc.*, **48**, 251–257.
179. Tressl, I., De Wannemacker, G., Quérel, C.R., Petrov, I., Vanhaecke, F., Moens, L. and Taylor, P.D.P. (2004) Validated measurements of the uranium isotopic signature in human urine samples using magnetic sector-field inductively coupled plasma mass spectrometry. *Environ. Sci. Technol.*, **38**, 581–586.
180. Bijlsma, J.A., Slottje, P., Huizink, A.C., Twisk, J.W.R., Witteveen, A., van der Voet, G.B., de Wolff, F.A., Moens, L., Vanhaecke, F. and Smid, T. (submitted) Urinary uranium concentrations in a large cohort of professional assistance workers: an assessment of potential exposure to depleted uranium during the 1992 Air Disaster in Amsterdam. *New Engl. J. Med.*
181. Walczyk, T. and von Blanckenburg, F. (2005) Deciphering the iron isotope message of the body. *Int. J. Mass. Spectrom.*, **242**, 117–134.
182. Krayenbuehl, P.A., Walczyk, T., Schoenberg, R., von Blanckenburg, F. and Schulthess, G. (2005) Hereditary chromatosis is reflected in the iron composition of blood. *Blood*, **105**, 3812–3816.
183. Ohno, T., Shinohara, A., Chiba, M. and Hirata, T. (2005) Precise Zn isotopic ratio measurements of human red blood cell and hair samples by multiple collector ICP mass spectrometry. *Anal. Sci.*, **21**, 425–428.
184. Outridge, P.M., Chenery, S.R., Babaluk, J.A. and Reist, J.D. (2002) Analysis of geological Sr isotope markers in fish otoliths with subannual resolution using laser ablation-multicollector-ICP-mass spectrometry. *Environ. Geol.*, **42**, 891–899.
185. Outridge, P.M., Davis, W.J., Stewart, R.E.A. and Born, E.W. (2003) Investigation of the stock structure of Antarctic walrus (*Odobenus rosmarus rosmarus*) in Canada and Greenland using dental Pb isotopes derived from local geochemical environments. *Arctic*, **56**, 82–90.

Chapter 7

Alternative and Mixed Gas Plasmas

Andrew Fisher and Steve J. Hill

7.1 Introduction

In the vast majority of routine applications utilising an inductively coupled plasma (ICP), argon is used as the plasma gas. This reflects its relatively low cost (in most countries), its available in bulk with high purity and the fact that it has a sufficiently high ionisation energy (15.76 eV) to ensure that the majority of analytes will be at least partially ionised for ICP-MS analyses. Despite this, numerous gases have been added to, or have replaced argon for both MS and OES based plasmas. In some instances this is understandable, as in the case of the halogens that are at best only poorly ionised in argon. The use of a helium plasma (ionisation energy 24.59 eV) facilitates the determination of the halogens, since it is far more ionising. The presence of other gases can make the plasma more energetic and hence facilitate atomisation and subsequently ionisation or, in some cases, the alternative gas can be used to overcome interferences. The interferences may be spectral or physical in nature and may well be completely different for ICP-OES and ICP-MS instruments. This means that although the introduction of a particular gas may be beneficial for one system, it may serve no purpose or perhaps even be detrimental to the performance of the other. Examples of spectral interferences include the determination of phosphorus and sulphur by ICP-OES where these analytes have several analytical lines in the ultraviolet (UV) region that are interfered with by argon lines [1]. Similarly, analytes whose most sensitive lines are above 350 nm (where the argon possesses a structured background) tend to have relatively poor limits of detection (LODs). The majority of gases introduced have been molecular, although a few articles, notably those involving helium or xenon, have used atomic gases. However, many laboratories are limited by the cost of gases such as xenon.

The alternative gases are usually introduced via a gas blender and a mass flow controller. This instrumental arrangement facilitates very accurate and reproducible concentrations (between 0% and 100%) of the alternative gas to be bled into the normal argon flow. Some instrument manufacturers have added a facility to their equipment that enables alternative gases to be introduced without recourse to external blenders and mass flow controllers. The alternative gas may be bled into any of the three plasma gas flows, although introduction to the nebuliser (injector) and the coolant (plasma) gas flows is the most common. Other modifications to instrumentation may also be required. Some radio-frequency (rf) generators may cope adequately with the introduction of alternative gases, but others may

have a relatively poor impedance-matching network and hence be less tolerant. This will lead to excessive reflected powers, instability and possible plasma extinction. The frequency at which the generator operates has also been found to have an effect, with higher-frequency (hf) generators being more stable than lower frequency ones. Standard 40.68 MHz generators are therefore usually more suitable than 27.12 MHz generators and tend to operate with lower forward power [2]. It should be noted that plasmas operating with mixed gases tend to require higher forward powers than all-argon plasmas, although this difference in power is not as large as the early studies seemed to indicate. The hf generators (e.g. 54 and 64 MHz) have also been used. Modifications to the torch design may also be necessary for the introduction of some gases.

It is often necessary to light the plasma using only argon and then introduce the alternative gas gradually to the relevant gas inlet to allow the impedance-matching network to compensate. Attempting to light the plasma with the alternative gas is likely to lead to failure and may even result in damage to the torch. The exceptions to the above generalisations are the low/reduced pressure (and power) helium ICPs.

Several reviews have been published describing the application of mixed gas plasmas, including comprehensive accounts by Sheppard and Caruso [3], Durrant [4] and Montaser and van Hoven [5].

It should be noted that rigorous optimisation of plasma parameters is required to obtain optimum performance from the mixed or alternative gases since very different observation heights/sampling depths, different powers and different gas flow rates may be required when compared with all-argon plasmas. It is necessary to use multivariate procedures such as Simplex optimisation to determine how all the different parameters interact as well as doing univariate searches to determine effects of the individual parameters. It is also important to quote the criterion that is being optimised. This is because the use of an alternative gas may lead to an increase in sensitivity of an analyte, but if the background noise level is increased by a similar factor, there may be no overall improvement in figures of merit (FoMs), such as LOD. It is therefore important to quote whether it is the analyte signal, the signal-to-noise ratio, signal-to-background ratio, etc. that is being optimised. The use of a multivariate approach for optimisation may also overcome confusion arising from the fact that the introduction of an alternative gas often requires completely different operating parameters. Comparing LODs with and without an alternative gas using the same operating conditions will often indicate that the alternative gas has a detrimental effect. If however, LODs are compared under optimal conditions for each gas mix, then a completely different result may be obtained. This chapter discusses the uses of alternative gases that have been introduced to plasmas for both OES and MS instrumentation, and overviews their effects, benefits and disadvantages. The effects and benefits are quantified in terms of FoMs, which include LODs, precision, signal-to-background and signal-to-noise ratios, as well as plasma temperatures, electron densities and thermal conductivity. It is these properties of the plasma that are responsible for sample volatilisation, excitation and ionisation. A recent article by Bai *et al.* analysed the parameters of several mixed gas ICPs [6]. These authors found that when helium was added, the electron temperature increased but that the electron density is almost constant. Introducing xenon, however, was found to increase the electron density, but decrease the electron temperature. The effects of several other gases introduced to the plasma were also discussed.

Table 7.1 Physical properties of commonly used plasma gases

Plasma gas	Nominal isotopic mass	Isotopic abundance (%)	Ionisation energy (eV)	Thermal conductivity ($\text{J K}^{-1} \text{m}^{-1} \text{s}^{-1}$)	Metastable energy (eV)
Helium	4	99.999	24.59	0.141 ^a	$^1\text{S}_0 = 20.16$ $^3\text{S}_0 = 19.82$
Neon	20	90.51	21.56	0.0461 ^b	$^3\text{P}_0 = 16.76$ $3\text{P}_2 = 16.62$
	21	0.27			
	22	9.22			
Argon	36	0.337	15.76	0.0162 ^b	$3\text{P}_0 = 11.75$ $3\text{P}_2 = 11.55$
	38	0.0063			
	40	99.6			
Krypton	78	0.35	13.99	0.0086 ^b	$3\text{P}_0 = 10.56$ $3\text{P}_2 = 9.92$
	80	2.25			
	82	11.6			
	83	11.5			
	84	57.0			
	86	17.3			
Hydrogen	1	99.985	13.60	0.166 ^a	
	2	0.015			
Nitrogen	14	99.634	14.53	0.0237 ^b	
	15	0.366			
Oxygen	16	99.762	13.62	0.0242 ^b	
	17	0.038			
	18	0.2			

At ^a273 K and ^b293 K.

Plasmas in spectrochemistry have most commonly been formed using argon or a mixture of argon and nitrogen [7]. Table 7.1 gives some of the relevant characteristics for a variety of gases that have been used to form plasmas for both optical and mass spectrometry. Ideally, the gas should have:

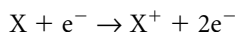
- (a) a high ionisation energy to facilitate the ionisation of elements with high ionisation potentials such as F, Cl, Br, I, As, Se, P and S;
- (b) high thermal conductivity to transfer heat from the outer region of the plasma, where coupling of the rf or microwave energy takes place, to the central core. However, if the thermal conductivity is too high, a large plasma becomes difficult to maintain due to rapid cooling by conduction to the surrounding atmosphere;
- (c) isotopes that do not interfere with, or give rise to any interferences with, the isotopic masses of analytically important elements;
- (d) electrical resistivity that falls in a suitable range to allow effective coupling and power dissipation;
- (e) low cost.

7.2 Ionisation effects

ICPs have maximum temperatures of around 10 000 K. At this temperature the gas forming the plasma has sufficient energy for partial ionisation to result, hence the formation of the plasma. For example, argon, hydrogen and nitrogen are calculated to be approximately 2% ionised at 10 000 K, assuming that only thermal ionisation prevails, reflecting the similarity in their ionisation energies. At the same temperature, the gases helium, neon, krypton and xenon would be approximately 0.01%, 0.1%, 5% and 15% ionised, respectively. However, these figures are not necessarily borne out in practise, for instance the degree of ionisation for the helium plasma is predicted to be extremely low, even at 10 000 K, so that formation of a plasma would be unlikely. Experimentally determined values of $T_{\text{rot}} \approx 2000\text{--}2500\text{ K}$, $T_{\text{exc}} \approx 4000\text{--}6000\text{ K}$ and $n_e \approx 4 \times 10^{13}\text{--}2 \times 10^{14}\text{ cm}^{-3}$ also yield widely divergent predictions for the extent of ionisation in a helium plasma. This indicates that local thermodynamic equilibrium (LTE) does not prevail in the helium ICP, nor always in plasmas formed with other gases.

Once atoms are formed in the ICP there are several pathways by which they can be ionised. The main mechanisms are:

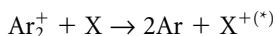
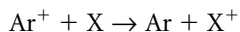
- (a) *Thermal ionisation*, caused by collisional energy exchange between atoms, ions and electrons:



- (b) *Penning ionisation*, caused by collisions between ground state atoms and argon metastable species:



- (c) *Charge-transfer ionisation*, caused by the transfer of charge between ions and atoms:



Ionisation energies for potential plasma gases are in the order $\text{He} > \text{Ne} \gg \text{Ar} > \text{N} > \text{Kr} > \text{O} > \text{Xe}$. Helium has proved popular as a plasma gas in microwave-induced plasma (MIP) generation by virtue of its ionisation energy and large number of metastable states that are involved in Penning ionisation, making it a more ionising plasma than would be expected just from consideration of the equilibrium temperature. Conversely, nitrogen plasmas are dominated by NO^+ , which dominates the upper limit of ionisation.

A convenient measure of the ionising capability of a plasma is the ionisation temperature, T_{ion} . For a typical argon plasma operated at 2 kW forward power and an observation height of 16 mm, $T_{\text{ion}} = 8730\text{ K}$ and $n_e = 4 \times 10^{15}\text{ cm}^{-3}$. The degree of ionisation, calculated using the Saha equation and assuming LTE, that would be expected in such a plasma,

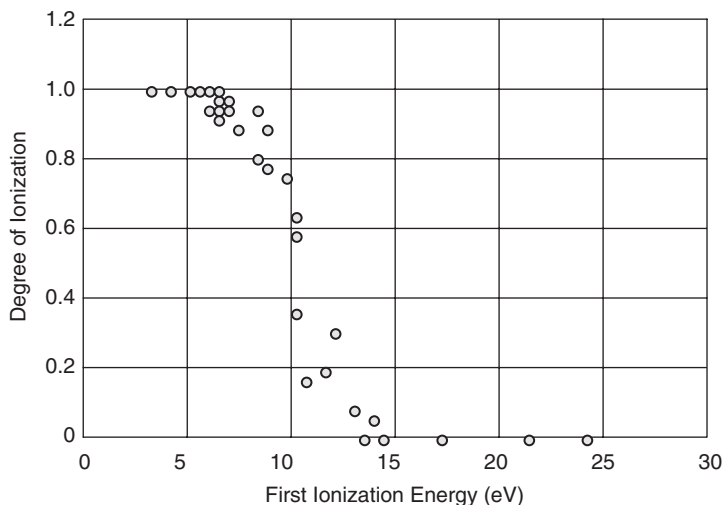


Figure 7.1 Plot of degree of ionisation against ionisation potential.

for elements with different ionisation potentials, is plotted in Fig. 7.1. It is evident that the degree of ionisation is over 90% for elements with first ionisation energies less than 9 eV. The ease with which elements are ionised follows the periodic trend of the elements, with the alkali and alkaline earth elements most easily ionised and the halogens least. However, since most elements have first ionisation energies of less than 9 eV the ICP is a suitable ion source for most element determinations. It is the metalloids, non-metals and halogens that are not ionised to such a large degree.

Temperature measurements have also been made for ICPs formed with molecular gases [7]. However, comparison between argon and molecular gas plasmas is hampered by lack of comparable experimental data. For instance, forward power and observation height will have a profound influence on the values for T_{ion} and n_e , and these variables tend to differ between groups and workers. In addition, the thermometric species (i.e. the way in which the temperature measurement was made) differs between workers, with different thermometric species often yielding substantially different values for temperature, even in the same plasma. However, it is generally agreed that the best method for the measurement of n_e is the Stark broadening of the H_{β} line, which is independent of thermal equilibrium. T_{ion} can then be calculated using the Saha equation and empirical measurements of selected atom/ion line ratios. In general, the degree of ionisation is poorer in molecular gas plasmas compared with argon, but can be improved somewhat by increasing the power.

Of all the gases used to form plasmas one would expect helium and neon to be the most favourable for ionisation since they have the highest ionisation energies of all the gases. There is limited experimental data available for helium plasmas (and none that is comparable for neon plasmas), so a definitive comparison is impossible. However, values for n_e are generally lower in helium than in argon plasmas, and T_{rot} is much lower, showing that the helium plasma is far from being in LTE. Another major problem in the operation

of a helium plasma is the propensity for a severe secondary discharge to occur in the expansion chamber. This causes an increase in the magnitude and spread of ion energies, making it difficult to find compromise ion-focusing conditions for analytes of widely differing m/z . It is also necessary to use a much higher pumping capacity and/or smaller sampling orifice due to the lower mass and reduced gas kinetic temperature of helium compared with argon [7].

7.3 Thermal conductivity

The thermal conductivities of the noble gases are in the order $\text{He} > \text{Ne} > \text{Ar} > \text{Kr} > \text{Xe}$, reflecting the relative viscosities of the gases (Table 7.1). As temperature increases, the thermal conductivities of these monatomic gases increase almost linearly up to the temperature at which ionisation occurs, and then rise more steeply because of the onset of ionisation to anywhere between 6000 and 10 000 K. The thermal conductivity of helium is the greatest of the monatomic gases so it is difficult to form a helium plasma with comparable thermal characteristics to an argon plasma. Heat is conducted away from the skin rapidly so that it becomes difficult to maintain the plasma or achieve a high power density.

The thermal conductivity of a diatomic gas is largely determined by the heat capacity of the gas, which is comprised of translational, rotational and vibrational components. At ambient temperatures diatomic gases are only translationally and rotationally excited, and this effectively determines the heat capacity of the gas. As the temperature increases, the molecule will begin to be vibrationally excited and the heat capacity will rise accordingly. When vibrational excitation is very great, the gas will begin to dissociate causing a further rapid and very large increase in heat capacity. The heat capacity will then decline as the gas becomes more and more dissociated until, upon complete dissociation, the heat capacity attains that of any monatomic gas. Subsequently the heat capacity will rise again as the gas becomes ionised. At ambient temperatures the thermal conductivity of hydrogen, nitrogen and oxygen are of the same order as the monatomic gases, but these differences become magnified greatly as the gases dissociate. Dissociation of oxygen and hydrogen starts at about 2500 K and is effectively complete at about 5000 K. The temperature at between 2 and 10 mm above the load coil in an oxygen plasma has been determined to be approximately 7000–10 000 K so such a plasma would be expected to be mainly comprised of monatomic species. However, it is reasonable to suppose that mixing of dissociated and un-dissociated gas and temperature gradients within the plasma, preclude such a simple interpretation. In comparison, the dissociation of nitrogen occurs between approximately 5000 and 9000 K, corresponding to a maximum thermal conductivity at around 7500 K. This overlaps the experimentally determined temperatures of approximately 7000–9000 K at between 10 and 20 mm above the load coil, so considerable dissociation and recombination are expected to occur at such temperatures.

Hence, plasmas formed entirely with molecular gases can be expected to have quite different thermal characteristics compared with plasmas formed with monatomic gases, and in practice they require much higher forward powers to sustain them. Such plasmas are typically operated at around 3 kW. However, molecular gas plasmas offer more efficient energy transfer from the skin to the central channel, and are often advantageous for decomposition of refractory or organic samples.

7.4 Use of alternative gases (mixed gas plasmas) in ICP-OES

7.4.1 Introduction of nitrogen

Nitrogen is one of the more popular gases to be introduced into plasmas. In the early days of plasma spectrochemistry, when the Greenfield torch was in common use, nitrogen was often used as a coolant for the plasma torches. This is because very high flow rates were required (up to 70 l min^{-1}) and nitrogen is substantially cheaper than argon. Since the vast majority of torches used nowadays are of the Fassel design, which is less tolerant of gases other than argon, nitrogen is used less routinely, but has still found several applications. In the past, numerous articles discussed the use of nitrogen plasmas and nitrogen as an addition to argon plasmas. These articles tended to use forward powers of several kW (some $>10\text{ kW}$), but more recently, powers of $1.2\text{--}2\text{ kW}$ have become more common.

The introduction of nitrogen into one or more of the plasma gas flows can have different effects depending on whether the plasma is a source for emission spectrometry or mass spectrometry and on which of the three gas flows it is introduced. The properties of the plasma with nitrogen addition have been reviewed in some detail [8].

The introduction of nitrogen to the nebuliser gas alters the physical shape of the plasma considerably, with a much wider annulus (central channel) and a shorter fireball being obtained, although the external diameter is unaffected. The wider central channel leads to reduced sample–plasma interaction [9,10]. If, however, the nitrogen is used to sustain the plasma, or is introduced to the coolant gas flow, a narrower central channel is produced, which leads to increased sample–plasma interaction. Increasing sample–plasma interaction assists in sample decomposition. It has been noted in the literature that nitrogen has been introduced successfully during the analysis of slurries and solids [11]. It has also been noted that introduction of nitrogen to the nebuliser gas does not assist in the decomposition of refractory slurry particles [12]. Introduction to the auxiliary gas flow affects both the central channel and the external diameter of the plasma [13]. The fundamental properties of the plasma are described by the temperatures (rotational, translational, electron and excitation), spectral line width and electron number density. Molecular gas ICPs tend to have higher temperatures than mixed gas ones. Comparison of an Ar–N₂ plasma and a N₂ plasma indicates that the rotational temperature for Ar–N₂ is $4500\text{--}5000\text{ K}$ whereas for N₂ it is $6000\text{--}8700\text{ K}$. Similarly, the excitation temperature has been reported to be $4500\text{--}7500\text{ K}$ for a mixed gas plasma, but $6000\text{--}9500\text{ K}$ for a N₂ plasma. The molecular gas ICPs tend to be closer to LTE than all-argon plasmas, and several studies of the electron number density of nitrogen plasmas have been made. In general, it has been found that the overall effects depended on whether the nitrogen was added to the nebuliser or auxiliary gas flow and on the amount added. A study by Sesi *et al.* [13] found that the addition of nitrogen depresses the electron concentration in the central channel and upper zones of the plasma. Addition to the nebuliser gas causes the largest decrease in electron density in the central channel. This was attributed to the higher heat capacity of nitrogen in comparison with argon (i.e. the nitrogen acts as an ‘energy sink’). Introduction to the auxiliary gas flow increased the electron density in the toroidal region. It was concluded that most of the energy was coupled from the load coil into the torus and that only a small proportion reached the central channel directly. Diffusional processes are relied on to transfer the

energy from the torus into the central channel and it was thought that the nitrogen 'sinks the energy' faster than it can be transferred.

The background spectral features for Ar-N₂ plasmas below 300 nm are basically the same as for an all-argon plasma, but are more complex between 300 and 500 nm. This may lead to problems when determining thallium at 351.9 nm and chromium at 425.4 nm. Similar background spectra are obtained using an ICP sustained by nitrogen.

7.4.2 Introduction of hydrogen

As with nitrogen addition, the introduction of hydrogen causes a thermal pinch effect on the plasma. The introduction of hydrogen via the nebuliser gas offers the greatest potential for the modification of the thermo-chemical properties of the plasma. A number of authors have reported improved detection limits and increased plasma temperatures and electron densities [14–18]. In the study by Shibata and co-workers [18], the hydrogen was introduced to the carrier gas that transports the analyte aerosol from a tungsten furnace electrothermal vaporiser into the plasma of an ICP-MS instrument. An optical fibre was used to obtain information on the electron number density ($n_e = 10^{13} \text{ cm}^{-3}$) and the excitation temperature ($T_{\text{exc}} = 5400 \text{ K}$) in the interface region. These values are higher than those obtained without hydrogen. The increase in n_e and T_{exc} resulted in enhanced ionisation of the analytes Ag, Bi, In, Pb, Te and Tl. The ion signals increased as the flow rate of hydrogen increased and the overall enhancement was dependent on the ionisation energy of the analyte. The use of hydrogen as an ad-mix to the carrier gas for electrothermal vaporisation (ETV) ICP-AES has been reported by Matousek and Mermet [19]. These authors found that enhancements in ionisation were achieved and hence the emission intensity of Cr(I) (an atom line) decreased, whereas the intensity for Cr(II) (an ion line) was enhanced. There was an overall improvement in analytical performance because the improved precision relative standard deviation (RSD) more than compensated for the increased background continuum emission. These authors also concluded that increased electron densities and excitation temperatures were achieved. The introduction of hydrogen (like nitrogen) to the nebuliser gas leads to plasma shrinkage and a widening of the central channel. The electron number density in the lower part of the plasma has been found to increase when hydrogen is introduced to either the nebuliser or the auxiliary gas flows. This has been attributed to an increase in the localised plasma power density. There is, however, a depression in the electron number density in higher regions of the plasma when hydrogen is introduced via the nebuliser gas flow. The increased plasma power density leads to an increase of approximately 1500 K in the electron temperature.

Although high levels of hydrogen (>15% v/v) have caused plasma instability, they have also been found to aid in the volatilisation of slurry particles. Data from Goodall [12] indicated that the recovery of several analytes from a firebrick slurry improved from approximately 60% in the absence of hydrogen to over 80% when 10% hydrogen was introduced through the nebuliser gas. Simplex optimisation of the procedure indicated that 6.08% v/v hydrogen yielded the best recovery for titanium. The increased ability to decompose refractory slurries was reflected in higher rotational temperatures in the plasma. This was attributed to the high thermal conductivity of hydrogen gas, which enables increased

energy transfer from the torus of the plasma to the annulus [16]. This has been supported by subsequent work by Sesi *et al.*, who found that the kinetic temperature throughout the entire plasma, in the presence of hydrogen in the nebuliser gas, increased by approximately 2000 K [13]. This increase is even larger if hydrogen is added to the auxiliary flow.

7.4.3 Introduction of hydrocarbon gases

Early work on the introduction of methane to the plasma via the nebuliser gas flow was carried out by Alder and Mermet [20]. By measuring the Stark-broadened H line at 486 nm they concluded that the presence of methane decreased the electron density from 6.1×10^{15} to $4.9 \times 10^{15} \text{ cm}^{-3}$.

Hydrocarbon gases have also been introduced to plasmas for atomic fluorescence determinations [21]. Typical operating parameters for ICP-AFS include a forward power of 300–700 W and a much higher observation height than for atomic emission spectrometry (AES) measurements. Introduction of 10 ml min^{-1} propane minimises the formation of metal oxides that have a dissociation energy of 4–6 eV. Introduction of 50 ml min^{-1} propane was found to be necessary before the refractory elements Mo, Ta, Ti and V fluoresced.

7.4.4 Introduction of halocarbon gases

Some of the gases described previously (e.g. nitrogen and hydrogen) modify the thermal properties of the plasma but the halocarbons modify the chemical environment, forming intermediate volatile species from refractory oxides. Halogenated gases have therefore been used as an aid to volatilisation during ETV sample introduction to both ICP-AES and ICP-MS plasmas [22–27]. Halocarbon gases have also been introduced to the plasma directly [28]. Up to 4.5% freon 116 (hexafluoroethane) was introduced to the nebuliser flow, although higher concentrations were found to attack the injector and auxiliary tubes of the torch. It was found that the freon could be used as an aid to particle decomposition during slurry analysis [28]. A slurry of firebrick (ECRM 776-1) was aspirated and the presence of 4% freon enabled a Ti recovery of close to 100% to be obtained compared with only 68% in its absence. It was also noted that the emission intensity decreased as the amount of freon increased and that the calibration curves deviated from linearity at higher analyte concentrations. It is this deviation from linearity that led to the increased recovery of the titanium from the slurry. The cause of the deviation was attributed to the formation of a classical mass action buffer system involving metal fluorides. This was confirmed by the identification of AlF in the plasma.

7.4.5 Introduction of oxygen

Oxygen has been introduced to both ICP-AES and ICP-MS plasmas. It has been found that certain interferences (e.g. the CN bands) can be removed by the addition of oxygen, although this can also be achieved using higher forward power. It has also been noted that the spectrum between 300 and 500 nm for an O_2 -Ar plasma is less complex than for either an N_2 -Ar or an all-Ar plasma.

The plasma temperatures for an O₂–Ar plasma tend, on the whole, to be slightly higher than for an all-Ar plasma, but lower than for N₂–Ar or air–Ar plasmas (excitation temperature ~1500 K lower, rotational temperature ~900 K lower). The excitation temperature has been reported to be 3500–6800 K [29] and the rotational temperature 4000–5000 K [30]. The overall effect depends on the amount of oxygen added, but the highest excitation temperature was observed when 10% oxygen was introduced to the coolant flow (6800 K), dropping to 4200 K when the coolant gas is pure oxygen. The electron number density measurements mirror this pattern, with very high density being observed with 10% O₂ in the coolant (much higher than for an argon plasma), dropping substantially when the argon coolant is replaced entirely by oxygen. Similarly, the net signal intensity and signal-to-noise ratio for the high excitation energy cadmium line is optimal at 10% added oxygen, but higher percentages have an adverse effect [31]. A recent application of a mixed argon–oxygen plasma has been reported by Edlund and co-workers [32]. These workers studied the effects of oxygen addition to each of the three gas flows of the plasma during the analysis of biodiesel diluted 1:4 with kerosene. A nebuliser flow rate of 0.35 l min⁻¹ oxygen and 0.8 l min⁻¹ argon was found to be the most efficient method of oxygen addition. The effect was to improve the LODs for the analytes which was attributed to an increase in signal-to-noise ratio arising from the decreased emission signal from carbon and carbon-containing compounds. A recent article by Chirinos *et al.*, has compared argon, argon–oxygen and argon–helium plasmas [33]. These authors used a direct injection, high-efficiency nebuliser (DIHEN) to introduce microlitre volumes of sample and then measured the Mg(II) 280.27 nm/Mg(I) 285.213 nm intensity ratios. It was found that small amounts of He or O₂ (5%) added to the coolant gas flow increased the ion to atom emission ratio (i.e. made the plasma more energetic). Since the plasma had improved excitation conditions, potential spectroscopic and matrix interferences were minimised.

Plasmas made entirely of oxygen have very high temperatures (excitation temperature of 6000–11 000 K and electron temperatures of 6500–10 500 K) [34]. As with most molecular gas ICPs, the oxygen plasma is regarded as being closer to LTE than an argon plasma. Electron density in the middle of an oxygen plasma has been found to be $5 \times 10^{15} \text{ cm}^{-3}$ under typical operating conditions.

7.4.6 Introduction of helium and other noble gases

In many countries, these gases are substantially more expensive than argon. The use of neon, xenon and krypton has therefore been relatively limited, although helium has found several applications. Helium has a very high thermal conductivity when compared with argon, and so an increase in kinetic temperature is obtained, although the electron temperature and the electron concentration appear to be relatively unaffected [13]. It is the increase in kinetic temperature that leads to the enhancement of the ionisation potential of the plasma and it is this property that makes helium so useful when the halogens or other hard-to-ionise analytes are to be determined. Introduction of approximately 17% helium to the nebuliser gas appears to increase the electron density in the annulus but decrease it in the lower regions of the torus. Both of these changes are slight, however. A small reduction in electron density is obtained when helium is added to the auxiliary gas flow, the shape of the plasma is found not to change dramatically. Helium ICPs have been developed but sustaining

them is far more difficult than for argon plasmas. This is because of helium's high electrical resistivity and high thermal conductivity. Often the discharge is sustained at reduced pressure [35], but atmospheric helium plasmas have also been sustained. The fundamental properties of atmospheric-pressure helium ICPs have been reported by Cai *et al.* [36]. Using high resolution Fourier transform spectrometry, these authors found that the line widths for Fe were similar to those in an argon plasma, but that the H and He line widths in a dry plasma were larger than those from a wet plasma. The excitation temperature was dependent on the energy levels of the thermometric species and increased in the presence of water vapour, but was found to be lower than that in an argon plasma. Similarly, the rotational temperature was also substantially lower than that found in an argon plasma. The appearance of an annular helium plasma differs markedly to that of an argon plasma. It tends to be filament shaped and have a pinkish tinge to it. Often specialised torches are required, although a helium plasma can be formed in a modified Fassel torch. It has also been found that the electron number density of a helium plasma ($4.8 \times 10^{13} \text{ cm}^{-3}$) is approximately 25 times less than for a comparable argon plasma [37]. Increasing the forward power from 1.5 to 2.5 kW increases the electron number density by a factor of 2 and raises the rotational temperature by 400 K. No improvements in the LOD were reported and at increased power, the plasma extended to an excess of 30 cm in length [38].

The atomic emission spectra of xenon, neon and krypton from 200 to 900 nm have been determined in a sealed ICP-AES by Jacksier and Barnes [39]. The plasma power was only 350 W.

7.4.7 Air plasmas for ICP-AES

Air ICPs are obviously cheap to operate and can withstand higher solvent and analyte loadings than their argon counterparts. These advantages encouraged two instrument manufacturers to develop commercial instrumentation for process control applications, although these instruments are now no longer available. Often, modifications to the torch and the generator are necessary to form the plasma. Several articles have been published on this subject, including one by Yang and Barnes [40] and another by Meyer and Barnes [41]. Abdallah and Mermet [42] used a 6 kW, 54 MHz generator together with a specially designed torch surrounded by a seven-turn load coil to produce an air plasma.

A low-power air-Ar plasma has been reported by Tang *et al.* [43] that was sustained on a commercial 40.7 MHz spectrometer. The molecular bands from CN to C₂ were eliminated even when organic solvents were introduced. Detection limits of analytes in isobutyl methyl ketone (IBMK) were superior or comparable to those found in a pure argon plasma. As an application, waste oil diluted in xylene was analysed.

7.4.8 Carbon dioxide plasmas

There have been very few attempts to generate a carbon dioxide plasma. Yang *et al.* [44] were successful in their attempt and generated a carbon dioxide plasma using a power of 2.3 kW. The background spectrum between 190 and 900 nm was investigated and it was

discovered that the spectrum was rich in molecular bands (CO , CN , CO^+ and C_2) below 520 nm, but above this wavelength, the background spectrum was relatively flat.

7.4.9 Multiple gas plasmas

Although it is not common, there have been reports of plasmas that have a mixture of alternative gases introduced to them. One example includes the ternary mixture of argon, helium and nitrogen [45]. The authors determined the effects of the mixture on seven different analytes (Ba, Ca, Cd, Fe, Mg, Y and Zn). It was concluded that the ternary mixture improved the signal-to-background ratio because the helium suppressed the increase in background signal caused by the nitrogen.

7.5 Mixed gas plasmas for use with ICP-MS

Different plasma gases will have different isotopic compositions, as indicated in Table 7.1. The atomic masses of these isotopes will greatly influence the interferences in the mass spectrum of a plasma, particularly when a complex matrix is present. Such spectroscopic interferences are caused by atomic or molecular ions having the same nominal mass as the analyte of interest, thereby interfering with analysis by causing an erroneously large signal at the mass-to-charge (m/z) ratio of interest. One type of interference is caused by overlapping isotopes of different elements. These interferences, termed isobaric interferences, are easy to predict and well documented so they can easily be overcome by using alternative isotopes or elemental equations for analysis. The second category is that of molecular or polyatomic ion interferences caused by polyatomic ions formed from precursors in the plasma gas, entrained atmospheric gases, water, acids used for dissolution and the sample matrix. The polyatomic ions so formed may then result in interferences on analytes with the same nominal m/z .

Interferences caused by the plasma gas, entrained gases and water are present regardless of whether a sample is being analysed and are dependent to a large extent on the isotopic composition of the plasma gas. For instance, consider a plasma comprised of argon, which has the isotopes ^{36}Ar , ^{38}Ar and ^{40}Ar . Entrained atmospheric air will contribute the isotopes of nitrogen and oxygen, and if water is nebulised into the plasma then all the isotopes of hydrogen and oxygen will also be present from this source and it is possible to observe many polyatomic ions in the mass spectrum up to the Ar_2^+ species at m/z 80. Many of the polyatomic ions at lower m/z interfere with the determination of transition elements, the interference of ArO^+ on Fe at mass-to-charge ratio (m/z) 54, 56 and 58 being a particular example. In comparison, if helium is used as the plasma gas then the polyatomic ions will be confined to the mass spectrum below HeO^+ at m/z 22, and hence, far fewer interferences arise.

There is also the possibility that molecular ions may form from constituents of the sample matrix in combination with the plasma gas, entrained atmospheric gases and water. Matrix elements that cause particular problems are Cl, K, Na, Ca, Mg, Al, Si, S and P since they are often found at high concentrations in many samples or acids that are used for dissolution. In addition, individual samples can cause particular problems, such as the interference of $^{196}\text{Pt}^1\text{H}$ on ^{197}Au when determining ^{197}Au in platinum bullion.

7.5.1 Introduction of nitrogen

Nitrogen addition to MS-based plasmas has been successful in overcoming many interferences. Several articles have introduced nitrogen as an ad-mix to either the nebuliser or the coolant gas flows to overcome polyatomic interferences [46–52]. There is disagreement between authors as to which of the argon flows the nitrogen should be introduced. Additions to both the nebuliser and coolant have advantages and disadvantages. The advantage of adding nitrogen to the coolant flow are claimed to be better analytical utility, but it may lead to reduced plasma stability and, for some instruments, a possible increase in reflected power. Introduction to the nebuliser gas flow causes less plasma disturbance and is more efficient; that is, less nitrogen is required to obtain the same results when compared with introduction to the coolant (3–4% v/v compared with 5–10% v/v). Again, introduction of nitrogen causes a change in the shape of the plasma and hence re-optimisation of the nebuliser flow rate and sampling depth will be necessary to ensure that maximum sensitivity is obtained.

Several interferences have been overcome. The majority of these are chloride-based polyatomic interferences such as those by $^{40}\text{Ar}^{35}\text{Cl}^+$ on $^{75}\text{As}^+$ and by $^{40}\text{Ar}^{37}\text{Cl}^+$ on $^{77}\text{Se}^+$. The mechanism by which these interferences are overcome appears to be direct competition between argon and nitrogen to combine with the chloride. As the amount of nitrogen increases, the amount of $^{40}\text{Ar}^{35}\text{Cl}^+$ decreases, but the amount of $^{14}\text{N}^{37}\text{Cl}^+$ increases. This is not a problem unless vanadium at m/z 51 ($^{14}\text{N}^{37}\text{Cl}^+$) or titanium at m/z 49 ($^{14}\text{N}^{35}\text{Cl}^+$) is also being determined. In addition to these polyatomic interferences being overcome, the addition of nitrogen may also decrease the amount of metal oxide (MO^+) interference and also decrease interferences from ArO^+ ($^{56}\text{Fe}^+$), CCl^+ ($^{47}\text{Ti}^+$ or $^{49}\text{Ti}^+$), ClO^+ ($^{51}\text{V}^+$) and Cl_2^+ (Ge). It should be noted that the amount of MO^+ increases again if over 5% v/v nitrogen is added to the nebuliser gas. There appears to be no evidence of MN^+ or M^{2+} formation. Introduction of nitrogen to the auxiliary gas flow appears to yield no beneficial effects [53]. There have been several more recent reports that reconfirmed the original findings [54–57]. Nitrogen introduction techniques therefore facilitate the accurate determination of analytes such as arsenic in samples such as seawater, clinical materials and other matrices containing high levels of chloride.

Instead of focusing on practical applications, some researchers have concentrated on the more theoretical aspects of nitrogen addition. Lam and Horlick assessed the effects of sampler–skimmer cone separation by comparing an all-Ar plasma with a 5% nitrogen-in-Ar plasma (the nitrogen being introduced to the coolant flow) [58]. Generally, as the separation distance increased (from 0.61 to 1.18 cm) for an all-Ar plasma, the response of the analyte and interferent species fell, although the exceptions were ArN^+ and ArOH^+ , which increased. The same was not found for the N_2 -Ar plasma. The response increased when the separation increased to 0.84 cm before decreasing again at higher separation distances. Again, the exceptions were ArN^+ and ArOH^+ . This implies that the addition of nitrogen was having an effect on the dimensions of the barrel shock and Mach disc position within the interface and that this had implications for the mechanism of polyatomic ion removal. More recently, nitrogen has been used to sustain (in part) the plasma during ICP-MS analyses [57]. Nitrogen replaced argon in the nebuliser and auxiliary flows and was also present in the coolant, although argon was also added to this flow to sustain a stable plasma. It was found that nitrogen-containing polyatomic interferences increased, but that

the Ar^+ signal was weak. Analytes such as arsenic and selenium that are adversely affected by argon-containing polyatomic interferences could therefore be determined. It was, however, noted that the analytical sensitivity in the nitrogen plasma was similar to that in an argon plasma for those analytes with low ionisation energy (<6.5 eV) but was poorer for those with ionisation energy >6.5 eV.

Nitrogen has a mixed effect on the sensitivity of analyte determinations. Some workers have described enhancements, others have reported suppressions and some have found both, depending on the amount of nitrogen added or on the mass of the analyte. It is worth repeating here that direct comparisons with all argon plasmas can be difficult unless optimised conditions are used. Similarly, if a multivariate optimisation procedure is used, the analyst should determine what is being optimised (e.g. analyte signal, signal-to-background ratio, signal-to-noise ratio or detection limits). Introduction of 4% v/v to the nebuliser flow rate has been found to decrease the overall sensitivity (by a factor of about 3). Despite this drop in sensitivity, for analytes where the introduction of nitrogen helps overcome a serious interference effect, the LOD is normally improved.

Non-spectroscopic interferences have also been removed using nitrogen. An example of this was reported by Xiao and Beauchemin [59], who found that the suppression of signals of analytes throughout the mass range by 0.1 M sodium solutions in an argon plasma could be removed if 10% nitrogen was introduced to the coolant gas flow. A reduction of mass discrimination effects compared with an all-argon plasma were also reported. A mixed nitrogen–argon plasma has also been reported to both increase sensitivity and decrease mass discrimination effects in an article that described the determination of lead isotope ratio measurements in samples by LA-ICP-MS [60]. In another study, Holliday and Beauchemin used a 4% nitrogen–96% argon plasma to determine molybdenum in seawater diluted twofold with de-ionised water [61]. By altering the sampling depth from within the plasma to 2 mm away from optimal sensitivity, robust operating conditions could be obtained that suffered far less from non-spectroscopic interferences. The authors concluded that although the formation of $^{40}\text{Ar}^{35}\text{Cl}^+$ was partially inhibited, the presence of so much chloride still prohibited the direct determination of $^{75}\text{As}^+$ in this particular matrix. The determination should, however, still be possible when somewhat less chloride is present.

7.5.2 Introduction of hydrogen

The effect of introducing hydrogen to ICP-MS plasmas have been discussed by several workers [62–64]. It has been found that the addition of hydrogen leads to signal suppression of heavier analytes relative to the lighter ones. It also degrades the signal-to-background and signal-to-noise ratios. It can, however, be used to remove some polyatomic interferences, for example it decreased MO^+ polyatomics to one-tenth of that obtained in the absence of hydrogen, but was found to have no effect on ArCl^+ , ArO^+ or ClO^+ [64]. LODs achieved under optimised conditions were fivefold better for ^{155}Gd when using hydrogen addition. There is a possibility of MH^+ formation, but this was found to be negligible unless very high concentrations of analyte were present and was therefore not a problem for natural samples. Interestingly, much of the work performed on the addition of hydrogen to ICP-MS instrumentation has concentrated on its introduction to dry plasmas (i.e. where samples are introduced via a desolvation device or by ETV). The hydrogen that would normally be

obtained from an aqueous matrix is therefore not present unless it is added directly via one of the gas flows. Hartley *et al.* [63] discussed this and concluded that hydrogen had to be added to ensure sufficient energy transfer from the torus to the central channel.

7.5.3 Introduction of hydrocarbon gases

Hydrocarbon gases have been introduced to the nebuliser gas flow of ICP-MS plasmas to overcome polyatomic interferences. Several gases have been used, including methane and ethane. Methane has been used by several workers including Allain *et al.* [65], Wang *et al.* [48] and Hill *et al.* [66]. Care must be taken to avoid carbon produced as a decomposition product from clogging the sampling cone, leading to excessive signal drift. Methane introduced through the nebuliser flow was particularly successful at reducing interferences arising from argon and chlorine combinations and hence facilitated the determination of arsenic and selenium. Introduction of up to 1% v/v methane was admissible to the plasma before instability occurred. Simplex optimisation of the working conditions indicated that a relatively low power (1250 W) and a high nebuliser flow rate (1 l min^{-1}) were required [66].

Introduction of methane to the coolant gas flow was far less successful. The plasma became less tolerant and could withstand concentrations of only 0.2% v/v before becoming very unstable. In addition, interferences were not reduced and ArO^+ actually increased, thereby deteriorating the Fe detection limit. Introduction to the auxiliary flow was also unsuccessful, although to a lesser extent than introduction to the coolant flow. The introduction of ethene to the nebuliser gas flow at a concentration of up to 0.5% v/v has also been achieved. This proved to be successful in overcoming numerous polyatomic interferences, although a constant flow of water into the plasma was required to prevent the accumulation of carbon particles on the sampling cone. Ebdon *et al.* have described the utilisation and advantages of ethene introduction [67]. The interference arising from ArCl^+ could be eliminated completely even at chloride concentrations of 33 mg ml^{-1} . Optimisation indicated that a higher nebuliser flow was required but that normal powers could be used. Similarly, a higher nebuliser flow rate was required to decrease the interference from ArO^+ on iron determinations. The LOD for iron was therefore improved. Similar improvements were obtained for the LODs of $^{63}\text{Cu}^+$ and $^{62}\text{Ni}^+$ (removal of NaAr^+ and Na_2O^+ , respectively). In addition to these interferences being removed, the addition of ethene also removed the interference effects exerted by ClO^+ , thereby facilitating vanadium determinations; that is, the formation of ClO^+ was reduced to 0.2% of its original value and polyatomic interferences arising from digestion acids (SO_2^+ , S_2^+ and PO_2^+) were overcome. In some cases, the improvements in LOD were substantial; for example, the use of ethene removed the PO_2 interferent during Cu determinations and improved the LOD by a factor of over 100. Overall, the use of ethene was shown to be far more beneficial for ICP-MS determinations when compared with either hydrogen or methane.

7.5.4 Introduction of oxygen

The only real use for oxygen in ICP-MS is to burn off carbon produced during aspiration of organic solvents or from samples with a high dissolved/suspended solids content. If carbon from such samples is not burned away from the cones, the sample cone may become

clogged, which leads to excessive signal drift until, when blocking is complete, no ions reach the detector and hence no signal is obtained. There are two main problems associated with the introduction of oxygen to ICP-MS determinations: it may exacerbate polyatomic interferences (e.g. MO^+ or ArO^+) and, equally importantly, it may have a severely deleterious effect on the cone. An excess of oxygen will burn a large hole through a standard nickel cone, which would curtail its useful lifetime substantially (possibly decreasing it to only a few minutes if a large excess is introduced). A balance between the amount of organic material and the amount of oxygen introduced is therefore required. The amount of oxygen introduced to the nebuliser flow varies according to the organic solvent/sample being analysed, but is typically 2%–5%, although much higher proportions (20%) have also been reported [68]. Platinum-tipped cones may be used as these have a higher resistance to oxidative attack. Applications where oxygen has been introduced are common and so only a few select examples are given here [69, 70]. The facility to introduce oxygen to assist in the analysis of organic solvents has now been adopted by instrument manufacturers who have incorporated a calibrated 'alternative' gas inlet, thus allowing accurate additions.

A more extreme case using a plasma in which the nebuliser and auxiliary gas flows were comprised of oxygen but with argon in the coolant flow to maintain stability has been sustained by Uchida and Ito [71]. The plasma operated at a power of 2.4 kW and maximum signal was obtained with a nebuliser flow of 1.41 l min^{-1} . The sensitivity of the technique was found to be inferior to that of Ar or N_2 plasmas and decreased further with increasing mass number of the analyte. In addition, it was found that there was a higher ratio of doubly charged to singly charged ions and the ratio of MO^+ to M^+ also increased.

7.5.5 Introduction of helium and other noble gases

For ICP-MS studies, the use of helium has several advantages. It is more ionising, therefore hard-to-ionise elements such as the halogens may be determined more readily. It can also circumvent many of the troublesome polyatomic interferences associated with argon (e.g. ArO^+ on ^{56}Fe , ArCl^+ on ^{75}As and ArNa^+ on ^{63}Cu , etc.). The major drawback is that of cost. Few laboratories can afford to use helium at flow rates of several litres per minute for extended periods of time. Several articles have been published recently involving the application of helium ICP-MS both to atmospheric-pressure plasmas [72–74] and to reduced-pressure plasmas [75]. Whereas most reduced-pressure plasmas have been coupled to gas chromatography [76,77], some reports have indicated that solutions may be nebulised, although the need for desolvation systems was highlighted [78,79]. An alternative sample introduction method has been described by Hayashi and co-workers who used ETV to introduce $10 \mu\text{l}$ aliquots of hair digests [80]. Four analytes were determined simultaneously with precision of better than 10% RSD. LODs were at the sub-ppb level. Nam *et al.* [81] indicated that the atmospheric helium plasma might be prone to matrix effects. Increasing concentrations of sulphate, sodium and uranium were found to enhance the signals of As and Br, but this could be corrected by the use of Se as an internal standard. Likewise, the addition of helium will generally improve the ionisation characteristics of an argon plasma.

Xenon has been introduced at $10\text{--}37 \text{ ml min}^{-1}$ to the nebuliser gas of an ICP-MS instrument [82]. It was found that its presence reduced the interference effects exerted by species such as N_2^+ , HN_2^+ , NO^+ , ArH^+ , ClO^+ , ArC^+ , ClOH^+ , ArN^+ and ArO^+ , thereby facilitating

determination of ^{28}Si , ^{29}Si , ^{39}K , ^{41}K , ^{51}V , ^{52}Cr , ^{54}Cr , ^{54}Fe and ^{58}Fe . Xenon has also been introduced at 1.5% to the nebuliser flow to try and elucidate the charge-transfer reactions that occur between xenon ions and iron atoms [83]. It was concluded that xenon had little effect on the electron number density or the iron atom-line emission intensities, but that the iron ion-line intensities were enhanced. A recent publication has described the use of a neon-based plasma for LA-ICP-MS measurements of solid samples [84]. Although the overall picture was complicated by the very different operating conditions required between the neon and argon plasmas (especially the nebuliser gas flow), it was concluded that sensitivity was reduced when compared with argon plasmas. However, it was also noted that the presence of argon-based interferences (e.g. $^{63}\text{Cu}^{40}\text{Ar}^+$ and $^{65}\text{Cu}^{40}\text{Ar}^+$) were reduced in the neon plasma, thus facilitating the determination of $^{103}\text{Rh}^+$ and $^{105}\text{Pd}^+$ in a copper sulphide sample. Similarly, a nickel sulphide sample was analysed for $^{98}\text{Ru}^+$ and $^{100}\text{Ru}^+$ which would otherwise have suffered interferences from $^{58}\text{Ni}^{40}\text{Ar}^+$ and $^{60}\text{Ni}^{40}\text{Ar}^+$, respectively.

7.5.6 Air plasmas for ICP-MS

Uchida and Ito [85] have used an air plasma as an ion source for mass spectrometry. The coolant and nebuliser flows were made up completely of air, but argon at a flow rate of 1.5 l min^{-1} was required in the auxiliary gas to sustain a stable plasma. Using a modified torch, the analyte signal was found to increase with increasing power, but 2 kW was found to be sufficient to maintain a stable discharge. Under optimised conditions, N^+ , O^+ and NO^+ gave strong signals, but Ar^+ was very weak. The air ICP-MS therefore yielded results comparable to the nitrogen ICP-MS. Sensitivity was found to be improved for analytes with low ionisation energy ($<6.5\text{ eV}$) but inferior for analytes with higher ionisation energy when compared with an all-Ar plasma. These results are also similar to those achieved using a nitrogen plasma.

7.6 Low-pressure plasmas

Reduced-pressure ICPs have been studied using AES principally to investigate excitation processes within the plasma [86–90]. Smith and Denton [91] have performed a study of the effects of pressure on the operation of an ICP. They observed that plasmas of most gases would form easily under reduced pressure even without initial excitation from a tesla coil.

There are a number of advantages of using low-pressure ICPs coupled with mass spectrometry. First, the removal of entrained air from the plasma-sampling interface results in fewer polyatomic interferences in the background spectra. Second, because it is easy to form a plasma in almost any gas, careful selection of the gas can reduce unwanted isobaric interferences. Third, low-pressure ICPs can be sustained with low gas flows, therefore reducing the gas consumption. However, the main advantage of the low-pressure plasma has been its use as a tunable ion source for mass spectrometry, yielding both atomic and molecular ions. Traditionally, plasma sources have been operated at atmospheric pressure and used to atomise the total sample, producing mostly atomic ions. If qualitative determination of molecular structure or weight are required, it is necessary to use an alternative ion source such as electron impact (EI), electron ionisation (ESI), chemical ionisation (CI)

or fast atom bombardment (FAB) – see Chapter 8. These sources, in combination with MS-MS experiments, have traditionally bridged the gap between total ionisation or partial fragmentation of molecules; however, some of the sources used for qualitative analysis (i.e. EI, CI, ESI and FAB) cannot be used satisfactorily to provide atomic ions because of their propensity for cluster formation.

Plasma source mass spectrometry, which is dominated by the atmospheric-pressure ICP, has been the choice of many groups for trace element speciation. The use of such a technique has many advantages. First, the high-energy ionisation source coupled to mass spectrometry has yielded detection limits, for many elements, in the sub-picogram range [92]. Another advantage of using such a high-energy source is its ability to quantify an unknown species by calibrating the instrument with a known compound that has at least one element in common with the unknown species. This is possible because the compounds are completely atomised to their constituent elements in the plasma source. A major disadvantage of such techniques is that qualitative identification of analyte species has relied on comparison of chromatographic retention times, requiring a pure standard of the analyte in question, or the use of an alternative technique. This has effectively limited the technique to the analysis of known compounds.

Evans and Caruso investigated the possibility of forming argon and helium low-pressure ICPs using commercially available atmospheric-pressure ICP-MS instrumentation [93]. Using this instrumentation, it was possible to sustain a 0.5 l min^{-1} , 350 W argon ICP at 0.2 mbar. However, it should be noted that both plasmas operated with reflected power readings of greater than 30 W, suggesting the ICP generator and matching network were not ideally suited to the task. Nevertheless, a similar instrument was later used for the analysis of halogenated compounds, with detection limits in the low picogram range, using gaseous sample introduction via a gas chromatograph [94].

Since these initial investigations, low-pressure ICP-MS has been applied to the analysis of non-metallic elements, using continuous sample introduction [95] and ETV [96]. Subsequently, Evans *et al.*, investigated the use of a low-pressure ICP-MS as a dual source for mass spectrometry, providing both trace level elemental analysis and qualitative information of a series of organohalides and organometallic compounds [97]. This required only moderate alteration to a commercially available ICP-MS instrument. Only atomic ions were observed in the mass spectrum when using a 1 l min^{-1} argon low-pressure ICP operated at 200 W, but molecular fragments were observed on removing the argon supply and sustaining a 3.5 ml min^{-1} helium low-pressure ICP at forward powers between 15 and 50 W. However problems do exist when using commercial ICP-MS instrumentation for the production and monitoring of ions from the low-pressure ICP, especially when operating in the molecular mode. These can be summarised as follows:

- (a) The rf generator, matching network and load-coil configuration were inadequate to sustain such a low-pressure helium plasma. This is to be expected since they were designed to sustain a $12\text{--}18 \text{ l min}^{-1}$ atmospheric argon plasma at between 1000 and 2000 W.
- (b) The ion-sampling interface was designed for sampling ions from an atmospheric-pressure plasma.
- (c) The quadrupole analyser of the mass spectrometer had a mass range from 5 to 255 m/z – this was inadequate for the analysis of many organometallic species, which have molecular masses exceeding this.

These problems were addressed by O'Connor *et al.* [98] in the design and construction of a dedicated low-pressure ICP-MS instrument. The improved rf power coupling and modified generator used in this study resulted in a stable 3 ml min^{-1} , 6 W low-pressure helium plasma being used for the production of molecular ions. However, problems still remained in the production of molecular ions at low levels, resulting in calibration of the analyte of interest by using the instrument in the atomic mode. This was addressed by addition of reagent gases to the low-pressure plasma [75]. The addition of 6 ml min^{-1} of helium to the 3 ml min^{-1} helium low-pressure plasma was shown to yield only atomic ions from a series of organohalides introduced via gas chromatography. On the introduction of 0.07 ml min^{-1} of isobutane to the plasma, fragmentation spectra similar to those produced by electron-impact mass spectrometry were observed for several halogenated compounds. The addition of 1 ml min^{-1} isobutane to the low-pressure plasma resulted in the production of only the molecular ions of these compounds. Moreover, the addition of isobutane was seen to stabilise the production of the molecular ions, enabling linear calibration of the instrument in atomic and molecular mode. Fig. 7.2 shows the resulting spectra of dibromobenzene from a low-pressure ICP-MS operating in (a) atomic mode and (b) molecular mode.

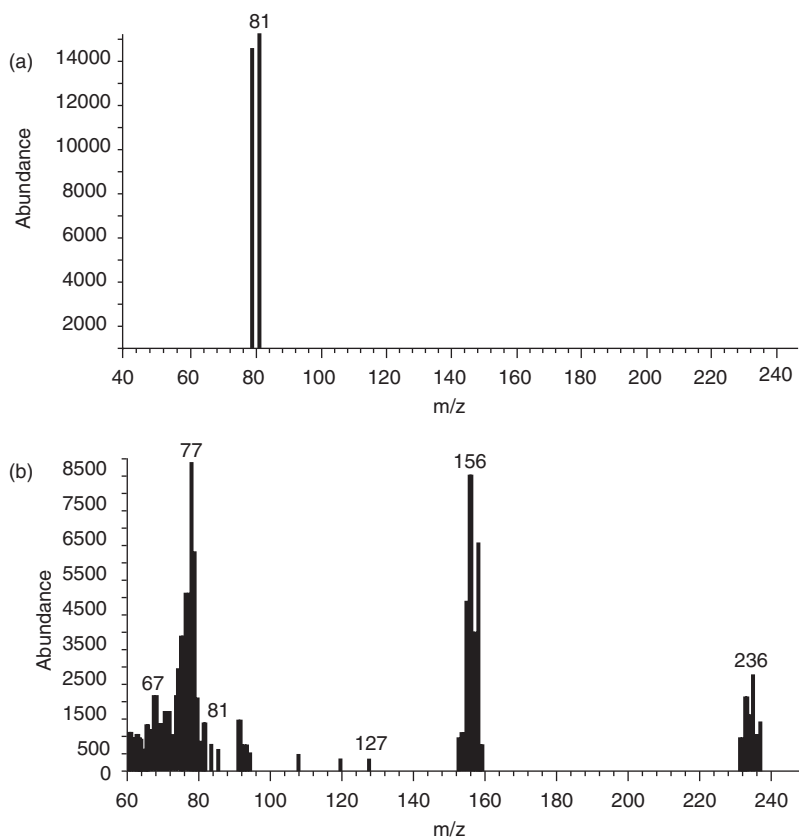


Figure 7.2 Spectra of dibromobenzene from a low-pressure ICP-MS operating in (a) atomic mode and (b) molecular mode.

7.7 Low-power plasmas

The use of a low-power 'cool' plasma was first described by Jiang *et al.* [99]. The ICP was effectively cooled by increasing the sampling depth, from 10 to 30 mm, so the plasma was cooled by air entrainment. On doing this the background spectra from the ICP changed from one which consisted mainly of Ar^+ , ArH^+ and O^+ to one dominated by NO^+ , O_2^+ and H_3O^+ . This reduction in argon-associated polyatomics enabled the analysis of potassium isotope ratios. However, a dual-slope calibration plot suggested that the analyte in the cool plasma suffered a self-enhancing matrix effect. In addition, when the plasma was cooled in this fashion a loss in sensitivity, compared with the normal operation mode, was reported.

7.8 Conclusions

Mixed gas plasmas have several advantages over all-argon plasmas. The thermal conductivity of many of the alternative gases is higher than that of argon and therefore there is often improved heat transfer from the torus of the plasma to the central channel. This means that many plasmas that contain an alternative gas (the exception being nitrogen, but only when it is introduced to the nebuliser flow) are more efficient at decomposing particles and other solids. These plasmas have therefore found use in the analysis of slurries and aerosol particles. Many mixed gas plasmas offer improved sensitivity over all-Ar plasmas but the operating parameters are often very different. Optimisation using a multivariate technique is therefore very important. Introduction to ICP-MS instruments facilitates the determination of many analytes that, under normal circumstances, suffer from polyatomic interferences. As well as overcoming spectral interferences, mixed gases can also be used to overcome interferences such as mass discrimination effects in plasma-mass spectrometry.

The use of molecular gas and helium ICPs may also offer many advantages (e.g. helium facilitates the determination of halogens and other hard-to-ionise analytes). Molecular-gas ICPs are also closer to LTE than argon plasmas. The main drawback to the use of mixed gas and alternative-gas plasmas is that often the instrumentation (matching network and torch) needs to be modified to sustain a stable discharge. This, added to the fact that many of the gases introduced (e.g. noble gases and helium) are less readily available, adds to the cost of analysis.

References

1. Mermet, J.M. and Trassy, C. (1981) A spectrometric study of a 40 MHz inductively coupled plasma. 5. Discussion of spectral interferences and line intensities. *Spectrochim. Acta*, **36B**, 269.
2. Meyer, G.A. and Barnes, R.M. (1984) Inductively coupled plasma discharge in flowing non-argon gas at atmospheric pressure for spectrochemical analysis. US Patent 4,482,246.
3. Sheppard, B.S. and Caruso, J. (1994) Plasma-mass spectrometry-consider the source. *J. Anal. Atom. Spectrom.*, **9**, 145.
4. Durrant, S.F. (1993) Alternatives to all argon plasmas in inductively coupled plasma-mass spectrometry (ICP-MS) – an overview. *Fresen. J. Anal. Chem.*, **347**, 389.
5. Montaser, A. and van Hoven, R.L. (1987) Mixed gas, molecular gas and helium inductively coupled plasmas for analytical atomic spectrometry – a critical review. *Crit. Rev. Anal. Chem.*, **18**, 45.

6. Bai, K.H., You, S.J., Chang, H.Y. and Uhm, H.S. (2002) Plasma parameters analysis of various mixed gas inductively coupled plasmas. *Phys. Plasmas*, **9**, 2831–2838.
7. Evans, E.H., Giglio, J.J., Castellano, T.M. and Caruso, J.A. (1995) *Inductively Coupled and Microwave Induced Plasmas for Mass Spectrometry*, Royal Society of Chemistry, Cambridge.
8. Montaser, A. and Van Hoven, R.L. (1987) *Basic Concepts and Characteristics of ICP-AES. Part 1: Methodology, Instrumentation and Performance*. (Ed. P.W.J.M. Boumans), John Wiley, New York.
9. Montaser, A., Fassel, V.A. and Zalewski, J. (1981) A critical comparison of argon and argon–nitrogen plasmas as excitation sources for atomic emission spectrometry, *Appl. Spectrosc.*, **35**, 292.
10. Lam, J.W.H. and Horlick, G. (1990) A comparison of argon and mixed gas plasmas for inductively coupled plasma-mass spectrometry. *Spectrochim. Acta*, **45B**, 1313.
11. Raeymaekers, B., Graule, T., Broekaert, J.A.C., Adamas, F. and Tschopel, P. (1988) Characteristics of nebulised suspensions of refractory oxide powders used for the production of ceramics and their evaporation behaviour in an ICP. *Spectrochim. Acta*, **43B**, 9223.
12. Goodall, P.S. (1991) Slurry nebulisation using mixed gas plasmas. PhD Thesis, Polytechnic South West, UK.
13. Sesi, N.N., MacKenzie, A., Shanks, K.E., Yang, P. and Hieftje, G.M. (1994) Fundamental studies of mixed gas inductively coupled plasmas. *Spectrochim. Acta*, **49B**, 1259.
14. Walters, P.E. and Barnardt, C.A. (1988) The role of desolvation and hydrogen addition on the excitation features of the inductively coupled plasma. *Spectrochim. Acta*, **43B**, 325.
15. Murillo, M. and Mermet, J.M. (1989) Improvement of the energy transfer with added hydrogen in inductively coupled plasma atomic emission spectrometry. *Spectrochim. Acta*, **44B**, 359.
16. Ebdon, L. and Goodall, P. (1992) Slurry atomisation using hydrogen modified inductively coupled plasmas. *J. Anal. Atom. Spectrom.*, **7**, 1111.
17. Murillo, M., Amaro, R. and Fernandez, A. (2003) Influence of hydrogen gas over the interference of acids in inductively coupled plasma atomic emission spectrometry. *Talanta*, **60**, 1171.
18. Shibata, N., Fudugawa, N. and Kubota, M. (1992) Effects of hydrogen mixed with argon carrier gas in electrothermal vaporization inductively coupled plasma mass spectrometry. *Spectrochim. Acta*, **47B**, 505.
19. Matousek, J.P. and Mermet, J.M. (1993) The effect of hydrogen in electrothermal vaporization inductively coupled plasma atomic emission spectrometry. *Spectrochim. Acta*, **48B**, 835.
20. Alder, J.F. and Mermet, J.M. (1973) A spectroscopic study of some radio frequency mixed gas plasmas. *Spectrochim. Acta*, **28B**, 421.
21. Demers, D.R. (1985) Hollow cathode lamp excited inductively coupled plasma atomic fluorescence spectrometry – update. *Spectrochim. Acta*, **40B**, 93.
22. Kirkbright, G.F. and Snook, R.D. (1979) Volatilization of refractory compounds forming elements from a graphite electrothermal atomization device for sample introduction into an inductively coupled argon plasma. *Anal. Chem.*, **51**, 1938.
23. Kirkbright, G.F. and Li-Xing, Z. (1982) Volatilization of some elements from a graphite rod direct sample insertion device into an inductively coupled argon plasma for optical emission spectrometry. *Analyst*, **107**, 617.
24. Barnes, R.M. and Fodor, P. (1983) Analysis of urine using inductively coupled plasma emission spectroscopy with graphite rod electrothermal vaporization. *Spectrochim. Acta*, **38B**, 1191.
25. Ng, K.C. and Caruso, J.A. (1983) Volatilization of zirconium, vanadium, uranium and chromium using electrothermal vaporization carbon cup sample vaporization into an inductively coupled plasma. *Analyst*, **108**, 476.
26. Ren J.M. and Salin, E.D. (1994) Direct solid sample analysis using furnace vaporization with freon modification and inductively coupled plasma atomic emission spectrometry. 1. Vaporization of oxides and carbides. *Spectrochim. Acta*, **49B**, 555.

27. Zaray, G., Varga, I. and Kantor, T. (1994) Halocarbon assisted slurry vaporization in inductively coupled plasma atomic emission spectrometry for the analysis of silicon nitride powders. *J. Anal. Atom. Spectrom.*, **9**, 707.
28. Ebdon, L. and Goodall, P. (1992) Thermochemical effects in hexafluoroethane (freon 116) modified argon inductively coupled plasmas. *Spectrochim. Acta*, **47B**, 1247.
29. Ishii, I. and Montaser, A. (1990) Radial excitation temperatures in argon–oxygen and argon–air inductively coupled plasmas. *J. Anal. Atom. Spectrom.*, **5**, 57.
30. Ishii, I. and Montaser, A. (1991) A tutorial discussion on measurements of rotational temperatures in inductively coupled plasmas. *Spectrochim. Acta*, **46B**, 1197.
31. Choot, E.H. and Horlick, G. (1986) Spectral characteristics of argon–nitrogen, argon–oxygen and argon–helium mixed gas plasmas. 2. *Spectrochim. Acta*, **41B**, 907.
32. Edlund, M., Visser, H. and Heitland, P. (2002) Analysis of biodiesel by argon–oxygen mixed-gas inductively coupled plasma optical emission spectrometry. *J. Anal. Atom. Spectrom.*, **17**, 232–235.
33. Chirinos, J.R., Kahen, K., O'Brien, S.E. and Montaser, A. (2002) Mixed gas inductively coupled plasma atomic emission spectrometry using a direct injection high efficiency nebulizer. *Anal. Bioanal. Chem.*, **372**, 128–135.
34. Yang, P. and Barnes, R.M. (1989) A low power oxygen inductively coupled plasma for spectrochemical analysis. 2. Plasma diagnostics. *Spectrochim. Acta*, **44B**, 1093.
35. Smith, T.R. and Denton, M.B. (1985) On the operation of inductively coupled plasmas as a function of pressure. *Spectrochim. Acta*, **40B**, 1227.
36. Cai, M.X., Ishii, I., Clifford, R.H., Montaser, A., Palmer, B.A. and Layman, L.R. (1994) Fundamental properties of helium inductively coupled plasmas measured by high resolution-Fourier transform spectrometry. *Spectrochim. Acta*, **49B**, 1081.
37. Chan, S. and Montaser, A. (1989) Determination of electron number density *via* Stark Broadening with an improved algorithm. *Spectrochim. Acta*, **44B**, 175.
38. Ishii, I., Tan, H., Chan, S. and Montaser, A. (1991) Helium ICP-AES effects of induction frequency and forward power on plasma formation and analytical and fundamental properties. *Spectrochim. Acta*, **46B**, 901.
39. Jacksier, T. and Barnes, R.M. (1994) Atomic emission spectra of xenon, krypton and neon spectra from 200 to 900 nm by sealed inductively coupled plasma atomic emission spectrometry. *Appl. Spectrosc.*, **48**, 65.
40. Yang, P. and Barnes, R.M. (1989) A low power oxygen inductively coupled plasma for spectrochemical analysis. 1. Computer simulation. *Spectrochim. Acta*, **44B**, 1081.
41. Meyer, G.A. and Barnes, R.M. (1985) Analytical inductively coupled nitrogen and air plasmas. *Spectrochim. Acta*, **40B**, 893.
42. Abdallah, M.H. and Mermet, J.M. (1982) Comparison of temperature measurements in ICP and MIP with argon and helium as plasma gas. *Spectrochim. Acta*, **37B**, 391.
43. Tang, Y.O., Du, Y.P., Shao, J.C., Liu, C., Tao, W. and Zhu, M.H. (1992) Air argon inductively coupled plasma for organic solution analysis-spectral characteristics and analytical performance. *Spectrochim. Acta*, **47B**, 1353.
44. Yang, P.Y., Barnes, R.M., Vecchiarelli, J. and Uden, P.C. (1990) Low power nitrogen and carbon dioxide plasmas for spectrochemical analysis. *Appl. Spectrosc.*, **44**, 531.
45. Wagatsuma, K. and Hirokawa, K. (1994) Analytical performance of inductively coupled plasma emission spectrometry using argon–nitrogen binary and argon–helium–nitrogen ternary gas mixture system. *Anal. Sci.*, **10**, 469.
46. Evans, E.H. and Ebdon, L. (1989) Simple approach to reducing polyatomic ion interferences on arsenic and selenium in inductively coupled plasma mass spectrometry. *J. Anal. Atom. Spectrom.*, **4**, 299.
47. Evans, E.H. and Ebdon, L. (1990) Effect of organic solvents and molecular gases on polyatomic ion interferences in inductively coupled plasma mass spectrometry. *J. Anal. Atom. Spectrom.*, **5**, 425.

48. Wang, J., Evans, E.H. and Caruso, J.A. (1992) Addition of molecular gases to argon gas flows for the reduction of polyatomic ion interferences in inductively coupled plasma mass spectrometry. *J. Anal. Atom. Spectrom.*, **7**, 929.
49. Branch, S., Ebdon, L., Ford, M.J., Foulkes, M.E. and O'Neill, P. (1991) Determination of arsenic in samples with high chloride content by inductively coupled plasma mass spectrometry. *J. Anal. Atom. Spectrom.*, **6**, 151.
50. Lam, J.W.H. and McLaren, J.W. (1990) The use of aerosol processing and nitrogen–argon plasmas for the reduction of oxide interferences in inductively coupled plasma mass spectrometry. *J. Anal. Atom. Spectrom.*, **5**, 419.
51. Akatsuka, K., McLaren, J.W., Lam, J.W. and Berman, S.S. (1992) Determination of iron and 10 other trace elements in the open ocean seawater reference material NASS-3 by inductively coupled plasma mass spectrometry. *J. Anal. Atom. Spectrom.*, **7**, 889.
52. Hill, S.J., Ford, M.J. and Ebdon, L. (1992) Simplex optimization of nitrogen–argon plasmas in inductively coupled plasma mass spectrometry for the removal of chloride based interferences. *J. Anal. Atom. Spectrom.*, **7**, 719.
53. Ford, M.J. (1994) Fundamental studies of mixed gas plasmas in ICP-MS. PhD. Thesis, University of Plymouth, UK.
54. Tanaka, T., Yonemura, K., Obara, K. and Kawaguchi, H. (1993) Inductively coupled plasma mass spectrometry with low power nitrogen and oxygen plasmas. *Anal. Sci.*, **9**, 765.
55. Laborda, F., Baxter, M.J., Crews, H.M. and Dennis, J. (1994) Reduction of polyatomic interferences in inductively coupled plasma mass spectrometry by selection of instrumental parameters and using an argon–nitrogen plasma-effect on multi-element analysis. *J. Anal. Atom. Spectrom.*, **9**, 227.
56. Van der Velde-Koerts, T. and Deboer, J.L.M. (1994) Minimization of spectral interferences in inductively coupled plasma mass spectrometry by simplex optimization and nitrogen addition to aerosol carrier gas for multi-element environmental analysis. *J. Anal. Atom. Spectrom.*, **9**, 1093.
57. Uchida, H. and Ito, T. (1995) Inductively coupled nitrogen plasma mass spectrometry assisted by adding argon to the outer gas. *J. Anal. Atom. Spectrom.*, **10**, 843.
58. Lam, J.W. and Horlick, G. (1990) Effects of sampler–skimmer distance in inductively coupled plasma mass spectrometry. *Spectrochim. Acta*, **45B**, 1327.
59. Xiao, G. and Beauchemin, D. (2001) Mixed Ar–N₂ plasmas: Simple antidotes to matrix effects in ICP-MS. *Can. J. Anal. Sci. Spect.*, **46**, 28–37.
60. Crowe, S.A., Fryer, B.J., Samson, I.M. and Gagnon, J.E. (2003) Precise isotope ratio determination of common Pb using quadrupole LA-ICP-MS with optimized laser sampling conditions. *J. Anal. Atom. Spectrom.*, **18**, 1331–1338.
61. Holliday, A.E. and Beauchemin, D. (2003) Preliminary investigation of direct seawater analysis by inductively coupled plasma mass spectrometry using a mixed gas plasma, flow injection and external calibration. *J. Anal. Atom. Spectrom.*, **18**, 1109–1112.
62. Hutton, R.C., Bridenne, M., Coffre, E., Marot, Y. and Simondet, F. (1990) Investigations into the direct analysis of semiconductor grade gases by inductively coupled mass spectrometry. *J. Anal. Atom. Spectrom.*, **5**, 463.
63. Hartley, J.H.D., Hill, S.J. and Ebdon, L. (1993) Analysis of slurries by inductively coupled plasma mass spectrometry using desolvation to improve transport efficiency and atomisation efficiency. *Spectrochim. Acta*, **48B**, 1421.
64. Ebdon, L., Ford, M.J., Goodall, P. and Hill, S.J. (1993) Hydrogen addition to the nebulizer gas for the removal of polyatomic ion interferences in inductively coupled plasma mass spectrometry. *Microchem. J.*, **48**, 246.
65. Allain, P., Jaunault, L., Mauras, Y., Mermet, J.M. and Delaporte, T. (1991) Signal enhancement of elements due to the presence of carbon containing compounds in inductively coupled plasma mass spectrometry. *Anal. Chem.*, **63**, 1497.

66. Hill, S.J., Ford, M.J. and Ebdon, L. (1992) Investigations into the applications of methane addition to the nebulizer gas in inductively coupled plasma mass spectrometry for the removal of polyatomic interferences. *J. Anal. Atom. Spectrom.*, **7**, 1157.
67. Ebdon, L., Ford, M.J., Hutton, R.C. and Hill, S.J. (1994) Evaluation of ethene addition to the nebuliser gas in inductively coupled plasma mass spectrometry for the removal of matrix gas derived and support gas derived polyatomic ion interferences. *Appl. Spectrosc.*, **48**, 507.
68. Evans, E.H. and Ebdon, L. (1991) Comparison of normal and low flow torches for inductively coupled plasma mass spectrometry using optimised operating conditions. *J. Anal. Atom. Spectrom.*, **6**, 421.
69. Cairns, W.R.L., Hill, S.J. and Ebdon, L. (1996) Directly coupled high performance liquid chromatography inductively coupled plasma mass spectrometry for the determination of organometallic species in tea. *Microchem. J.*, **54**, 88.
70. Rivas, C., Ebdon, L. and Hill, S.J. (1996) Effect of different spray chambers on the determination of organotin compounds by high performance liquid chromatography inductively coupled plasma mass spectrometry. *J. Anal. Atom. Spectrom.*, **11**, 1147.
71. Uchida, H. and Ito, T. (1997) Analytical characteristics of inductively coupled oxygen plasma-mass spectrometry assisted by adding argon to the outer gas. *Anal. Sci.*, **13**, 391.
72. Zhang, H., Nam, S.H., Cai, M.X. and Montaser, A. (1996) Atmospheric pressure helium inductively coupled plasmas for elemental mass spectrometry. *Appl. Spectrosc.*, **50**, 427.
73. Nam, S.H., Zhang, H., Cai, M.X., Lim, J.S. and Montaser, A. (1996) Status report on helium inductively coupled plasma mass spectrometry. *Fresen. J. Anal. Chem.*, **355**, 510.
74. Okino, A., Ishizuki, H., Hotta, E. and Shimada, R. (1996) Development of helium ICP-MS using an enhanced vortex flow torch. *Bunseki Kagaku*, **45**, 473.
75. O'Connor, G., Ebdon, L. and Evans, E.H. (1997) Low pressure inductively coupled plasma ion source for molecular and atomic mass spectrometry: the effect of reagent gases. *J. Anal. Atom. Spectrom.*, **12**, 1263.
76. Rosenkranz, B., O'Connor, G. and Evans, E.H. (2000) Low pressure inductively coupled plasma ion source for atomic and molecular mass spectrometry: investigation of alternative reagent gases for organomercury speciation in tissue and sediment. *J. Anal. Atom. Spectrom.*, **15**, 7–12.
77. Milstein, L.S., Waggoner, J.W., Sutton, K.L. and Caruso, J.A. (2000) Mixed gas helium/argon low power/reduced pressure ICP as a tunable ionization source for mass spectrometric detection of organotin compounds. *Appl. Spectrosc.*, **54**, 1286–1290.
78. Castillano, T.M., Giglio, J.J., Evans, E.H. and Caruso, J.A. (1997) Solution nebulization into a low-pressure helium inductively coupled plasma with mass spectrometry detection. *J. Anal. Atom. Spectrom.*, **12**, 383.
79. Hayashi, H., Furuzawa, S., Tanaka, T. and Hiraide, M. (2004) Low pressure helium inductively coupled plasma mass spectrometry: sample aerosol introduction through a capillary interface from a vibrating mesh nebulizer. *J. Anal. Atom. Spectrom.*, **19**, 773–774.
80. Hayashi, H., Honda, T., Iwata, T., Tanaka, T. and Hiraide, M. (2003) Simultaneous determination of trace elements in minute samples by electrothermal vaporization/low pressure helium ICP-MS. *Anal. Sci.*, **19**, 791–793.
81. Nam, S.H., Masamba, W.R.L. and Montaser, A. (1994) Helium inductively-coupled plasma-mass spectrometry-studies of matrix effects and the determination of arsenic and selenium in urine. *Spectrochim. Acta*, **49B**, 1325.
82. Smith, F.G., Wiederin, D.R. and Houk, R.S. (1991) Argon xenon plasma for alleviating polyatomic ion interferences in inductively coupled plasma mass-spectrometry. *Anal. Chem.*, **63**, 1458.
83. Bricker, T.M., Smith, F.G. and Houk, R.S. (1995) Charge transfer reactions between xenon ions and iron atoms in an argon–xenon inductively coupled plasma. *Spectrochim. Acta*, **50B**, 1325.
84. Petibon, C.M., Longerich, H.P., Horn, I. and Tubrett, M.N. (2002) Neon inductively coupled plasma for laser ablation-inductively coupled plasma-mass spectrometry. *Appl. Spectrosc.*, **56**, 658–664.

85. Uchida, H. and Ito, T. (1997) Evaluation of an inductively coupled air–argon plasma as an ion source for mass spectrometry. *J. Anal. Atom. Spectrom.*, **12**, 913.
86. Fannin, H.B. and Seliskar, C.J. (1987) Energy-transfer and ionisation processes in a reduced-pressure argon ICP. *Appl. Spectrosc.*, **41**, 1216.
87. Fleitz, P.A. and Seliskar, C.J. (1987) Characterization of OH radical 306.4 nm emission in argon and helium reduced-pressure ICPs. *Appl. Spectrosc.*, **41**, 679.
88. Wolnik, K.A., Miller, D.C. and Fricke, F.L. (1985) Characterization of bromine and chlorine atomic emission in a reduced-pressure inductively coupled (27 MHz) helium plasma. *Appl. Spectrosc.*, **39**, 930.
89. Miller, D.C., Seliskar, C.J. and Davidson, T.M. (1985) Hydrogen isotope analysis using a reduced-pressure ICP torch. *Appl. Spectrosc.*, **39**, 13.
90. Miller, D.C., Fannin, H.B., Fleitz, P.A. and Seliskar, C.J. (1986) Fundamental chemical processes in a low-density 27-MHz helium ICP. *Appl. Spectrosc.*, **40**, 611.
91. Smith, T.R. and Denton, M.B. (1985) On the operation of inductively coupled plasmas as a function of pressure. *Spectrochim. Acta*, **40B**, 1227.
92. Hieftje, G.M. and Norman, L.A. (1992) Plasma source-mass spectrometry. *Int. J. Mass Spectrom. Ion Proc.*, **118/119**, 519.
93. Evans, E.H. and Caruso, J.A. (1993) Low-pressure inductively-coupled plasma source for mass-spectrometry. *J. Anal. Atom. Spectrom.*, **8**, 427.
94. Castellano, T.M., Giglio, J.J., Evans, E.H. and Caruso, J.A. (1994) Evaluation of low-pressure inductively-coupled plasma-mass spectrometry for the analysis of gaseous samples. *J. Anal. Atom. Spectrom.*, **9**, 1335.
95. Yan, X., Tanaka, T. and Kawaguchi, H. (1996) Reduced-pressure inductively coupled plasma mass spectrometry for non-metallic elements. *Appl. Spectrosc.*, **50**, 182.
96. Yan, X., Tanaka, T. and Kawaguchi, H. (1996) Electrothermal vaporization for the determination of halogens by reduced pressure inductively coupled plasma mass spectrometry. *Spectrochim. Acta*, **51B**, 1345.
97. Evans, E.H., Pretorius, W., Ebdon, L. and Rowland, S.J. (1994) Low-pressure inductively-coupled plasma ion-source for molecular and atomic mass-spectrometry. *Anal. Chem.*, **66**, 3400.
98. O'Connor, G., Ebdon, L., Evans, E.H., Ding, H., Olson, L. and Caruso, J.A. (1996) Feasibility study of low pressure inductively coupled plasma mass spectrometry for qualitative and quantitative speciation. *J. Anal. Atom. Spectrom.*, **11**, 1151.
99. Jiang, S.J., Houk, R.S. and Stevens, M.A. (1988) Alleviation of overlap interferences for determination of potassium isotope ratios by inductively coupled plasma mass-spectrometry. *Anal. Chem.*, **60**, 217.

Chapter 8

Electrospray Ionization Mass Spectrometry: A Complementary Source for Trace Element Speciation Analysis

Helle R. Hansen and Spiros A. Pergantis

8.1 Introduction

Over the past decade we have witnessed the rapid development of a wide range of hyphenated analytical techniques for the purpose of trace and ultra-trace element speciation analysis [1]. These techniques are mainly based on high-resolution separation techniques coupled on-line with sensitive element-specific detectors. High-performance liquid chromatography (HPLC) is used extensively because most metal and metalloid species are non-volatile. In special cases, however, gas chromatography (GC) can be used for the separation of volatile species or non-volatile metal species that have been derivatized into volatile forms. The element species eluting from the HPLC or GC column are detected on-line using sensitive, element-specific detectors such as inductively coupled plasma (ICP) – atomic emission spectroscopy, atomic absorption spectrometry, atomic fluorescence spectrometry, or ICP-mass spectrometry (ICP-MS). In particular, ICP-MS has dominated this area of analysis as a result of its superior sensitivity and selectivity. Even though the use of this type of hyphenated techniques has proven extremely powerful in detecting and identifying a wide range of arsenic, selenium, antimony, tin, mercury, lead, and chromium species, directly in biological and environmental samples at trace or ultra-trace levels, it is recognized that the approach has shortcomings and fundamental limitations [2]. These limitations arise from the fact that identification of element species is based on matching chromatographic retention times of the unknown element species with those of well-characterized standards. Thus the approach requires the use of a wide range of suitable element species standards. Unfortunately, however, only a limited number of standards are currently commercially available for most elements. This necessitates either their synthetic preparation or the isolation of the naturally occurring species from their corresponding matrices. Limitations, however, persist even when suitable standards are available, as the possibility for misidentification of element species resulting from species co-elution cannot be dismissed [2]. In addition, even though the approach has proven extremely successful for detecting the presence of known element species in crude biological and environmental extracts, it fails to provide direct structural information for the characterization of novel species.

It is for these reasons that alternative and/or complementary analytical techniques are required. Various mass spectrometric techniques, which have been used with great success

for the characterization of organic molecules and biomolecules, are now attracting considerable attention for the purpose of element speciation analyses. For example, fast-atom bombardment [3], thermospray [4], and desorption chemical ionization [5] MS have been used with varying degrees of success in the past for arsenic speciation analysis in samples of environmental origin. However, it has become clear that electrospray ionization (ES) mass spectrometry (MS) and tandem mass spectrometry (MS/MS) are the molecular mass spectrometric techniques that exhibit the greatest potential in this respect [6]. ES-MS/MS has emerged as one of the most powerful analytical techniques for trace level detection and structural characterization of a wide range of organic compounds and biomolecules. This is mainly because it allows for the direct and efficient transition of analyte ions from the liquid to the gas phase. This is of major importance as most biomolecules are insufficiently volatile and thermally labile to be vaporized directly into the gas phase in order to be mass analysed. Even though the need to characterize biomolecules (e.g. proteomics analysis) has been the driving force for the rapid development of ES-MS/MS instrumentation, it is now well established that ES is also extremely efficient in generating gas-phase ions of inorganic, organometallic, and organometalloid compounds. As a result, the technique has attracted the attention of researchers interested in identifying metals and metalloid species present at trace levels in environmental and biological samples. Amongst them are those involved in the development and application of HPLC–ICP-MS techniques for the purpose of element speciation analysis. In fact, it is now viewed that ES-MS and ICP-MS are extremely well suited for complementing each other, allowing for advanced element speciation analysis. For example, the majority of element speciation papers published in one of the leading atomic spectrometry journals, that is *Journal of Analytical Atomic Spectrometry*, clearly demonstrate the complementarity between HPLC–ICP-MS and HPLC–ES-MS/MS. In addition, current research efforts are being made towards the development of novel mass spectrometric instrumentation which incorporates both an atomic source (i.e. ICP) and a molecular source (i.e. ES) [7]. We, therefore, consider it to be of importance to the readers of this book to include a chapter on ES-MS; a complementary source for element speciation analysis.

More specifically, the aim of this chapter is to provide an interpretative description of the fundamental principles of ES-MS and MS/MS, to overview a limited range of state-of-the-art instrumentation currently in use, and finally present examples of the use of these techniques in the field of element speciation analysis. In doing so it is not our intention to provide exhaustive references to all investigators who have made important contributions in these fields of research.

8.1.1 *Historical aspects of ES-MS*

Even though the electrospray process had been known for over a century, Chapman, in the late 1930s, was credited as being the first to conduct experiments involving this process [8]. Dole *et al.* [9] and Mack *et al.* [10] were the first to develop electrospray into a practical method for introducing ionized compounds into a mass spectrometer, including successful ionization of several high-mass compounds. The modern day development of ES as a source for MS, however, was first detailed by Yashimata and Fenn [11]. In their pioneering work they reported on the observation of both positive and negative inorganic ions. The potential of the technique, however, was not recognized until several years later when Fenn *et al.* [12]

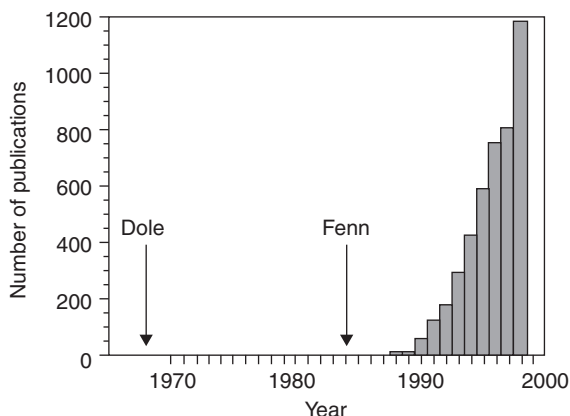


Figure 8.1 A list of the number of publications per year that were associated with 'electrospray' and 'mass spectrometry', compiled using an on-line Chemical Abstracts search (taken with permission from Stewart [13]).

demonstrated the essentials of the technique, especially its capability for multiple charging of analyte ions and the technique's application for the ionization of biological macromolecules and polymers. A gauge of the impact of these milestones on the establishment of ES-MS as an essential analytical technique for the characterization of compounds can be viewed in Fig. 8.1 which contains the number of ES-MS publications per year, for the last 30 years. In fact, John Fenn was awarded part of the 2002 Nobel Prize in Chemistry for his work on the development and application of ES-MS for the analysis of biomolecules.

Today ES is the predominant mass spectrometric technique used for the determination of a wide range of analytes present at trace level in biological, environmental, food, clinical, and pharmaceutical samples.

8.1.2 The role of ES-MS in biomolecule analysis

In order to take full advantage of the capabilities of ES-MS for element speciation analysis it is important to first have some knowledge of the advances that have so far been achieved using this technique for the analysis of a wide range of biomolecules in diverse matrices. Of course this section only provides brief reference to limited areas of application, and for this reason the reader is encouraged to seek more specialized texts in order to gain detailed knowledge of the rapid advancement of ES-MS in the area of biomolecule analysis. Knowledge of these advancements is surely to contribute towards the more productive use of ES-MS for element speciation analysis.

ES-MS is one of the two mass spectrometric techniques, the other being matrix-assisted laser desorption ionization (MALDI), to have revolutionized the role of MS in biological and biochemical research. Both are currently used for the high-precision determination of relative molecular masses of large biomolecules such as proteins, as well as the much smaller peptides. These determinations allow for protein identification (proteomics analysis), detection of mutations within proteins, detection of post-translational modifications, structure

confirmation, and eventual correction of the protein sequences derived from their DNA sequence. Without going into much detail protein identification by ES-MS generally consists of three steps [14,15]. Initially, the protein is cleaved enzymatically. Subsequently, the mixture of resulting peptides is separated, using HPLC or two-dimensional gel electrophoresis, and introduced into the ES tandem mass spectrometer. The objective is to identify a maximum number of peptides. Finally, in the last step, to compare the obtained tandem mass spectra generated from several peptides with databases generated by the application of the rules of cleavage to all the known sequences. In general, by using this approach, protein identification can be achieved from the identification of three to six of its peptides. Improved reliability of protein identification is achieved when using more than one different enzymatic digestions.

Another important application of ES-MS (and of MALDI) is the identification and localization of post-translational modifications in proteins. For example, disulfide bridges play an important role in establishing and preserving the three-dimensional structure of proteins, it is therefore of importance to determine if such bridges exist in a protein, as well as which cysteine residues participate in their formation. This can be quite conveniently accomplished by using ES-MS/MS to analyse peptides resulting from a protease digestion of the non-reduced protein, followed by the analysis of the peptides resulting from an identical digestion of the protein that has undergone disulfide bridge reduction. In comparing the two mass spectra it is evident that ions corresponding to peptides connected by a bisulfide bridge will disappear when the protein has been reduced, yielding two new peptides both containing cysteine residues.

ES-MS is being used extensively for the verification of the structure and purity of synthetic peptides, as well as for rapidly verifying the fidelity and homogeneity of proteins produced by genetic engineering.

Most recently attempts are being made to use ES-MS to monitor non-covalent interactions between biomolecules [16]. These interactions are categorized as intra-ionic interactions influencing the three-dimensional structure of an ion, as interactions between identical or structurally similar species resulting in the formation of multimeric species, and finally as specific interactions between structurally dissimilar species which are related by biological function. The literature contains many examples of all three categories of interactions.

8.2 Mechanistic aspects of electrospray ionization

8.2.1 Formation of charged droplets

The ES source can be considered as a special type of electrochemical cell. It consists of two electrodes placed approximately 1–3 cm apart: the first, a metal capillary (typically 0.2 mm o.d. \times 0.1 mm i.d.) through which the liquid sample is introduced, and the second a plate, with an orifice, that functions as a counter-electrode and the entrance to the mass analyser. In order to generate charged droplets from the liquid sample a high potential in the range of 3–6 kV is applied across the two electrodes, under atmospheric pressure conditions. This potential sets up an electric field at the capillary tip, which partially penetrates the surface of the liquid emerging from the capillary. In most ES configurations the capillary is set to a voltage between ± 3 –6 kV, while the counter-electrode is grounded. A positive voltage is applied in order to generate positively charged droplets that subsequently give rise to positively

charged gas-phase ions, whereas a negative voltage is applied to generate negatively charged gas-phase ions.

The sample liquid, delivered to the capillary at a relatively low flow rate of 1–10 $\mu\text{l}/\text{min}$, ‘experiences’ the electric field resulting from the potential applied across the two electrodes. Assuming a positive voltage is applied to the capillary and the counter-electrode is grounded, positive ions migrate towards the emerging liquid front, while negative ions migrate towards the capillary, and in some cases lose their charge through electrochemical discharge against the wall of the metal capillary. This electrophoretic separation of positive and negative ions leads to the accumulation of positive ions on the liquid surface, which causes destabilization of the liquid front as it is pulled downfield by the grounded counter-electrode. This gives rise to a liquid cone, referred to as the Taylor cone after the researcher who was amongst the first to describe how the competing forces of electric fields and liquid surface tension affect the cone’s stability. Under a sufficiently high electric field, a liquid filament, micrometers in diameter, is emitted from the Taylor cone tip. As this liquid filament travels towards the grounded counter-electrode it becomes unstable and gives off individual droplets, the surface of which contain an excess of positive ions. The diameter of these charged droplets is dependent on a number of parameters, most importantly the applied voltage, the solution flow rate, solvent properties such as surface tension, and solution conductivity. Also, the frequency of this process is dependent on the magnitude of the electric field, the solution surface tension, and solution conductivity.

As already discussed, one of the critical steps in the formation of charged droplets is the electrophoretic separation of positive and negative ions in solution. The resulting excess of positive electrolyte ions in the sprayed droplets is assessed quantitatively by measuring the capillary current which is generally in the range from 10 to 100 nA. It is reported that higher currents generally result from electric discharge. On the basis of theory and experimental measurements the following equation has been proposed for the capillary current (I) [17]:

$$I \approx \text{constant} \times (\gamma K V_f \epsilon / \epsilon_0)^{1/2} \quad (8.1)$$

where γ = surface tension, K = conductivity of solution, ϵ_0 = permittivity of vacuum, ϵ = permittivity of solution, V_f = flow rate of solution, and constant = 18 for liquids such as water, acetonitrile, and formamide. This equation is considered to be valid when solutions containing electrolyte concentrations of $<10^{-3}\text{ M}$ are electrosprayed at flow rates of a few $\mu\text{l}/\text{min}$. It is also well established that electrolyte concentrations $>10^{-5}\text{ M}$ are required in order for the ES process to occur [18,19]. The charge balance equation derived by Kebarle [20] allows for the calculation of the charge Q (moles of charge per litre volume of charged droplets) resulting from a solution delivered at a volumetric flow of V_f , having a total droplet current of I .

$$I/F = [Q] V_f \quad (8.2)$$

F = Faraday’s constant, corresponding to the charge in coulombs of 1 mol of elementary charges. Based on Equations (8.1) and (8.2) it can be argued that the charge resulting from a solution containing 10^{-5} M electrolyte and one with 10^{-3} M , will be at least 10 times greater for the latter solution. The scenario is even worse when the increased electrolyte concentration is due to buffers, other additives or matrix components present in the sample solution.

As described already the electrospray source produces a continuous current, and therefore an electrochemical oxidation reaction must be occurring at the metal capillary. This can occur by removing negative ions (from the sample solution) or by creating positive ions (from metal capillary). Also, an electrochemical reduction must be taking place at the counter-electrode by removal of positive ions. In support of this Blades *et al.* [21] reported that Zn^{2+} ions were produced when a Zn capillary tip was used. Also, Van Berkel [22] has shown that some compounds, not normally ionized by ES, undergo solution electrochemical oxidation (in the positive mode) or electrochemical reduction (in the negative mode) during ES ionization. This has been shown to occur with high-molecular-weight polycyclic aromatic hydrocarbons (PAHs), carotenoids, and porphyrins. Also recently the occurrence of electrochemical reactions have been reported to have an undesirable effect on the quantification of metal analytes such as Ag^+ , Cu^{2+} , and Hg^{2+} .

8.2.2 Electrospray sources

A schematic representation of a typical ES ionization source is shown in Fig. 8.2a. As mentioned previously a positive potential applied to the capillary while the counter-electrode is at ground potential will generate positively charged droplets. A negative potential applied to the capillary will result in the formation of negatively charged droplets. In an alternative design the capillary is at ground potential while the counter-electrode is held at high negative potential thus forming positively charged droplets, in which case negatively charged droplets can be obtained when applying a high positive potential to the counter-electrode while having the capillary at ground potential. The limitation with conventional ES ionization sources is that they are only capable of accommodating flow rates between 1 and 10 $\mu\text{l}/\text{min}$ and cannot be used for solvents of high surface tension (i.e. water).

To overcome these restrictions pneumatically assisted electrospray has been developed. This technique is often referred to as 'ionspray'. In addition to the applied potentials a gas flow is added via an outer capillary in order to enhance nebulization efficiency (i.e. aerosol formation (Fig. 8.2b)). The applied potentials, however, remain responsible for charging the droplet surface. One of the major advantages of pneumatically assisted nebulization ES is that it provides for a very efficient and routine interface between conventional HPLC (1 ml/min mobile-phase flow rates) and ES-MS, and as a result has been adopted by most ES manufacturers.

Progress, however, has also been made in achieving efficient ES ionization at reduced nl/min flow rates. Wilm *et al.* [23] developed an ES source that operates at low nl/min flow rates producing charged droplets, with nanometer diameters, through a 1–2 μm i.d. capillary. This type of ES is referred to as nanospray. The main feature of nanospray is that flow rates are governed solely by the ES process (i.e. applied potentials and solvent properties). Nanospray is reported to be more efficient by two orders of magnitude, relative to conventional ES sources, in converting condensed-phase analyte ions into gas-phase ions. This type of source also allows for improved analysis of solutions having high salt contents [23].

One further recent improvement to the conventional ES source involves placing the capillary diagonal or at right angles to the source axis (Fig. 8.2c). Such a configuration reduces the amount of solvent and neutral contaminants introduced into the mass spectrometer. This type of configuration takes advantage of the fact that only the charged droplets/ions are extracted from the mass spectrometer.

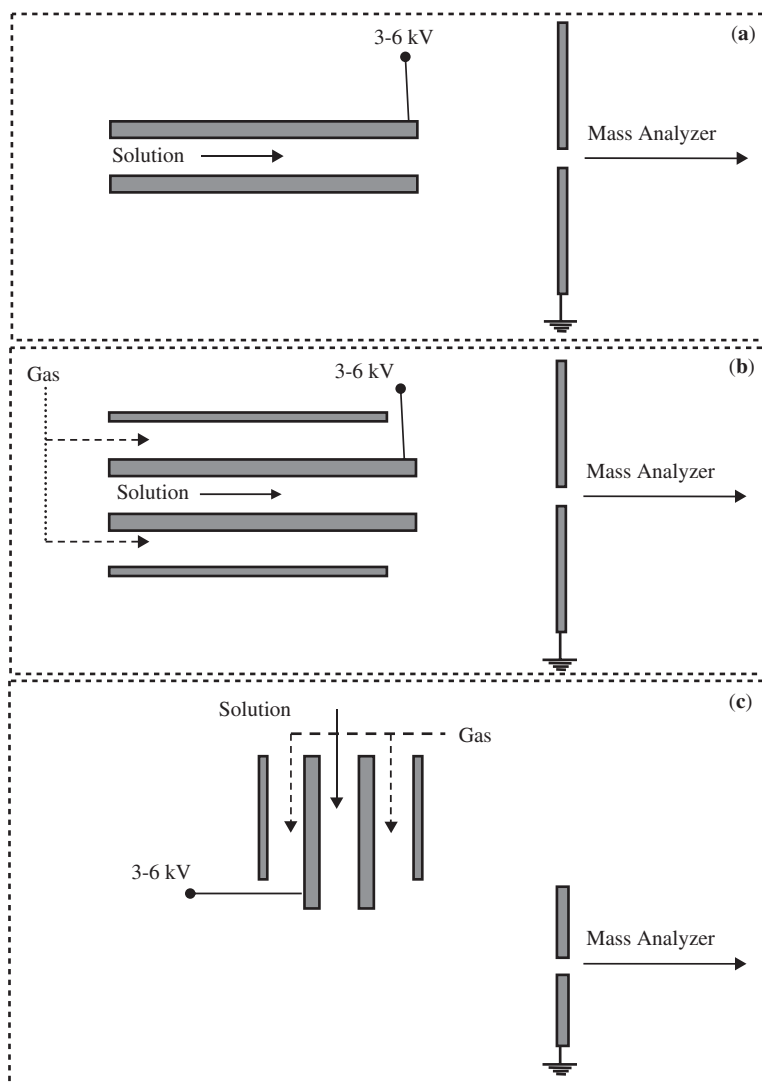


Figure 8.2 Versions of typical electrospray sources: (a) conventional ES source, (b) added sheath gas for sample introduction at high flow rates (up to 1 ml/min), (c) orthogonal sample introduction (most commonly adopted configuration).

8.2.3 Droplet disintegration

Droplets formed under electrospray conditions (flow rate from 0.5 to 10 $\mu\text{l}/\text{min}$ and total electrolyte concentrations below 10^{-3}M) have radii in the order of 0.2–2 μm . It is believed that these charged droplets contain approximately 50 000 singly charged ions, corresponding to a charge of $Q \approx 10^{-14}\text{C}$. The electric field they experience causes them to move

towards the counter-electrode, while undergoing size reduction because of solvent evaporation promoted from the heat supplied from the ambient air. It is now common to employ heated gases in order to assist with this process. A direct result of droplet shrinkage is an increase in the droplet's charge density. As solvent evaporation continues the repulsive forces resulting from the increased charge density overcome the solvent surface tension holding the droplet together (after $\sim 100 \mu\text{s}$). The Rayleigh equation gives the condition under which droplets undergo Coulombic fission. It is estimated that droplet fission occurs at approximately 80% of the Rayleigh limit.

$$q = 8\pi\sqrt{\epsilon_0\gamma R^3} \quad (8.3)$$

q = charge; ϵ_0 = permittivity of vacuum; γ = surface tension; and R = Rayleigh limit (droplet diameter).

Upon fission the parent droplet does not split evenly into smaller droplets. It is believed that because droplets experience shear forces as they travel through a dense gas they vibrate. The vibrations result in surface protrusions that have high charge densities. As a result these protrusions give rise to a jet of microdroplets having a radius of approximately $0.1 \mu\text{m}$ (roughly one-tenth of the radius of the parent). The initial jet of droplets is believed to consist of approximately 20 droplets carrying off 2% of the mass of the parent droplet and 15% of its charge. Kebarle and Tang [17] proposed a detailed droplet decomposition scheme which illustrates the cascade of Coulombic fissions and the time required for the generation of offspring microdroplets. The parent droplet, having lost 2% of its mass and 15% of its charge, also continues to shrink and release offspring droplets.

Efficient formation of microdroplets in the nanometer range is crucial for ES-MS as larger droplets within the micrometer range are reported to maintain their charge and as a result do not give rise to gas-phase ions. Therefore the rate of solvent evaporation is very important and as a consequence solvent vapour pressure needs to be taken into consideration. As a result solvents with low vapour pressure require elevated temperatures in order to achieve acceptable electrospray sensitivity. Droplet temperature is about 10°C lower than source gas temperature as a result of solvent evaporation.

8.2.4 Gas-phase ion formation

According to the charge residue model (CRM) gas-phase ions are generated from small charged droplets following solvent evaporation to the point where no more solvent can be lost [9,24,25]. As a result the dry charged residue that remains from a solution containing a single electrolyte (AX) will be $(A^+)_m(AX)_n$. The values of m and n depend on the charged droplets resulting through parent droplet fission. It is expected that parent droplets give rise to species with high m and n values, whereas, subsequent offspring droplets give A^+ and $(A^+)_m(AX)_n$ species with low m and n values.

An alternative model used to explain the formation of gas-phase ion during the ES process is the ion evaporation model (IEM), proposed by Iribarne [26] and Thomson [27]. According to this model gas-phase ions A^+ are emitted directly from highly charged droplets having a radius in the 10–20 nm range. The IEM theory, however, does not exclude the

formation of ions according to the CRM. In fact it is proposed that small ions (A^+) are produced via IEM, whereas $(A^+)_m(AX)_n$ ion species ($x > 1$ or 2 or 3 and $n \gg 1$) are formed via CRM.

8.2.5 *Sampling electrosprayed ions*

Introduction of gas-phase ions produced by ES into a mass analyser requires an atmospheric pressure interface, which is usually based on a two- or three-stage differential pumping system. Various different configurations have been used. Typically these consist of a sampling plate with a narrow orifice through which gases expand. The resulting jet expansion is skimmed through a second plate and the remaining ion beam is then guided using a series of ion optics into a mass analyser. Other configurations involve the use of a heated capillary tube as the first stage in extracting ions from atmospheric pressure regions and guiding them into the high vacuum stage of the mass spectrometer. This approach also provides improved solvent evaporation from the analyte ions. Sampling and skimmer plates are placed directly after the heated capillary. Ion optics follow in order to guide the ions into the mass analyser. Current practice involves the use of a curtain gas supplied in-front of the sampling plate or a heated gas coming from around the sampling plate towards the aerosol generated from the electrospray capillary. The function of these gases, which can be heated in most cases, is to prevent neutral species (mainly solvent molecules) from entering the expansion region of the interface, to minimize van der Waals cluster formation, and to assist in the drying of the electrosprayed droplets.

8.3 Mass analysers used with ES

Several different types of mass analysers have been used in conjunction with ES. The analyser performance characteristics that are most important include their resolution, transmission efficiency, and upper m/z limit. In the case of trace element speciation analysis the first two are of paramount importance. In order to provide a clear understanding of the operation and advantages associated with each type we will briefly devote a section to two important analysers used with ES-MS/MS. It is assumed that the principles of operation of the quadrupole mass analyser are known as it is the main analyser used with ICP-MS. Thus no additional information will be provided here regarding the operation of this in particular analyser.

8.3.1 *Quadrupole: time-of-flight analysers*

The ES Quadrupole time-of-flight (QqToF) mass spectrometer was only commercialized about a decade ago, however, it has achieved widespread acceptance and is now considered to be one of the most advanced tandem mass spectrometers. This is because of the combination of high sensitivity, high resolution, and high mass accuracy for ions detected in the single MS mode as well as for product ions detected in the MS/MS mode.

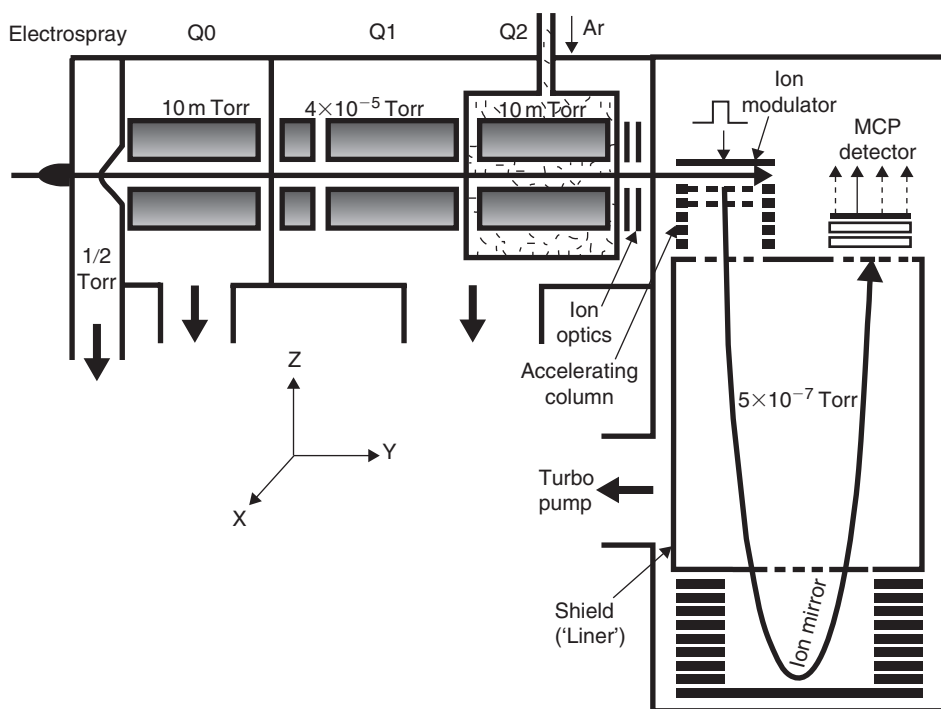


Figure 8.3 Schematic diagram of a QqToF mass spectrometer (permission from Chernushevich *et al.*, [28]).

The instrument shown in Fig. 8.3 contains a series of three quadrupoles (Q_0 , Q_1 , and Q_2) followed by a reflecting ToF analyser [28]. Quadrupoles Q_0 and Q_2 are rf only, the former acting as an ion guide and for collisional cooling, and the latter functioning as a collision cell. In some commercial instruments hexapoles are used instead of Q_0 and Q_1 , however the basic principles remain the same.

When operated in the MS/MS parent ion mode Q_1 is set to only transmit the parent ion of interest. The mass transmission window being usually $1\text{--}3\ m/z$ wide. Parent ions are accelerated to energies between 20 and 200 eV prior to entrance into the collision cell (Q_2), where they undergo collision-induced dissociation (CID) as a result of energetic collisions with a neutral gas, typically N_2 or Ar. Prior to exiting the collision cell the product ions are collisionally cooled and focused. Subsequently, the product ions leaving the collision cell are re-accelerated to several tens of eV per unit charge. The product ions are then focused by using ion optics into a parallel beam. This beam enters the modulator region continuously, while it is field-free. In order to introduce the product ions into the ToF analyser a pulsed electric field is applied at a frequency of several kilohertz per charge. The force experienced by the ions is perpendicular to their motion, thus causing them to accelerate in the x -direction thus forcing them to enter the field-free region of the ToF analyser where separation is achieved (Fig. 8.3). A single-stage reflectron is used to compensate for the initial spatial and energy spread of the ions.

In the single MS mode Q_1 is operated in the rf-only mode, while the ToF is used to separate ions based on their m/z ratio. This is the preferred arrangement because of the high resolution and mass accuracy afforded by the ToF analyser.

One of the attractive features of the ToF analyser relative to scanning analysers is its relatively high duty cycle. However, even though ions are recorded in parallel (quasi-simultaneously) duty cycles between 5% and 30% are achieved. The duty cycle is dependent on the ion m/z , discriminating against low-mass ions. This discrimination, however, only occurs in the ion modulator and not in the drift tube.

Another attractive feature of the QqToF instrument is its high resolution, which is far superior to that of triple quadrupole instruments. Resolution of about 10 000 (based on $m/\Delta m$, where Δm is the full-peak width at half-maximum) are routinely achieved. Such high resolution allows for the complete or partial separation of peaks with the same nominal mass. This provides interference reduction and in some cases improved signal-to-noise ratios as the chemical background is removed. High resolution also provides information on the charge-state of multiply charged species as a result of being able to determine their isotopic spacing.

Because the detailed discussion of the factors affecting resolution of orthogonal injection ToF mass spectrometers is beyond the scope of this chapter, a detailed discussion can be found in the work of Dodonov *et al.* [29].

High mass resolution and the simplicity of the mass calibration scale are the two main reasons that allow for high-accuracy measurements with the ToF of the QqToF instrument. High resolution is important as it reduces the possibility of mass peaks overlapping, which could affect the centroid of the peak significantly. The straightforward physics of the ToF mass analyser provides for accurate and simple mass calibration. A mass accuracy of better than 5 ppm can be achieved as long as there are no underlying interferences, there are sufficient ion statistics to measure the peak centroid, and the calibration function has been accurately measured.

8.3.2 Quadrupole ion trap mass analyser

One of the latest mass analysers to be used in conjunction with ES for tandem mass spectrometric analysis is the quadrupole ion trap (IT). This device allows for ion storage, mass analysis, and functions as a tandem mass analyser and can therefore be used to elucidate ion structures and to study their gas-phase chemistry of ions. The significance and elegance of this device was recognized in 1989 when the Nobel Prize in Physics was awarded to its inventor Paul [30,31].

The IT consists of three electrodes, one being the ring electrode and the other two almost identical electrodes are the end caps [32]. The ring electrode resembles a napkin holder ring both in shape and size. While the two end-cap electrodes can be envisioned as inverted small saucers. The hyperboloidal geometry of the electrode internal surface gives rise to a quadrupole field and a parabolic potential well within the IT cavity when an rf potential is applied to the ring electrode, while the end-cap electrodes are kept at ground potential. Such a potential well is required in order to trap ions of all masses in a three-dimensional 8-shaped trajectory. However, due to the kinetic energy of the ions entering the trap few would actually be maintained within the potential well without some other means of slowing them down or cooling them. This is accomplished having an inert gas, such as He, within the analyser to a pressure of approximately 10^{-3} Torr (0.13 Pa). Ions with increasing m/z ratio are expelled from the trap to a detector by increasing the rf potential. This scanning approach is referred to as the mass-selective instability mode.

Improvements in the operation of the IT can be obtained by applying an additional rf potential to one of the end caps, with a frequency that matches the frequency of ion oscillation. It should be noted that this frequency is different from the rf frequency applied to the ring electrode, however, it is characteristic of the m/z of the ion. Therefore by applying the correct resonance frequency, in addition to reducing the scan rate of the ring electrode rf potential, ions can be ejected selectively and with higher efficiency from the IT. This mode of operation is referred to as the resonance ejection mode. Also, by the application of a low-amplitude ac resonance signal across the end-cap electrodes the ion kinetic energies of the trap ions can be increased thus leading to ion dissociation as a result of their many collisions with the He damping gas. Product ions are ejected through holes in the end-cap electrode, from low to high m/z , by choosing amplitudes of the fundamental rf potential that sequentially make ion trajectories unstable.

State-of-the-art ITs used in combination with ES are now capable of reaching an upper mass range of 4000–6000 m/z . Resolutions of up to 5000 have been reported for commercial IT instruments.

8.4 Element speciation using ES-MS

8.4.1 Arsenic

The use of ES-MS techniques for the detection of arsenic species is fairly new. The initial comprehensive study by Corr and Larsen [6] on the detection of organoarsenic species by liquid chromatography (LC) coupled to ES-MS/MS has been followed by numerous papers by various research groups reporting on the use of ES for arsenic speciation analysis. In the last few years ES-MS and ES-MS/MS techniques have provided the vast majority of new methods for the targeted identification and quantification of a large number of arsenic species. In addition, these techniques have been used to obtain invaluable data for the identification of a novel group of organoarsenicals (i.e. the thio-arsenic compounds).

8.4.1.1 Recognizing As-containing peaks by ES-MS

The detection of arsenic compounds by ES-MS is complicated by the fact that As is monoisotopic and therefore no characteristic isotopic pattern exists in order to reveal its presence in the recorded electrospray mass spectra. This difficulty, however, can be overcome to some extent by simultaneous recording arsenic atomic ions (m/z 75) and molecular mass spectral data for arsenic compounds when using a HPLC coupled with a single quadrupole ES-MS system [33,34]. By applying a high fragmentor voltage (source voltage) the ES-MS may operate as an element-specific detector, however, Pedersen and Francesconi [33] noted that different organoarsenicals gave inconsistent quantities of atomic ions at m/z 75 (4–25%). Furthermore, they observed that inorganic arsenic (As(III) and As(V)) did not show any signal for arsenic atomic ions, hence caution needs to be taken when using m/z 75 as an indicator of the presence of arsenic. In fact several research groups failed all together to optimize their ES-MS system to act as an element-specific detector. Later Kuehnelt *et al.* [35] showed that the ability to detect arsenic atomic ions of four dimethylarsinoylribosides

(arsenosugars) was dependent on the purity of the nitrogen drying gas used. This finding seems to explain the controversy in the successful detection of m/z 75 ions. Using a purity of at least 99.999% all investigated arsenic compounds gave a signal at m/z 75. Although it has recently been shown by Francesconi and co-workers, that even though it is possible to fragment arsenosugars to $^{75}\text{As}^+$ in the ES source region, especially when pure arsenic standards and high-purity N_2 -curtain gas is used, difficulties still exist regarding the unequivocal detection of arsenic-containing compounds eluting from a LC column when crude extracts containing many other organic compounds are analysed [36].

Product ion and fragment ion data characteristic of many known organoarsenicals have been described [33,37–39] and this information may be used as a database for the identification of certain arsenic compounds. The presence of certain common fragment or product ions such as m/z 91 ($[\text{AsO}]^+$), m/z 107 ($[\text{AsS}]^+$) or m/z 237 (characteristic of dimethylarsinoylriboside) may give a rather good indication if the chromatographic peak contains an As compound. However, an element-specific detector is still required for the conclusive detection of arsenic.

8.4.1.2 Parallel HPLC-ICP-MS and single quadrupole HPLC-ES-MS

In recent years HPLC-ICP-MS is most commonly used in a complementary fashion with HPLC-ES-MS, as the elemental detector, especially when the ES-MS fails to detect the As atomic ions. The value of single quadrupole HPLC-ES-MS compared to HPLC-ICP-MS for quantification has been evaluated. It appears from the quantitative results by Pedersen and Francesconi [33] that quantification of four arsenosugars by ES-MS is most reliable when based on the protonated molecule (i.e. $[\text{M} + \text{H}]^+$). Madsen *et al.* [34] obtained quantitative results for four arsenosugars within 5–14% of the HPLC-ICP-MS data when using the $[\text{M} + \text{H}]^+$ for quantification. The ES ionization process is observed to be more affected by the matrix than in ICP ionization, and quantification of arsenic compounds using the standard addition approach generally provides more accurate results than when using external calibration [40].

Hansen *et al.* [41] first reported the use of simultaneous ICP-MS and ES-MS detection by splitting the flow of their LC system post-column (1 part into the ICP-MS, 4 parts into the ES-MS) (Fig. 8.4). Application of the simultaneous set-up gave the first indication of a thio-containing organoarsenical (dimethyl arsinothioyl acetate) from the m/z 197 and m/z 199 isotopic ratio matching that of ^{32}S to ^{34}S . This species was present as a natural metabolite in urine of sheep feeding on arsenosugar-containing seaweed. Limited fragmentation was obtained by adjusting the fragmentor voltage (source CID) on the single quadrupole ES-MS (Fig. 8.4). The authors then synthesized a standard analogue and the shared identity of the compound present in the urine samples and the standard was confirmed by tandem MS. The finding was very important as it directed focus onto this novel group of thio-arsenic compounds. This has resulted in the identification of several thio-arsenicals by the application of ES-MS techniques [42–44].

A similar recent successful application of simultaneous ICP-MS and single quadrupole ES-MS detection after HPLC separation is the characterization of the arsenic-glutathione complexes $(\text{R}_n\text{As(III)(GS)}_{(n-1)})$ where $n = 0\text{--}3$ [45]. Prior to this study, the evidence of

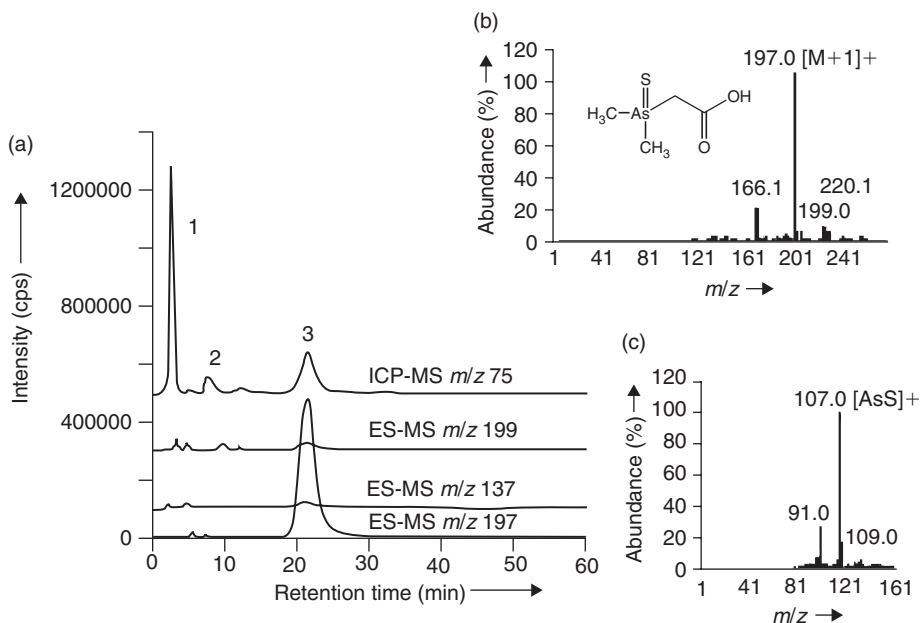


Figure 8.4 Simultaneous elemental detection by ICP-MS (m/z 75) and molecular detection by ES-MS (m/z 199, 198, 137, and 197 by full scan mode) of dimethyl arsinothioyl acetate (peak 3) present as a metabolite in a urine sample A. The data was obtained by splitting the flow of the anion-exchange-LC system post-column. Mass spectrum of peak 3 at fragmentor voltage (100 V B and 240 V C). Figure taken from Hansen *et al.* [41].

their occurrence in biological tissues was derived indirectly by comparison of results from experiments with and without glutathione (GSH) inhibitors. In the relevant study, the stability of the $R_nAs(III)(GS)_{(n-1)}$ complexes on several HPLC columns was studied. A very important finding of the study was that the complexes were extremely unstable and would not have been observed previously due to the 'harsh' conditions often used in 'routine' work.

8.4.1.3 Application of ES-MS/MS for identification of As species in crude matrices

Tandem MS/MS techniques have shown to be a suitable tool for the identification of new arsenic species in biological samples. In order to minimize the matrix effect, sample cleanup procedures are typically employed as demonstrated in the study by McSheehy *et al.* [37]. They applied multidimensional chromatography before analytical anion- and cation-exchange chromatography, collection of the individual peaks eluting from the columns, and subsequent determination of the collected fractions by ES-QqToF-MS/MS (direct infusion). The applied tandem MS techniques lead to the identification of 15 arsenic

species in the clam *Tridacna derasa* and at least two of the species were novel, as argued in the critical review by Francesconi and Kuehnelt [46].

It may be argued that with an increased number of operational cleanup steps, the risk that material is lost or arsenic species are transformed increases and the sample cleanup procedure should generally be kept to a minimum. This may be achieved by direct coupling of HPLC to ES-MS/MS as demonstrated by Francesconi and Pergantis [36]. They identified the important arsenic-containing nucleoside, 5'-dimethylarsinoyladenine (a suggested key intermediate in the biotransformation of arsenate to arsenosugars), in the same species of clam (*Tridacna derasa*) as in the study by McSheehy *et al.* [37]. In the relevant study the sample cleanup procedure was kept to a minimum and the selectivity of HPLC-ES-MS/MS operated in the selected reaction monitoring mode (SRM) as a tool suited for searching for well-known organoarsenicals present *in vivo* in crude extracts was demonstrated. The SRM results provided definitive evidence for the presence of 5'-dimethylarsinoyladenine (m/z 372) in a clam and by measuring three precursor ion/product ion transitions (m/z 372 \rightarrow 237 (collision energy of 26 eV), 372 \rightarrow 178 (33 eV), and 372 \rightarrow 145 (46 eV)), maximum selectivity was achieved and the HPLC-ES-SRM-MS/MS system could detect the 5'-dimethylarsinoyladenine compound as low as 0.3 $\mu\text{g As/l}$ (standard addition method see below). Such a low limit of detection (LOD) approaches the LODs of HPLC-ICP-MS.

A recent study evaluated the performance of HPLC-ES-SRM-MS/MS as a method for the identification and quantification of more than 20 arsenic species in complex matrices [39]. The chromatographic set-up in this study allowed for the identification of 28 known organoarsenic species. CID breakdown curves were initially constructed for each arsenic species by recording the product ion spectra in the positive ion mode at various collision energies between 5 and 60 eV. The CID breakdown curves were used to optimize the SRM conditions for each individual standard. Calibration curves were obtained for each species (1–50 $\mu\text{g As/l}$) by following two selected fragmentation reactions. The limits of detection were calculated from the linear regression and additionally from the standard deviation obtained for blank measurements. The LODs from the linear regression were between 0.9–6.8 $\mu\text{g As/l}$ for most of the standards however a few standards (4 standards) showed higher LODs (from 9.8 to >50 $\mu\text{g As/l}$). The LODs obtained on the measured blanks were generally lower than those obtained by linear regression approaching the LODs of HPLC-ICP-MS (0.001–6.6 $\mu\text{g As/l}$). When applying the HPLC-ES-SRM-MS/MS methodology to crude extracts of marine reference materials, interference with the quantification using external calibration was observed due to signal suppression caused by co-eluting matrix components. Consequently, application of the standard addition method along with a combined cation–anion-exchange HPLC method compensated for such matrix effects. However, the results of the study demonstrated that major matrix effects cannot be fully compensated by the standard addition method without adequate chromatographic separation of the analyte from the interfering matrix component.

8.4.2 Selenium

Se is an essential element which in excess may cause toxic effects to humans and animals, however, in most cases it is associated with diseases related to its deficiency. Because of large variability of Se supplements with respect to bio-availability and anti-cancer prevention

efficacy, large attention has been given to Se speciation over the last decade. Since most of selenium species present are non-volatile, the coupling of HPLC with ICP-MS has been the primary analytical tool in these studies. However, the method has with the appearance of many unknown Se compounds in the recorded chromatograms revealed an increased demand for molecular MS techniques capable of identifying Se species in Se-enriched materials and other biological samples. ES-MS, either as an HPLC detector or in the infusion mode, using triple quadrupole and QqToF systems, has been applied for the identification of non-volatile seleno-compounds as discussed below.

8.4.2.1 Recognizing Se-containing peaks by ES-MS

The natural isotopic distribution of selenium (^{74}Se (0.9%), ^{76}Se (9.0%), ^{77}Se (7.6%), ^{78}Se (23.6%), ^{80}Se (49.7%), and ^{82}Se (9.2%) (natural isotope abundance in brackets)) should theoretically reveal Se-containing compounds rather easily by the appearance of their characteristic isotopic pattern in the ES-MS mass spectra. However, poor sensitivity in the presence of a complex matrix, the presence of multiple Se-atoms, and the formation of doubly charged ions of high-molecular-weight Se species (as selenium-containing proteins) may make the recognition of the Se isotopic pattern difficult. For low-molecular-weight Se species, however, the characteristic isotopic pattern of Se may be recognized more easily. McSheehy *et al.* [47] concluded, on the background of their work on the identification of γ -glutamyl-Se-methyl-selenocysteine in garlic, that CID-ES-MS/MS performed on the individual Se isotopes allows for the identification of seleno-compounds in natural products without the need for an authentic standard. Their compound identity was based on CID of four ions corresponding to the different selenium isotopes ^{76}Se , ^{77}Se , ^{78}Se , and ^{80}Se in the infusion mode after a two-dimensional chromatographic sample cleanup procedure had been applied. It may be argued if ES-MS/MS can allow for the identification of novel seleno-compounds without harmonizing CID fragmentation pattern between the analyte and a standard. A remark in the conclusion made by McSheehy *et al.* [47] is that γ -glutamyl-Se-methyl-selenocysteine had already been proposed to be present in garlic prior to their study (see below) by comparing chromatographic retention time and ES-MS mass spectrum of the analyte with that of a synthesized standard [48].

8.4.2.2 Parallel HPLC-ICP-MS and HPLC-ES single quadrupole MS

Kotrebai *et al.* [48] analysed Se-enriched garlic and yeast sample extracts by ion-pair (IP) HPLC-ICP-MS and ion pairing-HPLC single quadrupole ES-MS. In this study certain standards (seleno-methionine (Se-Met), Se-adenosyl-selenohomocysteine, γ -glutamyl-Se-methyl-selenocysteine) were available and the occurrence of Se-Met and Se-adenosyl-selenohomocysteine in yeast extract and γ -glutamyl-Se-methyl-selenocysteine in garlic extract was based on the comparison of chromatographic retention times and molecular mass with these standards. A second major Se-peak was observed in the chromatogram of garlic and this peak was tentatively identified as γ -glutamyl-Se-selenomethionine based on its molecular weight. However, as no standard was available for comparison of chromatographic retention time and mass spectra this identification was rather inconclusive.

8.4.2.3 ES-MS/MS analysis after chromatographic purification (heart-cutting)

Prior the study by Kotrebai *et al.* [48], the group of Lobinski [49] reported the novel identification of Se-adenosyl-homoselenocysteine as a major Se-compound present in yeast using pneumatically assisted electrospray tandem MS. At this stage no standard of Se-adenosyl-homoselenocysteine was available and due to the relative high detection limits of ES-MS (compared to ICP-MS) and the vulnerability of the ES-MS ionization to the presence of salts, parallel detection by HPLC-ICP-MS and HPLC-ES-MS was unsuccessful. Instead, the compound of interest (as detected by using HPLC-ICP-MS) was pre-concentrated by reversed-phase (RP) fraction collection (heart-cutting) and freeze-drying, and separately analysed by off-line ES-MS/MS. The characteristic natural abundance Se isotopic pattern was recognized in the resulting mass spectra, the fragmentation pattern of the compound was established by CID-MS/MS and the identity of the compound tentatively identified as Se-adenosyl-homoselenocysteine. As no such standard was available the ultimate confirmation of its identity was obtained by comparing its CID fragmentation pattern with that of its sulphur analogue (^{32}S -adenosylhomocysteine). The CID mass spectrum of the molecular peak of ^{32}S -adenosylhomocysteine showed identical intense signals at m/z 136 and m/z 250 corresponding to the Se-free fragments of the Se-containing molecular ion (Fig. 8.5).

8.4.2.4 Parallel HPLC-ICP-MS and HPLC-ES-MS/MS analysis

A study by Infante *et al.* [50] demonstrates how the combination of RP-IP chromatography with ICP-MS and SRM-ES tandem MS allowed the identification of Se-methylselenocysteine (SeMC) in selenized yeast (minor species) and in Selenium MCTM tablets (major species). Apart from comparing the chromatographic retention time, molecular mass (m/z 184, $[\text{M} + \text{H}]^+$) and isotopic pattern of the unknown Se compound in the extract of the Selenium MCTM tablets with those of a SeMC standard, specific transitions from the precursor ion (m/z 184) to two product ions were measured (SRM; $184 \rightarrow 95$ and $184 \rightarrow 167$) and provided further proof for the occurrence of SeMC in the SeleniumMCTM tablets. Only by using the selectivity of the RP-IP-HPLC-ES-SRM-MS/MS method allowed for the identification of SeMC as a minor Se compound in an extract of selenized yeast for the first time. The obtained ratio of the transition intensities for the sample (2.2) was similar to that obtained for the SeMC standard (2.4). The existence of SeMC may be relevant to the cancer preventive activity of Se yeast since the metabolism of this species, mostly studied in animals, indicates that SeMC is not incorporated into any proteins in place of methionine.

8.4.2.5 Selenium-containing proteins

Selenoproteins incorporate the amino acid selenocysteine, a cysteine analogue in which a selenium atom is found instead of sulphur. Proteins containing selenium in the form of a selenomethionine residue are classified as selenium-containing proteins. ES-QqToF-MS has been successfully applied in combination with ICP-MS and MALDI-ToF-MS to identify selenium-containing proteins in selenized yeast [51]. As discussed above, ES-MS may not be

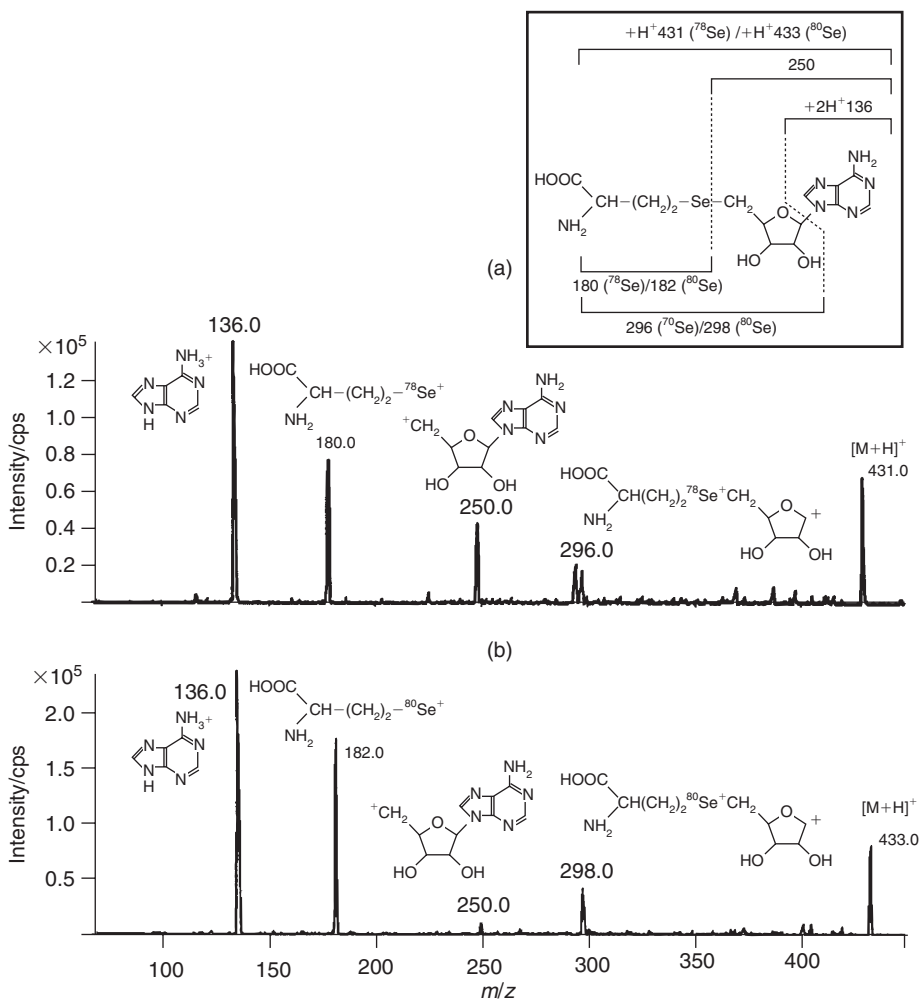


Figure 8.5 CID spectra (product ion scan) of the Se-containing molecular ion (a) m/z 431 (^{78}Se) and (b) m/z 433 (^{80}Se) present in a purified extract of selenium-enriched yeast (taken from Casiot *et al.* [49]).

suitable for identifying target ions of high-molecular-weight seleno-compounds due to poor detection limits obtained in the presence of a complex matrix, complex isotopic pattern due to the presence of multiple Se-atoms or due to the formation of multiply charged ions. MALDI-ToF-MS on the other hand suffer less from these interferences and may serve as a complementary technique to ES-MS/MS. Encinar *et al.* [51] reported for the first time the identification of two seleno-compounds with molecular masses exceeding 1000 Da in their work on selenized yeast. First they identified Se-containing fractions by size-exclusion-ICP-MS. The water-soluble protein fraction was treated with trypsin and subject to RP HPLC-ICP-MS. The different Se-containing fractions were collected, pooled, freeze-dried, and re-dissolved before being subject to analysis by MALDI-ToF-MS and ES-QToF-MS/MS.

The molecular mass of the Se-compound in each fraction was determined by MALDI-ToF-MS and structural information of each compound was obtained by CID-ES-MS/MS. The knowledge of the sequence of a few peptides allowed for a database search as the yeast genome is completely sequenced. In the database source, Se-methionine was naturally replaced by methionine. In this way, the stress-induced protein SIP18 (8874 Da) was identified as the relevant protein. SIP18 contains 79 amino acids of which 11 are methionine residues in which sulphur atoms can be replaced by Se. Following MALDI-ToF-MS results obtained directly on the water-soluble protein fraction (no enzymatic treatment) isolated by size exclusion chromatography confirmed the occurrence of a protein in the region of 9 kDa. Without the detailed study described above, the identity of this group of peaks would have been impossible to interpret as belonging to the SIP-18 protein in which two to nine methionine residues were replaced with selenomethionine.

The methodology developed was applied on one other water-soluble fraction and the database source revealed that the relevant protein was the heat-shock protein HSP12, a protein with a molecular mass at 11693 Da which contains 109 amino acids residues including one methionine. Hence, in this selenium-containing protein only one methionine residue was replaced by selenomethionine.

8.4.3 Antimony

In contrast to HPLC-ICP-MS, ES-MS has only been used in a limited number of antimony speciation studies. More specifically, ES-MS has been applied mainly for the determination of the relative molecular masses of complexes formed *in vitro* between Sb and various organic ligands. The absence of ES-MS for the speciation of Sb in 'real' samples is especially notable in the literature. In this respect HPLC-ICP-MS is leading the way; however, lack of appropriate standards is limiting the progress that can be made by using this approach.

8.4.3.1 Recognizing Sb-containing peaks by ES-MS

For several reasons it is believed that ES-MS can have a significant impact on Sb speciation analysis. Antimony has two naturally occurring isotopes (i.e. ^{121}Sb (57.2%) and ^{123}Sb (42.7%)), which provide a characteristic pattern in ES-MS spectra thus making it relatively straightforward to recognize antimony-containing peaks. These isotopes should also be useful if ES-MS is to be used as an element-specific detector for antimony (m/z 121 and 123), an approach which to our knowledge has not been fully exploited so far. Thus, Zheng *et al.* [52] observed very low-intensity signals at m/z 121 and m/z 123 when analysing trimethylated Sb compounds on an ES-ToF-MS instrument when applying a cone voltage (also referred to as source voltage or fragmentor voltage) of 100 V. No comment about this observation was made, presumably due to the very low intensities of the elemental ions. The electrospray behaviour of inorganic Sb(V) and Sb(III) (potassium hexahydroxyantimonate and Sb(III)tartrate, respectively) was also studied by Zheng *et al.* [52], but the ability to detect the elemental ions was not reported. Also, in the case of Sb speciation analysis in complex matrices (e.g. biological or environmental samples), the selectivity of ES-MS/MS, and its potential to achieve low limits of detection, has not been exploited so far.

8.4.3.2 *Sb interaction with biomolecules*

Sb(III) has a strong affinity for thiols and the interaction between antimony and the low-molecular-mass thiol trypanothione has been documented *in vitro* by using ES-MS as a complementary technique to nuclear magnetic resonance (NMR) [53–54]. Sun *et al.* [55] first used ES-MS complementary to NMR to characterize Sb(III)(GS)₃ and later Wehmeier *et al.* [55] detected Sb(III)(GS)₃ and (Me)Sb(III)(GS)₂ by using direct infusion ES-MS and hydride generation-cold trap-ICP-MS. Apart from detecting the chemically synthesized complexes, both complexes were also identified in sewage samples (spiked with Sb(III)) suggesting that these complexes may play an important role as intermediates in the biomethylation of antimony. Wehmeier *et al.* [56] tested various chromatographic systems (anion exchange and RP) for the elution of the Sb–GSH complexes but found that the compounds were irreversibly retained under all tested conditions, demonstrating the difficult task of performing chromatography on antimony species. Antimony also possesses a high affinity for organic molecules with vicinal cis-diols, which has been used in the synthesis of the antimonial anti-leishmanial agent meglumine antimonate (glucantime) (characterized by NMR and ES-MS [57]). The ability of antimony to form complexes with biomolecules possessing vicinal hydroxyl groups is currently being studied in our group by the use of ES-MSⁿ, and HPLC-ES-MS/MS and HPLC-ICP-MS [58].

8.4.3.3 *Complexation behaviour of Sb*

The important contribution of ES-MS towards our improved understanding of the chemistry of Sb with various organic ligands should be stressed. Lintschinger *et al.* [59] showed by using ES-MS that (CH₃)₃SbCl₂ was prone to form complexes with organic molecules present in its solvent. More specifically, in the presence of acetic acid in a MeOH–water–CH₃COOH (50:49:1) solvent system this compound was detected solely as a positively charged trimethylantimony acetic acid ester ($[(\text{CH}_3)_3\text{Sb}-\text{OOC}-\text{CH}_3]^+$) (indicated by two ion peaks observed at *m/z* 225 and 227). In the absence of acetic acid (MeOH–water, 1:1 solvent system) the following trimethylantimony species were detected: $[(\text{CH}_3)_3\text{SbOH}]^+$, $[(\text{CH}_3)_3\text{SbOH} + \text{H}_2\text{O}]^+$, $[(\text{CH}_3)_3\text{SbCl} + \text{MeOH}]^+$, and $[(\text{CH}_3)_3\text{SbOH} + \text{MeOH}]^+$. Similar complexation behaviour was observed for Sb(V) and Sb(III) with citric acid, as reported by Zheng *et al.* [60].

The ability of Sb(III) to complexate with ethylene diamine tetra-acetic acid (EDTA) is extensively used to obtain chromatographic separation between Sb(III) and Sb(V). The chromatographic system most often employed with ICP-MS consists of a strong anion-exchange column (Hamilton PRP-X100) and a mobile phase of EDTA (10–20 mM). The use of the complexing ligand, EDTA, allows for the successful elution of Sb(III) from this column. However, it is expected that when using such a strong complexing ligand in the mobile phase, most trivalent organoantimony species present in a sample will dissociate and form the Sb(III)–EDTA complex. This limits our ability to carry out meaningful and detailed speciation analysis. Some preliminary work has been carried out in our group using HPLC-ES-MS to characterize the complexation behaviour of inorganic Sb(III) and Sb(V) with ligands commonly used in the mobile phase (i.e. EDTA and citric acid). The objective is the development of an HPLC-ES-MS/MS method suitable for the quantification of Sb(III) and Sb(V). The ability of Sb(V) and Sb(III) to form complexes with the organic ligands in the mobile phase (i.e. Sb(V)–citrate (*m/z* 361–363) and Sb(III)–EDTA (*m/z* 409–411) formed and

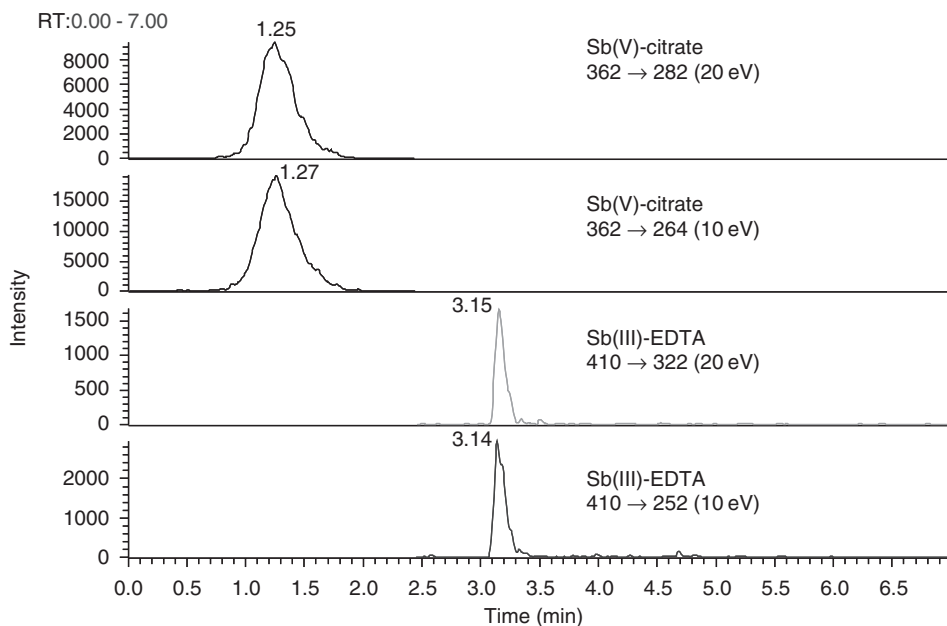


Figure 8.6 Anion-exchange (Hamilton PRP-X100 pre-column) HPLC-SRM-ES-MS chromatogram of Sb(V) and Sb(III) (25 µg Sb/l of each) with a mobile phase of 4 mM citric acid (10% MeOH) (0–2.4 min) and of 2 mM EDTA (30% MeOH) (2.5–5 min).

detected, respectively) is used to achieve separation and detection of the two (Fig. 8.6). In order to optimize the method for application on samples containing a complex matrix, two selected fragmentation reactions were followed in the SRM mode for each species and it is estimated that the LOD for both Sb(V)–citrate and Sb(III)–EDTA is below 6 µg/l.

8.4.4 Tin

Interest in speciation and determination of organotin compounds has grown in the last decades because of their multiple use and toxicological properties. Due to the volatile nature of derivatized organotin compounds, gas chromatographic separation has most frequently been employed with an elemental detector rather than HPLC separation. However, HPLC has also been used with element-specific detection, such as ICP-MS. The potential of Sn speciation using liquid injection and a molecular detector as atmospheric pressure chemical ionization (APCI)-MS [61], ion–electron impact (EI) MS [62], or ES-MS (see below) has been explored to a certain extent.

8.4.4.1 Recognizing Sn-containing peaks by ES-MS

The mass spectra of the organotins are very characteristic, in that tin has 10 stable isotopes (^{112}Sn (1.0), ^{114}Sn (0.7), ^{115}Sn (0.3), ^{116}Sn (14.5), ^{117}Sn (7.7), ^{118}Sn (24.2), ^{119}Sn (8.6),

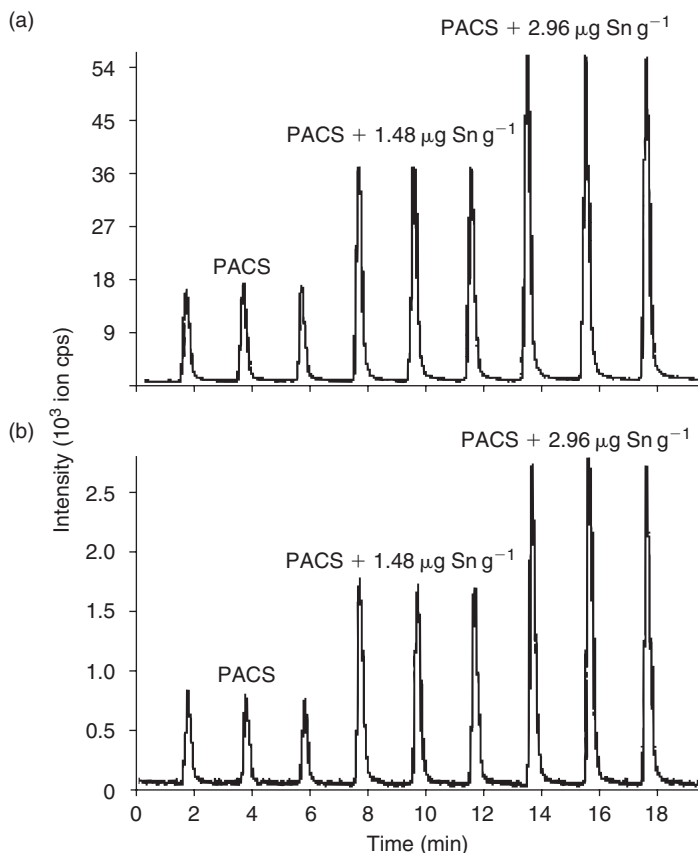


Figure 8.7 Elemental mode detection by monitoring m/z 120 (a) and MS/MS mode detection (SRM; m/z 291 \rightarrow 235 (10 eV) (b) of TBT in PACS-1 sediment reference material (taken from Corr [62]).

^{120}Sn (32.6), ^{122}Sn (4.6), and ^{124}Sn (5.8)), thereby providing a clear and distinct mass spectral pattern, making it relatively straightforward to recognize the Sn-containing peaks (assuming that only one Sn-atom is present and the Sn-compound is not multiple charged). The ability of both ES-MS and ES-MS/MS instruments to detect the elemental ion of tin has been explored. In a comprehensive study by Corr [63] a tandem ES-MS instrument was optimized to detect the molecular ion, elemental ion, and product ions of tributyltin (TBT). Especially the effect of optimizing the curtain gas flow rate and declustering or fragmentor voltage (or source voltage) was discussed in relation to obtaining a clear signal of the molecular TBT and the elemental ion of Sn. The best signal of the non-complexed molecular ion was obtained by applying 25 V declustering voltage, whereas a declustering voltage of 250 V was applied (along with a relatively elevated curtain gas flow) for the detection of the tin atomic ions. More specifically, at a declustering voltage of 250 V certain hydrogen adducts of Sn were observed (i.e. SnH_3^+ , SnH^+) and only when increasing the voltage to 350 V was the final hydrogen eliminated from Sn for predominant detection of Sn^+ at m/z 120 (however, the sensitivity was only 25% compared to that observed

using 250 V). Corr [63] applied the element (using a declustering voltage of 350 V) and SRM mode for quantification of TBT in NRCC harbour reference material (PACC-1) and obtained values differing by only 1.6% and 2.4% from the certified values of TBT (elemental mode and SRM mode, respectively) (Fig. 8.7). Quantification was performed by using the standard addition method in both modes (elemental and SRM, Fig. 8.7). TBT was detected in the standard reference material at 0.13 $\mu\text{g Sn/l}$.

Wu *et al.* [64] optimized a single quadrupole ES-MS instrument as an element detector for Sn in TBT. They also observed the formation of Sn-hydrogen adducts. By applying a fragmentor voltage of 100 V the main ion of Sn detected was at m/z 123 (SnH_3^+) but increasing the fragmentor voltage to 150 V allowed for predominant detection of m/z 121 (SnH^+) (hence the last hydrogen could not be eliminated). This study describes in detail the effect of optimizing the capillary voltage and the fragmentor voltage for TBT detection. The LOD obtained for TBT by direct liquid injection (20 μl) was 2.5 $\mu\text{g Sn/l}$ (M^+), but by coupling solid-phase microextraction (SPME) to the HPLC-ES-MS, a lower detection limit was achieved (0.1 $\mu\text{g Sn/l}$). The improved LOD was due to effective analyte–matrix separation and desalting achieved by the SPME system as well as the high extraction efficiency of the SPME.

8.5 Conclusions

It is clear that ES-MS has already exhibited significant potential in the field of element speciation analysis. In particular, it has been used, and is still used, extensively for arsenic and selenium speciation analysis, in which case its contributions have been of major impact. For several other metals and metalloids, even though it has found limited application so far, it has already made significant contributions to improve our understanding of their speciation. It is clear from recent publications in the area of element speciation that HPLC-ICP-MS and HPLC-ES-MS/MS must be used, in a complementary fashion, in the many cases where challenging identification problems exist. It is therefore of major importance for the element speciation community to follow the rapid advances currently being made in the development of new advanced MS instrumentation and the methodologies used for the analysis of biological and environmental systems.

References

1. Feldmann, J. (2005) What can the different current-detection methods offer for element speciation? *Trend Anal. Chem.*, **24**(3), 228–242.
2. Francesconi, K.A. and Sperling, M. (2005) Speciation analysis with HPLC-mass spectrometry–time to take stock. *Analyst*, **130**(7), 998–1001.
3. Pergantis, S.A., Francesconi, K.A., Goessler, W. and Thomas-Oates J.E. (1997) Characterization of arsenosugars of biological origin using fast atom bombardment tandem mass spectrometry. *Anal. Chem.*, **69**(23), 4931–4937.
4. Cullen, W.R. and Dodd, M. (1989) Arsenic speciation in clams of British Columbia. *Appl. Organomet. Chem.*, **3**(1), 79–88.
5. Cullen, W.R., Eigendorf, G.K. and Pergantis, S.A. (1993) Desorption chemical ionization mass-spectrometry of arsenic compounds present in the marine and terrestrial environment. *Rapid Commun. Mass Spectrom.*, **7**(1), 33–36.

6. Corr, J.J. and Larsen, E.H. (1996) Arsenic speciation by liquid chromatography coupled with ionspray tandem mass spectrometry. *J. Anal. Atom Spectrom.*, **11**, 1215–1224.
7. Hieftje, G.M. (2005) *European Winter Conference on Plasma Spectrochemistry*, 30 Jan.–3 Feb. 2005, Budapest, Hungary.
8. Chapman, S. (1937) Carrier mobility spectra of spray electrified liquids. *Phys. Rev.*, **52**, 184–190.
9. Dole, M., Mack, L.L., Hines, R.L., Mobley, R.C., Ferguson, L.D. and Alice, M.B. (1968) Molecular beams of macroions. *J. Chem. Phys.*, **49**(5), 2240–2249.
10. Mack, L.L., Kralik, P., Rheude, A. and Dole, M. (1970) Molecular beams of macroions. II. *J. Chem. Phys.*, **52**(10), 4977–4986.
11. Yashimata, M. and Fenn, J.B. (1984) Electrospray ion-source – another variation on the free jet theme. *J. Chem. Phys.*, **88**(20), 4451–4459.
12. Fenn, J.B., Mann, M., Meng, C.K., Wong, S.F. and Whitehouse, C.M. (1989) Electrospray ionization for mass-spectrometry of large biomolecules. *Science*, **246**(4926), 64–71.
13. Stewart, I.I. (1999) Electrospray mass spectrometry: a tool for elemental speciation. *Spectrochim. Acta B Atom. Spectrom.*, **54**(12), 1649–1695.
14. Yates, J.R., Speicher, S., Griffin, P.R. and Hunkapiller, T. (1993) Peptide mass maps – a highly informative approach to protein identification. *Anal. Bio. Chem.*, **214**(2), 397–408.
15. Pappin, D.J., Hojrup, C.P. and Bleasbly, A.J. (1993) Rapid identification of proteins by peptide-mass fingerprinting. *Curr. Biol.*, **3**(6), 327–332.
16. Gaskell, S.J. (1997) Electrospray: principles and practice. *J. Mass Spectrom.*, **32**(12), 1378.
17. Kebarle, P. and Tang, L. (1993) From ions in solution to ions in the gas-phase – the mechanism of electrospray mass-spectrometry. *Anal. Chem.*, **65**(22), A972–A986.
18. Hayati, I., Bailey, A.I. and Tadros, T.F. (1987) Investigation into the mechanisms of electrohydrodynamic spraying of liquids. 1. Effect of electric-field and the environment on pendant drops and factors affecting the formation of stable jets and atomization. *J. Colloid Interf. Sci.*, **117**(1), 205–221.
19. Ikonomou, M.G., Blades, A.T. and Kebarle, P. (1991) Electrospray ion spray – a comparison of mechanisms and performance. *Anal. Chem.*, **63**(18), 1989–1998.
20. Kebarle, P. (2000) A brief overview of the present status of the mechanisms involved in electrospray mass spectrometry. *J. Mass Spectrom.*, **35**, 804–817.
21. Blades, A.T., Ikonomou, M.G. and Kebarle, P. (1991) Mechanism of electrospray mass-spectrometry-electrospray as an electrolysis cell. *Anal. Chem.*, **63**(19), 2109–2114.
22. Van Berkel, G.J. (1997) In *Electrospray Ionization Mass Spectrometry* (Ed. R.D. Cole), John Wiley and Sons, New York, p. 67.
23. Wilm, M., Neubauer, G. and Mann, M. (1996) Parent ion scans of unseparated peptide mixtures. *Anal. Chem.*, **68**(3), 527–533.
24. Schmelzensen-Redeker, G., Bütfering, L. and Röllgen, F.W. (1989) Desolvation of ions and molecules in thermospray mass spectrometry. *Int. J. Mass Spectrom. Ion Process.*, **90**(2), 139–150.
25. Nehring, H., Thiebes, S., Bütfering, L. and Röllgen, F.W. (1993) Cluster ion formation in thermospray mass spectrometry of ammonium salts. *Int. J. Mass Spectrom. Ion Process.*, **128**(3), 123–132.
26. Iribarne, J.V. and Thomson, B.A. (1976) On the evaporation of small ions from charged droplets. *J. Chem. Phys.*, **64**(6), 2287–2294.
27. Thomson, B.A. and Iribarne, J.V. (1979) Field-induced ion evaporation from liquid surfaces at atmospheric-pressure. *J. Chem. Phys.*, **71**(11), 4451–4463.
28. Chernushevich, I.V., Loboda, A.V. and Thomson, B.A. (2001) An introduction to quadrupole–time-of-flight mass spectrometry. *J. Mass Spectrom.*, **36**(8), 849–865.
29. Dodonov, A.F., Loboda, A.V., Kozlovski, V.I., Soulimenkov, I.V., Raznikov, V.V., Zhen, Z., Horwath, T. and Wollnik, H. (2000) High-resolution electrospray ionization orthogonal-injection time-of-flight mass spectrometer. *Eur. J. Mass Spectrom.* **6**, 481–490.
30. Paul, W. and Steinwedel, H. (1956) German Patent 944900.

31. Paul, W. and Steinwedel, H. (1960) US Patent 2939952.
32. McLuckey, S.A., Van Berkel, G.J., Goeringer, D.E. and Glish, G.L. (1994) Ion trap mass spectrometry using high-pressure ionization. *Anal. Chem.*, **66**(44), A737–A743.
33. Pedersen, S.N. and Francesconi, K.A. (2000) Liquid chromatography electrospray mass spectrometry with variable fragmentor voltages gives simultaneous elemental and molecular detection of arsenic compounds. *Rapid Commun. Mass Spectrom.*, **14**, 641–645.
34. Madsen, A.D., Goessler, W., Pedersen, S.N. and Francesconi, K.A. (2000) Characterization of an algal extract by HPLC-ICP-MS and LC-electrospray MS for use in arsenosugar speciation studies. *J. Anal. Atom. Spectrom.*, **15**, 657–662.
35. Kuehnelt, D., Goessler, W. and Francesconi, K.A. (2003) Nitrogen purity influences the occurrence of As⁺ ions in HPLC-ESIMS. Analysis of four common arsenosugars. *Rapid Commun. Mass spectrom.*, **17**, 654–659.
36. Francesconi, K.A. and Pergantis, S.A. (2004) Application of selected reaction monitoring tandem mass spectrometry to the quantitative determination of an arsenic-containing nucleoside in a crude biological extract. *Analyst*, **129**, 398–399.
37. McSheehy, S., Szpunar, J., Lobinski, R., Haldys, V., Tortajada, J. and Edmonds, J.S. (2002) Characterization of arsenic species in kidney of the clam *Tridacna derasa* by multidimensional liquid chromatography-ICP-MS and electrospray time-of-flight tandem mass spectrometry. *Anal. Chem.*, **74**, 2370–2378.
38. McSheehy, S., Pohl, P., Velez, D. and Szpunar, J. (2002) Multidimensional liquid chromatography with parallel ICPP MS and electrospray MS/MS detection as tool for characterization of arsenic species in algae. *Anal. Bioanal. Chem.*, **372**, 457–466.
39. Nischwitz, V. and Pergantis, S.A. (2005) Liquid chromatography online with selected reaction monitoring electrospray mass spectrometry for the determination of organoarsenic species in crude extracts of marine reference materials. *Anal. Chem.*, **77**, 5551–5563.
40. Sanchez, D., Geislinger, A., Gomez-Ariza, J.L. and Francesconi, K.A. (2002) Determination of an arsenosugar in oyster extracts by liquid chromatography-electrospray mass spectrometry and liquid chromatography-ultraviolet photo-oxidation-hydride generation atomic fluorescence spectrometry. *Analyst*, **127**, 60–65.
41. Hansen, H.R., Pickford, R., Thomas-Oates, J., Jaspars, M. and Feldmann, J. (2004) 2-dimethylarsinothiyl acetic acid identification in a biological sample: the first occurrence of a mammalian arsiniothiyl metabolite. *Angew. Chem. Int. Ed.*, **43**, 337–340.
42. Hansen, H.R., Raab, A., Jaspars, M., Milne, B.F. and Feldmann, J. (2004) Sulfur-containing arsenical mistaken for dimethylarsinous acid (DMA(III)) and identified as a natural metabolite in urine: major implications for studies on arsenic metabolism and toxicity. *Chem. Res. Toxicol.*, **17**, 1086–1091.
43. Schmeisser, E., Raml, R., Francesconi, K.A., Kuehnelt, D., Lindberg, A.-L., Soeroes, C. and Goessler, W. (2004) Thio arsenosugars identified as natural constituents of mussels by liquid chromatography-mass spectrometry. *Chem. Commun.*, **16**, 1824–1825.
44. Nischwitz, V., Kanaki, K. and Pergantis, S.A. (2006) Mass spectrometric identification of novel arsiniothiyl-sugars in marine bivalves and algae. *J. Anal. At. Spectrom.*, **21**, 33–40.
45. Raab, A., Meharg, A.A., Jaspars, M., Genny, D.R. and Feldmann, J. (2004) Arsenic–glutathione complexes – their stability in solution and during separation by different HPLC modes. *J. Anal. At. Spectrom.*, **19**, 183–190.
46. Francesconi, K.A. and Kuehnelt, D. (2004) Determination of arsenic species: a critical review of methods and applications, 2000–2003. *Analyst*, **129**, 373–395.
47. McSheehy, S., Yang, W., Pannier, F., Szpunar, J., Lobinski, R., Auger, J. and Potin-Gautier, M. (2000) Speciation analysis of selenium in garlic by two-dimensional high-performance liquid chromatography with parallel inductively coupled plasma mass spectrometric and electrospray tandem mass spectrometric detection. *Anal. Chim. Acta*, **421**, 147–153.

48. Kotrebai, M., Birringer, M., Tyson, J.F., Block, E. and Uden, P.C. (1999) Identification of the principal selenium compounds in selenium-enriched natural sample extracts by ion-pair liquid chromatography with inductively coupled plasma- and electrospray ionization-mass spectrometric detection. *Anal. Commun.*, **36**, 249–252.
49. Casiot, C., Vacchina, V., Chassaigne, H., Szpunar, J., Potin-Gautier, M. and Lobinski, R. (1999) An approach to the identification of selenium species in yeast extracts using pneumatically-assisted electrospray tandem mass spectrometry. *Anal. Commun.*, **36**, 77–80.
50. Infante, H.G., O'Connor, G., Rayman, M., Wahlen, R., Entwisle, J., Norris, P., Hearn, R., and Catterick, T. (2004) Selenium speciation analysis of selenium-enriched supplements by HPLC with ultrasonic nebulisation ICP-MS and electrospray MS/MS detection. *J. Anal. At. Spectrom.*, **19**, 1529–1538.
51. Encinar, J.R., Ouerdane, L., Buchmann, W., Tortajada, J., Lobinski, R. and Szpunar, J. (2003) Identification of water-soluble selenium-containing proteins in selenized yeast by size-exclusion-reversed-phase HPLC/ICPMS followed by MALDI-TOF and electrospray Q-TOF mass spectrometry. *Anal. Chem.*, **75**, 3765–3774.
52. Zheng, J., Takeda, A. and Furuta, N. (2001) Investigating the electrospray mass spectra of inorganic and organic antimony compounds. *J. Anal. At. Spectrom.*, **16**, 62–67.
53. Yan, S., Li, F., Ding, K. and Sun, H. (2000) Complexation of antimony(III) by trypanothione. *Angew. Chem. Int. Ed.*, **39**, 4260–4262.
54. Yan, S., Li, F., Ding, K. and Sun, H. (2003) Reduction of pentavalent antimony by trypanothione and formation of a binary and ternary complex of antimony(III) and trypanothione. *J. Biol. Inorg. Chem.*, **8**, 689–697.
55. Sun, H., Cheong, S. and Cheng, W.S. (2000) Interaction of antimony tartrate with the tripeptide glutathione. Implication for its mode of action. *Eur. J. Biochem.*, **267**, 5450–5457.
56. Wehmeier, S., Raab, A. and Feldmann, J. (2004) Investigations into the role of methylcobalamin and glutathione for the methylation of antimony using isopically enriched antimony(V). *Appl. Organometal. Chem.*, **18**, 631–639.
57. Roberts, W.I., McMurray, W.J. and Rainey, P.M. (1998) Characterization of the antimonial antileishmanial agent meglumine antimonate (glucantime). *Antimicrob. Agent. Ch.*, **42**, 1076–1082.
58. Hansen, H.R. and Pergantis, S.A. (2006) Mass spectrometric identification and characterization of antimony complexes with ribose containing biomolecules and an RNA oligomer. *Anal. Bioanal. Chem.* 385, 821–833.
59. Lintschinger, J., Schramel, O. and Kettrup, A. (1998) The analysis of antimony species by using ESI-MS and HPLC-ICP-MS. *Fresen. J. Anal. Chem.*, **361**, 96–102.
60. Zheng, J., Iijima, A. and Furuta, N. (2001) Complexation effect of antimony compounds with citric acid and its application to the speciation of antimony(iii) and antimony(v) using HPLC-ICP-MS. *J. Anal. At. Spectrom.*, **16**, 812–818.
61. White, S., Catterick, T., Fairman, B. and Webb, K. (1998) Speciation of organo-tin compounds using liquid chromatography-atmospheric pressure ionisation mass spectrometry and liquid chromatography-inductively coupled plasma mass spectrometry as complementary techniques. *J. Chromatogr. A*, **794**, 211–218.
62. Lawson, G. and Ostah, N. (2000) Comparison of the tandem mass spectrometry analysis of compounds of general structure R₂R'SnPh, RR'SnPh₂ with R₄Sn analogues. *Appl. Organometal. Chem.*, **14**, 874–881.
63. Corr, J.J. (1997) Measurement of molecular species of arsenic and tin using elemental and molecular dual mode analysis by ionspray mass spectrometry. *J. Anal. At. Spectrom.*, **12**, 537–546.
64. Wu, J., Mester, Z. and Pawliszyn, J. (2001) Determination of tributyltin by automated in-tube solid-phase microextraction coupled with HPLC-ES-MS. *J. Anal. At. Spectrom.*, **16**, 159–165.

Chapter 9

Geological Applications of Plasma Spectrometry

Douglas L. Miles and Jennifer M. Cook

9.1 Introduction

Modern earth sciences span topics ranging in scale from the origin of the solar system and the physical and chemical evolution of the Earth over a period of 4.5 billion years, the formation and disappearance of ocean basins and the weathering of continents, to the isotopic composition of a single grain of the mineral zircon, which is less than 100 μm across. An understanding of geochemical processes – for example the role of fluids in the cycling of elements through the geosphere – helps to underpin our search for minerals and hydrocarbons, sheds light on the changes in climate that have occurred throughout Earth's history, and is increasingly important in guiding our decisions about how and where to dispose of the ever-growing quantities of stable and radioactive waste we generate.

Because of the range and complexity of the geological and geochemical processes they seek to unravel, earth scientists have an insatiable appetite for data on the chemical composition of the rocks, sediments, minerals and fluids they study. Geochemists have always been quick to pioneer the use of new analytical techniques, often long before commercially manufactured instruments based on them were available. For example, Victor Goldschmidt – regarded as the father of modern geochemistry – exploited the potential of X-ray spectroscopy very effectively in the 1920s [1]. More recently, much of the early work on inductively coupled plasma–mass spectrometry (ICP-MS) was done in geological research institutes and surveys, and in university earth science departments. Such synergy has greatly benefited both the earth sciences, by yielding geochemical information previously unobtainable, and the wider analytical community, by advancing our understanding of the capabilities and limitations of a new technique.

Atomic spectrometric techniques have been employed in geochemical analysis for many decades. X-ray fluorescence spectrometry (XRFS), which is ideally suited to the analysis of solid materials, is widely used for the determination of major and trace elements in geological samples, where its inherent precision is particularly valuable in the determination of the major components of silicate and other rocks. Optical emission spectrometry, in which the emission spectra of analyte elements in a solid sample are generated by an electrical discharge between two electrodes, was used extensively in geochemical analysis [2] in the 1940s, 1950s and 1960s, often supplanting the titrimetric, colorimetric and flame photometric methods [3–5] used at

the time for the determination of trace elements. The sensitivity and multi-element capability of dc arc optical emission spectrometry and its applicability to the direct analysis of solids made it attractive to geochemists, in spite of somewhat poor precision because of the instability of the excitation source. This well-recognised limitation prompted one of the most significant collaborative studies in early postwar geochemistry [6] and led to the production of two famous reference materials: the granite G-1 and the diabase W-1.

The development of atomic absorption spectrometry (AAS) in the 1960s did not eclipse the use of emission spectrometry in geochemical analysis as much as it did in some other fields, largely because of the limitation in AAS of having to determine one element at a time and the need to dissolve solid samples prior to analysis. Nevertheless, AAS was quickly adopted as an analytical technique for geological materials [7,8]. It still provides a convenient means of determining certain elements that are important in geochemistry and mineral exploration, such as As, Sb, Au and Hg, and is widely used.

The development of the ICP, initially as an excitation source for optical emission spectrometry, rekindled interest in emission spectrometric methods and had an early impact on geochemical analysis in the 1970s, when commercial ICP-AES (Auger electron spectroscopy) instruments became available. Its multi-element capability, good sensitivity for many geologically significant elements and the relatively good precision stemming from a more stable source counterbalanced the fact that it required liquid samples. Over the next 20 years it became established as a major analytical technique in the earth sciences, as it did in many other fields.

The subsequent development of ICP-MS, with its even greater and more uniform sensitivity for many elements, together with its ability to determine individual isotopes, heralded a second explosion of interest in ICP spectrometry among earth scientists. Its rapid acceptance as a potentially powerful geoanalytical technique was doubtless aided in part by the fact that, in the UK, much of the pioneering development work was accomplished by Alan Gray and Alan Date [9,10] when the latter was on the staff of the then Institute of Geological Sciences, now the British Geological Survey (BGS). Several of the early applications papers on ICP-MS reflect its geological associations [11–14].

Three excellent general textbooks on ICP spectrometry [15–17] cover the field up to roughly the beginning of the 1990s and reflect the strong geochemical background of many of their authors. Two more recent books on ICP-MS [18,19] provide an update on developments over the last decade. Various reviews of geoanalytical applications of plasma spectrometry have been published [20,21,22,23], including several in a special issue of the *Journal of Geochemical Exploration* published in 1992 [24 (includes Refs. 25,26)]. On the broader aspects of analytical geochemistry, Potts' tome [27] remains a classic and a slimmer book edited by Gill [28] is a useful addition to the literature. The proceedings of a number of geoanalytical conferences [29–34, 35,36], some concerned specifically with plasma spectrometric applications, provide further valuable sources of information. Articles on geochemical applications of ICP techniques appear regularly in *Geostandards and Geoanalytical Research*, formerly *Geostandards Newsletter*, as does a comprehensive annual bibliographic review of the literature concerned with the analysis of geological reference materials. The analysis of geological materials by various techniques is reviewed annually in applications reviews in *Analytical Chemistry* and in the *Atomic Spectrometry Update: Environmental Analysis*, which appears in each February issue of the *Journal of Analytical Atomic Spectrometry*.

This brief chapter cannot be a comprehensive account of the role of ICP spectrometry in the earth sciences, but it aims to provide general advice to those unfamiliar with handling geological materials and to highlight some of the areas covered in the recent and rapidly expanding literature. It concentrates on the application of plasma spectrometric techniques to the analysis of geological solids. The analysis of waters, which is frequently an integral part of many geochemical investigations [37], is covered in Chapter 10.

9.2 Sampling and sample preparation

9.2.1 Sampling

The importance of sampling and sample preparation in geochemical analysis cannot be over emphasised. Unless sufficient thought is devoted to devising appropriate sampling schemes, and unless suitable procedures are used to prepare samples, any subsequent analytical effort – no matter how powerful and sophisticated the technique – will be wasted.

A detailed discussion of sampling strategies and sample preparation methods is beyond the scope of this chapter, but both they and the subsequent analytical procedures must be seen as interrelated steps on the journey through any geochemical investigation. Typically, the stages involved are:

- (1) Definition of the problem or theory to be investigated.
- (2) Formulation of an investigative strategy.
- (3) Sample collection.
- (4) Physical and/or chemical preparation of samples.
- (5) Analysis.
- (6) Evaluation of sampling and data quality.
- (7) Data interpretation and derivation of geochemical information.

Such a scheme is often used iteratively, in which case step 6 is especially important. After an initial sampling and analysis phase – often referred to in geochemical surveys as an orientation study [38] – the quality and suitability of the data obtained are assessed. Valuable lessons are often learnt at this stage as the new information brings to light problems or ambiguities that could not have been foreseen at the planning stage. The sampling and analytical methodologies are then revised as necessary before the main survey is undertaken.

Factors to be considered in devising a sampling scheme include:

- The type of material being collected in relation to the geological environment being studied, for example is it planned to collect a particular size or density fraction of a sediment in order to increase the likelihood of detecting economically important mineral deposits?
- The size of sample that should be collected, bearing in mind the heterogeneity of the source material and also the preparative and analytical techniques to be employed.
- The number and spatial distribution of samples [39].

- Whether special precautions need to be taken to avoid the chemical composition of samples changing during and after collection (e.g. oxidation or contamination from sampling equipment).
- How the precision or bias in any sampling scheme will be estimated.
- What quality assurance procedures will be used to ensure that samples are correctly, unambiguously and securely identified, and tracked through the analytical process.

Properly devised sampling schemes have always been important in, for example, mineral exploration, where typically the aim is to locate a relatively small area containing economically viable amounts of the desired substance present at concentrations significantly higher than those in the vastly greater volume of rock that makes up the surrounding countryside. Often the sampling techniques used and the media sampled are chosen so as to enhance the contrast between barren and mineralised areas. The need for well thought out geochemical sampling schemes has been given an added boost in recent years with the realisation that past industrial activity in many countries has left a legacy of contaminated land that cannot be safely redeveloped until the nature and extent of the contamination has been reliably delineated. The extremely heterogeneous nature of most of these sites adds to the many problems associated with sampling them.

In contrast to the voluminous literature on the estimation of analytical error, there are relatively few articles dealing with the uncertainty introduced into geochemical data by different field sampling schemes. Ramsey, Thompson and their colleagues have called attention to the need for a comprehensive framework and methodology concerned with the quality of sampling to be established [40]. They have drawn helpful analogies between analytical measurements and sampling procedures over concepts such as uncertainty, trueness, bias, accuracy, error, precision, internal quality control, proficiency testing and collaborative trials, and also proposed a role for reference sampling targets by analogy with reference materials. They had earlier highlighted the importance of considering both sampling variance and analytical variance in relation to natural geochemical variance in order to assess the overall fitness for purpose of data arising from a combination of the two operations [41–44]. They also pointed out the merits of using robust [45,46] rather than classical analysis of variance (ANOVA) when analysing data, in order to moderate the effects of outlying values. To illustrate some of these points they investigated the bias of different sampling protocols employed on an area of land contaminated by lead smelting in the 14th to 16th centuries [47–51], carrying out the analyses by ICP-AES. Ramsey [52] has published a tutorial review of sampling as a source of measurement uncertainty. An approach for optimising contaminated land investigations using measurement uncertainty to judge fitness for purpose was demonstrated by two case studies [53]. This has proved useful, especially in demonstrating the value of *in situ* measurement techniques, showing that they can be more cost effective despite the higher uncertainty of the measurements they produce [54]. Alternative approaches to the estimation of uncertainty arising from sampling have been described [55–57]. Recently, Ramsey has identified 12 issues that impact on the quality of environmental sampling and its associated uncertainty [58]. *In situ* measurements have allowed the direct study of heterogeneity, which is usually the factor limiting the uncertainty arising from sampling [59]. The wider field of geostatistical error management has been discussed in detail by Myers [60], mainly in the context of mapping areas compromised by hazardous wastes.

9.2.2 Sample preparation

9.2.2.1 Comminution

Once samples¹ have been collected according to an appropriate protocol, some form of sample preparation is almost always required prior to analysis. The aim of this very important step is to change the physical form of the geological material to make it compatible with the chosen analytical technique, but without changing its chemical composition. Whatever the subsequent treatment, the first stage is usually mechanical comminution of solid samples to produce a powder. The twin dangers during crushing and grinding, as with virtually all other sample preparation procedures, are that the chemical composition of the test material will be modified by contamination from the equipment or, less commonly, by loss of volatile analytes and that the original composition will be fractionated in some way so that the final powder will not be truly representative of the starting material, for example, by some minerals being more easily broken down than others or by density effects. Changes in oxidation state can also occur at this stage.

Most solid geological samples are composed of several minerals or other discrete phases. The resultant powder will thus be a heterogeneous mixture of particles derived from the various components. It is therefore essential to ensure that it is thoroughly mixed before sub-sampling for further treatment. If a sample has been stored for some time or subjected to vibration, differences in density, size, shape or magnetic properties between particles can cause selective settling. The problems of sub-sampling bulk particulate materials were examined in detail by Gy [63] in the 1960s and 1970s, largely in the context of mineral extraction and processing. Ingamells and Switzer [64] proposed the use of a 'sampling constant' in geochemical analysis to minimise sub-sampling errors. Many of the processes involved in the preparation of samples of contaminated land [65] are equally applicable to geological samples. Ramsey and co-workers have shown that it is possible to estimate and minimise the portion of measurement uncertainty that arises in sample preparation [66,67].

In practice, the aim of the primary reduction stages of sample preparation is to produce powders with uniform physical characteristics. It is usual to start with fairly large samples weighing between a half and several kilograms and to treat the whole sample initially, having first removed with a rock splitter weathered material and zones contaminated by equipment, hammer paint, cutting lubricant, drilling fluid, etc. and taken sub-samples from which thin sections can be made for later mineralogical examination. Depending on the nature of the geochemical investigation, it may be appropriate to separate mineralised vein material from the country rock at this point.

Typically, the first reduction stage involves reducing fist-sized lumps of rock to c. 4 mm particles in a mechanical jaw crusher. Some contamination of the sample by metal worn from the fixed and reciprocating plates of the crusher is inevitable. This can be minimised

¹ For convenience, and in line with common parlance, the term 'sample' is used loosely and interchangeably in this chapter rather than in the context of the strict IUPAC [61,62] hierarchy of terms which defines *sample* as a portion of material selected from a larger quantity of material. A *composite sample* may be made up of a number of *increments* or *primary samples* that are combined. The *laboratory sample* is the sample or sub-sample received by the laboratory. This may be processed to yield the *test* or *analytical sample*, from which a *test* or *analytical portion* is removed and analysed.

by using hardened chrome steel, which may contribute a few to tens of parts per million (ppm) of Cr and Mn and up to hundreds of ppm of Fe. Physical fractionation of the particulate product is sometimes observed during crushing, for example, when comminuting hornfelses or mica-rich rocks, and it is always important to mix the crushed material thoroughly before successively riffle splitting it to obtain a several hundred gram sub-sample, which is then taken on to the grinding or milling stages.

The coarsely crushed material may be reduced to fine powder in a vibrating cup mill, also known as a swing mill, Tema mill, ring and puck mill or shatter box in the USA. This consists of a circular pot with a shallow cylindrical cavity carrying one or more freely moving rings and a smaller solid puck. Sample is poured into the spaces between the mill elements, the lid firmly clamped on and the whole assembly subjected to rapid eccentric orbital motion within a safety enclosure. Particles are ground between the inner walls of the pot and the ring and puck. Various materials are used in the construction of vibrating cup mills. Hardened chrome steel has good wear resistance but contributes significant amounts of Fe, Cr, Mn, Ni, Co and V. Tungsten carbide is very hard and usually causes less contamination, but still contributes W and Co. Where it is essential to reduce contamination to the absolute minimum (e.g. for trace element studies) samples have traditionally been ground in mills made of the natural silicate material agate. While agate contributes negligible amounts of metallic contaminants, it is far less hard wearing than steel and prone to fracture. Its lower density means increased grinding times and it is extremely expensive – a single 100 ml capacity agate milling vessel can cost *c.* \$1000. Mills made of aluminium–silicon–oxynitride alloys (e.g. Syalon 101) are now available. In trials [68], this material exhibited high wear resistance, good durability, a milling efficiency intermediate between that of agate and steel, and low contamination potential, although contributions from its rare earth oxide additives (Y or Er) were detected.

A vibrating cup mill will reduce many solid geological materials to a 150 μm powder within 15 min. When a very fine powder, for example, $<30 \mu\text{m}$, is required, particle size can be reduced further by using a planetary ball mill such as the Fritsch P5. Typically, up to 25 g of powder is placed in the shallow cylindrical milling vessel, which also contains four freely moving solid spheres. The charged and capped milling vessels, usually in sets of four or eight, are securely clamped to a table that spins and counter-rotates them at high speed for typically 20–30 min. Similar factors of cost, durability and the likelihood of contamination govern the choice of construction materials for ball mills as with other milling equipment.

Apart from the ever-present problem of contamination, special care needs to be taken over the comminution of certain types of sample, such as bentonite, siliceous limestones, boulder clay and those consisting of hard particles dispersed in a softer matrix. Paradoxically, hard materials usually mill well because of preferential fracturing, whereas difficulty can be experienced with softer, more elastic minerals. Samples that are to be analysed for their precious metal content require special attention to avoid problems caused by the nugget effect (see Section 9.6).

The physical preparation of geological samples may be all that is required for some analytical techniques, such as XRFs, which are applied directly to solid materials. However, for analysis by ICP spectrometry, it is usually necessary to bring samples into solution. As we shall see shortly, this is not always a straightforward task for geological materials, some components of which can be extremely resistant to acid attack. As an alternative to dissolution, the introduction into the ICP of finely ground solids ($<5 \mu\text{m}$) in the form of a

slurry therefore has some attractions. Jarvis and co-workers [69,70] have discussed the role of slurry nebulisation in geochemical analysis by ICP spectrometry and demonstrated its use in the determination of gold and the platinum group elements (PGEs) [71] and the rare earth elements (REEs) [72]. Ebdon *et al.* [73] have reviewed slurry nebulisation in plasmas. Alternatively, electrothermal vaporisation (ETV) can be utilised for the direct analysis of slurries or solids by plasma spectrometry [74]. These sample introduction techniques tend to be limited to specialist applications and should be regarded as being complementary to other approaches [75].

In a novel and potentially powerful and information-rich approach to the direct analysis of fine particles by ICP spectrometry, Thompson [76] and co-workers modified the electronics of a standard ICP-AES system and investigated the time-resolved signals obtained from dilute suspensions (0.3 g l^{-1}) of refractory oxide and silicate minerals introduced by means of a Babington-type nebuliser. A fast multichannel analogue-to-digital converter and data acquisition system was connected directly to the anodes of the photomultiplier tubes via virtual-earth preamplifiers, enabling individual element channels to be sampled at a frequency of 20 kHz. They demonstrated that individual particles in a mixture of finely ground zircon, olivine and albite could be identified during their brief (*c.* 0.5 ms) passage through the observation zone of the ICP from, respectively, their Zr, Fe and Al signals. Moreover, they showed it was possible to distinguish between particles of orthopyroxene and clinopyroxene on the basis of the relative proportions of their Ca, Fe and Si signals. One would think that this approach could have application in process control in industry, as well as being useful to those studying particle generation in laser ablation (LA).

9.2.2.2 Sample decomposition and dissolution

While the direct injection of fine particles into the ICP, either as slurries, suspensions or as the products from LA events, has important applications in certain areas of geochemical analysis, at present by far the most common form in which geological materials are introduced into the plasma is as nebulised solutions. The preparation of these solutions is a major consumer of time and resources in the overall geoanalytical process. Like the preceding sample collection stage, it is a crucial process to which considerable thought, care and often ingenuity must be devoted to ensure that the analytical data subsequently obtained are fit for purpose.

There is a voluminous literature on the decomposition of geological and environmental materials. Detailed discussion of the topic is beyond the scope of this chapter. Extensive guidance can be found in books by Bock [77], Šulcek and Povondra [78], and other reviews [79–81, 82].

During the dissolution of any type of sample prior to analysis there is the danger that its chemical composition will be modified, either by contamination from equipment or reagents or by loss of analytes through, for example, volatilisation. A very real problem with geological materials is the incomplete dissolution of some phases. Analysts unfamiliar with handling geological samples should reflect on the fact that some mineral grains will have existed virtually unchanged for hundreds of millions of years, during which time they will have been subjected to high temperatures and pressures and been in contact with aggressive fluids. They are thus some of the most refractory solids known and extreme measures may be needed to render them into solution.

Because of the variety and complexity of geological materials, one must choose a sample decomposition technique that is compatible with the aims of the investigation, the mineralogy of the material, the elements to be determined and the analytical technique to be used. Sample decomposition procedures designed to produce solutions suitable for analysis by ICP spectrometry can be broadly grouped into three types:

- Complete or partial dissolution with acids other than hydrofluoric acid.
- Complete or partial dissolution with acid mixtures including hydrofluoric acid.
- Fusion at high temperature with a suitable flux, followed by dissolution.

Dissolution techniques should never be applied uncritically. They hide many pitfalls for the unwary geoanalyst. Regrettably but understandably, few reports highlighting problems with sample dissolution and the difficulties in data interpretation that can flow from them have made it to the open literature. Those that have repay reflection [83–90].

9.2.2.2.1 *Decomposition with acids*

Treatment of samples with concentrated inorganic acids, either separately or in combination, is probably the most commonly used decomposition technique in geochemistry. The key distinction between acid dissolution procedures is whether or not hydrofluoric acid is included to attack the silicate lattice.

Concentrated inorganic acids are readily available commercially in varying degrees of purity, which escalate along with their cost. Those of the highest purity may be used without further treatment to dissolve geological materials, even when data on many trace elements are being sought at concentrations down to tens of parts per billion in the solid. However, for certain elements (e.g. Pb) when full advantage of the great sensitivity of ICP-MS is being taken to determine them at ultra-trace levels, or for certain isotopic measurements, additional purification and digestion under clean-room conditions may be required to reduce contamination from acids and apparatus to acceptable levels. Full procedural blanks should be run frequently with all batches of samples analysed so that data quality may be monitored. In practice, lower limits of measurement for several of the first row transition elements (e.g. Cu and Zn) are limited by a combination of contamination from the acid and digestion process and matrix-related polyatomic interferences.

Concentrated hydrochloric and nitric acids are occasionally used on their own to dissolve some minerals. Both will attack carbonates readily. The oxidising character of nitric acid means that it is to be preferred for the dissolution of, for example, sulphides, tellurides and arsenides. Conversely, hydrochloric acid is better at dissolving iron and manganese oxides, borates and sulphates other than barite. However, these acids are most frequently used combined together as *aqua regia*, which is a mixture of three parts concentrated HCl plus one part concentrated HNO₃, to dissolve, or, more correctly, leach, a wide range of geological materials. The effectiveness of hot, fresh *aqua regia* is due partly to its strong oxidising character, the complexing ability of the chloride ion and the catalytic effect of the nascent chlorine produced. It is widely used to leach samples from mineral exploration surveys, where the aim is usually to identify anomalously high concentrations of target or pathfinder elements that indicate the presence of economically viable deposits.

While hydrochloric, nitric and also perchloric acids will all attack a wide range of minerals to varying degrees, only hydrofluoric acid² will break the strong Si–O bonds and disrupt the lattice of silicate minerals sufficiently to dissolve them. Hydrofluoric acid is rarely used on its own, partly because the fluorides of the some major elements, especially calcium, are not particularly soluble. Because of its ability to dissolve silica, hydrofluoric acid must be handled in plastic rather than glass apparatus. Sample decomposition procedures involving hydrofluoric acid should be carried out in polytetrafluoroethylene (PTFE), perfluoro-alkoxyalkane (PFA) or platinum vessels.

Hydrofluoric acid is typically used in conjunction with nitric and perchloric acids. The former, being a strong oxidising acid, will attack sulphides. The latter, also a strong oxidising agent when hot and concentrated, has a high boiling point and allows the acid mixture to be heated sufficiently to drive off the volatile SiF₄ and residual HF if the decomposition is carried out in open vessels. This loss of silica greatly reduces the total salt content of the final solutions, which is especially advantageous if analysis is to be carried out by ICP-MS. Perchlorates, other than those of some of the alkali metals, are generally very soluble, but they can also be unstable in anhydrous form and may spontaneously combust. For this reason, decompositions involving perchloric acid must be carried out in special fume cupboards where the exhaust gases are scrubbed with water and where wash-down systems are incorporated to avoid the build-up of potentially hazardous perchlorates in the hood and ducting.

Typically, residues of rock solutions derived from mixed acid digestions are dissolved in hydrochloric or nitric acid and then diluted to give solutions which are *c.* 5% (v/v) with respect to the acid. Where analysis is to be carried out by ICP-AES alone the choice of acid is not critical. However, nitric acid should be used if the solutions are to be analysed by ICP-MS, to avoid additional polyatomic interferences involving chlorine.

Because sample decomposition is often the rate-limiting step in the overall analytical process, advantage may be taken of the economies of scale that can be achieved during dissolution with acid mixtures in open vessels by processing large batches of samples in PTFE tubes or Savillex® PFA vials fitted into a programmable heating block. A typical procedure routinely used in the authors' laboratory for batches of 50–120 samples is given below:

- (1) Weigh 0.1 ± 0.0005 g of each sample into uniquely numbered, 18 mm diameter PTFE test tubes.
- (2) Add 1 ± 0.1 ml HF to each tube and swirl. Place the sample tubes into the hot-block and leave for at least 4 h at 50°C.
- (3) Remove the tubes from the hot-block and allow to cool to approximately room temperature. Dispense 0.8 ± 0.1 ml HNO₃ and 0.4 ± 0.1 ml HClO₄ into each tube. Swirl and replace in the hot-block.

²Safety note: Hydrofluoric acid is one of the most dangerous reagents found in the geoanalytical laboratory. It should be used only by those aware of the hazards and trained to handle it safely wearing appropriate protective clothing. It attacks by absorption through the skin, causing excruciating pain which can develop up to several hours after exposure. Affected areas should be washed with copious amounts of water immediately and an HF antidote consisting of calcium gluconate gel massaged into the affected area. Repeated applications of the gel may be necessary. A recurrence of pain some hours after exposure may indicate severe internal damage and medical help should be sought immediately.

- (4) Set the heating program to run for 5 h at 100°C, then 1 h at 140°C, followed by 6 h at 190°C. The cooler upper parts of the PTFE tubes above the hot-block encourage a degree of refluxing of the acid mixture. Care is required here to avoid baking the residue and forming insoluble fluorides [91].
- (5) Remove the tubes from the hot-block once they are cool enough to handle. Allow them to cool to approximately room temperature then add 1 ± 0.1 ml 50% HNO_3 .
- (6) Warm the tubes gently in the hot-block at 50°C for at least 30 min. Check that the solutions appear clear. Gentle swirling may help to encourage difficult samples into solution.
- (7) When the dissolution is complete, add 9 ml deionised water to each tube using an automatic pipette. Cap the tubes securely and shake vigorously.
- (8) Pour the contents of each tube into labelled clear polystyrene vials and cap securely.
- (9) Examine each solution to check for precipitates or any undissolved sample and record the details.
- (10) Procedural blanks, reference materials and duplicate dissolutions of the same sample should be included randomly within each batch at a frequency of not less than one for every ten samples.

Where decompositions involving $\text{HF}/\text{HNO}_3/\text{HClO}_4$ mixtures are carried out in open vessels, the volatile fluorides of other elements, including As, B, Cr, Ge, Sb and Ti, may be lost in addition to SiF_4 . To avoid this, decomposition may be carried out in sealed PTFE bombs and excess HF complexed by the addition of a saturated solution of boric acid. This will protect glass and quartz components of the ICP sample introduction apparatus from attack, but the total salt content of the solutions will be high and considerable dilution will be required.

9.2.2.2.2 *Decomposition by fusion*

Certain oxide and silicate minerals, such as cassiterite, chromite, corundum, rutile, spinel, zircon, tourmaline and beryl, are resistant to attack from hot acid mixtures. Fusion of the powdered sample with a suitable flux at high temperature, followed by dissolution of the melt, must therefore be employed to achieve complete decomposition. Several compounds have been used as fluxes, especially alkali metal borates, carbonates, oxides and hydroxides. Fusion with lithium metaborate was proposed by Ingamells [92] and is widely used, sometimes in conjunction with lithium tetraborate. It will successfully break down most – but not necessarily all [93,94] – silicate and accessory minerals. All fusion methods require a degree of manipulative skill and experience to obtain consistent results across the broad range of geological materials. An early review [95] of fusion using lithium metaborate gives an insight into some of the practicalities. Several factors need to be considered, including choice of crucible material in relation to cost, flux and sample type, ratio of flux to sample, fusion temperature and mode of dissolution of the melt. A typical procedure [16] involves thoroughly mixing 0.5 g of powdered rock with 1.5 g of lithium metaborate in a platinum crucible, heating for 30–45 min at 1000°C in a muffle furnace while swirling the melt occasionally, cooling to room temperature and immersing the crucible in dilute nitric acid on a magnetic stirrer for 1–2 h to dissolve the melt.

From the point of view of subsequent analysis by ICP spectrometry, especially ICP-MS, all fusion methods have the disadvantage that the presence of the flux raises the salt

content of the final solutions significantly. Greater dilution is therefore required prior to measurement than is necessary for solutions derived from acid digestion, and detection limits are degraded accordingly. However, with the much greater sensitivity of the current generation of ICP-MS instruments, acceptable limits of quantification can be achieved for many geologically important trace and REEs on a routine basis (see Section 9.5). There is evidence [81,87] that elements such as Pb and Zn may be lost by volatilisation during fusion. There is also the possibility that trace amounts of some analytes, present as contaminants in the flux, will be introduced. Careful assessment of data from the analysis of procedural blanks is therefore essential. Depending on the flux used, the determination of certain elements (e.g. Li and B) is obviously precluded. Moreover, contamination of the sample introduction system from the high concentrations of Li and especially B will make subsequent determination of those elements difficult at trace levels without rigorous cleaning.

Fluxes other than lithium borates are quite commonly used to prepare geological materials for the determination of particular suites of elements. Alkali metal carbonates have been used to fuse samples to be analysed for B [96–98], W and Mo [99]. Sodium hydroxide has a long history as a flux in the analysis of silicates [4,5] and was used by Walsh [100] in a preparation scheme for the determination of the REEs. This combined acid attack with fusion of the insoluble residue likely to include resistant minerals such as zircon, sphene and garnet, which can contain a significant proportion of the REEs (see Section 9.5). Fusion with sodium hydroxide requires a high flux to sample ratio, but it can be carried out in inexpensive nickel or zirconium crucibles and does not introduce into the final solution high concentrations of elements not already present in geological materials (e.g. Na). For similar reasons, an allied technique, sintering with sodium peroxide at 450°C, has the advantage that most geological samples can be completely decomposed by this method relatively rapidly, but high blanks may reduce its applicability to the measurement of elements at low abundances [82]. In the authors' experience, this technique has proved particularly good at attacking minor phases. When used in combination with glassy carbon crucibles, it contributes much lower levels of contamination from nickel or zirconium. This in turn reduces the levels of interferences from these elements. The reductive fusion that forms the basis of the fire assay technique for the determination of Au and the PGEs is discussed in Section 9.6.

9.2.2.2.3 *Microwave-assisted decomposition*

The decomposition of solid materials by acids and other reagents in closed vessels at elevated temperatures and pressures assisted by microwave radiation is often used as a sample preparation technique in the biomedical and environmental fields [101]. It has attracted attention in analytical geochemistry too, but the perceived advantages of most microwave systems need to be balanced against some important logistical considerations. An evaluation [102] of the dissolution of 51 geological reference materials with an $\text{HNO}_3/\text{HCl}/\text{HF}$ mixture in polycarbonate bottles in a microwave oven showed that, while many samples were completely dissolved, those containing minerals resistant to such acid attack, for example chromite, corundum, quartz, rutile and zircon, were not. A comparison [81] between lithium metaborate fusion, digestion with HF/HClO_4 in open vessels and digestion with $\text{HF}/\text{HNO}_3/\text{HClO}_4$ in sealed containers in a microwave oven showed little difference in the

elemental concentrations measured for nine reference materials between the open vessel and microwave digestion techniques, apart from higher values for chromium from some samples. Neither procedure was suitable for the dissolution of resistant mineral phases, resulting in low recoveries of elements such as Cr, Hf and Zr from some materials. The same workers carried out a detailed evaluation [103] of the use of two microwave systems, one incorporating a pressure monitoring and control system, in the determination of Au and the PGEs in seven geological reference materials. Despite a thorough investigation of a range of acid mixtures and heating cycles, they were unable to find a set of conditions that would allow the complete dissolution of all types of material. In several cases, insoluble residues remained which required subsequent fusion.

The picture that emerges about the suitability of most current laboratory microwave systems for aiding the dissolution of geological materials is that, while the moderately increased pressures (*c.* 5–15 bar) and temperatures inside sealed microwave vessels may speed up dissolution rates significantly, these effects are not sufficient to overcome the chemical and thermodynamic barriers to the dissolution of several geochemically important minerals. These remain largely resistant to attack, as they do during digestion with the same acid mixtures in open vessels [82].

A point in favour of microwave systems, which they share with all other sealed bomb-type digestion equipment, is the ability to retain volatile analytes, which may be crucial in some investigations. However, the fact that microwave-assisted dissolution is not as widely used in the preparation of geological materials for analysis as might be expected can be traced in part to manipulative and logistical factors. Most microwave systems consist of 6–12 specially designed vessels mounted in a carousel within the oven. Typically, these need to be charged with sample and reagents and then sealed carefully, often with the aid of a tool to apply a constant torque to the caps. At the end of a microwave irradiation cycle the vessels must be cooled before they can be opened safely. If no further microwave-assisted treatment is required, the digests are removed and taken on to the next stage of preparation.

At this point, the microwave vessels need to be thoroughly cleaned before the next set of samples can be added. This is not always a quick or straightforward task because of the insoluble residues generated by some materials. Investment in a second set of vessels will enable irradiation to continue while one set is being cleaned, but the actual throughput of samples attainable is still relatively low compared to the large numbers many geoanalytical laboratories are used to receiving. Because of the need to include procedural blanks, quality control standards or reference materials in the dissolution procedure, the number of actual samples that can be processed is further reduced. Other considerations include the initial capital cost and the fact that HClO_4 cannot be used with some systems because of the danger of reaction with the plastic used in their construction.

A radically different microwave system that may find significant application in the preparation of geological samples has recently been introduced by the Milestone company [18]. Instead of a conventional oven holding a small number of individual sealed vessels, their UltraCLAVE™ apparatus consists of a single 4.21 titanium–nitride-coated stainless steel vessel which is pressurised with nitrogen or argon up to 200 bar. Into this can be placed many tens of samples in conventional containers, which may be open or loosely capped to allow for equalisation of pressure. Microwave radiation from the magnetron enters the pressure vessel through a microwave-transparent port. The system offers the

possibility of processing large numbers of samples rapidly at pressures and temperatures where real improvements in the efficiency of acid digestion can be expected.

9.2.2.2.4 Selective extraction schemes

While total dissolution of geological samples may be the aim in many circumstances, the differential solubility of component phases may be turned to advantage in some investigations where information on the association of elements with particular phases is being sought, for example, to establish which metals are bound in sulphides, carbonate cements or oxide, and amorphous oxyhydroxide coatings. In some cases it may be sufficient to attack samples with mineral acids that leave the silicate lattice relatively intact. If more detailed information on the distribution of analytes between phases is required, selective extraction schemes, such as that proposed by Tessier and co-workers [104], may be used. These involve sequential dissolution of the sample with a variety of reagents, including weak acids, and oxidising, reducing and complexing agents. Such procedures have been used for many years in exploration geochemistry [105–108] and are now being applied in the environmental field [109–113]. However, several different schemes have been published and they all yield data that are heavily method dependent and need to be interpreted with care [114–116]. Because of the difficulty in comparing data obtained from different procedures, the European Commission has proposed a three-step sequential extraction scheme, commonly referred to as the BCR method, in which the exchangeable, reducible and oxidisable fractions are methodologically defined [117]. With modifications [118], it has been successfully used to provide reproducible inter-laboratory data for several soil and sediment reference materials [119,120] and is commonly applied as a reference method [121]. A very weak partial leach, based on the generation of hydrogen peroxide by the action of the enzyme glucose oxidase on dextrose [122], has been used for mineral exploration.

Procedures that combine non-specific extraction with chemometric data processing may offer an alternative approach [123–125]. The experimental design is based on sequential extractions using increasing concentrations of nitric acid, which simplifies the chemical analysis of the resulting solutions compared to many other sequential extraction schemes. Recently the method has been modified by substituting *aqua regia* as the extractant, on the grounds that it is more effective in dissolving iron oxides [126].

Chemical extraction tests are often used to evaluate the amount of bioaccessible metals and metalloids in potentially contaminated soils. In practice, however, they only give a broad idea of the easily mobilised fraction. Consequently, physiologically based extraction tests (PBET) have been devised to simulate the leaching of a solid matrix in the human gastrointestinal tract [127,128]. The test is essentially a two-stage sequential extraction using various enzymes at 37°C to mimic conditions in the stomach and small intestine. The BioAccessibility Research Group of Europe (BARGE) has undertaken a comparison of techniques [129] and the status of such *in vitro* methods has been summarised by Wragg and Cave [130]. At present these tests are only validated against animal or human studies for a handful of elements.

The inherent multi-element capability of ICP spectrometry makes it a particularly appropriate and powerful technique for the analysis of solutions derived from sequential extraction schemes. Some care needs to be taken to ensure that no artefacts are introduced into the data as a result of interferences from the different matrices. One approach is to evaporate the original solutions and take up the solutes in dilute nitric acid. In preparing solutions for analysis by ICP-MS quite large dilution factors may also be necessary.

9.3 Determination of major elements

It is a convention in geochemistry to distinguish between those elements that make up the bulk of the minerals in a rock – the major elements – and those present in very small amounts – the trace elements. Somewhat arbitrarily, a concentration greater than *c.* 0.1% by mass is often used to delineate major elements, while trace elements are taken to be those present below 0.1%. Occasionally, one may come across the term minor element referring to those elements present at concentrations between 0.1% and 1% but, given the great range in composition of geological materials and the fact that an element may be a major element in one type of rock and a trace element in another, such fine distinctions are not particularly helpful.

Geological materials vary enormously in their overall composition but, in the majority of silicate rocks, the elements Si, Ti, Al, Fe, Mn, Ca, Mg, Na, K and P constitute the major components. Expressed as their oxides, and summed together with the weight lost on heating the ground rock sample to high temperature, thus driving off CO₂ and H₂O derived, respectively, from carbon and hydroxyl ions, they typically constitute $100 \pm 0.5\%$ of the mass. This calculation is traditionally used as a first check on the likely reliability of any analytical data and is an indication of the levels of accuracy and precision expected of the determination of major elements in geological materials. In many geochemical laboratories, XRFS is routinely used to determine the ten major elements in rock samples. Measurements are carried out on glass discs made by fusing finely ground rock with 5–10 times its mass of a suitable flux, such as a 2 + 1 mixture of lithium tetraborate and metaborate. Fusion of the sample to a glass removes mineralogical and particle size effects, reduces surface roughness and produces a truly homogeneous solid. Provided that calibration has been carried out with suitable standards and appropriate corrections made for the mutual interference of elements, XRFS will yield accurate and precise data for major components on a routine basis.

The detection capability of ICP-AES is more than adequate to allow all the major elements to be determined once in solution, but the technique's typical precision of *c.* 1–3% relative standard deviation (RSD) would suggest that significantly poorer quality data might be obtained compared to that generated by XRFS. An approach that has been used successfully to improve the precision of ICP-AES measurements is to choose appropriate elements as internal standards for groups of analytes and to ratio their signals, thus smoothing out some of the fluctuations. For example [131], Ga has been used as an internal standard for Si, Al and Mg, Cd for Fe and Ca, and Li for Na and K. In order to retain Si and avoid the damaging effects of HF on the ICP sample introduction system, sample preparation for the determination of the major elements by ICP-AES requires fusion. However, advantage may be taken of this step to supply the Li internal standard, from the lithium metaborate, and to introduce the Ga as a 1% addition of Ga₂O₃ to the flux. In order to avoid the need for a separate fusion step, some laboratories will forego data on Si and determine the remaining major elements on solutions derived from the same mixed acid attack that is used to prepare samples for trace element determination. This can be a realistic compromise when the highest levels of accuracy are not required, but it must be remembered that values for titanium in particular may be affected by incomplete dissolution. Detailed recommendations about the choice of spectral lines for the determination of the major elements may be found in Thompson and Walsh [16].

In a detailed and objective assessment of the overall precision of methods for the determination of the major elements [132], it was found that XRFS using fused glass discs

yielded a value of 0.23% relative, compared to 0.43% relative for ICP-AES with internal standardisation following fusion. For many purposes, both techniques would therefore provide adequate data. In practice, the choice of method will largely be dictated by the instruments that a laboratory possesses.

The accurate determination of major elements at percentage levels in geological materials has not been a realistic role for ICP-MS up to now, although it has been attempted using a combination of pulse counting and analogue modes of detection [133,134]. However, the much greater sensitivity of modern ICP-MS instruments combined with the wider dynamic ranges afforded by the latest generation of detectors make it a feasible proposition. Moreover, improved cone design, variable mass resolution and collision cells can all be used to reduce background signals from the many polyatomic ions prevalent in this region of the mass spectrum. However, the precision obtainable in the measurement of major elements by ICP-MS is unlikely to match that of ICP-AES and certainly XRFs.

9.4 Determination of trace elements

By far the single most attractive feature of plasma spectrometric techniques that endeared them to analytical geochemists from the outset is their ability to detect a very wide range of trace elements, once they are in solution, at geologically realistic concentrations. Over the 35 years that ICP-AES instruments have been commercially available, this technique has reached the position – analogous to that attained earlier by XRF spectrometry – where it is widely regarded as a powerful and reliable geoanalytical workhorse. Its capabilities and limitations, in terms of tolerance to the composition and concentration of sample matrices, limits of quantitation and the resultant precision that is realistically obtainable in the determination of over 40 elements are well known. There is now a wealth of information available in the literature [16,25,135] to guide the budding geoanalyst through the minefields of plasma operating conditions, line selection, and the assessment and correction of spectral interferences.

The intensity of their spectral lines is such that many trace elements in unmineralised rock samples can be determined by ICP-AES directly in solutions derived from a mixed acid attack or a lithium metaborate fusion. Boron can be determined following fusion with alkali metal carbonates [96–98]. The REEs can be determined after fusion followed by preconcentration and separation from the matrix by cation-exchange (see Section 9.5.2). The hydride-forming elements (e.g. As, Se and Sb) can be determined by ICP-AES using appropriate sample introduction procedures. However, where alternative methods for determining these elements are available in a laboratory, such as atomic absorption or atomic fluorescence, it may be more economic and efficient overall to use them rather than tie up a powerful multi-element ICP-AES instrument in the measurement of a small number of analytes.

In mineralised rocks, a wider range of trace elements can be detected using ICP-AES, making it often the technique of choice for the rapid analysis of large numbers of samples from mineral exploration surveys. A further strength of ICP-AES is its sensitivity for the geochemically important light elements, Li, Be and B, which exceeds that of alternative techniques such as XRFs.

However, in unmineralised rocks, the limits of detection routinely attainable by ICP-AES are not really adequate to permit the direct determination of a number of geochemically important trace elements at their typical concentrations, either because of lack of

intensity of their main spectral lines or interference from matrix elements (e.g. Bi, Cd, Hf, Ta, Nb, Pb, Mo, W, Sn, Ag, U, Th, Au and the PGEs).

The greater sensitivity and wider elemental coverage offered by ICP-MS made it, from its earliest days [11], an attractive and potentially powerful technique for the determination of trace elements in geological materials. In the 25 or so years since its initial development, that promise has largely been fulfilled. Provided that samples can be brought into solution, or their vaporised constituents introduced into the plasma by alternative means, a large number of elements can be determined directly down to concentrations corresponding to a few tens of parts per billion in the solid. If some form of separation or preconcentration is employed prior to analysis, the limits of detection for many geologically important trace elements can be lowered further.

There are a number of types of interference that can invalidate geochemical trace element data obtained by ICP-MS analysis unless they are avoided or corrected. A major category of these are the signals detected at m/z ratios corresponding to isotopes of elements of interest but which are generated by ions other than those of the analyte. These include:

- Direct coincidence of two or more isotopes of different elements, for example the overlap of $^{58}\text{Fe}^+$ on $^{58}\text{Ni}^+$ or $^{114}\text{Sn}^+$ on $^{114}\text{Cd}^+$.
- Background signals – sometimes very large, but confined largely to the region of the mass spectrum below 80 m/z – caused by ions derived from the main elements and impurities present in the plasma as solutions are being nebulised, for example $^{40}\text{Ar}^{40}\text{Ar}^+$ at $^{80}\text{Se}^+$, $^{40}\text{Ar}^{14}\text{N}^1\text{H}^+$ at $^{55}\text{Mn}^+$, $^{40}\text{Ar}^{12}\text{C}^+$ at $^{52}\text{Cr}^+$ and $^{82}\text{Kr}^+$ at $^{82}\text{Se}^+$.
- Polyatomic ions derived from combinations of elements present in the plasma and samples, for example $^{40}\text{Ar}^{23}\text{Na}^+$ at $^{63}\text{Cu}^+$ and $^{94}\text{Zr}^{16}\text{O}^1\text{H}^+$ at $^{111}\text{Cd}^+$.
- Oxide ions (MO^+), for example $^{35}\text{Cl}^{16}\text{O}^+$ at $^{51}\text{V}^+$, $^{44}\text{Ca}^{16}\text{O}^+$ at $^{60}\text{Ni}^+$, $^{135}\text{Ba}^{16}\text{O}^+$ at $^{151}\text{Eu}^+$, $^{140}\text{Ce}^{16}\text{O}^+$ at $^{156}\text{Gd}^+$ and $^{143}\text{Nd}^{16}\text{O}^+$ at $^{159}\text{Tb}^+$.
- Doubly charged ions, for example $^{138}\text{Ba}^{2+}$ at $^{69}\text{Ga}^+$.

Other types of interference include suppression of signals from ions of lighter elements in the presence of high concentrations of heavier elements caused by space-charge effects, and non-linear variations in sensitivity during an analytical run related to salt deposition on the sampling cone.

Fortunately, many of these types of interference are now well documented. There is specific guidance available in the literature [17,18] on, for example, choosing which isotopes to measure in order to avoid or minimise polyatomic interferences [136–138], avoiding certain acids (e.g. H_2SO_4 and HCl) in the final solution so as not to generate additional solvent-related polyatomic ions, or limiting the total concentration of dissolved solutes to reduce drift. However, to ensure that the accuracy of data produced by ICP-MS analysis of geological materials is not compromised, eternal vigilance needs to be exercised over interference effects; especially when a laboratory is faced with analysing materials which differ markedly from those it is familiar with. The powerful multi-element capability of ICP-MS can be of immense assistance here, enabling a semi-quantitative picture of a sample's overall composition to be obtained rapidly, thus allowing the significance of potential interferences to be assessed. Similarly, inspection of the apparent isotopic abundances of individual analyte elements can be a valuable early warning of interferences at particular m/z ratios.

The precision of ICP-MS measurements depends to a large extent on the geoanalyst's ability to correct for changes in sensitivity, which vary in a complex fashion with both mass and time over an analytical run. Many laboratories base their corrections on only two or three internal standards to cover the whole of the mass range because of the difficulty of identifying other suitable elements. Enriched isotopes have been used [134] to expand the pool of useable internal standards and obtain a more even mass distribution. These, combined with regular measurements of a solution to monitor instrument sensitivity, gave improved precision for many analytes.

Further developments in instrumentation have meant that some of the polyatomic interferences which limit the determination of certain trace elements by ICP-MS can now, in principle, be overcome. Coupling an ICP source to a single- or double-focusing magnetic sector mass spectrometer [139–141], the latter usually in a reverse Nier–Johnson configuration, provides far greater mass resolution than is obtainable with a quadrupole. This enables the signals from some interfering polyatomic ions to be resolved from those of analyte isotopes occurring at very similar, but not identical, m/z ratios. For example, a mass resolution of *c.* 2500 allows the signal from $^{40}\text{Ar}^{16}\text{O}^+$ at 55.957 m/z to be resolved from that of $^{56}\text{Fe}^+$ at 55.935 m/z and that of $^{35}\text{Cl}^{16}\text{O}^+$ at 50.964 from $^{51}\text{V}^+$ at 50.944. However, mass resolutions approaching 10 000, which is roughly the limit achievable with most current commercial instruments, are needed to separate $^{40}\text{Ar}^{35}\text{Cl}^+$ from $^{75}\text{As}^+$, $^{40}\text{Ar}^{40}\text{Ar}^+$ from $^{80}\text{Se}^+$ and $^{143}\text{Nd}^{16}\text{O}^+$ from $^{159}\text{Tb}^+$. Magnetic sector ICP mass spectrometers also offer improved limits of detection compared to quadrupole systems because of high ion transmission and the low background count rate arising from their different ion beam geometries. This high sensitivity has been utilised in the measurement of Cd, Pb and U in Antarctic snow cores [142] at the picogram per gram level, but their greatest current and potential use in geological applications is probably in the precise measurement of isotope ratios (see Section 9.7).

Other strategies for overcoming polyatomic interferences include the use of cold/cool plasma techniques [143] and mixed gas, for example argon–nitrogen, plasmas [144–146]. Collision or reaction cells [147,148], which up to now have tended to be used to solve specific interference problems, may in the future be used more widely to reduce background polyatomic interferences.

The determination of specific groups of trace elements of particular interest to earth scientists is discussed in the following sections.

9.5 Determination of the rare earth and other incompatible trace elements

9.5.1 Background

The coherent yet subtly varying nature of the chemistry of the REEs,³ which derives from the steady filling of their shielded 4*f* sub-shell and a consequential decrease in ionic radius,

³The term 'rare earth elements' is sometimes taken to include the lanthanides and the other trivalent Group III elements, Sc and Y. Here it is used in its widely accepted geochemical sense to cover the elements La–Lu.

makes them an especially important group of trace elements to geochemists interested in unravelling the complexities of petrogenetic processes [149]. The REEs, together with the high field-strength elements, HFSEs (Nb, Ta, Zr and Hf) and elements such as U, Th, Ba, Rb and Cs, are referred to as incompatible because they are not readily accommodated in the structures of the main igneous or metamorphic minerals. Their large ionic radii, in the case of Rb and Cs, or high polarising power mean that they tend to be excluded from the ferromagnesian, plagioclase and other minerals that crystallise first from magmas. They thus tend to be preferentially concentrated in later crystallising accessory minerals. Within the REEs, the degree of incompatibility decreases from the larger light REEs (LREEs) to the smaller, more compatible heavy REEs (HREEs).

Most REEs exhibit an oxidation state of +3. The two exceptions are cerium, which can form Ce^{4+} in oxidising environments, and europium, which can exist as Eu^{2+} under reducing conditions. Since Eu^{2+} has a similar radius to Ca^{2+} , it can substitute for Ca in plagioclase and become depleted in the melt. A negative europium anomaly is thus a valuable indicator of the oxygen fugacity prevailing during magma fractionation and mineral formation.

Nowadays, interest in REE geochemistry extends far beyond the domain of classical petrogenesis [150]. Data on the REE content of geological materials can provide diagnostic information on ore formation, mineral alteration, the provenance of detrital grains and even shed light on the origin of archaeological artefacts. They have been used as geochemical tracers in studies of water–rock interaction and regional groundwater movement [151–153], and can help us unravel the hydrothermal processes occurring at mid-ocean ridges [154]. Fresh impetus has been given to studies of the mobility of REEs in the environment by their use as analogues for the actinides in studies concerning the disposal of radioactive waste. Thus the demand for the measurement of REEs at trace levels in geological materials has never been greater.

Before the advent of ICP techniques, established methods for determining REEs included instrumental neutron activation analysis (INAA) and isotope dilution–thermal ionisation mass spectrometry (ID-TIMS). These are relatively time-consuming and expensive techniques but they do possess the necessary sensitivity to detect the REEs at the low concentrations at which they occur in the geosphere. The analytical requirements for the REEs can be gauged from their average concentrations in chondritic meteorites, which can be said to represent the composition of the Earth's primordial mantle. These are [155], in $\mu\text{g g}^{-1}$: La (0.24), Ce (0.64), Pr (0.1), Nd (0.47), Sm (0.15), Eu (0.058), Gd (0.2), Tb (0.37), Dy (0.25), Ho (0.057), Er (0.17), Tm (0.025), Yb (0.16) and Lu (0.025). The so-called chondrite-normalised values can be calculated from REE concentrations measured in terrestrial igneous rocks, so ironing out the saw-tooth pattern that would otherwise arise when such data are plotted. In groundwaters, the REEs are typically present at or below $\mu\text{g l}^{-1}$ levels. Their concentrations in seawater are very low, c. $0.1\text{--}5\text{ ng l}^{-1}$, and some form of pre-concentration, for example, complexation and adsorption onto C_{18} resin [156] or the use of ion chromatography [157], is required prior to measurement.

9.5.2 Determination of the REEs by ICP-AES

Inherently, ICP-AES has good sensitivity for the REEs. However, its performance for many of the REEs is compromised by the complexity of their emission spectra, together with a number of severe interferences from major elements. Thus, to obtain reliable data by

ICP-AES down to chondritic abundance levels, the REEs must be separated from the matrix elements; this is usually achieved by cation-exchange, following dissolution of the sample.

In one of the first ICP-AES methods published [100], still widely used, 4 ml of HClO_4 and 15 ml of HF were added to 0.5 g of powdered rock sample in a platinum crucible, evaporated to incipient dryness, cooled and dissolved in 20 ml of 25% HCl. The solution was filtered and the residue ignited to 800°C in a silver crucible before being fused at 800–850°C with NaOH. The cooled melt was dissolved in 25 ml of 25% HCl, combined with the acid digest filtrate and diluted to about 100 ml to reduce the acid strength to <10% HCl. The resulting solution was loaded onto columns containing Dowex AG 50W-X8 resin in its acid form and rinsed through with 450 ml of 1.7 M HCl. This was discarded as it contains the major and most of the trace elements. The REEs were then eluted with 600 ml of 4 M HCl. After the addition of a few mls of nitric acid, the eluted solution was evaporated to dryness and taken up in 5 ml of 10% nitric acid.

The complex emission spectra of the REEs require careful examination in advance of line selection and measurement by ICP-AES. Walsh [100] provides an evaluation of the alternative wavelengths, taking into account the relative abundances of the REEs encountered in geological materials, as well as their analytical sensitivity and spectral interferences. Other compilations are available [13,25]. Calibration is usually performed using synthetic multi-element mixtures of the REEs and Y, often obtained commercially. It has been estimated [25] that a precision of 3% RSD and an accuracy of better than ± 5 –10% can be obtained for most elements using the cation-exchange ICP-AES method. This is probably as good as much of the data in many of the published compilations of the REE content of reference materials.

9.5.3 *Determination by the REEs by ICP-MS*

Very early in the application of ICP-MS to geochemical analysis, it was appreciated that the simple nature of the REE mass spectrum, combined with superior detection limits, would allow the determination of all the REEs in silicate rocks without separation from the matrix [11]. Data indicated that most of the REEs could be quantified down to 10 times chondritic values, using a dilution factor of 500 on a sample subjected to a HF/HClO_4 attack [158].

It is important to appreciate that in many rocks the majority of the REEs, particularly the HREEs, reside in minerals such as zircon, sphene, garnet, apatite and monazite. Many of these minerals are not completely dissolved by a conventional open vessel HF/HClO_4 attack (see Section 9.2.2.2). In some of the early descriptions of the application of ICP-MS techniques to the measurement of the REEs [12,158–161] great reliance was placed on the ability of an HF-based attack to render all the sample into solution. In many cases this was probably true because of the mineralogical composition of the reference materials selected. There was also resistance to adopting a method involving fusion because of the high salt content of the final solution. However, Hall and Plant [85] tell the cautionary tale of the reporting of misleading data produced from samples which had been subjected only to an HF/HClO_4 leach. To obtain reliable data for the REEs and other elements such as Zr and Hf from samples of unknown composition, complete dissolution needs to be ensured, either by a ‘mini-fusion’ of the insoluble residue or fusion of the entire sample [25].

Whereas the salt content of solutions analysed by ICP-AES is usually limited to 1–2%, ICP-MS is less tolerant of high total dissolved solids (TDS) and their concentration is usually kept below 0.2%. Using the ion-exchange separation technique developed for ICP-AES is one way to ensure that the final solution has low TDS ($<0.001\%$) and will permit the determination of REEs down to well below chondritic abundance in most geological materials [158]. The efficiency of recovery of the REEs through the ion-exchange process may be monitored by the use of a pure Tm spike [162,163]. However, with the superior sensitivity and stability afforded by the latest generation of quadrupole ICP-MS instruments, acceptable detection limits can be achieved by analysing fusion-based digests directly, even with large dilution factors. A combination of sample decomposition with sodium peroxide and ICP-MS [20,82,164] has been shown to be a simple and robust procedure for the determination of the REE present at chondrite-normalised abundances of greater than one, together with other geochemically important elements, such as Hf, Nb, Ta, Th, Y and Zr. Meisel *et al.* [164] selected a sample:flux ratio of 1:6 and performed the sodium peroxide sinter/fusion in glassy carbon crucibles. Separation may still be required to determine the REE at very low abundances [165]. Alternative strategies, such as the use of ultrasonic and microconcentric desolvating nebulisers [166], an external correction procedure [167] and ID multiple collector (MC)-ICP-MS [168], have also been explored. In reality, the procedural blanks may well control the detection limit that can be achieved, whichever method is selected.

Each of the REEs has at least one isotope free from isobaric interference in the mass range 139 (La) to 175 (Lu). This region is almost free from polyatomic ions formed from matrix elements. However, the formation of oxide ions (MO^+), 16 mass units higher than the parent isotope, is a common feature in ICP mass spectra, particularly for refractory elements such as the REEs. Thus oxides of the LREEs will interfere with the determination of the HREEs. This is compounded by the fact that in the geosphere the abundance of the LREEs is normally greater than that of the HREEs, and is particularly serious for rocks in which the LREEs are enriched. Moreover, barium, often present in rocks at $>100\text{ }\mu\text{g g}^{-1}$, also forms a series of BaO^+ ions which interfere with both isotopes of Eu.

On modern ICP-MS instruments the operating conditions can be optimised so that the oxide levels are no more than 1% for CeO^+ which, along with La, has the greatest oxide ion yield of the REEs [169]. For any particular set of instrumental conditions, the production of oxides remains relatively constant [170]. Therefore single-element solutions of Ba and the REEs can be analysed and used to correct for oxide formation. A suggested list of isotopes and the corrections required are given in Table 9.1. A more comprehensive account of possible interferences, which also serves to demonstrate the additional polyatomic ions encountered when samples are prepared in HCl, is given by Dulski [169]. Potential interferences from oxychlorine ions, arising from the use of perchloric acid in sample preparation, have also been reported [171].

ICP-MS calibrations are typically performed using matrix-matched synthetic multi-element solutions of REE and Y, which can be prepared from single-element standards and are available commercially as a certified mixed standard. Usually one or more internal standards (e.g. In and Re) are added to the dissolved samples, blanks and reference materials to monitor signal suppression and drift in sensitivity throughout the analytical run. In some laboratories an REE monitor solution is inserted every 5–10 samples and used to correct for changes in signal sensitivity, primarily due to progressive blocking of the cones. Other

Table 9.1 Suggested isotopes for the quantification of the REEs by ICP-MS

Element	Mass	Interferences/comments
La	139	Virtually monoisotopic (99.9% abundant)
Ce	140	Major isotope
Pr	141	Monoisotopic
Nd	146	17.2% abundant
Sm	147	15% abundant
Eu	153	$^{137}\text{Ba}^{16}\text{O}^+$
Tb	159	$^{143}\text{Nd}^{16}\text{O}^+$
Gd	160	^{160}Dy (2.34%), $^{144}\text{Nd}^{16}\text{O}^+$, $^{144}\text{Sm}^{16}\text{O}$
Dy	163	24.9% abundant, $^{146}\text{Nd}^{16}\text{O}^{16}\text{H}^+$, $^{147}\text{Sm}^{16}\text{O}$
Ho	165	Monoisotopic
Er	166	33.6% abundant, $^{150}\text{Nd}^{16}\text{O}^+$, $^{150}\text{Sm}^{16}\text{O}$
Tm	169	Monoisotopic
Yb	172	21.9% abundant
Lu	175	97.4% abundant

workers have modelled non-linear drift using frequent measurements on a solution of a dissolved rock, and then used a spreadsheet macro to make corrections [172].

9.5.4 Determination of other incompatible elements

One of the Earth's fundamental geodynamic cycles is the formation of oceanic lithosphere at mid-ocean ridges and its later injection back into the mantle at convergent plate boundaries. Studies of the evolution of the mantle-crust system over geologic time rely heavily on geochemical data to shed light on the various melting and fractionation processes that give rise to the observed compositions of crustal rocks. In addition to the REEs [173], other incompatible elements, such as the large ion lithophile elements (LILEs) and especially the high field-strength elements (HFSEs), are valuable tools for probing the origins of magmas and their melting histories.

Two pairs of HFSEs, Zr and Hf, and Nb and Ta, are used extensively in such studies because of their similar charges and virtually identical ionic radii. It is subtle changes in their abundance ratios that are of particular interest to geochemists. Hence the quality and comparability of analytical values for these elements within and between datasets are of crucial importance. Until relatively recently, different techniques had to be employed to determine the individual HFSE. Either XRFS or the more sensitive spark-source mass spectrometry (SSMS) was widely used to measure Nb. INAA was used to determine Hf and Ta, while Zr was usually measured by XRFS. Detailed comparisons between methods [174] have suggested that there are discrepancies, for example between values for Nb obtained by SSMS and XRFS.

As with the REEs, a major consideration in the determination of the HFSEs by ICP techniques is the need to ensure complete dissolution of their resistant host minerals such as zircon [85]. Although it is possible to determine Zr and Nb by ICP-AES directly in solutions

following lithium metaborate fusion with detection limits corresponding to 1 and 2.5 ppm, respectively, in the original solid [175], Hf and Ta suffer from a number of spectral interferences and their detection limits are inadequate. Thus separation from the matrix elements and preconcentration is necessary before the HFSEs can be determined by ICP-AES. Watkins and Nolan [176] modified their REE cation-exchange separation method, by adding oxalic acid to the 6 M nitric acid elutant, and were able to determine Hf down to $0.2 \mu\text{g g}^{-1}$ by ICP-AES, in addition to the REEs, Y and Sc.

The advent of ICP-MS opened up the possibility of determining all the HFSEs by a single technique. Lower limits of detection and improved precision should enable smaller variations in Nb:Ta ratios to be used with greater confidence in unravelling the geochemical processes and complex histories of mantle source regions [177]. Nevertheless, separation of the HFSEs from the matrix elements was often necessary prior to measurement by ICP-MS, in order to reduce the TDS in the final solution to an acceptable level. Hall [175] used cupferron to separate the analytes from a lithium metaborate fusion solution prior to analysis.

Systematic variations in the Nb:Ta ratios of basaltic and andesitic rocks, obtained from ICP-MS measurements, have been used to constrain the source in a Cambrian arc-back arc system [178]. Although the need for complete dissolution was recognised, an HF/HClO₄ digestion was used. This avoided the inherently higher reagent blanks of a LiBO₂ fusion and the analytical problems arising from the resulting high TDS matrix, and also the difficulties of determining Li and B at low levels in subsequent samples because of contamination of the instrument by the flux. Problems with the stability of Nb and Ta in dilute nitric acid solutions were encountered. The addition of 2% HNO₃, 0.5% HCl and 0.1% HF to stabilise solutions containing more than 4 ppb Ta and 100 ppb Nb was recommended. For lower concentrations of these elements, the addition of 2% HNO₃ and 0.5% HCl together was sufficient to keep them in solution. As well as the HFSEs, the REEs and the LILEs were determined in solutions which represented a 1000-fold dilution of the original sample. Rh, In and Re were used as internal standards. Limits of quantitation of $0.07 \mu\text{g g}^{-1}$ for Nb and $0.02 \mu\text{g g}^{-1}$ for Ta were achieved. Memory effects were observed, especially for Ta. The poor washout characteristics of the HFSEs have been noted and wash procedures involving nitric acid spiked with two drops of HF per 300 ml [179], or a 60–90 s surfactant wash, followed by a 180 s wash with 2% nitric acid [134] have been used to reduce the blank signal to an acceptable level.

In the authors' laboratory, 42 major, minor and trace elements, including the REEs, Y, Zr, Nb, Hf, Ta, U and Th, are determined by ICP-MS after fusion with sodium peroxide to ensure complete dissolution:

- (1) Weigh 0.2 g of finely ground sample into uniquely numbered glassy carbon crucibles and add 1.0 g of sodium peroxide flux using a metal spatula. Mix carefully until the fine loose sample powder coats the coarse flux grains.
- (2) Fuse in a preheated furnace at 480°C for 1 h, unless there is a significant organic component, that may ignite. In this case, either ignite the sample first or heat slowly from ambient to 480°C.
- (3) Remove the crucibles from the furnace and allow to cool on an appropriate surface.
- (4) Transfer the crucibles to a fume cupboard. Add deionised water dropwise to the fused materials in the crucible until the reaction subsides. Continue to add water until the crucible is about two-thirds full (20 ml) and leave for 1 h to leach.

- (5) Partially fill clean 250 ml plastic volumetric flasks with 12.5 ml of 50% HCl and 1 ml of conc. HF. Carefully pour the contents of each crucible into a numbered volumetric flask via a plastic funnel, transferring as much of the solid as possible. Rinse the crucible and funnel with a few mls of deionised water.
- (6) Add 12.5 ml of 50% HCl to each crucible and leave for 15 min.
- (7) Carefully pour the contents of each crucible into the correct volumetric flask. Rinse the crucible three times with a minimal amount of 1% HCl, transferring the washings to the volumetric flask. Make up to volume with deionised water. The final solution is in 5% HCl with a trace of HF.
- (8) Leave until fully dissolved: this may take between 1 and 12 h depending on the sample type. Transfer to a plastic bottle for storage.
- (9) Before analysis dilute the sample solutions fourfold with 1% nitric acid, giving a total dilution of 5000. During aspiration of the sample, add indium and rhenium internal standards at a nominal concentration of 10 ng ml^{-1} via a T-piece, giving an overall dilution of 10 000 in the plasma.
- (10) Prepare matrix-matched calibration standards, that is in 20% v/v sodium peroxide, 1% HCl and 1% HNO_3 .
- (11) Include matrix-matched monitor solutions containing most of the elements of interest at 10 ng ml^{-1} at regular intervals throughout the analytical run and use these to correct for instrumental drift.
- (12) Include two blanks, two duplicate samples and two reference materials with each batch of 20 samples prepared.

9.6 Determination of gold and the PGEs

At concentrations of $1\text{--}10 \text{ ng g}^{-1}$, the average crustal abundances of gold and the PGEs (Pt, Pd, Rh, Ru, Ir and Os) are some of the lowest in the Periodic Table. Their determination in unmineralised rocks therefore presents a great challenge to any analytical technique. Moreover, their distribution is particularly heterogeneous in that they often occur as discrete particles of the native metal or as solid solutions or metallic inclusions in other minerals (e.g. chromites and sulphides). This nugget effect means that quite large amounts of material may need to be collected to provide a representative sample and has implications for subsequent sample preparation and analysis [180].

Geochemically, Au and the PGEs are classed as highly siderophilic elements. Their behaviour and distribution in the Earth can thus shed light on the evolution of the core–mantle equilibrium. Moreover, the upper mantle appears to contain an excess of PGEs over what would be expected at equilibrium [181] and it is thought that this may have been introduced as a ‘late veneer’ by meteorite bombardment during the Earth’s early history. High concentrations of some of the PGEs, particularly Ir, have been linked to later impact events that are thought to have had major consequences for life on our planet. The fractionation of Au and the PGEs that has been noted during partial mantle melting and their resultant variable signature in different rock types can potentially help us understand the subduction history of different parts of the lithosphere. However, all studies of these elements have been hampered in the past by the lack of reliable data on their concentrations in unmineralised rocks.

This situation is being slowly rectified as more sensitive methods of analysis, including ICP spectrometry, are applied to their measurement.

Nowadays, apart from their use in coinage and jewellery, Au and the PGEs have important uses in electronics, industrial catalysts, glass for cathode-ray tubes and liquid-crystal displays, road vehicle catalytic converters and as anti-cancer agents. The growing use of Pt, Pd and Rh, especially in automobile catalysts – 3.9 million ounces of Pt in 2005, of which only 0.8 million ounces were recovered – has triggered interest in the natural background levels and cycles of these elements in the environment and how they might be perturbed by anthropogenic inputs [182,183–185]. Hence there is an increasing requirement for ultra-sensitive analytical methods for the PGEs over and above the traditional needs of mineral exploration.

Because the PGEs occur at such low concentrations, they can be determined usually only after separation from the rock matrix and preconcentration, although INAA offers a means of measuring Au down to ng g^{-1} levels directly. As they often occur in minerals that are resistant to acid attack, some sort of fusion is required to bring them into solution. Fire assay remains the mining industry standard for precious metal determinations because it is able to deal with large sample masses and is amenable to a range of analytical finishes. The ascendancy of ICP-MS predicted by Hall and Bonham-Carter [186] is reflected in more recent reviews [187–189] of methods for the determination of Au and the PGEs in geological and related materials.

Fire assay is an ancient technique that has been used to separate and refine noble metals since the third millennium BC. There are several references to it in the Bible. In Proverbs 17:3 we read, 'The fining pot is for silver and the furnace for gold: but the Lord trieth the hearts'. The lead fire assay procedure is a reductive fusion technique, in which finely ground sample is intimately mixed with litharge and a reductant such as wood charcoal or flour, and a flux typically containing sodium carbonate, borax, silica and possibly calcium fluoride to improve fluidity, and heated in a fire clay crucible in a furnace at *c.* 1050°C for about 45 min. The exact composition of the flux will depend on the type of sample being analysed [190]. The aim is to produce a melt of two dispersed, immiscible phases: one of molten lead formed by reduction of the litharge (PbO) and a liquid borosilicate slag. Gold and the PGEs have high solubilities in molten lead and are scavenged into it. The melt is poured into a warmed iron mould where the lead, because of its higher specific gravity, collects at the bottom. The solidified mass is turned out and the lead button separated from the glassy slag and mechanically cleaned. The next stage is to remove the lead from the noble metals by an oxidative process known as cupellation. The lead button is placed on a shallow dish called a cupel, historically made of compressed bone ash, which has been preheated in a furnace to *c.* 1000°C. Within 30–45 min the lead is rapidly oxidised to molten lead oxide, most of which is absorbed by the cupel, and a small amount is volatilised. The noble metals remain on the cupel as a small bead or prill. Recovery of Au, Pt and Pd is regarded as quantitative but some Os, Ir and Ru are lost as their volatile oxides during cupellation. Where the concentration of noble metals in the samples is expected to be low, silver is added to the initial charge either as powdered metal or, more commonly, as silver nitrate solution. This helps to prevent the loss of trace amounts of Au and PGEs and produces a prill large enough to handle. Gold is sometimes added instead of silver if the former is not to be determined and Rh is to be measured [191].

The silver or gold prill obtained from lead fire assay is used as the starting point for many of the analytical techniques subsequently used to determine noble metals, including AAS and

ICP spectrometry, after dissolution of the prill. The superior detection capabilities of ICP-MS make it an attractive technique for the simultaneous determination of Au, Pt and Pd. In the ICP-MS procedure developed by Hall and Pelchat [192] the silver prill derived from a 10 g sample is dissolved in 0.5 ml of 3 M HNO_3 in a graduated test tube. This is heated for 30 min in a water bath at 90°C. Once the prill has dissolved, 0.5 ml of 2.5 M HCl is added to precipitate excess silver. The solution is heated for a further 10–15 min to avoid low recovery of Pd, made up to 5 ml with water, mixed and centrifuged. On a 10 g sample this procedure yields detection limits of 2, 0.1 and 0.5 $\mu\text{g g}^{-1}$ for Au, Pt and Pd, respectively. This method has been used for regional geochemical mapping in Jamaica [193] and the Shetland Islands [194] and to investigate lithostratigraphic and structural controls on the distribution of gold in the Southern Uplands of Scotland [195].

An alternative fusion technique involving collection into nickel sulphide, rather than lead, was developed [196] in the 1970s based on the earlier work of Williamson and Savage [197]. The fusion mixture typically consists of 5–20 g of pure nickel powder, depending on the amount of sample taken, *c.* 10 g of sulphur, and a flux typically consisting of a 2:1 mixture of borax to sodium carbonate, and silica as required. As with lead fire assay, the precise make-up of the charge is usually calculated from previous knowledge of the overall sample composition. After fusion at *c.* 1000°C and pouring into an iron mould, the NiS button is separated from the slag. There is no cupellation step. Instead, the PGE sulphides are separated from the nickel sulphide by dissolution of the latter in a large quantity (400–600 ml) of hot concentrated HCl in the presence of H_2S and filtered off. The PGEs are collected quantitatively by this method but some gold is lost. This procedure was initially adopted for use with INAA by sealing the filter paper containing the PGEs in a vial and irradiating [198]. In order to avoid the dissolution step and to minimise the high background radiation from ^{58}Co derived from the large mass of nickel normally used, later workers [199] investigated the possibility of directly irradiating a small nickel sulphide button [200].

For subsequent measurement by solution techniques, the separated PGE sulphides are dissolved in a mixture of HCl and H_2O_2 as used in the first application of ICP-MS to the determination of the PGEs [201]. Detailed investigations of the losses of the PGEs that can occur during the various stages of nickel sulphide collection and subsequent dissolution have been carried out [202–205]. Coprecipitation with tellurium can be used to improve the recovery [202,206]. Comparison between lead and nickel sulphide fire assay collections followed by ICP-MS determination [207] indicates that the former gives good recoveries for Au, Pt and Pd, and that the latter gives the highest recoveries for Ir, Os, Rh and Ru. In particular, high base metal content in a sample can impede the recovery of Au, and possibly also Pd, from a nickel sulphide assay [208]. Proposed modifications to the nickel sulphide method include the addition of iron to the fusion charge, to produce a button that dissolves more easily in HCl [209], and a new flux mixture that incorporates sodium metaphosphate to achieve complete dissolution of chromite minerals [210].

Both lead and nickel sulphide collection involve the use of large amounts of solid reagents that are difficult to purify, so ultra-low-level determinations of Au and the PGEs may be blank limited. Fire assay is rightly regarded as a skilled craft as much as a scientific procedure; considerable experience is required to achieve consistent fusions across a broad range of rock types. Accordingly, there have been numerous investigations of other procedures to determine Au and the PGEs in order to avoid the fire assay step and its reliance on skilled staff. These have included dry chlorination [211], fusion with sodium peroxide followed by coprecipitation

with Te [212,213], slurry nebulisation [71] and various combinations of microwave digestion, alkali fusion and ion-exchange preconcentration [103,214–217]. Opinions vary about whether anion- or cation-exchange resins provide better recovery. A combination of ID, high pressure asher acid attack, on-line cation-exchange separation of the PGEs and ICP-MS detection has been advocated for measurements of high accuracy and low uncertainties [218–219]. Recovery of the noble metals with an *aqua regia* leach is heavily dependent on the nature of the rock sample, although good recoveries of Pd and Au are usually achieved [220]. Direct LA of a <1 g nickel sulphide button has been explored [221].

Once the PGEs and Au have been separated from the rock matrix, concentrated and brought into solution, their determination by ICP-MS is relatively straightforward. They lie in two separate regions of the ICP mass spectrum: ^{96}Ru to ^{110}Pd and ^{184}Os to ^{198}Pt . All have at least one isotope free from isobaric overlap and are relatively free from interferences from polyatomic ions, especially after separation by fire assay. High levels of Ni, sometimes carried through from the fire assay procedure, and Cu from high copper samples may give rise to interferences on Ru, Rh and Pd via $^{61}\text{Ni}^{40}\text{Ar}^+$, $^{64}\text{Ni}^{37}\text{Cl}^+$, $^{63}\text{Cu}^{40}\text{Ar}^+$ and $^{65}\text{Cu}^{40}\text{Ar}^+$ [202]. Where samples have been fused in zirconium crucibles, for example using sodium peroxide, a range of ZrO^+ and ZrOH^+ ions may interfere with some isotopes of Pd. Although modern high-resolution ICP-MS instruments are capable of separating some of the potential interfering polyatomic ions [222–223], the determination of Pd remains a challenge unless chemical separation is employed. Various isotopes have been used as internal standards, including ^{111}Cd , ^{203}Tl , ^{115}In and ^{187}Re .

In many ways, the analysis of geological materials for the PGEs by ICP spectrometry epitomises many of the problems of the determination of trace elements in geochemistry. It highlights the fact that the final detection step is rarely the limiting factor, apart from sensitivity considerations. Much greater problems are associated with reliably separating trace analytes from rocks of widely varying composition and preconcentrating them with no, or at least quantifiable, losses. It is these stages that tax the ingenuity of the geoanalyst and trap the unwary.

9.7 Measurement of isotope ratios

The capability to determine the isotopic, rather than just the elemental, composition of geological materials is immensely valuable. Precise measurement of the abundance of two isotopes linked by a radioactive decay chain of known half-life provides earth scientists with one of their most important tools: the ability to date geological events. The isotopic signatures of elements in geological materials can indicate different origins or components that are not apparent from measurements of their bulk chemical composition. In geochemical analysis, as elsewhere, the technique of ID can be harnessed to yield some of the most reliable analytical data obtainable.

Isotope geology is a major area of the earth sciences which is only touched on very briefly here. It is a field to which ICP spectrometry has already made significant contributions, particularly since magnetic sector ICP-MS instruments became more widely available. The potential capability of ICP-MS to determine isotope ratios was one of the drivers in its early development [224] and was used by geochemical laboratories soon after commercial instruments became available [225–227]. The basic principles and key instrumental parameters involved in determining isotope ratios by ICP-MS can be found in Chapter 6 of this volume.

It is the level of precision needed in the measurement of isotope ratios for dating purposes that makes this the most exacting application for ICP-MS because the variations in the isotope ratios that must be detected are very small. For example, in the widely used Rb–Sr geochronometer, where ^{87}Rb undergoes β -decay to ^{87}Sr , which is measured as a ratio against the stable ^{86}Sr isotope, the value and uncertainty ($2s$) of a measured $^{87}\text{Sr}/^{86}\text{Sr}$ ratio might be 0.710235 ± 20 . Variations in the fourth decimal place are significant geochemically and ratios therefore need to be determined with precisions of $\sim 0.003\%$ RSD. Traditionally, such measurements are the province of TIMS which, with care and appropriate correction for mass fractionation caused by differential evaporation rates of light and heavy isotopes from the filament, can yield data of the necessary precision.

Measurements of isotope ratios on ICP quadrupole mass spectrometers have not really been able to attain the levels of precision needed for geochronological interpretation, although they have provided valuable data in other areas as we shall see later. Two fundamental factors combine to limit the precision obtainable: the noise in the ICP ion source and the sequential nature of the ion beam detection. Examination of the noise-power spectra of the ICP has shown how judicious selection of signal acquisition parameters can minimise the deleterious effects of non-random noise and yield precisions of $\sim 0.05\%$ RSD for the ^{107}Ag – ^{109}Ag isotope ratio [228]. Subsequent investigations [229] of sources of noise and offset in the mass spectrometer (e.g. mass scale shift, dead time and mass bias) enabled ^{206}Pb – ^{207}Pb ratios to be measured with a precision of $\sim 0.04\%$ RSD, compared to the 0.1 – 0.5% RSD precision typical of many published lead isotope ratio measurements by quadrupole ICP-MS [230].

Even when operated to yield their highest possible precision, it is clear that quadrupole ICP mass spectrometers cannot match the performance of TIMS [231], but the latter technique is by no means free from drawbacks either. Extensive preparation and chemical treatment of samples is required to separate the analyte elements from the rock matrix so that a small amount in sufficiently pure form can be deposited on the filament. This has then to be loaded, usually 10–15 at a time, into the sample magazine of the mass spectrometer and pumped down to vacuum. Overall analysis times are of the order of 1–2 h per sample. Corrections have to be made for the mass fractionation of isotopes during vaporisation from the filament. This is done by monitoring the signals from a pair of stable isotopes of the analyte which therefore have an accurately known ratio. Such a correction cannot be made when determining lead isotope ratios by TIMS because only ^{204}Pb can be regarded as stable. Thermal ionisation from a filament is limited in its ability to ionise isotopes of elements, such as Re, Os, Hf and W, which have a high first ionisation potentials. It was the ability of the ICP to ionise refractory elements that prompted early workers [232,233] to apply the technique to the measurement of the isotope ratios of Re and Os, introducing the latter into the ICP as volatile OsO_4 .

What would be highly desirable therefore would be to combine the ease of solution sample introduction at atmospheric pressure into an ICP ion source with the stability and ion detection capability of the magnetic sector mass spectrometers commonly used in TIMS. This was first achieved [139] by coupling an ICP to a double-focusing magnetic sector mass spectrometer fitted with a single Faraday detector and a pulse-counting electron multiplier. On this instrument, which was aimed mainly at high-resolution elemental analysis, isotope ratio measurements had to be performed sequentially. In 1992, the coupling of an ICP source to a double-focusing magnetic sector mass spectrometer fitted with seven Faraday detectors, allowing true simultaneous isotope ratio measurements, was reported [234].

The high precisions that could be achieved in the measurement of Pb, Sm–Nd and Lu–Hf isotope ratios with a multiple-collector instrument were soon demonstrated [235,236] and the exciting possibilities it offered quickly recognised by earth scientists [237].

Over the last decade, MC-ICP-MS has revolutionised high precision isotope measurement in the earth sciences [238,239]. The isotopic compositions and atomic weights of elements such as Mo, Te, Sn and W, which have high first ionisation potentials, have been determined precisely by MC-ICP-MS as a prelude to exploring their use in isotope geology [240]. The ability to obtain very precise Hf isotope data has considerably advanced our understanding of the early evolution of the Earth, the Moon and other planetary bodies [241–243]. The technique has also opened up extensive possibilities for the investigation of the variations in stable isotope ratios in natural materials that occur through physical, chemical or biological processes, such as those of Li, B, Ca, Fe, Ni, Cu, Zn, Ge, Se, Mo, Cd, Sb, Hg and Tl [244,245]. Geochemical applications of magnetic sector ICP-MS, with single and multiple collectors, have been reviewed [246].

Factors limiting the precision and accuracy of isotope measurements are discussed by Becker [247] and Albarède *et al.* [248]. To obtain accurate data, a number of corrections must be applied, of which one of the most important is mass bias. In ICP-MS this is often achieved by internal normalisation, using two stable isotopes, or standard-sample bracketing [246]. In some cases, isotopes of an adjacent element may be used; the classic example of this is monitoring the ratio of ^{203}Tl : ^{205}Tl added to the sample solution to correct the mass bias on Pb isotopes [249]. Strategies for optimising instrumental parameters to minimise mass bias have been explored [250,251]. For the best accuracy and precision it is still necessary to employ efficient chemical separation procedures prior to measurement to ensure that samples and standards are in an equivalent matrix. As a result, many of the separation schemes devised for use with TIMS are being re-evaluated for MC-ICP-MS.

While geochronology places the most stringent demands on the measurement of isotope ratios by ICP-MS, somewhat less precise estimates of isotopic abundances in geological materials can be extremely helpful as tracers in a system, distinguishing components that have different origins or histories. This capability was utilised by early workers in the typing of galena samples from different ore deposits [225,226]. The abundances of the two isotopes of lithium vary sufficiently to the extent that their different signatures in various minerals can be identified by quadrupole ICP-MS measurement [252]. Similarly, the ratios of the two stable isotopes of boron may vary enough [253] so that measurement by quadrupole ICP-MS can yield data which would indicate either a marine or non-marine origin of some evaporites [254]. Measurements of ^{206}Pb / ^{207}Pb abundances in soils and atmospheric aerosols by a combination of quadrupole ICP-MS and TIMS has enabled two different sources of petrol-derived lead to be distinguished from that contributed by the underlying carbonate bedrock [255]. More recently, quadrupole ICP-MS has been used to identify sources of depleted and enriched uranium, which can be clearly differentiated from natural background signatures [256,257].

9.8 Laser ablation

The geosphere is heterogeneous at all scales from tectonic plates measured in thousands of kilometres to defects in crystal lattices at an atomic scale. Earth scientists are especially

interested in correlating variations in chemical composition with structure and morphology. A great deal of analytical data is displayed and interpreted in a two- or three-dimensional context, ranging from geochemical maps of entire countries to plots of elemental zonation within individual mineral grains. Despite the proven value and power of ICP spectrometry in geochemistry in terms of sensitivity and speed of analysis, in its most widely used form – as a technique for the analysis of homogeneous solutions – it requires the analyst to disaggregate and dissolve heterogeneous solids and thus throw away a wealth of spatial information it cannot tap directly into.

Earth scientists currently have at their disposal a range of powerful ‘microbeam’ techniques [258,259] to aid them in their quest for spatially resolved data on the chemical composition of geological materials at the micrometre scale. These include electron probe microanalysis (EPMA) [260] and its proton analogue, proton-induced X-ray emission (PIXE) [261], secondary ion mass spectrometry (SIMS) and its close relative the ion microprobe [262,263], accelerator mass spectrometry (AMS) [264,265], synchrotron X-ray fluorescence spectrometry (SXRF) [266,267] and Auger electron spectroscopy [268]. In these techniques, the sample is bombarded with a beam of X-rays (SXRF), electrons (EPMA and AES), protons (PIXE) or ions, typically of oxygen or caesium (SIMS and AMS), and the resultant X-rays or sputtered ions detected.

A common feature of most microbeam methods is the need for geological samples to be specially prepared with a very smooth and polished surface. In addition, it may be necessary in some cases to coat them with a thin layer of gold or carbon to make them conducting. Sample preparation requirements for, say, ion microprobe analysis are quite stringent and may involve ultrasonic cleaning prior to coating to remove traces of polishing compounds. The vacuum levels in the sample chamber are typically several orders of magnitude lower than those needed in EPMA or electron microscopy and place constraints on the type of mounting medium. Techniques such as AMS and SXRF require access to large specialised facilities, while application of the sensitive high-resolution ion microprobe (SHRIMP) [269] is limited by the high cost and relative scarcity of such instruments. The spatial resolution and sensitivity for different elements varies considerably between techniques. For example, until the relatively recent development of synthetic multilayered analysers [270], the detection limits attainable by EPMA for geologically important light elements, such as Li, Be and B, were poor. Nevertheless, present microbeam techniques provide the geochemist with an impressive array of tools with which to study micro-scale variations in the composition of rocks and minerals. They can truly be said to have revolutionised our knowledge of mineralogy and petrology over the last 40 years.

However, there is great scope in the earth sciences for an analytical technique which combines the high spatial resolution of modern microbeam methods with good multi-element sensitivity across the Periodic Table following little or no sample preparation, and all at moderate cost. Coupling laser ablation sample introduction with ICP spectrometric detection goes a long way to fulfilling these criteria, and accounts for the present high level of interest in the earth sciences in the technique, and in LA-ICP-MS in particular. An especially attractive feature of LA-ICP compared to many other probe techniques is the lack of need for careful preparation of the sample surface, which does not have to be ground flat and polished or given a conductive coating. Moreover, no high-vacuum technology is involved in the ablation cell, which operates at atmospheric pressure. Samples are simply placed in small (c. 20–50 ml) chamber fitted with a window transparent to the wavelength of the laser. The beam is focused

through this, usually via an objective lens or, preferably, through a specially adapted microscope. The cell is flushed with argon or helium, which carries the ablated material to the injector tube of the ICP torch. Much more is understood about the processes involved in ablation since a number of significant reviews [271–274] were published a decade or so ago. Current insights into these processes are contained in several recent authoritative reviews [275–277], including one devoted to the analysis of inclusions [278].

Relatively soon after the first report of laser action in ruby [279] it was recognised that the intense power densities generated by a focused laser beam could be used to vaporise small amounts of material for chemical analysis, either directly by spectroscopic examination of the light emitted from the excited vapour [280] or indirectly by introducing the ablated material into another analytical system such as ICP-AES [281]. Studies with LA-ICP-AES systems demonstrated the potential value of the technique in the earth sciences [282–284], including its use in geochemical exploration [285–287] and the analysis of individual fluid inclusions [288–290]. They also shed early light on the complex processes involved in laser–solid interaction [291], the variable composition of ablation products [292,293] and problems of calibration [294].

However, the combination of LA with more sensitive ICP mass spectrometric detection holds even greater attractions for geoanalysts. Gray [14] was the first to report the use of LA as a means of sample introduction for ICP-MS. He used a ruby laser emitting a *c.* 1 mm beam. The wavelength of the laser is a key parameter in LA-ICP-MS. While early work on both LA-ICP-AES and LA-ICP-MS was carried out with the ruby laser operating at 694 nm, later applications [295–297] and initially most commercial LA-ICP-MS systems [298,299] tended to use the Nd:YAG laser operating at its fundamental infrared frequency of 1064 nm. Independent parallel research in the early 1990s at the BGS [300] and the Memorial University of Newfoundland [301–303] demonstrated that superior performance could be obtained by using a frequency quadrupled Nd:YAG operating in the far ultraviolet (UV) region at 266 nm. This was later confirmed by other workers using both Nd:YAG and excimer lasers [304–307]. Infrared (IR) lasers couple energy very poorly to many minerals because of their variable transparency to visible and near-IR radiation. Consequently, the ablation characteristics vary with sample matrix and a significant proportion of the ablation products consist of angular fragments ejected as a result of thermo-mechanical shock. UV radiation couples more efficiently to transparent material, resulting in a more controllable ablation process and a higher proportion of very small particles that can be reproducibly transported to the ICP.

Commercial LA systems now typically employ frequency quadrupled or quintupled Nd:YAG solid state lasers operating at 266 and 213 nm respectively. They have the advantage of compact size, ease of handling and low maintenance. While this type of laser predominates in current LA-ICP applications, partly because of ease of operation, a number of workers have evaluated the use of UV excimer lasers [306,308–312]. Although they can be relatively expensive to maintain and require care in setting up, they are becoming increasingly popular for certain applications because of their characteristic flat-top beam profile and high energy output. An argon fluoride laser operating in the far UV at 193 nm has been shown to generate only minor matrix-dependent element fractionation effects [311,313] and preliminary results from an in-house F₂He mixed gas 157 nm laser system were encouraging [314]. On the other hand, a 193 nm Nd:YAG laser system has been developed recently [315]. Its performance was sufficiently impressive that it has been converted into a commercial product.

One of the limitations of LA-ICP-MS is that the signal intensities measured do not always reflect the composition of the sample. This so-called elemental fractionation needs to be controlled to obtain quantitative results. Differences in ablation and transport behaviour between different constituents of a sample and between different samples and calibrants, have been investigated by several workers [273,306,316–318]. There is evidence that some of these effects were related to the melting points of analyte elements and their oxides [319–321], and to solid–liquid transitions and zone refinement processes occurring at the ablation site [322]. Early empirical approaches to minimising elemental fractionation included actively refocusing the laser on the sample as the ablation proceeded [316,323] or using low laser power initially and then gradually increasing it, which has been used in the authors' laboratory to control crater size [300] or gently ablate material to open an individual fluid inclusion [324]. Recent research has led to an improved understanding of the processes involved in LA-ICP-MS and these have greatly assisted the geoanalyst in reducing fractionation effects to an acceptable level. One significant factor is the particle size distribution produced during the ablation process; this is related to laser wavelength and the absorption characteristics of sample. The particle size of ablated material has been shown to decrease with decreasing wavelength from 266 to 213 to 193 nm in silicate glasses [325]. Smaller particles are produced if the ablation is performed in an atmosphere of helium rather than argon. Because of the nature of the induced-plasma at the ablation site, this effect is much greater at 193 nm than 266 nm [275]. Smaller particles are transported more efficiently to the ICP than larger ones, resulting in enhanced sensitivity when LA at 193 nm is performed in helium [326]. Once the ablated particles reach the ICP, it is equally important that they are fully vaporised and ionised in the plasma. Various workers have demonstrated the influence of particle size on fractionation effects arising in the ICP [327–329].

In early studies of LA-ICP-MS, lasers were used in both the fixed-Q [330] and Q-switched modes [297,298], but experience has shown that the latter mode is now generally to be preferred. Typical operating parameters for a Q-switched, frequency-quadrupled Nd:YAG laser would be 10 ns pulses of 1–5 mJ energy at repetition rates of c. 10 Hz. The use of femtosecond laser pulses to reduce elemental fractionation has been explored recently [331,332]. With ultra-short pulses, less of the photon energy is able to dissipate in the crystal lattice, so it is converted into kinetic energy in the ablated vapour rather than heat in the sample. A comparison of the performance of femtosecond and nanosecond 266 nm lasers in silicates and zircons provided evidence of reduced fractionation from a shorter pulse [332].

In many geological applications of LA-ICP-MS, it is often important to achieve the highest possible spatial resolution in analysis. Because of their shorter wavelength, lasers operating in the UV are capable of being focused to produce smaller ablation pits than IR lasers. Early commercial systems equipped with IR lasers typically produced craters 100 μm in diameter [299]; this was subsequently improved to c. 30 μm [333]. Craters as small as 6–10 μm in diameter were ablated in metal samples using a frequency doubled Nd:YAG laser operating at 532 nm [334], while several lanthanides have been determined in monazite using sub-micron diameter ablation pits created by the BGS LA system [335] operating at 266 nm [336]. With the enhanced sensitivity of modern ICP-MS instruments, more information than ever can be acquired from small spot sizes, and crater diameters are seldom a limiting factor. Sampling strategies may involve a line traverse, spot traverse or depth profiling [276], depending on the application, with spot sizes between 10 and 400 μm .

In the practical application of LA-ICP-MS to the analysis of geological materials it is vital to be able to observe samples clearly in the ablation cell in order to be able to choose the precise spot on which to focus the laser beam. A serious shortcoming of the first generation of commercial LA systems was the design and quality of their viewing optics, which were not adequate for observing complex mineralogical structures. Although it is still only research instruments, such as those found in the UK, Canada and Switzerland, that have modified petrological microscopes incorporated in their optical chain, sample observation facilities have improved in the latest generation of commercial systems, and are only a limitation for very complex samples.

Detection limits are directly related to the amount of material ablated and vary inversely with the volume of the ablation pit. They also depend on the sensitivity of the ICP-MS measurement step. This has been improved for heavy elements [316] by the addition of 0.4 ml min^{-1} of nitrogen to the plasma carrier gas, and in some instruments by modifying the cones of the ion extraction interface and lowering the pressure in the first expansion stage [337]. Typically, detection limits for many elements lie in the range of $0.1\text{--}10 \mu\text{g g}^{-1}$ for an individual $25 \mu\text{m}$ crater using a quadrupole ICP-MS instrument. However, figures of merit depend on the application, the LA system and operating conditions, and the ICP-MS instrument used for quantification. Lower limits of detection can be achieved by rastering the laser beam across a solid sample, creating a pseudo-continuous signal, but obviously only at the cost of sacrificing spatial resolution. Sector-field instruments can often provide higher sensitivities for a limited number of elements and are able to resolve some spectral interferences, although they are not capable of scanning as rapidly as quadrupoles. The measurement of isotope ratios by instruments fitted with multiple collectors (LA-MC-ICP-MS) is increasingly popular as more of these instruments become available. Theoretically, a time of flight (TOF) mass spectrometer should be an ideal detector because of its ability to sample all isotopes virtually simultaneously [338]. However, current TOF-ICP-MS instruments are not as sensitive as quadrupole ICP-MS for LA analysis.

Calibration and quantification present significant problems in LA-ICP-MS. Contributing factors include: our incomplete understanding of the precise mechanisms of laser–solid interaction and the potential for elemental fractionation during the ablation process; progressive defocusing of the laser beam at the sample surface as ablation proceeds; the influence of the transport of ablated material from the sample chamber to the ICP; the transient nature of the pulse of ablated material, which makes optimisation of the ICP-MS difficult; and the difficulty of obtaining solid standards that are both truly homogeneous on a sub-micron scale and which have similar ablation characteristics to those of the sample material.

A number of different approaches have been taken to calibration in LA-ICP-MS. Initially, these typically involved ablating solid standards made from certified reference materials, CRMs [296,330], previously analysed natural materials [266,339] or mixtures of pure salts [333] sometimes spiked with trace element solutions [340], which were finely ground and pressed into pellets [299,330,341] or fused into glass discs [299,342,343]. Sinters of finely ground zircon in a quenched albite glass have been used as standards for ablation with a Nd:YAG IR laser, where the crater size was large compared to the individual particles [344]. Direct ablation of the NIST 600 series of certified reference glasses has been widely used for calibration [303,345–347], and these materials are becoming almost the *de facto* means of calibration for LA-ICP and EMPA (electron microprobe analysis). Because of their importance

to these techniques, a Working Group of the International Association of Geoanalysts (IAG) was established to characterise the NIST glasses further, and a compilation of existing and new data on the composition of NIST SRM 610 and SRM 612 has been published [348]. One of the major advantages of glasses prepared from natural or synthetic materials is that they are likely to be relatively homogeneous on the scale suitable for LA. However, even these glasses are not entirely homogeneous for all elements. The extent and nature of compositional heterogeneity in the NIST SRM glasses was found to be related to the process of manufacture [349].

Calibrating with liquid standards is attractive because they can be prepared for any combination of elements at different concentrations, as well as simplifying the optimisation of the instrument. Isotope spikes for on-line ID can be introduced easily and a standard addition method of analysis can be applied if required. A novel approach [294,300] employed a dual gas-flow sample introduction system in which the output from the ablation cell, together with conventionally nebulised aqueous solutions, were aspirated simultaneously into the plasma via a mixing cell, thereby maintaining virtually constant bulk plasma conditions. The use of liquid standards has not been widely accepted as a method for matrix-independent calibration, except for the analysis of fluid inclusions, because of concerns over elemental fractionation and the fact that the nebulised particle size distribution is different from that generated in the ablation cell. In an alternative dual-flow approach to the optimisation of plasma operating conditions [350], an ETV sample introduction system was modified to produce a continuous stream of metallic vapour which was mixed with the ablation cell carrier stream just prior to the ICP torch. A similar approach [351] using a Mistral IR desolvating nebuliser to generate a dried aerosol stream for plasma optimisation also explored the potential of such a system for calibration. An attempt has been made to devise a universal calibration strategy for LA-ICP-MS based on the addition of different amounts of a polymer to conventional aqueous standards in order to match their absorption coefficient to that of the solid samples being ablated [352]. If the LA system employed can generate a stoichiometric aerosol with a particle size distribution that can be fully atomised in the plasma, then matrix-independent calibrations using liquid standards, with a desolvating nebuliser to reduce potential oxide inferences [353] has many advantages including the possibilities of ID.

Internal standardisation, in which the signal from an appropriate isotope of a major component of the standards and samples being ablated is monitored to correct for corresponding variations in analyte signals, is almost invariably used to improve the precision and accuracy of LA-ICP-MS measurements. It allows corrections to be made for variations in the mass of ablated material, ablation behaviour and instrument drift. Commonly used isotopes include ^{29}Si , ^{27}Al , ^{43}Ca , ^{44}Ca , ^{55}Mn and ^{137}Ba [303,333,341,346,354] and added ^{115}In [355]. However, cluster analysis of multi-element data from the ablation of NIST 612 glass [356] has shown that elements can be grouped according to their ablation behaviour and that it is important to choose an internal standard from within the same group. Due attention must be paid to data acquisition and reduction strategies when dealing with the transient signals generated in LA-ICP-MS [357].

The development of LA-ICP-MS has been driven, to a large extent, by its use as a microprobe to explore of the heterogeneity of geological materials, as well as its capacity to provide multi-elemental data with minimal sample preparation. Geochemical applications of LA-ICP-MS are many and varied: two particularly important areas are the analysis of fluid

inclusions (Section 9.8.1) and the measurement *in situ* of isotope ratios (Section 9.8.2). In the past few years, applications of LA-ICP-MS have included studies of chalcophile elements [358], trace elements in diamonds and indicator minerals [359] and placer gold [360] as an aid in exploration, REEs in single mineral grains [300,361] and in calcite cement from a Mississippi-Valley-type Pb–Zn deposit [347], trace element partitioning in natural [345, 362–364] and synthetic minerals and glasses [266,302,354], the distribution of trace elements [365] and precious metals [366] in sulphides, trace element affinities in coal [367], the pressure dependence of REE distribution in garnets [368], hydrothermal alteration of monazite [369], the distribution of the PGEs and Re between metallic phases of iron meteorites [370], trace elements in garnets [346] and sapphires [312]. The practicalities of bulk analysis of silicate rocks by ablating lithium borate fused glass discs normally prepared for XRF analysis have been revisited [371,372]. However, the use of LA-ICP-MS for the multi-element analysis of geological materials is now so widespread that many articles on geochemical applications contain very limited analytical information.

9.8.1 Analysis of fluid inclusions

An important application of LA-ICP-MS is in the analysis of fluid inclusions in minerals. These are extremely small cavities, typically $<100\ \mu\text{m}$ in size, that contain tiny amounts of the ancient fluids from which the mineral was formed. A knowledge of the elemental and isotopic composition of the fluids in these geological ‘time capsules’ can thus be of immense help to geochemists in unravelling the complexities of fluid–rock interactions, especially the processes by which metals are concentrated into major economic ore deposits.

Analysis of the contents of fluid inclusions presents a number of difficulties. Not only are inclusions very small but within a single mineral grain there may be several generations of inclusion formed at widely different times. Some may represent conditions when the mineral originally crystallised, others may contain fluids that were introduced during later hydrothermal events that modified the composition of the solid phase. Moreover, because they comprise liquid and gas, they are not readily amenable to the wide range of powerful surface analysis techniques, such as PIXE, EPMA and SXRF. For many years, analyses of fluid inclusions relied on crush-leach or decrepitation procedures in which the contents of large numbers of inclusions were liberated simultaneously by mechanical abrasion or heating [373]. Not only did the fluid released by these methods thus represent some averaged composition derived from unknown proportions of different generations of inclusions, but there was also the danger that its composition might be modified prior to analysis by interaction with the freshly exposed mineral surfaces. Nonetheless, valuable geochemical information about the formation of rocks [374] and the composition of high temperature crustal fluids [375] has been derived from the analysis of such composite samples. This has been greatly aided by the ability of ICP spectrometry to provide multi-element data on small volume samples [376–379].

Clearly, the analysis of individual fluid inclusions is highly desirable in order to avoid many of the limitations and uncertainties associated with crush-leach and decrepitation methods. Techniques such as microthermometry and laser Raman spectroscopy [380] are commonly used to measure the total salinity of single inclusions and their molecular gas content. Methods used with limited success to determine elemental composition have

included EPMA, PIXE, SXRFs and proton-induced gamma-ray emission (PIGE) [381], and direct observation of the emission from a laser-induced plasma using a spectrometer fitted with an intensified photo-diode array detector [382]. Early applications of LA-ICP-AES to the analysis of individual fluid inclusions [288–290] demonstrated the potential utility of this approach, but were limited partly by the laser systems used and partly by the sensitivity of the ICP-AES detection stage.

Far greater sensitivity is now offered by ICP-MS detection, but the analysis of individual fluid inclusions puts particular demands on the LA system, both in terms of capability and mode of operation. Good facilities for the microscopic observation of samples by reflected and transmitted light are essential so that inclusions can be clearly identified and the laser beam positioned precisely. The usual analytical protocol is to use the laser as a microdrill and gently ablate a small hole into the sub-surface inclusion. Because of the small size of the inclusions, this hole typically needs to be $<5\text{ }\mu\text{m}$ in diameter at the breakthrough point, thus the laser must be capable of being focused down to a *c.* $2\text{ }\mu\text{m}$ spot and of having its power output finely controlled. In the authors' laboratory [383] a modified ablation cell incorporating a heated stage is used to facilitate homogenisation of multiphase (solid + liquid + gas) inclusions prior to ablation. A lower power, shielded, 'cool' plasma is used to provide increased sensitivity for Fe and the alkali metals, partly by drastically reducing the background signals. Various strategies have been adopted to mimic the ablation of fluid inclusions for calibration purposes. These have included sealing standard solutions in glass microcapillary tubes [384] and growing halite crystals containing synthetic fluid inclusions [324]. It has been shown that the latter procedure is unnecessary and that covering tiny containers with Parafilm [385] or Sellotape [324] provides a suitable alternative. Internal standardisation obviously cannot be used because it is not possible to add an internal standard to the natural inclusions being analysed. Aqueous standard solutions are therefore used to provide relative response factors for the elements of interest. Final quantification is achieved by normalising the data to the concentration of a major element, for example Na, the concentration of which is measured independently by, for example, microthermometry [373]. It is important to be able to monitor analyte signals during the ablation process so that the integration period can be chosen to coincide with the release of fluid from an inclusion. The type of software used to resolve transient signals in coupled high-performance liquid chromatography (HPLC)-ICP-MS is equally suitable for LA-ICP-MS.

In principle, LA-ICP-MS is ideally suited to the quantitative analysis of fluid and melt inclusions. Its ability to analyse individual inclusions has stimulated many studies of ore-forming processes [278]. Although quartz has often been the host mineral [385,386], inclusions in minerals such as halite [387] and fluorite [388] have also been investigated. International conferences devoted to research on fluid inclusions are held in Europe and North America on a regular basis [389] and it is evident that LA-ICP-MS will continue to make an impact in this branch of geochemistry for many years to come.

9.8.2 *In situ determination of isotope ratios*

Differences in the ablation behaviour of different elements (e.g. U and Pb) from the same sample currently limit the usefulness of LA-ICP-MS in the measurement of isotope ratios

for geochronology. This is nonetheless a major growth area for the application of the technique in the earth sciences. While not capable of achieving the high precision obtainable by TIMS, it offers an alternative to SHRIMP for the *in situ* determination of isotope ratios in minerals at high spatial resolution. Fractionation effects between isotopes of the same element in a sample are, however, quite small compared to other sources of uncertainty in the overall measurement, for example the instability of the ICP source, or the detection step involving a quadrupole mass filter. Thus $^{207}\text{Pb}/^{206}\text{Pb}$ isotope ratios in zircon, monazite and other minerals have been measured successfully [273,317,390–393]. Ages deduced from these ratios for concordant grains were in good agreement ($\pm 1\text{--}2\%$) with those derived from conventional U–Pb measurements by TIMS and, despite being less precise, are perfectly adequate for provenance studies of detrital minerals in sedimentary rocks. By keeping the beam of a frequency quadrupled Nd:YAG laser continuously focused on the sample surface as ablation proceeded, Hirata and Nesbit [316] were able to reduce and correct for fractionation effects between Pb and U, to the extent that they could obtain U–Pb ages on concordant zircons that were within about 1% of those measured by SHRIMP, *albeit* with poorer precision. Use of the soft ablation technique improved the precision by a factor of 2–3 [394]. Recent developments in U–Pb geochronology in zircons measured by LA-ICP-MS are summarised by Sylvester [276].

A combination of LA into an ICP source coupled to a double-focusing mass spectrometer fitted with multiple ion detectors [395] greatly increases the potential scope of the technique by enabling isotope ratios to be measured with high precision approaching that obtained with TIMS. Because the ICP ionises a broad range of elements efficiently, it opens up the possibility of making isotope ratio measurements of elements such as W and Hf, which are difficult to ionise using TIMS (see Section 9.9). As a result, laser ablation multiple collector ICP-MS (LA-MC-ICP-MS) is now the method of choice for the measurement of Hf isotopes in zircons [396]. It has also been used to make precise measurements of the $^{87}\text{Sr}/^{86}\text{Sr}$ ratios in two neighbouring and apparently similar feldspar phenocrysts in a porphyritic basalt [397]. Systematic differences of ~ 0.0004 between their isotope ratios provided evidence for magma mixing. The measurement of Sr isotopes is fraught with difficulty because of isobaric interferences from rubidium in the samples and krypton in the argon gas [250]. However, LA-MC-ICP-MS can provide a very cost effective screening tool to identify regions of interest prior to expensive chemical separation and measurement by TIMS for samples requiring the ultimate precision. The technique has been employed to determine osmium isotope ratios of iridosmines *in situ* with precisions comparable to those obtainable with negative TIMS and thus helped to shed light on mantle–crust evolution [398]. The range of isotope systems studied using this technique continues to grow (e.g. those of Cu [399] and Fe [400]) and it is clear that LA-MC-ICP-MS will be a key tool in the development of isotope geoscience in the next decade.

9.9 Future trends

Measurement of the elemental and isotopic composition of geological materials continues to pose some of the greatest challenges to any analytical technique. Earth scientists wish to determine virtually the entire Periodic Table down to vanishingly small concentrations in a huge variety of complex, heterogeneous and often refractory matrices. Ideally, we would also like such miracles wrought on hundreds of samples per day at very low cost!

Plasma spectrometry has already had an enormous impact on analytical geochemistry, generating data on a scale and of a quality only dreamed of a few decades ago. It has provided information, especially about trace constituents, that has greatly enhanced our understanding of fundamental geological processes. It has aided our search for new mineral resources and helped us to assess the impact of man's activities on the environment.

Analysis by ICP-AES is regarded as routine in many geological laboratories. The instrumentation is for the most part robust and reliable and the underlying spectroscopy is well understood. It is unlikely that we shall witness any revolutionary developments in this area in the near future, but the continuing evolutionary improvements in instrument performance that will flow from, for example, new detectors and sample introduction systems will be welcomed in the earth sciences as elsewhere [401].

The greater sensitivity and isotopic measurement capability of ICP-MS made it attractive to geochemists from the outset and it has manifestly fulfilled much of its early promise for elemental analysis. The current generation of quadrupole instruments are much more stable and reliable than their predecessors and workers new to the field have a wealth of documented information on interference effects and operating conditions to draw on. There will be continued improvements in the performance of such instruments, but the greatest change we can expect to see in the application of ICP-MS to geological investigations will be in the much wider use of single- and multi-collector magnetic sector mass spectrometers, especially for isotope ratio measurements. This is already starting to happen.

Depending on their particular configuration, these instruments can offer high mass resolution as a means of resolving analyte signals from those of polyatomic ions with very similar m/z ratios (see Section 9.4). Alternatively, if they are fitted with multiple detectors, they can provide truly simultaneous detection of ions from a small number of selected isotopes, allowing isotope ratios to be measured with precisions approaching those of TIMS but with much faster sample throughput. They also offer the possibility of easier measurement of the isotopic abundance of elements such as Hf and W, which have high first ionisation potentials, making them difficult to determine by TIMS. The attraction to isotope geologists is that the immobility of Hf means that the Lu–Hf geochronometer is quite resistant to later resetting, while the short-lived ($t_{1/2} = 9$ million years) ^{182}Hf – ^{182}W system has great potential in studies of accretion and differentiation in the early solar system [402]. The current generation of these mass spectrometers being installed in some laboratories incorporates laminated magnets which permit the entire mass range to be scanned at speeds approaching that of quadrupole instruments.

TOF mass spectrometers offer an alternative approach to the detection of ions from an ICP source. They have been in development for a number of years [403] and the first generation of commercial TOF-ICP-MS instruments appeared over 5 years ago. Their full capabilities have yet to be proven, but with their high ion transmission and simultaneous detection they would appear to have considerable potential in the detection of small transient signals such as those generated by LA [404], and possibly for isotope ratio measurement. In visualising what an earth science ICP-MS laboratory will look like in the future, one cannot but hear the now little-used term, coined by Alan Gray in the mid-1970s, 'plasma source mass spectrometry' echoing down the years.

Because of the predominantly solid nature of geological materials, we can expect to see a continued growth of interest in LA techniques coupled with various types of mass spectrometer. These offer the prospect of direct multi-element and isotopic measurements on

heterogeneous solids at micrometre scale resolution without the need for lengthy and resource-consuming sample preparation. Although the technique already offers superior detection limits compared with other solid-sampling techniques, further developments are still required [277]. More flexible laser systems [405] may help us gain a better understanding of the ablation process itself and of subsequent particle transport mechanisms. This calls to mind the early days of ETV-AAS when our understanding at a fundamental level of the kinetics of analyte and matrix vaporisation and the mechanisms of atom cloud formation was incomplete. The situation is therefore not new. We have stumbled around among the trees of empirical data and instrumental artefacts in the past, before emerging on the high ground of a coherent model from which to look down and see the woods. There is no reason why this should not happen again with LA.

Another trend that is set to continue is the use of ICP-MS as a detector in the acquisition of information on chemical species and their movement through geochemical cycles. Nowadays it is relatively easy to couple an ICP-MS instrument to chromatographic systems such as gas chromatography (GC), HPLC or capillary electrophoresis [406]. Although much of the work thus far has been concerned with the speciation of aqueous and biological samples, levels of organotin and methylmercury species in sediments are monitored for regulatory purposes and there is growing interest in the speciation of As, Cr and Se in soils and sediments. ID as a calibration strategy for the study of elemental speciation is likely to facilitate studies of species and their interconversion in the environment [407].

As in other areas of analysis in recent years, there has been a growing recognition in the geoanalytical field for the need for appropriate quality control and quality assurance procedures [408] to ensure the reliability and fitness for purpose of data [409,410]. CRMs have for a long time played an important role in geochemical analysis and, to an extent, the geological community is fortunate that so many exist [411–414]. However, the number of analytes for which different CRMs are certified varies greatly, as do their concentrations; there are far fewer certified values for important trace constituents, such as the PGEs and some of the incompatible elements, than for major components. This situation is slowly being rectified and ICP-MS has played an important role in increasing the range of data available [415]. It is expected that this trend will continue, but it will be equally vital to avoid the circularity that can arise when CRM values for trace constituents, derived from only one technique having the required sensitivity, are then used to validate later procedures and measurements involving that method.

As well as having a range of CRMs at their disposal, analytical laboratories have the option to participate in one or more of the many proficiency testing schemes that exist. These provide a mechanism by which laboratories can regularly assess their performance and improve the accuracy of their data [416]. Across the whole range of analytical measurement there are probably of the order of a hundred proficiency testing schemes currently operating worldwide. It is important that a laboratory chooses one that caters for its particular field in terms of sample type, analyte range, and data presentation and feedback. The GeoPT proficiency testing scheme [417], run by the IAG, was set up specifically to cater for the needs of geoanalytical laboratories. Currently, over 70 organisations take part and this number is expected to rise steadily as regulatory and accreditation agencies increasingly expect laboratories to participate in such schemes as part of their overall quality system. The IAG also organised the first proficiency test for microprobe laboratories [418]. Because of the difficulty of finding a mineral that was sufficiently homogeneous for

such an exercise, fragments of a basaltic glass, prepared by fusing and quenching a natural basalt, were distributed. The majority of the data reported were obtained by EPMA and LA-ICP-MS, although data from ion probe measurements and bulk analyses were also made available. The results for Ba, Cs, Ni, Sc, Sr, U and a number of REE determined by LA-ICP-MS were comparable to the data obtained from bulk chemical analysis.

Earlier in this chapter, the importance of appropriate preparation of geological samples prior to analysis was stressed. This is a major consumer of time and effort in laboratories and is often the ultimate source of many of the shortcomings in data derived from ICP spectrometric measurement. As the analytical power and speed of ICP instruments increase, sample preparation becomes ever more the rate-limiting step. At a time when automation, artificial intelligence and robotics are so widely integrated into countless industrial and scientific processes – from building motor cars to analysing the human genome – it is interesting to speculate on why so many of the apparently simple and repetitive processes in geological sample preparation are not routinely automated. Batch processing under human control seems to be the norm in many laboratories. There are isolated cases in the literature of one or more preparative steps being automated [419] but the practice is not widespread. Some aspects of physical comminution have been successfully automated [420] and commercially available systems are in use in a few laboratories to prepare pressed-powder pellets and fused glass discs for X-ray analysis. However, the high temperatures and extremely corrosive reagents and fumes frequently involved in the treatment of geological samples constrain the design and materials that can be used to construct a robust, fully automated system for preparing sample solutions. Some of the best-documented examples are the automated fusion and dissolution systems set up many years ago in the Centre de Recherches Pétrographiques et Géochimiques [421] and the Bureau de Recherches Géologiques et Minières [422] in France.

The aggressive conditions involved in the chemical aspects of geological sample preparation may account in part for why it is not routinely automated or placed on-line with analytical instruments, as it is, for example, in environmental or biomedical analysis. The highly variable nature of geological materials and the need for experienced judgement during their preparation are further contributory factors. Nonetheless, if more effort and ingenuity could be successfully brought to bear on this vital area, the rewards would be considerable. If we can send a robot spectrometer to Mars to do some geochemical analysis, one would hope that more modest progress could be made nearer home.

References

1. Mason, B. (1992) *Victor Moritz Goldschmidt: Father of Modern Geochemistry*, The Geochemical Society, San Antonio.
2. Taylor, S.R. and Ahrens, L.H. (1960) Spectrochemical analysis. In *Methods in Geochemistry* (Eds. A.A. Smales and L.R. Wager), Interscience Publishers, New York, pp. 81–110.
3. Shapiro, L. and Brannock, W.W. (1962) Rapid analysis of silicate, carbonate and phosphate rocks. *US Geol. Surv. Bull.*, **1144-A**.
4. Shapiro, L. and Brannock, W.W. (1956) Rapid analysis of silicate rocks. *US Geol. Surv. Bull.*, **1036-C**.
5. Riley, J.P. (1958) The rapid analysis of silicate rocks and minerals. *Anal. Chim. Acta*, **19**, 413–428.
6. Fairbairn, H.W. (1951) A cooperative investigation of precision and accuracy in chemical, spectrochemical and modal analysis of silicate rocks. *US Geol. Surv. Bull.*, 980.

7. Angino, E.E. and Billings, G.K. (1967) *Atomic Absorption Spectrometry in Geology*, Elsevier, Amsterdam.
8. Langmyhr, F.J. and Paus, P.E. (1968) The analysis of inorganic siliceous materials by atomic absorption spectrophotometry and the hydrofluoric acid decomposition technique. Part 1. The analysis of silicate rocks. *Anal. Chim. Acta*, **43**, 397–408.
9. Date, A.R. and Gray, A.L. (1981) Plasma source mass spectrometry using an inductively coupled plasma and a high resolution quadrupole mass filter. *Analyst*, **106**, 1255–1267.
10. Gray, A.L. and Date, A.R. (1983) Inductively coupled plasma source mass spectrometry using continuum flow ion extraction. *Analyst*, **108**, 1033–1050.
11. Date, A.R. and Gray, A.L. (1985) Determination of trace elements in geological samples by inductively coupled plasma source mass spectrometry. *Spectrochim. Acta*, **40B**, 115–122.
12. Doherty, W. and Vander Voet, A. (1985) The application of inductively coupled plasma mass spectrometry to the determination of rare earth elements in geological materials. *Can. J. Spectrosc.*, **30**, 135–141.
13. Lichte, F.E., Meier, A.L. and Crock, J.G. (1982) Determination of rare earth elements in geological materials by inductively coupled argon plasma/atomic emission spectrometry. *Anal. Chem.*, **59**, 1150–1157.
14. Gray, A.L. (1985) Solid sample introduction by laser ablation for inductively coupled plasma source mass spectrometry. *Analyst*, **110**, 551–556.
15. Date, A.R. and Gray, A.L. (1989) *Applications of Inductively Coupled Plasma Mass Spectrometry*, Chapman & Hall, London.
16. Thompson, M. and Walsh, J.N. (1989) *Handbook of Inductively Coupled Plasma Spectrometry*, Chapman & Hall, London.
17. Jarvis, K.E., Gray, A.L. and Houk, R.S. (1992) *Handbook of Inductively Coupled Plasma Mass Spectrometry*, Chapman & Hall, London.
18. Montaser, A. (Ed.) (1998) *Inductively Coupled Plasma Mass Spectrometry*, Wiley-VCH, New York.
19. Nelms, S.M. (Ed.) (2005) *ICP Mass Spectrometry Handbook*, Blackwell Publishing, Oxford.
20. Longerich, H.P., Jenner, G.A., Fryer, B.J. and Jackson, S.E. (1990) Inductively coupled plasma-mass spectrometric analysis of geological samples: a critical evaluation based on case studies. *Chem. Geol.*, **83**, 105–118.
21. Falkner, K.K., Klinkhammer, G.P., Ungerer, C.A. and Christie, D.M. (1995) Inductively coupled plasma mass spectrometry in geochemistry. *Ann. Rev. Earth Planet. Sci.*, **23**, 409–449.
22. Jarvis, I. and Jarvis, K.E. (1992) Plasma spectrometry in the earth sciences: techniques, applications and future trends. *Chem. Geol.*, **95**, 1–33.
23. Linge, K.L. (2005) Recent developments in trace element analysis by ICP-AES and ICP-MS with particular reference to geological and environmental samples. In Hergt *et al.*, *Geostand. Geoanal. Res.*, **29**, 5–52.
24. Hall, G.E.M. (1992) Geoanalysis. *J. Geochem. Explor.*, **44**, 1–349.
25. Jarvis, I. and Jarvis, K.E. (1992) Inductively coupled plasma-atomic emission spectrometry in exploration geochemistry. *J. Geochem. Explor.*, **44**, 139–200.
26. Hall, G.E.M. (1992) Inductively coupled plasma mass spectrometry in geoanalysis. *J. Geochem. Explor.*, **44**, 201–249.
27. Potts, P.J. (1987) *A Handbook of Silicate Rock Analysis*, Chapman & Hall, London.
28. Gill, R. (Ed.) (1997) *Modern Analytical Geochemistry. An Introduction to Quantitative Chemical Analysis Techniques for Earth, Environmental and Materials Scientists*, Addison Wesley Longman, Harlow, pp. xii + 329.
29. Potts, P.J., Dupuy, C. and Bowles, J.F.W. (1990) Microanalytical methods in mineralogy and geochemistry. *Chem. Geol.*, **83**, 1–148.
30. Jarvis, I., Potts, P.J. and Jarvis, K.E. (1995) Analytical spectroscopy in the earth sciences. *Chem. Geol.*, **124**, 1–160.

31. Jarvis, I. and Jarvis, K.E. (1992) Plasma spectrometry in the earth sciences. *Chem. Geol.*, **95**, 1–198.
32. Hall, G.E.M. (1993) Geoanalysis 90: an international symposium on the analysis of geological materials. *Geol. Surv. Can. Bull.*, **451**.
33. Ramsey, M.H. (1995) Geoanalysis 94: an international symposium on the analysis of geological and environmental materials. *Analyst*, **120**, 1227–1541.
34. Kane, J.S. (1997) Geoanalysis 97: the third international conference on the analysis of geological and environmental materials. *Analyst*, **122**, 1177–1292.
35. Carignan, J., Télouk, P. and Valladon, M. (Eds.) (2001) Special issue – conference proceedings of Geoanalysis 2000. *Geostand. Newslett.*, **25**, 185–474.
36. Kane, J., Hämäläinen, L., Niskavaara, H., Ramsey, M. and Sandstrom, H. (Eds.) (2004) Special issue – Geoanalysis 2003. *Geostand. Geoanal. Res.*, **28**, 7–136 and 191–341.
37. Hall, G.E.M., Vaive, J.E. and Pelchat, J.-C. (1996) Performance of inductively coupled plasma mass spectrometric methods used in the determination of trace elements in surface waters in hydrogeochemical surveys. *J. Anal. Atom. Spectrom.*, **11**, 779–786.
38. Rose, A.W., Hawkes, H.E. and Webb, J.S. (1979) *Geochemistry in Mineral Exploration*, Academic Press, London.
39. Ramsey, M.H. (2002) Appropriate rather than representative sampling, based on acceptable levels of uncertainty. *Accred. Qual. Assur.*, **7**, 274–280.
40. Thompson, M. and Ramsey, M.H. (1995) Quality concepts and practices applied to sampling – an exploratory study. *Analyst*, **120**, 261–270.
41. Thompson, M. and Maguire, M. (1993) Estimating and using sampling precision in surveys of trace constituents of soils. *Analyst*, **118**, 1107–1110.
42. Ramsey, M.H., Thompson, M. and Hale, M. (1992) Objective evaluation of precision requirements for geochemical analysis using robust analysis of variance. *J. Geochem. Explor.*, **44**, 23–36.
43. Ramsey, M.H. (1993) Sampling and analytical quality control (SAX) for improved error estimation in the measurement of Pb in the environment using robust analysis of variance. *Appl. Geochem.* (Suppl. 2), 149–153.
44. Ramsey, M.H. (1994) Error estimation in environmental sampling and analysis. In *Environmental Sampling for Trace Analysis* (Ed. B.A. Markert), VCH, Weinheim, pp. 93–108.
45. Analytical Methods Committee (1989) Robust statistics – how not to reject outliers. Part 1. Basic concepts. *Analyst*, **114**, 1693–1697.
46. Analytical Methods Committee (1989) Robust statistics – how not to reject outliers. Part 2. Inter-laboratory trials. *Analyst*, **114**, 1699–1702.
47. Ramsey, M.H., Argyraki, A. and Thompson, M. (1995) Estimation of sampling bias between different sampling protocols on contaminated land. *Analyst*, **120**, 1353–1356.
48. Argyraki, A., Ramsey, M.H. and Thompson, M. (1995) Proficiency testing in sampling: pilot study on contaminated land. *Analyst*, **120**, 2799–2803.
49. Ramsey, M.J. (1997) Measurement uncertainty arising from sampling: implications for the objectives of geoanalysis. *Analyst*, **122**, 1255–1260.
50. Ramsey, M.J., Argyraki, A. and Thompson, M. (1995) On the collaborative trial in sampling. *Analyst*, **120**, 2309–2312.
51. Ramsey, M.H. and Argyraki, A. (1997) Estimation of measurement uncertainty from field sampling: implications for the classification of contaminated land. *Sci. Total Environ.*, **198**, 243–258.
52. Ramsey, M.H. (1998) Sampling as a source of measurement uncertainty: techniques for quantification and comparison with analytical sources. *J. Anal. Atom. Spectrom.*, **13**, 97–104.
53. Ramsey, M.H., Taylor, P.D. and Lee, J.-C. (2002) Optimized contaminated land investigation at minimum overall cost to achieve fitness-for-purpose. *J. Environ. Monit.*, **4**, 809–814.
54. Taylor, P.D., Ramsey, M.H. and Potts, P.J. (2004) Balancing measurement uncertainty against financial benefits: a comparison of in situ and ex situ analysis of contaminated land. *Env. Sci. Technol.*, **38**, 6824–6831.

55. De Zorzi, P., Belli, M., Barbizzi, S., Menegon, S. and Deluisa, A. (2002) A practical approach to assessment of sampling uncertainty. *Accred. Qual. Assur.*, **7**, 182–188.
56. Kurfurst, U., Desaulles, A., Rehnert, A. and Muntau, H. (2004) Estimation of measurement uncertainty by the budget approach for heavy metal content in soils under different land use. *Accred. Qual. Assur.*, **9**, 64–75.
57. Minkinen, P. (2004) Practical applications of sampling theory. *Chemometr. Intell. Lab. Syst.*, **74**, 85–94.
58. Ramsey, M.H. (2004) Sampling the environment: twelve key questions that need answers. *Geostand. Geoanal. Res.*, **28**, 251–261.
59. Taylor, P.D., Ramsey, M.H. and Potts, P.J. (2005) Spatial contaminant heterogeneity: quantification with scale of measurement at contrasting sites. *J. Environ. Monit.*, **7**, 1364–1370.
60. Myers, J.C. (1997) *Geostatistical Error Management: Quantifying Uncertainty for Environmental Sampling and Mapping*, Van Nostrand Reinhold, New York.
61. Horwitz, W. (1990) Nomenclature for sampling in analytical chemistry (Recommendations 1990). *Pure Appl. Chem.*, **62**, 1193–1208.
62. ISO 11074–2: 1998, ISO, Geneva.
63. Gy, P.M. (1982) *Sampling of Particulate Materials—Theory and Practice*, Elsevier, Amsterdam.
64. Ingamells, C.O. and Switzer, P. (1973) A proposed sampling constant for use in geochemical analysis. *Talanta*, **20**, 547–568.
65. Allen, M. (2003) Initial sample preparation. In *Chemical Analysis of Contaminated Land* (Eds. K.C. Thompson and C.P. Nathanail), Blackwell Publishing, Oxford, pp. 34–63.
66. Lyn, J.A., Ramsey, M.H., Fussell, R.J. and Wood, R. (2003) Measurement uncertainty from physical sample preparation: estimation including systematic error. *Analyst*, **128**, 1391–1398.
67. Lyn, J.A., Ramsey, M.H., Damant, A. P. and Wood, R. (2005) Optimising uncertainty in physical sample preparation. *Analyst*, **130**, 1507–1512.
68. Allen, M.A. (1998) Comminution of geological samples using Syalon based milling vessels: comparison with established sample preparation methods. *Anal. Commun.*, **35**, 75–78.
69. Jarvis, K.E. and Williams, J.G. (1989) The analysis of geological samples by slurry nebulization inductively coupled plasma-mass spectrometry (ICP-MS). *Chem. Geol.*, **77**, 53–63.
70. Jarvis, K.E. (1992) Role of slurry nebulization for the analysis of geological samples by inductively coupled plasma spectrometry. *Chem. Geol.*, **95**, 73–84.
71. Totland, M., Jarvis, I. and Jarvis, K.E. (1993) Determination of the platinum-group elements and gold in solid samples by slurry nebulisation ICP-MS. *Chem. Geol.*, **104**, 175–188.
72. Jarvis, K.E. (1989) Determination of rare earth elements in geological samples by inductively coupled plasma mass spectrometry. *J. Anal. Atom. Spectrom.*, **4**, 563–570.
73. Ebdon, L., Foulkes, M. and Sutton, K. (1997) Slurry nebulization in plasmas. *J. Anal. Atom. Spectrom.*, **12**, 213–229.
74. Vanhaecke, F. (2005) Electrothermal vaporization as a means of sample introduction in ICP-MS. In *ICP Mass Spectrometry Handbook* (Ed. S.M. Nelms), Blackwell Publishing, Oxford, pp. 215–227.
75. Sturgeon, R.E. and Lam, J.W. (1999) The ETV as a thermochemical reactor for ICP-MS sample introduction. *J. Anal. Atom. Spectrom.*, **14**, 785–791.
76. Knight, K., Chenery, S., Zochowski, S.W., Thompson, M. and Flint, C.D. (1996) Time-resolved signals from particles injected into the inductively coupled plasma. *J. Anal. Atom. Spectrom.*, **11**, 53–56.
77. Bock, R. (1979) *A Handbook of Decomposition Methods in Analytical Chemistry*, International Textbook Company, Glasgow.
78. Šulcek, Z. and Povondra, P. (1989) *Methods of Decomposition in Inorganic Analysis*, CRC Press, Boca Raton, NJ.
79. Chao, T.T. and Sanzalone, R.F. (1992) Decomposition techniques. *J. Geochem. Explor.*, **44**, 65–106.

80. Jarvis, I. (1992) Sample preparation for ICP-MS. In *Handbook of Inductively Coupled Plasma Mass Spectrometry* (Eds. K.E. Jarvis, A.L. Gray and R.S. Houk), Chapman & Hall, London, pp. 172–224.
81. Totland, M., Jarvis, I. and Jarvis, K.E. (1992) An assessment of dissolution techniques for the analysis of geological samples by plasma spectrometry. *Chem. Geol.*, **95**, 35–62.
82. Yu, Z., Robinson, P. and McGoldrick, P. (2001) An evaluation of methods for the chemical decomposition of geological materials for trace element determination using ICP-MS. *Geostand. Newslett.*, **25**, 199–217.
83. Hall, G.E.M., Vaive, J.E., Coope, J.A. and Weiland, E.F. (1989) Bias in the analysis of geological materials for gold using current methods. *J. Geochem. Explor.*, **34**, 157–171.
84. Hall, G.E.M. (1990) Are your REE results total? *Explore*, **68**, 18–20.
85. Hall, G.E.M. and Plant, J.A. (1992) Analytical errors in the determination of high field strength elements and their implications in tectonic interpretation studies. *Chem. Geol.*, **95**, 141–156.
86. Hall, G.E.M. and Vaive, J.E. (1992) Bias in the analysis of geological materials for gold using current methods – reply. *J. Geochem. Explor.*, **42**, 388–390.
87. Jarvis, K. (1990) A critical evaluation of two sample preparation techniques for low-level determination of some geologically incompatible elements by inductively coupled plasma mass spectrometry. *Chem. Geol.*, **83**, 89–103.
88. McHugh, J.B. and O’Leary, R.M. (1992) Bias in the analysis of geological materials for gold using current methods, by G.E.M. Hall *et al.* Comments. *J. Geochem. Explor.*, **42**, 387–388.
89. Cook, J.M., Robinson, J.J., Chenery, S.R.N. and Miles, D.L. (1997) Determining cadmium in marine sediments by inductively coupled plasma mass spectrometry: attacking the problem or the problems with the attack? *Analyst*, **122**, 1207–1210.
90. Cook, J.M., Gardner, M.J., Griffiths, A.H., Jessep, M.A., Ravenscroft, J.E. and Yates, R. (1997) The comparability of sample digestion techniques for the determination of metals in sediments. *Mar. Poll. Bull.*, **34**, 637–644.
91. Croudace, I.W. (1980) A possible error source in silicate wet-chemistry caused by insoluble fluorides. *Chem. Geol.*, **31**, 153–155.
92. Ingamells, C.O. (1964) Rapid chemical analysis of silicate rocks. *Talanta*, **11**, 665–666.
93. Cremer, M. and Schlocker, J. (1976) Lithium metaborate decomposition of rocks, minerals and ores. *Am. Mineral.*, **61**, 318–321.
94. Feldman, C. (1983) Behavior of trace refractory minerals in the lithium metaborate fusion-acid dissolution procedure. *Anal. Chem.*, **55**, 2451–2453.
95. Ingamells, C.O. (1970) Lithium metaborate flux in silicate analysis. *Anal. Chim. Acta*, **52**, 323–334.
96. Owens, J.W., Gladney, E.S. and Knab, D. (1982) Determination of boron in geological materials by inductively-coupled plasma emission spectrometry. *Anal. Chim. Acta*, **135**, 169–172.
97. Walsh, J.N. (1985) Determination of boron at trace levels in rocks by inductively coupled plasma spectrometry. *Analyst*, **110**, 959–962.
98. Hall, G.E.M. and Pelchat, J.-C. (1986) Inductively coupled plasma emission spectrometric determination of boron and other oxo-anion forming elements in geological materials. *Analyst*, **111**, 1255–1260.
99. Hall, G.E.M., Park, C.J. and Pelchat, J.C. (1987) Determination of tungsten and molybdenum at low levels in geological materials by inductively coupled plasma mass spectrometry. *J. Anal. Atom. Spectrom.*, **2**, 189–196.
100. Walsh, J.N., Buckley, F. and Barker, J. (1981) The simultaneous determination of the rare-earth elements in rocks using inductively coupled plasma source spectrometry. *Chem. Geol.*, **33**, 141–153.
101. Kingston, H.M. and Haswell, S.J. (Eds.) (1997) *Microwave Enhanced Chemistry: Fundamentals, Sample Preparation, and Applications*, American Chemical Society, Washington DC.

102. Lamothe, P.J., Fries, T.L. and Consul, J.J. (1986) Evaluation of a microwave oven system for the dissolution of geologic samples. *Anal. Chem.*, **58**, 1881–1886.
103. Totland, M.M., Jarvis, I. and Jarvis, K.E. (1995) Microwave digestion and alkali fusion procedures for the determination of the platinum-group elements and gold in geological materials by ICP-MS. *Chem. Geol.*, **124**, 21–36.
104. Tessier, A., Campbell, P.G.C. and Bisson, M. (1979) Sequential extraction procedure for the speciation of particulate trace metals. *Anal. Chem.*, **51**, 844–851.
105. Chao, T.T. (1984) Use of partial dissolution techniques in geochemical exploration. *J. Geochem. Explor.*, **20**, 101–135.
106. Hall, G.E.M. and Bonham-Carter, G.F. (Eds.) (1998) Selective extractions. *J. Geochem. Explor.*, **61**, 1–232.
107. Church, S.E., Mosier, E.L. and Motooka, J.M. (1987) Mineralogical basis for the interpretation of multi-element (ICP-AES), oxalic acid and aqua regia partial digestions of stream sediments for reconnaissance exploration geochemistry. *J. Geochem. Explor.*, **29**, 207–233.
108. Fonseca, E.C. and Martin, H. (1986) The selective extraction of Pb and Zn in selected mineral and soil samples, application in geochemical exploration (Portugal). *J. Geochem. Explor.*, **26**, 231–248.
109. Davidson, C.M., Thomas, R.P., McVey, S.E., Perala, R., Littlejohn, D. and Ure, A.M. (1994) Evaluation of a sequential extraction procedure for the speciation of heavy metals in sediments. *Anal. Chim. Acta*, **291**, 277–286.
110. Li, X., Coles, B.J., Ramsey, M.H. and Thornton, I. (1995) Sequential extraction of soils for multi-element analysis by ICP-AES. *Chem. Geol.*, **124**, 109–123.
111. Li, X., Coles, B.J., Ramsey, M.H. and Thornton, I. (1995) Chemical partitioning of the new National Institute of Standards and Technology Standard Reference Materials (SRM 2709–2711) by sequential extraction using inductively coupled plasma atomic emission spectrometry. *Analyst*, **120**, 1415–1419.
112. Hall, G.E.M., Vaive, J.E. and Button, P. (1997) Detection of past underground nuclear events by geochemical signatures in soils. *J. Geochem. Explor.*, **59**, 145–162.
113. Marin, B., Valladon, M., Polvé, M. and Monaco, A. (1997) Reproducibility testing of a sequential extraction scheme for the determination of trace metal speciation in a marine reference sediment by inductively coupled plasma-mass spectrometry. *Anal. Chim. Acta*, **342**, 91–112.
114. Hall, G.E.M., Vaive, J.E., Beer, R. and Hoashi, M. (1996) Selective leaches revisited, with emphasis on the amorphous Fe oxyhydroxide phase extraction. *J. Geochem. Explor.*, **56**, 59–78.
115. Hall, G.E.M., Gauthier, G., Pelchat, J.-C., Pelchat, P. and Vaive, J.E. (1996) Application of a sequential extraction scheme to ten geological certified reference materials for the determination of 20 elements. *J. Anal. Atom. Spectrom.*, **11**, 787–796.
116. McCarty, D.K., Moore, J.N. and Marcus, W.A. (1998) Mineralogy and trace element association in an acid mine drainage iron oxide precipitate: comparison of selective extractions. *Appl. Geochem.*, **13**, 165–176.
117. Quevauviller, Ph., Rauret, G., López-Sánchez, J.-F., Rubio, R., Ure, A. and Muntau, H. (1997) Certification of trace metal extractable contents in a sediment reference material (CRM 601) following a three-step sequential extraction procedure. *Sci. Total Environ.*, **205**, 223–234.
118. Sahuquillo, A., López-Sánchez, J.F., Rubio, R., Rauret, G., Thomas, R.P., Davidson, C.M. and Ure, A.M. (1999) Use of a certified reference material for extractable trace metals to assess sources of uncertainty in the BCR three-stage sequential extraction procedure. *Anal. Chim. Acta*, **382**, 317–327.
119. Pueyo, M., Rauret, G., Lück, D., Yli-Halla, M., Muntau, H., Quevauviller, Ph. and López-Sánchez, J.F. (2001) Certification of the extractable contents of Cd, Cr, Cu, Ni, Pb and Zn in a freshwater sediment following a collaboratively tested and optimized three-step sequential extraction procedure. *J. Environ. Monit.*, **3**, 243–250.

120. Quevauviller, Ph. (2002) Operationally-defined extraction procedures for soil and sediment analysis. Part 3: New CRMs for trace-element extractable contents. *Trends Anal. Chem.*, **21**, 774–785.
121. Marguá, E., Salvadó, V., Queralt, I. and Hidalgo, M. (2004) Comparison of three-stage sequential extraction and toxicity characteristic leaching tests to evaluate metal mobility in mining wastes. *Anal. Chim. Acta*, **524**, 151–159.
122. Clark, J.R. (1993) Enzyme-induced leaching of B-horizon soils for mineral exploration in areas of glacial overburden. *Trans. Inst. Min. Metall.*, **102**, B19–B29.
123. Cave, M.R. and Wragg, J. (1997) Measurement of trace element distributions in soils and sediments using sequential leach data and a non-specific extraction system with chemometric data processing. *Analyst*, **122**, 1211–1221.
124. Cave, M.R. and Harmon, K. (1997) Determination of trace metal distributions in iron oxide phases of red bed sandstones by chemometric analysis of whole rock and selective leach data. *Analyst*, **122**, 501–512.
125. Cave, M.R., Milodowski, A.E. and Friel, E.N. (2004) Evaluation of a method for identification of host physico-chemical phases for trace metals and measurement of their solid-phase partitioning in soil samples by nitric acid extraction and chemometric mixture resolution. *Geochemistry: Exploration, Environment, Analysis*, **4**, 71–86.
126. Palumbo-Roe, B., Cave, M.R., Klinck, B.A., Wragg, J., Taylor, H., O'Donnell, K.E., Shaw, R.A. (2005) Bioaccessibility of arsenic in soils developed over Jurassic ironstones in eastern England. *Environmental Geochemistry and Health*, **27**, 121–130.
127. Ruby, M.V., Davis, A., Schoof, R., Eberle, S. and Sellstone, C.M. (1996). Estimation of lead and arsenic bioavailability using a physiologically based extraction test. *Env. Sci. Technol.*, **30**, 422–430.
128. Cave, M.R., Wragg, J., Palumbo, B. and Klinck, B.A. (2003). Measurement of the bioaccessibility of arsenic in UK soils. R&D Technical Report P5-062/TR/02, Environment Agency, Bristol.
129. Oomen, A.G., Hack, A., Minekus, M., Zeijdner, E., Cornelis, C., Schoeters, G., Verstraete, W., Van de Wiele, T., Wragg, J., Rempelberg, C.J.M., Sips, A.J.A.M. and Van Wijnen, J.H. (2002) Comparison of five *in vitro* digestion models to study the bioaccessibility of soil contaminants. *Env. Sci. Technol.*, **36**, 3326–3334.
130. Cave, M.R. and Wragg, J. (2002). *In vitro* methods for the measurement of the oral bioaccessibility of selected metals and metalloids in soils: a critical review. R&D Technical Report P5-062/TR/01, Environment Agency, Bristol.
131. Walsh, J.N. (1992) Use of multiple internal standards for high-precision, routine analysis of geological samples by inductively coupled plasma-atomic emission spectrometry. *Chem. Geol.*, **95**, 113–121.
132. Ramsey, M.H., Potts, P.J., Webb, P.C., Watkins, P., Watson, J.S. and Coles, B.J. (1995) An objective assessment of analytical method precision: comparison of ICP-AES and XRF for the analysis of silicate rocks. *Chem. Geol.*, **124**, 1–19.
133. Hutton, R.C., Eaton, A.N. and Gosland, R.M. (1990) Application of a dual-mode detection system for ICP-MS. Part 1: Determination of majors, minors and traces in geostandards. *Appl. Spectrosc.*, **44**, 238–242.
134. Eggs, S.M., Woodhead, J.D., Kinsley, L.P.J., Mortimer, G.E., Sylvester, P., McCulloch, M.T., Hergt, J.M. and Handler, M.R. (1997) A simple method for the precise determination of ≥ 40 trace elements in geological samples by ICPMS using enriched isotope internal standardisation. *Chem. Geol.*, **134**, 311–326.
135. Thomas, P. (2003) Metal analysis. In *Chemical Analysis of Contaminated Land* (Eds. K.C. Thompson and C.P. Nathanail), Blackwell Publishing, Oxford, p. 84.
136. Jarvis, K.E., Gray, A.L. and McCurdy, E. (1989) Avoidance of spectral interference on europium in inductively coupled plasma mass spectrometry by sensitive measurement of the doubly charged ion. *J. Anal. Atom. Spectrom.*, **4**, 743–747.

137. Evans, E.H. and Giglio, J.J. (1993) Interferences in inductively coupled plasma mass spectrometry. A review. *J. Anal. Atom. Spectrom.*, **8**, 1–18.
138. Garbe-Schönberg, C.-D. (1993) Simultaneous determination of thirty-seven trace elements in twenty-eight international rock standards by ICP-MS. *Geostand. Newslett.*, **17**, 81–97.
139. Bradshaw, N., Hall, E.F.H. and Sanderson, N.E. (1989) Inductively coupled plasma as an ion source for high-resolution mass spectrometry. *J. Anal. Atom. Spectrom.*, **4**, 801–803.
140. Becker, J.S. and Dietze, H.-J. (1997) Double-focusing sector field inductively coupled plasma mass spectrometry for highly sensitive multi-element and isotopic analysis. *J. Anal. Atom. Spectrom.*, **12**, 881–889.
141. Moens, L. and Jakubowski, N. (1998) Double-focusing mass spectrometers in ICPMS. *Anal. Chem.*, **70**, 251A–256A.
142. Barbante, C., Bellomi, T., Mezzadri, G., Cescon, P., Scarponi, G., Morel, C., Jay, S., Van de Velde, K., Ferrari, C. and Boutron, C.F. (1997) Direct determination of heavy metals at picogram per gram levels in Greenland and Antarctic snow by double focusing inductively coupled plasma mass spectrometry. *J. Anal. Atom. Spectrom.*, **12**, 925–931.
143. Tanner, S.D., Paul, M., Beres, S.A. and Denoyer, E.R. (1995) The application of cold-plasma conditions for the determination of trace levels of Fe, Ca, K, Na and Li by ICP-MS. *At. Spectrosc.*, **16**, 16–18.
144. Lam, J.W.H. and Horlick, G. (1990) A comparison of argon and mixed gas plasmas for inductively coupled plasma-mass spectrometry. *Spectrochim. Acta*, **45B**, 1313–1325.
145. Lam, J.W.H. and McLaren, J.W. (1990) Use of aerosol processing and nitrogen–argon plasmas for reduction of oxide interference in inductively coupled plasma mass spectrometry. *J. Anal. Atom. Spectrom.*, **5**, 419–424.
146. Evans, E.H. and Ebdon, L. (1990) Effect of organic solvents and molecular gases on polyatomic ion interferences in inductively coupled plasma mass spectrometry. *J. Anal. Atom. Spectrom.*, **5**, 425–430.
147. Tanner, S.D., Baranov, V.I. and Bandura, D.R. (2002) Reaction cells and collision cells for ICP-MS: a tutorial review. *Spectrochim. Acta*, **57B**, 1361–1452.
148. Koyanagi, G.K., Bohme, D.K. and Bandura, D.R. (2005) Collision and reaction cells. In *ICP Mass Spectrometry Handbook* (Ed. S.M. Nelms), Blackwell Publishing, Oxford, pp. 336–351.
149. Bea, F. (1996) Residence of REE, Y, Th and U in granites and crustal protoliths: implications for the chemistry of crustal melts. *J. Petrol.*, **37**, 521–552.
150. Henderson, P. (1984) *Rare Earth Element Geochemistry*, Elsevier, Amsterdam.
151. Smedley, P.L. (1991) The geochemistry of rare earth elements in groundwater from the Carnmenellis area, southwest England. *Geochim. Cosmochim. Acta*, **55**, 2767–2779.
152. Fee, J.A., Gaudette, H.E., Lyons, W.B. and Long, D.T. (1992) Rare-earth element distribution in Lake Tyrrell groundwaters, Victoria, Australia. *Chem. Geol.*, **96**, 67–93.
153. Johannesson, K.H., Stetzenbach, K.J. and Hodge, V.F. (1997) Rare earth elements as geochemical tracers of regional groundwater mixing. *Geochim. Cosmochim. Acta*, **61**, 3605–3618.
154. German, C.R., Klinkhammer, G.P., Edmond, J.M., Mitra, A. and Elderfield, H. (1990) Hydrothermal scavenging of rare-earth elements in the ocean. *Nature*, **345**, 516–518.
155. Evensen, N.M., Hamilton, P.J. and O’Nions, R.K. (1978) Rare-earth abundances in chondritic meteorites. *Geochim. Cosmochim. Acta*, **42**, 1199–1212.
156. Shabani, M.B., Akagi, T. and Masuda, A. (1992) Preconcentration of trace rare-earth elements in seawater by complexation with bis(2-ethylhexyl) hydrogen phosphate and 2-ethylhexyl dihydrogen phosphate adsorbed on a C₁₈ cartridge and determination by inductively coupled plasma mass spectrometry. *Anal. Chem.*, **64**, 737–743.
157. Haley, B.A. and Klinkhammer, G.P. (2003) Complete separation of rare earth elements from small volume seawater samples by automated ion chromatography: method development and application to benthic flux. *Marine Chemistry*, **82**, 197–220.

158. Jarvis, K.E. (1988) Inductively coupled plasma mass spectrometry: a new technique for the rapid or ultra-trace level determination of the rare-earth elements in geological materials. *Chem. Geol.*, **68**, 31–39.
159. Date, A.R. and Hutchison, D. (1987) Determination of rare earth elements in geological samples by inductively coupled plasma source mass spectrometry. *J. Anal. Atom. Spectrom.*, **2**, 269–276.
160. Lichte, F.E., Meier, A.L. and Crock, J.G. (1987) Determination of the rare-earth elements in geological materials by inductively coupled plasma mass spectrometry. *Anal. Chem.*, **59**, 1150–1157.
161. Jenner, G.A., Longerich, H.P., Jackson, S.E. and Fryer, B.J. (1990) ICP-MS – a powerful tool for high-precision trace-element analysis in earth sciences: evidence from analysis of selected USGS reference materials. *Chem. Geol.*, **83**, 133–148.
162. Klinkhammer, G., German, C.R., Elderfield, H., Greaves, M.J. and Mitra, A. (1994) Rare earth elements in hydrothermal fluids and plume particulates by inductively coupled plasma mass spectrometry. *Mar. Chem.*, **45**, 179–186.
163. Barrat, J.A., Keller, F., Amossé, J., Taylor, R.N., Nesbitt, R.W. and Hirata, T. (1996) Determination of rare earth elements in sixteen silicate reference samples by ICP-MS after Tm addition and ion exchange separation. *Geostand. Newslett.*, **20**, 133–139.
164. Meisel, T., Schöner, N., Paliulionyte, V. and Kahr, E. (2002) Determination of rare earth elements, Y, Th, Zr, Hf, Nb and Ta in geological reference materials G-2, G-3, SCo-1 and WGB-1 by sodium peroxide sintering and inductively coupled plasma-mass spectrometry. *Geostand. Newslett.*, **26**, 53–61.
165. Rao, T.P. and Kala, R. (2004) On-line and off-line preconcentration of trace and ultratrace amount of lanthanides. *Talanta*, **63**, 949–959.
166. Jain, J.C., Field, M.P., Neal, C.R., Ely, J.C. and Sherrell, R.M. (2000) Determination of the REE in geological reference materials DTS-1 (Dunite) and PCC-1 (Peridotite) by ultrasonic and microconcentric desolvating nebulisation ICP-MS. *Geostand. Newslett.*, **24**, 65–72.
167. Olive, V., Ellam, R.M. and Wilson L. (2001) A protocol for the determination of the rare earth elements at picomole level in rocks by ICP-MS: results on geological reference materials USGS PCC-1 and DTS-1. *Geostand. Newslett.*, **25**, 219–228.
168. Kent, A.J.R., Jacobsen, B., Peate, D.W., Waight, T.E. and Baker, J.A. (2004) Isotope dilution MC-ICP-MS rare earth element analysis of geochemical reference materials NIST SRM 610, NIST SRM 612, NIST SRM 614, BHVO-2G, BHVO-2, BCR-2G, JB-2, WS-E, W-2, AGV-1 and AGV-2. *Geostand. Geoanal. Res.*, **28**, 417–429.
169. Dulski, P. (1994) Interferences of oxide, hydroxide and chloride analyte species in the determination of rare earth elements in geological samples by inductively coupled plasma-mass spectrometry. *Fresen. J. Anal. Chem.*, **350**, 194–203.
170. Longerich, H.P., Fryer, B.J., Strong, D.F. and Kantipuly, C.J. (1987) Effects of operating conditions on the determination of the rare earth elements in inductively coupled plasma-mass spectrometry (ICP-MS). *Spectrochim. Acta*, **42B**, 75–92.
171. Longerich, H.P. (1993) Oxychlorine ions in inductively coupled plasma mass spectrometry: effect of chlorine speciation as Cl^- and ClO_4^- . *J. Anal. Atom. Spectrom.*, **8**, 439–444.
172. Cheatham, M.M., Sangrey, W.F. and White, W.M. (1993) Sources of error in external calibration ICP-MS analysis of geological samples and an improved non-linear drift correction procedure. *Spectrochim. Acta*, **48B**, E487–E506.
173. Benoit, M., Polvé, M. and Ceuleneer, G. (1996) Trace element and isotopic characterization of mafic cumulates in a fossil mantle diapir (Oman ophiolite). *Chem. Geol.*, **134**, 199–214.
174. Jochum, K.P., Seufert, H.M. and Thirlwall, M.F. (1990) High-sensitivity Nb analysis by spark-source mass spectrometry (SSMS) and calibration of XRF Nb and Zr. *Chem. Geol.*, **81**, 1–16.
175. Hall, G.E.M., Pelchat, J.C. and Loop, J. (1990) Determination of zirconium, niobium, hafnium and tantalum at low levels in geological materials by inductively coupled plasma mass spectrometry. *J. Anal. Atom. Spectrom.*, **5**, 339–349.

176. Watkins, P.J. and Nolan, J. (1992) Determination of rare-earth elements, yttrium, scandium and hafnium using cation-exchange separation and inductively coupled plasma-atomic emission spectrometry. *Chem. Geol.*, **95**, 131–139.
177. Green, T.H. (1995) Significance of Nb/Ta as an indicator of geochemical processes in the crust-mantle system. *Chem. Geol.*, **120**, 347–359.
178. Münker, C. (1998) Nb/Ta fractionation in a Cambrian arc/back arc system, New Zealand: source constraints and applications of refined ICPMS techniques. *Chem. Geol.*, **144**, 23–45.
179. McGinnis, C.E., Jain, J.C. and Neal, C.R. (1997) Characterization of memory effects and development of an effective wash protocol for the measurement of petrogenetically critical trace elements in geological samples by ICP-MS. *Geostand. Newslett.*, **21**, 289–305.
180. Malik, H. and Parry, S.J. (1992) Importance of the sampling constant for the determination of gold in heterogeneous materials. *Analyst*, **117**, 1347–1349.
181. Pattou, L., Lorand, J.P. and Gros, M. (1996) Non-chondritic platinum-group element ratios in the Earth's mantle. *Nature*, **379**, 712–715.
182. Farago, M.E., Kavanagh, P., Blanks, R., Kelly, J., Kazantzis, G., Thornton, I., Simpson, P.R., Cook, J.M., Delves, H.T. and Hall, G.E.M. (1998) Platinum concentrations in urban road dust and soil and in blood and urine in the United Kingdom. *Analyst*, **123**, 451–454.
183. Zereini, F. and Alt, F. (Eds.) (2000) *Anthropogenic platinum group element emissions: their impact on man and environment*, Springer-Verlag, Berlin, Heidelberg, Germany.
184. Barbante, C., Veyseyre, A., Ferrari, C., Van de Velde, K., Morel, C., Capodaglio, G., Cescon, P., Scarponi, G. and Boutron, C. (2001) Greenland snow evidence of large scale atmospheric contamination for platinum, palladium and rhodium. *Environ. Sci. Technol.*, **35**, 835–839.
185. Merget, R. and Rosner, G. (2001) Evaluation of the health risk of platinum group metals emitted from automotive catalytic converters. *Sci. Total Environ.*, **270**, 165–173.
186. Hall, G.E.M. and Bonham-Carter, G.F. (1988) Review of methods to determine gold, platinum and palladium in production-oriented geochemical laboratories, with application of a statistical procedure to test for bias. *J. Geochem. Explor.*, **30**, 255–286.
187. Reddi, G.S. and Rao, C.R.M. (1999) Analytical techniques for the determination of precious metals in geological and related materials. *Analyst*, **124**, 1531–1540.
188. Barefoot, R.R. (1998) Determination of the precious metals in geological materials by inductively coupled plasma mass spectrometry. *J. Anal. Atom. Spectrom.*, **13**, 1077–1084.
189. Barefoot, R.R. and Van Loon, J.C. (1999) Recent advances in the determination of the platinum group elements and gold. *Talanta*, **49**, 1–14.
190. Haffty, J., Riley, L.B. and Goss, W.D. (1977) A manual of fire assaying and determination of the noble metals in geological materials. *US Geol. Surv. Bull.*, **1445**.
191. Suominen, M., Kontas, E. and Niskavaara, H. (2004) Comparison of silver and gold inquarting in the fire assay determination of palladium, platinum and rhodium in geological samples. *Geostand. Geoanal. Res.*, **28**, 131–136.
192. Hall, G.E.M. and Pelchat, J.C. (1994) Analysis of geological materials for gold, platinum and palladium at low ppb levels by fire assay-ICP mass spectrometry. *Chem. Geol.*, **115**, 61–72.
193. Simpson, P.R., Robotham, H. and Hall, G.E.M. (1990) Regional geochemical orientation studies for platinum in Jamaica. *Trans. Inst. Mining Metall.*, **99**, B183–B187.
194. Flight, D.M.A., Hall, G.E.M. and Simpson, P.R. (1994) Regional geochemical mapping of Pt, Pd and Au over an obducted ophiolite complex, Shetland Islands, northern Scotland. *Trans. Inst. Mining Metall.*, **103**, B68–B78.
195. Stone, P., Cook, J.M., McDermott, C., Robinson, J.J. and Simpson, P.R. (1995) Lithostratigraphic and structural controls on distribution of As and Au in southwest Southern Uplands, Scotland. *Trans. Inst. Mining Metall.*, **104**, B111–B119.
196. Robért, R.V.D., van Wyk, E. and Palmer, R. (1971) Concentration of the noble metals by a fire-assay technique using Nickel Sulphide as the collector, Report No 1371, National Institute for Metallurgy, Johannesburg.

197. Williamson, J.E. and Savage, J.A. (1965) The determination of osmiridium in Witwatersrand ores. *J. S. Afr. Inst. Min. Metall.*, **65**, 343–356.
198. Hoffman, E.L., Naldrett, A.J., Van Loon, J.C., Hancock, R.G.V. and Manson, A. (1978) The determination of all the platinum group elements and gold in rocks and ore by neutron activation analysis after preconcentration by a nickel sulphide fire-assay technique on large samples. *Anal. Chim. Acta*, **102**, 157–166.
199. Asif, M., Parry, S.J. and Malik, H. (1992) Instrumental neutron activation analysis of a nickel sulphide fire assay button to determine the platinum group elements and gold. *Analyst*, **117**, 1351–1353.
200. Asif, M. and Parry, S.J. (1989) Elimination of reagent blank problems in the fire-assay preconcentration of the platinum group elements and gold with a nickel sulphide bead of less than one gram mass. *Analyst*, **114**, 1057–1059.
201. Date, A.R., Davis, A.E. and Cheung, Y.Y. (1987) The potential of fire assay and inductively coupled plasma source mass spectrometry for the determination of platinum group elements in geological materials. *Analyst*, **112**, 1217–1222.
202. Jackson, S.E., Fryer, B.J., Gosse, W., Healey, D.C., Longerich, H.P. and Strong, D.F. (1990) Determination of the precious metals in geological materials by inductively coupled plasma mass-spectrometry (ICP-MS) with nickel sulfide fire-assay collection and tellurium coprecipitation. *Chem. Geol.*, **83**, 119–132.
203. Reddi, G.S., Rao, C.R.M., Rao, T.A.S., Lakshmi, S.V., Prabhu, R.K. and Mahalingam, T.R. (1994) Nickel sulfide fire assay-ICPMS method for the determination of platinum-group elements: a detailed study on the recovery and losses at different stages. *Fresen. J. Anal. Chem.*, **348**, 350–352.
204. McDonald, I., Hart, R.J. and Tredoux, M. (1994) Determination of the platinum-group elements in South African kimberlites by nickel sulphide fire-assay and neutron activation analysis. *Anal. Chim. Acta*, **289**, 237–247.
205. Frimpong, A., Fryer, B.J., Longerich, H.P., Chen, Z. and Jackson, S.E. (1995) Recovery of precious metals using nickel sulfide fire assay collection: problems at nanogram per gram concentrations. *Analyst*, **120**, 1675–1680.
206. Juvonen, R., Lakomaa, T. and Soikkeli, L. (2002) Determination of gold and the platinum group elements in geological samples by ICP-MS after nickel sulphide fire assay: difficulties encountered with different types of geological samples. *Talanta*, **58**, 595–603.
207. Juvonen, R., Kallio, E. and Lakomaa, T. (1994) Determination of precious metals in rocks by inductively coupled plasma mass spectrometry using nickel sulfide concentration. Comparison with other pre-treatment methods. *Analyst*, **119**, 617–621.
208. Juvonen, R., Bartha, A., Lakomaa, T.M., Soikkeli, L.A., Bertalan, E., Kallio, E.I. and Ballók, M. (2004) Comparison of recoveries by lead fire assay and nickel sulfide fire assay in the determination of gold, platinum, palladium and rhenium in sulfide ore samples. *Geostand. Geoanal. Res.*, **28**, 123–130.
209. Sun, Y. and Sun, M. (2005) Nickel sulfide fire assay improved for pre-concentration of platinum group elements in geological samples: a practical means of ultra-trace analysis combined with inductively coupled plasma-mass spectrometry. *Analyst*, **130**, 664–669.
210. Bédard, L.P. and Barnes, S.-J. (2004) Improved platinum-group element extraction by NiS fire assay from chromitite ore samples using a flux containing sodium metaphosphate. *Geostand. Geoanal. Res.*, **28**, 311–316.
211. Perry, B.J., Van Loon, J.C. and Speller, D.V. (1992) Dry-chlorination inductively coupled plasma mass spectrometric method for the determination of platinum group elements in rocks. *J. Anal. Atom. Spectrom.*, **7**, 883–888.
212. Enzweiler, J., Potts, P.J. and Jarvis, K.E. (1995) Determination of platinum, palladium, ruthenium and iridium in geological samples by isotope dilution inductively coupled plasma mass spectrometry using a sodium peroxide fusion and tellurium coprecipitation. *Analyst*, **120**, 1391–1396.

213. Jin, X. and Zhu, H. (2000) Determination of platinum group elements and gold in geological samples with ICP-MS using a sodium peroxide fusion and tellurium co-precipitation. *J. Anal. Atom. Spectrom.*, **15**, 747–751.
214. Chen, Z., Fryer, B.J., Longerich, H.P. and Jackson, S.E. (1996) Determination of the precious metals in milligram samples of sulfides and oxides using inductively coupled plasma mass spectrometry after ion exchange preconcentration. *J. Anal. Atom. Spectrom.*, **11**, 805–809.
215. Jarvis, I., Totland, M.M. and Jarvis, K.E. (1997) Assessment of Dowex 1-X8-based anion-exchange procedures for the separation and determination of ruthenium, rhodium, palladium, iridium, platinum and gold in geological samples by inductively coupled plasma mass spectrometry. *Analyst*, **122**, 19–26.
216. Jarvis, I., Totland, M.M. and Jarvis, K.E. (1997) Determination of the platinum-group elements in geological materials by ICP-MS using microwave digestion, alkali fusion and cation-exchange chromatography. *Chem. Geol.*, **143**, 27–42.
217. Rehkiämper, M. and Halliday, A.N. (1997) Development and application of new ion-exchange techniques for the separation of the platinum group and other siderophile elements from geological samples. *Talanta*, **44**, 663–672.
218. Meisel, T., Fellner, N. and Moser, J. (2003) A simple procedure for the determination of platinum group elements and rhenium (Ru, Rh, Pd, Re, Os, Ir and Pt) using ID-ICP-MS with an inexpensive on-line matrix separation in geological and environmental materials. *J. Anal. Atom. Spectrom.*, **18**, 720–726.
219. Meisel, T. and Moser, J. (2004) Platinum-group element and rhenium concentrations in low abundance reference materials. *Geostand. Geoanal. Res.*, **28**, 233–250.
220. Gowing, C.J.B. and Potts, P.J. (1991) Evaluation of a rapid technique for the determination of precious metals in geological samples based on a selective aqua regia leach. *Analyst*, **116**, 773–779.
221. Jarvis, K.E., Williams, J.G., Parry, S.J. and Bertalan, E. (1995) Quantitative determination of the platinum-group elements and gold using NiS fire assay with laser ablation-inductively coupled plasma-mass spectrometry (LA-ICP-MS). *Chem. Geol.*, **124**, 37–46.
222. Rauch, S., Motelica-Heino, M., Morrison, G.M. and Donard, O.F.X. (2000) Critical assessment of platinum group element determination in road and urban river sediments using ultrasonic nebulisation and high resolution ICP-MS. *J. Anal. Atom. Spectrom.*, **15**, 329–334.
223. Pretorius, W., Chipley, D., Kyser, K. and Helmstaedt, H. (2003) Direct determination of trace levels of Os, Ir, Ru, Pt and Re in kimberlite and other geological materials using HR-ICP-MS. *J. Anal. Atom. Spectrom.*, **18**, 302–309.
224. Date, A.R. and Gray, A.L. (1983) Progress in plasma source mass spectrometry. *Spectrochim. Acta*, **38B**, 29–37.
225. Smith, R.G., Brooker, E.J., Douglas, D.J., Quan, E.S.K. and Rosenblatt, G. (1984) The typing of Au and base-metal occurrences by plasma/mass spectrometry: initial results. *J. Geochem. Explor.*, **21**, 385–393.
226. Strong, D.F. and Longerich, H.P. (1985) The inductively coupled plasma/mass spectrometer (ICP-MS). *Geosci. Can.*, **12**, 72–75.
227. Lichte, F.E., Wilson, S.M., Brooks, R.R., Reeves, R.D., Holzbecher, J. and Ryan, D.E. (1986) New method for the measurement of osmium isotopes applied to a New Zealand Cretaceous/Tertiary boundary shale. *Nature*, **322**, 816–817.
228. Begley, I.S. and Sharp, B.L. (1994) Occurrence and reduction of noise in inductively coupled plasma mass spectrometry for enhanced precision in isotope ratio measurement. *J. Anal. Atom. Spectrom.*, **9**, 171–176.
229. Begley, I.S. and Sharp, B.L. (1997) Characterisation and correction of instrumental bias in inductively coupled plasma quadrupole mass spectrometry for accurate measurement of lead isotope ratios. *J. Anal. Atom. Spectrom.*, **12**, 395–402.

230. Quétel, C.R., Thomas, B., Donard, O.F.X. and Grousset, F.E. (1997) Factorial optimization of data acquisition factors for lead isotope ratio determination by inductively coupled plasma mass spectrometry. *Spectrochim. Acta*, **52B**, 177–187.
231. Pin, C., Telouk, P. and Imbert, J.-L. (1995) Direct determination of the samarium:neodymium ratio in geological materials by inductively coupled plasma quadrupole mass spectrometry with cryogenic desolvation. Comparison with isotope dilution thermal ionization mass spectrometry. *J. Anal. Atom. Spectrom.*, **10**, 93–98.
232. Lindner, M., Leich, D.A., Borg, R.J., Russ, G.P., Bazan, J.M., Simons, D.S. and Date, A.R. (1986) Direct laboratory determination of the ^{187}Re half-life. *Nature*, **320**, 246–248.
233. Richardson, J.M., Dickin, A.P., McNutt, R.H., McAndrew, J.I. and Beneteau, S.B. (1989) Analysis of a rhenium-osmium solid-solution spike by inductively coupled plasma mass spectrometry. *J. Anal. Atom. Spectrom.*, **4**, 465–471.
234. Walder, A.J. and Freedman, P.A. (1992) Isotopic ratio measurement using a double focusing magnetic sector mass analyser with an inductively coupled plasma as an ion source. *J. Anal. Atom. Spectrom.*, **7**, 571–575.
235. Walder, A.J., Platzner, I. and Freedman, P.A. (1993) Isotope ratio measurement of lead, neodymium and neodymium-samarium mixtures, hafnium and hafnium-lutetium mixtures with a double focusing multiple collector inductively coupled plasma mass spectrometer. *J. Anal. Atom. Spectrom.*, **8**, 19–23.
236. Walder, A.J. and Furuta, N. (1993) High-precision lead isotope ratio measurement by inductively coupled plasma multiple collector mass spectrometry. *Anal. Sci.*, **9**, 675–680.
237. Halliday, A.N., Lee, D.-C., Christensen, J.N., Walder, A.J., Freedman, P.A., Jones, C.E., Hall, C.M., Yi, W. and Teagle, D. (1995) Recent developments in inductively coupled plasma magnetic sector multiple collector mass spectrometry. *Int. J. Mass Spectrom. Ion Process.*, **146/147**, 21–33.
238. Rehkämper, M., Schönbachler, M. and Stirling, C.H. (2001) Multiple collector ICP-MS: introduction to instrumentation, measurement techniques and analytical capabilities. *Geostand. Newslett.*, **25**, 23–40.
239. Halliday, A.N., Lee, D.C., Christensen, J.N., Rehkämper, M., Yi, W., Luo, X.Z., Hall, C.M., Balentine, C.J., Pettke, T. and Stirling, C.H. (1998) Applications of multiple collector-ICPMS to cosmochemistry, geochemistry and paleoceanography. *Geochim. Cosmochim. Acta*, **62**, 919–940.
240. Lee, D.-C. and Halliday, A.N. (1995) Precise determinations of the isotopic compositions and atomic weights of molybdenum, tellurium, tin and tungsten using ICP magnetic sector multiple collector mass spectrometry. *Int. J. Mass Spectrom. Ion Process.*, **146/147**, 35–46.
241. Lee, D.-C., Halliday, A.N., Snyder, G.A. and Taylor, L.A. (1997) Age and origin of the moon. *Science*, **278**, 1098–1103.
242. Thirlwall, M. and Walder, A.J. (1995) *In situ* hafnium isotope ratio analysis of zircon by inductively coupled plasma multiple collector mass spectrometry. *Chem. Geol.*, **122**, 241–247.
243. Blichert-Toft, J. (2001) On the Lu–Hf isotope geochemistry of silicate rocks. *Geostand. Newslett.*, **25**, 41–56.
244. De Laeter, J.R. (2005) The role of isotopic reference materials for the analysis of “non-traditional” stable isotopes. *Geostand. Geoanal. Res.*, **29**, 53–61.
245. Lipschutz, M.E., Wolf, S.F., Culp, F.B. and Hanchar, J.M. (2005) Geochemical and cosmochemical materials. *Anal. Chem.*, **77**, 3717–3736.
246. Gäbler, H.-E. (2002) Applications of magnetic sector ICP-MS in geochemistry. *J. Geochem. Explor.*, **75**, 1–15.
247. Becker, J.S. (2002) State-of-the-art and progress in precise and accurate isotope ratio measurements by ICP-MS and LA-ICP-MS. *J. Anal. Atom. Spectrom.*, **17**, 1172–1185.
248. Albarède, F., Telouk, P., Blichert-Toft, J., Boyet, M., Agranier, A. and Nelson, B. Precise and accurate isotopic measurements using multiple-collector ICPMS. (2004). *Geochim. Cosmochim. Acta*, **68**, 2725–2744.

249. Longerich, H.P., Fryer, B.J. and Strong, D.F. (1987) Determination of lead isotope ratios by inductively coupled plasma-mass spectrometry (ICP-MS). *Spectrochim. Acta*, **42B**, 39–48.
250. Horstwood, M.S.A. and Nowel, G.M. (2005) Multi-collector devices. In *ICP Mass Spectrometry Handbook* (Ed. S.M. Nelms), Blackwell Publishing, Oxford, pp. 54–68.
251. Andréen, H., Rodushkin, I., Stenberg, A., Malinovsky, D. and Baxter, D.C. (2004) Sources of mass bias and isotope ratio variation in multi-collector ICP-MS: optimisation of instrumental parameters based on experimental observations. *J. Anal. Atom. Spectrom.*, **19**, 1217–1224.
252. Grégoire, D.C., Acheson, B.M. and Taylor, R.P. (1996) Measurement of lithium isotope ratios by inductively coupled plasma mass spectrometry: application to geological materials. *J. Anal. Atom. Spectrom.*, **11**, 765–772.
253. Grégoire, D.C. (1987) Determination of boron isotope ratios in geological materials by inductively coupled plasma mass spectrometry. *Anal. Chem.*, **59**, 2479–2484.
254. Aggarwal, J.K. and Palmer, M.R. (1995) Boron isotope analysis. A review. *Analyst*, **120**, 1301–1307.
255. Erel, Y., Veron, A. and Halicz, L. (1997) Tracing the transport of anthropogenic lead in the atmosphere and in soils using isotopic ratios. *Geochim. Cosmochim. Acta*, **61**, 4495–4505.
256. Chenery, S.R.N., Ander, E.L., Perkins, K.M. and Smith, B. (2002) Uranium anomalies identified using G-BASE data – natural or anthropogenic? A uranium isotope pilot study. British Geological Survey Internal Report, IR/02/001, 34 pp.
257. Howe, S.E., Davidson, C.M. and McCartney, M. (2002) Determination of uranium concentration and isotopic composition by means of ICP-MS in sequential extracts of sediment from the vicinity of a uranium enrichment plant. *J. Anal. Atom. Spectrom.*, **17**, 497–501.
258. Hawthorne, F.C. and Martin, R.F. (1995) Microbeam techniques in the earth sciences. *Can. Mineral.*, **33**, 201–508.
259. Potts, P.J., Bowles, J.F.W., Reed, S.J.B. and Cave, M.R. (Eds.) (1995) *Microprobe Techniques in the Earth Sciences*, Chapman & Hall, London.
260. Reed, S.J.B. (1995) Electron probe microanalysis. In *Microprobe Techniques in the Earth Sciences* (Eds. P.J. Potts, J.F.W. Bowles, S.J.B. Reed and M.R. Cave), Chapman & Hall, London, pp. 49–89.
261. Halden, N.M., Campbell, J.L. and Teesdale, W.J. (1995) PIXE analysis in mineralogy and geochemistry. *Can. Mineral.*, **33**, 293–302.
262. Reed, S.J.B. (1989) Ion microprobe analysis—a review of geological applications. *Mineral. Mag.*, 3–24.
263. Hinton, R.W. (1995) Ion microprobe analysis in geology. In *Microprobe Techniques in the Earth Sciences* (Eds. P.J. Potts, J.F.W. Bowles, S.J.B. Reed and M.R. Cave), Chapman & Hall, London, pp. 235–289.
264. Rucklidge, J. (1995) Accelerator mass spectrometry in environmental geoscience. *Analyst*, **120**, 1283–1290.
265. Wilson, G.C., Rucklidge, J.C. and Kilius, L.R. (1995) Ultrasensitive trace-element analysis with accelerator mass spectrometry: the current state of the art. *Can. Mineral.*, **33**, 237–242.
266. Dalpé, C., Baker, D.R. and Sutton, S.R. (1995) Synchrotron X-ray-fluorescence and laser-ablation ICP-MS microprobes: useful instruments for analysis of experimental run-products. *Can. Mineral.*, **33**, 481–498.
267. Smith, J.V. (1995) Synchrotron X-ray sources: instrumental characteristics. New applications in microanalysis, tomography, absorption spectroscopy and diffraction. *Analyst*, **120**, 1231–1245.
268. Nesbitt, H.W. and Pratt, A.R. (1995) Applications of Auger-electron spectroscopy to geochemistry. *Can. Mineral.*, **33**, 243–259.
269. Compston, W., Williams, I.S. and Meyer, C. (1986) U–Pb geochronology of zircons from Lunar breccia 73217 using a sensitive high mass-resolution ion microprobe. *J. Geophys. Res.*, **89**(Suppl.), B434–B525.
270. Raudsepp, M. (1995) Recent advances in the electron-probe micro-analysis of minerals for the light elements. *Can. Mineral.*, **33**, 203–218.

271. Darke, S.A. and Tyson, J.F. (1993) Interaction of laser radiation with solid materials and its significance to analytical spectrometry. A review. *J. Anal. Atom. Spectrom.*, **8**, 145–209.
272. Perkins, W.T. and Pearce, N.J.G. (1995) Mineral microanalysis by laserprobe inductively coupled plasma mass spectrometry. In *Microprobe Techniques in the Earth Sciences* (Eds. P.J. Potts, J.F.W. Bowles, S.J.B. Reed and M.R. Cave), Chapman & Hall, London, pp. 291–325.
273. Ludden, J.N., Feng, R., Gauthier, G., Stix, J., Shi, L., Francis, D., Machado, N. and Wu, G. (1995) Applications of LAM-ICP-MS analysis to minerals. *Can. Mineral.*, **33**, 419–434.
274. Russo, R.E. (1995) Laser ablation. *Appl. Spectrosc.*, **49**, 14A–28A.
275. Vogt, C. and Latkoczy, C. (2005) Laser ablation ICP-MS. In *ICP Mass Spectrometry Handbook* (Ed. S.M. Nelms), Blackwell Publishing, Oxford, pp. 228–258.
276. Sylvester, P.J. (2005), Laser ablation ICP-MS developments and trends for 2003. In Hergt J.M. *et al.*, *Geostand. Geoanal. Res.*, **29**, 5–52.
277. Günther, D. and Hattendorf, B. (2005) Solid sample analysis using laser ablation inductively coupled plasma mass spectrometry. *Trend. Anal. Chem.*, **24**, 255–265.
278. Heinrich, C.A., Pettke, T., Halter, W.E., Aigner-Torres, M., Audétat, A., Günther, D., Hattendorf, B., Bleiner, D., Guillong, M. and Horn, I. (2003). Quantitative multi-element analysis of minerals, fluid and melt inclusions by laser-ablation inductively-coupled-plasma mass-spectrometry. *Geochim. Cosmochim. Acta*, **67**, 3473–3496.
279. Maiman, T.H. (1960) Stimulated optical radiation in ruby. *Nature*, **187**, 493–494.
280. Ferguson, H.I.S., Mentall, J.E. and Nicholls, R.W. (1964) Laser excitation of powdered solids. *Nature*, **204**, 1295.
281. Thompson, M., Goulter, J.E. and Sieper, F. (1981) Laser ablation for the introduction of solid samples into an inductively coupled plasma for atomic emission spectrometry. *Analyst*, **106**, 32–39.
282. Darke, S.A., Long, S.E., Pickford, C.J. and Tyson, J.F. (1989) Laser ablation system for solid sample analysis by inductively coupled plasma atomic emission spectrometry. *J. Anal. Atom. Spectrom.*, **4**, 715–719.
283. Lin, S. and Peng, C. (1990) Studies on the application of laser sampling–inductively coupled plasma atomic emission spectrometry to the determination of rare earth and refractory elements. *J. Anal. Atom. Spectrom.*, **5**, 509–514.
284. Moenke-Blankenburg, L. and Günther, D. (1992) Laser microanalysis of geological samples by atomic emission spectrometry (LM-AES) and inductively coupled plasma atomic emission spectrometry (LM-ICP-AES). *Chem. Geol.*, **95**, 85–92.
285. Hale, M. and Thompson, M. (1983) Laser ablation inductively coupled plasma spectrometry for geochemical exploration. *Trans. Inst. Min. Metall. B.*, **92**, B23–B27.
286. Hale, M., Thompson, M. and Wheatley, M.R. (1984) Laser ablation of stream-sediment pebble coatings for simultaneous multi-element analysis in geochemical exploration. *J. Geochem. Explor.*, **21**, 361–371.
287. Thompson, M., Hale, M. and Coles, B. (1992) Geochemical reconnaissance using stream-sediment pebble coatings and laser ablation ICP-AES. *Trans. Inst. Mining Metall. B.*, **101**, B9–B14.
288. Ramsey, M.H., Coles, B.J., Wilkinson, J.J. and Rankin, A.H. (1992) Single fluid inclusion analysis by laser ablation inductively coupled plasma atomic emission spectrometry: quantification and validation. *J. Anal. Atom. Spectrom.*, **7**, 587–593.
289. Rankin, A.H., Ramsey, M.H., Coles, B., Van Langevelde, F. and Thomas, C.R. (1992) The composition of hypersaline, iron-rich granitic fluids based on laser-ICP and synchrotron-XRF microprobe analysis of individual fluid inclusions in topaz, Mole granite, eastern Australia. *Geochim. Cosmochim. Acta*, **56**, 67–79.
290. Wilkinson, J.J., Rankin, A.H., Mulshaw, S.C., Nolan, J. and Ramsey, M.H. (1994) Laser ablation-ICP-AES for the determination of metals in fluid inclusions: an application to the study of magmatic ore fluids. *Geochim. Cosmochim. Acta*, **58**, 1133–1146.

291. Chan, W.T. and Russo, R.E. (1991) Study of laser–material interactions using inductively coupled plasma–atomic emission spectrometry. *Spectrochim. Acta*, **46B**, 1471–1486.
292. Thompson, M., Chenery, S. and Brett, L. (1990) Nature of particulate matter produced by laser ablation—implications for tandem analytical systems. *J. Anal. Atom. Spectrom.*, **5**, 49–55.
293. Chenery, S., Hunt, A. and Thompson, M. (1992) Laser ablation of minerals and chemical differentiation of the ejecta. *J. Anal. Atom. Spectrom.*, **7**, 647–652.
294. Thompson, M., Chenery, S. and Brett, L. (1989) Calibration studies in laser ablation microprobe-inductively coupled plasma atomic emission spectrometry. *J. Anal. Atom. Spectrom.*, **4**, 11–16.
295. Arrowsmith, P. (1987) Laser ablation of solids for elemental analysis by inductively coupled plasma mass spectrometry. *Anal. Chem.*, **59**, 1437–1444.
296. Imai, N. (1990) Quantitative analysis of original and powdered rocks and mineral inclusions by laser ablation inductively coupled plasma mass spectrometry. *Anal. Chim. Acta*, **235**, 381–391.
297. Jackson, S.E., Longerich, H.P., Dunning, G.R. and Fryer, B.J. (1992) The application of laser-ablation microprobe-inductively coupled plasma-mass spectrometry (LAM-ICP-MS) to *in situ* trace-element determinations in minerals. *Can. Mineral.*, **30**, 1049–1064.
298. Broadhead, M., Broadhead, R. and Hager, J.W. (1990) Laser sampling ICP-MS: semi-quantitative determination of sixty-six elements in geological samples. *Atom. Spectrosc.*, **11**, 205–209.
299. Perkins, W.T., Fuge, R. and Pearce, N.J.G. (1991) Quantitative analysis of trace elements in carbonates using laser ablation inductively coupled plasma mass spectrometry. *J. Anal. Atom. Spectrom.*, **6**, 445–449.
300. Chenery, S. and Cook, J.M. (1993) Determination of rare earth elements in single mineral grains by laser ablation microprobe-inductively coupled plasma mass spectrometry—preliminary study. *J. Anal. Atom. Spectrom.*, **8**, 299–303.
301. Longerich, H.P., Jackson, S.E., Fryer, B.J. and Strong, D.F. (1993) Machinations—The laser ablation microprobe inductively coupled plasma-mass spectrometer. *Geosci. Can.*, **20**, 21–27.
302. Jenner, G.A., Foley, S.F., Jackson, S.E., Green, T.H., Fryer, B.J. and Longerich, H.P. (1993) Determination of partition coefficients for trace elements in high pressure–temperature experimental run products by laser ablation microprobe-inductively coupled plasma-mass spectrometry (LAM-ICP-MS). *Geochim. Cosmochim. Acta*, **58**, 5099–5103.
303. Fryer, B.J., Jackson, S.E. and Longerich, H.P. (1995) The design, operation and role of the laser-ablation microprobe coupled with an inductively coupled plasma-mass spectrometer (LAM-ICP-MS) in the earth sciences. *Can. Mineral.*, **33**, 303–312.
304. Geertsens, C., Briand, A., Chartier, F., Lacour, J.-L., Mauchien, P., Sjöström, S. and Mermet, J.-M. (1994) Comparison between infrared and ultraviolet laser ablation at atmospheric pressure – implications for solid sampling inductively coupled plasma spectrometry. *J. Anal. Atom. Spectrom.*, **9**, 17–22.
305. Jeffries, T.E., Perkins, W.T. and Pearce, N.J.G. (1995) Comparisons of infrared and ultraviolet laser probe microanalysis inductively coupled plasma mass spectrometry in mineral analysis. *Analyst*, **120**, 1365–1371.
306. Bea, F., Montero, P., Stroh, A. and Baasner, J. (1996) Microanalysis of minerals by an excimer UV-LA-ICP-MS system. *Chem. Geol.*, **133**, 145–156.
307. Figg, D. and Kahr, M.S. (1997) Elemental fractionation of glass using laser ablation inductively coupled plasma mass spectrometry. *Appl. Spectrosc.*, **51**, 1185–1192.
308. Russo, R.E., Mao, X.L., Chan, W.T., Bryant, M.F. and Kinard, W.F. (1995) Laser ablation sampling with inductively coupled plasma atomic emission spectrometry for the analysis of prototypical glasses. *J. Anal. Atom. Spectrom.*, **10**, 295–301.
309. Ducreux-Zappa, M. and Mermet, J.-M. (1996) Analysis of glass by UV laser ablation inductively coupled plasma atomic emission spectrometry. Part 1. Effects of the laser parameters on

- the amount of ablated material and the temporal behaviour of the signal for different types of laser. *Spectrochim. Acta*, **51B**, 321–332.
310. Ducreux-Zappa, M. and Mermet, J.-M. (1996) Analysis of glass by UV laser ablation inductively coupled plasma atomic emission spectrometry. Part 2. Analytical figures of merit. *Spectrochim. Acta*, **51B**, 333–341.
311. Günther, D., Frischknecht, R., Heinrich, C.A. and Kahlert, H.-J. (1997) Capabilities of an argon fluoride 193 nm excimer laser for laser ablation inductively coupled plasma mass spectrometry microanalysis of geological materials. *J. Anal. Atom. Spectrom.*, **12**, 939–944.
312. Guillon, M. and Günther, D. (2001) Quasi 'non-destructive' laser ablation-inductively coupled plasma-mass spectrometry fingerprinting of sapphires. *Spectrochim. Acta*, **56B**, 1219–1231.
313. Sylvester, P.J. and Ghaderi, M. (1997) Trace element analysis of scheelite by excimer laser ablation-inductively coupled plasma-mass spectrometry (ELA-ICP-MS) using a synthetic silicate glass standard. *Chem. Geol.*, **141**, 49–65.
314. Telouk, P., Rose-Koga, E.F. and Albarede, F. (2003) Preliminary results from a new 157 nm laser ablation ICP-MS instrument: new opportunities in the analysis of solid samples. *Geostand. Newslett.*, **27**, 5–11.
315. Horn I., Günther D. and Guillon M. (2003) Evaluation and design of a solid-state 193 nm OPO-Nd:YAG laser ablation system. *Spectrochim. Acta*, **58B**, 1837–1846.
316. Hirata, T. and Nesbitt, R.W. (1995) U–Pb isotope geochronology of zircon: evaluation of the laser probe-inductively coupled plasma mass spectrometry technique. *Geochim. Cosmochim. Acta*, **59**, 2491–2500.
317. Feng, R., Machado, N. and Ludden, J. (1993) Lead geochronology of zircon by LaserProbe-inductively coupled plasma mass spectrometry (LP-ICPMS). *Geochim. Cosmochim. Acta*, **57**, 3479–3486.
318. Morrison, C.A., Lambert, D.D., Morrison, R.J.S., Ahlers, W.W. and Nicholls, I.A. (1995) Laser ablation-inductively coupled plasma-mass spectrometry: an investigation of elemental responses and matrix effects in the analysis of geostandard materials. *Chem. Geol.*, **119**, 13–29.
319. Jeffries, T.E., Pearce, N.J.G., Perkins, W.T. and Raith, A. (1996) Chemical fractionation during infrared and ultraviolet laser ablation inductively coupled plasma mass spectrometry – implications for mineral microanalysis. *Anal. Commun.*, **33**, 35–39.
320. Outridge, P.M., Doherty, W. and Gregoire, D.C. (1996) The formation of trace element-enriched particulates during laser ablation of refractory materials. *Spectrochim. Acta*, **51B**, 1451–1462.
321. Outridge, P.M., Doherty, W. and Grégoire, D.C. (1997) Ablative and transport fractionation of trace elements during laser sampling of glass and copper. *Spectrochim. Acta*, **52B**, 2093–2102.
322. Cromwell, E.F. and Arrowsmith, P. (1995) Fractionation effects in laser ablation inductively coupled plasma mass spectrometry. *Appl. Spectrosc.*, **49**, 1652–1660.
323. Cousin, H., Weber, A., Magyar, B., Abell, I. and Günther, D. (1995) An auto-focus system for reproducibly focusing in laser ablation inductively coupled plasma mass spectrometry. *Spectrochim. Acta*, **50B**, 63–66.
324. Moissette, A., Shepherd, T.J. and Chenery, S.R. (1996) Calibration strategies for the elemental analysis of individual aqueous fluid inclusions by laser ablation inductively coupled plasma mass spectrometry. *J. Anal. Atom. Spectrom.*, **11**, 177–185.
325. Guillon, M., Horn, I. and Günther, D. (2003) A comparison of 266 nm, 213 nm and 193 nm produced from a single solid state Nd:YAG laser for laser ablation ICP-MS. *J. Anal. Atom. Spectrom.*, **18**, 1224–1230.
326. Horn, I. and Günther, D. (2003) The influence of ablation carrier gases Ar, He and Ne on the particle size distribution and transport efficiencies of laser ablation induced aerosols: Implications for LA-ICP-MS. *Applied Surface Science*, **207**, 144–157.

327. Figg, D.J., Cross, J.B. and Brink, C. (1998) More investigations into elemental fractionation resulting from laser ablation-inductively coupled plasma-mass spectrometry on glass samples. *Applied Surface Science*, **129**, 287–291.
328. Guillon, M. and Günther, D. (2002) Effect of particle size distribution of ICP-induced elemental fractionation in laser ablation-inductively coupled plasma-mass spectrometry. *J. Anal. Atom. Spectrom.*, **17**, 831–837.
329. Aeschliman, D.B., Bajic, S.J., Baldwin, D.P. and Houk, R.S. (2003) High-spread digital photographic study of an inductively coupled plasma during laser ablation: comparison of dried solution aerosols from a microconcentric nebulizer and solid particles from laser ablation. *J. Anal. Atom. Spectrom.*, **18**, 1008–1014.
330. Jarvis, K.E. and Williams, J.G. (1993) Laser ablation inductively coupled plasma mass spectrometry (LA-ICP-MS): a rapid technique for the direct, quantitative determination of major, trace and rare-earth elements in geological samples. *Chem. Geol.*, **106**, 251–262.
331. Russo, R.E., Mao, X., Gonzalez, J.J. and Mao, S.S. (2002) Femtosecond laser ablation ICP-MS. *J. Anal. Atom. Spectrom.*, **17**, 1072–1075.
332. Poitrasson, F., Mao, X., Mao, S.S., Freydis, R. and Russo, R.E. (2003) Comparison of ultraviolet femtosecond and nanosecond laser ablation inductively coupled plasma-mass spectrometry analysis in glass, monazite and zircon. *Anal. Chem.*, **75**, 6184–6190.
333. Pearce, N.J.G., Perkins, W.T., Abell, I., Duller, G.A.T. and Fuge, R. (1992) Mineral microanalysis by laser ablation inductively coupled plasma mass spectrometry. *J. Anal. Atom. Spectrom.*, **7**, 53–57.
334. Huang, Y., Shibata, Y. and Morita, M. (1993) Micro laser ablation-inductively coupled plasma mass spectrometry. 1. Instrumentation and performance of micro laser ablation system. *Anal. Chem.*, **65**, 2999–3003.
335. Flint, C.D., Chenery, S.R.N. and O'Grady, P. (1992) UK Patent 2,254,444.
336. Poitrasson, F. and Chenery, S.R.N. (1995) A high spatial resolution laser inductively coupled plasma mass spectrometer and its application for fluid-accessory mineral interaction studies [Abstract]. *Terra Nova*, **7**(Suppl. 1), 344.
337. Günther, D., Longerich, H.P., Jackson, S.E. and Forsythe, L. (1996) Effect of sampler orifice diameter on dry plasma inductively coupled plasma mass spectrometry (ICP-MS) backgrounds, sensitivities and limits of detection using laser ablation sample introduction. *Fresen. J. Anal. Chem.*, **355**, 771–773.
338. Leach, A.M. and Hieftje, G.M. (2000) Methods for shot-to-shot normalization in laser ablation with an inductively coupled plasma time-of-flight mass spectrometer. *J. Anal. Atom. Spectrom.*, **15**, 1121–1124.
339. Imai, N. (1992) Microprobe analysis of geological materials by laser ablation inductively coupled plasma mass spectrometry. *Anal. Chim. Acta*, **269**, 263–268.
340. Pearce, N.J.G., Perkins, W.T. and Fuge, R. (1992) Developments in the quantitative and semi-quantitative determination of trace elements in carbonates by laser ablation inductively coupled plasma mass spectrometry. *J. Anal. Atom. Spectrom.*, **7**, 595–598.
341. Williams, J.G. and Jarvis, K.E. (1993) Preliminary assessment of laser ablation inductively coupled plasma mass spectrometry for quantitative multi-element determination in silicates. *J. Anal. Atom. Spectrom.*, **8**, 25–34.
342. Perkins, W.T., Pearce, N.J.G. and Fuge, R. (1992) Analysis of zircon by laser ablation and solution inductively coupled plasma mass spectrometry. *J. Anal. Atom. Spectrom.*, **7**, 611–616.
343. Fedorowich, J.S., Richards, J.P., Jain, J.C., Kerrich, R. and Fan, J. (1993) A rapid method for REE and trace element analysis using laser sampling ICP-MS on direct fusion whole-rock glasses. *Chem. Geol.*, **106**, 229–249.
344. Bédard, L.P., Baker, D.R. and Machado, N. (1997) A new technique for the synthesis of geochemical reference samples for laser ablation-ICP-MS analysis of zircons. *Chem. Geol.*, **138**, 1–7.

345. Bea, F., Pereira, M.D. and Stroh, A. (1994) Mineral/leucosome trace-element partitioning in a peraluminous migmatite (a laser ablation-ICP-MS study). *Chem. Geol.*, **117**, 291–312.
346. Fedorowich, J.S., Jain, J.C. and Kerrich, R. (1995) Trace-element analysis of garnet by laser-ablation microprobe ICP-MS. *Can. Mineral.*, **33**, 469–480.
347. Kontak, D.J. and Jackson, S. (1995) Laser-ablation ICP-MS microanalysis of calcite cement from a Mississippi-valley-type Zn–Pb deposit, Nova Scotia: dramatic variability in REE content on macro- and micro-scales. *Can. Mineral.*, **33**, 445–467.
348. Pearce, N.J.G., Perkins, W.T., Westgate, J.A., Gorton, M.P., Jackson, S.E., Neal, C.R. and Chenery, S.R.N. (1997) A compilation of new and published major and trace element data for NIST SRM 610 and SRM 612 glass reference materials. *Geostand. Newslett.*, **21**, 115–144.
349. Eggins, S.M. and Shelley, J.M.G. (2002) Compositional heterogeneity in NIST SRM 610–617 glasses. *Geostand. Newslett.*, **26**, 269–286.
350. Doherty, W., Outridge, P.M. and Grégoire, D.C. (1996) Technique for the introduction of dry atomic vapours for improved optimization and diagnostic studies of laser ablation inductively coupled plasma spectrometry. *J. Anal. Atom. Spectrom.*, **11**, 1123–1126.
351. Günther, D., Cousin, H., Magyar, B. and Leopold, I. (1997) Calibration studies on dried aerosols for laser ablation inductively coupled plasma mass spectrometry. *J. Anal. Atom. Spectrom.*, **12**, 165–170.
352. Masters, B.J. and Sharp, B.L. (1997) Universal calibration strategy for laser ablation inductively coupled plasma mass spectrometry based on the use of aqueous standards with modified absorption coefficients. *Anal. Commun.*, **34**, 237–239.
353. Halicz, L. and Günther, D. (2004) Quantitative analysis of silicates using LA-ICP-MS with liquid calibration. *J. Anal. Atom. Spectrom.*, **19**, 1539–1545.
354. Stix, J., Gauthier, G. and Ludden, J.N. (1995) A critical look at quantitative laser-ablation ICP-MS analysis of natural and synthetic glasses. *Can. Mineral.*, **33**, 435–444.
355. Perkins, W. (1992) Role of inductively coupled plasma mass spectrometry in natural environment research. *J. Anal. Atom. Spectrom.*, **7**, 25N–34N.
356. Longerich, H.P., Günther, D. and Jackson, S.E. (1996) Elemental fractionation in laser ablation inductively coupled plasma mass spectrometry. *Fresen. J. Anal. Chem.*, **355**, 538–542.
357. Longerich, H.P., Jackson, S.E. and Günther, D. (1996) Laser ablation inductively coupled plasma mass spectrometric transient signal data acquisition and analyte concentration calculation. *J. Anal. Atom. Spectrom.*, **11**, 899–904.
358. Guo, X. and Lichte, F.E. (1995) Analysis of rocks, soils and sediments for the chalcophile elements by laser ablation-inductively coupled plasma mass spectrometry. *Analyst*, **120**, 2707–2711.
359. Watling, R.J., Herbert, H.K., Barrow, I.S. and Thomas, A.G. (1995) Analysis of diamonds and indicator minerals for diamond exploration by laser ablation-inductively coupled plasma mass spectrometry. *Analyst*, **120**, 1357–1364.
360. Outridge, P.M., Doherty, W. and Grégoire, D.C. (1998) Determination of trace element signatures in placer gold by laser ablation-inductively coupled plasma-mass spectrometry as a potential aid for gold exploration. *J. Geochem. Explor.*, **60**, 229–240.
361. Chenery, S., Williams, T., Elliott, T.A., Forey, P.L. and Werdelin, L. (1996) Determination of rare earth elements in biological and mineral apatite by EPMA and LAMP-ICP-MS. *Mikrochim. Acta*, **13**, 259–269.
362. Klemme, S., van der Laan, S.R., Foley, S.F. and Günther, D. (1995) Experimentally determined trace and minor element partitioning between clinopyroxene and carbonatite melt under upper mantle conditions. *Earth Planet. Sci. Lett.*, **133**, 439–448.
363. Foley, S.F., Jackson, S.E., Fryer, B.J., Greenough, J.D. and Jenner, G.A. (1996) Trace element partition coefficients for clinopyroxene and phlogopite in an alkaline lamprophyre from Newfoundland by LAM-ICP-MS. *Geochim. Cosmochim. Acta*, **60**, 629–638.

364. Jeffries, T.E., Perkins, W.T. and Pearce, N.J.G. (1995) Measurements of trace elements in basalts and their phenocrysts by laser probe microanalysis inductively coupled plasma mass spectrometry (LPMA-ICP-MS). *Chem. Geol.*, **121**, 131–144.
365. Watling, R.J., Herbert, H.K. and Abell, I.D. (1995) The application of laser ablation-inductively coupled plasma-mass spectrometry (LA-ICP-MS) to the analysis of selected sulfide minerals. *Chem. Geol.*, **124**, 67–81.
366. Chenery, S., Cook, J.M., Styles, M. and Cameron, E.M. (1995) Determination of the three-dimensional distributions of precious metals in sulfide minerals by laser ablation microprobe-inductively coupled plasma-mass spectrometry (LAMP-ICP-MS). *Chem. Geol.*, **124**, 55–65.
367. Querol, X. and Chenery, S. (1995) Determination of trace element affinities in coal by laser ablation microprobe-inductively coupled plasma mass spectrometry. In *European Coal Geology* (Eds. M.K.G. Whateley and D.A. Spears), Vol. 82, Geological Society, London, pp. 147–155.
368. Bea, F., Montero, P., Garuti, G. and Zacharini, F. (1998) Pressure-dependence of rare earth element distribution in amphibolite- and granulite-grade garnets. An LA-ICP-MS study. *Geostand. Newslett.*, **21**, 253–270.
369. Poitrasson, F., Chenery, S. and Bland, D.J. (1996) Contrasted monazite hydrothermal alteration mechanisms and their geochemical implications. *Earth Planet. Sci. Lett.*, **145**, 79–96.
370. Hirata, T. and Nesbitt, R.W. (1997) Distribution of platinum group elements and rhenium between metallic phases of iron meteorites. *Earth Planet. Sci. Lett.*, **147**, 11–24.
371. Günther, D., Quadt, A.V., Wirt, W., Cousin, H. and Dietrich, V. J. (2001) Elemental analyses using laser ablation-inductively coupled plasma-mass spectrometry (LA-ICP-MS) of geological materials fused with $\text{Li}_2\text{B}_4\text{O}_7$ and calibrated without matrix-matched standards. *Microchimica Acta*, **136**, 101–107.
372. Eggins, S.M. (2003). Laser ablation ICP-MS analysis of geological materials prepared as lithium borate glasses. *Geostand. Newslett.*, **27**, 147–162.
373. Shepherd, T.J., Rankin, A.H. and Alderton, D.H.M. (1985) *A Practical Guide to Fluid Inclusion Studies*, Chapman & Hall, London.
374. Banks, D.A., Davies, G.R., Yardley, B.W.D., McCaig, A.M. and Grant, N.T. (1991) The chemistry of brines from an Alpine thrust system in the Central Pyrenees: an application of fluid inclusion analysis to the study of fluid behaviour in orogenesis. *Geochim. Cosmochim. Acta*, **55**, 1021–1030.
375. Banks, D.A., Yardley, B.W.D., Campbell, A.R. and Jarvis, K.E. (1994) REE composition of an aqueous magmatic fluid: a fluid inclusion study from the Capitan Pluton, New Mexico, USA. *Chem. Geol.*, **113**, 259–272.
376. Thompson, M., Rankin, A.H., Walton, S.J., Halls, C. and Foo, B.N. (1980) The analysis of fluid inclusion decrepitate by inductively-coupled plasma atomic emission spectroscopy: an exploratory study. *Chem. Geol.*, **30**, 121–133.
377. Bottrell, S.H., Yardley, B. and Buckley, F. (1988) A modified crush-leach method for the analysis of fluid inclusion electrolytes. *Bull. Minéral.*, **111**, 279–290.
378. Ghazi, A.M., Vanko, D.A., Roedder, E. and Seeley, R.C. (1993) Determination of rare earth elements in fluid inclusions by inductively coupled plasma-mass spectrometry (ICP-MS). *Geochim. Cosmochim. Acta*, **57**, 4513–4516.
379. Coles, B.J., Gleeson, S.A., Wilkinson, J.J. and Ramsey, M.H. (1995) Improved detection limits for transient signal analysis of fluid inclusions by inductively coupled plasma atomic emission spectrometry using correlated background correction. *Analyst*, **120**, 1421–1425.
380. Dubessy, J., Poty, B. and Ramboz, C. (1989) Advances in C–O–H–N–S fluid geochemistry based on micro-Raman spectrometric analysis of fluid inclusions. *Eur. J. Mineral.*, **1**, 517–534.
381. Roedder, E. (1990) Fluid inclusion analysis – Prologue and epilogue. *Geochim. Cosmochim. Acta*, **54**, 495–507.

382. Boiron, M.C., Dubessy, J., Andre, N., Briand, A., Lacour, J.A., Mauchien, P. and Mermet, J.M. (1991) Analysis of mono-atomic ions in individual fluid inclusions by laser-induced plasma emission spectroscopy. *Geochim. Cosmochim. Acta*, **55**, 917–923.
383. Shepherd, T.J. and Chenery, S.R. (1995) Laser ablation ICP-MS elemental analysis of individual fluid inclusions: an evaluation study. *Geochim. Cosmochim. Acta*, **59**, 3997–4007.
384. Ghazi, A.M., McCandless, T.E., Vanko, D.A. and Ruiz, J. (1996) New quantitative approach in trace elemental analysis of single fluid inclusions: applications of laser ablation inductively coupled plasma mass spectrometry (LA-ICP-MS). *J. Anal. Atom. Spectrom.*, **11**, 667–674.
385. Günther, D., Audétat, A., Frischknecht, R. and Heinrich, C.A. (1998) Quantitative analysis of major, minor and trace elements in fluid inclusions using laser ablation-inductively coupled plasma mass spectrometry. *J. Anal. Atom. Spectrom.*, **13**, 263–270.
386. Stoffell, B., Wilkinson, J.J. and Jeffries, T.E. (2004). Metal transport and deposition in hydrothermal veins revealed by 213 nm UV laser ablation microanalysis of single fluid inclusions. *Am. J. Sci.*, **304**, 533–557.
387. Shepherd, T.J., Ayora, C., Cendón, D.I., Chenery, S.R. and Moissette, A. (1998) Quantitative solute analysis of single fluid inclusions in halite by LA-ICP-MS and cryo-SEM-EDS: complementary microbeam techniques. *Eur. J. Mineral.*, **10**, 1097–1108.
388. Gagnon, J.E., Samson, I.M., Fryer, B.J. and Williams-Jones, A.E. (2004). The composition and origin of hydrothermal fluids in an NYF-type granitic pegmatite, South Platte District, Colorado: evidence from LA-ICP-MS analysis of fluorite- and quartz-hosted fluid inclusions. *Can. Mineral.*, **42**, 1331–1355.
389. Kontak, D.J., Anderson, A.J. and Marshall, D.D. (2004). PACROFI VIII. *Can. Mineral.*, **42**, 1273–1274.
390. Fryer, B.J., Jackson, S.E. and Longerich, H.P. (1993) The application of laser ablation microprobe-inductively coupled plasma-mass spectrometry (LAM-ICP-MS) to *in situ* (U)–Pb geochronology. *Chem. Geol.*, **109**, 1–8.
391. Machado, N. and Gauthier, G. (1996) Determination of Pb-207/Pb-206 ages on zircon and monazite by laser-ablation ICP-MS and application to a study of sedimentary provenance and metamorphism in southeastern Brazil. *Geochim. Cosmochim. Acta*, **60**, 5063–5073.
392. Scott, D.J. and Gauthier, G. (1996) Comparison of TIMS (U–Pb) and laser ablation microprobe ICP-MS (Pb) techniques for age determination of detrital zircons from Paleoproterozoic metasedimentary rocks from northeastern Laurentia, Canada, with tectonic implications. *Chem. Geol.*, **131**, 127–142.
393. Horn, I., Rudnick, R.L. and McDonough, W.F. (2000) Precise elemental and isotope ratio determination by simultaneous solution nebulization and laser ablation-ICP-MS: application to U–Pb geochronology. *Chem. Geol.*, **164**, 281–301.
394. Hirata, T. (1997) Soft ablation technique for laser ablation-inductively coupled plasma mass spectrometry. *J. Anal. Atom. Spectrom.*, **12**, 1337–1342.
395. Walder, A.J., Abell, I.D., Platzner, I. and Freedman, P.A. (1993) Lead isotope ratio measurement of NIST 610 glass by laser ablation inductively coupled plasma mass spectrometry. *Spectrochim. Acta*, **48B**, 397–402.
396. Woodhead, J., Hergt, J., Shelley, M., Eggins, S. and Kemp, R. (2004) Zircon Hf-isotope analysis with an excimer laser, depth profiling, ablation of complex geometries, and concomitant age estimation. *Chem. Geol.*, **209**, 121–135.
397. Christensen, J.N., Halliday, A.N., Lee, D.-C. and Hall, C.M. (1995) *In situ* Sr isotopic analysis by laser ablation. *Earth Planet. Sci. Lett.*, **136**, 79–85.
398. Hirata, T., Hattori, M. and Tanaka, T. (1998) *In-situ* osmium isotope ratio analyses of iridosmines by laser ablation-multiple collector-inductively coupled plasma mass spectrometry. *Chem. Geol.*, **144**, 269–280.

399. Jackson, S.E. and Günther, D. (2003) The nature and sources of laser induced isotopic fractionation in laser ablation-multicollector-inductively coupled plasma-mass spectrometry. *J. Anal. Atom. Spectrom.*, **18**, 205–212.
400. Košler, J., Pedersen, R.B., Kruber, C. and Sylvester, P.J. (2005) Analysis of Fe isotopes in sulfides and iron meteorites by laser ablation high-mass resolution multi-collector ICP mass spectrometry. *J. Anal. Atom. Spectrom.*, **20**, 192–199.
401. Mermet, J.M. (2005) Is it possible, necessary and beneficial to perform research in ICP-atomic emission spectrometry? *J. Anal. Atom. Spectrom.*, **20**, 11–16.
402. Lee, D.-C. and Halliday, A.N. (1996) Hf–W isotopic evidence for rapid accretion and differentiation in the early solar system. *Science*, **274**, 1876–1879.
403. Hieftje, G.M., Myers, D.P., Li, G., Mahoney, P.P., Burgoyne, T.W., Ray, S.J. and Guzowski, J.P. (1997) Towards the next generation of atomic mass spectrometers. *J. Anal. Atom. Spectrom.*, **12**, 287–292.
404. Mahoney, P.P., Li, G. and Hieftje, G.M. (1996) Laser ablation-inductively coupled plasma mass spectrometry with a time-of-flight mass analyzer. *J. Anal. Atom. Spectrom.*, **11**, 401–405.
405. Omenetto, N. (1998) Role of lasers in analytical atomic spectroscopy: where, when and why. *J. Anal. Atom. Spectrom.*, **13**, 385–399.
406. Krupp, E., Seby, F., Martín-Doimeadios, R.R., Holliday, A., Moldován, M., Köllensperger, G., Hann, S. and Donard, O.F.X. (2005) Trace metal speciation with ICP-MS detection. In *ICP Mass Spectrometry Handbook* (Ed. S.M. Nelms), Blackwell Publishing, Oxford, pp. 259–335.
407. Rodríguez-González, P., Marchante-Gayón, J.M., Alonso, J.I.G. and Sanz-Medel, A. (2005) Isotope dilution analysis for elemental speciation: A tutorial review. *Spectrochim. Acta*, **60B**, 151–207.
408. Richardson, J.M., Lightfoot, P.C. and de Souza, H. (1996) Current geoscience laboratories geoanalytical programs and their quality assurance underpinnings. *Geostand. Newslett.*, **20**, 141–156.
409. Thompson, M. and Fearn, T. (1996) What exactly is fitness for purpose in analytical measurement? *Analyst*, **121**, 275–278.
410. Kane, J.S. (1997) Analytical bias: the neglected component of measurement uncertainty. *Analyst*, **122**, 1283–1288.
411. Kane, J.S. (1992) Reference samples for use in analytical geochemistry: their availability, preparation and appropriate use. *J. Geochem. Explor.*, **44**, 37–63.
412. Potts, P.J., Tindle, A.G. and Webb, P.C. (1992) *Geochemical Reference Material Compositions: Rocks, Minerals, Sediments, Soils, Carbonates, Refractories and Ores Used in Research and Industry*, Whittles Publishing, Latheronwheel.
413. Roelandts, I. (1996) Geochemical reference materials: update 1996. *Spectrochim. Acta*, **51B**, 1435–1441.
414. Valladon, M. (2004) Geostandards and geoanalytical research bibliographic review 2003. *Geostand. Geoanal. Res.*, **28**, 449–478.
415. Kane, J.S., Beary, E.S., Murphy, K.E. and Paulsen, P.J. (1995) Impact of inductively coupled plasma mass spectrometry on certification programs for geochemical reference materials. *Analyst*, **120**, 1505–1512.
416. Lawn, R.E., Thompson, M. and Walker, R.F. (1997) *Proficiency Testing in Analytical Chemistry*, The Royal Society of Chemistry, Cambridge.
417. Thompson, M., Potts, P.J., Webb, P.C. and Kane, J.S. (1997) GeoPT – a proficiency test for geoanalysis. *Analyst*, **122**, 1249–1254.
418. Potts, P.J., Thompson, M. and Wilson, S. (2002) G-Probe-1 – an international proficiency test for microprobe laboratories – Report on round 1: February 2002 (TB-1 basaltic glass). *Geostand. Newslett.*, **26**, 197–235.
419. Torres, P., Ballesteros, E. and Luque de Castro, M.D. (1995) Microwave-assisted robotic method for the determination of trace metals in soil. *Anal. Chim. Acta*, **308**, 371–377.

-
420. Wilson, S.A. and McGregor, R. (1989) The physical preparation of geologic samples for chemical analysis using laboratory robotics. *Anal. Lett.*, **22**, 647–668.
 421. Govindaraju, K. and Mevelle, G. (1987) Fully automated dissolution and separation methods for inductively coupled plasma atomic emission spectrometry rock analysis. Application to the determination of rare earth elements. *J. Anal. Atom. Spectrom.*, **2**, 615–621.
 422. Borsier, M. (1992) Automated analysis of geological materials: what, how and why? *Chem. Geol.*, **95**, 93–98.

Chapter 10

Environmental and Clinical Applications of Inductively Coupled Plasma Spectrometry

Anne P. Vonderheide, Baki B.M. Sadi, Karen L. Sutton, Jodi R. Shann and Joseph A. Caruso

10.1 Introduction

In recent years, inductively coupled plasma (ICP) spectrometry has emerged as an ideal instrumental analysis system for elemental analysis and speciation studies in environmental and clinical samples. Among the various plasma sources, ICP acts as a very efficient atomization, excitation, and ionization source, all in one, and has been successfully hyphenated to both mass spectrometric (MS) and atomic emission spectroscopic (AES) techniques. Both ICP-MS and ICP-AES offer excellent sensitivity for most elements with detection limits in the low parts per trillion range and parts per billion range, respectively. Both metals and many non-metal analytes of environmental and clinical interest can be analyzed offering the analyst a very robust, yet a flexible analytical tool for often difficult to determine trace elements.

Both ICP-AES and ICP-MS offer multi-elemental analysis capability. Modern ICP-AES instrumentation enables rapid sequential or, with the availability of charged coupled device multi-element detectors, true simultaneous analysis for minor, trace, and ultratrace constituents. The high resolution of modern ICP-AES instruments enables removal of many inter-element interferences. ICP-MS is now widely found in many well-equipped analytical laboratories and its applications for environmental and clinical analysis are numerous. Sensitivity is far greater than ICP-AES by up to three orders of magnitude for many elements. The ability to perform both semi-quantitative and fully quantitative analyses is also an attractive feature. It has been demonstrated that ICP-AES and ICP-MS instruments as detectors for chromatographic separations offer a far more sensitive alternative to traditional chromatographic detectors such as the ultraviolet (UV) absorption and refractive index detector [1]. This is particularly useful when information regarding the chemical form or 'speciation' of an element is required. High-performance liquid chromatography (HPLC), gas chromatography (GC), supercritical fluid chromatography, and capillary electrophoresis (CE) have all been successfully coupled to ICP-AES and ICP-MS instruments. Recent developments in element-specific detection of non-metals and robust plasmas as well as interface modification for handling high organic solvent load allows the ICP-AES-MS to be an excellent element-specific detection system for typical reversed-phase chromatographic separation of organic compounds [2,3]. It eliminates the necessity of often-tedious derivatization steps involved in

conventional absorption/fluorescence detection for analytes containing non-metallic elements such as the halogens (Cl, Br, I) or S, P, etc. Hyphenation capability of reversed-phase high-performance liquid chromatography (RPHPLC) separation techniques with ICP spectrometric detection systems also allows them to be a very powerful element selective screening system for speciation analysis in proteomic and metallomic research.

The widespread use of plasma spectrometry in environmental and clinical analysis is indicated by the volume of papers published each year. The annual Atomic Spectrometry Updates published in the *Journal of Analytical Atomic Spectrometry* give a comprehensive review of the use of ICP-AES and ICP-MS for air, water, soils, plants, and geological sample analysis. The aim of this chapter is to provide an overview of the analyses that have been performed with regard to air and water samples as well as clinical analysis in biological samples.

10.2 Analysis of air

10.2.1 Introduction

The study of air is a particular area of environmental analysis which requires analytical techniques of high sensitivity. Two major areas of air analysis may be defined. The first concerns anthropogenic air pollution where particulate matter and gaseous pollutants enter the environment as a result of processes such as electrical power generation, thermal waste, waste destruction, ore production, industrial melting processes, and vehicle pollution. In urban and industrial areas, air quality may be particularly poor. Therefore, studies concerning the cause, effect, transport, and control of air pollution are of importance. The second area of air analysis is concerned with occupational exposure in the work place. With the introduction of air quality regulations for the workplace, it is necessary to quantify the amount of hazardous elements in order to measure actual worker exposure. Exposure to metals in the workplace may occur due to forging, molding, welding, painting, abrasive blasting, and acid and alkali cleaning. In addition to the above-mentioned areas, air samples from emission sources and or the headspace of various biological samples can also be analyzed for toxic volatile (organic) compounds containing metals, some metalloids and non-metals by ICP spectrometric techniques.

Airborne particulates usually have a wide elemental composition range with different concentrations. The particles may be varied in size with complex matrices. Toxic elements are rarely found alone in industrial type environments; therefore the ratio of certain elements in airborne particulate matter at a particular site may provide an indication as to the source of the exposure, especially where multiple sources of an analyte occur. A slight but discernable change in isotope ratios for stable isotopes such as hydrogen, carbon, nitrogen, and oxygen can provide useful information in assessing the impact of anthropogenic activities on global climate changes [4].

10.2.2 Sampling

Air particulates are usually collected upon filters before sample treatment may begin. Several types are available and these filters are normally of very small pore size (approximately

0.8 μm) so that very small airborne particles are collected. Portable air samplers are the most commonly used means for air sampling and may require either low- or high-volume air samplers depending on the volume of air that is sampled per unit time. After samples are collected, the filters are normally kept in clean rooms at 20°C to maintain the filter integrity.

10.2.3 Sample preparation

Samples, once collected on the filters, are commonly digested using various methods involving acid dissolution techniques. Airborne particulate samples often have complex matrices and are therefore notoriously difficult to digest and may require harsh acidic conditions, usually involving nitric acid, aqua regia, perchloric acid and hydrofluoric acid. Temperatures in the region of 300–550°C have been used although care should be taken to avoid evaporative losses for the more volatile elements.

Nitric acid addition to a sample serves to breakdown any organic component and to cause metal oxidation while hydrochloric acid reacts with heavy metals. Both open vessel and closed pressurized acid decomposition procedures have been described in the literature for the complete digestion of air particulates along with the collection filters. For open vessel digestion, the quantity, type of acid and the duration of digestion depend on the matrix type of the particle. For some samples, aqua regia may suffice while for harder to dissolve matrices, perchloric acid and hydrofluoric acids may be necessary. The closed vessel method of acid digestion is more popular than the open vessel acid digestion method as it enables higher temperatures and pressures to be used which, in turn, results in a more complete digestion. In addition, open vessel digestion is time consuming and may potentially introduce contamination or evaporative losses of some elements [5]. The closed vessel is usually a high pressure ‘bomb’ into which concentrated acids are introduced. These acids are usually nitric acid, perchloric acid, hydrochloric acid, hydrofluoric acid, or a combination of these. It should be noted that, for the analysis of airborne particulates by the complete digestion of the filters and samples, blank contributions from impurities in the filters might be problematic. Hydrofluoric acid is very aggressive and, while very effective for the breakdown of ‘difficult’ matrices, it may damage parts of the ICP-MS or ICP-AES instrument. For this reason, HF is normally evaporated after dissolution is complete.

Microwave-assisted dissolution of airborne particulates samples and the collection filters is now increasing in popularity. The microwave-assisted dissolution technique is faster than conventional methods of acid dissolution. In addition, due to the compact design and automation, it offers an improvement in terms of quantity of reagents, handling, and sample exposure time to the open environment. A continuous flow microwave dissolution technique has been described by Beary *et al.* [6] for the determination of lead in selected reaction monitoring mode (SRM) 2676 ‘Toxic Metals on Air Filters’. The airborne particulates are introduced into the system as a slurry. An injection loop is filled with the slurry, which is subsequently injected into a carrier stream of HNO_3 , HClO_4 or HF.

10.2.4 Interferences

As previously mentioned, the presence of acids during open vessel, closed vessel and microwave dissolution may result in spectral interferences. For example, As and V may be

difficult to accurately determine if significant Cl^+ , ClO^+ and ArCl^+ are present, owing to the use of HClO_4 and HCl . In addition, many elements present in airborne particulate matter such as As, Ca, K, Se and S are difficult to determine owing to the formation of polyatomic ions from clustering reactions during the ion extraction step. The formation of ArO^+ generates a signal at m/z 56, which makes Fe determination difficult at the major isotope. However, the recent advent of collision/reaction cell technology in quadrupole-based ICP-MS instruments, and high-resolution sector field ICP-MS (SF-ICP-MS) instruments have been successful in many cases in minimizing isobaric and polyatomic interferences for many elements and will be discussed in more detail in the water analysis section.

10.2.5 Applications

Studies regarding the analysis of airborne particulate matter are numerous. These applications are varied; some of the more interesting applications of ICP-AES and ICP-MS in air analysis are mentioned in Table 10.1 [7–16]. Analysis of non-metals such as carbon, sulfur, phosphorus and halogens in air samples by ICP techniques is a very fast-paced advancement in recent years. Schwarz and Heumann have developed a GC-ICP-MS method for online detection of brominated and iodinated volatile organic compounds in air samples [17]. Absolute detection limits for iodinated, brominated and chlorinated volatile organic compounds were 0.5 pg, 10 pg, and 50 pg, respectively. A cryosampling system together with a low temperature GC-ICP-MS method have been developed for the determination of phosphine emission from a tobacco factory for industrial hygiene purposes [18]. Pecheyran *et al.*, used a similar technique to analyze non-metallic species of selenium, arsenic, and phosphorus in the air samples [19]. The method uses a small volume of air samples and was successfully applied for the determination of the metalloid species in atmospheres of urban and rural locations. Determination of iodine in the ambient air was carried out by selectively monitoring ^{129}I using an ICP-MS technique [20]. This technique was used to determine the anthropogenic release of this long-lived radionuclide, which is a definitive indicator of certain nuclear activities.

10.3 Analysis of water

10.3.1 Introduction

ICP-AES and ICP-MS are techniques well suited for the determination of trace elements in water samples, as the low levels of most elements in these samples eliminates the use of other, less sensitive, analytical techniques. There is a considerable volume of literature concerning the analysis of various water samples, and a complete review of this work is not possible in this section, however, the annual 'Environmental Analysis' Atomic Spectrometry Update is a comprehensive review of the publications in this area. Many different types of water samples have been analyzed, the majority of samples coming under the heading of 'natural waters', which include spring, river, and stream waters [6,21]. More specifically, ground water, estuarine water, wastewater, sediment pore waters, rain and river water, as well as snow have all been analyzed. The analysis of seawater and brines [22] represent an interesting sample

Table 10.1 Applications of air analysis with plasma spectrometric detection

Sample type	Elements analyzed	Collection method	Sample preparation technique	Sample analysis technique	Reference
Fly ash	Cu, Zn, Pb, Mn	Collected from cement works	Slurry nebulization and wet digestion (Concentration HNO ₃)	ICP-AES	[7]
Brown haze	Na, Mg, Al, Si, S, Cl, K, Ca, Ti, Mn, Fe, Ni, Cu, Zn, As, Pb	PM ₁₀ Hi-volume sampler and a versatile air pollution sampler	HNO ₃ extraction with ultrasonication	ICP-MS	[8]
Airborne particulate matter	Pb, Cd, Ni	A six-stage cascade impactor	Microwave-assisted acid digestion	ICP-MS	[9]
Total suspended particulate	Cr, Cu, Mn, Ni, Pb, Zn, Cd, V, Mo	High-volume sampler	Open vessel HNO ₃ (3N) digestion	ICP-AES	[10]
Urban aerosol	Pt, Pd, Rh	A six-stage cascade impactor	Microwave-assisted acid digestion	ICP-SFMS	[11]
Indoor dust	Ca, Fe, Al, Mg, Na, Ti, K, Zn, Cu, P, Mn, Ba, V, Sr, Cr, Ni, Pb, Zr, Y	Bag filter and vacuum cleaner	HNO ₃ digestion in autoclave	ICP-AES	[12]
Airborne particulate matter	Na, Mg, Al, Si, S, Cl, K, Ca, Ti, V, Cr, Mn, Fe, Cu, Zn, Br, Pb	Regenerated cellulose membrane filter	Water and dilute acid (0.1 M HCl) extraction	ICP-AES	[13]
Fine urban particles	Mg, Ca, Ti, V, Mn, Fe, Co, Ni, Cu, Cd, Pb	A high-volume sampling system	A sequential extraction protocol	ICP-AES	[14]
Arctic air	Mn, Fe, Co, Ni, Ag, Cd, Sn, Sb, Pb	Cascade impactor	Electrothermal vaporization (ETV)	ETV-ICP-MS	[15]
Particulate matter from power plant emissions	As, Ba, Be, Cd, Co, Cr, Cs, Cu, Ga, Ge, Mn, Ni, P, Pb, Rb, Sb, Sn, Sr, Tl, V, Zn	An iso-kinetic probe nozzle	A microwave digestion method using an acid mixture of HNO ₃ –HCl–HF in a closed vessel	ICP-MS	[16]
Air filters	Pb	Cellulose filters	Continuous flow microwave digestion	ICP-MS	[6]

application as the high dissolved solids concentration (3–4% by weight) may cause problems owing to spectral interferences. This will be discussed in more detail in Section 10.3.3.

10.3.2 Sample collection and preparation

The collection and preparation of a water sample may initially seem to be facile and is not described in many articles concerning water analysis. However, the type of water to be collected, stabilization of the sample, and sample transport must be considered if accurate analytical results are to be attained. Collection of water samples is normally performed using screw-topped 'polyethylene' or poly(ethylene terephthalate) bottles. Depending on the analysis, certain containers, which are sources of contamination and may cause erroneous analytical results, must be avoided.

After collection, many water samples are filtered using membrane filters of a low pore size (usually 0.4–0.5 μm). Filters should be acid cleaned 24 h prior to use. This removes any particulate matter which may interfere with the subsequent plasma analysis. The presence of particulates may cause blockages in flow injection preconcentration systems and in the nebulizer of the instrument sample introduction system. Acidification of the sample is also often necessary to prevent deposition of metal ions onto the surface of the collection vessel. At low pH values, most metal ions are more soluble and, thus, the addition of acids (usually HCl or HNO_3) to a pH of 1–2 is desirable.

10.3.3 Sample clean-up and interference removal

The use of ICP-MS and ICP-AES for the analysis of ultratrace levels in water samples is normally preceded by a sample clean-up procedure. With samples with a high dissolved solid content matrix loading, such as in seawater, the determination of trace elements may be problematic. A high dissolved solid (salt) content may result in restriction of the sampler and skimmer cone orifices (in the case of ICP-MS) owing to prolonged buildup of solids. This ultimately affects the sensitivity and precision of an analysis as well as the long-term stability. A water sample matrix may also contain significant amounts of Na, Cl, Ca, C, N, S, and P particularly so for seawater samples. The presence of these elements causes polyatomic ion interferences when ICP-MS is used as the method of detection. Ionization suppression and enhancement effects may also be seen for ICP-AES analyses when such easily ionizable elements are present. A complete removal of these species is thus highly desirable.

The analysis of water samples, therefore, requires matrix separation prior to sample analysis. Application of anion-exchange resins, matrix modification, precipitation, desolvation, thermal vaporization, chromatographic coupling, and different modifications in the sample introduction systems using modified capillaries are some of the frequently used techniques for matrix separation and interference removal. Methods based on liquid chromatography have also been used to achieve matrix elimination.

In addition to above-mentioned techniques, collision/reaction cell technology [23–26] and high-resolution SF-ICP-MS [27] are the most recent applications in isobaric and polyatomic interference removal in ICP-based instruments. Collision/reaction cell ICP-MS utilizes a multi-pole ion guide contained in a cell and the cell is pressurized with a gas flow.

Ions sampled from the plasma undergo an interaction with the gas prior to MS analysis [28]. Conditions are adjusted to remove interferences while allowing the analyte to remain. Subsequently, it is essential to aim for the elimination of the interference while maintaining minimal scattering of the analyte ion. Removal of an interferent can be accomplished by collisional dissociation (collision energy must be higher than bond-dissociation energy), chemical reaction or energy discrimination. Koppenaal and Eiden compiled a list of publications showing a rapid rise in the number of application of collision reaction cells in ICP-MS instruments over the last decade [29]. SF-ICP-MS instruments with a resolving power ($\Delta m/m$) of as high as 10 000 are sufficient to overcome the large majority of the isobaric and polyatomic interferences. The substantial loss in ion transmission efficiency observed on increasing mass resolution can be overcome by using multi-collector ICP-MS (MC-ICP-MS) instruments that use multiple detectors instead of a single one [27]. Moldovan *et al.*, presents a nice review focusing on the application of SF-ICP-MS and MC-ICP-MS in environmental research [27].

10.3.4 Preconcentration

Many elements in environmental samples are present at very low concentration levels, below the limits of detection (LODs) of ICP-AES and ICP-MS instruments. A method to concentrate the analytes of interest from a large volume of sample solution is therefore desirable and is known as 'preconcentration'. Only very rarely do environmental water samples require dilution before analysis by a plasma spectrometric technique.

Preconcentration may be achieved by one or a combination of a number of methods which may be separated into four major categories: ion exchange, chelating ion exchange, co-precipitation, and solvent extraction. Often flow injection analysis is used to perform on-line preconcentration and is based on the injection of a plug of the sample into a continuously flowing carrier stream. The signal obtained for the analysis is therefore transient, requiring the use of time resolved acquisition software. A detailed description of the different preconcentration techniques used in water analysis is given in the previous edition by Sutton and Caruso [30].

10.3.5 Hydride generation

Liquid samples are normally introduced into the plasma in analytical techniques such as ICP-MS and ICP-AES by pneumatic nebulization. This process is, at best, only 1–2% efficient, so much of the analyte is transported to waste and does not undergo atomization, excitation and ionization. In addition, energy is needed to desolvate the liquid aerosol. The transport of higher percentages of analytes into the plasma may be achieved by the formation of volatile compounds. In this way, detection limits may be improved and the analyte of interest may be separated from the matrix.

Hydride generation (HG) techniques have been applied to certain elements in water samples. There are two methods for HG. The first involves the addition of acid. Hydrochloric acid is the obvious acid for the reduction of metals, however, this may often be problematic owing to the formation of isobaric interferences such as ArCl^+ which may

interfere with As and Se determination. This reaction is not advantageous as it only works for the reduction of As(V), Sb(V), and Se(VI) with the addition of potassium iodide and tin chloride. The other method uses sodium borohydride, NaBH_4 , to reduce metals to their hydrides in a faster and more efficient reaction. It has been used for the reduction of metal species such as Se, Pb, Hg, As, Sb, Cd and Sn in water samples. After the hydride has been formed, it must be directed towards the plasma detector. This is commonly achieved by a continuous method where the NaBH_4 and the aqueous sample are pumped into a mixing tee, where they may react to form the hydride, before passing into a gas-liquid separator. A gas-liquid separator is commonly a Scott-type double pass spray chamber which removes the liquid from the gaseous analyte. The gaseous species are swept into the plasma by the nebulizer gas flow. Such a continuous flow system may be incorporated into a flow injection system. This offers several advantages including lower sample volumes (500–1000 μl), and lower reagent consumption. The optimization of such a flow injection system is important to achieve a high analytical throughput to the plasma. Parameters for optimization include sample volume, purge gas flow rate, acid and reductant concentrations, and liquid flow rate. The addition of organic solvents, such as alcohols, has been shown to be beneficial for the reduction of polyatomic interferences with HG-ICP-MS and to give enhancement of the analytical signal.

10.3.6 *Elemental speciation studies*

Traditional analytical techniques involving plasma source detection usually focus on the total concentration of an element in a sample. This may not, however, yield significant information as to the complex biogeochemistry of the system and their environmental impact. It requires a further step toward elemental speciation. This is because the uptake, accumulation, transports, and interaction of the different metals and metalloids in nature are strongly influenced by their specific elemental form [27]. The oxidation state of the element and the organic compounds that it may be part of, have a significant effect upon the toxicity of the species. This is of particular interest with water samples where elements may find their way into an aqueous system by a wide variety of pathways, both natural and anthropogenic. The identification and quantification of toxic species is essential for environmental monitoring.

Elemental speciation studies have been reviewed in detail [1,31,32] for ICP methods of detection. The separation of particular species is usually achieved using some form of separation technique, for example, liquid chromatography (including reversed-phase, ion-pairing, ion-exchange and size-exclusion chromatography (SEC)), CE [33], field flow fractionation [34], supercritical fluid chromatography and GC [35,36]; all have been used in elemental speciation analysis. After the species have been separated, they must be detected using analytical instrumentation such as ICP-MS or ICP-AES equipped with time resolved data acquisition facilities.

Speciation of many elements has been performed in various types of water samples (bottled water, tap water, fresh water, tube-well water, surface water, ground water, waste water, industrial discharge water, well water, lake water, river water, estuarine water, seawater, etc.) including arsenic [37–45], chromium [46–51], iron [47,52], lead [53–55], mercury [56–60], platinum [61,62], selenium [50,63–67], tin [56,68–70], and vanadium [71–73]. A literature survey was conducted to show the application of ICP-MS and ICP-AES in

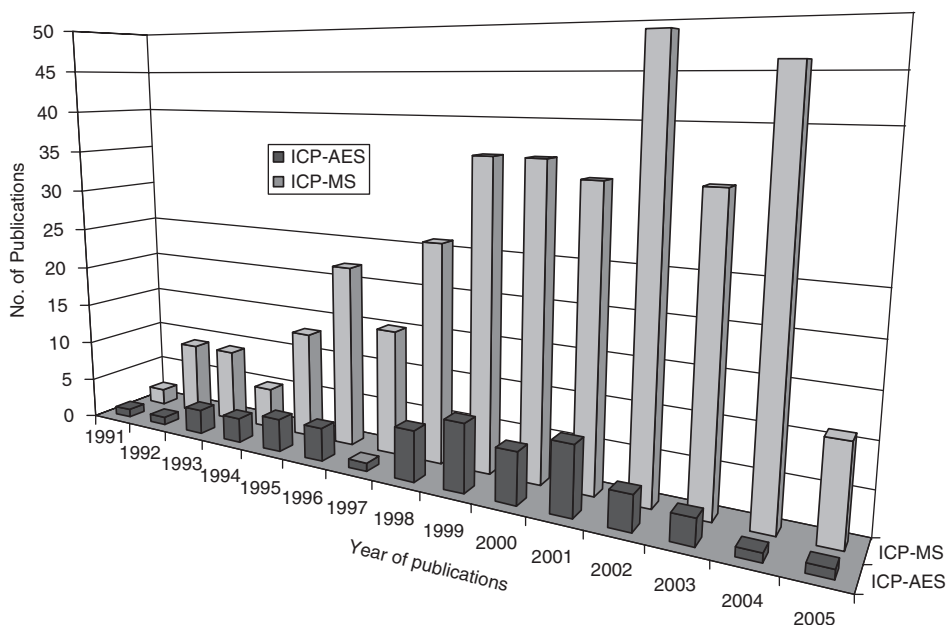


Figure 10.1 ICP-MS/AES in Elemental Speciation Publication History, 1991–2005 (to date). Compiled from SciFinder Scholar Database.

elemental speciation studies between 1991 and 2005 using SciFinder Scholar (Version 2004, Copyright © 2003, American Chemical Society). For ICP-MS, 349 references were found containing both of the concepts ‘Inductively coupled plasma mass spectrometry’ and ‘elemental speciation’. Whereas, 59 references were found for ICP-AES containing both of the concepts ‘Inductively coupled plasma atomic emission spectrometry’ and ‘elemental speciation’. As shown in Fig. 10.1, while the general trend for the number of publications for the application of ICP-AES in elemental speciation is decreasing after 2001, those for ICP-MS are still increasing.

10.3.7 Analysis of non-metals

ICP-based techniques are primarily used in the analysis of trace metals and metalloids. At the same time, both ICP-AES and ICP-MS were recognized as excellent element-specific detectors for chromatographic separations and have since then become important analytical tools for speciation analysis, a fast growing field in analytical chemistry with big impact on life and environmental sciences. On the other hand many organic compounds of environmental, biological, and clinical interests do not have suitable chromophores that result in absorption above 200 nm and thus cannot be analyzed with popular UV detectors. Chromatographic separation followed by pre- or post-column detection using fluorescence tagging requires often complex and time-consuming derivatization steps. Moreover, vulnerability of the refractive index detectors to minor changes in the mobile phase or other experimental conditions limits

Table 10.2 Applications of speciation of non-metals in water samples using plasma spectrometric detection

Sample type	Element species		Analytical technique	Absolute detection limit	Reference
River water	P	Aminomethylphosphonic acid, glyphosate, and glufosinate	HPLC-ICP-MS	25–32 ng l ⁻¹	[74]
River water	P	Aminomethylphosphonic acid, glyphosate, and glufosinate	CE-ICP-MS	0.11–0.19 mg l ⁻¹	[76]
Tap water	P	Diazinon, disulfoton, terbofos and fonofos	GC-ICP-MS	200 ng l ⁻¹	[75]
Water	S	S ²⁻ , SO ₃ ²⁻ , SO ₄ ²⁻ and S ₂ O ₃ ²⁻	IC-ICP-MS	0.4–7.71 ng S	[77]
Drinking water	S	SO ₄ ²⁻	IC-ICP-MS	0.03 µg as S	[78]
Drinking water; river waters	I	2-Iodophenol; 4-iodophenol; 2,4,6-triiodophenol	GC-ICP-MS	0.07–0.12 ng l ⁻¹	[79]
Fresh water and sea water	I	Iodide, iodate and organo-iodine	HPLC-ICP-MS	0.2 µg l ⁻¹	[80]
Wastewater; groundwater; wastewater from coal pyrolysis process	I	Iodine species associated with humic substances	SEC-ICP-MS	–	[81]
Seawater; air	Cl, Br, I	CH ₃ I; C ₂ H ₅ I; 2-C ₃ H ₇ I; 1-C ₃ H ₇ I; CH ₂ ClI; 2-C ₄ H ₉ I; i-C ₄ H ₉ I; 1-C ₄ H ₉ I; CH ₂ I ₂ CH ₃ Br; C ₂ H ₅ Br; 2-CH ₃ H ₇ Br; CH ₂ Br ₂ ; CHBrCl ₂ ; CHBr ₂ Cl; CH ₂ BrI; CHBr ₃ CH ₂ BrCl; CHBrCl ₂ ; CH ₂ ClI; 1,2-C ₂ H ₄ BrCl; 2,1-C ₃ H ₆ BrCl; CHBr ₂ Cl; 1,3-C ₃ H ₆ BrCl	GC-ECD-ICP-MS	0.5 pg as I; 10 pg as Br; 50 pg as Cl	[17]
Wastewaters of industrial and communal origin	Cl, Br, I	Halogens (I, Cl, Br) species associated with humic substances	SEC-ICP-MS	–	[82]
Groundwater; seepage water from soil; brown water	I	I–HS species; Br–HS species and Cl–HS species	SEC-ICP-MS; SEC-ICP-IDMS	–	[83]
Surface water	Br	Br ⁻ ; BrO ₃ ⁻	HPLC-ICP-MS	35–50 pg as Br	[84]

the use of such universal detection system from analyzing the native and underivatized organic compounds. As a result, exploring the capability of ICP-AES and ICP-MS in element-specific detection of non-metals such as sulfur, phosphorus and the halogens often present in such organic compounds has become a cutting edge research frontier. More recent applications of ICP-AES and ICP-MS in speciation of non-metals in water samples are summarized in Table 10.2 [17,74–84].

10.4. Analysis of clinical samples

10.4.1 Introduction

The relationship between elements and the human body can be varied; some are essential, having well-established biological function, while others are toxic. Metal ions, in particular, are known to act as oxidative agents in cells. Since oxidative stress can cause cytotoxicities that compromise health, the presence of certain metals in the human body is considered a risk factor and/or a bioindicator of disease. The distribution and concentration patterns of elements in the body are also informative. Essential element patterns can be used to assess the overall health and status of individuals, and the adequacy of their diets. Alternatively, the distribution of toxic elements allows the forensic determination of occupational or environmental exposure and the potential route of entry into the body.

ICP-MS, is the most commonly used detection technique for elemental analysis of clinical samples. Clinical samples are defined as those extraneous to the human patient that include urine, organ tissue, blood and blood fractions. Many papers specifically delineate whole blood from plasma and serum. Blood plasma is the liquid portion of whole blood in which blood cells are suspended. Plasma is an aqueous solution that contains proteins, nutrients, metabolic end products, hormones, and inorganic electrolytes. Serum is plasma that has had the clotting factors (such as fibrin) removed.

Within these typically complex clinical matrices, analysis is facilitated by the low detection limits and high specificity of ICP-MS. Given this and the instrument's ability to provide reliable stable isotopic data, ICP-MS [85,86] is now routinely used to determine the concentrations of single or multiple elements present, as well as their form (i.e. species). In fact, the volume of samples analyzed by ICP-MS is currently so great that instrument operators in clinical laboratories are considered to have a high risk of exposure due to nebulization [87].

For a review of all atomic spectroscopic techniques used on clinical samples (including ICP-MS), see Taylor *et al.* [88–92]. This section will first summarize the recent literature available on the routine analysis of single/multiple elements in varying clinical matrices, followed by a discussion of instrument differences in ion detection and sample introduction that alleviate problems of resolution and interference. These basics significantly contribute to the final section of this chapter, an overview of elemental speciation by ICP-MS.

The most common clinical use of ICP-MS is the measurement of total elemental concentration in specific cell types or tissues; less is known about the spatial elemental distribution within cells or the whole body. For example, in a recent article, Lombaert *et al.* [93] exposed human blood cells to tungsten carbide and metallic cobalt in an effort to study the effects of these *in vivo*. In this way, they could study the mechanism of toxicity in support

of the current theory of induced apoptosis [93]. Similarly, Frisk *et al.* [94] studied the effects of selenium, mercury or cadmium on the growth of human erythroleukemia cells; ICP-MS was used to measure the trace element contents of the cells and results indicated selenium protection against cadmium toxicity [95]. Lin *et al.*, used ICP-MS to measure lead concentrations in cells of a human lung carcinoma tumor to study the element's effect on nucleotide excision repair [96]. The binding and diffusion of drugs in cells has also been studied; Liang and Huang used ICP-MS to measure the influx of cisplatin to human lung adenocarcinoma A₅₄₉ cells [97]. Finally, Bredfeldt *et al.*, investigated the effects of arsenic on human urothelial cells in an effort toward a greater understanding of how arsenic affects cellular proteins and consequently, a better understanding of the mechanism of toxicity and carcinogenesis of arsenic [98].

10.4.2 Single element/multi-element

The selectivity of ICP-MS is a distinct advantage when the chemical background of a sample is as diverse as blood or urine. Blood is a particularly difficult matrix as it contains 6–8% proteins and 1% inorganic salts [99]. Even with the degree of selectivity that the ICP-MS can provide, sample components capable of contaminating the system or disrupting analytical results are generally removed prior to analysis.

The number of studies that measure a single element – usually when investigating the metabolic processes that control uptake, bioaccumulation and excretion of a specific trace element or when biomonitoring body fluids or tissues following exposure – are too numerous to cite here. Instead, Table 10.3 provides an abbreviated summary. It should be noted that an individual element may pose a unique problem, which may not be exclusive to the analysis of clinical samples. For example, the biggest difficulty in the analysis of Hg is the memory effect; for As and Se, it is the interference of argon-based polyatomic ions. Various sample preparation and instrumental schemes have been designed to eliminate matrix and plasma-based interferences. Subsequently, many of the papers categorized in Table 10.3 were chosen because they are focused on element-specific dilemmas. Table 10.4 identifies those studies that took advantage of the multi-element capability of ICP-MS for the simultaneous investigation of several elements.

10.4.3 Types of mass spectrometers in use

The most common ICP-MS is equipped with a quadrupole mass filter, which has limited mass spectral resolution. Thus, the determination of several isotopes, in particular those with mass-to-charge ratios less than 80, is prone to spectral interferences especially when analyzing heavy matrix materials such as clinical samples. Overall, interferences arise from atoms associated with the plasma gas, the solvent and associated reagents, and the sample matrix. A double focusing (SF) mass spectrometer can alleviate some of this interference. This type of MS contains two devices for focusing the beam of ions: an electrostatic analyzer and a magnetic analyzer. As a result, this instrument offers much better resolution. Moreover, for isotopes where interferences do not pose significant problems, SF instruments may be operated in medium- and low-resolution modes, which makes its detection

Table 10.3 Applications of ICP-MS for single element analysis in clinical samples

Element	Matrix	Summary comments	Reference
As	Urine, bone	Arsenic is measured in urine in support of epidemiological studies; it is measured in skeleton to determine individuals engaged in copper smelting.	[202,203]
Al	Blood, urine	This element is relatively nontoxic to healthy humans due to rapid excretion; however, it has been found to cause dementia and anemia in patients with renal disease.	[204,205]
Au	Serum	Gold compounds are used in the treatment of rheumatoid arthritis; the monitoring of serum of such patients is necessary to suppress side effects.	[206]
B	Serum, urine	Boron is considered to affect bone development and the function and composition of the brain, skeleton and immune systems.	[207,208]
Be	Urine	Pulmonary disease and lung cancer have been linked to beryllium; ICP-MS can be used in the analysis of urine as an indicator of worker exposure.	[209]
Ca	Urine, blood, faeces	Calcium is an essential element for humans for proper bone and teeth development; Cool plasma was used in this work to alleviate the ^{40}Ar interference at calcium's major isotope.	[210]
Cd	Urine, blood, faeces	Cadmium is considered a heavy metal and carcinogenic for humans; incorporated Cd becomes bound to the cysteine-rich metallothionein and accumulates in the soft tissues of the kidney and liver.	[211–217]
Cu	Blood	Copper is an essential element and a constituent of important metalloproteins and metalloenzymes.	[218]
Hg	Blood, urine, hair	Mercury is a toxic element and ICP-MS may be used to measure lethal exposure due to occupation or accident. In one recent interesting case report, ICP-MS was used to determine Hg in gastric contents at autopsy to determine cause of death [219].	[220–229]
I	Urine, serum, faeces	Iodine deficiency can lead to endocrine disease. Reduced maternal thyroid concentrations during pregnancy can affect foetal neurological development.	[230–233]
Mo	Blood, urine	Molybdenum is an essential trace element that contributes to the function of 11 known enzymes. ICP-MS may be used to study the metabolism, functions and distributions as its concentration is generally below 1 ppm.	[234–238]
Na	Blood	Sodium is a serum electrolyte that plays an important role in regulating osmotic pressure and the distribution of water. It is routinely determined to support diagnoses of circulatory, renal and nervous system functions.	[239]
Pt	Blood, urine	Long-term pharmacokinetic behavior of platinum in patient blood/urine studied after platinum drug administration. Platinum also studied in clinical samples to determine pollution exposure of humans as a result of vehicle catalysts [240,241].	[242–248]

Table 10.3 (Continued)

Element	Matrix	Summary comments	Reference
Pb	Blood, urine, teeth, hair, bone	Lead negatively affects human health as it binds to some specific proteins present in the erythrocytes. Biological monitoring is therefore needed for people occupationally exposed or for lead poisoning.	[249–257]
Pu	Urine	Plutonium is measured as an indicator of exposure; this element is considered more radiologically than chemically toxic.	[258–260]
Se	Blood, urine	Selenium is an essential element with a narrow range of optimal concentration. It is required for the functioning of many enzymes, particularly glutathione peroxidase which protects against oxidative stress by scavenging damaging peroxides. Se deficiency can lead to serious diseases.	[261–270]
Th	Urine	Thorium is considered a radionuclide with high toxicity.	[271]
Tl	Blood, urine	Thallium is a highly toxic element that can affect the central nervous system and lead to symptoms such as headache and fatigue.	[272]
Tl	Lung tissue	Thallium is used to diagnose myocardial infarction and thyroid tumors. As such, the concentration of this element may be measured in human lung cancer cells.	[273]
U	Serum, urine, vomit, hair	The toxicity of uranium results from the fact that it is a heavy element, rather than radiation dose.	[274–279]
W	Plasma	Sodium tungstate plays a helpful part in the long-term treatment of diabetes; ICP-MS may be used to monitor for this element in blood plasma and to determine the percentage binding of W to human plasma proteins.	[280]
Zn	Iris tissue	Zinc is an essential nutrient and the most abundant trace element in the eye. It is known to bind to melanin in pigmented tissues; a deficiency will result in night blindness.	[281]

limits considerably lower than those obtained by quadrupole based instrumentation. Many unique applications have been based on these benefits and, in some cases, use of such a mass spectrometer is essential [100].

SF instruments have found many applications in the analysis of clinical samples, due primarily to the advantages discussed in the previous paragraph [101]. For example, an SF MS was used to study the concentrations of Cd, Co, Cu, Fe, Mn, Rb, V and Zn in brain tissue. This work was in support of a hypothesis that imbalances in essential and toxic metals that are related to neurodegenerative disorders. Medium resolution was employed to reduce interferences, however, Cd analysis was performed in low-resolution mode, resulting in lower detection limits [102]. Melo and co-workers monitored Mn, Cu and Zn in the

Table 10.4 Applications ICP-MS for multiple element analysis in clinical samples

Elements	Matrix	Reference
Cu, Pb, Se, Zn	Serum	[282]
Ba, Sn, Te, U, Fe, Cu, Mo, Gd, Cd, Nd, Dy, Yb, Lu, Tl, Th, Mn, Co, Ni, Rb, Y, La, Ce, Pr	Bone	[283]
Cs, I, Sr, Th, U, Ca, Cu, Fe, K, Mn, Se, Zn	Tissue	[284]
Cd, Co, Cu, Hg, Pb, Pd, Pt, Rb, Rh, Se, Tl, W, Zn	Blood	[285–287]
As, Se, Hg, Zn, Pb, Ni, Cd, Mn, Cu, Fe	Hair/skin/nails	[288]
B, Sc, V, Cr, Mn, Ni, As, Mo, Se, Al, Ag, Cd, Te, Cs, Ba, Bi	Brain tissue	[289]
Bi, Cd, Co, Cs, Cu, Fe, Hg, Mn, Mo, Pb, Rb, Sb, Sn, Sr, Tl, Zn	Brain/liver tissue	[290]
As, Ca, Cd, Co, Cr, Cu, Fe, Mg, Mn, Ni, P, Pb, Sb, Se, Tl, V, Zn	Hair	[291]
Mn, Mo	Brain, serum	[292,293]
Ca, Cr, Co, Cu, Fe, Mg, Mn, Mo, Ni, Zn	Hair	[294]
Au, Ag, Cd, Co, Cr, In, Ni, Pb, Pt	Hair	[295]
As, Cd, Pb, Tl	Blood/urine	[296]
Fe, Zn	Faeces	[297]
Ag, Al, As, Au, B, Ba, Bi, Ca, Cd, Cr, Co, Cu, Fe, Ge, Hg, K, Li, Mg, Mn, Mo, Na, Ni, P, Pb, Sb, Se, Sn, Sr, Th, V, Zn	Hair	[298]
As, Se	Faeces	[299]
Al, Co, Cu, Fe, Mn, Zn	Serum	[300]
Al, As, Be, B, Cd, Co, Cu, Fe, Mn, Mo, Ni, Pb, Li, Rb, Se, Sr, Zn	Blood	[301]
Ag, Al, As, Ba, Be, Bi, Cd, Co, Cr, Cu, Ga, Li, Mg, Mn, Mo, Pb, Rb, Sb, Se, Sn, Sr, Tl, U, Zn	Blood/urine	[302]
Cu, Zn, Mn, Rb, Mg	Serum/thoracic empyemata	[303]
Cd, Pb	Blood/urine	[304–309]
Ag, Cd, Pb, Sb	Liver tissue	[310]
As, Se	Urine	[311]
Cd, Cs, Cu, Fe, Mg, Mn, Ru, Se, Sr, Zn	Blood and placenta tissue	[312]
Ag, Al, As, Ca, Cd, Co, Cu, Fe, Hg, Mg, Mn, Pb, Se, V, Zn	Aortic valve tissue	[313]
Ce, Dy, Er, Eu, Gd, Ho, La, Lu, Nd, Pr, Sm, Tb, Tm, Yb, Y	Serum/hair	[314,315]
Cd, Cu, Hg, Mg, Pb, Se, Zn	Blood	[316]
Cu, Se, Zn	Leukocytes separated from maternal blood	[317,318]
Cd, Hg, Pb	Blood	[319]
Ba, Cd, Cu, Pb, Zn	Saliva	[320]
As, Cu, Mo, Ni, Pb, Se, Zn	Urine	[321]
Th, U	Blood/urine/hair	[322–325]
Pd, Pt, Rh	Urine	[326,327]
Ti, Zr	Serum	[328]
Al, Cd, Co, Cu, Li, Mn, Mo, Ni, Pb, Pt Rb, Sb, Se, Zn	Serum	[329,330]
Ce, Nd, Sm	Hair	[331]
Ag, Al, As, Au, Ba, Bi, Cd, Ce, Co, Cr, Cs, Cu, Hg, I, La, Li, Mn, Mo, Ni, Pb, Pt, Rb, Sb, Se, Sr, Th, Ti, Tl, V, W, Zn, Zr	Liver, kidney, bone	[332]

Table 10.4 (Continued)

Elements	Matrix	Reference
Ag, Au, Al, As, Ba, Be, Bi, Cd, Co, Cs, Cu, Hg, Mo, Ni, Pb, Rb, Sb, Se, Sn, Sr, Te, Tl, U, Zn	Urine	[333]
Al, As, Cd, Co, Cr, Cu, Hg, Mn, Mo, Ni, Pb, Se, Tl	Urine/blood	[334]
Cu, Zn	Blood/urine	[335,336]
Actinides	Urine	[337]
Co, Cs, Cu, Pb, Rb, Sr, Zn	Blood	[338]
Cd, Cu, Hg, Pb, Se, Zn	Blood	[339]
Bi, Cd, Hg, Pb, Pd, Pt, Sb, Sn, Te, Tl, W	Urine	[340]
Cd, Co, Cu, Ga, Hg, Mo, Ni, Pb, Pd, Pt, Rb, Rh, Sb, Se, Sn, Tl, W, Zn	Urine	[341]
Ba, Be, Bi, Ca, Cd, Cs, Cu, La, Li, Mg, Mo, Pb, Rb, Sb, Sn, Sr, Tl, Zn	Synovial fluids of osteo-arthritic knee joints	[342]
Br, Ca, Mg, Rb, Sr, Zn	Serum	[343]
Bi, Ni	Urine	[344]
Ag, As, Ca, Cd, Ce, Co, Cr, Cu, Fe, Hg, I, K, Mg, Mn, Na, Ni, Pb, Rb, Sb, Se, Sn, Sr, U, V, Zn	Thyroid tissue	[345]
Sb, As, Cd, Cr, Pb, Hg, Se	Hair	[346]
Cr, Ni	Blood	[347,348]
Se, Zn	Hair	[349]
Cu, Fe, Mg, Mn, Pb, Sr, Zn	Tooth enamel	[350]
Ca, Cu, Mg, Zn, Sr, Al, Ba, Pb, U, Ce, La, Pr	Teeth	[351]
Cd, Pb, Zn, Se, Cu, Ca, Co, Mo, Mn	Placenta	[352]
Ag, Cd, Co, Pb, Sb	Liver tissue	[353]
Sb, Ba, Be, Cs, Co, Pb, Mn, Mo, Pt, Tl, Sn, W	Urine	[354]
Li, Na, Cr, Mn, Ni, Cu, Zn, Sr, Cd, Ba, Mg, Al, Ca, Fe, Ni	Hair/plasma	[355]
Cu, Pb	Urine	[356]
Cu, Fe, Ni, Pb, Zn	Blood	[357]
Ca, K	Serum	[358]
Mg, Ca, Ga, Mn, Fe, Cu, Zn	Saliva	[359]
I, Pt	Serum	[360]

cerebrospinal fluid of healthy subjects and patients with multiple sclerosis; they found significant differences in manganese and copper concentrations [103]. Other examples are given in the Table 10.5.

The use of a multi-collector detector with a SF instrument is another means by which specific advantages can be gained in the analysis of clinical samples, especially in the investigation of isotope ratios. As discussed earlier in this chapter, these instruments have multiple detectors and so they possess the ability of detecting and measuring multiple ion signals simultaneously. This instrumentation has been used in the analysis of Zn in faeces [104] and Fe in whole blood [105].

Utilizing a time-of-flight mass spectrometer in conjunction with an ICP ionization source has been found to yield unique advantages in the analysis of clinical samples. The

Table 10.5 Applications of different types of MS detection systems for analyzing clinical samples

Element	Matrix	Resolution	Reference
Al	Serum	Medium	[205]
Ca	Urine	Medium	[361–363]
Cd	Urine	Low	[364]
Fe	Faeces, Serum	Medium	[365,366]
Pb	Blood, bone	Low	[367–369]
Pt	Urine, serum, tissue	Low	[370]
Pu	Urine	Low	[371,372]
U	Urine	Low	[373,374]
V	Blood, urine	Medium	[375]
Se	Plasma	Low/high	[376]
Sr	Bone/urine	Low/medium	[377,378]
Zn	Faeces, urine, serum	Medium	[379,380]
Cd, Co, Cu, Fe, Mn, Rb, V, Zn	Brain tissue	Low/medium	[102]
Cr, Ni, V	Urine	Medium	[381]
Co, Cr, Cu, Fe, Mn, Ni, Sc, V, Zn	Urine	Medium	[382]
Fe, Cu, Zn	Serum	Medium	[383]
Cu, Mn, Zn	Cerebrospinal fluid	Low	[103]
Au, Ir, Pd, Pt	Blood	Low	[384]
60 elements	Blood/hair/nails	Low/medium/high	[385–387]
Al, Cd, Co, Cr, Cu, Fe, Mn, Ni, Pb, Pt, Tl, V, Zn	Blood/urine	Low/medium	[388]
Al, As, Cd, Cr, Co, Cu, Hg, Mn, Ni, Pb, Sb, Se, Tl, Zn	Blood/urine	Low/medium/high	[389]
Al, Ca, Cd, Co, Cr, Cu, Fe, Mn, Mo, Pb, Rb, Sr, U, Zn	Serum	Low/high	[390]
Th, U	Urine	Low	[391,392]
Cd, Cu, Pb, Zn	Urine	Low/medium/high	[393]
Ag, Al, Cd, Cu, Cr, Mn, P, Fe, S, Si, Sn, Ti, U, Zn	Serum	Low/medium	[394]
Cd, Co, Cr, Ni, Pb, Rb, Sb, Se, V, Pd, Pt, Rh	Urine	Medium	[381,395]
As, Se	Urine	Low	[396]
Pd, Pt	Urine	High	[397]
Al, Ca, Cr, Mn, Fe, Co, Cu, Zn, Se, Rb, Sr, Mo, Cd, Pb, U	Urine	Low	[398]
As, Cd, Hg, Pb, Th, U, Al, Cu, Cr, Mn, Ni	Serum	Low/medium	[399]
Cu, Pb	Serum/urine	Low/medium/high	[400]
	Serum	Medium	[401]

operation of this type of mass spectrometer is based on the fundamental principle that the kinetic energy of an ion is directly proportional to its mass and velocity. Therefore, if ions of different mass are given the same kinetic energy by an accelerating voltage, the velocities of the ions will differ over a fixed flight path. The resulting simultaneous nature of sampling ions offers distinct advantages in the analysis of transient signals. Additionally, the mass

Table 10.6 Applications of collision reaction cell technology in MS analysis of clinical samples

Element	Matrix	Cell gas	Reference
Cr, V	Urine, serum	Ammonia	[402]
Se	Urine, serum	Methane	[403]
Se	Plasma, urine, faeces	Methane	[404]
Se	Serum, urine, tissue	Hydrogen	[405]
Cr	Urine	Ammonia	[406]
As, Ba, Be, Co, Cd, Cu, Cr, In, Li, Mn, Mo, Ni, Pb, Pt, Rh, Sb, Se, Sn, Ti, U, V, W	Urine	Helium/hydrogen	[407]
Ca	Serum	Hydrogen	[408]
P, S	Colorectal tissue	Oxygen	[108]
Fe	Serum	Carbon monoxide	[366]

resolution obtained by such instrumentation lies between that of a quadrupole and a SF instrument. Benkhedda *et al.*, took advantage of the higher resolution obtainable with this instrument in the determination of the platinum group metals (Pt, Rh, and Pd) in urine and serum samples [106]. This group additionally employed ultrasonic nebulization to enhance the sensitivity of the method. Centineo and co-workers used the ICP-TOF-MS for the simultaneous determination of seven elements in urine (As, Be, Ge, Hg, Sb, Se, and Sn); they additionally employed HG in the sample introduction scheme to increase sensitivity [107].

Collision/reaction cell technology has also found many applications in the analysis of clinical samples as a means to remove interferences [26] and Table 10.6 summarizes this work. A collision cell consists of an ion guide operated in an rf only mode (no mass discrimination). Implementing the reaction cell necessitates lower ion energies and a narrower ion energy distribution for successful manipulation of the ions entering the cell. This can be accomplished by using platinum shield plate and bonnet (shield torch). Specific interferences may be removed by collision-induced dissociation, reaction or energy discrimination.

In a quite recent application, Bandura *et al.*, used a reaction cell for the determination of phosphorus and sulfur in biological samples [108]. Phosphorylation and de-phosphorylation of cell proteins are essential signaling processes that regulate a wide variety of cellular events; sulfur is a convenient internal standard as many target proteins of peptides contain cysteine or methionine residues. Oxygen was used in the reaction cell, transforming the analytes to their corresponding oxides, PO^+ and SO^+ , and hence removing them from the mass region of interference. The sulfur/phosphorus ratio was detected in cell cultures and was shown to provide a distinguishable difference between malignant cell lines and primary cultures. The method was applied to the analysis of colorectal adenocarcinoma tissues.

10.4.4 Sample introduction

Laser ablation is an attractive sample introduction technique for samples that are solid in nature and limited in quantity. A single laser pulse ablates a portion of the sample which is then swept into the plasma. The SF instrument is typically combined with this sample

introduction technique as it offers the greatest sensitivity in the analysis of a small sample size. Rodushkin and Axelsson used this technique for the determination of 55 elements in hair and nail samples. Chronological variations and depth distribution patterns were investigated in the nail samples and element distributions were measured along the hair strand [109]. Others have applied this technique to human teeth; Cox *et al.* [110], Lochner *et al.* [111], and Lee *et al.* [112] investigated the profiling of several elements whereas Hoffmann *et al.*, focused solely on Hg (due to amalgam fillings) in determining its potential migration [113], Ghazi *et al.*, studied gallium diffusion across human root dentin and Budd *et al.*, investigated lead distribution [114]. In other matrices, Prohaska *et al.*, utilized LA-ICP-MS in the determination of strontium in bones [115] and Legrand applied it in the determination of mercury in human hair [116]. Finally, Neilsen and co-workers used LA-ICP-MS in combination with gel electrophoresis to study the speciation of cobalt-binding serum proteins [117].

Electrothermal vaporization (ETV) is a second sample introduction technique that is particularly suited to situations where there is a limited sample size. It is typically more sensitive than the conventional nebulization/spray chamber arrangement because of the increased efficiency of sample transport to the plasma. ETV coupled to ICP-MS was recently utilized by Parsons *et al.*, in the determination of lead in a blood matrix [118]. Isotope dilution was utilized with this instrumental scheme for the determination of mercury [119], cadmium, copper, and lead in urine [120,121]. Pozebon and co-workers used ETV-ICP-MS for the determination of arsenic, selenium and lead in urine [122]. Human hair and serum were investigated for concentrations of lanthanides by ETV-ICP-MS by Buseth and co-workers [123]. Turner *et al.*, used ETV in the ICP-MS determination of selenium in serum [124,125] and in this case, its employment was found to help circumvent the signal suppression that ordinarily resulted from the high levels of sodium and organic compounds inherent in this matrix. Yu *et al.*, also utilized the advantages of ETV in the analysis of blood for aluminum, titanium and vanadium [126]. The samples were taken from patients that underwent joint replacement arthroplasty; the analysis was performed in an effort to monitor degradation of prosthetic materials composed of an alloy of these elements.

10.4.5 Speciation of elements

Elemental speciation is defined as the analyses that lead to determination of the distribution of an element's particular chemical species in a sample. This may be further associated with oxidation state (cationic or anionic), organometallic nature (characterized by the presence of a strong metal-carbon covalent bond) or complex form (entails the use of coordination bonds binding metals to ligands). Different species or forms of a single element are often markedly different in their toxicity, bioavailability, distribution, physiological function, diagnostic utility, and/or therapeutic potential [127]. A recent review by Templeton discusses this subject in more detail and demonstrates how the species determines distribution within the organism or governs transport across various biological barriers [128]. A second excellent review by Gomez-Ariza *et al.*, specifically discusses analytical techniques in the area of metallomics, an extension of elemental speciation that constitutes the investigation of biomolecules in which numerous biological ligands are bound to trace elements [129]. Elemental separation techniques are subsequently divided

into the determination of individual chemical species and elemental association to key biomolecules (DNA, RNA, polypeptides, proteins, etc.) [130]. Analytical techniques follow this division [131] and are discussed in the following sections in this order.

Most components of biological matrices are not volatile. However, volatile species of a few elements have been discovered to be constituents of clinical samples, whether artificial or natural. For these instances, the coupling of GC to ICP-MS detection has been shown to be an attractive technique for their analysis. Gui-Bin and co-workers used GC-ICP-MS for the determination of tin species in the blood and urine [132] and organs [133] of exposed patients. GC-ICP-MS was used by Feldmann *et al.*, to analyze volatile metal and metalloid compounds in human breath [134] while Rodriguez-Fernandez *et al.*, coupled the GC to a SF instrument to specifically monitor the sulfur-containing components of human breath [135]. In a similar vein, St. Remy and co-workers monitored total homocysteine in human serum by GC coupled to a SF-ICP-MS for sulfur-specific detection [136]. In both cases, medium resolution was necessary to separate $^{32}\text{S}^+$, the major sulfur isotope, from O_2^+ at the same nominal mass.

For those constituents of clinical samples that are not volatile, electrophoretic techniques may be applied. Alternative types have been employed in the speciation of Cr, Ga, In, Pt and V incubated in serum samples [137], however, CE is the most widely employed. It has shown nice results in the investigation of selenium [138] and iodine [139] species in serum, arsenic species in urine [140], and metallothioneins [141]. It has also been successfully used to study the interaction between platinum anticancer drugs and human serum albumin [142]. However, although CE yields exceptional resolution, sensitivity may be limited due to its small injection volume. HPLC has therefore been employed much more extensively [143]. There exist many forms of liquid chromatography, including normal-phase, reversed-phase, ion-exchange, ion-pairing and size exclusion. Reversed-phase liquid chromatography entails the use of a non-polar stationary phase with a polar mobile phase. Separation is based on strong hydrophobic interactions between the stationary phase and the analytes. Ion-pairing chromatography is a modification of reversed-phase chromatography and is used for analytes that are anionic or cationic. Ion-exchange chromatography is also a widely used separation method in the field of element speciation. Each of these types of HPLC has been extensively used in the determination of elemental species in clinical samples. Current focus is on the chromatographic separation of newly discovered species and identification of unknown species through complementary techniques, primarily of the elements of arsenic and selenium [144].

Several types of chromatography can be applied to the separation of arsenic species in clinical samples [145,146]. Arsenic speciation of urine is critical to properly evaluating a recent exposure to environmental and dietary arsenic. Ion-exchange chromatography is one of the most popular chromatographic techniques [147–157], however, others have employed ion-exclusion [158], reversed-phase [159,160], cation-exchange [161], ion-pairing [162], gel-permeation [163], and micellar-liquid chromatography [164]. In an interesting article, Mandal *et al.*, extended the speciation application to the analysis of nails and hair taken from people living in an arsenic affected area [165].

Like arsenic, many types of HPLC have been applied to the speciation of selenium in urine. Although much work has been done [166–168], the metabolites of selenium in the human body have yet to be completely elucidated and several types of HPLC have been employed in this investigation. These include anion-exchange [169,170], cation-exchange

[171,172] reversed-phase [173,174], gel-permeation [175], vesicle-mediated [176,177], and ion-pairing chromatography [178–182]. Marchante-Gayon *et al.*, additionally employed a collision cell in the speciation analysis to eliminate argon based interferences [183]. With respect to the selenium species in blood, Bendahl and co-workers used metal-ion affinity chromatography to separate selenoprotein P from other selenium-containing proteins in human plasma [184]. Both affinity and anion-exchange chromatography were used by Reyes *et al.*, in the speciation of selenium in human serum [185]. Michalke used only anion exchange in the analysis of serum from healthy patients and serum from cystic fibrosis patients; his results showed a significantly lowered concentration of selenocystine in sera of cystic fibrosis patients [186]. In a similar vein, Nyman and co-workers used anion exchange to separate selenium species in serum and prostate tissue of prostate cancer patients [187].

Various forms of HPLC have also found unique applications in the speciation of other elements. These works are summarized in the Table 10.7.

Several chromatographic techniques have been employed in the area of metallomics. These include size exclusion and fast protein as well as multi-dimensional techniques; all have been found to be relatively soft separation techniques in that they are not disruptive to the species. SEC is a variation of HPLC in which the separation is based on the differential degree of permeation of molecules of different sizes and shapes with respect to the pore size and packing geometry of the stationary phase. In general, this technique is used for high-molecular weight analytes and the retention behavior of the unknown may be correlated to molecular mass. This chromatography coupled to ICP-MS detection has been found to be of great use in the analysis of proteins as research efforts extend to the elucidation of reaction mechanisms and evaluation of binding capacities of different elements with biological entities.

Speciation studies of metals in biological tissues may elucidate mutagenic processes. Richarz and Bratter [188] used SEC-ICP-MS in the investigation of the speciation of trace elements in the brains of patients with Alzheimer's disease. Post-mortem samples from Alzheimer's disease brains and from brains of a control group were investigated to determine changes in the trace element distribution during the pathological process. Special emphasis was placed on metallothioneins and a comparison between Alzheimer's disease and control brains showed a significant difference concerning several metallothionein metal levels, leading to the assumption that oxidative processes occurred in Alzheimer's brain samples. In a later work, the same authors [189] investigated protein-bound trace elements in human cell cytosols (soluble proteins) of different organs as well as the same type of organ in different pathological states. This work was based on the assumption that the cells of different organs contain different proteins to perform their respective specialized functions; final identification of the proteins was performed by means of specific protein assays with collected fractions from the SEC column. Different elemental profiles were obtained for different organs of the same patient and for the same organ of patients with different diseases. Therefore, the authors concluded that metalloproteins and their bound metals may be used as biological markers for physiological differences or pathological changes in human tissue. In a similar vein, Boulyga utilized SEC-ICP-MS for comparative analysis of metal-containing species in cancerous and healthy human thyroid samples. This work was performed so as to estimate changes in metalloprotein speciation in pathological tissues; results showed a presence of species binding Cu, Zn, Cd and Pb in healthy thyroid tissue whereas these same species could not be detected in cancerous tissue.

Table 10.7 Applications of HPLC-ICP-MS in elemental speciation in clinical samples

Element	Matrix	Summary comments	Reference
Al, Fe	Serum	ICP-SF-MS was used to study the chemical forms of co-existing Al and Fe bound to human serum transferrin, an iron-binding glycoprotein.	[409]
V	Serum	The binding patterns of V to transferrin were studied. Transferrin is a glycoprotein that has two binding sites (C-lobe site and N-lobe site).	[410,411]
Sb	Blood, urine, hair	Patients with leishmaniasis were monitored after intramuscular administration to study the biotransformation of N-methyl meglumine antimoniate to Sb ⁺⁵ and Sb ⁺³ in the human body. HPLC-ICP-MS is also used for urinary analysis to support biomonitoring [412].	[412,413]
Cu, Fe, Zn	Serum	Ion-exchange chromatography coupled to ICP-SF-MS was used to monitor essential elemental differences between patients on haemodialysis and healthy volunteers.	[414]
I	Urine	Urine samples were investigated for the presence of 2,4,6-iodophenol, an anti-inflammatory drug, as well as its metabolites.	[415]
P, Si	Blood	P and Si were monitored with a SF-ICP-MS in the development of a method for organophosphorus pesticides in blood plasma and organosilicon compounds in the human body due to surgical implants or devices.	[416]
Au	Blood	The gold binding sites in red blood cells were studied; SEC indicated that gold was not bound principally to haemoglobin, but rather to a significantly higher-molecular weight species.	[417]
Fe	Serum	Four molecular forms of transferrins with different iron-binding states were separated and the percentage of iron saturation was determined.	[418]
Cd	Urine	Metallothioneins are low-molecular weight, cysteine-rich proteins which function in the metal detoxification process; the concentration of Cd bound to metallothioneins in urine can be studied.	[419]
B	Urine, blood	Clinical samples separated with a porous graphite carbon column and monitored with ICP-TOF-MS after boron neutron capture therapy (treatment for brain tumors) to determine boron drug metabolites.	[420]
U, Th, Am, Np, Pu	Urine	A novel matrix removal and gradient elution method was developed for the separation and simultaneous determination of ultratrace levels of five actinides.	[421]
Pt	Plasma	HPLC-ICP-MS was used in the analysis of plasma samples after platinum drug administration in an effort to classify biotransformation products, i.e., Pt adducts with plasma proteins, free platinum species.	[422–424]

Often SEC is applied in the study of the elemental association with biomolecules. Vanadium has shown promise medicinally as it may have anticancer effects as well as insulin-like properties. Chery and co-workers [190] speciated vanadium in serum with SEC-ICP-MS using a reaction cell pressurized with ammonia. Pb-bound ligands in human amniotic fluid were studied by SEC-ICP-MS in a work performed by Hall *et al.* [191] This work was done to support a study that examined maternal-faetal transfer of Pb by comparing Pb-bound ligands in amniotic fluid with those in maternal plasma. Using protein standards, Pb-containing ligand identifications included ceruloplasmin, pre-albumin, and a Zn-peptide; multi-element detection was employed to verify other known elements in each of the proteins.

The toxic activity of some trace metals such as Cd and Pb is thought to relate to their ability to compete with essential elements in proteins or to bind to DNA. Wang and co-workers used a magnetic sector ICP-MS coupled to the effluent of an SEC column in pursuit of identification of elements in the proteins of human serum as well as in DNA fragments [192]. Results showed that monitoring Cd, Cu and Zn in serum did not result in peaks in the appropriate molecular weight range for metallothioneins (~10 kDa) which promotes speculation that these elements are not stored in metallothioneins in serum or that the metallothioneins are bound to other larger proteins. Additionally, results indicated complete binding of Pb, Cd, Mn and Fe to DNA fragments as well as binding of Cr(VI) after reduction to Cr(III)/oxidation of DNA.

SEC-ICP-MS has also been applied for the investigation of drug-protein interactions and binding; such studies are critical for elucidating mechanisms of drug action, toxicity, and metabolism. For example, patients undergoing cisplatin chemotherapeutic treatment may experience a decrease of haemoglobin in the blood and Mandal *et al.*, therefore used this technique to study the interaction of cisplatin and haemoglobin [193]. SEC was used to separate free and protein-bound cisplatin and ICP to monitor simultaneously ^{195}Pt and ^{57}Fe . Results demonstrated the presence of haemoglobin bound platinum complexes which may explain the mechanism for the haemoglobin reduction. In a similar vein, Szpunar and co-workers studied the interactions of several Pt and Ru-based drugs with serum proteins [194].

Fast protein liquid chromatography (FPLC) is a second type of chromatography that has been frequently utilized in the speciation analysis of large biomolecules and is based on anion-exchange interaction. Cabezuelo *et al.* [195] used this chromatographic technique coupled to a SF-ICP-MS in medium resolution to conduct the speciation of basal aluminium in human serum. The speciation of this element is critical, as its excess has been documented to cause neurological and skeletal toxicity in renal failure patients [196]. Montes-Bayon extended the analyte list investigated with this instrumental setup; both low and medium resolution modes were employed in the determination of Ca, Sr, Fe, Cu, Zn, Se, Mn, Cr, Pb, Al and Sn [197]. Fernandes and co-workers [198] used FPLC with a quadrupole instrument equipped with a collision cell to study vanadium association to human serum proteins; the collision cell was employed to alleviate the chlorinated interference, $^{35}\text{Cl}^{16}\text{O}^+$.

Sun and Szeto investigated the binding of bismuth to serum proteins using FPLC and ICP-MS [199]. Bismuth complexes have been widely used in clinical treatment as anti-ulcer drugs, however, the mechanisms of the drug action are poorly understood and adverse affects have been diagnosed by detection of bismuth in the blood. The speciation of bismuth in blood and blood plasma and the mechanism whereby bismuth is transported into the

brain still remain unclear. In this work, the binding of bismuth to albumin and transferrin was investigated to determine the target of this element in blood plasma.

Bidimensional chromatography with ICP-MS detection was utilized by Pizarro and co-workers [200] in their evaluation of the protein binding of arsenic species in cardiovascular tissue. Inorganic arsenic has a high affinity for fibrous extracellular structures, insoluble structural proteins and fibrillary tissue with a high content of sulfhydryl groups. SEC was used to fractionate the cytosol and the collected samples were then further separated by FPLC. The resulting chromatograms showed that As is bound to biocompounds of different molecular mass through vicinal sulfur groups. Further, the monitoring of S, Cu and P present in the fractions show that As and Cu are usually bound to the same type of protein. Multi-dimensional chromatography was also applied by Koyama *et al.*, in the determination of selenium-containing proteins in human blood plasma [201]. The first column was a heparin affinity column and the second was a gel filtration column.

10.5 Conclusions

Environmental and clinical applications of ICP spectrometry have received a significant amount of attention in recent years. This is reflected in the volume of articles published each year and are reviewed annually in the Atomic Spectrometry Updates of the *Journal of Analytical Atomic Spectrometry*. The analysis of air involves the collection of particles on filters, subsequent digestion of the filters and particles, and analysis by plasma spectrometry. Various methods are available to the analyst for digestion and have been described in detail. The analysis of water samples is described, from sample collection to sample pretreatment and analysis. The preconcentration techniques currently available for the analysis of water samples enable the detection of ultratrace concentrations of many elements. HG is also available for increased sample throughput and speciation of samples may be achieved using chromatographic separation techniques. The robustness of ICP-MS to complex sample matrices as well as its compatibility for hyphenation to chromatographic separation techniques makes it an appropriate analytical tool for clinical analysis. The distribution and concentration pattern of the essential elements are informative in terms of overall health of an individual whereas the determination of concentration and speciation of toxic elements in clinical samples allows forensic investigation of occupational or environmental exposure as well as the potential route of entry into the human body. Finally, the recent advancement in non-metal analysis enriched the analytical capability of ICP spectrometric techniques toward element-specific detection of organic compounds of environmental and clinical interests. These latest advancements in the versatility of analytical applications might lead to parallel elemental-molecular mass spectrometric techniques to address more complicated analytical challenges.

References

1. Sutton, K.L., Sutton, R.M.C. and Caruso, J.A. (1997) Inductively coupled plasma mass spectrometric detection for chromatography and capillary electrophoresis. *J. Chromatogr. A*, **789**, 85–126.

2. Cornelis, R., Caruso, J.A., Crews, H. and Heumann, K.G. (Eds.) (2005) *Handbook of Elemental Speciation, II: Species in the Environment, Food, Medicine and Occupational Health*. Wiley Publishers, New York, USA.
3. Axelsson, B.O., Jornten-Karlsson, M., Michelsen, P. and Abou-Shakra, F. (2001) The potential of inductively coupled plasma mass spectrometry detection for high-performance liquid chromatography combined with accurate mass measurement of organic pharmaceutical compounds. *Rapid Commun. Mass Spectrom.*, **15**, 375–385.
4. Butler, O.T., Cook, J.M., Harrington, C.F., Hill, S.J., Rieuwerts, J. and Miles, D.L. (2005) Atomic spectrometry update. Environmental analysis. *J. Anal. Atom. Spectrom.*, **20**, 130–157.
5. Wang, C.F., Yang, J.Y. and Ke, C.H. (1996) Multi-element analysis of airborne particulate matter by various spectrometric methods after microwave digestion. *Anal. Chim. Acta*, **320**, 207–216.
6. Beary, E.S., Paulsen, P.J., Jassie, L.B. and Fassett, J.D. (1997) Determination of environmental lead using continuous-flow microwave digestion isotope dilution inductively coupled plasma mass spectrometry. *Anal. Chem.*, **69**, 758–766.
7. Halmos, P., Borszeki, J., Szabo, S. and Halmos, E. (2005) Direct analysis of fly ash materials by inductively coupled plasma atomic emission spectrometry using slurry nebulization. *Microchem. J.*, **79**, 25–28.
8. Senaratne, I. and Shooter, D. (2004) Elemental composition in source identification of brown haze in Auckland, New Zealand. *Atmos. Environ.*, **38**, 3049–3059.
9. Alvarez, F.F., Rodriguez, M.T., Espinosa, A.J.F. and Daban, A.G. (2004) Physical speciation of arsenic, mercury, lead, cadmium and nickel in inhalable atmospheric particles. *Anal. Chim. Acta*, **524**, 33–40.
10. Abdul-Wahab, S.A. and Yaghi, B. (2004) Total suspended dust and heavy metal levels emitted from a workplace compared with nearby residential houses. *Atmos. Environ.*, **38**, 745–750.
11. Kanitsar, K., Koellensperger, G., Hann, S., Limbeck, A., Puxbaum, H. and Stingeder, G. (2003) Determination of Pt, Pd and Rh by inductively coupled plasma sector field mass spectrometry (ICP-SFMS) in size-classified urban aerosol samples. *J. Anal. Atom. Spectrom.*, **18**, 239–246.
12. Pedersen, E.K., Bjørseth, O., Syversen, T. and Mathiesen, M. (2003) A screening assessment of emissions of volatile organic compounds and particles from heated indoor dust samples. *Indoor Air*, **13**, 106–117.
13. Kyotani, T. and Iwatsuki, M. (2002) Characterization of soluble and insoluble components in PM_{2.5} and PM₁₀ fractions of airborne particulate matter in Kofu city, Japan. *Atmos. Environ.*, **36**, 639–649.
14. Espinosa, A.J.F., Rodriguez, M.T., Rosa, F.J.B.d.I. and Sanchez, J.C.J. (2002) A chemical speciation of trace metals for fine urban particles. *Atmos. Environ.*, **36**, 773–780.
15. Ludke, C., Hoffmann, E., Skole, J. and Kriews, M. (1999) Determination of trace metals in size fractionated particles from arctic air by electrothermal vaporization inductively coupled plasma mass spectrometry. *J. Anal. Atom. Spectrom.*, **14**, 1685–1690.
16. Bettinelli, M., Spezia, S., Baroni, U. and Bizzarri, G. (1998) Determination of trace elements in power plant emissions by inductively coupled plasma mass spectrometry: comparison with other spectrometric techniques. *Microchem. J.*, **59**, 203–218.
17. Schwarz, A. and Heumann, K.G. (2002) Two-dimensional on-line detection of brominated and iodinated volatile organic compounds by ECD and ICP-MS after GC separation. *Anal. Bioanal. Chem.*, **374**, 212–219.
18. Pavageau, M., Pecheyran, C., Demange, M. and Donard, O.F.X. (2003) Phosphine emission measurements from a tobacco factory using cryogenic sampling and GC-ICP-MS analysis. *J. Anal. Atom. Spectrom.*, **18**, 323–329.
19. Pecheyran, C., Quétel, C.R., Lecuyer, F.M.M. and Donard, O.F.X. (1998) Simultaneous determination of volatile metal (Pb, Hg, Sn, In, Ga) and nonmetal species (Se, P, As) in different atmospheres by cryofocusing and detection by ICPMS. *Anal. Chem.*, **70**, 2639–2645.

20. Farmer, O.T., Barinaga, C.J. and Koppenaal, D.W. (1998) Determination of I-129 in ambient air by inductively coupled plasma mass spectrometry (ICP/MS). *J. Radioanal. Nucl. Ch.*, **234**, 153–157.
21. Hidalgo, M.M., Gomez, M.M. and Palacios, M.A. (1996) Trace enrichment and measurement of platinum by flow injection inductively coupled plasma mass spectrometry. *Anal. Bioanal. Chem.*, **354**, 420–423.
22. Hastings, D.W., Emerson, S.R. and Nelson, B.K. (1996) Determination of picogram quantities of vanadium in calcite and seawater by isotope dilution inductively coupled plasma mass spectrometry with electrothermal vaporization. *Anal. Chem.*, **68**, 371–377.
23. Koppenaal, D.W., Eiden, G.C. and Barinaga, C.J. (2004) Collision and reaction cells in atomic mass spectrometry: development, status, and applications. *J. Anal. Atom. Spectrom.*, **19**, 561–570.
24. Tanner, S.D., Baranov, V.I. and Bandura, D.R. (2002) Reaction cells and collision cells for ICP-MS: a tutorial review. *Spectrochim. Acta B*, **57**, 1361–1452.
25. Tanner, S.D., Baranov, V.I. and Vollkopf, U. (2000) A dynamic reaction cell for inductively coupled plasma mass spectrometry (ICP-DRC-MS). *J. Anal. Atom. Spectrom.*, **15**, 1261–1269.
26. McCurdy, E. and Woods, G. (2004) The application of collision/reaction cell inductively coupled plasma mass spectrometry to multi-element analysis in variable sample matrices, using He as a non-reactive cell gas. *J. Anal. Atom. Spectrom.*, **19**, 607–615.
27. Moldovan, M., Krupp, E.M., Holliday, A.E. and Donard, O.F.X. (2004) High resolution sector field ICP-MS and multicollector ICP-MS as tools for trace metal speciation in environmental studies: a review. *J. Anal. Atom. Spectrom.*, **19**, 815–822.
28. Eiden, G.C., Barinaga, C.J. and Koppenaal, D.W. (1997) Beneficial ion/molecule reactions in elemental mass spectrometry. *Rapid Commun. Mass Sp.*, **11**, 37–42.
29. Koppenaal, D.W. and Eiden, G.C. (2004) Foreword: collision and reaction cell techniques in atomic mass spectrometry. *J. Anal. Atom. Spectrom.*, **19**, 15N.
30. Sutton, K.L. and Caruso, J.A. (1997) *Inductively Coupled Plasma Spectrometry and Its Applications*, Sheffield, UK.
31. Leon, C.A.P.d., Montes-Bayon, M. and Caruso, J.A. (2002) Elemental speciation by chromatographic separation with inductively coupled plasma mass spectrometry detection. *J. Chromatogr. A*, **974**, 1–21.
32. Ackley, K.L., Sutton, K.L. and Caruso, J.A. (2000) *Comprehensive Analytical Chemistry*. Ed. D. Barcelo. Volume XXXIII, Elemental speciation, new approaches for trace element analysis. Elsevier, Amsterdam.
33. Olesik, J.W., Kinzer, J.A., Grunwald, E.J., Thaxton, K.K. and Olesik, S.V. (1998) The potential and challenges of elemental speciation by capillary electrophoresis-inductively coupled plasma mass spectrometry and electrospray or ion spray mass spectrometry. *Spectrochim. Acta B*, **53**, 239–251.
34. Lyven, B., Hasselov, M., Turner, D.R., Haraldsson, C. and Andersson, K. (2003) Competition between iron- and carbon-based colloidal carriers for trace metals in a freshwater assessed using flow field-flow fractionation coupled to ICPMS. *Geochim. Cosmochim. Ac.*, **67**, 3791–3802.
35. Wuilloud, J.C.A., Wuilloud, R.G., Vonderheide, A.P. and J.A. Caruso (2004) Gas chromatography/plasma spectrometry – an important analytical tool for elemental speciation studies. *Spectrochim. Acta B*, **59**, 755–792.
36. Jitaru, P., Infante, H.G. and Adams, F.C. (2004) Simultaneous multi-elemental speciation analysis of organometallic compounds by solid-phase microextraction and multicapillary gas chromatography hyphenated to inductively coupled plasma-time-of-flight-mass spectrometry. *J. Anal. Atom. Spectrom.*, **19**, 867–875.
37. Sanchez-Rodas, D., Gomez-Ariza, J.L., Giraldez, I., Velasco, A. and Morales, E. (2005) Arsenic speciation in river and estuarine waters from southwest Spain. *Sci. Total Environ.*, **345**, 207–217.
38. Jitmanee, K., Oshima, M. and Motomizu, S. (2005) Speciation of arsenic(III) and arsenic(V) by inductively coupled plasma-atomic emission spectrometry coupled with preconcentration system. *Talanta*, **66**, 529–533.

39. Hollibaugh, J.T., Carini, S., Gurleyuk, H., Jellison, R., Joye, S.B., LeClerc, G., Meile, C., Vasquez, L. and Wallschlaeger, D. (2005) Arsenic speciation in Mono Lake, California: response to seasonal stratification and anoxia. *Geochim. Cosmochim. Ac.*, **69**, 1925–1937.
40. Yasuyuki, S., Katsuaki, T., Sumiko, K., Chieko, U., Hiroe, I. and Masatoshi, M. (2005) Analysis of diphenylarsinic acid in human and environmental samples by HPLC-ICP-MS. *Appl. Organomet. Chem.*, **19**, 276–281.
41. Kenji, K., Yasuo, S., Chiseko, S., Mutsuo, I., Koichi, K., Osamu, S., Hiroyasu, I., Masatoshi, M., Takafumi, O. and Toshikazu, K. (2005) Determination of diphenylarsinic acid and phenylarsonic acid, the degradation products of organoarsenic chemical warfare agents, in well water by HPLC-ICP-MS. *Appl. Organomet. Chem.*, **19**, 287–293.
42. Bednar, A.J., Garbarino, J.R., Burkhardt, M.R., Ranville, J.F. and Wildeman, T.R. (2004) Field and laboratory arsenic speciation methods and their application to natural-water analysis. *Water Res.*, **38**, 355–364.
43. Xie, Q., Kerrich, R., Irving, E., Liber, K. and Abou-Shakra, F. (2002) Determination of five arsenic species in aqueous samples by HPLC coupled with a hexapole collision cell ICP-MS. *J. Anal. Atom. Spectrom.*, **17**, 1037–1041.
44. Shraim, A., Sekaran, N.C., Anuradha, C.D. and Hirano, S. (2002) Speciation of arsenic in tube-well water samples collected from West Bengal, India, by high-performance liquid chromatography–inductively coupled plasma mass spectrometry. *Appl. Organomet. Chem.*, **16**, 202–209.
45. Ellwood, M.J. and Maher, W.A. (2002) An automated hydride generation-cryogenic trapping-ICP-MS system for measuring inorganic and methylated Ge, Sb and As species in marine and fresh waters. *J. Anal. Atom. Spectrom.*, **17**, 197–203.
46. Balarama, K.M.V., Chandrasekaran, K., Rao, S.V., Karunasagar, D. and Arunachalam, J. (2005) Speciation of Cr(III) and Cr(VI) in waters using immobilized moss and determination by ICP-MS and FAAS. *Talanta*, **65**, 135–143.
47. Yeh, C.-F. and Jiang, S.-J. (2004) Speciation of V, Cr and Fe by capillary electrophoresis – bandpass reaction cell inductively coupled plasma mass spectrometry. *J. Chromatogr. A.*, **1029**, 255–261.
48. Yalcin, S. and Apak, R. (2004) Chromium(III, VI) speciation analysis with preconcentration on a maleic acid-functionalized XAD sorbent. *Anal. Chim. Acta*, **505**, 25–35.
49. Gine, M.F., Gervasio, A.P.G., Lavorante, A.F., Miranda, C.E.S. and Carrilho, E. (2002) Interfacing flow injection with capillary electrophoresis and inductively coupled plasma mass spectrometry for Cr speciation in water samples. *J. Anal. Atom. Spectrom.*, **17**, 736–738.
50. Martinez-Bravo, Y., Roig-Navarro, A.F., Lopez, F.J. and Hernandez, F. (2001) Multielemental determination of arsenic, selenium and chromium(VI) species in water by high-performance liquid chromatography – inductively coupled plasma mass spectrometry. *J. Chromatogr. A.*, **926**, 265–274.
51. Chang, Y.-L. and Jiang, S.-J. (2001) Determination of chromium species in water samples by liquid chromatography-inductively coupled plasma-dynamic reaction cell-mass spectrometry. *J. Anal. Atom. Spectrom.*, **16**, 858–862.
52. Yan, X.-P., Hendry, M.J. and Kerrich, R. (2000) Speciation of dissolved iron(III) and iron(II) in water by on-line coupling of flow injection separation and preconcentration with inductively coupled plasma mass spectrometry. *Anal. Chem.*, **72**, 1879–1884.
53. Garcia-Sanchez, R., Feldhaus, R., Bettmer, J. and Ebdon, L. (2001) Lead speciation in rainwater samples by modified fused silica capillaries coupled to a direct injection nebulizer (DIN) for sample introduction in ICP-MS. *J. Anal. Atom. Spectrom.*, **16**, 1028–1034.
54. Ebdon, L., Hill, S.J. and Rivas, C. (1998) Lead speciation in rainwater by isotope dilution-high performance liquid chromatography-inductively coupled plasma-mass spectrometry. *Spectrochim. Acta B.*, **53**, 289–297.
55. Heisterkamp, M. and Adams, F.C. (2001) Gas chromatography – inductively coupled plasma – time-of-flight mass spectrometry for the speciation analysis of organolead compounds in environmental water samples. *Anal. Bioanal. Chem.*, **370**, 597–605.

56. Monperrus, M., Tessier, E., Veschambre, S., Amouroux, D. and Donard, O. (2005) Simultaneous speciation of mercury and butyltin compounds in natural waters and snow by propylation and species-specific isotope dilution mass spectrometry analysis. *Anal. Bioanal. Chem.*, **381**, 854–862.
57. Lambertsson, L. and Bjoern, E. (2004) Validation of a simplified field-adapted procedure for routine determinations of methyl mercury at trace levels in natural water samples using species-specific isotope dilution mass spectrometry. *Anal. Bioanal. Chem.*, **380**, 871–875.
58. Bravo-Sanchez, L.R., Encinar, J.R., Fidalgo, M., Jose, I. and Sanz-Medel, A. (2004) Mercury speciation analysis in sea water by solid phase microextraction – gas chromatography – inductively coupled plasma mass spectrometry using ethyl and propyl derivatization. Matrix effects evaluation. *Spectrochim. Acta B*, **59**, 59–66.
59. Demuth, N. and Heumann, K.G. (2001) Validation of methylmercury determinations in aquatic systems by alkyl derivatization methods for GC analysis using ICP-IDMS. *Anal. Chem.*, **73**, 4020–4027.
60. Blanco, R.M., Villanueva, M.T., Uria, J.E.S. and Sanz-Medel, A. (2000) Field sampling, preconcentration and determination of mercury species in river waters. *Anal. Chim. Acta*, **419**, 137–144.
61. Hann, S., Stefanka, Z., Lenz, K. and Stingeder, G. (2005) Novel separation method for highly sensitive speciation of cancerostatic platinum compounds by HPLC-ICP-MS. *Anal. Bioanal. Chem.*, **381**, 405–412.
62. Lustig, S., Michalke, B., Beck, W. and Schramel, P. (1998) Platinum speciation with hyphenated techniques: high performance liquid chromatography and capillary electrophoresis on-line coupled to an inductively coupled plasma-mass spectrometer – application to aqueous extracts from a platinum treated soil. *Anal. Bioanal. Chem.*, **360**, 18–25.
63. Darrouzes, J., Bueno, M., Lespes, G. and Potin-Gautier, M. (2005) Operational optimisation of ICP – octopole collision/reaction cell – MS for applications to ultratrace selenium total and speciation determination. *J. Anal. Atom. Spectrom.*, **20**, 88–94.
64. Wallschläger, D. and London, J. (2004) Determination of inorganic selenium species in rain and sea waters by anion exchange chromatography-hydride generation-inductively-coupled plasma-dynamic reaction cell-mass spectrometry (AEC-HG-ICP-DRC-MS). *J. Anal. Atom. Spectrom.*, **19**, 1119–1127.
65. Yu, C., Cai, Q., Guo, Z.-X., Yang, Z. and Khoo, S.B. (2004) Simultaneous speciation of inorganic selenium and tellurium by inductively coupled plasma mass spectrometry following selective solid-phase extraction separation. *J. Anal. Atom. Spectrom.*, **19**, 410–413.
66. Bueno, M. and Potin-Gautier, M. (2002) Solid-phase extraction for the simultaneous preconcentration of organic (selenocystine) and inorganic [Se(IV), Se(VI)] selenium in natural waters. *J. Chromatogr. A*, **963**, 185–193.
67. Wallschläger, D. and Roehl, R. (2001) Determination of inorganic selenium speciation in waters by ion chromatography-inductively coupled plasma-mass spectrometry using eluant elimination with a membrane suppressor. *J. Anal. Atom. Spectrom.*, **16**, 922–925.
68. Tseng, C.M., Amouroux, D., Brindle, I.D. and Donard, O.F.X. (2000) Field cryofocussing hydride generation applied to the simultaneous multi-elemental determination of alkyl-metal(loid) species in natural waters using ICP-MS detection. *J. Environ. Monitor.*, **2**, 603–612.
69. Amouroux, D., Tessier, E. and Donard, O.F.X. (2000) Volatilization of organotin compounds from estuarine and coastal environments. *Environ. Sci. Technol.*, **34**, 988–995.
70. Tao, H., Rajendran, R.B., Quetel, C.R., Nakazato, T., Tominaga, M. and Miyazaki, A. (1999) Tin speciation in the femtogram range in open ocean seawater by gas chromatography/inductively coupled plasma mass spectrometry using a shield torch at normal plasma conditions. *Anal. Chem.*, **71**, 4208–4215.
71. Fan, Z., Hu, B. and Jiang, Z. (2005) Speciation analysis of vanadium in natural water samples by electrothermal vaporization inductively coupled plasma optical emission spectrometry after separation/preconcentration with thenoyltrifluoroacetone immobilized on microcrystalline naphthalene. *Spectrochim. Acta B*, **60**, 65–71.

72. Wuilloud, R.G., Wuilloud, J.C., Olsina, R.A. and Martinez, L.D. (2001) Speciation and preconcentration of vanadium(v) and vanadium(iv) in water samples by flow injection-inductively coupled plasma optical emission spectrometry and ultrasonic nebulization. *Analyst*, **126**, 715–719.
73. Wann, C.-C. and Jiang, S.-J. (1997) Determination of vanadium species in water samples by liquid chromatography-inductively coupled plasma mass spectrometry. *Anal. Chim. Acta*, **357**, 211–218.
74. Sadi, B.B.M., Vonderheide, A.P. and Caruso, J.A. (2004) Analysis of phosphorus herbicides by ion-pairing reversed-phase liquid chromatography coupled to inductively coupled plasma mass spectrometry with octapole reaction cell. *J. Chromatogr. A*, **1050**, 95–101.
75. Vonderheide, A.P., Meija, J., Montes-Bayon, M. and Caruso, J.A. (2003) Use of optional gas and collision cell for enhanced sensitivity of the organophosphorus pesticides by GC-ICP-MS. *J. Anal. Atom. Spectrom.*, **18**, 1097–1102.
76. Wuilloud, R.G., Shah, M., Kannamkumarath, S.S. and Altamirano, J.C. (2005) The potential of inductively coupled plasma-mass spectrometric detection for capillary electrophoretic analysis of pesticides. *Electrophoresis*, **26**, 1598–1605.
77. Divjak, B. and Goessler, W. (1999) Ion chromatographic separation of sulfur-containing inorganic anions with an ICP-MS as element-specific detector. *J. Chromatogr. A*, **844**, 161–169.
78. Dudoit, A. and Pergantis, S.A. (2001) Ion chromatography in series with conductivity detection and inductively coupled plasma mass spectrometry for the determination of nine halogen, metalloid and nonmetal species in drinking water. *J. Anal. Atom. Spectrom.*, **16**, 575–580.
79. Wuilloud, R.G., Wuilloud, J.C.A., Vonderheide, A.P. and Caruso, J.A. (2003) Determination of iodinated phenol species at parts-per-trillion concentration levels in different water samples by solid-phase microextraction/offline GC-ICP-MS. *J. Anal. Atom. Spectrom.*, **18**, 1119–1124.
80. Schwehr, K.A. and Santschi, P.H. (2003) Sensitive determination of iodine species, including organo-iodine, for freshwater and seawater samples using high performance liquid chromatography and spectrophotometric detection. *Anal. Chim. Acta*, **482**, 59–71.
81. Radlinger, G. and Heumann, K.G. (2000) Transformation of iodide in natural and wastewater systems by fixation on humic substances. *Environ. Sci. Technol.*, **34**, 3932–3936.
82. Heumann, K.G., Radlinger, G., Erbes, M., Heiber, I., Obst, U., Filip, Z. and Claus, H. (2000) Ageing of dissolved halogenated humic substances and the microbiological influence on this process. *Acta Hydroch. Hydrob.*, **28**, 193–201.
83. Radlinger, G. and Heumann, K.G. (1997) Determination of halogen species of humic substances using HPLC/ICP-MS coupling. *Anal. Bioanal. Chem.*, **359**, 430–433.
84. Seubert, A., Schminke, G., Nowak, M., Ahrer, W. and Buchberger, W. (2000) Comparison of on-line coupling of ion-chromatography with atmospheric pressure ionization mass spectrometry and with inductively coupled plasma mass spectrometry as tools for the ultra-trace analysis of bromate in surface water samples. *J. Chromatogr. A*, **884**, 191–199.
85. Sturup, S. (2004) The use of ICPMS for stable isotope tracer studies in humans: a review. *Anal. Bioanal. Chem.*, **378**, 273–282.
86. Griffin, I.J. (2002) Using stable isotopes and isotope ratio mass spectrometry to study mineral metabolism in humans. *J. Anal. Atom. Spectrom.*, **17**, 1186–1193.
87. Moreton, J.A. and Delves, H.T. (1999) Use of Virkon as a disinfectant for clinical samples carrying a high risk of infection in inductively coupled plasma mass spectrometry. *J. Anal. Atom. Spectrom.*, **14**, 893–894.
88. Taylor, A., Branch, S., Halls, D.J., Owen, L.M.W. and White, M. (1999) Clinical and biological materials, foods and beverages. *J. Anal. Atom. Spectrom.*, **14**, 717–781.
89. Taylor, A., Branch, S., Halls, D.J., Owen, L.M.W. and White, M. (2000) Clinical and biological materials, foods and beverages. *J. Anal. Atom. Spectrom.*, **15**, 451–487.
90. Taylor, A., Branch, S., Fisher, A., Halls, D. and White, M. (2001) Atomic spectrometry update. Clinical and biological materials, foods and beverages. *J. Anal. Atom. Spectrom.*, **16**, 421–446.

91. Taylor, A., Branch, S., Halls, D., Patriarca, M. and White, M. (2002) Atomic spectrometry update. Clinical and biological materials, foods and beverages. *J. Anal. Atom. Spectrom.*, **17**, 414–455.
92. Taylor, A., Branch, S., Halls, D., Patriarca, M. and White, M. (2004) Atomic spectrometry update. Clinical and biological materials, foods and beverages. *J. Anal. Atom. Spectrom.*, **19**, 505–556.
93. Lombaert, N., Boeck, M.D., Decordier, I., Cundari, E., Lison, D. and Kirsch-Volders, M. (2004) Evaluation of the apoptogenic potential of hard metal dust (WC-Co), tungsten carbide and metallic cobalt. *Toxicol. Lett.*, **154**, 23–34.
94. Frisk, P., Yaqob, A., Nilsson, K., Carlsson, J. and Lindh, U. (2000) Differences in the growth inhibition of cultured K-562 cells by selenium, mercury or cadmium in two tissue culture media (RPMI-1640, Ham's F-10). *BioMetals*, **13**, 101–111.
95. Frisk, P., Yaqob, A., and Lindh, U. (2002) Indications of selenium protection against cadmium toxicity in cultured K-562 cells. *Sci. Total Environ.*, **296**, 189–197.
96. Lin, Y.W., Chuang, S.M. and Yang, J.L. (2003) Persistent activation of ERK1/2 by lead acetate increases nucleotide excision repair synthesis and confers anti-cytotoxicity and anti-mutagenicity. *Carcinogenesis*, **24**, 53–61.
97. Liang, X. and Huang, Y. (2002) Physical state changes of membrane lipids in human lung adenocarcinoma A549 cells and their resistance to cisplatin. *Int. J. Biochem. Cell B.*, **34**, 1248–1255.
98. Bredfeldt, T.G., Kopplin, M.J. and Gandolfi, A.J. (2004) Effects of arsenite on UROtsa cells: low-level arsenite causes accumulation of ubiquitinated proteins that is enhanced by reduction in cellular glutathione levels. *Toxicol. Appl. Pharm.*, **198**, 412–418.
99. Moens, L. (1997) Applications of mass spectrometry in the trace element analysis of biological materials. *Anal. Bioanal. Chem.*, **359**, 309–316.
100. Jakubowski, N., Moens, L. and Vanhaecke, F. (1998) Sector field mass spectrometers in ICP-MS. *Spectrochim. Acta B.*, **53**, 1739–1763.
101. Marchante-Gayon, J.M., Muniz, C.S., Alonso, J.I.G. and Sanz-Medel, A. (1999) Multielemental trace analysis of biological materials using double focusing inductively coupled plasma mass spectrometry detection. *Anal. Chim. Acta*, **400**, 307–320.
102. Gellein, K., Garruto, R.M., Syversen, T., Sjobakk, T.E. and Flaten, T.P. (2003) Concentrations of Cd, Co, Cu, Fe, Mn, Rb, V and Zn in formalin-fixed brain tissue in amyotrophic lateral sclerosis and parkinsonism-dementia complex of guam determined by high-resolution ICP-MS. *Biol. Trace Elem. Res.*, **96**, 39–60.
103. Melo, T.M., Larsen, C., White, L.R., Aasly, J., Sjobakk, T.E., Flaten, T.P., Sonnewald, U. and Syversen, T. (2003) Manganese, copper, and zinc in cerebrospinal fluid from patients with multiple sclerosis. *Biol. Trace Elem. Res.*, **93**, 1–8.
104. Ingle, C., Langford, N., Harvey, L., Dainty, J.R., Armah, C., Fairweather-Tait, S., Sharp, B., Rose, M., Crews, H. and Lewis, J. (2002) An ICP-MS methodology using a combined high-resolution/multi-collector detector system for the measurement of total zinc and zinc isotope ratios in faecal samples from a human nutrition study. *J. Anal. Atom. Spectrom.*, **17**, 1502–1505.
105. Stenberg, A., Malinovsky, D., Rodushkin, I., Andren, H., Ponter, C., Ohlander, B. and Baxter, D.C. (2003) Separation of Fe from whole blood matrix for precise isotopic ratio measurements by MC-ICP-MS: a comparison of different approaches. *J. Anal. Atom. Spectrom.*, **18**, 23–28.
106. Benkhedda, K., Dimitrova, B., Infante, H.G., Ivanova, E. and Adams, F.C. (2003) Simultaneous on-line preconcentration and determination of Pb, Rh and Pt in urine, serum and road dust by flow injection combined with inductively coupled plasma time-of-flight mass spectrometry. *J. Anal. Atom. Spectrom.*, **18**, 1019–1025.
107. Centineo, G., Bayon, M.M. and Sanz-Medel, A. (2000) Flow injection analysis with inductively coupled plasma time-of-flight mass spectrometry for the simultaneous determination of elements forming hydrides and its application to urine. *J. Anal. Atom. Spectrom.*, **15**, 1357–1362.
108. Bandura, D.R., Ornatsky, O.I. and Liao, L. (2004) Characterization of phosphorus content of biological samples by ICP-DRC-MS: potential tool for cancer research. *J. Anal. Atom. Spectrom.*, **19**, 96–100.

109. Rodushkin, I. and Axelsson, M.D. (2003) Application of double focusing sector field ICP-MS for multielemental characterization for human hair and nails. Part III. Direct analysis by laser ablation. *Sci. Total Environ.*, **305**, 23–39.
110. Cox, A., Keenan, F., Cooke, M. and Appleton, J. (1996) Trace element profiling of dental tissues using laser ablation-inductively coupled plasma-mass spectrometry. *Anal. Bioanal. Chem.*, **354**, 254–258.
111. Lochner, F., Appleton, J., Keenan, F. and Cooke, M. (1999) Multi-element profiling of human deciduous teeth by laser ablation-inductively coupled plasma-mass spectrometry. *Anal. Chim. Acta*, **401**, 299–306.
112. Lee, K.M., Appleton, J., Cooke, M., Keenan, F. and Sawicka-Kapusta, K. (1999) Use of laser ablation inductively coupled plasma mass spectrometry to provide element versus time profiles in teeth. *Anal. Chim. Acta*, **395**, 179–185.
113. Hoffmann, E., Stephanowitz, H., Ullrich, E., Skole, J., Ludke, C. and Hoffmann, B. (2000) Investigation of mercury migration in human teeth using spatially resolved analysis by laser ablation-ICP-MS. *J. Anal. Atom. Spectrom.*, **15**, 663–667.
114. Ghazi, A.M., Shuttleworth, S., Angulo, S.J. and Pashley, D.H. (2000) New applications for laser ablation high resolution ICP-MS (LA-HR-ICP-MS): quantitative measurements of gallium diffusion across human root dentin. *J. Anal. Atom. Spectrom.*, **15**, 1335–1341.
115. Prohaska, T., Latkoczy, C., Schultheis, G., Teschler-Nicola, M. and Stingeder, G. (2002) Investigation of Sr isotope ratios in prehistoric human bones and teeth using laser ablation ICP-MS and ICP-MS after Rb/Sr separation. *J. Anal. Atom. Spectrom.*, **17**, 887–891.
116. Legrand, M., Lam, R., Jensen-Fontaine, M., Salin, E.D. and Chan, H.M. (2004) Direct detection of mercury in single human hair strands by laser ablation inductively coupled plasma mass spectrometry (LA-ICP-MS). *J. Anal. Atom. Spectrom.*, **19**, 1287–1288.
117. Neilsen, J.L., Abildtrup, A., Christensen, J., Watson, P., Cox, A. and McLeod, C.W. (1998) Laser ablation inductively coupled plasma-mass spectrometry in combination with gel electrophoresis: a new strategy for speciation of metal binding serum proteins. *Spectrochim. Acta B.*, **53**, 339–345.
118. Parsons, P.J., Zhou, Y., Palmer, C.D., Aldous, K.M. and Brockman, P. (2002) Atomization and vaporization of lead from a blood matrix using rhodium-coated tungsten filaments with pseudo-simultaneous electrothermal atomic absorption and inductively coupled plasma mass spectrometric measurements. *J. Anal. Atom. Spectrom.*, **18**, 4–10.
119. Lee, K.H., Jiang, S.J. and Liu, H.W. (1998) Determination of mercury in urine by electrothermal vaporization isotope dilution inductively coupled plasma mass spectrometry. *J. Anal. Atom. Spectrom.*, **13**, 1227–1231.
120. Chang, C.C. and Jiang, S.J. (1997) Determination of copper, cadmium and lead in biological samples by electrothermal vaporization isotope dilution inductively coupled plasma mass spectrometry. *J. Anal. Atom. Spectrom.*, **12**, 75–80.
121. Lee, K.H., Liu, S.H. and Jiang, S.J. (1998) Determination of cadmium and lead in urine by electrothermal vaporization isotope dilution inductively coupled plasma mass spectrometry. *Analyst*, **123**, 1557–1560.
122. Pozebon, D., Dressler, V.L. and Curtius, A.J. (1998) Determination of arsenic, selenium and lead by electrothermal vaporization inductively coupled plasma mass spectrometry using iridium-coated graphite tubes. *J. Anal. Atom. Spectrom.*, **13**, 7–11.
123. Buseth, E., Wibetoe, G. and Martinsen, I. (1998) Determination of endogenous concentrations of the lanthanides in body fluids and tissues using electrothermal vaporization inductively coupled plasma mass spectrometry. *J. Anal. Atom. Spectrom.*, **13**, 1039–1049.
124. Turner, J., Hill, S.J., Evans, E.H. and Fairman, B. (1999) The use of ETV-ICP-MS for the determination of selenium in serum. *J. Anal. Atom. Spectrom.*, **14**, 121–126.

125. Turner, J., Hill, S.J., Evans, E.H., Fairman, B. and Briche, C.S.J.W. (2000) Accurate analysis of selenium in water and serum using ETV-ICP-MS with isotope dilution. *J. Anal. Atom. Spectrom.*, **15**, 743–746.
126. Yu, L., Koirtiyohann, R., Rueppel, M.L., Skipor, A.K. and Jacobs, J.J. (1997) Simultaneous determination of aluminium, titanium and vanadium in serum by electrothermal vaporization-inductively coupled plasma mass spectrometry. *J. Anal. Atom. Spectrom.*, **12**, 69–74.
127. Sanz-Medel, A. (1998) Trace element analytical speciation in biological systems: importance, challenges and trends. *Spectrochim. Acta B.*, **53**, 197–211.
128. Templeton, D.M. (2003) The importance of trace element speciation in biomedical science. *Anal. Bioanal. Chem.*, **375**, 1062–1066.
129. Gomez-Ariza, J.L., Garcia-Barrera, T., Lorenzo, F., Bernal, V., Villegas, M.J. and Oliveira, V. (2004) Use of mass spectrometry techniques for the characterization of metal bound to proteins (metalloomics) in biological systems. *Anal. Chim. Acta*, **524**, 15–22.
130. Sanz-Medel, A., Montes-Bayon, M. and Sanchez, M.L.F. (2003) Trace element speciation by ICP-MS in large biomolecules and its potential for proteomics. *Anal. Bioanal. Chem.*, **377**, 236–247.
131. Szpunar, J. (2000) Bio-inorganic speciation analysis by hyphenated techniques. *Analyst*, **125**, 963–988.
132. Gui-Bin, J., Qun-Fang, Z., and Bin, H. (2000) Tin compounds and major trace elements in organotin-poisoned patient's urine and blood measured by gas chromatography-flame photometric detector and inductively coupled plasma-mass spectrometry. *B. Environ. Contam. Tox.*, **65**, 277–284.
133. Gui-Bin, J., Qun-Fang, Z. and Bin, H. (2000) Speciation of organotin compounds, total tin, and major trace metal elements in poisoned human organs by gas chromatography-flame photometric detector and inductively coupled plasma-mass spectrometry. *Environ. Sci. Technol.*, **34**, 2697–2702.
134. Feldmann, J., Riechmann, T. and Hirner, A.V. (1996) Determination of organometallics in intra-oral air by LT-GC/ICP-MS. *Anal. Bioanal. Chem.*, **354**, 620–623.
135. Rodriguez-Fernandez, J., Montes-Bayon, M., Pereiro, R. and Sanz-Medel, A. (2001) Gas chromatography double focusing sector-field ICP-MS as an innovative tool for bad breath research. *J. Anal. Atom. Spectrom.*, **16**, 1051–1056.
136. Remy, R.R.d.l.F.S., Montes-Bayon, M. and Sanz-Medel, A. (2003) Determination of total homocysteine in human serum by capillary gas chromatography with sulfur-specific detection by double-focusing ICP-MS. *Anal. Bioanal. Chem.*, **377**, 299–305.
137. Lustig, S., Lampaert, D., Cremer, K.D., Kimpe, J.D., Cornelis, R. and Schramel, P. (1999) Capability of flatbed electrophoresis (IEF and native PAGE) combined with sector field ICP-MS and autoradiography for the speciation of Cr, Ga, In, Pt, and V in incubated serum samples. *J. Anal. Atom. Spectrom.*, **14**, 1357–1362.
138. Michalke, B. and Schramel, P. (1998) Application of capillary zone electrophoresis-inductively coupled plasma mass spectrometry and capillary isoelectric focusing-inductively coupled plasma mass spectrometry for selenium speciation. *J. Chromatogr. A.*, **807**, 71–80.
139. Michalke, B. and Schramel, P. (1999) Iodine speciation in biological samples by capillary electrophoresis – inductively coupled plasma mass spectrometry. *Electrophoresis*, **20**, 2547–2553.
140. Holderbeke, M.V., Zhao, Y., Vanhaecke, F., Dams, R. and Sandra, P. (1999) Speciation of six arsenic compounds using capillary electrophoresis-inductively coupled plasma mass spectrometry. *J. Anal. Atom. Spectrom.*, **14**, 229–234.
141. Minami, T., Ichida, S. and Kubo, K. (2002) Study of metallothionein using capillary zone electrophoresis. *J. Chromatogr. B.*, **781**, 303–311.
142. Timerbaev, A.R., Aleksenko, S.S., Polec-Pawlak, K., Ruzik, R., Semenova, O., Hartinger, C.G., Oszwaldowski, S., Galanski, M., Jarosz, M. and Keppler, B.K. (2004) Platinum metallodrug-protein

- binding studies by capillary electrophoresis-inductively coupled plasma-mass spectrometry: characterization of interactions between Pt(II) complexes and human serum albumin. *Electrophoresis*, **25**, 1988–1995.
143. Guntinas, M.B.C., Bordin, G. and Rodriguez, A.R. (2002) Identification, characterization and determination of metal-binding proteins by liquid chromatography: a review. *Anal. Bioanal. Chem.*, **374**, 369–378.
144. Kotrebai, M., Tyson, J.F., Block, E. and Uden, P.C. (2000) High-performance liquid chromatography of selenium compounds utilizing perfluorinated carboxylic acid ion-pairing agents and inductively coupled plasma and electrospray ionization mass spectrometric detection. *J. Chromatogr. A.*, **866**, 51–63.
145. Suzuki, K.T., Mandal, B.K. and Ogra, Y. (2002) Speciation of arsenic in body fluids. *Talanta*, **58**, 111–119.
146. Chatterjee, A., Shibata, Y., Yoshinaga, J. and Morita, M. (2001) Estimation of arsenobetaine in the NIES candidate certified references material no. 18 human urine by HPLC-ICP-MS using different chromatographic conditions. *Appl. Organomet. Chem.*, **15**, 306–314.
147. Wei, Z., Brockhoff-Schwegel, C.A. and Creed, J.T. (2000) Application of sample pre-oxidation or arsenite in human urine prior to speciation via on-line photo-oxidation with membrane hydride generation and ICP-MS detection. *Analyst*, **125**, 1215–1220.
148. Wei, Z., Brockhoff-Schwegel, C.A. and Creed, J.T. (2001) A comparison of urinary arsenic speciation via direct nebulization and on-line photo-oxidation-hydride generation with IC separation and ICP-MS detection. *J. Anal. Atom. Spectrom.*, **16**, 12–19.
149. Sloth, J.J., Larsen, E.H. and Julshamn, K. (2004) Selective arsenic speciation analysis of human urine reference materials using gradient elution ion-exchange HPLC-ICP-MS. *J. Anal. Atom. Spectrom.*, **19**, 973–978.
150. Mandal, B.K., Ogra, Y. and Suzuki, K.T. (2001) Identification of dimethylarsinous and monomethylarsonous acids in human urine of the arsenic-affected areas in West Bengal, India. *Chem. Res. Toxicol.*, **14**, 371–378.
151. Lintschinger, J., Schramel, P., Hatalak-Rauscher, A., Wendler, I. and Michalke, B. (1998) A new method for the analysis of arsenic species in urine by using HPLC-ICP-MS. *Anal. Bioanal. Chem.*, **362**, 313–318.
152. Samanta, G., Chowdhury, U.K., Mandal, B.K., Chakraborti, D., Sekaran, N.C., Tokunaga, H. and Ando, M. (2000) High performance liquid chromatography inductively coupled plasma mass spectrometry for the speciation of arsenic compounds in urine. *Microchem. J.*, **65**, 113–127.
153. Ritsema, R., Dukan, L., Navarro, T.R.I., Leeuwen, W.V., Oliveira, N., Wolfs, P. and Lebre, E. (1998) Speciation of arsenic compounds in urine by LC-ICP-MS. *Appl. Organomet. Chem.*, **12**, 591–599.
154. Goessler, W., Schlagenhaufen, C., Kuehnelt, D., Greschönig, H. and Irgolic, K.J. (1997) Can humans metabolize arsenic compounds to arsenobetaine? *Appl. Organomet. Chem.*, **11**, 327–335.
155. Wrobel, K., Wrobel, K., Parker, B., Kannamkumarath, S.S. and Caruso, J.A. (2002) Determination of As(III), As(V), monomethylarsonic acid, dimethylarsinic acid and arsenobetaine by HPLC-ICP-MS: analysis of reference materials, fish tissue and urine. *Talanta*, **58**, 899–907.
156. Ebdon, L., Fisher, A., Roberts, N.B. and Yaqoob, M. (1999) Determination of organoarsenic species in blood plasma by HPLC-ICP-MS. *Appl. Organomet. Chem.*, **13**, 183–187.
157. Kavanagh, P., Farago, M.E., Thornton, I., Goessler, W., Kuehnelt, D., Schlagenhaufen, C. and Irgolic, K.J. (1998) Urinary arsenic species in Devon and Cornwall residents, UK. A pilot study. *Analyst*, **123**, 27–29.
158. Nakazato, T., Taniguchi, T., Tao, H., Tominaga, M. and Miyazaki, A. (2000) Ion-exclusion chromatography combined with ICP-MS and hydride generation ICP-MS for the determination of arsenic species in biological matrices. *J. Anal. Atom. Spectrom.*, **15**, 1546–1552.
159. Moldovan, M., Gomez, M.M., Palacios, M.A. and Camara, C. (1998) Arsenic speciation in water and human urine by HPLC-ICP-MS and HPLC-MO-HG-AAS. *Microchem. J.*, **59**, 89–99.

160. Meza, M.M., Kopplin, M.J., Burgess, J.L. and Gandolfi, A.J. (2004) Arsenic drinking water exposure and urinary excretion among adults in the Yaqui Valley, Sonora, Mexico. *Environ. Res.*, **96**, 119–126.
161. Hulle, M.V., Zhang, C., Schotte, B., Mees, L., Vanhaecke, F., Vanholder, R., Zhang, X.R. and Cornelis, R. (2004) Identification of some arsenic species in human urine and blood after ingestion of Chinese seaweed *Laminaria*. *J. Anal. Atom. Spectrom.*, **19**, 58–64.
162. Lai, V.W.M., Sun, Y., Ting, E., Cullen, W.R. and Reimer, K.J. (2004) Arsenic speciation in human urine: are we all the same? *Toxicol. Appl. Pharm.*, **198**, 297–306.
163. Shibata, Y., Tsuzuku, K., Komori, S., Umedzu, C., Imai, H. and Morita, M. (2005) Analysis of diphenylarsinic acid in human and environmental samples by HPLC-ICP-MS. *Appl. Organomet. Chem.*, **19**, 276–281.
164. Ding, H., Wang, J., Dorsey, J.G. and Caruso, J.A. (1995) Arsenic speciation by micellar liquid chromatography with inductively coupled plasma mass spectrometric detection. *J. Chromatogr. A.*, **694**, 425–431.
165. Mandal, B.K., Ogra, Y. and Suzuki, K.T. (2003) Speciation of arsenic in human nail and hair from arsenic-affected area by HPLC-inductively coupled argon plasma mass spectrometry. *Toxicol. Appl. Pharm.*, **189**, 73–83.
166. Gammelgaard, B., Madsen, K.G., Bjerrum, J., Bendahl, L., Jons, O., Olsen, J. and Sidenius, U. (2003) Separation, purification and identification of the major selenium metabolite from human urine by multi-dimensional HPLC-ICP-MS and APCI-MS. *J. Anal. Atom. Spectrom.*, **18**, 65–70.
167. Bendahl, L. and Gammelgaard, B. (2004) Separation and identification of Se-methylselenogalactosamine – a new metabolite in basal human urine – by HPLC-ICP-MS and CE-nano-ESI-MSMS. *J. Anal. Atom. Spectrom.*, **19**, 950–957.
168. Gammelgaard, B. and Bendahl, L. (2004) Selenium speciation in human urine samples by LC- and CE-ICP-MS – separation and identification of selenosugars. *J. Anal. Atom. Spectrom.*, **19**, 135–142.
169. Gammelgaard, B. and Jons, O. (2000) Determination of selenite and selenate in human urine by ion chromatography and inductively coupled plasma mass spectrometry. *J. Anal. Atom. Spectrom.*, **15**, 945–949.
170. Sawyer, S., Zhang, X., Vanhaecke, F., Cornelis, R., Moens, L. and Dams, R. (1997) Speciation of six arsenic compounds using high-performance liquid chromatography-inductively coupled plasma mass spectrometry with sample introduction by thermospray nebulization. *J. Anal. Atom. Spectrom.*, **12**, 1047–1052.
171. Gammelgaard, B., Jessen, K.D., Kristensen, F.H. and Jons, O. (2000) Determination of trimethylselenonium ion in urine by ion chromatography and inductively coupled plasma mass spectrometry. *Anal. Chim. Acta*, **404**, 47–54.
172. Gammelgaard, B., Jons, O. and Bendahl, L. (2001) Selenium speciation in pretreated human urine by ion-exchange chromatography and ICP-MS detection. *J. Anal. Atom. Spectrom.*, **16**, 339–344.
173. Cao, T.H., Cooney, R.A., Woznichak, M.M., May, S.W. and Browner, R.F. (2001) Speciation and identification of organoselenium metabolites in human urine using inductively coupled plasma mass spectrometry and tandem mass spectrometry. *Anal. Chem.*, **73**, 2898–2902.
174. Quijano, M.A., Gutierrez, A.M., Perez-Conde, M.C. and Camara, C. (1999) Determination of selenium species in human urine by high performance liquid chromatography and inductively coupled plasma mass spectrometry. *Talanta*, **50**, 165–173.
175. Chatterjee, A., Tao, H., Shibata, Y. and Morita, M. (2003) Determination of selenium compounds in urine by high-performance liquid chromatography-inductively coupled plasma mass spectrometry. *J. Chromatogr. A.*, **997**, 249–257.
176. LaFuente, J.M.G., Dlaska, M., Sanchez, M.L.F. and Sanz-Medel, A. (1998) Organic and inorganic selenium speciation in urine by on-line vesicle mediated high-performance liquid chromatography-hydride generation-inductively coupled plasma mass spectrometry. *J. Anal. Atom. Spectrom.*, **13**, 423–429.

177. LaFuente, J.M.G., Marchante-Gayon, J.M., Sanchez, M.L.F. and Sanz-Medel, A. (1999) Urinary selenium speciation by high-performance liquid chromatography-inductively coupled plasma mass spectrometry: advantages of detection with a double-focusing mass analyser with a hydride generation interface. *Talanta*, **50**, 207–217.
178. Wrobel, K., Wrobel, K., Kanamkumarath, S.S. and Caruso, J.A. (2003) Identification of selenium species in urine by ion-pairing HPLC-ICP-MS using laboratory synthesized standards. *Anal. Bioanal. Chem.*, **377**, 670–674.
179. Yang, K.L. and Jiang, S.J. (1995) Determination of selenium compounds in urine samples by liquid chromatography-inductively coupled plasma mass spectrometry with an ultrasonic nebulizer. *Anal. Chim. Acta*, **307**, 109–115.
180. Gammelgaard, B., Bendahl, L., Sidenius, U. and Jons, O. (2002) Selenium speciation in urine by ion-pairing chromatography with perfluorinated carboxylic acids and ICP-MS detection. *J. Anal. Atom. Spectrom.*, **17**, 570–575.
181. Zheng, J., Ohata, M. and Furuta, N. (2002) Reversed-phase liquid chromatography with mixed ion-pair reagents coupled to ICP-MS for the direct speciation analysis of selenium compounds in human urine. *J. Anal. Atom. Spectrom.*, **17**, 730–735.
182. Zheng, J., Shibata, Y. and Tanaka, A. (2002) Study of the stability of selenium compounds in human urine and determination by mixed ion-pair reversed-phase chromatography with ICP-MS detection. *Anal. Bioanal. Chem.*, **374**, 348–353.
183. Marchante-Gayon, J.M., Feldmann, I., Thomas, C. and Jakubowski, N. (2001) Speciation of selenium in human urine by HPLC-ICP-MS with a collision and reaction cell. *J. Anal. Atom. Spectrom.*, **16**, 457–463.
184. Bendahl, L., Sidenius, U. and Gammelgaard, B. (2000) Determination of selenoprotein P in human plasma by solid phase extraction and inductively coupled plasma mass spectrometry. *Anal. Chim. Acta*, **411**, 103–108.
185. Reyes, L.H., Marchante-Gayon, J.M., Alonso, J.I.G. and Sanz-Medel, A. (2003) Quantitative speciation of selenium in human serum by affinity chromatography coupled to post-column isotope dilution analysis ICP-MS. *J. Anal. Atom. Spectrom.*, **18**, 1210–1216.
186. Michalke, B. (2004) Selenium speciation in human serum of cystic fibrosis patients compared to serum from healthy persons. *J. Chromatogr. A.*, **1058**, 203–208.
187. Nyman, D.W., Stratton, M.S., Kopplin, M.J., Dalkin, B.L., Nagle, R.B. and Gandolfi, A.J. (2004) Selenium and selenomethionine levels in prostate cancer patients. *Cancer Detect. Prev.*, **28**, 8–16.
188. Richarz, A.N. and Bratter, P. (2002) Speciation of trace elements in the brain of individuals with Alzheimer's disease with special emphasis on metallothioneins. *Anal. Bioanal. Chem.*, **372**, 412–417.
189. Richarz, A.N., Wolf, C. and Bratter, P. (2003) Determination of protein-bound trace elements in human cell cytosols of different organs and different pathological states. *Analyst*, **128**, 640–645.
190. Chery, C.C., Cremer, K.D., Cornelis, R., Vanhaecke, F. and Moens, L. (2003) Optimisation of ICP-dynamic reaction cell-MS as a specific detector for the speciation of vanadium at therapeutic levels in serum. *J. Anal. Atom. Spectrom.*, **18**, 1113–1118.
191. Hall, G.S., Zhu, X. and Martin, E.G. (1999) Determination of Pb-bound ligands in human amniotic fluid by HPSEC-ICP-MS. *Anal. Commun.*, **36**, 93–95.
192. Wang, J., Houk, R.S., Dreessen, D. and Wiederin, D.R. (1998) Identification of inorganic elements in proteins in human serum and in DNA fragments by size exclusion chromatography and inductively coupled plasma mass spectrometry with a magnetic sector mass spectrometer. *J. Am. Chem. Soc.*, **120**, 5793–5799.
193. Mandal, R., Teixeira, C. and Li, X.F. (2003) Studies of cisplatin and haemoglobin interactions using nanospray mass spectrometry and liquid chromatography with inductively coupled plasma mass spectrometry. *Analyst*, **128**, 629–634.

194. Szpunar, J., Makarov, A., Pieper, T., Keppler, B.K. and Lobinski, R. (1999) Investigation of metalldrug-protein interactions by size-exclusion chromatography coupled with inductively coupled plasma mass spectrometry (ICP-MS). *Anal. Chim. Acta.*, **387**, 135–144.
195. Cabezuelo, A.B.S., Montes-Bayon, M., Gonzalez, E.B., Alonso, J.I.G. and Sanz-Medel, A. (1998) Speciation of basal aluminium in human serum by fast protein liquid chromatography with inductively coupled plasma mass spectrometric detection. *Analyst*, **123**, 865–869.
196. Sanz-Medel, A., Cabezuelo, A.B.S., Milacic, R. and Polak, T.B. (2002) The chemical speciation of aluminum in human serum. *Coordin. Chem. Rev.*, **228**, 373–383.
197. Montes-Bayon, M., Cabezuelo, A.B.S., Gonzalez, E.B., Alonso, J.I.G. and Sanz-Medel, A. (1999) Capabilities of fast protein liquid chromatography coupled to a double focusing inductively coupled plasma mass spectrometer for trace metal speciation in human serum. *J. Anal. Atom. Spectrom.*, **14**, 947–951.
198. Fernandes, K.G., Montes-Bayon, M., Gonzalez, E.B., Castillo-Busto, E.D., Nobrega, J.A. and Sanz-Medel, A. (2005) Complementary FPLC-ICP-MS and MALDI-TOF for studying vanadium association to human serum proteins. *J. Anal. Atom. Spectrom.*, **20**, 210–215.
199. Sun, H. and Szeto, K.Y. (2003) Binding of bismuth to serum proteins: implications for targets of Bi(III) in blood plasma. *J. Inorg. Biochem.*, **94**, 114–120.
200. Pizarro, I., Gomez, M., Camara, C., Palacios, M.A. and Roman-Silva, D.A. (2004) Evaluation of arsenic species-protein binding in cardiovascular tissues by bidimensional chromatography with ICP-MS detection. *J. Anal. Atom. Spectrom.*, **19**, 292–296.
201. Koyama, H., Omura, K., Ejima, A., Kasanuma, Y., Watanabe, C. and Satoh, H. (1999) Separation of selenium-containing proteins in human and mouse plasma using tandem high-performance liquid chromatography columns coupled with inductively coupled plasma-mass spectrometry. *Anal. Biochem.*, **267**, 84–91.
202. Amarasiriwardena, C.J., Lupoli, N., Potula, V., Korrick, S. and Hu, H. (1998) Determination of total arsenic concentration in human urine by inductively coupled plasma mass spectrometry: a comparison of the accuracy of three analytical methods. *Analyst*, **123**, 441–445.
203. Oakberg, K., Levy, T. and Smith, P. (2000) A method for skeletal arsenic analysis, applied to the chalcolithic copper smelting site of Shiqmin, Israel. *J. Archaeol. Sci.*, **27**, 895–901.
204. Graske, A., Thuvander, A., Johannisson, A., Gadhasson, I., Schutz, A., Festin, R. and Glynn, A.W. (2000) Influence of aluminium on the immune system – an experimental study on volunteers. *BioMetals.*, **13**, 123–133.
205. Muniz, C.S., Marchante-Gayon, J.M., Alonso, J.I.G. and Sanz-Medel, A. (1998) Comparison of electrothermal atomic absorption spectrometry, quadrupole inductively coupled plasma mass spectrometry and double-focusing sector field inductively coupled plasma mass spectrometry for the determination of aluminium in human serum. *J. Anal. Atom. Spectrom.*, **13**, 283–287.
206. Higashiura, M., Uchida, H., Uchida, T. and Wada, H. (1995) Inductively coupled plasma mass spectrometric determination of gold in serum: comparison with flame and furnace atomic absorption spectrometry. *Anal. Chim. Acta*, **304**, 317–321.
207. Sun, D.H., Ma, R.L., McLeod, C.W., Wang, X.R. and Cox, A.G. (2000) Determination of boron in serum, plasma and urine by inductively coupled plasma mass spectrometry (ICP-MS). Use of mannitol-ammonia as diluent and for eliminating memory effect. *J. Anal. Atom. Spectrom.*, **15**, 257–261.
208. Bellato, A.C.S., Gine, M.F. and Menegario, A.A. (2004) Determination of B in body fluids by isotope dilution inductively coupled mass spectrometry with direct injection nebulization. *Microchem. J.*, **77**, 119–122.
209. Apostoli, P. and Schaller, K.H. (2001) Urinary beryllium – a suitable tool for assessing occupational and environmental beryllium exposure. *Int. Arch. Occ. Env. Hea.*, **74**, 162–166.
210. Patterson, K.Y., Veillon, C., Hill, A.D., Moser-Veillon, P.B. and O'Haver, T.C. (1999) Measurement of calcium stable isotope tracers using cool plasma ICP-MS. *J. Anal. Atom. Spectrom.*, **14**, 1673–1677.

211. Infante, H.G., Sanchez, M.L.F. and Sanz-Medel, F. (1998) Vesicle-assisted determination of ultratrace amounts of cadmium in urine by electrothermal atomic absorption spectrometry and inductively coupled plasma mass spectrometry. *J. Anal. Atom. Spectrom.*, **13**, 899–903.
212. Ikeda, M., Zhang, Z.W., Moon, C.S., Shimbo, S., Watanabe, T., Nakasuka, H., Matsuda-Inoguchi, N. and Higashikawa, K. (2000) Possible effects of environmental cadmium exposure on kidney function in the Japanese general population. *Int. Arch. Occ. Env. Hea.*, **73**, 15–25.
213. Diemer, J., Vogl, J., Quetel, C.R., Linsinger, T., Taylor, P.D.P., Lamberty, A. and Pauwels, J. (2001) SI-traceable certification of the amount content of cadmium below the ng/g level in blood samples by isotope dilution ICP-MS applied as a primary method of measurement. *Anal. Bioanal. Chem.*, **370**, 492–498.
214. Boer, J.L.M.d., Joode, P.D. and Ritsema, R. (1998) Direct inductively coupled plasma mass spectrometric determination of cadmium in urine with special attention to matrix correction. *J. Anal. Atom. Spectrom.*, **13**, 971–975.
215. Hwang, T.J. and Jiang, S.J. (1997) Determination of cadmium by flow injection isotope dilution inductively coupled plasma mass spectrometry with vapour generation sample introduction. *J. Anal. Atom. Spectrom.*, **12**, 579–584.
216. Mota, J.P.V., Campa, M.R.F.d.l., Alonso, J.I.G. and Sanz-Medel, A. (1999) Determination of cadmium in biological and environmental materials by isotope dilution inductively coupled plasma mass spectrometry: effect of flow sample introduction methods. *J. Anal. Atom. Spectrom.*, **14**, 113–120.
217. Crews, H.M., Owen, L.M., Langford, N., Fairweather-Tait, S.J., Fox, T.E., Hubbard, L. and Philips, D. (2000) Use of the stable isotope Cd-106 for studies of dietary cadmium absorption in humans. *Toxicol. Lett.*, **112–113**, 201–207.
218. Beattie, J.H., Reid, M.D., Harvey, L.J., Dainty, J.R., Majsak-Newman, G. and Fairweather-Tait, S.J. (2001) Selective extraction of blood plasma exchangeable copper for isotope studies of dietary copper absorption. *Analyst*, **126**, 2225–2229.
219. Labat, L., Dumestre-Toulet, V., Goulle, J.P., and Lhermitte, M. (2004) A fatal case of mercuric cyanide poisoning. *Forensic Science International* **143**, 215–217.
220. Nixon, D.E., Burritt, M.F. and Moyer, T.P. (1999) The determination of mercury in whole blood and urine by inductively-coupled plasma mass spectrometry. *Spectrochim. Acta B*, **54**, 1141–1153.
221. Moreton, J.A. and Delves, H.T. (1998) Simple direct method for the determination of total mercury levels in blood and urine and nitric acid digests of fish by inductively coupled plasma mass spectrometry. *J. Anal. Atom. Spectrom.*, **13**, 659–665.
222. Vahter, M., Akesson, A., Lind, B., Bjors, U., Schutz, A. and Berglund, M. (2000) Longitudinal study of methylmercury and inorganic mercury in blood and urine of pregnant lactating women, as well as in umbilical cord blood. *Environ. Res.*, **84**, 186–194.
223. Bettinelli, M., Spezia, S., Ronchi, A. and Minoia, C. (2002) Determination of total urinary mercury by on-line sample microwave digestion followed by flow injection cold vapour inductively coupled plasma mass spectrometry or atomic absorption spectrometry. *Rapid Commun. Mass Sp.*, **16**, 1432–1439.
224. Apostoli, P., Cortesi, I., Mangili, A., Elia, G., Drago, I., Gagliardi, T., Soleo, L., Valente, T., Sciarra, G.F., Aprea, C., Ronchi, A. and Minoia, C. (2002) Assessment of reference values for mercury in urine: the results of an Italian polycentric study. *Sci. Total Environ.*, **289**, 13–24.
225. Knight, R., Haswell, S.J., Lindow, S.W. and Batty, J. (1999) Determination of mercury in hair by coupled CVAA-ICP-MS. *J. Anal. Atom. Spectrom.*, **14**, 127–129.
226. Jian, L., Goessler, W. and Irgolic, K.J. (2000) Mercury determination with ICP-MS: signal suppression with acids. *Anal. Bioanal. Chem.*, **366**, 48–53.
227. Gill, U.S., Schwartz, H.M. and Bigras, L. (2002) Results of multiyear international interlaboratory comparison program for mercury in human hair. *Arch. Environ. Cont. Tox.*, **43**, 466–472.

228. Shuqin, C., Hangting, C. and Xianjin, Z. (1999) Determination of mercury in biological samples using organic compounds as matrix modifiers by inductively coupled plasma mass spectrometry. *J. Anal. Atom. Spectrom.*, **14**, 1183–1186.
229. Hintelmann, H., Falter, R., Ilgen, G. and Evans, R.D. (1997) Determination of artifactual formation of monomethylmercury (CH_3Hg^+) in environmental samples using stable Hg^{2+} isotopes with ICP-MS detection: calculation of contents applying species specific isotope addition. *Anal. Bioanal. Chem.*, **358**, 363–370.
230. Wardley, C.J., Cox, A., McCleod, C. and Morris, B.W. (1999) A longitudinal study of iodine excretion in normal pregnancy determined by inductively coupled plasma mass spectrometry. *J. Anal. Atom. Spectrom.*, **14**, 1709–1710.
231. Nacapricha, D., Muangkaew, S., Ratanawimarnwong, N., Shiowatana, J. and Grudpan, K. (2001) Continuous and stopped flow injection for catalytic determination of total iodine in urine. *Analyst*, **126**, 121–126.
232. Michalke, B., Schramel, P. and Hasse, S. (1996) Separation of free iodide from other I-species in human serum – Quantification in serum pools and individual samples. *Anal. Bioanal. Chem.*, **354**, 576–579.
233. Jahreis, G., Hausmann, W., Kiessling, G., Franke, K. and Leiterer, M. (2001) Bioavailability of iodine from normal diets rich in dairy products – results of balance studies in women. *Exp. Clin. Endocr. Diab.*, **109**, 163–167.
234. Keyes, W.R. and Turnlund, J.R. (2002) Determination of molybdenum and enriched Mo stable isotope concentrations in human blood plasma by isotope dilution ICP-MS. *J. Anal. Atom. Spectrom.*, **17**, 1153–1156.
235. Luong, E.T., Houk, R.S. and Serfass, R.E. (1997) Chromatographic isolation of molybdenum from human blood plasma and determination by inductively coupled plasma mass spectrometry with isotope dilution. *J. Anal. Atom. Spectrom.*, **12**, 703–708.
236. Turnlund, J.R. and Keyes, W.R. (2004) Plasma molybdenum reflects dietary molybdenum intake. *J. Nutr. Biochem.*, **15**, 90–95.
237. Iversen, B.S., Menne, C., White, M.A., Kristiansen, J., Christensen, J.M. and Sabbioni, E. (1998) Inductively coupled plasma mass spectrometric determination of molybdenum in urine from a Danish population. *Analyst*, **123**, 81–85.
238. Minoia, C., Gatti, A., Aprea, C., Ronchi, A., Sciarra, G., Turci, R. and Bettinelli, M. (2002) Inductively coupled plasma mass spectrometric determination of molybdenum in urine. *Rapid Commun. Mass Sp.*, **16**, 1313–1319.
239. Long, S.E. and Vetter, T.W. (2002) Determination of sodium in blood serum by inductively coupled plasma mass spectrometry. *J. Anal. Atom. Spectrom.*, **17**, 1589–1594.
240. Farago, M.E., Kavanagh, P., Blanks, R., Kelly, J., Kazantzis, G., Thornton, I., Simpson, P.R., Cook, J.M., Delves, H.T. and Hall, G.E.M. (1998) Platinum concentrations in urban road dust and soil, and in blood and urine in the United Kingdom. *Analyst*, **123**, 451–454.
241. Schramel, P., Wendler, I. and Lustig, S. (1995) Capability of ICP-MS (pneumatic nebulization and ETV) for Pt-analysis in different matrices at ecologically relevant concentrations. *Anal. Bioanal. Chem.*, **353**, 115–118.
242. Gamelin, E., Allain, P., Maillart, P., Turcant, A., Delva, R., Lortholary, A. and Larra, F. (1995) Long-term pharmacokinetic behavior of platinum after cisplatin administration. *Cancer Chemoth. Pharm.*, **37**, 97–102.
243. Morrison, J.G., White, P., McDougall, S., Firth, J.W., Woolfrey, S.G., Graham, M.A. and Greenslade, D. (2000) Validation of a highly sensitive ICP-MS method for the determination of platinum in biofluids: application to clinical pharmacokinetic studies with oxaliplatin. *J. Pharmaceut. Biomed.*, **24**, 1–10.
244. Levi, F., Metzger, G., Massari, C. and Milano, G. (2000) Oxaliplatin: pharmacokinetics and chronopharmacological aspects. *Clin. Pharmacokinet.*, **38**, 1–21.

245. Sessa, C., Capri, G., Gianni, L., Peccatori, F., Grasselli, G., Bauer, J., Zucchetti, M., Vigano, L., Gatti, A., Minoia, C., Liati, P., Bosch, S.B.d., Bernareggi, A., Camboni, G. and Marsoni, S. (2000) Clinical and pharmacological phase I study with accelerated titration design of a daily times five schedule of BBR3464, a novel cationic triplatinum complex. *Ann. Oncol.*, **11**, 977–983.
246. Sessa, C., Minoia, C., Ronchi, A., Zucchetti, M., Bauer, J., Borner, M., Jong, J.d., Pagani, O., Renard, J., Weil, C. and D'Incalci, M. (1998) Phase I clinical and pharmacokinetic study of the oral platinum analogue JM216 given daily for 14 days. *Ann. Oncol.*, **9**, 1315–1322.
247. Andersson, A. and Ehrsson, H. (1995) Stability of cisplatin and its monohydrated complex in blood, plasma and ultrafiltrate – implications for quantitative analysis. *J. Pharmaceut. Biomed.*, **13**, 639–644.
248. Bettinelli, M. (2005) ICP-MS determination of Pt in biological fluids of patients treated with antitumor agents: evaluation of analytical uncertainty. *Microchem. J.*, **79**, 357–365.
249. Budd, P., Montgomery, J., Evans, J. and Barreiro, B. (2000) Human tooth enamel as a record of the comparative lead exposure of prehistoric and modern people. *Sci. Total Environ.*, **263**, 1–10.
250. Bonnefoy, C., Menudier, A., Moesch, C., Lachatre, G. and Mermet, J.M. (2002) Validation of the determination of lead in whole blood by ICP-MS. *J. Anal. At. Spectrom.*, **17**, 1161–1165.
251. Bergdahl, I.A., Sheveleva, M., Schutz, A., Artamonova, V.G. and Skerfving, S. (1998) Plasma and blood lead in humans: capacity-limited binding to aminolevulinic acid dehydratase and other lead-binding components. *Toxicol. Sci.*, **46**, 247–253.
252. Danadevi, K., Rozati, R., Banu, B.S., Rao, P.H. and Grover, P. (2003) DNA damage in workers exposed to lead using comet assay. *Toxicology*, **187**, 183–193.
253. Schutz, A., Olsson, M., Jensen, A., Gerhardsson, L., Borjesson, J., Mattsson, S., and Skerfving, S. (2005) Lead in finger bone, whole blood, plasma urine in lead-smelter workers: extended exposure range. *Int. Arch. Occ. Env. Hea.*, **78**, 35–43.
254. Chen, S., Zhang, Z., Yu, H., Liu, W. and Sun, M. (2002) Determination of trace lead by hydride generation-inductively coupled plasma-mass spectrometry. *Anal. Chim. Acta*, **463**, 177–188.
255. Aro, A., Amarasiriwardena, C., Lee, M.L., Kim, R. and Hu, H. (2000) Validation of K X-ray fluorescence bone lead measurements by inductively coupled plasma mass spectrometry in cadaver legs. *Med. Phys.*, **27**, 119–123.
256. Yoshinaga, J., Yoneda, M., Morita, M. and Suzuki, T. (1995) Lead in prehistoric, historic and contemporary Japanese: stable isotope study by ICP mass spectrometry. *Appl. Geochem.*, **13**, 403–413.
257. Hinnners, T.A., Hughes, R., Outridge, P.M., Davis, W.J., Simon, K. and Woolard, D.R. (1998) Interlaboratory comparison of mass spectrometric methods for lead isotopes and trace elements in NIST SRM 1400 bone ash. *J. Anal. Atom. Spectrom.*, **13**, 963–970.
258. Baglan, N., Cossonnet, C., Pitet, P., Cavadore, D., Exmelin, L. and Berard, P. (2000) On the use of ICP-MS for measuring plutonium in urine. *J. Radioanal. Nucl. Ch.*, **243**, 397–401.
259. Kuwabara, J. and Noguchi, H. (2002) Development of rapid bioassay method for plutonium. *J. Radioanal. Nucl. Ch.*, **252**, 273–276.
260. Inn, K.G.W., McCurdy, D., Kuruvilla, L., Barss, N.M., Pietrzak, R., Kaplan, E., Inkret, W., Efurd, W., Rokop, D., Lewis, D., Gautier, P. and Bell, R.T. (2001) Intercomparison study of inductively coupled plasma mass spectrometry, thermal ionization mass spectrometry and fission track analysis of microBq quantities of Pu-239 in synthetic urine. *J. Radioanal. Nucl. Ch.*, **249**, 121–131.
261. Delves, H.T. and Sieniawska, C.E. (1997) Simple method for the accurate determination of selenium in serum by using inductively coupled plasma mass spectrometry. *J. Anal. Atom. Spectrom.*, **12**, 387–389.
262. Sieniawska, C.E., Mensikov, R. and Delves, H.T. (1999) Determination of total selenium in serum, whole blood and erythrocytes by ICP-MS. *J. Anal. Atom. Spectrom.*, **14**, 109–112.
263. Labat, L., Dehon, B. and Lhermitte, M. (2003) Rapid and simple determination of selenium in blood serum by inductively coupled plasma-mass spectrometry (ICP-MS). *Anal. Bioanal. Ch.*, **376**, 270–273.

264. Abou-Shakra, F.R., Rayman, M.P., Ward, N.I., Hotton, V. and Bastian, G. (1997) Enzymatic digestion for the determination of trace elements in blood serum by inductively coupled plasma mass spectrometry. *J. Anal. Atom. Spectrom.*, **12**, 429–433.
265. Gammelgaard, B., and Larsen, E.H. (1998) Sensitivities of selenite, selenate, selenomethionine and trimethylselenonium ion in aqueous solution and in blood plasma – ETAAS compared with ICP-MS. *Talanta*, **47**, 503–507.
266. Tinggi, U., Gianduzzo, T., Francis, R., Nicol, D., Shahin, M. and Scheelings, P. (2004) Determination of selenium in red blood cells by inductively coupled plasma mass spectrometry (ICP-MS) after microwave digestion. *J. Radioanal. Nucl. Ch.*, **259**, 469–472.
267. Mestek, O., Suchanek, M., Vodickova, Z., Zemanova, B. and Zima, T. (1997) Comparison of the suitability of various atomic spectroscopic techniques for the determination of selenium in human whole blood. *J. Anal. Atom. Spectrom.*, **12**, 85–89.
268. Gammelgaard, B. and Jons, O. (1999) Determination of selenium in urine by inductively coupled plasma mass spectrometry: interferences and optimization. *J. Anal. Atom. Spectrom.*, **14**, 867–874.
269. Nixon, D.E., Moyer, T.P. and Burritt, M.F. (1999) The determination of selenium in serum and urine by inductively coupled plasma mass spectrometry: comparison with Zeeman graphite furnace atomic absorption spectrometry. *Spectrochim. Acta. B.*, **54**, 931–942.
270. Dhindsa, H.S., Bermingham, M.A., Mierzwa, J. and Sullivan, D. (1998) Plasma selenium concentrations in a Sikh population in Sydney, Australia. *Analyst*, **123**, 885–887.
271. Roth, P., Werner, E., Wendler, I. and Schramel, P. (1996) Application of ICP-MS for the assessment of thorium excretion in urine. *Appl. Radiat. Isotopes*, **47**, 1055–1056.
272. Sabbioni, E., Minoia, C., Ronchi, A., Hansen, B.G., Pietra, R. and Balducci, C. (1994) Trace element reference values in tissues from inhabitants of the European Union. VIII. Thallium in the Italian population. *Sci. Total Environ.*, **158**, 227–236.
273. Hanada, T., Isobe, H., Saito, T., Ogura, S., Takekawa, H., Yamazaki, K., Tokuchi, Y. and Kawakami, Y. (1998) Intracellular accumulation of thallium as a marker of cisplatin cytotoxicity in nonsmall cell lung carcinoma. *Cancer*, **83**, 930–935.
274. Caddia, M. and Iversen, B.S. (1998) Determination of uranium in urine by inductively coupled plasma mass spectrometry with pneumatic nebulization. *J. Anal. Atom. Spectrom.*, **13**, 309–313.
275. Lorber, A., Karpas, Z. and Halicz, L. (1996) Flow injection method for determination of uranium in urine and serum by inductively coupled plasma mass spectrometry. *Anal. Chim. Acta*, **334**, 295–301.
276. Muramatsu, Y., Yoshida, S., Ban-nai, T. and Akashi, M. (2004) Determination of radionuclides in human and environmental samples from the criticality accident in Tokai-mura, Japan. *J. Radioanal. Nucl. Ch.*, **262**, 129–134.
277. Werner, E., Roth, P., Wendler, I., Schramel, P., Hellmann, H. and Kratzel, U. (1997) Feasibility of ICP-MS for the assessment of uranium excretion in urine. *J. Radioanal. Nucl. Ch.*, **226**, 201–203.
278. Haldiman, M., Baduraux, M., Eastgate, A., Froidevaux, P., O'Donovan, S., Gunten, D.V. and Zoller, O. (2001) Determining picogram quantities of uranium in urine by isotope dilution inductively coupled plasma mass spectrometry. Comparison with alpha spectrometry. *J. Anal. Atom. Spectrom.*, **16**, 1364–1369.
279. Au, W.W., McConnell, M.A., Wilkinson, G.S., Ramanujam, V.M.S. and Alcock, N. (1998) Population monitoring: experience with residents exposed to uranium mining/milling waste. *Mutat. Res.*, **405**, 237–245.
280. Lamer-Dechamps, S.L., Pourcheret, P., Perez, J.L. and Bressolle, F. (2003) Validation of an inductively coupled plasma-mass spectrometry method to quantify tungsten in human plasma. Determination of percentage binding to proteins. *Clin. Chim. Acta*, **327**, 39–46.
281. Kokkinou, D., Kasper, H.U., Bartz-Schmidt, K.U. and Schraermeyer, U. (2004) The pigmentation of human iris influences the uptake and storing of zinc. *Pigm. Cell Res.*, **17**, 515–518.

282. Gine, M.F., Bellato, A.C.S. and Menegario, A.A. (2004) Determination of trace elements in serum samples by isotope dilution inductively coupled plasma mass spectrometry using on-line dialysis. *J. Anal. Atom. Spectrom.*, **19**, 1252–1256.
283. Stuart-Williams, H.L.Q., Schwarcz, H.P., White, C.D. and Spence, M.W. (1996) The isotopic composition and diagenesis of human bone from Teotihuacan and Oaxaca, Mexico. *Palaeogeogr. Palaeocl.*, **126**, 1–14.
284. Kawamura, H., Parr, R.M., Dang, H.S., Tian, W., Barnes, R.M. and Iyengar, G.V. (2000) Analytical quality assurance procedures developed for the IAEA's Reference Asian Man Project (Phase 2). *J. Radioanal. Nucl. Ch.*, **245**, 123–126.
285. Barany, E.I., Bergdahl, I.G., Bratteby, L.E., Lundh, T., Samuelson, G., Schutz, A., Skerfving, S. and Oskarsson, A. (2002) Trace element levels in whole blood and serum from Swedish adolescents. *Sci. Total Environ.*, **286**, 129–141.
286. Barany, E., Bergdahl, I.A., Bratteby, L.E., Lundh, T., Samuelson, G., Schutz, A., Skerfving, S. and Oskarsson, A. (2002) Relationships between trace element concentrations in human blood and serum. *Toxicol. Lett.*, **134**, 177–184.
287. Barany, E.I., Bergdahl, I.G., Bratteby, L.E., Lundh, T., Samuelson, G., Schutz, A., Skerfving, S. and Oskarsson, A. (2002) Trace elements in blood and serum of Swedish adolescents: relation to gender, age, residential area, and socioeconomic status. *Environ. Res.*, **89**, 72–84.
288. Samanta, G., Sharma, R., Roychowdury, T. and Chakraborti, D. (2004) Arsenic and other elements in hair, nails and skin-scales of arsenic victims in West Bengal, India. *Sci. Total Environ.*, **326**, 33–47.
289. Srivastava, R.A.K. and Jain, J.C. (2002) Scavenger receptor class B type I expression and elemental analysis in cerebellum and parietal cortex regions of the Alzheimer's disease brain. *J. Neurol. Sci.*, **196**, 45–52.
290. Krachler, M., Radner, H. and Irgolic, K.J. (1996) Microwave digestion methods for the determination of trace elements in brain and liver samples by inductively coupled plasma mass spectrometry. *Anal. Bioanal. Chem.*, **355**, 120–128.
291. Violante, N., Senofonte, O., Marsili, G., Meli, P., Soggiu, M.E. and Caroli, S. (2000) Human hair as a marker of pollution by chemical elements emitted by a thermoelectric power plant. *Microchem. J.*, **67**, 397–405.
292. Cszsma, I., Andrasi, W., Lasztity, A., Bertalan, E. and Gawlik, D. (2003) Determination of Mo and Mn in human brain samples by different techniques. *J. Anal. Atom. Spectrom.*, **18**, 1082–1087.
293. Gutensohn, K., Beythien, C., Bau, J., Fenner, T., Grewe, P., Koester, R., Padmanaban, K. and Kuehn, P. (2000) *In vitro* analyses of diamond-like carbon coated stents: reduction of metal ion release, platelet activation and thrombogenicity. *Thromb. Res.*, **99**, 577–585.
294. Senofonte, O., Violante, N., D'Ilio, S., Caimi, S., Peri, A. and Caroli, S. (2001) Hair analysis and the early detection of imbalances in trace elements for members of expeditions in Antarctica. *Microchem. J.*, **69**, 231–238.
295. D'Ilio, S., Violante, N., Senofonte, O. and Caroli, S. (2000) Occupational exposure of goldsmith workers of the area of Rome to potentially toxic metals as monitored through hair analysis. *Microchem. J.*, **67**, 343–349.
296. Nixon, D.E. and Moyer, T.P. (1996) Routine clinical determination of lead, arsenic, cadmium and thallium in urine and whole blood by inductively coupled plasma mass spectrometry. *Spectrochim. Acta B.*, **51**, 13–25.
297. Ingle, C.P., Langford, N., Harvey, L.J., Dainty, J.R., Turner, P.J., Sharp, B.L. and Lewis, D.J. (2004) Comparison of three different instrumental approaches to the determination of iron and zinc isotope ratios in clinical samples. *J. Anal. Atom. Spectrom.*, **19**, 404–406.
298. Miekeley, N., Carneiro, M.T.W. and Silveira, C.L.P.d. (1998) How reliable are human hair reference intervals for trace elements. *Sci. Total Environ.*, **218**, 9–17.

299. Krushevska, A., Kotrebai, M., Lásztity, A., Barnes, R.M. and Amarasiriwardena, D. (1996) Application of tertiary amines for arsenic and selenium signal enhancement and polyatomic interference reduction in ICP-MS analysis of biological samples. *Anal. Bioanal. Chem.*, **355**, 793–800.
300. Huang, C. and Beauchemin, D. (2003) Direct multielemental analysis of human serum by ICP-MS with on-line standard addition using flow injection. *J. Anal. Atom. Spectrom.*, **18**, 951–952.
301. Forrer, R., Gautschi, K. and Lutz, H. (2001) Simultaneous measurement of the trace elements Al, As, B, Be, Cd, Co, Cu, Fe, Li, Mn, Mo, Ni, Rb, Se, Sr, and Zn in human serum and their reference ranges by ICP-MS. *Biol. Trace Elem. Res.*, **80**, 77–93.
302. Falk, H., Geerling, R., Hattendorf, B., Krenzel-Rothensee, K. and Schmidt, K.P. (1997) Capabilities and limits of ICP-MS for direct determination of element traces in saline solutions. *Anal. Bioanal. Chem.*, **359**, 352–356.
303. Domej, W., Krachler, M., Goessler, W., Maier, A., Irgolic, K.J. and Lang, J.K. (2000) Concentrations of copper, zinc, manganese, rubidium, and magnesium in thoracic empyemata and corresponding sera. *Biol. Trace Elem. Res.*, **78**, 53–66.
304. Ikeda, M., Zhang, Z.W., Shimbo, S., Watanabe, T., Nakatsuka, H., Moon, C.S., Matsuda-Inoguchi, N. and Higashikawa, K. (2000) Urban population exposure to lead and cadmium in east and south-east Asia. *Sci. Total Environ.*, **249**, 373–384.
305. Ikeda, M., Zhang, Z.W., Shimbo, S., Watanabe, T., Nakatsuka, H., Moon, C.S., Matsuda-Inoguchi, N. and Higashikawa, K. (2000) Exposure of women in general populations to lead via food and air in east and southeast Asia. *Am. J. Ind. Med.*, **38**, 271–280.
306. Watanabe, T., Zhang, Z.W., Moon, C.S., Shimbo, S., Nakatsuka, H., Matsuda-Inoguchi, N., Higashikawa, K. and Ikeda, M. (2000) Cadmium exposure of women in general populations in Japan during 1991–1997 compared with 1977–1981. *Int. Arch. Occ. Env. Hea.*, **73**, 26–34.
307. Zhang, Z.W., Shimbo, S., Ochi, N., Eguchi, M., Watanabe, T., Moon, C.S. and Ikeda, M. (1997) Determination of lead and cadmium in food and blood by inductively coupled plasma mass spectrometry: a comparison with graphite furnace atomic absorption spectrometry. *Sci. Total Environ.*, **205**, 179–187.
308. Shimbo, S., Zhang, Z.W., Moon, C.S., Watanabe, T., Nakatsuka, H., Matsuda-Inoguchi, N., Higashikawa, K. and Ikeda, M. (2000) Correlation between urine and blood concentrations, and dietary intake of cadmium and lead among women in the general population of Japan. *Int. Arch. Occ. Env. Hea.*, **73**, 163–170.
309. Zhang, Z.W., Shimbo, S., Watanabe, T., Sriamujata, S., Banjong, O., Chitchumroonchokchai, C., Nakatsuka, H., Matsuda-Inoguchi, N., Higashikawa, K. and Ikeda, M. (1999) Non-occupational lead and cadmium exposure of adult women in Bangkok, Thailand. *Sci. Total Environ.*, **226**, 65–74.
310. Lyon, T.D.B., Patriarca, M., Howatson, A.G., Fleming, P.J., Blair, P.S. and Fell, G.S. (2002) Age dependence of potentially toxic elements (Sb, Cd, Pb, Ag) in human liver tissue from paediatric subjects. *J. Environ. Monitor.*, **4**, 1034–1039.
311. Anderson, S.L. and Pergantis, S.A. (2003) Sequential hydride generation/pneumatic nebulisation inductively coupled plasma mass spectrometry for the fractionation of arsenic and selenium species. *Talanta*, **2003**, 821–830.
312. Osada, H., Watanabe, Y., Nishimura, Y., Yukawa, M., Seki, K. and Sekiya, S. (2002) Profile of trace element concentration in the faeto-placental unit in relation to foetal growth. *Acta Obstet. Gyn. Scan.*, **81**, 931–937.
313. Nystrom-Rosander, C., Lindh, U., Thelin, S., Lindquist, O., Friman, G. and Ilback, N.G. (2002) Trace element changes in sclerotic heart valves from patients undergoing aortic valve surgery. *Biol. Trace Elem. Res.*, **88**, 9–24.
314. Inagaki, K. and Haraguchi, H. (2000) Determination of rare earth elements in human blood serum by inductively coupled plasma mass spectrometry after chelating resin preconcentration. *Analyst*, **125**, 191–196.

315. Ming, Y. and Bing, L. (1998) Determination of rare earth elements in human hair and wheat flour reference materials by inductively coupled plasma mass spectrometry with dry ashing and microwave digestion. *Spectrochim. Acta B.*, **53**, 1447–1454.
316. Osman, K., Zejda, J.E., Schutz, A., Mielzynska, D., Elinder, C.G. and Vahter, M. (1998) Exposure to lead and other metals in children from Katowice district, Poland. *Int. Arch. Occ. Env. Hea.*, **71**, 180–186.
317. Mahomed, K., Williams, M.A., Woelk, G.B., Mudzamiri, S., Madzime, S., King, I.B. and Bankson, D.D. (2000) Leukocyte selenium, zinc and copper concentrations in preeclamptic and normotensive pregnant women. *Biol. Trace Elem. Res.*, **75**, 107–118.
318. Zhang, Y., Zhao, Y., Wang, J., Zhu, H., Liu, Q., Fan, Y., Wang, N., Liu, A., Liu, H., Ou-Yang, L., Zhao, J. and Fan, T. (2004) Effects of zinc, copper and selenium on placental cadmium transport. *Biol. Trace Elem. Res.*, **102**, 39–50.
319. Vahter, M., Counter, S.A., Laurell, G., Buchanan, L.H., Ortega, F., Schutz, A. and Skerfving, S. (1997) Extensive lead exposure in children living in an area with production of lead-glazed tiles in Ecuadorian Andes. *Int. Arch. Occ. Env. Hea.*, **70**, 282–286.
320. Menegario, A.A., Packer, A.P. and Gine, M.F. (2001) Determination of Ba, Cd, Cu, Pb, and Zn in saliva by isotope dilution direct injection inductively coupled plasma mass spectrometry. *Analyst*, **126**, 1363–1366.
321. Wang, J., Hansen, E.H. and Gammelgaard, B. (2001) Flow injection on-line dilution for multi-element determination in human urine with detection by inductively coupled plasma mass spectrometry. *Talanta*, **55**, 117–126.
322. Tolmachev, S.Y., Kuwabara, J. and Noguchi, H. (2004) Flow injection chromatography with ICP-MS for thorium and uranium determination in human body fluids. *J. Radioanal. Nucl. Ch.*, **261**, 125–131.
323. Al-Jundi, J., Werner, E., Roth, P., Hollriegel, V., Wendler, I. and Schramel, P. (2004) Thorium and uranium contents in human urine: influence of age and residential area. *J. Environ. Radioactiv.*, **71**, 61–70.
324. Mohagheghi, A.H., Shanks, S.T., Zigmond, J.A., Simmons, G.L. and Ward, S.L.A. (2005) A survey of uranium and thorium background levels in water, urine, and hair and determination of uranium enrichments by ICP-MS. *J. Radioanal. Nucl. Ch.*, **263**, 189–195.
325. Ting, B.G., Paschal, D.C., Jarrett, J.M., Pirkle, J.L., Jackson, R.J., E.J. Sampson, Miller, D.T. and Caudill, S.P. (1999) Uranium and thorium in urine of United States residents: reference range concentrations. *Environ. Res.*, **81**, 45–51.
326. Caroli, S., Alimonti, A., Petrucci, F., Bocca, B., Krachler, M., Forashiere, F., Sacerdote, M.T. and Mallone, S. (2001) Assessment of exposure to platinum-group metals in urban children. *Spectrochim. Acta B.*, **56**, 1241–1248.
327. Palacios, M.A., Gomez, M., Moldovan, M. and Gomez, B. (2000) Assessment of environmental contamination risk by Pt, Rh and Pd from automobile catalyst. *Microchem. J.*, **67**, 105–113.
328. Kunze, J., Koelling, S., Reich, M. and Wimmer, M.A. (2000) Use of ultrasonic nebulizer with desolvator membrane for the determination of titanium and zirconium in human serum by means of inductively coupled plasma-mass spectrometry. *Anal. Bioanal. Chem.*, **366**, 165–166.
329. Alimonti, A., Petrucci, F., Fiorvanti, S., Laurenti, F. and Caroli, S. (1997) Assessment of the content of selected trace elements in serum of term and pre-term newborns by inductively coupled plasma mass spectrometry. *Anal. Chim. Acta*, **342**, 75–81.
330. Alimonti, A., Petrucci, F., Laurenti, F., Papoff, P. and Caroli, S. (2000) Reference values for selected trace elements in serum of term newborns from the urban area of Rome. *Clin. Chim. Acta*, **292**, 163–173.
331. Li, B., Sun, Y. and Yin, M. (1999) Determination of cerium, neodymium and samarium in biological materials at low levels by isotope dilution inductively coupled plasma mass spectrometry. *J. Anal. Atom. Spectrom.*, **14**, 1843–1848.

332. Benes, B., Jakubec, K., Smid, J. and Spevackova, V. (2000) Determination of thirty-two elements in human autopsy tissue. *Biol. Trace Elem. Res.*, **75**, 195–203.
333. Komaromy-Hiller, G., Ash, K.O., Costa, R. and Howerton, K. (2000) Comparison of representative ranges based on U.S. patient population and literature reference intervals for urinary trace elements. *Clin. Chim. Acta*, **296**, 71–90.
334. White, M.A. and Sabbioni, E. (1998) Trace element reference values in tissues from inhabitants of the European Union. X. A study of 13 elements in blood and urine of a United Kingdom population. *Sci. Total Environ.*, **216**, 253–270.
335. Inagaki, K., Mikuriya, N., Morita, S., Haraguchi, H., Nakahara, Y., Hattori, M., Kinoshita, T. and Saito, H. (2000) Speciation of protein-binding zinc and copper in human blood serum by chelating resin pre-treatment and inductively coupled plasma mass spectrometry. *Analyst*, **125**, 197–203.
336. Szpunar, J., Bettner, J., Robert, M., Chassaigne, H., Cammann, K., Lobinski, R. and Donard, O.F.X. (1997) Validation of the determination of copper and zinc in blood plasma and urine by ICP-MS with cross-flow and direct injection nebulization. *Talanta*, **44**, 1389–1396.
337. Bouvier-Capely, C., Ritt, J., Baglan, N. and Cossonnet, C. (2004) Potentialities of mass spectrometry (ICP-MS) for actinides determination in urine. *Appl. Radiat. Isotopes*, **60**, 629–633.
338. Krachler, M., Lindschinger, M., Watzinger, N., Eber, B. and Wallner, S. (2000) Impact of mechanical vascular injury on whole blood and plasma concentrations of trace elements and electrolytes in patients with coronary heart disease. *J. Trace Elem. Exp. Med.*, **13**, 185–194.
339. Pamphlett, R. (2001) Blood levels of toxic and essential metals in motor neuron disease. *NeuroToxicology*, **22**, 401–410.
340. Schramel, P., Wendler, I. and Angerer, J. (1997) The determination of metals (antimony, bismuth, lead, cadmium, mercury, palladium, platinum, tellurium, thallium, tin and tungsten) in urine samples by inductively coupled plasma-mass spectrometry. *Int. Arch. Occ. Env. Hea.*, **69**, 219–223.
341. Barany, E., Bergdahl, I.A., Schutz, A., Skerfving, S. and Oskarsson, A. (1997) Inductively coupled plasma mass spectrometry for direct multi-element analysis of diluted human blood and serum. *J. Anal. Atom. Spectrom.*, **12**, 1005–1009.
342. Krachler, M., Domej, W. and Irgolic, K.J. (2000) Concentrations of trace elements in osteoarthritic knee-joint effusions. *Biol. Trace Elem. Res.*, **75**, 253–263.
343. Gerotto, M., Andrea, E.D., Bortoli, A., Marchiori, M., Palonta, M. and Troncon, A. (1995) Interface effects and their control in ICP-MS analysis of serum and saline solutions. *Microchem. J.*, **51**, 73–87.
344. Wang, J. and Hansen, E.H. (2001) Interfacing sequential injection on-line preconcentration using a renewable micro-column incorporated in a 'lab-on-valve' system with direct injection nebulization inductively coupled plasma mass spectrometry. *J. Anal. Atom. Spectrom.*, **16**, 1349–1355.
345. Boulyga, S.F., Becker, J.S., Malenchenko, A.F. and Dietze, H.J. (2000) Application of ICP-MS for multielement analysis in small sample amounts of pathological thyroid tissue. *Microchim. Acta*, **134**, 215–222.
346. Morton, J., Carolan, V.A. and Gardiner, P.H.E. (2002) Removal of exogenously bound elements from human hair by various washing procedures and determination by inductively coupled plasma mass spectrometry. *Anal. Chim. Acta*, **455**, 23–34.
347. Alimonti, A., Petrucci, F., Santucci, B., Cristaudo, A. and Caroli, S. (1995) Determination of chromium and nickel in human blood by means of inductively coupled plasma mass spectrometry. *Anal. Chim. Acta*, **306**, 35–41.
348. Danadevi, K., Rozati, R. and Grover, P. (2003) Semen quality of Indian welders occupationally exposed to nickel and chromium. *Reprod. Toxicol.*, **17**, 451–456.
349. LeBlanc, A., Dumas, P. and Lefebvre, L. (1999) Trace element content of commercial shampoos: impact on trace element levels in hair. *Sci. Total Environ.*, **229**, 121–124.
350. Reitznerova, E., Amarasiwardena, D., Kopcakova, M. and Barnes, R.M. (2000) Determination of some trace elements in human tooth enamel. *Anal. Bioanal. Chem.*, **367**, 748–754.

351. Brown, C.J., Chenery, S.R.N., Smith, B., Mason, C., Tomkins, A., Roberts, G.J., Sserunjogi, L. and Tiberindwa, J.V. (2004) Environmental influences on the trace element content of teeth-implications for disease and nutritional status. *Arch. Oral Biol.*, **49**, 705–717.
352. Osman, K., Akesson, A., Berglund, M., Bremme, K., Schutz, A., Ask, K. and Vahter, M. (2000) Toxic and essential elements in placentas of swedish women. *Clin. Biochem.*, **33**, 131–138.
353. Patriarca, M., Lyon, T.D.B., Delves, H.T., Howatson, A.G. and Fell, G.S. (1999) Determination of low concentrations of potentially toxic elements in human liver from newborns and infants. *Analyst*, **124**, 1337–1343.
354. Paschal, D.C., Ting, B.G., Morrow, J.C., Pirkle, J.L., Jackson, R.J., Sampson, E.J., Miller, D.T. and Caldwell, K.L. (1998) Trace metals in urine of United States residents: reference range concentrations. *Environ. Res.*, **76**, 53–59.
355. Dombovari, J., Becker, J.S. and Dietze, H.J. (2000) Multielemental analysis in small amounts of environmental reference materials with inductively coupled plasma mass spectrometry. *Anal. Bioanal. Chem.*, **367**, 407–413.
356. Wang, J.H. and Hansen, E.H. (2002) FI/SI on-line solvent/back extraction preconcentration coupled to direct injection nebulization inductively coupled plasma mass spectrometry for the determination of copper and lead. *J. Anal. Atom. Spectrom.*, **17**, 1284–1289.
357. Huang, C.C., Yang, M.H. and Shih, T.S. (1997) Automated on-line sample pretreatment system for the determination of trace metals in biological samples by inductively coupled plasma mass spectrometry. *Anal. Bioanal. Chem.*, **69**, 3930–3939.
358. Murphy, K.E., Long, S.E., Rearrick, M.S. and Ertas, O.S. (2002) The accurate determination of potassium and calcium using isotope dilution inductively coupled 'cold' plasma mass spectrometry. *J. Anal. Atom. Spectrom.*, **17**, 469–477.
359. Watanabe, M., Asatsuma, M., Ikui, A., Ikeda, M., Yamada, Y., Nomura, S. and Igarashi, A. (2005) Measurements of several metallic elements and matrix metalloproteinases (MMPs) in saliva from patients with taste disorder. *Chem. Senses*, **30**, 121–125.
360. Patriarca, M., Kratochwill, N.A. and Sadler, J. (1999) Simultaneous determination of Pt and I by ICP-MS for studies of the mechanism of reaction of diiodoplatinum anticancer complexes. *J. Anal. Atom. Spectrom.*, **14**, 633–637.
361. Sturup, S., Hansen, M. and Molgaard, C. (1997) Measurements of Ca-44:Ca-43 and Ca-42:Ca-43 isotopic ratios in urine using high resolution inductively coupled plasma mass spectrometry. *J. Anal. Atom. Spectrom.*, **12**, 919–923.
362. Field, M.P., Shapses, S., Cifuentes, M. and Sherrell, R.M. (2003) Precise and accurate determination of calcium isotope ratios in urine using HR-ICP-SFMS. *J. Anal. Atom. Spectrom.*, **18**, 727–733.
363. Sturup, S. (2002) Uncertainty calculation on the determination of calcium absorption in nutritional experiments with enriched stable isotopes and detection by double focusing sector field ICP-MS with a shielded torch. *J. Anal. Atom. Spectrom.*, **17**, 1–7.
364. Mota, J.P.V., Encinar, J.R., Campa, M.R.F.d.I., Alonso, J.I.G. and Sanz-Medel, A. (1999) Determination of cadmium in environmental and biological reference materials using isotope dilution analysis with a double focusing ICP-MS: a comparison with quadrupole ICP-MS. *J. Anal. Atom. Spectrom.*, **14**, 1467–1473.
365. Ingle, C., Langford, N., Harvey, L., Dainty, J.R., Armah, C., Fairweather-Tait, S., Sharp, B., Crews, H., Rose, M. and Lewis, J. (2002) Development of a high-resolution ICP-MS method, suitable for the measurement of iron and iron isotope ratios in acid digests of faecal samples from a human nutrition study. *J. Anal. Atom. Spectrom.*, **17**, 1498–1501.
366. Vanhaecke, F., Balcaen, L., Wannemacker, G.D. and Moens, L. (2002) Capabilities of inductively coupled plasma mass spectrometry for the measurement of Fe isotope ratios. *J. Anal. Atom. Spectrom.*, **17**, 933–934.
367. Smith, D., Illustre, R.P. and Osterloh, J.D. (1998) Methodological considerations for the accurate determination of lead in human plasma and serum. *Am. J. Ind. Med.*, **33**, 430–438.

368. Gwiazda, R., Woolard, D. and Smith, D. (1998) Improved lead isotope ratio measurements in environmental and biological samples with a double focussing magnetic sector inductively coupled plasma mass spectrometer. *J. Anal. Atom. Spectrom.*, **13**, 1233–1238.
369. Woolard, D., Franks, R. and Smith, D.R. (1998) Inductively coupled plasma magnetic sector mass spectrometry method for stable lead isotope tracer studies. *J. Anal. Atom. Spectrom.*, **13**, 1015–1019.
370. Hann, S., Koellensperger, G., Kanitsar, K., Stingeder, G., Brunner, M., Erovic, B., Muller, M. and Reiter, C. (2003) Platinum determination by inductively coupled plasma-sector field mass spectrometry (ICP-SFMS) in different matrices relevant to human biomonitoring. *Anal. Bioanal. Chem.*, **376**, 198–204.
371. Ting, B.G., Pappas, R.S. and Paschal, D.C. (2003) Rapid analysis for plutonium-239 in urine by magnetic sector inductively coupled plasma-mass spectrometry using Aridus desolvation introduction system. *J. Anal. Atom. Spectrom.*, **18**, 795–797.
372. Pappas, R.S., Ting, B.G. and Paschal, D.C. (2004) Rapid analysis for plutonium-239 in 1 ml of urine by magnetic sector inductively coupled plasma mass spectrometry with a desolvating introduction system. *J. Anal. Atom. Spectrom.*, **19**, 762–766.
373. Krystek, P. and Ritsema, R. (2002) Determination of uranium in urine – measurement of isotope ratios and quantification by use of inductively coupled plasma mass spectrometry. *Anal. Bioanal. Chem.*, **374**, 226–229.
374. Schramel, P. (2002) Determination of U-235 and U-238 in urine using sector field inductively coupled plasma mass spectrometry. *J. Chromatogr. B*, **778**, 275–278.
375. Yang, L., Sturgeon, R.E., Prince, D. and Gabos, S. (2002) Determination of vanadium in biological fluids using HR-ICP-MS. *J. Anal. Atom. Spectrom.*, **17**, 1300–1303.
376. Featherstone, A.M., Townsend, A.T., Jacobson, G.A. and Peterson, G.M. (2004) Comparison of methods for the determination of total selenium in plasma by magnetic sector inductively coupled plasma mass spectrometry. *Anal. Chim. Acta*, **512**, 319–327.
377. Latoczy, C., Prohaska, T., Stingeder, G. and Teschler-Nicola, M. (1998) Strontium isotope ratio measurements in prehistoric human bone samples by means of high-resolution inductively coupled plasma mass spectrometry (HR-ICP-MS). *J. Anal. Atom. Spectrom.*, **13**, 561–566.
378. Vonderheide, A.P., Zoriy, M.V., Izmer, A.V., Pickhardt, C., Caruso, J.A., Ostapczuk, P., Hille, R. and Becker, J.S. (2004) Determination of Sr-90 at ultratrace levels in urine by ICP-MS. *J. Anal. Atom. Spectrom.*, **19**, 675–680.
379. Sturup, S. (2000) Application of HR-ICP-MS for the simultaneous measurement of zinc isotope ratios and total zinc content in human samples. *J. Anal. Atom. Spectrom.*, **15**, 315–321.
380. Helal, A.I., Zahran, N.F. and Rashad, A.M. (2002) Isotopes and concentrations of Zn in human blood and serum by ICP-MS. *Int. J. Mass Spectrom.*, **213**, 217–224.
381. Alimonti, A., Petrucci, F., Krachler, M., Bocca, B. and Caroli, S. (2000) Reference values for chromium, nickel and vanadium in urine of youngsters from the urban area of Rome. *J. Environ. Monitor.*, **2**, 351–354.
382. Townsend, A.T. (2000) The accurate determination of the first row transition metals in water, urine, plant, tissue and rock samples by sector field ICP-MS. *J. Anal. Atom. Spectrom.*, **15**, 307–314.
383. Muniz, C.S., Marchante, J.M., Alonso, J.I.G. and Sanz-Medel, A. (1999) Accurate determination of iron, copper and zinc in human serum by isotope dilution analysis using double focusing ICP-MS. *J. Anal. Atom. Spectrom.*, **14**, 1505–1510.
384. Begerow, J., Turfeld, M. and Dunemann, L. (1997) Determination of physiological palladium, platinum, iridium and gold levels in human blood using double focusing magnetic sector field inductively coupled plasma mass spectrometry. *J. Anal. Atom. Spectrom.*, **12**, 1095–1098.
385. Rodushkin, I., Odman, F. and Branth, S. (1999) Multielement analysis of whole blood by high resolution inductively coupled mass spectrometry. *Anal. Bioanal. Chem.*, **364**, 338–346.

386. Rodushkin, I., Odman, F., Olofsson, R. and Axelsson, M.D. (2000) Determination of 60 elements in whole blood by sector field inductively coupled plasma mass spectrometry. *J. Anal. Atom. Spectrom.*, **15**, 937–944.
387. Rodushkin, I. and Axelsson, M.D. (2000) Application of double focusing sector field ICP-MS for multielemental characterization of human hair and nails. Part II. A study of the inhabitants of northern Sweden. *Sci. Total Environ.*, **262**, 21–36.
388. Begerow, J., Turfeld, M. and Dunemann, L. (2000) New horizons in human biomonitoring of environmentally and occupationally relevant metals – sector-field ICP-MS vs. electrothermal AAS. *J. Anal. Atom. Spectrom.*, **15**, 347–352.
389. Schramel, P. and Wendler, I. (1998) Capabilities of double focussing magnetic sector-ICP-MS for the determination of trace elements in body fluids (blood, blood serum, urine) at the example of control materials. *Anal. Bioanal. Chem.*, **361**, 487–491.
390. Muniz, C.S., Fernandez-Martin, J.L., Marchante-Gayon, J.M., Alonso, J.I.G., Cannata-Andia, J.B. and Sanz-Medel, A. (2001) Reference values for trace and ultratrace elements in human serum determined by double-focusing ICP-MS. *Biol. Trace Elem. Res.*, **82**, 259–272.
391. Pappas, R.S., Ting, B.G., Jarrett, J.M., Paschal, D.C., Caudill, S.P. and Miller, D.T. (2002) Determination of uranium-235, uranium-238 and thorium-232 in urine by magnetic sector inductively coupled plasma mass spectrometry. *J. Anal. Atom. Spectrom.*, **17**, 131–134.
392. Pappas, R.S., Ting, B.G. and Paschal, D.C. (2003) A practical approach to determination of low concentration uranium isotope ratios in small volumes of urine. *J. Anal. Atom. Spectrom.*, **18**, 1289–1292.
393. Townsend, A.T., Miller, K.A., McLean, S. and Aldous, S. (1998) The determination of copper, zinc, cadmium and lead in urine by high resolution ICP-MS. *J. Anal. Atom. Spectrom.*, **13**, 1213–1219.
394. Riondato, J., Vanhaecke, F., Moens, L. and Dams, R. (1997) Determination of trace and ultra-trace elements in human serum with a double focusing magnetic sector inductively coupled plasma mass spectrometer. *J. Anal. Atom. Spectrom.*, **12**, 933–937.
395. Krachler, M., Alimonti, A., Petrucci, F., Forastiere, F. and Caroli, S. (1998) Influence of sample pre-treatment on the determination of trace elements in urine by quadrupole and magnetic sector inductively coupled plasma mass spectrometry. *J. Anal. Atom. Spectrom.*, **13**, 701–705.
396. Krachler, M., Alimonti, A., Petrucci, F., Irgolic, K.J., Forastiere, F. and Caroli, S. (1998) Analytical problems in the determination of platinum-group metals in urine by quadrupole and magnetic sector field inductively coupled plasma mass spectrometry. *Anal. Chim. Acta*, **363**, 1–10.
397. Townsend, A.T. (1999) The determination of arsenic and selenium in standard reference materials using sector field ICP-MS in high resolution mode. *Anal. Bioanal. Chem.*, **364**, 521–526.
398. Begerow, J., Turfeld, M. and Dunemann, L. (1997) Determination of physiological palladium and platinum levels in urine using double focusing magnetic sector field ICP-MS. *Anal. Bioanal. Chem.*, **359**, 427–429.
399. Muniz, C.S., Marchante-Gayon, J.M., Alonso, J.I.G. and Sanz-Medel, A. (1999) Multi-elemental trace analysis of human serum by double-focussing ICP-MS. *J. Anal. Atom. Spectrom.*, **14**, 193–198.
400. Schramel, P. and Wendler, I. (1998) Some investigations on stability and precision of an HR-ICP-MS. *J. Anal. Atom. Spectrom.*, **360**, 152–155.
401. Vanhaecke, F., Moens, L. and Dams, R. (1997) Applicability of high-resolution ICP-mass spectrometry for isotope ratio measurements. *Anal. Chem.*, **69**, 268–273.
402. Nixon, D.E., Neubauer, K.R., Eckdahl, S.J., Butz, J.A. and Burritt, M.F. (2002) Evaluation of a tunable bandpass reaction cell for an inductively coupled plasma mass spectrometer for the determination of chromium and vanadium in serum and urine. *Spectrochim. Acta B*, **57**, 951–966.

403. Nixon, D.E., Neubauer, K.R., Eckdahl, S.J., Butz, J.A. and Burritt, M.F. (2003) Evaluation of a tunable bandpass reaction cell for an inductively coupled plasma mass spectrometer for the determination of selenium in serum and urine. *Spectrochim. Acta B.*, **58**, 97–110.
404. Sloth, J.J., Larsen, E.H., Bugel, S.H. and Moesgaard, S. (2003) Determination of total selenium and Se-77 in isotopically enriched human samples by ICP-dynamic reaction cell-MS. *J. Anal. Atom. Spectrom.*, **18**, 317–322.
405. Reyes, L.H., Gayon, J.M.M., Alonso, J.I.G. and Sanz-Medel, A. (2003) Determination of selenium in biological materials by isotope dilution analysis with an octapole reaction system ICP-MS. *J. Anal. Atom. Spectrom.*, **18**, 11–16.
406. Chang, Y.L. and Jiang, S.J. (2001) Determination of chromium in water and urine by reaction cell inductively coupled plasma mass spectrometry. *J. Anal. Atom. Spectrom.*, **16**, 1434–1438.
407. Heitland, P. and Koster, H.D. (2004) Fast, simple and reliable routine determination of 23 elements in urine by ICP-MS. *J. Anal. Atom. Spectrom.*, **19**, 1552–1558.
408. Simpson, L.A., Hearn, R., Merson, S. and Catterick, T. (2005) A comparison of double-focusing sector field ICP-MS, ICP-OES and octapole collision cell ICP-MS for the high-accuracy determination of calcium in human serum. *Talanta*, **65**, 900–906.
409. Nagaoka, M.H. and Maitani, T. (2000) Binding patterns of co-existing aluminium and iron to human serum transferrin studied by HPLC-high resolution ICP-MS. *Analyst*, **125**, 1962–1965.
410. Nagaoka, M.H., Yamazaki, T. and Maitani, T. (2002) Binding patterns of vanadium ions with different valence states to human serum transferrin studied by HPLC/high resolution ICP-MS. *Biochem. Bioph. Res. Co.*, **296**, 1207–1214.
411. Nagaoka, M.H., Akiyama, H. and Maitani, T. (2004) Binding patterns of vanadium to transferrin in healthy human serum studied with HPLC/high resolution ICP-MS. *Analyst*, **129**, 51–54.
412. Krachler, M. and Emons, H. (2001) Urinary antimony speciation by HPLC-ICP-MS. *J. Anal. Atom. Spectrom.*, **16**, 20–25.
413. Miekeley, N., Mortari, S.R. and Schubach, A.O. (2002) Monitoring of total antimony and its species by ICP-MS and on-line chromatography in biological samples from patients treated for leishmaniasis. *Anal. Bioanal. Chem.*, **372**, 495–502.
414. Muniz, C.S., Marchante-Gayon, J.M., Alonso, J.I.G. and Sanz-Medel, A. (2001) Speciation of essential elements in human serum using anion-exchange chromatography coupled to post-column isotope dilution analysis with double focusing ICP-MS. *J. Anal. Atom. Spectrom.*, **16**, 587–592.
415. Wuilloud, R.G., Selar, N., Kannamkumarath, S.S. and Caruso, J.A. (2004) Determination of 2,4,6-triiodophenol and its metabolites in human urine by anion-exchange chromatography with ICP-MS detection. *J. Anal. Atom. Spectrom.*, **19**, 1442–1447.
416. Carter, J., Ebdon, L. and Evans, E.H. (2004) Speciation of silicon and phosphorus using liquid chromatography coupled with sector field high resolution ICP-MS. *Microchem. J.*, **76**, 35–41.
417. Zhang, Y., Hess, E.V., Pryhuber, K.G., Dorsey, J.G., Tepperman, K. and Elder, R.C. (1995) Gold binding sites in red blood cells. *Inorg. Chim. Acta*, **229**, 271–280.
418. Harada, K., Kuniyasu, A., Nakayama, H., Nakayama, M., Matsunaga, T., Uji, Y., Sugiuchi, H. and Okabe, H. (2002) Separation of human serum transferrins with different iron-binding states by high-performance liquid chromatography using a pyridium polymer column. *J. Chromatogr. B.*, **767**, 45–51.
419. Infante, H.G., Sanchez, M.L.F. and Sanz-Medel, A. (1999) Cadmium-bound species in human urine using high-performance liquid chromatography-vesicular hydride generation-inductively coupled plasma mass spectrometry. *J. Anal. Atom. Spectrom.*, **14**, 1343–1348.
420. Svantesson, E., Capala, J., Markides, K.E. and Pettersson, J. (2002) Determination of boron-containing compounds in urine and blood plasma from boron neutron capture therapy patients. The importance of using coupled techniques. *Anal. Chem.*, **74**, 5358–5363.

421. Hang, W., Zhu, L., Zhong, W. and Mahan, C. (2004) Separation of actinides at ultra-trace level from urine matrix using extraction chromatography-inductively coupled plasma mass spectrometry. *J. Anal. Atom. Spectrom.*, **19**, 966–972.
422. Cairns, W.R.L., Ebdon, L. and Hill, S.J. (1996) A high performance liquid chromatography – inductively coupled plasma-mass spectrometry interface employing desolvation for speciation studies of platinum in chemotherapy drugs. *Anal. Bioanal. Chem.*, **355**, 202–208.
423. Galettis, P., Carr, J.L., Paxton, J.W. and McKeage, M.J. (1999) Quantitative determination of platinum complexes in human plasma generated from the oral antitumour drug JM216 using directly coupled high-performance liquid chromatography-inductively coupled plasma mass spectrometry without desolvation. *J. Anal. Atom. Spectrom.*, **14**, 953–956.
424. Vacchina, V., Torti, L., Allievi, C. and Lobinski, R. (2003) Sensitive species-specific monitoring of a new triplatinum anti-cancer drug and its potential related compounds in spiked human plasma by cation-exchange HPLC-ICP-MS. *J. Anal. Atom. Spectrom.*, **18**, 884–890.

Chapter 11

Applications of Plasma Spectrometry in Food Science

Helen M. Crews, Paul Robb and Malcolm J. Baxter

11.1 Introduction

Plasma spectrometry has many applications in food science and is used in the analysis of a wide range of samples in the 'plough to plate' food chain. Food science in the broadest sense can be extended to include soil chemistry, plant uptake and, at the other end of the food chain, to include studies into the metabolic fate of particular elements or elemental species when certain foods are consumed by humans or animals. Samples analysed by plasma spectrometry can vary from the relatively simple and well defined, for example a single fruit or vegetable, through to complex, highly processed whole meals, diets, digesta, excreta or other biological samples. The establishment of routine automated analytical methods using inductively coupled plasma-atomic emission spectrometry (ICP-AES) and inductively coupled plasma-mass spectrometry (ICP-MS) have permitted multi-element measurements of most elements in the Periodic Table. Advantages of plasma spectrometry include the abilities to perform speciation studies when coupled with separation techniques, to measure isotopic composition (ICP-MS) in nutritional studies and to identify sources of environmental exposure.

The most commonly encountered plasma methods in food science are ICP-AES and ICP-MS (together with hyphenated techniques based on these methods). ICP-AES has largely superseded direct current plasma (DCP) spectrometry because a major drawback of DCPs is the lack of ease by which they may be incorporated into totally automated systems [1]. In a review by Taylor *et al.*, in 1997 the two ICP techniques each accounted for approximately 10% of publications concerned with analysis of foods and beverages with atomic absorption techniques cited in most of the remaining articles [2]. In atomic spectrometry reviews of foods and beverages by the same group in 2003, 2004 and 2005 [3–5] the percentage of ICP-AES articles remained at around 10% whilst publications in which ICP-MS was used had risen to over 30%. When compared to ICP-AES, ICP-MS has lower detection limits but is more expensive, due to its initial and running costs [6]. In addition, good quality analytical work requires a specialised staff who are also able to assess both multi-element and multi-isotopic data. The point is well made that purpose-written software can facilitate data gathering and manipulation but visual inspection by an experienced analyst remains essential and this applies to both ICP-MS and ICP-AES. Although ICP-AES has lower running costs, better tolerance to total

salt content in test solutions and less severe matrix effects when compared with ICP-MS [7,8], spectral overlap can be a problem. Some of the advantages of ICP-MS include fewer spectral interferences than ICP-AES [9], improved sensitivity and a wider dynamic range. The wide dynamic concentration range and speed of measurement makes this a particularly powerful tool for surveillance, legislative and emergency work.

In this chapter some of the common interferences are described in some detail before practical aspects of food analysis, including sample preparation, pre-treatment, quantification, quality control and the application of plasma methods to speciation studies are discussed. Some future trends for plasma spectrometry in food science are also considered.

11.2 Analytical challenges

Spectral interferences in ICP-MS take the form of isobaric interferences (i.e. overlap of isotopes of the same unit mass) or polyatomic species resulting from the overlap of the analyte peak by molecular fragments present in the plasma or formed from plasma and matrix components, or doubly charged species that appear at mass positions $m/2$. Spectral overlap remains a significant challenge for users of ICP-AES. Plasma-source methods of analysis are therefore not without problems and caution may be needed when dealing with complex real samples such as foods where matrix effects and interferences can occur.

Whilst quadrupole-based ICP-MS instruments show only unit mass resolution (peak width approximately 0.5μ over the entire mass spectrum), ICP-sector field MS (ICP-SFMS) permits measurements at a higher mass resolution [10]. Plasma source time-of-flight MS instruments can achieve resolution figures that are better than conventional quadrupole systems but their resolution is inferior to SF instruments and insufficient for separation of important ICP-MS isobars such as ^{52}Cr with $^{40}\text{Ar}^{12}\text{C}$ and ^{56}Fe with $^{40}\text{Ar}^{16}\text{O}$ [11].

11.2.1 Isobaric overlap in ICP-MS

Quadrupole ICP-MS (the most common form of ICP-MS currently in use in food science) has unit mass resolution, which means that isotopes with similar atomic masses will be detected as the same isotope. Consequently, particular care may be needed when performing isotope ratio measurements and these are an important tool in human nutrition studies [12,13]. In most cases, however, isotopes free from isobaric interferences can be chosen and In is the only element that does not have at least one isotope free of isobaric overlap (^{113}In , relative abundance 4.28%, is overlapped by ^{113}Cd , relative abundance 12.26%, and ^{115}In , relative abundance 95.72%, is overlapped by ^{115}Sn , relative abundance 0.35%). This particular isobaric problem can be severe since In is frequently employed as an internal standard and could therefore cause difficulties in Cd isotopic ratio studies or low-level Sn measurements. Both of these elements are important in food science and alternative internal standards can be used in most cases. Isobaric interferences and their abundances are predictable from isotope tables and can often be avoided.

The use of an Ar plasma precludes measurement of the main isotope of Ca, ^{40}Ca , but levels of this element in foods are usually high enough to allow the use of the next most abundant isotope, ^{44}Ca . However, for multi-isotope nutritional studies, the inability to

measure all Ca isotopes is a disadvantage. The use of cool plasma conditions (obtained by using a low-radio frequency power and increased nebuliser flow rate) leads to a substantial reduction in the intensity of Ar^+ and Ar-based ions. This can make the determination of K, Ca and Fe possible but the use of a cool plasma also brings disadvantages: elements characterised by high ionisation potential are no longer efficiently ionised, the signal intensity of other types of molecular interferences such as oxide ions increase and matrix effects become more pronounced [10]. Thus for food analyses where matrices are most commonly complex cool plasmas are not routinely used.

11.2.2 Polyatomic and doubly charged species interferences in ICP-MS

When samples are introduced into the plasma by nebulisation of aqueous solutions the major plasma species are H, O and Ar. However, in the presence of solvent acids, for example in digested foods, C, N, Cl, S or P ions may also be present. These species can form polyatomic species, which are usually binary but may include the addition of a hydrogen atom [14–16]. In such cases, only some of the isotopes in the lower mass range, 1–84 m/z , are affected. Table 11.1 gives some of the polyatomic species that may be important in the analysis of food samples (taken from [17,18]).

Table 11.1 Examples (non-exclusive) of polyatomic interferences of importance in food science [17,18]

Isotope	Natural abundance (%)	Potential interferences
^{26}Mg	11.01	$^{12}\text{C}^{14}\text{N}$
^{39}K	100	^{38}ArH
^{42}Ca	0.647	$^{40}\text{Ar}^{1}\text{H}_2$, $^{40}\text{Ar}^2\text{H}$
^{44}Ca	2.086	$^{12}\text{C}^{16}\text{O}_2$
^{46}Ca	0.004	$^{14}\text{N}^{16}\text{O}_2$, $^{32}\text{S}^{14}\text{N}$
^{48}Ca	0.187	$^{32}\text{S}^{16}\text{O}$, $^{34}\text{S}^{14}\text{N}$
^{50}Cr	4.345	$^{36}\text{Ar}^{14}\text{N}$
^{52}Cr	83.789	$^{40}\text{Ar}^{12}\text{C}$, $^{36}\text{Ar}^{16}\text{O}$, $^{35}\text{Cl}^{16}\text{O}^1\text{H}$
^{53}Cr	9.501	$^{37}\text{Cl}^{16}\text{O}$
^{54}Cr	2.365	$^{40}\text{Ar}^{14}\text{N}$, $^{37}\text{Cl}^{16}\text{O}^1\text{H}$
^{54}Fe	5.8	$^{40}\text{Ar}^{14}\text{N}$, $^{37}\text{Cl}^{16}\text{O}^1\text{H}$
^{56}Fe	91.72	$^{40}\text{Ar}^{16}\text{O}$
^{57}Fe	2.2	$^{40}\text{Ar}^{16}\text{O}^1\text{H}$
^{63}Cu	69.17	$^{40}\text{Ar}^{23}\text{Na}$, $^{31}\text{P}^{16}\text{O}_2$
^{65}Cu	30.83	$^{33}\text{S}^{16}\text{O}_2$, $^{32}\text{S}^{33}\text{S}$
^{64}Zn	48.6	$^1\text{H}^{31}\text{P}^{16}\text{O}_2$, $^{32}\text{S}^{16}\text{O}_2$, $^{32}\text{S}_2$
^{67}Zn	4.1	$^{35}\text{Cl}^{16}\text{O}_2$
^{70}Zn	0.6	$^{40}\text{Ar}^{14}\text{N}^{16}\text{O}$, $^{35}\text{Cl}_2$
^{76}Se	9.36	$^{36}\text{Ar}^{40}\text{Ar}$, $^{40}\text{Ar}^{36}\text{S}$
^{77}Se	7.63	$^{40}\text{Ar}^{37}\text{Cl}$
^{80}Se	49.61	$^{40}\text{Ar}_2$, $^{40}\text{Ar}^{40}\text{Ca}$, $^{32}\text{S}^{16}\text{O}_3$
^{82}Se	8.73	$^{34}\text{S}^{16}\text{O}_3$

For some analyses (e.g. analysis of diluted wines), the authors' experience is that any contribution to the low mass range signal from water can be reduced by using a cooled spray chamber, thus reducing the water loading of the plasma [19]. When polyatomic species are generated by reagent solutions and do not involve sample components, blank subtraction may be sufficient to correct for their contribution. An alternative approach is to reduce the water loading on the plasma using techniques such as multiple cryogenic desolvation [10,20].

An important challenge in the use of ICP-MS in food science occurs with As measurements where $^{40}\text{Ar}^{35}\text{Cl}$ interferes with ^{75}As and the Cl contribution may arise from the sample (e.g. in seafood). Judicious use of the measured responses on masses 77 and 82, as well as that on 75 and the natural $^{35}\text{Cl}^{37}\text{Cl}$ isotopic ratio allow calculation of the Cl contribution to the ^{75}As signal. The $^{40}\text{Ar}^{37}\text{Cl}$ contribution on ^{77}Se also needs to be taken into account and this may be calculated from the $^{77}\text{Se}^{82}\text{Se}$ ratio. Although these calculations can be performed automatically by instrument software, the usefulness of this approach is limited by counting statistics, so that at low levels of As this method of correction is relatively ineffective. Other approaches can be used to overcome the problem, such as separation of the Cl from the analyte by chromatographic techniques [21,22] or hydride generation for elements such as As and Se. De-salting has also been reported as eliminating OCl^+ , HOCl^+ and ArCl^+ interferences during the determination of Se and other elements in serum using a Sephadex G-25 gel filtration column. However, it was also reported that Cu and Zn were partially retained by the Sephadex gel used in that work [23].

Adding N_2 to the Ar plasma gas supply has been reported as reducing polyatomic interferences for elements such as V, As and Se, all of which can suffer from Cl interferences [24–26]. Cryogenic desolvation has also been used to reduce the Cl load in the plasma [20].

Levels of oxide species in the plasma can be significant, particularly for the lighter elements. Elements whose bond strengths are above about 500 kJ mol^{-1} (e.g. P, Mo, Si, Ba and some of the rare earths) can show ratios of $\text{MO}^+:\text{M}^+$ from about 0.1% up to a few per cent for the most refractory species [27]. Some of these elements are present in significant quantities in food (e.g. P), while many others (e.g. rare earths), are found at much lower concentrations and the analyst needs to be aware of this problem. Although oxide levels are, in part, a function of instrument design [28], levels are normally stable enough to be corrected for with the use of standard solutions.

The effect of doubly charged species is generally much less serious than that of oxides and other polyatomic species. In food science investigations, interferences from doubly charged species are most likely to be encountered in the analysis of samples with a high mineral content. If, for example, Ga was being assessed as a soil splash indicator in herbage analysis then $^{138}\text{Ba}^{2+}$ could cause a problem where Ba was present at high levels because the doubly charged species coincides with $^{69}\text{Ga}^+$.

In the last few years progress has been made in tackling the problem of spectral interferences using multiple collision cell (MCC) or dynamic reaction cell (DRC) systems [10]. These are discussed in detail elsewhere in this book but essentially they involve an 'interaction of the ion beam with a gas or mixture of gases that enables the chemical removal of polyatomic interferences through collisional dissociation and selective ion-molecule reactions. The quadrupole of the DRC also provides an active cut-off of gas-phase reaction products from the cell, which leads to an efficient reduction of otherwise potential interferences at higher masses' [6]. Taylor and colleagues commented in 2005 [5] that the use of DRCs with quadrupole ICP mass spectrometers had increased in the field of clinical and biological

analyses and also that some laboratories are using sector-field instruments with their higher resolving power to remove polyatomic spectral overlaps and thereby improve accuracy.

11.2.3 Ionisation interferences in ICP-MS

Elements such as Na, K, Cs, Mg and Ca have been shown to enhance the analyte signal for several elements measured across the mass range while others such as B, Al and U cause signal suppression [29]. Some elements that induce signal enhancement or suppression are commonly encountered in food science where, for example, significant quantities of Ca, Na, K and Al may be present in test samples. ICP-MS appears to be more susceptible to ionisation suppression effects than ICP-AES [30,31] but these effects could be compensated for by stable isotope dilution (ID) or internal standardisation. The validity of correction by internal standardisation relies on the internal standard being suppressed to the same extent as the analyte therefore care is needed in choosing the appropriate internal standard(s), which must be present in negligible quantities in the test material(s).

Prohaska *et al.* [32] used ICP-SFMS very successfully to measure 16 trace elements in human milk and infant formulae. Their article is a good example of how to evaluate appropriate nebulisation systems and internal standards to minimise the impact of potential interferences, both spectral and non-spectral. Acid digests of the samples were measured and the isotopes used (including internal standards), and limits of detection (LODs) are given in Table 11.2. The LODs included the whole sample preparation procedure and reagents used, and were 3 times the standard deviation of an average of $n = 10$ blank solutions. Values were

Table 11.2 Selected isotopes and LODs for milk and milk powder samples measured using ICP-SFMS, (adapted from Prohaska *et al.* [32]) compared with some LODs for ICP-OES milk powder determinations [33]

Isotope	Internal standard	LOD milk ng/g liquid	LOD milk powder ng/g solid	LOD ICP-OES milk powder ng/ml (λ nm)
^{27}Al	^{115}In	10	50	
^{45}Sc	^{187}Re	0.13	0.67	
^{47}Ti	^{115}In	2.7	13	
^{51}V	^{103}Rh	0.07	0.33	
^{52}Cr	^{103}Rh	0.8	4.0	2.0 (267.716)
^{55}Mn	^{115}In	0.8	4.0	0.4 (257.610)
^{56}Fe	^{115}In	35	173	7.0 (259.940)
^{59}Co	^{103}Rh	0.07	0.33	
^{60}Ni	^{103}Rh	0.13	0.67	
^{63}Cu	^{115}In	1.3	6.7	6.0 (327.396)
^{75}As	^{115}In	1.3	6.6	
^{109}Ag	^{187}Re	0.13	0.67	
^{114}Cd	^{115}In	0.07	0.33	
^{195}Pt	^{187}Re	0.01	0.03	
^{197}Au	^{187}Re	0.05	0.27	
^{208}Pb	^{115}In	0.27	1.3	

expressed on the basis of 1.5 g liquid milk or 0.30 g milk powder [32]. For comparison, data for a few elements (Cr, Mn, Fe and Cu) are provided for milk powder measured using ICP-OES following partial digestion with hydrochloric acid [33]. Calcium, K, Mg, Na, P and Zn were also determined.

11.2.4 Interferences in ICP-AES

Interferences in ICP-AES have been known since soon after the initial launch of the technique. Spectral overlap remains a limitation although selection of minimal interference lines is a straightforward solution in many cases. As ICP-AES involves the emission of ion lines as well as atom lines, the analyst has a wider choice of wavelengths than is the case with other emission techniques. However, more emission lines can mean more overlap and a general increase in the complexity of the emission spectrum. Improvements in monochromator and instrument design to improve spectral resolution have also played their part in dealing with this problem. Where unique emission line selection is not practicable, mathematical corrections can be performed to compensate for interferences, but these may be complicated by partial spectral overlap in some instances. The emission spectrum contains a background continuum and elements such as Al can influence detection limits of several other elements.

Examples of spectral interferences of importance in food science include the Cu interference on a relatively sensitive Zn line at 213.85 nm, Mg on the 202.55 nm Zn line and Cr on the 206.20 nm Zn line. In addition Al will generate a continuum between 190 and 220 nm which will affect detection limits [34]. Other examples include the measurement of Fe in fertilisers, where Ca, P and K interfere [35], and the measurement of Co in plant and animal tissues, where the Fe line interferes at 238.863 nm [36]. Matrix effects in ICP-AES are well documented and the need to matrix match standards and samples, at least approximately, is well known. In wine analyses, ethanol may be added to standards to assist matrix matching (e.g. Ref. [37]). Internal standardisation can help in such circumstances, particularly if signal suppressants are present (e.g. Na or Ca), but other remedial action may be required. One example of this is provided by Moon *et al.*, where sodium levels in food digests had to be reduced to below 150 mg l⁻¹ before K levels were determined by ICP-AES [38].

11.2.5 Other sources of error

Although ICP-MS and ICP-AES are powerful techniques, care is still needed to ensure adequate quality control when performing measurements over a wide concentration range and a thorough evaluation of the accuracy and precision may be required for each element. Consequently, it can take considerable effort to develop robust methods which account for all possible matrix and any associated interferences while still being able to take advantage of the speed and sensitivity offered by the approach. Additionally, large amounts of data can be generated (including isotopic information in ICP-MS) which require careful processing and such procedures can be very time-consuming. Regardless of the type of matrix, analysis of the samples most frequently encountered in food science can be considered in a number of discrete stages, namely sample collection and storage, preparation, pre-treatment, quantification, quality control and reporting.

11.3 Sample collection and storage

Effective accounts of sampling and sample preparation methods have been published by Woittiez and Sloof [39], Jarvis [40] and Reilly [41]. Some useful guidance in specific areas can be found in a bibliography published by Thomas and Schofield [42]. Sampling protocols can be complex and the design of a suitable sampling scheme will vary according to the nature of a given investigation. Samples taken for legislative or statutory purposes may have to be taken by specially qualified personnel using prescribed methods and detailed records of how each test sample was obtained and the subsequent custody chain can sometimes be as important as the performance of a satisfactory analysis. A review of international legislation on trace elements as contaminants in food has been published by Berg and Licht [43].

Any sub-samples taken for analysis should be representative of the bulk matrix and all test material should be stored in a way that prevents degradation or contamination either from external sources or the containers used to hold the material pending measurement. The type of laboratory test containers used to hold materials will depend on the element(s) of interest, particularly when such analytes are ubiquitous in the environment (e.g. Al, Pb and Zn). Care is needed to prevent contamination and clean, inert containers are an essential requirement for all analyses. In some instances steps may have to be taken to prevent physical damage to samples (e.g. soft fruit), while in transit to the analytical facility and an inert inner package (e.g. a plastic bag), may have to be held in a rigid Al foil case while in transit. On receipt, full details of all samples should be registered and appropriate reference numbers allocated to samples to ensure traceability before the samples are stored at a suitable temperature until required for use. Effective storage is particularly important where there is the risk of microbial spoilage of the test samples.

11.3.1 *Uncertainty associated with sampling*

It has been recognised that the quality of a measurement is affected by the sampling processes and procedures as well as the analysis. In fact, it is typical for sampling to make a larger contribution than analysis to the uncertainty associated with the result of a chemical measurement [44]. This is often neglected due to several factors. These are a lack of standard procedures for the quantitative assessment of sampling in the food sector, a perception that gaining information about sampling quality is difficult and expensive and a lack of communication between samplers and analysts. A well-characterised sample should be produced following a prescribed or agreed sampling protocol and methods for assessing the performance of such protocols are being developed [45]. Samples, particularly those with a legislative or regulatory impact should, wherever possible, be analysed by a method validated by collaborative trial [46] or by single laboratory validation following recognised protocols [44].

11.4 Sample preparation

There have been several reviews of sample preparation and recent texts, as well as covering the generic needs for total element determinations also consider the impact of sample preparation on studies involving different sample fractions or discrete forms or species of

elements [3–6,47–49]. In general the aim of sample preparation is to produce a homogeneous bulk material that will allow representative sub-samples to be taken as required. For speciation studies the aim is also to try and ensure that the procedures maintain the integrity of the species under investigation. Fresh foods may have to be prepared as for the table and the authors' experience is that using stainless steel knives and clean plastic chopping boards minimises contamination problems. Domestic blenders, coffee grinders and food processors fitted with stainless steel, Ti or ceramic blades can be extremely effective at homogenising food samples while minimising contamination. Larger quantities of materials (100 g or more) may require the use of catering or industrial-scale food blenders. If the suite of elements to be analysed does not include volatile elements (e.g. Hg), then samples can be freeze dried before homogenisation. Removal of water can improve detection limits in some cases and the resulting friable dried matter can be much easier to mix and homogenise than the fresh matrix. However, freeze drying is unlikely to be effective for foods such as raw cereals or root vegetables because the resulting dried material is relatively hard to crush. Ensuring that the test material has been fully homogenised is difficult although performing measurements in duplicate can help with this. The following examples illustrate the way in which most common samples encountered in food science can be prepared. None of the following can be guaranteed for all matrix/analyte combinations but they have proved robust over many years of use in the authors' laboratory.

11.4.1 Liquid foods

Milk, many wines and most other beverages only need to be shaken well before sub-samples are taken. Sparkling wines, beers, etc. should be de-gassed in an ultrasonic bath before mixing and those wines which form a precipitate, for example crusted port, some red wines, etc., may have to be decanted into another container before sub-sampling. If Pb is to be analysed in wines, then care may be needed to ensure that no contamination arises where Pb foil caps have been used, as these can leave deposits on the lip of the bottle. Wiping the outer lip of the bottle with a soft tissue and removing the sub-sample with a pipette has been found to be effective in such cases [19]. To improve LODs, samples such as milk can be freeze dried (if appropriate) and this can also help with longer-term storage.

11.4.2 Meat

Inedible material (e.g. skin, hair, etc.) should be removed and discarded before the edible flesh is sampled. A representative slice should be taken through the piece of meat with a clean stainless steel knife and the meat homogenised using a blender or equivalent. It is imperative that the blender is cleaned well between samples using, for example, dilute detergent followed by tap water and then pure water.

11.4.3 Fish and shellfish

The fish should be gutted, washed with pure water and portions of edible flesh taken for analysis (i.e. avoiding the head, fins and larger bones). Whether to include the skin or not

may depend on the type of fish and local dietary custom. Fish species that are normally eaten whole should be blended without deboning. Removal of edible flesh from shellfish can be awkward and time-consuming but wherever possible fresh samples should be analysed which have been washed free of sand, etc. If practicable, viscera should be removed. It should be noted that freezing some crustaceans can cause undesirable liquefaction of the flesh on thawing. This can cause problems, for example if brown and white crab meat needs to be analysed separately.

In all cases a food blender can be used to produce a satisfactory homogenate.

11.4.4 Vegetables

Gross surface contamination should be removed from both root and leafy vegetables by brushing or washing with pure water. Analyses in support of dietary intake studies may require that root vegetables that are customarily eaten whole (e.g. potatoes) should not be peeled but are scrubbed before pre-treatment and outer leaves which are not normally consumed should be discarded from leafy vegetables. However, peel and outer leaves may have to be analysed in plant uptake studies and removal of surface contamination should be undertaken using cleaning methods which approximate treatment prior to consumption as closely as possible. Dicing the prepared vegetables, either using a stainless steel knife or an automated dicer/chopper, can be helpful but further blending may be needed if smaller sample sizes are taken for analysis.

Mushrooms should be brushed clean before analysis, bearing in mind that local custom can dictate whether or not the outer skin is removed prior to consumption and that fungi can absorb significant amounts of water during washing.

11.4.5 Fruits

The outer skin or peel of fruit can be a useful indicator of surface contamination and may have to be analysed separately from the remaining edible portions of hard fruits such as apples, pears, etc. A stomacher-type blender is useful for homogenising soft fruit [50]. Freezing the pulp, allowing it to partially thaw and mixing the iced slurry well can also help produce a representative sample of flesh and juice.

11.4.6 Fats and oils

Oils need to be shaken well before sub-sampling but fats can probably be dealt with most effectively by melting and sub-sampling from the stirred molten bulk, although some fats may separate on melting, which can cause difficulties. Unless several different sources of fat are to be analysed as a homogenate, most fats will have been effectively mixed during preparation and a representative slice taken through the bulk will probably be adequate.

11.4.7 Cereals

Edible grains need to be separated from the chaff and analyses performed either on a sub-sample from a well-mixed bulk of individual grains or on a rough flour produced using a coffee grinder or equivalent.

11.4.8 Mixed foods/whole meals/diets

When a mixture of ingredients is to be analysed there are several options. Representative portions of the relevant food(s) can be combined in the laboratory or duplicate portions of the diet can be combined and stored until collected for analysis. In the latter case, test materials may have to be stored in an acid-cleaned plastic bucket (fitted with a lid) and the resulting mixture of food and drink prepared for measurement. Pre-treatment in such cases usually requires a large liquidiser or food processor.

11.5 Sample pre-treatment

Samples are normally pre-treated to allow efficient and quantitative introduction of the elements of interest into the analyser system. This can vary from simple dilution of liquids (e.g. wines) to more complex procedures involving dissolution in concentrated acids at high temperature and pressure or the use of solvent extraction, ligand and ion-exchange pre-concentration procedures. Clean-room facilities are strongly recommended for this stage of trace analysis and the purest reagents available should always be employed. Although laser-ablation (LA) techniques have been used on food matrices (e.g. Ref. [51]), the challenge of calibration means that the benefits of rapid sample preparation are sacrificed for semi-quantitative data.

11.5.1 Samples requiring minimal pre-treatment

Liquid samples offer the best opportunity for aspiration into the plasma source with minimal pre-treatment. Multi-element determinations (48 isotopes) have been performed on wine samples by ICP-MS following simple dilution with water and flow injection (FI) into a stream of 5% ethanol and 0.5% nitric acid [19]. Wine has also been analysed after dilution by Augagneur *et al.*, using ICP-MS [52]. Diluted sherry, which had undergone heat treatment, was analysed by ICP-AES [53]. Another example of minimal pre-treatment was provided by Al-Swaidan, who used direct aspiration of aqueous dilutions of orange, apple and pineapple fruit juices into an ICP-MS to determine Fe (between 4.49 and 8.19 mg kg⁻¹), Sn (between 5.16 and 200 mg kg⁻¹) and Pb (between 0.203 and 0.332 mg kg⁻¹) [54]. Dean *et al.*, prepared slurries of dried milk powder for analysis by ICP-MS when measuring Pb isotope ratios [55]. In this work, milk powder (5 g) was mixed with 0.1% Triton-X as dispersant in 200 ml of water and the pH adjusted to 7.4 with ammonia solution to prevent protein precipitation. The same method for slurries was used by Baxter *et al.*, to measure Al in infant formulae by ICP-MS [56]. Stuerup and Buechert used a similar approach when measuring Cu and I but

these workers dissolved milk powder (0.2 g sample plus 50 ml diluent) or whole milk (0.5 ml sample plus 9.5 ml diluent) in an alkaline solution of tetra-methylammonium hydroxide prior to analysis by ICP-MS [57].

Electrothermal vaporisation as a sample introduction method has been used in some food analyses (e.g. on both dissolved and slurried food samples) [58], and in the measurement of As in test solutions produced from plants [59]. In both cases, standard additions were the preferred method of calibration to eliminate matrix effects. Grégoire *et al.*, also obtained good results from the analysis of the certified reference materials (CRMs), LUTS-1 (lobster hepatopancreas) and SRM 1548 (selected reaction monitoring mode) (total diet) when measuring Mn, Co, Cr, Ni and Cu using ETV-ICP-MS [60].

11.5.2 Digestion of foods and related samples with acid(s)

The aim of all digestion methods is to transfer the element(s) of interest into the final solution quantitatively and efficiently, preferably with total decomposition of the bulk matrix and removal of potentially interfering species. While there are many different methods of achieving this, none of the methods developed to date are perfect for all elements and matrices. Quadrupole ICP-MS users sometimes prefer to avoid the use of HCl to minimise Cl interferences in As and Se measurements or avoid H₂SO₄ if cone blockage by salt formation is a problem. Safety constraints also limit the use of some acids (e.g. HClO₄ or HF, in some laboratories). Further pre-treatment may be needed in other circumstances; for example, where a redox cycle has to be used in the determination of As by hydride generation when it is necessary to ensure that all of the As is in a known oxidation state. Different types of heating have been used during the digestion of foods and related matrices. Negretti de Brätter *et al.*, compared microwave-based digestion and pressurised ashing systems, using different acid mixtures, for the determination of mineral and trace elements in total diet samples by ICP-AES [61]. These workers concluded that the best results were obtained from digestion with either nitric acid alone or with nitric acid and hydrogen peroxide (2:1) for both pressurised ashing and microwave-based digestion methods. Wet ashing with nitric acid and hydrogen peroxide was used by Muto *et al.*, to prepare freeze-dried food samples for measurement by ICP-MS when 13 elements were determined using In as the internal standard [62]. Shiraishi *et al.*, analysed duplicate diet samples for trace and ultra trace levels of Ba, Mo, Ni, Co, Cd, Cs, Tl, Pb, Bi, Th and U [63,64]. In their study, samples were dried and then dry ashed in a muffle furnace prior to digesting the ash with nitric acid (prepared in a sub-boiling still) and ultra-pure perchloric acid in a microwave oven. Sample solutions were taken to dryness on a hot plate before being dissolved in nitric acid and the diluted nitric acid digests were measured by ICP-MS with rhenium as internal standard. Good agreement was achieved between measured and certificate levels of elements in reference materials and the LODs (defined as 3 times the square of the error counts obtained for the blank solution) for Th and U were 1.3 and 2.9 pg ml⁻¹, respectively [64].

Microwave dissolution for preliminary breakdown of samples combined with an open-beaker digestion using nitric acid and hydrogen peroxide has been reported for the determination of 24 elements in some reference materials (oyster, liver and animal muscle) by ICP-MS [65]. Total sample preparation time was 2 h per sample with a five-element internal standard being used to compensate for instrument drift and matrix effects.

Compounded animal feed, imported gluten pellets, milk, some dairy products, and various animal tissues and fluids were analysed using low-pressure microwave dissolution with nitric acid following an incident in which animal feed became contaminated with Pb and other elements [66]. The use of microwave digestion (12 digests per run) permitted rapid sample throughput using a rapid microwave power programme which lasted 20 min. Pb, Cd, Mg, Zn, Cu, Fe, Co and Mn were determined in diluted nitric acid digests using ICP-MS. The high sample throughput achieved in this study was important in producing reliable data rapidly.

Some elements are particularly difficult to measure in biological matrices and special pre-treatment methods may be required. Sun *et al.*, reported the use of a mixture of acids (HNO_3 , HF, H_2O_2 and H_3BO_3) to pre-treat samples prior to measuring Al by ICP-AES [67]. They concluded that HF had to be present to ensure complete dissolution of the Al in the meat and shellfish they analysed. Cox *et al.*, developed a method for measuring ^{129}I by ICP-MS in which cabbage samples were homogenised, dried and then dry ashed for 6 h [68]. The ash was then refluxed with sulphuric acid for 30 min and iodine trapped as iodide in a U-tube containing NaHSO_3 . The ^{129}I was subsequently introduced into the plasma as iodine using NaNO_2 as oxidant with an LOD on a fresh weight basis of 1.4 ng kg^{-1} being achieved. Larsen and Ludwigsen performed iodine determinations on digests prepared using wet ashing in closed stainless steel bombs with a mixture of nitric and perchloric acids [69]. In this work iodine contamination at 9 ng per ashing was observed from the polytetra fluoroethylene (PTFE) liners of the reaction vessels. Nevertheless a detection limit (based on 3 times the standard deviation of reagent blanks) of 30 ng g^{-1} (dry mass) was obtained.

Another aspect of food science concerns food-packaging materials (e.g. polymers), which may contain low levels of the chemicals used in their manufacture, including catalyst residues. In polymers intended for food contact use, these substances may migrate (transfer) from the polymer into the food [70]. Consequently, there is a need to identify potential food contaminants in packaging materials. Trace elements have been determined by ICP-MS in a wide range of food contact polymers using microwave digestion with nitric and sulphuric acids, and the results were comparable to data obtained by LA-ICP-MS and neutron activation analysis (NAA) [16]. LA-ICP-MS allowed rapid multi-element screening of polymers prior to full quantitative analysis but the polymers required vigorous digestion procedures and ideally an alternative is needed for sulphuric acid if all the elements of interest are to be measured with adequate LODs by ICP-MS. Tin is a specific element which may enter some food packaged in cans. Although many tinned foods are found in cans with inner surfaces coated with lacquer, tomato soup and some other products containing tomatoes can be found in unlacquered cans. Tin levels have been measured in a variety of foods by Biego *et al.* [71] and Sumitani *et al.* [72].

11.5.3 Other techniques

Fusion methods have been used for many years in the analysis of metals, soils, etc. but have had relatively little use in food analysis by plasma spectrometry (e.g. Krushevskaya and Barnes [73] and Lásztity *et al.* [74]). The fusion reagents that are added to test samples can result in analytical solutions that are relatively high in dissolved salts and trace impurities, which can influence detection limits for some elements.

Speciation studies using ICP-MS or ICP-AES for element quantification need to remove the various element complexes and compounds without changing their chemical form [47,48]. Methanol is a popular solvent for use in Sn [75] and As [76] speciation studies. Supercritical-fluid extraction has also been used in studies of organotin species in fish [77] although the method has yet to achieve more widespread use. Enzymatic hydrolysis is often used to prepare samples for speciation measurements. For example, one of the most effective methods for degrading whole yeast samples, yeast extracts and specific yeast fractions for Se analysis has been achieved by proteolysis using protease and lipase followed by treatment with pronase XIV [78]. Compounds containing peptide bonds are broken down to selenoaminoacids (mostly selenomethionine – SeMet) and inorganic Se.

11.5.4 Pre-concentration methods and removal of interferences

When low LODs are required it may be necessary to pre-concentrate the elements of interest and this is particularly challenging in speciation studies [47]. Ion-exchange is a well-established method of pre-concentration (e.g. Ref. [79]) and offers the possibility of use in speciation studies where the oxidation state of the element(s) of interest needs to be preserved. Recent developments in this field have included on-line pre-concentration in the multi-element analysis of biological fluids, (e.g. Cd, Cu, Mn, Ni and Pb [80]). One advantage of isolation of the elements of interest is the possibility of separating the analyte from bulk ions in the test solution, such as Na, K and Ca, which can reduce interferences and improve sensitivity. Another method of preventing interferences is to use hydride generation techniques for those elements that form volatile hydrides plus Hg, which can be volatilised under hydride generation conditions. A significant disadvantage of multi-element hydride generation measurements is that the experimental conditions used may have to be a compromise and may lead to elevated background levels of Hg from some of the reagents used.

11.6 Quantification

There are several textbooks and reviews that describe the principles of plasma source spectrometry (e.g. Refs. [17,18,41,81–83]). However, the ability to acquire both multi-element and multi-isotopic data rapidly is a major advantage of ICP-MS. Although ICP-AES allows the analyst to carry out multi-element determinations, compared with ICP-MS it has limited sensitivity for some of the analytes. The advantages of internal standardisation for compensating for the effects of changes in viscosity, surface tension and aerosol characteristics of standards and samples are well established. An early comparison between ICP-MS and ICP-AES for the analysis of four biological reference materials showed that the sensitivity of ICP-MS for elements above mass 80 was superior to that obtainable by ICP-AES [84]. However, at that time the precision of ICP-MS for multi-element analysis was poor compared to ICP-AES. Since then, better quadrupoles have become available and more stable instruments have evolved. Current experience is that accurate and precise multi-element analysis of CRMs is possible [26,32]. It is of note that the addition of 8% nitrogen

to the aerosol carrier (nebuliser) gas flow reduced polyatomic interferences and improved the measurement of ^{51}V , ^{53}Cr , $^{67,68}\text{Zn}$, ^{75}As and ^{77}Se [26]. However, this was accompanied by an increase in LOD when the nitrogen was added, although this did not cause any problems with the multi-element determinations reported.

11.6.1 *Practical considerations*

There is a great temptation to maximise the perceived benefit of an analysis by obtaining as much information as possible from each test sample. With plasma-source techniques, which can enable the determination of most of the elements of interest in the Periodic Table, it has been said that it is just as easy to measure 20 elements as one. Automated procedures and readily available multi-element standards mean that this can be the case but caution is necessary as data processing becomes much more of a challenge as the number of elements studied is increased. Monitoring multiple isotopes or emission lines can give the analyst additional confidence in the final results although problems can occur when working close to LODs, when uncertainties can be relatively high.

11.6.2 *Data analysis*

Software provided by instrument manufacturers is usually very effective at generating mg l^{-1} concentrations in the test solutions analysed and can make the appropriate corrections for interferences and perform internal standardisation, etc. However, multi-element analyses in support of food science may require considerably more data processing before results can be reported as mg kg^{-1} in the commodity or other test material. When multi-element analyses are performed it is wise to use at least three reagent blanks in case spot contamination or an instrument 'glitch' causes an erroneous value to be recorded from one measurement. Although instrument software can accommodate blank correction for a single sample, it is not possible to use the mean of several blanks that may have been included in the test batch.

If spike or reference material recoveries are also to be assessed, and perhaps used to correct the test data, then additional software is required. Single-element measurements can be processed with simple spreadsheets but more complex data (e.g. 40 isotopes in 50 test samples) require purpose-written software. Spreadsheet macros offer a flexible approach to dealing with this problem, allowing large numbers of elements/isotopes and test samples to be processed in each batch. The disadvantage of this approach is that the macros have to be written in-house as none are, as yet, commercially available. Even with efficient software tools, data processing from multi-element analyses can be a lengthy process and can take as long as the pre-treatment processes used in the earlier stages of the analysis. The analytical community is currently giving some thought to methods for reporting measurement certainty [44] and this will almost inevitably require analysts to develop methods for assessing the reliability of each value quoted in a test report. Yet more data processing seems inevitable although visual inspection of data by an experienced analyst remains an important tool.

11.6.3 Isotope ratio measurements

Sample throughput for ICP-MS is rapid and in contrast to ICP-AES enables the determination of several isotopes in each acid solution prepared for analysis. This is a positive attribute when compared with isotopic determinations involving, for example, thermal ionisation, secondary ionisation and fast atom bombardment MS [85] for which extensive cleanup and pre-concentration of samples may be required. The major criticism of ICP-MS for isotope ratio determinations is that it is less precise than the conventional MS methods and this is due to a combination of factors. These factors include relatively poor sensitivity and hence counting statistics, relatively ineffective dead-time corrections (the interval during which the detector and its associated counting electronics are unable to resolve successive pulses, resulting in a non-linear response above count rates typically $>1 \times 10^6$ counts per second), mass bias effects (when the observed or measured isotope ratio differs from the true value as a function of the difference in mass between two isotopes), resolution (directly related to the quadrupole) and abundance sensitivity [13,83].

Thus the achievable precision is limited by Poisson ion-counting statistics for instruments as well as memory effects in the sample introduction system. Other factors, such as noise from the plasma and electronics, can lead to isotope ratio measurement precisions that are poorer than those which would be predicted from the counting statistics alone [83]. Begley and Sharp found that while an educated selection of acquisition parameters can give rise to a practical precision of about 0.05% for ^{107}Ag : ^{109}Ag ratio measurements, for example, precision is limited by inaccuracies associated with the operation of the quadrupole mass analyser and the statistical error arising from the random arrival of ions at the detector [86]. Sample matrix and size, as well as concentrations of each isotope of interest also influence the precision of measurements. New developments in ICP-MS and improvements in resolution [10] offer the prospect of much more precise isotope measurements that are finding applications in foods and biological materials [87–89].

Recent advances in MS have been accompanied by a massive increase in computing power and software development allowing complex mathematical equations to be solved quickly. The use of mathematical modelling for nutrition and mineral absorption studies is described for Se, Cu, Zn and Ca by Dainty and Fox [90]. In particular the uses of stable isotopes for quantifying Se in the investigation of Se status in humans [91] and its bioavailability from labelled foods have been reported [92–94]. For Se precisions of 1% or better are generally adequate for use in nutritional and clinical studies if Se concentrations are optimised as far as possible by judicious use of the isotope labels. The doses of isotope labels should be small enough not to perturb the steady-state conditions in the body of the volunteer but the detection limit of the ICP-MS instrument used to determine the isotopic enrichment must be taken into account when calculating experimental doses [91].

11.7 Quality control

It has been said that ‘all analytical results are wrong but it is just a question of by how much’ [95] and this statement applies to all forms of analysis. Effective analytical quality control must make sure that a given result is fit for its purpose but this presupposes that the end-user requirement is well defined. In theory, the end user of data should define the quality level

required and all the analyst then needs to do is to use established criteria to demonstrate that the necessary standard has been achieved. In practice, however, end users of data are not always aware of the technical limitations that can influence the final quality standard, particularly when multi-element analyses may require different standards for different elements over a wide concentration range.

Formal accreditation systems, such as those operated by the United Kingdom Accreditation Service (UKAS) [96], are essential quality control tools in many areas of food analysis but they rely on the analyst developing efficient measures of quality. Useful quality control criteria have been suggested for single analyte determinations by Thompson and Wood [97] but the scientific community has yet to agree generic criteria to apply to multi-analyte measurements. However, quality criteria for use in multi-element ICP-MS analyses of food have been discussed by Baxter *et al.* [98] and are now being referred to by other analysts (e.g. Leblanc *et al.* [99]).

Proficiency testing [46] is an external check of quality and is increasingly required as part of compliance with formal accreditation systems where a suitable scheme is available. It provides an independent and unbiased assessment of the performance of all aspects of the laboratory, both human and hardware. Some results [100] suggest that whilst the use of accredited methods may have little effect on the accuracy of results generated by a laboratory, continued participation in a proficiency scheme such as the Food Analysis Performance Assessment Scheme (FAPAS®) can, with appropriate corrective action improve performance for individual laboratories. Good analytical performance may not necessarily depend on the equipment available but how it is used. Having the experience available to interpret a technique is invaluable and a well-developed method, however old, will still perform adequately when employed for its original application but may not be suitable for new applications.

An important part of the process of gaining and transferring experience is internal quality control (IQC), which Thompson and Wood [97] define in their article on IUPAC/AOAC harmonised guidelines for IQC as 'routine analytical procedures that enable the analytical chemist to accept a result or group of results as fit for purpose or reject the results and repeat the analysis'. However, it must always be recognised that quality data generated for one application may be totally inadequate for use in another.

Wherever possible, IQC criteria should be established in advance of a study to cover all the different types of matrix, analyte and analyte concentration that might be encountered. This inevitably assumes that either the analytical problem being investigated is well characterised or that quality criteria can be established in advance by a relatively small number of cost-effective experiments. In practice, however, this is not always possible and, for example, an analytical survey containing a large number of different analyte/food combinations could generate tens of thousands of data points. Establishing rigid criteria for such a survey might not be possible until many of the analyses have been completed. At the opposite end of the scale, analysing several elements in a small number of samples could mean that establishing all of the necessary quality criteria before the work was performed was simply not cost-effective. Nevertheless it is vital that quality criteria are monitored so that details can be included in any test reports. Wherever possible analysts should establish routine IQC checks which allow problems to be identified at an early stage so that remedial action can be taken promptly.

The following criteria have been established for the analysis of food by ICP-MS [98] although some criteria have wider application to other plasma-source techniques.

11.7.1 *General observations*

There is no substitute for an experienced analyst and the 'art' of trace element measurement still remains an important, but sometimes almost indefinable, factor. Suitably qualified, experienced and highly motivated staff are essential prerequisites for good quality work.

11.7.2 *Instrument performance*

There is little point in proceeding with quantification of a test solution if the detection system cannot produce meaningful results. System suitability checks should be performed using, for example, tuning solutions or specific concentration standards to confirm that an adequate response can be achieved. In this case, suitable criteria can be established for selected elements in advance of any specific set of measurements with relative ease.

In the case of ICP-MS, severe instrument drift during the analytical run can indicate problems, particularly if the foods are rich in elements that can form solid deposits on instrument cones. Although internal standards can be used to correct for some drift, the effectiveness of any corrections should be assessed by measuring a mid-range calibration standard at the start and end of each test run. In the authors' laboratory an average ICP-MS run containing about 50 test solutions (made up of samples plus standards, etc.) will take about 5 h to measure. Experience obtained in the analysis of 40+ isotopes per food sample by ICP-MS has shown that the majority of check standard results should lie within $\pm 20\%$ of the initial value.

In theory, ICP-MS calibrations are linear over many (six to eight) orders of magnitude of concentration and a single calibration standard is all that is required. However, it is common practice in the authors' laboratory to use up to six calibration standards to bracket the concentration range expected in test solutions. Experience has shown that linear calibrations are achieved with calibration solutions in the range $<0.5\text{--}2000\ \mu\text{g l}^{-1}$ for pulse mode measurements and $<2000\text{--}50\,000\ \mu\text{g l}^{-1}$ for analogue mode measurements. Where wide concentration ranges are encountered in different samples within a batch, care is needed to ensure that cross-calibrations are effective and that excessively high or low standards do not distort the calibration graph in the region of interest.

11.7.3 *Limits of detection*

A good discussion of LODs and accuracy in trace element analysis in general has been published [101]. In practice, the LOD expressed as mg kg^{-1} of sample (see also Table 11.2) is strongly dependent on the material being analysed, the dissolution procedure and background levels of the analytes in reagents. Elevated LODs are effective indicators of possible contamination of the test samples or memory effects. The LODs given in Table 11.3 were obtained after multi-element analyses by ICP-MS of total diet survey (TDS) samples from the UK [102–104] and from France [99] that involved a wide variety of foods. For the UK samples elements were determined after sub-samples (0.5 g dry weight equivalent) were digested with nitric acid (5 ml) in microwave-digestion vessels. For the French samples about 0.6 g of the food composite samples were digested with nitric acid (3 ml) also in

a closed microwave system. The resultant digests were diluted and analysed by ICP-MS or HG-ICP-MS (hydride generation-inductively coupled plasma mass spectrometry) for some As, Se and Hg measurements. The LODs for the UK TDS samples were calculated from 3 times the standard deviation of the reagent blank corrected for sample weight and digest dilution [102–104]. The higher values quoted for the UK samples in this table arose

Table 11.3 Typical ICP-MS LODs (mg/kg fresh weight) for sample analyses from the 1994 UK, the 1997 UK and the 2000 French TDSs NA = not analysed [102–104,99]

Element	1994 UK TDS	1997 UK TDS	2000 French TDS
Li	0.002	NA	0.003
B	0.4	NA	NA
Mg	NA	NA	0.246
Al	0.27	0.04–0.1	0.114
Na	NA	NA	2.915
Ca	6.5	NA	7.65
Cr	0.1	0.01–0.09	0.015
Mn	0.01	NA	0.08
Fe	0.25	NA	NA
Co	0.001	NA	0.001
Ni	0.02	0.002–0.02	0.0315
Cu	0.02	0.002–0.02	0.019
Zn	0.3	0.04–0.3	0.0815
Ge	0.002	NA	NA
As (ICP-MS)	0.003	0.0004–0.003	0.0045
As (HG-ICP-MS)	0.002	NA	NA
Se (ICP-MS)	NA	NA	0.0225
Se (HG-ICP-MS)	0.003	0.0004–0.003	NA
Br	NA	0.03–0.2	NA
Sr	0.003	NA	NA
Mo	0.003	NA	0.003
Ru	0.002	NA	NA
Rh	0.0001	NA	NA
Pd	0.0003	NA	NA
Cd	0.001	0.0001–0.0009	0.0005
Sn	0.02	0.001–0.009	NA
Sb	0.001	NA	0.0005
I	NA	0.03–0.2	NA
Ba	0.008	NA	NA
Ir	0.001	NA	NA
Pt	0.0001	NA	NA
Au	0.0003	NA	NA
Hg (ICP-MS)	NA	NA	0.0055
Hg (HG-ICP-MS)	0.0006–0.002	0.0004–0.003	NA
Tl	0.001	NA	NA
Pb	0.01	0.0006–0.005	0.005
Bi	0.0001	NA	NA

primarily because of the higher sample dilutions that were needed to measure nutrient elements in some samples or when relatively low abundance isotopes were monitored to minimise interference effects (e.g. Ca). It should be noted that instrument detection limits were lower (on average, approximately 100-fold) than those shown in the table. For the French TDS samples the LOD was quoted as corresponding to twice the limit of quantification [99]. The ICQ criteria for both French and UK studies were similar to those described by Baxter *et al.* [98].

11.7.4 Spike and reference material recoveries

Each test run should also include spiked blanks and reference materials. Semi-quantitative analyses of typical samples prior to the main study can give an indication of the levels of each element in the food. Consequently, spike levels can be set approximately equal to the concentrations in the test material. In addition, analysing digested reference materials such as peach leaves, oyster tissue and bovine liver allows the analyst to assess overall method performance. Table 11.4 shows an example of the level of agreement that can be obtained between certificate values and a selection of measured data for the reference material National Institute of Standards and Technology (NIST 1547) (peach leaves) [98]. However, it should be noted that these data are the mean of 80 measurements and some variation is expected for these elements in individual batches. Acceptance criteria such as those established by the authors and used for accreditation purposes are very useful; for example, all reference material measured values to be within $\pm 40\%$ of the certificate value with 75% being within $\pm 20\%$ of those quoted by the certification body. However, it is important to

Table 11.4 Reference material results for NIST 1547 (peach leaves) obtained using ICP-MS ($n = 80$) (Baxter *et al.* [98])

Element	Measured	Certified (indicative)
B	30	29
Mg	4300	4320
Al	250	249
Ca	16 000	15 600
Cr	0.90	(1.0)
Mn	110	98
Fe	210	220
Co	0.07	(0.07)
Ni	0.71	0.69
Cu	3.3	3.7
Zn	20	17.9
Se (HG-ICP-MS)	0.14	0.12
Mo	0.05	0.06
Cd	0.03	(0.03)
Sn	0.2	(0.2)
Pb	0.90	0.87

use several different reference materials when complex matrices such as mixed diets are to be analysed [98,99,102].

CRMs for speciation analyses are still not widely available, with greatest efforts being made to produce CRMs for As and Se (e.g. Ref. [105]).

11.7.5 Replicate analyses

It is very important to undertake appropriate replicate analyses when dealing with complex matrices, such as foods, which are difficult to homogenise. A minimum of a 10% audit of samples should be re-analysed in a separate batch to identify batch-specific errors. Agreement between replicates should be better than $\pm 20\%$ or twice the LOD. The latter criterion is important in low-level measurements and is equivalent to some definitions of limit of determination or quantification [99].

11.7.6 Reporting results

Raw data generated by multi-analyte measurement techniques are complex and in some, but by no means all, cases are difficult to present in an easy-to-read format. Basic principles of what information should be included in a test report are given by formal accreditation agencies (e.g. UKAS [96]), and these cover the need to uniquely identify all materials tested, provide IQC information and a full list of measured data as required by the end user. In surveys where element levels are reported in a range of similar commodities, the maximum, minimum and mean values can be useful. However, a single large high or low value can distort the distribution and hence the mean value. In such circumstances, reporting the median value can be useful if a 'typical' concentration is required.

11.8 Speciation studies

There have been many reports on speciation studies in food and several texts provide an excellent overview of methods for trace metal speciation, some of the problems associated with the techniques and their applications [106–110]. In the most recent text [110] applications are described for speciation in food and biological samples including for example Al, As, Cd, Cr, Pb, Hg, Mo and Se species. Topical examples of speciation studies are given below. These are works with As, studies involving chromatographic coupling to plasmas and studies of Se bioavailability and speciation.

11.8.1 Arsenic speciation

Arsenic, particularly in fish, is a good example of the requirement to determine both total levels of the element and the chemical form, and where there is a need in legislative processes for speciation data to be available to facilitate meaningful decisions based on the differences

between the various As species that may be present in food [111]. Total As levels have been determined in foods by ICP-MS [112] and higher levels are generally found in fish. Inorganic forms of As [As(III) and As(V)] are much more toxic than forms such monomethylarsonic acid and dimethylarsinic acid, which are in turn more toxic than arsenocholine and arsenobetaine. The latter is frequently reported as the main organoarsenic compound in fish and has been isolated, for example, from seafood products using anion-exchange chromatography coupled to ICP-MS [76] and by reversed-phased chromatography (RPC) ICP-MS from blue mussels [113]. A recent publication has investigated the use of CE-ICP-MS to speciate As in fish and oyster tissues following microwave extraction of the As species using an 80% *v/v* methanol-water mixture [114]. Under these conditions 100% of the total As in tissues was extracted and both known and unknown species were found.

Hansen *et al.*, isolated seven As species using anion- and cation-exchange systems with ICP-MS [115]. Arsenic has also been monitored following high-performance liquid chromatography (HPLC) ICP-MS to determine the presence of the growth promoter 4-hydroxy-3-phenyl-arsonic acid in chicken tissue [22]. Arsenic species have been measured in chicken meat [116] using anion-exchange with ICP-MS and in rice using a Dionex IonPac AS7 column [105]. The latter study was part of a European Commission project to investigate the feasibility of producing CRMs for As and Se species. Vela and Heitkemper [117] studied total and speciated As in infant foods of terrestrial origin. Of the foods they studied – purée infant food products including rice cereals, fruits and vegetables – rice cereal would contribute most to the daily As intake with inorganic As accounting for approximately 48% of the As in the cereals analysed. Sample treatment with trifluoroacetic acid was an efficient and mild method for extraction of As species.

11.8.2 Applications using HPLC

Other authors have reported the use of HPLC with direct-injection nebulisation ICP-MS to determine As, Sn, Pb and Hg species [118,119], the role of chemical speciation on the determination of Hg in cod by ICP-MS [120] and the use of ion-pairing and RPC-ICP-MS for the measurement of organolead compounds [121]. Al and other element species have been measured by size-exclusion chromatography (SEC) ICP-MS in tea [122,123] and in intestinal digesta [124]. Inorganic halogen species have also been determined in water and soup using liquid chromatography (LC) ICP-MS [125] and bromate in bread by ion-exchange chromatography (IC) ICP-MS [126,127]. Iodine speciation in commercially available seaweed (consumed not only in Asia but increasingly in Europe and some African countries) was investigated using several chromatographic techniques with ICP-MS, including SEC, IC-HPLC and RP-HPLC [128]. Not only were iodine species extracted but also information on the association of I with the various seaweed components was obtained. For example iodide was the most predominant species in one product (Kombu), but a more complex distribution of I was found in another (Wakame) including the chemical forms mono-iodotyrosine and di-iodotyrosine probably bound to proteins.

Perhaps most progress has been made in the application of HPLC-ICP-MS to the separation and characterisation of some metal-binding proteins. In 1980, gel permeation chromatography was coupled to the nebuliser of an Ar plasma AES [129] and Co, Cu, Fe, Mn, P, Zn and C were determined simultaneously in a mixture of proteins. However, some

problems were encountered with adsorption of protein on to stainless steel tubing, making absolute quantification of the elements impossible.

The potential of ICP-MS for speciation studies was explored further and in 1987 protein standards were used to characterise HPLC coupled to ICP-MS [130] and a scavenger column containing Chelex 100 ensured that buffers were free of the elements of interest. A mixed-protein standard, which included vitamin B₁₂, was separated using SEC and the ⁵⁹Co signal monitored by ICP-MS. A comparison of the ultraviolet response with the ICP-MS response clearly showed the Co associated with vitamin B₁₂ [130]. In a separate experiment, SEC was used to analyse a mixture of equine metallothionein and ferritin, and ¹¹⁴Cd was monitored. The specificity of ICP-MS enabled detection of Cd in the metallothionein standard. This methodology was used by the same group to study the speciation of Cd in retail samples of pig kidney. Crews *et al.*, were able to show that the majority of soluble Cd in pig kidney was associated with a metallothionein-like protein that survived both cooking and *in vitro* gastrointestinal digestion [131]. This work also demonstrated that ICP-MS was sensitive enough to permit the study of Cd at endogenous levels. For example, the raw kidney contained 0.22 mg Cd kg⁻¹ fresh weight and Cd concentrations of 2 ng ml⁻¹ could be measured, on-line, in fractions separated by SEC.

Multi-element HPLC-ICP-MS has also been reported (e.g. Ref. [132]) in which simultaneous data acquisition for up to eight elements was performed following separation of metalloproteins in cytosolic extracts by SEC. Problems were encountered when optimising the HPLC and ICP-MS systems, and compromise conditions had to be established. Although a higher ionic strength mobile phase (0.25 M NaCl, 0.06 M Tris-HCl, pH 7.5 in 0.05% sodium azide) gave better chromatographic separation of the protein standard, direct aspiration of the high-salt buffer compromised the elemental analysis of the protein by ICP-MS. Sodium caused severe ion suppression, resulting in loss of attenuation and reduced sensitivity, and background counts for Cu, Zn and, to a lesser extent, Cd were elevated, giving poorer LODs. The high salt content caused deposition of solids on the torch and standard Meinhard nebuliser, which Mason *et al.* [132] postulated as being the cause of both the instability in the analyte signal and the irreproducibility of analyses that they experienced. The use of a lower ionic strength buffer (0.06 M Tris-HCl, 0.05% sodium azide, pH 7.5) gave fewer theoretical plates but similar values for peak tailing and symmetry, and was used for the remainder of the study. Relative LODs for ¹¹⁴Cd, for example, of approximately 500 to 2000 pg ml⁻¹, depending on the metallothionein concentration, were reported. The necessity to 'optimise compromise conditions' for HPLC-ICP-MS is a common feature of speciation studies using this technique.

Owen *et al.* [133] used multi-isotopic analysis to investigate the feasibility of on-line measurement of elements associated with proteins and to determine isotope ratios of Zn following the labelling of chicken meat with stable Zn. SEC-ICP-MS measurement of mixtures of thyroglobulin, gammaglobulin, ovalbumin, myoglobulin, vitamin B₁₂, metallothionein and ferritin were achieved. While no quantitative data were reported, the results indicated that SEC-ICP-MS should be useful for assessing the associations between proteins and elements. The results obtained for Zn isotope ratios measured by direct nebulisation ICP-MS, FI-ICP-MS and following RPC-ICP-MS were generally in good agreement. Measurements by FI-ICP-MS of the ⁶⁴Zn:⁶⁷Zn ratio in enzyme digests of chicken meat, which had been intrinsically labelled with ⁶⁷Zn, were compared with those obtained using thermal ionisation mass spectrometry (TIMS). The value obtained by TIMS was 3.05, which compared well with the value of 3.09 obtained by ICP-MS [133]. More recently, gel

filtration coupled to ICP-MS has been used to investigate the Cu, Zn and Cd content of freshwater mussels and its relationship to metallothionein concentrations during an evaluation of potential reference materials [134,135].

11.8.3 Selenium speciation

Interest in Se, and the number of publications concerning its chemical form in foods and dietary supplements, is both vast and increasing [91]. Not only is Se an essential element it also has toxic effects as well as postulated anti-cancer activity [93] and this latter has led to a surge in interest in the chemical forms of selenium and their bioavailability from the diet. Interest in dietary uptake of Se has also focused food and dietary supplements. In 2005 an excellent review of current MS strategies for Se speciation was produced by Goenaga Infanta *et al.* [136]. They note that the analytical methods have predominantly been based on coupling various chromatographic or electrophoretic separations to ICP-MS although recently electrospray ionisation and matrix-induced laser desorption have also been used for confirmation and/or identification of Se-compounds. The authors critically describe strategies for the determination of Se and its species with special reference to high-Se yeast, garlic, onions and Brazil nuts. An outline of the detailed analytical procedures used to measure Se species in selenized yeast was described by Polatajko *et al.* [137] and in another publication Goenaga Infanta *et al.* [78] report the analysis of Se-enriched supplements. These articles are among several that have recently investigated Se speciation in Se-enriched yeast (e.g. Refs. [93,94,138–141]), and in fact some 40 references are cited in the review by Goenaga Infanta *et al.* [136]. These authors concluded that for yeast studies, 'despite the increasing use of ID techniques for validation of methodologies for Se speciation analysis, the accurate determination of Se-compounds identified in Se-yeast, other than SeMet, still remains a challenge. This is due to a lack of commercially available isotopically enriched Se-containing species (to perform IDMS) and of speciated yeast CRMs for validation of measurements of target Se-containing species.' They also note that information available on molecules that bind or incorporate Se is scarce because of the complexity of the system and the low concentration of individual Se-compounds (even in high-Se yeast).

This complexity is also present when dietary intake, both *in vitro* and *in vivo* studies are undertaken. For example *in vitro* gastrointestinal digests of microwave-cooked cod were analysed by Crews *et al.* [142], who used anion-exchange HPLC-ICP-MS to investigate Se speciation. They were able to show clear separation of 10 ng ml⁻¹ solutions of seleno-L-methionine, seleno-D,L-cystine, sodium selenite and sodium selenate. Analysis of *in vitro* gastrointestinal digests using the same technique indicated that selenite accounted for approximately 12% of the total Se present. The major peak was unidentified but was thought to be associated with an organoselenium compound. When seleno-L-methionine, seleno-D,L-cystine, sodium selenite and sodium selenate were added to the *in vitro* digestion enzymes, marked changes in some retention times were observed. This effect, combined with possible suppression of the ⁸²Se signal by organic species, highlights some of the practical difficulties associated with this type of study.

In vivo studies with human volunteers demonstrated that Se from trout fish fed with intrinsically labelled ⁷⁴Se (as yeast pellets) provided a highly bioavailable form of dietary Se

Table 11.5 Total intake (μg) of Se (standard deviation) and mean percentage retention (standard deviation) of Se from different test meals and selenate reference dose; *n* = number of volunteers (adapted from [94])

Test meal	Total Se intake (μg)	% retention	Selenate dose	
			Total Se intake (μg)	% retention
Cooked fish <i>n</i> = 12	115.5 (5.1)	85.3 (7.3)	72.4 (1.6)	65.4 (13.2)
Salted fish <i>n</i> = 11	128.7 (1.3)	86.2 (5.6)	72.8 (1.7)	57.5 (9.9)
Yeast <i>n</i> = 12	151.3 (1.1)	59.3 (12.5)	73.0 (4.1)	66.4 (13.1)

for humans regardless of the method of preparing the fish for consumption (cooking or enzyme and salt treatment) [94]. The Se isotope measurements in cooked and salted fish (dried yeast as a test diet was also investigated) as well as urine and faecal samples from volunteers were undertaken using hydride generation-ICP-MS. Retention of Se from test meals including trout fish and yeast not significantly different but was greater for the fish than that from ingested selenate. Table 11.5 compares mean retention of Se from each of the test meals by volunteers with that from selenate reference doses administered as a drink. Retention was calculated as the difference between dietary intake and faecal and urinary recovery expressed as a percentage of the absorbed dose. Apparent absorption was calculated as the difference between intake and faecal recovery and expressed as a percentage of the total dose.

Other work from the same group [89] investigated intrinsically labelled wheat (hydroponic culture using ⁷⁷Se), garlic (hydroponic culture using ⁸²Se) and cod (⁸²Se administered via sprats which had been labelled using selenious acid) and found that Se absorption from wheat and garlic was higher than from fish and that inter-individual variation between the volunteers (*n* = 10) was low. The form of Se and food constituents appeared to be key – labelled selenite given with garlic test meals resulted in the highest blood plasma concentrations and selenite given with fish the lowest.

Changes in the chemical form of Se were observed in a study of the manufacture of Se-enriched sourdough bread for use in a human nutrition study [143]. Selenium incorporation into rye seedlings, which were then dried, fermented and the resulting plant biomass ground for use in production of the bread, was measured using HPLC-ICP-MS and HG-ICP-MS. Rye seedlings not enriched by exposure to selenite were used as a control. Fermented sourdough bread is popular in Poland and many Eastern European countries and could provide a good source of Se in areas where Se intake is low. At each key stage of production the mean level of total Se was measured (mg/kg) and found to be as follows: rye seeds prior to germination 0.85; control plant biomass 0.99; Se-enriched plant biomass 55.27; control bread 0.06 and Se-enriched bread 3.56. Fig. 11.1 shows chromatograms of Se speciation for selenite and SeMet standards, the Se profile in rye seeds and in the germinated enriched seedling biomass.

The enriched sourdough bread was fed to 24 volunteers (results not yet available) and Fig. 11.2 shows the Se speciation profile for the enriched and control bread. In the enriched bread SeMet accounted for 42% of the eluting peak area. Subsequent work using

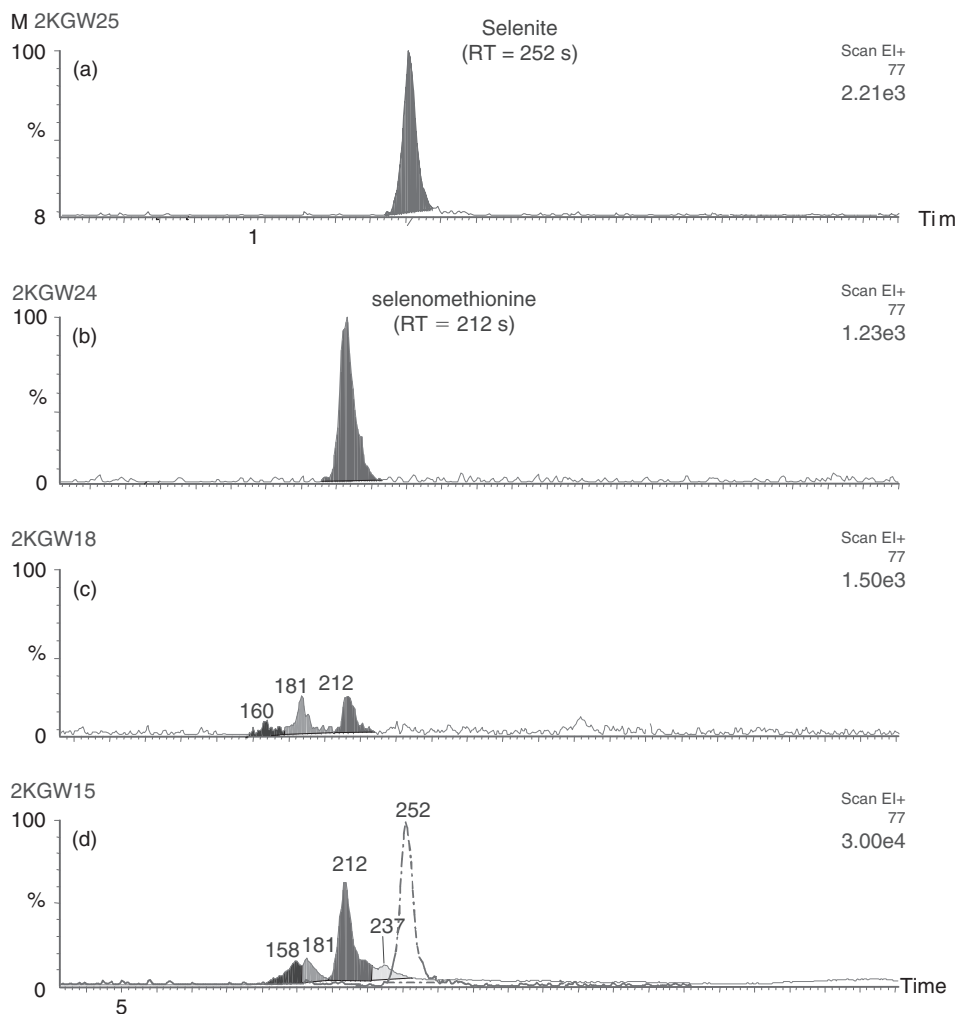


Figure 11.1 Chromatograms showing the various stages of selenium biotransformation and incorporation during the rye seedling germination process: (a) selenite standard (b) selenomethionine standard (c) selenium profile in seeds (d) selenium profile in germinated seedling biomass. The dotted line indicates the predicted elution time of selenite, had it been present in the test solution (adapted from [143]).

^{75}Se -labelling, electrophoretic separation and γ -scintillation counting with HPLC-ICP-MS analysis of different enzyme digests confirmed that there had been complete bio transformation of inorganic Se (selenite) into organic forms during germination of the rye seedlings [144]. Selenium was incorporated into a wide range of proteins (10–85 kDa), mainly through a non-specific route, probably substituting for S as and when required. Irrespective of the extraction procedure used SeMet was found in the biomass.

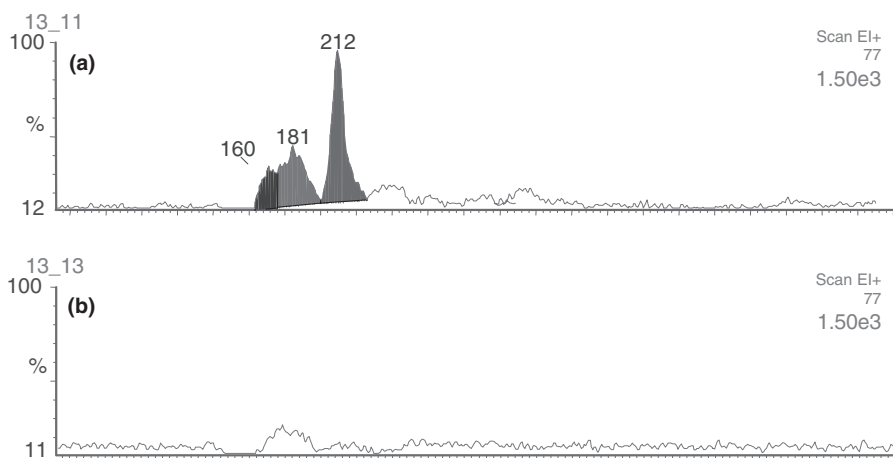


Figure 11.2 Chromatograms obtained from the wheat/rye sourdough breads fed to volunteers in the human study: (a) selenium profile in 'enriched' bread (b) selenium profile in 'control'(adapted from [143]).

11.9 Future trends

Plasma-source methods of metal and other element analysis already have widespread use in food science, both in monitoring the quality of food and in understanding the processes which occur during processing, storage and on digestion. Much of this routine work is likely to continue. However, there are some areas where developments are likely.

The use of MCC or DRC systems as well as the fact that affordable high resolution ICP-MS instruments are coming onto the market which will reduce the impact of many interferences that currently restrict some measurements. However, it remains to be seen whether these devices will also suffer from poorer detection limits. Quality control criteria for multi-analyte determinations are being investigated and these will lead to general improvements in analytical quality. A better appreciation of measurement certainty for all elements measured by plasma spectrometry is likely to become a pressing need in the coming years.

With more sophisticated instruments much less operator intervention is required but experienced operators will still be needed to solve the practical problems that occur with the rich diversity of sample types encountered in food science. Data processing is becoming quicker as faster computer systems are used to perform calculations and further improvement in interference correction may be possible.

Hyphenated techniques, such as capillary electrophoresis ICP-MS or AES (e.g. Refs. [145–148]), are also likely to become more common with dual element/organic molecule analysers being a likely development, which will enhance speciation studies even further. Analytes such as organophosphorous pesticides can be determined with LODs as the compound yielding an enhancement of 130- to 230-fold over flame photometric detection [148].

Stable-isotope tracers have proved to be an invaluable tool in nutrition studies and this is likely to be a future growth area although such studies can be costly and this fact may be prohibitive. Such studies do have the advantage that they can be performed using intrinsically

labelled foods on all age groups and even sensitive populations can be studied (e.g. the elderly or infants), without introducing any additional hazards. This will be particularly important in improving the scientific understanding of the interaction of metals and metal species *in vivo*. Methods for differentiating metal species are likely to become more important in the routine screening of foods for toxic metals, such as As and Hg, and for nutrients, such as Se.

There is a general trend in analytical science towards methods based on the biological sciences, and plasma-source methods may find applications using, for example, enzymes to pre-treat foods, cell cultures to concentrate elements of interest or studies into metal behaviour on a cellular level.

Authenticity studies are another important area where plasma techniques will continue to play a role, although these are likely to still be restricted to the higher-value products or those for which the consumer pays a premium because of the name.

While single-element determinations using methods such as atomic absorption spectrometry (AAS) will continue to play an important role in this field, multi-element and multi-isotope measurements will remain important in food science, ensuring that plasma source-MS has a role to play for many years to come.

References

1. Crews, H.M. (1998) Trace element analysis for food authenticity studies. In *Analytical Methods of Food Authentication* (Eds. P.R. Ashurst and M.J. Dennis), Blackie Academic and Professional, London, pp. 270–291.
2. Taylor, A., Branch, S., Crews, H.M., Halls, D.J., Owen, L.M.W. and White, M. (1997) Atomic spectroscopy update – clinical and biological materials, food and beverages. *J. Anal. Atom. Spectrosc.*, **12**, 119R–221R.
3. Taylor, A., Branch, S., Halls, D., Patriarca, M. and White, M. (2003) Atomic spectroscopy update – clinical and biological materials, food and beverages. *J. Anal. Atom. Spectrosc.*, **18**, 385–427.
4. Taylor, A., Branch, S., Halls, D., Patriarca, M. and White, M. (2004) Atomic spectroscopy update – clinical and biological materials, food and beverages. *J. Anal. Atom. Spectrosc.*, **19**, 505–556.
5. Taylor, A., Branch, S., Halls, D., Patriarca, M. and White, M. (2005) Atomic spectroscopy update – clinical and biological materials, food and beverages. *J. Anal. Atom. Spectrosc.*, **20**, 323–369.
6. Cubadda, F. (2004) Inductively coupled plasma-mass spectrometry for the determination of elements and elemental species in food: a review. *J. AOAC Int.*, **87**, 173–204.
7. Barnes, R.M. (1993) Advances in inductively coupled plasma mass spectrometry: human nutrition and toxicology. *Anal. Chim. Acta*, **283**, 115–130.
8. Chang, S.K.C., Rayas-Duarte, P., Holm, E. and McDonald, C. (1993) Food. *Anal. Chem.*, **65**, 334R–363R.
9. Taylor, H.E. (1986) Inductively coupled plasma-mass spectrometry: an introduction. *Spectrosc.*, **1**, 20–22.
10. Vanhaecke, F. and Köllensperger, G. (2003) Detection by ICP-mass spectrometry. In *Handbook of Elemental Speciation: Techniques and Methodology* (Eds. R. Cornelis, H. Crews, J. Caruso and K. Heumann), John Wiley and Sons Ltd, Chichester, pp. 281–312.
11. Leach, A.M., McClenathan, D.M. and Hieftje, G.M. (2003) Plasma source time-of-flight mass spectrometry: a powerful tool for elemental speciation. In *Handbook of Elemental Speciation: Techniques and Methodology* (Eds. R. Cornelis, H. Crews, J. Caruso and K. Heumann), John Wiley and Sons Ltd, Chichester, pp. 313–333.
12. Mellon, F. and Sandström, B. (1996) *Stable Isotopes in Human Nutrition*, Academic Press, London.

13. Lowe, N.M. and Jackson, M.J. (2001) Advances in isotope methods for the analysis of trace elements in man, CRC Press London.
14. Douglas, D.J. and Houk, R.S. (1985) Inductively-coupled plasma mass spectrometry (ICP-MS). *Progr. Anal. Atom. Spectrosc.*, **8**, 1–18.
15. Tan, S.H. and Horlick, G. (1986) Background spectral features in inductively coupled plasma mass spectrometry. *Appl. Spectrosc.*, **40**, 445–460.
16. Fordham, P.J., Gramshaw, J.W., Castle, L., Crews, H.M., Thompson, D., Parry, S.J. and McCurdy, E. (1995) Determination of trace elements in food contact polymers by semi-quantitative inductively coupled plasma mass spectrometry. Performance evaluation using alternative multi-element techniques and in-house polymer reference materials. *J. Anal. Atom. Spectrom.*, **10**, 303–309.
17. Crews, H. (1996) Inductively coupled plasma-mass spectrometry. In *Progress in Food Contaminant Analysis* (Ed. J. Gilbert), Chapman & Hall, London, pp. 147–186.
18. Crews, H.M., Luten, J.B. and McGaw, B.A. (1996) Inductively coupled plasma mass spectrometry (ICP-MS). In *Stable Isotopes in Human Nutrition* (Eds. F. Mellon and B. Sandström), Academic Press, London, pp. 97–115.
19. Baxter, M.J., Crews, H.M., Dennis, M.J., Goodall, I. and Anderson, D. (1997a) The determination of the authenticity of wine from its trace element composition. *Food Chem.*, **60**(3), 443–450.
20. Alves, L.C., Wiederin, D.R. and Houk, R.S. (1992) Reduction of polyatomic ion interferences in inductively coupled plasma mass spectrometry by cryogenic desolvation. *Anal. Chem.*, **64**, 1164–1169.
21. Ebdon, L., Fisher, A.S., Worsfold, P.J., Crews, H.M. and Baxter, M.J. (1993) On-line removal of interferences in the analysis of biological materials by flow injection inductively coupled plasma mass spectrometry. *J. Anal. Atom. Spectrom.*, **8**, 691–695.
22. Dean, J.R., Ebdon, L., Foulkes, M.E., Crews, H.M. and Massey, R.C. (1994) Determination of the growth promoter 4-hydroxy-3-nitrophenyl-arsonic acid in chicken tissue by coupled high-performance liquid chromatography-inductively coupled plasma mass spectrometry. *J. Anal. Atom. Spectrom.*, **9**, 615–618.
23. Lyon, T.D.B., Fell, G.S., Hutton, R.C. and Eaton, A.N. (1988) Elimination of Cl interference on the determination of Se in serum by inductively coupled plasma mass spectrometry. *J. Anal. Atom. Spectrom.*, **3**, 601–604.
24. Evans, E.H. and Ebdon, L. (1990) Effect of organic solvents and molecular gases on polyatomic ion interferences in inductively coupled plasma mass spectrometry. *J. Anal. Atom. Spectrom.*, **5**, 425–430.
25. Branch, S., Ebdon, L., Ford, M., Foulkes, M. and O'Neill, P. (1991) Determination of arsenic in samples with high Cl content by inductively coupled plasma mass spectrometry. *J. Anal. Atom. Spectrom.*, **6**, 151–154.
26. Laborda, F., Baxter, M.J., Crews, H.M. and Dennis, J. (1994) Reduction of polyatomic interferences in inductively coupled plasma mass spectrometry by selection of instrumental parameters and using an Ar-nitrogen plasma: effect on multi-element analyses. *J. Anal. Atom. Spectrom.*, **9**, 727–736.
27. Gray, A.L. and Williams, J.G. (1987) Oxide and doubly charged ion response of a commercial inductively coupled plasma mass spectrometry instrument. *J. Anal. Atom. Spectrom.*, **2**, 81–82.
28. Gray, A.L. (1989) The origins, nebulisation and performance of ICP-MS systems. In *Applications of Inductively Coupled Plasma Mass Spectrometry* (Eds. A.R. Date and A.L. Gray), Chapman & Hall, London, pp. 1–42.
29. Beauchemin, D., McLaren, J.W. and Berman, S.S. (1987) Study of the effects of concomitant elements in inductively coupled plasma mass spectrometry. *Spectrochim. Acta*, **42B**(3), 467–490.
30. Olivares, J.A. and Houk, R.S. (1986) Suppression of analyte signal by various concomitant salts in inductively coupled plasma mass spectrometry. *Anal. Chem.*, **58**, 20–25.

31. Thompson, J.J. and Houk, R.S. (1987) A study of internal standardisation in inductively coupled plasma-mass spectrometry. *Appl. Spectrosc.*, **41**, 801–806.
32. Prohaska, T., Köllensperger, G., Krachler, M., De Winne, K., Stingeder, G. and Moens, L. (2000) Determination of trace elements in human milk by inductively coupled plasma sector field mass spectrometry (ICP-SFMS). *J. Anal. Atom. Spectrom.*, **15**, 335–340.
33. Kira, C.S., Maio, F.D. and Maihara, V.A. (2004) Comparison of partial digestion procedures for determination of Ca, Cr, Cu, Fe, K, Mg, Mn, Na, P and Zn in milk by inductively coupled plasma-optical emission spectrometry. *J. AOAC Int.*, **87**, 151–156.
34. Thompson, M. and Walsh, J.N. (1983) *A Handbook of Inductively Coupled Plasma Spectrometry*, Chapman & Hall, London.
35. Matilainen, R. and Tummavuori, J. (1996) Iron determination in fertilizers by inductively coupled plasma atomic emission spectrometry: study of spectral and interelement effects at different wavelengths. *J. AOAC Int.*, **79**(1), 22–28.
36. Uchida, T., Isoyama, H., Oda, H., Wada, H. and Uenoyama, H. (1993) Determination of ultra-trace metals in biological standards by inductively coupled plasma atomic-emission spectrometry with ultrasonic nebulization. *Anal. Chim. Acta*, **283**(2), 881–886.
37. Thiel, G. and Danzer, K. (1997) Direct analysis of mineral components in wine by inductively coupled plasma optical emission spectrometry (ICP AES). *Fresen. J. Anal. Chem.*, **357**(5), 553–557.
38. Moon, C.S., Zhang, Z.W., Shimbo, S., Hokimoto, S., Shimazaki, K., Saito, T., Shimizu, A., Imai, Y., Watanabe, T. and Ikeda, M. (1996) A comparison of the food composition table-based estimates of dietary element intake with the values obtained by inductively coupled plasma atomic emission spectrometry: an experience in a Japanese population. *J. Trace Elem. Med. Biol.*, **10**(4), 237–244.
39. Woittiez, J.R.W. and Sloof, J.E. (1994) Sampling and sample preparation. In *Determination of Trace Elements* (Ed. Z.B. Alfassi), VCH Publishers, Weinheim, pp. 59–107.
40. Jarvis, I. (1992) Sample preparation for ICP-MS. In *Handbook of ICP-MS* (Eds. K.E. Jarvis, A.L. Gray and R.S. Houk), Chapman & Hall, London, pp. 173–224.
41. Reilly, C. (2002) Metal contamination of food: its significance for food quality and human health. In *Metal Analysis of Food* (Ed. C. Reilly), Blackwell Science Ltd, Oxford, pp. 23–39.
42. Thomas, C.L.P. and Schofield, H. (1995) *Sampling Source Handbook. An Indexed Bibliography of the Literature of Sampling*, Butterworth-Heinemann, Oxford.
43. Berg, T. and Licht, D. (2002) International legislation on trace elements as contaminants in food: a review. *Food Addit. Contam.*, **19**, 916–927.
44. Brereton, P., Macarthur, R. and Crews, H.M. (2003) Food: sampling with special reference to legislation, uncertainty and fitness for purpose. In *Handbook of Elemental Speciation: Techniques and Methodology* (Eds. R. Cornelis, H. Crews, J. Caruso and K. Heumann), John Wiley and Sons Ltd, Chichester, pp. 47–58.
45. Commission Directive (2001) 2001/22/EC of 8 March 2001 laying down the sampling methods and methods of analysis for the official control of the levels of lead, cadmium, mercury and 3-MCPD in foodstuffs. *Off. J.*, **L077**, 0014–0021.
46. Thompson, M. and Wood, R. (1993) The international harmonised protocol for the proficiency testing of (chemical) analytical laboratories. *J. AOAC Int.*, **76**, 929–940.
47. Muñoz-Olivas, R. and Cámara, C. (2003) Sample treatment for speciation analysis in biological samples. In *Handbook of Elemental Speciation: Techniques and Methodology* (Eds. R. Cornelis, H. Crews, J. Caruso and K. Heumann), John Wiley and Sons Ltd, Chichester, pp. 73–94.
48. Bouyssiére, B., Szpunar, J., Potin-Gautier, M. and Lobinski, R. (2003) Sample preparation techniques for elemental speciation studies. In *Handbook of Elemental Speciation: Techniques and Methodology* (Eds. R. Cornelis, H. Crews, J. Caruso and K. Heumann), John Wiley and Sons Ltd, Chichester, pp. 95–118.
49. Pyrzynska, K. (2004) Analytical methods for the determination of trace metals in wine *Crit. Rev. Anal. Chem.*, **34**(2), 69–83.

50. Robb, P., Owen, L.M.W. and Crews, H.M. (1995) Stable isotope approach to fission product element studies and *in vitro* modelling of ruminant digestion using inductively coupled plasma mass spectrometry. *J. Anal. Atom. Spectrom.*, **10**, 625–629.
51. Durrant, S.F. and Ward, N.I. (1994) Laser ablation-inductively coupled plasma mass spectrometry (LA-ICP-MS) for the multielemental analysis of biological materials: a feasibility study. *Food Chem.*, **49**(3), 317–323.
52. Augagneur, S., Medina, B., Szpunar, J. and Lobinski, R. (1996) Determination of rare-earth elements in wine by inductively coupled plasma mass spectrometry using a microconcentric nebulizer. *J. Anal. Atom. Spectrom.*, **11**(9), 713–721.
53. LopezArtiguez, M., Camean, A.M. and Repetto, M. (1996) Determination of nine elements in sherry wine by inductively coupled plasma atomic-emission spectrometry. *J. AOAC Int.*, **79**(5), 1191–1197.
54. Al-Swaidan, H.M. (1988) Analysis of fruit juices by inductively coupled plasma-mass spectrometry. *Anal. Lett.*, **21**, 1469–1475.
55. Dean, J.R., Ebdon, L. and Massey, R.C. (1987) Selection of mode for the measurement of lead isotope ratios by inductively coupled plasma mass spectrometry and its application to milk powder analysis. *J. Anal. Atom. Spectrom.*, **2**, 369–374.
56. Baxter, M.J., Burrell, J.A., Crews, H.M. and Massey, R.C. (1991) Al levels in milk and infant formulae. *Food Addit. Contam.*, **8**, 653–660.
57. Stuerup, S. and Buechert, A. (1996) Direct determination of copper and iodine in milk and milk powder in alkaline solution by flow-injection inductively coupled plasma mass spectrometry. *Fresen. J. Anal. Chem.*, **354**(3), 323–326.
58. Fonseca, R.W. and Millerlhlh, N.J. (1996) Influence of sample matrix components on the selection of calibration strategies in electrothermal-vaporization inductively coupled plasma mass spectrometry. *Spectrochim. Acta B Atom. Spectrosc.*, **51B**(13), 1591–1599.
59. Vanhaecke, F., Boonen, S., Moens, L. and Dams, R. (1995) Solid sampling electrothermal vaporization inductively coupled plasma mass spectrometry for the determination of As in standard reference materials of plant origin. *J. Anal. Atom. Spectrosc.*, **10**(2), 81–87.
60. Grégoire, D.C., Millerlhlh, N.J. and Sturgeon, R.E. (1994) Direct analysis of solids by ultrasonic slurry electrothermal vaporization inductively coupled plasma mass spectrometry. *J. Anal. Atom. Spectrom.*, **9**(5), 605–610.
61. Negretti de Brätter, V.E., Brätter, P., Reinicke, A., Schulze, G., Alvarez, W.A.L. and Alvarez, N. (1995) Determination of mineral trace elements in total diet by inductively coupled plasma atomic emission spectrometry: comparison of microwave-based digestion and pressurised ashing systems using different acid mixtures. *J. Anal. Atom. Spectrom.*, **10**, 487–491.
62. Muto, H., Abe, T., Takizawa, Y., Kawabata, K., Yamaguchi, K. and Saitoh, K. (1994) Simultaneous multi-elemental analysis of daily food samples by inductively coupled plasma mass spectrometry. *Sci. Total Environ.*, **144**, 231–239.
63. Shiraishi, K., McInroy, J.F. and Igarashi, Y. (1990) Simultaneous multi-element analysis of diet samples by inductively coupled plasma mass spectrometry and inductively coupled plasma atomic emission spectrometry. *J. Nutr. Sci. Vitaminol.*, **36**, 81–86.
64. Shiraishi, K., Takaku, Y., Yoshimizu, K., Igarashi, Y., Masuda, K., McInroy, J.F. and Tanaka, G. (1991) Determination of thorium and uranium in total diet samples by inductively coupled plasma mass spectrometry. *J. Anal. Atom. Spectrom.*, **6**, 335–338.
65. Friel, J.K., Skinner, C.S., Jackson, S.E. and Longerich, H.P. (1990) Analysis of biological reference materials, prepared by microwave dissolution, using inductively coupled plasma mass spectrometry. *Analyst*, **115**, 269–273.
66. Crews, H.M., Baxter, M.J., Bigwood, T., Burrell, J.A., Owen, L.M., Robinson, C., Wright, C. and Massey, R.C. (1992) Pb in feed incidence—multi-element analysis of cattle feed and tissues by inductively coupled plasma-mass spectrometry and co-operative quality assurance scheme for Pb analysis of milk. *Food Addit. Contam.*, **9**, 365–378.

67. Sun, D.H., Waters, J.K. and Mawhinney, T.P. (1997) Microwave digestion with $\text{HNO}_3\text{—H}_2\text{O}_2\text{—HF}$ for the determination of total aluminium in seafood and meat by inductively coupled plasma atomic emission spectrometry. *J. Agr. Food Chem.*, **45**(6), 2115–2119.
68. Cox, R.J., Pickford, C.J. and Thompson, M. (1992) Determination of iodine 129 in vegetable samples by inductively coupled plasma mass spectrometry. *J. Anal. Atom. Spectrom.*, **7**, 635–640.
69. Larsen, E.H. and Ludwigsen, M.B. (1997) Determination of iodine in food-related certified reference materials using wet ashing and detection by inductively coupled plasma mass spectrometry. *J. Anal. Atom. Spectrom.*, **12**(4), 435–439.
70. Heckman J. (2005) Food packaging regulation in the United States and the European Union. *Regulatory Toxicology and Pharmacology*, **42**(1), 96–143.
71. Biego, G.H., Biantet, H., Joyeux, H. and Debry, G. (1996) Determination of tin content in fruits, vegetables and their juices according to packaging. *Sci. aliment.*, **16**(6), 623–630.
72. Sumitani, H., Snekan, S., Nakatani, A. and Tatsuka, K. (1993) Inductively coupled plasma-atomic emission spectrometric determination of tin in canned food. *J. AOAC Int.*, **76**(6), 1374–1377.
73. Krushevska, A.P. and Barnes, R.M. (1994) Determination of low silicon concentrations in food and coral soil by inductively coupled plasma atomic-emission spectrometry. *J. Anal. Atom. Spectrom.*, **9**(9), 981–984.
74. Lásztity, A., Kotrebai, M. and Barnes, R.M. (1996) Inductively coupled plasma spectrometry determination of marker elements for childhood soil ingestion. *Microchem. J.*, **54**(4), 452–464.
75. Kohri, M., Sato, K., Ide, K., Inoue, Y. and Okochi, H. (1997) Solid-phase extraction for the speciation of organotin compounds in shellfish samples. *Anal. Sci.*, **13**(1), 141–143.
76. Ybáñez, N., Velez, D., Tejedor, W. and Montoro, R. (1995) Optimisation of the extraction, clean-up and determination of arsenobetaine in manufactured seafood products by coupling liquid chromatography with inductively coupled plasma atomic emission spectrometry. *J. Anal. Atom. Spectrom.*, **10**, 459–465.
77. Kunar, U.T., Vela, N.P., Dorsey, J.G. and Caruso, J.A. (1993) Supercritical-fluid extraction of organo-tins from biological samples and speciation by liquid chromatography and inductively coupled plasma-mass spectrometry. *J. Chromatogr. A*, **655**(2), 340–345.
78. Goenaga Infante H., O'Connor, G., Rayman, M., Wahlen, R., Entwisle, J., Norris, P., Hearn, R. and Catterick, T. (2004) Selenium speciation analysis of selenium-enriched supplements by HPLC with ultrasonic nebulisation ICP-MS and electrospray MS/MS detection. *J. Anal. Atom. Spectrom.*, **19**, 1529–1538.
79. Boomer, D.W., Powell, M.J. and Hipfner, J. (1990) Characterization and optimisation of HPLC for on-line preconcentration of trace metals with detection by ICP-mass spectrometry. *Talanta*, **37**, 127–134.
80. LopezArtiguez, M., Camean, A. and Repetto, M. (1996) Preconcentration of heavy metals in urine using chelating ion-exchange resin and quantification by ICP-AES. *Atom. Spectrosc.*, **17**(2), 83–87.
81. Williams, J.G. (1992) Instrument options. In *Handbook of ICP-MS* (Eds. K.E. Jarvis, A.L. Gray and R.S. Houk), Chapman & Hall, London, pp. 58–80.
82. Williams, J.G. (1992) Sample introduction for liquids and gases. In *Handbook of ICP-MS* (Eds. K.E. Jarvis, A.L. Gray and R.S. Houk), Chapman & Hall, London, pp. 58–80.
83. Jarvis, K.E., Gray, A.L. and Houk, R.S. (1992) *Handbook of ICP-MS*, Chapman & Hall, London.
84. Pickford, C.J. and Brown, R.M. (1986) Comparison of ICP-MS with ICP-ES: detection power and interference effects experienced with complex matrices. *Spectrochim. Acta*, **41B**, 183–187.
85. Eagles, J., Fairweather-Tait, S.J., Mellon, F.A., Portwood, D.E., Self, R., Gotz, A., Heumann, K.G. and Crews, H.M. (1989) Comparison of fast-atom bombardment, thermal ionisation and inductively coupled plasma-mass spectrometry for the measurement of $^{64}\text{Zn}/^{67}\text{Zn}$ stable isotopes in human nutrition studies. *Rapid Commun. Mass Sp.*, **3**(6), 203–205.

86. Begley, I.S. and Sharp, B.L. (1994) Occurrence and reduction of noise in inductively coupled plasma-mass spectrometry for enhanced precision in isotope ratio measurements. *J. Anal. Atom. Spectrom.*, **9**, 171–176.
87. Crews, H.M., Owen, L.M., Langford, N., Fairweather-Tait, S.J., Fox, T.E., Hubbard, L. and Phillips, D. (2000) Use of the stable isotope ^{106}Cd for studying dietary cadmium absorption in humans. *Toxicol. Lett.*, **112–113**, 201–207.
88. Harvey, L.J., Majsak-Newman, G., Dainty, J.R., Lewis, D.J., Langford, N.J., Crews, H.M. and Fairweather-Tait, S.J. (2003) Adaptive responses in men fed low- and high-copper diets. *Brit. J. Nutr.*, **90**, 161–168.
89. Fox, T.E., Atherton, C., Dainty, J.R., Lewis, D.J., Langford, N.J., Baxter, M.J., Crews, H.M. and Fairweather-Tait, S.J. (2005) Absorption of selenium from wheat, garlic, and cod intrinsically labeled with Se-77 and Se-82 stable isotopes. *Int. J. Vitam. Nutr. Res.*, **75**, 179–186.
90. Dainty, J.R. and Fox, T.E. (2005) Modeling in Nutrition. The metabolism of selenium, copper, zinc and calcium using stable isotopes in humans. In *Handbook of Elemental Speciation II: Species in the Environment, Food, Medicine and Occupational Health* (Eds. R. Cornelis, H. Crews, J. Caruso and K. Heumann), John Wiley and Sons Ltd, Chichester, pp. 690–712.
91. Crews, H.M. (2001) Use of stable isotopes of selenium to investigate selenium status. In *Advances in Isotope Methods for the Analysis of Trace Elements in Man* (Eds. N.M. Lowe and M.J. Jackson), CRC Press London, pp. 129–150.
92. Sloth, J.J., Larsen, E.H., Bügel, S.H. and Moesgaard, S. (2003) Determination of total selenium and ^{77}Se in isotopically enriched human samples by ICP-dynamic reaction cell-MS. *J. Anal. Atom. Spectrom.*, **18**, 317–322.
93. Rayman, M. (2004) The use of high-selenium yeast to raise selenium status: how does it measure up? *Brit. J. Nutr.*, **92**, 557–573.
94. Fox, T.E., Van den Heuvel E.G.H.M., Atherton, C.A., Dainty, J.R., Lewis, D.J., Langford, N.J., Crews, H.M., Luten, J.B., Lorentzen, M., Sieling, F.W., van Aken-Schneyder, P., Hoek, M., Kotterman, M.J.J., van Dael, P. and Fairweather-Tait, S.J. (2004) Bioavailability of selenium from fish, yeast and selenate: a comparative study in humans using stable isotopes. *Eur. J. Clin. Nutr.*, **58**, 343–349.
95. Ramsey, M.H., Thompson, M. and Banerjee, E.K. (1987) Realistic assessment of analytical data quality from inductively coupled plasma atomic emission spectrometry. *Anal. Proc.*, **24**, 260–265.
96. United Kingdom Accreditation Service (1989) *General Criteria for Competence for Calibration and Testing Laboratories*, NAMAS Accreditation Standard M10, UKAS, Feltham.
97. Thompson, M. and Wood, R. (1995) Harmonised guidelines for internal quality control in analytical chemistry laboratories. *Pure Appl. Chem.*, **67**, 649–666.
98. Baxter, M.J., Crews, H.M., Robb, P. and Strutt, P. (1997b) Quality control in the multi-element analysis of foods using ICP-MS. In *Plasma Spectrometry. Progress and Developments* (Eds. G. Holland and S.D. Tanner), The Royal Society of Chemistry, Cambridge, pp. 95–108.
99. Leblanc, J.-C., Guérin, Noël, L., Calamassi-Tran, G., Volatier, J.-L. and Verger, P. (2005) Dietary exposure estimates of 18 elements from the 1st French Total Diet Study. *Food Addit. Contamin.*, **22**, 624–641.
100. Rose, M., Knaggs, M., Owen, L. and Baxter, M. (2001) A review of analytical methods for lead, cadmium, mercury, arsenic and tin determination used in proficiency testing. *J. Anal. Atom. Spectrom.*, **9**, 1101–1106.
101. Kirchmer, C.J. (1994) Limits of detection and accuracy in trace elements analysis. In *Determination of Trace Elements* (Ed. Z.B. Alfassi), VCH Publishers, Weinheim, pp. 39–58.
102. Ysart, G., Miller, P., Crews, H., Robb, P., Baxter, M., De L'argy, C., Lofthouse, S., Sargent, C. and Harrison, N. (1999) Dietary exposure estimates of 30 elements from the UK Total Diet Study. *Food Addit. Contam.*, **16**, 391–403.

103. Ysart, G., Miller, P., Croasdale, M., Crews, H., Robb, P., Baxter, M., De L'argy, C. and Harrison, N. (2000) 1997 UK Total Diet Study – dietary exposures to aluminium, arsenic, cadmium, chromium, copper, lead, mercury, nickel, selenium, tin and zinc. *Food Addit. Contam.*, **17**, 775–786.
104. Rose, M., Miller, P., Baxter, M., Appleton, G., Crews, H. and Croasdale, M. (2001) *J. Environ. Monitor.*, **3**, 361–365.
105. D'amato, M., Forte, G. and Caroli, S. (2004) Identification and quantification of major species of arsenic in rice. *J. AOAC Int.*, **87**, 238–243.
106. Batley, G.E. (1989) *Trace Element Speciation: Analytical Methods and Problems*, CRC Press, Boca Raton.
107. Krull, I.S. (1991) *Trace Metals Analysis and Speciation*, Elsevier, Amsterdam.
108. Caroli, S. (1996) *Element Speciation in Bioinorganic Chemistry*, John Wiley & Sons, Inc., New York.
109. Cornelis, R., Crews, H., Caruso, J. and Heumann, K. (2003) *Handbook of Elemental Speciation: Techniques and Methodology*, John Wiley and Sons Ltd, Chichester.
110. Cornelis, R., Crews, H., Caruso, J. and Heumann, K. (2005) *Handbook of Elemental Speciation II: Species in the Environment, Food, Medicine and Occupational Health*, John Wiley and Sons Ltd, Chichester.
111. Berg, T. (2003) Speciation and legislation. In *Handbook of Elemental Speciation: Techniques and Methodology* (Eds. R. Cornelis, H. Crews, J. Caruso and K. Heumann), John Wiley and Sons Ltd, Chichester, pp. 629–634.
112. Lásztity, A., Krushevska, A., Kotrebai, M., Barnes, R.M. and Amarasiriwardena, D. (1995) As determination in environmental, biological and food samples by inductively coupled plasma mass spectrometry. *J. Anal. Atom. Spectrom.*, **10**, 505–510.
113. Gailer, J., Francesconi, K.A., Edmonds, J.S. and Irgolic, K.J. (1995) Metabolism of arsenic compounds by the blue mussel *Mytilus edulis* after accumulation from seawater spiked with As compounds. *Appl. Organomet. Chem.*, **9**, 341–355.
114. Yeh, C.-F. and Jiang, S.-J. (2005) Speciation of arsenic compounds in fish and oyster tissues by capillary electrophoresis-inductively coupled plasma-mass spectrometry. *Electrophoresis*, **26**, 1615–1621.
115. Hansen, S.H., Larsen, E.H., Pritzl, G. and Cornett, C. (1992) Separation of seven arsenic compounds by high-performance liquid chromatography with on-line detection by hydrogen-Ar flame atomic absorption spectrometry and inductively coupled plasma mass spectrometry. *J. Anal. Atom. Spectrom.*, **7**, 629–634.
116. Polatajko, A. and Szpunar, J. (2004) Speciation of arsenic in chicken meat by anion-exchange liquid chromatography with inductively coupled plasma-mass spectrometry. *J. AOAC Int.*, **87**, 233–237.
117. Vela, N.P. and Heitkemper, D.T. (2004) Total arsenic determination and speciation in infant food products by ion chromatography-inductively coupled plasma-mass spectrometry. *J. AOAC Int.*, **87**, 244–252.
118. Shum, S.C.K., Neddersen, R. and Houk, R.S. (1992) Elemental speciation by liquid chromatography-inductively coupled plasma mass spectrometry with direct injection nebulization. *Analyst*, **117**, 577–582.
119. Shum, S.C.K., Pang, H.-M. and Houk, R.S. (1992) Speciation of mercury and Pb compounds by microbore column liquid chromatography-inductively coupled plasma mass spectrometry with direct injection nebulization. *Anal. Chem.*, **64**, 2444–2450.
120. Campbell, M.J., Vermeir, G., Dams, R. and Quevauviller, P. (1992) Influence of chemical species on the determination of mercury in a-biological matrix (cod muscle) using inductively coupled plasma mass spectrometry. *J. Anal. Atom. Spectrom.*, **7**, 617–621.
121. Al-Rashdan, A., Heitkemper, D. and Caruso, J.A. (1991) Lead speciation by HPLC-ICP-AES and HPLC-ICP-MS. *J. Chromatogr. Sci.*, **29**, 98–102.

122. Owen, L.M.W., Crews, H.M. and Massey, R.C. (1992) Al in tea: SEC-ICP-MS speciation studies of infusions and simulated gastrointestinal digests. *Chem. Spec. Bioavailab.*, **4**, 89–96.
123. Ødegard, K.E. and Lund, W. (1997) Multi-element speciation of tea infusion using cation-exchange separation and size-exclusion chromatography in combination with inductively coupled plasma mass spectrometry. *J. Anal. Atom. Spectrom.*, **12**, 403–408.
124. Owen, L.M.W., Crews, H.M., Bishop, N.J. and Massey, R.C. (1994) Aluminium uptake from some foods by guinea pigs and the characterisation of aluminium in *in vivo* intestinal digesta by SEC-ICP-MS. *Food Chem. Toxicol.*, **32**, 697–705.
125. Salov, V.V., Yoshinaga, J., Shibata, Y. and Morita, M. (1992) Determination of inorganic halogen species by liquid chromatography with inductively coupled Ar plasma mass spectrometry. *Anal. Chem.*, **64**, 2425–2428.
126. Dennis, M.J., Burrell, J.A., Mathieson, K., Willetts, P. and Massey, R.C. (1994) The determination of the flour improver potassium bromate in bread by gas chromatographic and ICP-MS methods. *Food Addit. Contam.*, **11**, 633–639.
127. Heitkemper, D.T., Kaine, L.A., Jackson, D.S. and Wolnik, K.A. (1994) Practical applications of element-specific detection by inductively coupled plasma atomic emission spectroscopy and inductively coupled plasma mass spectrometry to ion chromatography of foods. *J. Chromatogr. A*, **671**, 101–108.
128. Shah, M., Wuilloud, G., Kannamkumarath, S.S. and Caruso, J.A. (2005) Iodine speciation studies in commercially available seaweed by coupling different chromatographic techniques with UV and ICP-MS detection. *J. Anal. Atom. Spectrom.*, **20**, 176–182.
129. Morita, M., Uehiro, T. and Fuwa, K. (1980) Speciation and elemental analysis of mixtures by high performance liquid chromatography with inductively coupled Ar plasma emission spectrometric detection. *Anal. Chem.*, **52**, 349–351.
130. Dean, J.R., Munro, S., Ebdon, L., Crews, H.M. and Massey, R.C. (1987) Studies of metalloprotein species by directly coupled high-performance liquid chromatography inductively coupled plasma mass spectrometry. *J. Anal. Atom. Spectrom.*, **2**, 607–610.
131. Crews, H.M., Dean, J.R., Ebdon, L. and Massey, R.C. (1989) Application of high-performance liquid chromatography-inductively coupled plasma mass spectrometry to the investigation of Cd speciation in pig kidney following cooking and *in vitro* gastro-intestinal digestion. *Analyst*, **114**, 895–899.
132. Mason, A.Z., Storms, S.D. and Jenkins, K.D. (1990) Metalloprotein separation and analysis by directly coupled size exclusion high-performance liquid chromatography inductively coupled plasma mass spectroscopy. *Anal. Biochem.*, **186**, 187–201.
133. Owen, L.M.W., Crews, H.M., Hutton, R.C. and Walsh, A. (1992) Preliminary study of metals in proteins by HPLC-ICP-MS using multi-element time-resolved analysis. *Analyst*, **117**, 649–655.
134. High, K.A., Methven, B.A.J., McLaren, J.W., Siu, K.W.M., Wang, J., Klavervkamp, J.F. and Blais, J.S. (1995) Physico-chemical characterisation of metal binding proteins using HPLC-ICP-MS, HPLC-MA-AAS and electrospray-MS. *Fresen. J. Anal. Chem.*, **315**, 393–402.
135. High, K.A., Blais, J.S., Methven, B.A.J. and McLaren, J.W. (1995) Probing the characteristics of metal-binding proteins using high-performance liquid chromatography-atomic absorption and inductively coupled plasma mass spectrometry. *Analyst*, **120**, 629–634.
136. Goenaga Infanta, H., Hearn, R. and Catterick, T. (2005) Current mass spectrometry strategies for selenium speciation in dietary sources of high selenium. *Anal. Bioanal. Chem.*, **382**, 957–967.
137. Polatajko, A., Śliwka-Kaszyńska, M., Dernovics, M., Ruzik, R., Ruiz Encinar, J. and Szpunar, J. (2004) A systematic approach to selenium speciation in selenized yeast. *J. Anal. Atom. Spectrom.*, **19**, 114–120.
138. Kotrebai, M., Birringer, M., Tyson, J.F., Block, E. and Uden, P.C. (1999) Identification of the principal compounds in selenium-enriched natural sample extracts by ion-pair liquid

- chromatography with inductively coupled plasma- and electrospray ionization-mass spectrometric detection. *Anal. Commun.*, **36**, 249–252.
139. Uden, P.C., Totoe Boakye, H., Kahakachichi, C., Hafezi, R., Nolibos, P., Block, E., Johnson, S. and Tyson, J.F. (2004) Element selective characterization of stability and reactivity of selenium species in selenized yeast. *J. Anal. Atom. Spectrom.*, **19**, 65–73.
140. Larsen, E.H., Sloth, J., Hansen, M. and Moesgaard (2003) Selenium speciation and isotope composition in ⁷⁷Se-enriched yeast using gradient elution HPLC separation and ICP-dynamic reaction cell-MS. *J. Anal. Atom. Spectrom.*, **18**, 310–316.
141. Bendahl, L. and Gammelgaard, B. (2004) Separation of selenium compounds by CE-ICP-MS in dynamically coated capillaries applied to selenized yeast samples. *J. Anal. Atom. Spectrom.*, **19**, 143–148.
142. Crews, H.M., Clarke, P.A., Lewis, D.J., Owen, L.M.W., Strutt, P.R. and Izquierdo, A. (1996) Investigation of selenium speciation in *in vitro* gastrointestinal extracts of cooked cod by high-performance liquid chromatography-inductively coupled plasma mass spectrometry and electrospray mass spectrometry. *J. Anal. Atom. Spectrom.*, **11**, 1177–1182.
143. Bryszewska, M.A., Ambroziak, W., Diowks, A., Baxter, M.J., Langford, N.J. and Lewis, D.J. (2005) Changes in the chemical form of selenium observed during the manufacture of a selenium-enriched sourdough bread for use in a human nutrition study. *Food. Addit. Contam.*, **22**, 135–140.
144. Bryszewska, M.A., Ambroziak, W., Rudzinski, J. and Lewis, D.J. (2005) Characterisation of selenium compounds in rye seedling biomass using ⁷⁵Se-labelling/SDS-PAGE separation/ γ -scintillation counting, and HPLC-ICP-MS analysis of a range of enzymatic digests. *Anal. Bioanal. Chem.*, **382**, 1279–1287.
145. Liu, Y., Lopez-Avila, V., Zhu, J.J., Wiedner, D.R. and Beckert, W.F. (1995) Capillary electrophoresis coupled on-line with inductively coupled plasma mass spectrometry for elemental speciation. *Anal. Chem.*, **67**, 2020–2025.
146. Taylor, K.A., Sharp, B.L., Lewis, D.J. and Crews, H.M. (1998) Design and characterisation of a microconcentric nebuliser interface for capillary electrophoresis-inductively coupled plasma-mass spectrometry. *J. Anal. Atom. Spectrom.*, **13**(10), 1095–1100.
147. Michalke, B. (2005) Capillary electrophoresis-inductively coupled plasma-mass spectrometry: a report on technical principles and problem solutions, potential, and limitations of this technology as well as on examples of application. *Electrophoresis*, **26**, 1584–1597.
148. Wuilloud, R.G., Shah, M., Kannamkumarath, S.S. and Altamirano, J.C. (2005) The potential of inductively coupled plasma-mass spectrometric detection for capillary electrophoretic analysis of pesticides. *Electrophoresis*, **26**, 1598–1605.

This page intentionally left blank

Index

- Abel inversion, 46, 47
- accuracy, 68, 162, 174, 188, 189, 309, 304, 392
- actinides, 188, 189, 294, 353, 359, 390
- aerosol, 61, 65, 70, 98, 134, 304, 309, 342, 344
 - generation, 98
 - primary aerosol, 98, 101, 102, 111
 - Sauter diameter, 99
- air plasmas, 236, 242
- analysis
 - agricultural materials, 210
 - cereals, 396, 407
 - fats and oils, 395
 - fruit, 395
 - manufactured objects, 206, 207, 398, 400, 410
 - vegetables, 395
 - wines, 210, 211, 390, 392, 394, 396
 - air (airborne particulates), 339, 340, 341, 342
 - animal/fish tissue, 265, 394, 406–407
 - archaeological, 206–210, 294
 - biological, 184, 188, 193, 195, 214, 253, 304, 357
 - blood, 348, 349, 350, 352, 354, 359
 - certification/metrological, 185
 - clinical, 198, 265, 338
 - earth science, 277, 302, 304, 305, 306, 313
 - environmental materials, 187, 192, 211, 346
 - firebrick, 233, 234
 - metalloids, 200, 273, 289, 345, 346
 - food, 185, 195, 210, 214, 387
 - forensic, 212, 348, 361
 - geochronology, 202–206, 304, 312
 - geological materials, 278, 279, 281, 283 290, 294, 302, 308, 313
 - fluid inclusions, 310
 - silicate minerals, 283, 285, 286
 - proteomics, 7, 193, 253, 267, 269, 339, 358, 360
 - provenance, 206, 210
 - radioactive materials, 187, 189, 205, 206
 - soils/sediments, 188, 211, 190
 - tracer studies, 197–202
 - waters, 187, 189, 195, 211, 237, 239, 285, 294, 345, 347, 394, 341–3
- antimony, 251, 269–271, 359
- argon, 27, 28, 40, 41, 45, 70, 71, 99, 154, 200, 228, 229, 232, 239, 388
- arsenic, 113, 239, 251, 262–5, 314, 342, 349, 350, 352, 354, 357, 361, 406–407
- atomic absorption spectrometry, 1, 49, 115, 278, 413
- atomic fluorescence, 18, 19, 74, 234
- axial systems, 47, 64–5, 89–90
- background (see *also* interferences), 28, 291, 292, 311, 349, 392, 399, 403
 - correction, 11, 71, 79–80, 81, 87–8
 - in isotope ratio measurements, 174
- barrel shock, 138, 238
- bivariate plot, 207, 208, 209
- blank correction, 183
- blazed grating, 80
- Boltzmann equation, 31, 34, 43, 30
 - plot, 38, 41, 39–40
- boron, 107, 291, 304, 350

- cadmium, 19, 88, 185, 186, 198, 350, 352, 354, 359, 360, 408
- calcium, 29, 206, 285, 341, 350, 352, 392
- calibration, 70, 72, 147, 163, 173, 182–3, 308, 403
- drift, 32, 69, 75, 78, 82, 88, 90, 149, 186, 192, 241, 403
- internal standardisation, 70, 71, 290–91, 293, 299, 309, 311, 391, 392, 399
- spike calibration, 182–3
- capillary electrophoresis, 73, 98, 149, 338, 412
- carbon dioxide plasmas, 236–7
- certified reference materials, 68, 163, 185, 196, 308, 397
- channel plate, 153
- charged-coupled device, 49–55, 66
- charged-transfer, 28, 85, 86, 229, 242
- chemical vapour generation, 65, 113, 114, 344, 404
- chromatographic interfaces, 112, 195, 358
- chromatography, 73, 91, 112–13, 187, 192, 251, 263, 267, 314, 338–9, 345, 357, 360–61, 407, 408
- chromium, 233, 251, 345, 360
- collision cells, 21, 165, 166, 200, 213, 260, 343, 355, 390,
- comminution, 281, 282, 315
- cones
- contamination, 174–6, 183, 189, 282, 393, 394
- cool (low power) plasmas, 141, 153–4, 245, 293, 389
- copper, 136–7, 194, 208, 302, 350, 356
- counting statistics, 67, 171, 390, 401,
- sampling, 64, 118, 137, 138, 154, 165, 172, 195, 240
- skimmer, 137, 138, 139, 140, 172, 238, 343
- dark current, 85
- data analysis, 87, 280, 392, 400
- data manipulation, 6, 88
- decomposition/dissolution, 283, 287–9
- desolvation, 109, 106–107, 111–12, 120, 390
- detection limits, 5, 61, 72, 112, 189, 267, 308, 387, 398, 403–405,
- limit of determination, 64, 406
- detector dead time, 166, 303, 176–8
- detectors, 8, 66–8, 84–6
- channeltron (see also dynode), 177
- charge coupled, 49–50, 85
- charge injection, 18, 50, 66–7, 85–6,
- electron multiplier, 151–52
- ‘sag’, 177–8
- Faraday cup, 150–51, 166, 303
- multi-collector, 160, 212, 214, 215, 296, 304, 344, 353
- photodiode array, 85
- photomultipliers, 84–5, 283
- determination limit, 64
- direct-current plasma (DCP) 27, 387
- double-focusing sector mass analyzer, 144, 145–6, 165, 167
- drift, 32, 69–70, 75, 82, 88, 90, 146, 186, 192, 292, 299, 403
- droplet size, 101, 106, 111, 258
- duty cycle, 261
- dwell time, 178
- dynamic range, 71–2, 89, 182, 291
- dynamic reaction cell, 156, 166, 390
- dynode
- continuous, 151–2
- discrete, 84, 152, 177
- multiplier, 151–2
- echelle systems, 67, 69, 80–81, 83, 90
- Einstein equation, 31, 61
- electron-impact ionization, 28, 242
- electron multiplier (see also detectors), 151
- electron number density, 42, 44, 47–8, 136, 233, 236
- electrons, 85, 134, 151
- electrospray ionization, 251
- charged droplets, 254, 255
- charge balance equation, 255
- droplet disintegration, 257–8
- ion sampling, 259
- electrospray sources, 256, 257
- electrothermal vapourisation, 5, 114–15, 190, 200, 233, 283, 309, 356, 397
- error magnification curves, 182
- Fabry–Perot interferometry, 16, 20, 90
- Faraday cup collector, 150–51, 303
- figure of merit, 62, 63, 64
- fireball, 71, 137, 232
- flow injection technique, 81, 184, 343, 344, 345, 396
- gas flows, 62, 66, 70, 76, 78, 101, 108, 134, 137–8, 232, 238
- gas-phase ion formation, 8, 252, 258–9
- generators, see radio frequency generators
- geochronology, 202, 304, 312
- sample preparation, 281–9
- sampling, 279–80
- geological samples, 202, 205, 206, 277–9, 282, 288, 305, 315
- gold, 32, 33, 135, 208, 283, 299, 300, 301, 310, 350, 359
- helium, 45, 78, 91, 92, 226, 228, 229, 230–31, 235–6, 241

- hexapole, 72, 140–41, 165, 167, 213
- high resolution (see *also* sector field ICP-MS), 90, 166, 201, 236, 260–61, 293, 302, 338, 343, 412
- hydride generation, 65–6, 113–14, 291, 344–5, 355, 399, 404, 410
- hydrocarbon gases, 234, 240
- hydrofluoric acid, 284–5, 340
- impedance matching, 75, 99–100, 226–7
- indium, 29, 233, 299
- injectors, 76–78, 306
- instrument control, 87–8
- instrument drift, 69–70, 82, 397, 403
- instrument performance, 313, 403
- interferences
 - definitions, 234, 237, 292, 340–41, 388
 - double charge, 175, 390
 - ionisation, 391–2
 - isobaric, 388–9
 - polyatomic, 72, 141, 147, 150, 156, 238, 239, 245, 284, 293, 389–91
- internal standard, 290, 291, 293, 299, 309, 311, 391, 392
- iodine, 179, 213, 341, 350, 398, 407
- ion(s)
 - beam, 16, 140, 144, 146, 150, 154, 164, 166, 390
 - detection, 67, 72, 144, 150–53
 - energy, 135, 136, 141, 142, 145, 146
 - focusing, 140–41, 144, 145, 146, 150, 231
 - lens, 138, 140, 150, 173
 - sampling, 136, 137, 138, 142, 147, 243, 259
- ion source, 134–36, 141, 142, 145, 146, 147
- ion trap, 20, 149–50, 164, 168, 171, 173, 178, 230, 261
- ionisation, 134–6, 164, 228, 229–31, 242–3, 254
 - charge transfer, 135, 229
 - degree of ionisation, 136, 230
 - electron impact, 28, 171, 271
 - kinetic energy, 141–2, 147, 172, 261
 - penning, 29, 135, 136, 229
 - temperature, 30
 - thermal, 135, 164, 171, 229, 303
- iron, 9, 10, 35, 40, 187, 188, 199, 284, 289, 300, 301, 310, 345
- isotope
 - dilution, 160, 161, 185, 294
 - fractionation, 164, 167, 206, 212, 214–15
 - mass discrimination, 167, 172–4, 204, 207, 210, 239
 - mass scale shift, 174
 - natural abundances, 162, 186, 198, 207, 228, 267, 297, 302, 313, 388
 - ratio, 160, 169, 170, 302, 312, 401
 - spike calibration, 182–3, 191, 195
 - uncertainty in measurement, 170, 173, 183, 303
- isotopic composition, 161, 179, 180, 193, 198, 206, 207, 211
- kinetic energy discrimination, 156
- Langmuir probe, 92, 141
- lanthanide elements, 188–9
- laser, 115, 117, 306
 - ablation, 81, 115, 118, 168, 191, 207, 304, 307, 355
 - elemental fractionation, 116, 119, 307, 309
 - induced fluorescence, 45
 - neodymium-YAG, 117, 306
 - quantification/calibration, 119–20, 308
 - sampling, 118–19
 - spot size/resolution, 119, 307, 309
- lead, 163, 177, 208, 212, 300, 304, 311, 360
- light scattering, 45
 - Rayleigh scattering, 45
 - Thomson scattering, 45
- line (spectral)
 - broadening, 32
 - atomic lines, 40, 43–4, 50
 - collisional, 32, 45, 48
 - diagnostics, 49
 - doppler, 32, 33, 35, 42
 - hyperfine structure, 34, 37
 - intensity, 31, 32, 36, 38, 40, 41
 - ionic lines, 29, 43, 50
 - isolation, 79–81
 - stark, 34, 42, 230, 234
 - intensity, 31, 38, 41, 43, 61
 - line pair method, 40–41
 - optical thickness, 64, 89
 - pressure-broadened, 32, 33, 35
 - profile, 32–4
- load coil, 49, 74, 79, 231, 236, 243
- local thermal equilibrium (LTE), 34, 36, 43, 44, 61, 229, 230, 245
- low-gas-flow torches, see torches
- low power plasmas, 245
- low pressure plasmas, 242–4
- m/z ratios, 145, 146, 147, 237, 260, 261, 293, 313
- Mach disc, 137, 139, 238
- magnetic sector analyser, 144–5
- mass analysers, 142
- mass discrimination, 167, 168, 172–4, 181, 186, 204, 206, 207, 210
- mass flow controller, 69, 226
- matrix effects, 44, 48, 49, 190, 264, 265, 388, 392, 397

- Maxwell distribution function, 34, 46
mercury, 65, 188, 196, 345, 349, 356
metallomics, 2, 7, 356, 358
microbeam methods, 305
micro-plasmas, 90–93
microwave-induced plasmas (MIP), 27, 91, 229
mixed gas and molecular-gas plasmas, 226–45
 advantages and limitations, 227
 air, 236, 242
 electron number densities, 232, 233, 235, 236, 242
 halocarbon gases, 234
 helium, 226, 227, 229, 230, 231, 235–6, 237, 241–2
 hydrocarbon gases, 234, 240
 hydrogen, 228, 230, 231, 233–34, 239–40
 neon, 228, 229, 230, 235, 236, 242
 nitrogen, 229, 231, 232–3, 237, 238–9
 oxygen, 228, 231, 234–5, 237, 240–241
 physical characteristics, 228
 temperatures, 229, 230, 231, 232, 233, 235, 236
 xenon, 227, 235, 236, 241, 242
monochromator, 81, 82, 84, 90, 392
 Czerny–Turner, 81
 Ebert, 81
multiline diagnostics, 49–50
multipole reaction cell, 153, 154

nebuliser, 65, 99, 102, 108, 110, 113
 desolvation, 106, 111
 direct injection (DIN), 66, 105
 electrospray, 66, 107
 frit, 107
 jet impact, 107
 micro-flow nebulisers, 101, 105, 108, 109, 110–111, 112
 pneumatic, 62, 65, 70, 101–105, 109
 Babington (v-groove), 102, 103, 105, 106, 283
 concentric, 101, 102, 105
 cone-spray, 102, 104, 105, 106
 cross-flow, 102, 103, 105, 106
 HEN, DIHEN, 102, 235
 high-pressure, 103, 107, 137, 187, 340
 Meinhard, 103, 408
 oscillating capillary, 102, 107
 thermospray, 66, 107
 ultrasonic, 65, 99, 105–107
nitrogen, 28, 49, 79, 112, 228, 332–3, 238–9
noble gases, 73, 231, 235, 241, 245
noise, 109, 111, 148, 149, 152, 171
Nukiyama–Tanasawa equation, 101

octapole, 72, 165
optical thickness, 64, 89
organic solvents, 70, 74, 236, 241, 345
oscillator strength, 36, 39

oxygen, 79, 141, 228, 231, 234–5, 237, 240–41, 355

palladium, 187, 299, 302, 324
particle size distribution, 98, 99, 108, 109, 115, 118, 290, 307, 309
partition function, 30, 39, 41
penning ionization, 29, 98–9, 102, 135, 136, 229
photodiode array, 85
photomultipliers, 9, 43, 66, 84, 91, 283
Planck function, 30, 61, 135
plasma
 atmospheric-pressure, 136, 137, 142, 241, 243
 definition, 27
 dry plasma, 1, 11, 236, 239
 equilibrium, 27, 29–30
 low power (cool), 245, 311, 350, 389
 low pressure, 241, 242
 mixed gas plasmas, 226
 multiple gas plasmas, 237
 power modulation, 48, 244
plasma gas, 28, 64, 135, 172, 226, 228, 229, 232, 237, 390
plasma on a chip, 90–93
plasma perturbation, 48–9
platinum, 66, 187, 191, 237, 299, 302
poisson distribution, 171, 401
polychromators, 49, 71, 82, 90
 Paschen–Runge, 82, 83, 84
precision, 68–73, 107, 111, 115, 146, 162, 168, 178, 207, 291, 303
proficiency testing, 280, 314, 402

quadrupole mass spectrometers, 72, 114–15, 141, 143, 166, 259, 296, 304, 349, 388, 399
quality control, 401, 412
quantification, 399–400
 in LA-ICP-MS, 199

radio-frequency (rf) generators, 74–6, 134, 153, 227
 impedance matching network, 75, 227
 oscillator types, 75
 power modulation, 48, 244
 solid state, 85, 88
rare earth elements (see lanthanide elements), 188, 283, 293, 294
 radial plasma, 88
Rayleigh equation, 258
Rayleigh scattering, 45–6
reaction cells, 154, 165, 166, 200, 344, 355
reaction gas, 156, 166, 188, 200, 204, 213
reference materials, 163, 189, 195, 207, 273, 405–406

- resolution, 34, 72, 90, 146, 261
rubidium, 204, 210, 294, 299, 303, 312, 351
Russell's equation, 174
- Saha-Boltzmann distribution function, 30, 34, 43
Saha equation, 30, 43, 135, 229, 230
sample, definition, 281
sample introduction (see also chromatography; nebulisers), 15, 62, 65–6, 81, 98, 164, 188, 190, 205
 chemical vapour generation, 65, 113, 114, 344, 355, 404
 electrothermal vaporisation, 114, 190, 200, 283, 309, 356, 397
 flow injection, 81, 184, 343, 344, 345, 396
 laser ablation, 81, 115, 118, 168, 191, 207, 304, 307, 355
 plasma loading, 99–101, 111
sample preparation and pre-treatment, 279, 284, 340, 393, 396–9
 fusion methods, 286, 398
 microwave systems, 287, 288, 397, 407
sample transport efficiency, 102, 106, 107, 109, 111, 114, 118
 solid samples, 79, 98, 114, 190, 192, 242, 278, 281, 309
Schmidt cross-disperser, 83, 84
sea water, 187, 211, 347
sector field icp-ms, 165, 168, 171, 174, 178, 192, 201, 203, 204, 207, 210, 212, 344, 349, 391
selective extraction, 289
selectivity, 73, 108, 251, 349
selenium, 193, 239, 265–9, 358, 409–12
sensitivity, 61, 227, 238, 239, 241, 245, 259, 278, 305, 307, 338
shear gas, 64, 89
SHRIMP, 305, 312
signal-to-background ratio, 63, 148, 227, 239
SIMION algorithm, 140
skin effect, 75, 134
slurries, 232, 233, 234, 283
solid samples, 190–92
space-charge effects, 140, 173, 292, 14
spatial profiles, 13, 46–47
speciation, 88, 192–7, 345–6, 356–61, 399, 406–12
spectral interferences (see also interferences), 14, 72, 188, 189, 388, 392
spectral-line modulation, 16–17, 19
spectral overlap, 165, 168, 180, 388, 392
spectrometer, 3, 11, 19–20, 79–84
 high resolution, 90
spray chambers, 70, 86–7, 105, 108–12
 cyclonic, 109
 designs, 109–11
 desolvation, 111
 operation, mode of, 108–9
 Scott/Double Pass, 109, 345
stark effect, 34, 42
stray light, 45, 80
- tandem source, 17, 18, 153, 264, 272
technology transfer, 1, 6–8
temperature, 29, 30, 34–5, 35–42, 47–8, 69, 230, 235, 310, 315
 electron, 46, 41–2, 227
 excitation, 38–41
 gas, 137, 45, 92
 ionisation, 30, 34, 135, 136
 kinetic, 32, 34, 35–6, 71, 142, 235
 line pair method, 40–41, 44
 LTE, 34, 61, 229
 measurements, 35–42, 230
 rotational, 34, 36–8, 236
thallium, 233, 304, 351, 352, 354
thermal conductivity, 27, 228, 231, 235, 245
thermal pinch, 233
Thomson scattering, 45–6
thorium, 351
time of flight ms, 21, 146–9, 165, 259–61, 353
TIMS, 164–9, 172, 205, 198, 202, 303, 312, 408
tin, 195, 271–3, 357
torch, 73, 74, 76–9, 134
 demountable, 77, 78
 dimensions, 76, 78
 fassel, 76, 77, 232, 236
 greenfield, 76, 232
 low-gas-flow, 78
 micro-torch, 78
 water-cooled, 79
transition metals, 114, 237, 284
transition probability, 37, 39–42
- uncertainty, 170–78, 183–4, 186, 280, 393
uranium, 198, 205, 213, 311
- vacuum (pumps), 138, 140, 151
vapour generation, 65, 113, 114, 344, 355, 404
vapour loading, 99
viewing height, 70, 88, 99
- wavelength correction, 69
wavelength scanning, 81
- x-ray spectrometry, 277
 fluorescence (XRF), 277, 305
 proton-induced x-ray fluorescence (PIXE), 305
xenon, 227, 236, 241, 201, 202, 226, 235
- zinc, 215, 351, 408
zone of silence, 137–8

5ª edición

Química Orgánica



PEARSON
Prentice
Hall

L. C. Wade, Jr.

ÍNDICE DE CONTENIDOS

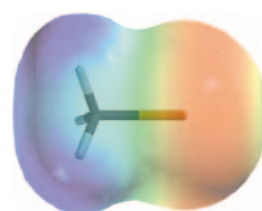
Prefacio xxii

Sobre el autor xxxvii

Capítulo 1

Introducción y revisión 1

- 1.1 Los orígenes de la química orgánica 1
- 1.2 Principios de la estructura atómica 3
- 1.3 La formación del enlace: la regla del octeto 6
- 1.4 Estructuras de Lewis 7
- 1.5 Enlace múltiple 8
 - Resumen: Modelos de enlace más frecuentes (sin carga) 9
- 1.6 La electronegatividad y la polaridad de enlace 9
- 1.7 Cargas formales 11
- 1.8 Estructuras iónicas 12
 - Resumen: Modelos de enlace más frecuentes en los compuestos e iones orgánicos 13
- 1.9 Resonancia 13
- 1.10 Fórmulas estructurales 17
- 1.11 Fórmulas moleculares y fórmulas empíricas 20
- 1.12 Ácidos y bases de Arrhenius 21
- 1.13 Ácidos y bases de Brønsted-Lowry 22
- 1.14 Ácidos y bases de Lewis 29
 - Glosario del Capítulo 1 32
 - Problemas 34

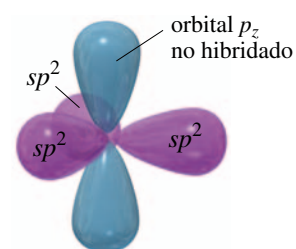


mapa del potencial electrostático del clorometano

Capítulo 2

Estructura y propiedades de las moléculas orgánicas 38

- 2.1 Propiedades ondulatorias de los electrones en los orbitales 38
- 2.2 Orbitales moleculares 40
- 2.3 Enlaces pi 43
- 2.4 Hibridación y geometría molecular 44
- 2.5 Representación de moléculas tridimensionales 47
- 2.6 Reglas generales de la hibridación y de la geometría 48
- 2.7 Rotación de enlaces 53
- 2.8 Isomería 54
- 2.9 Polaridad de enlaces y moléculas 57
- 2.10 Atracciones y repulsiones intermoleculares 60
- 2.11 Efecto de la polaridad en la solubilidad 64
- 2.12 Hidrocarburos 67
- 2.13 Compuestos orgánicos oxigenados 70
- 2.14 Compuestos orgánicos nitrogenados 72
 - Glosario del Capítulo 2 74
 - Problemas 76



átomo de carbono con hibridación sp^2 (vista lateral)

Capítulo 3

Estructura y estereoquímica de los alcanos 80

- 3.1 Clasificación de los hidrocarburos (revisión) 80
- 3.2 Fórmulas moleculares de los alcanos 81
- 3.3 Nomenclatura de los alcanos 82
Resumen: Reglas para la nomenclatura de los alcanos 87
- 3.4 Propiedades físicas de los alcanos 88
- 3.5 Aplicaciones y fuentes de los alcanos 90
- 3.6 Reacciones de los alcanos 92
- 3.7 Estructura y conformaciones de los alcanos 93
- 3.8 Conformaciones del butano 97
- 3.9 Conformaciones de los alcanos de cadena larga 99
- 3.10 Cicloalcanos 100
- 3.11 Isomería *cis-trans* en cicloalcanos 102
- 3.12 Estabilidad de los cicloalcanos: tensión de anillo 102
- 3.13 Conformaciones del ciclohexano 106
Estrategias para resolver problemas: Representación de las conformaciones de silla 109
- 3.14 Conformaciones de ciclohexanos monosustituídos 110
- 3.15 Conformaciones de ciclohexanos disustituídos 113
*Estrategias para resolver problemas: Reconocimiento de isómeros *cis* y *trans* 115*
- 3.16 Moléculas bicíclicas 117
Glosario del Capítulo 3 118
Problemas 122



Capítulo 4

El estudio de las reacciones químicas 124

- 4.1 Introducción 124
- 4.2 Cloración del metano 124
- 4.3 Reacción radicalaria en cadena 125
MECANISMO CLAVE: Halogenación radicalaria 127
- 4.4 Constantes de equilibrio y energía libre 129
- 4.5 Entalpía y entropía 131
- 4.6 Energías de disociación de enlace 133
- 4.7 Variación de entalpía en la reacción de cloración 135
- 4.8 Cinética y ecuación de velocidad 136
- 4.9 Energía de activación e influencia de la temperatura en la velocidad de reacción 138
- 4.10 Estados de transición 140
- 4.11 Velocidades en reacciones de varias etapas 141
- 4.12 Influencia de la temperatura en la reacción de halogenación 142
- 4.13 Halogenación de alcanos superiores 143
- 4.14 El postulado de Hammond 149
Estrategias para resolver problemas: Propuesta de un mecanismo de reacción 151
- 4.15 Inhibidores radicalarios 153
- 4.16 Intermedios reactivos 154
Resumen: Intermedios reactivos 160
Glosario del Capítulo 4 160
Problemas 163

Capítulo 5

Estereoquímica 167

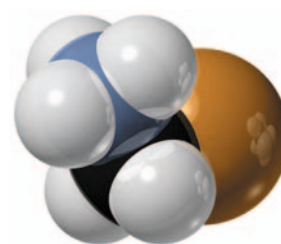
- 5.1 Introducción 167
- 5.2 Quiralidad 168
- 5.3 Nomenclatura (*R*) y (*S*) de átomos de carbono asimétricos 174
- 5.4 Actividad óptica 178
- 5.5 Discriminación biológica de los enantiómeros 183
- 5.6 Mezclas racémicas 184
- 5.7 Exceso enantiomérico y pureza óptica 186
- 5.8 Quiralidad de sistemas conformacionalmente móviles 187
- 5.9 Compuestos quirales sin átomos asimétricos 189
- 5.10 Proyecciones de Fischer 191
 - Resumen: Las proyecciones de Fischer y su uso 195
- 5.11 Diastereómeros o diastereoisómeros 195
 - Resumen: Tipos de isómeros 197
- 5.12 Estereoquímica de las moléculas con dos o más carbonos asimétricos 198
- 5.13 Compuestos *meso* 199
- 5.14 Configuración absoluta y relativa 201
- 5.15 Propiedades físicas de los diastereómeros 202
- 5.16 Resolución de enantiómeros 204
 - Glosario del Capítulo 5 207
 - Problemas 209



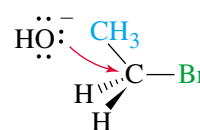
Capítulo 6

Haluros de alquilo: sustitución nucleofílica y eliminación 212

- 6.1 Introducción 212
- 6.2 Nomenclatura de haluros de alquilo 213
- 6.3 Aplicaciones y usos de los haluros de alquilo 215
- 6.4 Estructura de los haluros de alquilo 217
- 6.5 Propiedades físicas de los haluros de alquilo 218
- 6.6 Preparación de los haluros de alquilo 220
 - Resumen: Métodos de preparación de los haluros de alquilo 222
- 6.7 Reacciones de los haluros de alquilo: sustitución y eliminación 224
- 6.8 Sustitución nucleofílica bimolecular: la reacción S_N2 225
 - MECANISMO CLAVE: La reacción S_N2 225**
- 6.9 Generalidades sobre la reacción S_N2 227
 - Resumen: Reacciones S_N2 de haluros de alquilo 227
- 6.10 Factores que condicionan las reacciones S_N2 : fuerza de los nucleófilos 228
 - Resumen: Tendencias en la nucleofilia 230
- 6.11 Reactividad del sustrato en las reacciones S_N2 233
- 6.12 Estereoquímica de la reacción S_N2 236
- 6.13 Sustitución nucleofílica unimolecular: la reacción S_N1 238
 - MECANISMO CLAVE: La reacción S_N1 239**
- 6.14 Estereoquímica de la reacción S_N1 242
- 6.15 Reordenamientos en las reacciones S_N1 243
- 6.16 Comparación de las reacciones S_N1 y S_N2 246
 - Resumen: Sustituciones nucleofílicas 247



bromuro de etilo (1°)
el ataque es fácil



- 6.17 Eliminación unimolecular: la reacción E1 248
MECANISMO CLAVE: La reacción E1 248
Resumen: Reacciones mediadas por carbocationes 251
- 6.18 Eliminación bimolecular: la reacción E2 252
MECANISMO CLAVE: La reacción E2 252
- 6.19 Orientación en las reacciones de eliminación: la regla de Saytzeff 253
- 6.20 Estereoquímica de la reacción E2 255
- 6.21 Comparación de los mecanismos de eliminación E1 y E2 257
Resumen: Reacciones de eliminación 258
Estrategias para resolver problemas: Predicción de los productos resultantes de las sustituciones y eliminaciones 259
Resumen: Reacciones de los haluros de alquilo 261
Glosario del Capítulo 6 264
Problemas 267

Capítulo 7

Estructura y síntesis de alquenos 272

- 7.1 Introducción 272
- 7.2 Descripción de los orbitales del doble enlace en los alquenos 272
- 7.3 Elementos de insaturación 274
- 7.4 Nomenclatura de los alquenos 276
- 7.5 Nomenclatura de los isómeros *cis-trans* 278
Resumen: Reglas para nombrar los alquenos 280
- 7.6 Importancia comercial de los alquenos 281
- 7.7 Estabilidad de los alquenos 283
- 7.8 Propiedades físicas de los alquenos 289
- 7.9 Síntesis de alquenos mediante eliminación de haluros de alquilo 291
- 7.10 Síntesis de alquenos mediante deshidratación de alcoholes 300
MECANISMO CLAVE: Deshidratación de un alcohol catalizada por ácidos 300
- 7.11 Métodos industriales de síntesis de alquenos a alta temperatura 301
Estrategias para resolver problemas: Propuesta de mecanismos de reacción 303
Resumen: Métodos de síntesis de alquenos 306
Glosario del Capítulo 7 308
Problemas 310



Capítulo 8

Reacción de alquenos 314

- 8.1 Reactividad del doble enlace carbono-carbono 314
- 8.2 Adición electrofílica a alquenos 315
MECANISMO CLAVE: Adición electrofílica a alquenos 315
- 8.3 Adición de haluros de hidrógeno a alquenos 317
- 8.4 Adición de agua: hidratación de alquenos 322
- 8.5 Hidratación mediante oximercuriación-desmercuriación 324
- 8.6 Alcoximercuriación-desmercuriación 326
- 8.7 Hidroboración de alquenos 328
- 8.8 Hidrogenación catalítica de alquenos 333
- 8.9 Adición de carbenos a alquenos 336
- 8.10 Adición de halógenos a alquenos 338
- 8.11 Formación de halohidrinas 341
- 8.12 Epoxidación de alquenos 344
- 8.13 Apertura de epóxidos catalizada por ácidos 345
- 8.14 Hidroxilación de alquenos en *sin* 347
- 8.15 Ruptura oxidativa de alquenos 349

- 8.16 Polimerización de alquenos 352
[Estrategias para resolver problemas: Síntesis orgánica](#) 357
Resumen: Reacciones de alquenos 359
Glosario del Capítulo 8 363
Problemas 365

Capítulo 9

Alquinos 370

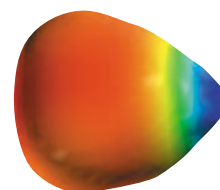
- 9.1 Introducción 370
9.2 Nomenclatura de alquinos 371
9.3 Propiedades físicas de los alquinos 372
9.4 Importancia comercial de los alquinos 372
9.5 Estructura electrónica de los alquinos 374
9.6 Acidez de los alquinos 375
9.7 Síntesis de alquinos a partir de acetiluros 378
9.8 Síntesis de alquinos mediante reacciones de eliminación 382
Resumen: Síntesis de alquinos 384
9.9 Reacciones de adición a alquinos 385
9.10 Reacciones de oxidación de alquinos 394
[Estrategias para resolver problemas: Síntesis en varias etapas](#) 396
Resumen: Reacciones de alquinos 397
Glosario del Capítulo 9 400
Problemas 401



Capítulo 10

Estructura y síntesis de alcoholes 405

- 10.1 Introducción 405
10.2 Estructura y clasificación de los alcoholes 405
10.3 Nomenclatura de los alcoholes y fenoles 407
10.4 Propiedades físicas de los alcoholes 411
10.5 Importancia comercial de los alcoholes 413
10.6 Acidez de los alcoholes y fenoles 415
10.7 Síntesis de alcoholes: introducción y revisión 418
Resumen: Síntesis previas de alcoholes 418
10.8 Reactivos organometálicos utilizados para la síntesis de alcoholes 420
10.9 Adición de reactivos organometálicos a compuestos carbonílicos 422
[MECANISMO CLAVE: Reacciones de Grignard](#) 423
Resumen: Reacciones de Grignard 429
10.10 Reacciones secundarias de compuestos organometálicos: reducción de haluros de alquilo 430
10.11 Reducción del grupo carbonilo: síntesis de alcoholes primarios y secundarios 432
Resumen: Reacciones de LiAlH_4 y NaBH_4 434
Resumen: Síntesis de alcoholes 435
10.12 Tioles (mercaptanos) 437
Glosario del Capítulo 10 440
Problemas 441



mapa de potencial
electrostático del metililitio

Capítulo 11

Reacciones de alcoholes 445

- 11.1 Estados de oxidación de los alcoholes y de los grupos funcionales relacionados 445
11.2 Oxidación de alcoholes 447
11.3 Métodos adicionales de oxidación de alcoholes 450

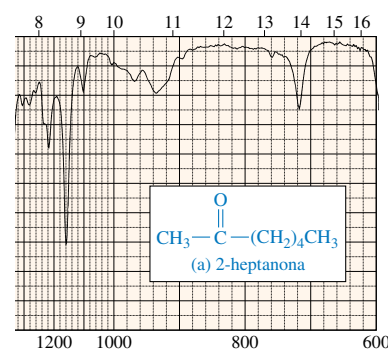
- 11.4 Oxidación biológica de alcoholes 452
- 11.5 Los alcoholes como nucleófilos y electrófilos: formación de tosilatos 454
Resumen: Reacciones S_N2 de tosilatos 456
- 11.6 Reducción de alcoholes 457
- 11.7 Reacciones de alcoholes con haluros de hidrógeno 457
- 11.8 Reacciones de alcoholes con haluros de fósforo 461
- 11.9 Reacciones de alcoholes con cloruro de tionilo 463
- 11.10 Reacciones de deshidratación de alcoholes 464
Estrategias para resolver problemas: Propuesta de mecanismos de reacción 468
- 11.11 Reacciones características de los dioles 472
- 11.12 Esterificación de alcoholes 474
- 11.13 Ésteres de ácidos inorgánicos 475
- 11.14 Reacciones de los alcóxidos 477
MECANISMO CLAVE: Síntesis de Williamson de éteres 478
Estrategias para resolver problemas: Síntesis en varias etapas 479
Resumen: Reacciones de alcoholes 482
Glosario del Capítulo 11 485
Problemas 486



Capítulo 12

Espectroscopía de infrarrojo y espectrometría de masas 490

- 12.1 Introducción 490
- 12.2 El espectro electromagnético 491
- 12.3 La región del infrarrojo 492
- 12.4 Vibraciones moleculares 493
- 12.5 Vibraciones activas e inactivas en el IR 495
- 12.6 Registro del espectro infrarrojo 496
- 12.7 Espectroscopía infrarroja de los hidrocarburos 499
- 12.8 Absorciones características de los alcoholes y las aminas 504
- 12.9 Absorciones características de los compuestos carbonílicos 505
- 12.10 Absorciones características de los enlaces C—N 511
- 12.11 Breve resumen de las frecuencias de tensión en el IR 513
- 12.12 Análisis e interpretación de los espectros de IR (problemas resueltos) 514
- 12.13 Introducción a la espectrometría de masas 519
- 12.14 Determinación de la fórmula molecular mediante espectrometría de masas 522
- 12.15 Modelos de fragmentación en la espectrometría de masas 526
Resumen: Modelos comunes de fragmentación de masas 530
Glosario del Capítulo 12 531
Problemas 533

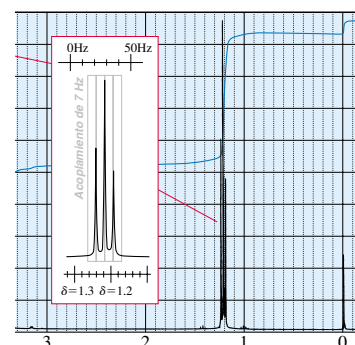


Capítulo 13

Espectroscopía de resonancia magnética nuclear 539

- 13.1 Introducción 539
- 13.2 Teoría de la resonancia magnética nuclear 539
- 13.3 Apantallamiento magnético por parte de los electrones 542
- 13.4 El espectrómetro de RMN 544
- 13.5 El desplazamiento químico 545
- 13.6 El número de señales 552
- 13.7 El área de los picos 553
- 13.8 Desdoblamiento espín-espín 556
Estrategias para resolver problemas: Representación de un espectro de RMN 561

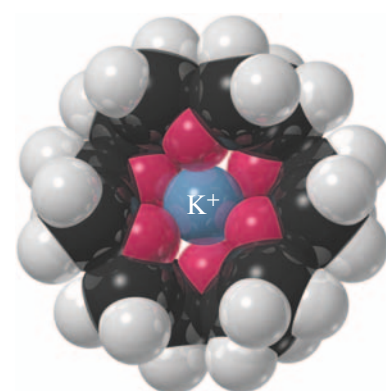
- 13.9 Acoplamientos complejos 565
- 13.10 Protones no equivalentes según la esteoquímica 568
- 13.11 Dependencia de la variable tiempo en la espectroscopía de RMN 571
Estrategias para resolver problemas: Interpretación de un espectro de RMN de protón 574
- 13.12 Espectroscopía de RMN de carbono-13 579
- 13.13 Interpretación de un espectro de RMN de carbono 584
- 13.14 Imágenes mediante resonancia magnética nuclear 587
Estrategias para resolver problemas: Problemas de espectroscopía 588
- Glosario del Capítulo 13 592
- Problemas 593



Capítulo 14

Éteres, epóxidos y sulfuros 600

- 14.1 Introducción 600
- 14.2 Propiedades físicas de los éteres 600
- 14.3 Nomenclatura de los éteres 605
- 14.4 Espectroscopía de los éteres 608
- 14.5 La síntesis de Williamson de éteres 610
- 14.6 Síntesis de éteres mediante alcoximercuriación-desmercuriación 612
- 14.7 Síntesis industrial: deshidratación bimolecular de alcoholes 612
Resumen: Síntesis de éteres 613
- 14.8 Ruptura de éteres con HBr y HI 613
- 14.9 Autooxidación de éteres 615
Resumen: Reacciones de éteres 616
- 14.10 Sulfuros (tioéteres) 616
- 14.11 Síntesis de epóxidos 619
Resumen: Síntesis de epóxidos 622
- 14.12 Apertura de epóxidos catalizada por ácidos 622
- 14.13 Apertura de epóxidos catalizada por bases 625
- 14.14 Orientación en la apertura de epóxidos 627
- 14.15 Reacciones de epóxidos con reactivos de Grignard y compuestos organolíticos 629
- 14.16 Resinas epoxi: el advenimiento de los pegamentos modernos 629
Resumen: Reacciones de epóxidos 631
- Glosario del Capítulo 14 632
- Problemas 634



éter 18-corona-6
solvatando el K^+

Capítulo 15

Sistemas conjugados, simetría orbital y espectroscopía ultravioleta 638

- 15.1 Introducción 638
- 15.2 Estabilidad de los dienos 638
- 15.3 Los sistemas conjugados según la teoría de orbitales moleculares 640
- 15.4 Los cationes alílicos 644
- 15.5 Adición 1,2 y 1,4 a dienos conjugados 645
- 15.6 Control cinético frente a control termodinámico en la adición de HBr a 1,3-butadieno 647
- 15.7 Radicales alílicos 649
- 15.8 Los orbitales moleculares del sistema alílico 651
- 15.9 Configuraciones electrónicas del radical, del catión y del anión alilo 652
- 15.10 Reacciones de sustitución S_N2 de haluros de alilo y de tosilatos 654
- 15.11 La reacción de Diels-Alder 655



MECANISMO CLAVE: La reacción de Diels-Alder 656

- 15.12 La reacción de Diels-Alder como ejemplo de una reacción pericíclica 663
- 15.13 Espectroscopía de absorción ultravioleta 666
- Glosario del Capítulo 15 672
- Problemas 675

Capítulo 16

Compuestos aromáticos 679

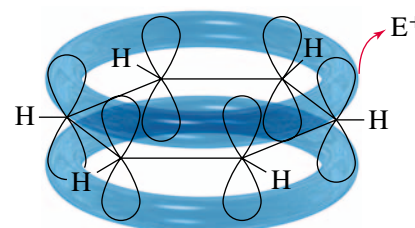
- 16.1 Introducción: el descubrimiento del benceno 679
- 16.2 Estructura y propiedades del benceno 679
- 16.3 Los orbitales moleculares del benceno 684
- 16.4 El ciclobutadieno según la teoría de orbitales moleculares 686
- 16.5 Compuestos aromáticos, antiaromáticos y no aromáticos 688
- 16.6 La regla de Hückel 689
- 16.7 Derivación de la regla de Hückel de la teoría de orbitales moleculares 691
- 16.8 Iones aromáticos 692
- 16.9 Compuestos aromáticos heterocíclicos 697
- 16.10 Hidrocarburos aromáticos polinucleares 702
- 16.11 Alótropos aromáticos del carbono 704
- 16.12 Compuestos heterocíclicos fusionados 706
- 16.13 Nomenclatura de los derivados del benceno 707
- 16.14 Propiedades físicas del benceno y de sus derivados 709
- 16.15 Espectroscopía de los compuestos aromáticos 710
- Glosario del Capítulo 16 713
- Problemas 715



Capítulo 17

Reacciones de compuestos aromáticos 722

- 17.1 Sustitución electrofílica aromática 722
- MECANISMO CLAVE: Sustitución electrofílica aromática 723**
- 17.2 Halogenación del benceno 723
- 17.3 Nitración del benceno 726
- 17.4 Sulfonación del benceno 726
- 17.5 Nitración del tolueno: efecto de la sustitución con grupos alquilo 728
- 17.6 Sustituyentes activadores *orto* y *para*-orientadores 730
- Resumen: Activadores *orto* y *para*-orientadores 733
- 17.7 Sustituyentes desactivadores *meta*-orientadores 734
- Resumen: Desactivadores *meta*-orientadores 737
- 17.8 Sustituyentes halogenados: desactivadores, pero *orto*, *para*-orientadores 737
- Resumen: Efectos orientadores de los sustituyentes 739
- 17.9 Efecto de múltiples sustituyentes sobre la sustitución electrofílica aromática 739
- 17.10 Alquilación de Friedel-Crafts 742
- 17.11 Acilación de Friedel-Crafts 746
- Resumen: Comparación de la alquilación y acilación de Friedel-Crafts 748
- 17.12 Sustitución nucleofílica aromática 750
- 17.13 Reacciones de adición de los derivados del benceno 754
- 17.14 Reacciones de las cadenas laterales de los derivados del benceno 757
- 17.15 Reacciones de los fenoles 761
- Resumen: Reacciones de los compuestos aromáticos 764
- Glosario del Capítulo 17 767
- Problemas 769



Capítulo 18

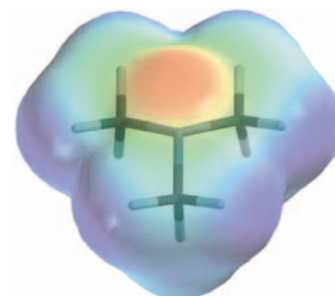
Cetonas y aldehídos 774

- 18.1 Compuestos carbonílicos 774
- 18.2 Estructura del grupo carbonilo 775
- 18.3 Nomenclatura de cetonas y aldehídos 775
- 18.4 Propiedades físicas de cetonas y aldehídos 778
- 18.5 Espectroscopía de cetonas y aldehídos 780
- 18.6 Importancia industrial de cetonas y aldehídos 787
- 18.7 Revisión de la síntesis de cetonas y aldehídos 787
- 18.8 Síntesis de cetonas y aldehídos a partir de 1,3-ditianos 791
- 18.9 Síntesis de cetonas a partir de ácidos carboxílicos 792
- 18.10 Síntesis de cetonas a partir de nitrilos 793
- 18.11 Síntesis de aldehídos y cetonas a partir de cloruros de ácido 793
Resumen: Síntesis de cetonas y aldehídos 795
- 18.12 Reacciones de cetonas y aldehídos: adición nucleofílica 797
MECANISMO CLAVE: Adiciones nucleofílicas a grupos carbonilo 800
- 18.13 La reacción de Wittig 800
- 18.14 Hidratación de cetonas y aldehídos 804
- 18.15 Formación de cianohidrinas 806
- 18.16 Formación de iminas 807
MECANISMO CLAVE: Formación de iminas 808
- 18.17 Condensaciones con hidroxilamina e hidrazinas 810
Resumen: Condensación de aminas con cetonas y aldehídos 811
- 18.18 Formación de acetales 811
MECANISMO CLAVE: Formación de acetales 812
Estrategias para resolver problemas: Propuesta de mecanismos de reacción 815
- 18.19 El uso de acetales como grupos protectores 817
- 18.20 Oxidación de aldehídos 818
- 18.21 Otras reducciones de cetonas y aldehídos 819
Resumen: Reacciones de cetonas y aldehídos 821
Glosario del Capítulo 18 824
Problemas 827

Capítulo 19

Aminas 836

- 19.1 Introducción 836
- 19.2 Nomenclatura de las aminas 837
- 19.3 Estructura de las aminas 839
- 19.4 Propiedades físicas de las aminas 841
- 19.5 Basicidad de las aminas 842
- 19.6 Efectos sobre la basicidad de las aminas 844
- 19.7 Sales de amonio 846
- 19.8 Sales de amonio y catalizadores de transferencia de fase 848
- 19.9 Espectroscopía de las aminas 849
- 19.10 Reacciones de las aminas con cetonas y aldehídos (revisión) 854
- 19.11 Sustitución aromática en arilaminas y piridina (revisión) 854
- 19.12 Alquilación de aminas con haluros de alquilo 858
- 19.13 Acilación de aminas con cloruros de ácido 859
- 19.14 Formación de sulfonamidas 861
- 19.15 Aminas como grupos salientes: la eliminación de Hofmann 862
- 19.16 Oxidación de aminas. La eliminación de Cope 865



mapa de potencial electrostático de la trimetilamina

- 19.17 Reacciones de aminas con ácido nitroso 868
- 19.18 Reacciones de las sales de diazonio aromáticas 870
- Resumen: Reacciones de las aminas 874
- 19.19 Síntesis de aminas 877
- Resumen: Síntesis de aminas 887
- Glosario del Capítulo 19 890
- Problemas 892

Capítulo 20

Ácidos carboxílicos 900

- 20.1 Introducción 900
- 20.2 Nomenclatura de los ácidos carboxílicos 900
- 20.3 Estructura y propiedades físicas de los ácidos carboxílicos 904
- 20.4 Acidez de los ácidos carboxílicos 906
- 20.5 Sales de ácidos carboxílicos 909
- 20.6 Fuentes comerciales de los ácidos carboxílicos 912
- 20.7 Espectroscopía de los ácidos carboxílicos 913
- 20.8 Síntesis de los ácidos carboxílicos 918
- Resumen: Síntesis de los ácidos carboxílicos 920
- 20.9 Reacciones de los ácidos carboxílicos y sus derivados. Sustitución nucleofílica en el grupo acilo 921
- 20.10 Condensación de los ácidos con los alcoholes: la esterificación de Fischer 922
- MECANISMO CLAVE: Esterificación de Fischer 923**
- 20.11 Síntesis y aplicaciones de los cloruros de ácido 925
- 20.12 Esterificación con diazometano 928
- 20.13 Condensación de ácidos con aminas: síntesis directa de amidas 928
- 20.14 Reducción de los ácidos carboxílicos 929
- 20.15 Alquilación de los ácidos carboxílicos para obtener cetonas 931
- Resumen: Reacciones de los ácidos carboxílicos 931
- Glosario del Capítulo 20 933
- Problemas 934

Capítulo 21

Derivados de los ácidos carboxílicos 940

- 21.1 Introducción 940
- 21.2 Estructura y nomenclatura de los derivados de ácido 941
- 21.3 Propiedades físicas de los derivados de ácidos carboxílicos 947
- 21.4 Espectroscopía de los derivados de ácidos carboxílicos 950
- 21.5 Interconversión entre los derivados de ácidos mediante sustitución nucleofílica en el grupo acilo 957
- MECANISMO CLAVE: Mecanismo de adición-eliminación en la sustitución nucleofílica en el grupo acilo 957**
- 21.6 Sustitución nucleofílica en el grupo acilo catalizada por ácidos 964
- Estrategias para resolver problemas: Propuestas de mecanismos de reacción 965**
- 21.7 Hidrólisis de los derivados de ácidos carboxílicos 968
- 21.8 Reducción de los derivados de ácidos 972
- 21.9 Reacciones de los derivados de ácidos con reactivos organometálicos 975
- 21.10 Resumen de la química de los cloruros de ácido 976
- 21.11 Resumen de la química de los anhídridos de ácido 978
- 21.12 Resumen de la química de los ésteres 981
- 21.13 Resumen de la química de las amidas 984
- 21.14 Resumen de la química de los nitrilos 987
- 21.15 Tioésteres 988

- 21.16 Ésteres y amidas del ácido carbónico 990
- Glosario del Capítulo 21 992
- Problemas 994

Capítulo 22

Sustituciones en alfa, y condensaciones de enoles y de iones enolato 1003

- 22.1 Introducción 1003
- 22.2 Enoles e iones enolato 1004
- 22.3 Halogenación en alfa de cetonas 1007
- 22.4 Bromación en alfa de ácidos: la reacción de HVZ (Hell-Volhard-Zelinsky) 1012
- 22.5 Alquilación de iones enolato 1013
- 22.6 Formación y alquilación de enaminas 1015
- 22.7 Condensación aldólica de cetonas y aldehídos 1017
- MECANISMO CLAVE: Condensación aldólica catalizada por una base 1018**
- 22.8 Deshidratación de aldoles 1020
- MECANISMO CLAVE: Deshidratación de un aldol 1021**
- 22.9 Condensaciones aldólicas cruzadas 1021
- Estrategias para resolver problemas: Propuesta de mecanismos de reacción 1022**
- 22.10 Ciclaciones aldólicas 1025
- 22.11 Diseño de síntesis utilizando condensaciones aldólicas 1026
- 22.12 La condensación de Claisen de ésteres 1027
- MECANISMO CLAVE: Condensación de Claisen 1028**
- 22.13 La condensación de Dieckmann: un tipo de ciclación de Claisen 1031
- 22.14 Condensaciones de Claisen cruzadas 1031
- 22.15 Síntesis empleando compuestos β -dicarbonílicos 1034
- 22.16 La síntesis malónica 1036
- 22.17 La síntesis acetilacética 1039
- 22.18 Adiciones conjugadas: la reacción de Michael 1042
- MECANISMO CLAVE: Adiciones 1,2 y 1,4 1043**
- 22.19 La anillación de Robinson 1046
- Estrategias para resolver problemas: Propuesta de mecanismos de reacción 1047**
- Resumen: Adiciones y condensaciones de enolatos 1049
- Glosario del Capítulo 22 1051
- Problemas 1052



Capítulo 23

Carbohidratos y ácidos nucleicos 1057

- 23.1 Introducción 1057
- 23.2 Clasificación de los hidratos de carbono 1058
- 23.3 Monosacáridos 1059
- 23.4 Diastereómeros *eritro* y *treo* 1062
- 23.5 Epímeros 1063
- 23.6 Estructura cíclica de los monosacáridos 1064
- 23.7 Anómeros de los monosacáridos. Mutarrotación 1068
- 23.8 Reacciones de los monosacáridos: reacciones secundarias en medio básico 1070
- 23.9 Reducción de los monosacáridos 1072
- 23.10 Oxidación de los monosacáridos. Los azúcares reductores 1073
- 23.11 Los azúcares no reductores: formación de glicósidos 1075
- 23.12 Formación de éteres y ésteres 1078
- 23.13 Reacciones con fenilhidrazina: formación de osazonas 1080
- 23.14 Acortamiento de la cadena: degradación de Ruff 1081

- 23.15 Alargamiento de la cadena: síntesis de Kiliani-Fischer 1081
Resumen: Reacciones de los azúcares 1083
- 23.16 La prueba de Fischer de la configuración de la glucosa 1085
- 23.17 Determinación del tamaño del anillo. Escisión de azúcares con ácido peryódico 1088
- 23.18 Disacáridos 1090
- 23.19 Polisacáridos 1095
- 23.20 Ácidos nucleicos: introducción 1098
- 23.21 Ribonucleósidos y ribonucleótidos 1100
- 23.22 La estructura del ácido ribonucleico 1102
- 23.23 La desoxirribosa y la estructura del ácido desoxirribonucleico 1102
- 23.24 Funciones adicionales de los nucleótidos 1106
Glosario del Capítulo 23 1108
Problemas 1111

Capítulo 24

Aminoácidos, péptidos y proteínas 1114

- 24.1 Introducción 1114
- 24.2 Estructura y estereoquímica de los α -aminoácidos 1115
- 24.3 Propiedades ácido-base de los aminoácidos 1119
- 24.4 Puntos isoeléctricos y electroforesis 1121
- 24.5 Síntesis de aminoácidos 1123
Resumen: Síntesis de aminoácidos 1127
- 24.6 Resolución de los aminoácidos 1128
- 24.7 Reacciones de los aminoácidos 1129
Resumen: Reacciones de aminoácidos 1131
- 24.8 Estructura y nomenclatura de péptidos y proteínas 1132
- 24.9 Determinación de la estructura de los péptidos 1136
- 24.10 Síntesis de péptidos en solución 1142
- 24.11 Síntesis de péptidos en fase sólida 1145
- 24.12 Clasificación de las proteínas 1151
- 24.13 Niveles de la estructura de las proteínas 1151
- 24.14 Desnaturalización de las proteínas 1154
Glosario del Capítulo 24 1156
Problemas 1158

Capítulo 25

Lípidos 1162

- 25.1 Introducción 1162
- 25.2 Ceras 1162
- 25.3 Triglicéridos 1163
- 25.4 Saponificación de grasas y aceites. Jabones y detergentes 1166
- 25.5 Fosfolípidos 1170
- 25.6 Esteroides 1171
- 25.7 Prostaglandinas 1174
- 25.8 Terpenos 1175
Glosario del Capítulo 25 1179
Problemas 1180



Capítulo 26

Polímeros sintéticos 1182

- 26.1 Introducción 1182
- 26.2 Polímeros de adición 1183
- 26.3 Estereoquímica de los polímeros 1189
- 26.4 Control estereoquímico de la polimerización. Catalizadores de Ziegler-Natta 1190
- 26.5 Gomas naturales y sintéticas 1190
- 26.6 Copolímeros de dos o más monómeros 1192
- 26.7 Condensación de polímeros 1192
- 26.8 Estructura y propiedades de los polímeros 1196
- Glosario del Capítulo 26 1198
- Problemas 1200

Apéndices

- 1A Posiciones de absorción de protones en RMN, en varios entornos estructurales 1204
- 1B Constantes de acoplamiento espín-espín 1205
- 1C Desplazamientos químicos de ^{13}C en los compuestos orgánicos 1205
- 2A Grupos de frecuencias características en el infrarrojo 1206
- 2B Absorciones en el infrarrojo características de los grupos funcionales 1209
- 3 Las reglas de Woodward-Fieser para predecir los espectros del ultravioleta-visible 1211
- 4A Métodos y sugerencias para proponer mecanismos 1215
- 4B Sugerencias para desarrollar síntesis de varios pasos 1218
- 5 Valores de $\text{p}K_{\text{a}}$ de compuestos representativos 1219

Esquemas de Mecanismos y Mecanismos clave

- CAPÍTULO 4 Halogenación vía radicales libres 127
- CAPÍTULO 6 Bromación alílica 221
 - La reacción $\text{S}_{\text{N}}2$ 225
 - Inversión de la configuración en las reacciones $\text{S}_{\text{N}}2$ 237
 - La reacción $\text{S}_{\text{N}}1$ 239
 - Racemización en las reacciones $\text{S}_{\text{N}}1$ 242
 - Transposición de hidruro en las reacciones $\text{S}_{\text{N}}1$ 244
 - Transposición de metilo en la reacción $\text{S}_{\text{N}}1$ 245
 - La reacción $\text{E}1$ 248
 - Reordenamientos en la reacción $\text{E}1$ 250
 - La reacción $\text{E}2$ 252
- CAPÍTULO 7 Deshidrohalogenación a través del mecanismo $\text{E}2$ 291
 - Estereoquímica de la reacción $\text{E}2$ 293
 - Dibromación $\text{E}2$ en la formación de un dibromuro vecinal 297
 - Deshidratación de un alcohol catalizada por un ácido 300
- CAPÍTULO 8 Adición electrofílica a alquenos 315
 - Adición iónica de HBr a un alqueno 316
 - Adición radicalaria de HBr a un alqueno 319
 - Hidratación de un alqueno catalizada por ácidos 323

	Oximercuriación de un alqueno	325
	Hidroboración de un alqueno	329
	Oxidación de un trialquilborano	332
	Adición de halógenos a alquenos	339
	Formación de halohidrinas	341
	Epoxidación de alquenos	344
	Apertura de epóxidos catalizada por ácidos	345
CAPÍTULO 9	Reducción de un alquino con un metal en amoniaco líquido	388
	Tautomería ceto-enólica catalizada por ácidos	392
CAPÍTULO 10	Reacciones de Grignard	423
	Reducción de un grupo carbonilo con hidruros	432
CAPÍTULO 11	Reacción de un alcohol terciario con HBr (S_N1)	458
	Reacción de un alcohol primario con HBr (S_N2)	458
	Reacción de alcoholes con PBr_3	462
	Revisión: Deshidratación de un alcohol catalizada por un ácido	464
	La transposición pinacolínica	472
	La síntesis de Williamson de éteres	478
CAPÍTULO 14	Ruptura de un éter con HBr	614
	Apertura de un epóxido catalizada por ácidos	622
	Apertura de un epóxido catalizada por ácidos en una solución alcohólica	623
	Apertura de un epóxido catalizada por bases	626
CAPÍTULO 15	Adición 1,2 y 1,4 a dienos conjugados	646
	Bromación alílica radicalaria	649
	La reacción de Diels-Alder	656
CAPÍTULO 17	Sustitución electrofílica aromática	723
	Bromación de benceno	723
	Nitración de benceno	726
	Sulfonación de benceno	727
	Alquilación de Friedel-Crafts	743
	Acilación de Friedel-Crafts	747
	Sustitución nucleofílica aromática (adición-eliminación)	751
	Sustitución nucleofílica aromática	753
	La reducción de Birch	756
CAPÍTULO 18	Adiciones nucleofílicas al grupo carbonilo	800
	La reacción de Wittig	802
	Hidratación de cetonas y aldehídos	804
	Formación de cianohidrinas	806
	Formación de iminas	808
	Formación de acetales	812
	Reducción de Wolff-Kishner	821
CAPÍTULO 19	Sustitución electrofílica aromática de la piridina	856
	Sustitución nucleofílica aromática de la piridina	857
	Acilación de una amina con un cloruro de ácido	859
	Eliminación de Hofmann	863
	Eliminación de Cope de un óxido de amina	867
	Diazoación de una amina	868
	Transposición de Hofmann	886
CAPÍTULO 20	Sustitución nucleofílica sobre el grupo acilo de un éster	922
	Esterificación de Fischer	923
	Esterificación con diazometano	928

CAPÍTULO 21	Mecanismo de adición-eliminación en la sustitución nucleofílica en el grupo acilo 957
	Transformación de un cloruro de ácido en un anhídrido 959
	Transformación de un cloruro de ácido en un éster 960
	Transformación de un cloruro de ácido en una amida 960
	Transformación de un anhídrido de ácido en un éster 961
	Transformación de un anhídrido de ácido en una amida 961
	Transformación de un éster en una amida (amonólisis de un éster) 962
	Transesterificación 967
	Saponificación de un éster 968
	Hidrólisis de una amida en medio básico 970
	Hidrólisis de una amida en medio ácido 971
	Hidrólisis catalizada por una base de un nitrilo 972
	Reducción de un éster por un hidruro 973
	Reacción de un éster con dos moles de un reactivo de Grignard 975
CAPÍTULO 22	Sustitución en alfa 1003
	Adición de un enolato a cetonas y aldehídos (condensación) 1003
	Sustitución de un enolato en un éster (condensación) 1004
	Tautomería ceto-enólica catalizada por una base 1004
	Tautomería ceto-enólica catalizada por un ácido 1005
	Halogenación promovida por una base 1008
	Pasos finales de la reacción del haloformo 1009
	Halogenación catalizada por un ácido 1011
	Condensación aldólica catalizada por una base 1018
	Condensación aldólica catalizada por un ácido 1020
	Deshidratación de un aldol 1021
	Condensación de Claisen 1028
	Adiciones 1,2 y 1,4 1043
CAPÍTULO 23	Formación de un hemiacetal cíclico 1064
	Epimerización de la glucosa catalizada por una base 1071
	Reordenamientos enodiol catalizados por una base 1072
CAPÍTULO 26	Polimerización radicalaria 1185
	Polimerización catiónica 1186
	Polimerización aniónica 1188

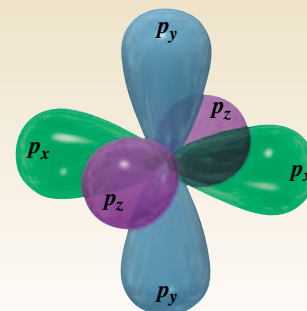
Soluciones de los problemas seleccionados A1

Créditos de las fotografías CF1

Índice I1

CAPÍTULO 1

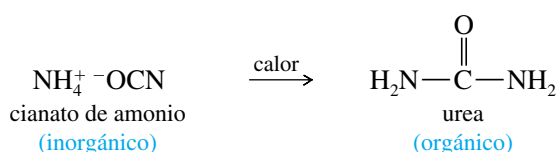
Introducción y revisión



La definición moderna de **química orgánica** es la *química de los compuestos de carbono*. ¿Qué tiene de especial el carbono que hay una rama de la química que se dedica a él? Al contrario que otros elementos, el carbono forma enlaces fuertes con otros átomos de carbono y con una gran variedad de otros elementos. Las cadenas y anillos de átomos de carbono son tan variadas que se puede formar una variedad interminable de moléculas. Esta diversidad de los compuestos de carbono es la base para la vida en la Tierra. Los seres vivos están formados de compuestos orgánicos complejos con funciones estructurales, químicas o genéticas.

El término **orgánico** literalmente significa «derivado de los organismos vivos». Originalmente, la ciencia de la química orgánica era el estudio de los compuestos que se extraían de los organismos vivos o productos naturales. Compuestos tales como azúcar, urea, levadura, ceras y aceites vegetales eran considerados «orgánicos» y se aceptó el **Vitalismo** como teoría que explicaba su origen: la creencia en que los productos naturales necesitaban una «fuerza vital» para ser creados. Por tanto, la química orgánica era el estudio de los compuestos que tenían esa fuerza vital. La química inorgánica era el estudio de los gases, rocas, minerales y de los compuestos que se podían obtener a partir de ellos.

En el siglo XIX, la experimentación demostró que los compuestos orgánicos se podían sintetizar a partir de compuestos inorgánicos. En 1828, el químico alemán Friedrich Wöhler convirtió el cianato de amonio, obtenido a partir de amoníaco y ácido ciánico, en urea simplemente calentando el cianato en ausencia de oxígeno.



La urea también proviene de los seres vivos y se creía que contenía la fuerza vital, a pesar de que el cianato de amonio es inorgánico y por tanto, según aquella creencia, no poseía la fuerza vital. Algunos químicos sostenían que esa fuerza vital provenía de las manos de Wöhler, pero la mayoría reconocieron la posibilidad de sintetizar compuestos orgánicos a partir de compuestos inorgánicos. También se llevaron a cabo otras síntesis, por lo que la teoría de la fuerza vital se descartó.

Desde que el Vitalismo se descartó a comienzos del siglo XIX, se podría pensar que esta idea habría ya desaparecido, pero estaríamos equivocados, ya que el Vitalismo hoy forma parte de la mentalidad de las personas que creen que los productos «naturales» (derivados de las plantas) son diferentes y más saludables que aquellos compuestos exactamente iguales, «artificiales», que han sido sintetizados.

Como químicos, sabemos que los compuestos derivados de las plantas y los compuestos sintetizados son idénticos. La única diferencia es el contenido en ^{14}C : los compuestos sintetizados a partir de derivados del petróleo tienen menor contenido del isótopo radioactivo ^{14}C ,

1.1

Los orígenes de la química orgánica



El corazón artificial Jarvik 7 está compuesto en gran parte de materiales orgánicos sintéticos.

ya que este isótopo ha ido desapareciendo con el tiempo. Los compuestos derivados de las plantas, al haber sido sintetizados recientemente a partir del CO_2 del aire, tienen un contenido más elevado en ^{14}C . Algunos suministradores importantes de productos químicos dan los análisis de los isótopos para confirmar que los «productos naturales» que distribuyen tienen mayor contenido en ^{14}C y son derivados de las plantas. Estos sofisticados análisis dan un aspecto de alta tecnología al Vitalismo del siglo XXI.

A pesar de que los compuestos orgánicos no necesitan una fuerza vital, todavía se diferencian de los compuestos inorgánicos. La característica que distingue a los compuestos orgánicos es que *todos* contienen uno o más átomos de carbono. Pero no todos los compuestos que contienen carbono son orgánicos, sustancias tales como: diamante, grafito, dióxido de carbono, cianato de amonio y carbonato de sodio son compuestos derivados de minerales, y tienen propiedades características de los compuestos inorgánicos. No obstante, la mayoría de los millones de compuestos que contienen carbono se clasifican como orgánicos.

Nosotros mismos estamos compuestos en gran parte por moléculas orgánicas y nos alimentamos de compuestos orgánicos. Las proteínas de nuestra piel, los lípidos de las membranas de nuestras células, el glucógeno de nuestro hígado y el DNA del núcleo de nuestras células son compuestos orgánicos. Nuestros cuerpos también están regulados y son defendidos por compuestos orgánicos complejos.

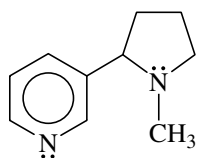
Los químicos han aprendido a diseñar y sintetizar muchas de estas moléculas complejas. Los productos sintéticos se utilizan como productos farmacéuticos, plásticos, pesticidas, pinturas y fibras. La mayoría de los avances más importantes en medicina se debe actualmente a los avances en química orgánica. Así, se sintetizan nuevos productos farmacéuticos para combatir enfermedades y se obtienen nuevos polímeros para elaborar dispositivos ortopédicos con los que sustituir órganos dañados. La química orgánica ha cerrado el ciclo, comenzó con el estudio de los compuestos derivados de «órganos» y ahora nos proporciona los productos farmacéuticos y materiales que necesitamos para salvar o reemplazar esos órganos.

Uno de los efectos de la nicotina es incrementar la concentración de una sustancia química en el sistema de estímulos cerebrales. La liberación de esta sustancia química hace que los fumadores se sientan bien y refuerza la necesidad de fumar.

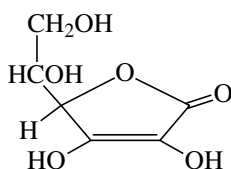
Una de las razones por las que los químicos sintetizan derivados de compuestos orgánicos complejos como la morfina es descubrir nuevas sustancias que mantengan sus propiedades útiles (analgésia) pero no las propiedades indeseables (adicción).



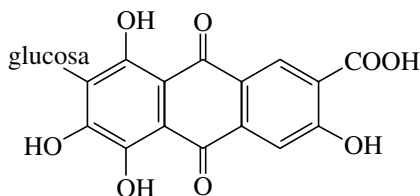
nicotina



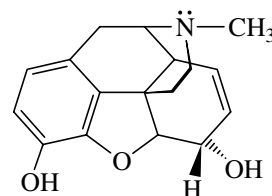
vitamina C



carmín



morfina



A continuación daré cuatro ejemplos de compuestos orgánicos aislados de organismos vivos: el tabaco contiene nicotina, un alcaloide que crea adicción; los escaramujos contienen vitamina C, esencial para prevenir el escorbuto; el carmín proviene de las cochinillas, insectos que suelen estar en las chumberas, y las adormideras contienen morfina, sustancia que mitiga el dolor pero provoca adicción.

Antes de comenzar el estudio de la química orgánica, se han de revisar algunos principios básicos. Muchos de los conceptos de estructura atómica y molecular son cruciales para entender la estructura y el enlace de los compuestos orgánicos.

1.2A Estructura del átomo

Los átomos están formados por protones, neutrones y electrones. Los protones están cargados positivamente y se encuentran, junto con los neutrones (sin carga), en el núcleo. Los electrones contienen una carga negativa de la misma magnitud que la carga positiva de los protones y se encuentran en el espacio que rodea al núcleo (Figura 1.1). Los protones y los neutrones tienen una masa parecida, aproximadamente unas 1800 veces la masa de un electrón. A pesar de que prácticamente toda la masa del átomo está concentrada en el núcleo, son los electrones los que participan en los enlaces químicos y en las reacciones.

Cada elemento se caracteriza por el número de protones que tiene en el núcleo (número atómico). El número de neutrones normalmente es parecido al número de protones, pero este número de neutrones puede variar. Los átomos que tienen el mismo número de protones pero diferente número de neutrones se llaman **isótopos**. Por ejemplo, el átomo de carbono más común es el que tiene seis protones y seis neutrones en el núcleo; su número másico (suma de protones y de neutrones) es 12, por lo que lo escribimos con el símbolo ^{12}C . Aproximadamente el 1% de los átomos de carbono tienen 7 neutrones y su número másico es 13, simbolizado por ^{13}C . Una fracción muy pequeña de átomos de carbono tiene ocho neutrones, por lo que su número másico es 14. El ^{14}C es un isótopo radioactivo, con un periodo de semidesintegración (tiempo que tarda una determinada masa de ese isótopo en desintegrarse y perder la mitad de su masa) de 5 730 años. Este tiempo de desintegración del ^{14}C se utiliza para determinar la edad de los materiales orgánicos de hasta unos 50 000 años de antigüedad.

1.2B Estructura electrónica del átomo

Las propiedades químicas de un elemento se determinan por el número de protones de su núcleo y el correspondiente número de electrones que hay alrededor del núcleo. Los electrones forman enlaces y determinan la estructura de las moléculas resultantes. Debido a que los electrones son muy pequeños y están en movimiento, se comportan simultáneamente como partículas y como ondas.

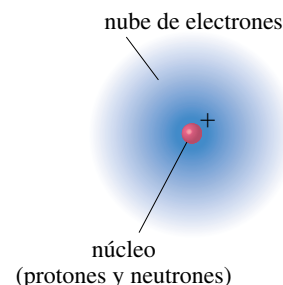
Los electrones que se encuentran moviéndose alrededor del núcleo se encuentran en **orbitales**. El principio de incertidumbre de Heisenberg dice que nunca se puede determinar con exactitud dónde se encuentra el electrón; sin embargo, se puede determinar la **densidad electrónica**, la probabilidad de encontrar al electrón en una determinada zona del orbital. Por tanto, un orbital es un estado de energía permitido para un electrón, con una función de probabilidad asociada que define la distribución de la densidad electrónica en el espacio.

Los orbitales atómicos se agrupan en «capas» o niveles diferentes a distintas distancias del núcleo. Cada capa se identifica por un número cuántico principal n , siendo $n = 1$ para la capa de menor energía (la que está más próxima al núcleo). Al aumentar n , las capas están más alejadas del núcleo, tienen una energía más alta y pueden contener más electrones. La mayoría de los elementos más comunes de los compuestos orgánicos se encuentran en las dos primeras filas (periodos) de la tabla periódica, lo que indica que sus electrones se encuentran en las dos primeras capas de electrones. La primera capa ($n = 1$) puede alojar dos electrones y la segunda capa ($n = 2$) puede alojar ocho.

La primera capa de electrones contiene solamente el orbital $1s$. Todos los orbitales s tienen simetría esférica, lo cual quiere decir que son no direccionales. La densidad electrónica del orbital $1s$ se representa en la Figura 1.2. Se puede observar que la densidad electrónica es más alta en las proximidades del núcleo y va disminuyendo exponencialmente según va aumentando la distancia al núcleo. Se podría comparar el orbital $1s$ con una cápsula de algodón, donde la semilla representaría el núcleo. La densidad del algodón es mayor en los lugares próximos a la semilla y su densidad va disminuyendo según se va alejando del núcleo.

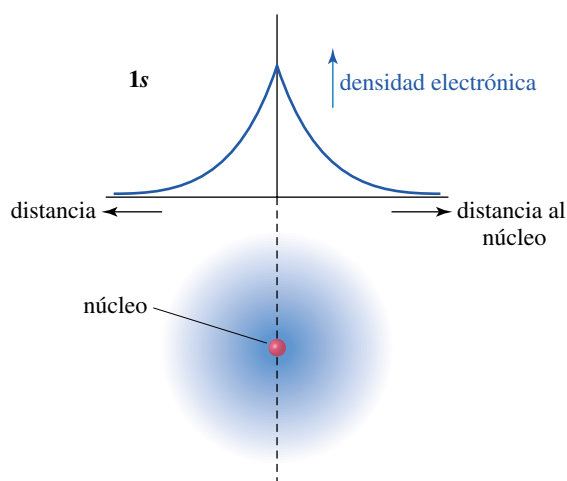
La segunda capa de electrones consta de orbitales $2s$ y $2p$. El orbital $2s$ posee simetría esférica igual que el $1s$, pero su densidad electrónica no es una simple función exponencial. El orbital $2s$ tiene una densidad electrónica más pequeña en las proximidades del

1.2 Principios de la estructura atómica



▲ Figura 1.1

El átomo tiene un denso núcleo, cargado positivamente, rodeado de una nube de electrones.

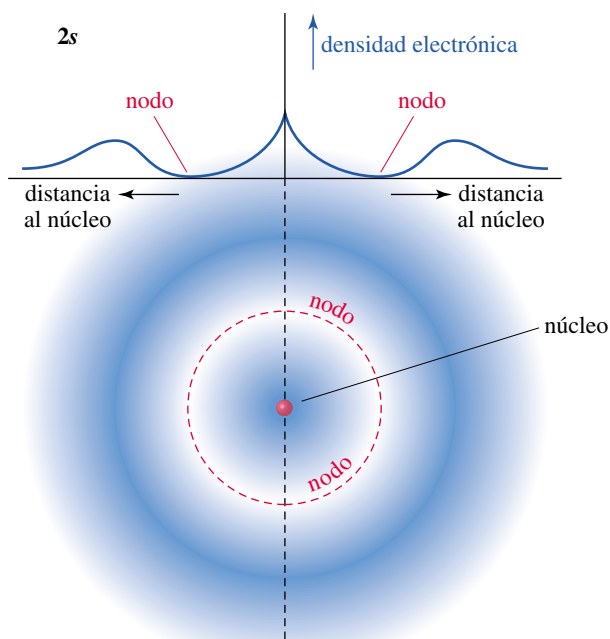


► Figura 1.2

Gráfico y diagrama del orbital atómico 1s. La densidad electrónica es más alta cerca del núcleo y disminuye exponencialmente al aumentar la distancia al núcleo en cualquier dirección.

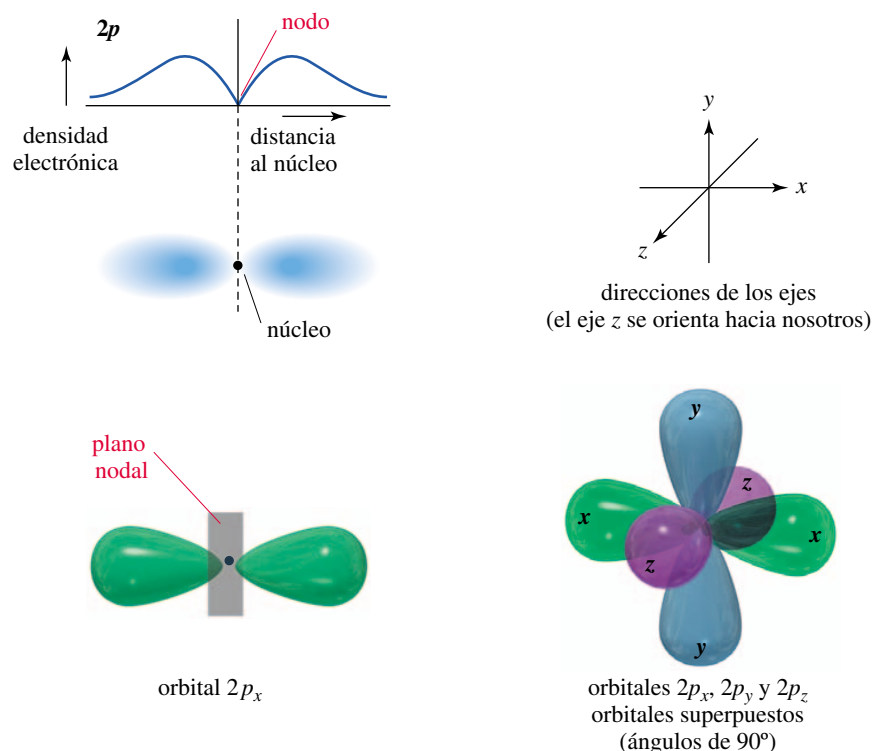
núcleo, ya que la mayor parte de la densidad electrónica está más alejada, más allá de una zona de densidad electrónica nula llamada **nodo**. Como la densidad electrónica del orbital 2s cerca del núcleo es menor que en el caso del orbital 1s, el orbital 2s tiene energía más alta. La Figura 1.3 muestra una representación gráfica del orbital 2s.

Además del orbital 2s, la segunda capa también contiene tres orbitales atómicos 2p, orientados cada uno de ellos en las tres direcciones del espacio. Estos tres orbitales reciben el nombre $2p_x$, $2p_y$ y $2p_z$, según su orientación a lo largo de los ejes x , y o z . Los orbitales 2p tienen una energía ligeramente superior a la de los orbitales 2s, debido a que la localización media de los electrones en los orbitales 2p se sitúa a una distancia más alejada del núcleo. Cada orbital p consta de dos lóbulos, uno a cada lado del núcleo, con un **plano nodal** en el núcleo. El plano nodal es una región (plana) del espacio que incluye el núcleo y tiene una densidad electrónica nula. Los tres orbitales 2p únicamente difieren en sus orientaciones espaciales, por lo que tienen la misma energía. Los orbitales que tienen la misma cantidad de energía reciben el nombre de **orbitales degenerados**. La Figura 1.4 muestra las formas de los tres orbitales atómicos 2p degenerados.



► Figura 1.3

Los orbitales 2s tienen una pequeña región de densidad electrónica elevada próxima al núcleo, pero la mayor parte de la densidad electrónica está alejada del núcleo, más allá del nodo o región de densidad electrónica cero.



◀ **Figura 1.4**

Orbitales $2p$. Hay tres orbitales $2p$, orientados unos con respecto a los otros perpendicularmente. Se nombran según su orientación a lo largo del eje x , y o z .

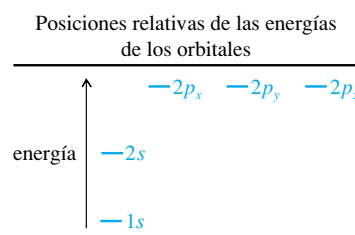
El *principio de exclusión de Pauli* dice que un orbital como máximo puede alojar dos electrones, de forma que sus espines estén apareados. La primera capa (un orbital $1s$) puede alojar dos electrones. La segunda capa (un orbital $2s$ y tres orbitales $2p$) puede alojar ocho electrones y la tercera capa (un orbital $3s$, tres orbitales $3p$ y cinco orbitales $3d$) puede alojar 18 electrones.

1.2C Configuraciones electrónicas de los átomos

Aufbau significa «construir» en alemán, y el *principio de aufbau* explica cómo establecer la configuración electrónica de un átomo en su estado fundamental (el de mayor estabilidad). Se comienza con el orbital de energía más baja y se van llenando ordenadamente de menor a mayor energía hasta que se han colocado todos los electrones. La Tabla 1.1 muestra las configuraciones electrónicas en estado fundamental de todos los elementos que forman parte de los dos primeros periodos de la tabla periódica.

TABLA 1.1 Configuraciones electrónicas de los elementos del primer y segundo periodo

Elemento	Configuración	Electrones de valencia
H	$1s^1$	1
He	$1s^2$	2
Li	$1s^2 2s^1$	1
Be	$1s^2 2s^2$	2
B	$1s^2 2s^2 2p_x^1$	3
C	$1s^2 2s^2 2p_x^1 2p_y^1$	4
N	$1s^2 2s^2 2p_x^1 2p_y^1 2p_z^1$	5
O	$1s^2 2s^2 2p_x^2 2p_y^1 2p_z^1$	6
F	$1s^2 2s^2 2p_x^2 2p_y^2 2p_z^1$	7
Ne	$1s^2 2s^2 2p_x^2 2p_y^2 2p_z^2$	8



► **Figura 1.5**

Primeras tres filas de la tabla periódica. La organización de la tabla periódica se debe al alojamiento de los electrones en los orbitales por orden creciente de energía. Para estos elementos representativos, el número de la columna corresponde al número de electrones de valencia.

El carbonato de litio, una sal de litio, es un antidepresivo que se utiliza para tratar el problema psiquiátrico conocido como manía. La manía está caracterizada por comportamientos tales como alteraciones del humor, sentimientos de grandeza, obsesiones y dificultad para dormir. No se sabe cómo actúa el carbonato de litio cuando estabiliza el humor de este tipo de pacientes.

Detalle de la tabla periódica

IA							gases nobles (VIII)
H	IIA	IIIA	IVA	VA	VIA	VIIA	He
Li	Be	B	C	N	O	F	Ne
Na	Mg	Al	Si	P	S	Cl	Ar

En la Tabla 1.1 se ilustran dos conceptos adicionales. Los **electrones de valencia** son los electrones que se encuentran en la capa más externa. El carbono tiene cuatro electrones de valencia, el nitrógeno cinco y el oxígeno seis. El helio tiene dos electrones de valencia y el neón tiene ocho, lo que corresponde, respectivamente, a la primera capa de valencia y a la segunda capa de valencia llenas. En general (para los elementos representativos), la columna o número de grupo de la tabla periódica corresponde al número de electrones de valencia (Figura 1.5). El hidrógeno y el litio tienen un electrón de valencia y los dos se encuentran en la primera columna (grupo IA) de la tabla periódica. El carbono tiene cuatro electrones de valencia y está en el grupo IVA de la tabla periódica.

Observad en la Tabla 1.1 que los electrones de valencia tercero y cuarto del carbono no están apareados, ocupan orbitales separados. A pesar de que el principio de exclusión de Pauli dice que dos electrones pueden ocupar el mismo orbital, los electrones se repelen uno a otro, y el apareamiento requiere energía adicional. La **regla de Hund** afirma que cuando hay dos o más orbitales de la misma energía, los electrones preferentemente se alojan en orbitales *diferentes* antes que aparearse en un mismo orbital. El primer electrón $2p$ (caso del boro) se coloca en un orbital $2p$, el segundo (caso del carbono) en un orbital diferente y el tercero (caso del nitrógeno) se coloca en el último orbital $2p$. El cuarto, quinto y sexto electrón $2p$ se aparearán, respectivamente, con los tres primeros electrones.

PROBLEMA 1.1

Escriba las configuraciones electrónicas de los elementos de la tercera fila que se muestra en la tabla periódica parcial de la Figura 1.5

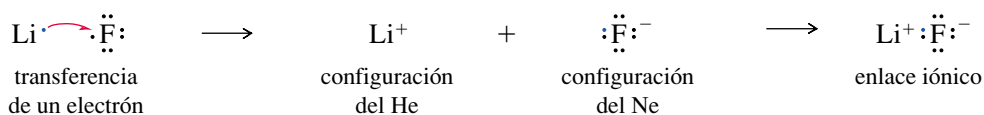
1.3

La formación del enlace: la regla del octeto

En 1915, G. N. Lewis propuso varias teorías nuevas para describir cómo se enlazaban los átomos unos a otros para formar moléculas. Una de esas teorías afirma que una capa llena de electrones es especialmente estable y que *los átomos transfieren o comparten electrones para que de esa forma las capas se llenen de electrones*. Una capa llena de electrones tiene la configuración de un gas noble como el He, Ne o Ar. A este principio se le dio el nombre de la **regla del octeto** porque una capa llena implica ocho electrones de valencia para los elementos de la segunda fila de la tabla periódica.

1.3A Enlace iónico

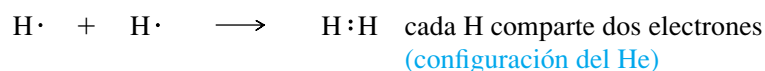
Hay dos formas en las que los átomos pueden interactuar para adquirir configuraciones de gas noble. Algunas veces los átomos adquieren configuraciones de gas noble transfiriendo electrones de un átomo a otro. Por ejemplo, el litio tiene un electrón más en su configuración que el helio, y el fluor tiene un electrón menos que la configuración del neón; el litio pierde fácilmente sus electrones de valencia y el fluor los gana fácilmente:



La transferencia de un electrón da a cada uno de los elementos la configuración de gas noble. Los iones resultantes tienen cargas opuestas y se atraen uno a otro formando un **enlace iónico**. El enlace iónico normalmente da lugar a la formación de grandes estructuras cristalinas en vez de moléculas individuales. El enlace iónico es muy frecuente en los compuestos inorgánicos, pero bastante inusual en los orgánicos.

1.3B Enlace covalente

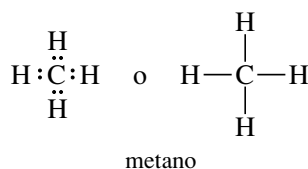
El **enlace covalente**, en el que se comparten electrones en lugar de transferirse, es la forma más habitual de enlace en los compuestos orgánicos. El hidrógeno, por ejemplo, necesita un segundo electrón para conseguir la configuración del gas noble helio. Si dos átomos de hidrógeno se unen y forman un enlace, «comparten» sus dos electrones y cada átomo tiene dos electrones en su capa de valencia.



El enlace covalente se estudiará con más detalle en el Capítulo 2.

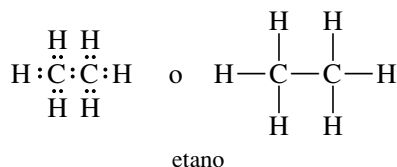
Una forma de simbolizar el enlace en una molécula covalente consiste en usar **estructuras de Lewis**. En una estructura de Lewis cada electrón de valencia se simboliza por un punto. Un par de electrones de enlace se simboliza por un par de puntos o por una línea (—). Se ha de intentar que todos los átomos tengan sus propias configuraciones de gas noble: dos electrones en el caso del hidrógeno y octetos para los elementos de la segunda fila de la tabla periódica.

Considere, por ejemplo, la estructura de Lewis del metano (CH_4):



El carbono contribuye con cuatro electrones de valencia y cada hidrógeno aporta uno, dando un total de ocho electrones. Todos estos ocho electrones rodean al carbono dando lugar a un octeto y cada átomo de hidrógeno comparte dos de los electrones.

La estructura de Lewis para el etano (C_2H_6) es más compleja:



Una vez más, se han colocado los electrones de valencia (14) y se han distribuido de forma que cada átomo de carbono quede rodeado por ocho electrones y cada hidrógeno por dos. La única estructura posible para el etano es la que se ha mostrado anteriormente, con los dos átomos de carbono compartiendo un par de electrones y cada átomo de hidrógeno compartiendo dos con uno de los carbonos. La estructura del etano muestra las características más importantes del carbono (su habilidad para formar enlaces fuertes carbono-carbono).

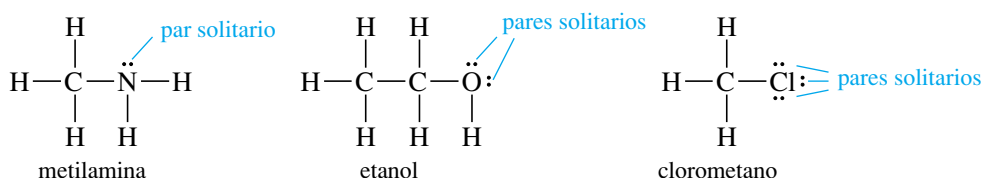
Los electrones de la capa de valencia que *no* son compartidos entre dos átomos reciben el nombre de **electrones no enlazantes**. Un par de electrones no enlazantes a menudo también es conocido como un **par solitario**. Los átomos de oxígeno, de nitrógeno y los halógenos (F, Cl, Br, I) normalmente tienen electrones no enlazantes en sus compuestos

1.4 Estructuras de Lewis

SUGERENCIA PARA RESOLVER PROBLEMAS

Las estructuras de Lewis son la forma de representar los enlaces en química orgánica. Aprender a representarlas de forma rápida y correctamente será muy útil a lo largo de este curso.

estables. Estos pares solitarios de electrones no enlazantes ayudan a determinar la reactividad de sus compuestos. Las estructuras de Lewis siguientes muestran un par solitario de electrones en el átomo de nitrógeno de la metilamina y dos pares solitarios en el átomo de oxígeno del etanol. Los átomos de los halógenos normalmente tienen tres pares solitarios, como se muestra en la estructura del clorometano.



Una estructura de Lewis correcta debería mostrar los pares solitarios de electrones. Los químicos orgánicos a menudo dibujan estructuras de Lewis omitiendo la mayoría o todos los pares solitarios de electrones. Éstas no son estructuras correctas de Lewis porque uno se ha de imaginar el número de electrones no enlazantes.

PROBLEMA 1.2

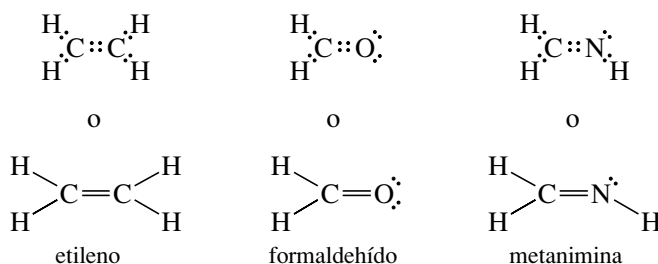
Dibuje las estructuras de Lewis de los siguientes compuestos:

- | | |
|--|--|
| (a) amoníaco, NH_3 | (b) agua, H_2O |
| (c) ión hidronio, H_3O^+ | (d) propano, C_3H_8 |
| (e) etilamina, $\text{CH}_3\text{CH}_2\text{NH}_2$ | (f) dimetil éter, CH_3OCH_3 |
| (g) fluoroetano, $\text{CH}_3\text{CH}_2\text{F}$ | (h) 2-propanol, $\text{CH}_3\text{CH}(\text{OH})\text{CH}_3$ |
| (i) borano, BH_3 | (j) trifluoruro de boro, BF_3 |

Explique qué es inusual en el enlace de los compuestos (i) y (j).

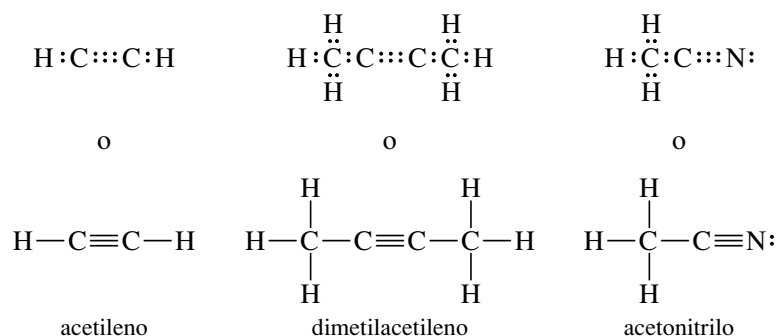
1.5 Enlace múltiple

Al representar las estructuras de Lewis en la Sección 1.4, se pusieron un par de electrones entre cada dos átomos. La compartición de un par de electrones entre dos átomos se conoce como **enlace sencillo**. Muchas moléculas comparten con sus átomos adyacentes dos o incluso tres pares de electrones; cuando se comparten dos pares se da el nombre de **enlace doble** y cuando se comparten tres pares se da el nombre de **enlace triple**. El etileno (C_2H_4) es un compuesto orgánico con un doble enlace. Cuando se representan las estructuras de Lewis para el etileno, la única forma de conseguir que los dos átomos de carbono tengan octetos es mediante la compartición de dos pares de electrones. El ejemplo siguiente muestra compuestos orgánicos con dobles enlaces. En cada caso, se comparten cuatro electrones (dos pares) entre dos átomos para formar octetos. Una doble línea (=) simboliza el doble enlace.



El acetileno, cuando se combina con el oxígeno, arde con una llama intensa que tiene diversas aplicaciones. Se puede utilizar para soldar las piezas de un puente bajo el agua o para reparar las tuberías de un oleoducto en Siberia.

El acetileno (C_2H_2) tiene un triple enlace. Su estructura de Lewis muestra los tres pares de electrones entre los dos átomos de carbono para que formen un octeto. Una línea triple (\equiv) simboliza el triple enlace.



Todas estas estructuras de Lewis muestran que el carbono normalmente forma cuatro enlaces en compuestos orgánicos neutros. El nitrógeno generalmente forma tres enlaces y el oxígeno dos. El hidrógeno y los halógenos normalmente forman un enlace. El número de enlaces que normalmente puede formar un átomo se conoce como **valencia**. El carbono es tetravalente, el nitrógeno trivalente, el oxígeno divalente, y el hidrógeno y los halógenos monovalentes. Si se recuerda el número usual de enlaces de estos elementos, se podrán escribir estructuras orgánicas con mucha facilidad. Si una estructura se representa de forma que cada átomo tenga el número de enlaces que le corresponden, la estructura de Lewis será correcta.

RESUMEN Modelos de enlace más frecuentes (sin carga)

	$\begin{array}{c} \\ -\text{C}- \\ \end{array}$	$\begin{array}{c} \cdot\cdot \\ -\text{N}- \\ \end{array}$	$\begin{array}{c} \cdot\cdot \\ -\text{O}- \\ \cdot\cdot \end{array}$	$-\text{H}$	$\begin{array}{c} \cdot\cdot \\ -\text{Cl}: \end{array}$
	carbono	nitrógeno	oxígeno	hidrógeno	halógenos
valencia:	4	3	2	1	1
pares solitarios:	0	1	2	0	3

SUGERENCIA PARA RESOLVER PROBLEMAS

Estos «números de enlaces usuales» pueden ser sencillos o estar combinados en dobles y triples enlaces. Por ejemplo, los tres enlaces del nitrógeno podrían corresponder a tres enlaces sencillos, a un enlace sencillo y uno doble, o a un triple enlace ($:\text{N}\equiv\text{N}:$). En los problemas hay que considerar todas las posibilidades.

PROBLEMA 1.3

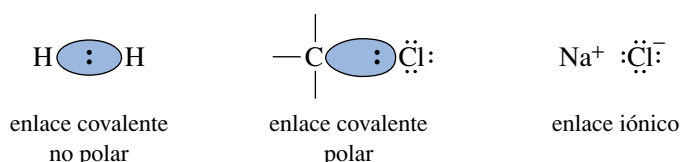
Escriba la estructura de Lewis para cada una de las siguientes fórmulas moleculares:

- | | | |
|---|---|----------------------------|
| (a) N_2 | (b) HCN | (c) HONO |
| (d) CO_2 | (e) H_2CNH | (f) HCO_2H |
| (g) $\text{C}_2\text{H}_3\text{Cl}$ | (h) HNNH | (i) C_3H_6 |
| (j) C_3H_4 (dos dobles enlaces) | (k) C_3H_4 (un triple enlace) | |

PROBLEMA 1.4

Rodee con un círculo los pares solitarios (pares de electrones no enlazantes) en las estructuras representadas en el Problema 1.3.

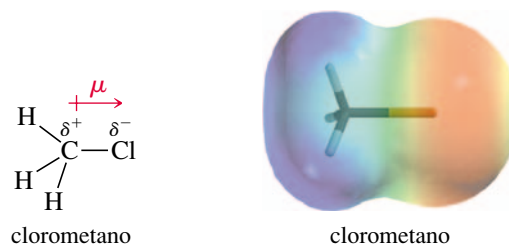
Un enlace cuyos electrones están igualmente compartidos por los dos átomos recibe el nombre de **enlace covalente no polar**. El enlace en la molécula de H_2 y el enlace $\text{C}-\text{C}$ en el etano son enlaces covalentes no polares. En la mayoría de enlaces entre dos elementos diferentes los electrones del enlace están atraídos de forma diferente por cada uno de los dos núcleos. Cuando la compartición del par de electrones del enlace no es igual para los dos átomos, a este enlace se le conoce como **enlace covalente polar**.



1.6 La electronegatividad y la polaridad de enlace

► **Figura 1.6**

El clorometano contiene un enlace polar carbono-cloro con una carga negativa parcial en el cloro y una carga positiva parcial en el carbono. El mapa de potencial electrostático muestra una región roja (rica en electrones) alrededor de la carga negativa parcial y una región azul (pobre en electrones) alrededor de la carga positiva parcial. El resto de colores indican valores intermedios de potencial electrostático.



Cuando el carbono se enlaza al cloro, por ejemplo, los electrones de enlace son atraídos más fuertemente hacia el átomo de cloro, por lo que el átomo de carbono adquirirá una pequeña carga positiva parcial y el átomo de cloro esa misma cantidad de carga pero de signo negativo. La Figura 1.6 muestra el enlace polar carbono-cloro del clorometano. Nosotros simbolizaremos la polaridad de enlace por una flecha que tenga como origen la carga positiva del enlace polar, y sobre este origen un signo positivo. La polaridad de un enlace se mide por su **momento dipolar** (μ), definido por el producto de la carga (separación de las cargas δ^+ y δ^-) y la longitud del enlace. El símbolo δ^+ significa «una pequeña cantidad de carga positiva» y el símbolo δ^- «una pequeña cantidad de carga negativa».

La Figura 1.6 también muestra un **mapa de potencial electrostático (MPE)** para el clorometano, que usa colores para representar la distribución de la carga calculada en una molécula. El rojo indica regiones ricas en electrones y el azul regiones pobres en electrones. El naranja, amarillo y verde indican niveles intermedios de potencial electrostático. En el clorometano, la región roja muestra la carga negativa parcial del cloro y la región azul indica la carga positiva parcial de los átomos de carbono y de hidrógeno.

A menudo se usan las **electronegatividades** como guía para predecir si un determinado enlace será polar y la dirección del momento dipolar. La escala de electronegatividad de Pauling, la que comúnmente utilizan los químicos orgánicos, se basa en las propiedades del enlace y es muy útil para predecir la polaridad de los enlaces covalentes. Los elementos con electronegatividades más altas atraen con más fuerza a los electrones de enlace. No obstante, en un enlace entre dos átomos diferentes, el átomo con la electronegatividad más alta es el extremo negativo del dipolo. La Figura 1.7 muestra las electronegatividades de Pauling para algunos de los elementos importantes de los compuestos orgánicos.

Obsérvese que la electronegatividad aumenta de izquierda a derecha a lo largo de la tabla periódica. El nitrógeno, el oxígeno y los halógenos son más electronegativos que el carbono; el sodio, el litio y el magnesio son menos electronegativos. La electronegatividad del hidrógeno es parecida a la del carbono, por lo que el enlace C—H normalmente se considera no polar. La polaridad de los enlaces y de las moléculas se tratará con más detalle en la Sección 2.9.

PROBLEMA 1.5

Haga uso de las electronegatividades para predecir los momentos dipolares de los siguientes enlaces:

- (a) C—Cl (b) C—O (c) C—N (d) C—S (e) C—B
(f) N—Cl (g) N—O (h) N—S (i) N—B (j) B—Cl

► **Figura 1.7**

Electronegatividades de algunos de los elementos que se encuentran en los compuestos orgánicos.

H 2.2						
Li 1.0	Be 1.6	B 1.8	C 2.5	N 3.0	O 3.4	F 4.0
Na 0.9	Mg 1.3	Al 1.6	Si 1.9	P 2.2	S 2.6	Cl 3.2
K 0.8						Br 3.0
						I 2.7

En los enlaces polares, las cargas parciales (δ^+ y δ^-) de los átomos del enlace son *reales*. Las **cargas formales** proporcionan un método de seguimiento de los electrones, pero pueden corresponder o no a cargas reales. En la mayoría de los casos, si la estructura de Lewis muestra que un átomo tiene una carga formal, quiere decir que tiene parte de esa carga. El concepto de carga formal ayuda a determinar qué átomos tienen mayor cantidad de carga en una molécula y ver que hay átomos cargados en moléculas que son neutras globalmente.

Para calcular las cargas formales, hay que contar cuántos electrones contribuyen a la carga de cada átomo y comparar ese número con el número de electrones de valencia que hay en el átomo neutro y aislado (dado por el número de grupo en la tabla periódica). Los electrones que contribuyen a la carga de un átomo son:

1. *Todos* sus electrones no compartidos (no enlazantes).
2. *La mitad* de los electrones (enlazantes) que comparte con otros átomos, o un electrón de cada par de enlace.

La carga formal de un átomo determinado puede ser calculada mediante la fórmula:

$$\text{carga formal (CF)} = [\text{número de grupo}] - [\text{electrones no enlazantes}] - \frac{1}{2}[\text{electrones compartidos}]$$

PROBLEMA RESUELTO 1.1

Calcule la carga formal (CF) de cada átomo de las estructuras siguientes:

(a) Metano (CH_4)

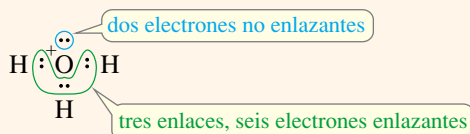


SOLUCIÓN

Cada átomo de hidrógeno del metano tiene un par enlazante de electrones (dos electrones compartidos). La mitad de los dos electrones compartidos es un electrón de valencia y es lo que el hidrógeno necesita para ser neutro. Los átomos de hidrógeno con un enlace son neutros formalmente: $\text{CF} = 1 - 0 - 1 = 0$.

El átomo de carbono tiene cuatro pares de electrones enlazantes (ocho electrones). La mitad de los ocho electrones compartidos, esto es, cuatro electrones son los que el carbono (grupo IVA) necesita para ser neutro. El carbono es formalmente neutro cuando tiene cuatro enlaces: $\text{CF} = 4 - 0 - \frac{1}{2}(8) = 0$.

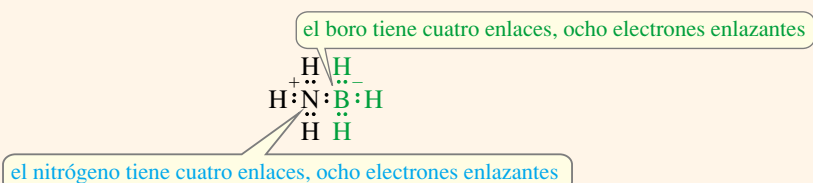
(b) Ión hidronio, H_3O^+



SOLUCIÓN

Cuando se representa la estructura de Lewis para este ión, se utilizan ocho electrones: seis del oxígeno y tres de los hidrógenos, menos uno porque el ión tiene una carga positiva. Cada hidrógeno tiene un enlace y es formalmente neutro. El oxígeno está rodeado por un octeto, con seis electrones enlazantes y dos electrones no enlazantes. La mitad de los electrones enlazantes más todos los electrones no enlazantes contribuyen a la carga: $6/2 + 2 = 5$; pero el oxígeno (grupo VIA) necesita seis electrones de valencia para ser neutro, por este motivo, el átomo de oxígeno tiene una carga formal de $+1$: $\text{CF} = 6 - 2 - \frac{1}{2}(6) = +1$.

(c) $\text{H}_3\text{N} - \text{BH}_3$



1.7 Cargas formales

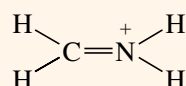
SOLUCIÓN

Éste es un compuesto neutro donde los átomos individuales están cargados formalmente. La estructura de Lewis muestra que tanto el nitrógeno como el boro tienen cuatro pares de electrones enlazantes. Los dos átomos, boro y nitrógeno, tienen $8/2 = 4$ electrones que contribuyen a sus cargas. El nitrógeno (grupo V) necesita cinco electrones de valencia para ser neutro, por lo que su carga formal es $+1$. El boro (grupo III) sólo necesita tres electrones de valencia para ser neutro, por lo que su carga formal es -1 .

$$\text{Nitrógeno: } CF = 5 - 0 - \frac{1}{2}(8) = +1$$

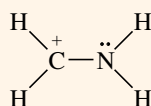
$$\text{Boro: } CF = 3 - 0 - \frac{1}{2}(8) = -1$$

(d) $[\text{H}_2\text{CNH}_2]^+$

**SOLUCIÓN**

En esta estructura, tanto el carbono como el nitrógeno tienen cuatro pares de electrones enlazantes. Con cuatro enlaces, el carbono es formalmente neutro; no obstante, el nitrógeno es del grupo V, por lo que su carga positiva formal es: $CF = 5 - 0 - 4 = +1$.

Este compuesto también podría ser representado con la siguiente estructura de Lewis:



En esta estructura, el átomo de carbono tiene tres enlaces con seis electrones enlazantes que, si se dividen entre dos, $6/2 = 3$, se observa que el carbono tiene un electrón menos de los cuatro que necesita para ser neutro formalmente: $CF = 4 - 0 - \frac{1}{2}(6) = +1$.

El nitrógeno tiene seis electrones enlazantes y dos electrones no enlazantes. Si se hace el cálculo $6/2 + 2 = 5$, se observa que el nitrógeno es neutro en esta segunda estructura:

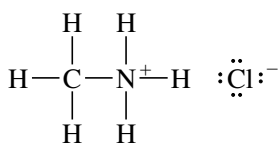
$$CF = 5 - 2 - \frac{1}{2}(6) = 0$$

El significado de estas dos estructuras de Lewis se discute en la Sección 1.9.

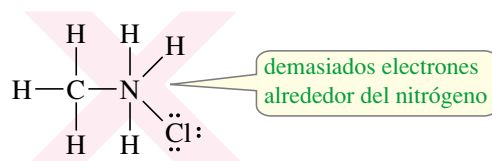
La mayoría de los compuestos orgánicos sólo contienen un número pequeño de elementos bastante comunes, normalmente con el octeto de electrones completo. La tabla resumen de la página siguiente indica la naturaleza de los enlaces más habituales, utilizando líneas para representar los pares de electrones enlazantes. Utilice estas reglas de cálculo de las cargas formales para comprobar las cargas que se dan en las estructuras. Si las estructuras se entienden bien, será fácil representar los compuestos orgánicos y sus iones de forma rápida y correcta.

1.8 Estructuras iónicas

Algunos compuestos orgánicos contienen enlaces iónicos. Por ejemplo, la estructura del cloruro de metilamonio ($\text{CH}_3\text{NH}_3\text{Cl}$) no se puede representar si solamente se utilizan enlaces covalentes; esto requeriría que el nitrógeno tuviese cinco enlaces, lo que implicaría diez electrones en la capa de valencia. La estructura correcta contiene un ión cloruro enlazado iónicamente al resto de la estructura.



cloruro de metilamonio



no se puede representar mediante enlaces covalentes

RESUMEN

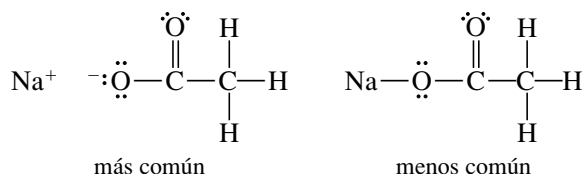
Modelos de enlace más frecuentes en los compuestos e iones orgánicos

Átomo	Electrones de valencia	Cargado positivamente	Neutro	Cargado negativamente
B	3		(no octeto) $\begin{array}{c} \text{—B—} \\ \end{array}$	$\begin{array}{c} \\ \text{—B—} \\ \end{array}$
C	4	$\begin{array}{c} + \\ \text{—C—} \\ \end{array}$ (no octeto)	$\begin{array}{c} \\ \text{—C—} \\ \end{array}$	$\begin{array}{c} \cdot\cdot \\ \text{—C—} \\ \end{array}$
N	5	$\begin{array}{c} \\ \text{—N}^+ \\ \end{array}$	$\begin{array}{c} \cdot\cdot \\ \text{—N—} \\ \end{array}$	$\begin{array}{c} \cdot\cdot \\ \text{—N—} \\ \end{array}$
O	6	$\begin{array}{c} \cdot\cdot \\ \text{—O}^+ \\ \end{array}$	$\begin{array}{c} \cdot\cdot \\ \text{—O—} \\ \end{array}$	$\begin{array}{c} \cdot\cdot \\ \text{—O—} \\ \end{array}$
halógeno	7	$\begin{array}{c} \cdot\cdot \\ \text{—Cl}^+ \\ \end{array}$	$\begin{array}{c} \cdot\cdot \\ \text{—Cl:} \end{array}$	$\begin{array}{c} \cdot\cdot \\ \text{:Cl:}^- \end{array}$

SUGERENCIA PARA RESOLVER PROBLEMAS

Esta tabla es muy importante. Haz un número de problemas suficientes como para familiarizarte con estos modelos de enlace, tal que puedas saber cuándo otros modelos son incorrectos o bien inusuales.

Algunas moléculas se pueden representar tanto en forma covalente como iónica. Por ejemplo, el acetato de sodio (NaOCOCH_3) se puede representar tanto con un enlace covalente como con un enlace iónico entre el sodio y el oxígeno. Como el sodio normalmente forma enlaces iónicos con el oxígeno (NaOH), la estructura con enlace iónico es la que se prefiere. En general, los enlaces entre átomos con gran diferencia de electronegatividad (2 o más) normalmente se representan como compuestos iónicos.



PROBLEMA 1.6

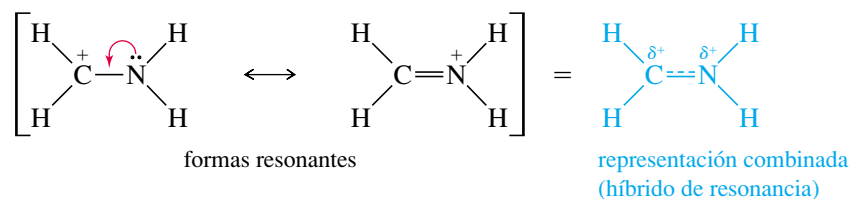
Dibuje las estructuras de Lewis de los siguientes compuestos e iones, diciendo cuál es su carga formal apropiada:

- | | |
|---|---------------------------------|
| (a) $[\text{CH}_3\text{OH}_2]^+$ | (b) NH_4Cl |
| (c) $(\text{CH}_3)_2\text{NH}_2\text{Cl}$ | (d) NaOCH_3 |
| (e) $^+\text{CH}_3$ | (f) $^-\text{CH}_3$ |
| (g) NaBH_4 | (h) NaBH_3CN |
| (i) $(\text{CH}_3)_2\text{O—BF}_3$ | (j) $[\text{HONH}_3]^+$ |
| (k) $\text{KOC}(\text{CH}_3)_3$ | (l) $[\text{H}_2\text{C=OH}]^+$ |

1.9A Híbridos de resonancia

Algunas de las estructuras de los compuestos no es adecuado representarlas mediante una sola estructura de Lewis. Cuando son posibles dos o más estructuras de enlace de valencia, que difieren sólo en la colocación de los electrones, la molécula suele mostrar características de las dos estructuras. A estas estructuras diferentes se las conoce como **estructuras de resonancia** o **formas resonantes**, ya que no son compuestos diferentes, sino formas diferentes de representar el mismo compuesto. La molécula real se dice que corresponde a un **híbrido de resonancia** de sus formas resonantes. En el Problema resuelto 1.1(d) se mostró cómo el ión $[\text{H}_2\text{CNH}_2]^+$ se podía representar por cualquiera de las siguientes formas de resonancia:

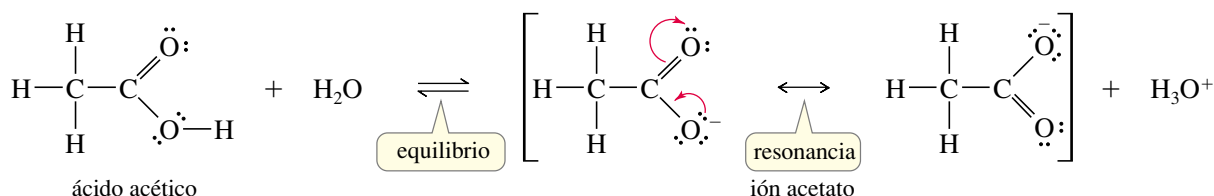
1.9 Resonancia



La estructura real de este ión es un híbrido de resonancia de las dos estructuras. En la molécula real, la carga positiva está **deslocalizada** (extendida) entre el átomo de carbono y el de nitrógeno. En la forma resonante de la izquierda, la carga positiva está en el carbono, pero el carbono no tiene un octeto. Los electrones no enlazantes del nitrógeno se pueden mover por el enlace (tal como indica la flecha roja) dando una segunda estructura con un doble enlace entre el nitrógeno que tiene carga positiva y el carbono que posee un octeto. La representación combinada de las dos formas de resonancia en una sola representación da lugar a una carga compartida entre el nitrógeno y el carbono.

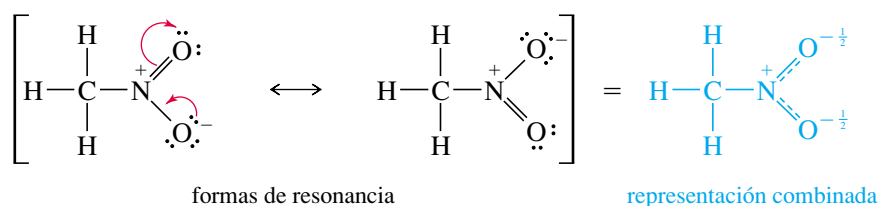
El extender la carga positiva sobre dos átomos hace que el ión sea más estable que en el caso de que la carga positiva estuviera localizada solamente sobre el carbono o sobre el nitrógeno. Se dice que este catión está **estabilizado por resonancia**. La resonancia es más importante cuando permite que una carga esté deslocalizada entre dos o más átomos, como en el ejemplo mencionado.

La estabilización por resonancia desempeña un papel crucial en la química orgánica, especialmente en la química de compuestos que tienen dobles enlaces. Se usará frecuentemente el concepto de resonancia a lo largo de este curso. Por ejemplo, la acidez del ácido acético (véase abajo) se incrementa por efecto de la resonancia. Cuando el ácido acético pierde un protón, el ión acetato resultante tiene una carga negativa deslocalizada sobre los dos átomos de oxígeno. Cada átomo de oxígeno posee la mitad de la carga negativa y su deslocalización estabiliza el ión. Cada uno de los enlaces carbono-oxígeno es intermedio entre un enlace doble y un enlace sencillo, por lo que se dice que su *orden de enlace* es de $1\frac{1}{2}$.



Se usará una sola flecha con doble punta entre las formas de resonancia (a menudo puestas entre corchetes) para indicar que la estructura real es un híbrido de las estructuras de Lewis representadas. Por otra parte, un equilibrio se representará por dos flechas con sentidos opuestos.

Algunas moléculas sin carga también tienen estructuras de resonancia estabilizadas con la misma carga formal positiva y negativa. Se pueden representar dos estructuras de Lewis para el nitrometano (CH_3NO_2), pero las dos estructuras tienen una carga positiva formal en el nitrógeno y una carga negativa en uno de los oxígenos. Por tanto, el nitrometano tiene una carga positiva en el átomo de nitrógeno y una carga negativa extendida por igual sobre los dos átomos de oxígeno. Los enlaces N—O están entre un enlace sencillo y uno doble, tal como se indica en la representación combinada siguiente:

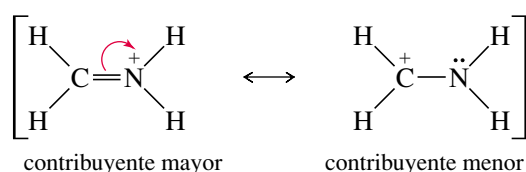


Recuerde que las formas de resonancia individuales no existen como especies químicas independientes. La molécula no «resuena» entre esas estructuras, es un híbrido con

características de ambas estructuras. Una analogía sería una mula, que es un híbrido de un caballo y un burro. La mula no «resuena» entre parecerse a un caballo o a un burro; simplemente es una mula, con el amplio dorso de un caballo y las grandes orejas de un burro.

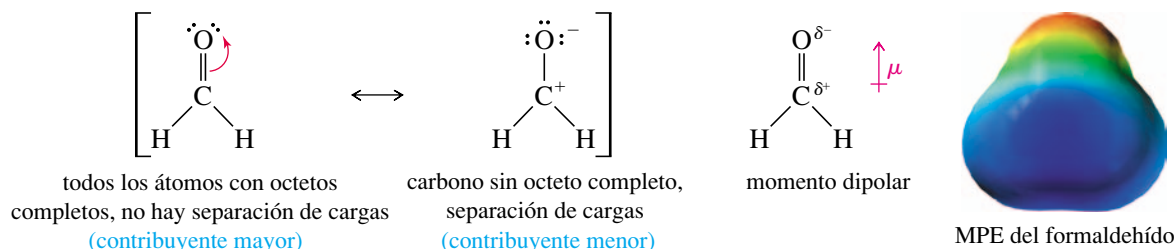
1.9B Contribución mayor o menor de las formas resonantes al híbrido de resonancia

Dos o más estructuras de Lewis correctas para un mismo compuesto pueden o no representar distribuciones de electrones de igual energía. A pesar de que formas de resonancia separadas no existen, se pueden estimar sus energías relativas como si existieran. La mayoría de las formas de resonancia estables son representaciones más cercanas de la molécula real que las menos estables. Las dos formas de resonancia del apartado anterior, para el ión acetato, tienen enlaces similares e idéntica energía. Lo mismo se puede decir para las dos formas de resonancia del nitrometano. Las formas de resonancia siguientes, por el contrario, tienen enlaces diferentes.



Las estructuras anteriores no tienen la misma energía estimada. La primera estructura tiene la carga positiva en el nitrógeno. La segunda tiene la carga positiva en el carbono, y el átomo de carbono no posee un octeto completo. La primera estructura es más estable ya que tiene un enlace adicional y todos los átomos tienen octetos completos. Muchos iones estables tienen una carga positiva en el átomo de nitrógeno con cuatro enlaces (*véase* la tabla resumen de la página 13). A la forma de resonancia más estable se la conoce como la **contribuyente mayor** y a la forma menos estable como la **contribuyente menor**. La estructura del compuesto real se parece más al contribuyente mayor que al contribuyente menor.

Muchas moléculas orgánicas tienen contribuyentes de resonancia mayor y menor. El formaldehído ($\text{H}_2\text{C}=\text{O}$) se puede representar con una carga negativa en el oxígeno, equilibrada por una carga positiva en el carbono. Esta forma de resonancia polar tiene mayor energía estimada que la estructura con doble enlace, porque tiene separación de cargas, menos enlaces y un átomo de carbono cargado positivamente con un octeto incompleto. La estructura con cargas separadas es solamente un contribuyente menor, pero ayuda a explicar por qué el enlace $\text{C}=\text{O}$ del formaldehído es muy polar, con una carga positiva parcial en el carbono y una carga negativa parcial en el oxígeno. El mapa de potencial electrostático (MPE) también muestra una región rica en electrones (rojo) alrededor del oxígeno y una región pobre en electrones (azul) alrededor del carbono en el formaldehído.



Cuando se representan las formas de resonancia, se intenta dibujar estructuras que sean lo más bajas posible en energía. Las mejores candidatas son las que tienen un número máximo de octetos y el máximo número de enlaces. Además, las estructuras tienen que tener la mínima cantidad de separación de cargas.

Sólo los electrones pueden estar deslocalizados. Al contrario que los electrones, los núcleos no pueden estar deslocalizados, deben permanecer en el mismo lugar, con las mismas distancias de enlace y los mismos ángulos en todos los contribuyentes a la resonancia. Las reglas generales siguientes serán útiles para representar estructuras de resonancias.

SUGERENCIA PARA RESOLVER PROBLEMAS

Para comparar las formas de resonancia se pueden utilizar los siguientes criterios, comenzando por el más importante:

1. Tantos octetos como sea posible.
2. Tantos enlaces como sea posible.
3. Si hay carga negativa se coloca en los átomos electronegativos.
4. La menor separación de cargas posible.

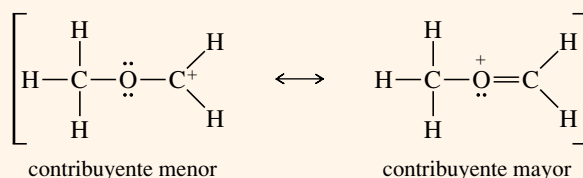
1. Todas las estructuras de resonancia deben ser estructuras de Lewis válidas para el compuesto.
2. Sólo se puede cambiar la posición de los electrones de una estructura a otra (los electrones de los dobles enlaces y pares solitarios son los que se cambian con más frecuencia). El núcleo no se puede cambiar de posición y los ángulos de enlace han de ser los mismos.
3. El número de electrones desapareados (si hay alguno) debe permanecer igual. La mayoría de los compuestos estables no tienen electrones desapareados y todos los electrones deben permanecer apareados en todas las estructuras de resonancia.
4. El contribuyente mayor a la resonancia es el que tiene menor energía.
Los buenos contribuyentes generalmente tienen todos los octetos satisfechos, con el máximo número de enlaces covalentes que sea posible y con una separación de cargas lo menor posible. Las cargas negativas son más estables en los átomos más electronegativos.
5. La estabilización por resonancia es más importante cuando sirve para deslocalizar una carga entre dos o más átomos.

PROBLEMA RESUELTO 1.2

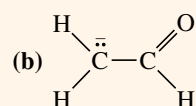
Para cada uno de los siguientes compuestos, represente las formas de resonancia importantes. Indique qué estructuras tienen contribuyentes mayores y menores, o si tienen la misma energía.

(a) $[\text{CH}_3\text{OCH}_2]^+$

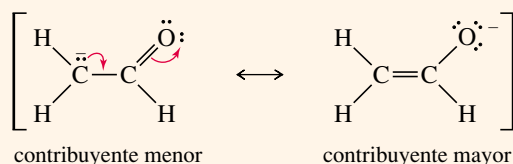
SOLUCIÓN



La primera estructura (menor) tiene un átomo de carbono con sólo seis electrones a su alrededor. La segunda estructura (mayor) tiene octetos en todos los átomos y un enlace adicional.



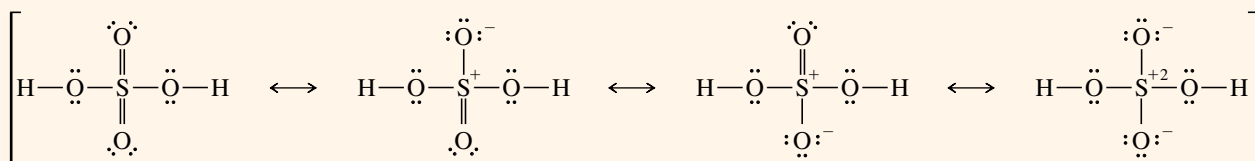
SOLUCIÓN



Las dos estructuras tienen octetos en el átomo de oxígeno y en el de carbono, y tienen el mismo número de enlaces. La primera estructura tiene la carga negativa en el carbono y la segunda la tiene en el oxígeno. El oxígeno es más electronegativo que el carbono, por lo tanto, la segunda estructura es el contribuyente mayor.

(c) H_2SO_4

SOLUCIÓN



La primera estructura, con más enlaces y menor separación de carga, es posible porque el azufre es un elemento de la tercera fila de la tabla periódica con orbitales *d* accesibles, lo que le da la posibilidad de expandir aparentemente su octeto. Por ejemplo, el SF_6 es un compuesto estable con 12 electrones alrededor del azufre. Sin embargo, algunos cálculos teóricos sugieren que la última estructura representada, con octetos en todos los átomos, podría ser la contribuyente mayor a la resonancia. No se puede predecir siempre el contribuyente mayor de un híbrido de resonancia.

PROBLEMA 1.7

Represente las formas de resonancia importantes de las siguientes moléculas e iones:

- (a) CO_3^{2-} (b) NO_3^- (c) NO_2^- (d) $\text{H}_2\text{C}=\text{CH}-\text{CH}_2^+$
 (e) $\text{H}_2\text{C}=\text{CH}-\text{CH}_2^-$ (f) SO_4^{2-} (g) $[\text{CH}_3\text{C}(\text{OCH}_3)_2]^+$

PROBLEMA 1.8

Para cada uno de los siguientes compuestos, represente las formas de resonancia importantes. Indique qué estructuras son las contribuyentes mayores y menores a la resonancia, o si tienen la misma energía.

- (a) $[\text{H}_2\text{CNO}_2]^-$ (b) $\text{H}_2\text{C}=\text{CH}-\text{NO}_2$ (c) $[\text{H}_2\text{COH}]^+$
 (d) H_2CNN (e) $[\text{H}_2\text{CCN}]^-$ (f) $\text{H}_2\text{N}-\overset{+}{\text{CH}}-\text{CH}=\text{CH}-\text{NH}_2$
 (g) $\text{H}-\overset{\text{O}}{\parallel}{\text{C}}-\overset{-}{\text{CH}}-\overset{\text{O}}{\parallel}{\text{C}}-\text{H}$ (h) $\text{H}-\overset{\text{O}}{\parallel}{\text{C}}-\text{NH}_2$

SUGERENCIA**PARA RESOLVER PROBLEMAS**

Cuando se representan formas de resonancia para iones, observe cómo se puede deslocalizar la carga entre varios átomos. Intente colocar una carga negativa sobre elementos electronegativos como el oxígeno y el nitrógeno. Intente, así mismo, colocar una carga positiva sobre todos los carbonos que sea posible, pero especialmente sobre los átomos que puedan alojar la carga positiva y tener un octeto completo; por ejemplo, el oxígeno (con tres enlaces) o el nitrógeno (con cuatro enlaces).

Los químicos orgánicos utilizan varias clases de fórmulas para representar los compuestos orgánicos. Algunas de estas fórmulas incluyen una notación específica que requiere una explicación. Las **fórmulas estructurales** indican qué átomos están enlazados a otros. Hay dos tipos de fórmulas estructurales: las estructuras de Lewis completas y las fórmulas estructurales condensadas. Además, hay varias formas de representar fórmulas estructurales condensadas. Según se ha visto, una estructura de Lewis simboliza un par de electrones enlazantes como un par de puntos o como una línea (—). Los pares solitarios de electrones se muestran como pares de puntos.

1.10**Fórmulas estructurales****1.10A Fórmulas estructurales condensadas**

Las **fórmulas estructurales condensadas** (Tabla 1.2) se representan sin mostrar todos los enlaces individuales. En una estructura condensada, cada átomo central se representa junto a los átomos a los que está enlazado. Los átomos enlazados a un átomo central a menudo se escriben a continuación del átomo central (CH_3CH_3 en lugar de $\text{H}_3\text{C}-\text{CH}_3$) incluso aunque no sea el orden del verdadero enlace. En muchos casos, si hay dos o más grupos idénticos, se puede utilizar un paréntesis y un subíndice para representar a todos estos grupos. Los electrones no enlazantes raramente se representan en las fórmulas estructurales condensadas.

TABLA 1.2 Ejemplos de fórmulas estructurales condensadas

Compuesto	Estructura de Lewis	Fórmula estructural condensada
etano	$\begin{array}{c} \text{H} & \text{H} \\ & \\ \text{H}-\text{C}- & \text{C}-\text{H} \\ & \\ \text{H} & \text{H} \end{array}$	CH_3CH_3
isobutano	$\begin{array}{c} \text{H} & \text{H} & \text{H} \\ & & \\ \text{H}-\text{C}- & \text{C}- & \text{C}-\text{H} \\ & & \\ \text{H} & & \text{H} \\ & & \\ & \text{H}-\text{C}-\text{H} \\ & & \\ & \text{H} & \end{array}$	$(\text{CH}_3)_3\text{CH}$
n-hexano	$\begin{array}{c} \text{H} & \text{H} & \text{H} & \text{H} & \text{H} & \text{H} \\ & & & & & \\ \text{H}-\text{C}- & \text{C}- & \text{C}- & \text{C}- & \text{C}- & \text{C}-\text{H} \\ & & & & & \\ \text{H} & \text{H} & \text{H} & \text{H} & \text{H} & \text{H} \end{array}$	$\text{CH}_3(\text{CH}_2)_4\text{CH}_3$

(continúa en la página siguiente)

TABLA 1.2 (continuación)

Compuesto	Estructura de Lewis	Fórmula estructural condensada
dietil éter	$ \begin{array}{ccccccc} & \text{H} & \text{H} & & \text{H} & \text{H} & \\ & & & & & & \\ \text{H} & - \text{C} & - \text{C} & - \ddot{\text{O}} & - \text{C} & - \text{C} & - \text{H} \\ & & & & & & \\ & \text{H} & \text{H} & & \text{H} & \text{H} & \end{array} $	$\text{CH}_3\text{CH}_2\text{OCH}_2\text{CH}_3$ o $\text{CH}_3\text{CH}_2-\text{O}-\text{CH}_2\text{CH}_3$ o $(\text{CH}_3\text{CH}_2)_2\text{O}$
etanol	$ \begin{array}{ccccccc} & \text{H} & \text{H} & & & & \\ & & & & & & \\ \text{H} & - \text{C} & - \text{C} & - \ddot{\text{O}} & - \text{H} \\ & & & & & & \\ & \text{H} & \text{H} & & & & \end{array} $	$\text{CH}_3\text{CH}_2\text{OH}$
alcohol isopropílico	$ \begin{array}{ccccccc} & \text{H} & & \ddot{\text{O}} & - \text{H} & \text{H} & \\ & & & & & & \\ \text{H} & - \text{C} & - \text{C} & - & \text{C} & - \text{H} \\ & & & & & \\ & \text{H} & \text{H} & & \text{H} & \end{array} $	$(\text{CH}_3)_2\text{CHOH}$
dimetilamina	$ \begin{array}{ccccccc} & \text{H} & & & \text{H} & & \\ & & & & & & \\ \text{H} & - \text{C} & - \ddot{\text{N}} & - & \text{C} & - \text{H} \\ & & & & & \\ & \text{H} & & & \text{H} & \end{array} $	$(\text{CH}_3)_2\text{NH}$

Cuando se escribe una fórmula estructural condensada para un compuesto que contiene enlaces dobles o triples, los enlaces múltiples con frecuencia se representan igual que en las estructuras de Lewis. La Tabla 1.3 muestra ejemplos de fórmulas estructurales condensadas que contienen enlaces múltiples. Observe que el grupo $-\text{CHO}$ de un aldehído y el grupo $-\text{COOH}$ de un ácido carboxílico se enlazan de forma diferente a como sugiere la notación condensada.

Como se puede observar en las Tablas 1.2 y 1.3, la diferencia entre una fórmula estructural de Lewis completa y una fórmula estructural condensada puede ser confusa. Los químicos con frecuencia representan las fórmulas con algunas partes condensadas y otras

TABLA 1.3 Fórmulas estructurales condensadas para dobles y triples enlaces

Compuesto	Estructura de Lewis	Fórmula estructural condensada
2-buteno	$ \begin{array}{ccccccc} & \text{H} & \text{H} & & \text{H} & & \\ & & & & & & \\ \text{H} & - \text{C} & - \text{C} & = \text{C} & - \text{C} & - \text{H} \\ & & & & & \\ & \text{H} & & \text{H} & \text{H} & \end{array} $	$\text{CH}_3\text{CHCHCH}_3$ o $\text{CH}_3\text{CH}=\text{CHCH}_3$
acetonitrilo	$ \begin{array}{ccccccc} & \text{H} & & & & & \\ & & & & & & \\ \text{H} & - \text{C} & - \text{C} & \equiv \text{N} & : \\ & & & & & & \\ & \text{H} & & & & & \end{array} $	CH_3CN o $\text{CH}_3\text{C}\equiv\text{N}$
acetaldehído	$ \begin{array}{ccccccc} & \text{H} & & \ddot{\text{O}} & & & \\ & & & & & & \\ \text{H} & - \text{C} & - & \text{C} & - \text{H} \\ & & & & & & \\ & \text{H} & & & & & \end{array} $	CH_3CHO o $\text{CH}_3\overset{\text{O}}{\underset{ }{\text{C}}}\text{H}$
acetona	$ \begin{array}{ccccccc} & \text{H} & & \ddot{\text{O}} & & \text{H} & \\ & & & & & & \\ \text{H} & - \text{C} & - & \text{C} & - & \text{C} & - \text{H} \\ & & & & & & \\ & \text{H} & & & & \text{H} & \end{array} $	CH_3COCH_3 o $\text{CH}_3\overset{\text{O}}{\underset{ }{\text{C}}}\text{CH}_3$
ácido acético	$ \begin{array}{ccccccc} & \text{H} & & \ddot{\text{O}} & & & \\ & & & & & & \\ \text{H} & - \text{C} & - & \text{C} & - \ddot{\text{O}} & - \text{H} \\ & & & & & & \\ & \text{H} & & & & & \end{array} $	CH_3COOH o $\text{CH}_3\overset{\text{O}}{\underset{ }{\text{C}}}-\text{OH}$ o $\text{CH}_3\text{CO}_2\text{H}$

completamente desarrolladas. El estudiante debería trabajar con las diferentes formas de representar las fórmulas para entender su significado.

PROBLEMA 1.9

Represente las estructuras de Lewis completas para las siguientes fórmulas estructurales condensadas:

- (a) $\text{CH}_3(\text{CH}_2)_3\text{CH}(\text{CH}_3)_2$ (b) $(\text{CH}_3)_2\text{CHCH}_2\text{Cl}$ (c) $\text{CH}_3\text{CH}_2\text{COCHCH}_2$
 (d) $\text{CH}_3\text{CH}_2\text{CHO}$ (e) CH_3COCN (f) $(\text{CH}_3)_3\text{CCOOH}$ (g) $(\text{CH}_3\text{CH}_2)_2\text{CO}$

1.10B Fórmulas lineoangulares

Otra forma de representar las estructuras orgánicas es la **fórmula lineoangular**, algunas veces llamada **estructura esquelética** o de barras. Las fórmulas lineoangulares con frecuencia se usan en los compuestos cíclicos y muy ocasionalmente en los lineales. En una fórmula lineoangular, los enlaces están representados por líneas y los átomos de carbono vienen dados por los vértices o puntos de encuentro de dos líneas, o el punto del principio o final de la línea en el caso de los extremos. Los átomos de nitrógeno, de oxígeno y los halógenos se escriben con su símbolo, pero los átomos de hidrógeno frecuentemente no se simbolizan a no ser que vayan unidos a elementos que se han simbolizado. Se supone que cada átomo de carbono tiene los suficientes átomos de hidrógeno para que el total de sus enlaces sea cuatro. Los electrones no enlazantes raramente se representan. La Tabla 1.4 muestra algunos ejemplos de estas representaciones lineoangulares.

TABLA 1.4 Ejemplos de representaciones lineoangulares

Compuesto	Estructura condensada	Fórmula lineoangular
hexano	$\text{CH}_3(\text{CH}_2)_4\text{CH}_3$	
2-hexeno	$\text{CH}_3\text{CH}=\text{CHCH}_2\text{CH}_2\text{CH}_3$	
3-hexanol	$\text{CH}_3\text{CH}_2\text{CH}(\text{OH})\text{CH}_2\text{CH}_2\text{CH}_3$	
2-ciclohexenona		
2-metilciclohexanol		
ácido nicotínico (vitamina, también llamada niacina)		

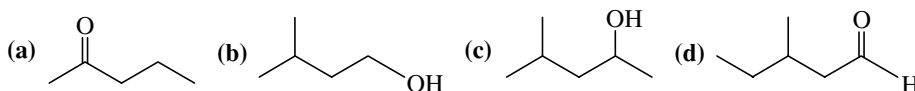
PROBLEMA 1.10

Escriba la estructura de Lewis correspondiente a las siguientes estructuras lineoangulares:

- (a)
- (b)
- (c)
- (d)
- (e)
- (f)
- (g)
- (h)

PROBLEMA 1.11

Represente las fórmulas estructurales condensadas correspondientes a las siguientes estructuras lineoangulares:



1.11

Fórmulas moleculares y fórmulas empíricas

Antes de poder escribir las posibles fórmulas estructurales de un compuesto, se necesita saber su fórmula molecular. La **fórmula molecular** simplemente informa del número de átomos de cada elemento que hay en una molécula de un compuesto. Por ejemplo, la fórmula molecular del 1-butanol es $C_4H_{10}O$.



1-butanol, fórmula molecular $C_4H_{10}O$

Cálculo de la fórmula empírica Las fórmulas moleculares se pueden determinar mediante un proceso que consta de dos pasos. El primer paso es la determinación de la **fórmula empírica**, o relación relativa entre los elementos presentes en la molécula. Suponga, por ejemplo, que en un compuesto desconocido, por análisis elemental cuantitativo, se encontró que contenía un 40.00% de carbono y un 6.67% de hidrógeno. La masa restante, 53.33%, se supone que era oxígeno. Para pasar esos números a una fórmula empírica, se puede seguir un procedimiento simple:

1. Suponga que la muestra contiene 100 g, por lo que los valores porcentuales dan el número de gramos de cada elemento. Dividiendo el número de gramos de cada elemento por la masa atómica se obtiene el número de moles de ese átomo en los 100 g de muestra.
2. Divida cada uno de los números de moles obtenidos en el paso anterior por el número más pequeño y redondee a la cifra entera más próxima. Este paso ha de conducir a la relación existente, expresada en números enteros, entre los elementos de la molécula.

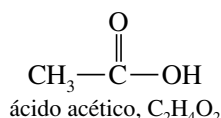
Para el compuesto desconocido, con los datos anteriores y siguiendo los pasos indicados, se obtendrían los siguientes resultados:

$$\begin{array}{lcl} \frac{40.0 \text{ g C}}{12.0 \text{ g/mol}} = 3.33 \text{ mol C;} & \frac{3.33 \text{ mol}}{3.33 \text{ mol}} = 1 \\ \frac{6.67 \text{ g H}}{1.01 \text{ g/mol}} = 6.60 \text{ mol H;} & \frac{6.60 \text{ mol}}{3.33 \text{ mol}} = 1.98 \approx 2 \\ \frac{53.3 \text{ g O}}{16.0 \text{ g/mol}} = 3.33 \text{ mol O;} & \frac{3.33 \text{ mol}}{3.33 \text{ mol}} = 1 \end{array}$$

En el primer cálculo se divide el número de gramos de carbono por 12, el número de gramos de hidrógeno por 1 y el número de gramos de oxígeno por 16. Se comparan los resultados dividiendo todos los valores obtenidos por el número más pequeño, 3.33. El resultado final da una relación de un átomo de carbono por dos de hidrógeno y uno de oxígeno. Este resultado nos dice que la fórmula empírica es $C_1H_2O_1$ o CH_2O , que muestra solamente la relación de los elementos. La fórmula molecular puede ser un múltiplo cualquiera de la fórmula empírica, porque cualquier múltiplo también tiene la misma relación numérica entre los átomos de sus elementos. Fórmulas moleculares posibles son CH_2O , $C_2H_4O_2$, $C_3H_6O_3$, $C_4H_8O_4$, etc.

Cálculo de la fórmula molecular ¿Cómo se sabe cuál es la fórmula molecular correcta? Se puede elegir el verdadero múltiplo de la fórmula empírica cuando se conoce la masa molecular. Las masas moleculares de una sustancia se pueden determinar por métodos como el *descenso crioscópico* o el *aumento ebulloscópico* de un disolvente cuando contiene la sustancia desconocida a una concentración molar. Si el compuesto es volátil, se puede convertir en gas y utilizar su volumen para determinar el número de moles por la *ley de los gases ideales*. En la actualidad existen métodos entre los que se incluye la *espectrometría de masas*, que será tratada en el Capítulo 11.

Para el ejemplo anterior (fórmula empírica: CH_2O) supondremos que la masa molecular es aproximadamente 60. La masa de una unidad de CH_2O es 30, por lo que el compuesto contendrá el doble número de átomos. La fórmula molecular será $\text{C}_2\text{H}_4\text{O}_2$. Este compuesto podría ser el ácido acético.



En los Capítulos 12, 13 y 15 se usarán técnicas espectroscópicas para determinar la estructura completa de un compuesto una vez que se conozca su fórmula molecular.

PROBLEMA 1.12

Escriba la fórmula empírica y la fórmula molecular a partir de los análisis elementales siguientes. En cada caso, proponga al menos una estructura que corresponda a la fórmula molecular.

	C	H	N	Cl	PM(*)
(a)	40.0%	6.67%	0	0	90
(b)	32.0%	6.67%	18.7%	0	75
(c)	37.2%	7.75%	0	55.0%	64
(d)	38.4%	4.80%	0	56.8%	125

(*) Peso molecular.

SUGERENCIA

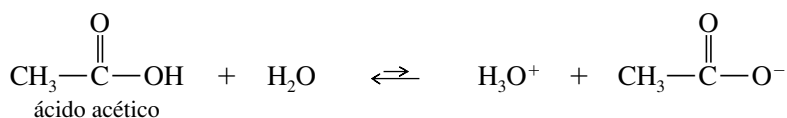
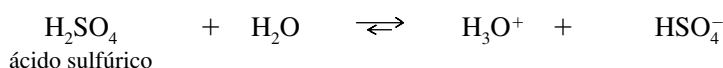
PARA RESOLVER PROBLEMAS

Si un análisis elemental no suma el 100%, el porcentaje que falta se supone que es de oxígeno.

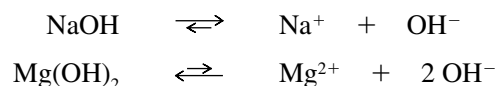
Las propiedades y la reactividad de los ácidos y de las bases son fundamentales para el estudio de la química orgánica. Hay que saber exactamente qué quieren decir los términos **ácido** y **base**. La mayoría de la gente estaría de acuerdo en que el H_2SO_4 es un ácido y el NaOH una base. ¿El BF_3 es un ácido o es una base? ¿El etileno ($\text{H}_2\text{C}=\text{CH}_2$) es un ácido o una base? Para responder a estas preguntas se necesitan entender las tres definiciones diferentes de los ácidos y de las bases: la definición de Arrhenius, la de Brønsted-Lowry y la de Lewis.

La primera clasificación de los compuestos ácidos se hizo basándose en su sabor agrio. Los términos latinos *acidus* (agrio) y *acetum* (vinagre) dieron lugar a los términos actuales de *ácido* y *ácido acético*. Los compuestos alcalinos (bases) eran sustancias que neutralizaban a los ácidos, tales como la caliza y las cenizas de las plantas (en árabe, *al kalai*).

La *teoría de Arrhenius* se desarrolló al final del siglo diecinueve y definía los ácidos como sustancias que se disocian en el agua para formar iones H_3O^+ . Se asumió que los ácidos más fuertes, tales como el ácido sulfúrico (H_2SO_4), se disociaban mucho más que los ácidos débiles, tales como el ácido acético (CH_3COOH).



Según la definición de Arrhenius, las bases son sustancias que se disocian en solución acuosa para formar iones hidroxilo. Por otra parte se consideró que las bases fuertes, tales como el NaOH , se disociaban más que las débiles o que aquellas que se disuelven moderadamente, como el $\text{Mg}(\text{OH})_2$.



La acidez o basicidad de una solución acuosa (agua) de una sustancia se mide por la concentración de H_3O^+ en dicha disolución. Este valor también permite conocer implícitamente la concentración de OH^- , ya que estas dos concentraciones están relacionadas entre sí por la constante de ionización del agua:

$$K_w = [\text{H}_3\text{O}^+][\text{OH}^-] = 1.00 \times 10^{-14} \quad (\text{a } 24^\circ\text{C})$$

1.12

Ácidos y bases de Arrhenius

En las soluciones neutras la concentración de $[\text{H}_3\text{O}^+]$ y de $[\text{OH}^-]$ son iguales,

$$[\text{H}_3\text{O}^+] = [\text{OH}^-] = 1.0 \times 10^{-7} \text{ M} \text{ en una solución neutra}$$

Las soluciones ácidas y básicas poseen un exceso de $[\text{H}_3\text{O}^+]$ o de $[\text{OH}^-]$, respectivamente.

$$\text{ácidas: } [\text{H}_3\text{O}^+] > 10^{-7} \text{ M} \text{ y } [\text{OH}^-] < 10^{-7} \text{ M}$$

$$\text{básicas: } [\text{H}_3\text{O}^+] < 10^{-7} \text{ M} \text{ y } [\text{OH}^-] > 10^{-7} \text{ M}$$

Como estas concentraciones pueden abarcar un amplio rango de valores, la acidez o basicidad de una solución normalmente se mide en escala logarítmica. El **pH** se define como el logaritmo (en base 10), cambiado de signo, de la concentración de H_3O^+ .

$$\text{pH} = -\log_{10}[\text{H}_3\text{O}^+]$$

Una solución neutra tiene un pH de 7, una solución ácida tiene un pH menor que 7 y una solución básica tiene un pH mayor que 7.

PROBLEMA 1.13

Calcule el pH de las siguientes soluciones:

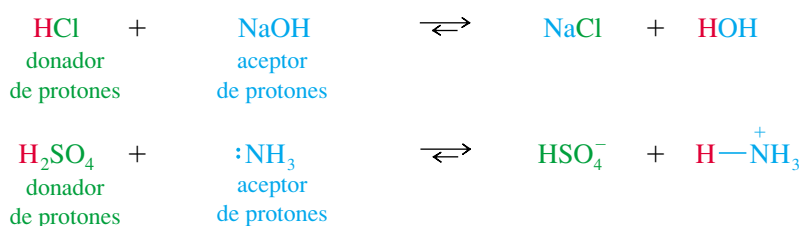
- (a) 5.00 g de HBr en 100 mL de solución acuosa.
- (b) 1.50 g de NaOH en 50 mL de solución acuosa.

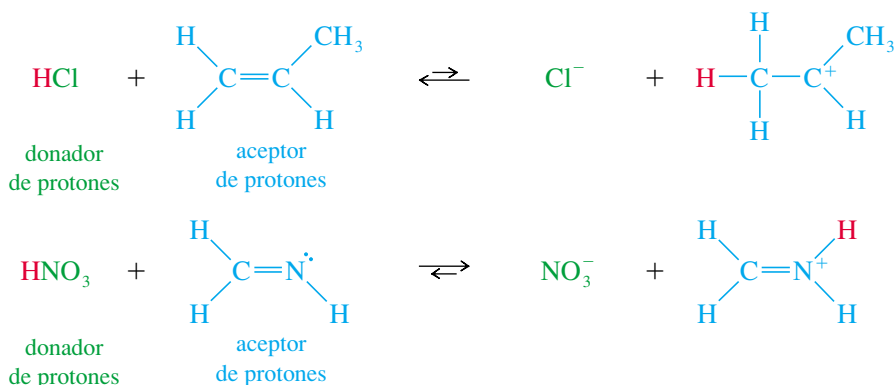
La definición de Arrhenius fue una contribución importante para poder entender muchos ácidos y muchas bases, pero no explica por qué un compuesto como el amoníaco (NH_3) neutraliza los ácidos, a pesar de no tener un ión hidróxido en su fórmula molecular. En la Sección 1.13 se explica una teoría más versátil de ácidos y bases que incluye al amoníaco y a una variedad más amplia de ácidos y bases orgánicos.

1.13 Ácidos y bases de Brønsted-Lowry

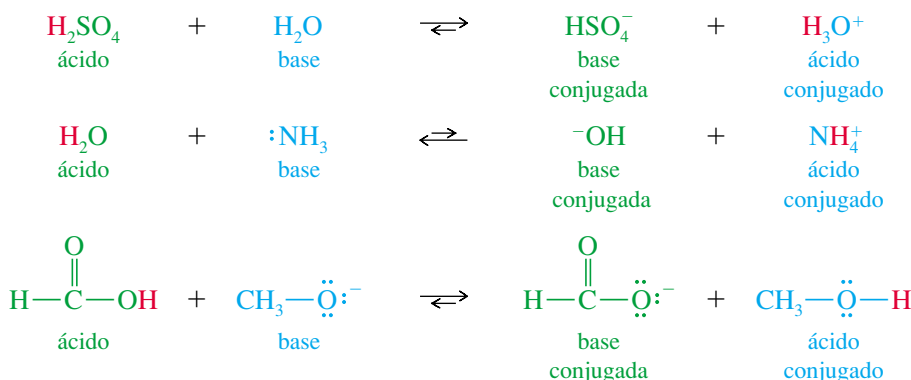
En 1923, Brønsted y Lowry definieron los ácidos y las bases teniendo en cuenta su capacidad de liberar o captar protones, respectivamente. Un **ácido de Brønsted-Lowry** es cualquier especie que puede donar un protón, y una **base de Brønsted-Lowry** es cualquier especie que puede aceptar un protón. Estas definiciones también incluyen todos los ácidos y bases de Arrhenius, ya que los compuestos que se disocian para dar H_3O^+ son donadores de protones y los compuestos que se disocian para dar OH^- son aceptores de protones (el ión hidróxido acepta un protón para formar H_2O).

Además de los ácidos y bases de Arrhenius, la definición de Brønsted-Lowry incluye también las bases que no tienen iones hidróxido, y que pueden aceptar protones. Observa los ejemplos siguientes de ácidos capaces de ceder protones a las bases. El NaOH es una base tanto si se considera la definición de Arrhenius o la de Brønsted-Lowry. Los tres ejemplos siguientes son bases de Brønsted-Lowry pero no bases de Arrhenius, ya que no tienen iones hidróxido.



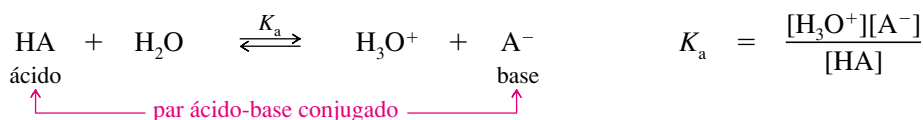


Cuando una base acepta un protón, se convierte en un ácido capaz de devolver ese protón. Cuando un ácido cede un protón, se convierte en una base capaz de aceptar de nuevo ese protón. Uno de los principios más importantes de la definición de Brønsted-Lowry es el concepto de **ácidos y bases conjugados**. Por ejemplo, el NH_3 y el NH_4^+ forman un par de ácido y base conjugados; el NH_3 es la base, cuando acepta un protón, se transforma en el ácido conjugado, NH_4^+ . Muchos compuestos (por ejemplo, el agua) pueden reaccionar como un ácido o como una base. A continuación se dan algunos ejemplos de pares ácido-base conjugados:



1.13A Fuerza de los ácidos

La fuerza de un ácido de Brønsted-Lowry se expresa de forma similar a la definición de Arrhenius, teniendo en cuenta su grado de ionización en agua. La reacción general de un ácido (HA) con agua es la siguiente:



A la K_a se la conoce con el nombre de *constante de disociación del ácido* y su valor indica la fuerza relativa del ácido. Cuanto más fuerte es el ácido, más se disocia, dando un valor de K_a mayor. Las constantes de disociación de un ácido varían en un intervalo amplio. Los ácidos fuertes se ionizan casi completamente en agua y sus constantes de disociación son superiores a 1. La mayoría de los ácidos orgánicos son ácidos débiles, con valores de K_a menores que 10^{-4} . Muchos compuestos orgánicos son ácidos extremadamente débiles; por ejemplo, el metano y el etano tienen un carácter ácido muy débil, su K_a es inferior a 10^{-40} .

Debido a este amplio margen de valores, las constantes de disociación ácida frecuentemente se expresan en escala logarítmica. El $\text{p}K_a$ de un ácido se define de forma parecida al pH: logaritmo (en base 10), con signo negativo, de la K_a .

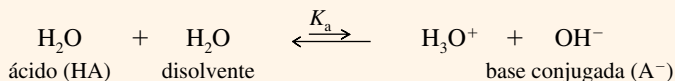
$$\text{p}K_a = -\log_{10} K_a$$

PROBLEMA RESUELTO 1.3

Calcule la K_a y el pK_a del agua.

SOLUCIÓN

El equilibrio que define la K_a del agua es:



El agua se comporta en esta disolución como ácido y como disolvente. La expresión del equilibrio es:

$$K_a = \frac{[\text{H}_3\text{O}^+][\text{A}^-]}{[\text{HA}]} = \frac{[\text{H}_3\text{O}^+][\text{OH}^-]}{[\text{H}_2\text{O}]}$$

Donde $[\text{H}_3\text{O}^+][\text{OH}^-] = 1.00 \times 10^{-14}$, constante del producto de ionización del agua.

La concentración de moléculas de H_2O en el agua simplemente es el número de moles de agua en 1 L (aproximadamente 1 kg).

$$\frac{1000 \text{ g/L}}{18 \text{ g/mol}} = 55.6 \text{ mol/L}$$

Haciendo la sustitución:

$$K_a = \frac{[\text{H}_3\text{O}^+][\text{OH}^-]}{[\text{H}_2\text{O}]} = \frac{1.00 \times 10^{-14}}{55.6} = 1.8 \times 10^{-16} \text{ M}$$

El logaritmo de 1.8×10^{-16} es -15.7 , por lo que el pK_a del agua es 15.7 .

**SUGERENCIA
PARA RESOLVER PROBLEMAS**

En la mayor parte de los casos, el pK_a de un ácido coincide con el valor del pH de un ácido disociado en un 50%. A un pH menor (más ácido), el ácido estará menos disociado; a un pH mayor (más básico), el ácido estará más disociado.

Los ácidos fuertes generalmente tienen valores de pK_a próximos a 0 y los ácidos débiles, como la mayoría de los ácidos orgánicos, tienen valores superiores a 4. *Los ácidos más débiles tienen valores de pK_a más elevados.* La Tabla 1.5 recoge los valores de K_a y pK_a de algunos de los compuestos inorgánicos y orgánicos más habituales. Observa que los valores de pK_a aumentan cuando los valores de K_a disminuyen.

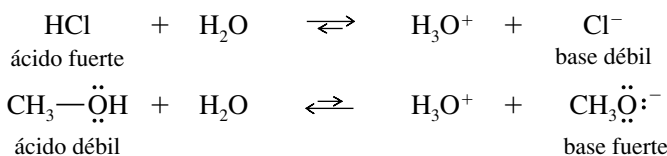
PROBLEMA 1.14

El amoníaco se encuentra en la Tabla 1.5 de dos formas, la forma básica y su ácido conjugado.

- Explique cómo el amoníaco puede actuar como base y como ácido. ¿Cuál de estas dos formas es más habitual en las soluciones acuosas?
- Explique por qué el agua puede actuar como ácido y como base.
- Explique por qué el metanol (CH_3OH) puede comportarse como ácido y como base. Escriba una ecuación para la reacción del metanol con el ácido sulfúrico.

1.13B Fuerza de las bases

La fuerza de un ácido es inversa a la fuerza de su base conjugada. Si un ácido (HA) es fuerte, su base conjugada (A^-) será débil, al ser estable en su forma aniónica; de lo contrario, el ácido HA no perdería fácilmente sus protones. Por lo tanto, la base conjugada de un ácido fuerte será una base débil. Por otra parte, si un ácido es débil, su conjugado es una base fuerte.

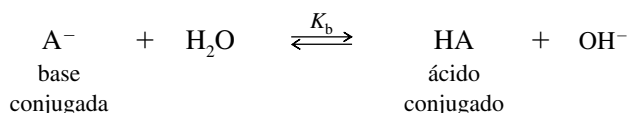


En la reacción de un ácido con una base, el equilibrio generalmente está desplazado hacia la formación de los ácidos y bases *débiles*. Por ejemplo, en las reacciones anteriores, el H_3O^+ es un ácido más débil que el HCl, pero un ácido más fuerte que el CH_3OH ; esto conlleva que el H_2O sea una base más fuerte que el Cl^- , pero más débil que el CH_3O^- .

TABLA 1.5 Fuerza relativa de algunos ácidos inorgánicos y orgánicos frecuentes, y sus bases conjugadas

	Ácido		Base conjugada	K_a	pK_a
ácidos fuertes	HCl ácido clorhídrico	$+ H_2O \rightleftharpoons H_3O^+ + Cl^-$	ion cloruro	1.6×10^2	-2.2
	HF ácido fluorhídrico	$+ H_2O \rightleftharpoons H_3O^+ + F^-$	ion fluoruro	6.8×10^{-4}	3.17
	$\begin{array}{c} O \\ \\ H-C-OH \end{array}$ ácido fórmico	$+ H_2O \rightleftharpoons H_3O^+ + \begin{array}{c} O \\ \\ H-C-O^- \end{array}$	ion formiato	1.7×10^{-4}	3.76
	$\begin{array}{c} O \\ \\ CH_3-C-OH \end{array}$ ácido acético	$+ H_2O \rightleftharpoons H_3O^+ + \begin{array}{c} O \\ \\ CH_3-C-O^- \end{array}$	acetano ion	1.8×10^{-5}	4.74
ácidos débiles	$H-C \equiv N:$ ácido cianhídrico	$+ H_2O \rightleftharpoons H_3O^+ + :C \equiv N:$	ion cianuro	6.0×10^{-10}	9.22
	$^+NH_4$ ion amonio	$+ H_2O \rightleftharpoons H_3O^+ + :NH_3$	amoniaco	5.8×10^{-10}	9.24
	CH_3-OH alcohol metílico	$+ H_2O \rightleftharpoons H_3O^+ + CH_3O^-$	metóxido ion	3.2×10^{-16}	15.5
	H_2O agua	$+ H_2O \rightleftharpoons H_3O^+ + HO^-$	ion hidróxido	1.8×10^{-16}	15.7
muy débil	NH_3 amoniaco	$+ H_2O \rightleftharpoons H_3O^+ + :\ddot{N}H_2$	ion amiduro	10^{-33}	33
no ácido	CH_4 metano	$+ H_2O \rightleftharpoons H_3O^+ + :\ddot{C}H_3$	anión metilo	$<10^{-40}$	>40

La fuerza de una base se mide de forma similar a la de los ácidos, usando la constante de equilibrio de la reacción de hidrólisis:



La constante de equilibrio (K_b) para esta reacción se conoce con el nombre de *constante de disociación de la base* para la base A^- . Debido a que esta constante tiene un amplio rango de valores, frecuentemente se expresa en forma logarítmica. El pK_b se define como el logaritmo (en base 10), cambiado de signo, de la K_b .

$$K_b = \frac{[HA][OH^-]}{[A^-]} \quad pK_b = -\log_{10} K_b$$

Cuando se multiplica K_a por K_b , se puede apreciar cómo la acidez de un ácido está relacionada con la basicidad de su base conjugada:

Las propiedades ácido-base de muchos productos naturales son importantes de cara a su aislamiento, a su distribución en el cuerpo y a justificar sus efectos terapéuticos. Por ejemplo, la morfina (p. 2), que se aísla de las adormideras (opio), llega al cerebro como base libre, en la que el nitrógeno no está cargado. Sin embargo, son sus especies cargadas las que actúan como analgésicas.

$$(K_a)(K_b) = \frac{[\text{H}_3\text{O}^+][\text{A}^-]}{[\text{HA}]} \frac{[\text{HA}][\text{OH}^-]}{[\text{A}^-]} = [\text{H}_3\text{O}^+][\text{OH}^-] = 1.0 \times 10^{-14}$$

constante del producto de ionización del agua

$$(K_a)(K_b) = 10^{-14}$$

Aplicando logaritmos:

$$\text{p}K_a + \text{p}K_b = -\log 10^{-14} = 14$$

El producto de K_a por K_b siempre es igual a la constante del producto iónico del agua, 10^{-14} . Si el valor de K_a es grande, el valor de K_b será pequeño; es decir, cuanto más fuerte es un ácido, más débil es su base conjugada. De forma similar, un valor pequeño de K_a (ácido débil) implica un valor grande de K_b (base fuerte).

Cuanto más fuerte es un ácido, más débil es su base conjugada.

Cuanto más débil es un ácido, más fuerte es su base conjugada.

Las reacciones ácido-base favorecen la formación de ácidos más débiles y/o bases más débiles.

SUGERENCIA PARA RESOLVER PROBLEMAS

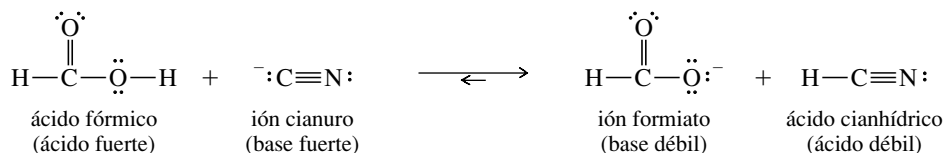
Un ácido donará un protón a la base conjugada de cualquier ácido que sea más débil (menor K_a o mayor $\text{p}K_a$).

PROBLEMA 1.15 (parcialmente resuelto)

Escriba las ecuaciones para las siguientes reacciones ácido-base. Utilice la información de la Tabla 1.5 para predecir si el equilibrio favorecerá a los reactivos o a los productos.

- | | |
|--|--|
| (a) $\text{HCOOH} + ^-\text{CN}$ | (b) $\text{CH}_3\text{COO}^- + \text{CH}_3\text{OH}$ |
| (c) $\text{CH}_3\text{OH} + \text{NaNH}_2$ | (d) $\text{NaOCH}_3 + \text{HCN}$ |
| (e) $\text{HCl} + \text{H}_2\text{O}$ | (f) $\text{H}_3\text{O}^+ + \text{CH}_3\text{O}^-$ |

Solución para (a): el ión cianuro es la base conjugada del HCN; puede aceptar un protón del ácido fórmico:



Observando la Tabla 1.5, se aprecia que el ácido fórmico ($\text{p}K_a = 3.76$) es un ácido más fuerte que el HCN ($\text{p}K_a = 9.22$) y que el cianuro es una base más fuerte que el formiato. Resultan favorecidos, pues, los productos ácido y base más débiles.

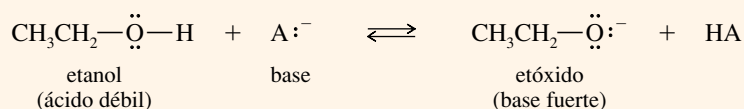
PROBLEMA RESUELTO 1.4

Cada uno de los compuestos siguientes puede actuar como un ácido. Escriba la reacción de cada compuesto con una base general (A^-) y la estructura de Lewis de la base conjugada que se obtiene.

- | | | |
|---------------------------------------|------------------------------|------------------------------|
| (a) $\text{CH}_3\text{CH}_2\text{OH}$ | (b) CH_3NH_2 | (c) CH_3COOH |
|---------------------------------------|------------------------------|------------------------------|

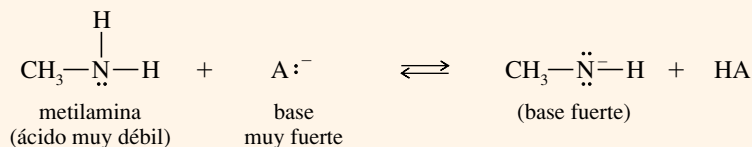
SOLUCIÓN

- (a) El etanol ($\text{CH}_3\text{CH}_2\text{OH}$) puede perder el protón del grupo $\text{O}-\text{H}$ para formar una base conjugada que es un ión orgánico análogo al ión hidroxilo.

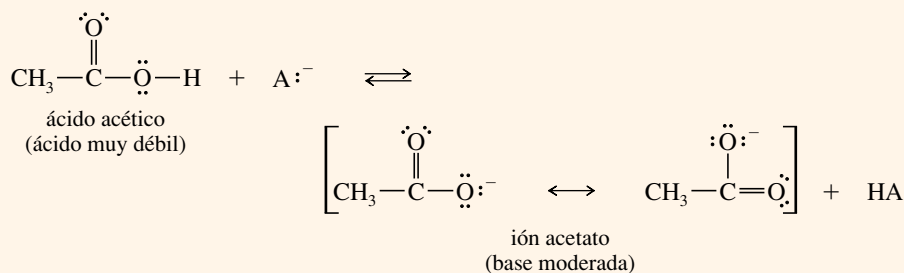


(Los protones del grupo $\text{C}-\text{H}$ son mucho menos ácidos que los protones del grupo $\text{O}-\text{H}$, porque el carbono es menos electronegativo que el oxígeno y, por lo tanto, la carga negativa es menos estable en el carbono.)

- (b) La metilamina (CH_3NH_2) es un ácido muy débil. Una base muy fuerte le puede sustraer un protón y dar lugar a una base conjugada fuerte.



- (c) El ácido acético (CH_3COOH) es un ácido moderadamente fuerte. Su base conjugada es el ión acetato que está estabilizado por resonancia.

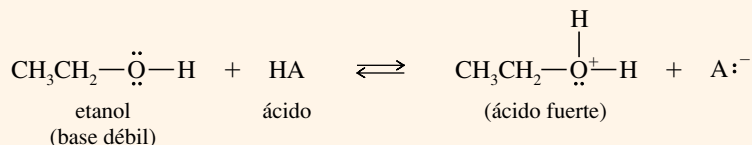


PROBLEMA RESUELTO 1.5

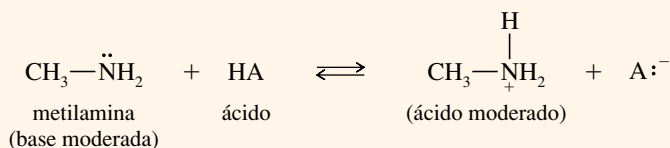
Cada uno de los compuestos del Problema resuelto 1.4 también pueden reaccionar como una base. Escriba la reacción de cada compuesto con un ácido general (HA) y las estructuras de Lewis del ácido conjugado que se obtiene.

SOLUCIÓN

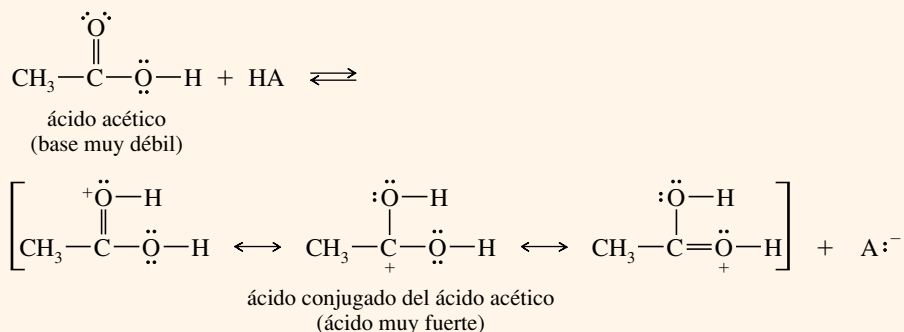
- (a) El etanol puede protonarse en su átomo de oxígeno. Observe que uno de los pares solitarios del oxígeno forma el nuevo enlace $\text{O}-\text{H}$.



- (b) El átomo de nitrógeno de la metilamina tiene un par de electrones que pueden enlazarse con un protón.



- (c) El ácido acético tiene electrones no enlazantes en los dos átomos de oxígeno. Cada uno de estos átomos de oxígeno podría protonarse, pero la protonación de oxígeno que forma parte del doble enlace está favorecida porque la protonación de este oxígeno da lugar a un ácido conjugado simétrico y estabilizado por resonancia.



PROBLEMA 1.16

El Problema resuelto 1.5(c) muestra la protonación del oxígeno con doble enlace del ácido acético. Escriba el producto obtenido de la protonación en el otro oxígeno (—OH). Explique por qué la protonación del oxígeno con doble enlace está favorecida.

PROBLEMA 1.17

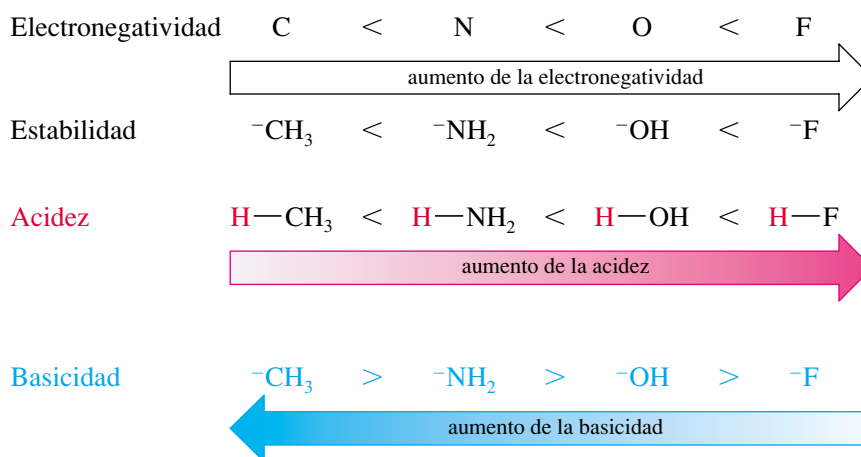
- (a) Ordene por orden decreciente de acidez el etanol, la metilamina y el ácido acético.
 (b) Ordene por orden decreciente de basicidad el etanol, la metilamina ($\text{p}K_b = 3.36$) y el ión etóxido ($\text{CH}_3\text{CH}_2\text{O}^-$). En cada caso, explique las razones de este orden.

1.13C Efectos estructurales en la acidez

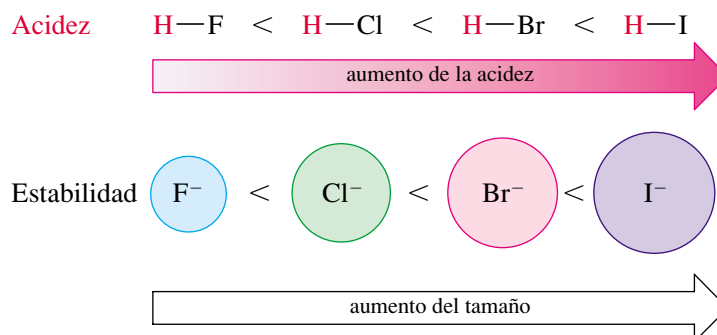
Cuando se observa una estructura, ¿cómo se puede predecir si el compuesto será un ácido fuerte o débil, o bien si no tendrá nada de carácter ácido? Según la teoría de Brønsted-Lowry, un ácido (HA) es un compuesto que ha de contener un átomo de hidrógeno que puede ser cedido como un protón. Un ácido fuerte debe formar una base conjugada estable (A^-) después de perder el protón.

La estabilidad de la base conjugada es una buena guía para conocer la fuerza del ácido. Los aniones más estables tienden a ser bases más débiles y sus ácidos conjugados tienden a ser ácidos más fuertes. Algunos de los factores que afectan a la estabilidad de las bases conjugadas son la electronegatividad, el tamaño y la resonancia.

Electronegatividad Cuanto más electronegativo sea un elemento, será capaz de adquirir una carga negativa con más facilidad, lo que dará lugar a una base conjugada más estable y a un ácido fuerte. La electronegatividad aumenta de izquierda a derecha en la tabla periódica.



Tamaño La carga negativa de un anión es más estable cuando se distribuye sobre una región del espacio más amplia. Si se considera una columna de la tabla periódica, la acidez aumenta hacia abajo, a medida que el tamaño de los elementos aumenta.



Estabilización por resonancia La carga negativa de una base conjugada puede estar deslocalizada entre dos o más átomos, y estabilizada por resonancia. Dependiendo de la electronegatividad que tengan esos átomos y de cómo se comparta esa carga, la deslocalización por resonancia con frecuencia es el efecto dominante que ayuda a la estabilización del anión. Observe las bases conjugadas siguientes:

Base conjugada	Ácido	pK _a
$\text{CH}_3\text{CH}_2-\ddot{\text{O}}:^-$ ión etóxido	$\text{CH}_3\text{CH}_2-\text{OH}$ etanol	15.9 (ácido débil)
$\left[\text{CH}_3-\overset{\text{O}}{\underset{\cdot\cdot}{\parallel}}\text{C}-\ddot{\text{O}}:^- \longleftrightarrow \text{CH}_3-\overset{\cdot\cdot}{\underset{\cdot\cdot}{\text{O}}}=\text{C}-\ddot{\text{O}}:^- \right]$ ión acetato	$\text{CH}_3-\overset{\text{O}}{\parallel}\text{C}-\text{OH}$ ácido acético	4.74 (ácido moderado)
$\left[\text{CH}_3-\overset{\text{O}}{\underset{\cdot\cdot}{\parallel}}\text{S}-\ddot{\text{O}}:^- \longleftrightarrow \text{CH}_3-\overset{\cdot\cdot}{\underset{\cdot\cdot}{\text{O}}}=\text{S}-\ddot{\text{O}}:^- \longleftrightarrow \text{CH}_3-\overset{\cdot\cdot}{\underset{\cdot\cdot}{\text{O}}}=\text{S}-\ddot{\text{O}}:^- \right]$ ión metanosulfonato	$\text{CH}_3-\overset{\text{O}}{\parallel}\text{S}-\text{OH}$ ácido metanosulfónico	-1.2 (ácido fuerte)

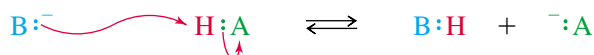
El ión etóxido es el más fuerte de las tres bases anteriores. El etóxido tiene una carga negativa localizada en un átomo de oxígeno; el ión acetato tiene una carga negativa compartida por dos átomos de oxígeno y el ión metanosulfonato tiene una carga negativa extendida sobre tres átomos de oxígeno. Los valores de los pK_a de los ácidos conjugados de esos aniones muestran que los ácidos son más fuertes si su desprotonación da lugar a bases conjugadas estabilizadas por resonancia.

PROBLEMA 1.18

Escriba las ecuaciones correspondientes a las reacciones ácido-base siguientes. Señale los ácidos y bases conjugados y justifique, si es el caso, su estabilización por resonancia escribiendo las posibles formas resonantes. Prediga si el equilibrio está desplazado hacia los reactivos o hacia los productos.

- (a) $\text{CH}_3\text{CH}_2\text{OH} + \text{CH}_3\text{NH}^-$ (b) $\text{CH}_3\text{CH}_2\text{COOH} + \text{CH}_3\text{NHCH}_3$
 (c) $\text{CH}_3\text{OH} + \text{H}_2\text{SO}_4$ (d) $\text{NaOH} + \text{H}_2\text{S}$
 (e) $\text{CH}_3\text{NH}_3^+ + \text{CH}_3\text{O}^-$ (f) $\text{CH}_3\text{O}^- + \text{CH}_3\text{COOH}$
 (g) $\text{CH}_3\text{SO}_3^- + \text{CH}_3\text{COOH}$

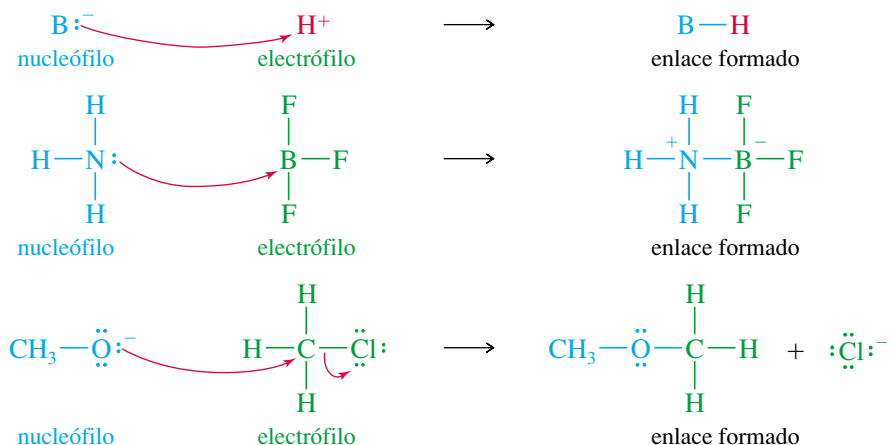
La definición de Brönsted-Lowry de ácidos y bases depende de la transferencia de un protón del ácido a la base. La base utiliza un par de electrones no enlazantes para formar un enlace con el protón. G. N. Lewis pensó que esta clase de reacciones no necesitaba obligatoriamente un protón para tener lugar. Una base podría usar su par solitario de electrones para enlazarse a algún otro átomo deficiente en electrones. En efecto, puede haber reacciones ácido-base desde el punto de vista de los *enlaces* que se forman y rompen, sin necesidad de que se transfiera un protón. La siguiente reacción muestra la transferencia del protón haciendo hincapié en los enlaces que se forman y que se rompen. Los químicos orgánicos utilizan de forma rutinaria flechas curvadas para mostrar el movimiento de los electrones que participan,



Las **bases de Lewis** son especies con electrones no enlazantes que pueden ser cedidos para formar nuevos enlaces. Los **ácidos de Lewis** son especies que pueden aceptar esos pares de electrones para formar nuevos enlaces. Debido a que un ácido de Lewis *acepta* un par de electrones, se le conoce como **electrófilo**, palabra derivada del griego, que significa «amante de electrones». A la base de Lewis se le llama **nucleófilo**, o «amante de los núcleos», ya que cede electrones a un núcleo que tenga un orbital vacío (o prácticamente vacío). En este libro, a veces se usan caracteres coloreados para enfatizar: azul para los nucleófilos, verde para los electrófilos y ocasionalmente rojo para los protones ácidos.

1.14 Ácidos y bases de Lewis

Las definiciones ácido-base de Lewis incluyen reacciones que no tienen ninguna relación con los protones. A continuación se muestran algunos ejemplos de reacciones ácido-base de Lewis. Observe que los ácidos y las bases de Brønsted-Lowry también están incluidos dentro de la definición de Lewis, siendo el protón un electrófilo. Las flechas curvadas (rojas) se usan para mostrar el movimiento de los electrones, generalmente desde el nucleófilo al electrófilo.

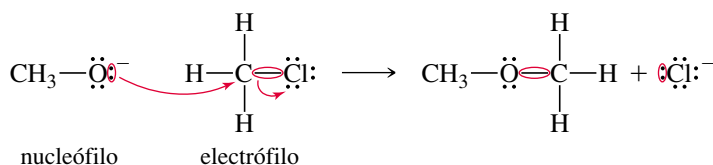


Algunos de los términos asociados con los ácidos y bases poseen significados específicos en química orgánica. Cuando un químico orgánico utiliza el término *base*, normalmente quiere decir «aceptor de protones» (una base de Brønsted-Lowry). De manera similar, el término *ácido* normalmente implica a un protón ácido (un ácido de Brønsted-Lowry). Cuando una reacción ácido-base implica la formación de un enlace con otro elemento (especialmente carbono), un químico orgánico denomina al donador de electrones *nucleófilo* (base de Lewis) y al aceptor de electrones, *electrófilo* (ácido de Lewis).

Las **flechas curvadas** se utilizan para mostrar el movimiento de un par de electrones *desde el donador de electrones al aceptor de electrones*. El movimiento de cada par de electrones implicado en formar o romper enlaces se indica por sus propias flechas separadas, como se muestra en las reacciones anteriores. En este libro, estas flechas curvadas se dibujan siempre en rojo. En la reacción anterior del CH_3O^- con CH_3Cl , una flecha curvada muestra el par solitario del oxígeno formando un enlace con el carbono; otra flecha curvada muestra que el par enlazante del $C-Cl$ se separa del átomo de carbono y se transforma en un par solitario formando el ión Cl^- .

SUGERENCIA PARA RESOLVER PROBLEMAS

Utilice una flecha curvada para cada par de electrones que participen en la reacción.



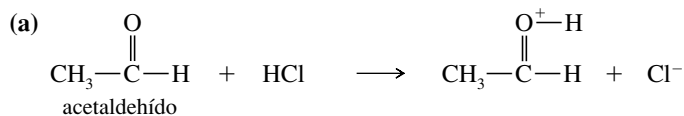
La flecha curvada se usa universalmente para seguir el camino del movimiento de los electrones en las reacciones; en este libro también se ha utilizado (en la Sección 1.9, por ejemplo) para seguir el movimiento de los electrones en las estructuras de resonancia, con objeto de representar el supuesto «flujo electrónico» cuando se pasaba de una estructura de resonancia a otra. Recuerde que los electrones no «fluyen» en las estructuras de resonancia, simplemente están deslocalizados. Este formalismo de las flechas nos ayuda, sin embargo, a comprender la interconversión entre las formas resonantes. Estas flechas curvadas se usan constantemente para seguir el camino de los electrones, tanto en el cambio de reactivos a productos como cuando imaginamos nuevas estructuras resonantes adicionales de un híbrido de resonancia.

PROBLEMA 1.19 (parcialmente resuelto)

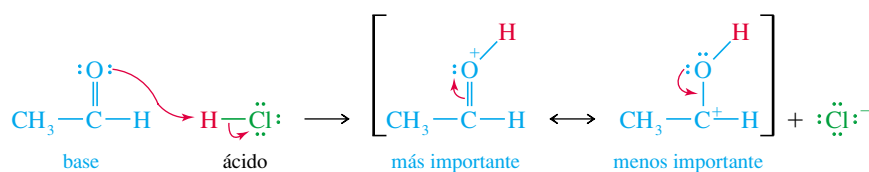
En las siguientes reacciones ácido-base:

- (1) Determine qué especies actúan como ácidos y cuáles como bases.
- (2) Utilice las flechas curvadas para mostrar el movimiento de los pares de electrones de las reacciones, así como el movimiento imaginario de electrones en los híbridos de resonancia de los productos.

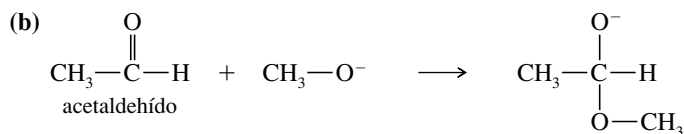
(3) Indique qué reacciones son las más apropiadas para poderlas incluir dentro de las reacciones ácido-base de Brønsted-Lowry.



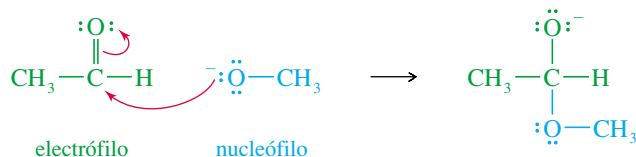
En esta reacción hay transferencia del protón del HCl al grupo C=O del acetaldehído, por tanto, es una reacción ácido-base de Brønsted-Lowry, donde el HCl actúa como ácido (donador de protones) y el acetaldehído actúa como base (aceptor de protones). Antes de dibujar una flecha curvada, recuerde que las flechas deben mostrar el movimiento de los electrones *desde* el donador del par de electrones (la base) *hasta* el aceptor del par de electrones (el ácido). Una flecha debe ir *desde* los electrones no enlazantes del acetaldehído *hasta* el átomo de hidrógeno del HCl y el enlace del ácido clorhídrico se ha de romper, con la formación del ión cloruro que ha captado los electrones del enlace H—Cl. Dibujar las flechas es fácil después de haber representado correctamente estructuras de Lewis de todos los reactivos y productos.



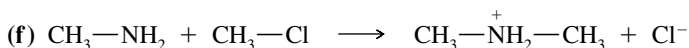
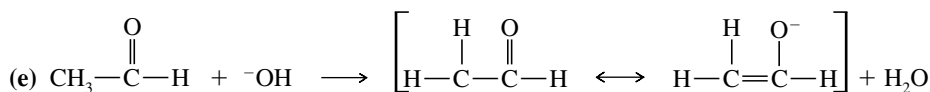
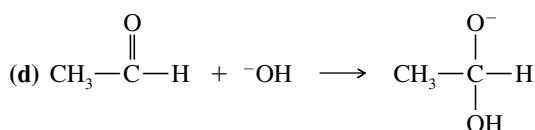
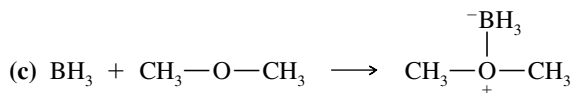
Las formas de resonancia del producto muestran que un par de electrones puede moverse entre el átomo de oxígeno y el enlace pi del C=O. La carga positiva está deslocalizada sobre los átomos de carbono y de oxígeno, con la mayor parte de la carga positiva sobre el oxígeno, ya que todos los octetos están completos en esa estructura de resonancia.



En este caso, ningún protón se ha transferido, por lo que no es una reacción ácido-base de Brønsted-Lowry. En su lugar, se ha formado un enlace entre el átomo de carbono del grupo C=O y el átomo de oxígeno del grupo CH₃—O[−]. Dibujar las estructuras de Lewis ayuda a ver que el grupo CH₃—O[−] (el nucleófilo en esta reacción) cede los electrones para formar el nuevo enlace con el acetaldehído (el electrófilo). Este resultado concuerda con la intuición de que un ión cargado negativamente es probablemente rico en electrones y por tanto un donador de electrones.



Observe que el acetaldehído actúa como nucleófilo (base) en (a) y como electrófilo en (b). Como la mayoría de los compuestos orgánicos, el acetaldehído puede ser tanto un ácido como una base. Actúa como una base si se le añade un ácido lo suficientemente fuerte para que ceda un par de electrones o capte un protón.



SUGERENCIA PARA RESOLVER PROBLEMAS

Las flechas curvadas se utilizan en los mecanismos para mostrar el *flujo de electrones* y no el movimiento de los átomos. Estas flechas curvadas se usarán constantemente a lo largo de este curso.

Glosario del Capítulo 1

Cada capítulo finaliza con un glosario que recoge los términos nuevos más importantes del capítulo. Estos glosarios son más que un diccionario en el que se buscan términos desconocidos conforme se los vaya encontrando (el índice sirve para este propósito). El glosario es una de las herramientas para revisar el capítulo, se puede leer cuidadosamente para saber si se entienden y se recuerdan todos los términos químicos mencionados. Cualquier concepto que no resulte familiar debería ser revisado volviendo a la página que aparece numerada en el mismo.

Ácido conjugado El ácido que resulta de la protonación de una base. (p. 23)

Ácido de Lewis, base de Lewis. Véase ácidos y bases.

Ácidos y bases (pp. 21-31)

(definiciones de Arrhenius)

(definiciones de Brønsted-Lowry)

(definiciones de Lewis)

Ácido: se disocia en agua para dar H_3O^+ .

Base: se disocia en agua para dar OH^- .

Ácido: donador de protones.

Base: aceptor de protones.

Ácido: aceptor de un par de electrones (electrófilo).

Base: donador de un par de electrones (nucleófilo).

Base conjugada La base que resulta de la pérdida de un protón de un ácido. (p. 23)

Cargas formales Método para hacer un seguimiento de las cargas, el cual permite mostrar qué carga habría en una determinada estructura de Lewis. (p. 11)

Densidad electrónica Probabilidad relativa de encontrar un electrón en una cierta región del espacio. (p. 3)

Electrófilo Aceptor de un par de electrones. (p. 29)

Electronegatividad Medida de la capacidad de un elemento para atraer electrones. Los elementos con electronegatividades más altas atraen a los electrones con más fuerza. (p. 10)

Electrones de valencia Electrones que se encuentran en la capa externa más alejada del núcleo. (p. 6)

Electrones no enlazantes Electrones de valencia que no se utilizan en el enlace. A un par de electrones no enlazantes con frecuencia se le denomina **par solitario**. (p. 7)

Enlace covalente Enlace que se forma por la compartición de electrones en la región que hay entre dos núcleos. (p. 7)

Enlace sencillo: enlace covalente en el que se comparte un par de electrones. (p. 8)

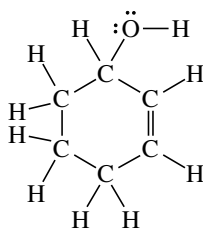
Enlace doble: enlace covalente en el que se comparte dos pares de electrones. (p. 8)

Enlace triple: enlace covalente en el que se comparte tres pares de electrones. (p. 8)

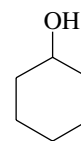
Enlace covalente polar Enlace covalente en el que los electrones se comparten de forma desigual. Cuando los electrones están igualmente compartidos se llama **enlace covalente no polar**. (p. 9)

Enlace iónico Enlace que se produce por la atracción de iones que tienen carga opuesta. El enlace iónico normalmente da lugar a la formación de una gran estructura cristalina en tres dimensiones. (p. 7)

Estructura de Lewis Fórmula estructural que muestra todos los electrones de valencia, con los enlaces simbolizados por líneas (—) o por pares de puntos, y los electrones no enlazantes simbolizados por puntos. (p. 7)



estructura de Lewis del 2-ciclohexenol



2-ciclohexenol
fórmula lineoangular equivalente

Flechas curvadas El dibujar flechas curvadas es un método que se utiliza para seguir el camino de los electrones cuando se mueven desde el nucleófilo al electrófilo (o dentro de una molécula) durante el transcurso de una reacción. (p. 30)

Fórmula empírica Relación numérica de los átomos en un compuesto. (p. 20). Véase también **fórmula molecular**.

Fórmula lineoangular (estructura esquelética o de barras) Fórmula estructural con enlaces representados por líneas; los átomos de carbono son los puntos de encuentro entre dos líneas o el final de la línea cuando está en el extremo de la cadena. Los átomos de nitrógeno, de oxígeno y los halógenos se representan, pero los átomos de hidrógeno no. Se supone que cada átomo de carbono tiene los hidrógenos suficientes para que en total tenga cuatro enlaces. (p. 19)

Fórmula molecular Número de átomos de cada elemento que forman parte de una molécula de un compuesto. La **fórmula empírica** simplemente da la relación de los átomos de los diferentes elementos. Por ejemplo, la fórmula molecular de la glucosa es $C_6H_{12}O_6$; su fórmula empírica es CH_2O . Ni la fórmula empírica ni la fórmula molecular dan información estructural. (p. 4)

Fórmulas estructurales Una **fórmula estructural completa** (tal como una estructura de Lewis) muestra todos los átomos y enlaces en la molécula. Una **fórmula estructural condensada** muestra cada átomo central y los átomos con los que está enlazado. Una **fórmula lineoangular** supone que hay un átomo de carbono donde dos líneas se encuentren, o donde la línea comience o termine. Véanse los ejemplos de la Sección 1.10. (p. 17)

Híbrido de resonancia Molécula o ión para el cual se pueden representar dos o más estructuras de Lewis válidas, diferenciándose solamente en la posición de los electrones de valencia. Estas estructuras de Lewis se conocen como **formas de resonancia** o **estructuras de resonancia**. Las formas de resonancia individuales no existen, pero se puede estimar sus energías relativas. A las estructuras más importantes (de energía más baja) se las conoce como **contribuyentes mayores**, y a las estructuras menos importantes (energía más alta), como **contribuyentes menores**. Cuando una carga se reparte entre dos o más átomos por resonancia, se dice que está **deslocalizada** y que la molécula está **estabilizada por resonancia**. (pp. 13-16)

Isótopos Átomos con el mismo número de protones pero diferente número de neutrones. Átomos del mismo elemento pero con diferentes masas atómicas. (p. 3)

Mapa de potencial electrostático (MPE) Representación molecular calculada por computador que utiliza colores para mostrar la distribución de carga en una molécula. En la mayoría de los casos, el MPE utiliza el color rojo para indicar las regiones ricas en electrones (potencial electrostático más negativo) y azul para indicar las regiones pobres en electrones (potencial electrostático más positivo). Los colores intermedios naranja, amarillo y verde indican regiones con potenciales electrostáticos intermedios. (p. 10)

Momento dipolar (μ) Medida de la polaridad de un enlace (o una molécula), proporcional al producto de la separación de cargas por la longitud de enlace. (p. 10)

Nodo Región de un orbital con densidad electrónica cero. (p. 4)

Nucleófilo Donador de par de electrones (base de Lewis). (p. 29)

Orbital Estado de energía permitida para un electrón que rodea a un núcleo; función de probabilidad que define la distribución de la densidad electrónica en el espacio. El *principio de exclusión de Pauli* afirma que un orbital sólo puede ser ocupado por dos electrones, como máximo, si los espines de éstos están apareados. (p. 3)

Orbitales degenerados Orbitales con energías idénticas. (p. 4)

Par solitario Par de electrones no enlazantes. (p. 7)

pH Medida de la acidez de una solución, definido como el logaritmo (en base 10), cambiado de signo, de la concentración de H_3O^+ . $pH = -\log_{10}[H_3O^+]$. (p. 22)

Plano nodal Región plana (plano) del espacio con densidad electrónica cero. (p. 4)

Química orgánica Definición nueva: química de los compuestos de carbono. Definición antigua: estudio de los compuestos derivados de los organismos vivos y sus productos naturales. (p. 1)

Regla de Hund Cuando hay dos orbitales o más con la misma energía (orbitales degenerados) vacíos, la configuración de energía más baja se consigue colocando los electrones en orbitales diferentes (con espines paralelos), mejor que colocándolos apareados en el mismo orbital. (p. 6)

Regla del octeto Los átomos generalmente se enlazan para que sus capas de valencia se completen con electrones (configuración de gas noble). Para los elementos de la segunda fila de la tabla periódica, esta configuración tiene ocho electrones de valencia. (p. 6)

Valencia Número de enlaces que normalmente forma un átomo. (p. 9)

Vitalismo Creencia en que la síntesis de compuestos orgánicos requiere la presencia de una «fuerza vital». (p. 1)

Pautas esenciales para resolver los problemas del Capítulo 1

1. Escribir e interpretar las fórmulas estructurales de Lewis, condensadas y lineoangulares. Indicar qué átomos tienen cargas formales.
2. Escribir formas de resonancia y usarlas para predecir la estabilidad.
3. Calcular fórmulas empíricas y moleculares de composiciones elementales.
4. Predecir la acidez y la basicidad relativa basada en la estructura, en el enlace y en la resonancia de los pares ácido-base conjugados.
5. Calcular, usar e interpretar los valores de K_a y pK_a .
6. Identificar nucleófilos (bases de Lewis) y electrófilos (ácidos de Lewis) y escribir ecuaciones de reacciones ácido-base de Lewis utilizando flechas curvadas para mostrar el flujo de los electrones.

Problemas

Es fácil engañarse a uno mismo pensando que se entiende la química orgánica cuando realmente no se entiende. Según se van leyendo a lo largo de este libro, todos los conceptos y las ideas pueden tener sentido, pero todavía no se ha aprendido a combinar y a usar esos conceptos e ideas. Un examen es un trance duro para darse cuenta de que realmente no se han entendido los contenidos.

La mejor forma de aprender química orgánica es aplicarla. Por supuesto se necesita leer y releer todo el material del capítulo, pero este nivel de entendimiento es justamente el comienzo. Se proponen problemas para poder trabajar con las ideas, aplicándolas a nuevos compuestos y reacciones que no se han visto con anterioridad. Al resolver problemas, uno se ve obligado a utilizar los conceptos y a entender lo que antes no se había comprendido, también se aumenta el nivel de autoestima y de habilidad para realizar los exámenes.

En cada capítulo se incluyen varias clases de problemas. Hay problemas dentro de los capítulos, que se introducen como ejemplos y explican cómo se han de resolver. Se ha de realizar ese tipo de problemas según se vaya leyendo el capítulo para asegurarse de que se han entendido los conceptos. Las soluciones de muchos de estos problemas se encuentran al final de libro. Los Problemas del final de cada capítulo proporcionan una experiencia adicional en el uso de los conceptos y obligan a pensar con detenimiento sobre las ideas expuestas en el texto. Para algunos de estos problemas se incluyen soluciones breves al final del libro, sin embargo, se pueden encontrar soluciones más detalladas de los mismos en el *Manual de Soluciones*.

Estudiar química orgánica sin resolver problemas es como lanzarse al aire sin paracaídas. Al principio parece divertido, pero después puede resultar duro para aquellos que carezcan de preparación.

1.20 Defina y ponga un ejemplo para cada término:

- | | | |
|------------------------------------|----------------------------|-------------------------------|
| (a) isótopos | (b) orbital | (c) nodo |
| (d) orbitales degenerados | (e) electrones de valencia | (f) enlace iónico |
| (g) enlace covalente | (h) estructura de Lewis | (i) electrones no enlazantes |
| (j) enlace sencillo | (k) enlace doble | (l) enlace triple |
| (m) enlace polar | (n) cargas formales | (o) formas de resonancia |
| (p) fórmula molecular | (q) fórmula empírica | (r) ácido y base de Arrhenius |
| (s) ácido y base de Brønsted-Lowry | (t) ácido y base de Lewis | (u) electrófilo |
| (v) nucleófilo | | |

1.21 Nombre el elemento que corresponda a cada configuración electrónica.

- (a) $1s^2 2s^2 2p^2$ (b) $1s^2 2s^2 2p^4$ (c) $1s^2 2s^2 2p^6 3s^2 3p^3$ (d) $1s^2 2s^2 2p^6 3s^2 3p^5$

1.22 Hay una pequeña sección de la tabla periódica que se debe conocer en química orgánica. Escriba de memoria esta parte, realizando los siguientes pasos:

- (a) Haga una lista, de memoria, de los elementos de las dos primeras filas de la tabla periódica, junto con su número de electrones de valencia.
 (b) Use esta lista para construir las dos primeras filas de la tabla periódica.
 (c) Los compuestos orgánicos a veces contienen azufre, fósforo, cloro, bromo y yodo. Añada estos elementos a la tabla periódica.

1.23 Para cada compuesto, diga si el enlace es covalente, iónico, o intermedio entre covalente e iónico.

- (a) NaCl (b) NaOH (c) CH_3Li (d) CH_2Cl_2 (e) NaOCH_3 (f) HCO_2Na (g) CF_4

1.24 (a) El PCl_3 y el PCl_5 son compuestos estables. Escriba la estructura de Lewis para los dos compuestos.

- (b) El NCl_3 es un compuesto conocido, pero todos los intentos de sintetizar el NCl_5 han fracasado. Escriba las estructuras de Lewis para el NCl_3 y una hipotética para el NCl_5 , y explique por qué el NCl_5 es una estructura improbable.

1.25 Escriba una estructura de Lewis para cada una de las especies.

- (a) N_2H_4 (b) N_2H_2 (c) $(\text{CH}_3)_4\text{NCl}$ (d) CH_3CN (e) CH_3CHO (f) $\text{CH}_3\text{S(O)CH}_3$
 (g) H_2SO_4 (h) CH_3NCO (i) $\text{CH}_3\text{OSO}_2\text{OCH}_3$ (j) $\text{CH}_3\text{C(NH)CH}_3$ (k) $(\text{CH}_3)_3\text{CNO}$

1.26 Escriba una estructura de Lewis para cada compuesto. Incluya todos los pares de electrones no enlazantes.

- (a) $\text{CH}_3\text{CHCHCH}_2\text{CHCHCOOH}$ (b) $\text{NCCH}_2\text{COCH}_2\text{CHO}$
 (c) $\text{CH}_2\text{CHCH(OH)CH}_2\text{CO}_2\text{H}$ (d) $\text{CH}_3\text{CH(CH}_3\text{)CH}_2\text{C(CH}_2\text{CH}_3\text{)}_2\text{CHO}$

1.27 Escriba la fórmula lineoangular de todos los compuestos del Problema 1.26.

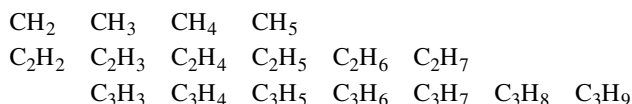
1.28 Escriba las estructuras de Lewis para:

- (a) dos compuestos de fórmula C_4H_{10} (b) dos compuestos de fórmula $\text{C}_2\text{H}_7\text{N}$
 (c) dos compuestos de fórmula $\text{C}_3\text{H}_8\text{O}_2$ (d) dos compuestos de fórmula $\text{C}_2\text{H}_4\text{O}$

1.29 Represente una fórmula estructural completa y una fórmula estructural condensada para:

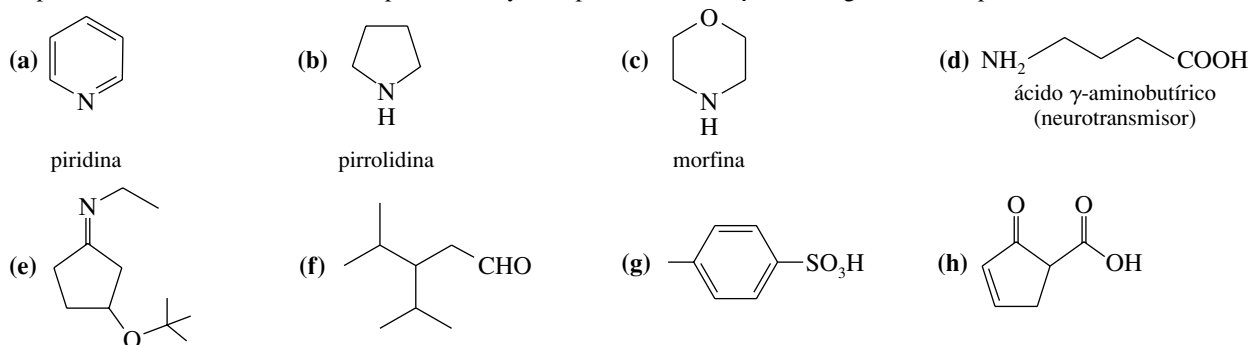
- (a) tres compuestos de fórmula $\text{C}_3\text{H}_8\text{O}$ (b) cinco compuestos de fórmula $\text{C}_3\text{H}_6\text{O}$

1.30 Alguna de las siguientes fórmulas moleculares corresponde a compuestos estables. Represente, cuando sea posible, una estructura estable para cada fórmula.



Proponga una regla general que dé el número de átomos de hidrógeno en los hidrocarburos estables.

1.31 Represente estructuras de Lewis completas, incluyendo pares solitarios, para los siguientes compuestos:



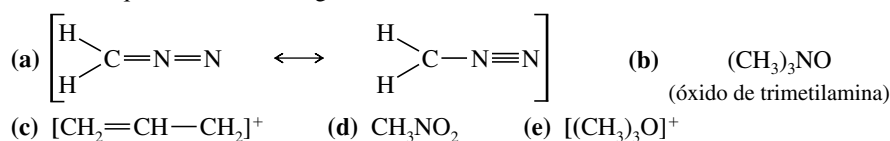
1.32 Escriba la fórmula molecular de todos los compuestos del Problema 1.31.

1.33 Un compuesto X, aislado de la lanolina (grasa de la lana de oveja), tiene un fuerte aroma a calcetines sucios sudados. Un análisis cuidadoso mostró que el compuesto X contenía un 62.0% de carbono y un 10.4% de hidrógeno. No se encontró nitrógeno ni halógenos.

- (a) Escriba la fórmula empírica del compuesto X.
 (b) La determinación del peso molecular mostró que el compuesto X tenía un peso molecular aproximadamente igual a 117; encuentre la fórmula molecular del compuesto X.
 (c) Hay muchas estructuras posibles que tienen esa fórmula molecular. Represente las fórmulas estructurales completas de cuatro de ellas.

1.34 Para cada una de las siguientes estructuras:

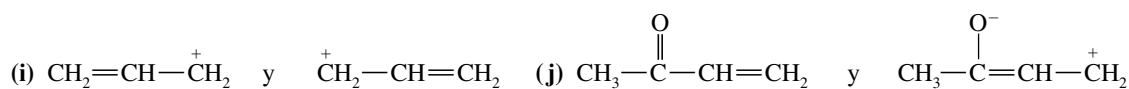
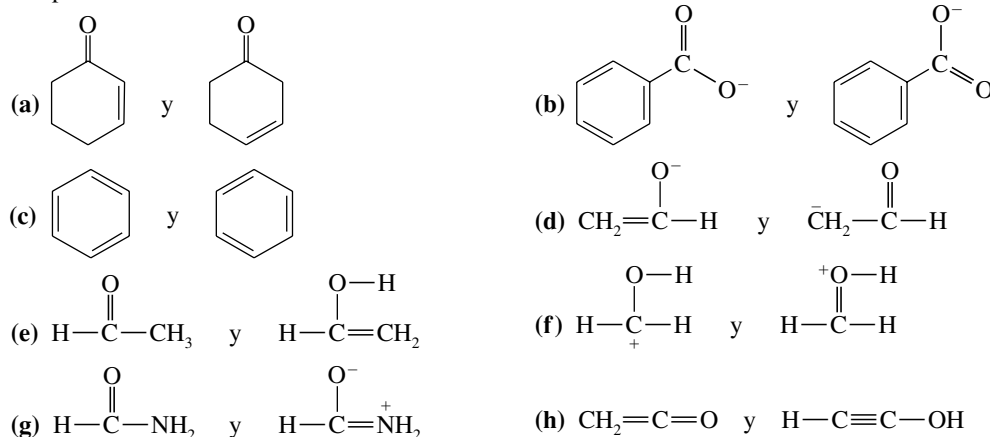
- (1) Represente una estructura de Lewis, poniendo también los electrones no enlazantes.
 (2) Calcule la carga formal de todos los átomos excepto del hidrógeno. Todos son eléctricamente neutros excepto aquellos en los que se indica su carga.



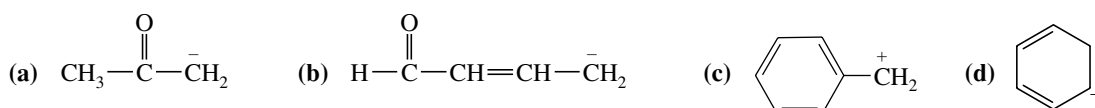
1.35 (1) Teniendo en cuenta la electronegatividad, establezca la dirección de los momentos dipolares de los siguientes enlaces.
 (2) En cada caso, prediga si el momento dipolar es relativamente grande o pequeño.

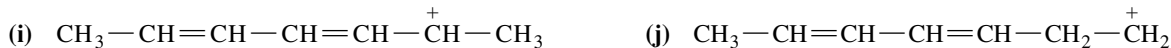
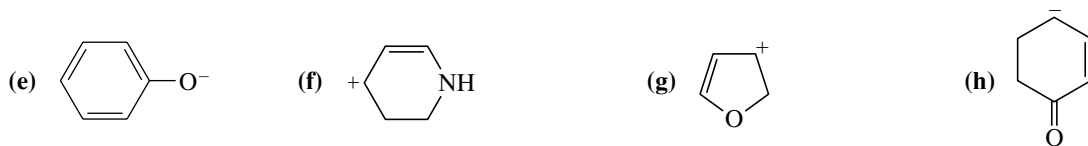
- (a) $\text{C}-\text{Cl}$ (b) $\text{C}-\text{H}$ (c) $\text{C}-\text{Li}$ (d) $\text{C}-\text{N}$ (e) $\text{C}-\text{O}$
 (f) $\text{C}-\text{B}$ (g) $\text{C}-\text{Mg}$ (h) $\text{N}-\text{H}$ (i) $\text{O}-\text{H}$ (j) $\text{C}-\text{Br}$

1.36 Determine si los siguientes pares de estructuras son diferentes compuestos o solamente formas de resonancia del mismo compuesto.



1.37 Represente las formas de resonancia importantes para mostrar la deslocalización de cargas en los iones siguientes:





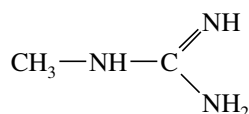
1.38

- (a) Represente las formas de resonancia para el SO_2 (conectividad $\text{O}-\text{S}-\text{O}$).
 (b) Represente las formas de resonancia para el ozono (conectividad $\text{O}-\text{O}-\text{O}$).
 (c) El dióxido de azufre tiene una forma de resonancia más que el ozono, explique por qué esa estructura no es posible para el ozono.

*1.39

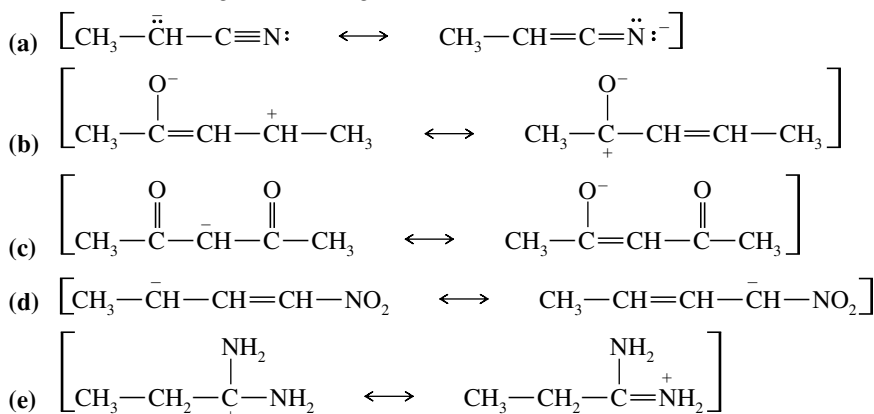
El compuesto siguiente puede protonarse en cualquiera de los átomos de nitrógeno, no obstante, uno de esos nitrógenos es mucho más básico que los otros.

- (a) Represente las formas de resonancia importantes de los productos de protonación de cada uno de los tres átomos de nitrógeno.
 (b) Determine qué átomo de nitrógeno es el más básico.



1.40

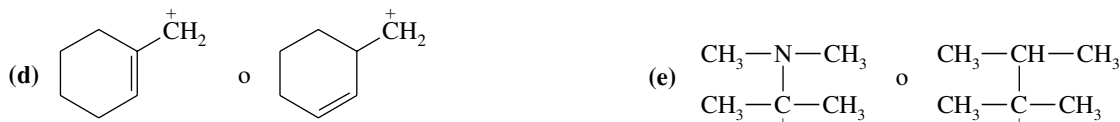
En los siguientes apartados de formas de resonancia, señale los contribuyentes mayor y menor, y diga qué estructuras tienen la misma energía. Si falta alguna forma de resonancia, añádala.



1.41

Para cada par de iones, determine cuál es más estable. Use formas de resonancia para explicar las respuestas.

- (a) $\text{CH}_3-\overset{+}{\text{CH}}-\text{CH}_3$ o $\text{CH}_3-\overset{+}{\text{CH}}-\text{OCH}_3$
 (b) $\text{CH}_2=\text{CH}-\overset{+}{\text{CH}}-\text{CH}_3$ o $\text{CH}_2=\text{CH}-\text{CH}_2-\overset{+}{\text{CH}}_2$
 (c) $\overset{-}{\text{CH}}_2-\text{CH}_3$ o $\overset{-}{\text{CH}}_2-\text{C}\equiv\text{N}:$



1.42

Ordene las siguientes especies por orden creciente de acidez, explicando las razones de este ordenamiento.



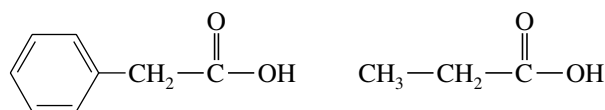
1.43

Ordene las siguientes especies por orden creciente de basicidad, explicando las razones de este ordenamiento.



1.44

La K_a del ácido fenilacético es 5.2×10^{-5} y el pK_a del ácido propiónico es 4.87.

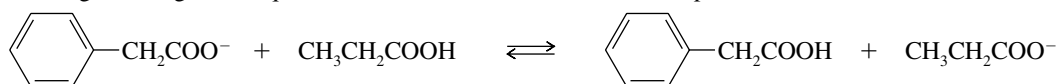


ácido fenilacético, $K_a = 5.2 \times 10^{-5}$ ácido propiónico, $pK_a = 4.87$

- (a) Calcule el pK_a del ácido fenilacético y la K_a del ácido propiónico.

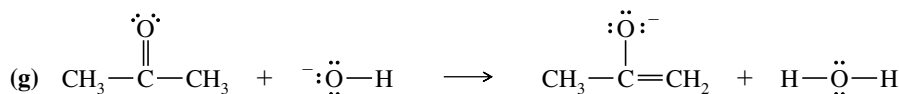
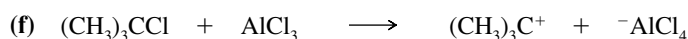
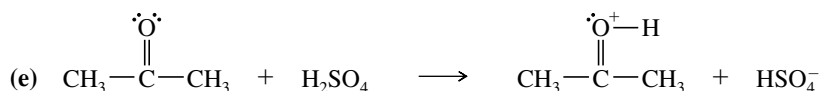
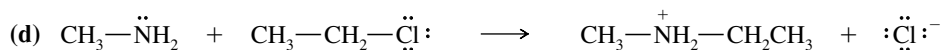
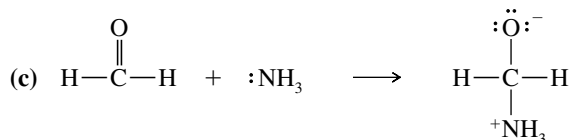
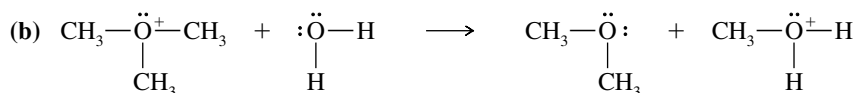
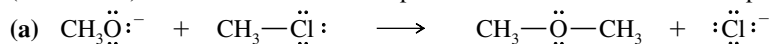
(b) ¿Cuál de los dos ácidos es el más fuerte? Calcule cuánto más fuerte es uno que otro.

(c) Prediga si el siguiente equilibrio favorecerá a los reactivos o a los productos.



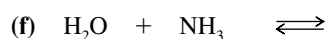
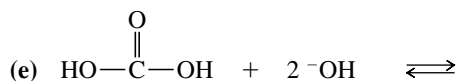
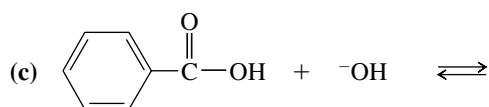
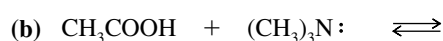
1.45

En las siguientes reacciones ácido-base clasifique los reactivos como ácidos de Lewis (electrófilos) o bases de Lewis (nucleófilos). Utilice flechas curvadas para indicar el movimiento de los pares de electrones en las reacciones.



1.46

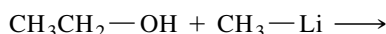
Prediga los productos de las siguientes reacciones ácido-base:



*1.47

El metilítio (CH_3Li) a menudo se usa como base en reacciones orgánicas.

(a) Prediga los productos de la siguiente reacción ácido-base:



(b) ¿Cuál es el ácido conjugado del CH_3Li ? ¿Qué es el CH_3Li ?, ¿una base fuerte o débil?

*1.48

En 1984, Edward A. Doisy de la Universidad de Washington extrajo 1 360 kg de ovarios de cerda para aislar unos pocos miligramos de estradiol puro, una potente hormona femenina. Doisy quemó 5.00 mg de esa preciada muestra en oxígeno y encontró que se obtenían 14.54 mg de CO_2 y 3.97 mg de H_2O .

(a) Determine la fórmula empírica del estradiol.

(b) La masa molecular del estradiol se determinó posteriormente y se encontró que era de 272. Determine la fórmula molecular del estradiol.

Chemsoft®

Química Orgánica

Recopilación

José A. - UHNMOSM



2009

Química Orgánica

Recopilación

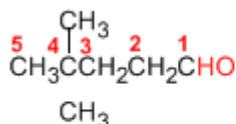
Índice.

- i. Nomenclatura de Aldehídos y Cetonas*
- ii. Preparación de Aldehídos y Cetonas*
- iii. Formación de Hidratos*
- iv. Formación de Hemiacetales*
- v. Formación de Acetales*
- vi. Formación de Acetales Cíclicos*
- vii. Acetales Como Grupos Protectores*
- viii. Formación de Iminas*
- ix. Formación de Oximas*
- x. Formación de Hidrazonas*
- xi. Formación de Azinas*
- xii. Formación de Semicarbazonas*
- xiii. Ensayo de la 2,4 - Dinitrofenilhidrazina*
- xiv. Formación de Cianhídrinas*
- xv. Reacción de Wittig*
- xvi. Oxidación de Baeyer Villiger*
- xvii. Problemas Nomenclatura Aldehídos y Cetonas*
- xviii. Problemas Resueltos de Aldehídos y Cetonas*
- xix. Teorías de Enoles y Enolatos*

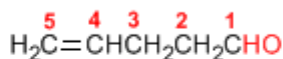
Nomenclatura de Aldehídos y Cetonas

Los aldehídos se nombran reemplazando la terminación **-ano** del alcano correspondiente por **-al**. No es necesario especificar la posición del grupo aldehído, puesto que ocupa el extremo de la cadena (localizador 1).

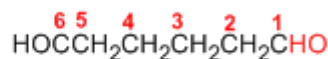
Cuando la cadena contiene dos funciones aldehído se emplea el sufijo **-dial**.



4,4-Dimetilpentanal

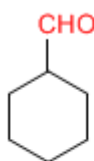


Hex-4-enal

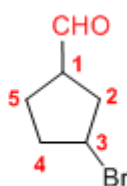


Pentanodial

El grupo **-CHO** unido a un ciclo se llama **-carbaldehído**. La numeración del ciclo se realiza dando localizador 1 al carbono del ciclo que contiene el grupo aldehído.



Ciclohexanocarbaldehído

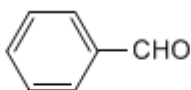


3-Bromociclopentanocarbaldehído

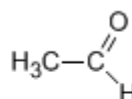
Algunos nombres comunes de aldehídos aceptados por la IUPAC son:



Formaldehído
(Metanal)

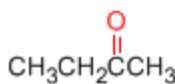


Benzaldehído
(Bencenocarbaldehído)

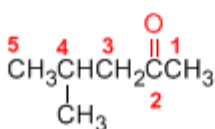


Acetaldehído
(Etanal)

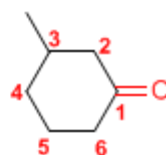
Las cetonas se nombran sustituyendo la terminación **-ano** del alcano con igual longitud de cadena por **-ona**. Se toma como cadena principal la de mayor longitud que contiene el grupo carbonilo y se numera para que éste tome el localizador más bajo.



Butanona

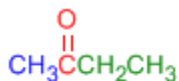


4-Metil-2-pentanona

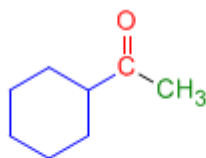


3-Metilciclohexanona

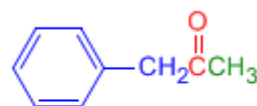
Existe un segundo tipo de nomenclatura para las cetonas, que consiste en nombrar las cadenas como sustituyentes, ordenándolas alfabéticamente y terminando el nombre con la palabra **cetona**.



Etil metil cetona



Ciclohexil metil cetona



Fenil metil cetona

[Siguiete >](#)

[\[Volver\]](#)

Charles Friedel (1832 - 1899)



Origen: Químico frances..

Lugar de nacimiento: Estrasburgo.

Formación: estudió química en la Universidad de Berlín entre 1895 y 1899, consiguiendo el doctorado este año.

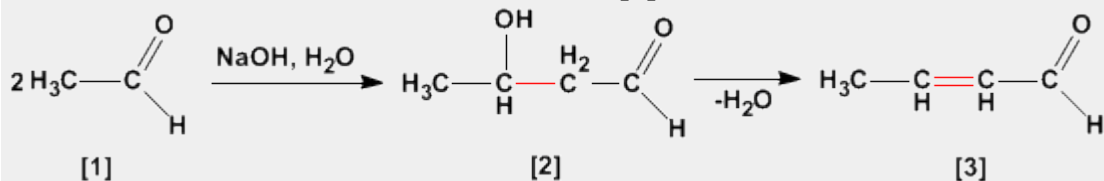
Docencia: Profesor en la Universidad de la Sorbona.

Investigación: Obtuvo el alcohol propílico. En 1877, Friedel y Crafts describieron por primera vez la reacción del benceno con un haloalcano en presencia de un ácido de Lewis. Esta reacción produce la alquilación del benceno y se conoce como alquilación de Friedl-Crafts.

Premio Nobel:

Aldólica (Condensación)

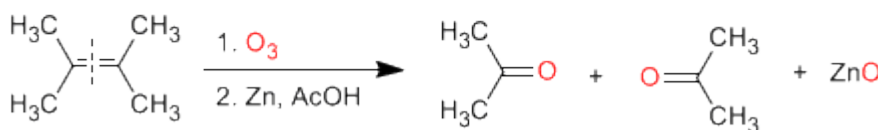
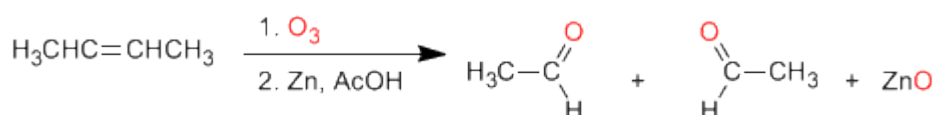
La condensación aldólica es una reacción de aldehídos o cetonas **[1]** que forma 3-hidroxicarbonilos (aldoles) **[2]**. El 3-hidroxialdehído **[2]** bajo condiciones de deshidratación por calentamiento rinde un aldehído alfa,beta-insaturado **[3]**.



Preparación de aldehídos y cetonas

Los aldehídos y cetonas pueden ser preparados por oxidación de alcoholes, ozonólisis de alquenos, hidratación de alquinos y acilación de Friedel-Crafts como métodos de mayor importancia.

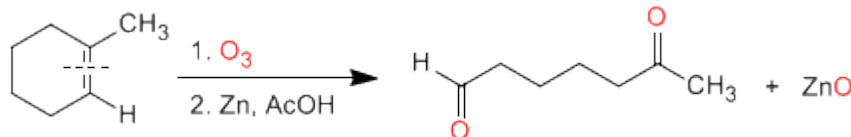
a) **Ozonólisis de alquenos:** Los alquenos rompen con ozono formando aldehídos y/o cetonas. Si el alqueno tiene hidrógenos vinílicos da aldehídos. Si tiene dos cadenas carbonadas forma cetonas.



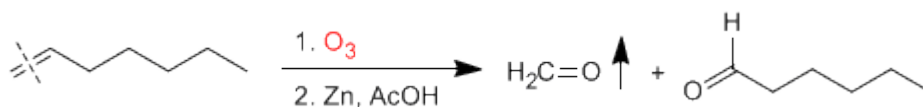
Ozonólisis

Los alquenos simétricos y terminales permiten la preparación de carbonilos mediante ozonólisis

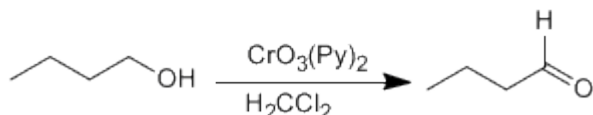
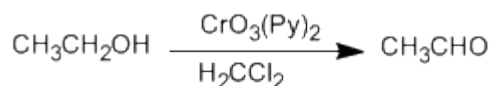
La ozonólisis de alquenos cíclicos produce compuestos dicarbonílicos:



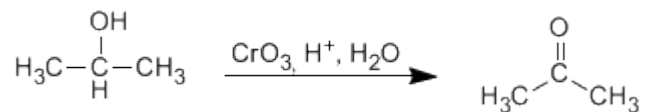
Los alquenos terminales rompen formando metanal, que separa fácilmente de la mezcla por su bajo punto de ebullición.



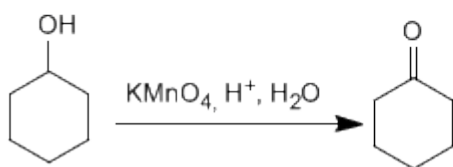
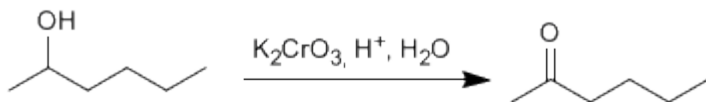
b) **Oxidación de alcoholes:** Los alcoholes primarios y secundarios se oxidan para dar aldehídos y cetonas respectivamente. Deben tomarse precauciones en la oxidación de alcoholes primarios, puesto que sobreoxidan a ácidos carboxílicos en presencia de oxidantes que contengan agua. En estos caso debe trabajarse con reactivos anhidros, como el clorocromato de piridino en diclorometano (PCC), a temperatura ambiente.



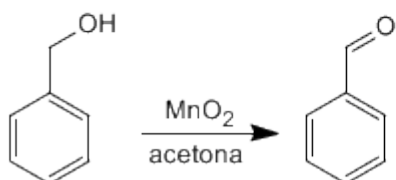
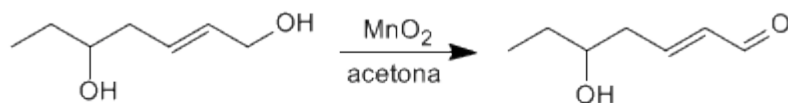
Los alcoholes secundarios dan cetonas por oxidación. Se emplean como oxidantes permanganato, dicromato, trióxido de cromo.



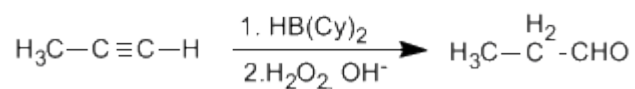
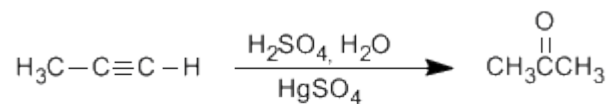
La oxidación supone la pérdida de dos hidrógenos del alcohol. Los alcoholes terciarios no pueden oxidar puesto que carecen de hidrógeno sobre el carbono.



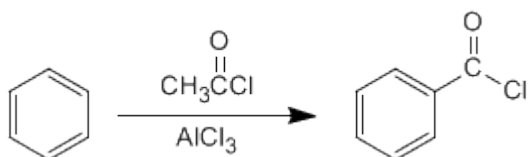
Los alcoholes alílicos y bencílicos se transforman en aldehídos o cetonas por oxidación con dióxido de manganeso en acetona. Esta reacción tiene una elevada selectividad y no oxida alcoholes que no se encuentren en dichas posiciones.



c) **Hidratación de alquinos:** Los alquinos se pueden hidratar Markovnikov, formando cetonas, o bien antiMarkovnikov, para formar aldehídos.



d) **Acilación de Friedel-Crafts:** La introducción de grupos acilo en el benceno permite la preparación de cetonas con cadenas aromáticas.



Otto Paul Hermann Diels (1876 - 1954)



Origen: Químico alemán.

Lugar de nacimiento: Königshütte (hoy Chorzów, Polonia).

Formación: estudió química en la Universidad de Berlín entre 1895 y 1899, consiguiendo el doctorado este año.

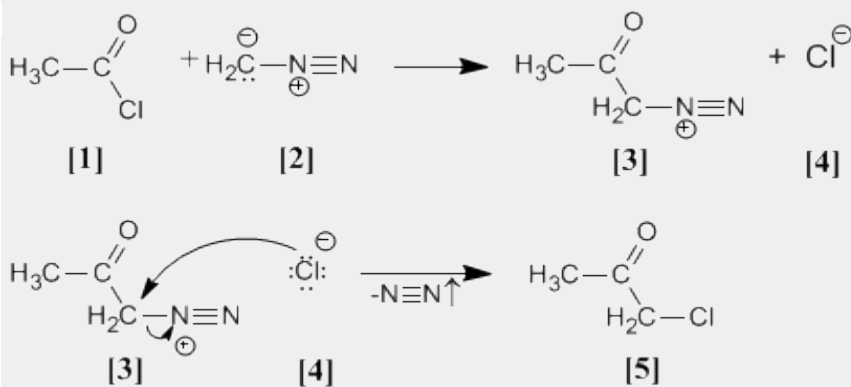
Docencia: profesor y jefe del departamento de química en la Universidad de Berlín. En 1916, tomó el puesto de profesor de Química en la Universidad de Kiel, cargo que no dejó hasta su jubilación en 1945.

Investigación: En 1906 descubrió el anhídrido malónico. Investigó en reacciones de deshidrogenación con selenio. Síntesis de α -dicetonas. Pero su trabajo más importante es la reacción de Diels - Alder.

Premio Nobel: En 1950 recibió el Premio Nobel junto a Kurt Alder

Arndt Eistert (Síntesis)

Cloruro de acetilo [1] se trata con diazometano [2] rindiendo la sal de diazonio [3]. El cloruro [4] producido reacciona con la sal de diazonio para dar la α -clorocetona [5].

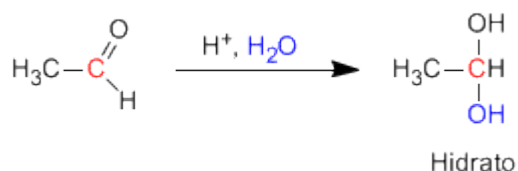


Síntesis de Arndt Eistert

Esta reacción permite transformar haluros de alcanoilo en cetonas halogenadas en su posición alfa.

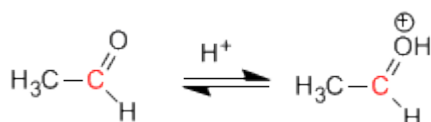
Formación de Hidratos

Los aldehídos y cetonas reaccionan en medio ácido acuoso para formar hidratos. El mecanismo consta de tres etapas. La primera y más rápida consiste en la protonación del oxígeno carbonílico. Esta protonación produce un aumento de la polaridad sobre el carbono y favorece el ataque del nucleófilo. En la segunda etapa el agua ataca al carbono carbonilo, es la etapa lenta del mecanismo. En la tercera etapa se produce la desprotonación del oxígeno formándose el hidrato final.

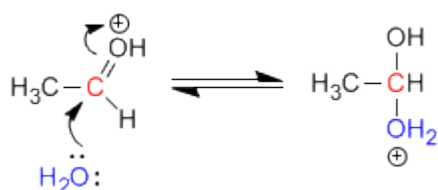


Mecanismo de la reacción

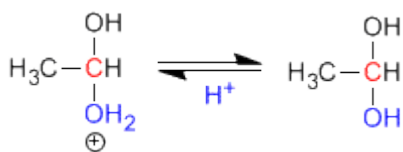
Etapa 1. Protonación del oxígeno carbonílico.



Etapa 2. Ataque nucleófilo del agua al carbonilo protonado.



Etapa 3. Desprotonación del hidrato





Origen: Químico estadounidense.

Lugar de nacimiento: Budapest

Formación: Se doctoró en la Universidad de Budapest en 1949

Docencia: Trabajó en el departamento de química orgánica de la Academia de Ciencias de Hungría y posteriormente en la Universidad de Cleveland.

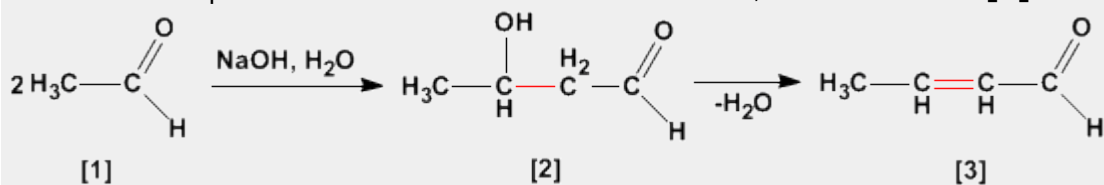
Industria: Trabajó en los laboratorios de la Dow Chemical de Ontario

Investigación: Olah consiguió preparar carbocationes estables utilizando componentes extremadamente ácidos.

Premio Nobel: En 1994 obtuvo el premio Nobel de Química por sus investigaciones sobre los carbocationes

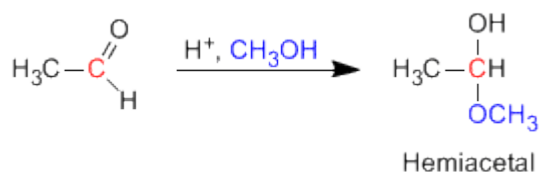
Aldólica (Condensación)

La condensación aldólica es una reacción de aldehídos o cetonas **[1]** que forma 3-hidroxicarbonilos (aldoles) **[2]**. El 3-hidroxialdehído **[2]** bajo condiciones de deshidratación por calentamiento rinde un aldehído alfa,beta-insaturado **[3]**.



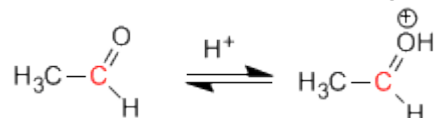
Formación de Hemiacetales

Los hemiacetales se forman por reacción de un equivalente de alcohol con el grupo carbonilo de un aldehído o cetona. Esta reacción se cataliza con ácido y es equivalente a la formación de hidratos.

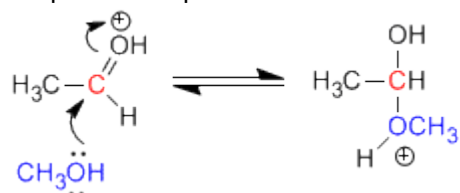


Mecanismo de la reacción:

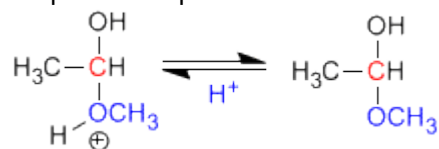
Eta 1. Protonación del oxígeno carbonílico.



Eta 2. Ataque nucleófilo del metanol al carbonilo protonado.



Eta 3. Desprotonación del hemiacetal



Otto Paul Hermann Diels (1876 - 1954)



Origen: Químico alemán.

Lugar de nacimiento: Königshütte (hoy Chorzów, Polonia).

Formación: estudió química en la Universidad de Berlín entre 1895 y 1899, consiguiendo el doctorado este año.

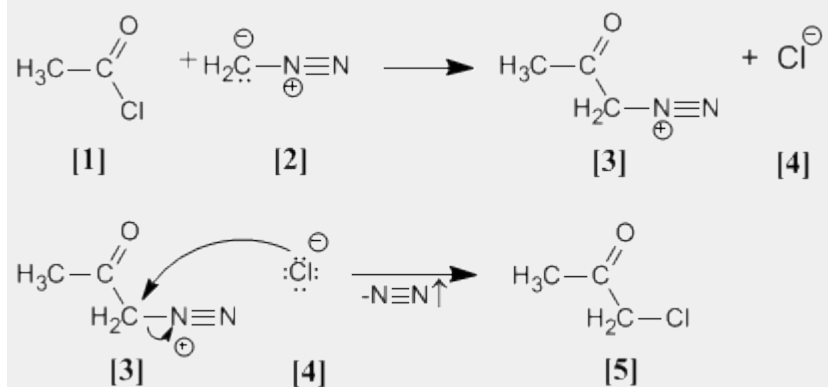
Docencia: profesor y jefe del departamento de química en la Universidad de Berlín. En 1916, tomó el puesto de profesor de Química en la Universidad de Kiel, cargo que no dejó hasta su jubilación en 1945.

Investigación: En 1906 descubrió el anhídrido malónico. Investigó en reacciones de deshidrogenación con selenio. Síntesis de α -dicetonas. Pero su trabajo más importante es la reacción de Diels - Alder.

Premio Nobel: En 1950 recibió el Premio Nobel junto a Kurt Alder

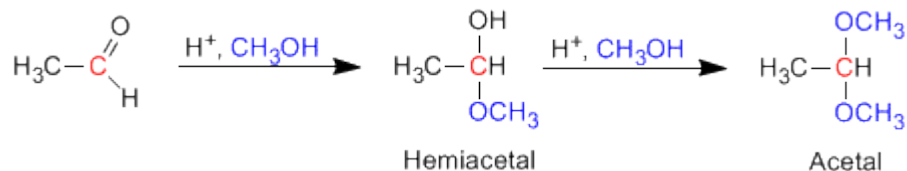
Arndt Eistert (Síntesis)

Cloruro de acetilo **[1]** se trata con diazometano **[2]** rindiendo la sal de diazonio **[3]**. El cloruro **[4]** producido reacciona con la sal de diazonio para dar la α -clorocetona **[5]**.



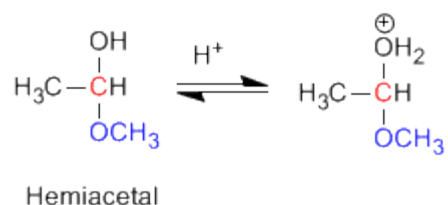
Formación de Acetales

Los aldehídos y cetonas reaccionan con alcoholes bajo condiciones de catálisis ácida, formando en una primera etapa hemiacetales, que posteriormene evolucionan por reacción con un segundo equivalente de alcohol a acetales.

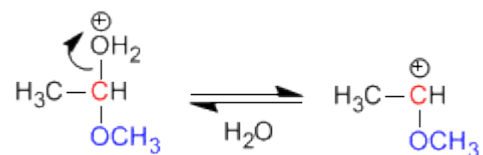


Mecanismo para la formación de acetales

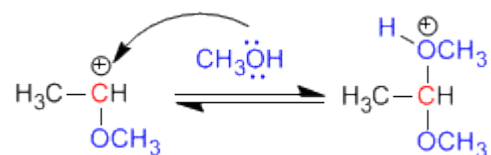
Etapa 1. Protonación del grupo hidroxilo



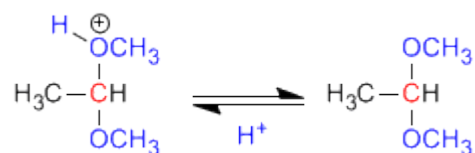
Etapa 2. Pérdida de agua.



Etapa 3. Ataque del alcohol al carbocatión



Etapa 4. Desprotonación del acetal



Otto Paul Hermann Diels (1876 - 1954)



Origen: Químico alemán.

Lugar de nacimiento: Königshütte (hoy Chorzów, Polonia).

Formación: estudió química en la Universidad de Berlín entre 1895 y 1899, consiguiendo el doctorado este año.

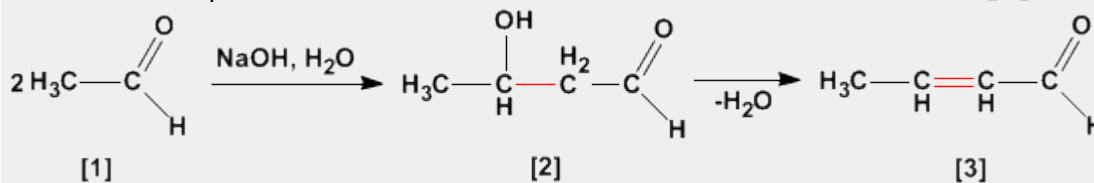
Docencia: profesor y jefe del departamento de química en la Universidad de Berlín. En 1916, tomó el puesto de profesor de Química en la Universidad de Kiel, cargo que no dejó hasta su jubilación en 1945.

Investigación: En 1906 descubrió el anhídrido malónico. Investigó en reacciones de deshidrogenación con selenio. Síntesis de α -dicetonas. Pero su trabajo más importante es la reacción de Diels - Alder.

Premio Nobel: En 1950 recibió el Premio Nobel junto a Kurt Alder

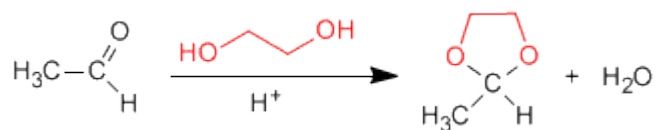
Aldólica (Condensación)

La condensación aldólica es una reacción de aldehídos o cetonas **[1]** que forma 3-hidroxicarbonilos (aldoles) **[2]**. El 3-hidroxialdehído **[2]** bajo condiciones de deshidratación por calentamiento rinde un aldehído alfa,beta-insaturado **[3]**.



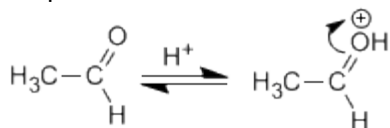
Formación de acetales cíclicos

Los 1,2- y 1,3-dioles reaccionan con aldehídos y cetonas formando acetales cíclicos. Los equilibrios se desplazan hacia el producto final eliminando el agua formada por destilación azeotrópica con benceno o tolueno.

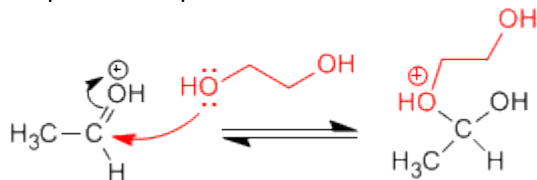


Mecanismo para la formación de acetales cíclicos:

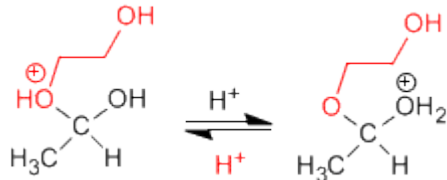
Etapa 1. Protonación del carbonilo



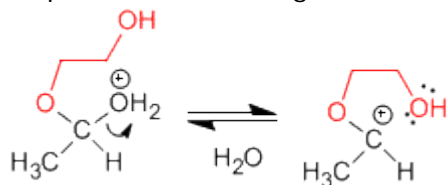
Etapa 2. Ataque nucleófilo del diol al carbonilo.



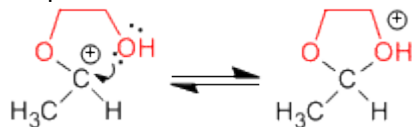
Etapa 3. Equilibrio ácido base entre el éter y el alcohol



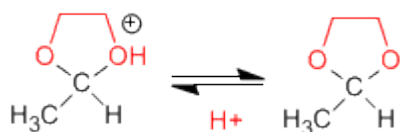
Etapa 4. Pérdida de agua



Etapa 5. Ciclación



Etapa 6. Desprotonación del acetal cíclico



Kurt Alder (1902 - 1958)



Origen: Químico alemán.

Lugar de nacimiento: Königshütte (hoy Chorzów, Polonia).

Formación: estudió en la Universidad de Kiel. Bajo la supervisión del químico alemán Otto Diels, su jefe e instructor en Kiel.

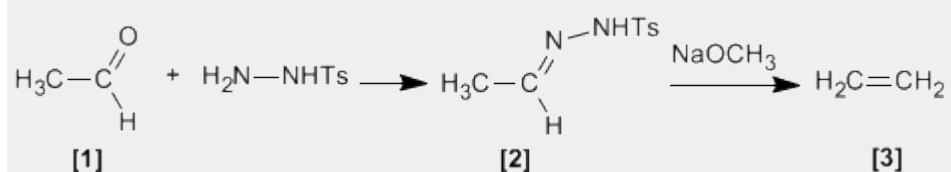
Docencia: Alder ejerció como profesor de química en las universidades de Kiel y Colonia.

Investigación: Alder se especializó en la síntesis diénica (conocida más tarde como la reacción Diels - Alder) que consiste fundamentalmente en el análisis y formación de compuestos orgánicos complejos. Ya en 1928 ambos fueron coautores de un ensayo sobre este proceso.

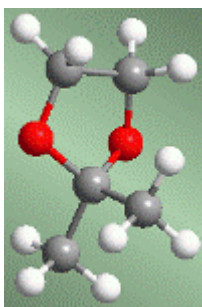
Premio Nobel: En 1950 recibió el Premio Nobel junto a Diels

Bamford Stevens (Reacción)

Tosilhidrazonas [2] de aldehídos o cetonas alifáticos [1] reaccionan con bases fuertes para dar alquenos [3].

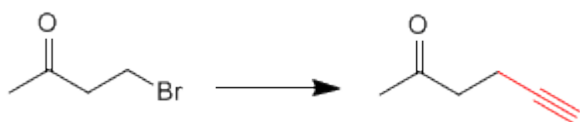


Acetales como grupos protectores

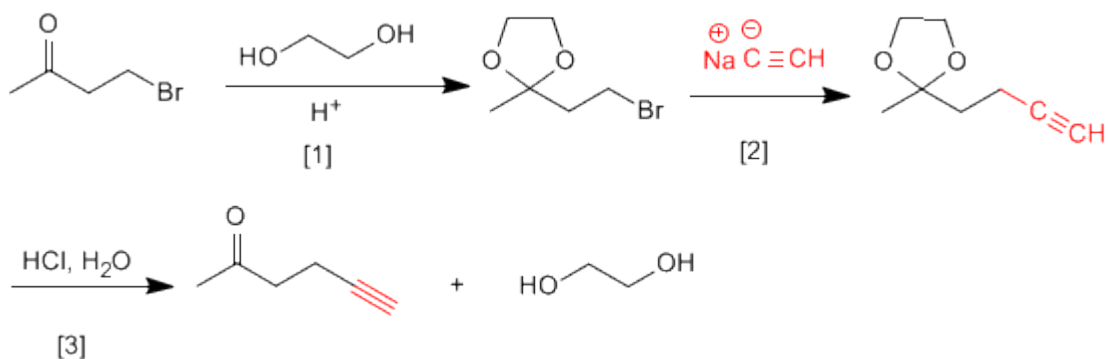


Los acetales pueden emplearse, por su estabilidad, como grupos protectores del carbonilo. El acetal es un éter, muy estable en medios básicos, aunque rompe en presencia de medios ácidos. En muchos procesos de síntesis el grupo carbonilo es incompatible con el reactivo utilizado. En estos casos debe protegerse para evitar que reaccione. La inestabilidad del acetal en medio ácido puede emplearse para desproteger el carbonilo.

Veamos algunos ejemplos:



Esta transformación requiere una sustitución, empleando como nucleófilo un acetiluro de sodio. El nucleófilo puede atacar también al grupo carbonilo, para evitarlo vamos a protegerlo.

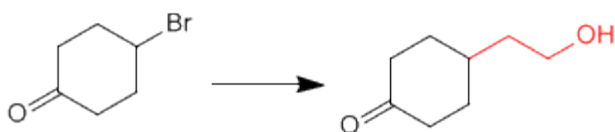


[1] Protección de la cetona.

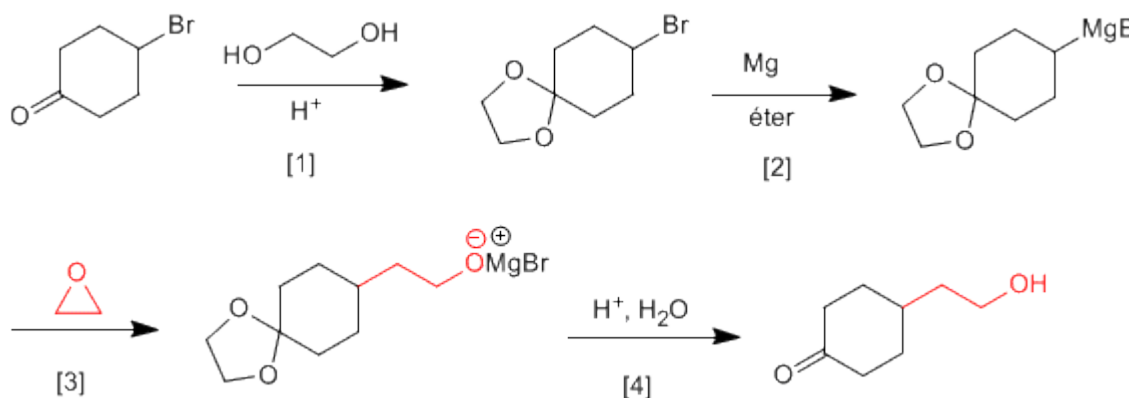
[2] Ataque del acetiluro al carbono del bromo.

[3] Desprotección del carbonilo

Veamos un segundo ejemplo:



Es necesario proteger la cetona antes de formar el organometálico para evitar la dimerización del compuesto.



- [1] Protección de la cetona.
 [2] Formación del magnesiano.
 [3] Apertura del oxaciclopropano.
 [4] Desprotección y protonación del alcóxido.

Otto Paul Hermann Diels (1876 - 1954)



Origen: Químico alemán.

Lugar de nacimiento: Königshütte (hoy Chorzów, Polonia).

Formación: estudió química en la Universidad de Berlín entre 1895 y 1899, consiguiendo el doctorado este año.

Docencia: profesor y jefe del departamento de química en la Universidad de Berlín. En 1916, tomó el puesto de profesor de Química en la Universidad de Kiel, cargo que no dejó hasta su jubilación en 1945.

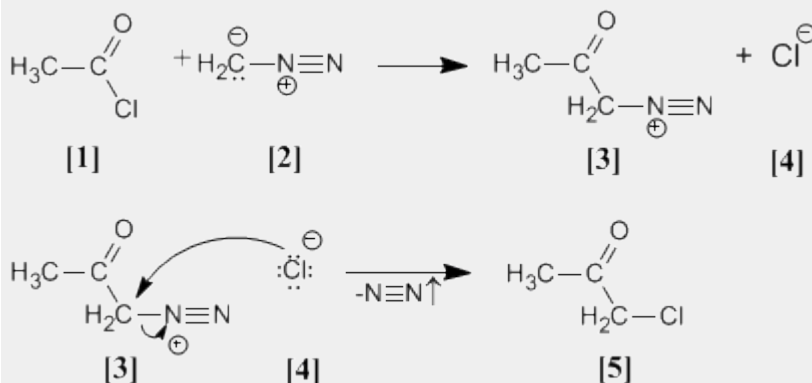
Investigación: En 1906 descubrió el anhídrido malónico.

Investigó en reacciones de deshidrogenación con selenio. Síntesis de α-dicetonas. Pero su trabajo más importante es la reacción de Diels - Alder.

Premio Nobel: En 1950 recibió el Premio Nobel junto a Kurt Alder

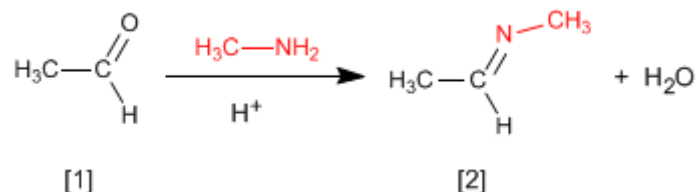
Arndt Eistert (Síntesis)

Cloruro de acetilo **[1]** se trata con diazometano **[2]** rindiendo la sal de diazonio **[3]**. El cloruro **[4]** producido reacciona con la sal de diazonio para dar la α-clorocetona **[5]**.



Formación de Iminas

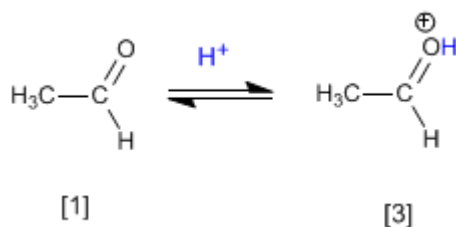
La reacción de aldehídos o cetonas **[1]** con aminas primarias genera iminas **[2]**. La reacción se favorece en un medio ligeramente ácido (pH=4.5).



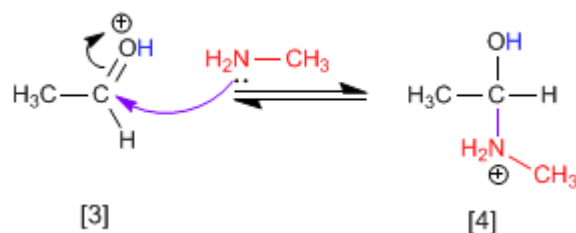
El control del pH es fundamental, puesto que se requiere la protonación del oxígeno del carbonilo para favorecer el ataque nucleófilo.

Mecanismo:

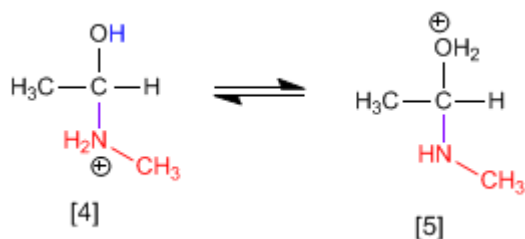
Etapas 1. Protonación del grupo carbonilo que aumenta la polaridad positiva sobre el carbono y favorece el ataque nucleófilo.



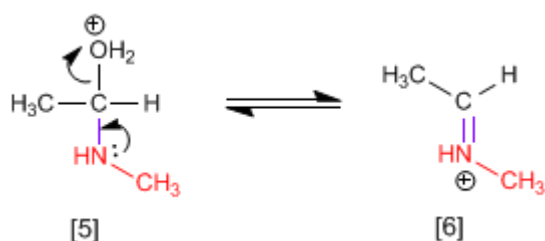
Etapas 2. Ataque nucleófilo de la amina primaria al carbono carbonilo.



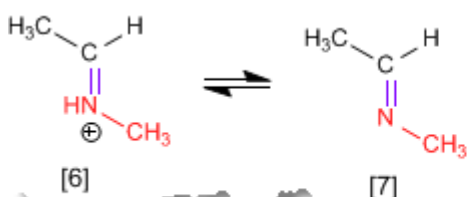
Etapas 3. Protonación del grupo hidroxilo para transformarlo en buen grupo saliente.



Etapas 4. Pérdida de agua y formación de la imina protonada.



Etapa 5. Desprotonación del catión.



George A. Olah (1927 -)



Origen: Químico estadounidense.

Lugar de nacimiento: Budapest

Formación: Se doctoró en la Universidad de Budapest en 1949

Docencia: Trabajó en el departamento de química orgánica de la Academia de Ciencias de Hungría y posteriormente en la Universidad de Cleveland.

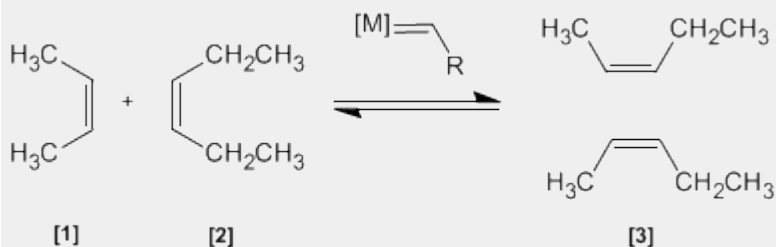
Industria: Trabajó en los laboratorios de la Dow Chemical de Ontario

Investigación: Olah consiguió preparar carbocationes estables utilizando componentes extremadamente ácidos.

Premio Nobel: En 1994 obtuvo el premio Nobel de Química por sus investigaciones sobre los carbocationes

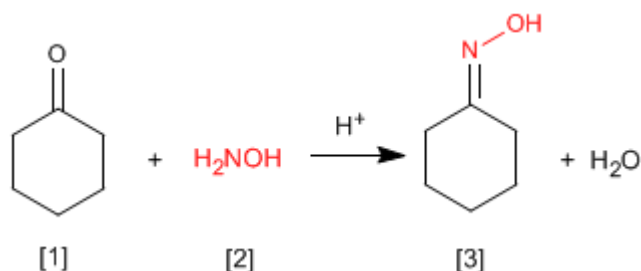
Metátesis de Alquenos

En esta reacción dos alquenos **[1]** y **[2]** son tratados con un metal de transición que actúa como catalizador, dando una mezcla de alquenos **[3]** (incluyendo isómeros Z/E). Este productos se obtiene por intercambio de grupos alquilideno.

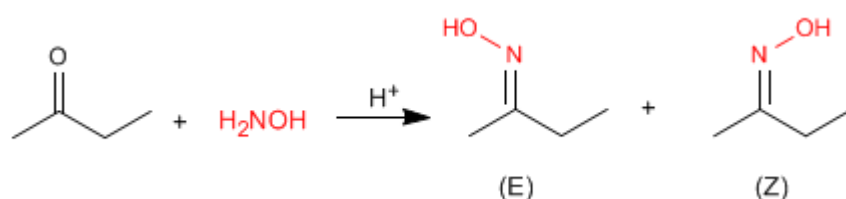


Formación de Oximas

Las oximas [3] se obtienen por reacción de aldehídos o cetonas [1] e hidroxilamina [2] en un medio débilmente ácido. El mecanismo es análogo al de formación de iminas.



Las oximas de aldehídos y cetona asimétricas presentan isomería Z/E dependiendo de la posición del hidroxilo.



Las iminas e hidrazonas (que comentaremos a continuación) también presentan esta característica.

George A. Olah (1927 -)



Origen: Químico estadounidense.

Lugar de nacimiento: Budapest

Formación: Se doctoró en la Universidad de Budapest en 1949

Docencia: Trabajó en el departamento de química orgánica de la Academia de Ciencias de Hungría y posteriormente en la Universidad de Cleveland.

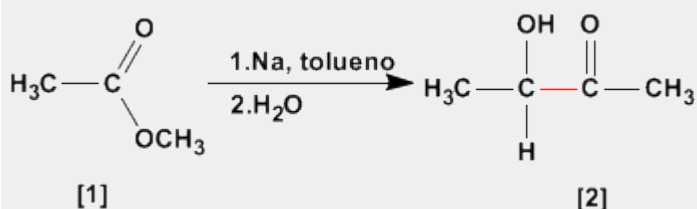
Industria: Trabajó en los laboratorios de la Dow Chemical de Ontario

Investigación: Olah consiguió preparar carbocationes estables utilizando componentes extremadamente ácidos.

Premio Nobel: En 1994 obtuvo el premio Nobel de Química por sus investigaciones sobre los carbocationes

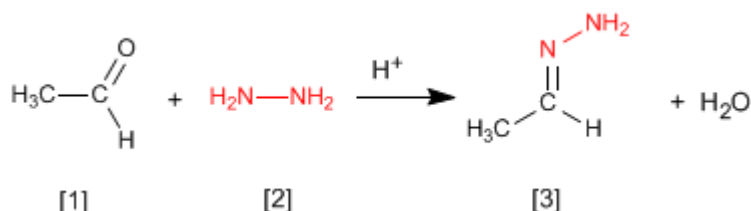
Aciloinica (Condensación)

La condensación aciloinica transforma esteres [1] en alfa-hidroxicetonas [2]. Esta reacción se realiza con sodio metal en disolvente inerte.

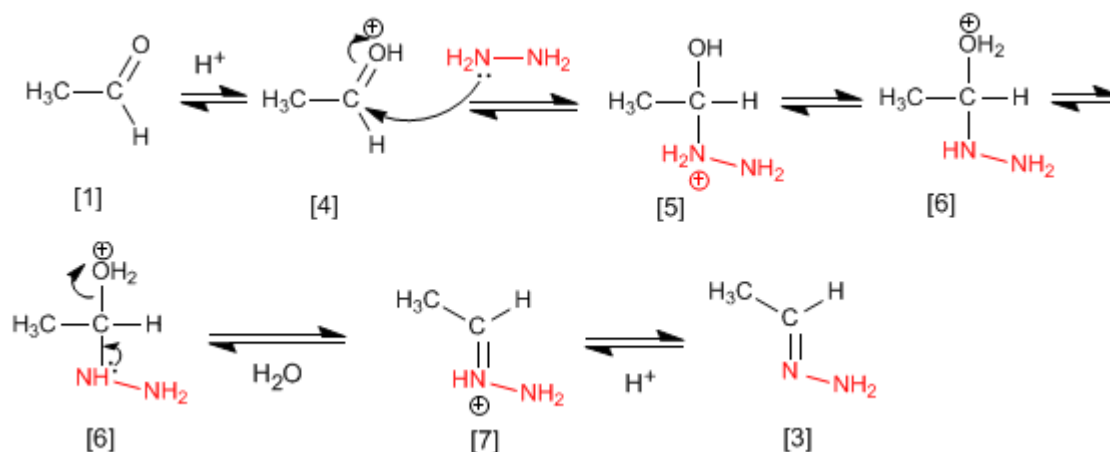


Formación de Hidrazonas

Las hidrazonas **[3]** se obtienen por reacción de aldehídos o cetonas **[1]** con hidrazina **[2]**. Igual que en el caso de las iminas y oximas requiere pH=4.



Aunque el mecanismo es análogo al de formación de iminas, comentaremos de nuevo los pasos.



El etanal **[1]** se protona formando su ácido conjugado **[4]**. La importante polaridad del carbono carbonilo de **[4]** favorece el ataque de la hidrazina **[2]** para formando el intermedio **[5]**. El compuesto **[5]** intercambia un protón entre el nitrógeno y el oxígeno, transformando el grupo hidroxilo en agua (buen grupo saliente). El intermedio **[6]** pierde una molécula de agua transformándose en **[7]**, cuya desprotonación da la hidrazona final **[3]**.

Kurt Alder (1902 - 1958)



Origen: Químico alemán.

Lugar de nacimiento: Königshütte (hoy Chorzów, Polonia).

Formación: estudió en la Universidad de Kiel. Bajo la supervisión del químico alemán Otto Diels, su jefe e instructor en Kiel.

Docencia: Alder ejerció como profesor de química en las universidades de Kiel y Colonia.

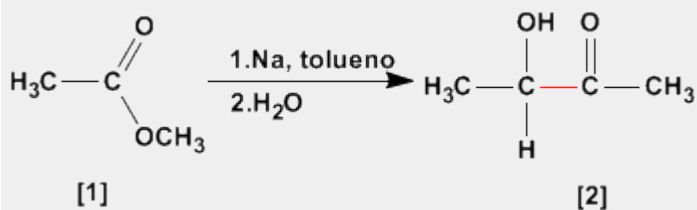
Investigación: Alder se especializó en la síntesis diénica (conocida más tarde como la reacción Diels - Alder) que consiste fundamentalmente en el análisis y formación de compuestos orgánicos complejos.

Ya en 1928 ambos fueron coautores de un ensayo sobre este proceso.

Premio Nobel: En 1950 recibió el Premio Nobel junto a Diels

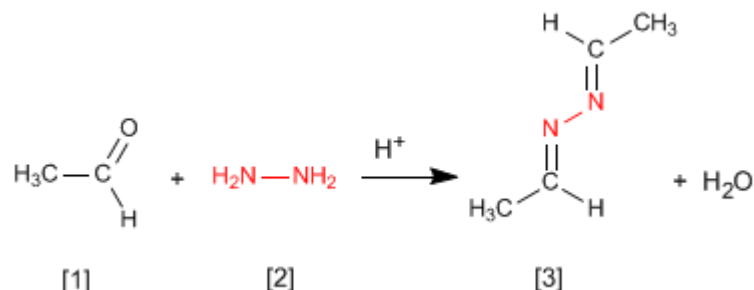
Aciloínica (Condensación)

La condensación aciloínica transforma esteres [1] en alfa-hidroxicetonas [2]. Esta reacción se realiza con sodio metal en disolvente inerte.



Formación de Azinas

La hidrazina [2] reacciona con dos moléculas de aldehído [1] para formar azinas [3].



El mecanismo es análogo al de formación de iminas, oximas e hidrazonas.

George A. Olah (1927 -)



Origen: Químico estadounidense.

Lugar de nacimiento: Budapest

Formación: Se doctoró en la Universidad de Budapest en 1949

Docencia: Trabajó en el departamento de química orgánica de la Academia de Ciencias de Hungría y posteriormente en la

Universidad de Cleveland.

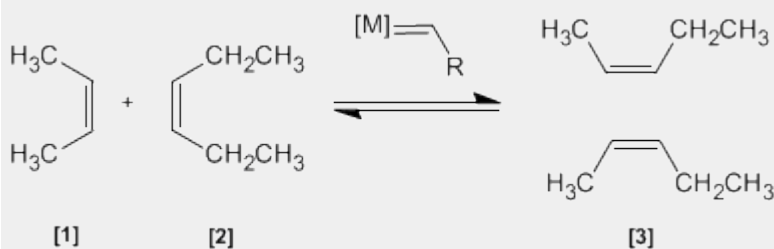
Industria: Trabajó en los laboratorios de la Dow Chemical de Ontario

Investigación: Olah consiguió preparar carbocationes estables utilizando componentes extremadamente ácidos.

Premio Nobel: En 1994 obtuvo el premio Nobel de Química por sus investigaciones sobre los carbocationes

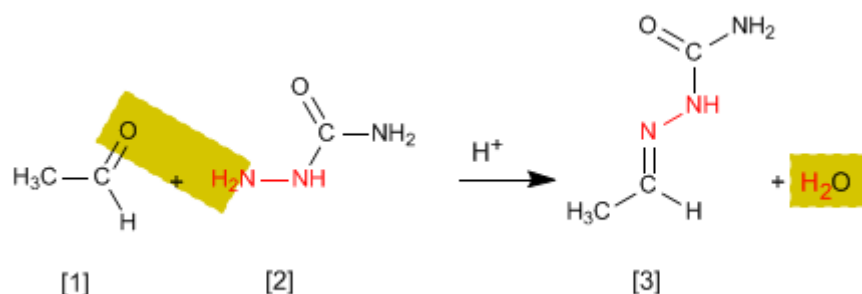
Metátesis de Alquenos

En esta reacción dos alquenos [1] y [2] son tratados con un metal de transición que actúa como catalizador, dando una mezcla de alquenos [3] (incluyendo isómeros Z/E). Este producto se obtiene por intercambio de grupos alquilideno.



Formación de Semicarbazonas

Las semicarbazonas [3] se obtienen por reacción de aldehídos o cetonas [1] con semicarbazida [2]. Veamos un ejemplo:



El mecanismo es análogo al de formación de iminas, oximas e hidrazonas.

Charles Friedel (1832 - 1899)



Origen: Químico frances..

Lugar de nacimiento: Estrasburgo.

Formación: estudió química en la Universidad de Berlín entre 1895 y 1899, consiguiendo el doctorado este año.

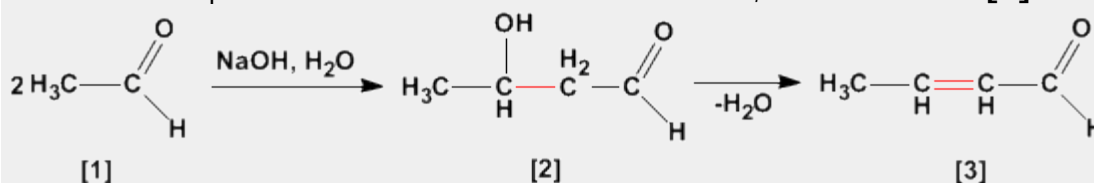
Docencia: Profesor en la Universidad de la Sorbona.

Investigación: Obtuvo el alcohol propílico. En 1877, Friedel y Crafts describieron por primera vez la reacción del benceno con un haloalcano en presencia de un ácido de Lewis. Esta reacción produce la alquilación del benceno y se conoce como alquilación de Friedl-Crafts.

Premio Nobel:

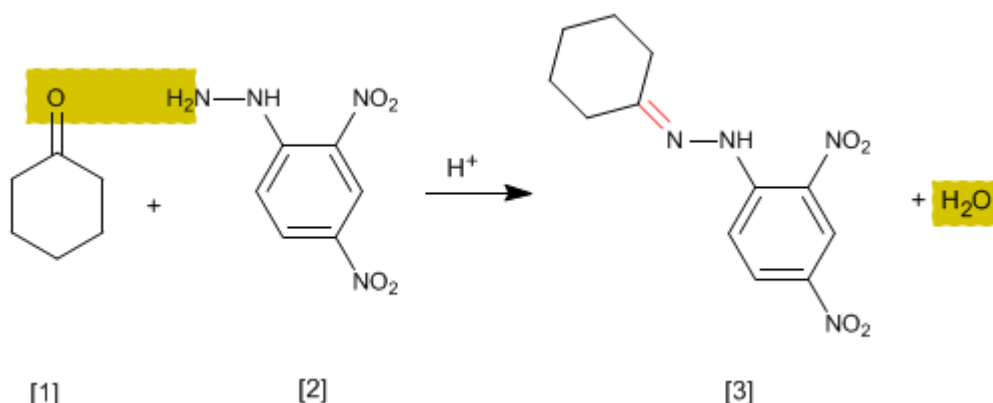
Aldólica (Condensación)

La condensación aldólica es una reacción de aldehídos o cetonas [1] que forma 3-hidroxicarbonilos (aldoles) [2]. El 3-hidroxiacetaldehído [2] bajo condiciones de deshidratación por calentamiento rinde un aldehído alfa,beta-insaturado [3].



Ensayo de la 2,4-Dinitrofenilhidrazina

Se trata de un ensayo analítico específico de aldehídos y cetonas. Los carbonilos **[1]** reaccionan con 2,4-Dinitrofenilhidrazina **[2]** formando fenilhidrazonas **[3]** que precipitan de color amarillo. La aparición de precipitado es un indicador de la presencia de carbonilos en el medio.



El mecanismo de la reacción es análogo al de formación de iminas.

Kurt Alder (1902 - 1958)



Origen: Químico alemán.

Lugar de nacimiento: Königshütte (hoy Chorzów, Polonia).

Formación: estudió en la Universidad de Kiel. Bajo la supervisión del químico alemán Otto Diels, su jefe e instructor en Kiel.

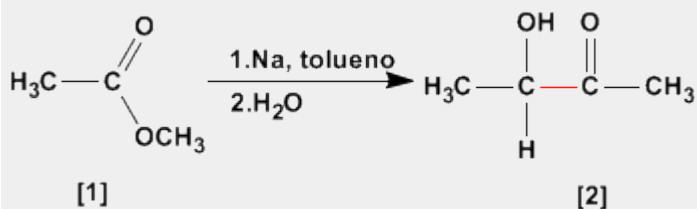
Docencia: Alder ejerció como profesor de química en las universidades de Kiel y Colonia.

Investigación: Alder se especializó en la síntesis diénica (conocida más tarde como la reacción Diels - Alder) que consiste fundamentalmente en el análisis y formación de compuestos orgánicos complejos. Ya en 1928 ambos fueron coautores de un ensayo sobre este proceso.

Premio Nobel: En 1950 recibió el Premio Nobel junto a Diels

Aciloinica (Condensación)

La condensación aciloinica transforma esteres **[1]** en alfa-hidroxicetonas **[2]**. Esta reacción se realiza con sodio metal en disolvente inerte.



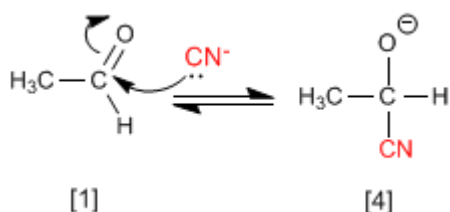
Formación de Cianhidrinas

Las cianhidrinas **[3]** se forman por reacción de aldehídos o cetonas **[1]** con ácido cianhídrico **[2]** y son compuestos que contienen un grupo ciano y un hidroxilo sobre el mismo carbono.

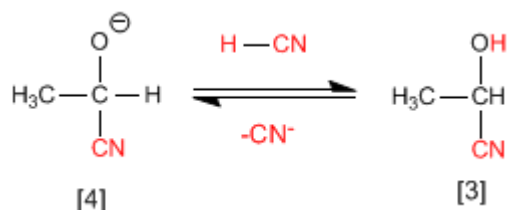


El mecanismo de la reacción transcurre en dos etapas:

Etapas 1. Los iones cianuro actúan como nucleófilos atacando al carbono carbonilo. El ácido cianhídrico es demasiado débil para generar cantidades importantes de cianuro, por ello, se añade cianuro de sodio o potasio al medio, garantizando la cantidad suficiente de cianuro para que la reacción transcurra en buen rendimiento.



Etapas 2. En este paso el ión alcóxido **[4]** se protona arrancando hidrógenos al ácido cianhídrico. En esta etapa se regeneran los iones cianuro.



Kurt Alder (1902 - 1958)



Origen: Químico alemán.

Lugar de nacimiento: Königshütte (hoy Chorzów, Polonia).

Formación: estudió en la Universidad de Kiel. Bajo la supervisión del químico alemán Otto Diels, su jefe e instructor en Kiel.

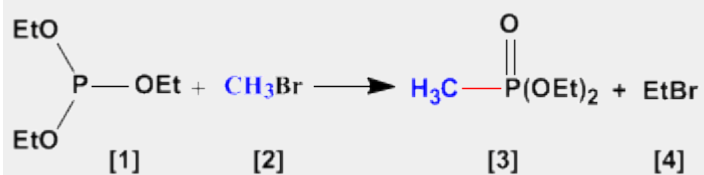
Docencia: Alder ejerció como profesor de química en las universidades de Kiel y Colonia.

Investigación: Alder se especializó en la síntesis diénica (conocida más tarde como la reacción Diels - Alder) que consiste fundamentalmente en el análisis y formación de compuestos orgánicos complejos. Ya en 1928 ambos fueron coautores de un ensayo sobre este proceso.

Premio Nobel: En 1950 recibió el Premio Nobel junto a Diels

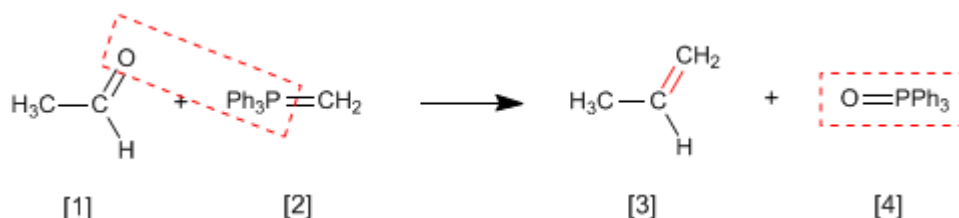
Arbuzov (Reacción)

La reacción de Arbuzov se emplea en la síntesis de fosfonatos **[3]** a partir de fosfitos **[1]**. Los fosfonatos obtenidos en la síntesis de Arbuzov se emplean como materiales de partida en la síntesis de Horner-Wittig.



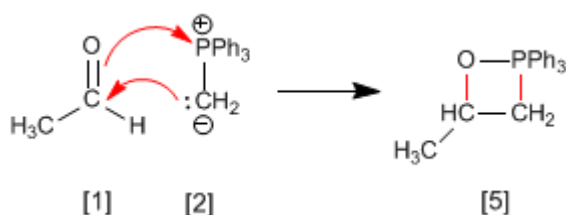
Reacción de Wittig

La reacción de Wittig emplea iluros de fósforo **[2]** para transformar aldehídos y cetonas **[1]** en alquenos **[3]**. Como subproducto se obtiene el óxido de trifenilfosfina **[4]**.

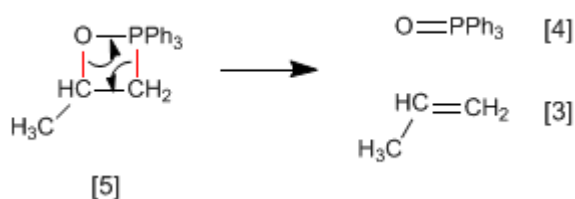


En el mecanismo de la reacción el iluro y el carbonilo se combinan para formar un oxafosfetano que rompe dejando libre el alqueno final.

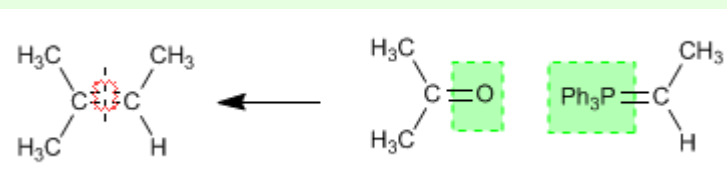
Etapas 1. El etanal y el iluro se combinan formando el fosfetano.



Etapas 2. El fosfetano rompe formando el alqueno y óxido de trifenilfosfina.

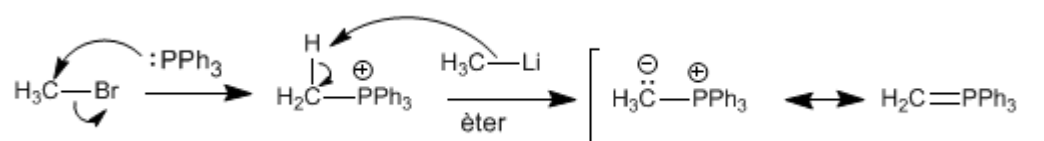


Ejemplo - Obtener mediante Wittig el 2-Metilbut-2-eno



Se rompe el alqueno por el doble enlace y a cada carbono se le agrega el grupo encerrado en verde.

Los **iluros de fósforo** se preparan mediante reacción de haloalcanos y trifenilfosfina, seguido de desprotonación del carbono con base fuerte (organometálicos de litio).



Charles Friedel (1832 - 1899)



Origen: Químico frances..

Lugar de nacimiento: Estrasburgo.

Formación: estudió química en la Universidad de Berlín entre 1895 y 1899, consiguiendo el doctorado este año.

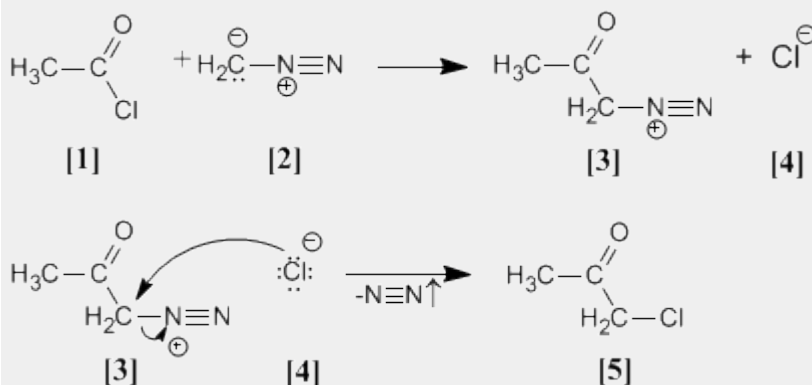
Docencia: Profesor en la Universidad de la Sorbona.

Investigación: Obtuvo el alcohol propílico. En 1877, Friedel y Crafts describieron por primera vez la reacción del benceno con un haloalcano en presencia de un ácido de Lewis. Esta reacción produce la alquilación del benceno y se conoce como alquilación de Friedl-Crafts.

Premio Nobel:

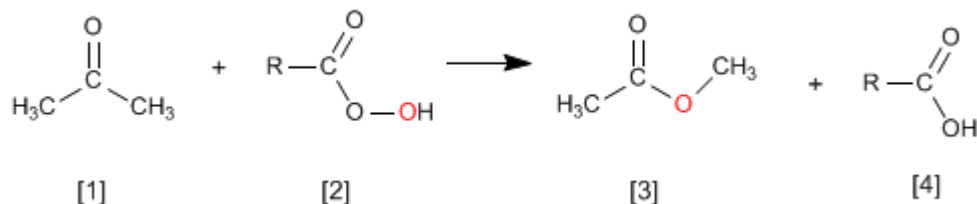
Arndt Eistert (Síntesis)

Cloruro de acetilo **[1]** se trata con diazometano **[2]** rindiendo la sal de diazonio **[3]**. El cloruro **[4]** producido reacciona con la sal de diazonio para dar la α -clorocetona **[5]**.

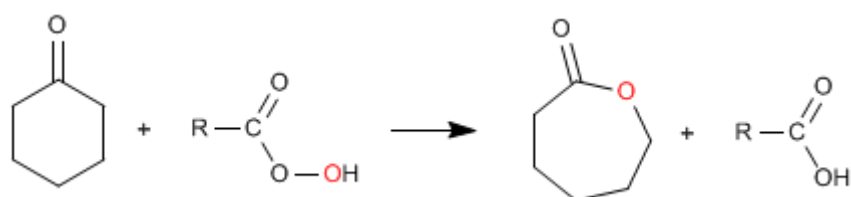


Oxidación de Baeyer Villiger

La reacción de cetonas **[1]** con perácidos **[2]** produce ésteres **[3]**. El oxígeno del perácido se inserta entre el carbono carbonilo y el carbono alfa de la cetona. Esta reacción fue descrita por Adolf von Baeyer y Victor Villiger in 1899.

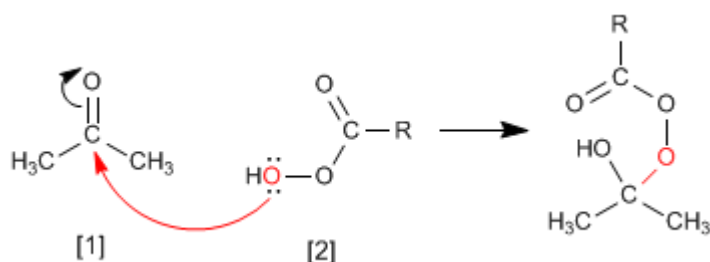


A partir de cetonas cíclicas se obtienen ésteres cíclicos (lactonas)

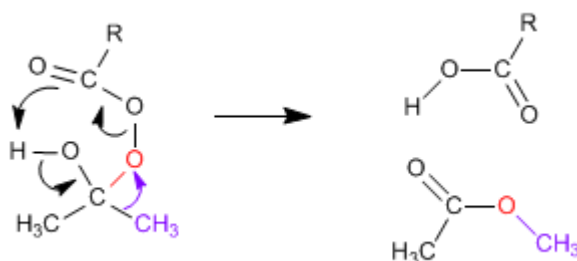


El mecanismo de Baeyer Villiger comienza con el ataque nucleófilo del perácido sobre el carbonilo, seguido de la migración del sustituyente desde el grupo carbonilo al oxígeno del perácido.

Etapas 1. Adición del perácido al carbonilo

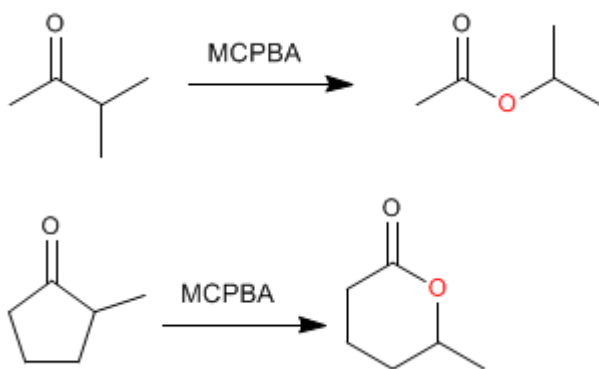


Etapas 2. Migración del sustituyente desde carbono carbonilo hacia el oxígeno (rojo)



Cuando la cetona tiene dos sustituyentes diferentes migra mejor el más sustituido. Existe un orden de migración que nos ayuda a decidir que sustituyente pasa a unirse al oxígeno del perácido.

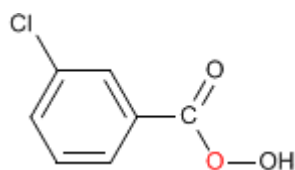
Orden de migración: H > carbono terciario > ciclohexilo > carbono secundario » fenilo > carbono primario > metilo



Como puede observarse en el orden de migración, el grupo que mejor migra, por su pequeño tamaño, es el hidrógeno, por ello, al tratar aldehídos con perácidos se produce la migración del hidrógeno formándose ácidos carboxílicos.



El **MCPBA** (Ácido meta-cloroperoxibenzoico) es un perácido ampliamente utilizado en la epoxidación de alquenos y también en Baeyer-Villger. La fórmula del MCPBA se muestra a continuación.



Charles Friedel (1832 - 1899)



Origen: Químico frances..

Lugar de nacimiento: Estrasburgo.

Formación: estudió química en la Universidad de Berlín entre 1895 y 1899, consiguiendo el doctorado este año.

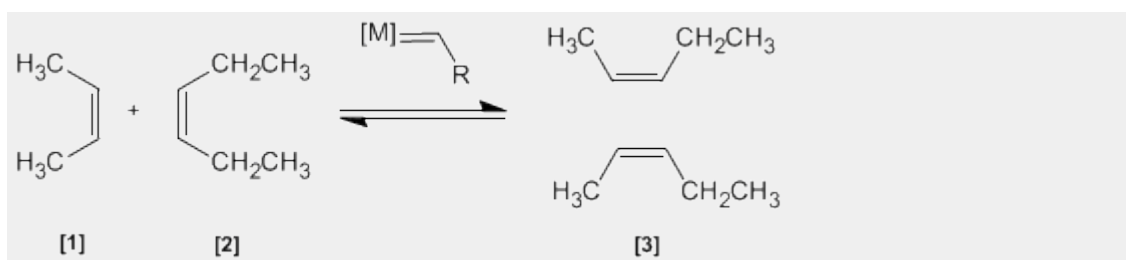
Docencia: Profesor en la Universidad de la Sorbona.

Investigación: Obtuvo el alcohol propílico. En 1877, Friedel y Crafts describieron por primera vez la reacción del benceno con un haloalcano en presencia de un ácido de Lewis. Esta reacción produce la alquilación del benceno y se conoce como alquilación de Friedl-Crafts.

Premio Nobel:

Metátesis de Alquenos

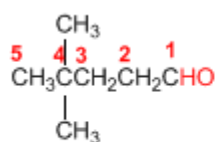
En esta reacción dos alquenos **[1]** y **[2]** son tratados con un metal de transición que actúa como catalizador, dando una mezcla de alquenos **[3]** (incluyendo isómeros Z/E). Este productos se obtiene por intercambio de grupos alquilideno.



Nomenclatura de Aldehídos y Cetonas - Reglas IUPAC

Regla 1. Los aldehídos se nombran reemplazando la terminación **-ano** del alcano correspondiente por **-al**. No es necesario especificar la posición del grupo aldehído, puesto que ocupa el extremo de la cadena (localizador 1).

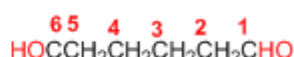
Cuando la cadena contiene dos funciones aldehído se emplea el sufijo **-dial**.



4,4-Dimetilpentanal

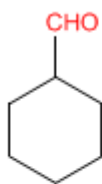


Hex-4-enal

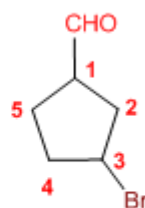


Hexanodial

Regla 2. El grupo **-CHO** se denomina **-carbaldehído**. Este tipo de nomenclatura es muy útil cuando el grupo aldehído va unido a un ciclo. La numeración del ciclo se realiza dando localizador 1 al carbono del ciclo que contiene el grupo aldehído.

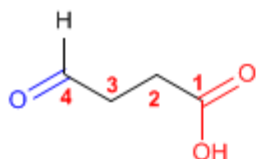


Ciclohexanocarbaldehído

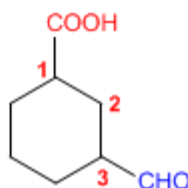


3-Bromociclopentanocarbaldehído

Regla 3. Cuando en la molécula existe un grupo prioritario al aldehído, este pasa a ser un sustituyente que se nombra como oxo- o formil-.



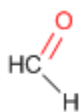
Ácido 4-oxobutanoico



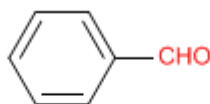
Ácido 3-formilciclohexanocarboxílico

Tanto **-carbaldehído** como **formil-** son nomenclaturas que incluyen el carbono del grupo carbonilo. **-carbaldehído** se emplea cuando el aldehído es grupo funcional, mientras que **formil-** se usa cuando actúa de sustituyente.

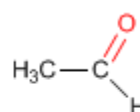
Regla 4. Algunos nombres comunes de aldehídos aceptados por la IUPAC son:



Formaldehído
(Metanal)

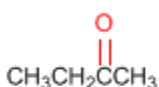


Benzaldehído
(Benceno**carbaldehído**)

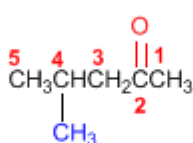


Acetaldehído
(Etanal)

Regla 5. Las cetonas se nombran sustituyendo la terminación **-ano** del alcano con igual longitud de cadena por **-ona**. Se toma como cadena principal la de mayor longitud que contiene el grupo carbonilo y se numera para que éste tome el localizador más bajo.



Butan**ona**

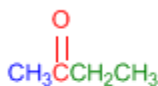


4-Metil-2-pentan**ona**

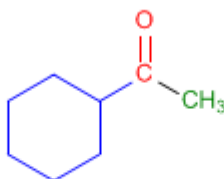


3-Metilciclohexan**ona**

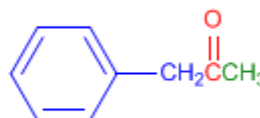
Regla 6. Existe un segundo tipo de nomenclatura para las cetonas, que consiste en nombrar las cadenas como sustituyentes, ordenándolas alfabéticamente y terminando el nombre con la palabra cetona.



Etil metil **cetona**

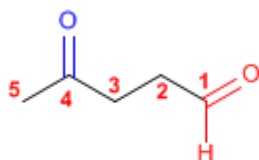


Ciclohexil metil **cetona**

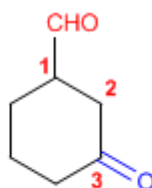


Fenil metil **cetona**

Regla 7. Cuando la cetona no es el grupo funcional de la molécula pasa a llamarse **OXO-**.



4-Oxopentan**al**

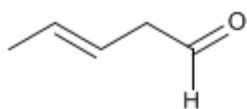


3-Oxociclohexano**carbaldehído**

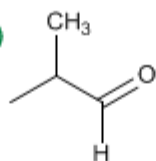
Nomenclatura de Aldehídos y Cetonas - Problema 9.1

Nombra los siguientes aldehídos y cetonas:

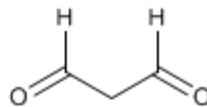
a)



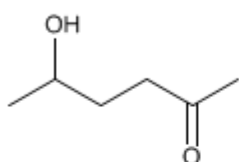
b)



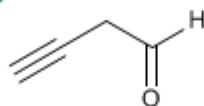
c)



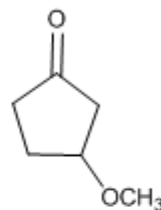
d)



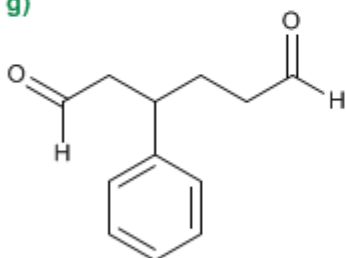
e)



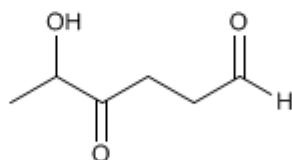
f)



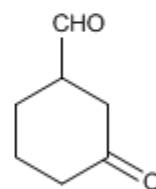
g)



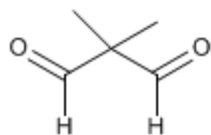
h)



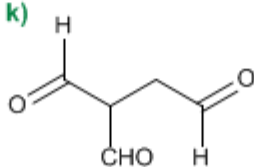
i)



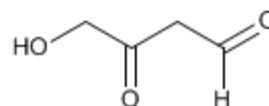
j)



k)

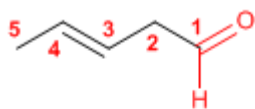


l)

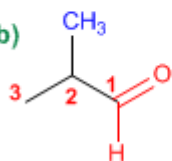


Solución

a)



b)



1. Cadena principal: 5 carbonos (pentano)

2. Numeración: comienza en el aldehído (grupo funcional)

Grupo funcional: aldehído

3. Nombre: Pent-3-enal

1. Cadena principal: 3 carbonos (propano)

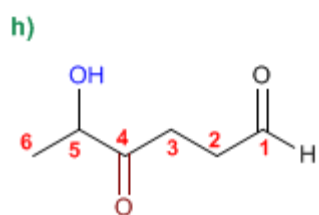
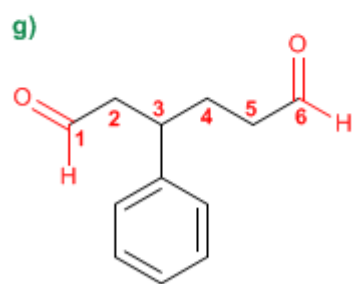
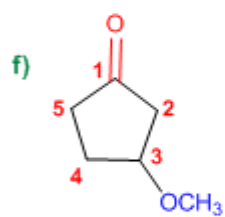
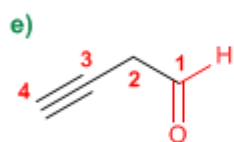
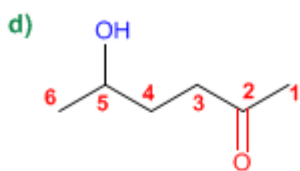
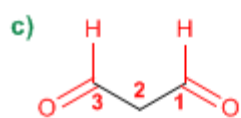
2. Numeración: localizador más bajo al aldehído.

3. Grupo funcional: aldehído

4. Sustituyentes: metilo en 2.

5. Nombre: 2-Metilpropanal

Los aldehídos y cetonas son prioritarios sobre alquenos y alquinos, y se numeran otorgándoles el localizador más bajo



1. Cadena principal: 3 carbonos (propano)
2. Grupo funcional: aldehído (dialdehído)
3. Nombre: Propanodial

1. Cadena principal: 6 carbonos (hexano)
2. Grupo funcional: cetona
3. Numeración: asignar el menor localizador a la cetona
4. Sustituyentes: hidroxí en 5.
5. Nombre: 5-Hidroxihexan-2-ona

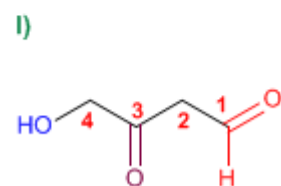
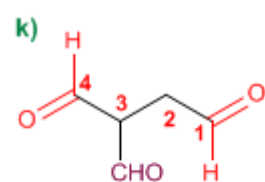
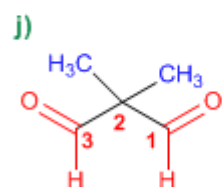
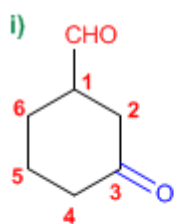
1. Cadena principal: 4 carbonos (butano)
2. Grupo funcional: aldehído
3. Numeración: asignar el menor localizador al aldehído
4. Nombre: But-3-inal

1. Cadena principal: ciclo de 5 miembros (ciclopentano)
2. Grupo funcional: cetona
3. Numeración: comienza en la cetona y prosigue hacia el sustituyente
4. Sustituyentes: metoxi en 3.
5. Nombre: 3-Metoxiciclopentanona

1. Cadena principal: 6 carbonos (hexano)
2. Grupo funcional: aldehído (dialdehído)
3. Numeración: comienza en el extremo que otorga al fenilo el localizador más bajo.
4. Sustituyentes: fenilo en 3.
5. Nombre: 3-Fenilhexanodial

1. Cadena principal: 6 carbonos (hexano)
2. Grupo funcional: aldehído
3. Numeración: asignar el menor localizador al aldehído
4. Sustituyentes: hidroxí en 5 y oxo en 4.
5. Nombre: 5-Hidroxí-4-oxohexanal

Los aldehídos son prioritarios sobre las cetonas que pasan a nombrarse como sustituyentes (oxo-)



1. Cadena principal: ciclo de 6 miembros (ciclohexano)
2. Grupo funcional: aldehído (-carbaldehído)
3. Numeración: menor localizador al grupo -CHO (este no se numera)
4. Sustituyentes: cetona (oxo-) en 3
5. Nombre: 3-Oxociclohexanocarbaldehído

1. Cadena principal: 3 carbonos (propano)
2. Grupo funcional: aldehído (dialdehído)
3. Sustituyentes: metilos en 2,2.
4. Nombre: 2,2-Dimetilpropanodial

1. Cadena principal: 4 carbonos (butano)
2. Grupo funcional: aldehído
3. Sustituyentes: formil en 3
4. Nombre: 3-Formilbutanodial

1. Cadena principal: 4 carbonos (butano)
2. Grupo funcional: aldehído
3. Numeración: asignar el menor localizador al aldehído
4. Sustituyentes: hidroxil en 4 y oxo en 3.
5. Nombre: 4-Hidroxil-3-oxobutanal

Nomenclatura de Aldehídos y Cetonas - Problema 9.2

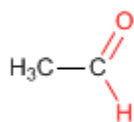
PRINT EMAIL

Dibuja la estructura de los siguientes aldehídos y cetonas:

- | | |
|---|----------------------------------|
| a) Etanal (acetaldehído) | g) 2,5-Dioxooctanodial |
| b) 3-Metilbutanal | h) 1,3-Ciclohexanodiona |
| c) Benzaldehído | i) 3-Metil-3-pental |
| d) 4-Hidroxiciclohexanocarbaldehído | j) 3-Oxobutanal |
| e) 3-Hidroxi-4-metil-5-oxociclohexanocarbaldehído | k) 3-Hidroxiciclopentanona |
| f) 2-Metil-2,5-octanodiona | l) 4-Etoxi-5-fenil-3-oxoheptanal |

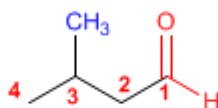
Solución

a)



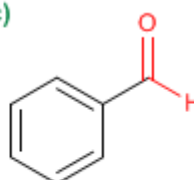
Etanal (acetaldehído)

b)

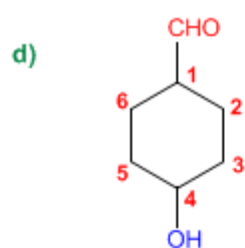


3-Metilbutanal

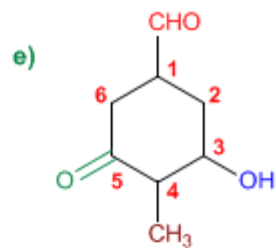
c)



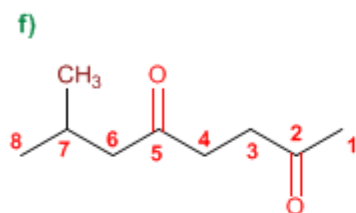
Benzaldehído



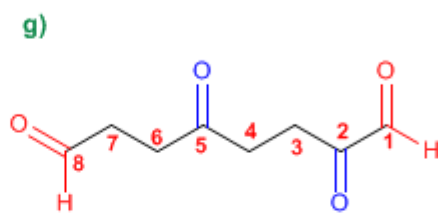
4-Hidroxiciclohexanocarbaldehído



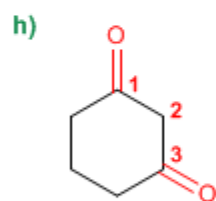
3-Hidroxi-4-metil-5-oxociclohexanocarbaldehído



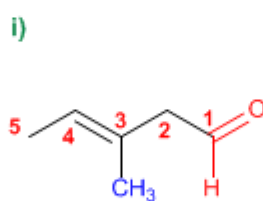
7-Metil-2,5-octanodiona



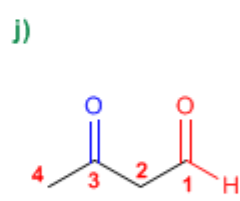
2,5-Dioxooctanal



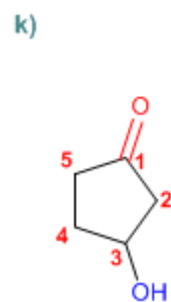
1,3-Ciclohexanodiona



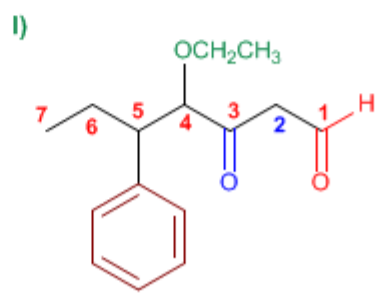
3-Metil-3-pentenal



3-Oxobutanal



3-Hidroxiciclopentanona

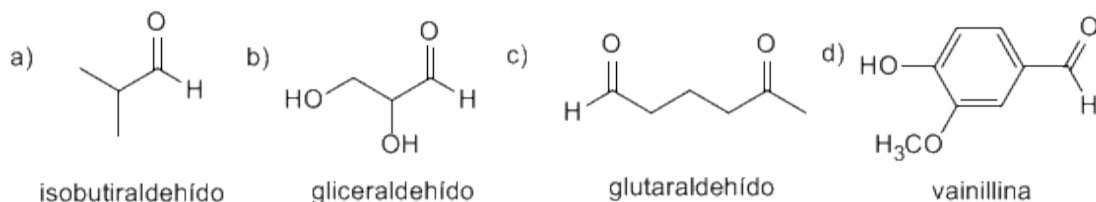


4-Etoxi-5-fenil-3-oxoheptanal

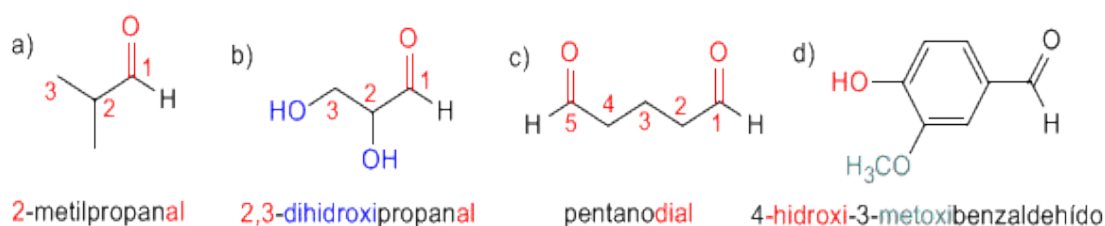
PROBLEMAS RESUELTOS DE ALDEHÍDOS Y CETONAS

Aldehídos y Cetonas: Problema 1

1) A continuación se dan nombres comunes y las fórmulas estructurales de algunos compuestos carbonílicos. Indique el nombre correspondiente según la IUPAC.



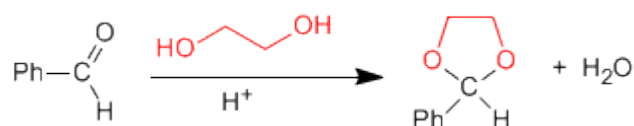
Solución



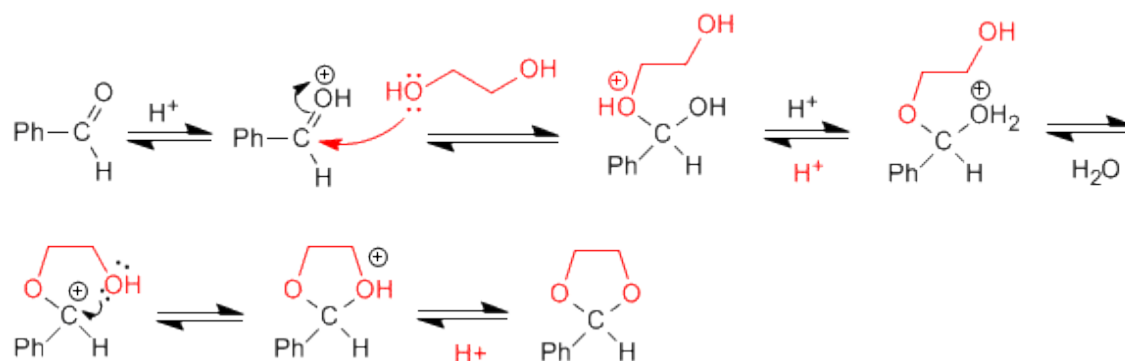
Aldehídos y cetonas: Problema 2

Dibuje la estructura del acetal que se forma cuando el benzaldehído se calienta con 1,2-etanodiol en medio ácido. Escriba un mecanismo detallado que justifique su formación. Describa paso a paso la hidrólisis de este acetal en medio ácido acuoso.

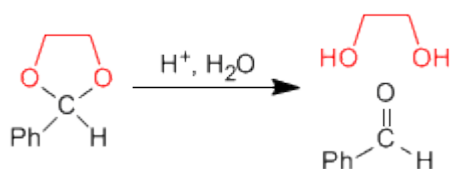
SOLUCIÓN



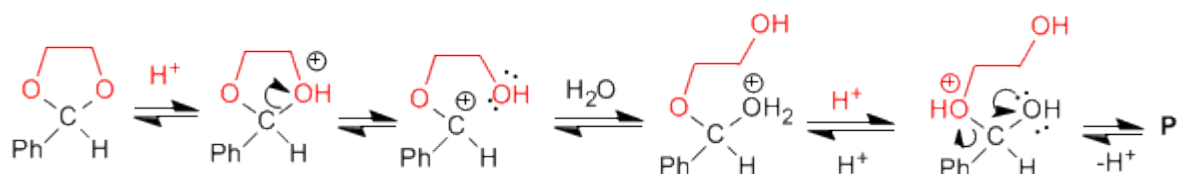
Mecanismo de formación del acetal:



La hidrólisis del acetal en medio ácido acuoso sigue es etapas inversas a la síntesis.



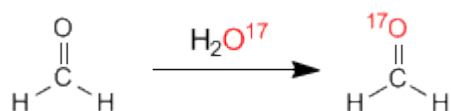
Mecanismo de hidrólisis del acetal cíclico.



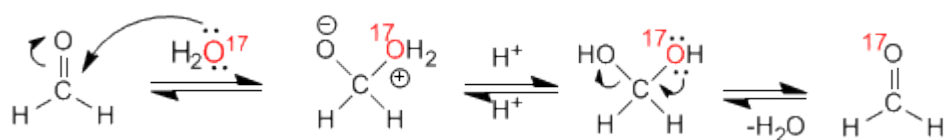
Aldehídos y Cetonas: Problema 3

Cuando se disuelve formaldehído en agua marcada con ^{17}O , se observa que después de unas horas tanto el hidrato del formaldehído como el formaldehído han incorporado el isótopo ^{17}O . Sugiera una explicación razonable de este hecho.

SOLUCION



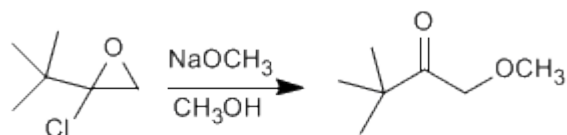
Mecanismo:



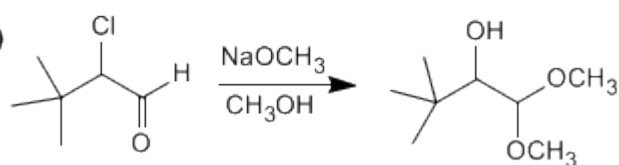
Aldehídos y Cetonas: Problema 4

Sugiera un mecanismo razonable para una de las siguientes reacciones:

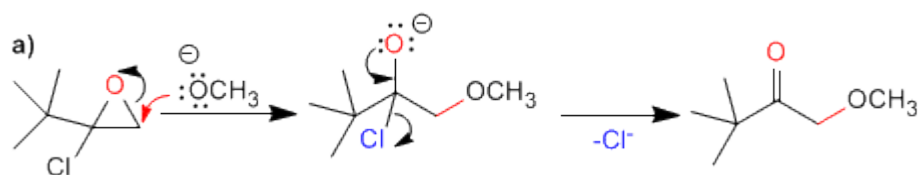
a)



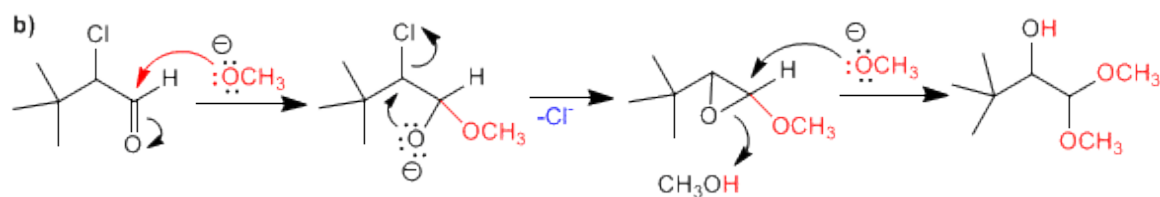
b)



SOLUCION



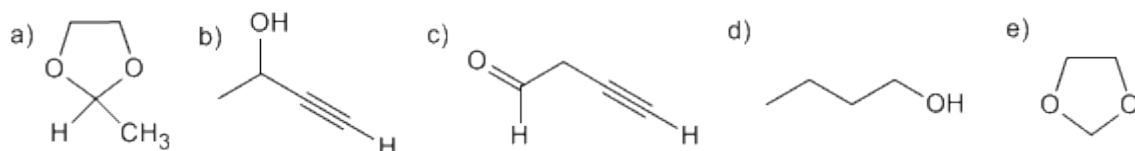
La primera etapa consiste en la apertura del oxaciclopropano sobre el carbono menos sustituido. En la segunda etapa, la cesión del par del oxígeno elimina el cloro, formándose un carbonilo.



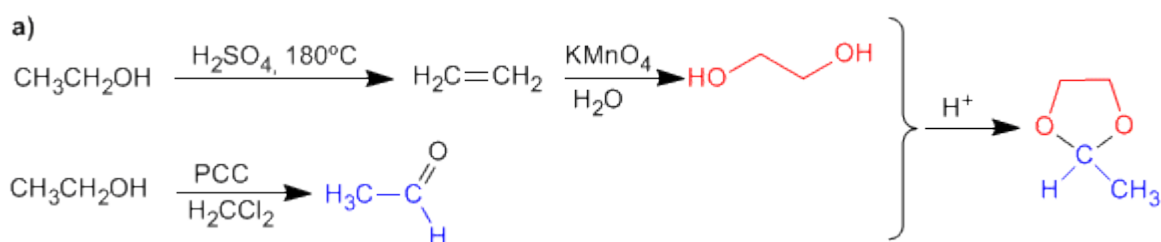
En el primer paso hay dos posibles posiciones de ataque; el carbono carbonilo y el carbono del cloro. Como el producto final no tiene metóxido en el carbono del cloro, atacamos al carbonilo. En la segunda etapa se produce una sustitución nucleófila intramolecular. Para terminar el metóxido abre el epóxido.

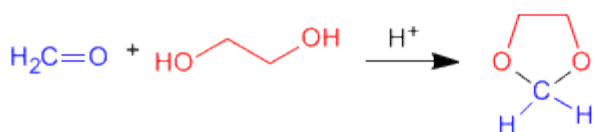
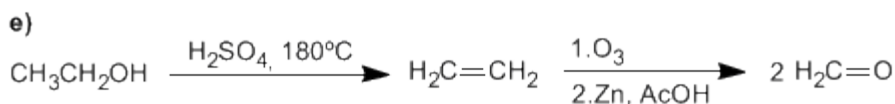
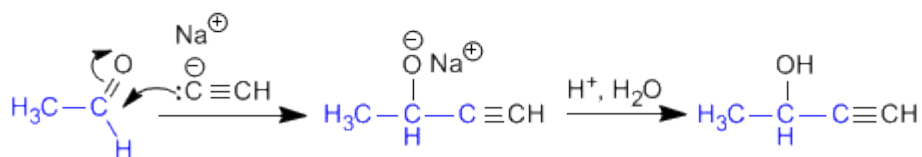
Aldehídos y Cetonas: Problema 5

Usando etanol como fuente de todos los átomos de carbono y los reactivos que necesite, describa una síntesis eficiente de cada una de las sustancias siguientes:

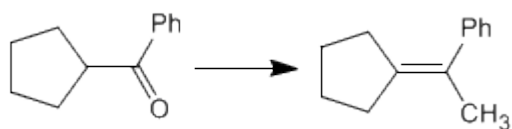


SOLUCIÓN





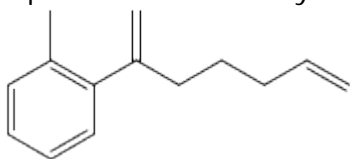
Utilizando los reactivos necesarios, indicar las etapas que permiten realizar la siguiente transformación:



[2] Isomerización en medio ácido, impulsada por la mayor estabilidad del alqueno interno.

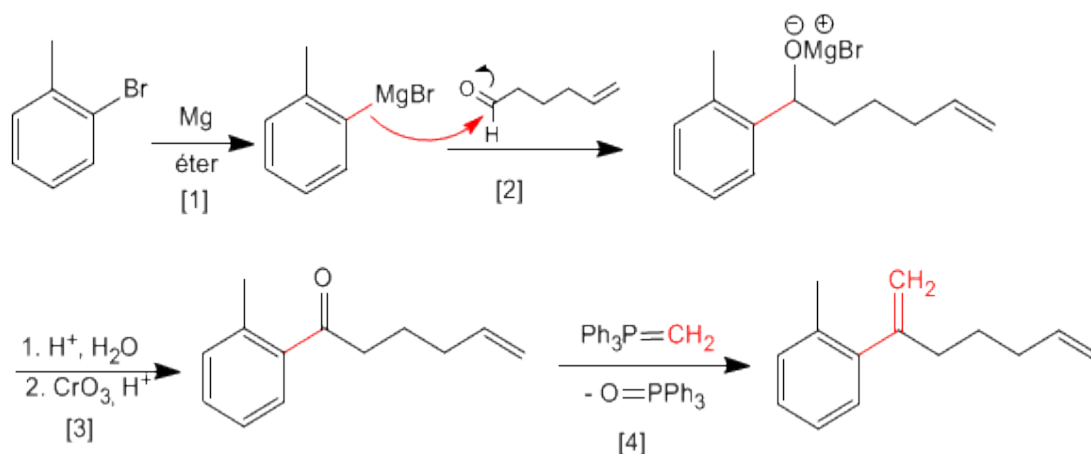
Aldehídos y Cetonas: Problema 7

A partir de 5-hexenal y o-bromotolueno obtener el siguiente producto.



Pueden ser necesarios reactivos orgánicos e inorgánicos adicionales.

SOLUCIÓN



[1] Formación del magnesiano

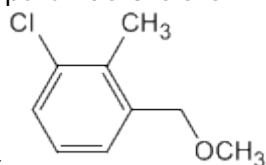
[2] Ataque nucleófilo del magnesiano al carbonilo.

[3] Hidrólisis y posterior oxidación del alcohol secundario.

[4] Reacción de Wittig entre la cetona y el trifenilmetilenfosforano.

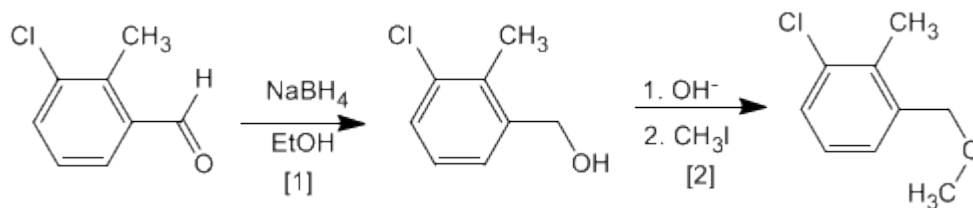
Aldehídos y Cetonas: Problema 8

Obtener a partir de 3-cloro-2-metilbenzaldehído y de los reactivos



necesarios
el compuesto siguiente:

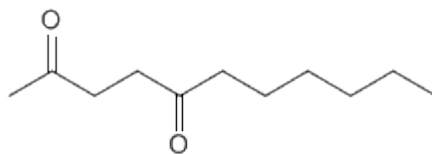
SOLUCIÓN



[1] Reducción del aldehído a alcohol

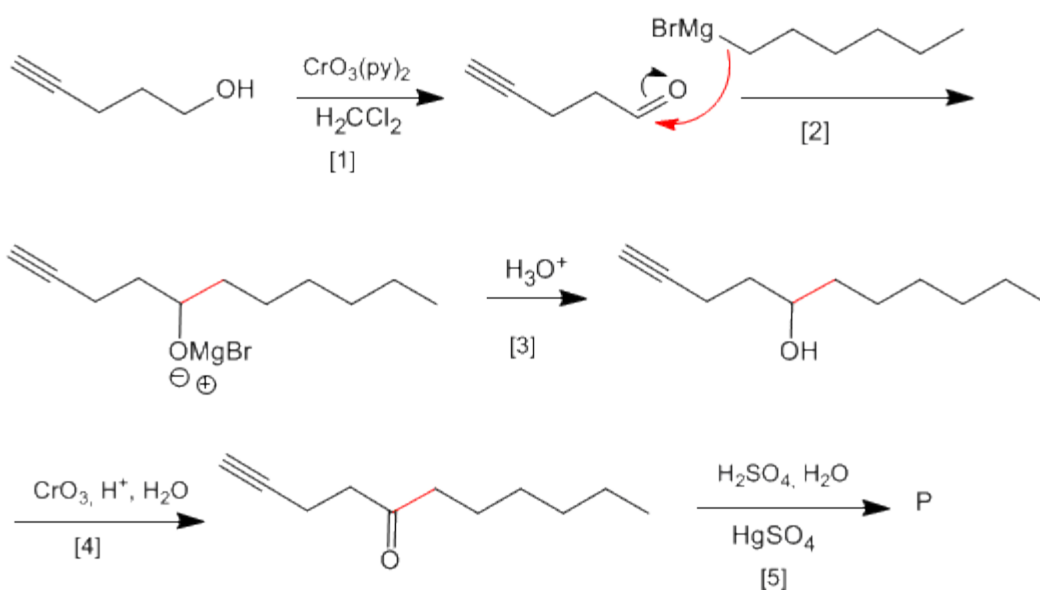
[2] Síntesis de Williamson de éteres.

Aldehídos y Cetonas: Problema 9



A partir de 4-pentin-1-ol obtener:

SOLUCIÓN

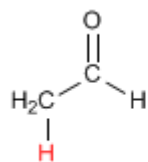


- [1] Oxidación del alcohol a aldehído
- [2] Formación del enlace carbono-carbono mediante organometálicos de magnesio
- [3] Protonación del alcohol
- [4] Oxidación del alcohol con Jones (Puedes utilizar también $\text{CrO}_3(\text{py})_2$)
- [5] Hidratación Markovnikov del alquino, para formar cetonas

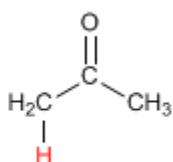
TEORÍA DE ENOLES Y ENOLATOS

Formación de Enolatos

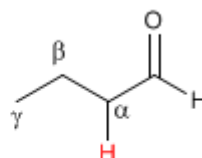
Los aldehídos y cetonas presentan hidrógenos ácidos en la posición vecina al grupo carbonilo, conocida como posición alfa. Estos hidrógenos presentan un pKa comprendido entre 18 y 21.



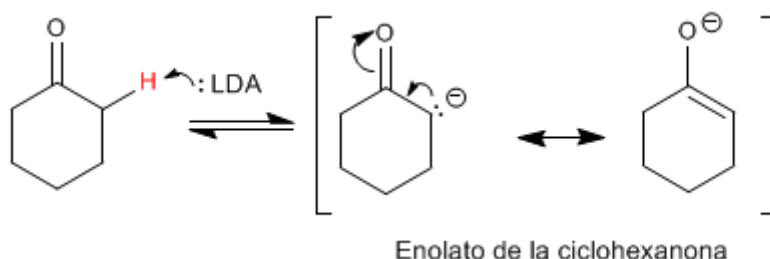
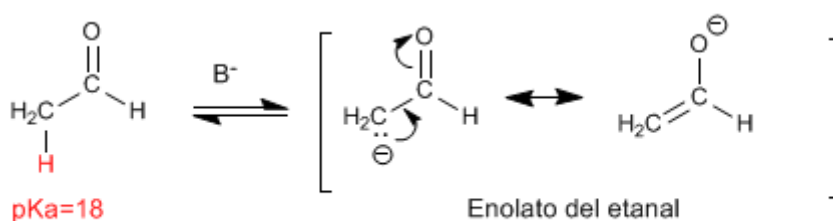
pKa=18



pKa=20-21



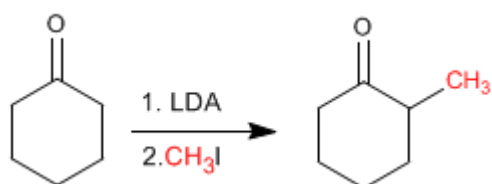
La acidez de los hidrógenos α es debida a la estabilización de la base conjugada (enolato) por resonancia.



Alquilación de Enolatos

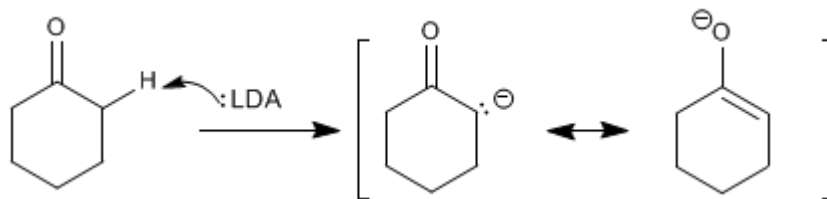
Los enolatos actúan como nucleófilos a través del carbono atacando a un gran número de electrófilos (haloalcanos, epóxidos, carbonilos, ésteres.....). En este punto nos fijaremos en la reacción entre enolatos y haloalcanos, que permite añadir cadenas carbonadas a la posición α de la cadena.

La Ciclohexanona se convierte en 2-Metilciclohexanona por tratamiento con LDA seguido de yoduro de metilo.

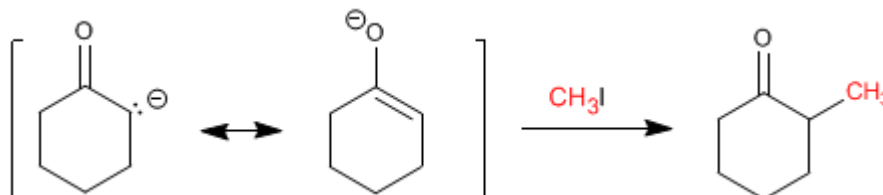


Etapas del mecanismo por el que se alquila la ciclohexanona:

Etapas 1. Formación del enolato

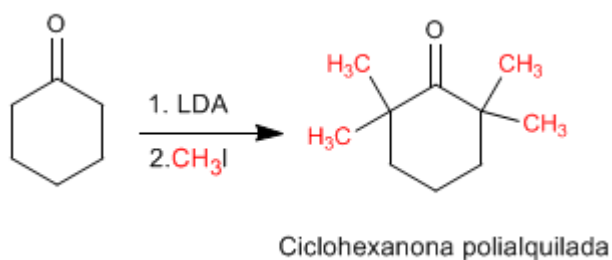


Etapas 2. Ataque nucleófilo del enolato sobre el haloalcano (Reacción de tipo S_N2)



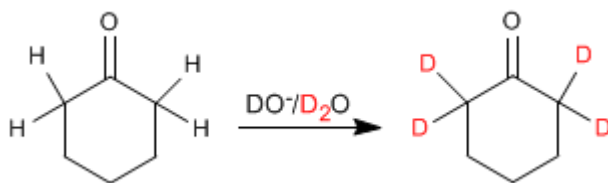
Las reacciones de alquilación tienen dos importantes problemas.

1. Competencia con la condensación aldólica. Los carbonilos en medio básico tienden a condensar para formar aldoles.
2. La reacción es difícil de controlar y tiende a polialquilar el carbonilo.



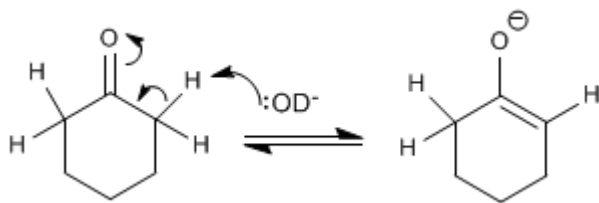
Intercambio hidrógeno - Deuterio

Los aldehídos y cetonas intercambian sus hidrógenos α por deuterios cuando se tratan con $\text{DO}^-/\text{D}_2\text{O}$ o con $\text{D}^+/\text{D}_2\text{O}$. En medios básicos la reacción transcurre a través de enolatos y en medios ácidos los intermediarios formados son enoles.

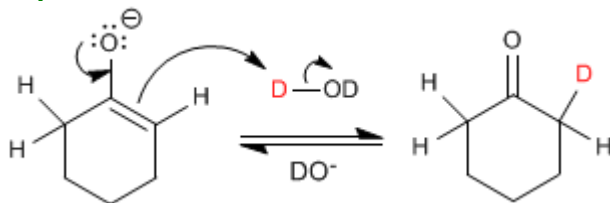


El mecanismo del intercambio hidrógeno-deuterio transcurre en los siguientes pasos:

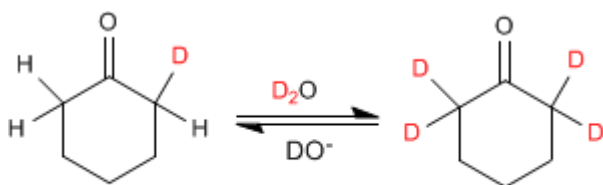
Etapas 1. Formación del enolato



Etapas 2. Transferencia del deuterio al enolato



Etapas 3. Sustitución del resto de hidrógenos



Halogenación de aldehídos y cetonas

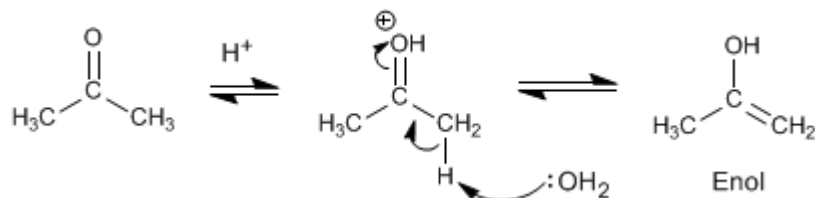
Los aldehídos y cetonas reaccionan con halógenos en medios ácidos o básicos produciéndose la sustitución de hidrógenos a por halógenos.

Halogenación de la propanona en medio ácido:

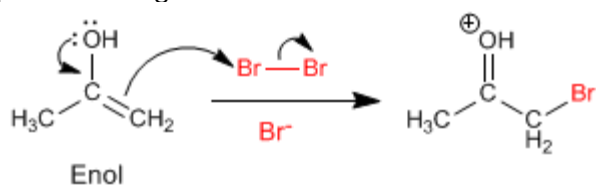


El mecanismo de halogenación en **medio ácido** tiene las siguientes etapas:

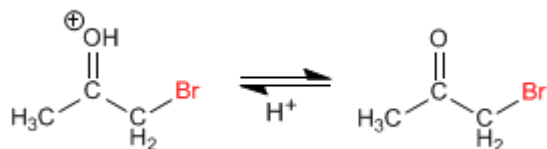
Etapas 1. Formación del enol



Etapas 2. Ataque nucleófilo del enol sobre el halógeno ayudado por la cesión del para del oxígeno.

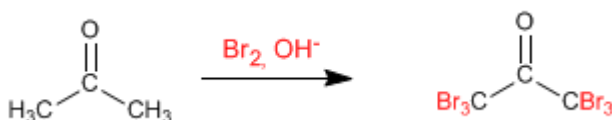


Etapa 3. Desprotonación



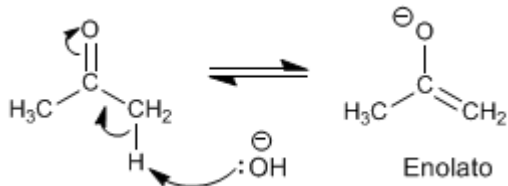
Trabajando con un equivalente de reactivo la halogenación para en una primera adición y no ocurren polihalogenaciones. El paso clave del mecanismo es la formación del enol y esta etapa requiere protonar el oxígeno del carbonilo. Una vez halogenada la posición α al oxígeno se vuelve menos básico, debido al efecto electronegativo del bromo, protonándose peor.

Halogenación de la propanona en **medio básico**:

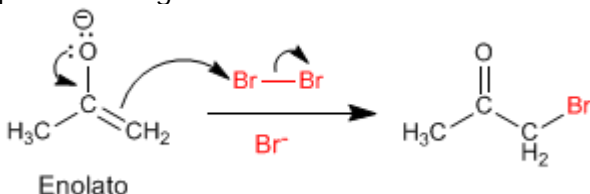


La halogenación en medio básico tiene el siguiente mecanismo:

Etapa 1. Formación del enolato



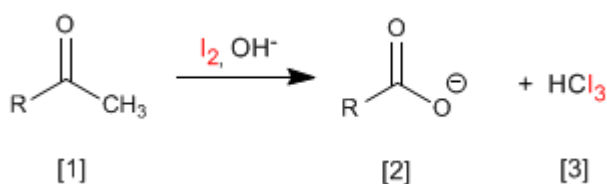
Etapa 2. Ataque nucleófilo del enolato sobre el halógeno ayudado por la cesión del par del oxígeno.



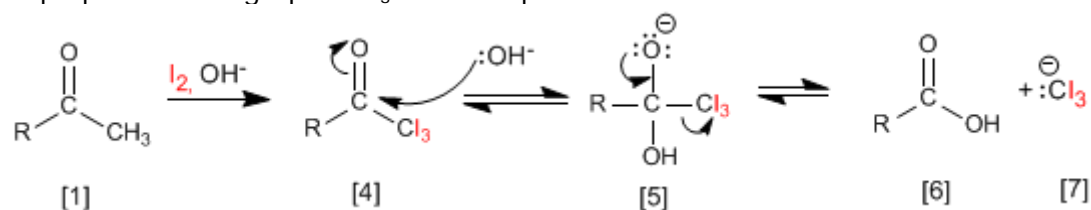
Este mecanismo se repite otras 5 veces sustituyendo todos los hidrógenos α por halógenos. En este caso la reacción no para puesto que el producto halogenado es más reactivo que la propanona de partida. La base arranca mejor los hidrógenos en el producto halogenado (son más ácidos), haciendo imposible parar la reacción.

Reacción del Haloformo (Yodoformo)

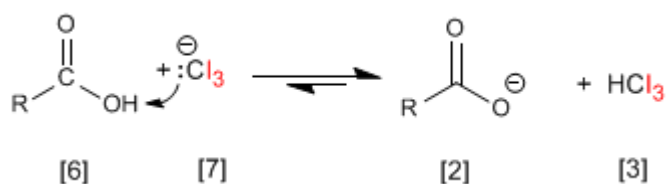
Las cetonas metílicas **[1]** reaccionan con halógenos en medios básicos generando carboxilatos **[2]** y haloformo **[3]**.



El mecanismo consiste en halogenar completamente el metilo, sustituyendo en una etapa posterior el grupo -CX₃ formado por -OH.



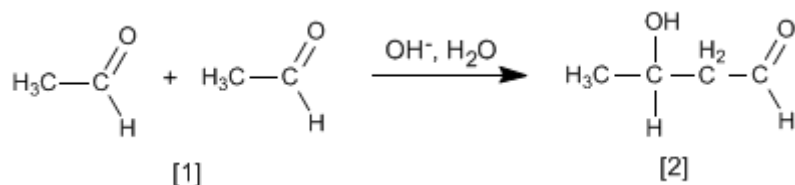
El grupo Cl₃⁻ es muy básico y desprotona el ácido carboxílico formándose yodoformo y el carboxilato.



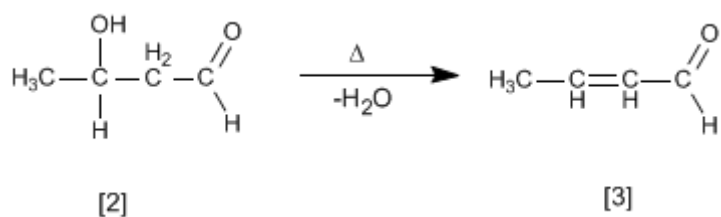
Esta reacción (con yodo) puede emplearse como ensayo analítico para identificar cetonas metílicas aprovechando que el yodoformo precipita de color amarillo.

Condensación Aldólica

Aldehídos y cetonas **[1]** condensan en medios básicos formando aldoles **[2]**. Esta reacción se denomina condensación aldólica.

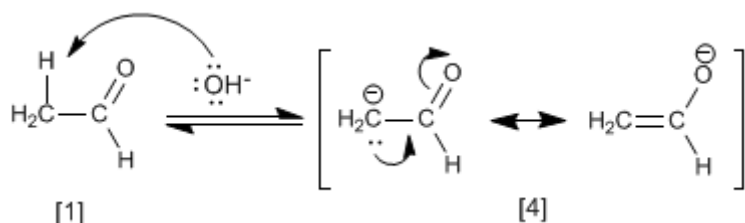


El aldol **[2]** formado deshidrata en el medio básico por calentamiento para formar un α,β-insaturado **[3]**.



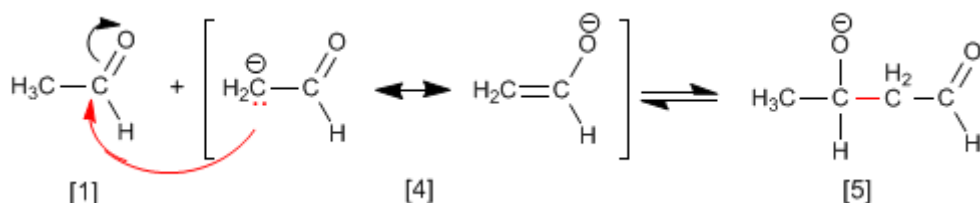
El mecanismo de la condensación aldólica transcurre con formación de un enolato, que ataca al carbonilo de otra molécula. En esta condensación se forma un enlace carbono-carbono entre el carbonilo de una molécula y el carbono α de la otra.

Etapas 1. Formación del enolato

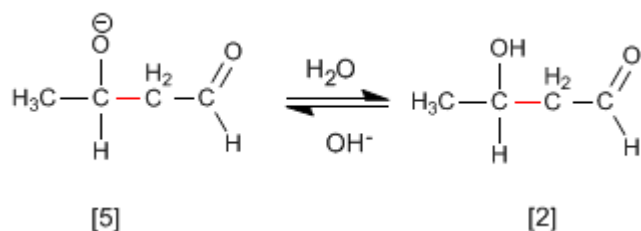


La base desprotona el carbono alfa del etanal [1] generando el enolato [4] estabilizado por resonancia.

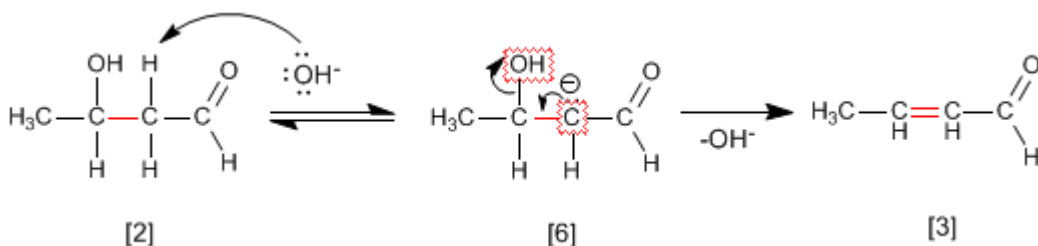
Etapas 2. Ataque nucleófilo del enolato sobre el carbonilo



Etapas 3. Protonación

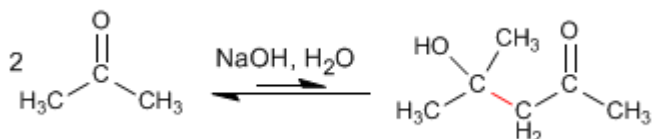


Etapas 4. Deshidratación del aldol

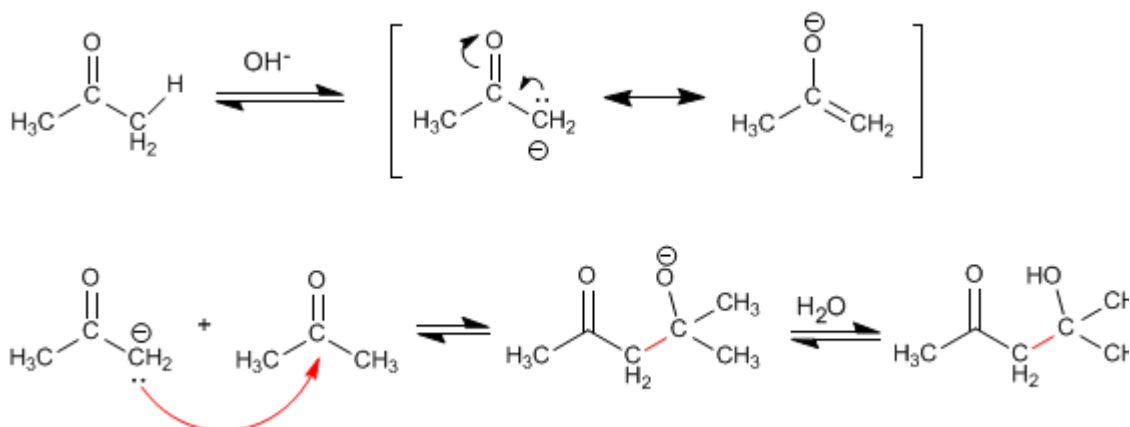


Condensación aldólica con cetonas

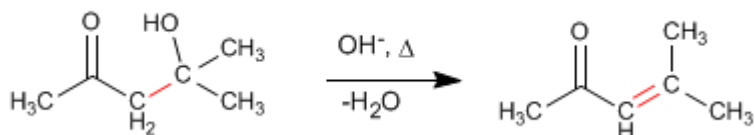
Las cetonas son menos reactivas que los aldehídos y dan un rendimiento muy bajo en la condensación aldólica. Así, dos moléculas de propanona condensan para formar el aldol correspondiente con un rendimiento del 2%. Se pueden conseguir porcentajes elevados del producto separándolo del medio de reacción según se va formando, o bien, calentando para deshidratarlo. De ambas formas los equilibrios de la aldólica se desplazan hacia el producto final.



Mecanismo de la reacción:

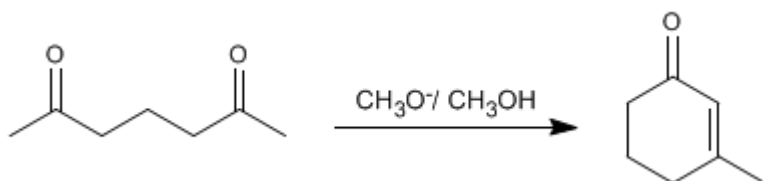


La deshidratación final permite el desplazamiento de los equilibrios. También se puede realizar una extracción del aldol del medio de reacción para favorecer la reacción.



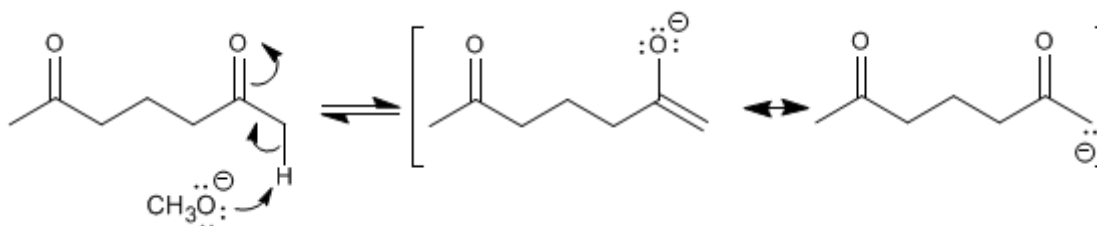
Condensación aldólica intramolecular

Los compuestos dicarbonílicos condensan mediante la aldólica intramolecular en medios básicos. En esta reacción se obtienen ciclos de cinco o seis miembros. Así, la 2,6-heptanodiona condensa con metóxido en metanol para formar el 3-metilciclohex-2-enona.

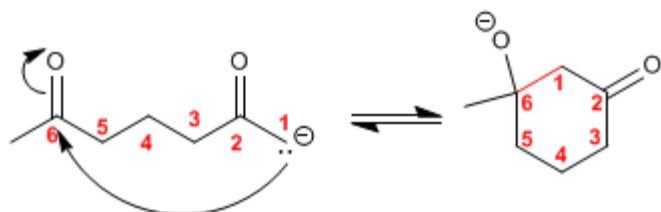


El mecanismo de la reacción transcurre a través de las siguientes etapas:

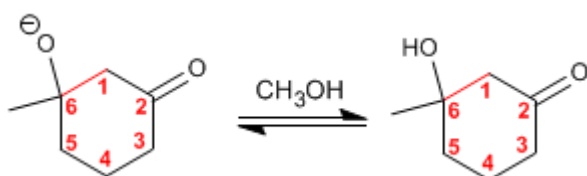
Etapa 1. Formación del enolato.



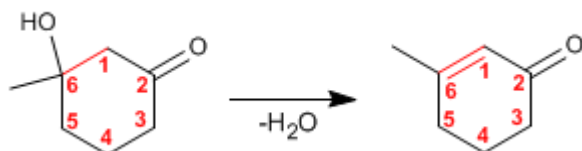
Etapa 2. Adición nucleófila intramolecular



Etapa 3. Protonación de la base del aldol



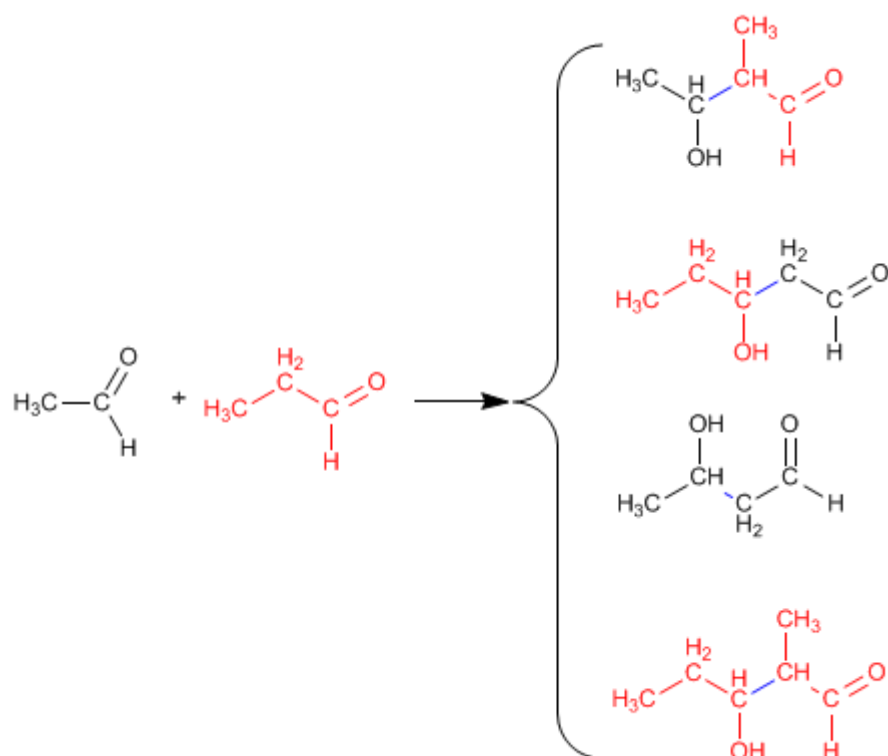
Etapa 4. Deshidratación del aldol



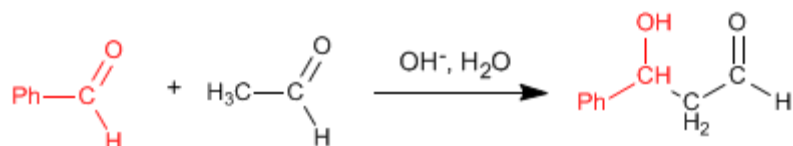
Condensación aldólica cruzada o mixta

La reacción entre dos carbonilos diferentes se llama aldólica cruzada o mixta. Esta reacción sólo tiene utilidad sintética en dos casos:

1. Sólo uno de los carbonilos puede formar enolatos.
 2. Uno de los carbonilos es mucho más reactivo que el otro.
- En el resto de situaciones la aldólica mixta genera mezclas de cuatro productos. Veamos como ejemplo la condensación del etanal y propanal.

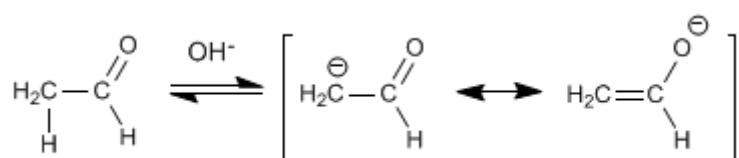


La condensación aldólica mixta del etanal con el benzaldehído genera un producto, cuando se trabaja en exceso de benzaldehído, debido a que el benzaldehído carece de hidrógenos en el carbono alfa y no puede formar enolatos.



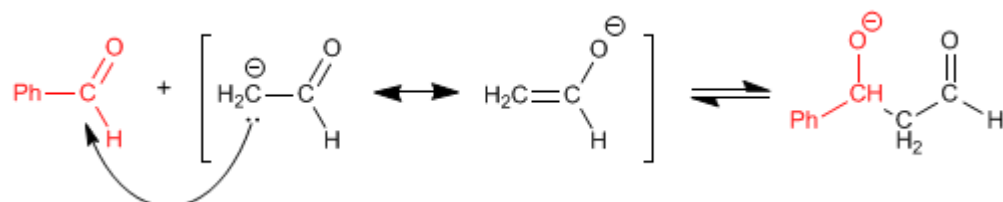
El mecanismo de esta reacción tiene lugar en las siguientes etapas:

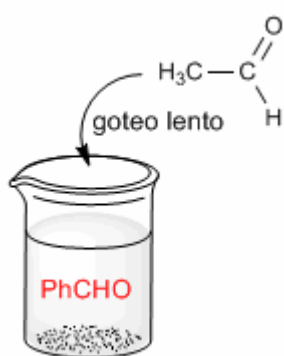
Etapla 1. Enolización del etanal



La formación de enolatos sólo puede tener lugar con el etanal, puesto que el benzaldehído carece de hidrógenos ácidos en el carbono alfa.

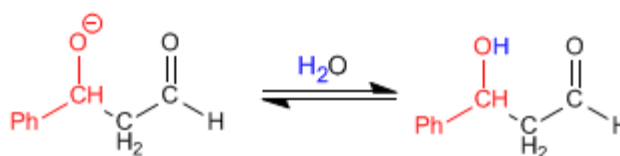
Etapla 2. Ataque nucleófilo del enolato al benzaldehído.





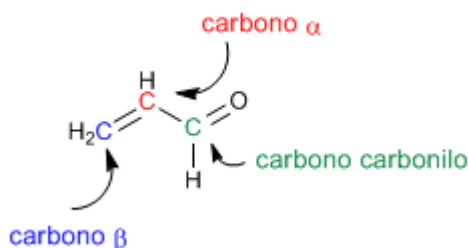
En esta etapa puede ocurrir el ataque del enolato de etanal sobre si mismo. Para evitarlo debe trabajarse en exceso de benzaldehído. Un procedimiento experimental muy usado para evitar la condensación del etanal consigo mismo es gotear lentamente el etanal sobre una disolución básica de benzaldehído

Etapa 3. Protonación



Síntesis de carbonilos alfa,beta-insaturados

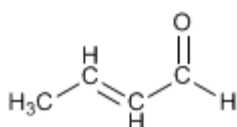
Los carbonilos α,β -insaturados son compuestos orgánicos que tienen un doble enlace entre las posiciones α,β de un aldehído o cetona.



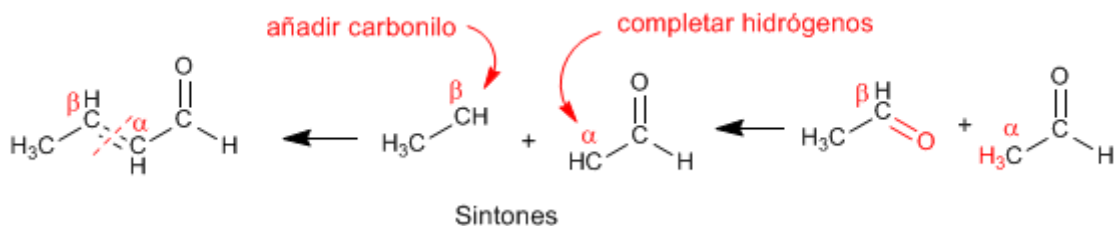
El propenal o acroleína es un carbonilo α,β -insaturado. Sus dos dobles enlaces conjugados le confieren una reactividad especial.

Existen 4 métodos importantes para la preparación de α,β -insaturados: condensación aldólica, halogenación del carbono α seguida de eliminación, oxidación de alcoholes alílicos y Wittig.

Método 1. Preparar mediante la condensación aldólica el siguiente compuesto.

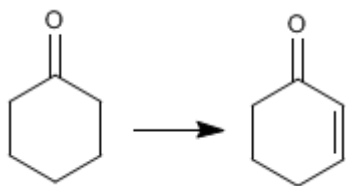


Empleamos la retrosíntesis para preparar el compuesto. Al ser de la familia de los α,β -insaturados se puede obtener mediante la condensación aldólica.

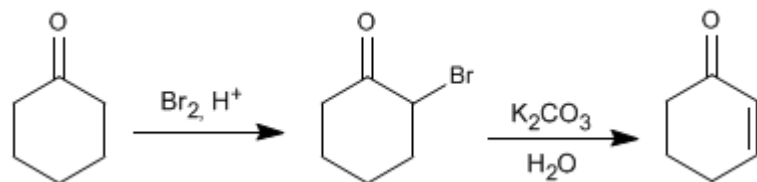


Para obtener los reactivos que forman el α,β -insaturado se rompe por el doble enlace, obteniéndose los sintones (equivalentes sintéticos). Los reactivos se obtienen añadiendo al carbono β un carbonilo y completando los hidrógenos que faltan en el carbono α .

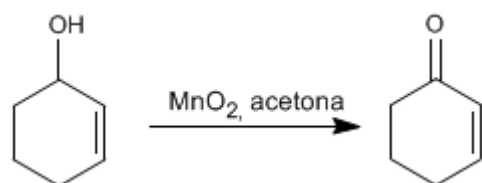
Ejemplo 2. Indicar como se puede realizar las siguiente transformación.



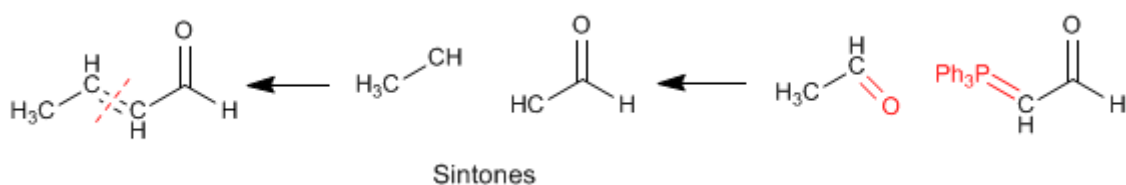
En una primera etapa se halogena la posición α del carbonilo. En la segunda etapa se realiza una eliminación que nos deja el producto final.



Método 3. La oxidación de alcoholes alílicos con dióxido de manganeso en acetona produce α,β -insaturados

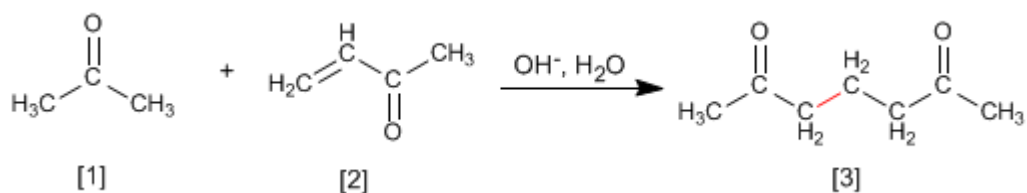


Método 4. Reacción de Wittig



Adición de Michael y anelación de Robinson

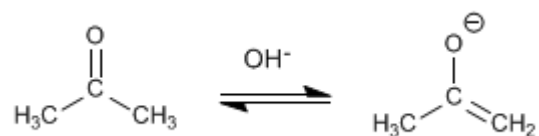
Los enolatos de aldehídos o cetonas se adicionan a los α,β -insaturados para formar 1,5-dicarbonilos. Esta reacción se denomina adición de Michael.



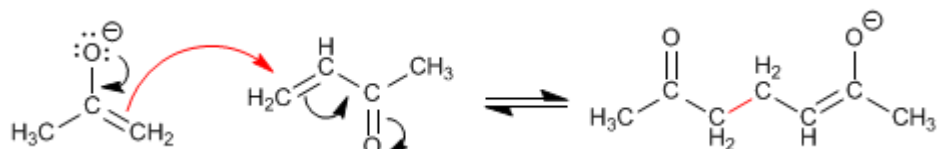
La propanona [1] reacciona con el α,β -insaturado [2] para formar el 1,5-dicarbonilo [3]

Mecanismo de la Adición de Michael:

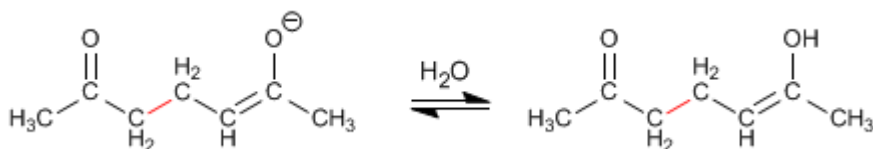
Etapla 1. Formación del enolato.



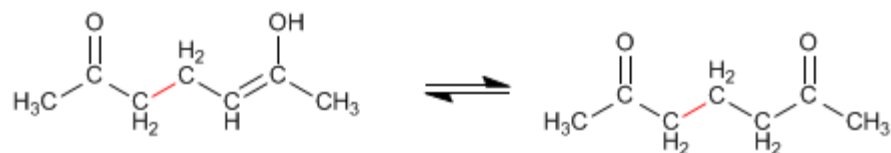
Etapla 2. Ataque nucleófilo del enolato al carbono β del α,β -insaturado.



Etapla 3. Equilibrio ácido-base



Etapla 4. Tautomería ceto-enol



El producto de Michael puede condensar mediante una aldólica intramolecular, formando un α,β -insaturado. El conjunto de la adición de Michael y la aldólica final se conoce como reacción de Robinson

Chemsoft ®

Química Orgánica

Recopilación : 2da Edición - 2009

José A.

Química Orgánica

Recopilación: 2da Edición

Diciembre 2009

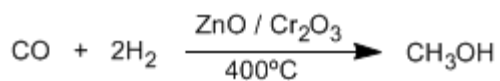
Índice:

- i. Alcoholes*
- ii. Éteres*
- iii. Aldehídos y Cetonas*
- iv. Enoles y Enolatos*
- v. Benceno*

SÍNTESIS Y REACTIVIDAD DE ALCOHOLES

Alcoholes - características generales

Los alcoholes son compuesto orgánicos que contienen el grupo hidroxilo (-OH). El metanol es el alcohol más sencillo, se obtiene por reducción del monóxido de carbono con hidrógeno.

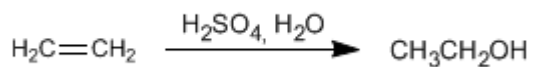


El metanol es un líquido incoloro, su punto de ebullición es 65°C, miscible en agua en todas las proporciones y venenoso (35 ml pueden matar una persona)

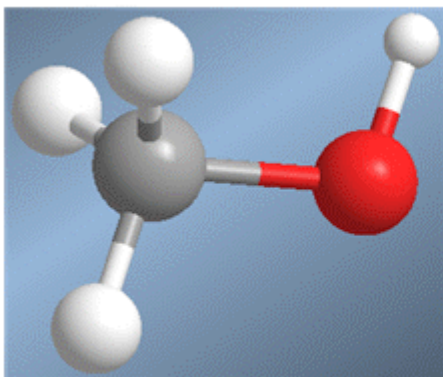
La mitad del metanol producido se oxida a metanal (formaldehído), material de partida para la fabricación de resinas y plásticos.

El etanol se obtiene por fermentación de materia vegetal, obteniéndose una concentración máxima de 15% en etanol. Por destilación se puede aumentar esta concentración hasta el 98%.

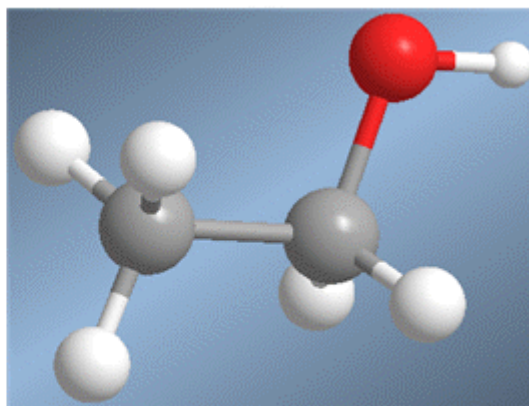
También se puede obtener etanol por hidratación del etileno (eteno) que se obtiene a partir del petróleo.



El etanol es un líquido incoloro, miscible en agua en todas proporciones, con punto de ebullición de 78°C. Es fácilmente metabolizado por nuestros organismos, aunque su abuso causa alcoholismo.



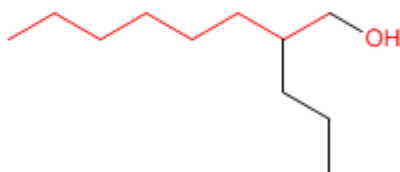
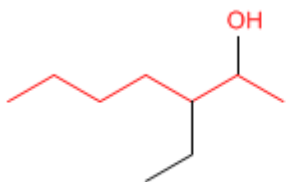
(metanol) CH_3OH



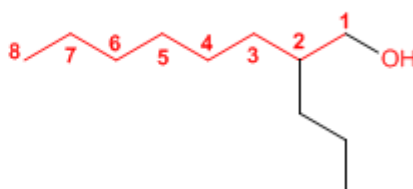
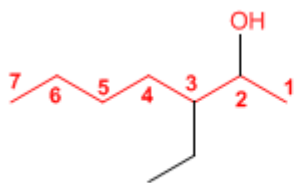
(etanol) $\text{CH}_3\text{CH}_2\text{OH}$

Nomenclatura de Alcoholes

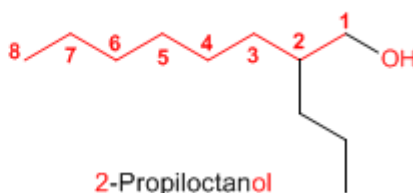
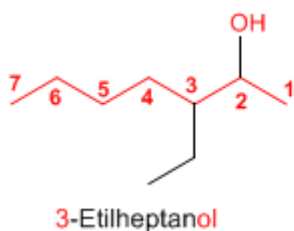
Regla 1. Se elige como cadena principal la de mayor longitud que contenga el grupo -OH.



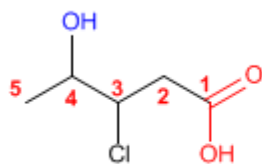
Regla 2. Se numera la cadena principal para que el grupo -OH tome el localizador más bajo. El grupo hidroxilo tiene preferencia sobre cadenas carbonadas, halógenos, dobles y triples enlaces.



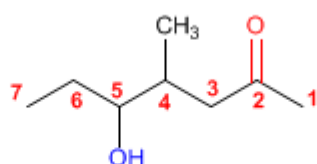
Regla 3. El nombre del alcohol se construye cambiando la terminación -o del alcano con igual número de carbonos por -ol



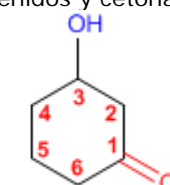
Regla 4. Cuando en la molécula hay grupos funcionales de mayor prioridad, el alcohol pasa a ser un mero sustituyente y se llama **hidroxi-**. Son prioritarios frente a los alcoholes: ácidos carboxílicos, anhídridos, ésteres, haluros de alcanoilo, amidas, nitrilos, aldehídos y cetonas.



Ácido 3-cloro-4-hidroxi-pentanoico

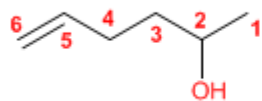


5-Hidroxi-4-metilheptanona

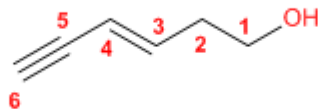


3-Hidroxiciclohexanona

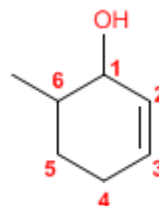
Regla 5. El grupo -OH es prioritario frente a los alquenos y alquinos. La numeración otorga el localizador más bajo al -OH y el nombre de la molécula termina en -ol.



Hex-5-en-2-ol



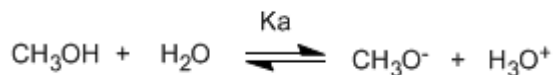
Hex-3-en-5-in-1-ol



6-Metilciclohex-2-en-1-ol

Acidez y basicidad de alcoholes

Los alcoholes son especies anfóteras (anfipróticas), pueden actuar como ácidos o bases. En disolución acuosa se establece un equilibrio entre el alcohol, el agua y sus bases conjugadas.



Escribiendo la constante del equilibrio (K_a)

$$K_a = \frac{[\text{H}_3\text{O}^+][\text{CH}_3\text{O}^-]}{[\text{CH}_3\text{OH}]} = 10^{-15.5}$$

El pequeño valor de la constante nos indica que el equilibrio está totalmente desplazado a la izquierda.


El logaritmo cambiado de signo de la constante de equilibrio nos da el pK_a del metanol, parámetro que indica el grado de acidez de un compuesto orgánico.

$$pK_a = -\log k_a = 15.5$$


El aumento del pK_a supone una disminución de la acidez. Así, el metanol con un pK_a de 15.5 es ligeramente más ácido que el etanol con pK_a de 15.9.

El pK_a de los alcoholes se ve influenciado por algunos factores como son el tamaño de la cadena carbonada y los grupos electronegativos

Al aumentar el tamaño de la cadena carbonada el alcohol se vuelve menos ácido.

CH_3OH	$pK_a = 15.5$	
$\text{CH}_3\text{CH}_2\text{OH}$	$pK_a = 15.9$	
$(\text{CH}_3)_2\text{CHOH}$	$pK_a = 17.1$	
$(\text{CH}_3)_3\text{COH}$	$pK_a = 18$	

Los grupos electronegativos (halógenos) aumentan la acidez de los alcoholes (bajan el pK_a)

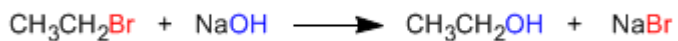
$\text{CH}_3\text{CH}_2\text{OH}$	$pK_a = 15.9$	
$\text{ClCH}_2\text{CH}_2\text{OH}$	$pK_a = 14.3$	
$\text{F}_3\text{CCH}_2\text{OH}$	$pK_a = 12.4$	

Síntesis de Alcoholes a partir de Haloalcanos

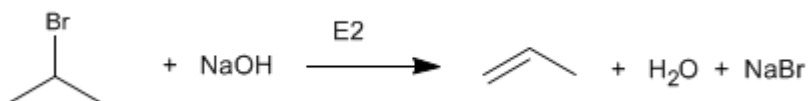
Los alcoholes se pueden obtener a partir de haloalcanos mediante reacciones S_N2 y S_N1

Síntesis de alcoholes mediante S_N2

Los haloalcanos primarios reaccionan con hidróxido de sodio para formar alcoholes. Haloalcanos secundarios y terciarios eliminan para formar alquenos.

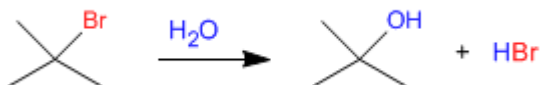


El bromuro de isopropilo (sustrato secundario) elimina al reaccionar con el ión hidróxido.



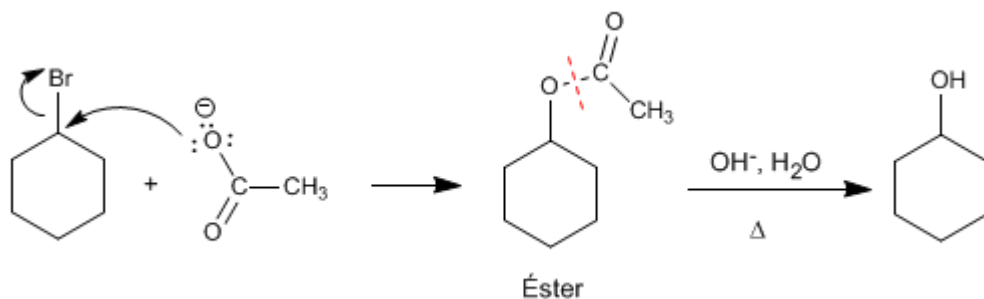
Síntesis de alcoholes mediante S_N1

Los sustratos secundarios y terciarios reaccionan con agua mediante mecanismo S_N1 para formar alcoholes.



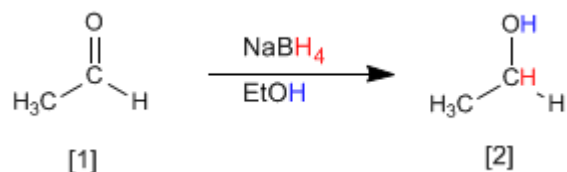
Hidrólisis de ésteres

Es un método interesante para preparar alcoholes a partir de haloalcanos secundarios. El haloalcano se convierte en éster por reacción con acetato de sodio, para después hidrolizarse en medio ácido o básico, obteniéndose el alcohol.



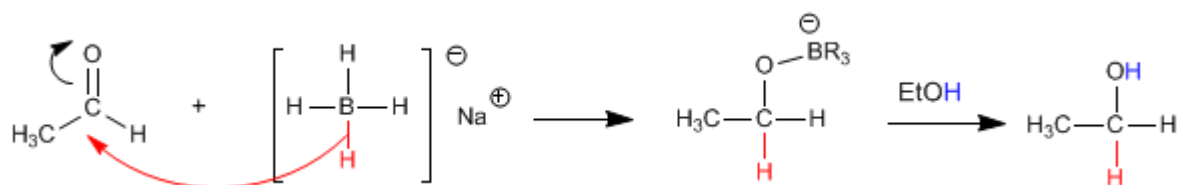
Síntesis de Alcoholes por reducción de carbonilos

Tanto el borohidruro de sodio (NaBH_4) como el hidruro de litio y aluminio (LiAlH_4) reducen aldehídos y cetonas a alcoholes.

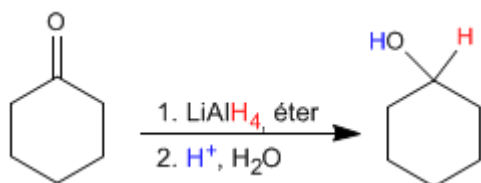


El etanal [1] se transforma por reducción con el borohidruro de sodio en etanol [2].

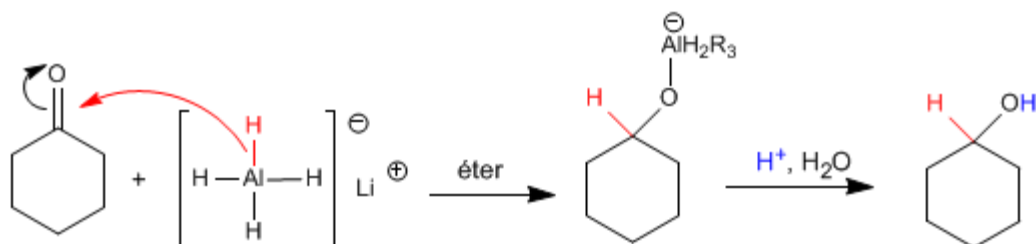
El mecanismo transcurre por ataque del hidruro procedente del reductor sobre el carbono carbonilo. En una segunda etapa el disolvente protona el oxígeno del alcóxido.



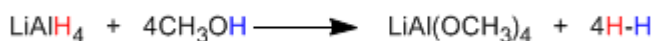
El hidruro de litio y aluminio trabaja en medio éter y transforma aldehídos y cetonas en alcoholes después de una etapa de hidrólisis ácida.



El mecanismo es análogo al del borohidruro de sodio.



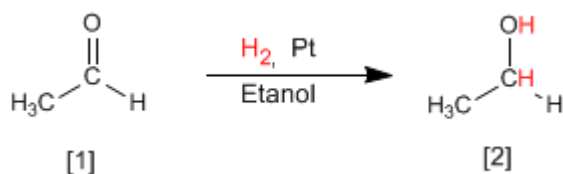
El reductor de litio y aluminio es más reactivo que el de boro, reacciona con el agua y los alcoholes desprendiendo hidrógeno. Por ello, debe disolverse en medios apróticos (éter).



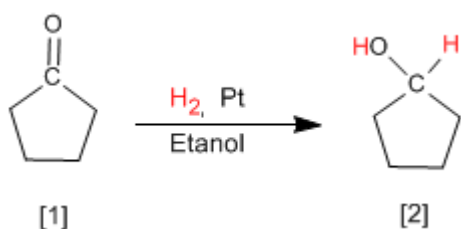
El reductor de boro, menos reactivo, descompone lentamente en medios próticos, lo que permite utilizarlo disuelto en etanol o agua.

Síntesis de Alcoholes por hidrogenación de Carbonilos

Otro método para preparar alcoholes consiste en la reducción de aldehídos o cetonas a alcoholes. El método más simple es la hidrogenación del doble enlace carbono-oxígeno, utilizando hidrógeno en presencia de un catalizador de platino, paladio, níquel o rutenio.



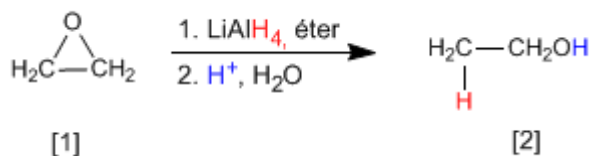
El etanal [1] se transforma por hidrogenación del doble enlace en etanol [2]



La ciclopentanona [1] se transforma por hidrogenación en ciclopentanol [2]

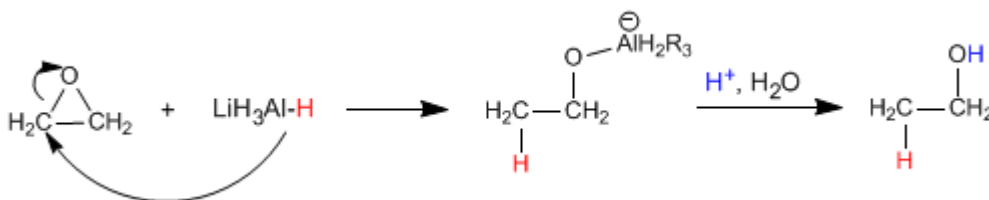
Síntesis de Alcoholes a partir de Epóxidos

Los alcoholes se pueden obtener por apertura de epóxidos (oxaciclopropanos). Esta apertura se puede realizar empleando reactivos organometálicos o el reductor de litio y aluminio.



El oxaciclopropano [1] se transforma por reducción con hidruro de litio y aluminio en etanol [2].

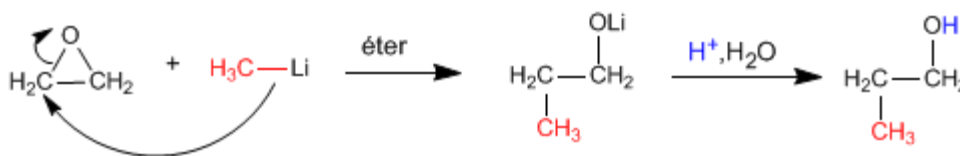
El mecanismo de la reacción comienza con el ataque del hidruro procedente del reductor sobre el carbono polarizado positivamente del epóxido, para terminar con la protonación del alcóxido.



Los reactivos de Grignard (organometálicos de magnesio) y los organolitícos reaccionan con oxaciclopropano para dar un alcohol primario.



El metillitio ataca al oxaciclopropano [1] para formar propan-1-ol [2].

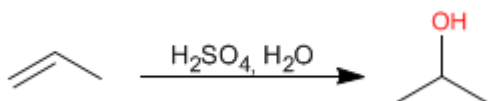


Síntesis de Alcoholes por Hidratación de Alquenos

Un método de síntesis para alcoholes, ya estudiado en la sección de alquenos, consiste en hidratar el alqueno. La adición del -OH puede ser en el carbono más sustituido del alqueno (Markovnikov), o bien, en el carbono menos sustituido (antiMarkovnikov).

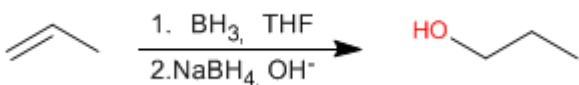
Hidratación Markovnikov

En esta hidratación el grupo hidroxilo va al carbono con más sustituyentes. Se emplea como reactivo sulfúrico acuoso, o bien, acetato de mercurio en agua, seguido de reducción con borohidruro de sodio.



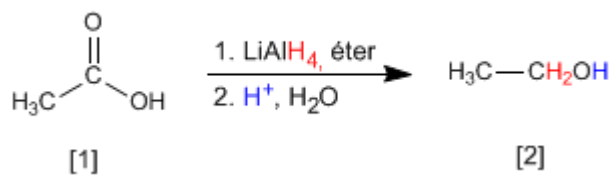
Hidratación antiMarkovnikov

El grupo hidroxilo se adiciona al carbono menos sustituido. El reactivo empleado es borano en THF seguido de oxidación con agua oxigenada en medio básico (hidroboración)

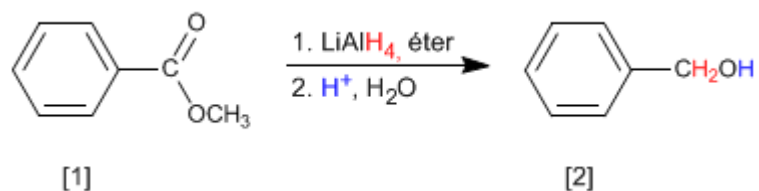


Síntesis de alcoholes por reducción de ácidos y ésteres

Los ácidos carboxílicos y los ésteres se reducen a alcoholes con el hidruro de litio y aluminio.
Reductores más suaves como el borohidruro de sodio son incapaces de reducir estos compuestos.



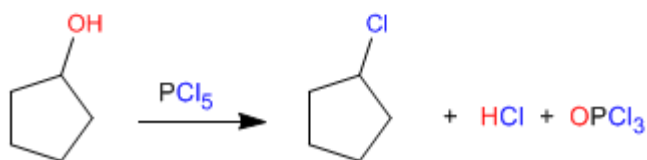
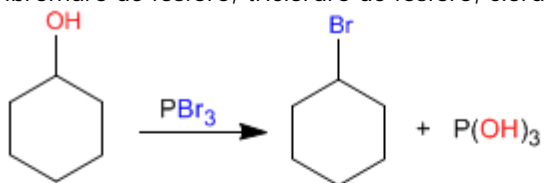
El ácido etanoico [1] se transforma por reducción con hidruro de litio y aluminio en etanol [2].



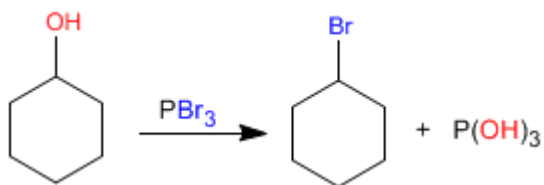
El benzoato de metilo [1] se transforma en alcohol bencílico [2] por reducción con hidruro de litio y aluminio.

Síntesis de Haloalcanos a partir de Alcoholes

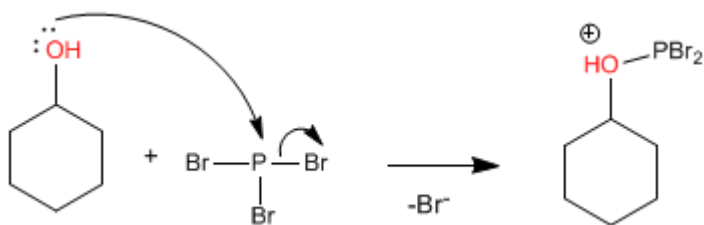
Los alcoholes primarios y secundarios pueden convertirse en haloalcanos con reactivos como: tribromuro de fósforo, tricloruro de fósforo, cloruro de tionilo y pentacloruro de fósforo.



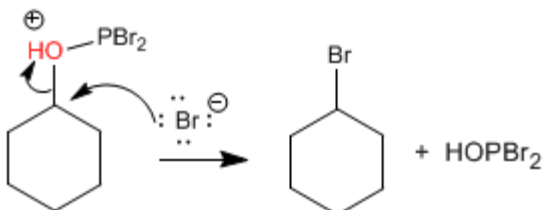
El mecanismo de estas reacciones es de tipo $\text{S}_{\text{N}}2$ y sólo los alcoholes primarios y secundarios reaccionan. Veamos el mecanismo de la primera reacción.



Etapas 1. Ataque del alcohol al tribromuro de fósforo



Etapas 2. Sustitución nucleófila bimolecular, actuando el bromuro como nucleófilo

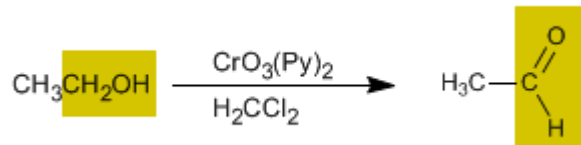


Todos los bromos del PBr_3 son reactivos y el mecanismo se repite dos veces más.

Oxidación de Alcoholes

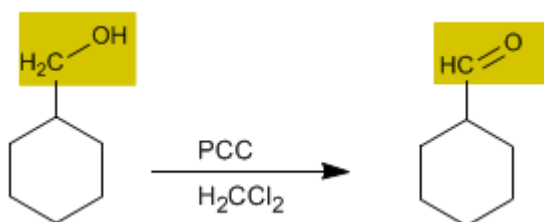
La oxidación de alcoholes forma compuestos carbonilos. Al oxidar alcoholes primarios se obtienen aldehídos, mientras que la oxidación de alcoholes secundarios forma cetonas.

Oxidación de alcoholes primarios a aldehídos



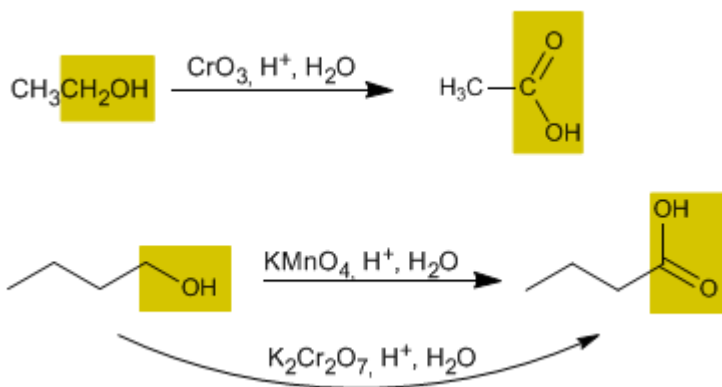
El trióxido de cromo con piridina en diclorometano permite aislar aldehídos con buen rendimiento a partir de alcoholes primarios.

Se conoce como PCC (clorocromato de piridinio) al trióxido de cromo con piridina y ácido clorhídrico en diclorometano. Este reactivo también convierte alcoholes primarios en aldehídos.



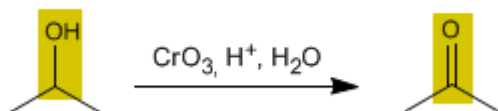
Oxidación de alcoholes primarios a ácidos carboxílicos

El trióxido de cromo en medio ácido acuoso (reactivo de Jones), el permanganato de potasio y el dicromato de potasio oxidan los alcoholes primarios a ácidos carboxílicos.



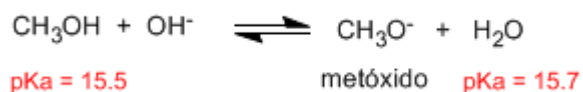
Oxidación de alcoholes secundarios a cetonas

Los oxidantes convierten los alcoholes secundarios en cetonas. No es posible la sobreoxidación a ácido carboxílico.

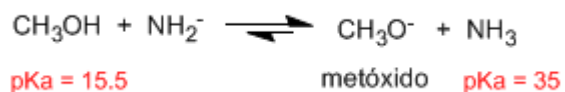


Formación de Alcóxidos a partir de Alcoholes

Los alcóxidos son las bases de los alcoholes, se obtienen por reacción del alcohol con una base fuerte.

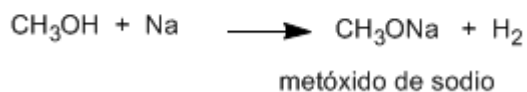
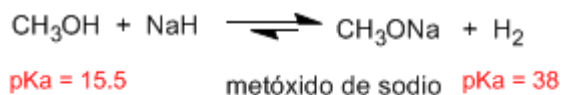


Los pKa de los ácidos conjugados son similares y el equilibrio no se encuentra desplazado. El ión hidróxido es una base demasiado débil para formar el alcóxido en cantidad importante.



El amiduro es una base muy fuerte y desplaza el equilibrio a la derecha, transformando el metanol en metóxido.

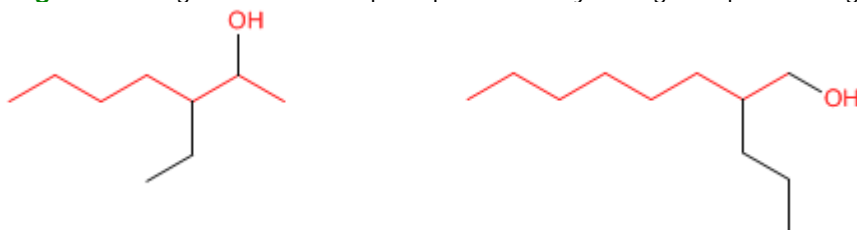
Otras bases fuertes que pueden ser usadas para formar alcóxidos son: hidruro de sodio, LDA, sodio metal.



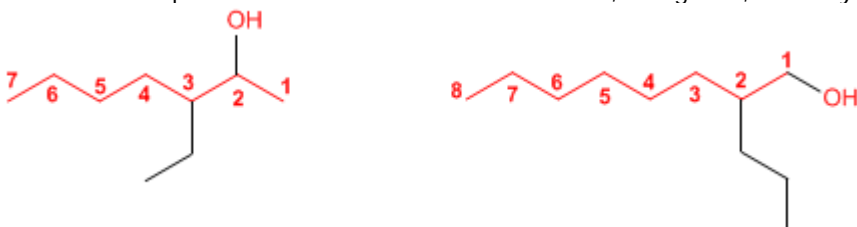
PROBLEMAS NOMENCLATURA - ALCOHOLES

Nomenclatura de Alcoholes - Reglas IUPAC

Regla 1. Se elige como cadena principal la de mayor longitud que contenga el grupo -OH.



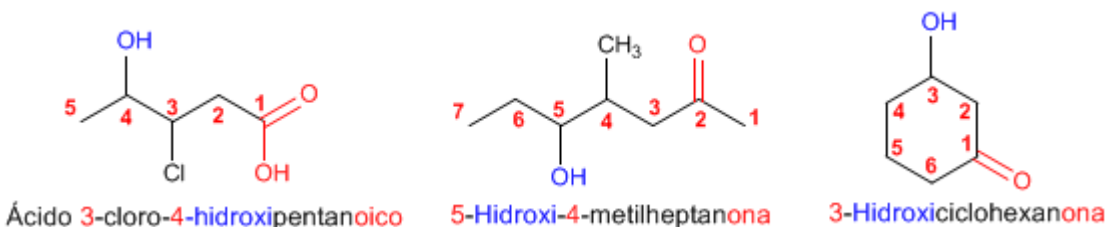
Regla 2. Se numera la cadena principal para que el grupo -OH tome el localizador más bajo. El grupo hidroxilo tiene preferencia sobre cadenas carbonadas, halógenos, dobles y triples enlaces.



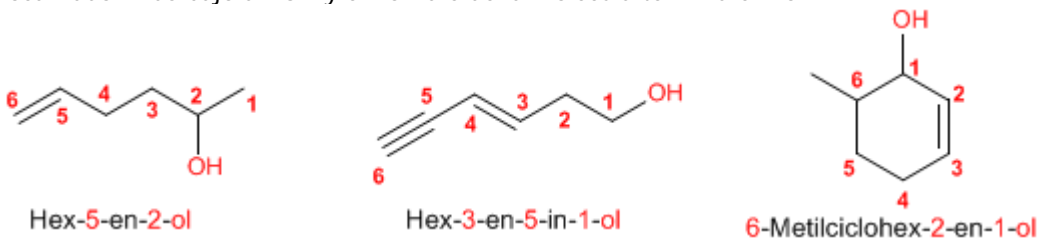
Regla 3. El nombre del alcohol se construye cambiando la terminación -o del alcano con igual número de carbonos por -ol



Regla 4. Cuando en la molécula hay grupos funcionales de mayor prioridad, el alcohol pasa a ser un mero sustituyente y se llama **hidroxi-**. Son prioritarios frente a los alcoholes: ácidos carboxílicos, anhídridos, ésteres, haluros de alcanoilo, amidas, nitrilos, aldehídos y cetonas.

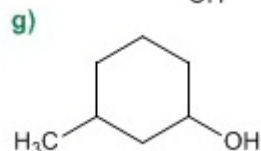
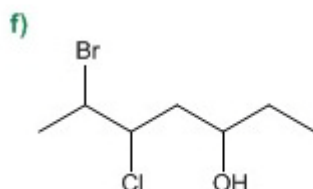
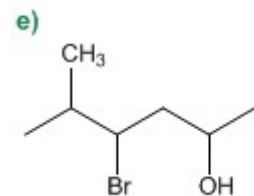
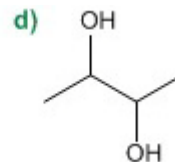
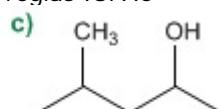
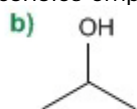
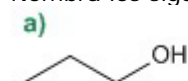


Regla 5. El grupo -OH es prioritario frente a los alquenos y alquinos. La numeración otorga el localizador más bajo al -OH y el nombre de la molécula termina en -ol.

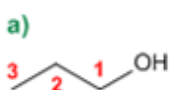


Nomenclatura de Alcoholes - Problema 0.1

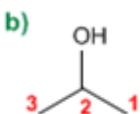
Nombra los siguientes alcoholes empleando reglas IUPAC



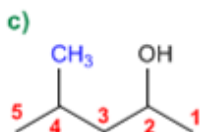
Solución:



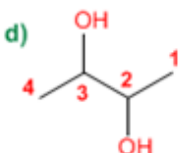
1. Cadena principal: la de mayor longitud que contenga el -OH (propano)
2. Numeración: otorga al -OH el localizador más bajo.
3. Sustituyentes: no
4. Nombre: Propan-1-ol



1. Cadena principal: la de mayor longitud que contenga el -OH (propano)
2. Numeración: indiferente.
3. Sustituyentes: no
4. Nombre: Propan-2-ol



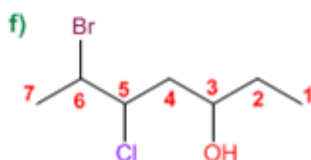
1. Cadena principal: la de mayor longitud que contenga el -OH (pentano)
2. Numeración: otorga al -OH el localizador más bajo (-OH preferente sobre cadenas)
3. Sustituyentes: metilo en 4
4. Nombre: 4-Metilpentan-2-ol



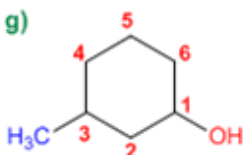
1. Cadena principal: mayor longitud (butano)
2. Numeración: comienza en uno de los extremos.
3. Sustituyentes: no
4. Nombre: Butano-2,3-diol



1. Cadena principal: mayor longitud (hexano)
2. Numeración: comienza en el extremo derecho, para otorgar al -OH el localizador más bajo.
3. Sustituyentes: bromo en posición 4 y metilo en 5.
4. Nombre: 4-Bromo-5-metilhexan-2-ol



1. Cadena principal: mayor longitud (heptano)
2. Numeración: comienza en extremo que otorga el localizador más bajo al -OH.
3. Sustituyentes: bromo en 6 y cloro en 5.
4. Nombre: 6-Bromo-5-cloroheptan-3-ol



1. Cadena principal: ciclo de seis miembros (ciclohexano)
2. Numeración: comienza en el carbono del -OH.
3. Sustituyentes: metilo en 3.
4. Nombre: 3-Metilciclohexanol

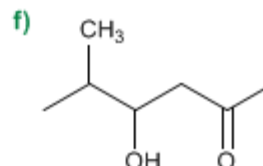
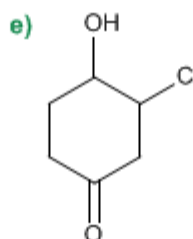
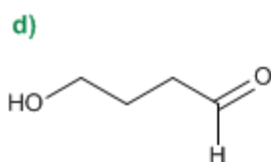
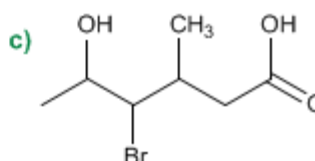
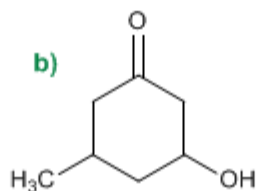
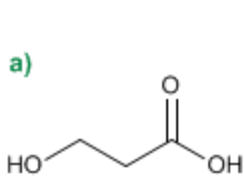
1. Cuando en una molécula hay más de un grupo -OH se pueden emplear los prefijos de cantidad di, tri, tetra, penta, hexa,..... La numeración debe otorgar los menores localizadores a los -OH.

2. El nombre del alcohol se construye comenzando por los sustituyentes, precedidos por sus respectivos localizadores, terminando en el nombre de la cadena principal. La terminación -o del alcano correspondiente se sustituye por -ol.

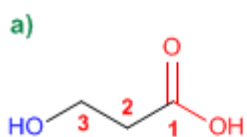
3. En el caso de alcoholes cíclicos no es necesario indicar la posición del grupo hidroxilo, puesto que siempre toma localizador 1.

Nomenclatura de Alcoholes - Problema 0.2

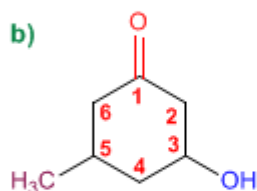
Nombra los siguientes moléculas, en las que el alcohol actúa como sustituyente.



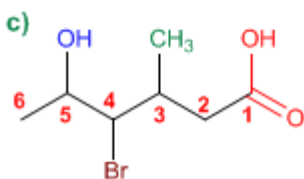
Solución



1. Cadena principal: más larga que contenga el grupo funcional (propano)
2. Grupo funcional: ácido carboxílico
3. Numeración: localizador más bajo al grupo ácido
4. Sustituyentes: grupo **hidroxi** en 3.
5. Nombre: **Acido 3-hidroxi**propanoico



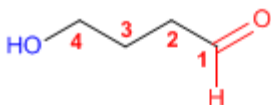
1. Cadena principal: ciclo de seis miembros (ciclohexano)
2. Grupo funcional: cetona
3. Numeración: localizador más bajo al grupo carbonilo
4. Sustituyentes: grupo **hidroxi** en 3 y **metilo** en 4.
5. Nombre: **2-Hidroxi-5-metilciclohexanona**



1. Cadena principal: más larga que contenga el grupo funcional (hexano)
2. Grupo funcional: ácido carboxílico
3. Numeración: asigna el localizador más bajo al grupo ácido.
4. Sustituyentes: **bromo** en 4, grupo **hidroxi** en 5 y **metilo** en 3
5. Nombre: **Acido 4-bromo-6-hidroxi-3-metilhexanoico**

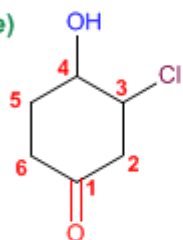
Los ácidos carboxílicos y las cetonas son prioritarios sobre los alcoholes.
El alcohol pasa a ser un sustituyente más de la molécula, ordenándose alfabéticamente con el resto de sustituyentes.

d)



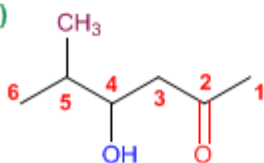
1. Cadena principal: más larga que contenga el grupo funcional (butano)
2. Grupo funcional: aldehído
3. Numeración: localizador más bajo al grupo carbonilo
4. Sustituyentes: grupo **hidroxi** en 4.
5. Nombre: **4-Hidroxibutanal**

e)



1. Cadena principal: ciclo de seis miembros
2. Grupo funcional: cetona
3. Numeración: localizador más bajo al carbonilo
4. Sustituyentes: **cloro** en 3 e **hidroxi** en 4.
5. Nombre: **3-Cloro-4-hidroxiciclohexanona**

f)



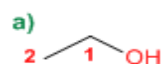
1. Cadena principal: más larga que contenga el grupo funcional (propano)
2. Grupo funcional: cetona
3. Numeración: localizador más bajo al grupo carbonilo
4. Sustituyentes: grupo **hidroxi** en 4 y **metilo** en 5.
5. Nombre: **3-Hidroxi-4-metilhexan-2-ona**

Nomenclatura de Alcoholes - Problema 0.3

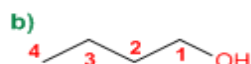
Dibujar la estructura de los siguientes alcoholes:

- | | |
|--------------------------|-----------------------------------|
| a) Etanol | i) Ciclopent-2-enol |
| b) Butanol | j) 2,3-Dimetilciclohexanol |
| c) 2-Metilpropan-1-ol | k) Octa-3,5-dien-2-ol |
| d) 2-Metilbutan-2-ol | l) Hex-4-en-1-in-3-ol |
| e) 3-Metilbutan-2-ol | m) 2-Bromohept-2-en-1,4-diol |
| f) 3-Metilbutan-1-ol | n) 2-Fenil-5-metilheptan-2-ol |
| g) 2,3-Pentanodiol | o) Alcohol bencílico |
| h) 2-Etil-pent-3-en-1-ol | p) 1,2,3-Propanotriol (glicerina) |

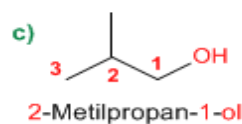
Solución:



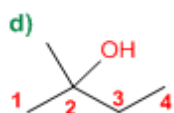
Etanol



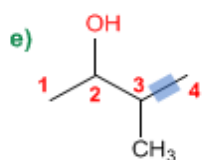
Butanol



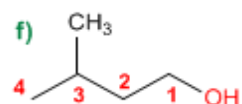
2-Metilpropan-1-ol



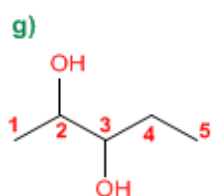
2-Metilbutan-2-ol



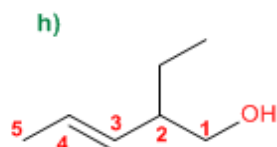
3-Metilbutan-2-ol



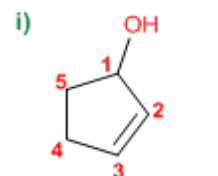
3-Metilbutan-1-ol



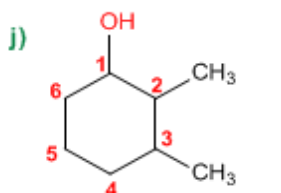
2,3-Pentanodiol



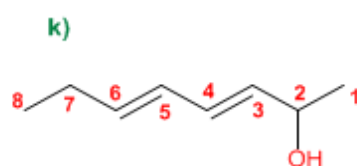
2-Etil-pent-3-en-1-ol



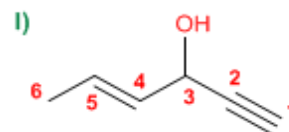
Ciclopent-2-enol



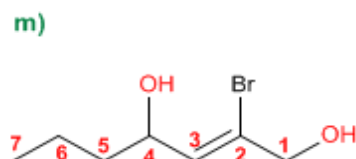
2,3-Dimetilciclohexanol



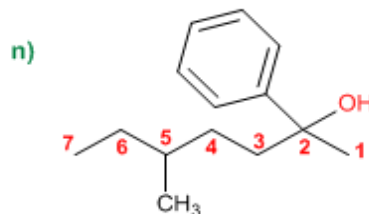
Octa-3,5-dien-2-ol



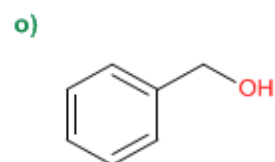
Hex-4-en-1-in-3-ol



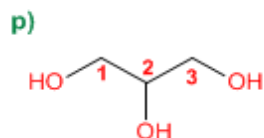
2-Bromohept-2-en-1,4-diol



2-Fenil-5-metilheptan-2-ol



Alcohol bencílico

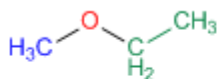


1,2,3-Propanotriol (glicerina)

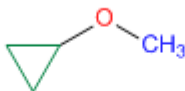
TEORÍA DE ÉTERES

Nomenclatura de éteres - epóxidos

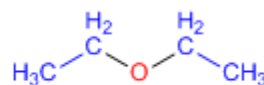
La nomenclatura de los éteres consiste en nombrar alfabéticamente los dos grupos alquilo que parten del oxígeno, terminando el nombre en éter. Veamos algunos ejemplos:



Etil metil éter

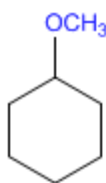


Ciclopropil metil éter

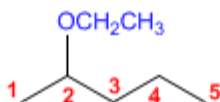


Dietil éter

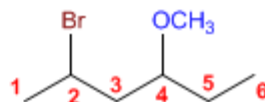
También se pueden nombrar los éteres como grupos alcoxi.



Metóxiciclohexano



2-Etoxi pentano

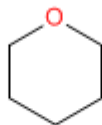


2-Bromo-4-metoxihexano

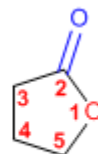
Los éteres cíclicos se forman sustituyendo $-CH_2-$ del ciclo por $-O-$. Este cambio se indica con el prefijo **oxa-**.



Oxaciclopropano



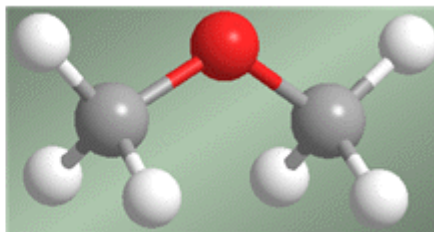
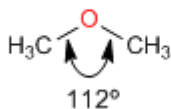
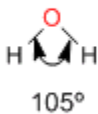
Oxaciclohexano



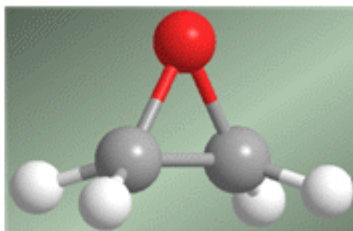
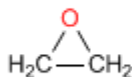
2-oxo-oxaciclopentano

Estructura y enlace en éteres y epóxidos

Los éteres son moléculas de estructura similar al agua y alcoholes. El ángulo entre los enlaces C-O-C es mayor que en el agua debido a las repulsiones estéricas entre grupos voluminosos.

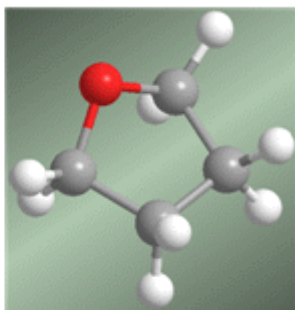
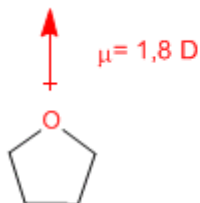


En el caso de los epóxidos la característica más relevante es la tensión del anillo, debida a ángulos de enlace muy distantes a los 109° .



El enlace C-O-C presenta un ángulo de 61° .

Los éteres son moléculas muy polares. Así, el Dietil éter presenta un momento dipolar de 1,2 D. Este momento dipolar es aún más importante en éteres cíclicos (oxaciclopropano, tetrahydrofurano) que presentan momentos dipolares sobre 1,8 D, similares al agua.



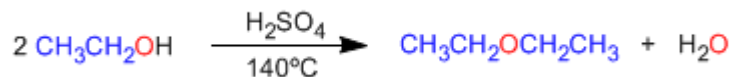
.....



Síntesis de éteres por condensación de alcoholes

1. Éteres a partir de alcoholes primarios

Los éteres simétricos pueden prepararse por condensación de alcoholes. La reacción se realiza bajo calefacción (140°C) y con catálisis ácida. Así, dos moléculas de etanol condensan para formar dietil éter.

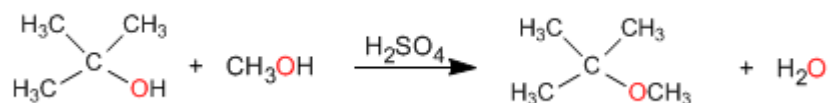


El mecanismo de la reacción transcurre en las siguientes etapas:



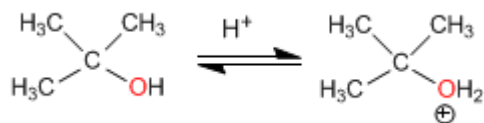
2. Uno de los alcoholes es secundario o terciario

En este caso la reacción transcurre en condiciones más suaves, a través de mecanismos $\text{S}_{\text{N}}1$.

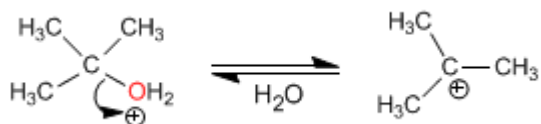


El mecanismo transcurre con formación de un carbocatión terciario de gran estabilidad

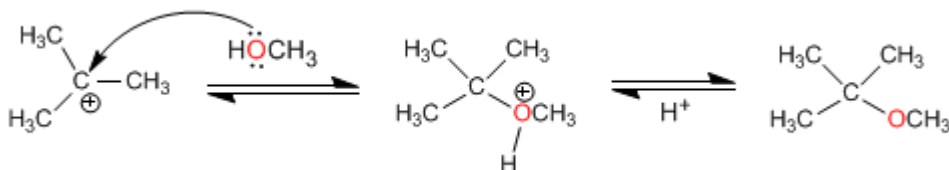
Etapa 1. Protonación del alcohol terciario



Etapa 2. Formación del carbocatión por pérdida de agua

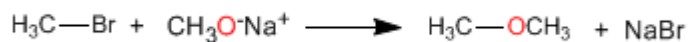


Etapa 3. Ataque nucleófilo del metanol



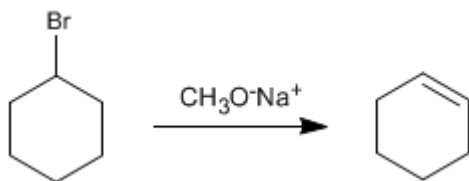
Síntesis de Williamson de los éteres

La reacción entre un haloalcano primario y un alcóxido (o bien alcohol en medio básico) es el método más importante para preparar éteres. Esta reacción es conocida como síntesis de Williamson.

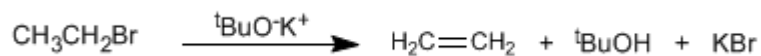


Esta reacción transcurre a través del mecanismo $\text{S}_{\text{N}}2$.

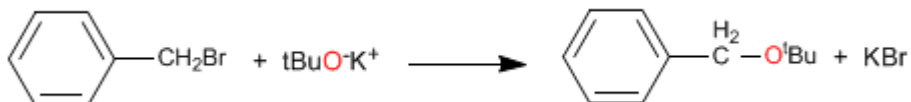
La importante basicidad de los alcóxidos produce reacciones de eliminación con sustratos secundarios y terciarios, formando alquenos en lugar de éteres.



Otra situación en la que Williamson no rinde éteres, es en el caso de emplear alcóxidos impedidos, como *tert*-butóxido de potasio. Debido a su gran tamaño el *tert*-butóxido elimina incluso con sustratos primarios.



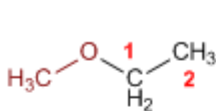
Con haloalcanos primarios y sobre todo con haloalcanos que carecen de hidrógenos β el rendimiento de Williamson es muy bueno.



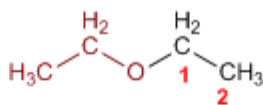
PROBLEMAS NOMENCLATURA - ÉTERES

Nomenclatura de Éteres - Reglas IUPAC

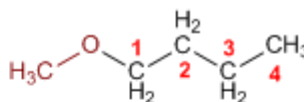
Regla 1. Los éteres pueden nombrarse como alcoxi derivados de alcanos (nomenclatura IUPAC sustitutiva). Se toma como cadena principal la de mayor longitud y se nombra el alcóxido como un sustituyente.



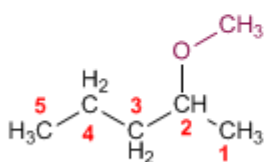
Metoxietano



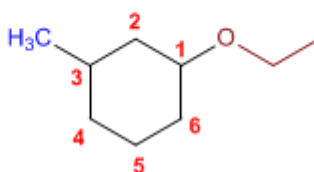
Etoxietano



1-Metoxibutano

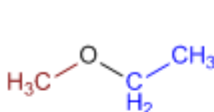


2-Metoxipentano

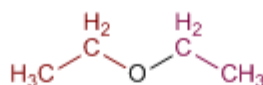


1-Etoxi-3-metilciclohexano

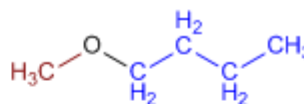
Regla 2. La nomenclatura funcional (IUPAC) nombra los éteres como derivados de dos grupos alquilo, ordenados alfabéticamente, terminando el nombre en la palabra éter.



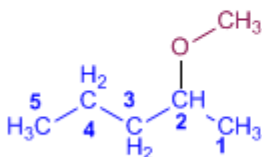
Etil metil éter



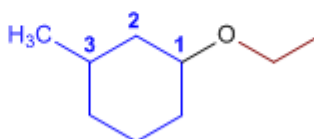
Dietil éter



Butil metil éter



Metil pent-2-il éter



Etil 3-metilciclohexil éter

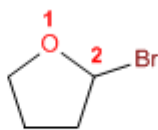
Regla 3. Los éteres cíclicos se forman sustituyendo un -CH₂- por -O- en un ciclo. La numeración comienza en el oxígeno y se nombran con el prefijo oxa- seguido del nombre del ciclo.



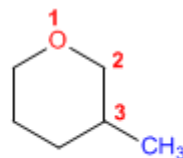
Oxaciclopropano



Oxaciclobutano



2-Bromooxaciclopentano

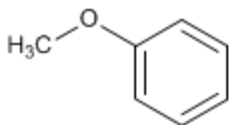


3-Metiloxaciclohexano

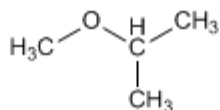
Nomenclatura de Éteres - Problema 0.1

Nombra los siguientes éteres:

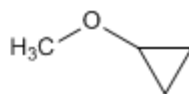
a)



b)



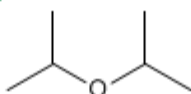
c)



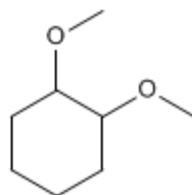
d)



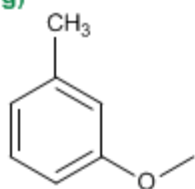
e)



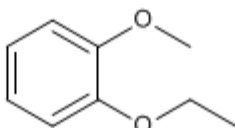
f)



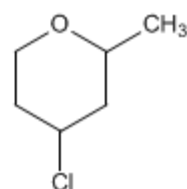
g)



h)

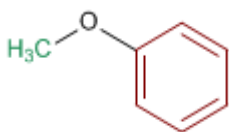


i)



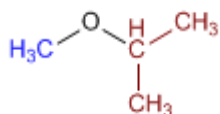
Solución:

a)



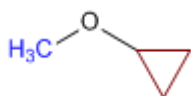
1. Sustituyentes: **fenil** y **metil**
2. Nombre: **Fenil metil** éter

b)



1. Sustituyentes: **isopropil** y **metil**
2. Nombre: **Isopropil metil** éter

c)



1. Sustituyentes: **ciclopropil** y **metil**
2. Nombre: **Ciclopropil metil** éter

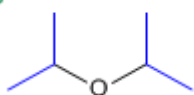
El nombre de los éteres se construye terminando en la palabra éter el nombre de las cadenas que parten del oxígeno. Estas cadenas se nombran como sustituyentes y se ordenan alfabéticamente. Obsérvese el espacio de separación entre las palabras.

d)



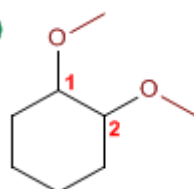
1. Sustituyentes: **etilo** y **propilo**
2. Nombre: **Etil propil** éter

e)



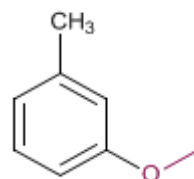
1. Sustituyentes: **isopropilos**
2. Nombre: **Diisopropil** éter

f)



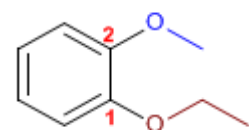
1. Cadena principal: ciclo de seis miembros (ciclohexano)
2. Numeración: otorga localizadores más bajos a sustituyentes
3. Sustituyentes: **metoxidos** en 1,2
4. Nombre: **1,2-Dimetoxiciclohexano**

g)



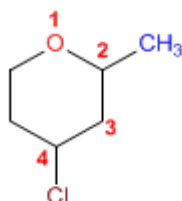
1. Cadena principal: Tolueno
2. Numeración: metilo y metóxido en meta.
3. Sustituyentes: **metoxido**
4. Nombre: **m-Metoxitolueno**

h)



1. Cadena principal: Benceno
2. Numeración: Comienza en el etoxi (antes alfabéticamente)
3. Sustituyentes: **etoxido** en 1 y **metoxido** en 2. (posición meta)
4. Nombre: **m-Etoximetoxibenceno**

i)



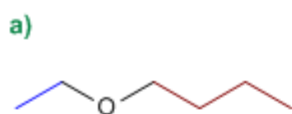
1. Cadena principal: ciclo de 6 miembros (oxaciclohexano)
2. Numeración: comienza en el oxígeno, prosigue a la derecha para otorgar a los sustituyentes los menores localizadores.
3. Sustituyentes: **cloro** y **metilo**
4. Nombre: **4-Cloro-2-metiloxa**ciclohexano

Nomenclatura de Éteres - Problema 0.2

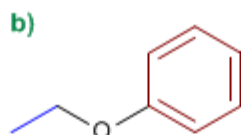
Dibuja las estructuras de los siguientes éteres:

- | | |
|--------------------------|----------------------------------|
| a) Butil etil éter | k) 2-Clorofenil fenil éter |
| b) Etil fenil éter | l) tert-butil isopropil éter |
| c) Difenil éter | m) 2-Metoxi-3-fenilbutan-1-ol |
| d) Divinil éter | n) Dietil éter |
| e) Isopropoxibutano | o) m-Etoxifenol |
| f) Bencil fenil éter | p) 2,3-Dimetiloxaciclopropano |
| g) Metoxiciclohexano | q) 3-Metoxioxaciclohexano |
| h) 4-Metoxipent-2-eno | r) 2-Etil-3-metiloxaciclopentano |
| i) 4-Etoxibut-1-ino | s) Ciclohexil ciclopropil éter |
| j) Ciclohexil fenil éter | t) 2-Metoxipentano |

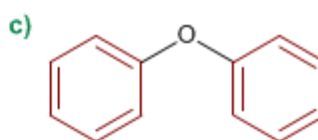
Solución



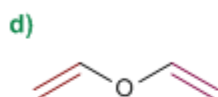
Butil etil éter



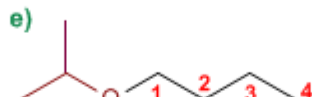
Etil fenil éter



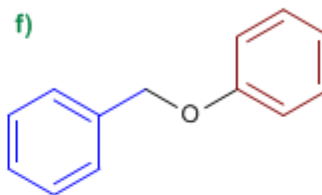
Difenil éter



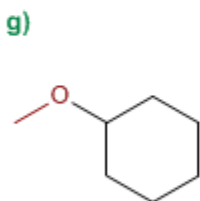
Divinil éter



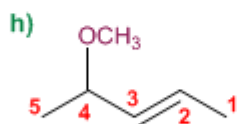
1-Isopropoxibutano



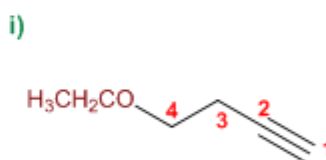
Bencil fenil éter



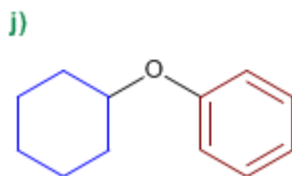
Metoxiciclohexano



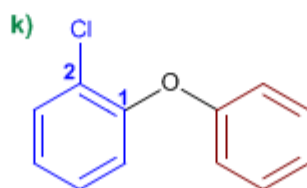
4-Metoxipent-2-eno



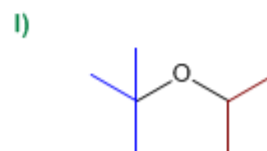
4-Etoxibut-1-ino



Ciclohexil fenil éter

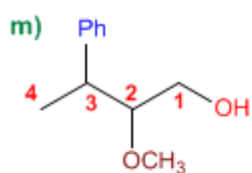


2-Clorofenil fenil éter

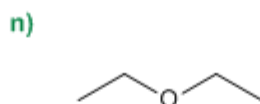


tert-butil isopropil éter

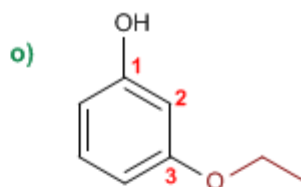
Los grupos alcóxido (metóxido, etóxido....) se ordenan alfabéticamente con los demás sustituyentes de la molécula y no tienen ninguna preferencia sobre ellos



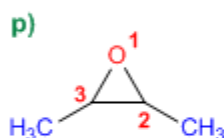
2-Metoxi-3-fenilbutan-1-ol



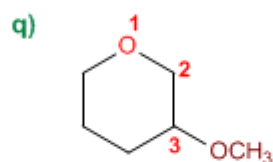
Dietil éter



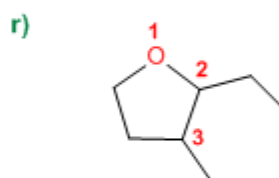
m-Etoxifenol



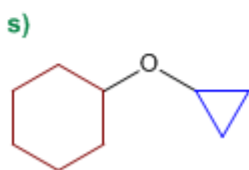
2,3-Dimetiloxa**c**ciclopropano



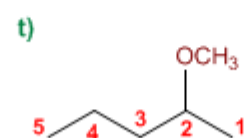
3-Metoxio**x**a**c**ciclohexano



2-Etil-3-metiloxa**c**ciclopentano



Ciclohexil **c**iclopropil éter

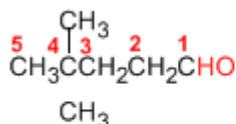


2-Metoxipentano

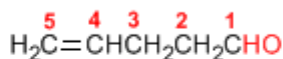
Nomenclatura de Aldehídos y Cetonas

Los aldehídos se nombran reemplazando la terminación **-ano** del alcano correspondiente por **-al**. No es necesario especificar la posición del grupo aldehído, puesto que ocupa el extremo de la cadena (localizador 1).

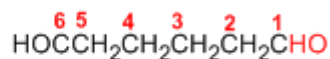
Cuando la cadena contiene dos funciones aldehído se emplea el sufijo **-dial**.



4,4-Dimetilpentanal

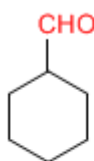


Hex-4-enal

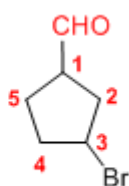


Pentanodial

El grupo **-CHO** unido a un ciclo se llama **-carbaldehído**. La numeración del ciclo se realiza dando localizador 1 al carbono del ciclo que contiene el grupo aldehído.



Ciclohexanocarbaldehído

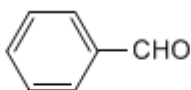


3-Bromociclopentanocarbaldehído

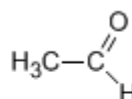
Algunos nombres comunes de aldehídos aceptados por la IUPAC son:



Formaldehído
(Metanal)

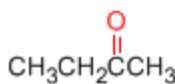


Benzaldehído
(Bencenocarbaldehído)

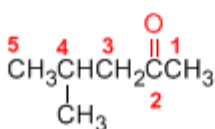


Acetaldehído
(Etanal)

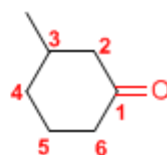
Las cetonas se nombran sustituyendo la terminación **-ano** del alcano con igual longitud de cadena por **-ona**. Se toma como cadena principal la de mayor longitud que contiene el grupo carbonilo y se numera para que éste tome el localizador más bajo.



Butanona

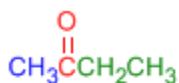


4-Metil-2-pentanona

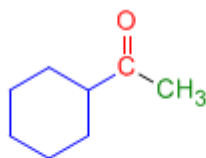


3-Metilciclohexanona

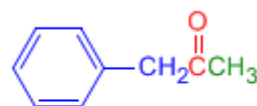
Existe un segundo tipo de nomenclatura para las cetonas, que consiste en nombrar las cadenas como sustituyentes, ordenándolas alfabéticamente y terminando el nombre con la palabra **cetona**.



Etil metil cetona



Ciclohexil metil cetona



Fenil metil cetona

[Siguiete >](#)

[\[Volver\]](#)

Charles Friedel (1832 - 1899)



Origen: Químico frances..

Lugar de nacimiento: Estrasburgo.

Formación: estudió química en la Universidad de Berlín entre 1895 y 1899, consiguiendo el doctorado este año.

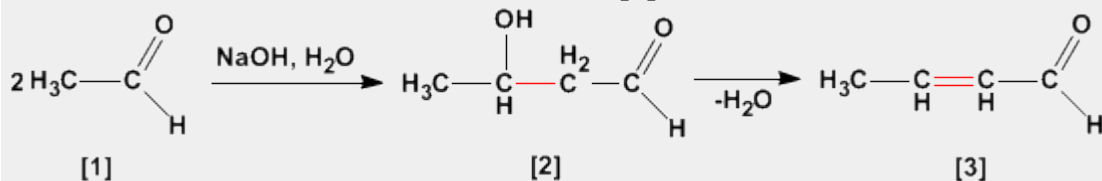
Docencia: Profesor en la Universidad de la Sorbona.

Investigación: Obtuvo el alcohol propílico. En 1877, Friedel y Crafts describieron por primera vez la reacción del benceno con un haloalcano en presencia de un ácido de Lewis. Esta reacción produce la alquilación del benceno y se conoce como alquilación de Friedl-Crafts.

Premio Nobel:

Aldólica (Condensación)

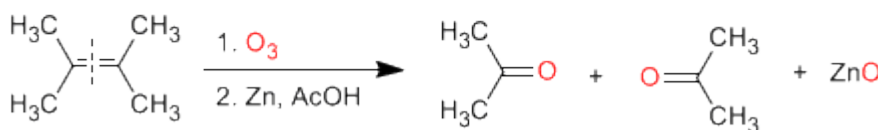
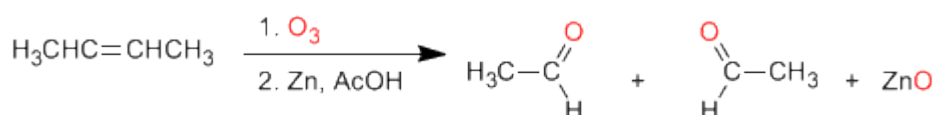
La condensación aldólica es una reacción de aldehídos o cetonas **[1]** que forma 3-hidroxicarbonilos (aldoles) **[2]**. El 3-hidroxialdehído **[2]** bajo condiciones de deshidratación por calentamiento rinde un aldehído alfa,beta-insaturado **[3]**.



Preparación de aldehídos y cetonas

Los aldehídos y cetonas pueden ser preparados por oxidación de alcoholes, ozonólisis de alquenos, hidratación de alquinos y acilación de Friedel-Crafts como métodos de mayor importancia.

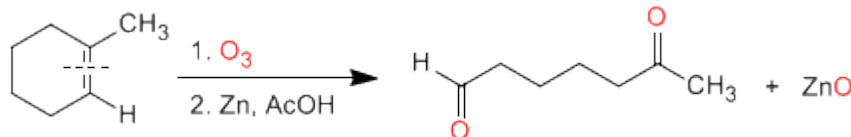
a) **Ozonólisis de alquenos:** Los alquenos rompen con ozono formando aldehídos y/o cetonas. Si el alqueno tiene hidrógenos vinílicos da aldehídos. Si tiene dos cadenas carbonadas forma cetonas.



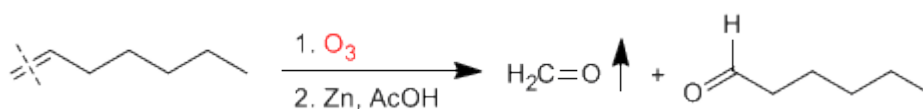
Ozonólisis

Los alquenos simétricos y terminales permiten la preparación de carbonilos mediante ozonólisis

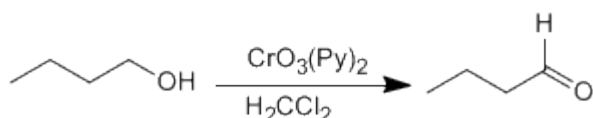
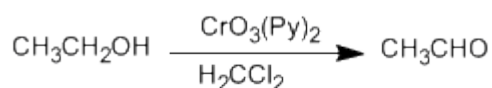
La ozonólisis de alquenos cíclicos produce compuestos dicarbonílicos:



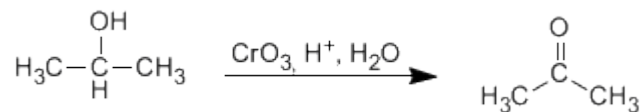
Los alquenos terminales rompen formando metanal, que separa fácilmente de la mezcla por su bajo punto de ebullición.



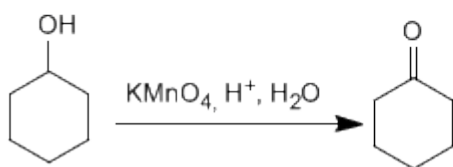
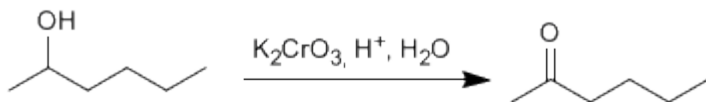
b) **Oxidación de alcoholes:** Los alcoholes primarios y secundarios se oxidan para dar aldehídos y cetonas respectivamente. Deben tomarse precauciones en la oxidación de alcoholes primarios, puesto que sobreoxidan a ácidos carboxílicos en presencia de oxidantes que contengan agua. En estos caso debe trabajarse con reactivos anhidros, como el clorocromato de piridino en diclorometano (PCC), a temperatura ambiente.



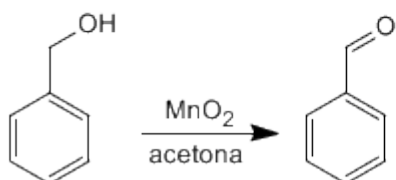
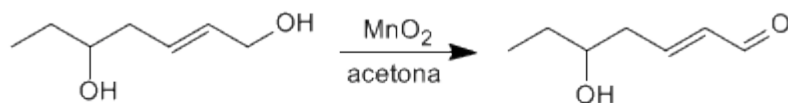
Los alcoholes secundarios dan cetonas por oxidación. Se emplean como oxidantes permanganato, dicromato, trióxido de cromo.



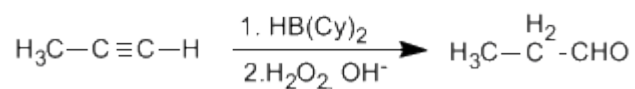
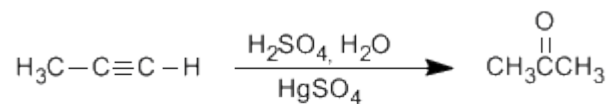
La oxidación supone la pérdida de dos hidrógenos del alcohol. Los alcoholes terciarios no pueden oxidar puesto que carecen de hidrógeno sobre el carbono.



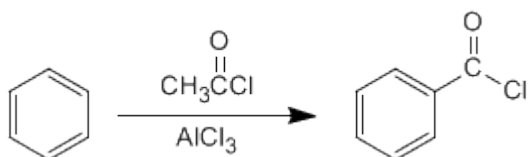
Los alcoholes alílicos y bencílicos se transforman en aldehídos o cetonas por oxidación con dióxido de manganeso en acetona. Esta reacción tiene una elevada selectividad y no oxida alcoholes que no se encuentren en dichas posiciones.



c) **Hidratación de alquinos:** Los alquinos se pueden hidratar Markovnikov, formando cetonas, o bien antiMarkovnikov, para formar aldehídos.



d) **Acilación de Friedel-Crafts:** La introducción de grupos acilo en el benceno permite la preparación de cetonas con cadenas aromáticas.



Otto Paul Hermann Diels (1876 - 1954)



Origen: Químico alemán.

Lugar de nacimiento: Königshütte (hoy Chorzów, Polonia).

Formación: estudió química en la Universidad de Berlín entre 1895 y 1899, consiguiendo el doctorado este año.

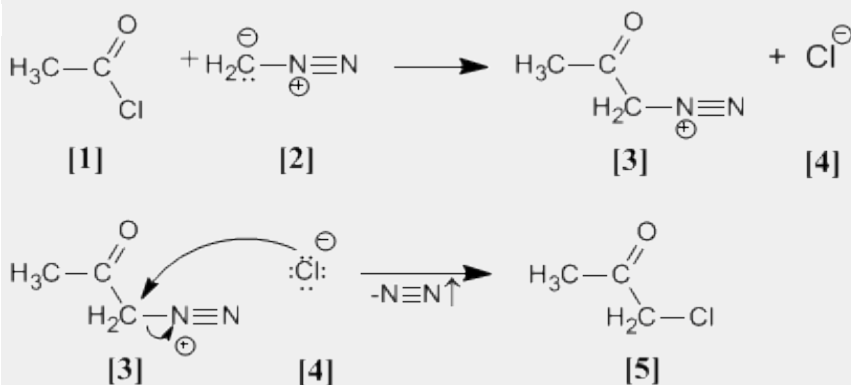
Docencia: profesor y jefe del departamento de química en la Universidad de Berlín. En 1916, tomó el puesto de profesor de Química en la Universidad de Kiel, cargo que no dejó hasta su jubilación en 1945.

Investigación: En 1906 descubrió el anhídrido malónico. Investigó en reacciones de deshidrogenación con selenio. Síntesis de α -dicetonas. Pero su trabajo más importante es la reacción de Diels - Alder.

Premio Nobel: En 1950 recibió el Premio Nobel junto a Kurt Alder

Arndt Eistert (Síntesis)

Cloruro de acetilo [1] se trata con diazometano [2] rindiendo la sal de diazonio [3]. El cloruro [4] producido reacciona con la sal de diazonio para dar la α -clorocetona [5].

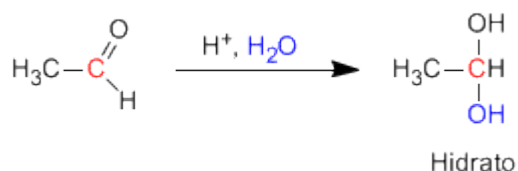


Síntesis de Arndt Eistert

Esta reacción permite transformar haluros de alcanoilo en cetonas halogenadas en su posición alfa.

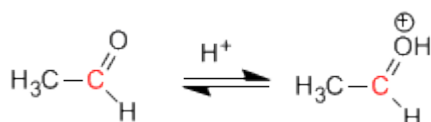
Formación de Hidratos

Los aldehídos y cetonas reaccionan en medio ácido acuoso para formar hidratos. El mecanismo consta de tres etapas. La primera y más rápida consiste en la protonación del oxígeno carbonílico. Esta protonación produce un aumento de la polaridad sobre el carbono y favorece el ataque del nucleófilo. En la segunda etapa el agua ataca al carbono carbonilo, es la etapa lenta del mecanismo. En la tercera etapa se produce la desprotonación del oxígeno formándose el hidrato final.

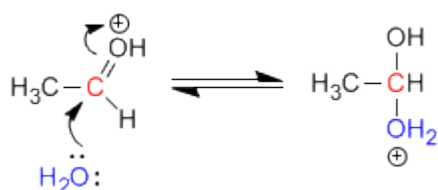


Mecanismo de la reacción

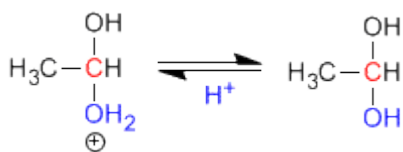
Etapa 1. Protonación del oxígeno carbonílico.



Etapa 2. Ataque nucleófilo del agua al carbonilo protonado.



Etapa 3. Desprotonación del hidrato





Origen: Químico estadounidense.

Lugar de nacimiento: Budapest

Formación: Se doctoró en la Universidad de Budapest en 1949

Docencia: Trabajó en el departamento de química orgánica de la Academia de Ciencias de Hungría y posteriormente en la Universidad de Cleveland.

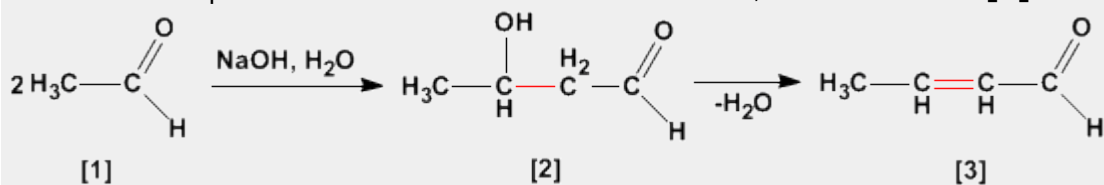
Industria: Trabajó en los laboratorios de la Dow Chemical de Ontario

Investigación: Olah consiguió preparar carbocationes estables utilizando componentes extremadamente ácidos.

Premio Nobel: En 1994 obtuvo el premio Nobel de Química por sus investigaciones sobre los carbocationes

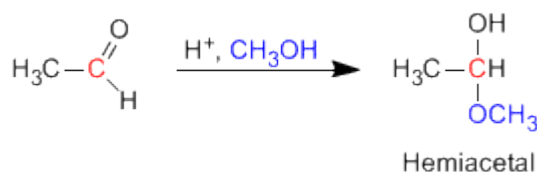
Aldólica (Condensación)

La condensación aldólica es una reacción de aldehídos o cetonas **[1]** que forma 3-hidroxicarbonilos (aldoles) **[2]**. El 3-hidroxialdehído **[2]** bajo condiciones de deshidratación por calentamiento rinde un aldehído alfa,beta-insaturado **[3]**.



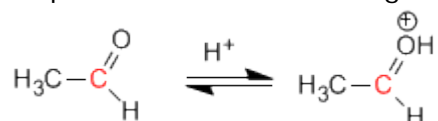
Formación de Hemiacetales

Los hemiacetales se forman por reacción de un equivalente de alcohol con el grupo carbonilo de un aldehído o cetona. Esta reacción se cataliza con ácido y es equivalente a la formación de hidratos.

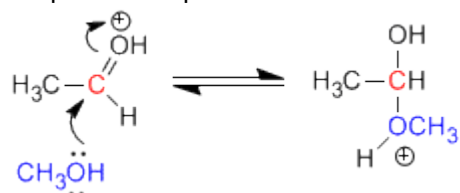


Mecanismo de la reacción:

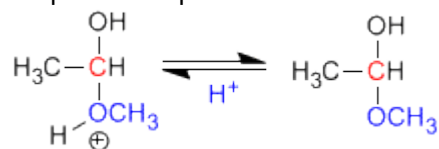
Eta 1. Protonación del oxígeno carbonílico.



Eta 2. Ataque nucleófilo del metanol al carbonilo protonado.



Eta 3. Desprotonación del hemiacetal



Otto Paul Hermann Diels (1876 - 1954)



Origen: Químico alemán.

Lugar de nacimiento: Königshütte (hoy Chorzów, Polonia).

Formación: estudió química en la Universidad de Berlín entre 1895 y 1899, consiguiendo el doctorado este año.

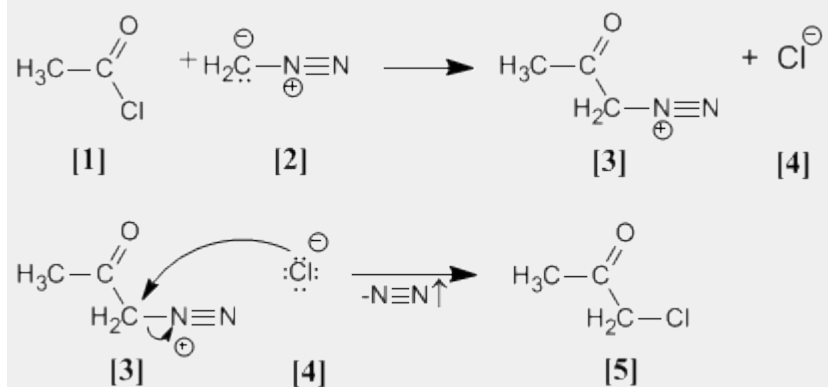
Docencia: profesor y jefe del departamento de química en la Universidad de Berlín. En 1916, tomó el puesto de profesor de Química en la Universidad de Kiel, cargo que no dejó hasta su jubilación en 1945.

Investigación: En 1906 descubrió el anhídrido malónico. Investigó en reacciones de deshidrogenación con selenio. Síntesis de α -dicetonas. Pero su trabajo más importante es la reacción de Diels - Alder.

Premio Nobel: En 1950 recibió el Premio Nobel junto a Kurt Alder

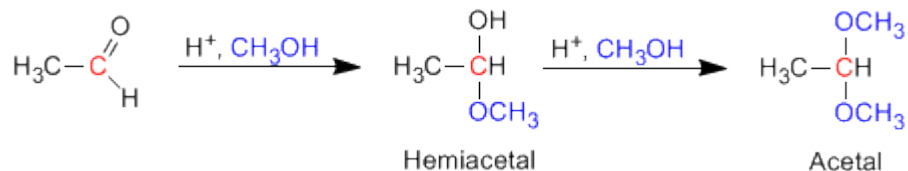
Arndt Eistert (Síntesis)

Cloruro de acetilo **[1]** se trata con diazometano **[2]** rindiendo la sal de diazonio **[3]**. El cloruro **[4]** producido reacciona con la sal de diazonio para dar la α -clorocetona **[5]**.



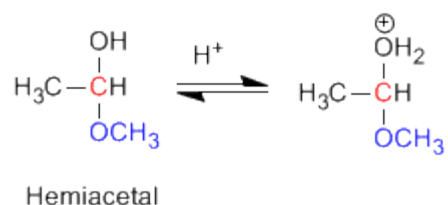
Formación de Acetales

Los aldehídos y cetonas reaccionan con alcoholes bajo condiciones de catálisis ácida, formando en una primera etapa hemiacetales, que posteriormene evolucionan por reacción con un segundo equivalente de alcohol a acetales.

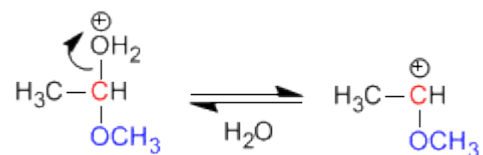


Mecanismo para la formación de acetales

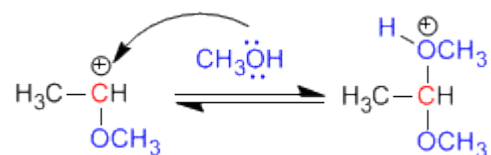
Etapa 1. Protonación del grupo hidroxilo



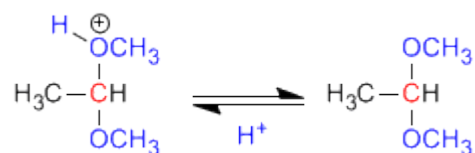
Etapa 2. Pérdida de agua.



Etapa 3. Ataque del alcohol al carbocatión



Etapa 4. Desprotonación del acetal



Otto Paul Hermann Diels (1876 - 1954)



Origen: Químico alemán.

Lugar de nacimiento: Königshütte (hoy Chorzów, Polonia).

Formación: estudió química en la Universidad de Berlín entre 1895 y 1899, consiguiendo el doctorado este año.

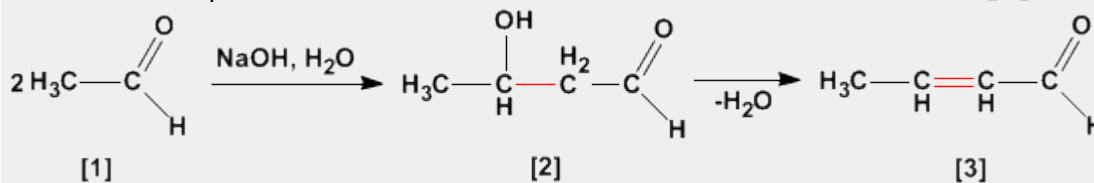
Docencia: profesor y jefe del departamento de química en la Universidad de Berlín. En 1916, tomó el puesto de profesor de Química en la Universidad de Kiel, cargo que no dejó hasta su jubilación en 1945.

Investigación: En 1906 descubrió el anhídrido malónico. Investigó en reacciones de deshidrogenación con selenio. Síntesis de α -dicetonas. Pero su trabajo más importante es la reacción de Diels - Alder.

Premio Nobel: En 1950 recibió el Premio Nobel junto a Kurt Alder

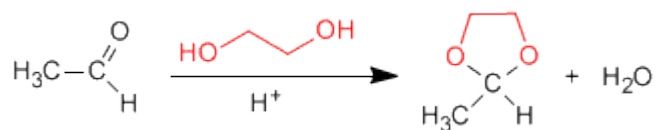
Aldólica (Condensación)

La condensación aldólica es una reacción de aldehídos o cetonas **[1]** que forma 3-hidroxicarbonilos (aldoles) **[2]**. El 3-hidroxialdehído **[2]** bajo condiciones de deshidratación por calentamiento rinde un aldehído alfa,beta-insaturado **[3]**.



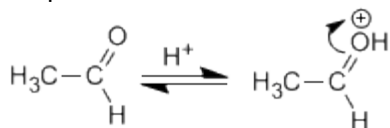
Formación de acetales cíclicos

Los 1,2- y 1,3-dioles reaccionan con aldehídos y cetonas formando acetales cíclicos. Los equilibrios se desplazan hacia el producto final eliminando el agua formada por destilación azeotrópica con benceno o tolueno.

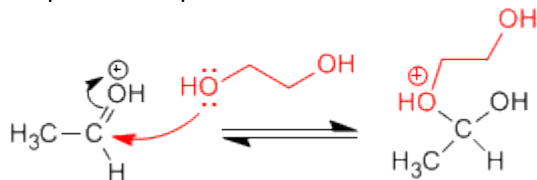


Mecanismo para la formación de acetales cíclicos:

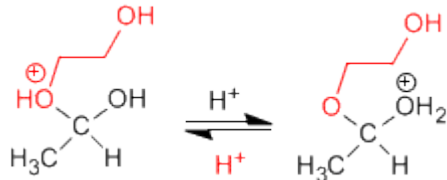
Etapa 1. Protonación del carbonilo



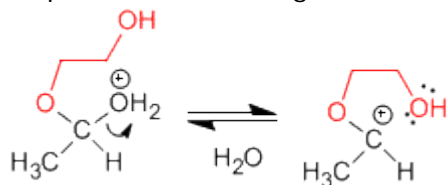
Etapa 2. Ataque nucleófilo del diol al carbonilo.



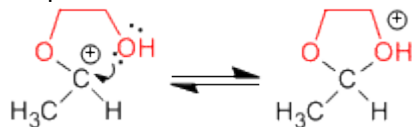
Etapa 3. Equilibrio ácido base entre el éter y el alcohol



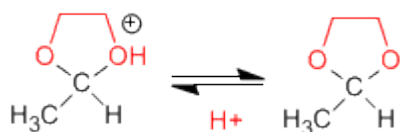
Etapa 4. Pérdida de agua



Etapa 5. Ciclación



Etapa 6. Desprotonación del acetal cíclico



Kurt Alder (1902 - 1958)



Origen: Químico alemán.

Lugar de nacimiento: Königshütte (hoy Chorzów, Polonia).

Formación: estudió en la Universidad de Kiel. Bajo la supervisión del químico alemán Otto Diels, su jefe e instructor en Kiel.

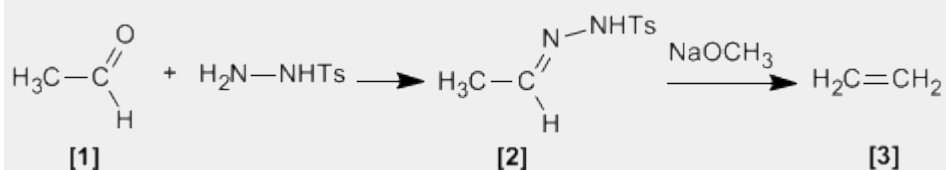
Docencia: Alder ejerció como profesor de química en las universidades de Kiel y Colonia.

Investigación: Alder se especializó en la síntesis diénica (conocida más tarde como la reacción Diels - Alder) que consiste fundamentalmente en el análisis y formación de compuestos orgánicos complejos. Ya en 1928 ambos fueron coautores de un ensayo sobre este proceso.

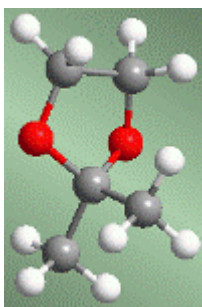
Premio Nobel: En 1950 recibió el Premio Nobel junto a Diels

Bamford Stevens (Reacción)

Tosilhidrazonas [2] de aldehídos o cetonas alifáticos [1] reaccionan con bases fuertes para dar alquenos [3].

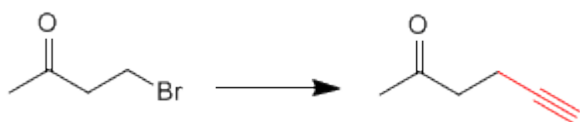


Acetales como grupos protectores

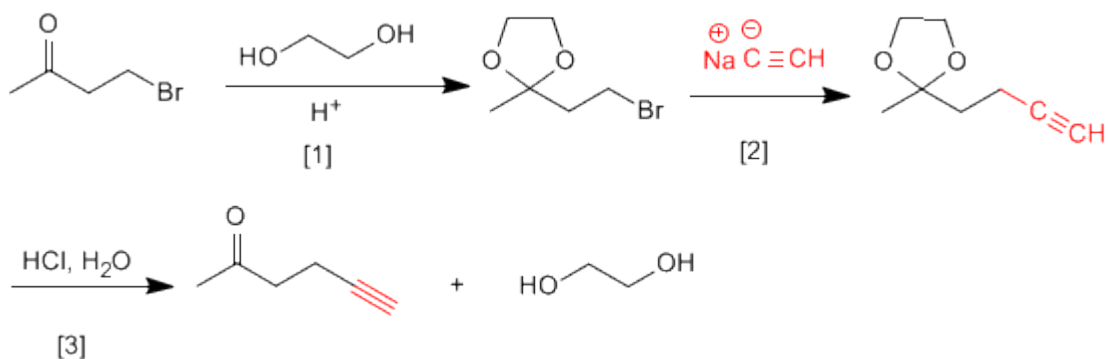


Los acetales pueden emplearse, por su estabilidad, como grupos protectores del carbonilo. El acetal es un éter, muy estable en medios básicos, aunque rompe en presencia de medios ácidos. En muchos procesos de síntesis el grupo carbonilo es incompatible con el reactivo utilizado. En estos casos debe protegerse para evitar que reaccione. La inestabilidad del acetal en medio ácido puede emplearse para desproteger el carbonilo.

Veamos algunos ejemplos:



Esta transformación requiere una sustitución, empleando como nucleófilo un acetiluro de sodio. El nucleófilo puede atacar también al grupo carbonilo, para evitarlo vamos a protegerlo.

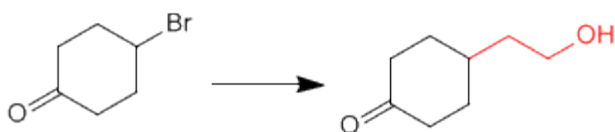


[1] Protección de la cetona.

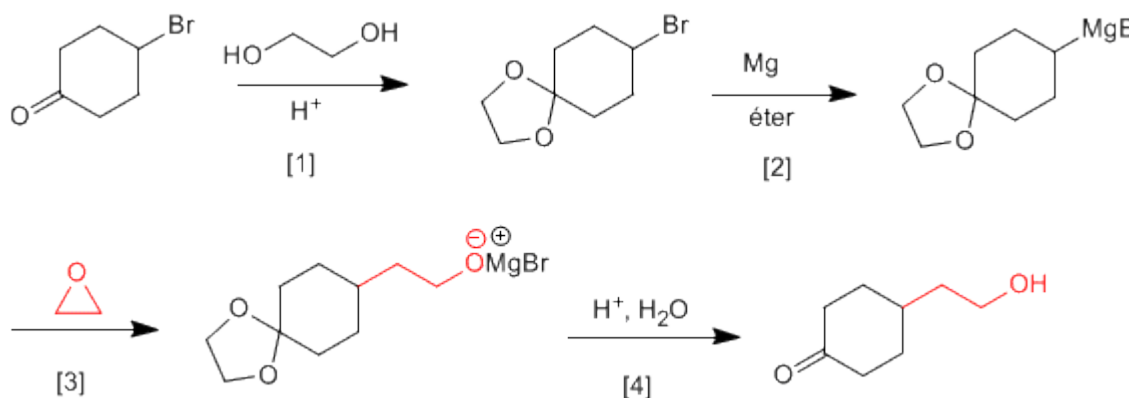
[2] Ataque del acetiluro al carbono del bromo.

[3] Desprotección del carbonilo

Veamos un segundo ejemplo:



Es necesario proteger la cetona antes de formar el organometálico para evitar la dimerización del compuesto.



- [1] Protección de la cetona.
 [2] Formación del magnesiano.
 [3] Apertura del oxaciclopropano.
 [4] Desprotección y protonación del alcóxido.

Otto Paul Hermann Diels (1876 - 1954)



Origen: Químico alemán.

Lugar de nacimiento: Königshütte (hoy Chorzów, Polonia).

Formación: estudió química en la Universidad de Berlín entre 1895 y 1899, consiguiendo el doctorado este año.

Docencia: profesor y jefe del departamento de química en la Universidad de Berlín. En 1916, tomó el puesto de profesor de Química en la Universidad de Kiel, cargo que no dejó hasta su jubilación en 1945.

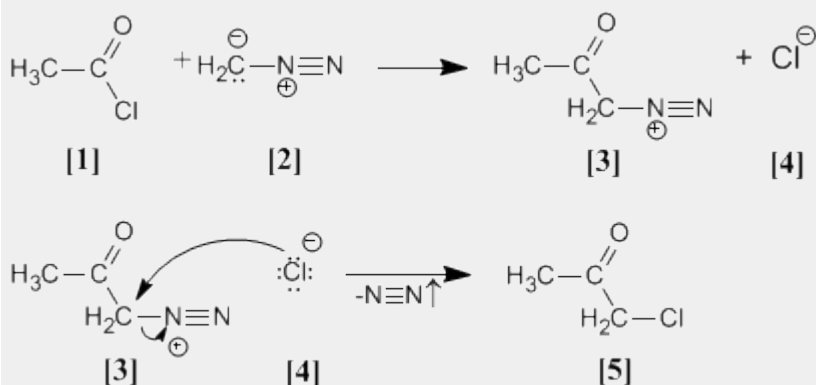
Investigación: En 1906 descubrió el anhídrido malónico.

Investigó en reacciones de deshidrogenación con selenio. Síntesis de α -dicetonas. Pero su trabajo más importante es la reacción de Diels - Alder.

Premio Nobel: En 1950 recibió el Premio Nobel junto a Kurt Alder

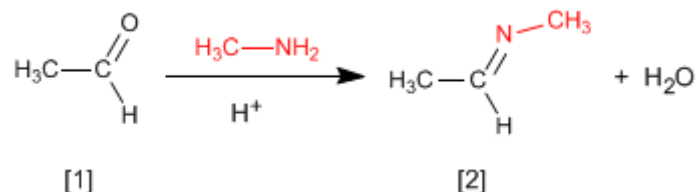
Arndt Eistert (Síntesis)

Cloruro de acetilo **[1]** se trata con diazometano **[2]** rindiendo la sal de diazonio **[3]**. El cloruro **[4]** producido reacciona con la sal de diazonio para dar la α -clorocetona **[5]**.



Formación de Iminas

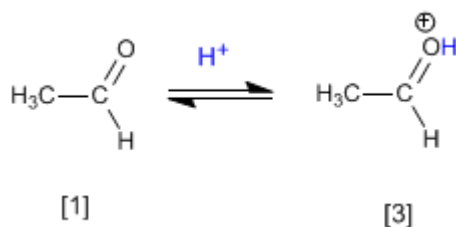
La reacción de aldehídos o cetonas **[1]** con aminas primarias genera iminas **[2]**. La reacción se favorece en un medio ligeramente ácido (pH=4.5).



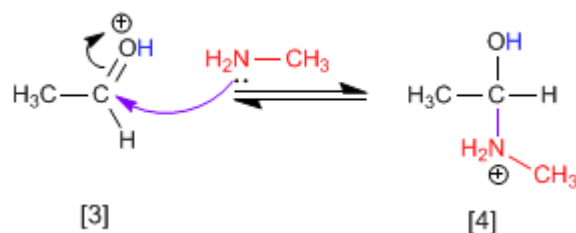
El control del pH es fundamental, puesto que se requiere la protonación del oxígeno del carbonilo para favorecer el ataque nucleófilo.

Mecanismo:

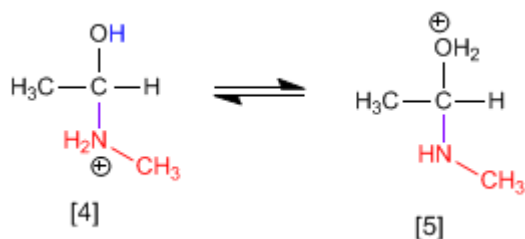
Etapas 1. Protonación del grupo carbonilo que aumenta la polaridad positiva sobre el carbono y favorece el ataque nucleófilo.



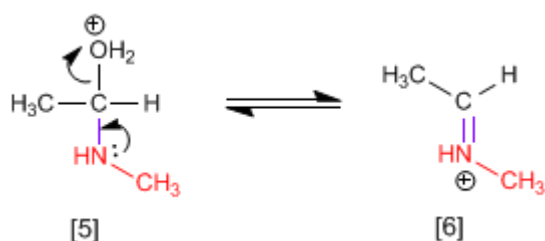
Etapas 2. Ataque nucleófilo de la amina primaria al carbono carbonilo.



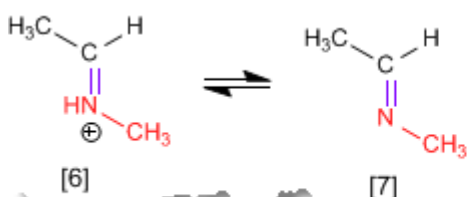
Etapas 3. Protonación del grupo hidroxilo para transformarlo en buen grupo saliente.



Etapas 4. Pérdida de agua y formación de la imina protonada.



Etapa 5. Desprotonación del catión.



George A. Olah (1927 -)



Origen: Químico estadounidense.

Lugar de nacimiento: Budapest

Formación: Se doctoró en la Universidad de Budapest en 1949

Docencia: Trabajó en el departamento de química orgánica de la Academia de Ciencias de Hungría y posteriormente en la Universidad de Cleveland.

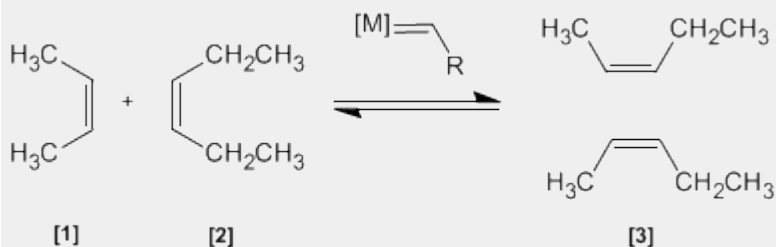
Industria: Trabajó en los laboratorios de la Dow Chemical de Ontario

Investigación: Olah consiguió preparar carbocationes estables utilizando componentes extremadamente ácidos.

Premio Nobel: En 1994 obtuvo el premio Nobel de Química por sus investigaciones sobre los carbocationes

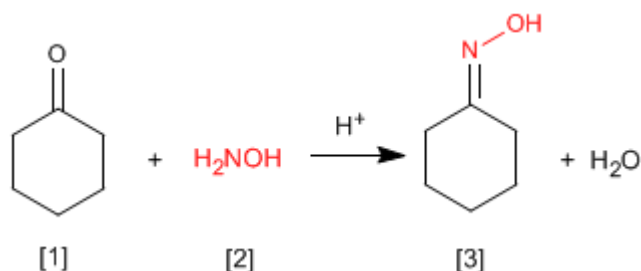
Metátesis de Alquenos

En esta reacción dos alquenos **[1]** y **[2]** son tratados con un metal de transición que actúa como catalizador, dando una mezcla de alquenos **[3]** (incluyendo isómeros Z/E). Este productos se obtiene por intercambio de grupos alquilideno.

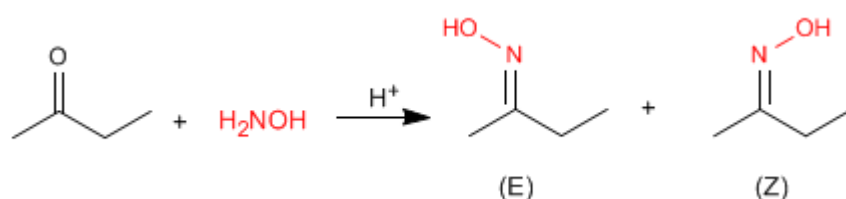


Formación de Oximas

Las oximas [3] se obtienen por reacción de aldehídos o cetonas [1] e hidroxilamina [2] en un medio débilmente ácido. El mecanismo es análogo al de formación de iminas.



Las oximas de aldehídos y cetona asimétricas presentan isomería Z/E dependiendo de la posición del hidroxilo.



Las iminas e hidrazonas (que comentaremos a continuación) también presentan esta característica.

George A. Olah (1927 -)



Origen: Químico estadounidense.

Lugar de nacimiento: Budapest

Formación: Se doctoró en la Universidad de Budapest en 1949

Docencia: Trabajó en el departamento de química orgánica de la Academia de Ciencias de Hungría y posteriormente en la Universidad de Cleveland.

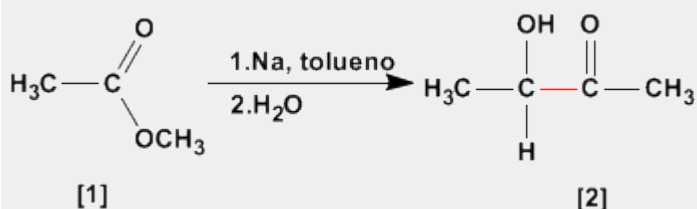
Industria: Trabajó en los laboratorios de la Dow Chemical de Ontario

Investigación: Olah consiguió preparar carbocationes estables utilizando componentes extremadamente ácidos.

Premio Nobel: En 1994 obtuvo el premio Nobel de Química por sus investigaciones sobre los carbocationes

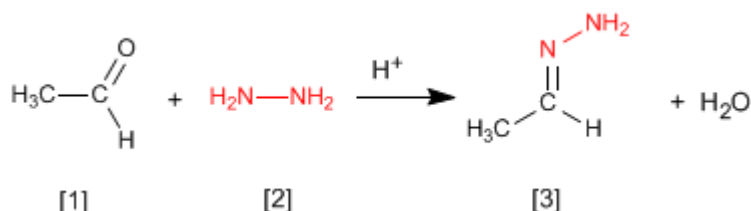
Aciloinica (Condensación)

La condensación aciloinica transforma ésteres [1] en alfa-hidroxicetonas [2]. Esta reacción se realiza con sodio metal en disolvente inerte.

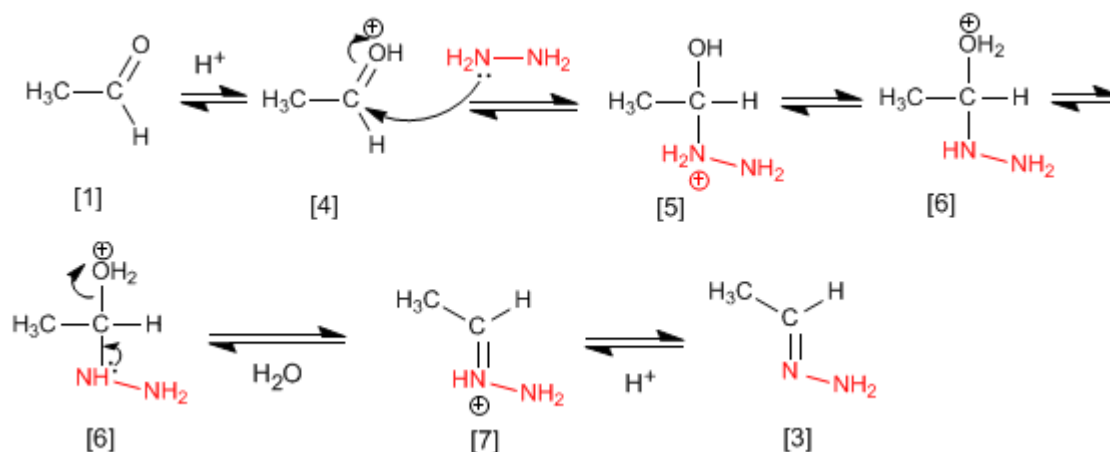


Formación de Hidrazonas

Las hidrazonas [3] se obtienen por reacción de aldehídos o cetonas [1] con hidrazina [2]. Igual que en el caso de las iminas y oximas requiere pH=4.



Aunque el mecanismo es análogo al de formación de iminas, comentaremos de nuevo los pasos.



El etanal [1] se protona formando su ácido conjugado [4]. La importante polaridad del carbono carbonilo de [4] favorece el ataque de la hidrazina [2] para formando el intermedio [5]. El compuesto [5] intercambia un protón entre el nitrógeno y el oxígeno, transformando el grupo hidroxilo en agua (buen grupo saliente). El intermedio [6] pierde una molécula de agua transformándose en [7], cuya desprotonación da la hidrazona final [3].

Kurt Alder (1902 - 1958)



Origen: Químico alemán.

Lugar de nacimiento: Königshütte (hoy Chorzów, Polonia).

Formación: estudió en la Universidad de Kiel. Bajo la supervisión del químico alemán Otto Diels, su jefe e instructor en Kiel.

Docencia: Alder ejerció como profesor de química en las universidades de Kiel y Colonia.

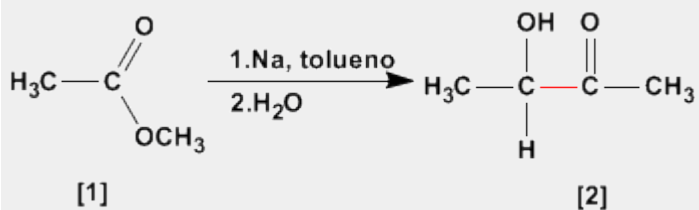
Investigación: Alder se especializó en la síntesis diénica (conocida más tarde como la reacción Diels - Alder) que consiste fundamentalmente en el análisis y formación de compuestos orgánicos complejos.

Ya en 1928 ambos fueron coautores de un ensayo sobre este proceso.

Premio Nobel: En 1950 recibió el Premio Nobel junto a Diels

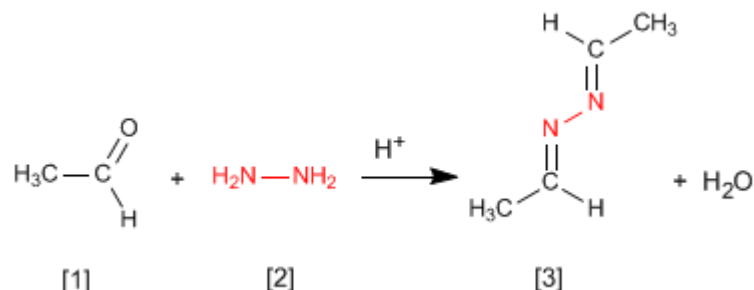
Aciloínica (Condensación)

La condensación aciloínica transforma esteres [1] en alfa-hidroxicetonas [2]. Esta reacción se realiza con sodio metal en disolvente inerte.



Formación de Azinas

La hidrazina [2] reacciona con dos moléculas de aldehído [1] para formar azinas [3].



El mecanismo es análogo al de formación de iminas, oximas e hidrazonas.

George A. Olah (1927 -)



Origen: Químico estadounidense.

Lugar de nacimiento: Budapest

Formación: Se doctoró en la Universidad de Budapest en 1949

Docencia: Trabajó en el departamento de química orgánica de la Academia de Ciencias de Hungría y posteriormente en la

Universidad de Cleveland.

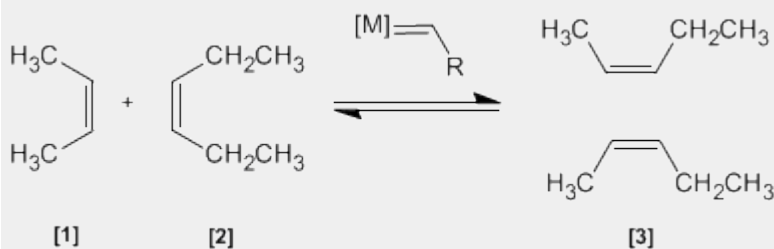
Industria: Trabajó en los laboratorios de la Dow Chemical de Ontario

Investigación: Olah consiguió preparar carbocationes estables utilizando componentes extremadamente ácidos.

Premio Nobel: En 1994 obtuvo el premio Nobel de Química por sus investigaciones sobre los carbocationes

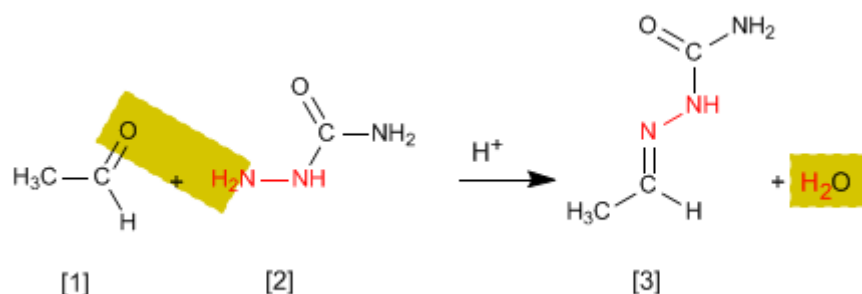
Metátesis de Alquenos

En esta reacción dos alquenos [1] y [2] son tratados con un metal de transición que actúa como catalizador, dando una mezcla de alquenos [3] (incluyendo isómeros Z/E). Este producto se obtiene por intercambio de grupos alquilideno.



Formación de Semicarbazonas

Las semicarbazonas [3] se obtienen por reacción de aldehídos o cetonas [1] con semicarbazida [2]. Veamos un ejemplo:



El mecanismo es análogo al de formación de iminas, oximas e hidrazonas.

Charles Friedel (1832 - 1899)



Origen: Químico frances..

Lugar de nacimiento: Estrasburgo.

Formación: estudió química en la Universidad de Berlín entre 1895 y 1899, consiguiendo el doctorado este año.

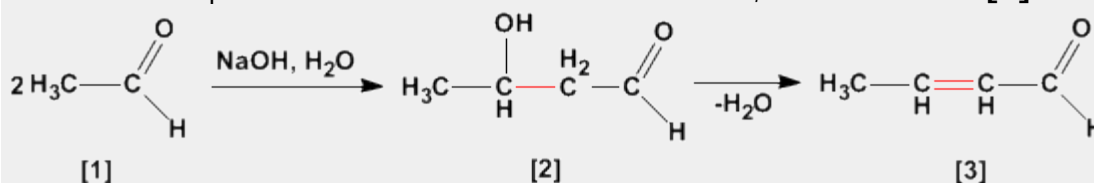
Docencia: Profesor en la Universidad de la Sorbona.

Investigación: Obtuvo el alcohol propílico. En 1877, Friedel y Crafts describieron por primera vez la reacción del benceno con un haloalcano en presencia de un ácido de Lewis. Esta reacción produce la alquilación del benceno y se conoce como alquilación de Friedl-Crafts.

Premio Nobel:

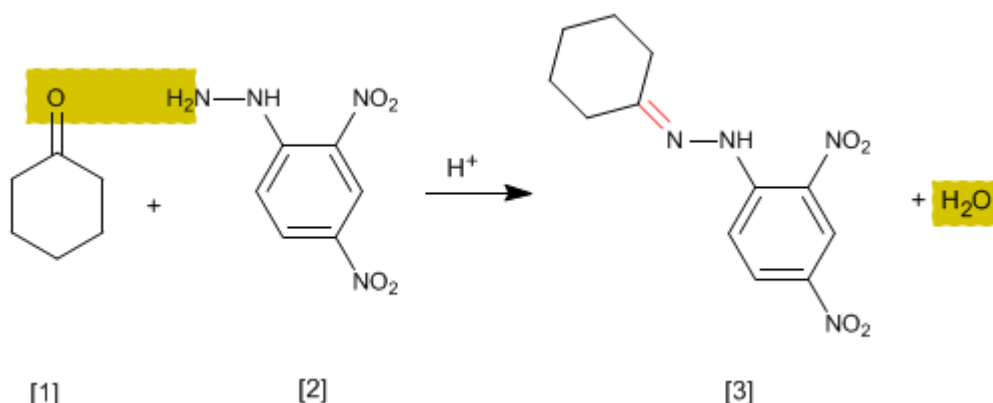
Aldólica (Condensación)

La condensación aldólica es una reacción de aldehídos o cetonas [1] que forma 3-hidroxicarbonilos (aldoles) [2]. El 3-hidroxialdehído [2] bajo condiciones de deshidratación por calentamiento rinde un aldehído alfa,beta-insaturado [3].



Ensayo de la 2,4-Dinitrofenilhidrazina

Se trata de un ensayo analítico específico de aldehídos y cetonas. Los carbonilos **[1]** reaccionan con 2,4-Dinitrofenilhidrazina **[2]** formando fenilhidrazonas **[3]** que precipitan de color amarillo. La aparición de precipitado es un indicador de la presencia de carbonilos en el medio.



El mecanismo de la reacción es análogo al de formación de iminas.

Kurt Alder (1902 - 1958)



Origen: Químico alemán.

Lugar de nacimiento: Königshütte (hoy Chorzów, Polonia).

Formación: estudió en la Universidad de Kiel. Bajo la supervisión del químico alemán Otto Diels, su jefe e instructor en Kiel.

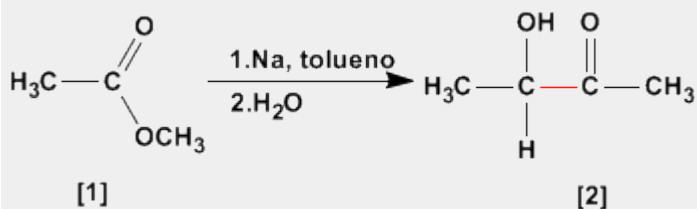
Docencia: Alder ejerció como profesor de química en las universidades de Kiel y Colonia.

Investigación: Alder se especializó en la síntesis diénica (conocida más tarde como la reacción Diels - Alder) que consiste fundamentalmente en el análisis y formación de compuestos orgánicos complejos. Ya en 1928 ambos fueron coautores de un ensayo sobre este proceso.

Premio Nobel: En 1950 recibió el Premio Nobel junto a Diels

Aciloinica (Condensación)

La condensación aciloinica transforma esteres **[1]** en alfa-hidroxicetonas **[2]**. Esta reacción se realiza con sodio metal en disolvente inerte.



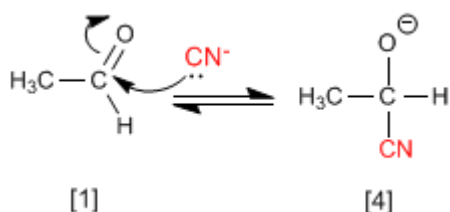
Formación de Cianhidrinas

Las cianhidrinas **[3]** se forman por reacción de aldehídos o cetonas **[1]** con ácido cianhídrico **[2]** y son compuestos que contienen un grupo ciano y un hidroxilo sobre el mismo carbono.

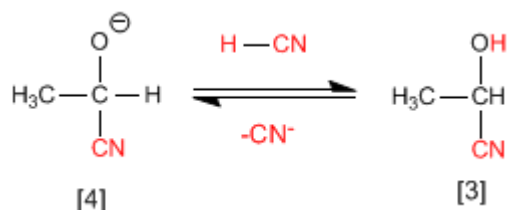


El mecanismo de la reacción transcurre en dos etapas:

Etapla 1. Los iones cianuro actúan como nucleófilos atacando al carbono carbonilo. El ácido cianhídrico es demasiado débil para generar cantidades importantes de cianuro, por ello, se añade cianuro de sodio o potasio al medio, garantizando la cantidad suficiente de cianuro para que la reacción transcurra en buen rendimiento.



Etapla 2. En este paso el ión alcóxido **[4]** se protona arrancando hidrógenos al ácido cianhídrico. En esta etapa se regeneran los iones cianuro.



Kurt Alder (1902 - 1958)



Origen: Químico alemán.

Lugar de nacimiento: Königshütte (hoy Chorzów, Polonia).

Formación: estudió en la Universidad de Kiel. Bajo la supervisión del químico alemán Otto Diels, su jefe e instructor en Kiel.

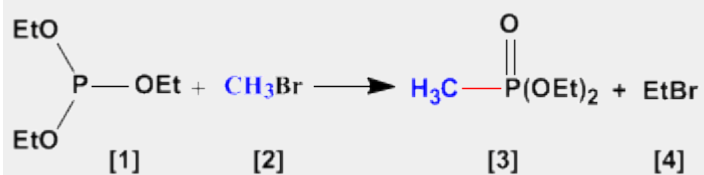
Docencia: Alder ejerció como profesor de química en las universidades de Kiel y Colonia.

Investigación: Alder se especializó en la síntesis diénica (conocida más tarde como la reacción Diels - Alder) que consiste fundamentalmente en el análisis y formación de compuestos orgánicos complejos. Ya en 1928 ambos fueron coautores de un ensayo sobre este proceso.

Premio Nobel: En 1950 recibió el Premio Nobel junto a Diels

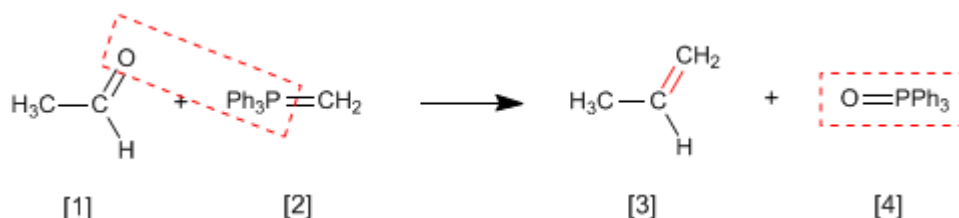
Arbuzov (Reacción)

La reacción de Arbuzov se emplea en la síntesis de fosfonatos **[3]** a partir de fosfitos **[1]**. Los fosfonatos obtenidos en la síntesis de Arbuzov se emplean como materiales de partida en la síntesis de Horner-Wittig.



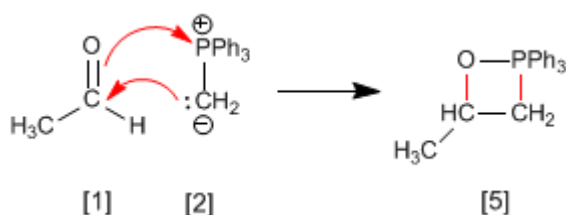
Reacción de Wittig

La reacción de Wittig emplea iluros de fósforo **[2]** para transformar aldehídos y cetonas **[1]** en alquenos **[3]**. Como subproducto se obtiene el óxido de trifenilfosfina **[4]**.

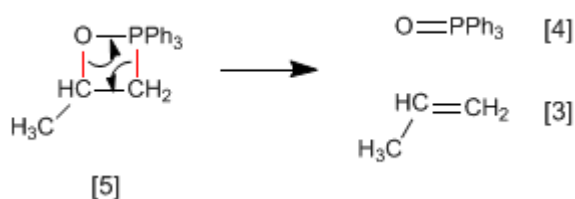


En el mecanismo de la reacción el iluro y el carbonilo se combinan para formar un oxafosfetano que rompe dejando libre el alqueno final.

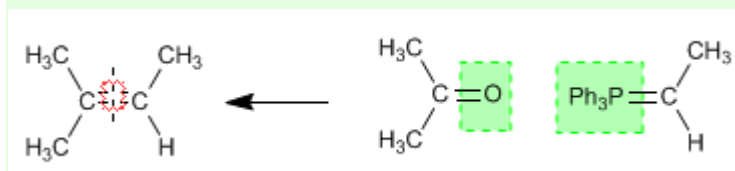
Etapas 1. El etanal y el iluro se combinan formando el fosfetano.



Etapas 2. El fosfetano rompe formando el alqueno y óxido de trifenilfosfina.

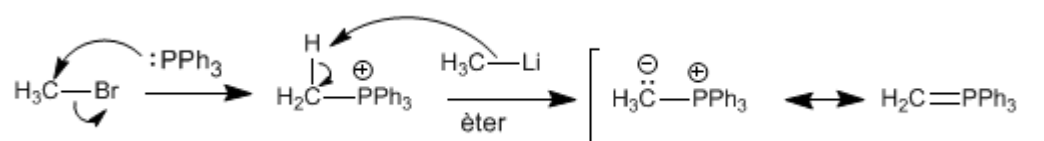


Ejemplo - Obtener mediante Wittig el 2-Metilbut-2-eno



Se rompe el alqueno por el doble enlace y a cada carbono se le agrega el grupo encerrado en verde.

Los **iluros de fósforo** se preparan mediante reacción de haloalcanos y trifenilfosfina, seguido de desprotonación del carbono con base fuerte (organometálicos de litio).



Charles Friedel (1832 - 1899)



Origen: Químico frances..

Lugar de nacimiento: Estrasburgo.

Formación: estudió química en la Universidad de Berlín entre 1895 y 1899, consiguiendo el doctorado este año.

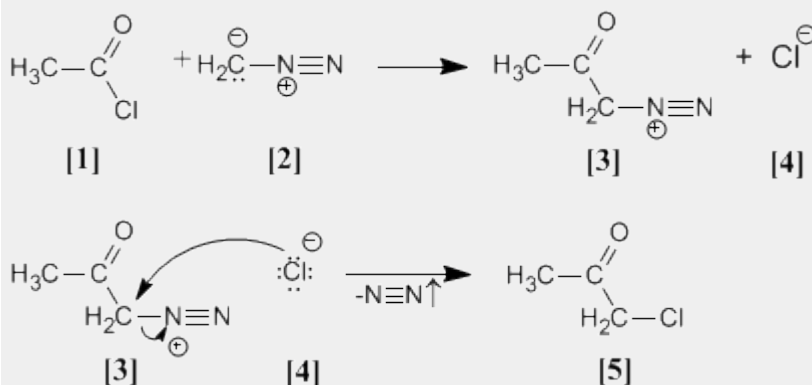
Docencia: Profesor en la Universidad de la Sorbona.

Investigación: Obtuvo el alcohol propílico. En 1877, Friedel y Crafts describieron por primera vez la reacción del benceno con un haloalcano en presencia de un ácido de Lewis. Esta reacción produce la alquilación del benceno y se conoce como alquilación de Friedl-Crafts.

Premio Nobel:

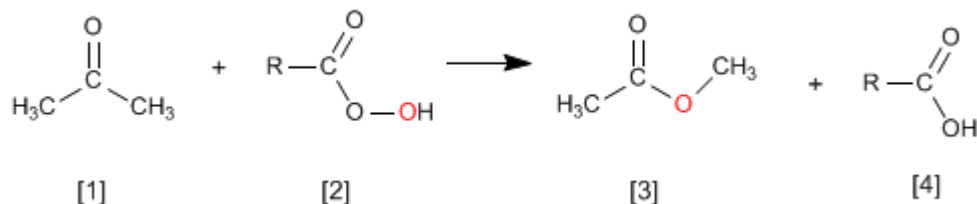
Arndt Eistert (Síntesis)

Cloruro de acetilo **[1]** se trata con diazometano **[2]** rindiendo la sal de diazonio **[3]**. El cloruro **[4]** producido reacciona con la sal de diazonio para dar la α -clorocetona **[5]**.

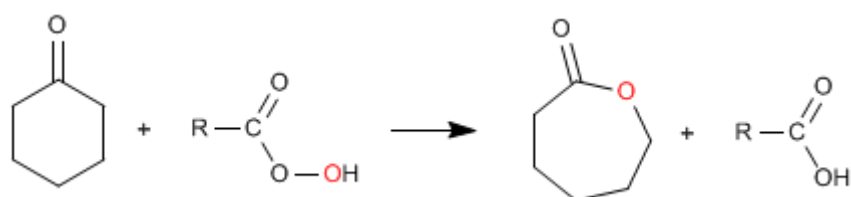


Oxidación de Baeyer Villiger

La reacción de cetonas **[1]** con perácidos **[2]** produce ésteres **[3]**. El oxígeno del perácido se inserta entre el carbono carbonilo y el carbono alfa de la cetona. Esta reacción fue descrita por Adolf von Baeyer y Victor Villiger in 1899.

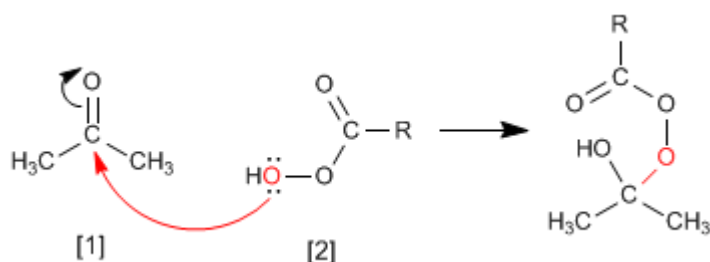


A partir de cetonas cíclicas se obtienen ésteres cíclicos (lactonas)

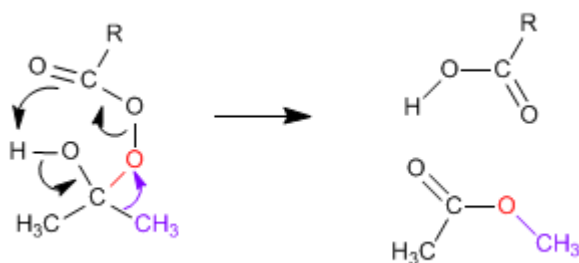


El mecanismo de Baeyer Villiger comienza con el ataque nucleófilo del perácido sobre el carbonilo, seguido de la migración del sustituyente desde el grupo carbonilo al oxígeno del perácido.

Etapas 1. Adición del perácido al carbonilo

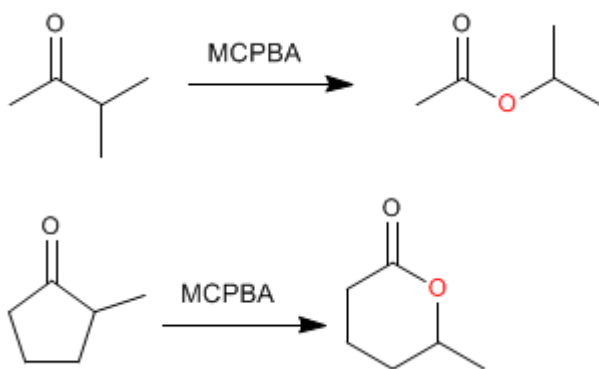


Etapas 2. Migración del sustituyente desde carbono carbonilo hacia el oxígeno (rojo)



Cuando la cetona tiene dos sustituyentes diferentes migra mejor el más sustituido. Existe un orden de migración que nos ayuda a decidir que sustituyente pasa a unirse al oxígeno del perácido.

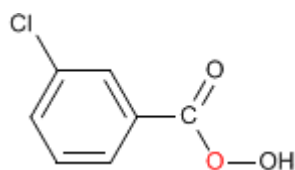
Orden de migración: H > carbono terciario > ciclohexilo > carbono secundario » fenilo > carbono primario > metilo



Como puede observarse en el orden de migración, el grupo que mejor migra, por su pequeño tamaño, es el hidrógeno, por ello, al tratar aldehídos con perácidos se produce la migración del hidrógeno formándose ácidos carboxílicos.



El **MCPBA** (Ácido meta-cloroperoxibenzoico) es un perácido ampliamente utilizado en la epoxidación de alquenos y también en Baeyer-Villger. La fórmula del MCPBA se muestra a continuación.



Charles Friedel (1832 - 1899)



Origen: Químico frances..

Lugar de nacimiento: Estrasburgo.

Formación: estudió química en la Universidad de Berlín entre 1895 y 1899, consiguiendo el doctorado este año.

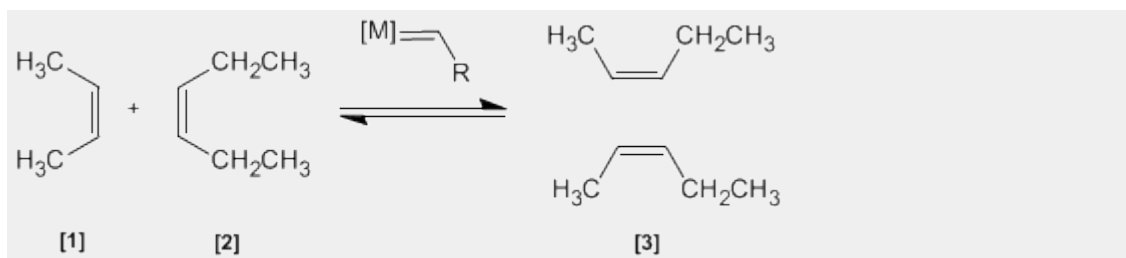
Docencia: Profesor en la Universidad de la Sorbona.

Investigación: Obtuvo el alcohol propílico. En 1877, Friedel y Crafts describieron por primera vez la reacción del benceno con un haloalcano en presencia de un ácido de Lewis. Esta reacción produce la alquilación del benceno y se conoce como alquilación de Friedl-Crafts.

Premio Nobel:

Metátesis de Alquenos

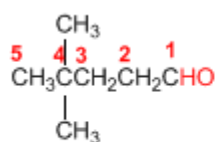
En esta reacción dos alquenos **[1]** y **[2]** son tratados con un metal de transición que actúa como catalizador, dando una mezcla de alquenos **[3]** (incluyendo isómeros Z/E). Este productos se obtiene por intercambio de grupos alquilideno.



Nomenclatura de Aldehídos y Cetonas - Reglas IUPAC

Regla 1. Los aldehídos se nombran reemplazando la terminación **-ano** del alcano correspondiente por **-al**. No es necesario especificar la posición del grupo aldehído, puesto que ocupa el extremo de la cadena (localizador 1).

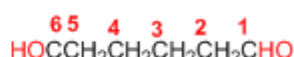
Cuando la cadena contiene dos funciones aldehído se emplea el sufijo **-dial**.



4,4-Dimetilpentanal

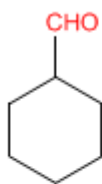


Hex-4-enal

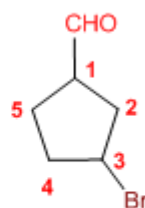


Hexanodial

Regla 2. El grupo **-CHO** se denomina **-carbaldehído**. Este tipo de nomenclatura es muy útil cuando el grupo aldehído va unido a un ciclo. La numeración del ciclo se realiza dando localizador 1 al carbono del ciclo que contiene el grupo aldehído.

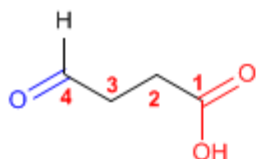


Ciclohexanocarbaldehído

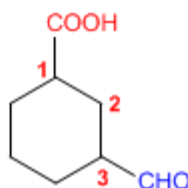


3-Bromociclopentanocarbaldehído

Regla 3. Cuando en la molécula existe un grupo prioritario al aldehído, este pasa a ser un sustituyente que se nombra como oxo- o formil-.



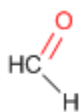
Ácido 4-oxobutanoico



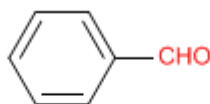
Ácido 3-formilciclohexanocarboxílico

Tanto **-carbaldehído** como **formil-** son nomenclaturas que incluyen el carbono del grupo carbonilo. **-carbaldehído** se emplea cuando el aldehído es grupo funcional, mientras que **formil-** se usa cuando actúa de sustituyente.

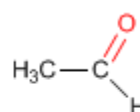
Regla 4. Algunos nombres comunes de aldehídos aceptados por la IUPAC son:



Formaldehído
(Metanal)

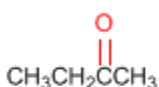


Benzaldehído
(Benceno**carbaldehído**)

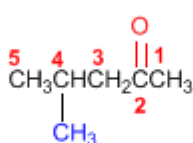


Acetaldehído
(Etanal)

Regla 5. Las cetonas se nombran sustituyendo la terminación **-ano** del alcano con igual longitud de cadena por **-ona**. Se toma como cadena principal la de mayor longitud que contiene el grupo carbonilo y se numera para que éste tome el localizador más bajo.



Butan**ona**

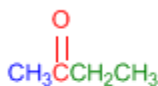


4-Metil-2-pentan**ona**

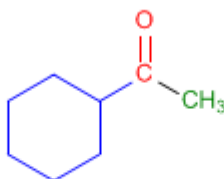


3-Metilciclohexan**ona**

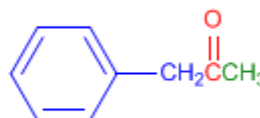
Regla 6. Existe un segundo tipo de nomenclatura para las cetonas, que consiste en nombrar las cadenas como sustituyentes, ordenándolas alfabéticamente y terminando el nombre con la palabra cetona.



Etil metil **cetona**

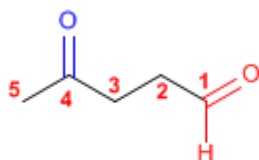


Ciclohexil metil **cetona**

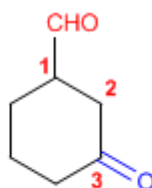


Fenil metil **cetona**

Regla 7. Cuando la cetona no es el grupo funcional de la molécula pasa a llamarse **OXO-**.



4-Oxopentan**al**

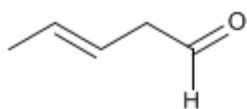


3-Oxociclohexano**carbaldehído**

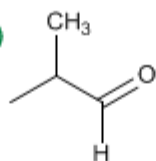
Nomenclatura de Aldehídos y Cetonas - Problema 9.1

Nombra los siguientes aldehídos y cetonas:

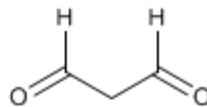
a)



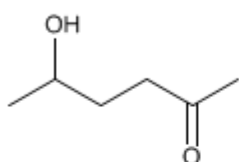
b)



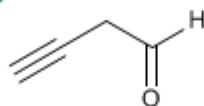
c)



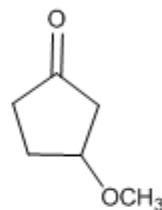
d)



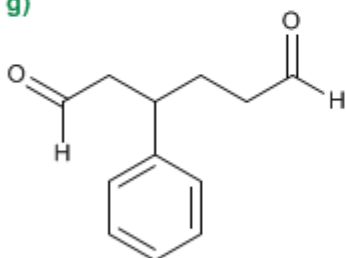
e)



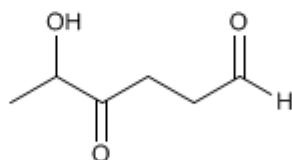
f)



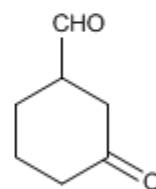
g)



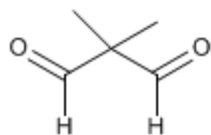
h)



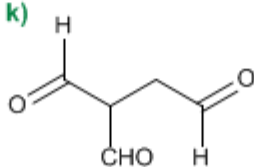
i)



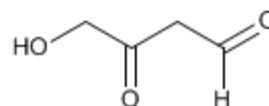
j)



k)

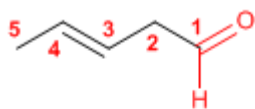


l)

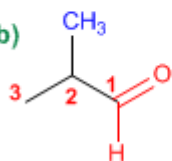


Solución

a)



b)



1. Cadena principal: 5 carbonos (pentano)

2. Numeración: comienza en el aldehído (grupo funcional)

Grupo funcional: aldehído

3. Nombre: Pent-3-enal

1. Cadena principal: 3 carbonos (propano)

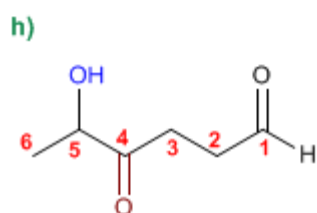
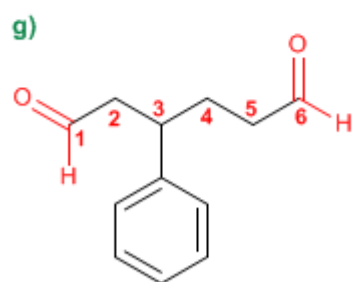
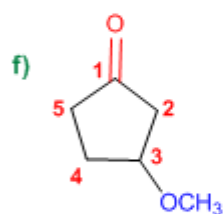
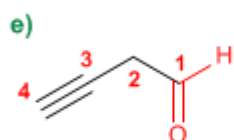
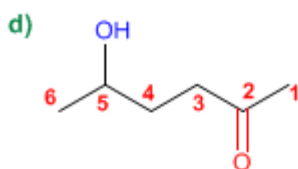
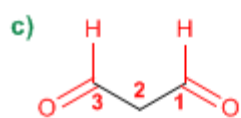
2. Numeración: localizador más bajo al aldehído.

3. Grupo funcional: aldehído

4. Sustituyentes: metilo en 2.

5. Nombre: 2-Metilpropanal

Los aldehídos y cetonas son prioritarios sobre alquenos y alquinos, y se numeran otorgándoles el localizador más bajo



1. Cadena principal: 3 carbonos (propano)
2. Grupo funcional: aldehído (dialdehído)
3. Nombre: Propanodial

1. Cadena principal: 6 carbonos (hexano)
2. Grupo funcional: cetona
3. Numeración: asignar el menor localizador a la cetona
4. Sustituyentes: hidroxí en 5.
5. Nombre: 5-Hidroxihexan-2-ona

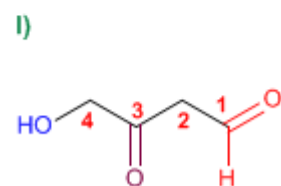
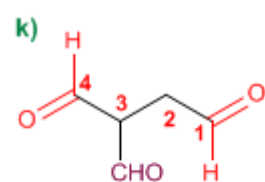
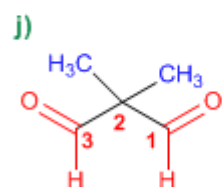
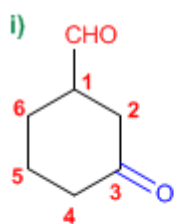
1. Cadena principal: 4 carbonos (butano)
2. Grupo funcional: aldehído
3. Numeración: asignar el menor localizador al aldehído
4. Nombre: But-3-inal

1. Cadena principal: ciclo de 5 miembros (ciclopentano)
2. Grupo funcional: cetona
3. Numeración: comienza en la cetona y prosigue hacia el sustituyente
4. Sustituyentes: metoxi en 3.
5. Nombre: 3-Metoxiciclopentanona

1. Cadena principal: 6 carbonos (hexano)
2. Grupo funcional: aldehído (dialdehído)
3. Numeración: comienza en el extremo que otorga al fenilo el localizador más bajo.
4. Sustituyentes: fenilo en 3.
5. Nombre: 3-Fenilhexanodial

1. Cadena principal: 6 carbonos (hexano)
2. Grupo funcional: aldehído
3. Numeración: asignar el menor localizador al aldehído
4. Sustituyentes: hidroxí en 5 y oxo en 4.
5. Nombre: 5-Hidroxí-4-oxohexanal

Los aldehídos son prioritarios sobre las cetonas que pasan a nombrarse como sustituyentes (oxo-)



1. Cadena principal: ciclo de 6 miembros (ciclohexano)
2. Grupo funcional: aldehído (-carbaldehído)
3. Numeración: menor localizador al grupo -CHO (este no se numera)
4. Sustituyentes: cetona (oxo-) en 3
5. Nombre: 3-Oxociclohexanocarbaldehído

1. Cadena principal: 3 carbonos (propano)
2. Grupo funcional: aldehído (dialdehído)
3. Sustituyentes: metilos en 2,2.
4. Nombre: 2,2-Dimetilpropanodial

1. Cadena principal: 4 carbonos (butano)
2. Grupo funcional: aldehído
3. Sustituyentes: formil en 3
4. Nombre: 3-Formilbutanodial

1. Cadena principal: 4 carbonos (butano)
2. Grupo funcional: aldehído
3. Numeración: asignar el menor localizador al aldehído
4. Sustituyentes: hidroxil en 4 y oxo en 3.
5. Nombre: 4-Hidroxil-3-oxobutanal

Nomenclatura de Aldehídos y Cetonas - Problema 9.2

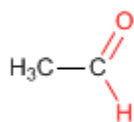
PRINT EMAIL

Dibuja la estructura de los siguientes aldehídos y cetonas:

- | | |
|---|----------------------------------|
| a) Etanal (acetaldehído) | g) 2,5-Dioxooctanodial |
| b) 3-Metilbutanal | h) 1,3-Ciclohexanodiona |
| c) Benzaldehído | i) 3-Metil-3-pental |
| d) 4-Hidroxiciclohexanocarbaldehído | j) 3-Oxobutanal |
| e) 3-Hidroxi-4-metil-5-oxociclohexanocarbaldehído | k) 3-Hidroxiciclopentanona |
| f) 2-Metil-2,5-octanodiona | l) 4-Etoxi-5-fenil-3-oxoheptanal |

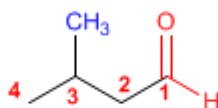
Solución

a)



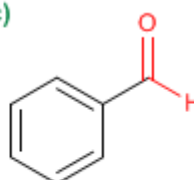
Etanal (acetaldehído)

b)

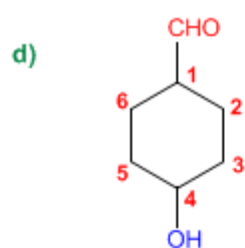


3-Metilbutanal

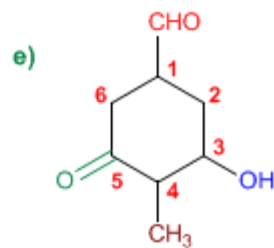
c)



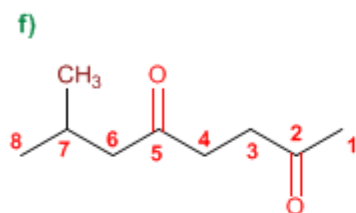
Benzaldehído



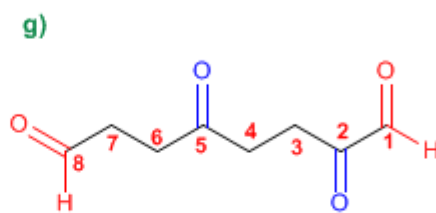
4-Hidroxiciclohexanocarbaldehído



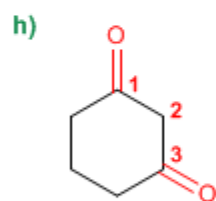
3-Hidroxi-4-metil-5-oxociclohexanocarbaldehído



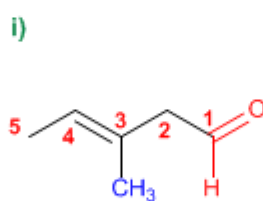
7-Metil-2,5-octanodiona



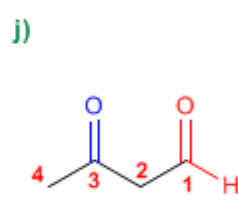
2,5-Dioxooctanal



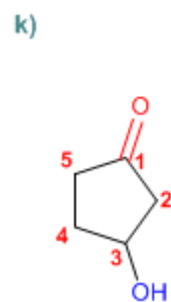
1,3-Ciclohexanodiona



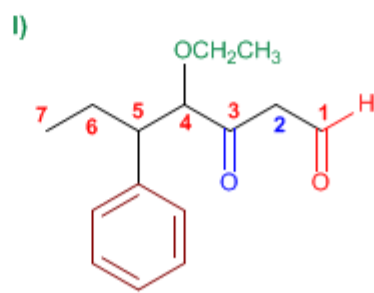
3-Metil-3-pentenal



3-Oxobutanal



3-Hidroxiciclopentanona

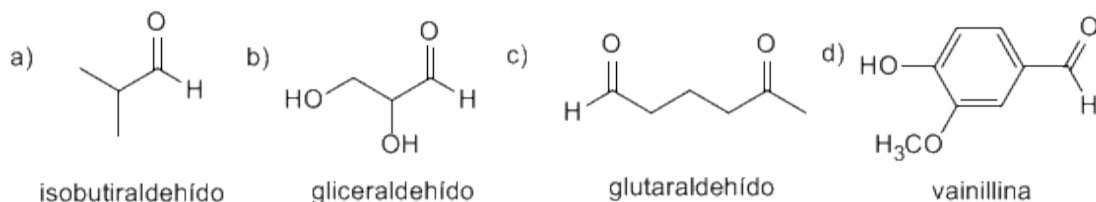


4-Etoxi-5-fenil-3-oxoheptanal

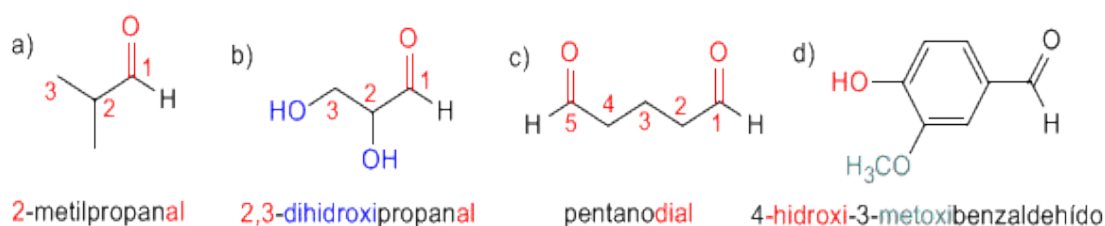
PROBLEMAS RESUELTOS DE ALDEHÍDOS Y CETONAS

Aldehídos y Cetonas: Problema 1

1) A continuación se dan nombres comunes y las fórmulas estructurales de algunos compuestos carbonílicos. Indique el nombre correspondiente según la IUPAC.



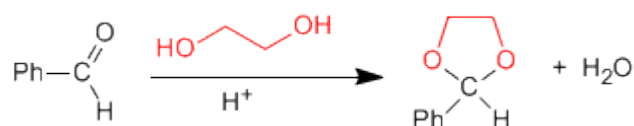
Solución



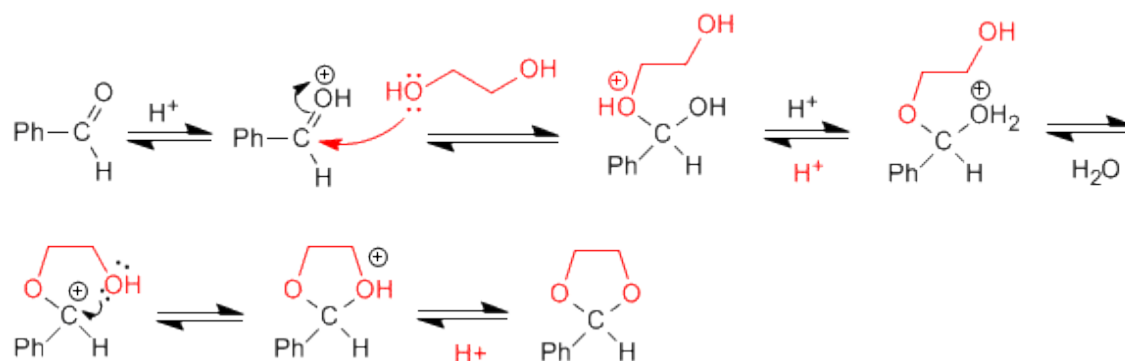
Aldehídos y cetonas: Problema 2

Dibuje la estructura del acetal que se forma cuando el benzaldehído se calienta con 1,2-etanodiol en medio ácido. Escriba un mecanismo detallado que justifique su formación. Describa paso a paso la hidrólisis de este acetal en medio ácido acuoso.

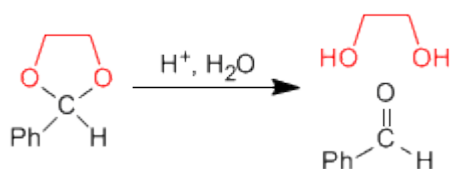
SOLUCIÓN



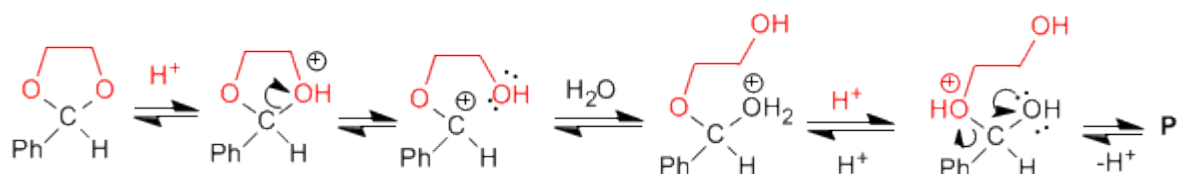
Mecanismo de formación del acetal:



La hidrólisis del acetal en medio ácido acuoso sigue es etapas inversas a la síntesis.



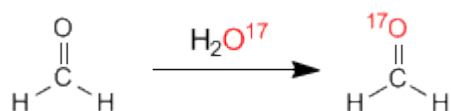
Mecanismo de hidrólisis del acetal cíclico.



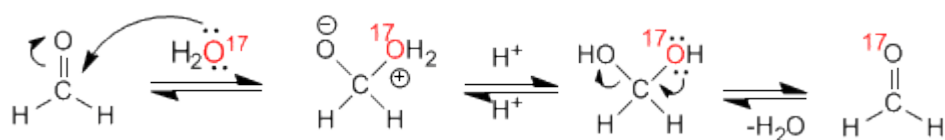
Aldehídos y Cetonas: Problema 3

Cuando se disuelve formaldehído en agua marcada con ^{17}O , se observa que después de unas horas tanto el hidrato del formaldehído como el formaldehído han incorporado el isótopo ^{17}O . Sugiera una explicación razonable de este hecho.

SOLUCION



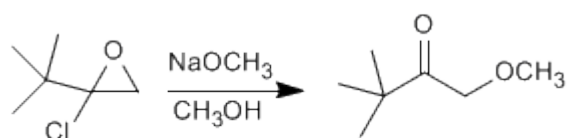
Mecanismo:



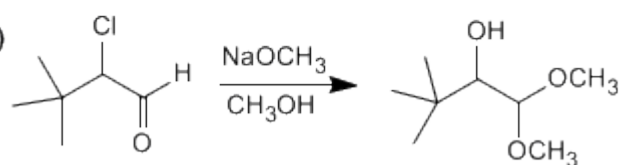
Aldehídos y Cetonas: Problema 4

Sugiera un mecanismo razonable para una de las siguientes reacciones:

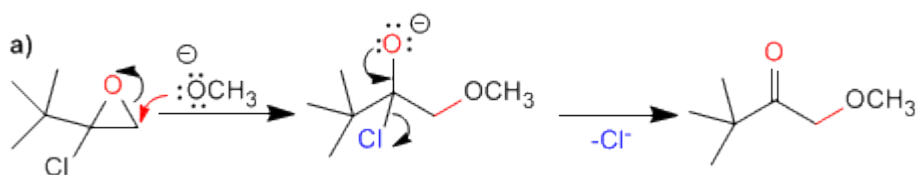
a)



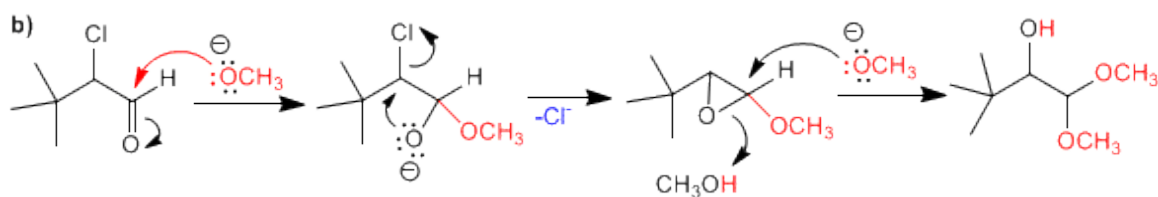
b)



SOLUCION



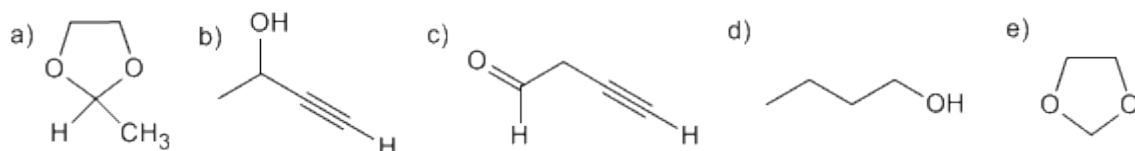
La primera etapa consiste en la apertura del oxaciclopropano sobre el carbono menos sustituido. En la segunda etapa, la cesión del par del oxígeno elimina el cloro, formándose un carbonilo.



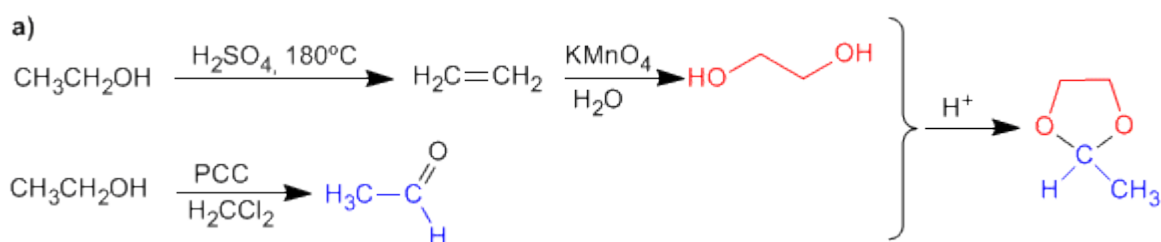
En el primer paso hay dos posibles posiciones de ataque; el carbono carbonilo y el carbono del cloro. Como el producto final no tiene metóxido en el carbono del cloro, atacamos al carbonilo. En la segunda etapa se produce una sustitución nucleófila intramolecular. Para terminar el metóxido abre el epóxido.

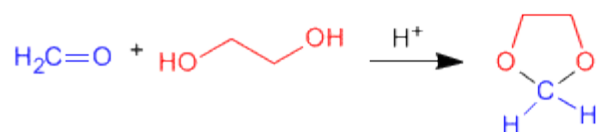
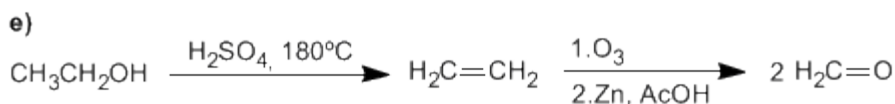
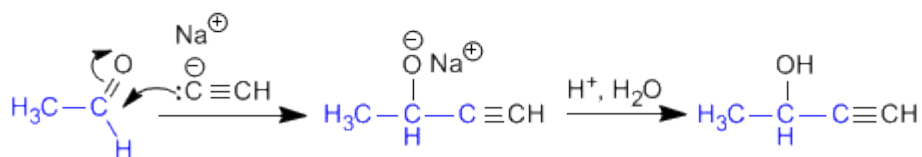
Aldehídos y Cetonas: Problema 5

Usando etanol como fuente de todos los átomos de carbono y los reactivos que necesite, describa una síntesis eficiente de cada una de las sustancias siguientes:

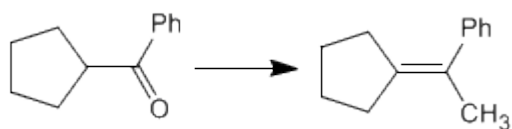


SOLUCIÓN

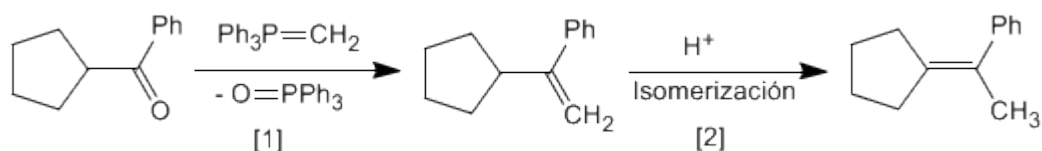




Utilizando los reactivos necesarios, indicar las etapas que permiten realizar la siguiente transformación:



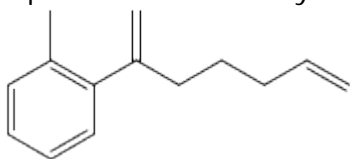
SOLUCIÓN



[2] Isomerización en medio ácido, impulsada por la mayor estabilidad del alqueno interno.

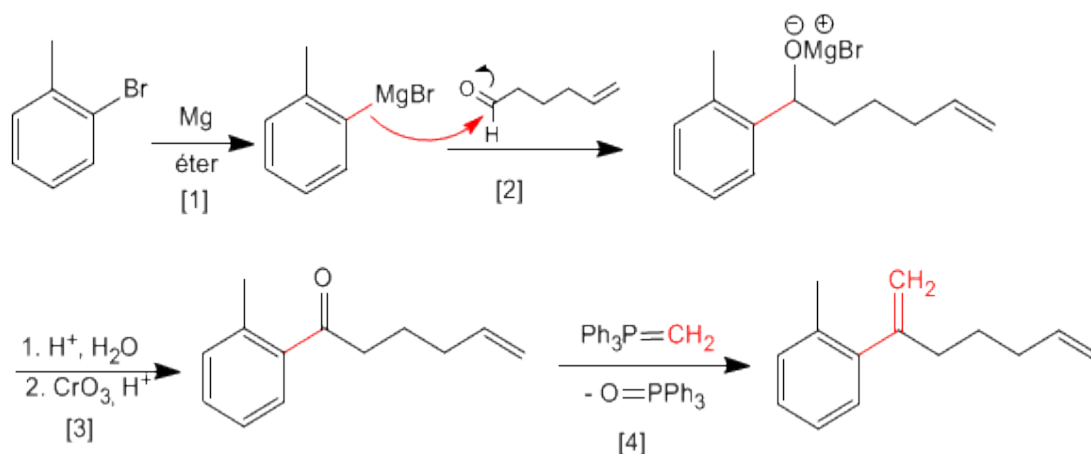
Aldehídos y Cetonas: Problema 7

A partir de 5-hexenal y o-bromotolueno obtener el siguiente producto.



Pueden ser necesarios reactivos orgánicos e inorgánicos adicionales.

SOLUCIÓN



[1] Formación del magnesiano

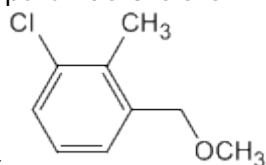
[2] Ataque nucleófilo del magnesiano al carbonilo.

[3] Hidrólisis y posterior oxidación del alcohol secundario.

[4] Reacción de Wittig entre la cetona y el trifenilmetilenfosforano.

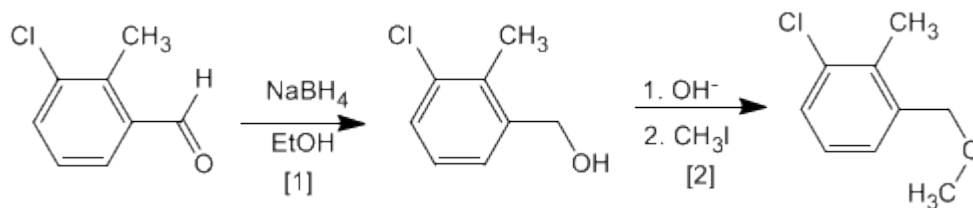
Aldehídos y Cetonas: Problema 8

Obtener a partir de 3-cloro-2-metilbenzaldehído y de los reactivos



necesarios
el compuesto siguiente:

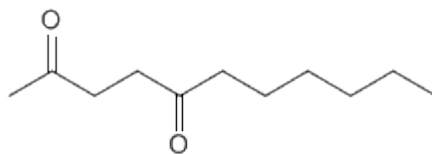
SOLUCIÓN



[1] Reducción del aldehído a alcohol

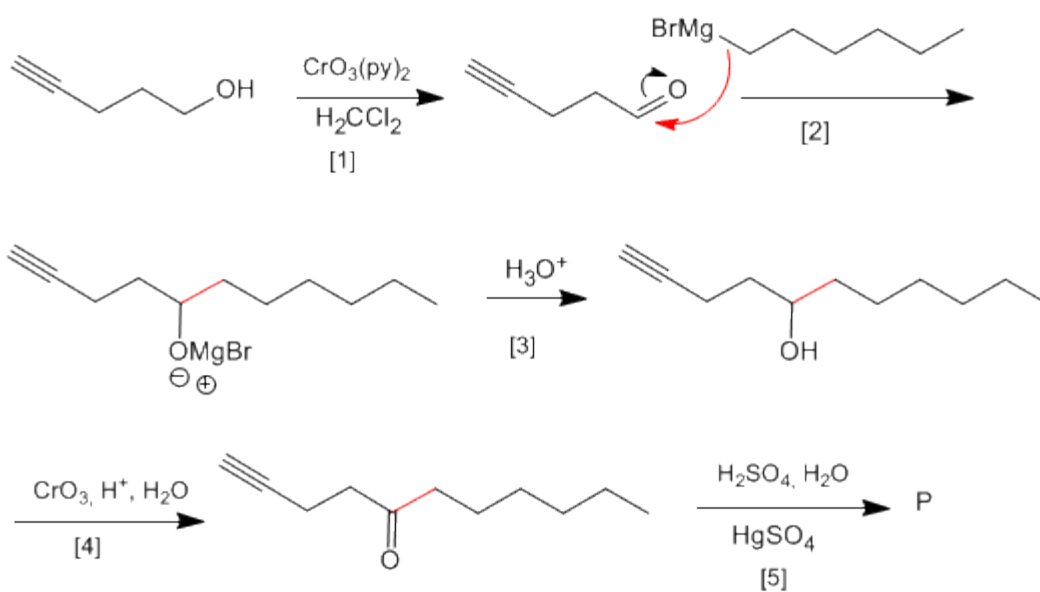
[2] Síntesis de Williamson de éteres.

Aldehídos y Cetonas: Problema 9



A partir de 4-pentin-1-ol obtener:

SOLUCIÓN

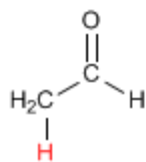


- [1] Oxidación del alcohol a aldehído
- [2] Formación del enlace carbono-carbono mediante organometálicos de magnesio
- [3] Protonación del alcohol
- [4] Oxidación del alcohol con Jones (Puedes utilizar también $\text{CrO}_3(\text{py})_2$)
- [5] Hidratación Markovnikov del alquino, para formar cetonas

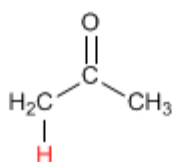
TEORÍA DE ENOLES Y ENOLATOS

Formación de Enolatos

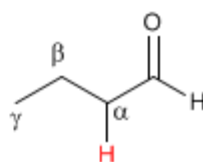
Los aldehídos y cetonas presentan hidrógenos ácidos en la posición vecina al grupo carbonilo, conocida como posición alfa. Estos hidrógenos presentan un pKa comprendido entre 18 y 21.



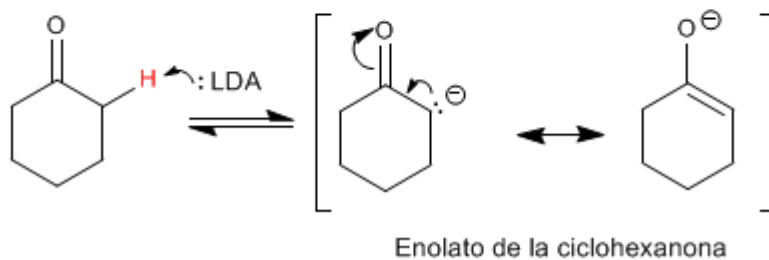
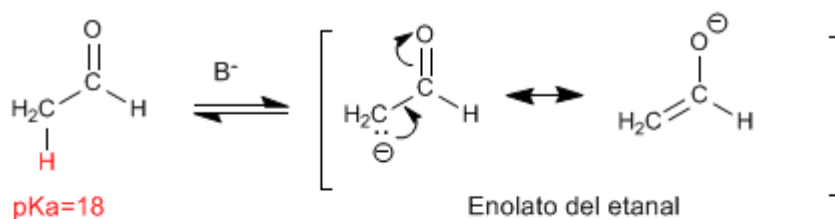
pKa=18



pKa=20-21



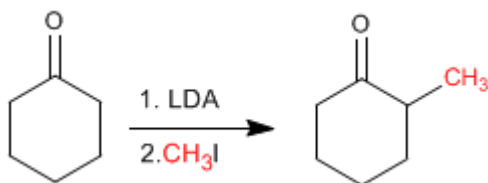
La acidez de los hidrógenos α es debida a la estabilización de la base conjugada (enolato) por resonancia.



Alquilación de Enolatos

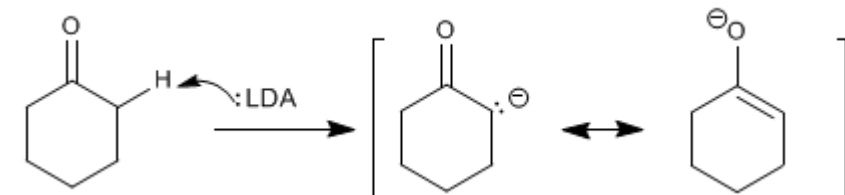
Los enolatos actúan como nucleófilos a través del carbono atacando a un gran número de electrófilos (haloalcanos, epóxidos, carbonilos, ésteres.....). En este punto nos fijaremos en la reacción entre enolatos y haloalcanos, que permite añadir cadenas carbonadas a la posición α de la cadena.

La Ciclohexanona se convierte en 2-Metilciclohexanona por tratamiento con LDA seguido de yoduro de metilo.

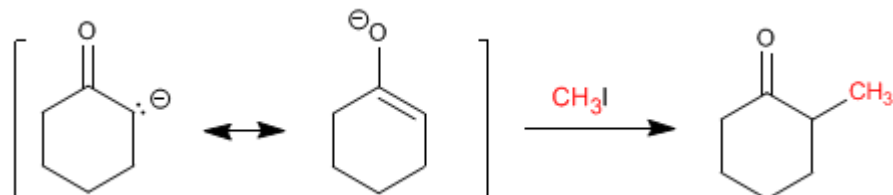


Etapas del mecanismo por el que se alquila la ciclohexanona:

Etapas del mecanismo

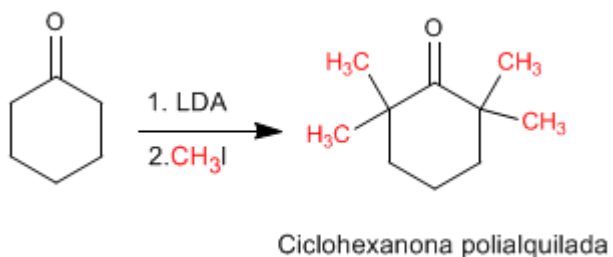


Etapas del mecanismo



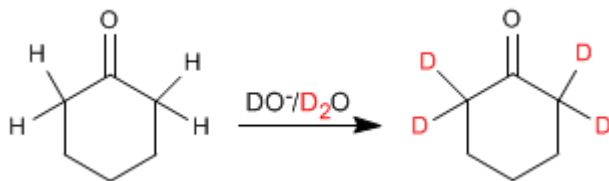
Las reacciones de alquilación tienen dos importantes problemas.

1. Competencia con la condensación aldólica. Los carbonilos en medio básico tienden a condensar para formar aldoles.
2. La reacción es difícil de controlar y tiende a polialquilar el carbonilo.



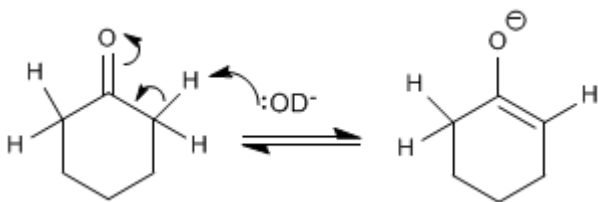
Intercambio hidrógeno - Deuterio

Los aldehídos y cetonas intercambian sus hidrógenos a por deuterios cuando se tratan con $\text{DO}^-/\text{D}_2\text{O}$ o con $\text{D}^+/\text{D}_2\text{O}$. En medios básicos la reacción transcurre a través de enolatos y en medios ácidos los intermediarios formados son enoles.

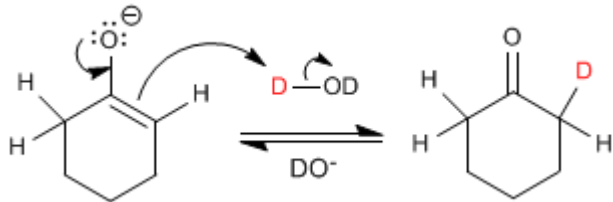


El mecanismo del intercambio hidrógeno-deuterio transcurre en los siguientes pasos:

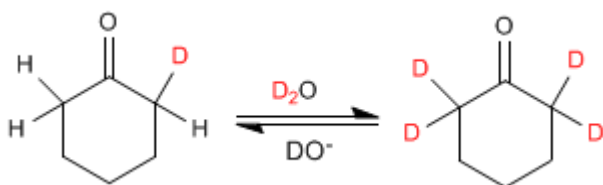
Etapas 1. Formación del enolato



Etapas 2. Transferencia del deuterio al enolato



Etapas 3. Sustitución del resto de hidrógenos



Halogenación de aldehídos y cetonas

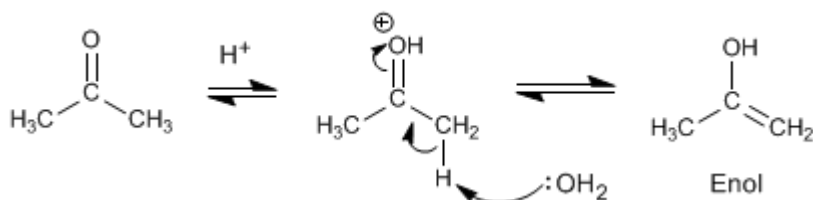
Los aldehídos y cetonas reaccionan con halógenos en medios ácidos o básicos produciéndose la sustitución de hidrógenos a por halógenos.

Halogenación de la propanona en medio ácido:

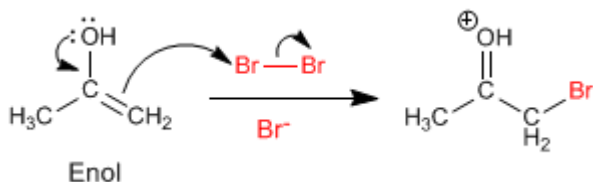


El mecanismo de halogenación en **medio ácido** tiene las siguientes etapas:

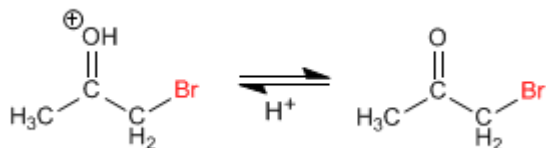
Etapas 1. Formación del enol



Etapas 2. Ataque nucleófilo del enol sobre el halógeno ayudado por la cesión del par del oxígeno.

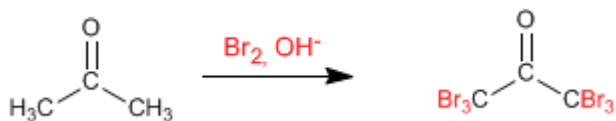


Etapas 3. Desprotonación



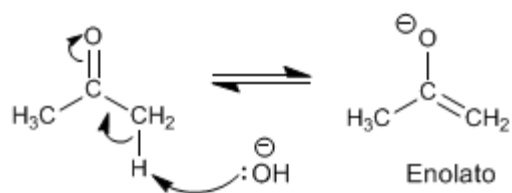
Trabajando con un equivalente de reactivo la halogenación para en una primera adición y no ocurren polihalogenaciones. El paso clave del mecanismo es la formación del enol y esta etapa requiere protonar el oxígeno del carbonilo. Una vez halogenada la posición α el oxígeno se vuelve menos básico, debido al efecto electronegativo del bromo, protonándose peor.

Halogenación de la propanona en **medio básico**:

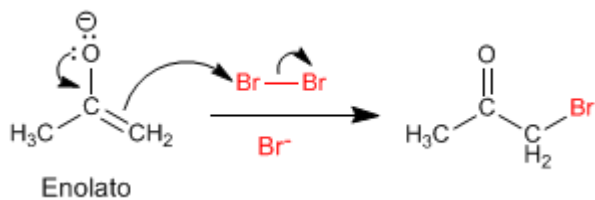


La halogenación en medio básico tiene el siguiente mecanismo:

Etapla 1. Formación del enolato



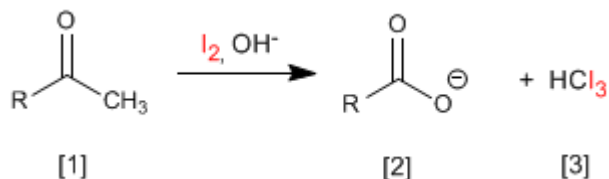
Etapla 2. Ataque nucleófilo del enolato sobre el halógeno ayudado por la cesión del para del oxígeno.



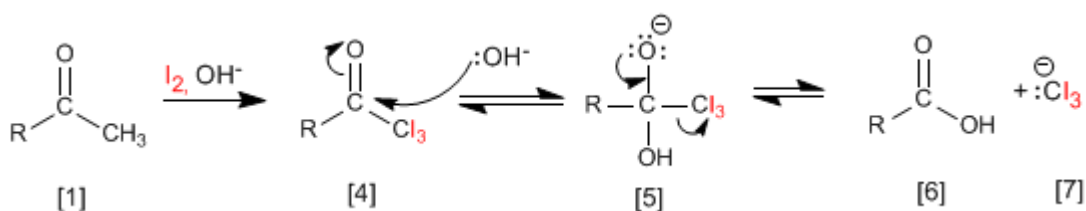
Este mecanismo se repite otras 5 veces sustituyendo todos los hidrógenos a por halógenos. En este caso la reacción no para puesto que el producto halogenado es más reactivo que la propanona de partida. La base arranca mejor los hidrógenos en el producto halogenado (son más ácidos), haciendo imposible parar la reacción.

Reacción del Haloformo (Yodoformo)

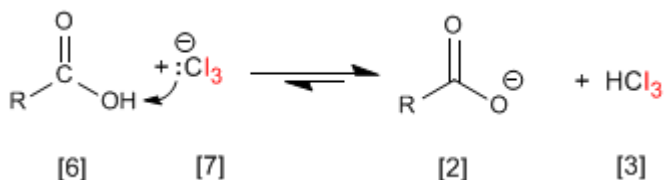
Las cetonas metílicas **[1]** reaccionan con halógenos en medios básicos generando carboxilatos **[2]** y haloformo **[3]**.



El mecanismo consiste en halogenar completamente el metilo, sustituyendo en una etapa posterior el grupo $-\text{CX}_3$ formado por $-\text{OH}$.



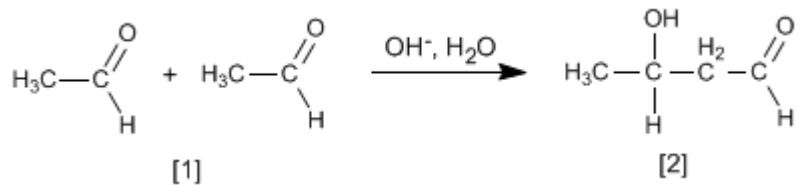
El grupo Cl_3^\ominus es muy básico y desprotona el ácido carboxílico formándose yodoformo y el carboxilato.



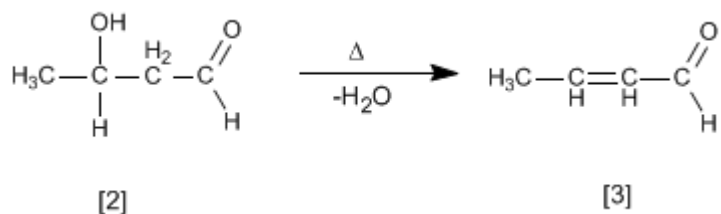
Esta reacción (con yodo) puede emplearse como ensayo analítico para identificar cetonas metílicas aprovechando que el yodoformo precipita de color amarillo.

Condensación Aldólica

Aldehídos y cetonas [1] condensan en medios básicos formando aldoles [2]. Esta reacción se denomina condensación aldólica.

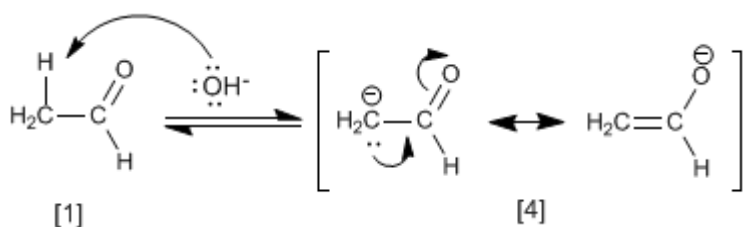


El aldol [2] formado deshidrata en el medio básico por calentamiento para formar un α,β -insaturado [3].



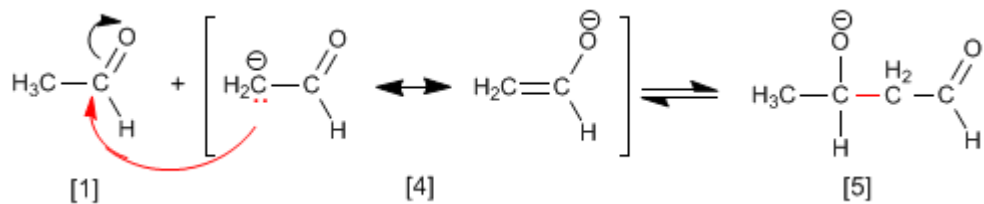
El mecanismo de la condensación aldólica transcurre con formación de un enolato, que ataca al carbonilo de otra molécula. En esta condensación se forma un enlace carbono-carbono entre el carbonilo de una molécula y el carbono α de la otra.

Etapa 1. Formación del enolato

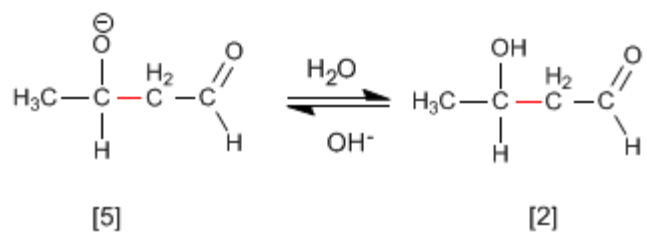


La base desprotona el carbono alfa del etanal [1] generando el enolato [4] estabilizado por resonancia.

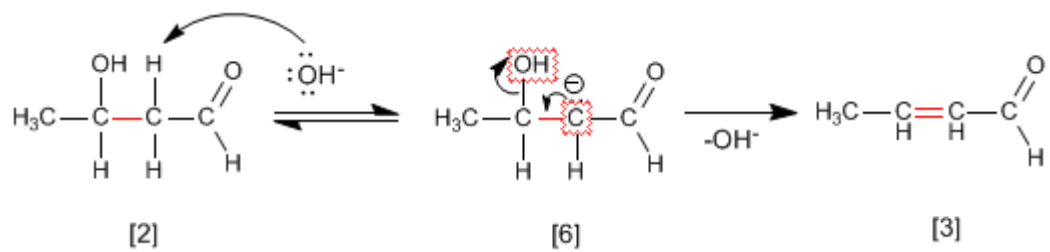
Etapa 2. Ataque nucleófilo del enolato sobre el carbonilo



Etapas 3. Protonación

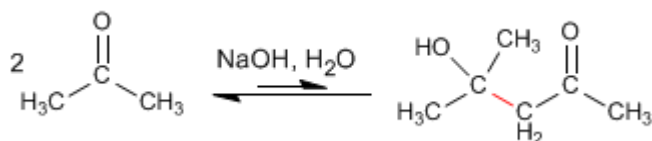


Etapas 4. Deshidratación del aldol

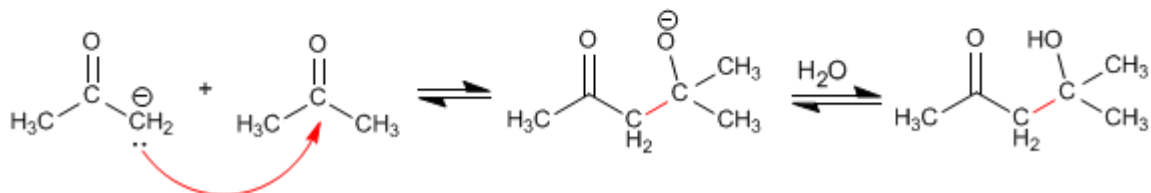
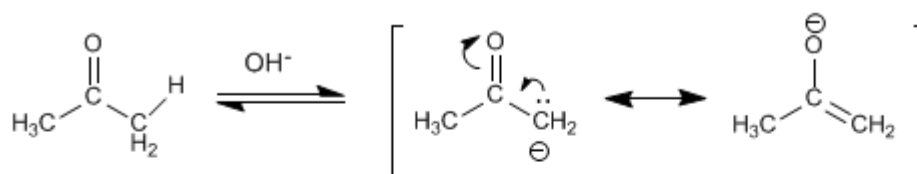


Condensación aldólica con cetonas

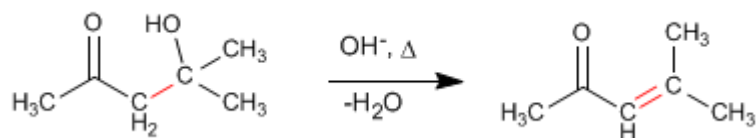
Las cetonas son menos reactivas que los aldehídos y dan un rendimiento muy bajo en la condensación aldólica. Así, dos moléculas de propanona condensan para formar el aldol correspondiente con un rendimiento del 2%. Se pueden conseguir porcentajes elevados del producto separándolo del medio de reacción según se va formando, o bien, calentando para deshidratarlo. De ambas formas los equilibrios de la aldólica se desplazan hacia el producto final.



Mecanismo de la reacción:



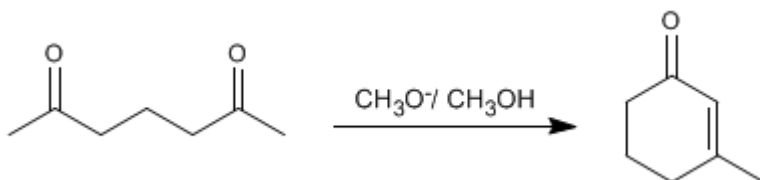
La deshidratación final permite el desplazamiento de los equilibrios. También se puede realizar una extracción del aldol del medio de reacción para favorecer la reacción.



Condensación aldólica intramolecular

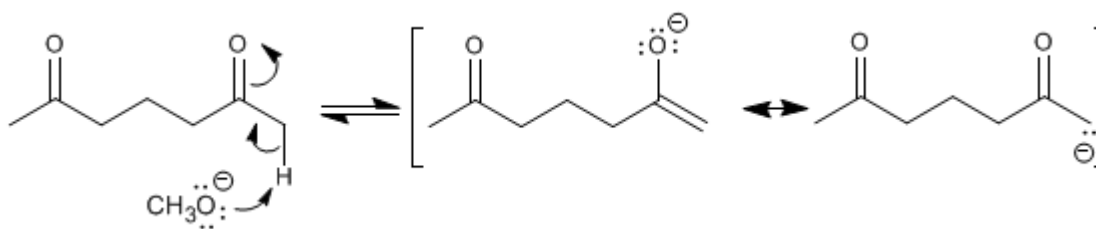
Los compuestos dicarbonílicos condensan mediante la aldólica intramolecular en medios básicos. En esta reacción se obtienen ciclos de cinco o seis miembros.

Así, la 2,6-heptanodiona condensa con metóxido en metanol para formar el 3-metilciclohex-2-enona.

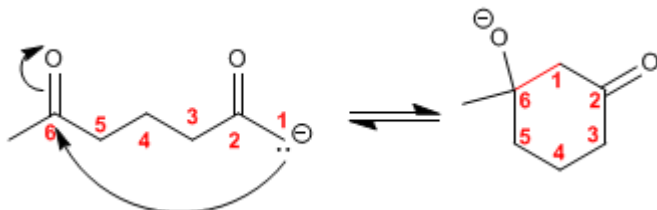


El mecanismo de la reacción transcurre a través de las siguientes etapas:

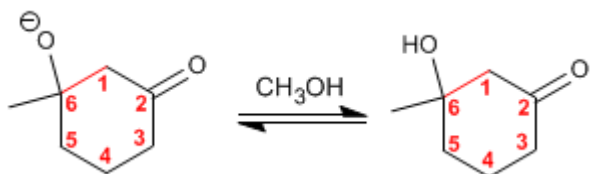
Etapas 1. Formación del enolato.



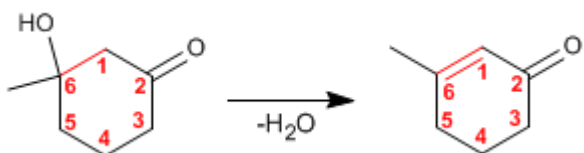
Etapas 2. Adición nucleófila intramolecular



Etapas 3. Protonación de la base del aldol



Etapas 4. Deshidratación del aldol

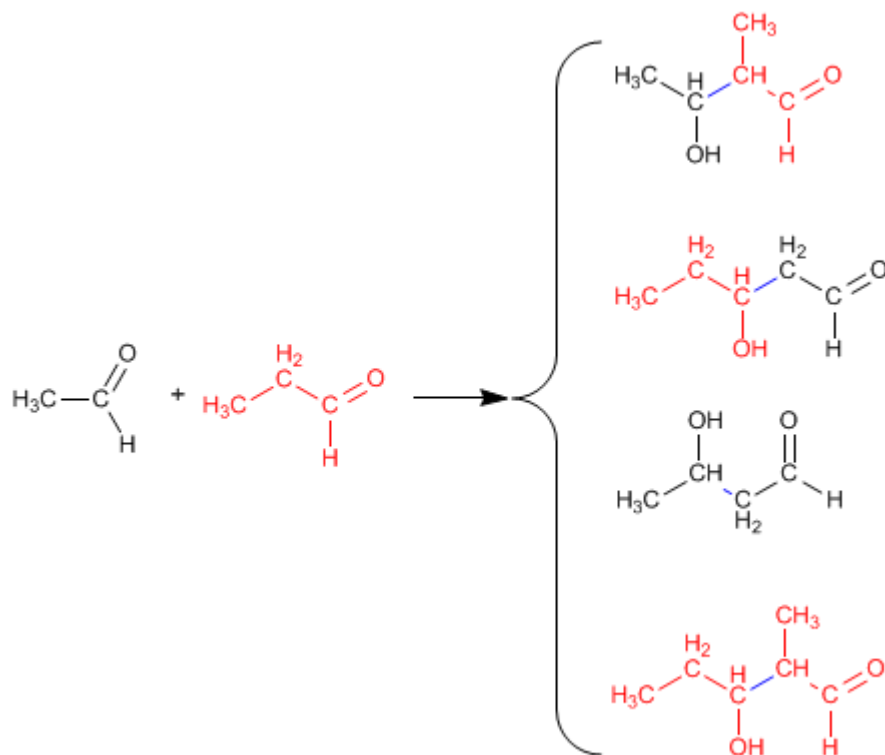


Condensación aldólica cruzada o mixta

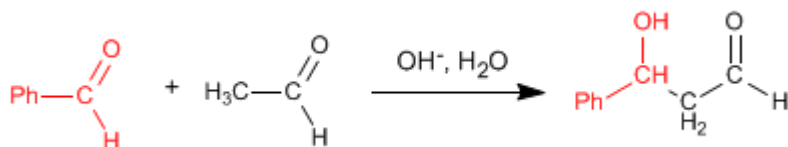
La reacción entre dos carbonilos diferentes se llama aldólica cruzada o mixta. Esta reacción sólo tiene utilidad sintética en dos casos:

1. Sólo uno de los carbonilos puede formar enolatos.
2. Uno de los carbonilos es mucho más reactivo que el otro.

En el resto de situaciones la aldólica mixta genera mezclas de cuatro productos. Veamos como ejemplo la condensación del etanal y propanal.

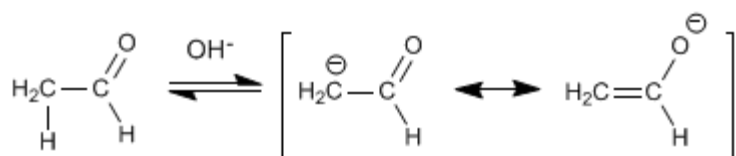


La condensación aldólica mixta del etanal con el benzaldehído genera un producto, cuando se trabaja en exceso de benzaldehído, debido a que el benzaldehído carece de hidrógenos en el carbono alfa y no puede formar enolatos.



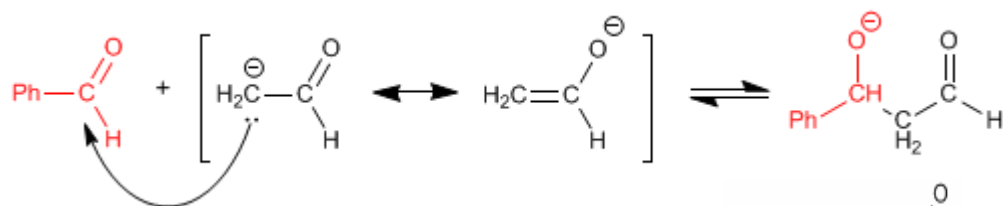
El mecanismo de esta reacción tiene lugar en las siguientes etapas:

Etapla 1. Enolización del etanal

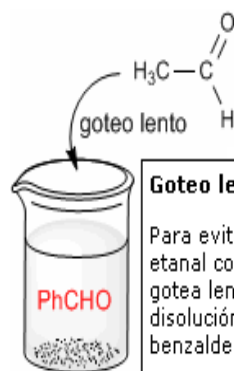
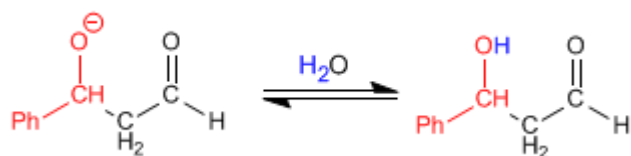


La formación de enolatos sólo puede tener lugar con el etanal, puesto que el benzaldehído carece de hidrógenos ácidos en el carbono alfa.

Etapla 2. Ataque nucleófilo del enolato al benzaldehído.



En esta etapa puede ocurrir el ataque del enolato de etanal sobre si mismo. Para evitarlo debe trabajarse en exceso de benzaldehído. Un procedimiento experimental muy usado para evitar la condensación del etanal consigo mismo es gotear lentamente el etanal sobre una disolución básica de benzaldehído

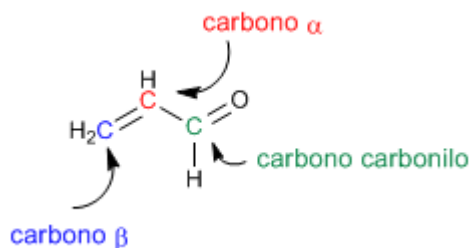


Goteo lento

Para evitar la condensación del etanal consigo mismo, se gotea lentamente sobre una disolución básica de benzaldehído.

Síntesis de carbonilos alfa,beta-insaturados

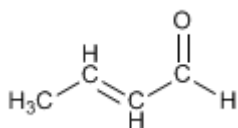
Los carbonilos α,β -insaturados son compuestos orgánicos que tienen un doble enlace entre las posiciones α,β de un aldehído o cetona.



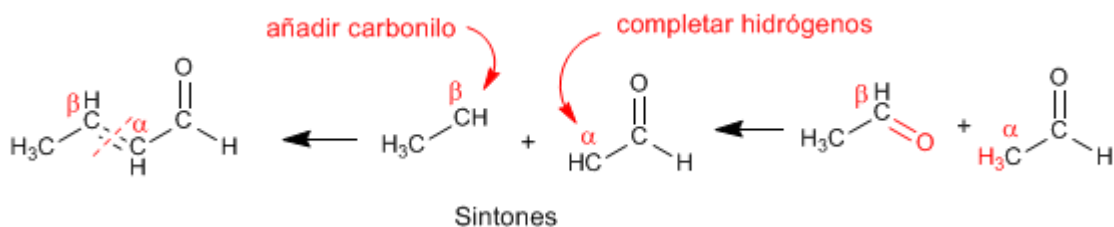
El propenal o acroleína es un carbonilo α,β -insaturado. Sus dos dobles enlaces conjugados le confieren una reactividad especial.

Existen 4 métodos importantes para la preparación de α,β -insaturados: condensación aldólica, halogenación del carbono α seguida de eliminación, oxidación de alcoholes alílicos y Wittig.

Método 1. Preparar mediante la condensación aldólica el siguiente compuesto.

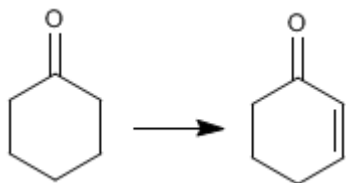


Empleamos la retrosíntesis para preparar el compuesto. Al ser de la familia de los α,β -insaturados se puede obtener mediante la condensación aldólica.

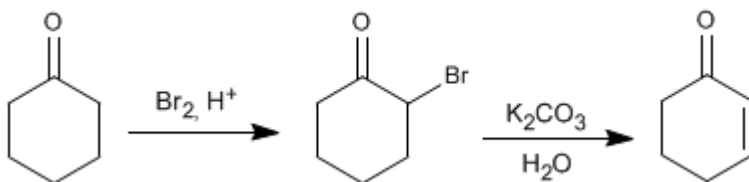


Para obtener los reactivos que forman el α,β -insaturado se rompe por el doble enlace, obteniéndose los sintones (equivalentes sintéticos). Los reactivos se obtienen añadiendo al carbono β un carbonilo y completando los hidrógenos que faltan en el carbono α .

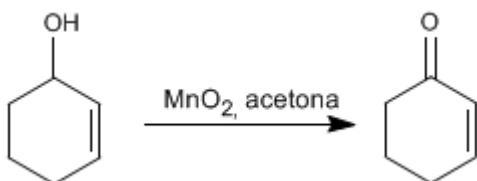
Ejemplo 2. Indicar como se puede realizar la siguiente transformación.



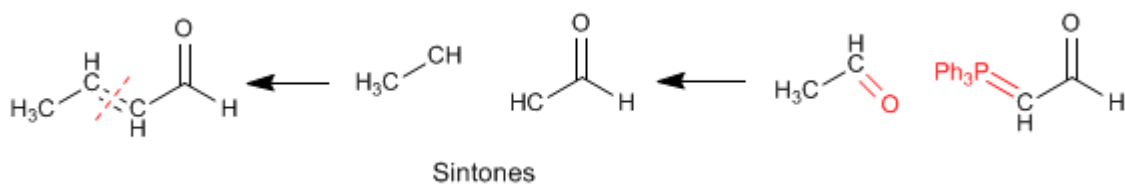
En una primera etapa se halogena la posición α del carbonilo. En la segunda etapa se realiza una eliminación que nos deja el producto final.



Método 3. La oxidación de alcoholes alílicos con dióxido de manganeso en acetona produce α,β -insaturados



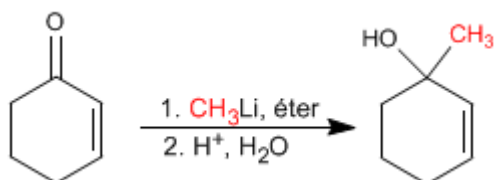
Método 4. Reacción de Wittig



Reactividad de carbonilos alfa,beta-insaturados

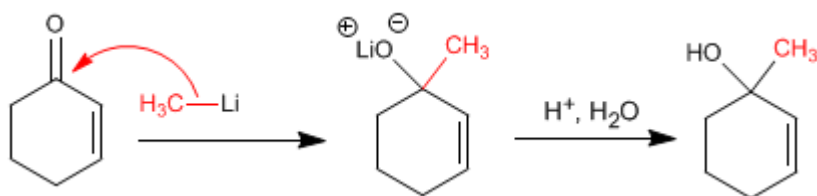
Los α,β -insaturados son compuestos que poseen dos posiciones electrófilas: el carbono carbonilo y el carbono β .

Adiciones 1,2. Los organometálicos de litio atacan al carbono carbonilo dando lugar a adiciones 1,2.



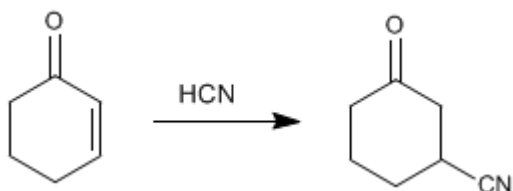
Los organometálicos de litio y magnesio atacan al carbono carbonilo de los α,β -insaturados

Mecanismo de la adición 1,2

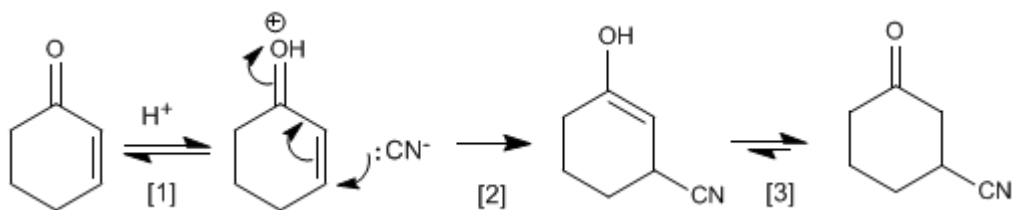


Adiciones 1,4. Los cupratos, cianuro y otros nucleófilos atacan al carbono β de los α,β -insaturados, dando adiciones 1,4.

El ácido cianhídrico da adiciones 1,4 con los α,β -insaturados. El ciano se une al carbono β .

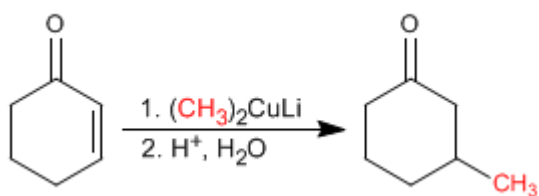


Mecanismo de adición del ácido cianhídrico a la Ciclohex-2-enona

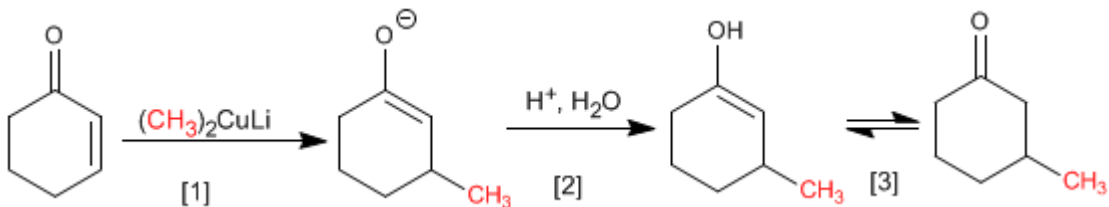


- [1] Protonación del carbonilo
- [2] Ataque nucleófilo del cianuro al carbono β .
- [3] Tautomería ceto-enol.

Los cupratos son organometálicos de cobre que se adicionan al carbono β de los α,β -insaturados.



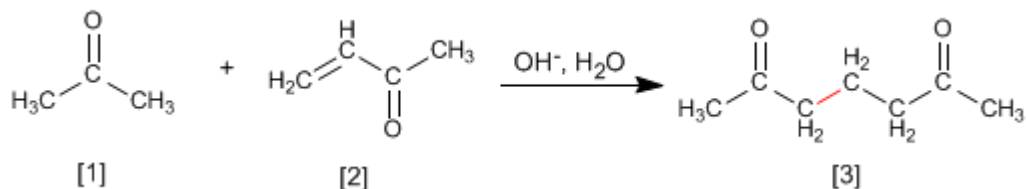
El mecanismo de la reacción comienza con el ataque nucleófilo del cuprato sobre el carbono β , formando un enolato, que se protona en la segunda etapa para dar un enol. El enol tautomeriza a cetona generando el producto final.



- [1] Adición nucleófila del cuprato.
- [2] Protonación del enolato
- [3] Tautomería ceto-enol

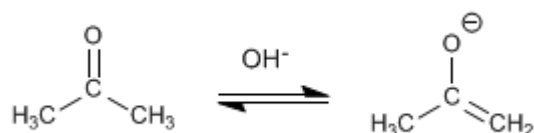
Adición de Michael y anelación de Robinson

Los enolatos de aldehídos o cetonas se adicionan a los α,β -insaturados para formar 1,5-dicarbonilos. Esta reacción se denomina adición de Michael.

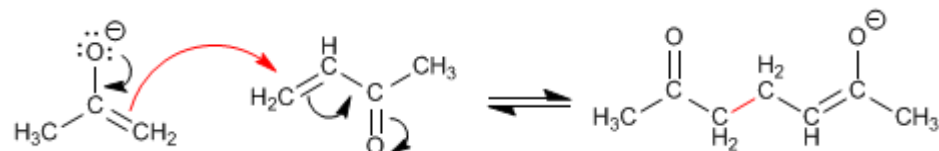


La propanona [1] reacciona con el α,β -insaturado [2] para formar el 1,5-dicarbonilo [3]
Mecanismo de la Adición de Michael:

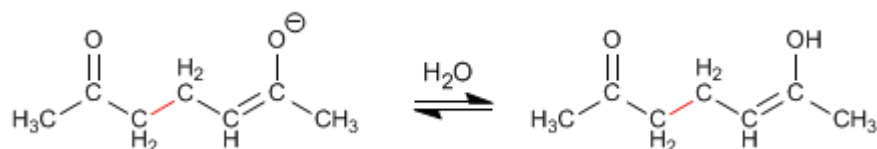
Etapla 1. Formación del enolato.



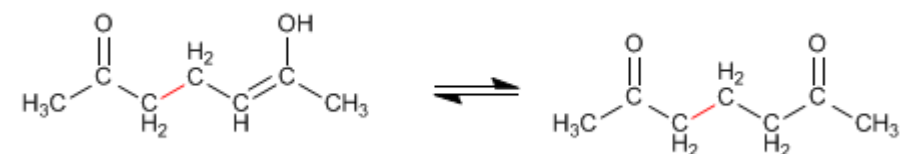
Etapla 2. Ataque nucleófilo del enolato al carbono β del α,β -insaturado.



Etapla 3. Equilibrio ácido-base



Etapla 4. Tautomería ceto-enol

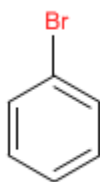


El producto de Michael puede condensar mediante una aldólica intramolecular, formando un α,β -insaturado. El conjunto de la adición de Michael y la aldólica final se conoce como reacción de Robinson

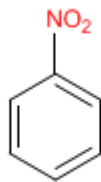
TEORÍA DEL BENCENO

Nomenclatura del Benceno

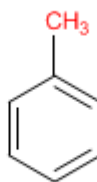
Los bencenos monosustituídos se nombran terminando el nombre del sustituyente en benceno.



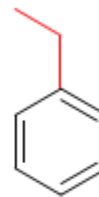
Bromobenceno



Nitrobenceno

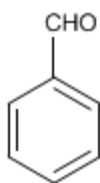


Metilbenceno

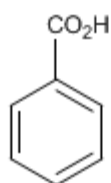


Etilbenceno

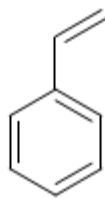
Algunos derivados monosustituídos del benceno tienen nombres comunes ampliamente aceptados.



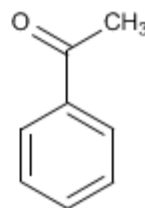
Benzaldehído



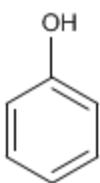
Ácido benzoico



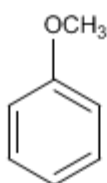
Estireno



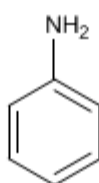
Acetofenona



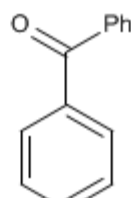
Fenol



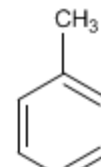
Anisol



Anilina

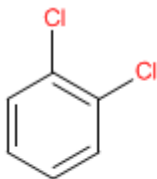


Benzofenona

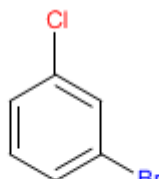


Tolueno

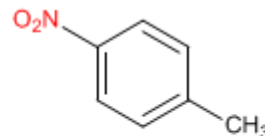
En bencenos disustituídos se emplean los prefijos *orto* (benceno 1,2-disustituído), *meta* (benceno 1,3-disustituído) y *para* (benceno 1,4-disustituído) para indicar la posición de los sustituyentes en el anillo.



o-Diclorobenceno
(1,2-Diclorobenceno)



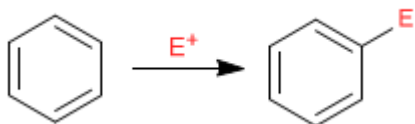
m-Bromoclorobenceno
(1-Bromo-3-clorobenceno)



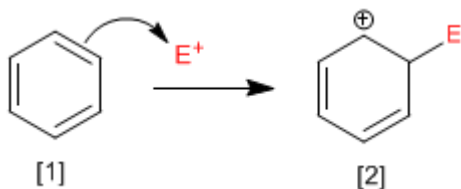
p-Nitrotolueno
(4-Nitrotolueno)

Sustitución Electrónica Aromática

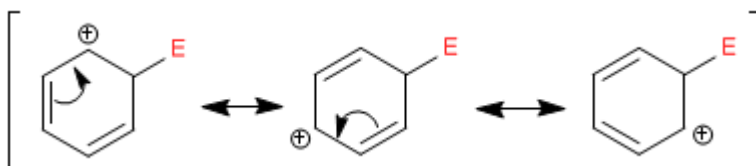
El benceno actúa como nucleófilo, atacando a un número importante y variado de electrófilos.



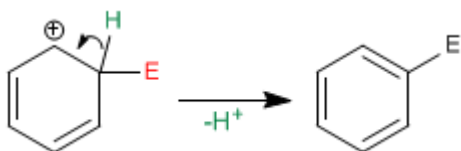
Etapas 1. En la primera etapa de la reacción el electrófilo acepta un par de electrones procedentes de la nube π del benceno, formándose un carbocatión estabilizado por resonancia.



El catión ciclohexadienilo [2] deslocaliza la carga positiva según las siguientes estructuras:

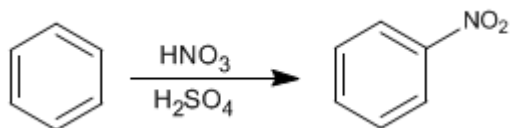


Etapas 2. En la segunda etapa el benceno recupera su aromaticidad por pérdida de un protón. Es una etapa rápida conocida como rearomatización del anillo.

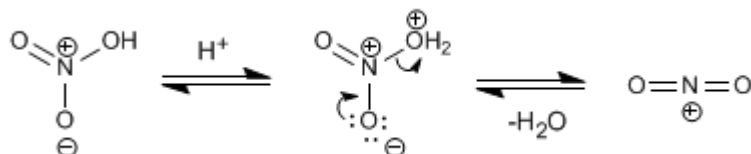


Nitración del Benceno

El benceno reacciona con la mezcla nítrico-sulfúrica adicionando grupos nitro.

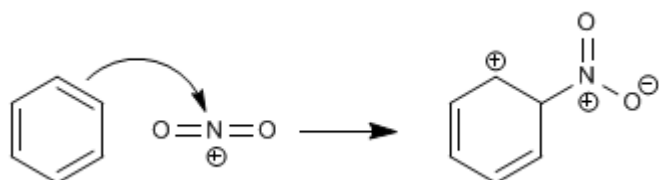


El electrófilo de esta reacción es el catión nitronio, NO_2^+ . Las concentraciones de este catión en el ácido nítrico son muy bajas para nitrar el benceno, por ello es necesario añadir ácido sulfúrico.

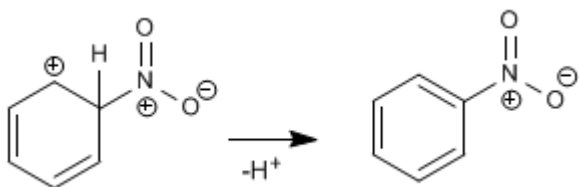


Mecanismo para la nitración del benceno:

Etapla 1. Ataque del benceno al catión nitronio

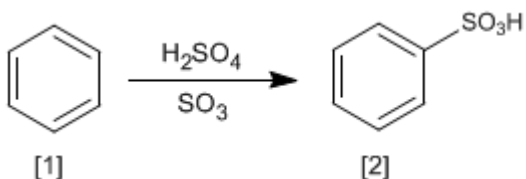


Etapla 2. Recuperación de la aromaticidad por pérdida de un protón



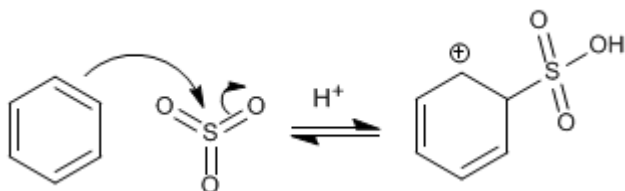
Sulfonación del Benceno

La reacción del benceno [1] con una disolución de trióxido de azufre en ácido sulfúrico produce ácidos bencenosulfónicos [2].

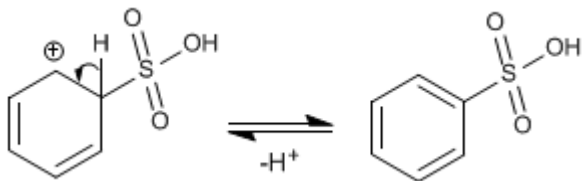


El mecanismo de la sulfonación tiene lugar con las siguientes etapas:

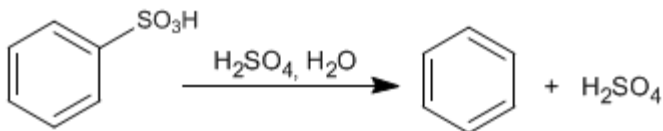
Etapas 1. Ataque del benceno al trióxido de azufre



Etapas 2. Recuperación de la aromaticidad por pérdida de un protón.

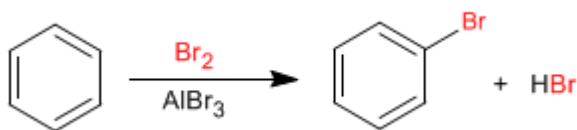


El mecanismo de la sulfonación es reversible, lo cual permite eliminar el grupo $-\text{SO}_3\text{H}$ por tratamiento con sulfúrico acuoso. Esta propiedad es utilizada para proteger posiciones del benceno, ocupándolas con el grupo $-\text{SO}_3\text{H}$.



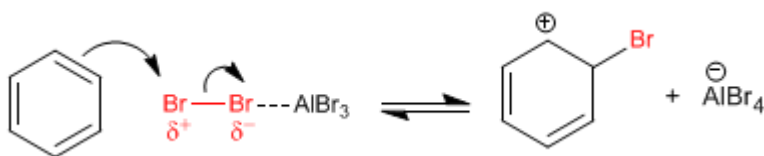
Halogenación del Benceno

El benceno reacciona con halógenos en presencia de ácidos de Lewis para formar derivados halogenados.

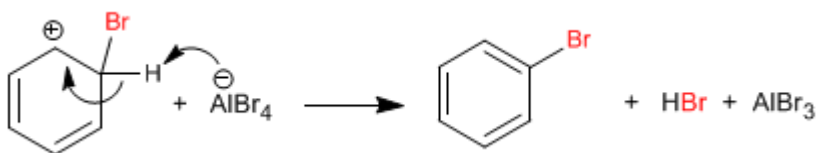


El mecanismo de la halogenación tiene lugar con las siguientes etapas:

Etapas 1. La molécula de bromo se polariza al interactuar con el ácido de Lewis. El benceno ataca al bromo polarizado positivamente para formar el catión ciclohexadienilo.



Etapas 2. Recuperación de la aromaticidad por pérdida de un protón.

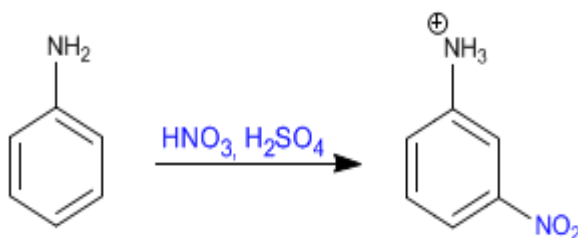


La cloración se puede llevar a cabo de forma similar a la bromación. La reacción con flúor y yodo se realiza muy poco frecuentemente. En el caso del flúor la reacción es difícil de controlar por su elevada reactividad. Por el contrario, el yodo reacciona lentamente y tiene un equilibrio desfavorable.

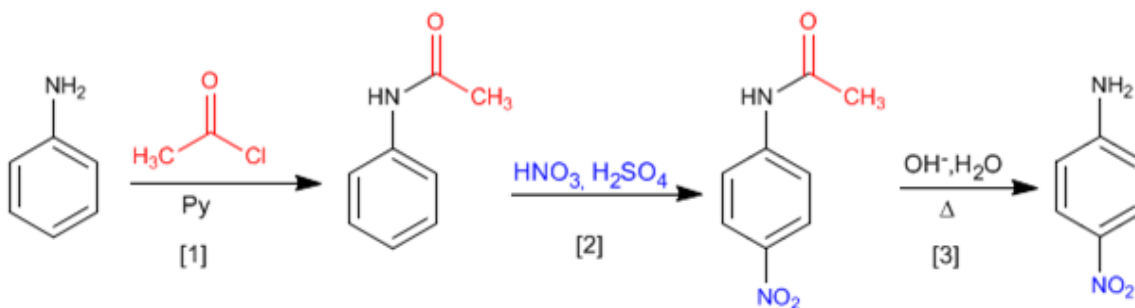
Benceno - Protección y desprotección del grupo amino

El grupo amino es un activante fuerte, que orienta a orto/para. Sin embargo, en medios ácidos se protona transformándose en un desactivante fuerte (sal de amonio) que orienta a posición meta. Se puede evitar la protonación del amino protegiéndolo con cloruro de etanoilo en piridina.

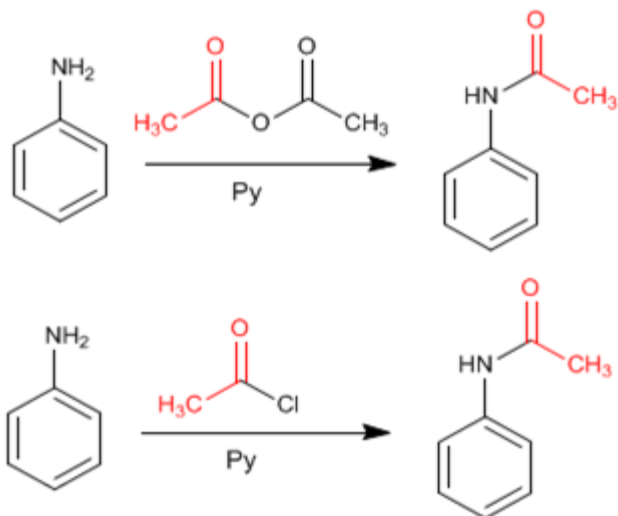
Nitración de la anilina sin protección del amino



Nitración de la anilina con protección del grupo amino, empleando cloruro de etanoilo

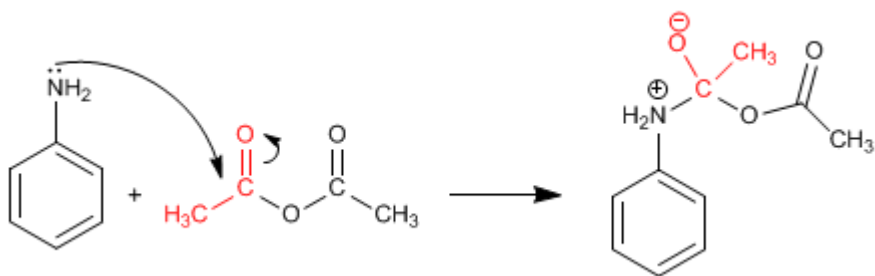


La protección del amino puede realizarse con anhídrido etanoico en piridina, o con cloruro de etanoilo en piridina

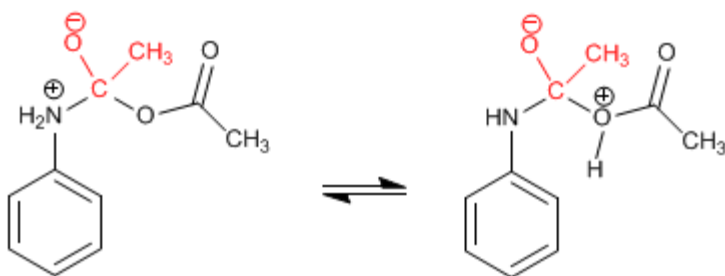


El producto final es una amida, mucho menos básica que la amina de partida y con menos tendencia a protonarse. El mecanismo de la reacción es el siguiente:

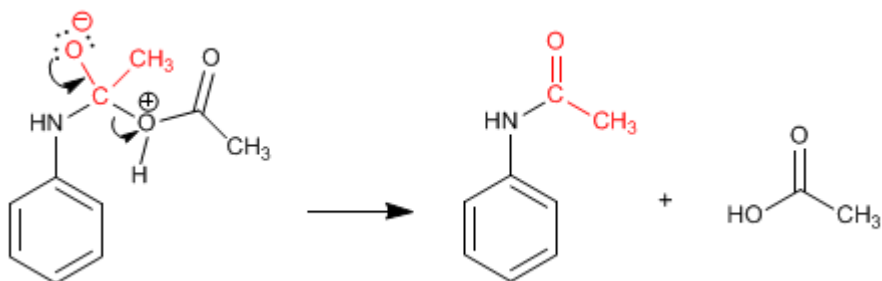
Etapla 1. Adición



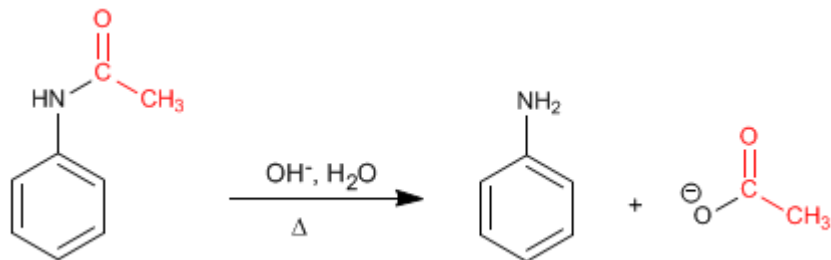
Etapla 2. Equilibrio ácido-base



Etapla 3. Eliminación

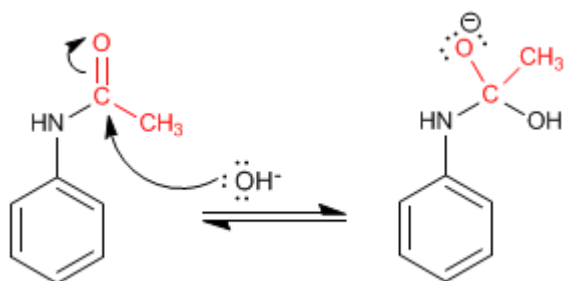


La amida formada se desprotege por hidrólisis ácida o básica, dejando libre la anilina.

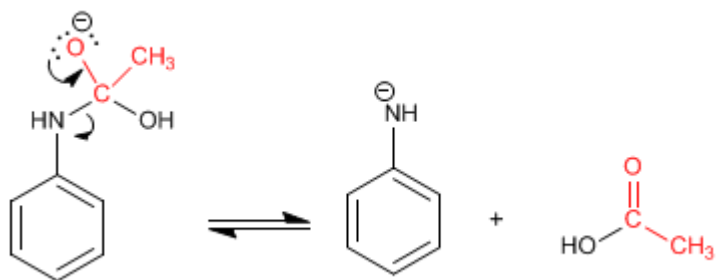


Mecanismo de desprotección en medio básico.

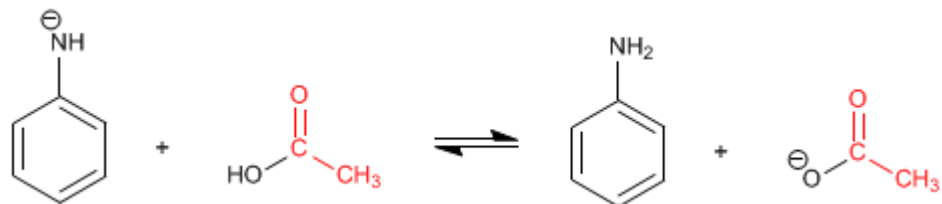
Etapla 1. Adición del grupo hidroxilo a la amida



Etapla 2. Eliminación

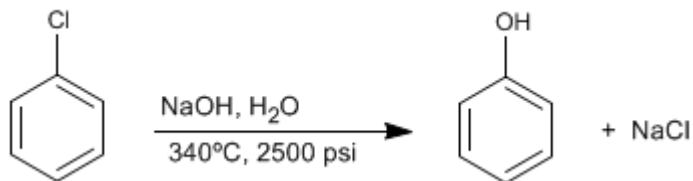


Etapla 3. Equilibrio ácido-base



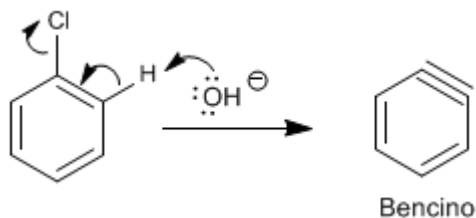
Sustitución nucleófila aromática: Bencino

Los bencenos halogenados reaccionan con sosa diluida en condiciones de alta presión y temperatura, para formar fenoles. Esta reacción no requiere grupos desactivantes en posición orto/para y sigue un mecanismo diferente al de la sustitución nucleófila aromática por adición-eliminación.

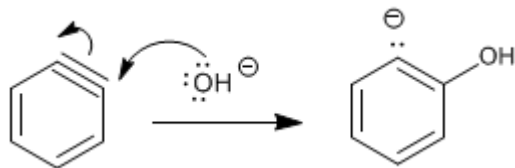


Esta reacción fue descubierta en 1928 por los químicos de la compañía Dow Chemical. El mecanismo consiste en la eliminación de HCl con formación de un intermedio inestable llamado bencino, el cual es atacado por los iones hidróxido del medio, para formar fenol.

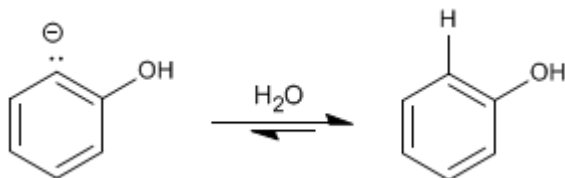
Etapas 1. Eliminación de HCl



Etapas 2. Adición del ion hidróxido al bencino



Etapas 3. Protonación



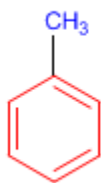
El mecanismo de esta reacción recibe el nombre de sustitución nucleófila aromática por eliminación-adición.

Cuando en el benceno existen sustituyentes produce mezclas, debido al ataque del nucleófilo sobre los dos carbonos del triple enlace.

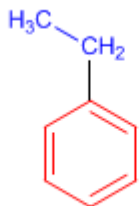
PROBLEMAS NOMENCLATURA - BENCENO

Nomenclatura de Benceno - Reglas IUPAC

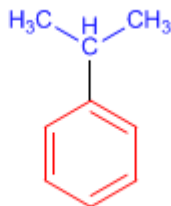
Regla 1. En bencenos monosustituídos, se nombra primero el radical y se termina en la palabra benceno.



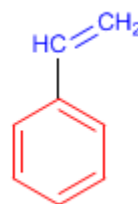
Metilbenceno



Etilbenceno

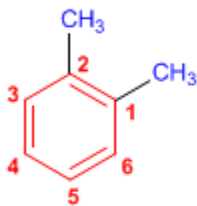


Isopropilbenceno



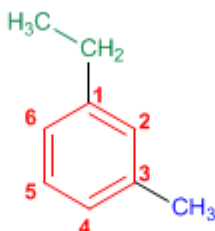
Vinilbenceno

Regla 2. En bencenos disustituídos se indica la posición de los radicales mediante los prefijos *orto-* (*o-*), *meta* (*m-*) y *para* (*p-*). También pueden emplearse los localizadores 1,2-, 1,3- y 1,4-.



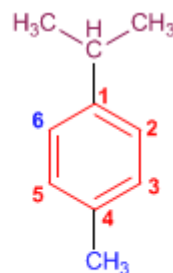
o-Dimetilbenceno

(1,2-Dimetilbenceno)



m-Etilmetilbenceno

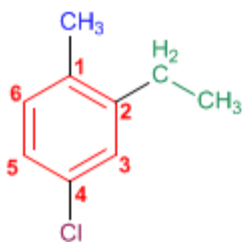
(1-Etil-3-metilbenceno)



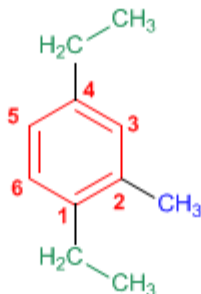
p-Isopropilmetilbenceno

(1-Isopropil-4-metilbenceno)

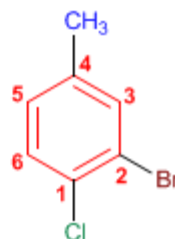
Regla 3. En bencenos con más de dos sustituyentes, se numera el anillo de modo que los sustituyentes tomen los menores localizadores. Si varias numeraciones dan los mismos localizadores se da preferencia al orden alfabético.



4-Cloro-2-etil-1-metilbenceno

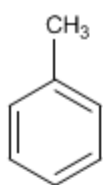


1,4-Dietil-2-metilbenceno

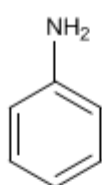


2-Bromo-1-cloro-4-metilbenceno

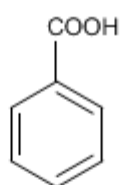
Regla 4. Existen numerosos derivados del benceno con nombres comunes que conviene saber:



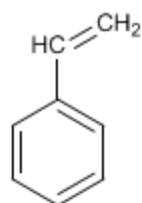
Tolueno



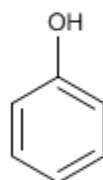
Anilina



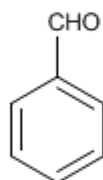
Ac. Benzoico



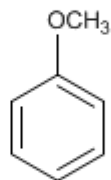
Estireno



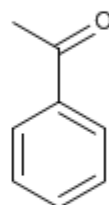
Fenol



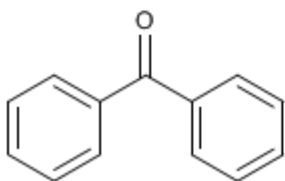
Benzaldehido



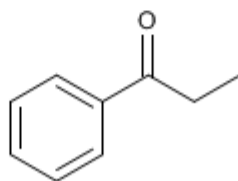
Anisol



Acetofenona



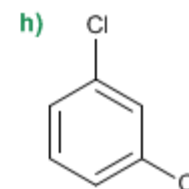
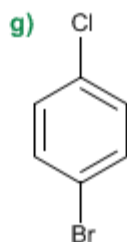
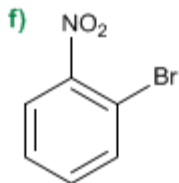
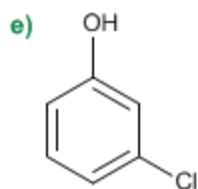
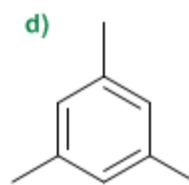
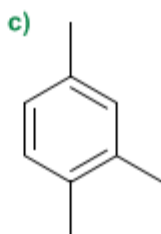
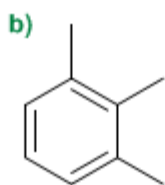
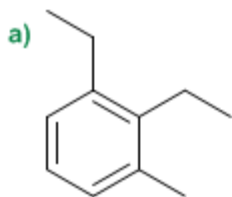
Benzofenona



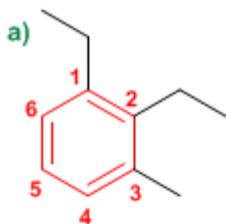
Propiofenona

Nomenclatura de Benceno - Problema 0.1

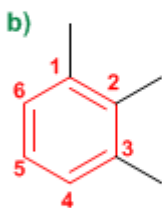
Nombra los siguientes derivados del benceno:



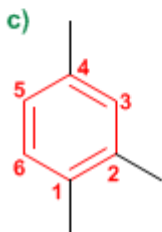
Solución



1. Cadena principal: benceno
2. Numeración: los sustituyentes deben tomar los menores localizadores, y además, se asignan los localizadores menores a los grupos que van antes en el orden alfabético (etilo antes que metilo)
3. Sustituyentes: etilos en 1,2 y metilo en 3.
4. Nombre: 1,2-Dietil-3-metilbenceno



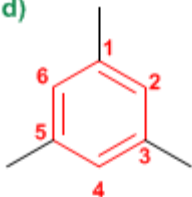
1. Cadena principal: benceno
2. Numeración: los sustituyentes deben tomar los menores localizadores.
3. Sustituyentes: metilos en posición 1,2,3.
4. Nombre: 1,2,3-Trimetilbenceno



1. Cadena principal: benceno
2. Numeración: los sustituyentes deben tomar los menores localizadores.
3. Sustituyentes: metilos en posición 1,2,4.
4. Nombre: 1,2,4-Trimetilbenceno

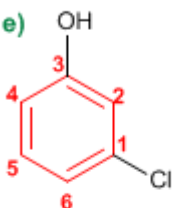
El anillo se numera para que los sustituyentes tomen los localizadores más bajos. En caso de empate se tiene en cuenta el orden alfabético

d)



1. Cadena principal: benceno
2. Numeración: se parte de un metilo y se numera en cualquier dirección.
3. Sustituyentes: metilos en 1,3,5.
4. Nombre: 1,3,5-Trimetilbenceno

e)



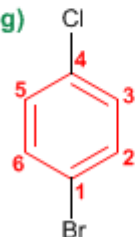
1. Cadena principal: benceno
2. Numeración: la numeración comienza en el cloro (va antes alfabéticamente) y prosigue por el camino más corto hacia el hidroxilo.
3. Sustituyentes: cloro en posición 1 e hidroxilo en posición 3 (posición meta)
4. Nombre: 1-Cloro-3-hidroxibenceno (*m*-Clorohidroxibenceno)

f)



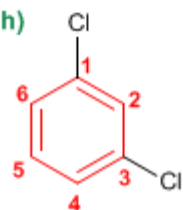
1. Cadena principal: benceno
2. Numeración: la numeración comienza en el bromo (preferencia alfabética)
3. Sustituyentes: bromo en posición 1 y nitro en posición 3 (posición orto)
4. Nombre: 1-Bromo-3-nitrobenzoceno (*o*-Bromonitrobenzoceno)

g)



1. Cadena principal: benceno
2. Numeración: comienza en el bromo (preferencia alfabética sobre el cloro)
3. Sustituyentes: bromo en 1 y cloro en 4 (posición para)
4. Nombre: 1-Bromo-4-clorobenceno (*p*-Bromoclorobenceno)

h)



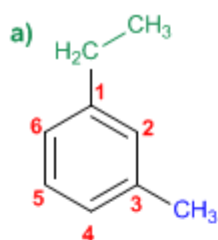
1. Cadena principal: benceno
2. Numeración: localizadores más bajos posibles a los cloros.
3. Sustituyentes: cloros en posición 1,3.
4. Nombre: 1,3-Diclorobenceno (*m*-Diclorobenceno)

Nomenclatura de Benceno - Problema 0.2

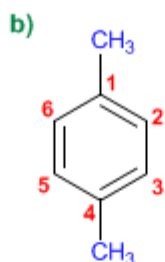
Formular los siguientes derivados del benceno:

- | | |
|---|---|
| a) 1-Etil-3-metilbenceno | k) 4,5-Difenil-1-octeno |
| b) <i>p</i> -Dimetilbenceno | l) 2-Fenil-4-metilhexeno |
| c) 1-Butil-3-etilbenceno | m) 1-(metiletil)-4-(2-metilpropil)benceno |
| d) <i>o</i> -Cloronitrobenceno | n) 6-Fenil-3-metilhexa-1,4-dieno |
| e) <i>m</i> -Bromoclorobenceno | o) <i>cis</i> -1-Fenil-1-buteno |
| f) <i>p</i> -Diisopropilbenceno | p) <i>trans</i> -2-Fenil-2-buteno |
| g) 1- <i>tert</i> -Butil-4-metilbenceno | q) 7-Etil-4,5-difenildec-5-en-1-ino |
| h) <i>o</i> -Alilvinilbenceno | r) <i>m</i> -Diciclohexilbenceno |
| i) <i>m</i> -Etilpropilbenceno | s) <i>p</i> -Ciclobutilciclobutilbenceno |
| j) 2-Etil-1,4-dimetilbenceno | t) 3-(1,1-Difeniletil)-3-metilhex-1-en-5-ino. |

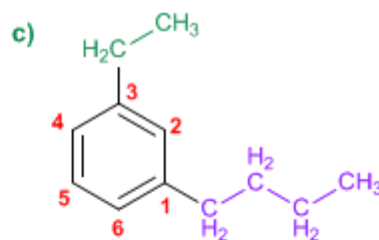
Solución



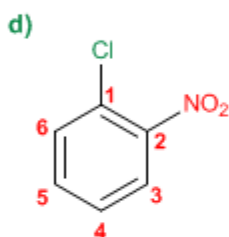
1-Etil-3-metilbenceno



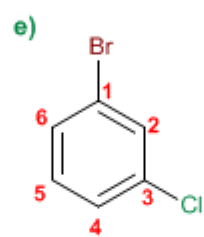
p-Dimetilbenceno



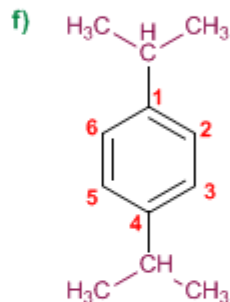
1-Butil-3-etilbenceno



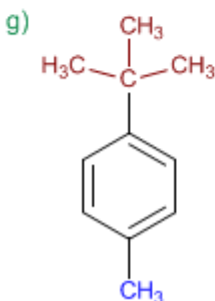
o-Cloronitrobenceno



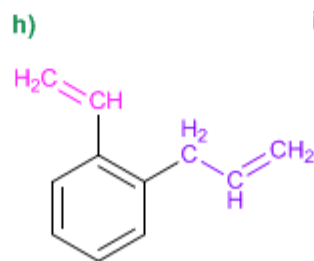
m-Bromoclorobenceno



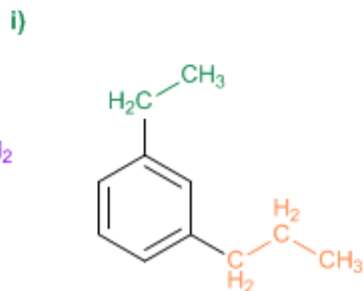
p-Diisopropilbenceno



1-*tert*-Butil-4-metilbenceno

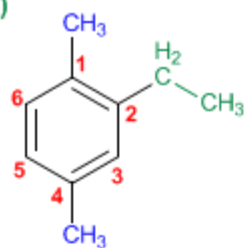


o-Alilvinilbenceno



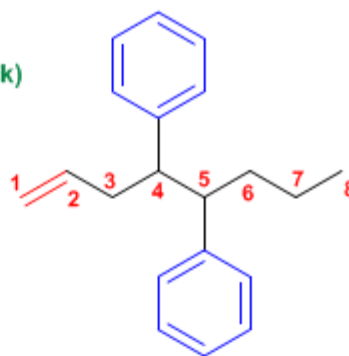
m-Etilpropilbenceno

j)



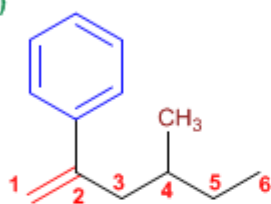
2-Etil-1,4-dimetilbenceno

k)



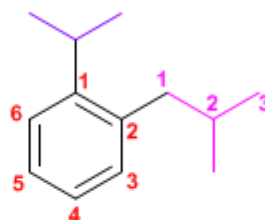
4,5-Difenil oct-1-eno

l)



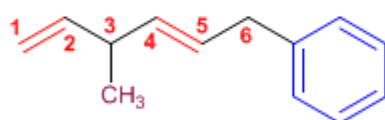
2-Fenil-4-metilhex-1-eno

m)



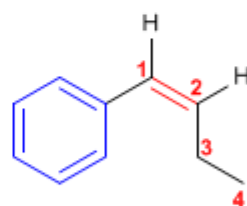
1-(metiletil)-2-(2-metilpropil)benceno

n)

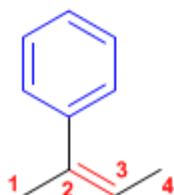


6-Fenil-3-metilhexa-1,4-dieno

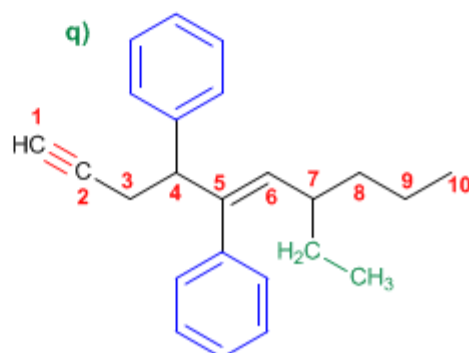
o)

*cis*-1-Fenil-1-butenó

p)

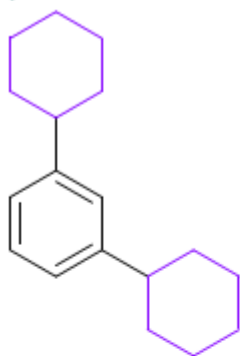
*trans*-2-Fenil-2-butenó

q)



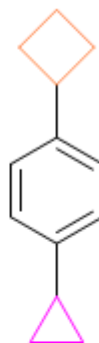
7-Etil-4,5-difenildec-5-en-1-ino

r)



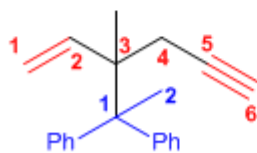
m-Diciclohexilbenceno

s)



p-Ciclobutilciclopropilbenceno

t)



3-(1,1-Difeniletil)-3-metilhex-1-en-5-ino.

Agradecimientos:

❖ <http://www.quimicaorganica.org>

❖ <http://www.taringa.net/perfil/jose07070012>